Wieslaw Kurdowski

Cement and Concrete Chemistry

Springer

Cement and Concrete Chemistry

Wieslaw Kurdowski

Cement and Concrete Chemistry

Springer

Wieslaw Kurdowski
Instytut Szkła I Materiałów Budowlanych
Kraków
Poland

ISBN 978-94-007-7944-0 ISBN 978-94-007-7945-7 (eBook)
DOI 10.1007/978-94-007-7945-7
Springer Dordrecht Heidelberg New York London

Library of Congress Control Number: 2014931241

© Springer Science+Business Media B.V. 2014
This work is subject to copyright. All rights are reserved by the Publisher, whether the whole or part of the material is concerned, specifically the rights of translation, reprinting, reuse of illustrations, recitation, broadcasting, reproduction on microfilms or in any other physical way, and transmission or information storage and retrieval, electronic adaptation, computer software, or by similar or dissimilar methodology now known or hereafter developed. Exempted from this legal reservation are brief excerpts in connection with reviews or scholarly analysis or material supplied specifically for the purpose of being entered and executed on a computer system, for exclusive use by the purchaser of the work. Duplication of this publication or parts thereof is permitted only under the provisions of the Copyright Law of the Publisher's location, in its current version, and permission for use must always be obtained from Springer. Permissions for use may be obtained through RightsLink at the Copyright Clearance Center. Violations are liable to prosecution under the respective Copyright Law.
The use of general descriptive names, registered names, trademarks, service marks, etc. in this publication does not imply, even in the absence of a specific statement, that such names are exempt from the relevant protective laws and regulations and therefore free for general use.
While the advice and information in this book are believed to be true and accurate at the date of publication, neither the authors nor the editors nor the publisher can accept any legal responsibility for any errors or omissions that may be made. The publisher makes no warranty, express or implied, with respect to the material contained herein.

Printed on acid-free paper

Springer is part of Springer Science+Business Media (www.springer.com)

Preface

Writing a book on the chemistry of cement and concrete is a very responsible task, and if we take into account very valuable works of Lea and principally of Taylor, even unusually responsible. His last book is of the highest value and, apart from its clear presentation of all important problems of cement chemistry, it contains a different and interesting Taylor's hypothesis, among others concerning the structure of C-S-H phase.

The progress in cement chemistry was particularly very quick in the last thirty years, principally because of the development of new methods and techniques, including the progress in scanning electron microscopy and introduction of some non-typical, quite new methods. To the latter ones I enclose the electrons Auger, which make possible to determine the superplasticizer layer on cement grains. In my book, I tried to present the maximum of interesting experimental results and linked them with hypotheses, leaving for the readers the last choice.

One of my goals was also to remind some scientists, which innovative works make possible the further development of cement chemistry and which were forgotten, particularly by young researches. A typical example is Professor Hans Kühl, who already in 1907 had established the accelerating effect of sodium hydroxide and of sulphate ions on the hardening of granulated blastfurnace slag. In 1908 H. Kühl obtained a German patent for the production of supersulphated cement, based on his discoveries. During the workshop "$Ca(OH)_2$ in Concrete" J. Gebauer reminded that the concrete from this cement, used to build the Beervlei Dam in South Africa, had after forty five years of exploitation the strength of 124 MPa. The most probable is that only "the lime saturation factor", which was also introduced by H. Kühl, is till now linked with his name.

The writing of this book would not be possible without numerous fruitful discussions with my friends, whom I present my warmest thanks. I owe particularly many to the discussions with the following professors: A. Bielański, H. F. W. Taylor, F. W. Locher, W. Wieker, and A. Małecki, as well as to Sorrentinos and to Mike George.

Without crucial help of Professor Wiesława Nocuń-Wczelik, who translated the majority of the book, appearing of the English version will be not possible.

I present my thanks to my young assistant Aleksandra Bochenek, who wrote the English version of all tables and figures, as well as text edition, and particularly the preparation of figures was a very laborious task.

I would like also to thank my former co-worker Barbara Trybalska for the beautiful scanning electron microscope photos that she took me when she worked with me in the AGH University of Science and Technology.

Kraków, September 2013 Wiesław Kurdowski

Acknowledgments

In the book there are many figures which enhance its value in a significant degree and make several phenomena much clearer for the readers. All these figures are touching very important and, in majority of cases, complicated processes or relations and were included in the papers of world–known authors.

I would like to present my warm thanks for all authors as well as for the publishers, being copyrights holders, who granted me permission to reproduce these figures in the book. First of all, I address my thanks to Elsevier, because the majority of figures are from the great journal "Cement and Concrete Research", as well as to American Ceramic Society, Presses des Ponts et Chaussées and Applied Science Publishers. I address also my thanks to Editions Septima, which edited the Proceedings of 7th International Congress on the Chemistry of Cements in Paris in 1980. However, I could not find neither Editions Septima nor the successors of this Publisher. The same was with the Liaison des Laboratoires des Ponts et Chaussées Publisher, to which I address also my deep thanks. I due also my great thanks to Chemical Publishing Company, INC. to grant me permission to reproduce some figures from the excellent book of F.M. Lea "The Chemistry of Cement and Concrete". All these figures are of crucial importance for my book.

Contents

1 Cement Kinds and Principles of their Classification 1
1.1 The History of Binders and Concrete 1
1.2 Principles of Cement Classification 10
References 19

2 Portland Cement Clinker 21
2.1 Portland Cement Clinker Burning 21
2.2 The Phase Systems Important for Cement Chemistry 32
2.2.1 The System $CaO–SiO_2–Al_2O_3$ 32
2.2.2 The System $CaO–Fe_2O_3–SiO_2$ 39
2.2.3 The System $CaO–Al_2O_3–Fe_2O_3$ 40
2.2.4 The System $CaO–SiO_2–Al_2O_3–Fe_2O_3$ 41
2.2.5 Departure from Equilibrium in the Clinkering Process 46
2.3 The Clinkering Process in Industrial Mixes 48
2.3.1 The Clinkering Process Modification in the Presence of Mineralizers 55
2.3.2 Clinkering Process in Rotary Kiln 63
2.4 Thermochemistry of Clinkering Process 69
2.5 Phase Composition of Portland Cements 72
2.5.1 Tricalcium Silicate and Alite Phase 77
2.5.2 Dicalcium Silicate and Belite Phase 88
2.5.3 $Ca_3 Al_2O_6$ and Aluminate Phase in Clinker 98
2.5.4 Ferrite Phase 103
2.5.5 Minor Phases 107
2.5.6 Methods of Clinker Phase Composition Determination 115
References 123

3 Hydration of Clinker Phases 129
3.1 Introduction 129
3.2 Silicate Hydration 131

3.2.1 Tricalcium Silicate Hydration 131
3.2.2 Dicalcium Silicate Hydration 147
3.2.3 C–S–H Phase 148
3.3 Hydration of Calcium Aluminates 166
3.3.1 The System $CaO–Al_2O_3–H_2O$ 166
3.3.2 Calcium Sulphoaluminate Hydrates and Other Aluminate Hydrated Phases 171
3.3.3 C_3A Hydration 179
3.3.4 C_3A Hydration in the Presence of Gypsum 186
3.3.5 Hydration of Different C_3A Polymorphs 188
3.4 Hydration of Ferrite Phase 190
3.5 Minor Hydrated Phases in Cement Paste 191
3.6 Heat of Hardening 192
References 200

4 Cement Hydration 205
4.1 Cement Hydration at Room Temperature 205
4.1.1 Paste Phase Composition 212
4.1.2 Role of Gypsum in Hydration and Disturbances of the Setting Process 213
4.1.3 Effect of Selected Compounds on Cement Hydration 226
4.1.4 The Effect of Grinding Aids 254
4.1.5 Chromium Reducers 256
4.2 Hydration of Cement in Hydrothermal Conditions 258
4.2.1 Phases in the $CaO–SiO_2–H_2O$ System 258
4.2.2 The Conditions of Formation and Structures of Some Selected Phases 259
4.2.3 Phase Composition of Cement Hydrated in Hydrothermal Conditions 265
References 272

5 The Properties of Cement Paste 279
5.1 The Rheological Properties of Concrete 280
5.2 Relationship Between the Microstructure and Strength of Cement Paste 303
5.3 Deformation of the Paste 332
5.3.1 Volume Changes of the Plastic Paste 333
5.3.2 Drying Shrinkage 341
5.3.3 Volume Changes of Concrete 348
5.3.4 Creep 349
5.3.5 Permeability of Paste 351
References 364

6 Concrete Properties 369
6.1 Effect of Cement Paste on Concrete Properties 369
6.2 Cement Paste–Aggregate Bond 374
6.3 Paste–Reinforcement Bond 386
6.4 Concrete Corrosion 392
6.4.1 Paste–Aggregate Reactions 396
6.4.2 Limestone Aggregates 412
6.4.3 Delayed Ettringite Formation 414
6.4.4 Corrosion of Concrete in the Chlorides Solutions 426
6.4.5 Sulphate Attack 441
6.4.6 Corrosion in Sea Water 454
6.4.7 Miscellaneous Corrosive Media 459
6.4.8 Carbonation of Concrete 460
6.4.9 Soft Waters 467
6.4.10 Action of Frost on Concrete 470
6.4.11 Corrosion of Steel in Concrete 478
6.5 Efflorescence of Concrete 485
6.6 Admixtures Modifying Paste and Concrete Properties 489
6.6.1 Water Reducing Admixtures (Plasticizers) 490
6.6.2 Superplasticizers 495
6.6.3 Shrinkage Reducing Admixtures 510
6.6.4 Air Entraining Agents 511
6.6.5 Permeability Reducing Admixtures 513
6.6.6 Viscosity Modifying Admixtures 514
6.7 Mineral and Chemical Composition of Aggregates 515
References 522

7 Mineral Additions for Cement Production 533
7.1 Classification 533
7.2 Metallurgical Slags 538
7.3 Slag Cements 548
7.4 Fly Ash 556
7.5 Cements with Fly Ash Addition 567
7.6 Silica Fume 573
7.7 Fillers 574
7.8 Metakaolinite 577
References 578

8 Hydration of Cements with Mineral Additions 585
8.1 Hydration of Slag 585
8.2 Fly Ash Hydration 590
References 600

9 Special Cements 603
9.1 Calcium Aluminate Cement 604
9.2 White and Coloured Cements 613
9.3 Expansive Cements 615
9.4 Rapid Hardening and Fast–Setting Cements 638
9.5 Low Energy Cements 641
9.5.1 Alinite Cements 647
9.6 Oilwell Cement 649
9.7 Sorel Cement 651
9.8 Very High Strength Pastes 652
References 655

10 New Concretes 661
10.1 Introduction 661
10.2 High Performance Concretes 662
10.3 Self Compacting Concrete 668
10.4 Reactive Powder Concretes 669
10.5 Polymer–Cement Concretes 672
References 674

Index 677

Chapter 1
Cement Kinds and Principles of their Classification

1.1 The History of Binders and Concrete

In the early period of civilisation the buildings were constructed by placing one heavy rock block on another, which were laying firmly due to friction forces only as like that of the famous edifices in Mycenae. With the civilisation development the different binders started to be used [1].

In Egypt the dried clay bricks without burning were linked with Nile slim (2). Such construction was effective in dry climatic zone only, because low moisture durability of these materials. Also the blocks in first stairs Djoser's pyramid were linked with clay (twentyseventh century before Christ) in Sakkara [2].

The plaster found wide application in ancient Egypt [2]. It was applied as mortar and to stucco decoration, for example in Tutankhamen's tomb, for finishing the tombstones of calcite (called alabaster). As mortar it was used in pyramids, in Giza. The beginning of its application is not establish; it is regarded that it falls in the period from 5,000 to 3,400 year before Christ [2]. The plaster application, instead of lime Jaworski explains by the lack of fuel, because the limestone are more easily accessible than gypsum raw materials [2].

The lime mortars were introduced to Egypt only about 300 year before Christ the Romans and the Greeks, which on turns did not know gypsum because of its limited usefulness in the humid climate of Italy and Greece.

The lime was applied very long ago by Greeks, and even earlier on Crete [2]. In turn from Greeks it was adopted by Romans. The correct technology of lime slacking and mixing it with sand. The mortar was mixed very carefully and compacted, which assured it a high density, thus to our times the edifices can be found in which inside the mortar non–carbonated calcium hydroxide is preserved [1].

Both Greeks and Romans knew the properties of some volcanic deposits, which finely ground and mixed with lime and sand give the mortars not only of higher strength, but also of higher durability on water influence, also of sea water [1]. Greeks applied for this purpose volcanic tuff from island of Santorin (known for to–day as Santorin earth), and Romans different raw materials and tuffs from the Neapolitan gulf. The origin of the best material was Pozzuoli (Puteoli) to whom the name was given pozzolana. Vitruvius writes about it: "There is a kind of sand,

W. Kurdowski, *Cement and Concrete Chemistry*,
DOI 10.1007/978-94-007-7945-7_1, © Springer Science+Business Media B.V. 2014

which in natural state has the extraordinary properties. It was discovered in a gulf in proximity of the Vesuvius mountain; blended with lime and broken stone hardens as well under water as in ordinary building" [1]. Probably also very long ago the Romans started to apply Rheine tuff, known as trass [1].

The Romans replaced also the natural pozzolana by the ground roofing–tiles, bricks and porcelain. Lea states that the name "cement" in the Late–Latin or Old–French languages was for the first time used to determine the materials which now are called artificial pozzolanas [1]. Later on this name was used for mortar produced from three components, and only recently the to–day mining was adopted.

To Romans we also owe the name "hydraulic cement" as they defined the binders hardening under water and thanks to the reaction with water [3]. Some blended materials, in order to better define their composition, was called pozzolanic cements.

There are proofs that already in buildings in Create the crushed ceramic pot-sherds (minoyen culture) were added to lime to give it the hydraulic properties [1]. On this basis the assumption was developed that Romans used firstly artificial pozzolanic materials, before they check the natural pozzolanas. Jaworski stats that in twelveth century before Christ Phoenician used hydraulic lime to mortar building the temple in Cyprus [2].Already about tenth century before Christ they used the bricks flour as the admixture giving to lime mortar hydraulic properties [2].

After the decay of Romans Empire the art of good binders production disappears. Lea cites the opinion of Viollet–le–Duc that in the period from nineth to eleventh centuries totally fell through the art of lime burning and it was applies as badly burned lumps, without the addition of crushed ceramic materials [1]. The quality of mortars became only improved in twelveth century, however, from fifteenth century their quality were already again very good, among others the washed sand, without clay impurities was used. There are proofs that in England from seventeenth century pozzolanas were again used. The mortars were still named cements which proofs can be found in Bartholomew Anglicus. However, the name "mortar" was also used already from the year 1290 [1].

During long time it was believed that the only one hydraulic binder is the mixture of lime with natural or artificial pozzolanas. It is proved by the Rondelet works on surprising level from 1805 and additionally, which underlines Lea, Rondelet cites the old authors, which were authorities, namely Pliny, Vitruvius, and saint Augustine [1]. The clarity of judgements, and also the extraordinary intuition of these authors surprises till today.

Revolution in the field of hydraulic binders production makes John Smeaton who made inquiries to the best material for the construction of the lighthouse in Eddystone Rock in 1756. He found that the better properties have the mortars of the lime burned from the raw material reach in clayey matter. It was equivalent to the discovery of hydraulic lime. Probably Smeaton was the first to use this name. Forty years later James Parker from Northfleet obtained a patent for the product from burned marl, which was named some years later as Roman cement. It was rapid setting cement. This cement started to be produced soon from the raw materials occurring near Boulogne.

The author of artificial hydraulic lime, produced by the burning of the interground mixture of choc and clay was L.J. Vicat, which published his results in 1818. He can be recognised as the predecessor of the technology of Portland cement production.

Joseph Aspdin is recognised as one of the inventor of Portland cement, which in 1824 patented the method of binder production from the burned mixture of limestone and clay, for the first time using the name Portland cement, because its colour resembled the stone from Portland. However, he burned the limestone at too low temperature, and the quality of product was bad.

Lea [1] and Bogue [3] state that the actual creator of Portland cement was Isaac Charles Johnson, which after several experiments established the correct proportion of clay and limestone, and also chose the advantageous, higher burning temperature. It happened at about 1845 year. It cannot be forgotten that he had taken advantage of the experiences of many his predecessors in England, chiefly J. Smeaton, Higgins, J. Parker and J. Frost, and also of Swede Bergmann, Dutchman J. John, and mainly L.J. Vicat.

Some authors claim that the higher burning temperature introduction we owe to Aspdin. Johnson applied this method in the factory in Gateshead, which he had taken after Aspdin leaved it in 1851 [4]. Johnson obtained a patent for improvement of Portland cement production in the year 1872. The Johnson achievement was recognised also by Michaelis, it is, however, the open matter to whom of two precursors of Portland cement producing—Aspdin or Johnson—this invention should be attributed [1, 4].

There are few information on the production of hydraulic lime in Poland. Górewicz states that it was used by the Teutonic knights for castle Malbork construction [5]. He states further the textile factory in Tomaszów Mazowiecki, which was build in 1828. The lime mortar was used for bonding of erratic boulders, from which the foundations were build. The significant importance ascribes Górewicz to the production, in the same period, of hydraulic lime used for the construction of Augustowski Channel. It was the hydraulic lime of excellent quality, and made of it mortars and concretes has today the compressive strength equal 15–50 MPa [5]. The hydraulic lime factory was erected in the neighbourhood of the foreseen channel location, and in the technology the advantage of L.J. Vicat works was taken [5]. During the production technology elaboration the experiments were made by professor Joseph Nowicki from Professional School in Warsaw.

Thirty years later the first cement plant on Polish Land was build in Grodziec and started production in 1857, which was the fifth working cement plant in the World (Fig. 1.1). In the twenty year of inter war period it was sell by the owner Stanislaw Ciechanowski to Solvay and significantly developed. In 1939 its capacity achieved 390 thousand tons per year [6].

Cement production on Polish Land increased quickly after the year 1884, and its development lasted till 1914. With exception of the small factory in Wejherowo, which was build in 1872, the remaining cement plants was erected after 1884 year—still in this year plant “Wysoka” in Łazy, in 1885 “Szczakowa” in Szczakowa and

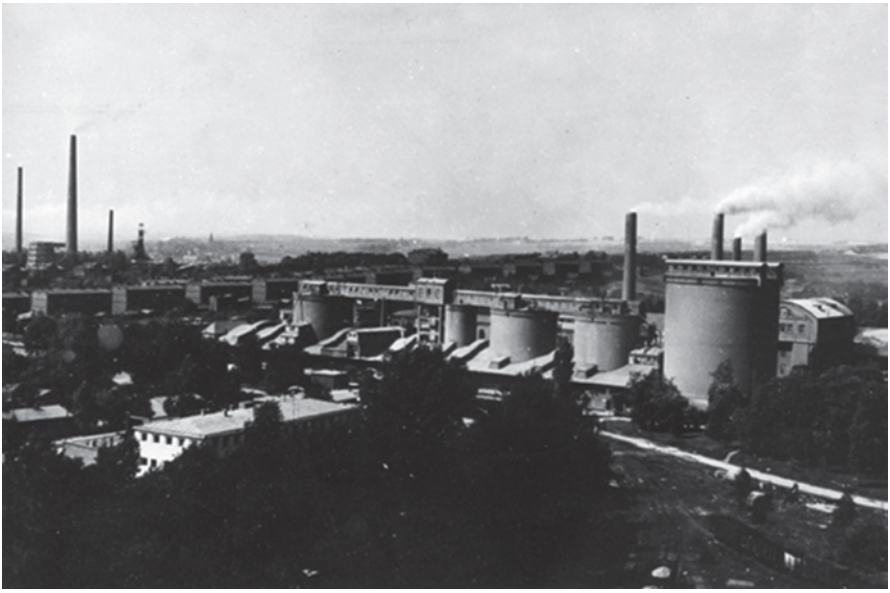


Fig. 1.1 Cement plant "Grodziec" in 1957, general view

"Bonarka" in Podgórze, near Kraków. In 1889 started the exploitation of "Goleszów" factory in Goleszów, and in 1894 "Firlay" in Lublin. During the years 1897–1898 further two cement plants were build, namely "Rudniki" near Częstochowa and "Klucze" near Rabsztyn. Very quickly further plants were erected, in total 15, but in this number the most ten in Russian Partition. During the First World War cement industry in Russian Partition was significantly destroyed, however, the remaining cement factories were not affected during war. From the year 1920 the progressive increase of cement production in Poland was noted, which, with the exception the crisis period, achieved a quick development (Fig. 1.2). The capacity was in year 1939 was equal 1.98 million, however the production was the highest in 1938 close to 1.72, due to the outbreak of the Second World War.

Cement from Poland was exported all over the world and was very well reputed. The new kinds of cement are introduced: high strength, with low heat of hydration [7]. As a curiosity can be reminded that people from cement plant "Saturn" patented the addition of siliceous fly ash to cement, which should increase the durability of concrete to sulphates.

After the Second World War there is a very quick development of cement industry in Poland. Already in the year 1948 cement production was higher than before the war, reaching 1.8 million ton and in 1955 was doubled, exceeding 3.8 million ton. The most tempestuous development period of cement industry was in the decennium 1965–1975, in which the production was increased from 8 to 16 million ton. The highest production was achieved in 1979, in which I was close to 23 million ton (Fig. 1.3).

Similar development was noted in others European countries and as an example cement production in Italy and Spain is given in Table 1.1, thanks to courtesy of

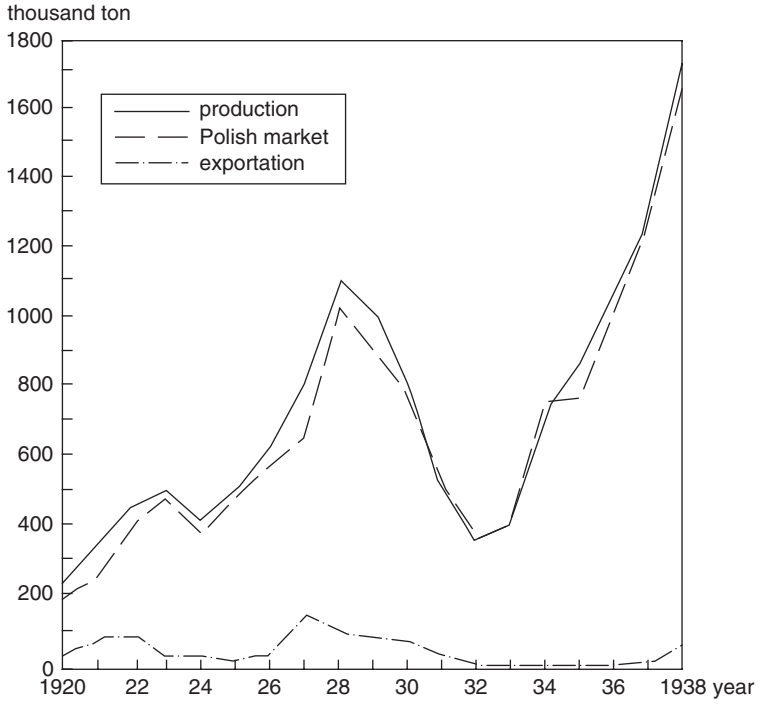


Fig. 1.2 Production and cement market in Poland in interwar period

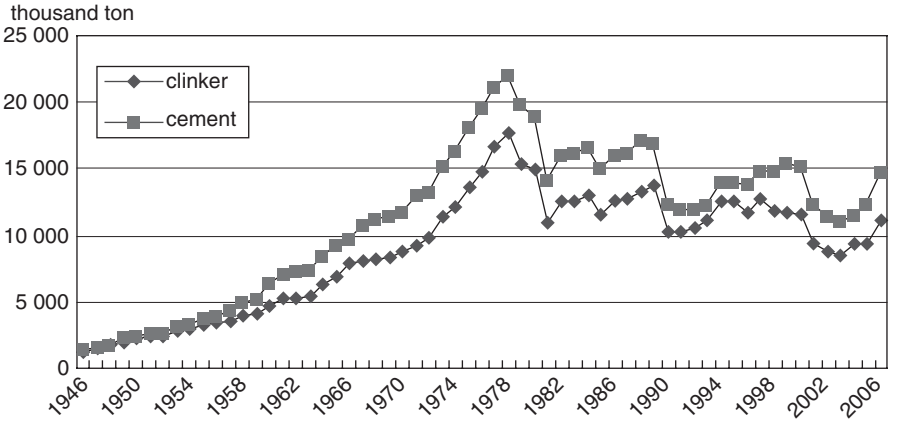


Fig. 1.3 Production of clinker and cement in Polish cement industry

Table 1.1 Cement production in Italy and Spain, thousand tone

Year	Italy			Spain		
1960	15.817					
		1964	22.935			
1965	20.733					
1970	33.126					
		1973	36.321		1973	22.247
1975	34.229			23.970		
1980	41.870			28.010	1978	30.230
		1981	42.996		1981	28.751
1985	37.266			21.880		
		1986	35.909			
1990	40.751			28.092		
		1994	33.084			
1995	34.019					
		1996	33.832			
2000	39.020					
2005	46.411					
2010	34.408					

Cement Associations of these countries. After 1980 significant fluctuations of cement production are typical, similarly as in Poland.

The economic crisis, which arrived in Poland after the 1979 embraced also cement industry. The quick decrease of cement market caused the diminution of its production (Fig. 1.3). The lowest level equal 14 million ton was in 1981, and after it was oscillating in the range from 15 to 16 million ton yearly. The change of political system in Poland brings the privatisation of cement industry, which takes place in the period from 1992 to 1998. The owners of about 90 % of production capacity of cement industry became the big concerns, namely Lafarge, Heilderberg, Cement Roadstone Holding, Cemex and Dyckerhoff. This privatisation was very successful and resulted in cement industry as modernisation, the elimination of wet method and the reconstruction of almost all factories, with introduction of modern technical solutions. The kilns with precalciners, the roller press, closed circuit in cement grinding, with the application of the most modern separators. In cement plant "Chełm" the world unique technology of clinker burning, without raw materials grinding and in "Ożarów" plant the biggest kiln in Europe for dry method was erected, with the capacity of 8,000 tpd. Also in "Górażdże" and "Kujawy" the very modern technological lines on world level were introduced and there are only the most important solutions. Others numerous, not mentioned smaller modernisation, gave the lowering of energy consumption in industry by 25 % and dust emission by 95 %.

The concrete history is also of great antiquity. Basing on Lea definition [1], which names concrete as an artificial conglomerate of gravel or broken stone with sand and lime or cement, we can relate the beginning of concrete use by people with lime binder. Thus we do not relate to concrete the ancient buildings composed of the

aggregate bind with clay, but we will link the concrete with lime binder. The most ancient concrete elements based on lime are the Yiftah in South Galilean in Israel which are dated back to 7,000 year before Christ. They were discovered in 1985 and are described by Malinowski and Garfinkel [8]. This housing from Neolithic epoch embraces several buildings in which the floors and parts of walls were made of lime concrete with aggregate of crushed limestone. Malinowski and Garfinkel [8] state the vast concrete floors surfaces testify of the mass application of lime binder which proves the good knowledge of their production. The concrete production was also well known of which testify its good quality and measured compressive strength was in the range from 15 to 40 MPa and in one case was even 60 MPa [8].

The next examples of ancient concrete were found in Lepen Whirl, in Danube bend, in Serbia [9, 10]. They are linked with buildings, which origin is dated back to 5,600 year before Christ and are concerning also mainly the floors in the fishermen cabins.

The numerous concrete constructions are linked with Roman times, because in ancient Rome the technology of good lime mortar production was well developed, including also the hydraulic lime, which was applied for concrete production. Many such examples are described by Vitruvius, using the Greek term *emplechton* as a name of today concrete precursor, which was called in Rome *opus caementitium*. However, probably Greeks were the first which used hydraulic binders for concrete production. It was the mixture of lime with volcanic ash from Nisiros island, but also from Pozzuoli, from Greek colony in Italy, near Napoli. With this binder the pieces of stone were mixed and this concrete served among others for the production of water cisterns of the volume of 600 m^3 in Athena's temple, in Rhodes island and in Piraeus port. They were also described by Pliny [1]. Instead of stone pieces Greek used also the crushed tiles, among others in maritime constructions in Delos and Rhodes. The Romans adopted these knowledge from Greeks at about 300 year before Christ, and in production of hydraulic lime they used principally the tuff from Pozzuoli. The proofs of the durability of these materials are among others the numerous concrete constructions on the sea embankment between Napoli and Gaeta "polished by sea water, but not destroyed" [1]. Great Roman concrete construction retained to our times are Colosseum (82 year before Christ), Pantheon (123 year before Christ), theatre in Pompeii for 20 thousand spectators 75 year before Christ). The dome in Pantheon, with the diameter of about 44 m, was also made of concrete.

Also in North America the ancient concrete was found. Already in 1785 the ruin of El Tajin town, located in state Veracruz in Mexico, was discovered, but only during its reconstruction in 1924 the destructed concrete roofs in different houses were found [11]. The building of these houses in which the concrete roofs were applied are dated 1,000 year before Christ. This concrete, examined by Cabera et al. [11] appeared to be light concrete from hydraulic lime binder, and sand as well as aggregate were obtained from pumice (Fig. 1.4).

Hydraulic binder was produced by adding volcanic tuff to the lime, disintegrated to powder. Thus it became evident that the use of concrete in North America is dated to the same times as Roman buildings and the base of this composite was also lime with the addition of volcanic tuff.



Fig. 1.4 Microstructure of light concrete from El Tajin under SEM

The production of good lime and also of concrete was significantly declined in Middle Ages and was developed only after the discovering of Portland cement. The most important dates in the history of the development of contemporary concrete are the following:

- 1867—Joseph Monier introduced the reinforcement of concrete,
- 1870—the production of precast elements begun,
- 1877—T. Hayatt constructed in London the house with the use of reinforced concrete,
- 1896—Feret proposed the formula for concrete strength calculation,
- 1907—Koenen introduced the prestressed concrete,
- 1924—Bolomey proposed the formula for concrete strength calculation, applied till today,
- 1929—Freyssinet constructed the reinforced concrete bridge, of the length of 180 m,
- 1980—the paste with reactive powders and very low w/c ratio started to be applied,
- 1980—Aïtcin was the first to introduce HPC,
- 1988—Aïtcin was the first to introduce the concrete from reactive powders,
- The end of eightieth—Okamura applied the self compacting concrete.

Parallel with cement production development the significant progress in cement chemistry was achieved. The real revolution we owe to French scientist Le Chatelier. This great chemist determined the phase composition of Portland cement clinker and the hypothesis of hydration process. Le Chatelier stated that, similarly as in the case of gypsum, the anhydrite cement components dissolve, the solution became oversaturated in relation to hydrates, which causes their crystallization [3].

The quick development of chemistry with the introducing of new research methods, and principally by Laue discovery in 1912 of the X–ray diffraction on the

crystal lattice. It was creating the base of modern cement chemistry. Further methods, which was the source of further new information, was the electronic microscopy coupled with X–ray microanalysis, infrared spectroscopy and nuclear magnetic resonance and recently atomic forces microscopy. These methods gave first of all the advancement of learning the structure of hydrates, including the C–S–H phase.

Many scientists had the significant contribution in the development of this discipline of science and at least some of them deserves to be mentioned. Parallel to Le Chatelier in Germany worked Michealis, who justified the importance of colloidal processes in cement hydration. The next was Eitel, which works are till today the source of important information of silicate chemistry [12]. Changed and significantly widen second edition of his book "Silicate Science", which was edited in 1966 is a beautiful achievement of the works of this author [13].

Probably even more important was the consecutive edition of chemistry of cement and concrete by English scientist F.M. Lea (first edition together with Desch) [14]. Impossible to omit also professor Hans Kühl from Berlin, which modulus of lime saturation are used till today [15]. He was also the inventor of the alkali activated granulated blast furnace slag as well as of supersulphated cement [16]. Similar position had after the Second World War Bogue and his method of phase composition calculation of Portland clinker is till now commonly used [3]. From many Russian scientists, which contribution to cement chemistry cannot be overestimated, it is necessary to mention P.P. Budnikov which works covered all important problems of binders chemistry [17], but the most important was linked with the chemistry of hydration processes. Finally the contribution of Hall Taylor [18] should be underlined, especially concerning the structure of C–S–H phase and the role of ettringite, which he differentiated into "good" and "wrong" [19].

Also in Poland, parallel to the cement industry development during the interwar period, several problems of cement chemistry were studied. They were concentrated in the chair of Cement Technology in Warsaw Technical University, under the scientific leadership of professor Zawadzki. There are principally the works of Konarzewski, concerning the formation of calcium silicates and ferrites [20, 21].

Good position had also the works of Eiger on cement hydration which was one of the first to present the hypothesis of solid solution C_3AH_6– C_3FH_6[1] [22]. He cooperated also with Zawadzki's chair, where the experiments linked with his works were executed. Eiger was the first, which has shown that the paste strength is directly proportional to the degree of cement hydration [23]. Eiger works were concerned also the most favourable cement grains size composition [21]. He participated in the Second Congress on Cement Chemistry in Stockholm in 1938. The importance of his works is testified by five citations in Lea's book, edited in 1971 [1].

In Poland, after the Second World War, the researches on cement chemistry were significantly developed with the formation in 1949 of the faculty of Ceramics in the University of Mining and Metallurgy in Kraków, and in 1954 of the Institute of Building Materials in Opole. Among the several scientists working in Cement Chemistry

[1] The author use the well known abbreviation: C – CaO, S – SiO_2, A – Al_2O_3, F – Fe_2O_3, M – MgO, H – H_2O, S – SO_3, N – Na_2O, K – K_2O

prof. George Grzymek, the author of complex technology of alumina oxide and rapid–hardening cement production [24, 25] and prof. Sulikowski, which works were devoted to the raw mix sintering and some disturbance of cement setting [26].

1.2 Principles of Cement Classification

Cement is a powder, which mixed with water forms plastic mass, easy to shape (paste), setting with time and hardening gradually with strength increase. In many standards the more exact Portland cement definitions were introduced. It is necessary because the name of cement is given to other binding materials, for example to anhydrite or magnesium oxychloride (the last is called Sorel cement).

Already Romans introduced first binders classification, dividing them to non–hydraulic and hydraulic. Frequently by defining the properties of these two kinds of binding materials there were customary assumed that the first sets only in the air, thus the setting process requires drying (lime) and the second under water. It is not exact and better as a base of division assumes their water durability. Since for example plaster of Paris sets under water, but is not water durable, while lime with ash addition gains gradually hydraulic properties, but initially, at least during 7 days should be cured in the moist air.

Presenting the rules of Portland cements classification and derived from them others kind of hydraulic binders, it must be underlined that the basis of this classification are their useful properties. In relation to this that cement is an intermediate product—the raw material for concrete production, these properties will concern the conventional "micro–concrete" or the mortar, sometimes paste, and now and again cement itself, for example phase composition. Some experts reckon the mortar to some kind of concrete, however, it is a subject of controversy.

Cement composition is the basis for division of cements into kinds: Portland, Slag, Pozzolanic; the last two with high addition of slag and pozzolana, respectively.

The hydraulic or pozzolanic additions bring about, that the pastes of these cements have usually different properties, particularly the rate of strength development (early strength), heat of hydration, resistance to corrosion factors. It found the expression in standards introduced at the end of seventies of twentieth century in France and Germany, in which Portland cements were divided into two groups: without and with additions. However, there is a pretty common opinion, particularly among cement producers, that the users should be interested only in paste (mortar) properties and to this should be limited their requirements. Thus the user can have the requirements concerning, for example, the rate of strength development, the strength immediately after heat treatment, heat of hydration, or setting time, but should not put conditions, what methods can be used by producer to fulfil these demands. Consequently in the past in the regulations of different cements applying, for example in France, grouped cements according to strength class and strength development rate and not on the basis of additions content or their lack. For example the paste of Portland cement without additions, having specific surface area

equal 280 m^2/kg, shows, under the suitable clinker phase composition, very similar properties to the paste of cement with the surface area equal 340 m^2/kg and with 30 % addition of fly ash.

In the European standards, above all in EN 197–1, another principle was adopted, dividing cement on kinds according to the quantity and kind of mineral additions. However, the division on class is common, independently of cement kind. These rules of division facilitate the classification of cements for concrete production, designated for constructions exploiting in different expositions.

The fundamental performance properties of cements, being the basis of classification are the following:

- the strength of the mortar after 28 days of hardening (class of cement),
- the rate of strength development: strength after 2 days of hardening, and exceptionally in the case of 32.5 N cement after 7 days,
- setting time.

There are few differences in the setting time in the world standards: initial setting time is in the range 40–90 min, the final is 6, 8, and 10 or 12 h. Much higher differences are embracing special cements beyond the standards (see Chap. 8). In EN 197–1 standard there is even no requirement for final setting time. This approach is, however, at least discussable.

From other important cement properties the following should be mentioned:

- heat of hydration,
- resistance to aggressive environment.

Resistance of concrete to external attack is only limited to the corrosion of sulphate water solution, in this connection only the C_3A content is normalised, respectively additionally the sum $2C_3A+C_4AF$. Exceptionally in France were normalised the requirements concerning cements designed to sea constructions (ciments "prise mer"). The composition of these cements should fulfil the following condition:

$$\frac{SiO_2 + Al_2O_3}{CaO + MgO} - \frac{2Al_2O_3}{100} \geq 0.31$$

Additionally the C_3A content $< 10\,\%$. They should also gave the positive results of the following long–term tests:

- the concrete cubes cured in open sea should not exhibit the properties worsening,
- the samples cured in sea water in laboratory should maintain good strength.

The following important property of cement is soundness. With this criterion three requirements are linked:

a. the volume change according to Le Chatelier test equal to standard requirement,
b. the content of MgO in clinker lower than 5 %,
c. limited to 3.5 % or 4 % SO_3 content.

The limit of MgO content is linked to the lack of respective standardised test of potential expansion, caused by the periclase from clinker. In ASTM standards the method of volume stability testing in autoclave was introduced, and after the United States also nine countries have adopted this method, among others Canada, Finland, Belgium and Argentine [27].

The objections towards the autoclave method were interposed, stating that it is too severe and not adopted to concrete. Mehta [28] states that in the conditions of this test the periclase is hydrated very quickly causing expansion, while in concrete this process is slow, proceeding gradually, without stress. Additionally the expansion in the paste is significant, but in concrete to low to cause cracks. For these reasons there is no correlation between the standard requirements for MgO content, which gives good result in autoclave test, and soundness of concrete. It is commonly considered that cements from clinker containing 7–8 % MgO do not cause expansion of concrete, neither in laboratory tests, nor in field trials. Gonnermann [29] found that the concrete cubes from cements containing 7–10 % MgO do not show the strength decrease even after 15 years water curing Gebauer [30] had published the first results of the research of concrete behaviour cured in open air and in laboratory. Concrete produced from cements containing 7.1 % MgO and showing expansion in autoclave higher than 7 %, did not show disadvantageous changes after 4 years. The degree of periclase hydration was 30 % and its crystals was seen in hydrated paste. Without doubt this problem needs further studies.

In connection with the requirements for concrete durability cements are divided also according to alkalis content (see Chap. 6). Cements with high and low alkalis content are distinguished and the threshold value is the sum $Na_2O + 0.658K_2O = 0.6$. Certainly there are cements with even lower content of alkalis.

In the past the division of cements on the basis of phase composition was applied, as follows: alite, alite–celite (Törnebohm called brownmillerite celite), alite–aluminate and others (Fig. 1.5) [31]. Such division, although fully justified, gives few information to the user—properties of several classes are very approximate, it has no application to cements with additions and for these reasons has no practical use. However, the chemists use it frequently enough for cement kind definition, especially in the case of special cements, which are discussed in Chap. 9.

The presented important principles of cements classification can be divided into three groups form the point of view of paste influence on concrete properties. They are the following:

1. the properties of concrete mix (chiefly consistency and workability, setting time, C_3A content, water demand),
2. concrete properties during hardening process (rate of strength development, strength after 28 days, heat of hydration, shrinkage), concrete durability (soundness, MgO, SO_3, C_3A, Na_2O_e[2], hydraulic or pozzolanic addition content).

On the end of aforementioned rules of classification the position should be taken on the methods of cement properties testing. It is, however, not necessary to justify that

[2] Na_2O_e we should call the sodium equivalent of alkalis total content, thus $Na_2O + 0.658K_2O$

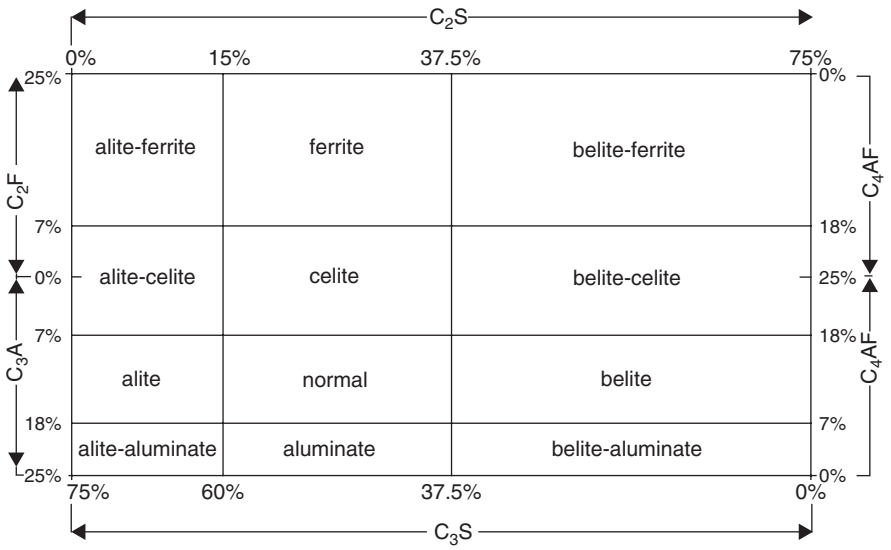


Fig. 1.5 Classification of cements on the basis of phase composition

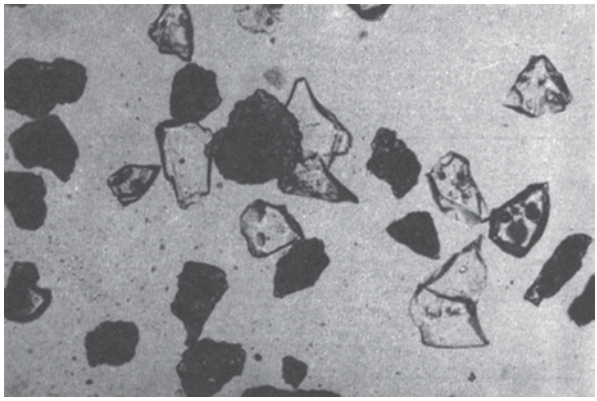


Fig. 1.6 Powder specimen of slag cement, *transparent grains*—slag, *dark grains*—clinker

the classification has only sense when there are suitable methods for determination of individual material properties with sufficient accuracy in relation to the requirements contained in this classification.

The basis for rate cements to individual kinds is cement composition based principally on chemical determinations, to which belong insoluble residue and loss on ignition. They are principally linked with cement additions. For quantitative slag content determination from long time the light microscopy is used, and the accuracy of this method is assessed to be ±5% (Fig. 1.6). Lastly also the methods of separation in heavy liquids are recommended, based on the density differences of individual cement components: clinker about 3.1 g/cm^3, slag 2.85 g/

Table 1.2 Requirements concerning the chemical composition of cements. (Content of Cr(VI) cannot exceed 2 mg/kg; in the case of higher chromium content it must be reduced by addition for example iron(II) sulphate)

Properties	Control test	Cement kind	Strength class	Required value
Loss on ignition	EN 196–2	CEM I	All	≤5.0%
		CEM II		
Insoluble residue	EN 196–2[a]	CEM I	All	≤5.0%
		CEM II		
Sulphates content (as SO_3)	EN 196–2	CEM I	32.5 N	≤3.5%
		CEM II[b]	32.5 R	
		CEM IV	42.5 N	
		CEM V	42.5 R	≤4.0%
			52.5 N	
			52.5 R	
		CEM III[c]	All	
Chlorides content	EN 196–2	All[d]	All	≤0.10%[e]
Pozzolanic activity	EN 196–5	CEM IV	All	Favourable result

[a] Determination of insoluble residue in hydrochloric acid and sodium carbonate
[b] Cement CEM III/B–T can contain up to 4.5% of sulphate in all strength classes
[c] Cement CEM III/C can contain up to 4.55 of sulphate
[d] Cement CEM III can contain more than 0.10% of chlorides, but in that case the maximal chlorides content must be given on package and/or in delivering document
[e] For prestressed concrete cements can be produced with lower chlorides content

cm^3, fly ash from hard coal about 2.6 g/cm^3. However it is a much more difficult method demanding well skilled laboratory staff. From the new methods the using of solubility differences of individual cement components in some solvents is proposed [32]. However these methods did not found practical application. For the content of siliceous fly ash

determination the method of insoluble residue is currently used (Table 1.2 and 1.3), which is multiplied by 1.25. This coefficient is the result of assumption that the siliceous fly ash contains 80% of glass.

The standard methods used for rheological studies of cement paste and water demand, assuring the normal consistency are not satisfying. Traditionally the Vicat apparatus is used, which gives no information about the initial concrete stiffening, so important for concrete mix producing and moulding. We have of course much better equipment, to which the viscometers with coaxial cylinders should be included, and also penetrometers of Bombled [33] and Banfill [34] (see also point 5.1). The methods with the use of these apparatus do not became so familiarised to bring about the conditions for standardisation. They are too sophisticated and need expensive equipment, which is important in standard methods [33]. Odler [35] proposed an interesting acoustic method of setting time measurement.

The initial paste stiffening can be detected with Vicat apparatus equipped additionally in hydraulic oil retarder of needle dip. This method is popular in Scandinavian countries, and the requirements for the paste are the same as for

Table 1.3 The requirements concerning the chemical and phase composition different cement class according to ASTM

Class	Loss on ignition max, %	Insoluble residue max, %	MgO max, %	SO_3 max, % $C_3A \leq 8$ $C_3A > 8$	C_3A max, %	Others[a], %
I II	3.0	0.75	6.0	3.0 3.5	–	–
II[b] IIA[b]	3.0	0.75	6.0	3.0	8.0	Al_2O_3 6.0 SiO_2 20.0 Fe_2O_3 6.0
III[c] IIIA[c]	3.0	0.75	6.0	3.5 4.5	15.0	–
IV	2.5	0.75	6.0	2.3	7.0	C_3S 35.0 Fe_2O_3 6.5 C_2S 40.0
V	3.0	0.75	6.0	2.3	5.0	$C_4AF+2C_3A<25.0$ or C_4AF+C_2F

[a] For all cement classes, when low alkalis content is demanded, $Na_2O+K_2O£0.60\%$; heat of hydration for class II is equal 290 kJ/kg after 7 days, class IV 250 after 7 and 280 kJ/kg after 28 days,

[b] $C_3S+C_3A<58\%$ for cements with moderated heat of hydration,

[c] For moderated sulphate resistance $C_3A<8\%$, for high sulphate resistance C_3A content $<5\%$. Mineral composition calculated according to Bogue formulae:

$S=SiO_2-SiO_2$ (insoluble) When $M_G<0.64$

$C=CaO-CaO$ (free) $-0.7\ SO_3$ $C_3S=4.07C-7.6S-4.48A-2.86F$

$C_3S=4.07C-7.6S-1.43F-6.72A$ $C_2S=2.87S-0.75C_3S$

$C_2S=287S-0.75C_3S$ $C_4AF=4.77A$

$C_3A=2.65A-1.69F$ $C_2F=1.7F-2.67A$

$C_4AF=3.04F$

$CaSO_4=1.7SO_3$

classic Vicat apparatus [36]. The sensitivity of this method is good and make possible to detect the false set, caused by the presence of low quantities of hemihydrate gypsum.

Bonin discussed the new results explaining the reasons of paste or concrete stiffening [37]. Apart of false set, occurring as the result of alkalis carbonation, which in turn react with calcium hydroxide with $CaCO_3$ precipitation, Bonin considers the case of cement paste stiffening, in which under moisture influence the rate of ettringite formation had changed [37].

On the good level is the method of strength measurement introduced by International Standard Organisation ISO in 1967, now embraced in the standard EN 196–1. The results are relatively close to the one obtained for the classic concrete, and accuracy and repeatability good. However, it is a long method and for cement class determination requires 28 days. It is the reason that there are continuous studies for quick method elaboration [38–40]. The majority of accelerated method use higher temperature of samples maturing (heat treatment). These methods are comparatively good for Portland cements, without mineral additions, however, cement with

additions have different behaviour during the heat treatment, giving very similar strength development during normal curing conditions [32]. In practise, in cement plants the strength is measured after 2 days, and, on the basis of "curve of strength development" typical for cement of this plant, the strength after 28 days is established. Two days is chosen because in the case of strength measured after shorter period there are greater errors in obtained results.

The method of differential calorimetry is one of the best method of cement heat of hydration measurements especially at early period [39]. In the world standards the method of the dissolution heat is also very popular [40]. This method is particularly suitable for long period of hydration, even for one year [41–43]. It cannot be used in the case of cements with the addition of slag or fly ash, which are not totally dissolved in the acids mixture.

In the standard EN establishing the methods of cements testing two methods of heat of hydration are given:

- in the part 196–8 the heat of dissolution,
- in the part 196–9 the semi–adiabatic method.

The heat measured with the second method after 41 h is the base for classing cement to the group "low heat of hydration" if the value is under 270 kJ/kg and to the "very low heat" if it is below 220 kJ/kg.

There are also other methods, particularly isothermal (called conductive), which are, however, particularly suitable for testing the early hydration process of cement [45].

The given classification principles are used in cement standards. In European standards cements are divided in five kinds (Table 1.4) The second kind has seven sub kind, in relation to type of mineral addition or some simultaneous additions (CEM II/A–M and CEM II B–M).

The standard EN 197–1 defines the properties of mineral additions to cement and in the case of limestone establishes the calcium carbonate content on the level at least equal 75 %, the clay content determined by methylene blue should not exceeds 1.2 % and organic carbon in the case of 0.55 and LL 0.2 %.

Also the ASTM standards distinguish traditionally five kinds of cements (Table 1.5). One of them is rapid hardening cement (Table 1.5, class III). With the introduction in USA cements with the addition of fly ash and slag further three kinds appeared.

Cement class I is applied for concrete construction, to which no special conditions are imposed. Cement class II has limited heat of hydration and moderate sulphate resistance. In this connection, beside of requirements concerning the composition, which refer to all kinds of cements, the requirements to some oxides content as well as C_3S and C_3A were introduced (Table 1.3).

In Table 1.4 the content of components in European cements, according to standard EN 197–1 was given. As a rule it was establish that the share of clinker and mineral additions is equal 100 %, and the gypsum content refers to the total and its addition, or anhydrite, is the result of normalised SO_3 content, which threshold values are 3.5 % or 4 % (Table 1.3)

Table 1.4 The kinds of European cements

Main kinds	Cement name		Main components, % mas									Secon–dary comp–onents
			Clinker K	Blast fur-nace slag S	Silica fume D[a]	Pozzolana natural P	industrial Q	Fly ash Siliceous V	calcareous W	Burnt shale T	Lime–stone L	LL	
CEM I	Portland cement	CEM I	95–100	–	–	–	–	–	–	–	–	–	0–5
CEM II	Portland slag cement	CEM II/A–S	80–94	6–20	–	–	–	–	–	–	–	–	0–5
		CEM II/B–S	65–79	21–35	–	–	–	–	–	–	–	–	0–5
	Portland silica fume cement	CEM II/A–D	90–94	–	6–10	–	–	–	–	–	–	–	0–5
	Portland pozzolana cement	CEM II/A–P	80–94	–	–	6–20	–	–	–	–	–	–	0–5
		CEM II/B–P	65–79	–	–	21–35	–	–	–	–	–	–	0–5
		CEM II/A–Q	80–94	–	–	–	6–20	–	–	–	–	–	0–5
		CEM II/B–Q	65–79	–	–	–	21–35	–	–	–	–	–	0–5
	Portland fly ash cement	CEM II/A–V	80–94	–	–	–	–	6–20	–	–	–	–	0–5
		CEM II/B–V	65–79	–	–	–	–	21–35	–	–	–	–	0–5
		CEM II/A–W	80–94	–	–	–	–	–	6–20	–	–	–	0–5
		CEM II/B–W	65–79	–	–	–	–	–	21–35	–	–	–	0–5
	Portland burnt shale cement	CEM II/A–T	80–94	–	–	–	–	–	–	6–20	–	–	0–5
		CEM II/B–T	65–79	–	–	–	–	–	–	21–35	–	–	–
CEM II	Portland limestone cement	CEM II/A–L	80–94	–	–	–	–	–	–	–	6–20	–	0–5
		CEM II/B–L	65–79	–	–	–	–	–	–	–	21–35	–	0–5
		CEM II/A–LL	80–94	–	–	–	–	–	–	–	–	6–20	0–5
		CEM II/B–LL	65–79	–	–	–	–	–	–	–	–	21–35	0–5
	Portland composite cement	CEM II/A–M	80–94	6–20									0–5
		CEM II/B–M	65–79	21–35									0–5
		CEM III/A	35–64	36–65	–	–	–	–	–	–	–	–	0–5
CEM III	Blast–furnace cement	CEM III/B	20–34	66–80	–	–	–	–	–	–	–	–	0–5
		CEM III/C	5–19	81–95	–	–	–	–	–	–	–	–	0–5
CEM IV	Pozzo–lanic[b] Cement	CEM IV/A	65–89	–	11–35					–	–	–	0–5
		CEM IV/B	45–64	–	36–55					–	–	–	0–5
CEM V	Composite cement [b]	CEM V/A	40–64	18–30	–	18–30			–	–	–	–	0–5
		CEM V/B	20–38	31–50	–	31–50			–	–	–	–	0–5

[a] The share of microsilica is limited to 10%

[b] In Portland composite cements CEM II/A–M and CEM II/B–M, in Pozzolanic cements CEM IV/A and CEM IV/B and in Composite cements CEM V/A and CEM V/B others components than clinker should be mentioned, for example CEM II/A–M(S–V–L).

Table 1.5 Kinds of cements produced in USA

Cement kind	Class	Strength min./max in MPa after days				Addition, %
		2	3	7	28	
Portland	I		12.4	19.3	27.6[a]	0
	IA (with air entraining agent)		10.0	15.5	22.1[a]	0
	II } (with moderate heat of hydration)		10.3	17.2	27.6[a]	0
	IIA }		6.9	11.7	22.1[b]	0
			8.3	13.8	22.1[a]	0
			5.5[b]	9.3[b]	17.7[a, b]	0
	III } (with high early strength)	12.4[c]	24.1			0
	IIIA }	10.0[c]	19.3			0
	IV (with low heat of hydration)			6.9	17.2	0
	V (high sulphate resistance)		8.3	15.2	20.7	0
Portland with slag addition[d]	J (SM)		12.4	19.3	24.1	25
Portland with pozzolana addition[d]	J (PM)A[e]		9.9	15.5	19.3	15
Pozzolanic	JP or P			10.3	20.7	15–40
Metallurgical	JS		8.3	13.8	19.3	25–65
Slag	S			4.1	10.3	70

[a] On special demand.
[b] Lower strength concerns cement with imposed heat of hydration or limited value of $C_3S + C_3A$.
[c] After one day of hardening.
[d] Clinker can be replaced by Portland cement, all kinds of cement with additions can be also produced in subclass with air entraining agent, additionally the variety: resistant to sulphates and limited heat of hydration can also be produced.
[e] Additionally the strength of cement with air entraining agent, but without mineral addition is as for J(SM). Clinker can be replaced by Portland or slag cement.

Table 1.6 Strength of different class of cements

Strength class	Compressive strength, N/mm^2				Initial setting time, min	Soundness, mm
	After 2 days	After 7 days	After 28 days			
32.5 N	–	≥16.0	≥32.5	≤52.5	≥75	≤10
32.5 R	≥10.0	–				
42.5 N	≥10.0	–	≥42.5	≤62.5	≥60	
42.5 R	≥20.0	–				
52.5 N	≥20.0	–	≥52.5	–	≥45	
52.5 R	≥30.0	–				

All kinds of cements are divided into six strength classes. Subclass N concerns cements with normal strength development, and class R rapid hardening cements (Table 1.6). The strength of all cements cannot be higher than 20 MPa of the value for given class, with the exception of class 52.5, which has no maximal threshold value.

References

1. Lea, F.M.: The Chemistry of Cement and Concrete, 3rd edn. Chemical Publishing Company, New York (1971)
2. Znaczko–Jaworski, S.Ł.: Oczierki Istorii Wiażuszczich Wieszczestw, Izd. Akadiemii Nauk SSSR, Moscow (1963). (in Russian: The History of Binding Materials)
3. Bogue, R.H.: The Chemistry of Portland Cement. Reinhold Publ. Corporation, New York (1947)
4. Gooding, P., Halstead, P.E.: 3rd ICCC* London, s. 1. London (1955)
5. Górewicz, J.: Cement Wapno Gips. 36, 277 (1983), 37, 113 (1984). (in Polish)
6. Selmach, M.: Cement Wapno Gips. 13, 217 (1957). (in Polish)
7. Grzymek, J.: Private Information
8. Malinowski, R., Garfinkel, Y.: Concrete Intern. 13, 62 (1991)
9. Srejovič, D.: Lepenski Vir. Srpskaknjizevna zadruga, Beograd (1969)
10. Bensted, J., Nichola, C.: Cement Wapno Beton, 73, 134 (2003)
11. Cabera, J.G., Rivera–Villarreal, I., Sri Ravindrarajah, R.: CANMET/ACI (red. V.M. Malhotra), vol. 2, p. 1215. (1997)
12. Eitel, W.: Physikalische Chemie der Silikate. L. Voss, Leipzig (1929)
13. Eitel, W.: Silicate Science. Academic Press, New York (1966)
14. Lea, F.M., Desch, C.H.: Die Chemie des Zementes und Betones. Verlag Technik GmbH, Berlin (1937)
15. Kühl, H.: Zement–Chemie. Verlag Technik, Berlin (1952)
16. Budnikow, P.P.: Izbrannyje Trudy, Izd. Akadiemii Nauk Ukraińskiej SSR, Kijew (1960). (in Russian: Book containing all papers)
17. Konarzewski, J.: Przemysł Chemiczny. 4, 165 (1932). (in Polish)
18. Konarzewski, J.: Roczniki Chemii. 11, 44 (1931)
19. Eiger, A.: Rev. Mat. Constr. Trav. Publ. (334), 141 (1937)
20. Eiger, A.: Cement. **5**, 231 (1935)
21. Eiger, A.: Tonind. Ztg**. 56**, 532, 558 (1932)
22. Grzymek, J.: 6th ICCC Moscow, t. III, s. 328. Moscow (1974)
23. Grzymek, J.: Silikattechnik. **2**, 81 (1959)
24. Sulikowski, J.: Cement. Produkcja i zastosowanie. Arkady, Warszawa (1981). (in Polish: Cement Production and Use)
25. Anamienko, N.F.: 8th ICCC Rio de Janeiro, vol. VI, p. 143. Rio de Janeiro (1986)
26. Mehta, P.K.: ASTM Publication. Special Technical Publication. (663), 35 (1953)
27. Gonnermann, H.F., Lerch, W., Whiteside, M.W.: PCA Research Laboratory Bulletin. (45), 1 (1953)
28. Gebauer, J.: 8th ICCC Rio de Janeiro, vol. VI, p. 154. Rio de Janeiro (1986)
29. Jung, W.N., Butt, J.M., Żurawlew, W.F., Okorokow, S.D.: Technologia materiałów wiążących. Budownictwo i Architektura, Warszawa (1957). (translated from Russian)
30. Dutron, P.: 8th ICCC Rio de Janeiro, vol. VI, p. 288. Rio de Janeiro (1986)
31. Bombled, J.P.: Rev. Mat. Constr. (637), 256 (1971)
32. Banfill, P.F.G.: 7th ICCC Paris, vol. IV, p. 324. Paris (1980)
33. Odler, I., Abdul–Maula, S., Hennicke, V.: 8th ICCC Rio de Janeiro, vol. VI, p. 328. Rio de Janeiro (1986)
34. Sweden State Regulations in Stockholm: B1/1960
35. Bonin, A.: 7th ICCC Paris, vol. II, pp. 11–209. Paris (1980)
36. Gaca, W.: Cement Wapno Gips. **28**, 141 (1963)
37. Kovács, R.: 8th ICCC Rio de Janeiro, vol. VI, p. 371. Rio de Janeiro (1986)
38. Relis, M., Soroka, L.: Mat. et Construc. **7**, 103 (1974)

39. Zielenkiewicz, W.: Analiza przebiegu efektów cieplnych w kalorymetrach nieizotermicznych i nieadiabatycznych. PWN, Warszawa (1966). (in Polish: The analysis of heat evolution in non–isothermic, non–adiabatic calorimeter)
40. Papadakis, M., Venuat, M.: Manuel du Laboratoire d'Essais des Ciments, Mortiers, Bétons. Eyrolles, Paris (1969)
41. de Jong, J., Marpuenie, L.: Instrum. Pract. 16, 45 (1962)
42. Zielenkiewicz, W., Kamiński, M.: Cem. Concr. Res. 12, 549 (1982)
43. Charreton, C.: Annales de ITBTP. (422), 100 (1984)

Chapter 2
Portland Cement Clinker

2.1 Portland Cement Clinker Burning

The main goal of the clinkering process is to produce the material of designed phase composition, which is called Portland cement clinker. Under the action of high temperature, parallel to the clinker phases formation, underwent the process of sintering and nodulization of material in the rotary kiln. It is of high technological importance, having the decisive influence on the rate of material transport and also on the quantity of dust carry off with gases in the kiln and in the cooler, then having its effect on heat consumption and kiln capacity.

Raw mix, composed of limestone, marl and small addition of iron corrective component is transformed, as the effect of several complicated reactions, in clinker containing from 55 to 65 % C_3S, 15–25 % C_2S, 8–12 % C_3A and 8–12 % $C_2(A, F)$.

It is convenient to follow the advancement of clinkering process by determining the free calcium oxide in the raw mix, called frequently "free lime". The content of this component on the beginning is increasing quickly, as a result of calcium carbonate decomposition, and then is gradually decreasing (Fig. 2.1), as the new compounds are formed with silica, alumina and iron.

In the process formation two stages can be distinguish: at the range of lower temperature to about 1300 °C, when the reactions proceed, as a rule, in the solid state, in the presence of very low quantities of the liquid phase, and at higher temperature, at which it is already about 25 % of the melt. It is assumed that the dicalcium silicate[1] and calcium aluminate and ferrite are formed principally as the result of reactions in the solid state. However, tricalcium silicate is formed by crystallization from the liquid phase.

The solid state reactions of $CaCO_3$ with SiO_2, Al_2O_3 and Fe_2O_3 was the object of numerous, systematic studies [1–4]. They belong to the reactions of solid phases with the formation of products interlayer between substrates. In the case of pressed sandwiches of CaO and silica as the first product the $2CaO \cdot SiO_2$ is formed and then—in CaO tablet—$3CaO \cdot SiO_2$ and in the SiO_2 tablet—rankinite $3CaO \cdot 2SiO_2$

[1] Dicalcium silicate is the orthosilicate with formula $Ca_2[SiO_4]$, and tricalcium silicate—orthosilicate with formula $Ca_3[SiO_4]O$.

W. Kurdowski, *Cement and Concrete Chemistry*,
DOI 10.1007/978-94-007-7945-7_2, © Springer Science+Business Media B.V. 2014

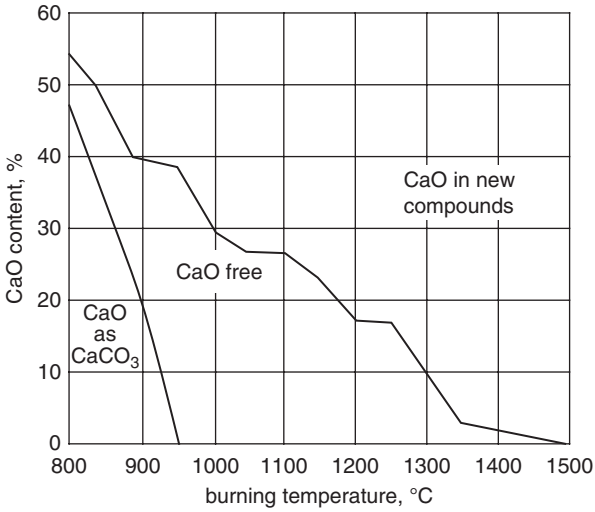


Fig. 2.1 Combination of lime during raw mix clinkering

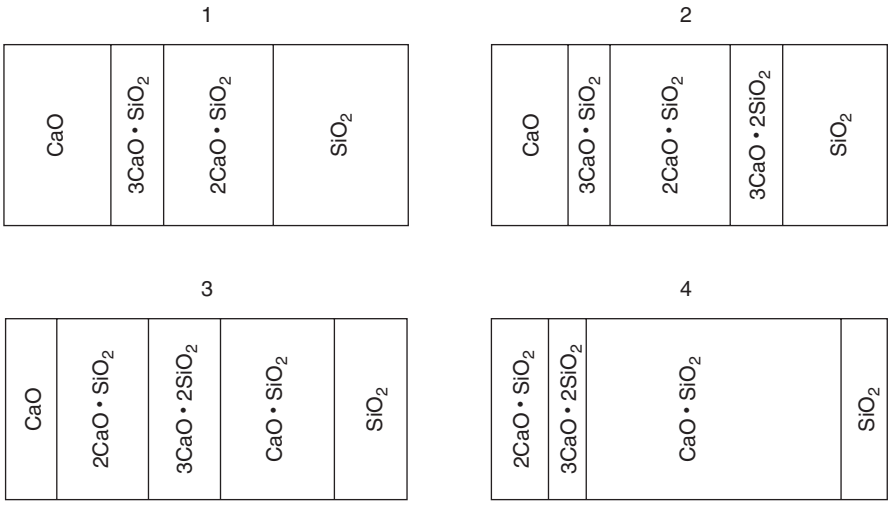


Fig. 2.2 The sequence of phases formation during the reaction of CaO with SiO_2 with molar ratio of substrates 1:1, 1–4 increase of the reaction time

(Fig. 2.2.). The change of products phase composition of the reaction versus time are shown in Fig. 2.3 [3].

The kinetic of this reaction was studied by Jander [3], which assumed that its rate is governing by the diffusion of one substrate (CaO) through the layer of the product formed to the surface of second substrate (SiO_2). Under different simplifying assumptions, using first Fick's law, Jander derived the formula

$$y^2 = kt \tag{2.1}$$

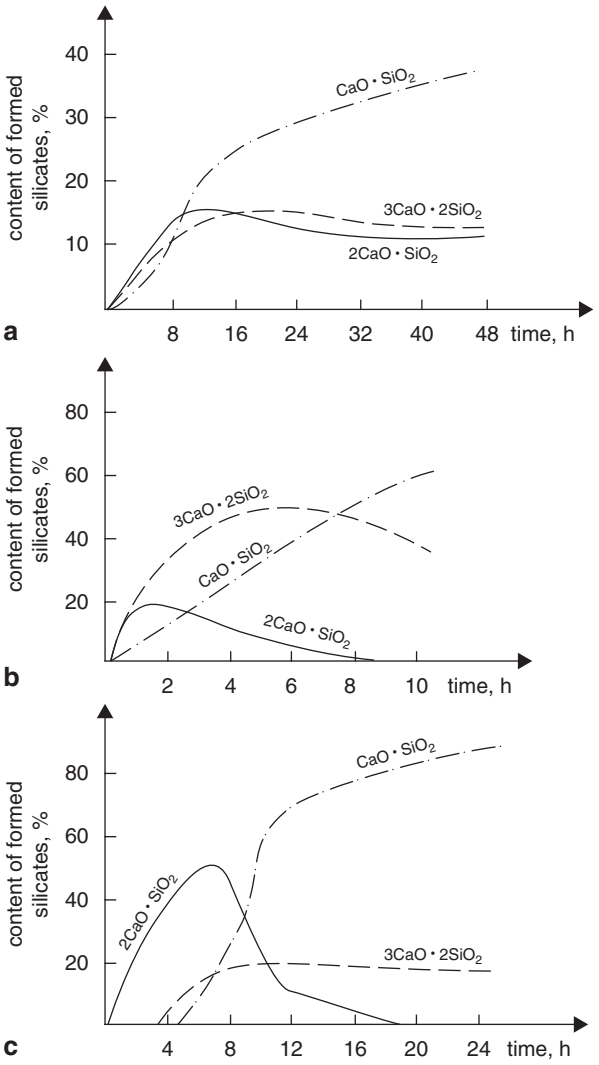


Fig. 2.3 The content of products in the function of CaO with SiO_2 reaction time in the mixture with molar ratio 1:1 (after [3]); **a** in dry air at 1000 °C, **b** in moist air at 1000 °C, **c** in dry air at 1200 °C

in which y was the product layer thickness, k—rate constant, t—time.

The layer thickness can be easily replaced by degree of transformation:

$$\alpha = \frac{\frac{4}{3}\pi r^3 - \frac{4}{3}\pi(r-y)^3}{\frac{4}{3}\pi r^3} \tag{2.2}$$

where r is the radius of substrate grain (SiO_2), covered with product layer. After introducing to the proceeding formula the expression is given

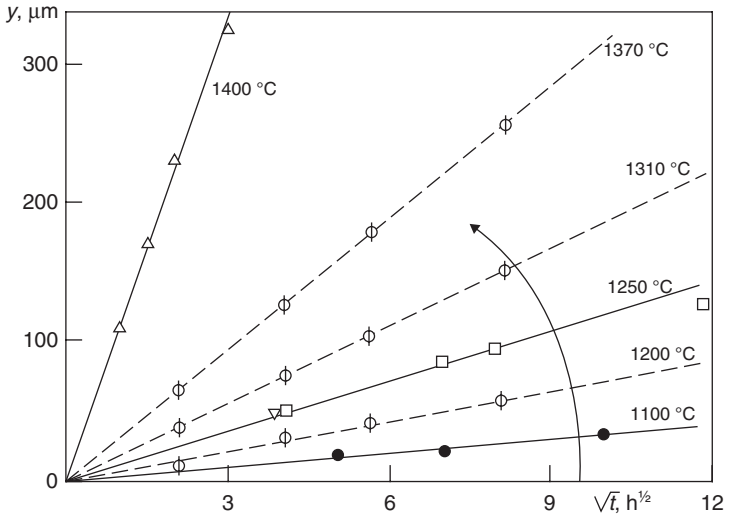


Fig. 2.4 The rate of product layer growing in relation to heating time in the mixtures: CaO++ SiO_2—*full line* and CaO+Al_2O_3—*broken line* (diagrammatic)

$$\left[1-(1-\alpha)^{1/3}\right]^2 = \left[k / r^2\right] t \tag{2.3}$$

in which α is the degree of transformation after time t, *k*—rate constant, *r*—radius of reacting grains.

The degree of transformation can be followed by free calcium oxide determination in the raw mixture. The experimental results for different time of reaction, put on the diagram of relation $\left[1-(1-\alpha)^{1/3}\right]^2$ for time give the straight lines, which coefficient of inclination is increasing with temperature.

Weisweiler et al. [5] studied the reaction advancement on the frontier of two tightly bordered tablets of CaO and SiO_2, prepared by hot pressing. Samples heated at the temperature range 1000–1450 °C gave the analogous to earlier established products sequence. However, simultaneously the glass formation of the approximate formula "CS_2" was found, at the temperature higher than 1300 °C. The product layers have thus the sequence: C/C_2S/CS/"CS_2"/S. The glass is formed as a result of calcium diffusion to the lattice of cristobalite or tridymite, in connection with polymorphic transformation of SiO_2. The rate of multiphase layer growing (*y*) in the function of reaction time (*t*) is well described by the Jander's formula $y^2 = kt$ (Fig. 2.4). Deja [6] researching the influence of different calcium silicates on the rate of tricalcium silicate formation found that it is the highest in the case of C_2S, and the slowest, when one of the substrate is a chain silicate.

Also in the case two–components mixtures, calcium carbonate or oxide with iron (III) oxide, in which ferrite are formed, and three components mix: CaO+Al_2O_3+Fe_2O_3, in which alumina–ferrites are formed, Jander's formula is well satisfied.

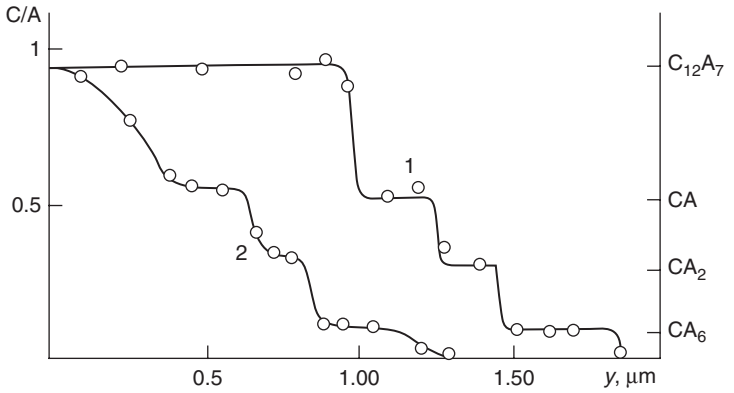


Fig. 2.5 Phase composition of reaction zone in corundum pulley [(after 9)]; *1* pulley heated in powdered CaO at 1370 °C, *2* pulley heated second time at the same temperature after removing CaO

First aluminate formed in the mixture $CaO+Al_2O_3$ is the monocalcium aluminate $CaO \cdot Al_2O_3$. At the temperature about 900 °C $C_{12}A_7$ appears, which is transformed in C_3A at the temperature higher than 1200 °C, in practice close to 1300 °C. The studies of reaction rate in the mixture $CaO+Al_2O_3$ with molar ratio 3:1, in which $Ca_3Al_2O_6$ is the final product, have shown that the Ginstling–Brounsteins' [7] formula is better fulfilled than Jander's equation:

$$\frac{(1-2\alpha)}{\left[3-(1-\alpha)^{2/3}\right]} = (k/r^2)t \tag{2.4}$$

Also in the case of this mixture the interpretation of the results is complicated, because apart of C_3A other phases appear among the products, namely: CA, $C_{12}A_7$, CA_2 and even CA_6. This complicated phase composition of reacting mixture is showing that the mobile component is CaO and the product layers onto Al_2O_3 grains are formed.

The mechanism of reaction in the solid state of the mixtures CaO with SiO_2 or Al_2O_3 was studied by many authors and all have confirmed the much higher mobility of the calcium ions than the others [5, 8, 9]. Also Rouanet [9], studying the phase composition of the reaction layer, formed in the corundum pulley immersed in powdered CaO, showed in Fig. 2.5 confirmed it. However, the XRD examination of the powder around the Al_2O_3 pulley, has shown the presence of thin layer of C_3A, which confirms the alumina ions diffusion in the opposite direction to calcium ions [9].

For the reason of low diffusion coefficients of silicon and aluminium the rate of reaction is determined by the calcium ions diffusion and oxygen, the last probably through the gaseous phase. Such mechanism of this process is confirmed by frequently observed in industrial mixtures the thin layers of $Ca_2[SiO_4]$ on quartz grains. On the Fig. 2.6 this layer, found by Moore [(after 10)], is shown in the specimen of the material sampled in industrial rotary kiln.

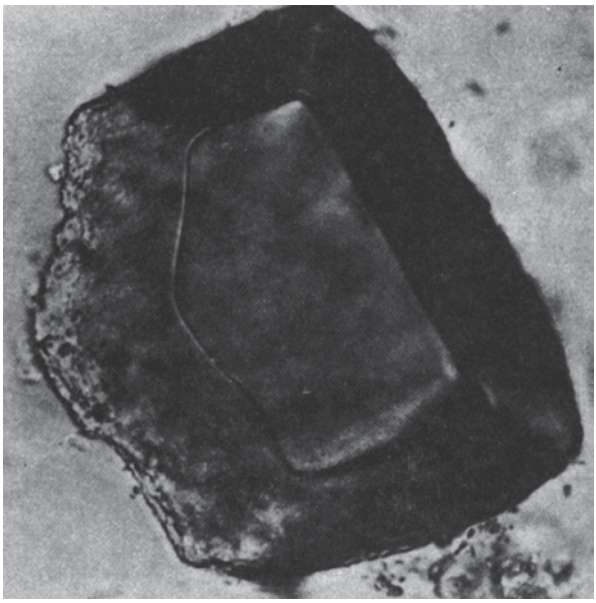


Fig. 2.6 The layer of C_2S on quartz grain. (After [10])

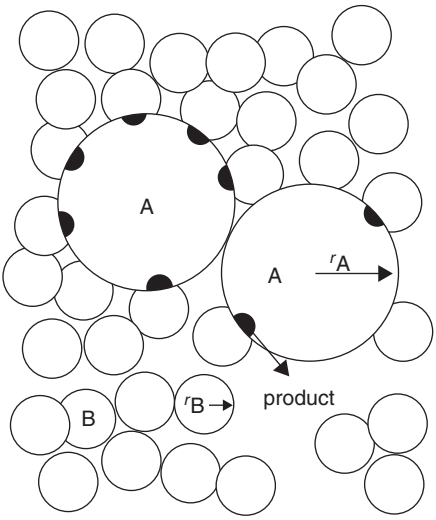


Fig. 2.7 The Komatsu's model of reaction in the solid state

The kinetic models of Jander and Ginstling were developed by Komatsu [11]. He had assumed that the reaction starts in the places of intergranular contact (Fig. 2.7). The fundamental role in the reaction has the number of these contacts, thus the fineness of the mixture. If the number of contacts is constant in time, the formula derived by Komatsu is reduced to Jander's equation, in which, however, the k constant is the function not only of the temperature but also the ratio of grains sizes r_A and r_B of both components as well as the content ratio of these components in the mixture.

The equations of reaction constant rate between the substrates A and B are the following:

when A/B > 1

$$k = k_0 \left[\frac{ax}{1+ax} \right]^{m_1} \tag{2.5}$$

when A/B < 1

$$k = k_0 \left[\frac{1}{1+ax} \right]^{m_2} \tag{2.6}$$

where:—A/B is the molar ratio of the substrates in the mixtures, $a = r^3_B \rho_B / (r^3_A \rho_A)$—mass ratio of single grain B to the grain A: r_A, r_B, ρ_A, ρ_B—grains diameters and densities of the components A and B, x—mass ratio of component A to the mass of component B.

The experimental results in the coordinate system log k–log$[ax/(1+ax)]$ and log k–log$[1/(1+ax)]$ should lay on two straight lines of inclination equal m_1 and m_2. Both lines should intersect in point k_0 if the mechanism of reaction is the same for both concentration ranges. Practical application of Komatsu's equation can be found in the paper of Haber and Ziółkowski [12].

From kinetic reason the composition of reacting mixtures is frequently very complicated and far from equilibrium. It should be reminded that the thermodynamic permits to determine the equilibrium phase composition of reaction mixture: this state has the lowest free enthalpy. This principle permits to find *a priori* the direction of reaction course or permits to determine the phases stability in determined thermodynamic conditions. The change of free enthalpy can be found from the Gibbs–Helmholtz's equation [13]:

$$\Delta G^0_T = \Delta H^0_{298} - T\Delta S^0_{298} + \int_{298}^{T} \Delta C_p \tag{2.7}$$

The standard enthalpy data (ΔH^0_{298}), standard entropy (S^0_{298}) and molal heat capacity (C_p) of substrates and products can be found in the tables [13] or on the Internet. Their changes as the result of reaction can be calculated as the sum of enthalpy (entropy) of products diminished by the sum of enthalpy (entropy) of substrates:

$$\Delta H^0_{298} = \sum \Delta H^0_{298} \text{ (of products)} - \sum \Delta H^0_{298} \text{ (of substrates)} \tag{2.8}$$

If there is no molal heat capacity as a function of temperature we can use the simplified formula: $C_p = a + bT + cT^{-2}$. The example of calculated values for the mixture $2CaO + SiO_2$ is shown in Fig. 2.8 [13]. However, the lack of some precise thermodynamic data is for the present the limitation of this method.

The reaction kinetic of models mixtures, of the composition close to industrial one and at the temperature corresponding to the real production processes, thus in

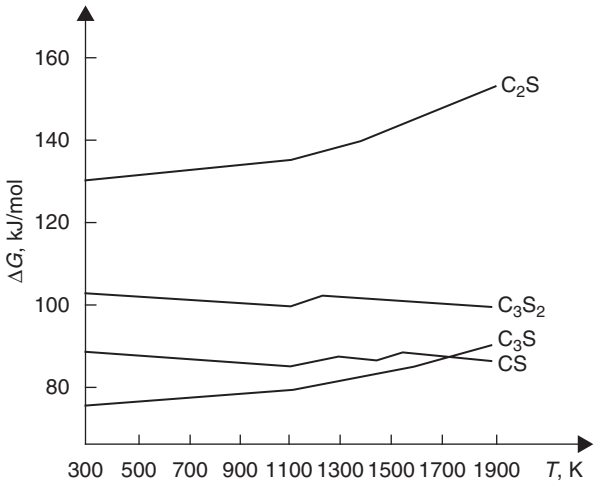


Fig. 2.8 ΔG^0 of the reaction of CaO with SiO_2 in the function of temperature for the mixture $2CaO+SiO_2$. (After [13])

the case of important content of liquid phase, was also studied. The liquid phase plays the main role in the formation process of tricalcium silicate. Kondo and Choi [14] have shown that the rate of CaO and $Ca_2[SiO_4]$ dissolution in the melt and crystallization of $Ca_3[SiO_4]O$ can be presented with the relation analogical to Jander's formula, in which the volumetric diffusion in the solid state was replaced by dissolution. It is as follows:

$$\left[1-(1-\alpha)^{1/3}\right]^2 = \frac{2D\Delta c}{r^2}t = kt \tag{2.9}$$

In this equation D is the diffusion coefficient, Δc—the concentration difference in diffusion layer, r—the radius of dissolving grains, and the remaining symbols as in Jander's equation.

The diffusion coefficient can be calculated from the equation:

$$D = \frac{RT}{6\pi\eta\delta N} \tag{2.10}$$

where: η—melt viscosity, δ—the radius of the particles under diffusion (the authors adopted 40 pm for Si^{4+}), R—gas constant, T—temperature, N—Avogadro's constant.

The simple formula for the calculation of free CaO in the clinkering process by Johansen [15] was given; he admitted that the limiting of the process rate factor is diffusion:

$$(1+\beta\alpha)^{2/3} - \frac{2}{3}\alpha = 1 - \left[\frac{2\gamma D\Delta c}{d_1}\right]\left[\frac{t}{r_0^2}\right] \tag{2.11}$$

where: α—is the degree of CaO transformation, β—coefficient dependent of sample composition and porosity, γ—volume fraction of liquid phase content in surface layer of the tablet, D—effective, two–dimensional coefficient of CaO diffusion, Δc—CaO concentration gradient in the reaction layer, d_1—density of CaO, t—time, r_0—the radius of CaO grains.

Applying this model Johansen calculated that at temperature of 1500 °C and heating time of 20 min the CaO grains of 80 μm diameter will react, which are corresponding to calcite grains equal 120 μm. It is in accordance with earlier Heilmann [16] research. On the base of experiments with the sandwiches ($C+C_3S$) and (C_3S+C_2S) Johansen and Christensen [17] applied the simpler formula, which gives the possibility to eliminate the grains diameter. The formula is:

$$x^2 = kt \tag{2.12}$$

simultaneously

$$k = 2D_m \beta c H \tag{2.13}$$

and

$$H = \frac{1}{C_1 - C_a} + \frac{1}{C_b - C_2} \tag{2.14}$$

In these formula x is the layer thickness of C_3S+C+melt or C_3S+C_2S+melt, k—rate constant, t—time, D_m—effective, two–dimensional coefficient of CaO diffusion, with the simultaneous diffusion $SiO_2+Al_2O_3$ etc. in opposite direction, in the melt, β—mass content of the melt in the C_3S layer, Δc—concentration difference of CaO (mass fraction) in the melt in equilibrium with C_3S+C or C_2S+C_3S, C_1, C_2—mass shares CaO in two, C_a, C_b—mass shares of CaO in C_3S layer on the surface of sandwich I–C_3S and of sandwich II–C_3S.

The sequence of phases appearing in the mixtures composed of natural raw materials was also examined. In the mixture of calcium carbonate with quartz and clay minerals first reactions are the dehydroxylation of the latters. The kaolinite dehydroxylation at the temperature close to 450 °C is transforming in metakaolinite, which has, in disturbed form, the structure of initial mineral [18]. It is presenting high reactivity with calcium carbonate and the reaction of these components will start at this range of temperatures. For these reasons the mixture of marl with kaolinite produce C_3S at 1100 °C and with illite even at 1000 °C [19].

The calcium carbonate starts to react with quartz at temperatures close to 600 °C, and it is probably linked with the increase of SiO_2 reactivity, caused by its polymorphic transformation at 573 °C. It is so called Hedvall's effect [20]. As the first phase calcium disilicate is formed. At the almost the same temperature the mono–calcium aluminate and ferrite $Ca_2[Fe_2O_5]$ will be formed. Some authors mention the CF appearing [21].

At the temperature range 600–700 °C the decarbonisation of calcium carbonate is beginning too. The reaction rate very low at the temperatures from 600 to 800 °C,

is gradually increasing, and many experimental works have confirmed the validity of Arrhenius equation [22]:

$$k = A \exp \frac{-E_a}{RT} \tag{2.15}$$

where: k—reaction rate constant, E_a—apparent activation energy, R—gas constant, T—absolute temperature, A—constant (lattice elements oscillation frequency).

During the reaction in the solid state the decomposition processes and polymorphic transformations of mineral components, which cause the lowering of apparent activation energy of reaction, are very important. The processes of clay minerals dehydroxylation, calcium carbonate decomposition, which cause the formation of phases *in statu nascendi*, frequently amorphous with different structural disorganisations, belong to them. For this primarily reason the rate of temperature rise is important. Low rate of heating, favouring the processes of crystallization and recrystallization, the decrease of reactivity of these phases is causing, for example of calcium oxide, formed of $CaCO_3$ decarbonisation, which causes the general rate decrease of clinkering process.

The aluminate $C_{12}A_7$ begins to appear at the temperature 800–1000 °C, which then is transformed in C_3A at the temperature range 1000–1200 °C. It should be underlined that in practise the large differences of temperature of individual phases appearing can be observed, which is understandable if the numerous changeable factors influencing these heterogeneous processes will be considered. There are principally: grains sizes, degree of raw meal homogenisation and presence of impurities. On Fig. 2.9 the ranges of different phases appearance, according to the literature, are presented.

Gehlenite is an intermediate phase formed at the temperature range of 800–1200 °C by some authors is mentioned. Starting from the temperature 950–1000 °C the formation of ferrites $C_2(A, F)$ can be observed.

The mixtures of natural raw materials contain always low quantity of alkalis, sulphates and chlorides, which eutectics of melting temperature lower than 700 °C is formed [23]. The liquid phase formation highly increases the rate of reactions, accelerating diffusion of several orders of magnitude. Higher amounts of liquid phase start to appear at the temperature of about 1200 °C and are linked with the eutectic $CF–CF_2$, and then at about 1280 °C. The last one corresponds to eutectic $C_2S–C_{12}A_7–C_2(A, F)$. Clinker's melt is corresponding to the invariable point $C_3S–C_2S–C_3A–C_4AF$, thus with the phases richer in lime, but poorer in alumina, which melting temperature is 1338 °C. MgO and R_2O lower the appearing of the liquid phase to 1260 °C [24].

The content of clinker melt is increasing with temperature, and its viscosity is decreasing. The content of liquid phase at chosen temperature (compare with Sect. 2.2) can be calculated from corresponding multicomponent systems. Lea and Parker [24] gave the simplified formulae, which permit the content of liquid phase calculation:

liquid phase content at 1340 °C = $6.1y + a + b$ (for A/F > 1.38)
liquid phase content at 1340 °C = $8.5x—5.22y + a + b$ (for A/F < 1.38)
liquid phase content at 1400 °C = $2.95x + 2.2y + a + b$
liquid phase content at 1450 °C = $3.0x + 2.25y + a + b$

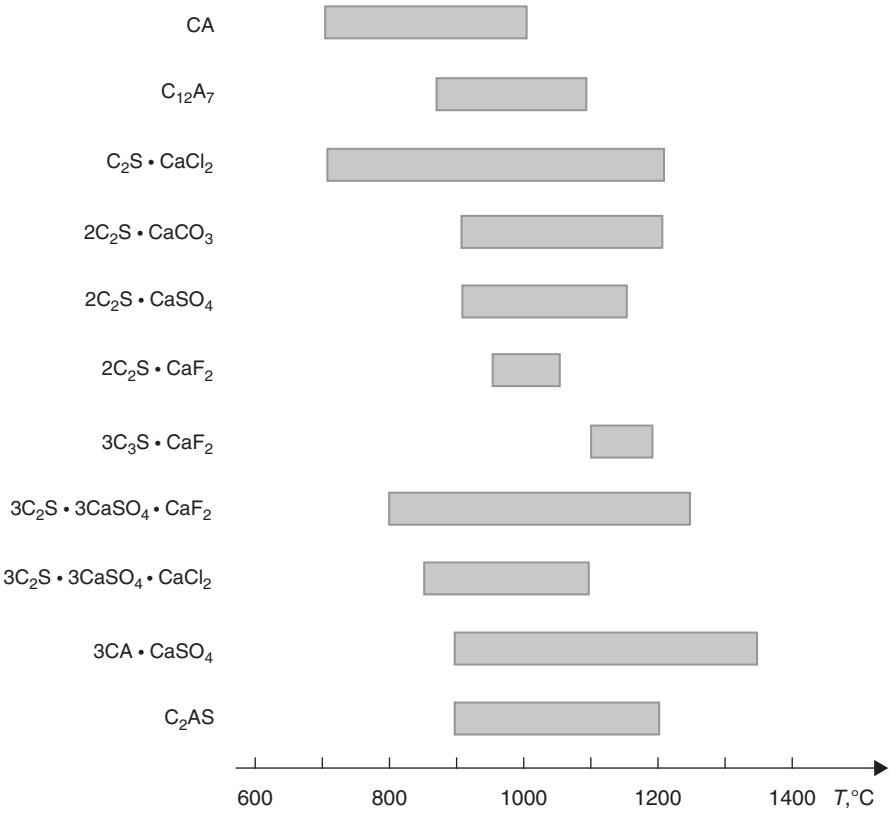


Fig. 2.9 The ranges of some intermediate phases appearing in clinkering process

In these equations x is Al_2O_3 content (%), y—is Fe_2O_3 (%), a—is MgO (%) under condition that it is lower than 2% (it results from 5–6% solubility of MgO in clinker's melt)[2], b—is the sum of $Na_2O + K_2O$ (%).

The liquid phase, its chemical composition and physical properties, and principally viscosity and surface tension, are very important, because in industrial process tricalcium silicate is crystallizing from this phase. Calcium oxide and dicalcium silicate are dissolved in the liquid phase which became oversaturated towards C_3S. The crystallization of tricalcium silicate begins at about 1300 °C, but in prevailing mass proceeds at 1450 °C, i.e. at maximum clinkering temperature.

The melt in eutectic point of the system CaO–SiO_2–Al_2O_3–Fe_2O_3 has at 1338 °C the composition: CaO—54.8%, Al_2O_3—22.7%, Fe_2O_3—16.5%, SiO_2—6%, which corresponds to the following phase composition: C_4AF—50.1%, C_3A—32.3%, C_2S—16.0%, C_3S—1.6%.

At temperature of 1450 °C the melt composition is changing as an effect of C_2S and C dissolution: CaO—56.3%, Al_2O_3—18.5%, Fe_2O_3—18.5%, SiO_2—6.7%. It

[2]Also the solubility in alite is 2%.

contains also MgO (till 2 %) and all containing in clinker amount of Na_2O, K_2O and SO_3. The three last components can form the own liquid phase (liquation phenomenon, Sect. 2.3).

2.2 The Phase Systems Important for Cement Chemistry

The chemical composition of clinker is complex, however, it is easy to notice that the sum of four components, CaO, SiO_2, Al_2O_3 and Fe_2O_3 is as a rule higher than 95 %. The processes of Portland cement clinker phases crystallization in the four components system can thus be presented. It is especially justified that MgO is not forming own compounds in the rich in calcium part of five–components system, but solid solutions with remaining clinker phases, or is present as periclase. However, the four–components system is seldom used, because the use of ternary systems is much more convenient. They are usually presented as the horizontal projection.

2.2.1 The System CaO–SiO_2–Al_2O_3

In order to understand this the most important ternary system in cement chemistry the two forming its sides two–components systems should be discussed: CaO–SiO_2 and CaO–Al_2O_3.

2.2.1.1 The System CaO–SiO_2

In this system (Fig. 2.10) four two–components phases are present: wollastonite $CaO \cdot SiO_2$, rankinite $3CaO \cdot 2SiO_2$ and orthosilicates: $2CaO \cdot SiO_2$ and $3CaO \cdot SiO_2$. Two of these phases, namely dicalcium silicate and wollastonite are melting congruently and two remaining incongruently. Tricalcium silicate is not only melting incongruently but also is not stable at temperature lower than 1250 °C and during cooling is decomposed to C_2S and C. Tricalcium silicate, as a phase of incongruent melting temperature, is not in equilibrium with the melt, but at 2070 °C is decomposed to the melt poorer in calcium oxide and some amount of CaO crystals.

Analogically, from the melt of the composition given by point *S* (Fig. 2.11), after achieving the liquidus temperature (T_1), phase CaO is crystallizing, and the melt composition is changing along the liquidus curve till the point *M*. This composition the melt will attain at 2070 °C. At this temperature the meritectic reaction starts:

$$CaO + \text{melt} \rightleftarrows 3CaO \cdot SiO_2 \tag{2.16}$$

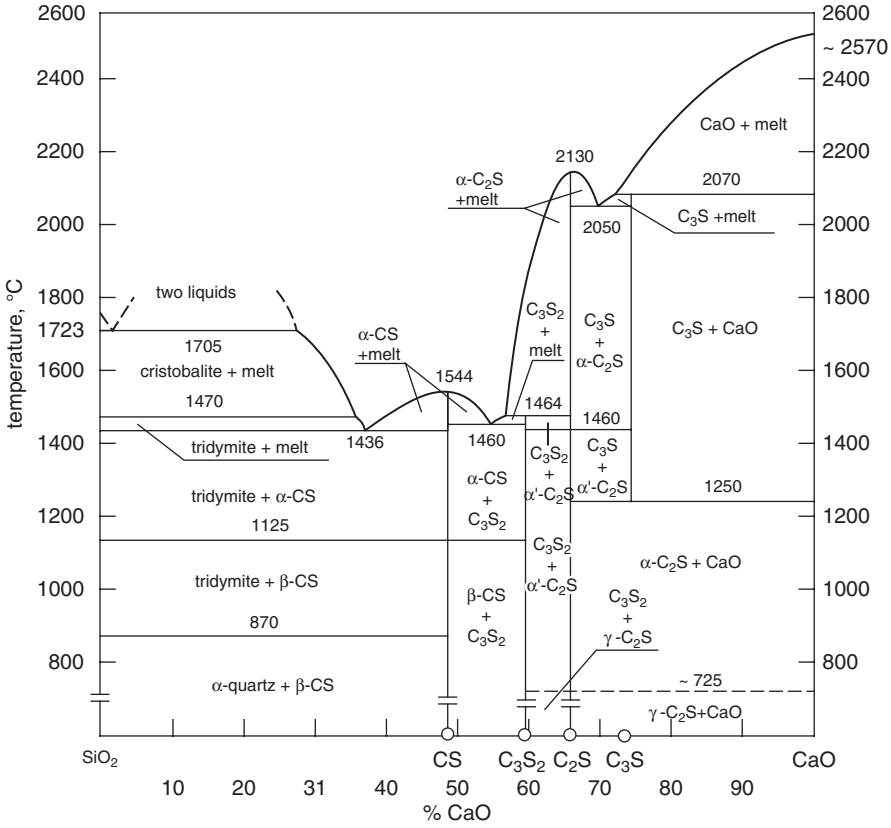


Fig. 2.10 The system CaO–SiO_2

It will proceed at constant temperature, as an exothermic reaction. The system will be invariable, as a result of Gibbs's phase rule[3].

One can reminds that the phase rule gives the equation:

$$f + s = n + 2 \tag{2.17}$$

where: *f*—the number of phases, *s*—number of degrees of freedom, *n*—number of components. The constant 2 is linked with the systems, in which the equilibrium is dependent only on two exterior factors: temperature and pressure.

The cases can be in which the number of these factors will be higher and then the constant will be also grater and for example in the case of taking into consideration the surface tension it will be 3. There are also cases in which the external pressure is much higher than the system vapour pressure, corresponding to existing

[3] Gibbs's phase rule can be found in Physical Chemistry, P. Atkins, Oxford University Press 1998.

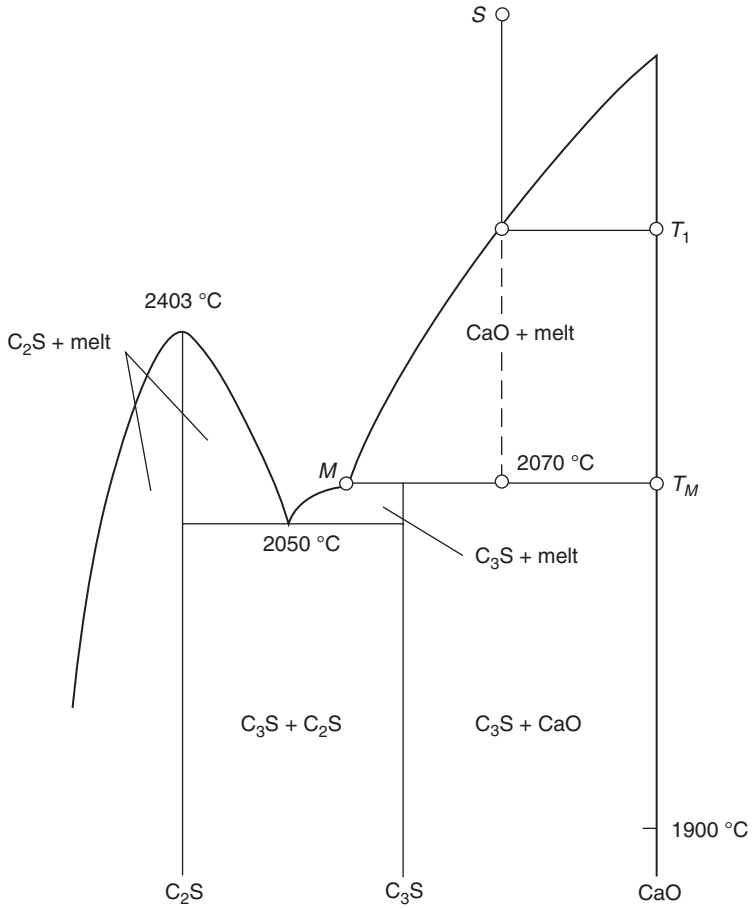


Fig. 2.11 Part of $CaO–SiO_2$ system

temperature. For non–metallic, inorganic systems the vapour pressure is extremely low, and are fulfilling this condition under 1000 hPa pressure, which is always the case[4]. Pressure establishing entails the number of freedom degrees decreasing of one:

$$f + s = n + 1 \tag{2.18}$$

It is so called reduced phase rule. Using this reduced phase rule one can easily calculates that during the meritectic reaction of C_3S formation the system is zero–variant:

[4]It is always some simplification. At higher temperature than 1500 °C the silica vapour pressure has a significant value and even more intensive chromium oxide which evaporates as well as sodium and potassium oxides.

$$f + 3 = 2 + 1$$

$$f = 0$$

The system will remain in the state as long as the melt or CaO will be exhausted, thus one phase will disappear and the system will become univariant.

Liquid phase appears in this system only at 1436 °C, which corresponds to the eutectic of wollastonite with SiO_2. In the mixtures richer in CaO more important is the eutectic of wollastonite with rankinite, which melting point is at 1460 °C.

2.2.1.2 The System $CaO–Al_2O_3$

Five compounds is formed in the system $CaO–Al_2O_3$: C_3A, $C_{12}A_7$, CA, CA_2 and CA_6 (Fig. 2.12). This system differentially to the system $CaO–SiO_2$ is the field of numerous controversial opinions. They concern among other CA and CA_2 melting mechanism, which according to some authors is incongruent [24, 25] and to the other ones congruent [26]. The differences are low, because practically the melt compositions are almost the same, as of the melting phase. Two remaining phases, C_3A and CA_6 are melting also incongruently.

Even more controversies the phases C_5A_3 and $C_{12}A_7$ were developing. The condition of these phases formation are now in significant degree explained. At the beginning it was considered that $C_{12}A_7$ must contain some amount of OH^- ions, which have the stabilizing effect, replacing oxygen: $Ca_{12}Al_{14}O_{32}(OH)_2$. Then after Glasser [27] has shown that the same role oxygen can play, and its excess is from 0.07 to 0.1 %. To the similar conclusion Zhmoidin [28] and Brisi [29] were arrived, and are stating that the amount of excess oxygen is increasing with the decrease of H_2O content. Other gases, for example CO_2 can be also absorbed by the melt. However, the reducing atmosphere, long heating of the melt at high temperature and rapid freezing gives C_5A_3 and glass. According to Brisi [29] C_5A_3 is stable under 1280 °C (Fig. 2.13) under low partial pressure of O_2 and H_2O. At temperature over 1280 °C $C_{12}A_7$ is formed, however, it does not appears under the lack of oxygen and trace of water vapour [29]. Brisi [29] is considering that it is also the equilibrium phase in the system $CaO–Al_2O_3$. The phase $C_{11}A_7CaX_n$, where X can be S, F_2, Cl_2 is known too. This phase should not contain the excess oxygen.

2.2.1.3 The System $CaO–Al_2O_3–SiO_2$

The most frequently we use the ternary system horizontal projection, on which the most important isotherms are marked. On the Fig. 2.14 the section of this system is presented, on which, apart of earlier discussed two–component compounds, mullite, without practical importance for cement chemistry, is shown. However, it is present in siliceous fly ash, but it belongs to inert compounds does not reacting with calcium hydroxide in water. Furthermore two ternary phases are formed in

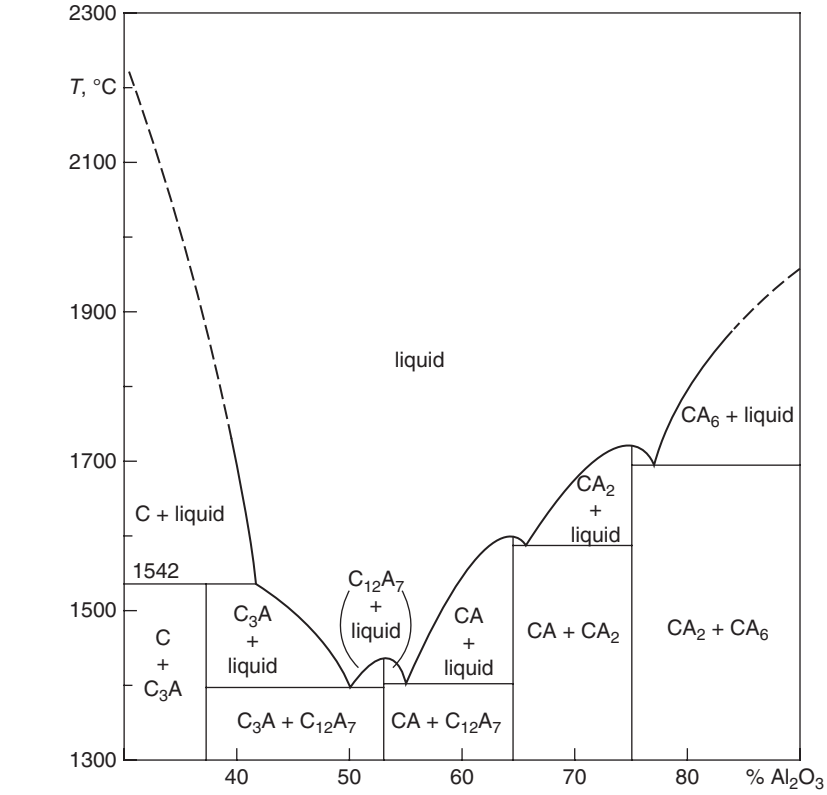


Fig. 2.12 The system CaO–Al_2O_3; in the totally free of water vapour atmosphere the phase $C_{12}A_7$ is not formed

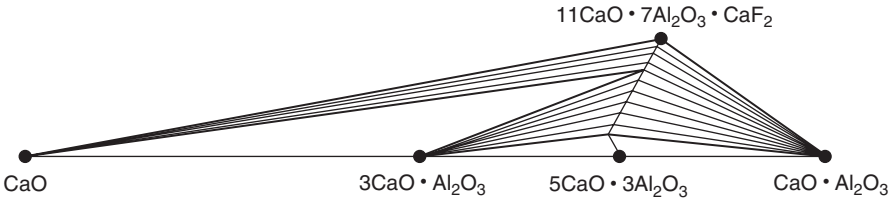


Fig. 2.13 Subsolidus in CaO–Al_2O_3–CaF_2 system at 1200 °C. (After [29])

this system, namely gehlenite $Ca_2Al[Al, SiO_7]$ and anorthite $Ca[Al_2Si_2O_8]$. Both are melting congruently, which simultaneously means that the points representing their composition are on the fields of their primary crystallization. More important is gehlenite, which is the phase of blastfurnace slag. It forms extensive solid solutions with akermanite $Ca_2Mg[Si_2O_7]$. These solid solutions belong to the melilite family.

The principles of crystallization processes analysis in the ternary system will be shown on the examples of dicalcium and tricalcium silicates crystallization on the

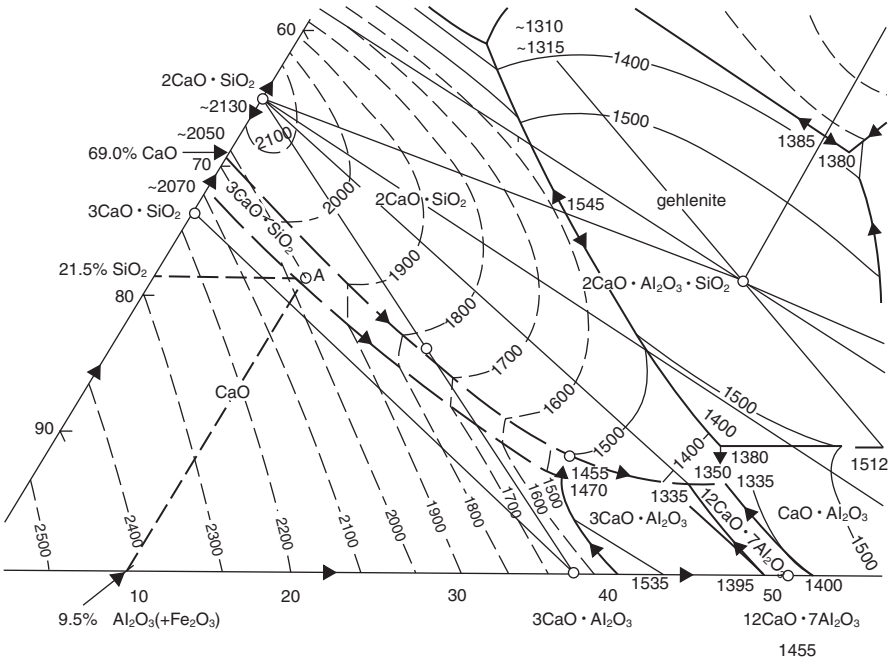


Fig. 2.14 Part of the system $CaO–SiO_2–Al_2O_3$

enlarged section of the ternary system $CaO–SiO_2–Al_2O_3$ (Fig. 2.15).This system represents very well the conditions of formation of white cement, which chemical composition is laying in this system.

Assume that we are cooling the melt of composition determined by point *S*. Because we are on the field of CaO primary crystallization then this phase will crystallize, and the melt composition will change along the straight line drowned from the point *S* to the vertex CaO. At point *M* the meritectic reaction equivalent to the resorption of CaO and crystallization of C_3S. To the point *N* all the amount of CaO crystals will be resorbed (melt composition is laying on the straight line *S*–C_3S) and the crystallization of C_3S from the melt will begin, thus we enter on the field of this phase. In the point *O* the double eutectic: C_3S, C_3A starts to form, thus these two phases simultaneously are formed and the melt composition is changed along the curve *TY*. After arriving to the triple point *Y* additionally the crystallization of C_2S will begin and the system became invariable. There are four phases and the number of degree of freedom became zero:

$$s = f - (n+1) = 4 - 4 = 0$$

Thus the process is ending in this point.

The process of melt cooling of composition *P* will proceed similarly, but will start by C_3S crystallization, because we are already on the field of this phase. From

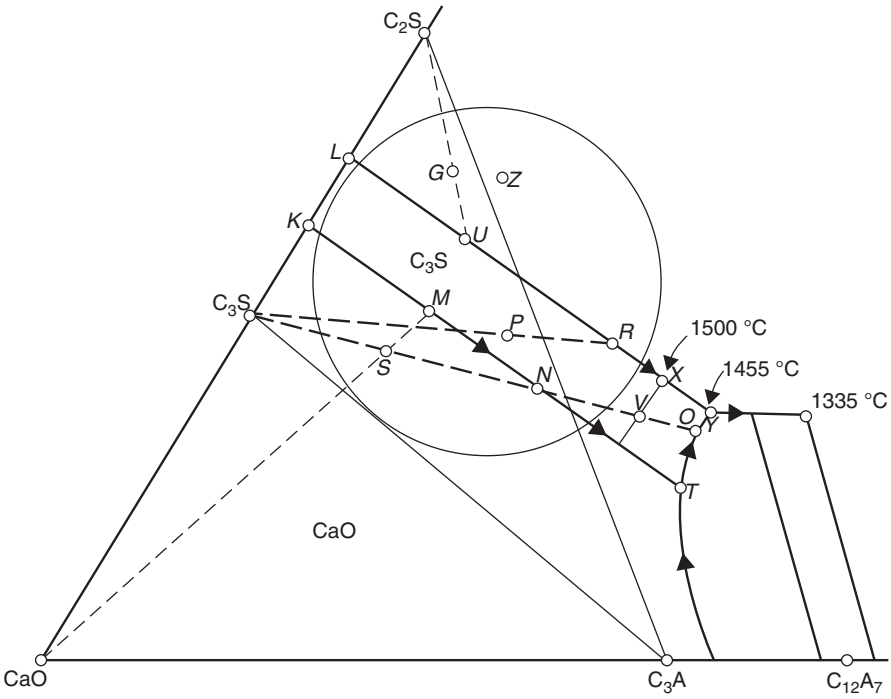


Fig. 2.15 Melts crystallization with the chemical composition represented by points *S, P, G* and *Z* in the system $CaO–SiO_2–Al_2O_3$ (schematically)

the point *R* C_2S will be also crystallizing, because the line *LY* is the eutectic curve of these two phases. The process will end similarly in *Y* because both of the initial melts composition are laying on the field of triangle C_3S, C_2S, C_3A. A little different situation will be in the case of melt given by point *G*. To the point *U* C_2S will crystallize and from *U* to *Y* C_3S and C_2S, and the melt composition will be changed along the curve *LY*. At point *Y* the crystallization of C_3A will start and all the melt will solidify. However, the peritectic liquid phase[5] of the composition given by point *Y*, laying out of the triangle C_3S, C_2S, C_3A will have too low content of calcium oxide for these three phases to be formed, C_3S partial resorption will undergo.

The melt of the starting composition given by the point *Z*, laying in the triangle C_2S, C_3A, $C_{12}A_7$ will have in the initial period the same crystallization course. However, after arriving to the point *Y* C_3S will be totally resorbed, the system will again became univariant and the crystallization will continue along curve *Y*—1335 °C. At that point of ternary eutectic the crystallization of $C_{12}A_7$, apart of C_2S and C_3A, will begin and the process will end.

[5]That it is not the eutectic point the arrows on curves are showing which all are not converging in point *Y*. The eutectic curve *Y*—1335, C_3A and C_2S, falls in the direction of the eutectic point 1335 of phases C_3A, C_2S, $C_{12}A_7$.

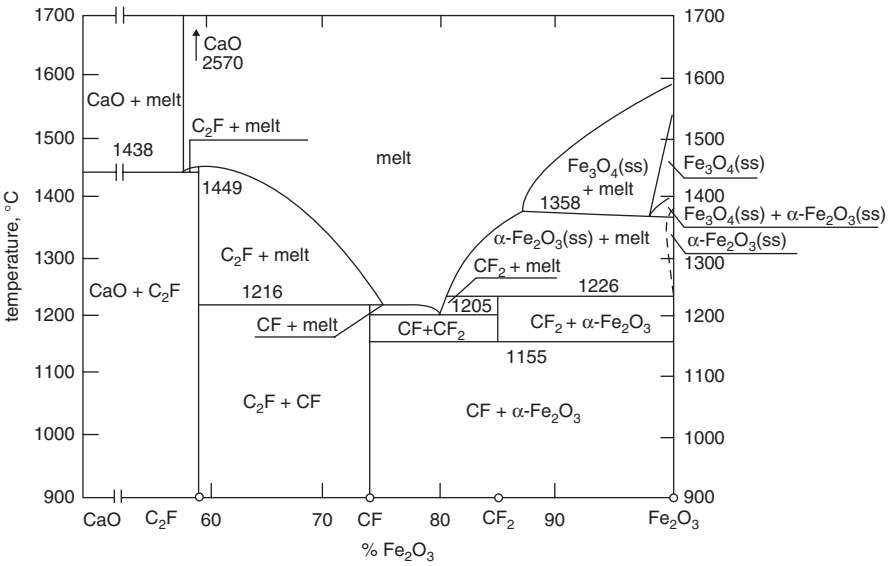


Fig. 2.16 The system CaO–Fe_2O_3

2.2.2 The System CaO–Fe_2O_3–SiO_2

2.2.2.1 The System CaO–Fe_2O_3

On the Fig. 2.16. the system CaO–Fe_2O_3 is shown, in which three phases: CF, C_2F and CF_2 are present. The only dicalcium ferrite is melting congruently at 1449 °C. The two remaining are incongruent and additionally CF_2 is decomposing in the solid state at 1155 °C, giving CF and hematite—α–Fe_2O_3.

The system CaO–Fe_2O_3 is binary only in the part rich in calcium oxide. The mixture rich in iron, even heated in air, easily lost the oxygen at higher temperatures with the magnetite formation, in which part of iron is reduced to Fe(II). Obviously, the iron reduction is much quicker in reducing atmosphere and then in the clinkering process even metallic iron can be formed (see Sect. 2.3.2 and 9.2).

In the ternary system CaO–Fe_2O_3–SiO_2 the region of the primary crystallization of CaO, C_3S and C_2S is important (Fig. 2.17). The crystallization process of the melts is ending in the invariant point 1405, in which, apart from earlier precipitated C_3S and C_2S C_2F is crystallizing. This system has no practical importance in cement chemistry, because of the marls (clays) use, the raw mixture will contain always some percent of Al_2O_3.

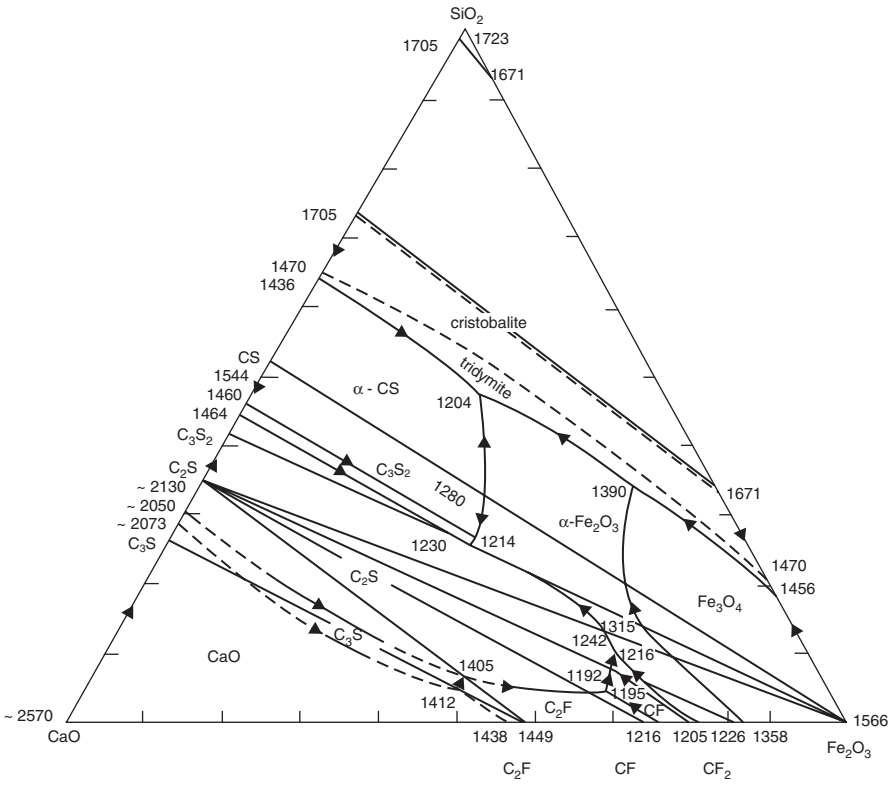


Fig. 2.17 The system $CaO–Fe_2O_3–SiO_2$

2.2.3 The System $CaO–Al_2O_3–Fe_2O_3$

This system is very important for understanding of quaternary system $CaO–SiO_2–Al_2O_3–Fe_2O_3$ and particularly for understanding of the ferrite phase composition in Portland cement clinker. The systems $CaO–Al_2O_3$ and $CaO–Fe_2O_3$ in Sects 2.2.1.2 and 2.2.2.1 were presented. However, in the system $Al_2O_3–Fe_2O_3$ of lower importance in cement chemistry the ordered solid solution of the composition close to $Al_2O_3 \cdot Fe_2O_3$ is formed, which in the narrow range of temperatures is stable. Both oxides have also limited miscibility in the solid state.

In the ternary system $CaO–Al_2O_3–Fe_2O_3$ the highest importance has the series of solid solutions extending from C_2F to C_6A_2F (Fig. 2.18).There are the solid solutions of C_2F with hypothetical "C_2A". The composition of alumina–ferrite phase in clinkers is depending from alumina ratio; for its medium value is close to C_4AF, for low (A/F < 1) is close to C_6AF_2 and for high to C_6A_2F. To the last one corresponds the limiting alumina ratio from 2.2 to 2.3 [30].

Majumdar [31] has shown that the solid solutions C_2F–"C_2A" are stable till the 70 % of mole"C_2A". Ferrite phase in equilibrium with solid solution of Fe_2O_3 in

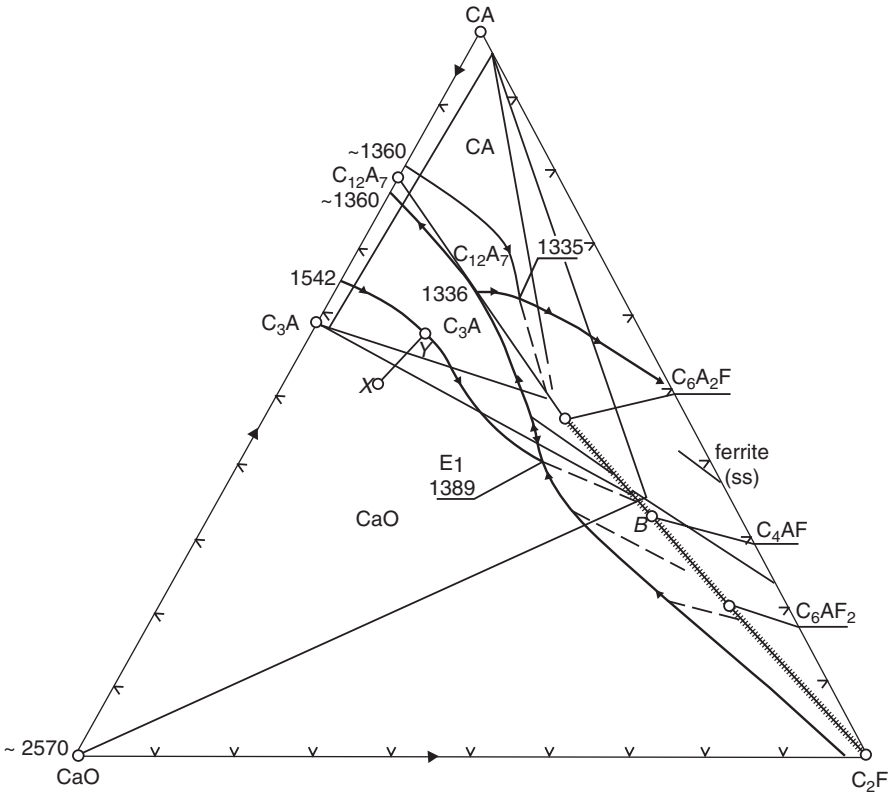


Fig. 2.18 Part of the system $CaO–Al_2O_3–Fe_2O_3$

C_3A (C_3A_{ss}) and CaO contains 48 mol. % "C_2A", thus has the composition close to C_4AF (Fig. 2.18) [31].

For the range of solid solutions $C_3(A_{1-x}F_x)$ the data are rather divergent [31–34]. Majumdar [31] and Moore [32] observed the increase of the dimension of unit cell beyond the composition C_6AF_2 then this limiting composition is not corresponding to the equilibrium (Fig. 2.19). However, Tartre [34] found the maximum saturation at the molar ratio Fe/(Al+Fe) higher than 10%. For higher ratio no change of unit cell parameters was observed [34].

2.2.4 The System $CaO–SiO_2–Al_2O_3–Fe_2O_3$

Only two part of this system will be shown: $CaO–C_2S–C_4AF$ (Fig. 2.20) and $CaO–C_2S–C_{12}A_7–C_4AF$ (Fig. 2.21). The first is very important for the Portland cement clinker having the alumina ratio lower than 0.64, in which the calcium aluminates are not formed and the alumina is bound in C_4AF. The C_3S field is ended in

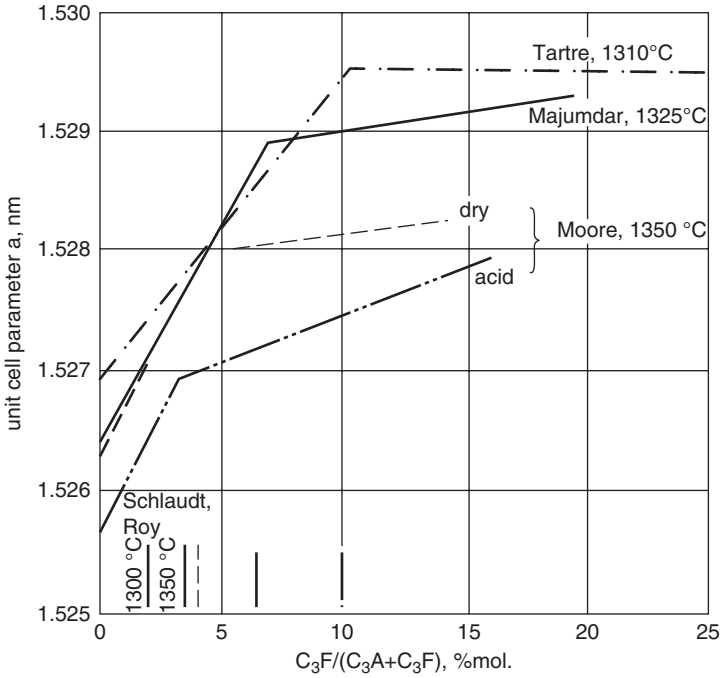


Fig. 2.19 The dependence of unit cell dimension of $C_3(A1-_xF_x)$ on C_3F content. (After [34])

eutectic *K*, in which CaO, C_3S and C_4AF are crystallizing and in peritectic point (*H*) in which C_2S, C_3S and C_4AF are crystallizing.

In the quaternary system (Fig. 2.21) the field of C_3S primary crystallization forms the flat, regular body limited by the fields of primary crystallization of CaO and C_2S. High importance have fields, upper C_3S–C_4AF and lower C_3A–C_3S which are separated by eutectic curve C_3S, C_3A, C_4AF, ending in the invariant points 1341 °C and 1338 °C. Both probably are the peritectic points and are lying in relation to the plane C_2S–C_3A–C_4AF, on the lime—poor side. It is resulting from the system that all composition, which are located in the volume with lower lime content in relation to the plane C_3S–C_3A–C_4AF will not have free CaO after burning. All mixtures located inside the tetrahedron C_3S–C_2S–C_3A–C_4AF will give, as the effect of equilibrium crystallization, this four phases in agreement with Bogue's method calculation. It is important that the point corresponding to the melt composition formed in the clinkering process was located in the C_3S side in relation to the limiting plane CaO–C_3S. In the case that this composition point being from the CaO side, this phase should be present as the solid phase, and its full resorption in the clinkering process will be hardly probable. Welch [36] states, that the limiting plane CaO–C_3S at the clinkering temperatures goes approximately through the point C_4AF, C_3S and *Z* (Fig. 2.21). On this basis Lea and Parker [24] defined the relation determining the maximum CaO content in the clinker[6]:

[6]Thus the lime saturation factor LSF = 100CaO/(2.8S + 1.18A + 0.65F). Till 2 % MgO:LSF = 100 (CaO + 0.75MgO)/(2.8S + 1.18A + 0.65F).

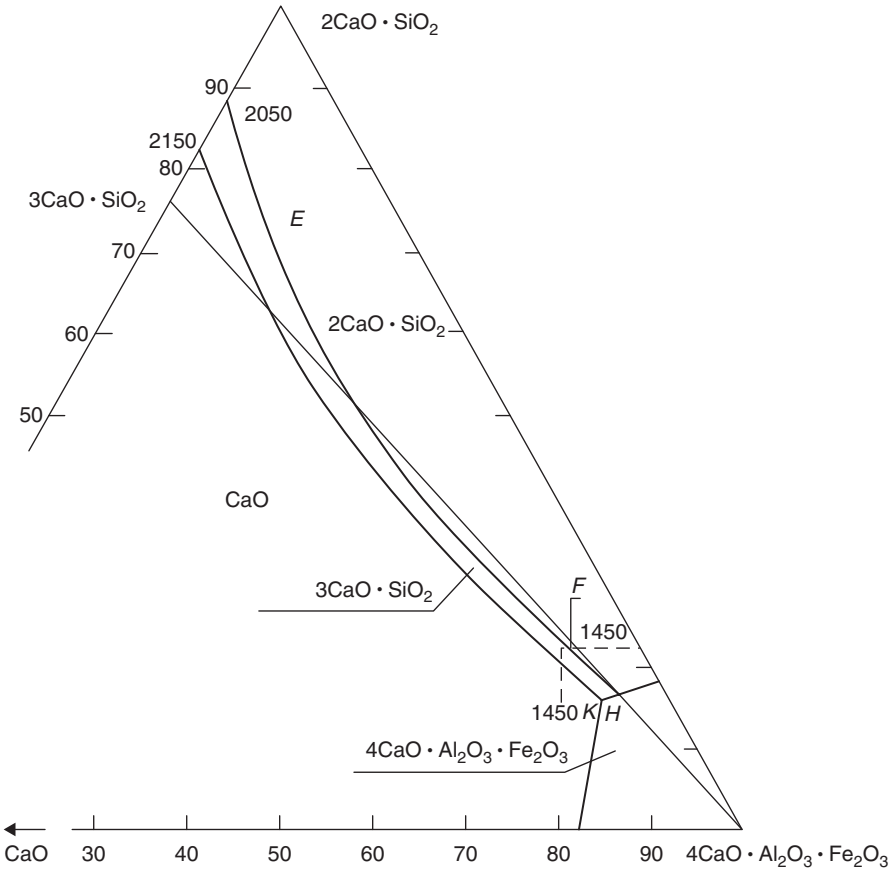


Fig. 2.20 The pseudo–ternary system CaO–C_2S–C_4AF

$$CaO = 2.80SiO_2 + 1.18Al_2O_3 + 0.65Fe_2O_3 \tag{2.19}$$

Lea and Parker were considering that this formula is valid only for alumina ratio higher than 0.64. However, as correctly Welch is stating, it is valid also for lower value of this ratio, since the earlier given plane is corresponding approximately to the plane C_3S–"C_2A"–C_4AF, and the line "C_2A"–C_4AF embraced, as it was explained earlier, all members of alumina–ferrite solid solutions, till C_2F.

2.2.4.1 Pseudosystem CaO–C_2S–$C_{12}A_7$–C_2F

This system is very close to the previous one (Fig. 2.22). The invariant point *1 at* 1342 °C in which the following phases are present: CaO–C_3S–C_3A–C_2(A, F)–melt correspond to the point 1341 °C in the system CaO–C_2S–$C_{12}A_7$–C_4AF (Fig. 2.21).

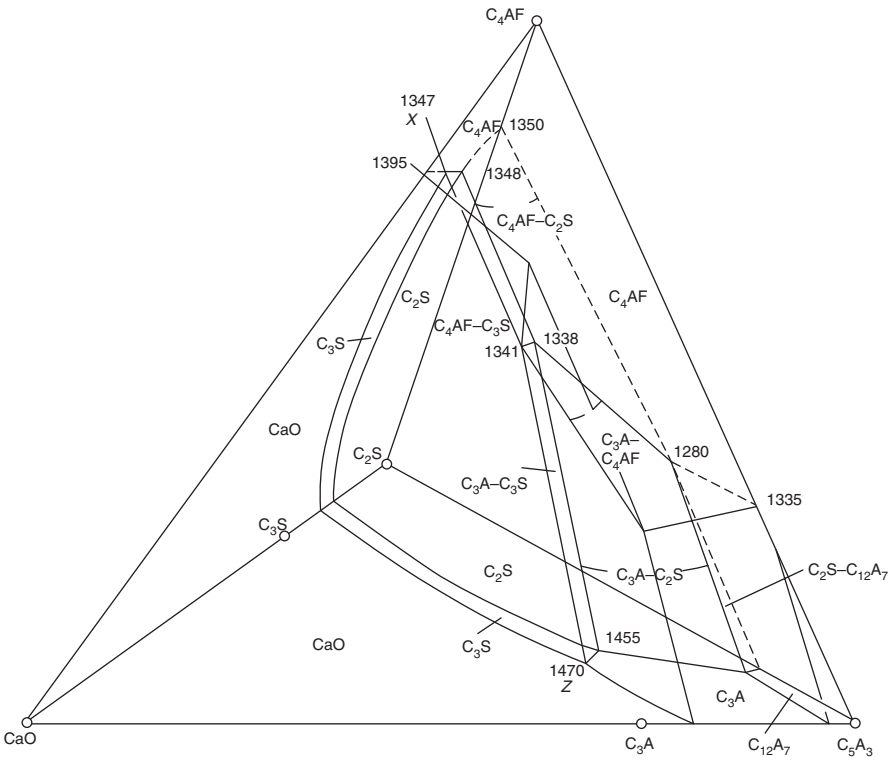


Fig. 2.21 The pseudosystem $CaO–SiO_2–Al_2O_3–Fe_2O_3$

The invariant point *2 at* 1338 °C $C_2S–C_3S–C_3A–C_2(A, F)$–melt has the same temperature. Both these points Swayze [37] treated as peritectic. In the equilibrium condition the clinkering process ends in point 2, and the composition of ferrite phase is $C_2A_{0.57}F_{0.43}$ which corresponds to the ratio A/F = 0.85. Both invariant points *1* and *2* are laying out of the tetrahedron $C_3S–C_2S–C_3A–C_6A_2F$, which means that the latter one phase cannot crystallize in the ternary system. Welch [36] points out that the plane $C_3S–C_2S–C_6A_2F$ coming out from the edge $C_3S–C_2S$ is crossing the fields $C_3S–C_3A$ above the points *1* and *2*, thus crystallization of the phase C_6A_2F is not possible.

2.2.4.2 The Influence of MgO

As Swayze [37] has shown 5% addition of MgO is insignificantly modifying the quaternary system (Fig. 2.23). It is slightly higher amount which can be dissoluted in the liquid phase in the region of studied compositions, in connection with this the low amount of periclase will crystallize.

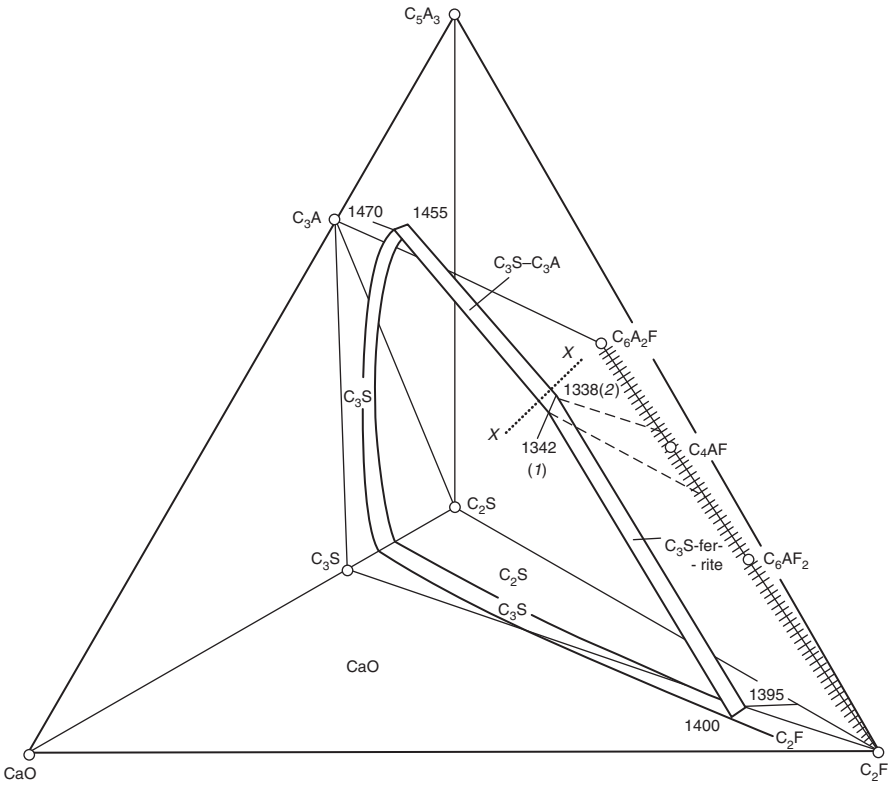


Fig. 2.22 Pseudosystem CaO–C_2S–$C_{12}A_7$–C_2F. (After [36])

The volumes of primary phases crystallization are similar to the system without MgO. However, the invariant points *1* and *2* were shifted to the points *A* and *B*, beyond the plane C_3S–C_2S–C_6A_2F, to the richer in Al_2O_3 volume of tetrahedron C_3S–C_2S–C_3A–C_2(A, F). Thus in the presence of 5 % MgO C_6A_2F is a stable product, crystallizing in both invariant points *A* and *B*. In the equilibrium condition the mixture of the composition corresponding to the Portland cement clinker will end the crystallization in point *B* [C_2S–C_3S–C_3A–C_2(A, F)]. In the equilibrium with the liquid phase, corresponding to the point *B*, C_6A_2F is. The composition of the ferrite phase will depend of the end of crystallization which can be in this point or in the invariant point *A*. In this later case in the solid phase exists CaO when ferrite starts to crystallize and contains less Al_2O_3 than C_4AF, then the C_3A will be formed. The calculation according the Bogue's method will give too low content of C_3A and to high of ferrite phase. However, in the earlier case C_3A will not be formed if A/F < 0.84. For higher value of alumina ratio small quantity of C_3A will crystallize and the ferrite phase will be richer in alumina than C_4AF. In this case the calculation according to Bogue's formulae will give too high C_3A content and too low ferrite phase.

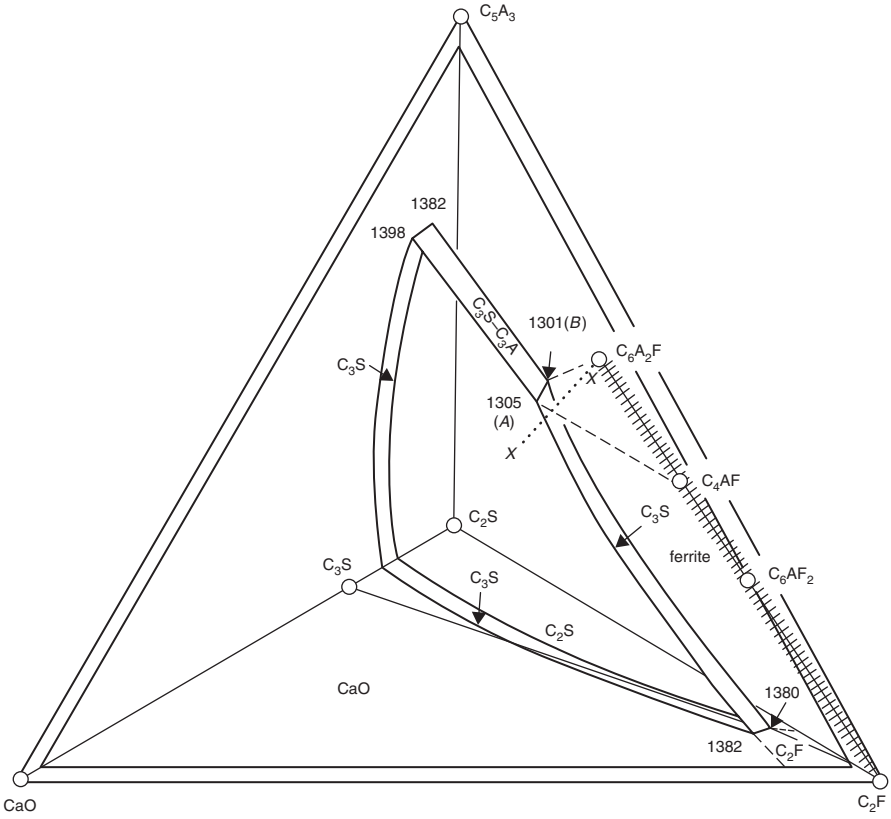


Fig. 2.23 The pseudosystem CaO–C_2S–C_5A_3–C_2F modified with 5% MgO. (After [36])

2.2.5 Departure from Equilibrium in the Clinkering Process

In this section the departure from equilibrium state linked with too low fineness of raw mix components or with insufficient homogenization, thus with lack of homogeneity of this mixture will be not discussed. They will be discussed in Sect. 2.3. This section will be limited to the lack of equilibrium in the crystallization process on clinker phase composition.

Discussing the crystallization of clinkering products in Sect. 2.2.1.3 it was assumed that during whole process the liquid phase was in equilibrium with solid phases. It means that earlier formed phases, e.g. CaO, crystallizing from the melt of composition *S* (Fig. 2.15) will be totally resorbed in invariant point *T* and crystallization will end in point *Y*. Similarly the melt crystallization of composition *P* will demand the resorption of earlier precipitated C_3S crystals. Similar dependences will occur in the case of melts crystallization in the ternary pseudo–system CaO–$2CaO \cdot SiO_2$–$4CaO \cdot Al_2O_3 \cdot Fe_2O_3$ (Fig. 2.20). If the cooling is rapid then the melt can

solidify as glass or its crystallization will proceed independently of earlier formed phases: CaO, C_3S or C_3S and C_2S. Lea [24] considers these cases for both systems shown on Fig. 2.15 and 2.20. In the system $CaO–Al_2O_3–SiO_2$ (Fig. 2.15) at 1500 °C the mixture *S* will contain the crystals C_3S and melt of the composition *V*, in which the line C_3S–*S* cross the isotherm 1500 °C. From the melt till point *O* C_3S will crystallize, and from this point, along the eutectic curve, C_3S and C_3A. The melt composition will change along the curve *OY* and in invariant point (it is the point *Y* in which the temperature = 1455 °C) the precipitation of C_2S will start and of remaining melt these three phases will crystallize. Part of C_3S will be simultaneously resorbed.

The mixture *G* of lower lime saturation will compose at 1500 °C of crystals C_3S and C_2S as well as of melt *X*, laying on the crossing point of binary eutectic C_3S and C_2S (the line separating their primary fields of crystallization) with isotherm 1500 °C. From this melt will further crystallize C_3S and C_2S until the melt will reach the composition *Y*. In this point C_3A precipitation will begin and the rest of melt will crystallize.

This advancement of process will be in the equilibrium conditions; in practice the cooling of clinker is too quick, to maintain the equilibrium of crystals with the melt. All melts composition: *V, X, O, Y* are laying on the lime–poor side of the triangle $C_3S–C_2S–C_3A$. The melts cannot thus crystallize with formation of these three phases only. The deficiency of lime in the melt will cause the partial resorption of earlier formed C_3S crystals. In the case of equilibrium lack of the melt with C_3S caused by rapid cooling clinker will contain more tricalcium silicate. C_2S, C_3A and $C_{12}A_7$ will crystallize from the remaining melt of composition *Y*. In this case the melt composition during crystallization will be shifted to the eutectic point 1335 °C. Clinker will also be richer in C_3S if the crystallization will end in the points *V* or *Y* and from a part or all melt glass will be formed. The composition of mixture *S* is: 69.5 % CaO, 20.5 % SiO_2, 10 % Al_2O_3, then after equilibrium crystallization should contain: 60 % C_3S, 13.5 % C_2S and 26.5 % C_3A. In the point *V* the precipitated C_3S crystals are already 68 %, in point *O*—69 %, and in *Y* 70.5 % C_3S and 6.5 % C_3A. Quenching will then give more C_3S of 8 %, 9 % or 10.5 % respectively.

The analysis of crystallization in the pseudo ternary system $CaO–C_2S–C_4AF$ (Fig. 2.20) shows that the results can be in this case opposite to the previous one. The mixture *E* of the composition 65.4 % CaO, 22.7 % SiO_2, 4.6 % Al_2O_3 and 7.3 % Fe_2O_3 at 1450 °C consists of the C_3S and C_2S crystals and melt *F*, which is the cross point of the limiting line of their primary fields with isotherm 1450 °C. The composition of this melt lies in the lime–richer side of the triangle $C_3S–C_4AF–C_2S$. During cooling of the melt in equilibrium with crystals its composition goes to *H*, where part of C_2S is resorbed in favour of C_3S and from the melt C_4AF is crystallizing. By rapid cooling and in the lack of equilibrium with the melt the solid phase will contain less C_3S and little CaO. In this case the end of crystallization is in point *K*. The crystallization in equilibrium gives 52.9 % C_3S (point *H*), 50.6 % C_3S, when the melt of composition *F* will crystallize independently, and only 41.1 % if melt *F* is solidifying as glass.

In average Portland cement clinker, in which the A/F ratio is significantly higher than in the last discussed examples, the C_3S content is higher in the case of rapid melt cooling. The opposite is for A/F < 0.64.

The field of Portland cement clinker marked in the system $CaO–Al_2O_3–SiO_2$ lies in principle inside the triangle $C_3S–C_2S–C_3A$ (Fig. 2.15). Fe_2O_3 was taken together with Al_2O_3. All compositions which are laying on left side of the line linking C_3S with the eutectic *T* will contain at 1470 °C two solid phases C_3S and C and the melt. In industrial condition the melt cooling is usually to quick, the produced clinker will always contain free CaO. The line $C_3S–T$ is defining the maximum content of CaO in industrial clinkers and this value should not be exceeded.

2.3 The Clinkering Process in Industrial Mixes

The clinkering process in industrial mixtures is in substantial degree dependent on the mineral compositions of raw materials, their fineness, and homogeneity of raw meal. Even in the perfectly produced raw meals at the initial period the reactions are limited to the small micro–areas, composed only of some raw material grains. Then the local eutectic are formed, accelerating the reactions in these micro–areas. They differ significantly between each other on degree of transformation and phase composition. Particular importance have the coarse grains of calcite and quartz. Under the influence of the liquid phase rich in CaO, the transformation of quartz into cristobalite takes place. Parallel, on the surface of SiO_2 grains the C_2S layer and the amorphous phase of the CaO/SiO_2 ratio lower than 1 are forming. Much favourable situation is in the case of clay minerals, and particularly with marls which contain frequently "all" clinker components. The content of liquid phase is constantly increasing and its composition is approaching to the clinker melt. However, important composition differentiates in it are occurring. The low diffusion rate of $[SiO_4]^{4-}$ and the increase of viscosity linked with these ions concentration rise, the melt surrounding C_2S crystals (pseudomorphose after quartz) is more acidic, which causes the further C_2S crystallization from the liquid phase. This acidic liquid phase is aggressive towards the alite phase, causing its crystals corrosion. However, in the neighbourhood of CaO grains liquid phase is oversaturated to alite, and its crystallization is favoured.

The clinker texture is definitely formed at the temperature range from 1300 to 1450 °C and during cooling process. The decisive influence has the alite crystallization condition at maximum clinkering temperature and then the interstitial matter crystallization from the melt, during clinker cooling.

Clinker melt, as it is known from microscopic observation, well wets the solid phase grains and forms the continuous phase enabling the diffusion transport to longer distances that it can be practically the case in the solid state. The rate of calcium oxide and dicalcium silicate dissolution in the melt is exponentially increasing with temperature. Quick heating of raw meal to the high temperatures is favourable and facilitates the nucleation process. However, the rate of temperature rise should be adjusted to the properties and primarily to the burnability of raw meal. Generally it can be assumed that lower rate of heating and lower burning temperature will be sufficient for the raw meal of good burnability.

It should be remember that the high oversaturation of clinker melt and high rate of C_3S can be easier obtained if CaO and C_2S are low crystallized, have defected structure and are composed of small crystallites. Then is possible, as Timashev [38] had shown, dispersive mechanism of dissolution which initial stage consists on breaking of porous CaO grains on singular crystallites. The eutectic liquid phase migrates inside the CaO sinters with high density (porosity lower than 14 %) with the rate of 1–1.5 mm/min and inside porous ones with the rate 7–10 mm/m. The experimental results of melt migration showed that the Altshuller's relation is fulfilled:

$$l = \sqrt{\frac{r\sigma\cos\theta}{2\eta}t} \tag{2.20}$$

where: l—depth of migration (cm), r—capillary diameter (cm), θ—wetting angle, t—migration time (s), η—liquid phase viscosity, (Pa · s), σ—surface tension ($N \cdot cm^{-1}$).

The CaO and C_2S crystals solubility depends on the diffusion rate of ions $Ca^{2+}$and $[SiO_4]^{4-}$ in the boundary layer. The rate of diffusion is increasing with temperature rise, because simultaneously the exponential lowering of clinker melt viscosity arises [14]. However, the C_2S dissolution process depends on chemical melt composition. Presence of Na^+ and K^+ ions in the melt causes the significant dissolution acceleration. This alkalis effect can be explained by the properties change of the acidic layer surrounding C_2S particles causing the acceleration of $[SiO_4]^{4-}$ ions diffusion. The advantageous effect of the surface tension melt lowering on the C_2S dissolution process, which improves these particles wetting by the melt, cannot also be excluded.

The simultaneous presence of sulphate ions with alkalis somewhat decrease the process rate, but it is farther much higher than for CaO. Thus it can be assumed that in industrial clinkers the C_2S dissolution rate is from three to five times higher than this of calcium oxide.

Different cations effect on the clinker melt viscosity is differentiated (Fig. 2.24). The addition of sodium and potassium significantly increases viscosity, but of magnesium and sulphates decreases it [38]. It is known that the increase of SiO_2 content in liquid phase is increasing its viscosity and CaO decreases it [14]. These relation can be explained on the basis of the melt constitution considerations. It is known that the melts viscosity depends on the elements dimensions of viscous flow. To this name atoms or more frequently groups of atoms belong, which are moving between them in the viscous flow. The activation energy of this flow is the function of the dimensions of moving elements and attracting forces thus the bonding forces in these elements [cohesion] and the interacting forces between them.

The ions are the small elements of viscous flow and cannot cause high viscosity. However, the clinker melts are composed also of larger elements, primarily of anions $[SiO_4]^{4-}$, which additionally show the polymerization tendency, forming dimers $[Si_2O_7]^{6-}$, trimmers $[Si_3O_9]^{6-}$ and bigger groups, bound by bridging oxygens. This tendency, however, has no practical importance in the clinker melt, in which the content of silica is low (compare the melt composition according to Timashev

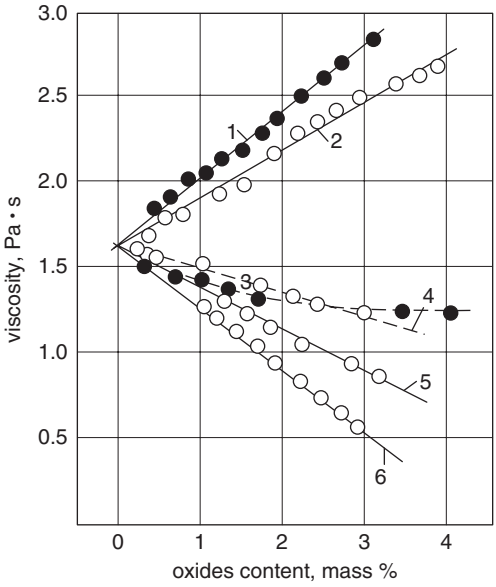


Fig. 2.24 The influence of some constituencies added to the clinker melt on its viscosity (Pa · s) (after [38]): *1* K_2O, *2* Na_2O, *3* MgO, *4* K_2SO_4, *5* Na_2SO_4, *6* SO_3

[38]) and the oxygen concentration is high. It was confirmed by Timashev [38] which measured the activation energy of silicon diffusion in the clinker melt. Very important is the effect of amphoteric components: Al^{3+} and Fe^{3+}, which can form the tetrahedra $[AlO_4]^{5-}$ or octahedra $[AlO_6]^{9-}$ groups, showing acidic or basic properties, respectively. This acidic–basic equilibrium is influencing the viscosity of clinker melt. The amphoteric ions are bonding stronger oxygen ions in tetrahedral coordination, however, in octahedral one they are easily decomposed on metal and oxygen ions, diminishing thereby the melt viscosity.

The acidic–basic equilibrium can be presented in the equation:

$$MO_4^{5-} \rightleftarrows M^{3+} + 4O^{2-} \tag{2.21}$$

$$K = \frac{\left[M^{3+}\right]\left[O^{2-}\right]^4}{\left[MO_4^{5-}\right]} \tag{2.22}$$

The ions Na^+ and K^+ shift the equilibrium in the left side, increasing the viscosity. However, at lower concentration of basic ions Fe^{3+} and Al^{3+} occupy the octahedral position. Particularly strong effect decreasing viscosity have the addition of sulphate anions, which shift the equilibrium on right. These anions are neutralizing the disadvantageous influence of sodium and potassium on the viscosity of clinker melt, which has high practical importance (Fig. 2.25) This favourable influence can be find only at the molar ratio $SO_3/R_2O \geq 1$. Sodium and potassium sulphates

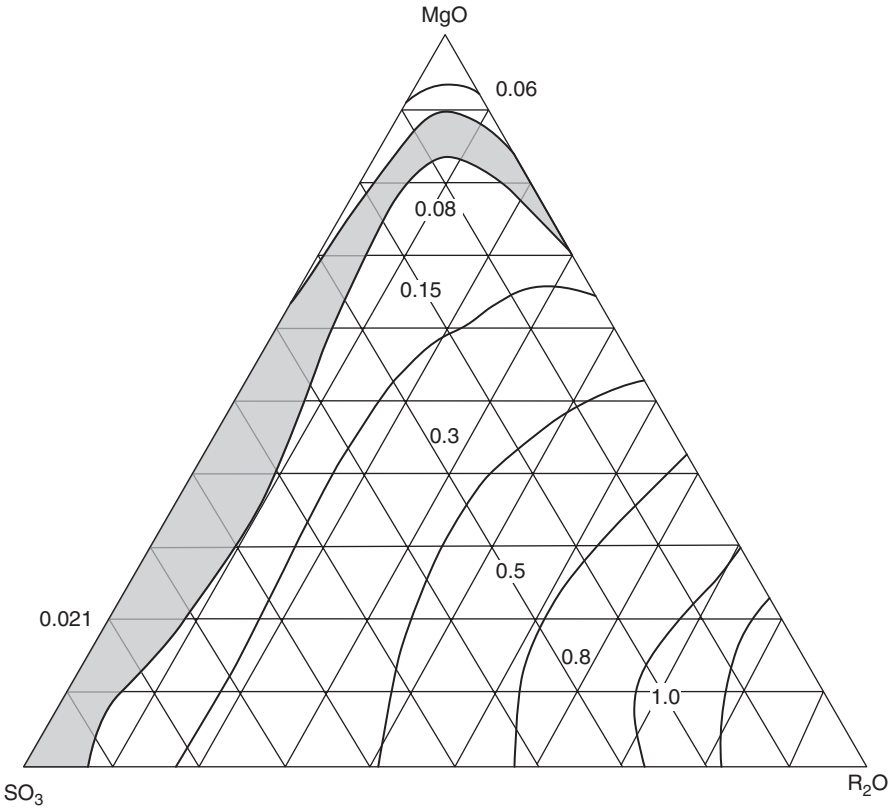


Fig. 2.25 Iso–viscosity curves (Pa · s) of clinker melt in relation to R_2O, MgO and SO_3 content (after [39]); the liquation field is *grey*

form the separate liquid phase, and particularly in the case of K_2SO_4 this liquation phenomenon is observed. MgO addition causes also the decrease of clinker melt viscosity, which additionally is diminishing the unfavourable effect of alkalis. The dependence of clinker liquid phase viscosity on the content of R_2O, MgO and SO_3 is shown on Fig. 2.25. The influence of these components on the properties of clinker melt finds the reflection in the free lime content lowering in the clinkering process (Fig. 2.26) [40]. Similarly to sulphur the phosphorus and boron are decreasing viscosity, which anions $[PO_4]^{3-}$ and $[BO_4]^{5-}$ are more acidic than $[SiO_4]^{4-}$.

Fluorine and chlorine up to 1 % have the strongest decreasing effect on the viscosity of clinker melt [41], but further increase of their content gives the quick increase of viscosity as a result of crystallization of clinker phases. As the infrared spectra has shown they increase also the share of octahedral groups $[MO_6]^{9-}$.

The initial oversaturation of the melt towards alite is low and principally the heterogeneous nucleation takes place, primarily as a result of the decrease of Gibbs free energy on phases boundary [42]. In this initial period alite nucleation can occur

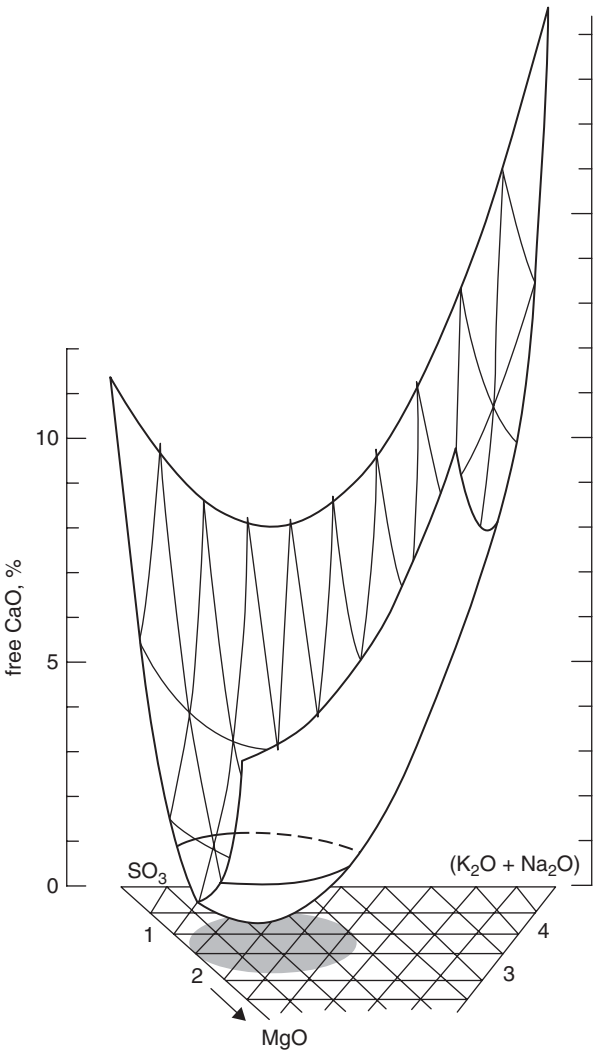


Fig. 2.26 The decrease of free lime content in clinkering process in relation to the minor components content. (After [40])

on C_2S particles, which results in the crystallization of C_3S on them. However the oversaturation is increasing quickly with the temperature rise and the viscosity of the liquid phase is decreasing, which permits the homogeneous nucleation, and the process is significantly accelerated. The point of view exists, that the homogeneous nucleation in clinkering is never appearing in the pure form.

Alite crystallizing from the melt has very differentiated morphology. Frequently of very disturbed constitution. Maki [42] distinguishes two periods of alite crystals growth: quick and in condition close to equilibrium. The crystals formed during the quick growth period contains the inclusions of liquid phase. They are usually in the core of crystals. In the similar conditions the inclusions of small crystals of C_2S and CaO as well as air bubbles can be formed. The latter, according to Maki, as

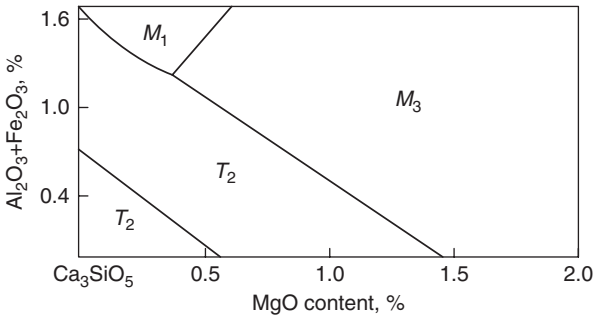


Fig. 2.27 The section of the system $CaO–SiO_2–MgO–Al_2O_3–Fe_2O_3$ showing stable polymorphic phase of C_3S after cooling (after [42]); molar ratio $Al_2O_3/Fe_2O_3 = 1$

a result of mechanical vibrations, caused by kiln rotations. The extended period of rapid growth gives very disturbed crystals, mostly without regular faces. However, the skeleton crystals in peculiar conditions are formed, when the oversaturation is higher in the vicinity of edges and corners, and lower in the middle regions of crystal faces. Further increase of differentiation of liquid phase oversaturation leads to the dendritic forms of crystals. After cooling, formed in these conditions alite crystals, are at the low temperature monoclinic M_1 if the MgO content in clinker is not too high (see Fig. 2.27).

Alite crystals formed in the period of slower growth do not contain inclusions, also the concentration of isomorphic substitutions is much lower. They form regular faces of hexagonal habit. After cooling they form phase M_3 which overgrow the core consisting of phase M_1 giving zonal constitution of crystals. From these growth conditions result also significantly higher dislocations number in the crystal cores. Extended holding of clinker at high temperatures causes, according to general rules, alite recrystallization thus the growth of large crystals at the expense of small, the latter became dissoluted [Ostwald's maturing]. During the recrystallization also the morphology of alite crystals is changing in the benefit of the forms with the faces composed of tetragonal prisms $(10\bar{1}1)$ and $(1\bar{1}02)$ [43]. It can be concluded on this basis that the growth in this period is occuring principally along the axis *c*. For this reason the *l/w* ratio in crystals where *l* is parallel to (0001) and *w* perpendicular to it gives the information about the growth condition. Crystals of zonal constitution, with the core composed of phase M_1 and the rim of phase M_3, have high ratio *l/w* from 3 to 4. However, in the conditions of easy nucleation and lower oversaturation small crystals are developed, practically composed of M_3, without inclusions, with *l/w* ratio from 2 to 3.

The decrease of foreign elements in the solid solution causes that in clinkers with low MgO content alite is present sometimes in phase T_2. It forms the overgrowth on M_3 giving the "reversed" laminar constitution of alite, it means that in this case the birefringence is lower on the crystal border (< 0.003) than in the core. The chemical composition equalization by the volumetric diffusion can give the homogeneous alite crystals, composed only of the phase T_2. At the low temperature the rate of crystal growth is always exceeding the rate of nuclei formation and the phase M_1 is formed. At higher temperatures and in the presence of earlier precipitated alite crystals, particularly of higher dimensions, the oversaturation of clinker melt is

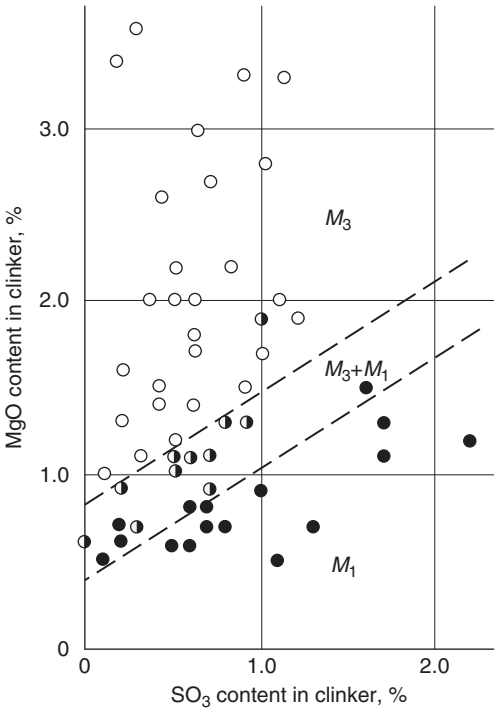


Fig. 2.28 Simultaneous influence of MgO and SO_3 on stabilization of alite different polymorphic modification in industrial clinkers. (After [42])

lowering and the equilibrium crystallization of phase M_3 occurs which overgrows the crystals M_1. Anomalous large crystals are formed as a result of crystallographic oriented intergrowth of smaller one. From the other components SO_3 has favourable influence on large crystals growth which is linked with the decrease of the liquid phase viscosity. After cooling they are principally composed of the phase M_1 and are distinguished by irregular skeleton shape, or even dendritic morphology. Common are the inclusions of interstitial matter and belite. To high SO_3 content causes the deterioration of alite crystallization condition and is decreasing its content. Thus the effect of MgO and SO_3 on the alite crystallization process are very different. Simultaneous effect of these both components on different alite phases stabilization occurring in clinker established by Maki [42] is presented on Fig. 2.28. High importance have, however, the clinkering conditions which can considerably change this picture.

The relation between the minor components concentration in the liquid phase and their content in alite crystals was investigated [44]. Maki [43] gives the content of minor components in alite of industrial clinkers, which is higher in the crystals core (M_1) then in surface layers (M_3). It is in good correlation with Burton's [44] relation, because in the initial period the rate of crystal growth is higher. Maki [43] has shown simultaneously that the recrystallization of alite in the condition close to equilibrium causes the significant decrease of foreign elements in its crystals.

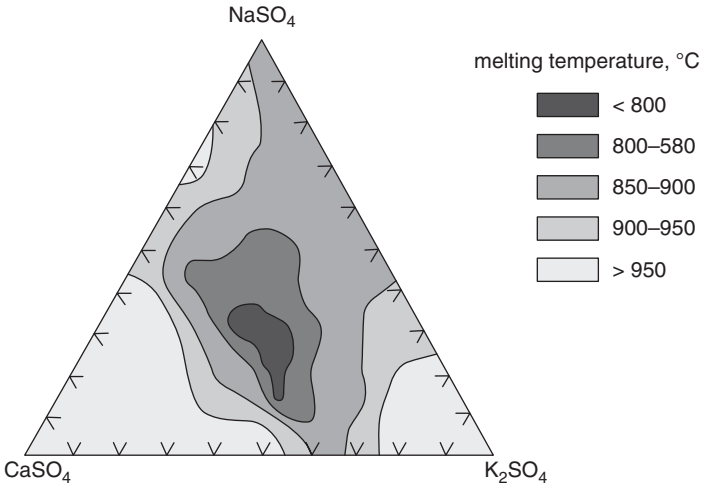


Fig. 2.29 Temperatures ranges of liquid phase formation in the system of sulphates sodium, potassium and calcium. (After [23])

2.3.1 The Clinkering Process Modification in the Presence of Mineralizers

The foreign elements occurring in raw materials have lower or higher influence on clinkering process. Three causes are given: earlier liquid phase formation (fluxes), intermediate phases formation and clinker melt properties modification. High part of minor elements are fluxes, thus influencing on liquid phase formation at lower temperatures. Typical example are sulphates or chlorides of sodium and potassium. In the system Na_2SO_4–K_2SO_4–$CaSO_4$ (Fig. 2.29) the liquid phase appears at 800 °C and in the presence of low chlorides content (Fig. 2.30) much earlier already at 700 °C [23].

There is the commonly accepted opinion that the Al_2O_3 and Fe_2O_3 are not the valuable clinker components, but principally behave as fluxes. They cause the high amount of liquid phase formation and at considerably lower temperature than in the binary system CaO–SiO_2. Although attributing to the phases C_3A and C_4AF low importance in cement hardening process is a significant simplification, it does not change the fact that the formation of alite, with acceptable in industrial practice rate, is possible thanks to the clinker melt only, which embraced principally calcium aluminates and ferrites.

The liquid phase formed due to local eutectic, accelerate the calcium carbonate decomposition and the reactions of calcium oxide with silica, as well as with alumina and iron oxides.

The common phenomenon linked with the mineralizers presence is the formation of new, untypical intermediates phases, which are not encountered in the mixtures

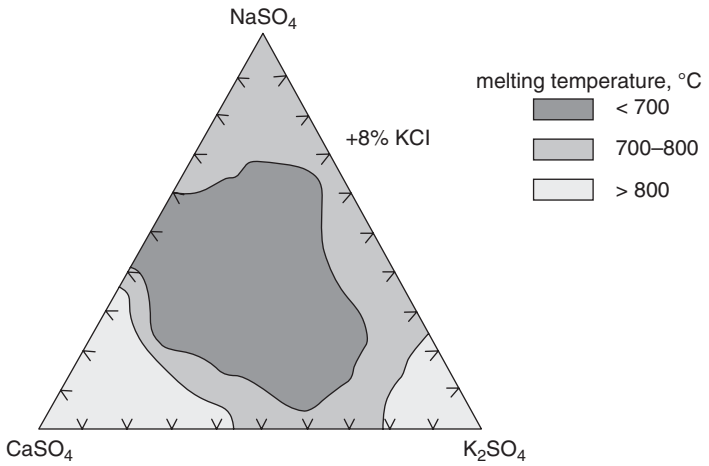


Fig. 2.30 The temperature ranges of liquid phase formation in the sodium, potassium and calcium sulphates system with 8 % of KCl addition. (After [23])

without these components. To these intermediate phases belong, among other, spurrite $Ca_5[SiO_4]_2(CO_3)$[7] or calcium sulpho–aluminate $3(CaO \cdot Al_2O_3) \cdot CaSO_4$ [45].

The studies have shown that in spurrite structure the individual SiO_4 tetrahedra as in dicalcium silicate are present [46]. Thus it is logic that the formation of this phase significantly accelerates belite crystallization. Trojer [47] found the chromite spurrite $(C_2S)_2CaCrO_4$, and Klucharov [48] the calcium chromite–aluminate $3CaO \cdot 3Al_2O_3 \cdot CaCrO_4$.

The mineralizers influence on liquid phase properties was discussed earlier and further information are completed in Sect. 2.5.5.5.

2.3.1.1 The Fluorine Effect on Clinkering Process

Fluorine is the earliest known and very effective mineralizer. In the mixtures of $CaCO_3$ with SiO_2 in the presence of CaF_2 at the temperature close to 600 °C, spurrite is formed, which is decomposed in C_2S and CaO at temperature insignificantly higher than 960 °C. Moreover in the system $CaO–SiO_2–CaF_2$ two new ternary phases are formed: $2(Ca_2[SiO_4] \cdot CaF_2$ and $3C_3S \cdot CaF_2$ [49]. First is formed at about 950 °C and at 1040 °C is decomposed in C_2S and CaF_2. The second is formed at 1130 °C and melts incongruently at 1175 °C, decomposing onto C_3S, $\alpha–C_2S$ and melt [50]. Gutt [50] gives the following scheme of these processes:

[7] B. Courtault was the first which found spurrite formation in the mixture of $CaCO_3$ with SiO_2 in the presence of CaF_2 [*Bull.Soc. Franc.Mineral.Crist.,* **1964 (4),** 527].

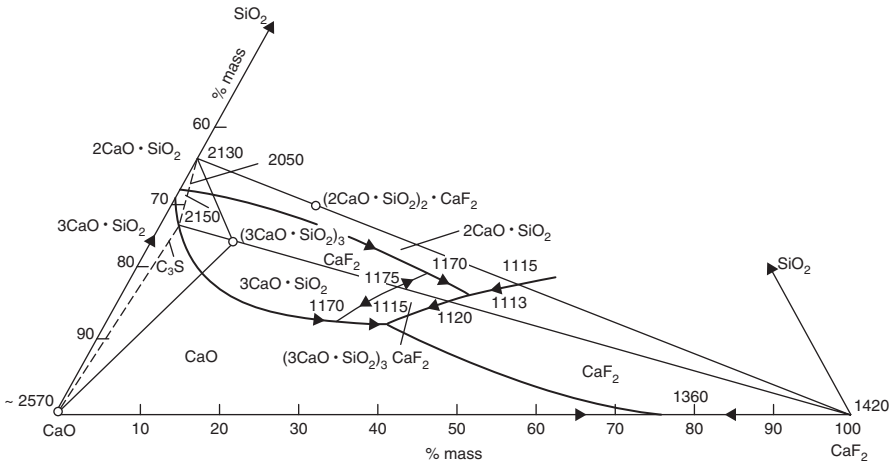
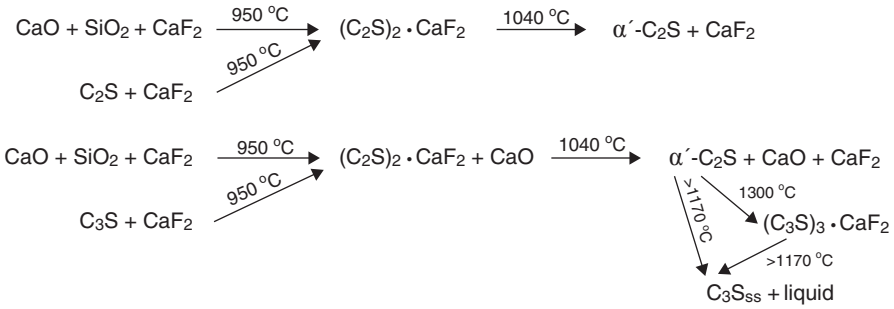


Fig. 2.31 The part of the system $CaO–SiO_2–CaF_2$. (After [50])



In the system $CaO–SiO_2–CaF_2$ the C_3S field became much larger and the temperature of invariant point is considerably lower and equal 1170 °C (Fig. 2.31). CaF_2 forms the eutectic with $(3CaO \cdot SiO_2)_3 \cdot CaF_2$ at 1115 °C.

In the multicomponent system C–S–A–F–M the highest rate of alite formation is at the CaF_2 addition lower than 1 % [17]. Further increase of this addition does not cause significant differences in the synthesis rate and even at 1500 °C this rate became lower. It was establish that the fluorine addition is neutralizing partially the unfavourable phosphorus effect [50].

Gilioli et al. [51] have shown that at the presence of $CaSO_4$ the fluoride phases are not formed. In this condition the fluoride ellestadite ($3C_2S \cdot 3CaSO_4 \cdot CaF_2$) is formed. The fluorine phases can be only formed when the ratio $F/SO_3 > 0.158$. However, when $F/SO_3 < 0.158$ the sulphate spurrite is formed ($2C_2S \cdot CaSO_4$). These authors also state that the compound $(C_3S)_3 \cdot CaF_2$ has the composition closer to the formula $19C \cdot 7S \cdot 2CaF_2$. Ellestadite formation was also studied by Damao Tong

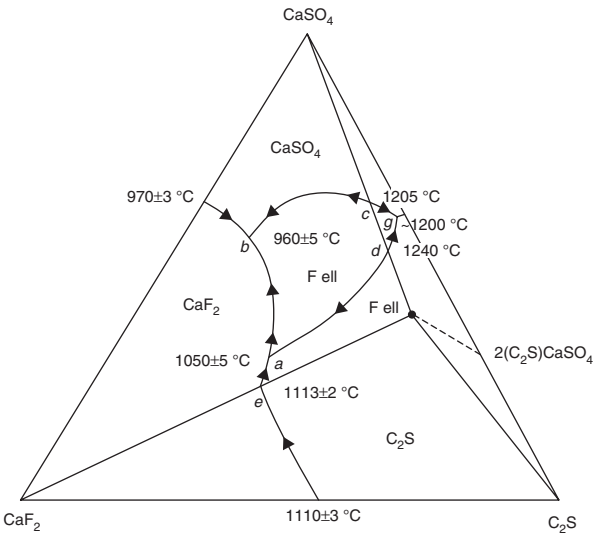


Fig. 2.32 The fluorine ellestadite (*F ell*) in the system $CaSO_4$–CaF_2–Ca_2SiO_4. (After [53])

and Zongshon Lin [52]. They found that $3C_2S \cdot 3CaSO_4 \cdot CaF_2$ is easily formed at 940 °C, thanks to development of eutectic melt at 910 °C. The fluoride ellestadite melt at 1225 °C, but the melting point became lowered to the temperature 1160–1180 °C at the presence of A, F, and M.

On the Fig. 2.32 the system $CaSO_4$–CaF_2–Ca_2SiO_4 is shown [53]. Fluoride ellestadite to the liquidus temperature is stable and melts incongruently, decomposing to C_2S and melt at 1240 °C. Low–temperature eutectic Ca_2SiO_4 with CaF_2 is at about 1113 °C. Fluorine ellestadite has no hydraulic properties and its presence in clinker is unfavourable. Probably, there is no possibility to avoid some low content of this phase in clinkers containing fluorine.

In the second half of seventieth the papers were publish concerning the application of double mineralizer $CaF_2 + CaSO_4$ [54, 55]. This two–components mineralizer appeared to be very effective and gave the possibility to produce clinker at low temperature: 1300–1350 °C [52]. Odler [56] obtained even clinker at 1230 °C.

At the presence of potassium in clinker another phase containing fluorine can be formed, namely $KF \cdot 2[Ca_6(SO_4)(SiO_4)_2O]$ [57]. Its structure is close to alite, but it does not react with water. This phase was found by Trivine and Vasquez [57] in the coating, on kiln lining.

In Aalborg cement plant in Denmark the two–component mineralizer was used of composition 1.5 % $CaSO_4$ + 0.3 % CaF_2 to produce clinker in the kilns using wet method [58]. The clinkering temperature was lowered as much as 200 °C, but the fuel economy was only 5 % [59]. However, the emission of NO_x was considerably lower. As fuel the pit–coke with high sulphur content was used. The SO_2 emission was kipping low by passing gases through the scrubber with lime slurry. The produced gypsum was partially used as cement setting retarder. Cement quality was very satisfying, equal to class 62.5 MPa.

There is the opinion that fluorine does not cause emission from rotary kilns which can be explained by high chemical affinity of this element to calcium, with which it forms easily not volatile CaF_2. Also Moir [60] ascribes F to the low volatile component, even lower than the sulphates and this opinion is generally accepted. However, Goswami et al. [61] ascribe fluorine to the volatile component, probably basing on volatile SiF_4. This paper is devoted to build–ups formation in cyclone preheaters, the fluorine was not added to the raw meal, but was present in limestone, at the level of 0.11 % [61]. The authors are stating that the reason of build–ups formation is spurrite, which they found in the material blocking cyclones. Anhydrite was also found. The chemical buildups composition was as follows:

F	0.10–0.29 %	Cl	0.02–0.05 %
K_2O	0.95–3.56 %	SO_3	0.60–0.85 %
Na_2O	0.13–0.16 %		

These authors [61] found also the fluorine and potassium concentrations in the kiln inlet and in the middle part of sintering zone. In the ring formed in the distance of 33 m from the hot kiln end 50 % of spurrite was found. Sylvine was found in the coating from the distance of 11.5–14.5 m from the cold kiln end. The sample from 14 m contained also spurrite. In the riser duct the anhydrite and chlorine silicate $Ca_3SiO_4Cl_2$ were found too. In the sampled specimens the fluorine content was from 0.17 to 0.38 % and chlorine 0.02 to 0.25 %. In the 8500 t/day capacity kiln in cement plant Ozarov in cyclone IV build–ups the formation of sylvine and spurrite was also found, despite of relatively low chlorine content in the raw material [62].

In the clinkers, the addition of fluorine to the raw meal, causes the phase $C_{11}A_7 \cdot CaF_2$ formation, thanks to C_3A decrease. The quantity of fluorine bound in clinker is proportional to this phase content. This phase was found in the ternary system C–A–S with CaF_2 addition. The phase $C_{11}A_7 \cdot CaF_2$ forms solid solution with $C_{11}A_7$. The phase equilibriums in the system $CaO–Al_2O_3–SiO_2$ in the presence of 5 % of $CaSiF_6$ was studied by Roy [63]. In this system the field of $C_{12}A_{7ss}$ [8] is significantly larger (Fig. 2.33). and in this connection the eutectic curve of this phase with gehlenite is appearing. Two Alkemade's lines linking C_3S with $C_{12}A_{7ss}$ and C_2AS with $C_{12}A_{7ss}$ show the new invariant point presence at 1360 °C. Also the C_3S field is enlarged and this phase became stable till 1200 °C.

2.3.1.2 Chlorine Influence on Clinkering Process

Chlorine is very effective mineralizer. The calcium chloride addition to the mixture $CaCO_3 + SiO_2$ causes the formation of two intermediate phases: calcium chloride silicate $Ca_3[SiO_4]Cl_2$ and mentioned earlier spurrite [64].

[8] $C_{12}A_{7ss}$ means the solid solution of $C_{11}A_7 \cdot CaF_2$ with $C_{12}A_7$.

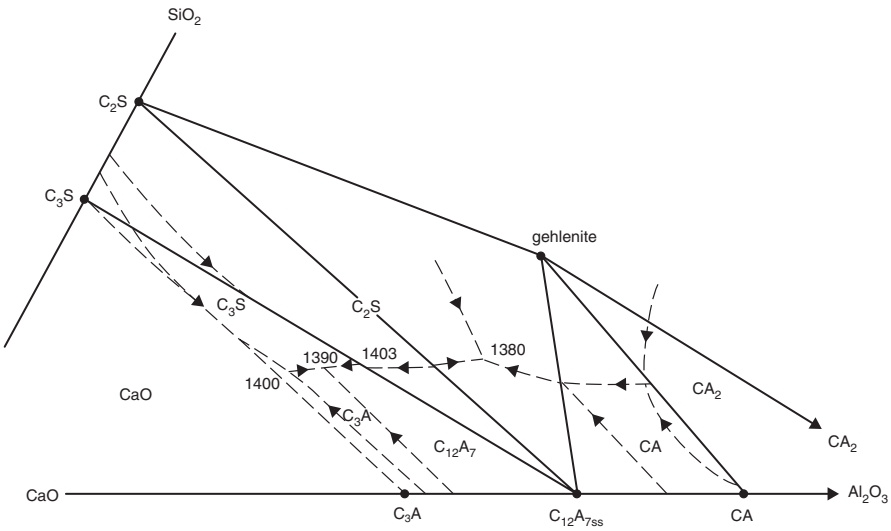


Fig. 2.33 Part of the system $CaO–Al_2O_3–SiO_2$ with 5% $CaSiF_6$ addition

Calcium chloride silicate is always formed in this mixture at 630 °C and its quantity is proportional to the $CaCl_2$ content. It is caused by the eutectic liquid phase formation with the following molar composition: 73.5% $CaCl_2$, 25% $CaCO_3$ and 1.5% CaO. Its melting point is at about 630 °C [65]. Examination under the high temperature microscope has shown the dissolution of silica in the liquid phase, and crystallization of $Ca_3[SiO_4]Cl_2$. Successively at 810 °C as the result of the eutectic mixture melting of the molar composition 48% $CaCO_3$ and 52% $Ca_3[SiO_4]Cl_2$ spurrite is formed. In CO_2 atmosphere spurrite is decomposed at 960 °C and a little earlier, because at 915 °C, calcium chloride silicate (Fig. 2.34). It corresponds to the liquid phase $CaCl_2–CaO–CO_2$. In air atmosphere spurrite is not formed, and chloride silicate is decomposed at about 1000 °C (eutectic point $CaCl_2$–CaO) (Fig. 2.35). Both phases are decomposed on α–C_2S and CaO, which favors their quick reaction to C_3S. The liquid phase formed in the system $CaCO_3–CaCl_2$ favors, through silica dissolution, quick reaction with lime, with $Ca_2[SiO_4]$ formation. Dicalcium silicate is coexisting with calcium chloride silicate and with spurrite, till the decomposition of these both intermediate phases.

In the micro–regions rich in silica the formation of cuspidine chlorine analog $Ca_4[Si_2O_7]Cl_2$ and also $Ca_2[SiO_4]Cl_2$ is possible. The first is decomposed at about 1000 °C and the second at 950 °C.

In the multicomponent or industrial mixes chlorine reacts principally with aluminate phase with formation of $C_{11}A_7 \cdot CaCl_2$. It is the stable phase and can exists in Portland cement clinker. Simultaneously alinite can in this conditions replace alite [67]. This phase contains aluminium and magnesium, but probably the last one is necessary for alinite formation. The alinite formulae given by several authors differ slightly. Massazza and Gilioli [69] give the following composition:

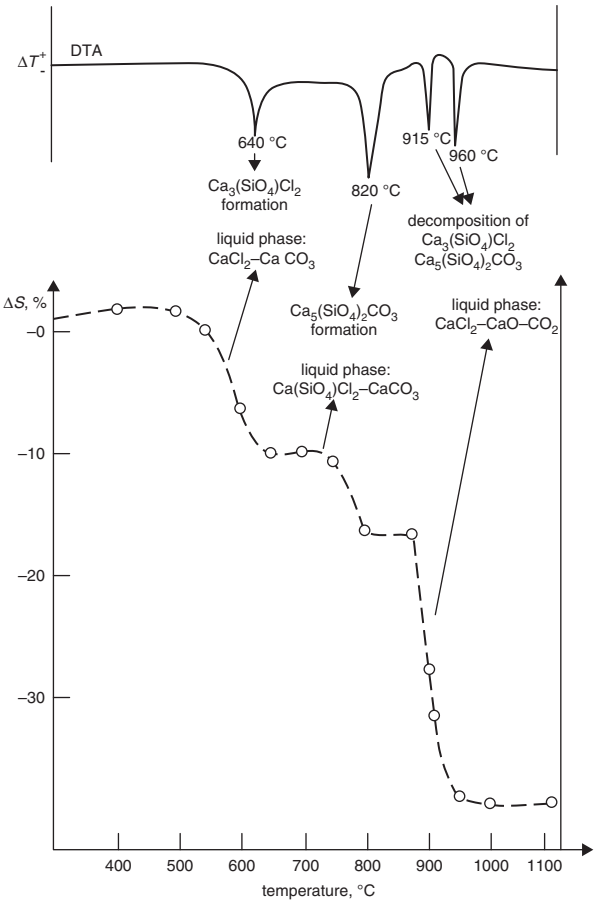


Fig. 2.34 DTA *curve* and the change of the surface of sample $5CaCO_3 + 2SiO_2 + 10\%$ Cl under high–temperature microscope, heated in CO_2 atmosphere. (After [66])

$$3[(CaO)_{0.875}(MgO)_{0.07}(CaCl_2)_{0.055}][(SiO_2)_{0.885}(Al_2O_3)_{0.115}]$$

This phase can also be formed in Portland cement clinker at higher chlorine content in raw meal [70]. However, chlorine is not a desirable component in clinkering process. The chloride compounds with potassium and sodium, which are quickly formed in rotary kiln, have high vapour pressure at high temperature and undergo sublimation in the sintering zone and condensation on meal particles in cyclone preheater, then returning to the kiln. Thus they have high partial pressure in the kiln gaseous phase and cause the disadvantageous phenomena of build–ups formations in the riser duct carrying the hot gases from the kiln to the preheater, up to its partial plugging.

2.3.1.3 Alkalis in Clinkering Process

Potassium and sodium introduced to the raw meal with clay minerals are not desirable in the process of clinker phases formation. However, at low temperature they

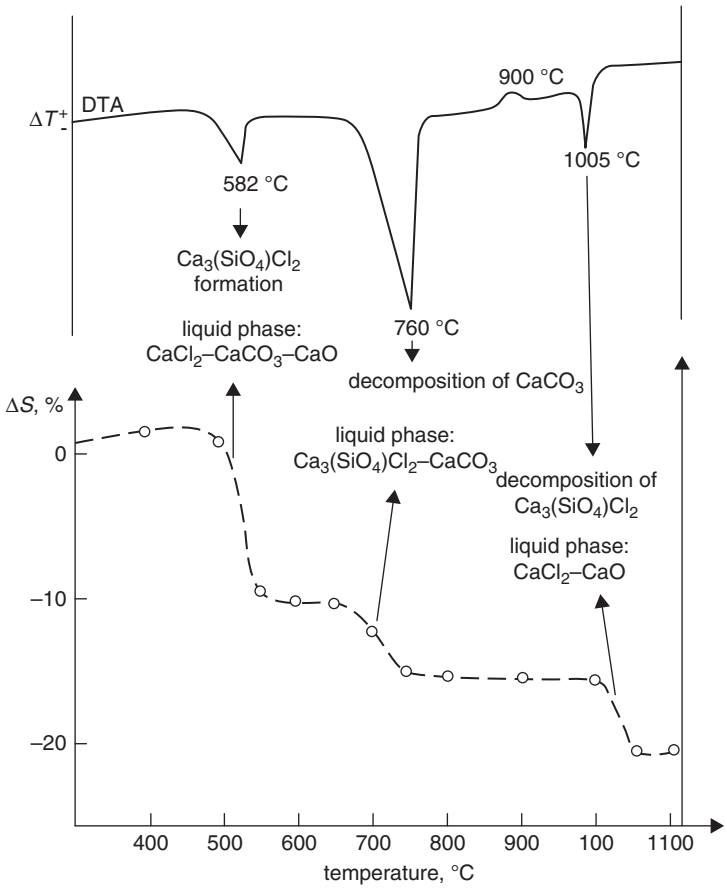


Fig. 2.35 DTA *curve* and the change of the sample $5CaCO_3+2SiO_2+10\,\%$ Cl surface under high–temperature microscope; heating in the air atmosphere. (After [66])

play the advantageous role, because they participate in the local eutectics formation and increase the degree of raw mixture transformation. In the presence of alkalis spurrite as an intermediate phase is formed. At the higher temperature potassium is formed solid solution in dicalcium silicate, which maximum content corresponds to the formula $K_2O \cdot 23CaO \cdot 12SiO_2$. This phase is reacting harder with calcium and the reaction of alite formation is delayed. This phase is decomposed reacting with anhydrite:

$$K_2O \cdot 23CaO \cdot 12SiO_2 + CaSO_4 \rightarrow K_2SO_4 + 12C_2S \tag{2.23}$$

At molar ratio $(K_2O+Na_2O)/SO_3 \leq 1$ sulphur is neutralizing disadvantageous alkalis effect, forming principally sulphates. Similarly sulphur neutralizes the unfavorable alkalis influence on properties of clinker melt (Sect. 2.3) The presence of alkalis in the multi–component system will give the slight modification of phases equilibrium. It was

established in the case of Na_2O [71]. The regular C_3A is in equilibrium with ferrite solid solution only in the range C_4AF–C_6A_2F. However, C_3A of lower symmetry containing sodium in solid solution, is coexisting with alumina low ferrites: from C_4AF to C_6AF_2.

Unfavorable alkalis influence consists also in their volatizing and the inner circuits formation in the kiln. It will be discussed in Sect. 2.3.2.

2.3.1.4 Sulphur in Clinkering Process

The action of sulphur as mineralizer is insignificant. The advantageous influence of this component consists principally on neutralizing of noxious effect of alkalis. In the case of sulphur excess, then when the molar ratio $(K_2O+Na_2O)/SO_3<1$, the phase $2CaSO_4 \cdot K_2SO_4$ is formed. At high sulphur excess the intermediate phase: $3CaO \cdot 3Al_2O_3 \cdot CaSO_4$ is formed. This phase develops with high rate already at 1000 °C and is decomposed at 1300 °C.

In the system CaO–SiO_2–$CaSO_4$ the compound $2C_2S \cdot CaSO_4$ is formed [72], stable at the range 1000–1200 °C. This is important in the production of expansive clinkers [73]. As it was mentioned earlier, at low quantities the sulphur presence has advantageous effect on clinkering process, principally by modification of the melt properties.

2.3.1.5 Phosphorus in Clinkering Process

Admissible content of phosphorus in clinker is 2% according to Nurse [74], and according to Gutt [50] 2.5%. Up to the content of about 2% good quality clinker is obtained, although the paste is setting slower. Higher content of phosphorus is significantly worsening its quality, because phosphorus decompose C_3S and the solid solution of C_3P in belite is formed of the composition: 7% P_2O_5, 66.5% CaO, 26.5% SiO_2. This composition is close to nagelschmidtite $7CaO \cdot P_2O_5 \cdot 2SiO_2$, but with lower C_2S content. Nurse [74] was considering that 1% P_2O_5 is decreasing C_3S content of 9.9% and increases the content of belite and solid solution of C_3P in belite of 10.9%. Gutt [50] was stating that 2% P_2O_5 can be the maximum content in solid solution in C_3S and that the field of primary crystallization of C_3S is extended up to 13% of P_2O_5.

2.3.2 Clinkering Process in Rotary Kiln

To the most important factors influencing the clinkering process in rotary kiln are the following:

- the rate of material temperature increase, particularly in the range from 800 °C to 1300 °C,
- the rate of clinker cooling in the range 1450–1250 °C,
- composition of gaseous atmosphere in the kiln.

- Other phenomena which can happen in the kiln and have also some effect on the processes occurring in the rotary kiln are the following:
- dropping downwards of non–combusted fuel onto the material,
- dropping downwards of the ash from fuel,
- mechanical effect of kiln movements.

The rate of temperature rise, after achieving by material the temperature of 800 °C, then the temperature of limestone decarbonisation, has an significant effect on further process development, principally on the reaction of alite formation. Low increase of temperature, thus the long residence time of material at 800–1200 °C, causes the sintering of CaO and its recrystallization. Larger CaO particles with lower porosity are causing its slower dissolution in the clinker melt which appears at the temperature slightly higher than 1250 °C. The melt oversaturation towards alite, necessary to its crystallization, is reached later and the process itself is slower.

The rate of clinker cooling, from maximum temperature (1450 °C) till the melt stiffening, has also high influence on clinker phase composition and thus on its properties. Lea [24] is discussing several examples of rapid clinker cooling of different composition, in which clinker is transformed to glass or crystallizes independently. It can be generally concluded that in the case of the majority of industrial clinkers rapid cooling gives the increase of alite content in comparison of crystallization in equilibrium conditions. The departures from equilibrium was discussed in Sect. 2.2.5.

In the case of variable rates of cooling, with different intensity, the recrystallization phenomena will also happen, which share will increase with the drop of this rate. The rate of cooling will have considerable influence on C_3A, brownmillerite and glass content, the two first phases are crystallizing from the melt as the latest ones. Cooling will have high influence on the content of minor components in solid solutions, which will decrease with the slow drop of temperature. It is known for example that the slow cooling causes alite surface decomposition and crystals of this phase will have the shells composed of very small belite crystallites (Fig. 2.70). Belite is also under significant transformation in the case of slow cooling which was discussed in Sect. 2.5.2. Finally slow clinker cooling causes usually the solid solution of SiO_2 in C_3A decomposition with the crystallisation of minute crystallites of belite (Fig. 2.77). Unfortunately there is a lack of research of the effect of clinker cooling rate, particularly in industrial condition, on phase composition, crystals morphology and clinker properties.

The composition of gas phase in the kiln depends on fuel composition and condition of combusting, which introduce to the kiln atmosphere CO_2, H_2O, CO and in minor share SO_2 and NO_x. In this gaseous atmosphere are also the highly volatile components to which belong principally chlorine, alkalis and some heavy metals (Tl, H).

The sintering of Portland cement clinker is running as a rule in oxidation atmosphere, with exception of special process, to which for example the production of white clinker belongs. These special processes are presented in Sect. 9.2. However, sometimes the disturbances in combustion process can occur which causes momentary appearing of reduction atmosphere, then containing low quantity of CO. In this condition superficial reduction of clinker grains, usually in the layer of low thickness, consisting in transformation of iron Fe^{3+} to lower oxidation degree Fe^{2+}

is occurring. It has insignificant effect on clinkering process and clinker properties, and the layer in which the reduction phenomena were occurring underwent quick oxidation still on the end of sintering zone.

The reduction phenomena can occur also even by maintaining oxidation atmosphere in the kiln in the case of fuel addition to the kiln feed. Also the fuel feeding to the riser duct carrying the hot gases from the kiln to the cyclone preheater can be reckon among these phenomena [75]. Similar condition can exists in the case of falling fuel from gas stream on clinker, e.g. coarse coal particles. These coke particles fall down usually in the intermediate zone, or in the beginning of sintering zone.

As a rule feeding of the fuel to the cyclone exchangers is linked with the maintaining of higher air excess in the kiln giving quick fuel combustion, still before material is approaching to the sintering zone. Also in the case of falling the fuel particles on clinker there is in the kiln sufficient oxygen amount, ensuring its quick combustion.

The exceptional situation can take place in the case of fuel mixing with raw mix, then when the nodulization of material in the kiln will cause the closing of part of coal in the nodule core. In this condition, despite oxidation atmosphere in the kiln, the oxidation reaction of this part of coal will be exceptionally difficult and we can observe the reduction phenomena in the clinker nodule core. It is occurring especially when on the nodules surface the shells of hardly sintered material are formed. These phenomena were observed in the case of the Lepol's grate [76]. The classic example of the fuel addition to the feed are the shaft kiln, but they are applied exceptionally seldom.

The influence of reducing atmosphere on phase composition and clinker properties was studies by several authors [76–81]. They state unanimously the gradual iron reduction, which leads to ferrite phase decomposition with C_3A and free CaO formation. Fe^{2+} can substitute Ca^{2+} in all clinker phases, obviously in accordance with its solubility in individual phases. Frequently the tendency of clinker to self–powdering, linked with γ–C_2S formation is listed.

The hypothesis was put forward by Woerman [76] that the burning of clinker in reducing condition is accelerating alite decomposition. It is caused by the presence of Fe^{2+} substituting Ca^{2+} in alite. During cooling, already in oxidizing condition, iron is transformed to higher oxidation degree, which favours the alite decomposition at the temperature close to 1180 °C. This process can be presented in simplified scheme:

$$\left(C, Fe^{2+}\right)_3 S \rightarrow C_2S + C_2F \tag{2.24}$$

Magnesium in solid solution counteracts this decomposition.

Vernet [81] rejects Woerman's hypothesis. He found that coal is reducing CaO, which is causing belite formation. This reduction is relatively quick at high temperature and at 1450 °C after 26 h of heating the reduction degree is higher than 41 %.

It seems that the results of these authors are not contradictory. Only the oxidation atmosphere during cooling must be taken into consideration. However, Vernet [81] confirmed once more the known fact of acceleration of C_2S polymorphic transformation, until γ phase formation in reducing condition.

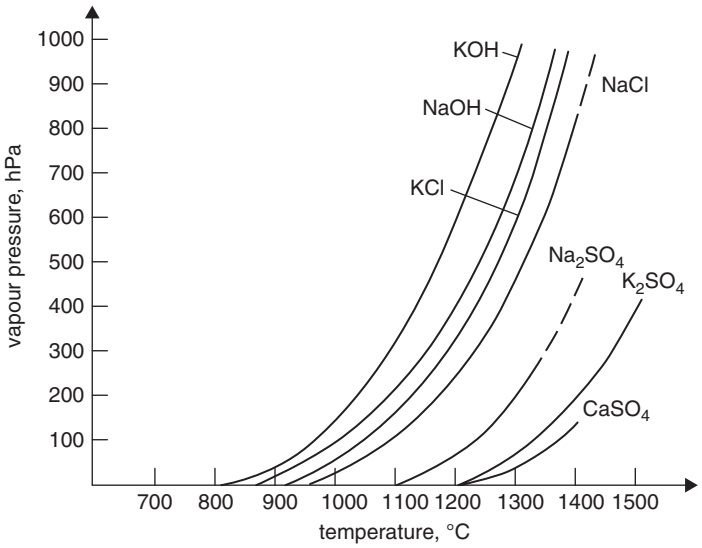


Fig. 2.36 Vapour pressure of some volatile compounds

Very high influence on kiln gaseous atmosphere have volatile raw mix components. Belong to them chlorine, alkalis, and some heavy metals. On Fig. 2.36 vapour pressure curves of some compounds are presented. These components are volatilized and with hot gases are swept to the inlet to cyclone preheater where they are largely reabsorbed on small raw material grains. In this part of the kiln system temperatures are relatively low of about 800 °C and the vapour pressure of these components is also low (Fig. 2.36). Thus they return to the kiln which causes the enrichment of gases in these components, and has important influence on the clinkering process.

It has particularly great importance in the modern kilns, i.e. short rotary kilns equipped with cyclones, which, on account of the intensive mass exchange in these preheaters, can be called "closed kilns". It creates condition for the intermediate phases formation which are frequently found in the rings occurring in industrial kilns [82–85]. Belong to them spurrite, sulphate spurrite and also calcium aluminate sulphate. Amafuji and Tsumagari [86] studied these problems, using modelling approach. They found the formation of secondary $CaCO_3$ at the temperatures range 750–900 °C, anhydrite in the range 530–1190 °C, sulphate spurrite in the range 1050–1150 °C. In gases of the composition close to found in industrial kilns at temperature > 700 °C primarily $CaSO_4$ is formed, spurrite at the temperature range 800–850 °C and sulphate spurrite at the range 900–1100 °C. K_2SO_4 presence provides for the development of $2CaSO_4 \cdot K_2SO_4$ at temperature 600–900 °C. Then all these phases are formed which are encountered in rings in industrial kilns. Kurdowski [87] found also the possibility of syngenite formation in the kilns using wet method, which can causes the ring formation in chain zone.

Great changes in clinker phase composition are caused by the dropping downwards of coal ash on clinker in the kiln. Using of fuel rich in ash provides a worsening of

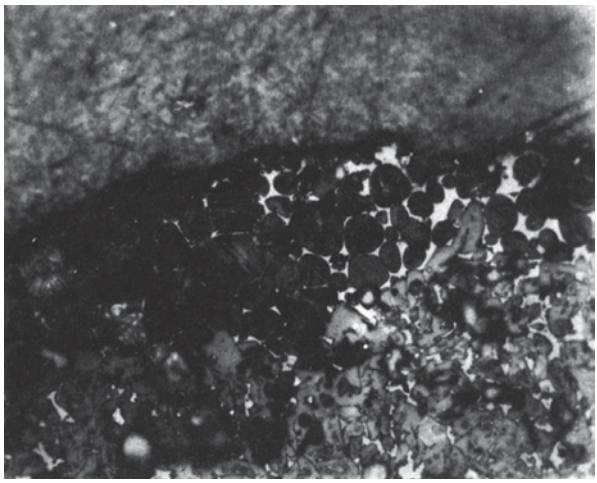


Fig. 2.37 Belite layer on clinker nodule (primary nodule surface = alite zone). (Photo C. Wieja)

clinker quality, because this ash cannot fully react with clinker, particularly in the case of this coal which simultaneously the temperature drop in sintering zone of the kiln will cause. In this condition belite layer on clinker nodules will be formed (Fig. 2.37).

Heilmann [16] and Christensen [88] the proceed of ash reaction with clinker have explained. At the temperature range 1450–1500 °C (Fig. 2.38) the ash is fully melted, but clinker contains two solid phases C_3S and C and the melt composition is laying on the curve M_a–M_b. Process is controlled by diffusion and during its progress two reaction regions are established: C_3S + melt M_a–M_b and C_2S + melt M_b–M_c–M_d–M_e nearby the ash liquid phase. During the process the mean clinker composition is laying on the line linking the points C_1 and A_2. In this connection freezing of clinker–ash sandwich from 1500 °C the sample will contain four zones Z_1—ash glass, Z_2—C_2S in this glass, Z_3—C_3S in glass and Z_4—clinker.

The studies of phase composition of material along the rotary kiln are seldom. It needs the shutdown of the kiln and sampling of the material after its cooling. What transformation underwent material during slow temperature drop is always the problem under discussion. On the Fig. 2.39 the results of Moore [10] study are presented. Obtained results confirm the purposefulness of such studies, however, very anxious and expensive.

The introducing of cyclone heat exchangers gives the possibility of relatively easy sampling of material in kiln inlet, at temperature of about 800 °C. Further technological development and application of precalciners permitted to obtain material after decarbonisation, which is feeded to the kiln. In the latter one only three zones remained: intermediate, sintering and cooling.

Wolter [89] studied the phase composition of raw mix after the precalcination, then after the material heating to about 900 °C. Material falling to the kiln has the following new phases: CaO, periclase, belite, spurrite, $C_{12}A_7$ and C_2(A, F). The CaO content was from 30 to 75 % and C_2S from 25 to 30 %. The components which were condensed on raw material grains from gaseous phase, namely KCl

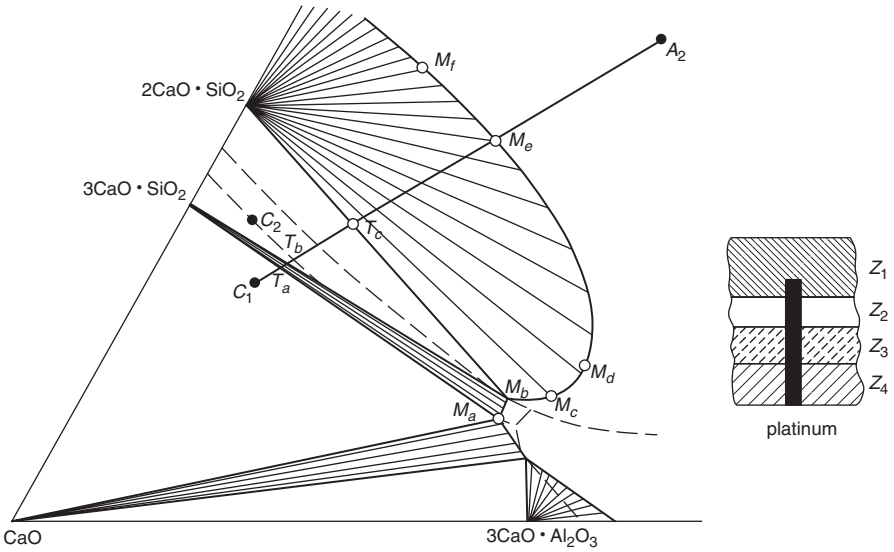


Fig. 2.38 Liquidus *curves* at 1500 °C in the part of the $CaO–Al_2O_3–SiO_2$. Fields of C_3S and C_3A primary crystallization are denoted by *dashed lines*. C_1 clinker composition (reduced to three oxides) and ash A_2 (according to [88]). At *right side* scheme of Heilmann experiment: ash–clinker sandwich Christensen N.H., Simonsen, "Diffusion in Portland Cement Clinker", J. Am Ceram. Soc. **53**, 361 (1970), published by John Wiley & Sons Ltd, reproduced with the permission of Wiley & Sons

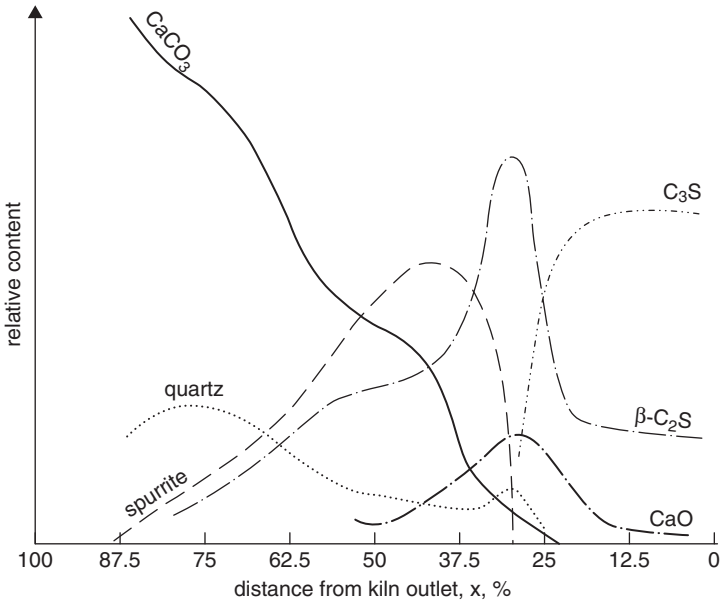


Fig. 2.39 The phase composition of material samples taken in rotary kiln. (According to [10])

(as sylvine), NaCl (halite), K_2SO_4 (arcanite), $K_3Na[SO_4]_2$ (aftitalite) and anhydrite are also found. In the clinker dust carried out of the kiln alite was found. The coal ash present in the dust typical round particles forms [87].

Wächtler and Jannsen [90] studied the material phase composition in the kiln with partial precalcination, and without its shut down. In the material from cyclone preheater spurrite, C_2F and aluminates: CA and $C_{12}A_7$ and free CaO were found. In the samples also these phases and additionally C_4AF were present. Then the gehlenite appears, C_2S and C_3A. Appearing of C_3A is accompanied with the disappearing of C_2F and CA. When C_3S appears the samples have already the composition of clinker.

In the second part of seventieth Humboldt introduced to the industry a very short kiln "Pyrorapid", with the extremely rapid temperature increase of burned material, which provides a very favourable quick reaction of CaO after decarbonisation with silica [91]. The clinker phases formation, particularly of alite, became accelerated. The phase composition of material in the kiln are shown in Fig. 2.40 [91].

In the rotary kiln the process of material nodulising, parallel to clinker formation is occuring. The studies have shown that for nodulising the surface tension of clinker melt is very important and its rise has advantageous effect [38]. It is shown on Fig. 2.41.

The quantity of dust in the kiln is increasing with the lowering of raw mix burnability, then with the lime saturation factor and silica ratio increase [92, 93] (Fig. 2.42). The situation is also worsening by the content of quartz silica and even by siliceous limestone increase. It was establish also that the sintering process depends in a high degree of alumina ratio. Mac Gregor [94] is stating that in the large rotary kiln the unfavourable temperature distribution in sintering zone is generated and the nodulising process is worsening. Also large alite crystals make this process more difficult [94]. The increase of raw mix fineness has the favourable effect on the fine fractions share in clinker, which is decreasing. Clinker grains can also be disintegrated during the cooling process as a result of high temperature gradient between the surface and the core of nodules, which causes the stress formation. However, it has low practical importance.

2.4 Thermochemistry of Clinkering Process

The experimental difficulties of direct clinkering heat measurements caused that they are seldom. Much frequently the indirect measurements were used, for example Eitel and Richter [95] the heat of oxides and clinker dissolution have measured, for the exothermic clinkering effect calculation. Many calculations have also been done on the basis of known specific heats and some heats of reactions.

The formulae for these calculations can be found in Babushkin et al. book [13]. The heats of several reactions, which constitute the overall clinkering process, are given in the Table 2.1, and specific heats of components participating in this process in Table 2.2. On the basis of these data the theoretical thermal balance of clinkering can be obtained and heat of this process can be calculated (Table 2.3).

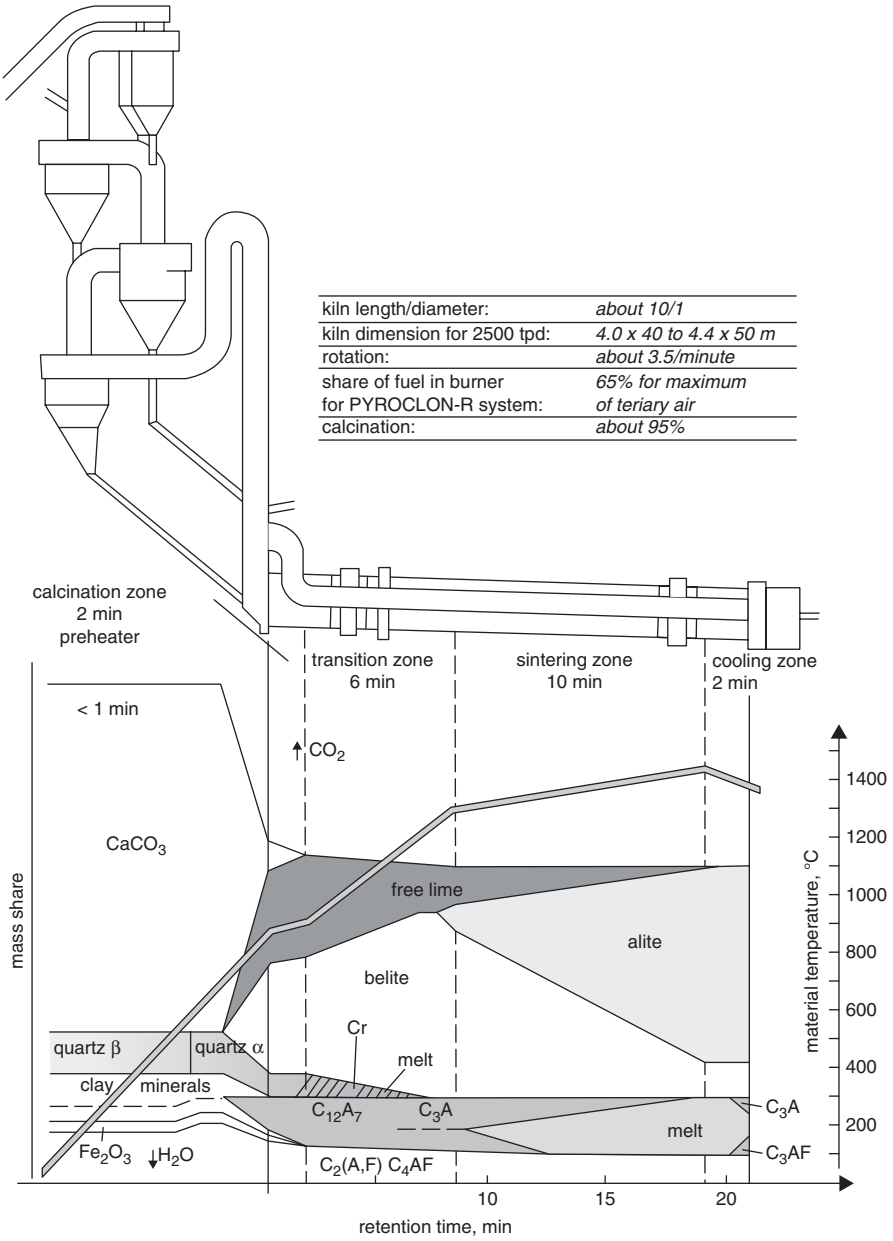


Fig. 2.40 The changes of material phase composition in the "Pyrorapid" kiln. (According to [91])

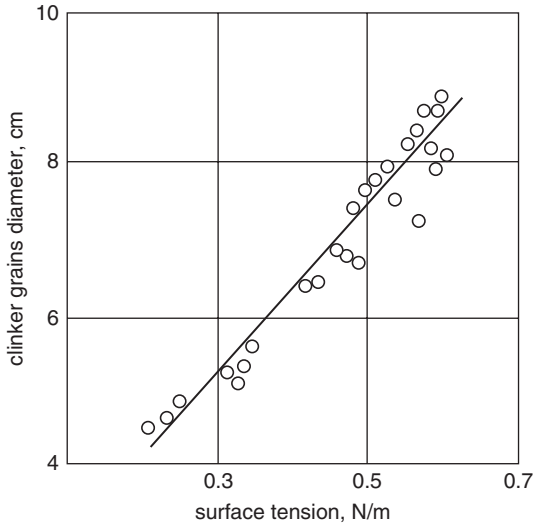


Fig. 2.41 The surface tension effect of clinker melt on the clinker grading. (According to [38])

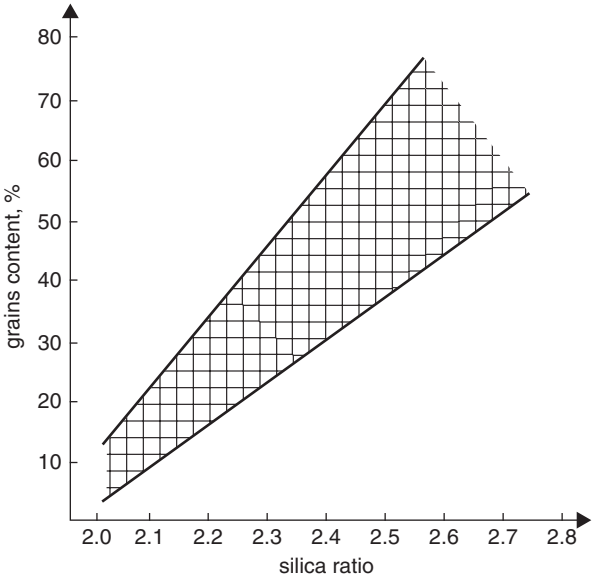


Fig. 2.42 Influence of silica ratio on the grains content of diameter < 5 mm in clinker

Clinker mineral composition was the following:

	Zur Strassen	Gygi
C_3S	191 g	673 g
C_2S	544 g	112 g
C_3A	265 g	103 g
C_4AF	–	113 g

Table 2.1 Heat of elemental reactions participating in clinkering process [96]

Dehydroxylation at temp. 450 °C	Kaolinite +907.7 933.7[a]	Montmorillonite +1316.1	Illite +347.5	$Ca(OH)_2$ +1.47
Decarbonation at temp. 900 °C	$CaCO_3$ +1766.9 +1645.5[b]	$MgCO_3$ +1356.6 +1395[b] +1214.2[c]		
Crystallization	C_3S −538.9 −528.4 −464.8[a]	C_2S −726.4 −716.0 −619.7[a]	C_3A −320.7 15.5 −347.5[a] 87.9[d]	C_4AF −229.0 −84.2 −108.9[a]

Melt formation + 104.7 kJ/kg of clinker. Metakaolinite recrystallization 301.5 ± 41.9 kJ/kg
[a] After Gygi [97]
[b] at 20 °C
[c] at 590 °C
[d] After Lea [24]

Table 2.2 Specific heat of some solid phase [kJ/kg · K]

Temperature range (°C)	Kind of substance											
	CaO	SiO_2	Al_2O_3	$CaCO_3$	C_3A	C_2S	C_3S	AS_2H_2	Meta–kaolinite	Clinker	Slag	CA
20–100	0.787			0.875		0.7913				0.787	0.837	
20–200	0.816			0.921		–				0.829	0.850	
20–300	0.842		0.972	0.980	0.887	0.8663	0.8667			0.867	0.863	0.931
20–400	0.854			1.022		0.8910	0.8918			0.892	0.934	
20–450	0.858	1.001		1.038		–		1.1724	0.996	0.909	0.942	
20–500	0.861	1.030	1.043	1.051	0.927	0.9149	0.9111		1.009	0.921	0.946	0.981
20–600	0.867			1.080		0.9341 0.9689	0.9337			0.938	0.963	
20–675	0.875			–		0.9689				–	–	
20–700	0.876	1.080	1.083	1.093	0.947	0.9743	0.9517		1.047	0.959	0.992	1.013
20–800	0.883					0.9952	0.9672			0.967	1.009	
20–900	0.891	1.101	1.108	1.114	0.958	1.0112	0.9798		1.080	0.988	1.017	1.0472
20–1000	0.896					1.0262	0.9965			0.997	1.030	
20–1100	0.901	1.114	1.133		0.971	1.0409	1.0074		1.110	1.013	1.047	1.0664
20–1200	0.904					1.0539	1.0133			1.030	1.076	
20–1300	0.909		1.157		0.983	1.0643	1.0212			1.097	1.160	1.0798
20–1400	0.913	1.135					1.0300		1.130	1.097		1.0853
20–1500	0.915	1.139	1.177				1.0363			1.131		

From data presented in Table 2.1. it can be concluded that the results given by different authors are changing in large range. Even in the case of so simple reaction as $MgCO_3$ decomposition at 590 °C the heat given by different authors is changing from 1050 to 1215 kJ/kg. In practice, thus with natural raw materials with

Table 2.3 Thermal balance of clinkering process, J/g of clinker

Processes	zur Strassen [96]	Gygi [97]	
Heating of 253 g kaolinite (20–450 °C)	−125.6	160 g kaolinite	−84.6
Heating of 123 g SiO_2 (20–450 °C)	−54.4	142 g SiO_2	−64.1
Heating of 1177 g $CaCO_3$ (20–450 °C)	−523.4	1221 g $CaCO_3$	−570.7
		37 g Fe_2O_3	−13.4
Decomposition of 253 g kaolinite at 450°C	−234.5	160 g kaolinite	−149.1
Heating 218 g metakaolinite (450–900 °C)	−134	138 g	−72.4
Heating 123 g SiO_2 (450–900 °C)	−67	142 g SiO_2	−77.0
Heating 1177 g $CaCO_3$ (450–900 °C)	−632.2	1221 g $CaCO_3$	−655.3
		37 g Fe_2O_3	−17.2
Decomposition of 1177 g $CaCO_3$ at 900°C	−1951.1	1221 g $CaCO_3$	−2022.3
Heating 218 g metakaolinite (900–1400 °C)	−134	138 g	−84.6
Recrystallization of 218 g metakaolinite at 1000°C	+67	–	
Heating 123 g SiO_2 (900–1400 °C)	−71.2	142 g SiO_2	−83.7
Heating 660 g CaO (900–1400 °C)	−314	37 g Fe_2O_3	−21.4
		685 g CaO	−325.3
Crystallization of 191 g C_3S at 1400°C	+88	673 g C_3S at 1450°C	
			312.8
Crystallization 544 g C_2S w 1400°C	+335	112 g C_2S[a]	+69.5
Liquid phase formation at 1400°C	−92.1		−108.9
Clinker cooling (1400–20 °C)	+1507.3	(1450–0 °C)	+1532.4
CO_2 cooling (900–20 °C)	+489.9		+519.2
Water vapour cooling (450–20 °C)	+29.3[b]		+12.6[c]
Clinkering heat	−1796		−1903.5

[a] Crystallization of 103 g of C_3A 36 J/g, 113 g C_4AF 12.1 J/g
[b] Related to vapour; if the liquidation is included +117 J/g, the clinkering heat will be −1679 J/g
[c] Water vapour condensation 49.4 J/g included in crystallization heat

changeable mineral composition and large changes of minor components content, the heat of reactions will also present high variability. For example, exothermic heat of clinker formation from different raw materials is in the range from 420 to 500 kJ/kg, however, in the case of slag and limestone is only 210–290 kJ/kg of clinker. It is admitted in all calculation that as a result of dehydroxylation

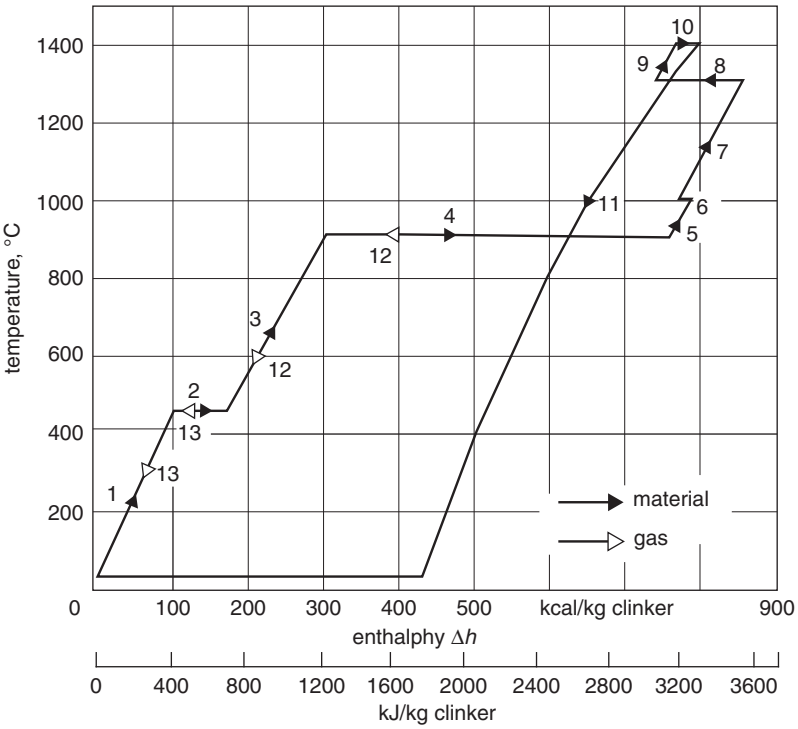


Fig. 2.43 Enthalpy of clinkering process: *1, 3, 5, 7, 9* heating of raw mix, *2* dehydroxylation kaolinite, *4* decarbonisation of $CaCO_3$, *6* mullite crystallization, *8* melt formation, *10* crystallization of clinker phases, *11* clinker cooling, *12* cooling of gaseous CO_2, *13* cooling of water vapour

of clay minerals the free oxides are formed and their heat of crystallization is calculated, namely α–Al_2O_3 and quartz. It is the reason that the heat of clinker phases crystallization is calculated using the oxides data. It is obviously a great simplification (Fig. 2.43).

Castanet and Sorrentino [98] measured the clinkering heat in the high–temperature calorimeter of Calvet. In the case of clinker composition 4.77% C_4AF, 11.07% C_3A, 21.28% C_2S, 55.7% C_3S and 4% of free CaO the heat was 1876 kJ/kg of clinker. There is a difference between measured and calculated heat of 322 kJ/kg of clinker. This difference is explained.

Zur Strassen [96] introduced also the empirical formulae for raw mixes of different mineral composition, which gives the possibility for approximate clinkering heat calculation, using their chemical composition. For classic raw mix, composed of limestone and clay this formula is as follows:

$$q_{cl} = 4.178\left(4.11\mathrm{A} + 6.48\mathrm{M} + 7.64\mathrm{C} - 5.116\mathrm{S} - 0.59\mathrm{F}\right) \tag{2.25}$$

where the symbols A, M, C etc. mean content of oxides (% mass) in clinker, and q_{cl}—heat of clinkering, J/g.

Table 2.4 Maximum coordination number in dependency on ionic radii of cation and anion

r_M/r_X	CN	Configuration
<0.15	2	linear or angular
0.15–0.22	3	triangular flat or pyramidal
0.22–0.41	4	Tetrahedral
0.41–0.73	4	quadratic flat
	6	octahedral
0.73–1.0	8	hexahedral (cube)
>1.0	12	cubic–octahedral

When the mineral composition of clay components is known it can be applied in the coefficient before A, as follows:

5.30A for kaolinite,
3.12A for montmorillonite,
3.92A for illite.

2.5 Phase Composition of Portland Cements

Portland cement clinker is composed of four principal phases: alite, which is close to tricalcium orthosilicate $Ca_3[SiO_4]O$, belite close to dicalcium orthosilicate $Ca_2[SiO_4]$, tricalcium aluminate $Ca_3[Al_2O_6]$ and ferrite $C_2(A, F)$. Chemical composition of these phases is complicated by solid solutions, which have the decisive influence on their reactivity with water. For the elements from which clinker phases are composed isomorphism is typical and very developed phenomenon. The highest concentration of isomorphic elements is encountered in tricalcium aluminate (about 12–13 %), and then in alumino–ferrites (about 10–11 %), belite (about 6 %), and the lowest in alite (about 4 %).

Before the discussion of particular dependencies which are encountered in clinker solid solutions it will be useful to remind general principles of solid solutions formation. In crystal chemistry significant importance have the interionic distances in the lattice, which is the basis for ionic radius determination[9]. The radii ratio of neighbouring ions in the lattice is deciding of the numbers of the closest neighbours, then of so called coordination number of ion. For example silicon ion is as a rule surrounded by four oxygen ions (CN = 4), located in the tetrahedron corners[10].

In the Table 2.4 the coordination numbers dependency of cation to anion radius ratio and in Table 2.5 the ionic radii of the elements the most often encountered in cement chemistry, are given. It should be remembered that the ionic radii, given in Table 2.5, depend on oxidation degree, and are decreasing with its rise,

[9] In cement crystal chemistry we have generally the ionic crystals. Other kinds of crystals are discussed in books on crystallography. In Polish: J. Chojnacki "Chemical and Physical crystallography" PWN, Warsaw 1961. In this book also the problem of ionic radii is presented.

[10] Structure of silicates: see E. Görlich "Silicate Chemistry", Geological Ed. Warsaw 1957 (in Polish), M. Handke "Crystal Chemistry of Silicates", Kraków 2005, (in Polish).

Table 2.5 The ionic radii of elements the most frequently encountered in cement chemistry

Ion	Ionic radius (pm)	Ion	Ionic radius (pm)
H^+	0	Ti^{4+}	68
Li^+	68	Cr^{3+}	63
B^{3+}	23	Cr^{6+}	52
O^{2-}	140	Mn^{3+}	66
F^-	133	Fe^{2+}	74
Na^+	97	Fe^{3+}	64
Mg^{2+}	66	Zn^{2+}	74
Al^{3+}	51	As^{3+}	58
Si^{4+}	42	Ba^{2+}	134
P^{5+}	35	Pb^{2+}	120
S^{6+}	30	OH^-[a]	130–180
Cl^-	181	$H2O$[a]	138[b]
K^+	133	$H3O^+$[a]	143(140)
Ca^{2+}	99		

[a] approximate values
[b] in ice

e.g. Fe^{2+}about 82 pm; Fe^{3+} about 67 pm, and of lattice type, then of CN. Given in Table 2.5 radii belong to the lattice type of NaCl.

Isomorphic substitutions are possible in the case of ions of approximate radii. For example Sr^{2+} with the radius 113 pm easily substitutes Ca^{2+} ($r = 99$ pm) in all clinker phases. The situation is more complicated if the substitution is regarding ions of different charge. Crystal as a whole must be electrically neutral. The different cases are then possible: group substitution, e.g. $[Ca^{2+}, Si^{4+} \rightleftarrows 2Al^{3+}$. Aluminium is substituting silicon in anionic sublattice, and calcium in cationic one. The examples of these substitutions can be alite $Ca_3[SiO_4]O$. All these are the solid solutions by substitution.

Another possibility is the location of ion in interstitial position, for example interstitial solid solution of Na^+ in C_3A. Still another possibility is the cationic vacancies formation. It is the substitution of calcium ions by chromium(III) in octahedral positions in C_3S with cationic vacancy formation (extraction solid solution).

Particular case of aluminium, substituting simultaneously Ca^{2+} and Si^{4+} in alite lattice is possible because the ionic radii ratio of Al^{3+} and O^{2-} equal 0.36 (51/140) is close to threshold value 0.41, separating CN = 4 from CN = 6.

The solid solutions formation provides to significant mother lattice defecting and frequently is stabilising the phases stable at high temperature. Lack of arrangement caused by solid solutions fulfils the role of ions thermal vibrations. It is the reason why solid solutions provide the increase of reactivity, because they cause the numerous disturbances in the mother lattice.

To solid solutions studies the chemical, X–ray diffraction and spectroscopy (IR and NMR) methods are used. Chemical methods in cement chemistry consist principally on free CaO determination in function of additive content increasing, for example MgO, which substitute calcium in solid solution.

In X–ray method Vegard's law is applied, which assume that the changes of unit cell is directly proportional to the increase of concentration of solid solution. Usually the measurements of the changes of inter–plane distance (d) in the function of introduced additive are conducted. Irrespectively of numerous departures from the Vegard's rule it has a significant experimental importance and give the possibility to establish maximum of component content in the solid solutions (Figs. 2.19 and 2.61).

Particular importance have the studies of infrared spectra, which give the possibility of analysing of so called "short–range ordering" (first coordination sphere), which is of fundamental importance in the case of solid solutions.

On the kind of isomorphic substitutions significant influence has the arrangement of external electronic shell of ion. It is linked with mixed kind of bonds, which never are pure ionic. Some share of covalent bond, which is always oriented in space, as the effect of hybridized orbitals formation, significantly facilitates the coordination polyhedron formation, in accordance with the directions of covalent bonds. The example can be the Si–O bond (only about 60% ionic), in which the hybridized orbitals sp^3 participate.

2.5.1 Tricalcium Silicate and Alite Phase

Tricalcium silicate is the most important component of Portland cement clinker. Its share as a rule is overpassing 55% and reactivity with water has the decisive effect on paste hardening. At room temperature C_3S is triclinic. The structures of different polymorphic phases of tricalcium silicate was determined by Jeffery [99]. The basis was the rhombohedral pseudo–structure with hexagonal unit cell [99]:

$a = 700$ pm	$c = 2500$ pm	$R3m$	$Z = 9$

The structure is composed of independent tetrahedra, bound by calcium ions. Tetrahedra are placed in the following manner: three SiO_4 tetrahedra and three calcium ions are lying on ternary axis. They are linked by two triplets of calcium ions (Fig. 2.44). These in turn are surrounded by further three oxygen atoms, not belonging to SiO_4 tetrahedra. Each oxygen atom is surrounded by six calcium ions, forming around them octahedra. The silica–oxygen tetrahedra are lying on all ternary axis, but they are positioned on different height. It causes the formation of irregular oxygen octahedra around the calcium ions and in the structure large voids remain, in which other atoms can locate themselves. This irregular calcium ions coordination, in which the bond length can differ from 254 to 324 pm and voids in the cationic sublattice are according to some authors the reason of significant reactivity of C_3S with water. On Fig. 2.45 the vertical intersection through the longer diagonal of unit cell, showing the cell base is presented and in Fig. 2.46 projection along the c axis on the base plane.

The structure of Jeffery is only simplified [100]. Studying the pseudo–hexagonal crystals Regourd [35] found the superstructure peaks, in case of which $a = 1400$ pm.

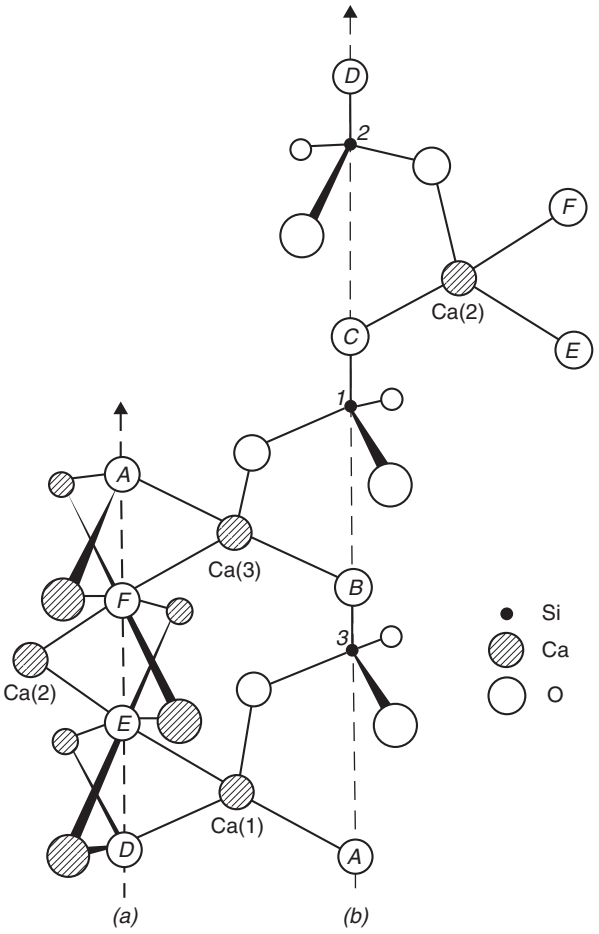


Fig. 2.44 Tricalcium silicate: two adjacent tetrahedra columns and linking them calcium ions. Total column can be obtained by superimposing of fragment *b* on top *a* (or *a* on *b*) etc. The full surrounding of calcium ions is not shown, two oxygen atoms is lacking, also for simplicity only one oxygen ion from the triplet in column *b* is shown. (According to [99])

Handke et al. [101] on the basis of infra–red and Raman spectroscopic studies advanced the hypothesis that the structure of triclinic C_3S seems to be laminar and is composed of the layers of $Ca_2[SiO_4]$ and CaO. The symmetry of single layer being close to the *R3m* symmetry, proposed by Jeffery. This laminar C_3S structure could explain its non–stoichiometry and easy decomposition into C_2S and CaO. In C_3S structure proposed by Belov et al. [102] the oxygen coordination number (CN=6) non belonging to SiO_4 tetrahedra is also close to octahedral coordination, existing in CaO crystals.

Tricalcium silicate several polymorphic phases forms, which structures are very similar. All transformations belong to the displacive type and in their occurring only small displacement of atoms, without breaking the primary coordination bonds takes place. Then they occur easily and the enthalpies of transformation are low. The high–temperature phases cannot be stabilised by quenching. Regourd [103] distinguishes seven polymorphic forms of tricalcium silicate, which are presented

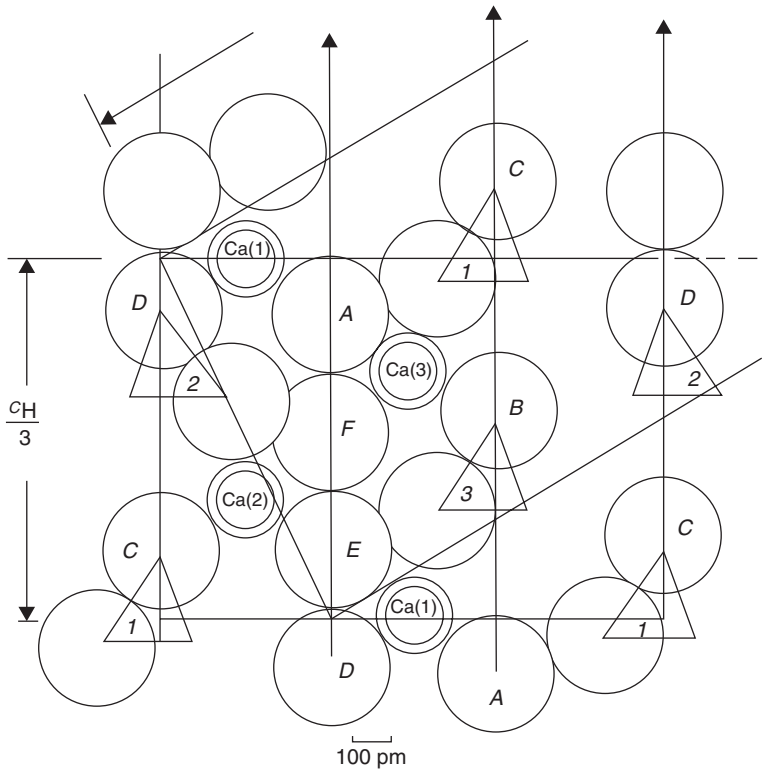


Fig. 2.45 Vertical intersection through the longer diagonal of hexagonal unit cell. (According to [99])

in Table 2.6. Phase triclinic 3 was described by Maki and Chromy [104]. Regourd [103] found this phase in samples containing 0.5 % of ZnO, but she states that it is "reversed" polymorphic phase monoclinic (II), in which the characteristic peaks 224, 404 and 620, 040 are reversed.

The stability range of individual C_3S polymorphic phases can be somewhat different depending on the method used for their establishing.

To distinguish the individual C_3S polymorphic phases with X–ray analysis the most important two range of 2θ angles are: 31–33° and 51–52°. Figure 2.47 shows the changes of peaks in dependence on temperature: at 1100 °C the lattice is trigonal and the parameters of hexagonal unit cell are: $a = 715$ pm, $c = 2556$ pm.

With temperature decrease three hexagonal planes 201[11], 204 and 220 give on X–ray pattern doublets and triplets, instead of single peak. At the studied temperature range peak 009 is not splitted. It means that the distance between the planes per-

[11] Planes 201 is not shown on the picture, it is the peak for the angle 29.5° which is splitted into doublet 401 and 221.

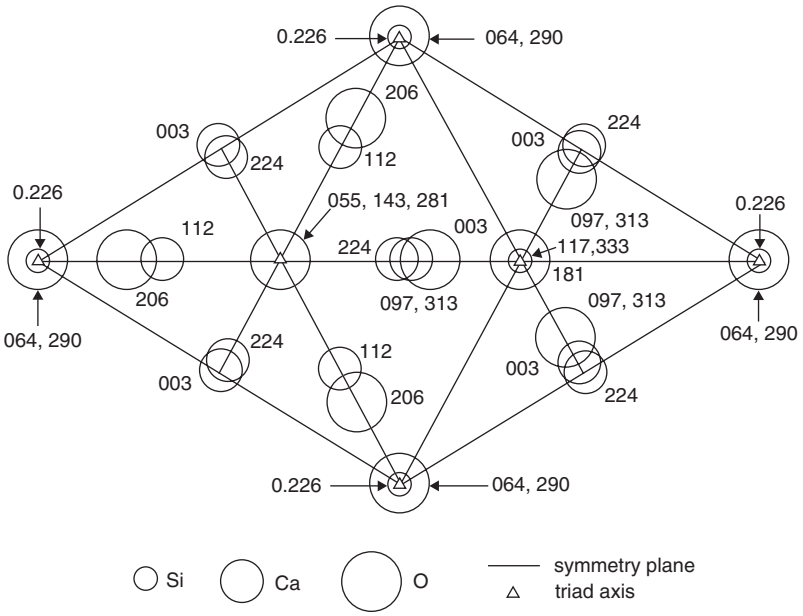


Fig. 2.46 C_3S unit cell projection along the c axis on the basic plane; atoms heights as thousandth of c cell dimension. (According to [99])

Table 2.6 Polymorph of C_3S (according to [99])

Transformation temperature (°C)	Method		
	XRD	Microscopy	DTA (enthalpy, J/g)
1070	R	R	–[a]
1060	M_{IIb}	M_3	–[a]
990	M_{IIa}	M_2, M_1	0.209
980	M_{Ia}		0.209
920	T_{III}		4.19
620	T_{II}	T_3, T_2	2.51
120	T_I	T_1	–

[a] On DTA curves the transformation $R \rightarrow M_3$ and $M_2 \rightarrow M_3$ are not found

pendicular to the *c* axis remains constant. However, the slip of these planes in the direction perpendicular to *c* axis occurs. The transformation of the rhombohedral into monoclinic plane at 1050 °C is continuous. The basis of the hexagonal unit cell became deformed. The pseudo–hexagonal unit cell parameters are as follows: $a = b = 713$ pm, $c = 2543$ pm, $\alpha = \beta = 90°$, $\gamma = 119.88°$. The transformation is probably of the second order and the formed structure is monoclinic.

The transformation at 990 °C is not continuous, unit cell is transformed without the symmetry change. Apart of base deformation of hexagonal unit cell the inclination of *c* axis in relation to the plane occurs, $\beta = 89.88°$. The range of stability of this monoclinic (M_I) polymorph is very small, equal only 10 °C. The transforma-

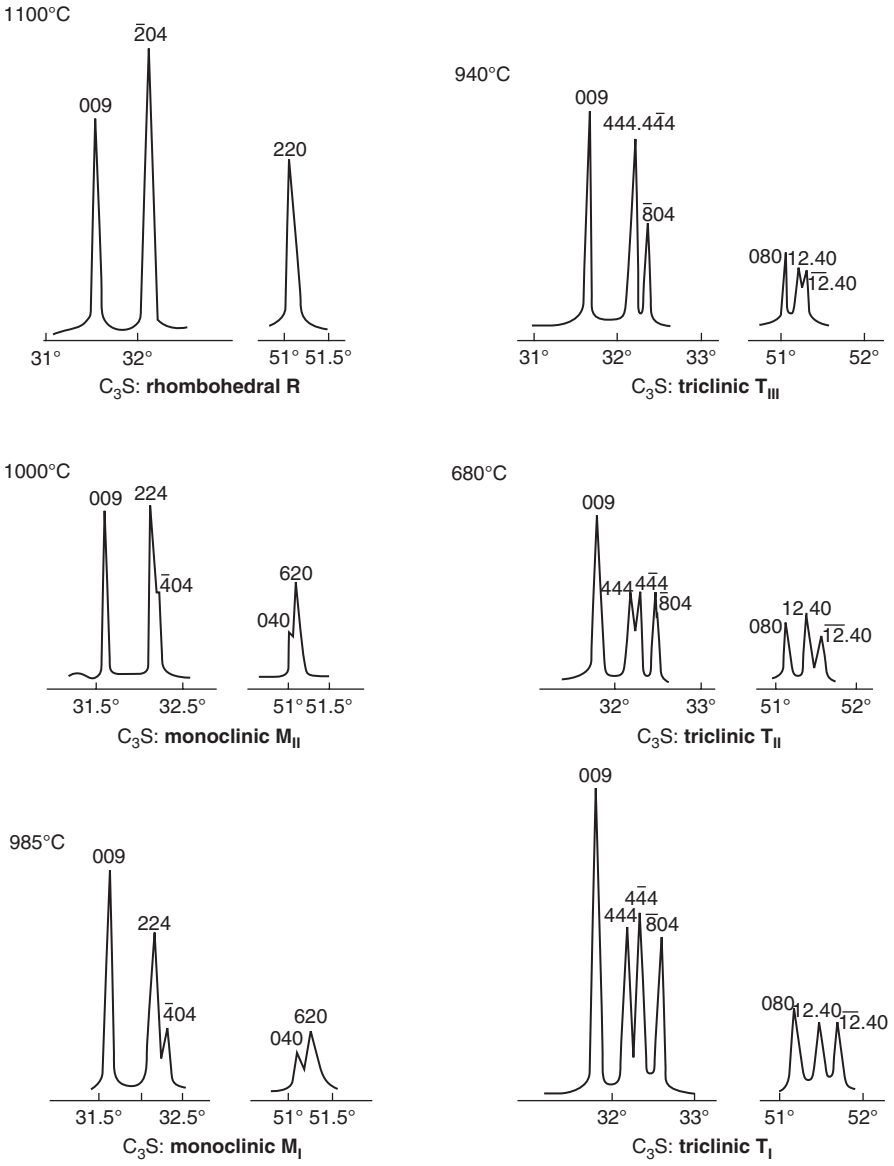


Fig. 2.47 C_3S X–ray pattern changes in the range 2θ: 31–33° and 51–52° in the function of temperature. (According to [35])

tion gives a very small peak on DTA curve at 990 °C. The phase M_I with addition of 1 % of Al_2O_3 is stabilised at room temperature [105].

The transformation at 980 °C is accompanied with symmetry change to triclinic: $M_I \rightarrow T_{III}$. Doublets are transformed into triplets. In hexagonal unit cell all three axis

Table 2.7 Content of different oxides, stabilising C_3S polymorphic phases after quenching from 1500 °C [42, 57, 88]

Oxide	Addition stabilising phase, %						Threshold solubility at temp. 1500°C, % mass
	T_I	T_{II}	T_{III}	M_I	M_{II}	R	
Cr_2O_3	0–1.4	–	–	–	–	–	1.4
Fe_2O_3	0–0.9	0.9–1.1	–	–	–	–	1.1
Ga_2O_3	0–0.9	0.9–1.9	–	–	–	–	1.9
Al_2O_3	0–0.45	0.45–1.0	–	–	–	–	1.0
MgO	0–0.55	0.55–1.45	–	1.45–2.0	–	–	2.0
Mn_2O_3	0–0.01	0.01–0.06	0.06[a]				0.06[a]
TiO_2	0–0.005	0.005–0.13	–	–	–	–	0.13[a]
BaO	0–0.5[a]	0.5–1.0[a]	1–1.05[a]	1.05–1.75$_a$			1.75[a]
ZnO	0–0.8	0.8–1.8	–	1.8–2.2	2.2–4.5	4.5–5.0	5.0[b]
La_2O_3	0–1.0			1.0–1.5		2.0–4.0	4.0
MgO + + Al_2O_3 + + TiO_2						0.93[c] 1.97 2.43	
MgO + + Al_2O_3 + + Mn_2O_3						2.02[c] 0.96 1.91	

[a] mole %, [b] at 1400°C,[c] regarded as synthetic alite

a, b and *c* are different. The crystal indices on X–ray pattern determination requires the doubling of *a* and *b* to 1400 pm.

At 940 °C pseudo–hexagonal cell parameters are: $a = 1433.9$ pm, $b = 1424$ pm, $c = 2541.2$ pm, $\alpha = 90.10°$, $\beta = 89.85°$, $\gamma = 119.76°$.

At 920 °C a high peak on DTA curve appears, but no symmetry and volume change of unit cell is observed. The distance between triplet lines is increasing. Similarly at 600 °C no symmetry changes occur, and no continuity in triplet peaks position changes appears.

The existence of superstructure during long X–ray study of T_I phase has been shown.

The tricalcium silicate solid solutions can stabilize different phases at low temperature. The increase of foreign elements in solid solution causes the stabilisation of phase stable at higher and higher temperature (Table 2.7). Among the single foreign elements phases stable at the highest temperature are stabilising only by ZnO. Zn^{2+} ion substitutes Ca^{2+} ion in the C_3S lattice [106]. ZnO addition is decreasing the transformations temperature. Further oxides which substitute CaO are MgO and BaO. At 1550 °C the maximum solubility of MgO is 2 %. When the content is higher periclase is appearing.

The solubility of BaO in C_3S is very limited and calcium is substituted and displaced [107]. To these solid solutions the formula $(Ca_{1-x}Ba_x)_3[SiO_4]O$ can be then described, x being ≤ 0.02 at 1600 °C. With low BaO content in solid solution the rate of C_3S hardening is increasing. Also Na_2O is substituting CaO in C_3S lattice and monoclinic structure is stabilised [108].

In clinkers, aluminium is the ion which the most frequently substitute Si. The Al_2O_3 solid solutions in C_3S were studied by Wörmann et al. [109] and Regourd [106]. They distinguish two kinds of solid solutions [109]. When the Al_2O_3 content does not exceed 0.45 % Al^{3+} is substituting for Si^{4+} in tetrahedra and simultaneously is occupying free octahedral positions assuring maintenance of electrical neutrality of the lattice. The formula of these solid solutions can be written:

$$Ca_3^{VI}Al_{x/4}^{VI'}\left[Si_{1-3x/4}Al_{3x/4}\right]^{IV}O_5 \tag{2.26}$$

where: $x \leq 0.02$; VI' is the octahedral vacancy. The phase T_I is stabilized.

When Al_2O_3 exceeds 0.45 % the Al^{3+} ions substitute in tetrahedra for Si and for Ca in octahedral positions. To these solutions corresponds the formula:

$$\left(Ca_{3-x/2}Al_{x/2}\right)^{VI}\left[Si_{1-x/2}\,Al_{x/2}\right]^{IV}O_5 \tag{2.27}$$

Simultaneously, in lower degree, aluminium ions can occupy the octahedral vacancies. Then the phase T_{II} is stabilised.

After exceeding 1 % Al_2O_3 the peaks of C_3A on X–ray pattern appear, thus it is the solubility limit at 1550 °C.

In the presence of Mg and also Ba the kind of Al substitutions is changed. In the presence of Ba the Al^{3+} are displaced from octahedral to tetrahedral positions, then they reach the acidic property [110].

On the Fig. 2.48 the volume occupied at 1550 °C by Ca_3SiO_5 in the system CaO–MgO–Al_2O_3–SiO_2 is shown [111]. It results from this system that also CaO is participating in these solid solutions. The system CaO–Al_2O_3–SiO_2 is the base of this four–components system and the edge C_3S–*L* is representing the solid solutions, which forms MgO in the system CaO–MgO–SiO_2. The range of solid solutions CaO *B*–*C* (0.14 % CaO) was increased to *B*'–*C*' (0.34 % CaO) under the influence of MgO at 1550 °C.

The ranges of solid solutions of MgO and Al_2O_3 remained unchanged and are 2 % and 1 % respectively. The solubility limit of Al_2O_3 does not depend on temperature whereas for MgO is highly increasing with temperature (1.5 % at 1420 °C).

Fe_2O_3 content in solid solution with C_3S can achieve maximum 1.1 % [109] In the range up to 0.8 % phase T_I is stabilized and above 0.8 % phase T_{II}. According to Fletcher [112] $3Fe^{3+}$ is substituting for $3Ca^{2+}$ and $6Fe^{3+}$ $6Si^{4+}$, however, the charge difference is compensated by one Fe^{3+} in interstitial position. Hahn et al. [111] give the formula:

$$\left(Ca_{1-x/6}Fe_{x/6}\right)_2^{IV}\left[Si_{1-x/2}Fe_{x/2}\right]^{IV}O_5 \tag{2.28}$$

valid for Ca/Fe = 1. When the atomic ratio Ca/Fe is in the interval 1–1.25 the substitution is as follows:

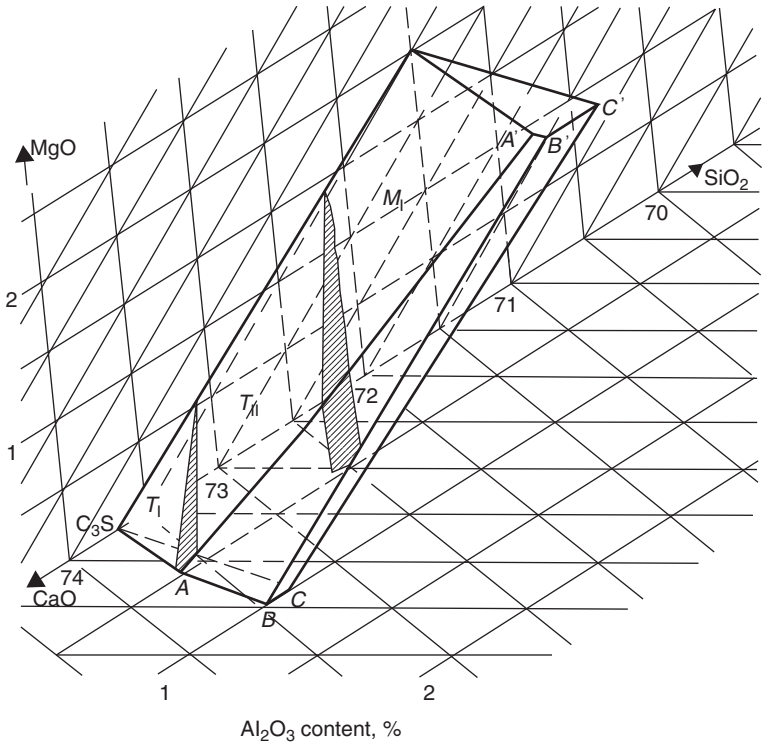


Fig. 2.48 The volume of primary crystallization of solid solutions Ca_3SiO_5 in CaO–MgO–Al_2O_3–SiO_2 system. (After [111])

$$\left(Ca_{3-x/2}Fe_{x/2}\right)^{IV}\left[Si_{1-x/2}Fe_{x/2}\right]^{IV}O_5 \tag{2.29}$$

However, Ca/Al is changing from 1 to 2.25, which provides the substitution of type II:

$$Ca_3^{VI}Al_{y/4}^{VI'}\left[Si_{1-3y/4}Al_{3y/4}\right]^{IV}O_5 \tag{2.30}$$

$T_I$and T_{II} are stabilized by single foreign ion, but M_I by arbitrary pairs from among three oxides: Al_2O_3, Fe_2O_3 and MgO. If Al occurs together with Fe then only Al is occupying the octahedral positions [100].

Chromium ion is substituting for silicon in C_3S lattice, and because it can occur on two oxidized levels, the calcium vacancies can be formed, according to the scheme:

$$\begin{aligned} 2Si^{4+} &\rightarrow 2Cr^{5+} + V_{Ca} \\ Si^{4+} &\rightarrow Cr^{4+} \end{aligned} \tag{2.31}$$

Boikova [113] the hypothesis is presenting that besides calcium also silicon vacancies can be formed:

$$\begin{aligned} 3Si^{4+} &\rightarrow 2Cr^{6+} + V_{Si} \\ 3Ca^{2+} &\rightarrow 2Cr^{3+} + V_{Ca} \end{aligned} \tag{2.32}$$

It is stated that the solid solutions $C_3S + Cr_2O_3$ are semiconductors of type *p* [114].

Toropov and Boikova [115, 116] have studied the solid solutions of tricalcium silicate with the rare earth silicates and yttrium as well as calcium germinates. Toropov stated that there are the substitutions $3Ca^{2+} \rightleftarrows 2Y^{3+}$, and in the structure vacancies are formed. Occupying of these vacancies caused the departure from the stoichiometry of tricalcium silicate. These studies have shown that the solid solutions can contain 7 mass % of $Y_2O_3 \cdot SiO_2$, 5 mass % of $La_2O_3 \cdot SiO_2$, 10 mass % of $Gd_2O_3 \cdot SiO_2$, 3 mass % of $Sc_2O_3 \cdot SiO_2$ and 7% of $Nd_2O_3 \cdot SiO_2$. Depending on La_2O_3 content successively the following C_3S phases are stabilized: up to 1.0% *T*, 1.5% *M*, 2% *R* [117]. There is a high similarity between Ca_3SiO_5 and Ca_3GeO_5, which are isomorphic [115, 118]. Tricalcium germinate also has six polymorphic phases: T_I, T_{II}, T_{III}, M_I and M_{II} and *R* [118].

Ti^{4+} substitutes for Si^{4+} in C_3S at 1600 °C till 0.14 mol % $3CaO \cdot TiO_2$ [114]. T_{II} phase is stabilized. Also Kondo [119] stated that in alite small quantities of $3CaO \cdot TiO_2$ up to 0.13 mol % solid solution can form; higher quantities caused C_3S decomposition to free CaO and calcium titanate. Manganese is formed solid solution with C_3S to very limited extent. Kondo [119] has determined the solubility of $3CaO \cdot MnO_2$ to be 0.06 mol %. Mn^{2+} ion up to 0.02 mol substitutes for Si^{4+} and in higher quantities Mn^{2+} substitutes for Ca^{2+} and Mn^{4+} for Si^{4+} in the 3:1 ratio. Kondo [119] does not exclude placing of manganese ions in the lattice defect, existing in the C_3S structure. At the $3CaO \cdot MnO_2$ concentration equal 0.01 mol the T_{II} phase is stabilizing and at higher concentration T_{III}.

Several works are devoted to the effect of C_3S solid solutions on hydraulic activity of this phase. There is a view that the reactivity with water of different C_3S phases are not linked with the polymorphism of this phase, but principally with the crystal structure defects, caused by solid solutions. Primarily the vacancies are listed, the presence of foreign elements [120], and dislocations [114, 121], as well as superficial defects [122]. It is much likely that very important are also the properties of minor elements [123]. The BaO solid solution is distinguished by quick hydration [123]. The solid solutions with Al and Fe assure the higher strength of mortars than the solution containing Mg [124].

Basing upon the studies of Gutt and Smith, Lea [24] is announcing that the solubility limit as solid solution of SO_3 in C_3S at 1310 °C is 2.9%. Ion S^{6+} substitutes for $2Ca^{2+} + ½Si^{4+}$ and solid solution has the composition: 92 mol % of C_3S and 8 mol % "$2CaSO_4 \cdot SiO_2$" [24].

Alite in clinker contains primarily in solid solution Al_2O_3, Fe_2O_3 and MgO, which stabilize phase M_I. Then, as it was mentioned earlier, alite in clinker forms the most frequently phase M_I and at higher MgO and SO_3 content phase $M_{III,}$ seldom

Table 2.8 Foreign ions content (mass %) the most frequently found in clinker phases

Phase	Oxide[a]						
	Al_2O_3	Fe_2O_3	MgO	SiO_2	Na_2O	K_2O	TiO_2
Alite	0.7–1.7	0.4–1.6	0.3–1.0	–	0.1–0.3	0.1–0.3	0.1–0.4
Belite	1.1–2.6	0.7–2.2	0.2–0.6	–	0.2–1.0	0.3–1.0	0.1–0.3
C_3A	–	4.4–6.0	0.4–1.0	2.1–4.2	0.3–1.7	0.4–1.1	0.1–0.6
Ferrite	–	–	0.4–3.8	1.2–6.0	0.0–0.5	0.0–0.1	0.9–2.6

[a]Additionally Mn_2O_3 in alite and belite 0.01–0.06, in ferrite to 0.06; SO_3 in alite 0.02–0.17, in belite 0.1–0.7% mass

Table 2.9 The foreign elements in alite crystals (mass %) in two industrial clinkers [100]

Oxide	Al_2O_3	Fe_2O_3	MgO	Na_2O	K_2O	TiO_2	SO_3
Alite monoclinic 3	0.8±0.1	0.6±0.2	0.98±0.07	0.20±0.02	0.20±0.02	0.12±0.05	0.02
Alite monoclinic 2 (pseudo–trigonal)	1.0±0.1	0.6±0.1	0.59±0.07	0.02±0.005	0.10±0.02	0.20±0.05	0.17±0.05

hexagonal (R) or triclinic (T_2) (see Fig. 2.28). Sometimes the inversed phase M_2 can be found [42].

The content of isomorphic foreign elements in alite is significant and the solid solutions formed have a very composed chemical composition. In connection with very limited quantity of ions which can be placed in voids, the solid solutions introduce many defects in the structure of this phase. The chemical composition of the main clinker phases in Table 2.8 is given. The determinations with electron microprobe have shown that the molar ratio C/S of alite in clinker is mostly higher than 3 and as the rule is in the range from 3.02 to 3.04 [125], which is just ascribed to solid solutions. The examples of foreign elements content in two alite crystals of different structure are given after Regourd [100] in Table 2.9.

The factors which influence on tricalcium silicate or alite decomposition were studied. The kinetic curve of C_3S decomposition are shown on Fig. 2.49. It was found that the rate of decomposition depends in high degree on the gaseous atmosphere surrounding the sample [126]. The induction period is linked with the formation of nuclei of CaO and $Ca_2[SiO_4]$. Glasser [22] calculated the nucleation rate as a function of time, using Avrami formulae:

$$\xi = 1 - \exp\left[-kt^n\right] \tag{2.33}$$

in which ξ is a volume fraction, which was transformed during the time *t, k*—constant, *n* depends upon the nucleation mechanism: for three–dimensional nucleation and growth $3 \leq n \leq 4$, for two–dimensional growth $2 \leq n \leq 3$.

The value of *n* can be assessed from experimental data by plotting log log [1/(1—ξ)] against log *t*. In this way, Mohan and Glasser (after 22) obtained values of *n* lying between 2 and 3 and concluded that the nucleation of decomposition product

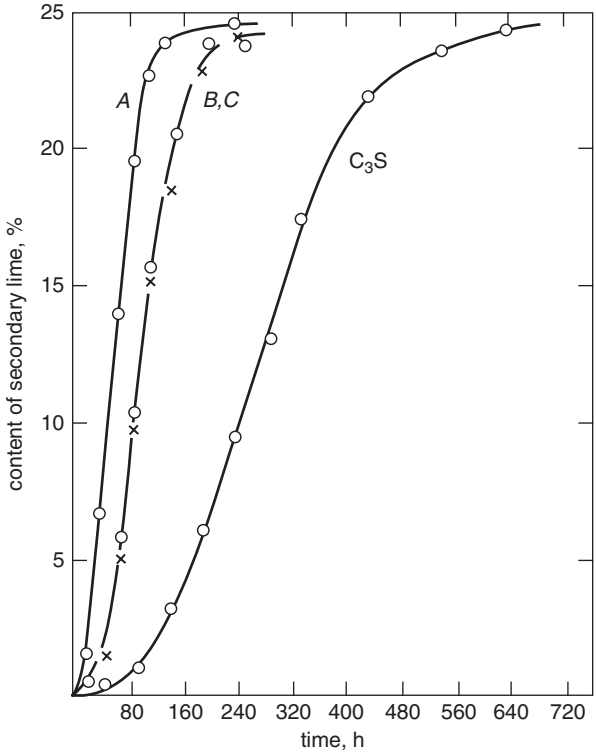


Fig. 2.49 Decomposition of C_3S compared with solid solutions nearly saturated in iron (*A, B, C*). In *A* and *B* iron was added as C_2F equivalent to 1.1 % Fe_2O_3; sintering temperature: *A* 1375–1400 °C, *B* 1550 °C. Curve *C* is for a sample containing 1.1 % Fe_2O_3. All samples had comparable surface areas: data are for 1075 °C. (According to 22)

was essentially a surface phenomenon. The influence of stoichiometric variations and linked with them defects were not found, however, the content of foreign ions have substantial effect. Fe caused the significant acceleration of alite decomposition while Mg and Na exhibited a progressively greater retarding influence, but Al had no appreciable effect. The influence of Fe is attributed to the Fe^{2+}/Fe^{3+} ratio which furnishes the driving force for diffusion of iron ions and causes the instability of C_3S structure.

The rate of C_3S decomposition, as of a process starting with surface nucleation, will considerably depend on the water vapour content in atmosphere surrounding the sample, even at 1050 °C. On the Fig. 2.50 the relation of time taken for C_3S to attain 50 % decomposition from P_{H_2O}. Glasser [22] proposes the mechanism based on the breaking of oxygen bonds:

$$\mathrm{Ca-O-Si+HOH \rightarrow Ca-OH\cdots\cdots HO-Si} \tag{2.34}$$

Subsequent elimination of water and rearrangement of Ca, Si and O lead to formation of the products phases Ca_2SiO_4 and CaO. Glasser [22] is stating also that the presence of molten sulphates is enhancing the decomposition of C_3S. They are formed globules on alite surface leading to its decomposition.

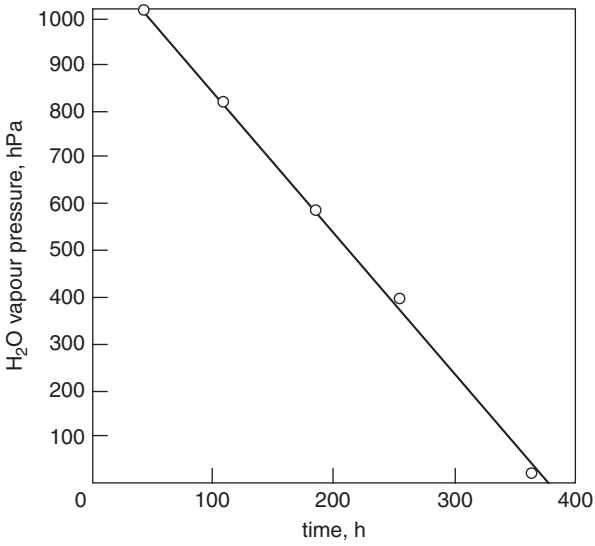


Fig. 2.50 The time taken for Ca_3SiO_5 to attain 50 % decomposition is shown as a function of P_{H_2O} in the ambient atmosphere. Data obtained at 1050 °C. (According to [22])

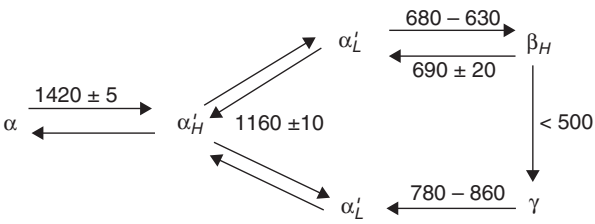


Fig. 2.51 Temperature (°C) transformation of different C_2S phases. (According to [127])

2.5.2 *Dicalcium Silicate and Belite Phase*

Polymorphism $Ca_2[SiO_4]$ and structures of phases stable at different range of temperature are relatively well known. On Fig. 2.51 the range of temperature of individual polymorphic phases stability after Niesel and Thormann [127] are shown. Dicalcium silicate forms four phases which are stable at different temperature ranges, however, fifth phase β is unstable. Nurse [128] gives the hypothetical system for C_2S in which phase β is thermodynamically stable, at high pressure.

All C_2S phases are formed of independent SiO_4 tetrahedra linked by calcium atoms, but the structural arrangement is changing in individual polymorphs (Fig. 2.52).

Phase γ stable at low temperature has the rhombic structure of olivine type and is frequently called calcio–olivine (see Table 2.10). Silicate tetrahedra are irregular and the distances Si–O change from 158.9 to 172.5 pm. These irregularities are probably caused by distortions of hexagonal arrangement of oxygen ions. Half of calcium ions is spaced in the cornets of unit cell, in the half of edge length and in the middle of all walls. The second half of calcium ions is arranged as in ol-

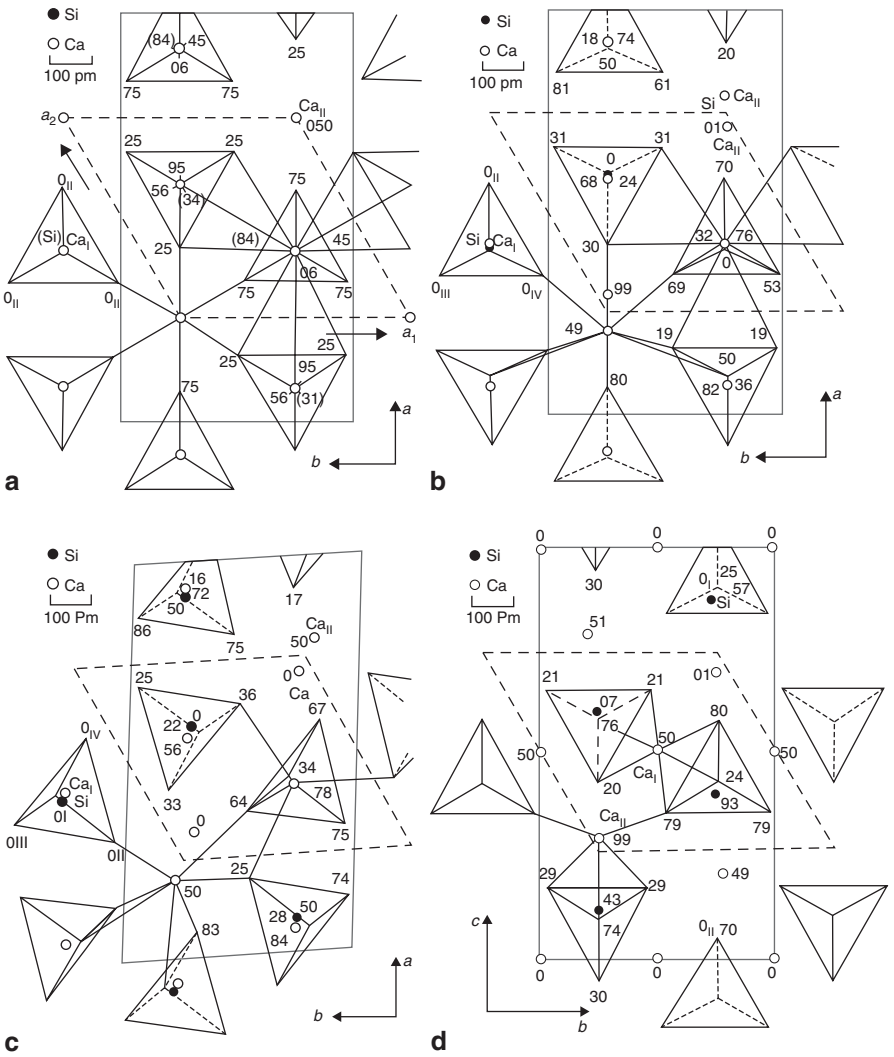


Fig. 2.52 The structure of C_2S phases: a) α, b) β, d) γ. (After [100])

ivine, between the silica–oxygen tetrahedra. All calcium ions have the octahedral coordination. Low coordination number of calcium explains higher molar volume of this low–temperature phase.

Phase α' appears in two forms: α'_H and α'_L which are stable at temperature range 1420–1160 °C and 1160–675 °C respectively. Their structures were determined for the samples stabilized with additions of SrO, BaO or B_2O_3 [130]. The distances Si–O in tetrahedron differ significantly (175, 177 and 167 pm) which is caused by the belonging of each oxygen atoms to the surrounding of two kinds of calcium

Table 2.10 Structure of $Ca_2[SiO_4]$ polymorphs (after [103])

Phase	Structure type	Space group	Number of "molecules" in unit cell	Calcium coordination	Lattice constants, nm
γ	olivine type	orthorhombic $\frac{P2_12_12_1}{cmn}$	4	Ca(1) = 6 Ca(2) = 6	a = 0.5091 b = 0.6782 c= 1.1371
β	strongly deformed low K_2SO_4 type	monoclinic $P11\frac{2_1}{n}$	4	Ca(1) = 6 + 6 Ca(2) = 8	a = 0.928 b = 0.548 c = 0.676 b = 94°33' stabilised by Ba
α'_L	slightly deformed low K_2SO_4 type	Orthorhombic $Ccm2_1$ (others groups possible)	16	Ca(1) = 10 Ca(2) = 9	a = 1.880 b= 1.107 c = 0.685 stabilised byBa
α	Alternative type	Hexagonal $P6_3mc$	2	Ca(1) = 4 + 9 Ca(2) = 6 + 3	a = 0.545 c = 3·0.720 stabilised by V_2O_5

ions. From among 32 calcium ions sixteen [Ca(1), Ca(2), Ca(3)] are located above and below SiO_4 tetrahedra, in direction of z axis and remaining sixteen [Ca(4), Ca(5), Ca(6)] are in the voids between tetrahedra. The coordination number for Ca(1), Ca(2) and Ca(3) is eight and for Ca(4), Ca(5) and Ca(6) six. Calcium ions Ca(1)–Ca(3) are probably more frequently substituted by foreign ions, because the latter cannot so easy occupy specific sites of ions Ca(4)–Ca(6), but are distributed statistically.

Phase β, the most important in cement chemistry, has the monoclinic structure established long ago (Table 2.10) [130, 131]. The unit cell is composed of SiO_4 tetrahedra in direction of y axis, and remaining four Ca [Ca(2)] ions are distributed between tetrahedra. The coordination number Ca(1) is six and Ca(2) eight. The coordination is changeable, however, the voids formed in the structure are smaller than in C_3S, the distances Si–O are 157, 160, 164 pm. Ca(1) is in the distance 230–275 pm from O^{2-}.

γ phase has the lowest density, comparable only with phase α and it is why the transformation β → γ leads to the decomposition into very small crystals. As it is shown in Fig. 2.51, sequence of transformations during cooling goes always trough phase β. It is not possible to obtain γ phase by cooling α'_L phase. Both transformation β → γ and γ → α'_L are reconstructive transformations.

Crystalline structure of the phases: α'_L, α'_H and α is very similar; the small displacements of elements are sufficient for transformation, without embracing the first coordination zone. The transformation $\alpha'_L \rightleftarrows \alpha'_H$ belongs to the kind order—disorder and have very low enthalpy (ΔH=720 J/mole) [130]. It consists of a very

small displacement of calcium atoms, which, however, leads to the superlattice (*a* and *b* reduplication), but the lattice remains rhombic.

In the case of α'_L two special groups are possible: *Pcmn, Pcan* and *Pnmn*, which are subgroups of *Pcmn*, to which belong also the crystals of α'_H phase.

The transformation $\alpha'_L \rightarrow \beta$ has higher enthalpy (several authors give the values from 1424 to 2722 J/mole) [130, 131], caused by breaking the bonds Ca–O, linked with the change of coordination number of calcium ions.

The transformation $\alpha \rightleftarrows \alpha'_H$ is causing the rotation of half tetrahedra (Fig. 2.52) and is classed among the demi–reconstructive transformation. Its enthalpy is 13482–14194 J/mole [130, 131].

The most important transformation in cement chemistry $\beta \rightarrow \gamma$ depends on many factors, and frequently the process is not complete. One of the most important factors was the fineness of β crystals which influence studied Yannaquis and Guinier [132]. β crystals smaller than 5 μm are stabilizing this phase at low temperature. Similar results obtained Gawlicki [133]. Chromy [134] has shown that the recrystallization, which depends on temperature and time of samples heating, cannot be forgotten. The crystals growth is enhancing the transformation to γ phase.

Lehmann with coworkers [135] have shown that the size of β crystals is governed by the fineness of α'_L particles. Coarse α'_L crystals are transformed at temperature range 630–680 °C in β phase which in turn gives at < 500 °C phase γ (Fig. 2.53). Small crystals of α'_L give small β particles which do not transform to γ. These conditions are fulfilled during the synthesis of C_2S as the reaction of CaO with SiO_2 at 1200 °C, at the range of stability of α′ phase [136, 137]. At this temperature the ratio of crystals rate growth to the nucleation rate is low, close to zero. Equally, the C_2S samples heated to 1550 °C, to the range of stability, give 90 % of β polymorph on quenching, because the passage through the transformation $\alpha \rightleftarrows \alpha'_H$ is very quick and the crystals remain small. However, when the samples are cooled slowly from the temperature 1550 to 1400 °C and later quenched, then 95 % of phase γ is obtained. Slow passage through the temperature range of transformation $\alpha \rightleftarrows \alpha'$ permits the crystals growth, which in spite of very quick cooling gives full transformation $\beta \rightarrow \gamma$. Growth of the α'_L crystals can be obtained by long heating of the sample at the range of α'_H stability, thus at 1160–1000 °C.

The stabilization of small β crystals can be explained if it will be admitted that the transformation of this phase in polymorph γ is the result of formation and growth of the nuclei of this phase. In each β crystal one nucleus of γ phase must be formed at least, however, the probability of its formation in a small crystal will be low and will increase with the volume of crystals. The process of nuclei of phase γ formation is linked with the thermal history of the sample, then with its heating at the range of the stability of polymorphs: α (above 1420 °C and α'_H (above 1160 °C). Its permits the explanation of particular role of temperature 1420 °C in the process of β polymorph stabilization, which was observed by different authors [138, 139]. According to Niesel and Thormann [127] 1160 °C is the most suitable temperature for the growth of α′–C_2S crystals. In the case of synthesis at 1160 °C β phase is produced, however, at higher temperature the mixture of β and γ is obtained.

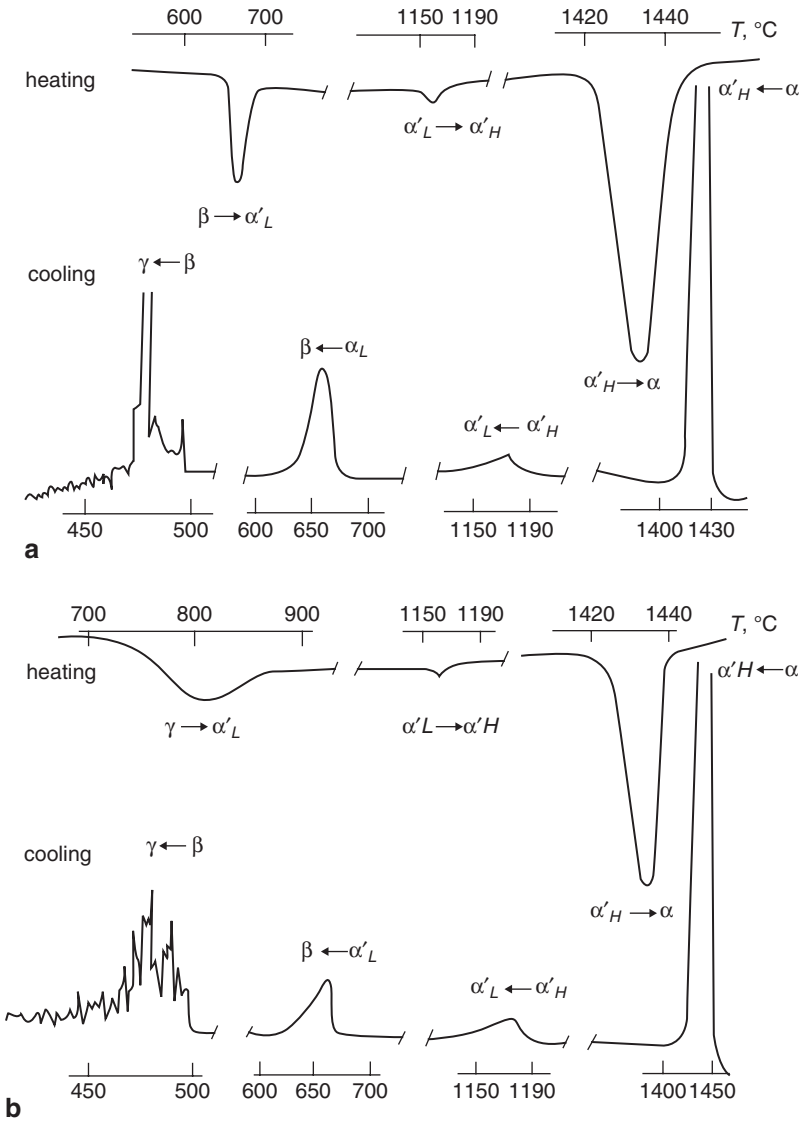


Fig. 2.53 DTA *curves* of C_2S: a) phase β, b) phase γ. (After [100])

The transformation process of β phase can be accelerated under crystals deformation and pressure [140]. For example the partial transformation of β to γ can be caused at room temperature through crushing of sample in hydraulic press. It accelerates probably nuclei formation of this phase as the result of crystals shearing. From the other side when the powdered sample of β phase is exposed to the hydrostatic pressure of 900 MPa no transformation is observed, because γ has lower

density than β polymorph and pressure does not enhance the transformation. Under high pressure β phase has a stability field, which does not exist under atmospheric pressure [141]. β phase is stable at room temperature under pressure of 2 MPa, and the transformation $\gamma \rightarrow \beta$ takes place under pressure of 1.7 MPa [141]. Roy [142] has established the ternary point for the phases γ, β and α under pressure of $1.9 \cdot 10^3$ MPa and at 410 °C [142].

Midgley [143] states, on the basis of thermal and XRD analysis, that dicalcium silicate forms one phase more— α'_m with monoclinic structure. According to this author the polymorphic transformation series will be as follows:

$$\gamma \xrightarrow[711°C]{} \alpha'_m \xrightarrow[979°C]{} \alpha'_L \tag{2.35}$$

Further transformation are the same as according to other authors. During cooling the form α'_m should transform at 676 °C in polymorph β. Midgley [143] obtained the α'_m specimens stabilized with 15–25 % $CaNaPO_4$ and 3.6 % K_2O. Other authors do not mention about this phase.

Solid solutions are very important in dicalcium silicate chemistry. In this phase much higher concentration of minor components can be present than in C_3S. The most known are the substitutions of calcium ions by K, Na, Mg, Fe, Ba, Sr, and the silicate anions by $[AlO_4]^{5-}$, $[FeO_4]^{5-}$, $[TiO_4]^{4-}$, $[SO_4]^{2-}$, $[BO_4]^{5-}$, $[PO_4]^{3-}$, $[CrO_4]^{2-}$. In the Table 2.11 data of different authors concerning the content of minor components are presented as well as the polymorphs $Ca_2[SiO_4]$ stabilized by the formed solid solutions. The minor elements which are stabilizing the phase β are mostly stabilizing also, at higher content, the phases α′ and α, stable at higher temperature.

No general conception of the mechanism of stabilizing by minor components was elaborated. It is believed that they increase the disorder degree of the dicalcium silicate structure, thus their action is similar to the thermal vibrations of ions at higher temperature. The conception of Dietzel and Tscheischvili [149], according to which the stabilizers should accomplish the following conditions: a) ions substituting for Ca^{2+} should have greater ionic radius, b) anions substituting for $[SiO_4]^{4-}$ should have smaller dimensions, did not remain valid. It cannot be accepted, as yet, a general regularity. For example Greene [150] considers that increasing the dimension *c* of unit cell by the solid solution of alkali and Al_2O_3 or Fe_2O_3 stabilizes the phase α. It is the effect of substitution of SiO_4 tetrahedra by $[AlO_4]^{5-}$ or $FeO_4]^{5-}$ groups.

The solid solutions of CaO and SiO_2 in dicalcium silicate are also know, which can be treated as the departure from stoichiometric composition. C_2S can contain in solid solution 1 % CaO and 1.5–2 % SiO_2 [133]. The CaO excess enhance the β stabilization and the excess of SiO_2 accelerates the transformation to γ phase. Schlaudt and Roy [151] consider that β–C_2S cannot be stabilized by substitution only the ions Ca^{2+}.

Lea [24] states that the small admixture of $CaSO_4$ equal 0.5 % is stabilizing β–C_2S and higher amount α′–C_2S. The range of solid solutions in α′–C_2S is 1.7 mol % $CaSO_4$ at 1000 °C and 1.1 % at 1200 °C. Also Struiliou and Arnould [152] studied

Table 2.11 The stabilizers of different C_2S phases

Phase	Content of minor component, % mass	According to
β	Mn_2O_3	Newmann and Wells [144]
	V_2O_3 , As_2O_3	Zerfoss and Davis [145]
	Na_2O 0.3% mol	Thilo and Funk [146]
	K_2O 0.3% mol	
	B_2O_3 0.1–0.25	Schwiete [147]
	V_2O_3 0.1–0.25	
	MgO 1.25 (Mg_2SiO_4)	
	B_2O_3 0.3	Lea [24]
	ZrO_2 5	
	Cr_2O_3 1	
	C_3P 1	
	$CaSO_4$ 0.5	
α′	Ba_2SiO_4 10% mol	Schwiete [147]
	Sr_2SiO_4 20% mol	
	$Ca_3(PO_4)_2$ 20% mol	
	$CaSO_4$ 1.1% mol	Lea [24]
	Al_2O_3 1	
	Fe_2O_3 1	
	B_2O_3 0.95	
	BaO 0.15–0.30	
	SrO 0.15–0.30	
	MgO 2	
	Ba_2SiO_4 18–28	Butt [148]
	Na_3BO_3 10	
	Na_3PO_4 10	
	Fe_2O_3 1.5	
	BaO 11	
	MgO 1.5	
α	$Ca_3(PO_4)_2$ 15	Gutt [50]
	Al_2O_3 2–3	Nurse [129]
	$Ca_3(PO_4)_2$ 34	Gutt [50]
	Ba_2SiO_4 34–54	Butt [148]
	Na_3BO_3 20	
	Na_3PO_4 20	
	Mg_2SiO_4 13.6	
	Fe_2SiO_4 5.6	
	Na_2O 2.8	

the synthesis of phase β using sulphate at 750 °C. They used the mixture of calcium nitrate and silica. Melting at 561 °C $Ca(NO_3)_2$ introduces liquid phase which significantly accelerates the reaction with SiO_2. After 20 min of heating at 780 °C the authors obtained, cooled sample composed of phase β. Addition of 6% $C\bar{S}H_2$ gives phase β of very poor crystallinity, which quickly reacted with water giving the strength close to Portland cement class 40.

However, significant part of authors are considering that the structure of C_2S is close–packed which considerably diminish the possibility of interstitial ions placing [135]. For this reason formation of silica or oxygen or finally calcium vacancies are

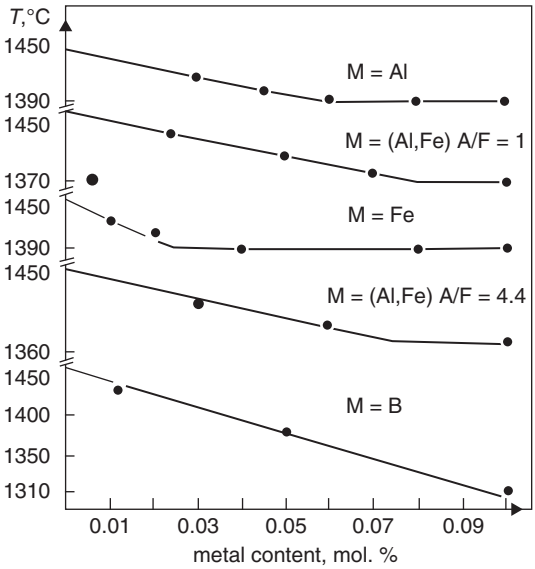


Fig. 2.54 Limits of C_2S solid solutions, determined on the basis of $\alpha'_H \rightarrow \alpha$ transformation. (After [35])

assumed [83, 140]. Yannaquis and Guinier [140] consider that the substitution of anions $[SiO_4]^{4-}$ by $[BO_4]^{5-}$ in phase β gives tetrahedral vacancies in order to preservation of electroneutrality of the crystal. In the structure the vacancies of Si^{4+} ions and two oxygen atoms are formed, then SiO_2.

Forest [83] is considering that to some solid solution in belite can be ascribed the formula: $Ca_2M_xSi_{1-x}O4_{-x/2}$. They are formed as the result of Si substitution with the oxygen vacancy formation: $2Si^{4+} + O^{2-} \rightarrow 2M^{3+}$. He considers that such solid solutions at temperature higher than the transformation point $\alpha'_H \rightarrow \alpha$ are formed. The threshold foreign ion content was established by determining the decrease of $\alpha'_H \rightarrow \alpha$ transformation temperature applying the DTA curves (Fig. 2.54). Phase β was produced using the following compositions [153]:

$$Ca_2B_{0.01}Si_{0.99}O_{3.995}$$
$$Ca_2Fe_{0.035}Al_{0.035}Si_{0.930}O_{3.965}$$
$$Ca_2Fe_{0.050}Al_{0.050}Si_{0.900}O_{3.950}$$

However, some peaks are shifted which is the proof of structure distortion. Similar observations were made by Görlich and Handke [154] which used infrared spectroscopy.

Also Na_2O and K_2O are stabilizing β phase [146]. Thilo and Funk [146] are stating that a very small Na_2O content (from 0.17 to 0.27%) is sufficient for phase β stabilization. This opinion is, however, not confirmed by others authors [127, 132]. However, the stabilization of polymorph β by covering the crystals with the glass coating is known, which assumes the formed internal stress.

Niesel and Thormann [127] describe the physical stabilization which consists in covering the dicalcium silicate crystals with the layers: $CaMoO_4$, $CaO \cdot WO_3$ [135] or $Ca_3Al_2O_6$, which prevents the transformation $\beta \rightarrow \gamma$ by rapid cooling, responding the temperature decrease of 1000 °C/min, but is cracking by slow temperature drop equal 10 °C/min.

Toropov [155] studied the solid solutions of silicates of rare earth elements with C_2S, namely yttrium, lanthanum and neodymium. The solubility of $Y_4[SiO_4]_3$ and $La_4[SiO_4]_3$ is high equal 35% mass, and in the case of $Nd_4[SiO_4]_3$ even 40%. It leads to the successive stabilization of polymorphs β, α′ and α.

Suzuki [156] used for stabilization double additions: $Na_2O + Al_2O_3$, $Na_2O + Fe_2O_3$ and $K_2O + Al_2O_3$, $K_2O + Fe_2O_3$. Additions Na–Fe and K–Fe stabilized phase α, however, Na–Al and K–Al give the mixture α + α′ or polymorph β. Exemplary samples compositions were the following:

$$\alpha \quad Ca_{1.80}\,Na_{0.18}\,Si_{0.82}\,Fe_{0.17}\,O_4$$
$$\alpha \quad Ca_{1.80}\,K_{0.19}\,Si_{0.87}\,Fe_{0.18}\,O_4$$
$$\beta \quad Ca_{1.88}\,K_{0.12}\,Si_{0.94}\,Fe_{0.08}\,O_4$$

Suzuki [156] found that α hydraulic activity was high and its rate of reaction with water surpassed significantly rate of β phase reaction with water.

Sodium and phosphorous are good double stabilizers [129]. The studies of the system Ca_2SiO_4–$CaNaPO_4$ have shown that for β polymorph only 0.5% $CaNaPO_4$ is sufficient and it is stable at room temperature till 10% of this stabilizer. Addition of 15–25% $CaNaPO_4$ gives α'_L–C_2S and 30–70% α'_H. The increase of stabilizers content causes the changes of unit cell dimensions, however, without the structure change.

In β phase stabilization process very important is reduction atmosphere. Polymorph β stabilized by Si substitution is stable in reduction condition. In the case when foreign ions substitute for Ca, the transformation $\beta \rightarrow \gamma$ is easy in this condition [151]. In reduction atmosphere Fe^{2+} can substitutes Ca^{2+}, giving solid solution which has no disadvantageous influence on transformation of C_2S to γ phase.

Boikova [157] was synthesizing belite phases of complicated composition using minor elements substituting for both: calcium and silicon. She produced the following stabilized phases: α′, α'_Z, and β. Apart the foreign elements also the special condition of thermal treatment was applied. Phase β was close to industrial belites, which can be regarded as the products of imperfect crystallization. These unstable belites have good hydraulic properties, close to the phase α′. Boikova [157] was considering that phase α′ is very susceptible to structural changes and by suitable isomorphic foreign ions and heat treatment conditions the production of more than two phases of this polymorph is possible. The hydraulic activity of α and α′ belites is significantly higher than β phase. It is here the decisive role the important distortion of these phases structure [157]. Exemplary compositions of α and α'_Z belites were the following:

$$\alpha \quad Ca_{1.94}Na_{0.06}K_{0.03}Mg_{0.02}Si_{0.92}Al_{0.05}Fe_{0.04}Ti_{0.006}Mn_{0.001}O_4$$
$$\alpha'_Z \quad Ca_{1.97}Na_{0.02}K_{0.04}Mg_{0.02}Si_{0.92}Al_{0.06}Fe_{0.03}O_4$$

Dicalcium silicate occurring in industrial products has a very complicated composition. The natural mineral bredigite [158] which is identical with α′ phase has the composition:

$$\left(Ca_{1.76}Mg_{0.26}Na_{0.01}\right)\left[Si_{0.95}S_{0.02}P_{0.01}\right]$$

and larnite, which structure is corresponding to phase β has the composition [159]:

$$\left(Ca_{2.01}Na_{0.01}\right)\left[Si_{0.97}S_{0.31}P_{0.01}\right]$$

Then for larnite and bredigite the following formulae can be assumed:

$$\begin{aligned} &\text{larnite} \quad Ca_2Si_{1-x}Al_xO_{4-x/2}\ (\text{traces Na, Mg, P, S}) \\ &\text{bredigite}\ Ca_{2-x}Mg_xSiO_4\ (x=0.22)\ (\text{traces Na, Al, P, S}) \end{aligned} \tag{2.36}$$

Also belites in clinkers are, as a rule, β phase containing different minor elements. However, on the XRD pattern some peaks are broadening and some shifted a little. The composition of these belites is unbalanced. Ca^{2+} is usually substituted by Mg^{2+}, K^+, Na^+, Cr^{3+}, Mn^{2+} and $[SiO_4]^{4-}$ by $[AlO_4]^{5-}$, $[FeO_4]^{5-}$[PO_4]$^{3-}$ and $[SO_4]^{2-}$ [129].

As it was aforementioned clinker contains phase β and seldom α′ [160,161]. The synthetic preparations obtained by Forest [83], of the formula $Ca_2M_xSi_{1-x}O_{4-x/2}$ with oxygen vacancies, are similar to belite. It turned out [100] that α′–C_2S contains more K_2O and less Al_2O_3. K_2O in clinker is principally in belite, albeit there are exceptions from this principle.

XRD belite identification in clinker is difficult, because its peaks show coincidences with C_3S and usually its content is too low for 120 peak, $2\theta = 31°$ (Cu K_α) to be analyzed. For clear separation of this peak should be at least 12 % of β–C_2S. Regourd [103] affirmed also the presence of α′–C_2S in clinker on the basis of 111 peak.

Different C_2S phases, in the case of low content of belite in clinker, is most convenient to identify using light microscopy. Among others, Metzger [161] applying this method found the presence of phase α′. The striations of belite crystals always observed in industrial clinkers due to polysynthetic twinning, are distinctly differentiate this phase from alite crystals and are formed in the polymorphic transformation process.

Belites formed in transformation α → α′ (or also α′ → β)[12] are presenting type I, however, linked with the transformation α′ → β type II, which are classified mainly on the basis of whether the evident lamellae are complex (at least two sets type I),

[12] There are also opinion about direct martensitic transformation α → β.

Table 2.12 Content of foreign elements (% mass) in β and α′–C_2S [100]

Phase	Oxide							
	Al_2O_3	Fe_2O_3	MgO	Na_2O	K_2O	TiO_2	SO_3	P_2O_5
β–C_2S	2.6±0.3	1.3±0.2	0.54±0.07	0.11±0.02	0.78±0.07	0.46±0.07	0.62±0.07	0.17±0.02
α′–C_2S	1.9±0.3	1.0±0.1	0.43±0.05	0.40±0.02	1.42±0.02	0.20±0.02	–	–

simple (only one set type II). Type I is by far the most commonly occurring in Portland cement clinker. Phase α can form the matrix between β–C_2S layers, and on the boundaries from solid solutions Al and Fe are released, forming ferrite [153]. Type III of belite without lamellae is seldom found.

Thanks to numerous measurements with electron microprobe there are many chemical analysis of belites in clinkers (Table 2.12). Midgley [162] gives also the following content of foreign elements in belites from industrial clinkers (mass %):

Na_2O	0.5–1.0	TiO_2	0.12–0.18
MgO	0.24–0.56	MnO_2	0.01–0.06
Al_2O_3	1.19–2.58	Fe_2O_3	0.69–2.16
K_2O	0.50–0.95		

2.5.3 $Ca_3Al_2O_6$ and Aluminate Phase in Clinker

The C_3A structure was well determined [163]. It is composed of $[AlO_4]^{5-}$ tetrahedra forming rings $[Al_6O_{18}]^{18-}$composed of six AlO_4 groups sharing corners (Fig. 2.55). Structure is cubic, $a=1526.3$, space group *Pa*3, and the number of "molecules" C_3A in the unit cell is $Z=24$. This unit cell can be presented as the assemblage of 64 subcells with $a=a/4$, which are clearly marked in the structure, because position of the metal ions majority is linked with this cell. Twisted rings $[Al_6O_{18}]^{18-}$ are positioned in such a manner that their axis are parallel to the triad axis of unit cell and are bonded with calcium ions. Inside the $[Al_6O_{18}]^{18-}$ rings there are holes of 147 pm radius, eight in each cell In farther 56 "subcells" these holes are occupied by calcium ions. The remaining 16 calcium ions are located at the corners of the subcells. Two types of calcium ions can be distinguished:

- Ca(1), Ca(2), Ca(3) at the corners of the subcells are octahedrally coordinated by the oxygen ions, and the bond length is in the range 238.8–235.4 pm.
- Ca(4), Ca(5), Ca(6) are located in central positions inside the ring with irregular coordination, in which the bond length is varying from 244.4 to 262.5 pm.

a) Cubic structure; numbers show the height of rings (in scale to 8). Rings with black tetrahedra correspond to rings *B* in *R*II and remaining *A*. All rings are identical in the phase *R*I. b) rings in remaining structures. Black tetrahedra correspond to

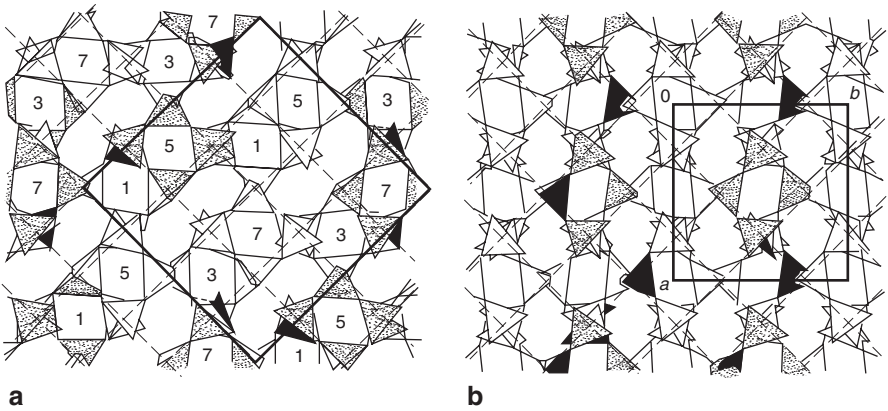


Fig. 2.55 C_3A structure, *rings* formed of six tetrahedra are shown. (After [164]):

rings *B* in monoclinic structure (analogical packing is in orthorhombic structure). Continuous lines show unit cells and dashed subcells.

Solid solutions of sodium ions, which have the formula $Ca_{9-x/2}Na_xAl_6O_{18}$, are significantly modifying the C_3A structure. Na^+ ions substitute in the structure calcium atoms and to maintain the lattice electroneutrality the second atom is located in the center of one ring. In dependency upon Na^+ ions concentration at room temperature the following forms are present (Fig. 2.56):

until 1.9 mass % Na_2O—cubic phase,
from 1.9 to 3.7% Na_2O—common occurrence of two phases: cubic and rhombic,
from 3.7 to 4.6% Na_2O—rhombic phase,
from 4.6 to 5.9% Na_2O—monoclinic phase

In 1980 Takeuchi [164] determined the structure of solid solutions containing 2.4, 3.8, 5.7% Na_2O. The structure had the structure cubic II, orthorhombic *O* and monoclinic respectively.

Cubic II phase of the composition $Ca_{8.688}Na_{0.625}Al_2O_{18}$ contains in the unit cell 69.5 Ca atoms and 5 Na atoms. Its unit cell is not space–centered, space group $P2_13$. Half sodium atoms is placed in the middle of Al_6O_{18} ring and half is substituting for Ca^{2+}in positions Ca(3) and Ca(4). The calcium polyhedra, in which sodium ions are substituting for calcium, are increasing, but the rings in which sodium ions are located, are decreasing. It leads to the unit cell decrease.

In the case of sodium concentration increasing up to 3.8 mass %, which corresponds to the formula $Ca_{8.375}Na_{0.875}Al_2O_{18}$, the change of structure to orthorhombic occurs (*Pbca*). Unit cell is decreasing to half and contains four "molecules" C_3A. *c* value remains unchanged, however, $a \neq b$, but both close to $c/\sqrt{2}$. In the case $c=0$ and $c=1/2$ the centers of rings are in this cell and have their axis parallel to pseudo ternary axis; one for $c=0$ and second for $c=1/2$. Sodium atoms partially substitute calcium atoms, but only in the sites Ca(5), and partially are located inside the rings.

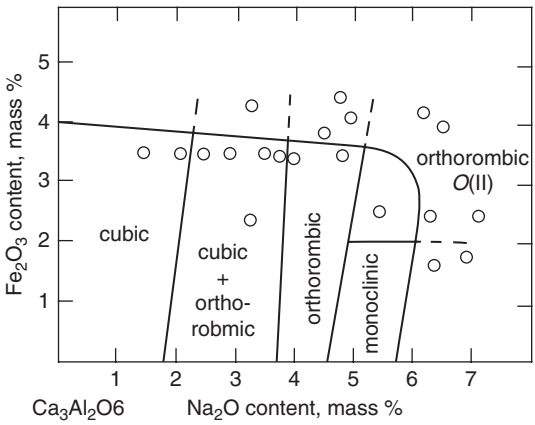


Fig. 2.56 Na_2O content and Fe_2O_3 threshold contents in different C_3A polymorphic phases, stable at room temperature. (After [165])

After exceeding the 4.6 % Na_2O content, which is the threshold value for rhombic phase, the change to monoclinic structure occurs. Takeuchi et al. [164] have determined the phase structure containing 5.7 % Na_2O. It is slightly modified in relation to the orthorhombic structure as result of separation calcium ions, occupying the sites Ca(5) onto two strictly defined sites Ca(5*A*) and Ca(5*B*). The bond length Ca(5*B*)–O is longer than in orthorhombic structure, and Ca(5*A*)–O is shorter, thus we have two groups of calcium polyhedral—bigger and smaller. It causes the increase of unit cell.

Takeuchi et al. [164] have shown that Na_2O is dissolving up to reaching the content 5.9 %, and limitation is the occupying of 75 % places in the center of rings. The possibility of substituting Ca itself could give higher sodium content. Exceeding the limiting value 5.9 % Na_2O, then formation of solid solutions NC_8A_3 (7.6 % Na_2O) is possible after the introduction of some Si^{4+} ions substituting Al^{3+} ions. Takeuchi et al. [164] studied the phase containing SiO_2 in such a quantity that ring has the formula: $Al_{5.535}Si_{0.475}O_{18}$, and found the possibility of Na_2O content increasing in solid solution to 6.6 %, by more frequently substituting the Ca sites. It seems to show that in the case of higher content of SiO_2 the concentration of Na_2O could be increased to 7.6 % [166]. Solid solution NC_8A_3, of orthorhombic structure, can be obtained by quenching of samples having temperature 1300 °C or even 600 °C [167]. Then these authors see the possibility of Ca substituting by Na up to 7.6 % Na_2O content, without silica participation. However, this hypothesis is not supported [166]. In the case of silica introduction it is possible substitution by Na^+ all calcium ions in sites Ca(5*B*) and occupation 75 % places in the rings [164, 166]. Presence of Si increases the range of orthorhombic phase stability. The excess of charge introduced with Si^{4+} is compensated by a decrease of Na occupancy inside the rings.

Also potassium can enter in the structure of C_3A, substituting for Ca^{2+}, however, without others foreign ions it is more difficult than in case of Na, and moreover potassium alone does not cause the change of cubic C_3A structure. Solid solution formation by K_2O is much easier in the presence of SiO_2 and Fe_2O_3. The orthorhombic phase was studied containing 2 % K_2O, 4.1 % SiO_2 and 10 % Fe_2O_3 [168].

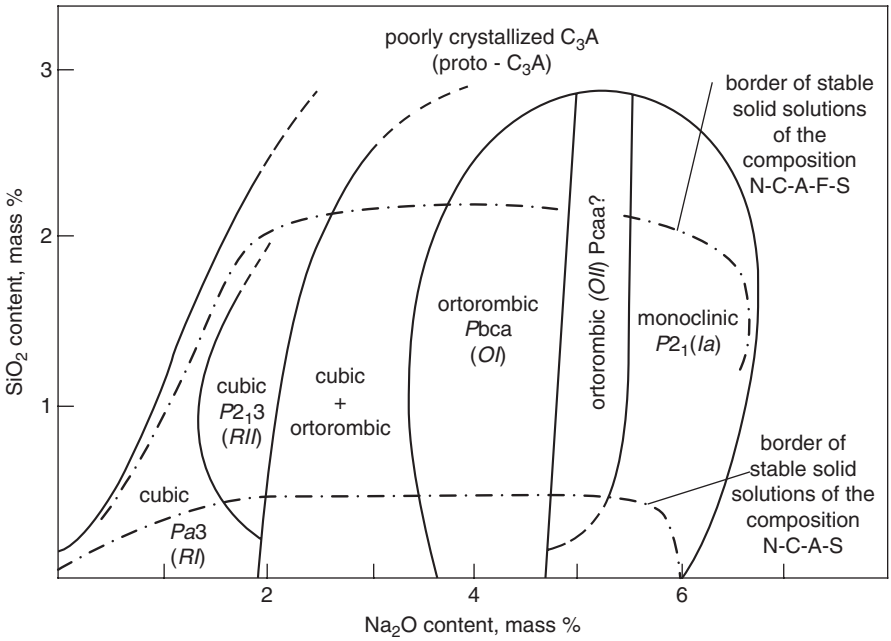


Fig. 2.57 Stable and unstable solid solutions C_3A. (After [165])

Glasser et al. [169] have obtained several non–stable phases C_3A stabilized by Na_2O and simultaneously by others foreign elements, however, by decisive stabilizing sodium effect, which they called proto–C_3A. They are distinguished by the absence of peaks typical for lattice surfaces $h+k+l \neq 4n$ (cubic cell) on the X–ray patterns. Proto–C_3A which are crystallizing from highly over–cooled melts rich in Fe_2O_3 and SiO_2 (20 % and 17 % respectively), contain much more ions Fe and Si in tetrahedral sites, thus it can occur in C_3A obtained in the conditions close to equilibrium (Fig. 2.57).

In reducing conditions the solubility of Fe^{2+} in C_3A is low [170]. Fe^{3+} has much higher solubility, and the maximum concentration at 1300 °C is 8 %, which corresponds 48 tetrahedral sites [169].

In the case of Na^+ Glasser et al. [169] propose the following mechanism of calcium ions substitutions:

$$\left[Ca_{72-n}Na_{2n}\right]_{72+n} Al_{48}O_{144} \tag{2.37}$$

And for simultaneous sodium substitution for calcium, and silicon for aluminium the following mechanism:

$$\left[\left(Ca_{72-(n+m)}\right)\left(Na_{2n+m}\right)\right]_{72+n}\left[\left(Al,Fe\right)_{48-m}Si_m\right]_{48}O_{144} \tag{2.38}$$

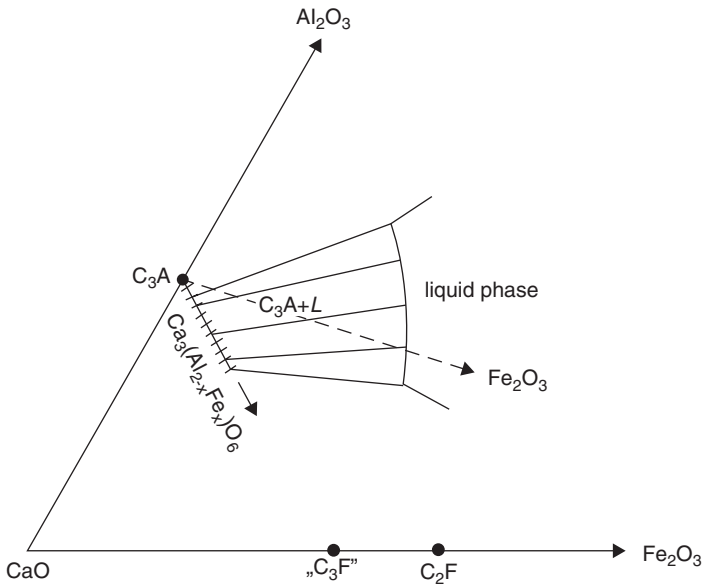


Fig. 2.58 The explanation of errors source in studying the solid solutions $Ca_3[Al2–_xFe_x]O_6$ when adding Fe_2O_3 to C_3A. (After [165]

However, in the case of Si alone (because it is possible):

$$\left(Ca_{72}\right)\left[\left(Al,Fe\right)_{48-z}\,Si_{3z/4}\right]_{48-z/4}\,O_{144} \tag{2.39}$$

It causes the tetrahedra vacancies, and some 6–member rings incomplete. However, it is low probably that these three mechanism are independent, particularly in the presence of Na. They will occur simultaneously, which gives for solid solutions the following formula:

$$\begin{aligned}&\left[\left(Ca,Mg\right)_{72-(n+m)}\,\left(Na_{2n+m}\right)\right]_{72+n}\\&\left[\left(Al,Fe\right)_{48-(m+z)}\,\left(Si_{m+3z/4}\right)\right]_{48-z/4}\,O_{144}\end{aligned} \tag{2.40}$$

Simultaneous introduction of Si with alkalis causes slower sodium and potassium occupancy of places inside the rings than in samples without silicon. Substitution of significant number of Al^{3+} ions by Fe^{3+} and Si^{4+} influence also on the range of cubic and orthorhombic solid solutions, which are then not only function of Na_2O concentration.

According to Lee et al. [165] solid solution $Ca_3[Al_{2-x}Fe_x]O_6$ can be only examined along the line linking C_3A with "C_3F". In the opposite case divergent results in the range of maximum Fe_2O_3 concentration are resulting from distribution of iron between C_3A_{ss} and liquid, being in equilibrium with this phase (Fig. 2.58), which

causes always the decreasing of iron content. In the case of double substitution Na + Fe the range of stability individual C_3A phases are dependent principally on Na^+ and are changing insignificantly (Fig. 2.56). However, in the case of higher Na and Fe concentration phase *O*(II) is stabilizing, which has the defined field of stability or quasi–stability. The results are shown in the Fig. 2.57, which has still somewhat speculative kind. The borders between phase *O*(I) and *O*(II) are changing insignificantly, depending of cooling rate. Instead of tetragonal phase, introduced by Regourd [100], Glasser et al. [169] were proposed phase *O*(II), because this phase was found after freezing of tetragonal phase.

In the case of reaction of sodium silicate and calcium–sodium silicate with C_3A at 1050–1150 °C the content of SiO_2 in C_3A is lower than 0.5 % [163]. It is in accordance with Regourd's results, which determined the highest solubility of SiO_2 as 0.3 %. However, C_3A static crystallization from eutectic melt C_3S–C_2S–C_3A–C_4AF gives the solid solution containing about 2 % SiO_2 [163]. From dynamic crystallization, which corresponds to the conditions of clinker formation, concentration of foreign elements can be even higher. In this dynamic conditions C_3A in clinker is formed, with high content of SiO_2 and Fe_2O_3. Produced by Glasser et al. [169] proto–tricalcium aluminates show significant importance of cooling process and prove that clinker phase composition must be regarded as dynamic system.

C_3A phase in Portland cement clinker has mainly cubic structure, however, in the case of higher sodium content it forms typical monoclinic crystals (Fig. 2.78). In clinkers, however, the most frequently cubic or orthorhombic phase, or the mixture of these phases are found. Goudrin [171] examining 60 different clinkers found just these three phase variants. In C_3A phases stabilization, apart of alkalis, SO_3 content is also influencing. C_3A in industrial clinkers has, with no doubt, the highest content of Fe_2O_3. SiO_2 content is always very high and usually exceeds 4 %. This SiO_2 content was not possible to obtained in synthetic specimens (Table 2.13).

The reaction rate of C_3A with water is lowering in the case of solid solutions, containing Na_2O (Fig. 2.59). Also Regourd [168] found significantly higher hydration rate of cubic phase than of orthorhombic, containing Na_2O and K_2O. It appeared that C_3A reactivity is decreasing with the degree of holes occupancy in the structure by Na^+ ions. However, the SiO_2 solid solution has higher reactivity with water than C_3A without foreign elements [174].

2.5.4 Ferrite Phase

Miscibility of C_2F with hypothetic "C_2A" is total, until the composition C_6A_2F.

Bertaut et al. (Fig. 2.60) [175] determined the structure of C_2F. The parameters of orthorhombic unit cell was: $a = 564$, $b = 1468$, $c = 539$ pm, spatial group *Pcmn*, cell contains four "molecules" of C_2F. Along the axis *b* the layers of octahedra FeO_6 follow in turn tetrahedra FeO_4. These octahedra and tetrahedra have no common oxygen atoms and are highly distorted. Ca^{2+} ions are situated in large holes between the oxygen ions and their coordination is very irregular. Calcium ions are surrounded by 9 oxygen atoms, however, one of them is relatively far (330 pm). Tetrahedral lay-

Table 2.13 Chemical composition of C_3A in industrial clinkers [100, 172]

Sample	Composition (% mass)								
	CaO	SiO_2	Al_2O_3	Fe_2O_3	MgO	TiO_2	SO_3	K_2O	Na_2O
Industrial clinker cooled in water	57.8	4.1	29.0	5.1	0.9	0.6	0.3	0.1	0.4
Industrial clinker slowly cooled	50.9 55.7	3.7 4.3	24.2 26.3	5.3 9.2	0.5 1.7	0.2 0.9	0.1 0.1	0.2 0.3	–
Industrial[a] clinker	55.5±0.8 55.5–57.9	5.5±0.1 2.9–4.9	28.4±0.6 26.4–31.1	4.8±0.4 4.9–1.3	0.9±0.1 0.4–1.3	0.4±0. 5 0.29–0.32	– –	 0.25–0.4	0.85±0.04 0.5–0.6
O(I) *C* *M*	53.2–56.6	4.4–5.3	28.8–25.5	5.5–8.0	0.6–1.9	0.80	–	0.82–1.9	1.10–2.42

[a] C_3A phases: *O*(I) rhombic, *C*—cubic, *M*—monoclinic

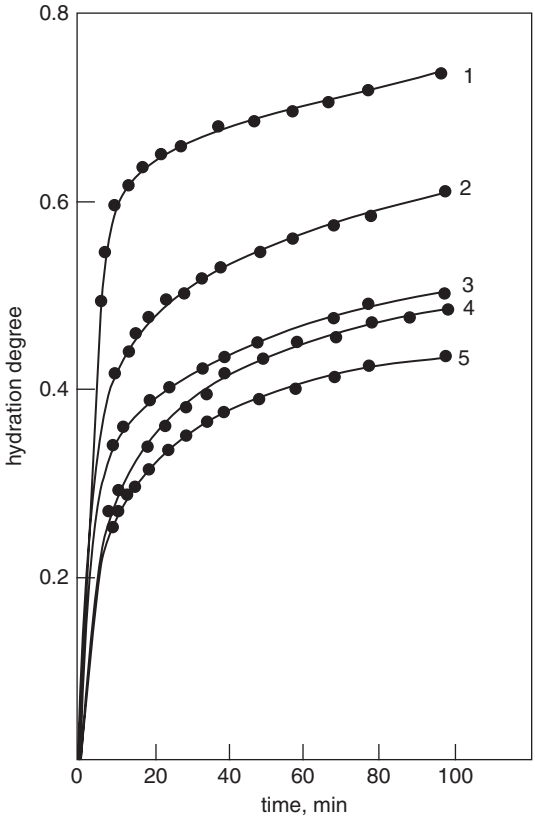


Fig. 2.59 Hydration rate of different C_3A phases: 1) cubic C_3A, 2) C_3A+2.4% Na_2O, 3) orthorhombic C_3A+3.8% Na_2O, 4) orthorhombic C_3A+4.8% Na_2O, 5) monoclinic C_3A+5.7% Na_2O. (After [173])

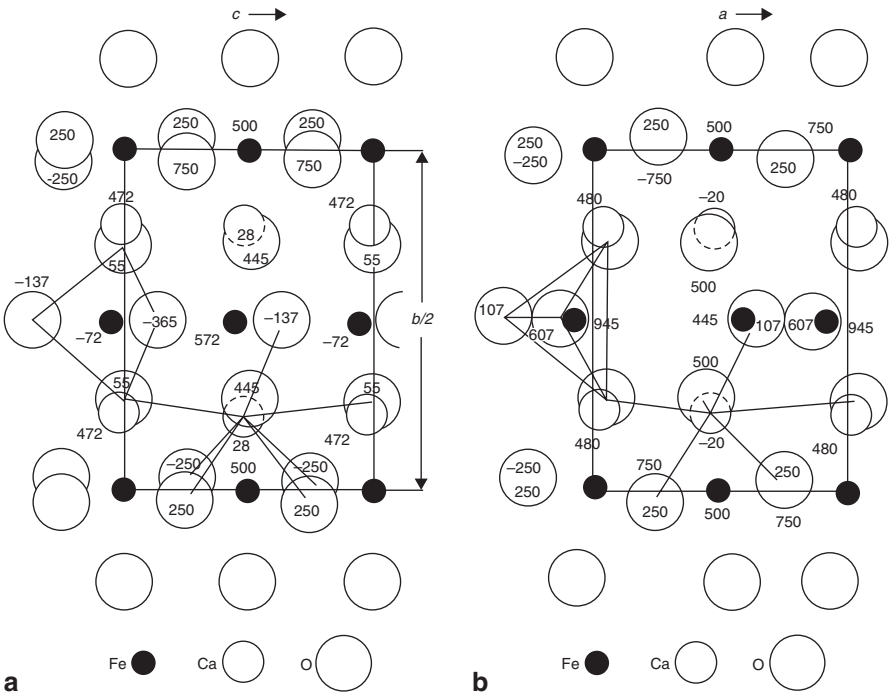


Fig. 2.60 $Ca_2Fe_2O_5$ structure: a) projection along axis *a* b) projection along axis *c* (after [175]). Tetrahedra have only common vertex, the same calcium octahedra

ers are composed of infinite tetrahedra chains parallel to axis *a*, but a little distorted to the plane *ac*, caused by the compression parallel to axis *a*.

Aluminum is divided uniformly between tetrahedra and octahedra until the composition $C_2F_{0.67}A_{0.33}$. However, in the case of higher aluminum content it substitute iron principally in tetrahedral layers, which causes decrease of tetrahedra dimensions in relation to octahedral layer and their such twisting that they occupy more symmetric position. Simultaneously calcium ions are a little shifted which causes higher symmetry and transformation of structure to the special group *Imma* [176]. In brownmillerite about 75 % Al is substituting Fe in tetrahedral sites, and about 25 % in octahedral [101]. C_4AF has the highest stability in this series of solid solutions [100].

Solid solutions $C_2F_{1-p}A_p$ studied, among others, Woermann et al. [177]. They found two discontinuities in the changes of unit cell parameters for $p = 0.30$ and 0.50 (Fig. 2.61). However, the change of inclination is very low. First discontinuity is linked with the polymorphic transformation of pure C_2F at 430 °C, which is caused by discontinuity in increase of the unit cell volume [100]. This polymorphic transformation does not appear in the case of solid solution for $p = 0.33$, for structure change from *Pnma* to *Imma*, which has shown Smith [176].

Magnesium oxide can form the solid solutions with $C_2F_{1-p}A_p$ phase. Two kinds of these solid solutions were found [177]. First, in which Mg^{2+} substitute Fe^{3+}, is

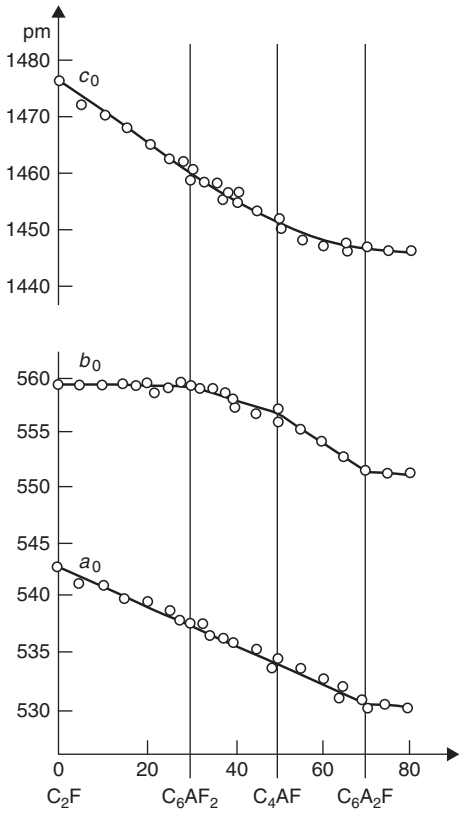


Fig. 2.61 Changes of unit cell parameters of ferrite phase $C_2F1-_pA_p$ in relation to Al_2O_3 content. (After [177])

extending to $p=0.50$. The lattice electroneutrality is preserved by introducing of one Mg ion in interstitial site for each two ions substituting iron [177]. The formula of solid solutions is the following:

$$Ca_2\left[Fe_{1-2x/3}Mg_x\right]_2O_5 \quad 0<x<0.023 \text{ at } 1400°C \tag{2.41}$$

When aluminium concentration $p\geq 0.49$ the 1/5 Mg substitutes Ca, while 4/5 Mg is continuing to form the solid solution of previous kind. These solid solutions are given by the formula:

$$\left(Ca_{1-x/5}Mg_{x/5}\right)_2\left[R_{1-8x/5}Mg_{4x/5}\right]_2O_5 \quad x=0.049 \text{ at } 1300°C \tag{2.42}$$

Also SiO_2 forms solid solutions with ferrite phase [35], substituting Al and Fe. Ti, Mn and Cr form similar solid solutions. Chromium on oxidation degree VI is occupying octahedral sites [178]. Ferrite rich in aluminium forms by rapid cooling glass phase [179].

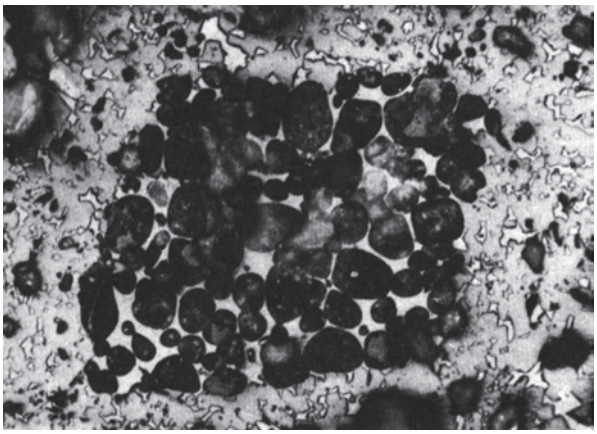


Fig. 2.62 Pseudo–morphose of CaO after calcite grain. (Photo C. Wieja)

Composition of ferrite phase in clinker depends in great degree on the A/F ratio and also on the burning conditions. The compositions are ranging from C_6AF_2 through C_4AF to C_6A_2F. Many authors found that in Portland cement clinkers of common composition ferrite phase has the composition close to brownmillerite [171, 180]. Ferrite phase has always the orthorhombic symmetry.

Analysis of ferrite phase composition using electron microprobe is difficult because of the small crystals and the intergrowth with C_3A or inclusions of microcrystalline belite. For ferrite phase separation salicylic acid and methanol were used according to the method of Yamaguchi and Takagi [181], or salicylic acid and sugar solution [100], and also maleic acid [168]. Brisi and Rolando [182] state that the $C_2(A, F)$ solid solutions are decomposed in the presence of CaF_2 and $CaCl_2$. Phases $C_{11}A_7 \cdot CaX_2$ and C_6AF_2 are then formed [182].

2.5.5 Minor Phases

2.5.5.1 Calcium Oxide

The presence of free lime can be very easily found under light microscope on polished section, without etching. Low amounts of humidity, which is always in the air is sufficient for very clear differentiating of these particles.

Calcium oxide forms in general agglomerations of round particles. Two kinds of calcium oxide can be distinguish in clinker. Primary free lime which did not reacted with others components because of errors in raw mix preparation, for example coarse limestone grains or insufficient homogenization, or to high lime saturation factor, or at least inadequate burning conditions. On Fig. 2.62 typical pseudo–morphose of CaO after calcite grain is shown. Second kind is the secondary free lime. It is formed as a result of alite decomposition. It is highly dispersed, making impression of amorphous.

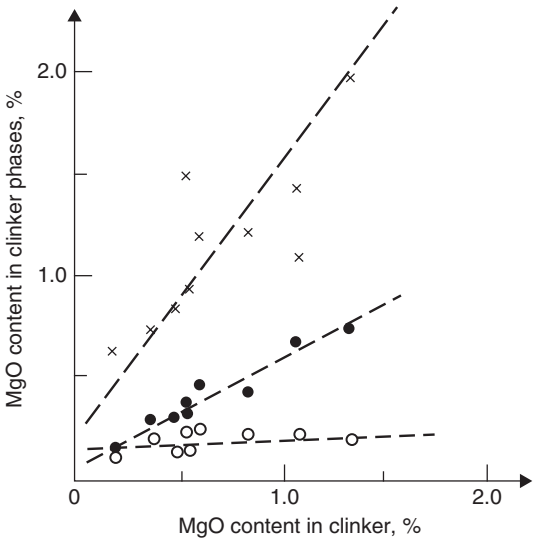


Fig. 2.63 Change of MgO content in clinker phases: alite (●), belite (○), interstitial matter (x) in relation to MgO amount in clinker. (After [183])

2.5.5.2 Periclase

The content of magnesium oxide in raw mix higher than 2 %, calculated for burned material, causes already periclase formation. The concentration of MgO in individual clinker phases in dependence of its content in clinker was studied by many authors. No regularities were found, but the maximum content of MgO in individual phases can be estimated. On the basis of electron microprobe analysis it can be assumed that 2 % MgO is in alite, 1 % in belite, 1 % in C_3A and 3.5 % in C_4AF. It gives the total MgO content in clinker of about 2 %. However, others authors state somewhat lower amounts, particularly in belite. According to them MgO content in belite does not exceed 0.2 % and in alite 1 % (Fig. 2.63) [183]. Further information can be found in tables 2.8 and 2.16. These divergences without doubt are caused by micro–heterogeneous clinker composition. In the case of higher MgO content in clinker periclase is formed. The dependence between periclase amount and MgO content in clinker was experimentally found by Boikova (Fig. 2.64) [68].

Periclase forms typical cubic crystals with very high coefficient of light reflection. MgO and CaO have cubic structure and the lattice of NaCl kind. Metal and oxygen ions are in octahedral coordination. Unit cell contains four "molecules" of CaO or MgO; $a = 479.7$ for CaO and 420.3 pm for MgO. The Mg^{2+} ionic radius is 78 pm and can be exactly situated between oxygen ions in hexagonal lattice of the most dense atoms packing. Calcium ion is larger (106 pm) and for this reason oxygen ions are a little extended. CaO structure is then less stable than MgO structure, and the last is much slower hydrated and is found in nature.

Moore [184] was XRD determining periclase in clinker, applying selective dissolution of silicates in boric acid, or successively added acetic acid, using rutile as inner standard.

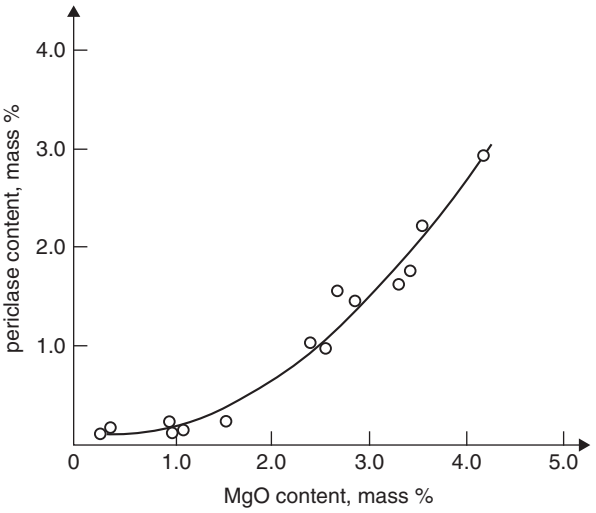


Fig. 2.64 Dependence on periclase and MgO content in clinker. (After [68])

2.5.5.3 Alkalis in Clinker

Alkalis show the biggest affinity to sulphur and form preferentially sulphates. In clinker K_2SO_4 [100, 185, 187] and Na_2SO_4 [168] are formed, and can also be present as $3K_2SO_4 \cdot Na_2SO_4$ and $2CaSO_4 \cdot K_2SO_4$ [186]. The presence of former to the last phase was mentioned by Regourd [168]. Trace amounts of alkali carbonates or potassium aluminate have also been reported to occur in some clinkers [207].

Also Mauder and Skalny [187] are considering that, apart from arcanite (K_2SO_4), the most frequently formed phases are aphthitalite $3K_2SO_4 \cdot Na_2SO_4$ and calcium langbeinite $2CaSO_4 \cdot K_2SO_4$. The last phase was identified with XRD after dissolution of calcium silicates in maleic acid, using peaks at 26.9°, 27.2° and 27.6° (Cu $K\alpha$) [187]. These authors state that the observation under SEM shows that the sodium and potassium sulphates are condensed from gaseous phase on the surface of clinker phases in rotary kiln [187]. In clinkers from short kilns with cyclone preheaters light plate crystals on clinker nodule surface can be easily found.

In 1986 Fundal [188] found new potassium phases. In laboratory clinkers rich in potassium $K_2O \cdot Al_2O_3$ and free potassium oxide were present. Both phases are highly hygroscopic which influence clinker properties.

In the case of higher alkalis content, when molar ratio $(K_2O + Na_2O)/SO_3$ excites 1, sodium forms preferentially solid solution in C_3A and potassium in belite. However, there are exceptions which were discussed in points 2.5.2 and 2.5.3.

The minor alkali phases are simultaneously the suggestion concerning sulphur compounds formed in clinker. Regourd [168] found by XRD in some industrial clinkers K_2SO_4 and $K_3Na[SO_4]_2$. Besides these minor phases Barnes and Ghose [183] found the highest concentration of sulphur in belite (compare point 2.5.2, Table 2.12). However, only in few experimental works, the "formally" calculated anhydrite (Bogue's formulae), is mentioned.

Table 2.14 Distribution of some minor components in clinker phases

Element	Content (% mass)			
	clinker	Alite	Belite	Interstitial matter
V_2O_5	0.4	0.6	0.0	0.0
As_2O_3	1.5	1.7	0.0	0.0
Cr_2O_3	0.4	0.2	–	0.8[a]
P_2O_5	1.0	1.0	1.8	0.2
TiO_2	0.9	0.7	1.2	2.0
BaO	0.7	0.3	1.4	0.2[b]
BaO	0.3	0.25	–	0.79[c]

[a] calculated as the difference between the content in clinker and alite
[b] in C_4AF
[c] in C_3A

2.5.5.4 Glass

Taking into account that determined content of principal clinker phases, namely C_3S, C_2S, C_3A, $C_2(A, F)$ is usually close to expected value, the glass presence was disputed. However, quenched clinkers in laboratory condition caused the decrease content principally of C_3A, and also of ferrite phase as well as of belite and glass formation in quantity of about 20% [189]. Regourd [168] found on XRD patterns of few clinkers the broad diffraction effect (glass halo) in the angles range 29–34°, confirming glass existence.

However, it is doubtful that industrial clinkers can ever contain a good deal of glass, because even very good grate coolers cannot assure such rapid cooling, as in laboratory.

It was established that in clinkers with low MgO and alkalis content less glass is formed [189]. Simultaneously it is known that rapid clinker cooling diminishes expansion in water solution of $MgSO_4$.

2.5.5.5 Minor Components

Except earlier mentioned elements others minor components do not form own phases, but solid solutions in principal clinker phases. The use of industrial by–products and untypical raw materials are introducing to clinker other foreign elements, which distribution in clinker phases was studied. In Table 2.14 the distribution of some foreign elements is presented [190]. As it results from these data vanadium is concentrated in alite, however, chromium and titanium principally in interstitial matter.

Manganese Oxide Mn_2O_3 occurs in higher amount when slags are used as raw materials. Manganese substitutes iron giving brownmillerite analogue $4CaO \cdot Al_2O_3 \cdot Mn_2O_3$ and both phases unlimited solid solutions are formed [191]. For this reason manganese is placed in clinker in ferrite phase. According to Lea [24] manganese has in this respect low effect on cement properties: from clinker containing up to 4% of Mn_2O_3

Table 2.15 Content of heavy metals in industrial clinkers; A, B and C different cement plants, from 2000 to 2010 [199]

Heavy metal	A				B				C			
	Year											
	2000	2002	2006	2010	2000	2002	2006	2010	2000	2002	2006	2010
	Content, mg/kg											
Zn	147	247	250	521	48	119	494	375	1703	1631	3069	782
Cr	37	32	34	42	31	29	93	74	42	33	133	113
Cu	11	18	40	127	8	10	79	103	33	47	123	338
Ni	17	21	20	25	14	23	32	30	22	26	45	46
Pb	6	16	28	10	<5	<5	28	8	280	276	371	65

very good cement is produced. Knöfel et al. [192] found that small manganese content about 0.5 % is increasing cement strength. Simultaneously the increase of alite content with rise of Mn_2O_3 to this value was found [192].

Titanium Oxide TiO_2 is introduced to clinker principally with clay minerals and also with iron corrective components. Usually the TiO_2 content in clinker is about 0.25 %. The influence of this oxide on properties of individual clinker phases was studied. Alite, in which titanium is substituting silicon, is hydrating slower at the beginning (up to three days) and then quicker [193]. Fierens [194] found lower reactivity of C_3A solid solutions with titanium. Titanium substitutes primarily iron in ferrite phase, then aluminium in C_3A, and only in the last order silicon in belite. Knöfel [195] established the distribution of TiO_2 in individual clinker phases and found 54 % of total quantity in $C_2(A, F)$, 23 % in C_3A, 15 % in belite and 8 % in alite. Similar values found Midgley [196]. Additionally Knöfel [195] the larger alite crystals in the case of TiO_2 addition in comparison with clinker without titanium, and also increase of cement strength found. Sychev et al. [197] state that TiO_2 can form in clinker neutral calcium titanates. Gaillard et al. [198] found that the content of TiO_2 in individual clinker phases can be calculated by using the empirical coefficients: in alite $= \%TiO_2 \cdot 0.7$, in belite $= \%TiO_2 \cdot 1.2$, in interstitial matter $= \%TiO_2 \cdot 2$. According Knöfel [195] the last empirical coefficient is equal 1.

Zinc, lead, cuprum In the last decade cement industry itroduced in increasing degree alternative fuels, among which the used tires and oils, wood waste, and municipal waste. Simultaneously as iron corrective component different byproduct are used, for example blastfurnace dust. These materials introduce to the kiln different minor components, heavy metals among others, which content in clinker increased multiply (Table 2.15). Clinkers analysis have shown that the highest increase is concerning primarily zinc, but also lead, cuprum, nickel and chromium, in minor degree (Table 2.15) [199]. These components influence on clinkering process and cement properties. They have relatively low vapour pressure and, in the case of kiln with cyclones preheaters, they remain practically totally in clinker (Table 2.16).

Heavy metals will have advantageous effect on clinkering if they will form eutectics in low temperature and will increase clinker melt content, as well as decrease

Table 2.16 Absorption degree of heavy metals in rotary kilns with cyclones preheaters

Metal	Metal quantity (g/h)		Absorption degree
	Feeded to the kiln	emission	
Pb	1198	0.754	99.94
Cd	90	1.119	99.87
Cr	2263	0.754	99.97
Co	796	0.477	99.94
Ti	180	0.052	99.97
V	12221	0.477	99.99
Ni	5288	0.477	99.99
Cu	2242	0.286	99.99
As	282	0.048	99.98

its viscosity. Timashev [39] studied the influence of some heavy metals and found that they can decrease clinker melt viscosity (Fig. 2.65). It has the advantageous effect on clinkering process by increasing the rate of CaO and C_2S dissolution and alite crystallization (Fig. 2.66). From the other side these components decrease the surface tension of clinker melt (Fig. 2.67) which causes the decrease of clinker nodules dimensions, formed in rotary kilns (Fig. 2.41).

Nowadays there is few studies concerning influence of heavy metals on clinkering process, however, some works were published, the most of them linked with zinc [200–203]. Bordoloi et al. [200] found that Zn has advantageous effect on clinkering process, but already 0.32% ZnO in clinker decrease significantly cement strength after 28 days of hardening. Also Murat and Sorrentino [203] establish the worsening of cement properties from clinker burned with zinc addition. Further increase of zinc in clinker (Table 2.15) caused increasing interest of studies concerning zinc influence on clinkering process [204–210]. High importance for this group of works has the study of Bolio–Arceo and Glasser [211] regarding the system CaO–ZnO–Al_2O_3 in which two three components phases $Ca_3ZnAl_4O_{10}$ and $Ca_6Al_4Zn_3O_{15}$ are formed. Gineys [210] presented the profound studies of zinc influence on clinkering process and cement properties. The results of this research can be summarized as follows: Zn is forming solid solutions with all clinker phases, but after exceeding the Zn content of 0.7% it forms its own two phases in clinker. Part of zinc in $Ca_6Al_4Zn_3O_{15}$ phase can be replaced by Mg [211]. The amount of Zn found by Gineys [210] in clinker phases was the following: in alite 1.40%, in belite 0.11%, in C_3A 0.43% and in brownmillerite 1.94%, when the total content of Zn in clinker was 0.7%. Kakali [207] found additionally the phase $2CaO \cdot ZnO \cdot SiO_2$, when the content of ZnO overpassed 1.5%.

The phase $Ca_6Al_4Zn_3O_{15}$ reacts violently with water, giving high heat of hydration [210]. Gineys [210] did not found disturbances in the hydration and hardening of cement till zinc content of 0.7%. However, the Zn content equal 3% caused significant retarding effect of cement hydration with decrease of strength after 2 and 28 days [210].

Some comments must be devoted to the phase $Ca_6Al_4Zn_3O_{15}$; Barbanyagre et al. [212] obtained the phase $Ca_{14}Al_{10}Zn_6O_{35}$, which, as it is seen from stoichiometric equation, has a very close chemical composition to the first, and, which is even more

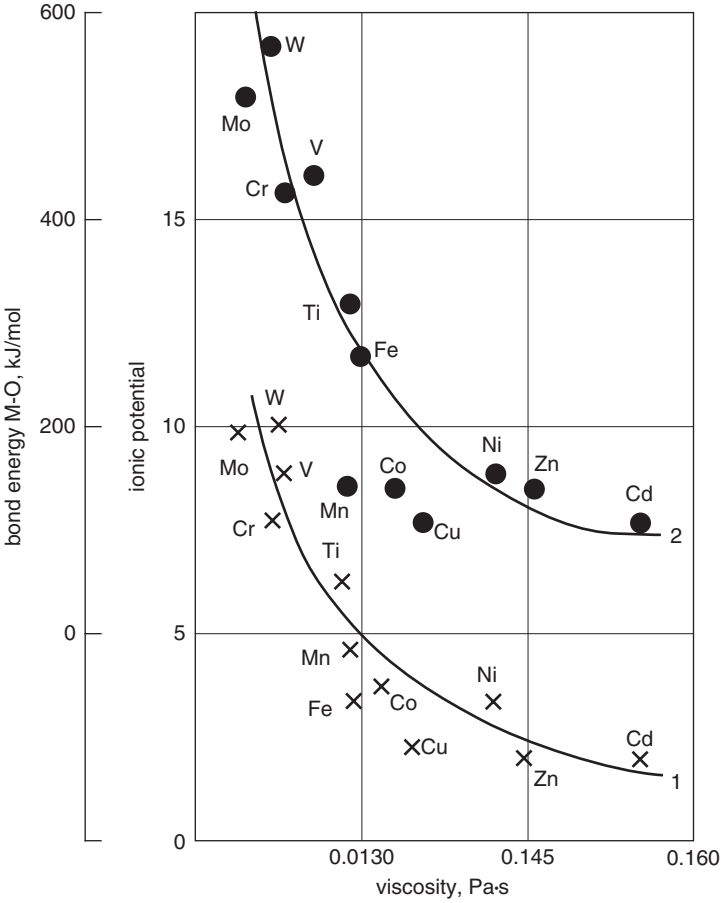


Fig. 2.65 Influence of some minor components on viscosity of clinker melt (after [39]); cation ionic potential (*z/r*) (*1*), bond energy (*2*)

important, very similar structure, thus its X–ray pattern is also very similar. The main difference is chiefly limited to the weak peak at d = 2.35084 (intensity 4.8 %), which is lacking on the X–ray pattern of $Ca_6Al_4Zn_3O_{15}$ and the last has relatively high peak at d = 1.52130 (intensity 21 %), which is not present on the X–ray pattern of the previous phase. From this reason the computer program X'Pert High Score Plus does not differentiate these phases and lives the choose to the experimenter.

The experiments in the Institute of Ceramics and Building Materials in Poland [213] have shown that zinc forms three phases: $Ca_6Al_4Zn_3O_{15}$, the last one containing Mg and $2CaO \cdot ZnO \cdot SiO_2$, when Zn content in clinker is equal 0.61 %. Cement produced from this clinker has normal properties, compressive strength equal 17.7 and 55.1 MPa, after 2 and 28 days respectively. The three phases: C_3A_2Z, $C_6A_2Z_3$ and $C_6A_2Z_{2.8}M_{0.2}$ were synthesized and their reaction in lime saturated water studied. All phases react quickly with water and the heat of hydration is high, for first two phases 186 J/g and about 200 J/g after 24 and 41 hours respectively. However,

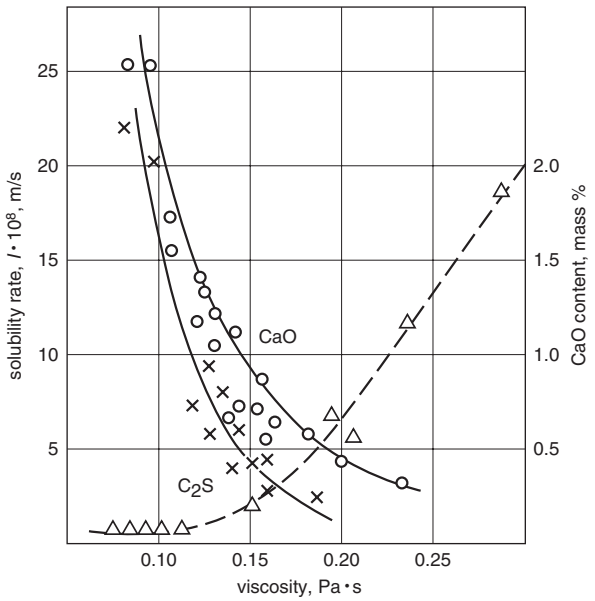


Fig. 2.66 Rate of calcium oxide and C_2S dissolution in clinker melt in relation to its viscosity. (After [39])

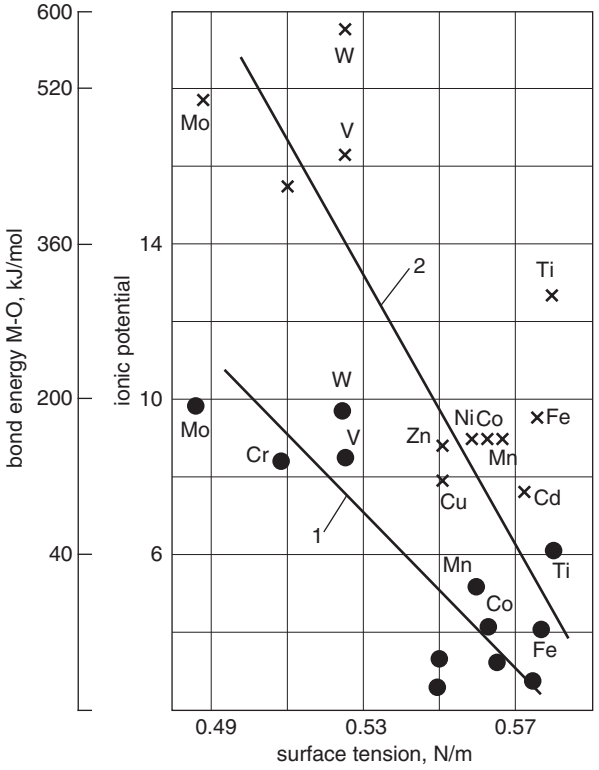


Fig. 2.67 Influence of some minor components on surface tension of clinker melt (after [39]); cation ionic potential (z/r) (*1*), bond energy (*2*)

heat of hydration of $C_6A_2Z_{2.8}M_{0.2}$ is about 300 J/g and 350 J/g after 24 and 41 hours respectively XRD patterns have shown that the hydration products were C_2AH_8 and C_3AH_6 as well as basic calcium zincate hydrate. The addition of these phases to Portland cement in quantity corresponding to 2% Zn caused rapid set with ettringite formation and low strength. [214]. The experiment with slag cement, without gypsum, gave the same result—low strength, but the phases causing rapid set was hydrated calcium aluminates: CAH_{10} and C_2AH_8 [214]. Cement from clinker burnt in small rotary kiln and containing 2,13% ZnO, has shown extremely long setting time. It was caused by ZnO content in clinker of about 0,5% beside of solid solutions and zincate phases.

Similarly cuprum enhances the clinkering process, however, worsens cement properties [215]. Chromium, barium, phosphorus, boron and titanium added in small quantities to raw materials increase cement strength after 3 days of hardening and barium also after 28 days [216].

2.5.6 Methods of Clinker Phase Composition Determination

Clinker phase composition has decisive influence on several properties of cement paste, thus also on concrete. The most important are the following:

- strength which depends principally on alite content (Fig. 2.68),
- sulfate resistance which depends principally on C_3A content,
- rheological paste properties, which depend chiefly on C_3A content.

In their studies authors are limiting the most frequently to the calculation of phase composition using Bogue's formulae (see note under Table 1.2). Newkirk [217] proposed the formulae taking into consideration the alkalis content, assuming that alkalis are forming firstly sulphates, and then $KC_{23}S_{12}$ (potassium) and NC_8A_3 (sodium).

According to Taylor [218] Bogue's formulae give to low values in the case of alite and tricalcium aluminate, too high for belite and relatively correct for ferrite phases. More close to reality results can be obtained with modified by Taylor [218] Bogue's formulae, which take into account the presence of minor components solid solutions in clinker phases. Taylor simplifying assumed that in clinker phases the quantity of minor components are on the level given in Table 2.17.

The calculation procedure is as follows. According to Bogue calculation CaO content must be corrected for free lime and bond in sulphates or $CaCO_3$. Then, if there is no more accurate data, it can be assumed that 67% of insoluble residue is composed of SiO_2 and 33% of Al_2O_3.

The system of equations is the following:

$$\begin{aligned}
\text{alite} &= 4.5131CaO - 8.5947SiO_2 - 6.8987Al_2O_3 - 1.5116Fe_2O_3 \\
\text{belite} &= -3.6133CaO + 10.0842SiO_2 + 5.1743Al_2O_3 + 1.0286Fe_2O_3 \\
C_3A &= 0.1320CaO - 0.3961SiO_2 + 3.6483Al_2O_3 - 3.9598Fe_2O_3 \\
C_4AF &= -0.0482CaO - 0.0084SiO_2 - 0.8292Al_2O_3 + 5.6298Fe_2O_3
\end{aligned} \tag{2.43}$$

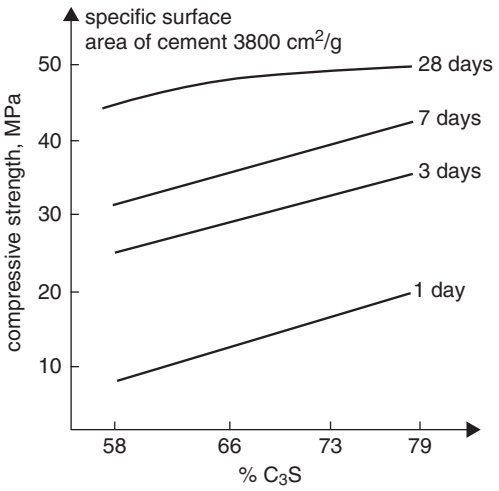


Fig. 2.68 Alite effect on cement strength. (Specific surface area of cement 380 m^2/kg)

One of the oldest, but always used experimental method for clinker analysis is optical microscopy. Taylor [218] is citing Aldrige [219], which states that the microscopy gives good results, if the operator has suitable experience. In this method the polished sections, etched with 1 % solution of nitrogen acid in absolute alcohol, are used. For interstitial matter differentiation, to which tricalcium aluminate forming dark interstitial matter and brownmillerite forming light one are numbered, 10 % water solution of KOH is used [220]. The etching time in first case is 2–15 s, in second 15 s. Ammonium dimethyl–citrate in combination with initial water etching is also used (together 5–10 s) [220].

Alite is forming usually hexagonal crystals, seldom of the trapezohedron or rhombohedron habitus [221] (Fig. 2.69). This morphology is depending from the

Table 2.17 Typical composition of clinker phases (after [218])

Phase	CaO	SiO_2	$Al2O_3$	Fe_2O_3	MgO	Na_2O	K_2O
Alite[a]	71.6	25.2	1.0	0.7	1.1	0.1	0.1
Belite[b]	63.5	31.5	2.1	0.9	0.5	0.1	0.9
C_3A cubic	56.6	3.7	31.3	5.1	1.4	1.0	0.7
C_3A rhombic[c]	53.9	4.3	28.9	6.6	1.2	0.6	4.0
C_3A, low in Fe[d]	58.1	4.6	33.8	1.0	1.0	0.4	0.5
Ferrite	47.5	3.6	21.9	21.4	3.0	0.1	0.2
Ferrite, low in Al[e]	46.0	3.5	15.2	29.8	2.8	0.1	0.2

[a] % of MgO = 0.667·% of MgO in clinker, however, not more than 2 %, % Fe_2O_3 = 0.25 % Fe_2O_3 in clinker, however, not more than 1.1 %; CaO = 71.6–1.4·(MgO in alite—1.1) The composition shoud be bring to 100 %

[b] Higher content of SO_3 in clinkers with high ratio $SO_3/(K_2O + Na_2O)$

[c] Orthorhombic or pseudotrigonal phase in clinker rich in alkalis

[d] In white clinkers

[e] In sulphate resistance clinker

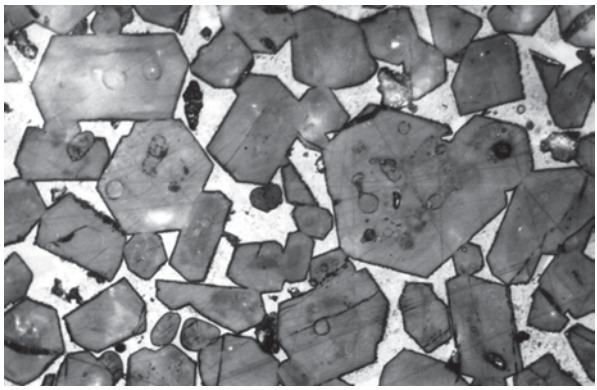


Fig. 2.69 Typical alite habitus, polygonal knitting is visible

one side of alite crystals morphology and from the other side—of the cutting direction of crystals by polished section surface. Frequently alite forms polygonal knits. By high melt oversaturation and rapid alite crystallization in this condition it contains frequently belite or interstitial matter inclusions. In the case of low cooling, for example in the core of big clinker nodule, alite crystals underwent surface decomposition, and became covered by microcrystalline shell of secondary belite (Fig. 2.70). In industrial clinkers alite crystallization condition are changing in micro–zones, even within one crystal, which frequently causes zoned crystals formation. These zones contain different foreign elements concentration, which is stabilising different polymorphs [222] (Fig. 2.71). Because of very different local conditions of crystals growth, alite dimensions primary formed in clinker are very differentiated. As a result of oversaturation decrease in late period of clinkering the small crystals are dissoluting in the melt, which causes the increase of neighbouring alite crystals. The process of dissolution and growth is taking place during temperature increase and decreasing of melt viscosity [222]. The initially formed crystals are smaller, the influence of Ostwald maturing is higher in clinker [222].

Belite is forming in clinker round crystals with typical striations. They are caused by polysynthetic twinning due to the transformation of phase α in α'_H and six configurations of twinning plates are possible. The best dimensions fitting of crystal lattices α and α'_H is when the plates direction is parallel to (010) and are crossing (0001) at an angle of 27° (Fig. 2.72). In the case of very rapid cooling from 1280 °C α phase became frozen and its crystals have smooth surface (Fig. 2.73). However, in the case of much slower cooling the process of secondary crystals melting took place, directly after the transformation to phase α'_H [222]. From the melt the secondary phase α'_H is precipitated, on partially melted primary crystals. This process can last till the total replacing of primary crystals by secondary α'_H phase which is causing only one set of striations, after next transformation in β phase [222] (Fig. 2.74). Known overlapping fingers forms of belite crystals respond to the initial stage of secondary melting (Fig. 2.75).

Belite crystals can form clusters in the places occupied by quartz grains, and in their core the typical “hole” can be present (Fig. 2.76). On the quartz grain initially

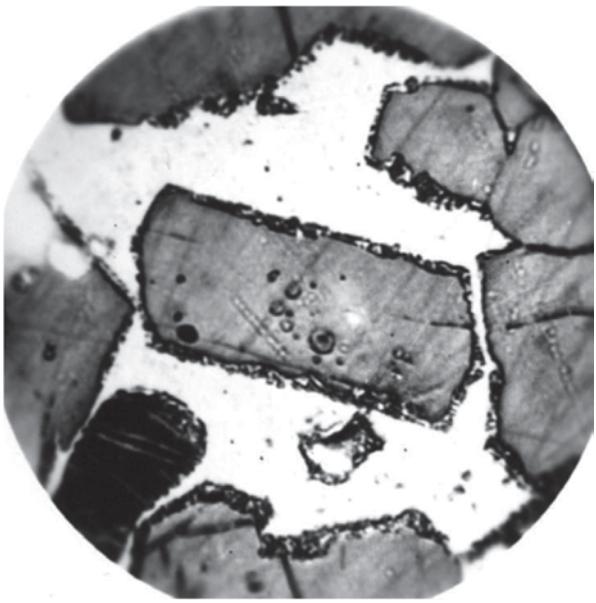


Fig. 2.70 Belite shell on alite crystals

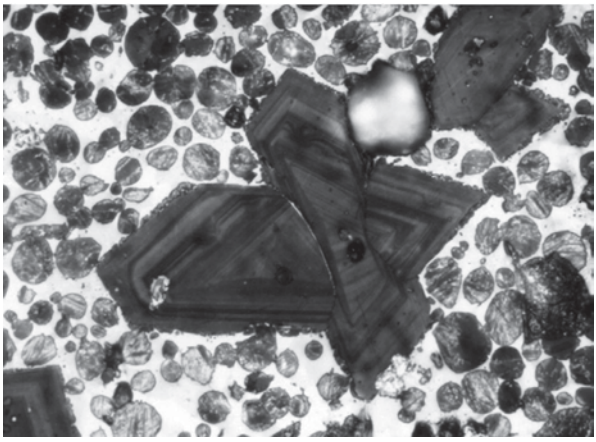


Fig. 2.71 Large zoned alite crystal

the shell of small belite crystals are formed, which are growing due to Ostwald maturing. Inside the belite shell wollastonite is crystallizing which forms eutectic with cristobalite, from polymorphic transformation of quartz, and liquid flows out of the shell. In dependence on CaO diffusion rate belite can be formed inside the shell or the "hole" can be filled with interstitial matter. Only seldom the dendritic belite crystals, secondary precipitated from the melt can be found.

Tricalcium aluminate which is dark interstitial matter forms most frequently cubic crystals, sometimes of large dimensions. In it the inclusions of very small secondary belite crystals can be found, formed by reaction of calcium with silica from

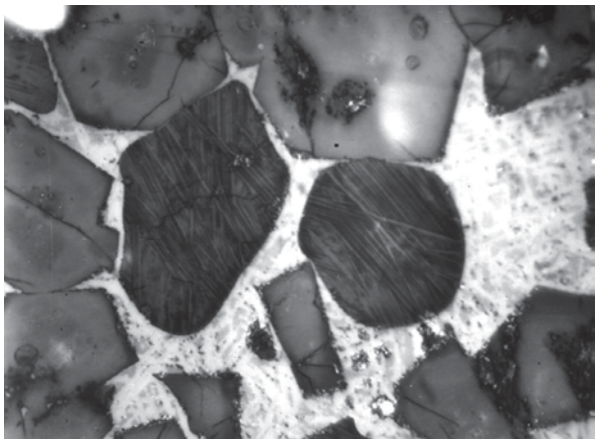


Fig. 2.72 Belite crystals with two–directions striations, correct alite and belite distribution, indicating good raw mix homogenisation

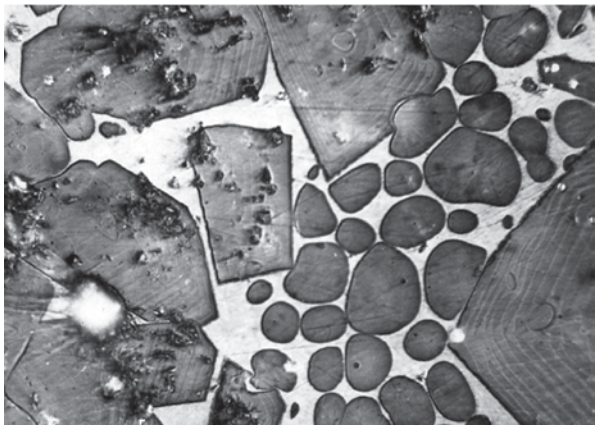


Fig. 2.73 α–C_2S phase, large zoned alite crystal

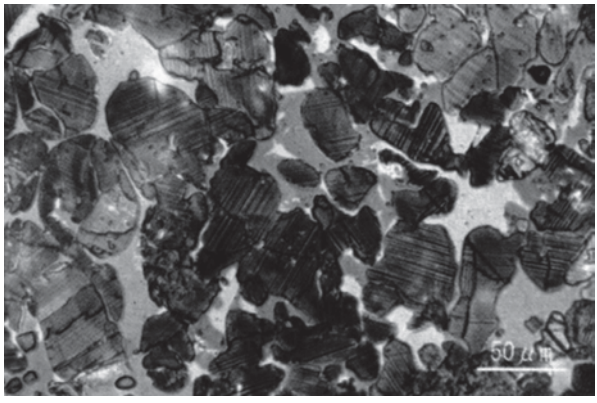


Fig. 2.74 Belite with striation in one direction. (After [211])

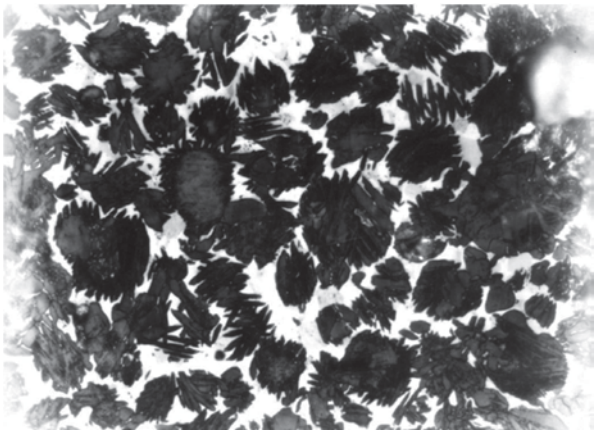


Fig. 2.75 Belite particles with overlapping fingers formation in industrial clinker

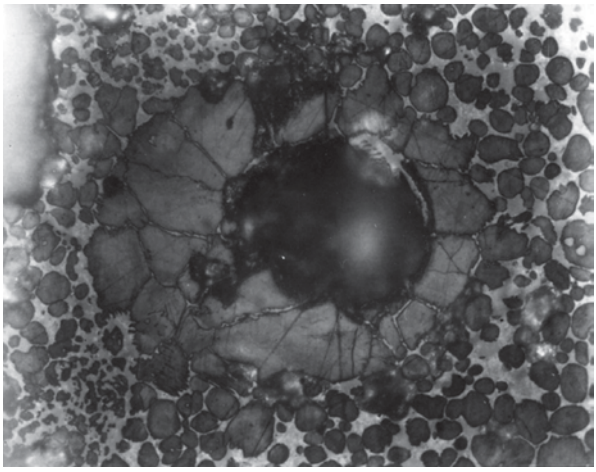


Fig. 2.76 Belite shell around the "*hole*". Pseudo–morphose after large quartz crystal

C_3A solid solution decomposition (Fig. 2.77). In clinkers rich in alkalis monoclinic tricalcium aluminate is formed (Fig. 2.78).

Brownmillerite forms as a rule very small crystals, sometimes concretions with tricalcium aluminate can be found. Seldom the idiomorphic prismatic crystals are formed.

From minor phases principally free lime should be mention, which can be dispersed in interstitial matter or can form pseudomorphoses after large calcite crystals (Figs 2.62, 2.79). CaO particles are visible on non–etched polished section surfaces as a result of air moisture effect.

In clinkers rich in magnesium cubic periclase crystals can be found, of high light reflecting power.

Analysis under light microscopy gives also the possibility of technological process correctness evaluation and explain the causes of possible disturbances. Proper raw mix preparation—homogenisation and fineness, gives in microscopic image the uniform distribution of alite and belite crystals, in amounts corresponding to

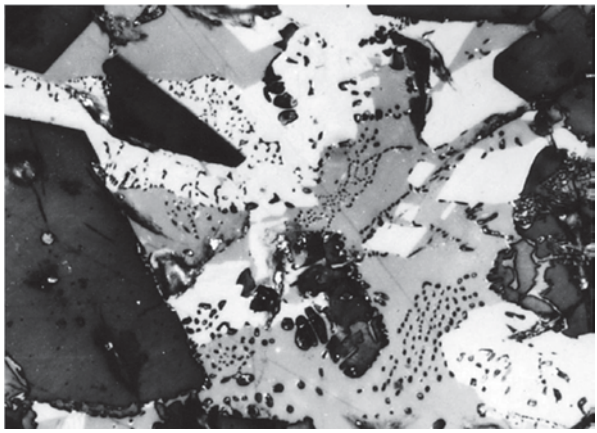


Fig. 2.77 Cubic tricalcium aluminate with belite micro–crystals inclusions

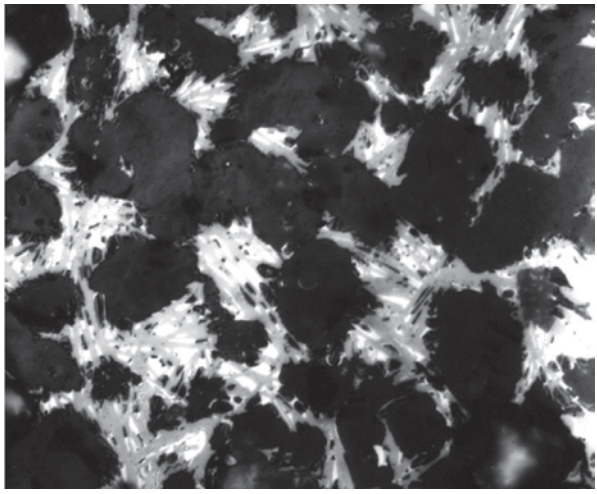


Fig. 2.78 Monoclinic tricalcium aluminate

their content in clinker (Fig. 2.72). Concentrations of belite close to surfaces occupied by alite are the proofs of inadequate homogenisation of raw mix (Fig. 2.80), however, the conglomerates of free lime surrounded by alite indicate too high lime saturation factor, at least local (Fig. 2.79). In turn large agglomerations of free lime particles, frequently of rhombohedral habitus (Fig. 2.62), indicate the presence in raw mix coarse limestone grains. However, the belite shell around the "hole" indicates the presence of coarse quartz grains (Fig. 2.76).

In the last two decades the unquestionable superiority in clinker phase composition has gained XRD. The inner standard is usually used, frequently rutile or corundum. The last one has advantage that it does not coincidence with clinker phases peaks in the range of 2θ till 60°. Taylor [218] states that this method is not useful for belite determination, because the coincidence of its peaks with alite, which cause that the weak ones must be used.

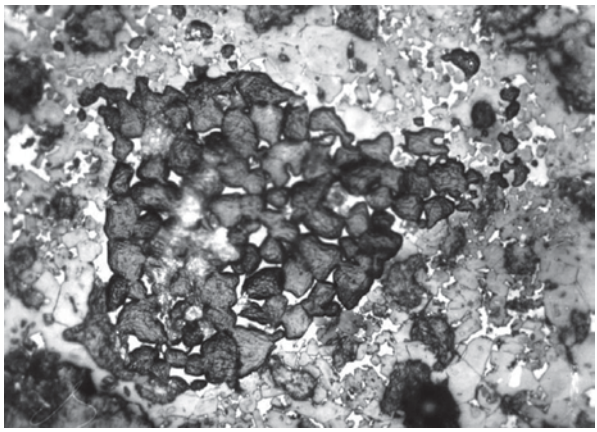


Fig. 2.79 Agglomeration of isomorphic CaO crystals in the place occupied previously by calcite

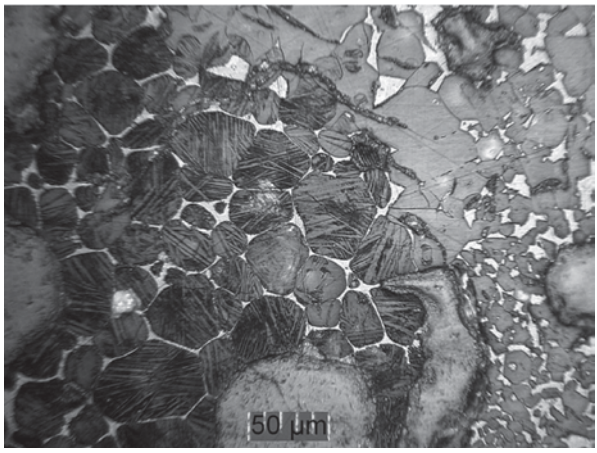


Fig. 2.80 Large surfaces occupied by alite and belite, incorrect raw mix homogenisation

In seventies XRD methods gained still greater popularity as the Rietveld [223] program was introduced. On the basis of the structure of all clinker phases the theoretical X–ray pattern can be calculated, which then is compared with the diffraction pattern of examined sample and correlated using the least square method. This method needs, however, the calibration curves determination for different clinker types, in order to take into account the matrix influence.

In order to examine particulary clinker phases, including minor phases, the dissolution of silicates or interstitial matter can be used. Taylor [218] is stating that for the dissolution of free lime, alite and belite the solution of silicic acid in methanol can be used. For this aim the solution of maleic acid in methanol was also applied. Guttrige [224], for aluminates and ferrites dissolution, used also the solution of sucrose or KOH in water.

References

1. Budnikov, P.P., Ginstling, A.M.: Reakcii w smiesiach twiordych wieszczestv. Strojizdat, Moscow (1965) (in Russian)
2. De Keyser, W.L.: Bull. Soc. Chim. Belg. **62**, 235 (1952)
3. Jander, W., Hoffman, E.Z.: Anorg. Chem. **218**, 211 (1934)
4. Kurdowski, W.: Silicates Ind., **30**, 500 (1965)
5. Weisweiler, W., Osen, E., Eck, J.: Cem. Concr. Res. **16**, 283 (1986)
6. Kurdowski, W., Deja, J.: 9th ICCC, New Delhi, t. II, p. 255, New Delhi (1992)
7. Zhuravlev, W.F., Lasotin, J.G., Tempelman, R.C.: Ż. prikł. chim. **21**, 887 (1948) (in Russian)
8. De Keyser, W.L.: Bull. Soc. Chim. Belg. **64**, 395 (1955)
9. Rouanet, A.: 8th ICCC Rio de Janeiro, t. II, p. 25, Rio de Janeiro (1986)
10. Moore, A.: Cement Technology. **7**(85), 134 (1976)
11. Deren, J., Pampuch, R., Haber, J.: Chemia ciała stałego. PWN, Warszawa (1975) (in Polish)
12. Haber, J., Ziółkowski, J.: Proc. 7th Int. Symp. Reactivity of Solids, Munich 1964, p. 162, Elsevier, Amsterdam (1965)
13. Babushkin, W.J., Matveev, G.M., Mchedlov–Petrossian, O.P.: Thermodynamics of Silicates, Strojizdat, Moscow (1986) (in Russian)
14. Kondo, R., Choi San–Heul: 5th ICCC Tokyo, t. I, p. 163, Tokyo (1968)
15. Johansen, V.: J. Am. Ceram. Soc. 56, 450 (1973)
16. Heilmann, T.: 4th ICCC Washington, t. I, p. 87. Washington (1960)
17. Johansen, V., Christensen, N.H.: Cem. Concr. Res. 9, 1 (1979)
18. Stoch, L.: Clay Minerals. Wydawnictwo Geologiczne, Warszawa (1974) (in Polish)
19. Tamas, F.D.: Cem. Concr. Res. 1, 27 (1971)
20. Hedvall, J.A.: Einführung in die Festkörper Chemie. Friedr. VJW EEG Sohn, Braunschweig (1952)
21. De Keyser, W.L.: Bull. Soc. Chim. Belg. 63, 40 (1954)
22. Glasser, F.P.: In: Barnes P. (ed.) Structure and Performance of Cements, chap. 2, Applied Science Publishers, London, p.69 (1983)
23. Ritzmann, H.: Zement–Kalk–Gips 24(8), 338 (1971)
24. Lea, F.M.: The Chemistry of Cement and Concrete. Chemical Publ. Comp. Inc., New York (1972)
25. Taylor, H.F.W.: In: Taylor HFW. (ed.) The Chemistry of Cements. Academic Press, London (1964)
26. Bogue, R.H.: The Chemistry of Portland Cement. Reinhold Publ. Corp., New York (1955)
27. Imlach, J.A., Dent–Glasser L.S., Glasser F.P.: Cem. Concr. Res. 1, 57 (1971)
28. Żmoidin, G.J., Chatterjee, A.K.: Cem. Concr. Res. 14, 386 (1984); 15, 442 (1985)
29. Brisi, C., Borlera, M.L.: Il Cemento, 80(3), 153 (1983); 81, 187 (1984)
30. Malquori, G., Cirilli, V.: 3rd ICCC London, p. 120. London (1955)
31. Majumdar, A.J.: Trans. Brit. Cer. Soc., 64(2), 105 (1965)
32. Moore, A.E.: Mag. Concr. Res. 18(55), 59 (1966)
33. Schlaudt, C.M., Roy, D.M.: Nature 206(4986), 819 (1965)
34. Tartre, P.: Nature 207(5000), 973 (1965)
35. Guinier, A., Regourd, M.: 5th ICCC Tokyo, vol. I, p. 1. Tokyo (1968)
36. Welch, J.H.: In: Taylor, HFW. (ed.) The Chemistry of Cements, p. 49. Academic Press, London (1964)
37. Swayze, M.A.: Am. J. Sci. 244(1), 65 (1946)
38. Butt, J.M., Timashev, W.W., Osokin, A.P.: 6th ICCC Moscow, vol. I, p. 132. Strojizdat, Moscow (1976) (in Russian)
39. Timashev, W.W.: 7th ICCC Paris, vol. I, p. I–3/1. Paris 1980
40. Wachtler, H.J., Zozula, P.W., Sychev, M.M., Shubina, J.J.: Sbor. Trud. Leningradzkogo Techn. Inst., p. 50, (1975) (in Russian)
41. Endell, K., Hendrikx, G.: Zement 31, 416 (1942)

42. Maki, J.: 8th ICCC Rio de Janeiro, vol. I, p. 34, Rio de Janeiro (1986)
43. Maki, J.: Cem. Concr. Res. 14, 413 (1984)
44. Burton, I.A., Prim R.C., Slichter W.P.: J. Chem. Phys. 21, 1987 (1953)
45. Chatterjee, T.K.: In: Ghosh, S.N. (ed.) w Advances in Cement Technology, p. 69. Pergamon Press, Oxford (1983)
46. Smith, J.V.: Acta Cryst. 13, 454 (1960)
47. Trojer, F.: Zement–Kalk–Gips 30, 40 (1977)
48. Klucharov, J.W., Caenko, N.S.: Nieorg. Mat. 4, 670 (1976) (in Russian)
49. Gutt, W., Osborne, G.J.: Trans. Brit. Ceram. Soc. 67, 125 (1968); 69, 125 (1970)
50. Gutt, W.: 5th ICCC Tokyo, vol. I, p. 93, Tokyo (1968)
51. Gilioli, C., Massazza, F., Pezzuoli, M.: Cem. Concr. Res. 9, 295 (1979)
52. Damao, T., Zongshon, L.: 8th ICCC Rio de Janeiro, vol. II, p. 117. Rio de Janeiro (1986)
53. Gimenez–Molina, S., Blanco–Varela, M.T., Marr, M., Glasser, F.P.: Adv. Cem. Res. (4), 81 (1991/2)
54. Osokin, A.P., Potapova, E.N.: Silikattechnik, 7, 229 (1989)
55. Blanco–Varela, M.T.: Cem. Concr. Res. 16, 97 (1986)
56. Odler, I., Zhang, H., Ceramics Bulletin: p. 43, 5. Seminarium Ceramiczne, Zakopane (1992)
57. Trivino, E., Vasquez, F.: Cem. Concr. Res. 12, 455 (1982)
58. Borgholm, H.E.: A new heat recovery and desulphurization plant for 4 wet kilns in Aalborg. Portland, Aalborg Portland (1992)
59. Borgholm, H.E., Herfort, D., Soren Rasmussen: World Cement Research (8), 27 (1995)
60. Moir, G.K., Glasser, F.P.: 9th ICCC New Delhi, vol. I, p. 794. New Delhi (1992)
61. Goswami, G., Mohaparta, B.N., Panda, J.D.: p. 375. VDZ Congress, Düsseldorf (1993)
62. Kurdowski, W., Sobon, M.: J. Therm. Anal. 112 (1992)
63. Roy, D.M., Sarkar, A.K.: In: Skalny Jan (ed.) w Cement Production and Use, p. 51. Franklin Pierce College Rindge, New Hampshire (1979)
64. Kurdowski, W., Garbacik, A.: Ceramika, nr 30, p. 47. PAN, Kraków (1980) (in Polish)
65. Poletaev, I.R., Ismailov, A.J., Ludomirska, A.P.: Ż. nieorg. chim. 21, 2281 (1976) (in Russian)
66. Garbacik, A.: Przyspieszenie procesu syntezy krzemianu dwuwapniowego przez dodatek chlorku wapniowego. Ph. D. Thesis, Academy of Mining and Metallurgy, Kraków (1980)
67. Nudelman, B., Bikbau, M., Sviecicki, A., Ilushin, W.: 7th ICCC Paris, vol. III, p. V–169. Paris (1980)
68. Boikova, A.: 8th ICCC Rio de Janeiro, vol. I, p. 19. Rio de Janeiro (1986)
69. Massazza, F., Gilioli C.: Il Cemento, 80, 101 (1983)
70. Kurdowski, W., Garbacik A.: 7th ICCC Paris, vol. IV, p. 702, Paris (1980)
71. Massazza, F.: 8th ICCC Rio de Janeiro, vol. II, p. 179. Rio de Janeiro (19860
72. Gutt, W., Smith, M.A.: Trans. Brit. Ceram. Soc. 66, 557 (1967); 67, 487 (1968)
73. Kurdowski, W., Thiel, A.: Beijing Internal Symp. on Cement and Concrete, p. 158. China Academic Publ., Beijing (1985)
74. Nurse, R.W.: J. Appl. Chem. 2, 708 (1952)
75. Kurdowski, W.: In: Ghosh, S.N. (ed.) Advances in Cement Technology, p. 115. Pergamon Press, Oxford (1983)
76. Woermann, E.: 4th ICCC Washington, vol. I, p. 119. Washington (1960)
77. Suzukawa, Y., Sasaki, T.: ibid., p. 83
78. Ponomarev, J.F., Gayadjourov, P.O., Zoubelhin, A.P., Kitaev, W.W.: 7th ICCC Paris, vol. II, pp. 1–166. Paris (1980)
79. Ono, M., Akita, M., Hikita, K.: ibid., vol. II, p. 1/124
80. Sylla, H.M.: Zement–Kalk–Gips 34, 618 (1981)
81. Vernet, C.: 8th ICCC Rio de Janeiro, vol. II, p. 146. Rio de Janeiro (19860
82. Chromy, S., Weber, M. Zement–Kalk–Gips 34, 453 (1981)
83. Forest, J.: Silicates Ind. 32, 373, 427 (1967)
84. Sylla, H.M.: Zement–Kalk–Gips 30, 487 (1977)
85. Trojer, F., Kozlowski, A.: Radex Rdsch. (5), 329 (1972)
86. Amafuji, M., Tsumagari, A.: 5th ICCC Tokyo, vol. I, p. 136. Tokyo (1968)

87. Kurdowski, W.: Cement–Wapno–Gips 39, 74 (1986)
88. Christensen, N.H., Simonsen, K.A.: J. Am. Ceram. Soc. 53, 361 (1970)
89. Wolter, A.: 8th ICCC Rio de Janeiro, vol. II, p. 89, Rio de Janeiro (1986)
90. Wächtler, H.J., Jannsen, W.: Silikattechnik 34, 205 (1983)
91. Wolter, A.: Zement–Kalk–Gips 43, 429 (1990)
92. Kurdowski, W.: Cement–Wapno–Gips 36, 133 (1983)
93. Fundal, E.: World Cement 10, 195 (1979)
94. Mac Gregor, F.: Rock Prod. 83, 152 (1980)
95. Eitel, W., Richter, H.: Zement 31, 505 (1942)
96. zur Strassen, H.: Zement 30, 231 (1941); Zement–Kalk–Gips, 10, 1 (1957)
97. Gygi, H.: 3rd ICCC London, p. 750. London (1955)
98. Castanet, R., Sorrentino, F.P.: 8th ICCC Rio de Janeiro, vol. II, p. 36. Rio de Janeiro (1986)
99. Jeffery, J.W.: Acta Cryst. 5, 26 (1952)
100. Regourd, M., Guinier, A.: 6th ICCC Moscow, vol. I, p. 25. Moscow (1974) (in Russian)
101. Handke, M., Ptak, M., Jurkiewicz, E.: Ann. Chim. Fr. **4**, 145 (1979)
102. Gołowiestnikow, I.L, Matsiejewa, R.G., Biełow, N.W.: Kristałłografija **20**, 721 (1975)
103. Regourd, M.: In: Barnes, P. (ed.) Structure and Performance of Cements, p. 109. Applied Science Publ., London (1983)
104. Maki, J., Chromy, S.: Cem. Concr. Res. **8**, 407 (1978)
105. Bigaré, M.: Rev. Mat. Constr. (598–599), 325; (600), 394 (1965)
106. Bigaré, M., Guinier, A., Mazieres, C., Regourd, M., Yannaquis, N., Eysel, W., Hahn, T., Woermann, E: J. Am. Ceram. Soc. **50**, 609 (1967)
107. Kurdowski, W., Wollast, R.: Silicates Ind. **35**, 153 (1970)
108. Yamaguchi, C., Uchikawa, H.: Zement–Kalk–Gips 14, 497 (1961)
109. Woermann, E., Hahn, T., Eysel, W.: Zement–Kalk–Gips **16**, 370 (1963)
110. Kurdowski, W., Handke, M., Siemiński, G.: 7th ICCC Paris, vol. II, p. I–282. Paris (1980)
111. Hahn, T., Eysel, W., Woermann, E.: 5th ICCC Tokyo, vol. I, p. 61. Tokyo (1968)
112. Fletcher, K.E.: Trans. Brit. Ceram. Soc. **64**, 377 (1965)
113. Boikova, A.L.: 5th ICCC Tokyo, vol. I, p. 234. Tokyo (1968)
114. Sakurai, T., Sato, T., Yoshinaga, A.: 5th ICCC Tokyo, vol. I, p. 300. Tokyo (1968)
115. Toropov, N.A.: 5th ICCC Tokyo, vol. I, p. 49. Tokyo (1968)
116. Toropov, N.A., Boikova, A.L.: Dokł. Akad. Nauk SSSR **154**, 1114 (1963); **156**, 1428 (1964) (in Russian)
117. Boikova, A.L.: Cemient **9**, 6 (1982)
118. Boikova, A.L., Toropo, N.A., Vavilonova, W.T.: Dokł. Akad. Nauk SSSR **159**, 654 (1967) (in Russian)
119. Kondo, R., Yoshida, K.: 5th ICCC Tokyo, vol. I, p. 262. Tokyo (1968)
120. Boikova, A.I.: Proc. ninth Conf. on the Silic. Ind. Budapest 1967, p. 41. Akadémiai Kiadó, (1968)
121. Toropov, N.A., Degen, M.G., Boikova, A.I.: Silikattechnik **22**, 400 (1971)
122. Fierens, P., Thauvoye, M., Yerhaegen, J.P.: Il Cemento **69**, 211 (1972)
123. Kurdowski, W.: Wpływ dodatku baru na własności klinkieru portlandzkiego, Ceramika, nr 18. PAN, Kraków (1972) (in Polish)
124. Mascolo, G., Marchese, B., Frigione, G., Sersale, R.: J. Am. Ceram. Soc. **56**, 222 (1973)
125. Terrier, P., Hornain, H., Socroun, G.: Rev. Mat. Constr. (630) (1968), 109; (640), 1 (1969)
126. Mohan, K., Glasser, F.P.: Cem. Concr. Res., **7**(1) 269, 379 (1977)
127. Niesel, K., Thormann, P.: Tonind. Ztg, **91**, 362 (1967)
128. Nurse, R.W.: 3rd ICCC London, p. 56. London (1955)
129. Suzuki, K., Yamaguchi, G.: 5th ICCC Tokyo, vol. I, p. 67. Tokyo (1968)
130. Midgley, H.: Acta Cryst. **5**, 307 (1952)
131. Eysel, W., Hahn, T.: Z. Krystall. **131**, 322 (1970)
132. Yannaquis, N., Guinier, A.: Bull. Soc. Franc. Miner. Crist. **82**, 126 (1959)
133. Gawlicki M., Ceramika/Ceramics, Z104, Kraków 2008 (in Polish)
134. Chromy, S.: Zement–Kalk–Gips **23**(8), 382 (1970)

135. Lehmann, H., Niesel, K., Thormann, P.: Tonind. Ztg **93**(6), 197 (1969)
136. Guinier, A., Yannaquis, N.: Comp. Rend. **244**, 2623 (1957)
137. Niesel, K.: Silicates Ind. **37**, 136 (1972)
138. Smith, D.K., Majumdar, A.J., Ordway, F.: Acta Cryst. **18**, 787 (1965)
139. Grzymek, J., Skalny, J.: Tonind. Ztg **91**(4), 128 (1967)
140. Yannaquis, N., Guinier, A.: 4th ICCC Washington, vol. I, p. 21. Washington (1960)
141. Roy, R.: 4th ICCC Washington, vol. I, p. 29. Washington (1960)
142. Roy, D.M.: J. Am. Ceram. Soc., **41**, 293 (1958)
143. Midgley, H.G.: 6th ICCC Moscow vol. I, p. 63. Moscow (1974) (in Russian)
144. Newmann, E.S., Wells, L.S.: J. Res. Nat. Bur. Stand. **34**, 137 (1946)
145. Zerfoss, S., Davis, H.M.: J. Am. Ceram. Soc. **26**, 302 (1943)
146. Thilo, E., Funk, H.: Z. Anorg. Allg. Chem. **273**, 28 (1953)
147. Schwiete, H.E., Krönert, W., Deckert, K.: Zement–Kalk–Gips **57**, 359 (1968)
148. Butt, J.M., Timashev, W.W.: Portłandcemientnyj klinkier, Izd. Lit. po Stroitielstwu, Moscow (1967)(in Russian)
149. Dietzel, A., Tscheischwili, L.: Ber. Deutsch. Keram. Ges. **30**, 151 (1953)
150. Green, K.T.: J. Res. Nat. Bur. Stand. **32**, 1 (1944)
151. Schlaudt, C.M., Roy, D.M.: J. Am. Ceram. Soc. **49**, 430 (1966)
152. Struillou, R., Arnould, M.: 7th ICCC Paris, vol. III, p. V–75, Paris (1980)
153. Regourd, M., Bigare, J., Forest, A., Guinier, A.: 5th ICCC Tokyo, vol. I, p. 427. Tokyo (1968)
154. Görlich, E., Handke, M.: Cement–Wapno–Gips **28**, 100 (1973) (in Polish)
155. Toropov, N.A., Fiedorov, N.F.: Ż. prik. chim. **35**, 2156, 2548 (1962) (in Russian)
156. Suzuki, K.: 7th ICCC Paris, vol. II, pp. 11–47, Paris (1980)
157. Boikova, A.: 7th ICCC Paris, vol. II, pp. 1–7, Paris (1980)
158. Midgley, H.G., Bennet, M.: Cem. Concr. Res., **1**, 413 (1971)
159. Sarker, S.L., Jeffery, J.W.: J. Am. Cer. Soc., **61**, 177 (1978)
160. Terrier, P., Hornain, H.: Rev. Mat. Constr. (619), 123, 135 (1967)
161. Metzger, A.T.: Zement–Kalk–Gips **6**, 269 (1953)
162. Midgley, H.G.: 5th ICCC Tokyo, vol. I, p. 226. Tokyo (1968)
163. Mondal, P., Jeffery, J.W.: Acta Cryst. **B31**, 689 (1975)
164. Takeuchi, Y., Nishi, F., Maki, J.: 7th ICCC Paris, vol. IV, p. 426, Paris (1980)
165. Lee, F.C., Banda, H.M., Glasser, F.P.: Cem. Concr. Res. **12**, 237 (1982)
166. Regourd, M.: 7th ICCC Paris, vol. IV, p. 415, Paris (1980)
167. Tavasci, B., Massazza, F.: Costa V., ibid., vol. IV, p. 452
168. Regourd, M.: Il Cemento **3**, 323 (1978)
169. Han, K.S., Gard, J.A., Glasser, F.P.: Cem. Concr. Res. **11**(1), 79 (1981)
170. Imlach, J.A., Glasser, F.P.: Trans. Brit. Ceram. Soc. **70**, 227 (1971); **72**, 221 (1973)
171. Goudrin, P., Demoulian, E.H., Hawthorn, F., Vernet, C.: 7th ICCC Paris, vol. II, pp. 11–212. Paris (1980)
172. Ghosh, S.N.: ibid. vol. II, pp. 11–18
173. Boikova, A.I., Domanski, A.L., Ponomaroya, V.A., Staickaya, G.P., Nikushchenko, V.M.: Cem. Concr. Res. **7**, 483 (1977)
174. Kurdowski, W., Wieja, K., Handke, M.: Ceramika, nr 38. PAN, Kraków (1989) (in Polish)
175. Bertaut, E.F., Blum, P., Sagnières, A.: Acta Cryst., **12**, 149 (1959)
176. Smith, D.K.: Acta Cryst. **15**, 1146 (1962)
177. Woermann, E., Hahn, T., Eysel, W.: Am. Ceram. Soc. Bull. **44**, 299 (1965)
178. Sakurai, T., Sato, T.: 5th ICCC Tokyo, vol. I, p. 221. Tokyo (1968)
179. Tartre, P.: Nature, **207**, 973 (1965)
180. Copeland, L.E., Brunauer, S., Kantro, D.L., Schultz, E.G., Weise, C.H.: Anal. Chem. **31**, 1521 (1959)
181. Yamaguchi, G., Takagi, S.: 5th ICCC Tokyo, vol. I, p. 181, Tokyo (1968)
182. Brisi, C., Rolando, P.: Ind. Ital. del Cemento **1**, 37 (1967)

183. Barnes, P., Ghose, A.: In: Barnes, P. (ed.) Structure and Performance of Cements, p. 172. Appl. Science Publ., London (1983)
184. Moore, E.: 7th Conference on the Silicate Industry, Budapest 1963, p. 669. Akademiai Kiadó, Budapest (1965)
185. Peterson, O.: Zement–Kalk–Gips **20**(2), 61 (1967)
186. Pollitt, H.W.W., Brown, A.W.: 5th ICCC Tokyo, vol. I, p. 322. Tokyo (1968)
187. Mauder, J.E., Skalny, J.: Ceram. Bull. **56**, 987 (1977)
188. Fundal, E.: 8th ICCC Rio de Janeiro, vol. II, p. 139. Rio de Janeiro (1986)
189. Nurse, R.W.: 5th ICCC Tokyo, vol. I, p. 77. Tokyo (1968)
190. Kurdowski, W.: 6th ICCC Moscow, vol. I, p. 203, Moscow 1974 (in Russian)
191. Guttmann, A., Gille, F.: Zement, **18**, 500, 537, 570 (1929)
192. Knöfel, D., Strunge, J., Bambauer, H.V.: Zement–Kalk–Gips **36**, 402 (1983)
193. Kondo, E., Yoshida, S.: 5th ICCC Tokyo, vol. I, p. 262. Tokyo (1968)
194. Fierens, P., Thauvoye, M., Verhaegen, J.P., Il Cemento, **71**, 3 (1974)
195. Knöfel, D.: Zement–Kalk–Gips **30**, 191 (1977)
196. Midgley, H.G.: 5th ICCC Tokyo, vol. I, p. 226, Tokyo (1968)
197. Syczov, M.M., Kornieev, W.J., Fiedorov, N.F.: Alit i bielit w portłandcemientnom klinkierie. Strojizdat, Moscow 1965 (in Russian)
198. Gaillard, J., Magnan, R., Vibert, C.: Rev. Mat. Constr. (680), 24 (1973)
199. Kalarus, D., Nocuń–Wczelik, W.: Cement Wapno Beton **74**, 75 (2008)
200. Bordoloi, D., Baruah, A. Ch., Barkakati, P., Borthakur, P. Ch.: Cem. Concr. Res. **28**, 329 (1998)
201. Kakali, G., Parissakis, G.: Cem. Concr. Res., **25**, 79 (1995)
202. Kakali, G., Tsivilis, S., Tsialtas, A.: Cem. Concr. Res. **28**, 3345 (1998)
203. Murat, M., Sorrentino, F.: Cem. Concr. Res. **26**, 377 (1996)
204. Fernandez, Olmo I., Chacon, E., Irabien, A.: Cem. Concr. Res. **31**, 1213, (2001)
205. Stephan, D., Mallmann, R., Knöfel, D., Härdtl, R.: Cem. Concr. Res. **29**, 1949 (1999)
206. Andrade, F.R.D., Maringolo, V., Kihara, Y.: Cem. Concr. Res. **33**, 63 (2003)
207. Kakali, G.: Cem. Concr. Res. **25**, 79 (1995)
208. Kolovos, K., Barafaka, S., Kakali, G., Tsivilis, S.: Ceramics **49**, 205, (2005)
209. Barbarulo, R., Sorrentino, F., Sing, C.: 12th ICCC. W3-09.5 Montreal, Canada, (2007)
210. Gineys, N.: Influence de la teneur en elements métallique du clinker sur les proprietes techniques et environnementales du ciment Portland, thèse, Université Lille Nord de Franç̧e, (2011)
211. Bolio–Arcero, H., Glasser, F.P.: Adv. Cem. Res. **10**, 25, (1998)
212. Barbanyagre, V.D., Timoshenko, T.I., Ilyinets, A.M., Shamshurov: Power Diffraction **12**, 22, (1997)
213. Matusiewicz, A., Bochenek, A., Szelag, H., Kurdowski, W.: Cement Wapno Beton **78**, 332, (2011)
214. Bochenek, A.: Unpublished results
215. Kakali, G., Parissakis, G., Bouras, D.: Cem. Concr. Res. **26**, 1473 (1996)
216. Kurdowski, W., Szumer, A., Silicates Ind. **33**, 183 (1968)
217. Newkirk, T.F.: 3rd ICCC London, p. 151. London (1955)
218. Taylor, H.F.W.: Cement Chemistry. Academic Press, London (1990)
219. Aldrige, L.P.: Cem. Concr. Res. **12**, 381 (1982)
220. Mikroskopie des Zementklinkers: Beton–Verlag GmbH, Düsseldorf (1965)
221. Kurdowski, W., Wieja, C.: Cement–Wapno–Gips **32**, 345 (1965)
222. Maki, I.: Cement–Wapno–Beton **73**, 65 (2006)
223. Rietveld, H.M.A.: J. Appl. Crystallogr. **2**, 65 (1969)
224. Gutteridge, W.A.: Cem. Concr. Res. **9**, 319 (1979)

Chapter 3
Hydration of Clinker Phases

3.1 Introduction

The reaction of cement with water is a very complex process; for a long time it has been the subject of numerous discussions and controversies. The contradictory opinions derived from the crystallization theory proposed by Le Chatelier and the colloidal concept announced by Michaelis return again and again in the renewed theories and reaction schemes. There are some serious questions as the mechanism of reaction, particularly at early age, is concerned; the factors leading to an apparent hindering of reaction in the so–called induction period are not completely understood.

These discussions and doubts result first of all from the complexity of reaction of unhydrous cement phases with water. This can be illustrated taking into account a simple, on a first appearance, example of gypsum hemihydrate hydration. This reaction served as a basis of Le Chatelier's crystallization theory. The uncomplicated, at first sight, reaction:

$$CaSO_4 \cdot 0.5H_2O + 1.5H_2O \rightarrow CaSO_4 \cdot 2H_2O \tag{3.1}$$

does not consists in the simple incorporation of water to the solid, but it is an effect of several unit processes, following each other, viz the dissolution of the solid phase with the formation of oversaturated solution of hemihydrate, nucleation of the new phase, and finally the crystal growth. Therefore, according to the Le Chatelier's theory the dissolution of solid phase and crystallization of hydrate from the solution takes place. After the initiation of reaction these two processes occur simultaneously and the rate of reaction is determined by the slowest one.

The studies of hydration process reveal that the mechanism at early age is more sophisticated [1]. It is not only the break down of the bonds in crystal structure by water molecules (an endothermic process with thermal effect corresponding to lattice energy) and the transport of ions (or molecules) into the solution with their simultaneous hydration (an exothermic process).

Just after the contact of water with the hemihydrate grains water molecules are absorbed by the solid and a type of solid solution in the sulphate hemihydrate

W. Kurdowski, *Cement and Concrete Chemistry*,
DOI 10.1007/978-94-007-7945-7_3, © Springer Science+Business Media B.V. 2014

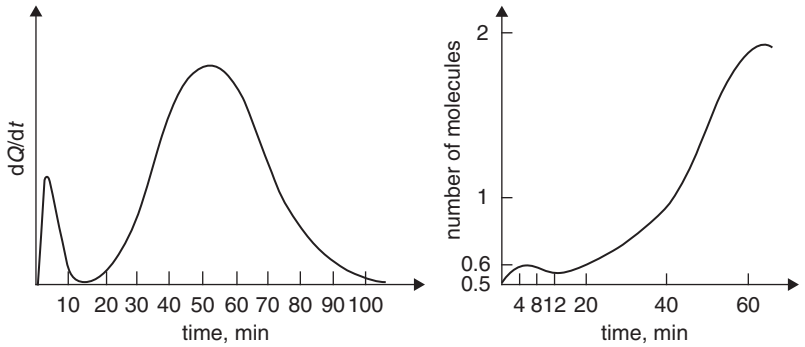


Fig. 3.1 H_2O content increase in the hydrating hemihydrate phase versus hydration time. (After [1])

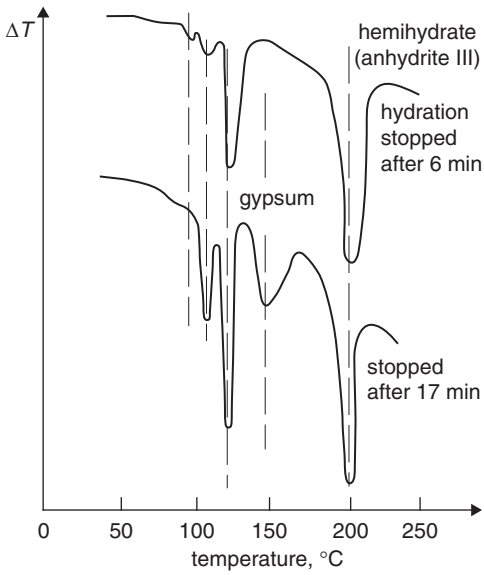


Fig. 3.2 DTA curves of hydrating hemihydrate after different hydration time. (After [1])

is formed (Fig. 3.1). This is proved by the change of water content in the range from 0.1 to 0.66 mol; this corresponds to the proportions from $CaSO_4 \cdot 0.1H_2O$ to $CaSO_4 \cdot 0.66H_2O$. As it was reminded by Magnan et al. [1], Flörke had proved that the additional water molecules can be located in the hemihydrate lattice along the *c* axis. In the second stage of the process the adsorption of water molecules occurs in the preferential positions in active centres on the surface of hemihydrate. In the third stage the layer of liquid poorly adherent to the solid, surrounds the hydrating grains.

The three endothermic peaks at temperatures 80, 110 and 120 °C respectively are attributed to the aforementioned three types of water (Fig. 3.2). In the loosely bound layer of water the dissolution of hemihydrate is facilitated and when the

supersaturation in relation to gypsum is attained, the heterogeneous nucleation of this phase on the surface of gypsum hemihydrate takes place. Simultaneously, the maximum concentration of Ca^{2+} and $[SO_4]^{2-}$ ions in the interface layer is achieved.

The complexity of any individual binder reaction with water is well illustrated on the example of gypsum hemihydrate hydration. The hydration process in the case of multiphase material as Portland cement is, must be much more complex. The reactions of individual cement phases with water occur simultaneously and interfere; the presence of minor components, first of all alkalis and sulphates, modifies further the composition of the liquid phase. Therefore the rate of hydration of basic cement phases is strongly affected.

It should be remember that the hydration of cementitious materials is a heterogeneous process; therefore among the rate controlling agents are not only the state parameters, such as temperature, pressure and concentration, but also the other factors. The most important are the fineness of the solid, the surface constitution and the presence of crystals structural defects.

The following unit processes can be distinguished in any hydration reaction mechanism:

- reactions at the phase boundaries,
- formation of nuclei, called nucleation,
- transport of mass from the substrates to the products; this occurs basically through diffusion,
- processes of hydrate crystals growth—crystallization.

The composition of the liquid phase co-existing with the solid, as it has been mentioned above, is of special importance in the hydration process. This system is far from the equilibrium and at the usual water content on the level 33 % approximately (w/c = 0.5), there are the micro–areas of different composition. Simultaneously, the diffusion becomes more and more difficult as the hydrates are formed. The gradients of concentrations appear, as well as the differences of temperature between the particular micro-areas. Therefore the image of the process becomes more sophisticated. To simplify this, we take into account the model, three-component systems: $CaO–SiO_2–H_2O$ or $CaO–Al_2O_3–H_2O$ which correspond to the calcium silicate or calcium aluminate hydration. However, the processes occurring in these simplified systems are complex, as one could conclude from the aforementioned considerations.

3.2 Silicate Hydration

3.2.1 Tricalcium Silicate Hydration

The tricalcium silicate hydration, and as a matter of fact, the tricalcium silicate hydrolysis is of special importance, because this phase is a dominant component of Portland cement clinker, constituting more than 60 %. Moreover, the tricalcium silicate hydration is often considered as a good model of cement reaction with water.

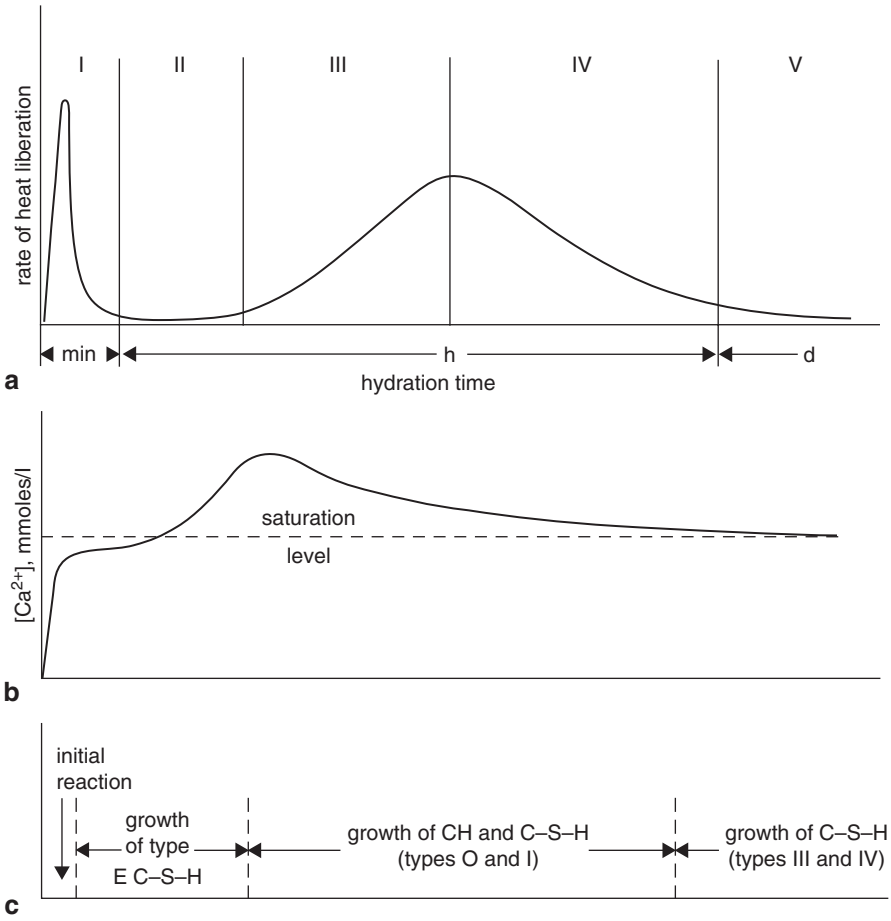


Fig. 3.3 Microcalorimetric curve of C_3S (**a**), change of Ca^{2+} ions concentration in the liquid phase (**b**), formation of hydrates (**c**). (According to [2])

The reaction of tricalcium silicate with water is a complex heterogeneous process with not fully recognized mechanism. It occurs with the formation of calcium silicate hydrate C–S–H and calcium hydroxide. The relationship between these two products is given by the schematic equation:

$$2C_3S + 6H \rightarrow C_3S_2H_3 + 3CH \tag{3.2}$$

This equation can be considered only as a starting point in the discussion dealing with the mechanism of reaction because, as it will be shown later, the C/S ratio in the C–S–H, as well as the H/S ratio are variable; calcium hydroxide is the only well defined hydrate phase.

It is convenient to use for the discussion of hydration process the microcalorimetric curve obtained in the isothermal conditions, reflecting the rate of heat evolution vs. time (Fig. 3.3). This curve can be compared with the plot of calcium ions

concentration in the liquid phase vs. time, basing on the approach presented by other authors. The hydrated phases formed in the reacting mixture are also indicated. The five stages of reaction can be distinguished on the calorimetric curve, namely: the pre–induction, induction (II), hydration rate increase, hydration rate decrease and low hydration rate respectively [2, 3]. Simultaneously one can notice that the process starts very quickly, independently that the total heat evolved during the first stage is not too high, however, the heat flux is rather intensive and the accompanying calcium ions concentration growth is rapid. A substantial amount of silica appears also and the C/S ratio is close to 3, but falls down quickly as a result of decreasing concentration of silica.

The initial stage of C_3S reaction with water arouses some controversial opinions and two hypotheses are presented:

- congruent dissolution,
- incongruent dissolution with the formation of silica rich layer on the surface of C_3S.

These hypotheses are difficult for the experimental verifications because of several reasons. At first the concentration of silica in the solution is very low (micromoles per kg) and cannot be precisely measured. Secondly, it is difficult to separate the C–S–H formed from the surface of C_3S crystals—the intensive stirring of the mixture is not sufficient. Additionally, the layer of C–S–H gel is very compact, tight and poorly permeable for the liquid phase.

The authors favouring the hypothesis of the incongruent dissolution are of the opinion that only the calcium ions are released into solution and the solid transforms into the "silicate skeleton" with low calcium content [2, 4, 5]. This product is absorbing calcium ions from the solution and the C–S–H is produced, as a result of topochemical reaction. The proof of this mechanism was based by these authors on the measured positive values of ξ potential [4].

In the middle eighties the strong experimental proofs supporting the hypothesis consisting in the C_3S congruent dissolution were published. This congruent dissolution was proved by Barret et al. [6] who found that the increase of C/S ratio in the solution above 3 should be attributed to the formation of C–S–H. Several experiments were carried out in the open and closed systems [7–9]: water was put through the C_3S layer on the filter in such a way that the contact between the liquid and solid was very short, about 0.11 s. The C and S concentrations are then only a little higher than the saturation level for C–S–H, at low nucleation rate. When the C–S–H precipitation is not possible, the C/S ratio in solution is equal 3. The crystallization of C–S–H gives immediately the C/S growth. The C–S–H composition was also examined and the known ratio C/S in the range between 1 and 2 was found, the H/S ratio was less variable, oscillating around 2.5.

The studies of Barret et al. [7] (closed system) allowed to establish the curves: of super–solubility, oversaturation of solution in relation to the C–S–H, as well as the curves of metastable equilibriums, corresponding to the supersaturated solutions. These curves were plotted in the $CaO–SiO_2–H_2O$ system at the temperature 21 °C (Fig. 3.4). It is worthwhile to remind also the classic Flint and Wells curve (Fig. 3.4). The two branches of this curve can be distinguished. The *CD* (Fig. 3.4) corresponds

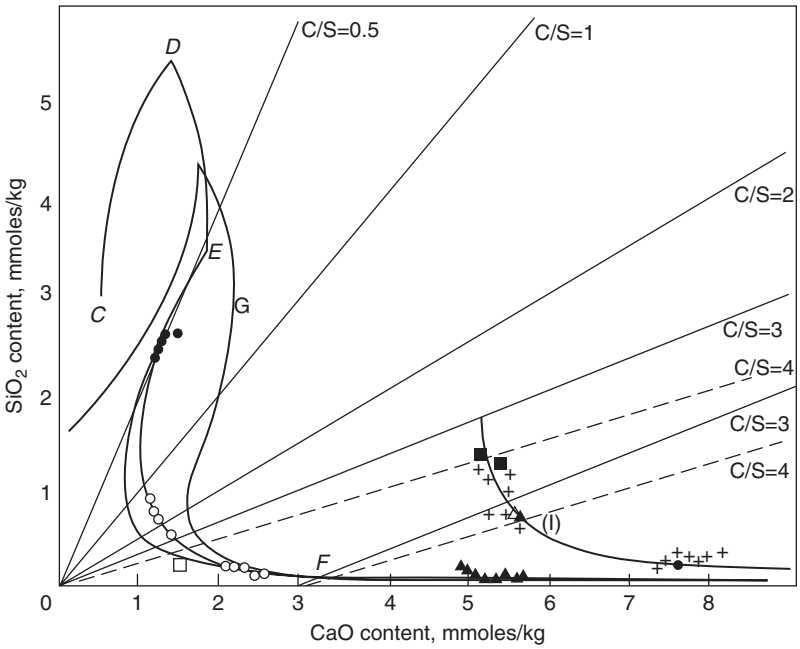


Fig. 3.4 Solubility curves of C–S–H in the system CaO–SiO_2–H_2O at temperature 25 °C [according to Flint and Wells, as well as Greenberg (G)]. The C_3S solubilities on the filter at 21 °C according to [9] are added: I—dissolution in water (+), in lime solution $3.06 \cdot 10^{-3}$ mol/kg (Δ) and $6.78 \cdot 10^{-3}$ mol/kg (■); experimental points for C–S–H: 500 mg in water (●), 250 mg in lime solution $3.95 \cdot 10^{-3}$ mol/kg (○), 50 mg in lime solution $2.88 \cdot 10^{-3}$ mol/kg (□) and $6.78 \cdot 10^{-3}$ mol/kg (▲)

to the solubility of silica gel with adsorbed calcium ions; *EF* is the C–S–H II solubility curve; *E* is an invariant point, corresponding to the equilibrium between these two phases and the solution. The C/S molar ratio of C–S–H increases continually from the point *F*, until the portlandite dissolution limit. In Fig. 3.4 the supersolubility curve (I), which is the limit between the low and high nucleation rate of C–S–H I, is plotted (Fig. 3.5). Between the I and *F* curves there is a field of the supersaturate, metastable solutions. The curve 1 is linking the [C] and [S] concentrations for the water to solid ratio = 1,000, and the curve 1' for the w/s = 100 (Fig. 3.5). The last one corresponds to a little higher supersaturation. The curves 2, 3 and 8 correspond to the $(C/S)_s$ ratio in the solution = 1. These curves can be obtained in the case when the C_3S is processed with the calcium hydroxide solution or when the filtrate (produced by separation of solid with hydrates) is stored separately.

Vernet [10] is also of the Barret's opinion that the curve I corresponds to certain dynamic state in which the concentration in the liquid phase results from the C_3S solubility and C–S–H crystallization rate (Fig. 3.6).

Jennings [11] was of the opinion that the curve I (*B* in Fig. 3.7), which according to Barret is the C–S–H supersolubility curve, is in fact the dissolution curve of the second C–S–H modification, different from the C–S–H which dissolves along the *A* curve (Fig. 3.7). He supports his view by presenting many results reported by different authors, which fit to the well–defined curve. Moreover, he

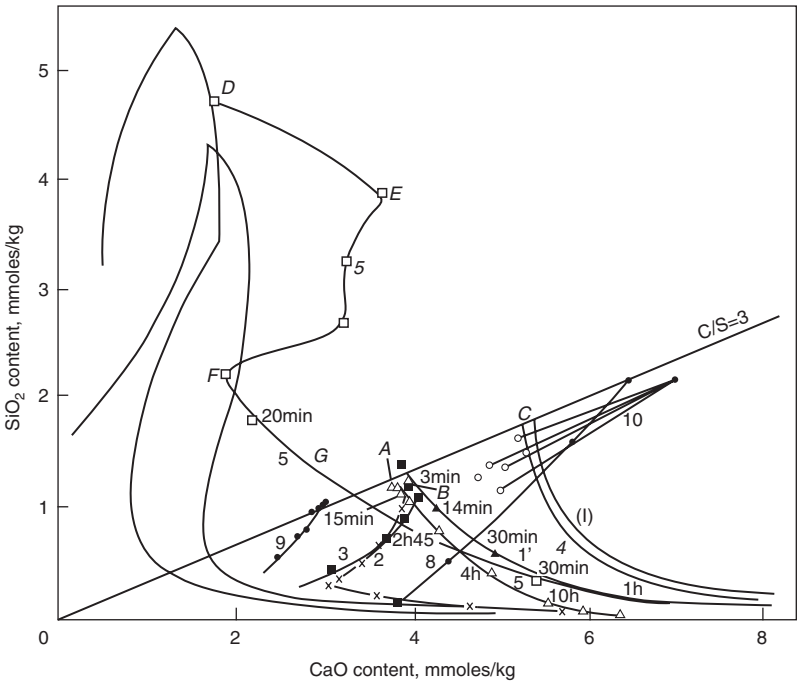


Fig. 3.5 The experimental results of Barret, Menetrier and Bertrandie [7] superposed on the C–S–H system: *1* W/C_3S = 1,000 (there is no possibility to saturate the liquid phase with calcium hydroxide); *1'* W/C_3S = 100; *2* C_3S + solution C = $3.95 \cdot 10^{-3}$ mol/kg, S = $1.19 \cdot 10^{-3}$ mol/kg; *3* primary solution; *5* C_3S processed with the solution rich in silica of concentration S = $4.70 \cdot 10^{-3}$ mol/kg, C = $1.75 \cdot 10^{-3}$ mol/kg; *8*, *9*, *10* two primary solutions with different composition from the left and right side of the curve I

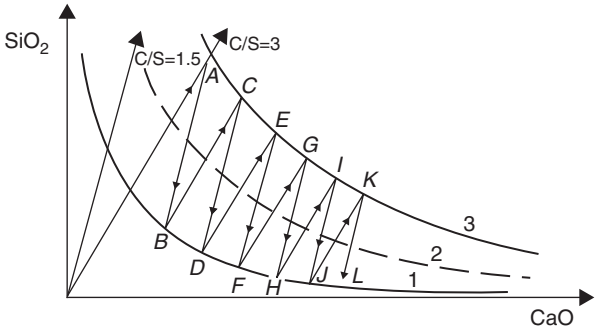


Fig. 3.6 C–S–H system (according to [10]): *1* solubility curve of C–S–H, *2* curve I, *3* solubility curve of alite. The precipitation of C–S–H with C/S about 1.5 is shown

is of the opinion, like Taylor (see [33]), that the metastable equilibrium (that is supersolubility) of this one C–S–H phase would give a "cloud" of points, and not the one curve. Jennings is not right because the supersaturation assuring the nuclei formation would give also the points situated along one curve, as it was proved by Barret [12].

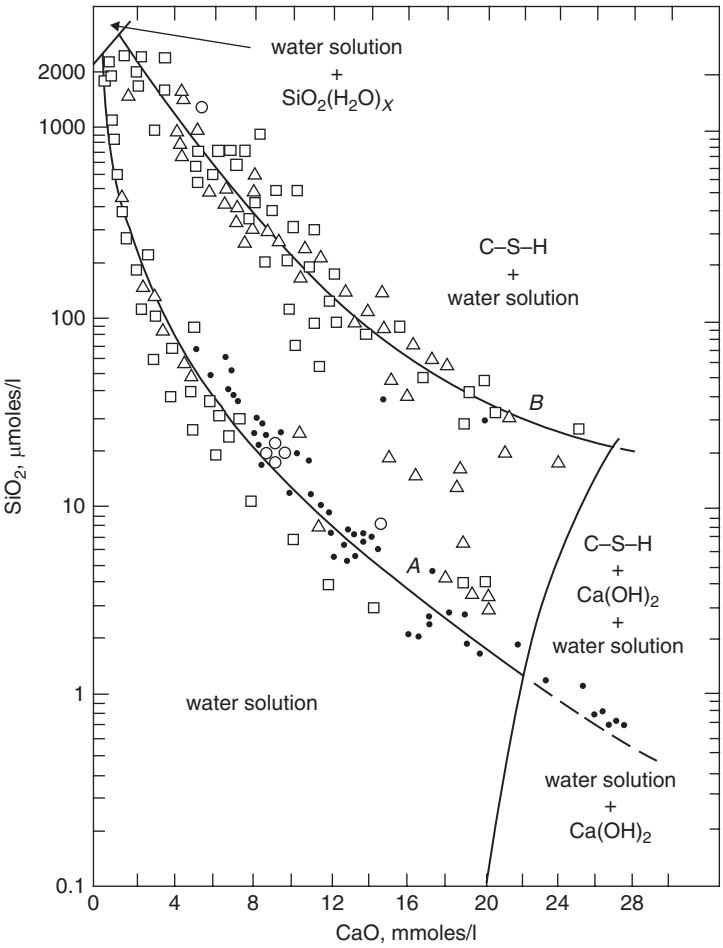


Fig. 3.7 Composition of liquid phase in the system $CaO–SiO_2–H_2O$ according to different authors. (After [11]) Jennings H.M., "Aqueous Solubility Relationships for Two Types of Calcium Silicate Hydrate", J. Am Ceram. Soc. 69, 614 (1986), published by John Wiley & Sons Ltd, reproduced with the permission of Wiley & Sons

Recently Chen, Jennings et al. [13] presented a detailed discussion relating to the equilibrium solubility curves of C–S–H in the $CaO–SiO_2–H_2O$ system, coming back to the idea of Jennings, modified in such a way that they put no attention to the *B* curve (Fig. 3.7) but to the series of curves *C, C', C''* (Fig. 3.8). These curves cover the experimental data of these authors and the previous results of many others, among them those of Barret and Bertrandie [7]. Chen et al. [13] conclude that these curves correspond to different metastable C–S–H modifications. These curves are reversible (*C, C', C''*) and relate to the C–S–H with different silicate chains length and different number of Ca–OH bonds in the C–S–H structure. They are reversible—it means that they can be produced by the de–calcification of C–S–H

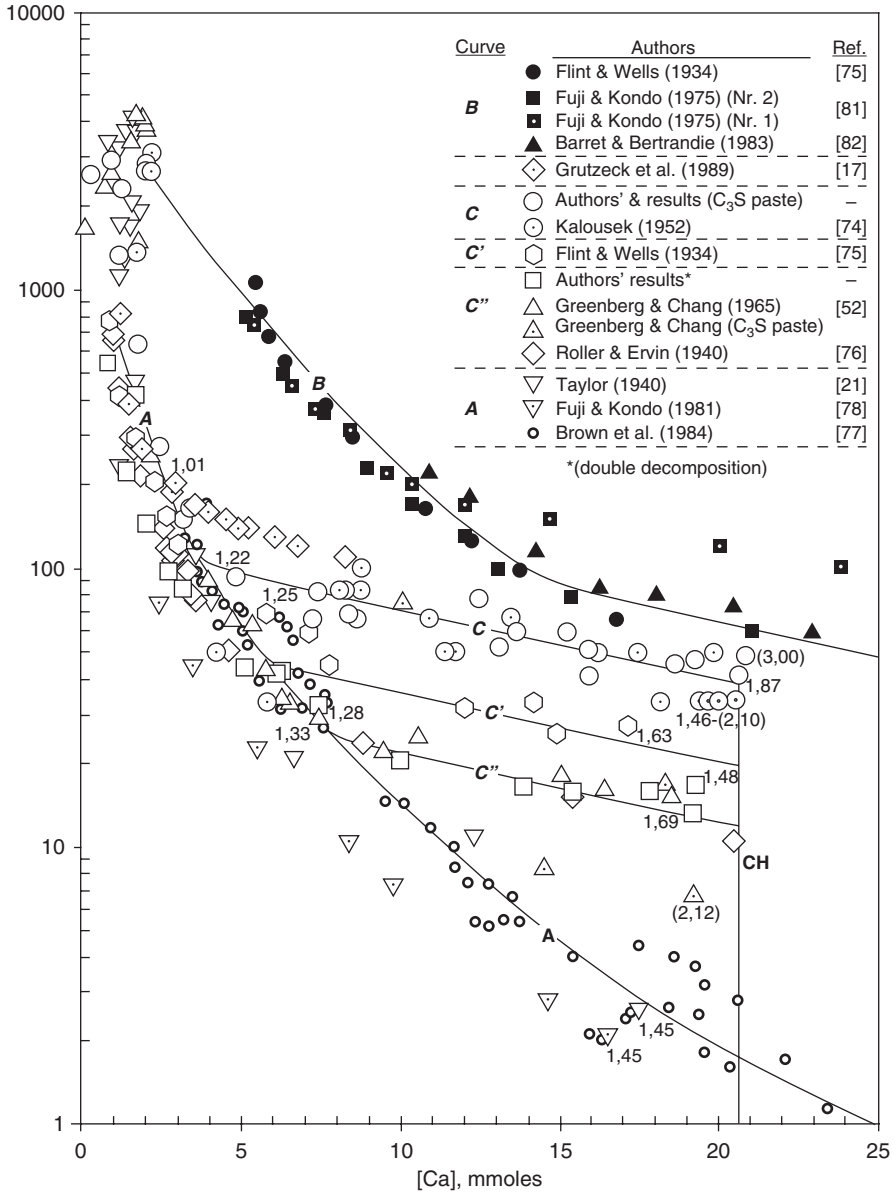


Fig. 3.8 The published solubility data in the $CaO–SiO_2–H_2O$ system (references in [13]). Bright spots correspond to the equilibrium with the metastable phases of C–S–H, dark spots relate to the equilibrium at early C_3S hydration stage. For some selected spots the C/S ratio is given; the values in brackets relate to the samples composed of C–S–H and CH. (According to [13])

with high C/S ratio (as a result of washing with water) or by secondary increasing of this ratio, caused by contact of C–S–H with saturated calcium hydroxide solution, assuring equilibrium.

This standpoint they explain not only by the reversibility of curves but also by the results obtained with the ^{29}Si nuclear magnetic resonance measurements. Underlining that the charge of anions in the chain can be equilibrated by the protons or Ca^{2+} cations, the authors are assuming that at growing Ca/Si ratio all protons in the Si–OH groups are replaced by the interlayer Ca^{2+} ions, before the "excess" calcium ions entering to the structure as Ca–OH. From the above consideration it results that the Si–OH and Ca–OH groups do not occur simultaneously and it was assumed that in the curve *A* intersection points with set of curves *C* the Ca–OH groups appear at one of curves *C* after living this intersection point.

Basing on this assumption the authors calculate the Ca–OH groups content from the balance of charge and subsequently the C/S ratio in C–S–H in the intersection points and along the curves. In the intersection points the C–S–H formula is $Ca_{6-x}(O_{18-2x}) \cdot nH_2O$; where x must not be an integer. Therefore the authors conclude that the limit values relate to the structure analogous to that of tobermorite, which does not contain Ca–OH groups, chain length is 2, C/S 1.5. The highest Ca–OH groups content corresponds to the curve *C* and decreases gradually along the curves *C'*, *C''* and finally *A*.

The congruent C_3S dissolution should result in the formation of saturated solution with the equilibrium as follows:

$$Ca_3SiO_5 + H_2O \rightleftarrows 3Ca^{2+}_{aq} + SiO^{4-}_4 + 2OH^-_{aq} \tag{3.3}$$

Stein [14] tried to calculate the calcium and silicate ions concentration in the solution from the thermodynamic equilibrium conditions. The results thus obtained were significantly higher than the experimental values. The similar inconsistency was found for C_3A too.

These discrepancies were explained by Barret [6] who assumed that the C_3S reaction with water would start from the surface hydroxylation of solid phase. Barret assumed the high value of free enthalpy of the hydroxylation process and into the solution are only released the ions resulting from this process. Based upon this assumption and the determination of ions concentration in the saturated C_3S_{sh}[1] solution gives the following value:

$$C_3S \rightarrow C_3S_{sh} - 75.2\ \text{kJ/mol} \tag{3.4}$$

The dissolution process corresponds to the reaction:

$$C_3S_{sh} \rightarrow Ca^{2+} + SiO^{2-}_3 - 15.38\ \text{kJ/mol} \tag{3.5}$$

The [C] and [S] concentrations calculated basing on above equations are consistent with the experimental data. In the opinion of this author the surface hydroxylation of C_3S and C_2S consists in the protonation of these phases and leads, as a consequence, to the release of OH^- ions into the solution. This process can be schematically written as follows:

$$(Ca_3SiO_5)_s + 4H_2O_l \rightarrow (Ca_3OHH_3SiO_4)^{\cdots\cdots}_s + 4OH^-_{aq} \tag{3.6}$$

[1] C_3S_{sh} means surface layer formed by hydroxylation.

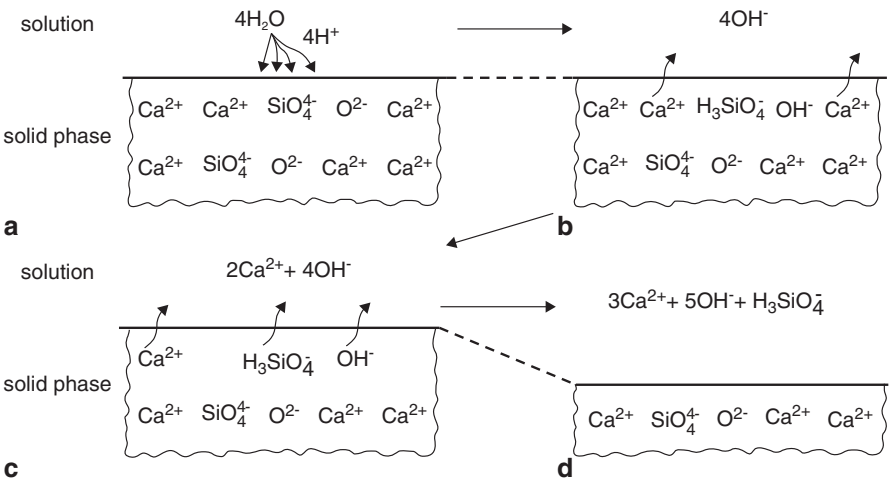


Fig. 3.9 The mechanism of C_3S dissolution as presented by Taylor based on the model proposed by Barret [15], the stage (**d**) equivalent to the stage (**a**). Details are given in text (pages 138-140)

s	index means the C_3S phase surface
l	the liquid phase
dots	the positive charges

Using the Kröger notation we have:

$$(3Ca_{Ca} + O_O + SiO_{4(SiO_4)})_s + 4H_2O_l \rightarrow (3Ca_{Ca} + OH_O^{\bullet} + H_3SiO_{4(SiO_4)}^{\bullet\bullet\bullet})_s + 4OH_{aq}^- \tag{3.7}$$

During the first contact with water the hydroxylation embraces all surface sites occupied by oxygen atoms (Fig. 3.9). It can be even supposed that a part of them was hydroxylated earlier, in the contact with atmospheric moisture. According to Barret [6] a strong electrostatic attraction will appear between the surface charges of solid phase and OH_{aq}^- groups released to the solution. This will be equivalent to the adsorption of the groups OH_{ad}^-. Simultaneously, the surface elements of solid phase $(2[Ca_{Ca}]_s + 4OH_{aq}^-)$ will be released into the solution, according to the reaction (Fig. 3.9c):

$$(Ca_{Ca})_s + 2OH_{ad}^- \rightleftarrows (V_{Ca}'')_s + Ca_{aq}^{2+} + 4OH_{aq}^- \tag{3.8}$$

Release of calcium ions to the solution must produce the cation vacancies. Assumption of this mechanism can explain the decreasing Ca/Si ratio on the C_3S surface, found by many authors in ESCA studies. It takes place within a few seconds after contact of C_3S with water (Fig. 3.10).

The further progress of the process needs the exposure of new oxygen site on the C_3S surface with the access of water and simultaneous OH^- groups formation. According to Barret this process will control the reaction rate of C_3S with water. Two mechanisms can be taken into account:

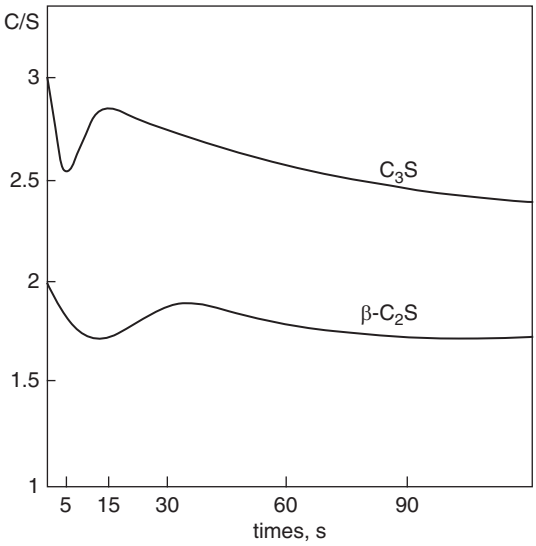


Fig. 3.10 Changes of C/S ratio measured with ESCA for C_3S and β–C_2S. (According to [6])

1. Dissolution of C_3S_{sh} layer with its hydroxylation (Fig. 3.9d)

$$2(Ca_3OHH_3SiO_4)_s^{\bullet\bullet\bullet\bullet} + 8OH_{ad}^- \rightleftarrows 6Ca_{aq}^{2+} + 10OH_{aq}^- + 2H_3SiO_{4(aq)}^- \tag{3.9}$$

Simultaneously the crystallization of C–S–H from the solution occurs. This mechanism belongs to the theory of crystallization "through solution".

Because, at pH from 12.6 to 12.9 there are mainly the $H_2SiO_{4(aq)}^{2-}$ ions in the solution, Barret considers the possibility of their formation directly on the C_3S surface with the simultaneous formation of oxygen vacancies:

$$(2V''_{Ca} + Ca_{Ca} + OH_O^{\bullet} + H_3SiO_{4(SiO_4)s}^{\bullet\bullet\bullet} \rightleftarrows (2V_{Ca}^{\bullet} + Ca_{Ca} + V_O^{\bullet\bullet} + H_2SiO_{4(SiO_4)}^{\bullet\bullet})_s + H_2O_l \tag{3.10}$$

2. The second mechanism consists in the diffusion of calcium ions in the solid phase toward the surface contact with the liquid phase and their subsequent reaction with the OH^- groups and, in the opposite direction, diffusion of protons. As a result the hydroxylation of oxygen lattice sites takes place.

This diffusion can occur or along the phase boundaries, when the C–S–H nuclei do not cover the whole C_3S surface, but they are formed on the active centres only, or can proceed through the continuous C–S–H layer (Fig. 3.11). This would result in the epitaxial growth of C–S–H on the nuclei formed earlier. This mechanism will correspond obviously to the topochemical process.

One can imagine another variety of this process, namely the nuclei formation in the C_3S phase, as a result of the rearrangement of its defected structure:

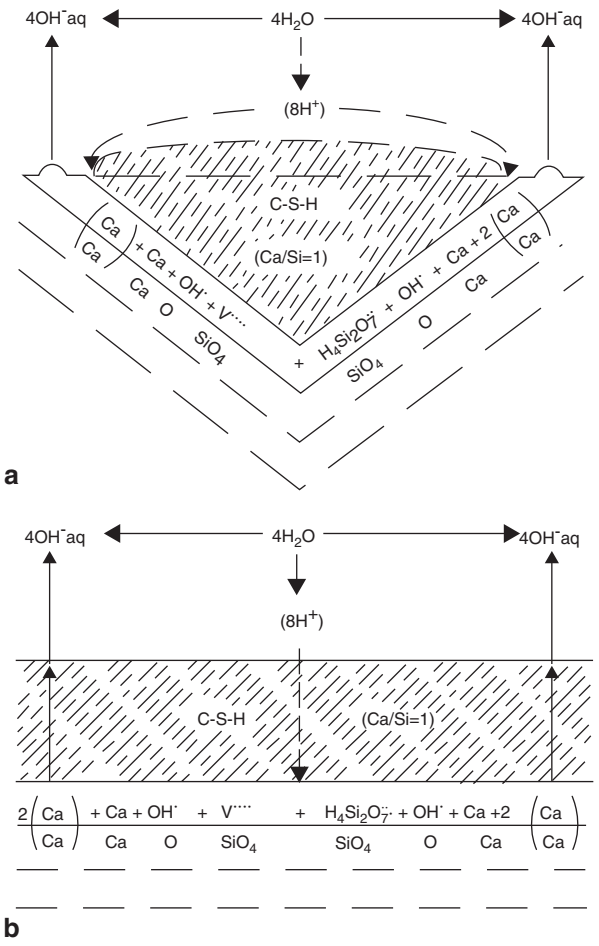


Fig. 3.11 The mechanism of C–S–H (C/S = 1) growth as shown schematically (according to [15]): (**a**) on open surface (individual nuclei), (**b**) on closed surface with the C–S–H layer in which the diffusion of H^+ and Ca^{2+} ions occurs

$$(V''_{Ca} + Ca_{Ca} + OH^{\bullet}_{O} + H_3SiO^{\bullet\bullet\bullet}_{4(SiO_4)} + V^{\bullet\bullet}_{O}) \tag{3.11}$$

with initial $H_4Si_2O_7^{2-}$ dimers formation, and subsequently of the $Ca_2(OH)_2H_4Si_2O_7$ phase.

In the later period of hydration the topochemical process cannot be rejected, in the light of collected experimental data. However, its role in hydration process seems to be significantly limited, if a very low volume diffusion rate is considered. Moreover, the variable ions Ca^{2+} and $H_2SiO_4^{2-}$ concentrations during the hydration cannot be explained basing on the topochemical mechanism. These concentrations correspond to the C_3S congruent dissolution, occurring simultaneously (sections *B–C, D–E, F–G*) and C–S–H crystallization (sections *A–B*, *C–D*… for C/S = 1.5) (see Fig. 3.6).

3.2.1.1 Induction Period

The hypotheses explaining the occurrence of the induction period, which has a very low heat evolution, are the subject of serious discussions. The following hypotheses are proposed:

- nucleation of CH and C–S–H,
- formation of poorly permeable C–S–H layer,
- supersaturation of solution in relation to CH.

As it has been shown by Barret [7], the nucleation of C–S–H occurs very quickly. It is provided also by the rapid drop of silica concentration in solution. Also the addition of CH nuclei, though it causes some acceleration of the process, does not eliminate the induction period [16]. There are some reports indicating the "poisoning" of the CH nucleation process by diluted silica solution and a slowed growth of calcium hydroxide crystals as a result of silicate anions adsorption on the 001 planes [17, 18]. However, this has not been proved in the case of C_3S hydration; a low CH crystallization rate is important because it prevent fast calcium ions removing from the solution.

The hypothesis relating the induction period with the formation of the low permeable C–S–H layer on the surface of C_3S was proposed by de Jong and Stein [14]. This hypothesis, close to the topochemical model, can be derived from the gel constitution of the hydration products, precipitated on C_3S surface. It is also compatible with aforementioned phenomenon of hindered C–S–H phase separation from the C_3S grain. At the C_3S–liquid phase boundaries the concentration of ions is the highest and thus the nucleation is the most probable. There is also a common opinion that C–S–H nucleation is heterogenic [12]. C–S–H phase on the surface of C_3S was observed by many authors [5, 19]. Initially the nuclei appear in spherical forms, which subsequently are transformed into the C–S–H II network. A view is presented that the primary C_3SH hydrate is formed initially and plays a role of the barrier layer. Subsequently it is transformed into the hydrate with low C/S ratio (0.8–1.5), more permeable and this means the end of the induction period (change of morphology and structure of primary hydrate). Other authors explain the end of the induction period by break up of the impermeable layer by osmotic pressure (Fig. 3.12). These hypothesis are based on the commonly known features of silica gel which behaves as an semipermeable membrane.

The *in situ* formation of such layers on cement grains can be observed under the high voltage electron microscope [20, 21]. According the hypothesis of Double et al. [20] these membranes are permeable for the calcium and OH^- ions released into solution, and water toward cement grains. However, they are not permeable for silicate anions, because of their large dimensions. This preferential diffusion leads to the formation of osmotic pressure inside the membrane and finally to its break–down (Fig. 3.12).

The silicate ions are released into solution and react with the calcium ones giving C–S–H phase. It is the end of induction period interfering with Ca^{2+} ions concentration decrease in the liquid phase due to the C–S–H crystallization. The phenomenon

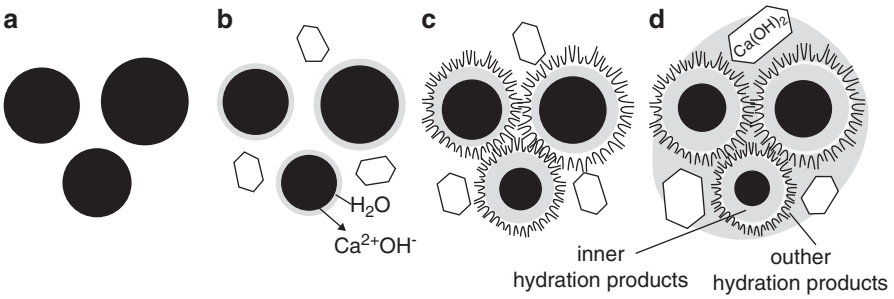


Fig. 3.12 The scheme of cement hydration (according to [20]): (**a**) cement grains in water, (**b**) gel layer formed on cement grains, (**c**) break–up of gel layer under the osmotic pressure and the growth of secondary C–S–H gel, (**d**) filling of pores in the paste after longer period of time, caused by gel formation

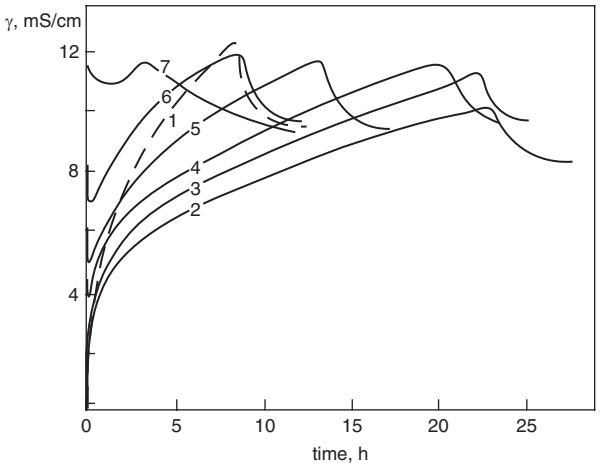


Fig. 3.13 Conductometric curves: *1* stirred C_3S suspension in water at w/C_3S = 20; *2* stoppage hydration after 2 h 30 min. and repeated water treatment, after the treatment with calcium hydroxide solutions with the concentrations *3*–$5.40 \cdot 10^{-3}$ mol/kg, *4*–$10.85 \cdot 10^{-3}$ mol/kg, *5*–$15.10 \cdot 10^{-3}$ mol/kg, *6*–$22 \cdot 10^{-3}$ mol/kg, *7*–$33.10 \cdot 10^{-3}$ mol/kg. (According to [6])

of osmosis should promote the formation of tubular crystals, which really have been found in the gel on cement grains [21, 22].

The formation of poorly permeable layer can be deduced from the results of Bertrandie reported by Barret [6]. The rate of Ca^{2+} ions concentration rise, caused by reaction of C_3S with liquid phase, decreases with time of preliminary hydration of this phase (Fig. 3.13). The thickness of the barrier decreases with the reduced w/c ratio in the paste too [6].

Taylor et al. [23] are assuming that after 12 h the hydration rate is controlled by diffusion. It is probable that the slowest stage can be silicon ions diffusion. Taylor et al. [23] suggest that water molecules are the "donors" of protons migrating from one oxygen atom to another in the C–S–H layer until the unchanged C_3S surface (Fig. 3.14). Then they combine with the O^{2-} and SiO_4^{4-} ions in C_3S phase; which make possible that a part of calcium and silicate ions can be released to the solution.

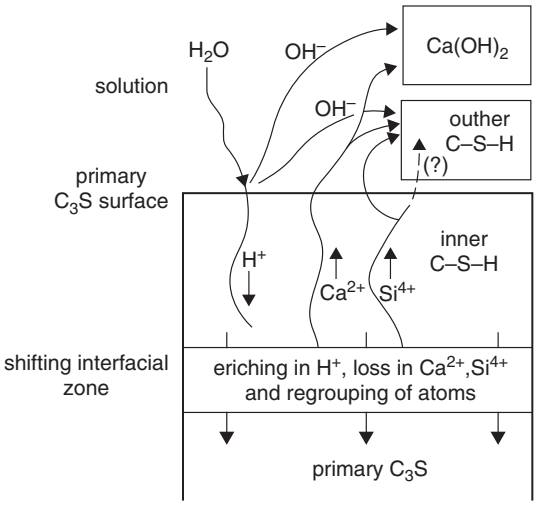


Fig. 3.14 The mechanism of C_3S hydration at later age proposed by Taylor. (According to [23]) Taylor H. F. W., Mohan K., Moir G. K, "Analytical Study of Pure and Extended Portland Cement Pastes: I, Pure Portland Cement Pastes", *J. Am. Ceram. Soc.,* **68**, 680 (1985). published by John Wiley & Sons Ltd, reproduced with the permission of Wiley & Sons

The results of Maycock et al. [24] as well as of Fierens and Verhaegen [25] are not consistent with the barrier layer hypothesis. These authors found a strong relationship between the induction period and the concentration of defects in the C_3S structure. Fierens and Verhaegen [25] have proved that the active centres on the C_3S surface induced by ultra violet radiation were the spots of preferred chemisorption of water molecules. The chemisorption of water leads to the formation of nuclei in these active centres and the dissolution of C_3S small amount. The induction period is ended when the C–S–H nuclei attain their critical size and the growth of crystals begins. This hypothesis is proved by the shortening of induction period when C_3S was primary treated with water vapour, which caused earlier nuclei hydrates formation.

Also Gauffinet et al. [26] are of the opinion that the induction period reflects the time needed for the C–S–H nucleation. It may be the homogenous nucleation but more preferable will be rather a heterogonous process, occurring on the C_3S surface. The first needs much higher supersaturation and as lower it would be as longer will be the induction period. Heterogeneous nucleation will proceed at much lower supersaturation and critical radius of nuclei, leading to further growth of crystals, is reduced too. At the beginning this growth is unconstrained and corresponds to this part of calorimetric curve which presents the increasing rate of hydration. Subsequently the rate of hydration decreases, as the unhydrous C_3S grains are covered with C–S–H layer and the process is diffusion controlled.

Finally, there are the experimental data supporting the hypothesis concerning the supersaturation of liquid phase with calcium hydroxide as a cause of induction period. Barret et al. [7, 12] have found that the rate of C_3S_{sh} dissolution decreases with growing concentration of calcium ions in the solvent filtrated through the C_3S layer. The release of calcium ions into the solution with the formation of calcium vacancies occurs according to the scheme:

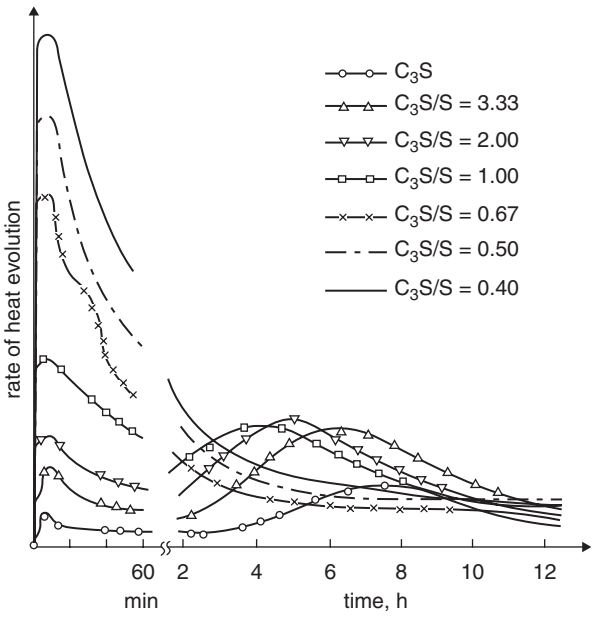


Fig. 3.15 Rate of heat evolution of C_3S reaction with water as a function of silica gel addition. (According to [27])

$$3Ca_{Ca} + OH_O^{\bullet} + H_3SiO_4^{\dddot{}} + 4(OH_{ad}^-) \rightleftarrows$$
$$\rightleftarrows 2Ca_{Ca} + V_{Ca}^{''} + OH_O^{\bullet} + H_3SiO_{4(SiO_4)}^{\dddot{}} + 2(OH_{ad}^-) + Ca_{aq}^{2+} + 2OH_{ad}^- \quad (3.12)$$

which can be presented by the following kinetic equation [15]:

$$\ln\left[1 - \frac{[C]}{K}\right] = -\frac{k}{K} \cdot t \quad (3.13)$$

$[C]$	is the concentration of calcium hydroxide in the solution
K	equilibrium constant
k	constant of reaction rate
t	time

The Ca^{2+} ions concentration in the solution plotted as a function of time gives a straight line, assuming the arbitrarily stipulated value of $K=40$. This line does not intersect the origin of coordinates, because some amounts of C–S–H with variable composition are formed.

Vernet et al. [10]. came to the similar conclusions deriving the formulae from which it can be deduced that the reduction of Ca^{2+} and OH^- ions concentration in solution is increasing the rate of C_3S dissolution (hydration).

Kurdowski and Nocuń [27] found that the active silica addition and reduction of Ca^{2+}concentration in the solution results in a substantial acceleration of C_3S reaction with water, leading to the elimination of induction period (Fig. 3.15). The

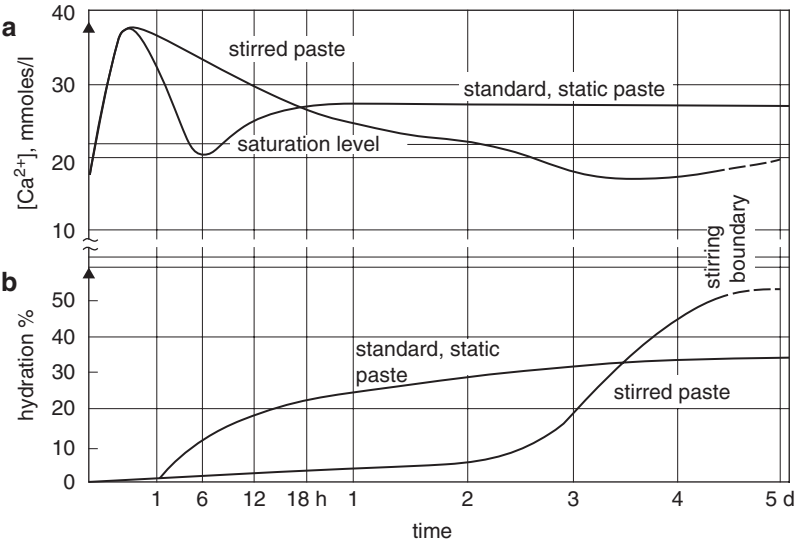


Fig. 3.16 C_3S hydration in the static and stirred C_3S paste (according to [28]): (**a**) Ca^{2+} ions concentration vs. time, (**b**) C_3S hydration degree (w/c = 0.3, temperature 20 °C)

authors are stating that the very high specific surface of amorphous silica is accelerating the rapid bonding of calcium ions with C–S–H formation. The similar conclusions can be found in the work of Ménétrier et al. [28]. They argue that the presence of *quasi*–stationary layer of supersaturated solution around the hydrating C_3S grain is a reason of C_3S reaction inhibition.

Interesting experimental data, proving the supersaturation as a source of induction period were reported by Bellina et al. [29]. Use of special "self–mixing" device, removing the hydrates caused by friction between grains, gave the surprising results. Supersaturation of the liquid phase lasts much longer—up to two days (for w/c = 0.3), which results in the reduction of the C_3S hydration degree of about four times. The lowering of supersaturation after this period of time is accompanied by a rapid increase of hydration rate (Fig. 3.16).

3.2.1.2 Post–Induction Period

Only a few percent of C_3S is hydrated up to the end of the induction period. After the end of induction period the increasing reaction rate begins. It is highly depending on the fineness of sample and the degree of defects in C_3S structure. The hydration of tricalcium silicate (hydrolysis) proceeds at high rate with simultaneous transformation of C–S–H II (also E, see Table 3.1) to C–S–H I (fibres). The crystallization of calcium hydroxide is intensive and the crystals of this phase grow quickly. Calcium hydroxide appears both on the C_3S surface and in the pores far from the silicate grains. C–S–H crystallizes mainly around the C_3S grains.

Table 3.1 Different forms of C–S–H phase [2]

Anion structure	Early product	Middle products		Late products	
TEM[a]					
Notation	E	0	I(I')	3	4
Morphology		Amorphous	Needles growing radially from the grains	Crumbled foils	Compact gel
SEM[b]					
Notation	II	I		II	IV
Morphology	Network	Needles growing radially from the grains		Undefined	Spherical aggregates
Presumed silicate anion condensation degree	Monomers? dimers	Dimers		Dimers (+polymers?) (pentamers + octamers?)	Polymers (+dimers), pentamers + octamers

[a] Transmission electron microscopy
[b] Scanning electron microscopy

The transition from the rapid to the gradually decreasing reaction rate is conventional and depends also on the calorimeter used and the conditions of measurements. It is characterized, however, primarily by transition to the diffusion controlled process, as a result of increasing C–S–H gel content and rising thickness of its layer formed around the anhydrous cores of grains. The supersaturation of solution decreases, which causes and the drop of the rate of crystallization processes.

Further densification of C–S–H phase and transformation to the type III and also IV, in the form of compact gel, leads to the significant reaction rate decrease. The formation of inner C–S–H begins. This is also the consequence of lower content both of anhydrous phases and of the liquid phase. The further growth of $Ca(OH)_2$ crystals is observed. Finally, one can conclude that there is less experimental data relating to the post–induction period.

3.2.2 Dicalcium Silicate Hydration

The hydration or more precisely the hydrolysis of C_2S occurs analogously as in the case of C_3S and can be schematically written as follows: $2C_2S + 4H \rightarrow C_3S_2H_3 + CH$. Therefore the amount of calcium hydroxide formed per "mole" of silicate is three times lower.

As it has been mentioned in Chap. 2, C_2S occurs mainly as β polymorph. The rate of its hydration is substantially lower, however, there is a common opinion that the mechanism of reaction is the same as in case of C_3S. The layer of hydrates on the C_2S surface is not observed under the electron microscope, even at very high magnification. After 24 h the β–C_2S surface is like the C_3S surface after 5 min. hydration

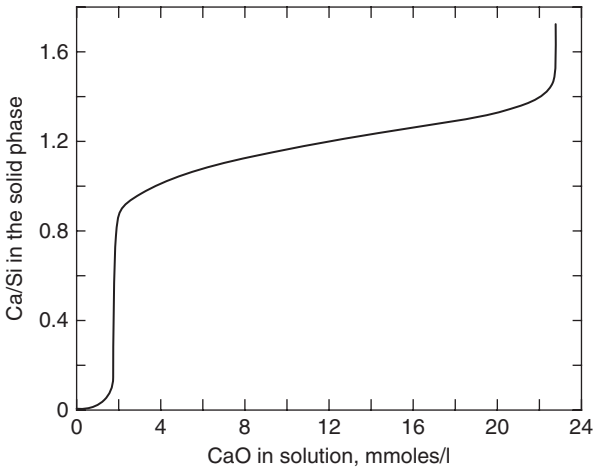


Fig. 3.17 CaO/SiO_2 molar ratio in the C–S–H phase as a function of Ca^{2+} concentration in the liquid phase

[30]. The low hydration rate, attributed to the different C_3S and C_2S structures is the reason of slow process, and the calcium ions concentration in the solution is low. As a result the $Ca(OH)_2$ crystals are usually large, while the C–S–H morphology is very similar. Some C_3S added causes the acceleration of C_2S hydration, because the nucleation of CH is accelerated and thus the C_2S dissolution process is accelerated.

As it results from the ESCA studies the C/S in the about 2 nm thick surface layer is decreasing rapidly, as in the case of C_3S hydration [31].

3.2.3 C–S–H Phase

Basic properties of Portland cement pastes are attributed to the C–S–H gel. Therefore this phase is a field of interest and the subject of numerous investigations [32]. However, in spite of this, the structure and chemical composition of C–S–H cause several discussions. It is the effect of colloidal constitution of this phase and variable, not well defined composition, depending on liquid phase composition, primarily of calcium ions concentration. Moreover, the morphology of this phase transforms as a function of hydration or maturing time of the samples.

First of all the C/S molar ratio changes depending on the saturation of the liquid phase in concrete, in relation to $Ca(OH)_2$ (Fig. 3.17). Especially in the case of cements with mineral additions, particularly siliceous fly ash or ground granulated blastfurnace slag, this ratio decreases and the sections of chains composed of $[SiO_4]^{4-}$ tetrahedra become longer [32].

The adjective “tobermorite–like” has been used to C–S–H for a long time, more or less between the Congresses in London and Tokyo (1953–1969) by many authors. This term was subsequently rejected because of the significant differences in chemical composition, degree of crystallinity and the silicate anion structure. From

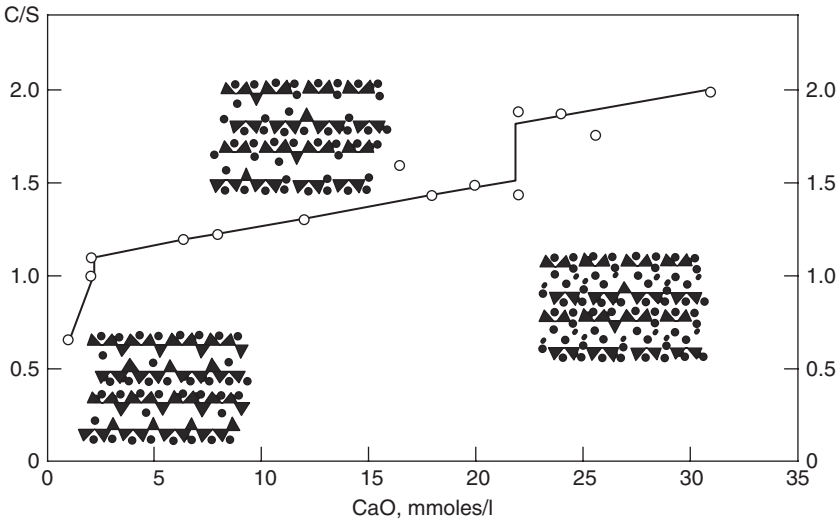


Fig. 3.18 C/S molar ratio of C–S–H phase according to the classification proposed by Nonat. (After [35])

this time the term C–S–H (*Calcium Silicate Hydrate*), proposed by Moore and firstly used by Taylor in written report [33], is commonly accepted. Nowadays there is no possibility to differentiate well defined phases in this group of nearly amorphous or semi–crystalline calcium silicate hydrates. It is considering as a group of different morphology and chemical composition varying in a large range. The attempts of C–S–H classification are often based on C/S ratio (Fig. 3.18).

C–S–H in equilibrium with the liquid phase in which the calcium ions concentration is increasing shows a variable C/S ratio, rising with this concentration. The change of C/S ratio in relation to the increase of calcium ions concentration in solution are shown in Fig. 3.17. Taylor [33] divided the C–S–H phase on two types: C–S–H (I) with C/S ratio <1.5 and C–S–H (II) with C/S ratio >1.5. This classification can be primarily explained by a discontinuity of C/S ratio with the change of calcium ions concentration in the solution [34]. The other discontinuity has been found by Damidot and Nonat at calcium ions concentration corresponding to 22 mmoles CaO/kg, in the C/S range from 1.5 to 1.8. Therefore they proposed the occurrence of three types of C–S–H, which for avoiding mistakes they called as follows: α–C–S–H ($0.66<C/S<1$), β–C–S–H ($1<C/S<1.5$), γ–C–S–H ($1.5<C/S<2$).

As can be deduced from XRD data the structures of these phases do not differ significantly and do not vary especially from the tobermorite structure (see Fig. 3.22).

There were also attempts to find the compatibility of this division with C–S–H morphology. C–S–H (I) forms crumbled foils, well visible under the microscope, while for C–S–H (II) typical are fibre crystals or corrugated foils. Differences in morphology is observed in the case of inner and outer product.

The development of investigation techniques, particularly the electron scanning microscopy, allowed to differentiate the other morphological types of the calcium

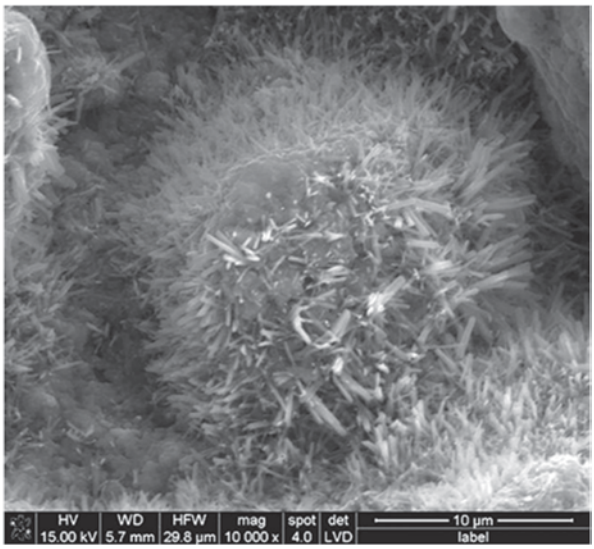


Fig. 3.19 The fibrous C–S–H crystals under SEM. (By the courtesy of B. Trybalska)

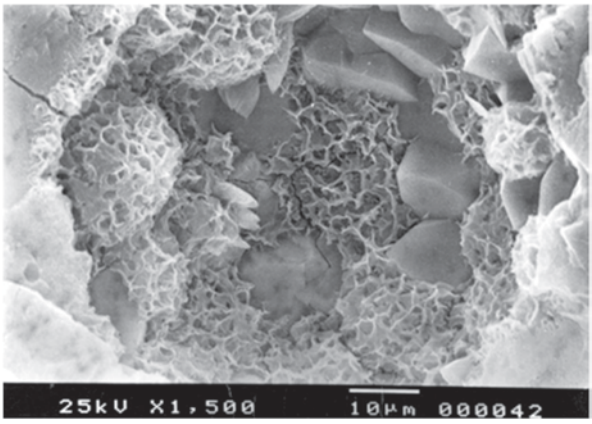


Fig. 3.20 C–S–H honeycomb constitution in the pastes produced from the ground granulated blastfurnace slag activated with Na_2SiO_3, the cracked slag grain is visible. (By the courtesy of B. Trybalska)

silicate hydrates, depending particularly on the different maturing time and kind of cements. Basing on the numerous studies, Diamond [36] distinguished four morphological forms of C–S–H phase: C–S–H I of fibrous microstructure (Fig. 3.19), C–S–H II with network constitution known as *honeycomb* (Fig. 3.20), corresponding to the C–S–H (I) phase according to Taylor, C–S–H III forming isometric particles and the C–S–H IV forming spherical agglomerates, corresponding to the inner C–S–H and distinguished under the electron microscope as compact gel.

According to Jennings et al. [37] the C–S–H III is composed of interlacing and interlocking mutually thin foils. This is another proof that different morphological varieties of C–S–H gel are not belonging to separate types, but to the series of continuously transforming forms derived from layer structure, which have tendency for coiling, twisting or, becoming fuzzy are forming fibres oriented in privileged

directions It is accepted that the C–S–H IV appears as an "inner" or late product of hydration, formed as a result of topochemical process.

Stark et al. [38], using environmental electron microscope, have shown that C–S–H forms generally fibres, short at the beginning, and then of increasing length with the rising of hydration time. It should be, however, remember that these observations relate to the advanced hydration, because the fibres are 200 nm long. At the beginning of reaction the C–S–H particles formed on the C_3S surface are much smaller and their dimensions, according to Nonat [39] are $30 \times 60 \times 5$ nm; therefore it is difficult to attribute them a fibrous morphology.

There are the other classification systems, irrespective of those proposed by Taylor or Diamond. One of them is attributed to the hydration period in which the C–S–H is formed. On this basis the following types can be distinguished: C–S–H E (early), formed at early stage of hydration, C–S–H 0, formed in a middle time and the later one C–S–H L (see Table 3.1). Finally Kondo [3] introduced the partition on the "outer" and "inner" C–S–H. The "inner" was formed in the space occupied earlier by C_3S or cement grain, while the "outer" one—in the area between the hydrating grains, occupied earlier by water. These two types of C–S–H phase have significantly different morphology. The conventionality of this division was pointed out by Taylor [32] who underlined the impossibility of differentiation between these two types with electron microprobe, particularly in case of fine cement grains. Therefore he proposed to use rather the term "undefined" product. Only in some exceptional cases of not fully hydrated C_3S the inner and outer C–S–H can be distinguish [32]. However, recently the modern electron microscopes of high resolving power and giving very high magnification do allow the characterization of inner and outer C–S–H [40]. The inner product is built of equidimensional particles less than 10 nm; containing the internal pores of the same diameter. The outer product crystallizes in a more oriented way and occurs as agglomerates of fibres with length attaining 100 nm; with capillary pores between them. The individual fibres are 10 nm long and 5 nm wide. Nonat [39] in turn, based on the experimental data, reveals that C–S–H precipitated on the surface of cement grains occurs as small layers of 30×60 nm, and 5 nm thick. According to Richardson [41], the inner product is composed of spherical 4–8 nm particles, as the hydration is occuring at 20 °C, but at higher temperatures they are smaller, equal about 3–4 nm. This author is of the opinion that the lowering of C/S in C–S–H in blended cement pastes causes the change of this phase morphology consisting in the transition from the fibrous to the corrugated foils. This indicates the transformation of crystallites (fibres) growing principally in one direction to the two–dimensional forms (foils). The foils are attributed mainly to the tobermorite–like structure.

The C–S–H structure was presented by Henderson and Bailey [42] already during the Rio de Janeiro Congress, based on the results of their studies with high definition electron microscope. Applying different conditions of specimens preparation they obtained two types of C–S–H. Single corrugated foils, 1 to 2 nm thick, and the others showing clearly space orientation, almost rectilinear multi–layer forms, which number reached six. The latter form of C–S–H, with $C/S = 1.7$ gave, at low magnification (38,000×), an image similar to the fibrous C–S–H (II) and revealed a pseudo–hexagonal microstructure. The thickness of single foil is in good agreement

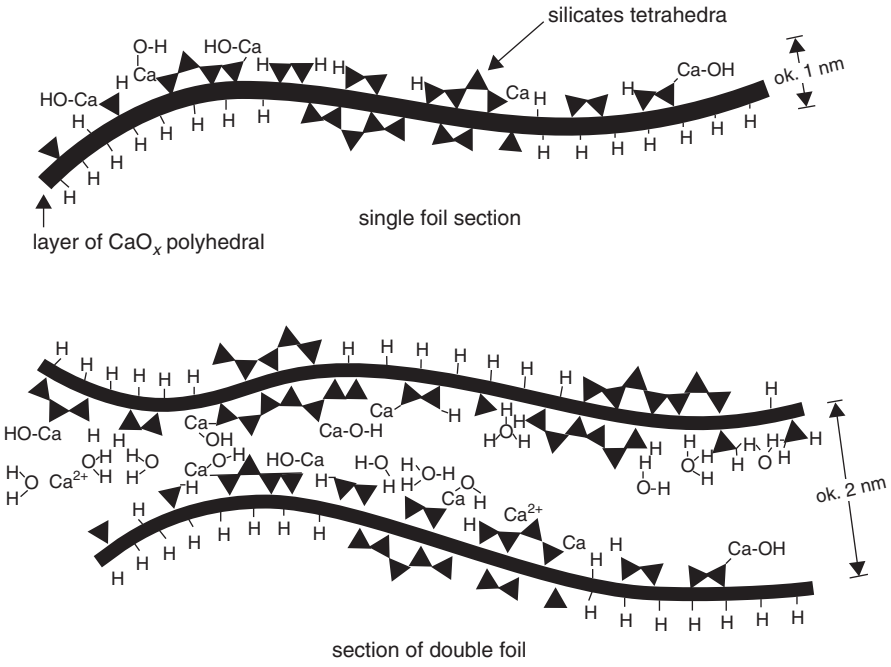


Fig. 3.21 The structure of C–S–H foil. (According to [42])

with the value calculated theoretically (1.1 nm), based on the length of Ca–O and Si–O bonds (0.235 nm and 0.27 nm respectively) (Fig. 3.21). The C–S–H particles are composed usually of the two, three, but sometimes also of four foils. The C–S–H is "nearly amorphous" when gives only three peaks on the XRD pattern, showing higher or lower broadening. In this material, determined in the past as a "tobermorite gel" [33], the short–range order only occurs. When there is a few peaks on the XRD pattern or there are only the diffuse peaks, such a C–S–H (I) is determined as a "semicrystalline" material, with no full three–dimensional ordering.

The XRD powder diffraction pattern of C–S–H (I) is better ordered and the peaks correspond to the two–dimensional, centred orthogonal lattice with $a \approx 560$, $b \approx 360$ pm. The strong basic peak in the range 0.9–1.4 nm can, but not must be present on the XRD pattern. Therefore the C–S–H was classified earlier as a disordered form of 1.4 nm tobermorite, because on its X–ray diffraction pattern there are peaks attributed to the *hk0* planes of tobermorite phase, and sometimes of broadened basic peak [33]. C–S–H (II) is more variable than C–S–H (I) and usually of lower degree of crystallinity than the later one. More crystalline C–S–H (II) is formed in the C_3S or β–C_2S pastes and the XRD pattern of this phase is similar to that for C–S–H (I) with the highest *d* value corresponding to about 0.9 nm [33]. According to Taylor [43], this phase is close to 1.4 nm tobermorite[2], because in some cases on the XRD

[2] In the tobermorite group which has the layer structure, the individual phases are distinguished taking on the basis of the basic interplanar spacing corresponding to the thickness of layers in the

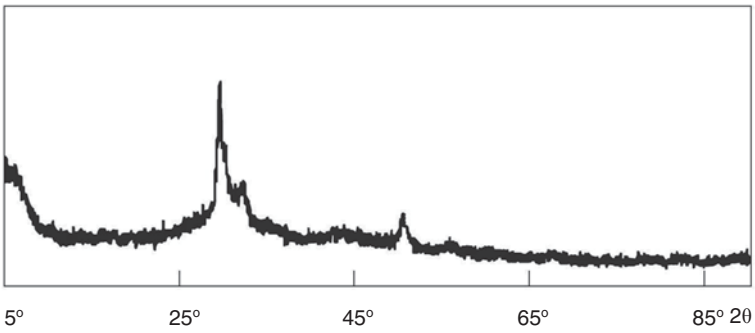


Fig. 3.22 XRD powder pattern of C–S–H. (According to [39])

pattern of this phase there were the peaks for *d* 0.307, 0.280 and 0.183 nm. At present this phase is determined as closely related to a disordered jennite.

Nonat [39] stated that the XRD patterns of C–S–H are, in all the range of C/S ratio, similar to the XRD pattern of 1.4 nm tobermorite. According to this author, C–S–H is a crystalline phase, but with extremely small crystals.

Taylor [32] has been pointed out that the results of C–S–H phase chemical composition determination are strongly affect by the conditions of these experiments. It was establish that the C/S ratio is increasing with the use of higher accelerating voltage in the scanning electron microscope or in electron microprobe. It has been found that the best conditions for the calcium silicate hydrates analysis are at the voltage of 10 kV. Taking into account the all possible sources of errors Taylor and Newbury [44] determined the C/S ratio in the C_3S paste as 1.7–1.8. The similar value can be accepted for β–C_2S paste. The same results have been obtained by Taylor [32] under the analytical electron microscope. Although these results scatter within a wider interval than the results obtained in earlier experiments, scattered from 1.2 to 2.0; but there is an opinion that these extreme values should be rejected because the sources of errors are unclear. However, more recently Richardson [45, 46], based on the numerous experiments with industrial cement samples, has shown a significant variability of C–S–H composition, in the interval from 0.7 to 2.3. This variability in the case of C_3S and β–C_2S pastes, having the mean C/S ratio equal 1.75, can be higher in the micro–areas, ranging from 1.2 to 2.1 [47, 48]. Formerly Lachowski and Diamond [49] proved the C/S high variability in C–S–H, in the range 1.1 to 2.3, however, the most of results was in the interval from 1.3 to 1.8. The experimental data reveal that the high C/S ratio is accompanied by higher concentration of Al, S and Fe. Therefore this C/S ratio is not too high as the quoted elements are included in the calculations. According to Lachowski and Diamond [49] the aluminum, sulphur and iron ions substitute Si in the C–S–H structure. Rayment and Majumdar [50] has come earlier to the similar conclusion concerning the isomorphic substitution in C–S–H. According to these authors [50] also Mg is substituting Ca.

structure. There are the following phases: 1.1 nm tobermorite, 1.4 nm tobermorite, 1.0 nm tobermorite, 1.26 nm tobermorite and 0.93 nm tobermorite.

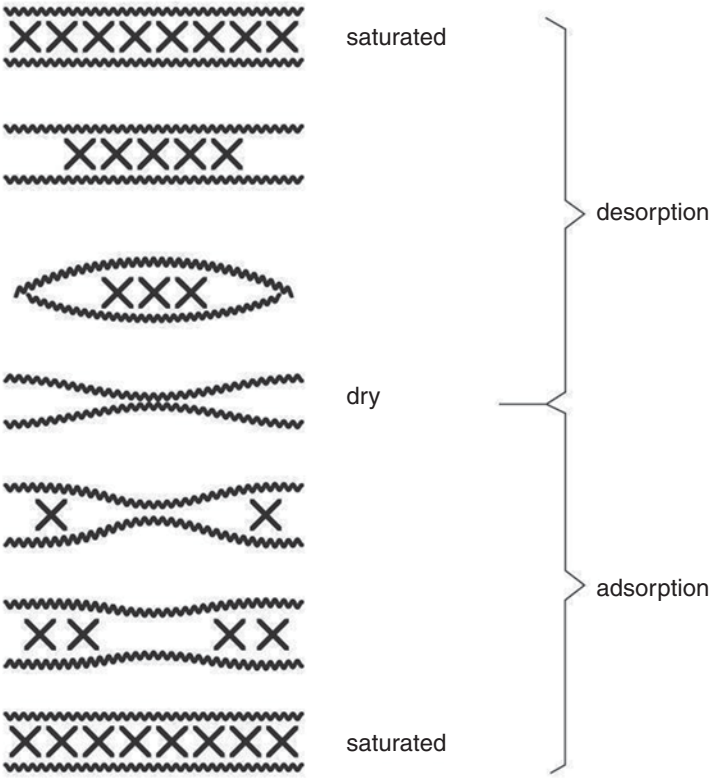


Fig. 3.23 Simplified model of the distances between the layers in C–S–H during subsequent drying and water adsorption [52] Buil P., OllivierJ. P., Chapter 3 in « La Durabilitė des Bėtons », page 87, fig. 3.23 « Influence du rapport E/C et de la taille mximale des granulats sur le coefficient de permėabilitė á l'eau des bėtons», Published by Presses de l'Ecole Nationale des Ponts et Chaussėes, reproduced with the permission of the Presses de l'Ecole Nationale des Ponts et Chaussėes

C–S–H in cement pastes reveals the C/S ratio in the range from 1.75 to 1.85 and these value do not alter neither with time nor with w/c, as it has been establish by Rayment and Lachowski [51] in numerous experiments. In the pastes of cement with slag or fly ash addition this C/S ratio is much lower.

Taylor studied also the H_2O/Ca ratio, which for full water saturation is from 2.3 to 2.5, at 11 % RH is 1.3–1.4 and for material dried at 110 °C—0.8–0.9 respectively. The research has shown that the interlayer water can be removed and reversibly taken again, depending on the environment humidity [52]. As it has been found in the NMR studies, water at the humidity exceeding 70 % RH is bound in C–S–H analogously as interlayer water in the swelling clay minerals and this water shows lower mobility than the adsorbed water [53]. It is in good agreement with the model proposed by Feldman (Fig. 3.23).

With trimethylsilylation procedure the presence of $[Si_2O_7]$ dimmers, as a main structural component of C–S–H phase, and a low amount of longer linear chain sec-

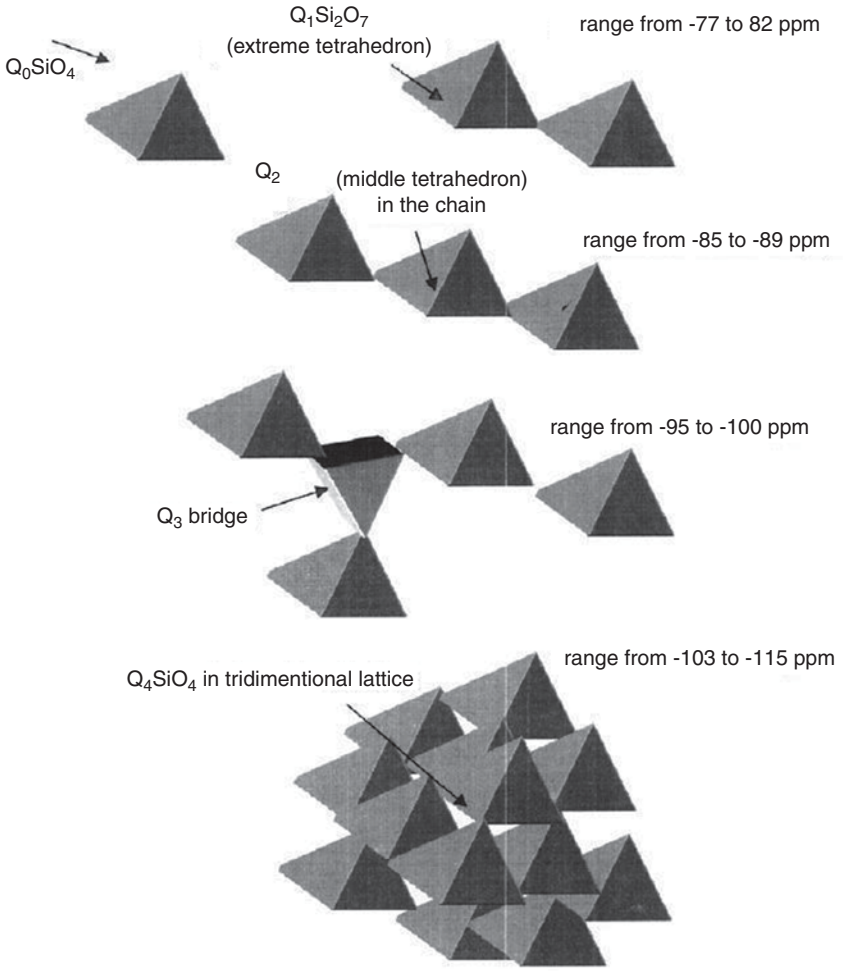


Fig. 3.24 Silicate anions with different number of oxygen bridges, as determined by ^{29}Si NMR

tions, called generally polymers, was detected. The other forms of silicate ions, such as trimers or tetramer rings were not found. The mean size of anion is increasing with hydration. The $[Si_5O_{16}]$ pentamers in the chains was also found [54].

The ^{29}Si nuclear magnetic resonance resulted in a significant progress in the studies of the silicate anion structure [55]. This method, as a "pure physical" one has a serious positive feature—it does not affect the examined structure. It gives the information about the environment of Si atoms; Q_0, Q_1, Q_2... mean the types of silicate anions, characterized by a number of oxygen bridges, that is by the number of bonded tetrahedra (Fig. 3.24). The data for the C_3S paste show that the percentage of Q_0 decreases, but Q_1 and a little later Q_2 appear (Fig. 3.25). Q_0 means the monomers attributed to the initial C_3S, Q_1 without Q_2, Q_3 and Q_4 means the presence of dimers. Q_1 together with Q_2 but without Q_3 and Q_4 means single chains or single rings. It is admitted that the C–S–H phase is composed mainly of dimmers and the pentamers

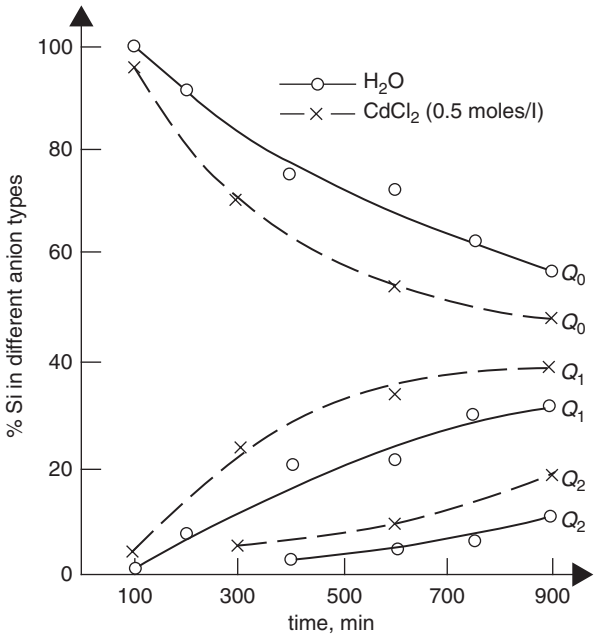


Fig. 3.25 Different silicate anions in the C_3S hydrating sample vs. time. (According to [55])

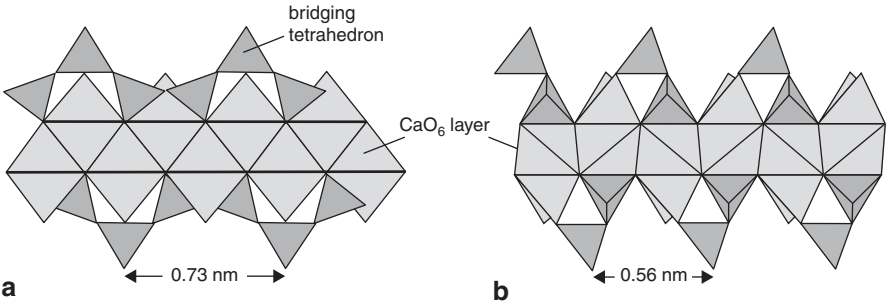


Fig. 3.26 Idealized 1.4 nm tobermorite structure (according to [13]); (**a**) the projection on the 210 plane, (**b**) on the 010 plane

and octamers appear steadily and their content increase with hydration time. In the pastes cured at higher temperatures the larger structural elements can be formed. Therefore in C–S–H there are the chains composed of $(3n-1)$ tetrahedra [32].

For the last 20 years after the work of Grutzeck et al. appeared [56], in which the results of C–S–H phase studies with NMR were presented, a significant progress of C–S–H structure knowledge has been observed. Although the cationic sublattice, composed of CaO_6 octahedra (the coordination number can attain 7) is thought to be the base of C–S–H structure, because as it has been already proved by Belov [57] the condensation of silicate anions is controlled by this sublattice, there are, however, the experimental proofs for the occurrence of chains with different length. The wollastonite chains are well compatible with the layers of CaO_6 octahedra [56]

(see Fig. 3.26 and 4.57). These chains are of a type called “dreierketten” i.e. they are kinked so as to repeat at intervals of three tetrahedra, and they surround the octahedral layer from the both sides. The two neighbouring tetrahedra are coordinated by calcium ions from the octahedral layer, while the third one, so–called the bridging tetrahedron, is bonding two adjacent Si_2O_7 dimers (Fig. 3.26). The shortage of some bridging tetrahedra in the chain, that means the occurrence of their fragments of different length: dimers, pentamers, octamers (generally, according to Taylor [32] the polymers composed of $3n-1$ tetrahedra) allows to explain the variable C/S in C–S–H. However, this hypothesis, proved by NMR, cannot explain whole changes range of this ratio, but only till C/S = 1.25.

For this reason some hypothetical models have been proposed, as a solution of this problem. In the oldest one the C–S–H phase was considered as a solid solution of $Ca(OH)_2$ in tobermorite [58]. In the second the C–S–H phase was presented as a defected 1.4 nm tobermorite structure, with the Ca^{2+} and OH^- ions between the layers [59].

During the Congress in Rio de Janeiro Taylor [32] proposed the model of C–S–H structure based on two extreme units: 1.4 nm tobermorite—for C–S–H I and jennite—for C–S–H II. In tobermorite two oxygen atoms from the non–bridging tetrahedra are coordinated by calcium ions [60], while in jennite only one oxygen atom is coordinated by the calcium ion from the layer, the second one—by the hydroxyl ions [61]. In the latter structure the charges of calcium ions in the layer are balanced with the charge of OH^-, and the protons in the silanol SiOH groups are substituted by calcium ions. 1.4 nm tobermorite has the formula $Ca_4H_4Si_6O_{18} \cdot 8H_2O$ corresponding to the ratio of C/S = 0.66, while jennite—$Ca_8H_4Si_6O_{18}(OH)_8Ca \cdot 6H_2O$, which gives C/S = 1.5. The 1.4 nm tobermorite structure is composed of central Ca–O layer in which all oxygen atoms are bonded with the silicate chain having the empirical formula Si_3O_9H.

In the structure of jennite only some oxygen atoms are bonded with the Si_3O_9H chains, the rest belongs to the OH^- groups. According to Taylor [32, 62] both phases can co-exist in the poorly ordered structure. Taylor supposes that there is a shortage of large number of tetrahedra in both types of layers which causes the formation of chains composed of 2, 5, 8,…, $(3n-1)$ tetrahedra. There are several lines of evidence supporting this hypothesis: conditions of C–S–H phase synthesis, the silicate anion structure, H_2O/Ca ratio, density of material dried in variable conditions, TG curves, peaks on XRD patterns, diffraction of electrons and finally the range of C/S ratio, as found experimentally using the analytical electron microscope.

Therefore Taylor [62] presented the hypothesis that the structure of C–S–H I could be formed by elimination of the part or all the bridging tetrahedra from tobermorite; the same operation with jennite structure would result in the transformation to the C–S–H II structure. These operations, after the removal of all the bridging tetrahedra, give the following ultimate formulae: $Ca_5H_2Si_4O_{16} \cdot 8H_2O$ (C/S = 1.25) and $Ca_9H_2Si_4O_{16}(OH)_8 \cdot 6H_2O$ (C/S = 2.2). According to Taylor [62] this system composed of two different structures transforms, as a result of mutual interaction, into the intermediate one, related structurally to jennite. Taylor [62] supposed that during paste maturing this composed of two structure constitution is disappearing, as the effect of mutual interaction, giving the intermediate composition, similar

structurally to jennite. Taylor [63] assumed that similar to the tobermorite–like and jennite–like areas can be quite freely limited and penetrate each other, even within the single layers. Therefore the base of this model relates to the very disordered C–S–H phase structure.

Cong and Kirkpatrick [64] reject the Taylor's model and suggest that the occurrence of C–S–H II with disordered jennite structure is very rare; they derive the C–S–H model from the defected tobermorite. Simultaneously they stipulate that some areas in the disordered tobermorite are structurally close to portlandite and these areas or layers are mixed in the structure with the tobermorite–like layers. The intensity of the attributed to Ca–OH bands in the spectrum increases with C/S ratio which indicates the increase of these areas in the C–S–H structure. The model proposed by Cong and Kirkpatrick includes basically only the C–S–H with C/S ratio lower than 1.5 and the "solid solutions tobermorite–portlandite" at higher C/S. On the other side, three years later, in 1999 Yu et al. [65], as well as Kirkpatrick and Cong in this group, reported the detailed results of C–S–H structure investigations by infrared spectroscopy and found that the results are confirming the similarity of the C–S–H structure to the 1.4 nm tobermorite and jennite structure. With the increasing C/S ratio occurs the removal of bridging tetrahedra and their substitution for the interlayer calcium ions, accompanied by the formation of silanol Si–OH groups. Further growth of C/S ratio results in the further removal of tetrahedra from the silicon–oxygen chains; this is equivocal to the formation of jennite or jennite–like areas.

Richardson and Groves [66, 67] propose a general model related to the two hypotheses: solid solution of CH in tobermorite and linked areas having the tobermorite or jennite structure. This model is given as a formula related to the wollastonite chains of variable length and different protonation; hydrogen occurs in the –OH groups bonded with Si atoms and finally a variable $Ca(OH)_2$ content in the solid solution. The formula is as follows:

$$Ca_X H_{2(N+1-X)} Si_N O_{(3N+1)} \cdot z Ca(OH)_2 \cdot m H_2O \tag{3.14}$$

N is the mean number of tetrahedra in the silicate chain
X the number of Ca^{2+} ions to balance the silicate chain charge
$2(N+1-X)$ the number of hydroxyl groups joined to the chains
z number of $Ca(OH)_2$ units in solid solution
m number of bond water molecules, apart from those occurring in the hydroxyl groups

Adapting the model to the experimentally determined chain length, that is to $3n-1$, the authors obtain the following formula:

$$Ca_X H_{(6n-2X)} Si_{(3n-1)} O_{(9n-2)} \cdot z Ca(OH)_2 \cdot m H_2O \tag{3.15}$$

These both formulae are in good compatibility with the polysilicate presented in the model proposed by Glasser et al. [68] and the second with C–S–H composed of the dimers only.

The alternate formula was given by Richardson [67]:

$$\left\{Ca_{2n}H_wSi_{(3n-1)}O_{(9n-2)}\right\}\cdot(OH)_{w+n(y-2)}\cdot Ca_{ny/2}\cdot mH_2O \tag{3.16}$$

in which w is the number of silanol groups, w/n—the degree of silicate chain protonation.

The extreme values of variables in these formulae, resulting from the layer structure and electrical neutrality of crystal are as follows:

$$\begin{aligned} &0 < y < 2,\ n(2-y) < w < 2n \\ &2 < y < 4,\ 0 < w < 2n \\ &4 < y < 6,\ 0 < w < n(6-y) \\ &X = 1/2\ (6n-w) \\ &z = 1/2\ [w+n(y-2)] \end{aligned} \tag{3.17}$$

In the formula 3.16, analysed on the point of view of T/CH model terms in the parentheses correspond exclusively to the tobermorite. It has very disordered layer structure, composed of the chains of the medium length equal $3n-1$. Dimers ($n=1$) during the polymerisation undergo joining by bridging tetrahedra with formation of pentamers ($n=2$) and longer chain sections. The Ca^{2+} ions appearing in amount $2n$ in brackets belong to the main layer, however, the part $n-(w/2)$ from the total $(n\cdot y)/2$ Ca^{2+} number, being outside the brackets are the interlayer calcium ions, indispensable for electric charge balance. Their position depends on the adapted structural arrangement. In case of T/CH model they belong to the CH layers situated between the silicate layers of tobermorite structure that is the ones forming the tobermorite layers; in the case of T/J model they constitute a part of main jennite layer, as Si–O—Ca–OH. These structural units can change in different areas in the C–S–H structure; causing therefore the changes of composition of this phase, observed under the transmission electron microscope. Designing by the symbols T or J the units derived from jennite or tobermorite phases it was possible to use in the schematically presented structures on Figs. 3.27 and 3.28 the denotation J2 and T2 which correspond to the dimers in these structures formed by removal of all bridging tetrahedra. In the adapted model presented by the formula 3.16, the degree of silicate chains protonation w/n can be variable too. Summarizing the discussion of the model proposed by Richardson and Groves [66, 67] it is worthwhile to notice that it does not introduce any new hypothesis but it is a generalization of previous T/J and T/CH models. This model, in comparison with that of Taylor, gives higher freedom in variable share of hydroxyl groups in the C–S–H structure. This is because in the "more generalized" structure the tobermorite groups occupy the positions being the mirror projections of jennite ones [65].

Nonat [35, 39] has proposed another C–S–H model, including all the range of C/S ratios, from 0.66 to 2; simultaneously, there is no need to assume its disordered structure. In this whole range of C/S ratio the XRD pattern of this phase is very similar to that for the 1.4 nm tobermorite; the basic plane d spacing shows small

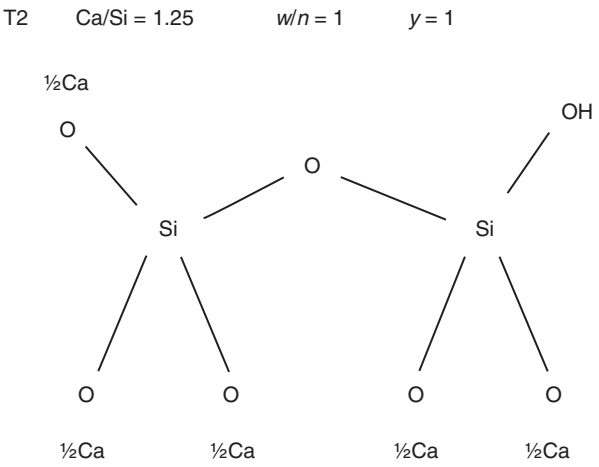


Fig. 3.27 Dimer in the tobermorite structure according to the model proposed by Richardson, with the mean degree of protonation of silicate chain SiO_4^{4-}

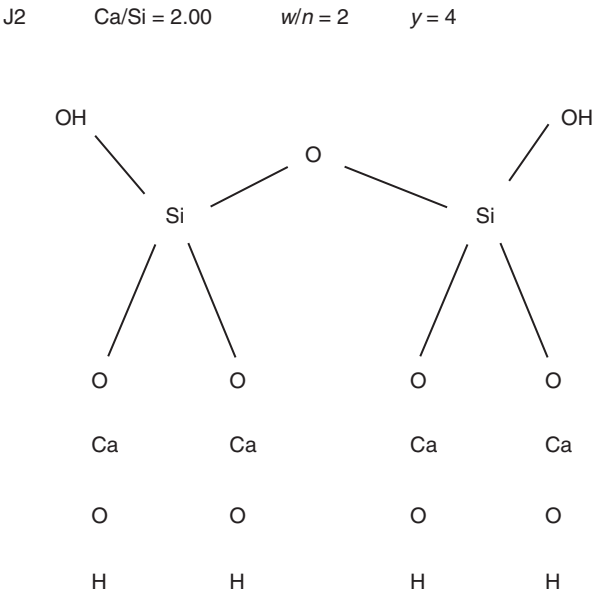


Fig. 3.28 The unit of jennite structure analogous to that shown in Fig. 3.27. (According to [67])

variations, even for high C/S ratio, close to 2. This model is based on tobermorite structure, in which the calcium ions from the main layer are not coordinated by OH^- ions. Nonat [39] has assumed that the interlayer positions in the tobermorite model are occupied by the calcium ions; their charges are balanced by the OH^- ions from the interlayer sites. Each missing bridging tetrahedron gives the sites for two OH^- ions in the structure and allows the acceptance of one $Ca(OH)_2$ group (Fig. 3.29). On the surface of C–S–H layers the acidic–basic equilibriums occur and the silanol groups Si–OH are formed; these groups form the complexes with calcium ions:

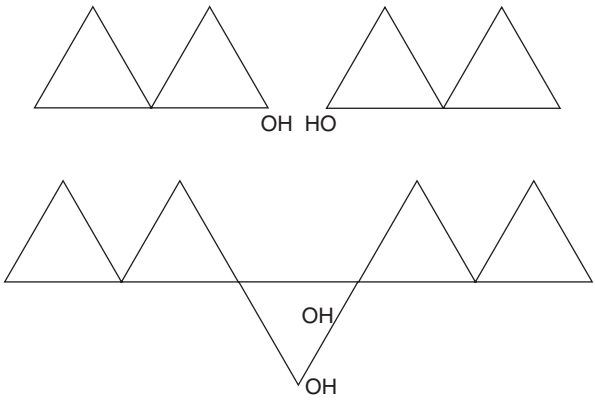


Fig. 3.29 Displacement of the silanol groups at the chain length change. (According to [35])

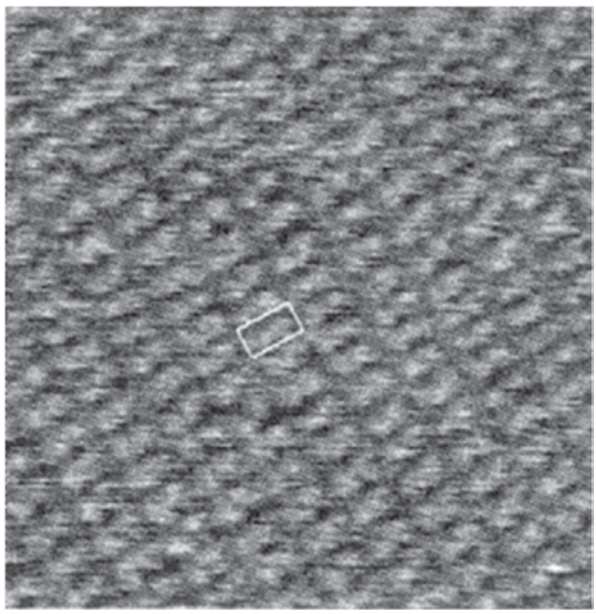


Fig. 3.30 Nanocrystallites of C–S–H (C/S = 1.5) under the AFM, formed on the surface of single calcite crystal. (According to [39])

$$-\mathrm{SiOH} + \mathrm{Ca}^{2+} \rightleftarrows -\mathrm{SiOCa}^{+} + \mathrm{H}^{+} \tag{3.18}$$

This model is in good agreement with the results of the spectroscopic investigations, because they give no possibility to distinguish whether the calcium ions are in the main layer, between the layers or in these two positions simultaneously.

The atomic force microscopy observations of the paste layer deposited on the single calcite crystal revealed that C–S–H gel is composed of the network of nanoparticles with the surface 60×30 nm^2 and 5 nm thick (Fig. 3.30). The rheological measurements have shown that this network reveals some elasticity under the

week stress [39]. The conclusion is that C–S–H is a gel, but composed of crystallites which gives known peaks on XRD pattern if the specimen is composed only of this phase (see Fig. 3.22).

Developing farther his model Nonat [35], notes that very high C–S–H surface area causes that the surface properties are at least as important as these attributed to the volume properties. Simultaneously the surface charge is changed with the variable calcium ions concentration in the solution [69]. At low Ca^{2+} ions concentration the C–S–H surface charge is negative, while at high concentration it is positive; the neutral zero point occurs at the concentration corresponding to 2 mmoles CaO per litre. This inversion of charge was presented by Viallis et al. [70] in the model including the two types of surface equilibrium related to the silanol groups present on the surface of silicate chains:

- the acid–base equilibrium of silanol groups –SiOH:

$$-\mathrm{SiOH} \rightleftarrows \mathrm{SiO^-} + \mathrm{H^+} \tag{3.19}$$

- the complexation of calcium by the surface –SiO groups:

$$-\mathrm{SiOH} + \mathrm{Ca^{2+}} \rightleftarrows \mathrm{SiOCa^+} + \mathrm{H^+} \tag{3.20}$$

At low concentration of calcium ions the first equilibrium prevails, at high concentration—the second one.

The model proposed by Nonat [35, 39] is based upon the following structural assumptions:

- the main layer is composed of dimers; their electric charge is balanced by two calcium ions, two free charges are linked with two protons: $Ca_2H_2Si_2O_7$;
- the two adjacent dimers can be bound by a bridging tetrahedron; in this case the bridging tetrahedron is linking also two protons, following the formula: $Ca_2H_2Si_2O_7(SiO_2)_x$, where $x<1$,
- the silanol groups can be partially ionized, their charges are balanced by the interlayer calcium ions, which gives:

$$\mathrm{Ca_2H_{2-p}Si_2O_7\left(SiO_2\right)_x\,Ca_{p/2}} \text{ or } \mathrm{Ca_2H_{2-p}Si_2O_7\left(SiO_2\right)_x\left(CaOH\right)_p},$$

- the $Ca(OH)_2$ particles can occupy the sites of missing bridging tetrahedra; this can be presented by the formula: $\mathrm{Ca_2H_{2-p}Si_2O_7\left(SiO_2\right)_x\,Ca_{p/2}},\ \left[\mathrm{Ca\left(OH\right)_2}\right]_y$.

Nonat [35, 39] gives the thermodynamic supplement to this model basing on the mass action law, related to the solution in equilibrium with the C–S–H phase and to the surface of this phase. The thermodynamic calculations comply well with the experimental results, as it is shown in Fig. 3.31.

Another approach to the C–S–H phase modelling was proposed by Jennings [91], which was taking into account the discrepancies occurring when the microstructure of this phase was evaluated based on the specific surface area and pore structure. It

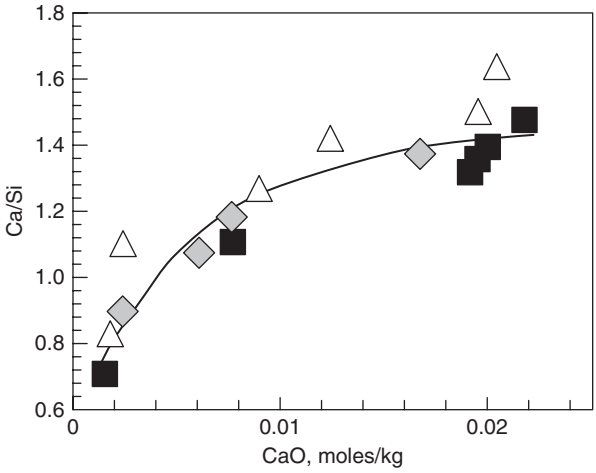


Fig. 3.31 C/S ratio measured and calculated based on the model (■, Δ). (According to [39])

has been shown that not only the different methods lead to the controversial results, but also one method, for example based on nitrogen adsorption measurements, gives significant differences in the case of apparent similar samples. Jennings [71] is reminding that Feldman's and Sereda's model, developed further by Daimon, reflects very well the C–S–H microstructure, proved by many experimental data, however, many problems remain unresolved. For example: why the specific surface area of C–S–H measured with different methods give significantly divergent values? Does this phase structure is homogenous in a scale exceeding 10 nm? And if it is not—if is it possible to quantify this inhomogeneity? These problems have not been elucidated also with help of the most modern methods, such as neutron scattering, low angle X-ray scattering or nuclear magnetic resonance. The tests of these discrepancies explaining takes Jennings [71] in his model, relating to the C–S–H microstructure in the range from 1 to 100 nm. The surface measurements by nitrogen adsorption reveal the occurrence of two types of C–S–H phase: one with the structure impermeable and the second permeable for nitrogen. Therefore the model proposed by Jennings and Tennis [72] assumes the presents of two types of C–S–H: one with more open constitution, accessible for the nitrogen molecules and the second of higher density to which they cannot migrate (Fig. 3.32).

According to Tennis and Jennings [72] hypothesis, there are the two types of C–S–H; high density C–S–H and low density C–S–H (Fig. 3.32). Jennings underlines that this model is well compatible with many experimental results and allow to elucidate many discrepancies. Both C–S–H types are built of spherical particles, however with a different packing density (Fig. 3.32); at more dense packing—HD C–S–H (*high density*)—the micropores are not accessible for nitrogen. The content of both C–S–H types in the cement paste depends on hydration conditions, and primarily of the w/c ratio, reaction temperature and the presence of mineral additions.

Richardson and Groves [66, 67] studied the solid solutions in the C–S–H phase. The Al^{3+} ions are the most important; they substitute silicon exclusively in the

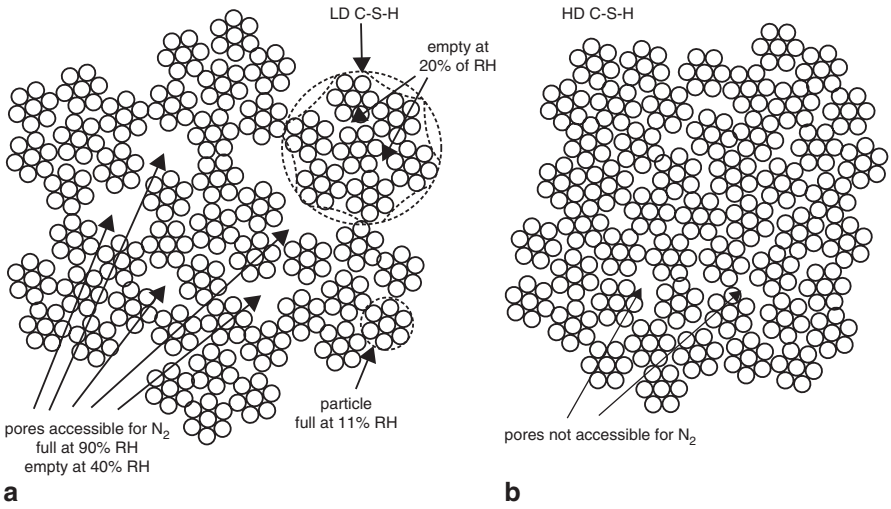


Fig. 3.32 Model of C–S–H gel of low (**a**) and high density (**b**). (According to [71, 72])

bridging tetrahedra. The monovalent ions can occur in the interlayer positions, balancing the shortage of charge resulting from the Al^{3+} substitution for Si^{4+}. These authors presume that the Na^+ and K^+ cations are present in the pastes of alkali activated slag in the interlayer positions. Others authors suppose also the possibility of solid solution formation by Fe^{3+}, as well as by SO_4^{2-} and CO_3^{2-}, however, the doubts cannot be excluded that it is caused by the nanometric mixture with AFm phase (see 3.3.2) [67, 73].

Many studies were devoted to the high adsorptive properties of C–S–H phase, relating to the very developed specific surface of this phase. The adsorption of chloride ions on the C–S–H phase was studied by Beaudoin et al. [74], which found that it is affected by the C/S ratio; the chemisorption is increasing with this ratio lowering. These authors detected the strongly bound chlorine which was not leached by water. Stade [75]. Found that the adsorption of potassium ions is depending on the C/S ratio and is increasing with this ratio reduction. This adsorption consists primarily on potassium ions bonding by the silanol groups, mainly from the outer surfaces of layers. The similar conclusions were drawn by Hong and Glasser [76]. These authors observed that C–S–H with low C/S ratio, particularly in the pastes produced from cements with mineral additions, was enriched with the sodium and potassium ions, as compared to C–S–H with high C/S, typical for ordinary Portland cement without additions. The bonds of these cations are relatively poor and that is why the desorption occurs quickly. The maximum amount of adsorbed ions and the chemical affinity of ions to the C–S–H surface are strongly affected by the ionic power[3] of the electrolyte, as it has been reported recently by Divet et al. [77]. The

[3] Ionic power $I = \Sigma_i c_i z_i^2$.

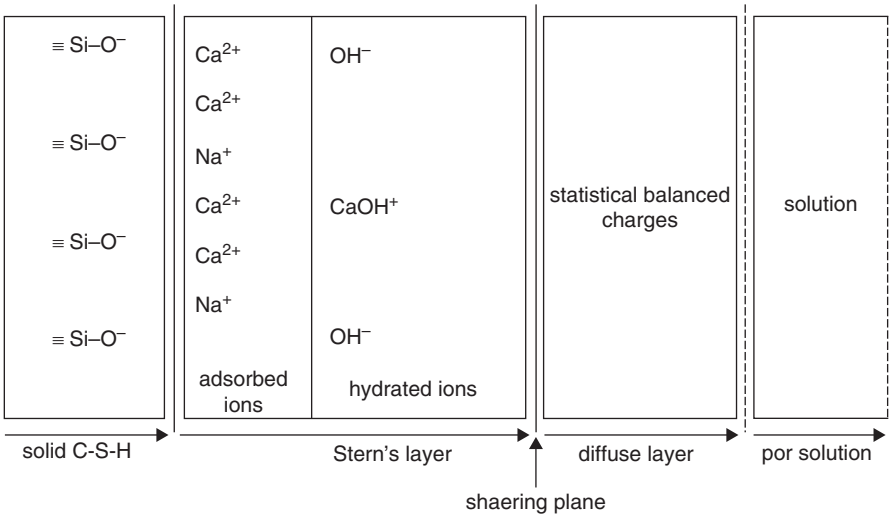


Fig. 3.33 Model of the double layer on the C–S–H surface loosely based on the model proposed by Divet [77]

relationship between the free ions in the solution and the adsorbed ones can be given by the Langmuir equation, which in the case of chloride can be written:

$$1/\left[Cl^-\right]_{ad} = 572 \cdot 1/\left[Cl^-\right]_{sol.} + 6.9 \tag{3.21}$$

In the case of sulphate ions:

$$1/\left[SO_4^{2-}\right]_{ad} = 74 \cdot 1/\left[SO_4^{2-}\right]_{sol.} - 0.23 \tag{3.22}$$

As can be calculated from the formula if the concentration of solution is on the level of 80 mmole/l the quantity of adsorbed chloride ions is 0.8 mmole/g C–S–H.

It should be underlined that the type of potential forming ions depends on the composition of the solution in the pores. At low calcium ions concentration the amount of these ions between the C–S–H layers is low and the surface charge of silicate anions is not balanced. In this case the negative centres on the C–S–H surface are balanced by the Na^+ and K^+ cations playing the potential forming role. Duchesne and Berube [78] proved the occurrence of Na^+ and K^+ ions in the double layer, at concentrations higher that the Ca^{2+} ions. In some cases the Ca^{2+} cations are the potential forming ions and the isoelectric point is attained at their concentration from 2 to 4 mmole/l [78].

It will be worthwhile to present a simplified model of double layer on the C–S–H surface in the paste, loosely based on Divet's et al. [77] model (Fig. 3.33). The adsorption phenomena consist in the exchange of anions in the Stern's external layer. The internal Stern's layer is composed mainly of Ca^{2+}, Na^+ and K^+ cations and the external one—from the OH^- and hydrated cations.

There is a much interest as the strength of C–S–H is concerned, because the properties of paste and concrete are strongly affected by this component. Taylor [63], considering the properties of C–S–H, relates to the definition of gel as a dispersion system in which the attracting forces (cohesion) among its dispersed elements are so strong that all the system reveals a rigid network and, at low stress it behaves as an elastic body.

Beaudoin et al. [79] studied the strength properties of pressed C–S–H specimens, as well as the strength of samples produced from C–S–H and CH. The strength was not affected by the C/S ratio in the range from 1 to 1.5, although the authors suspected that it is controlled by the polymers to dimers ratio.

Nonat [80], as well as Plassard et al. [81] studding the adhesion forces between the C–S–H layers concluded there are between them ionic bonds, being the consequence of the calcium ions presence. At low calcium ions concentration in the solution, the bonds: silanol group–water–silanol group (–OSiOH–H_2O–HOSiO–) between the C–S–H layers appear. A change of chemical bond takes place with increasing CH concentration: the silanol groups are increasing ionized with CH concentration and the negative charges formed are balanced by Ca^{2+}: –OSiO–Ca^{2+}–OSiO–, causing the reduction of interlayer space *c* between the two planes composed of calcium tetrahedra. The C–S–H density increases and the elasticity modulus became ten times higher.

Finally, Ulm et al. [82] have shown that the concrete and primarily the C–S–H phase, controlling its properties, can be classified as a porous material, complying the rules governing the mechanics of porous bodies. Nowadays the properties of these materials can be examined in the nanometric scale, as it has been shown by Nonat [80] and Plassard [81]. They are elastic bodies; to which the Biot modulus and coefficient (between 0.61 and 0.71 for C–S–H) could be applied [82].

3.3 Hydration of Calcium Aluminates

3.3.1 The System $CaO–Al_2O_3–H_2O$

There is a significant number of metastable calcium aluminate hydrates. Their identification is difficult because of a large number of polymorphs and high susceptibility to the formation of carboaluminates under the influence of CO_2, although they occur as well crystallized hydrates. In cement paste they can also form the nanometric mixtures with the C–S–H phase. Therefore it will be convenient to begin the discussion of calcium aluminate hydration from the presentation of the $CaO–Al_2O_3–H_2O$ system (Fig. 3.34).

In the C–A–H system, protected against the CO_2 influence, there is a large number of so–called hexagonal hydrates, crystallized in the form of hexagonal plates. These are the metastable phases, because cubic C_3AH_6 is the only stable calcium aluminate hydrate [83, 84]. This phase is, however, formed in the reaction of calcium aluminates with water only at temperature higher than 45 °C [85]. At lower temperatures

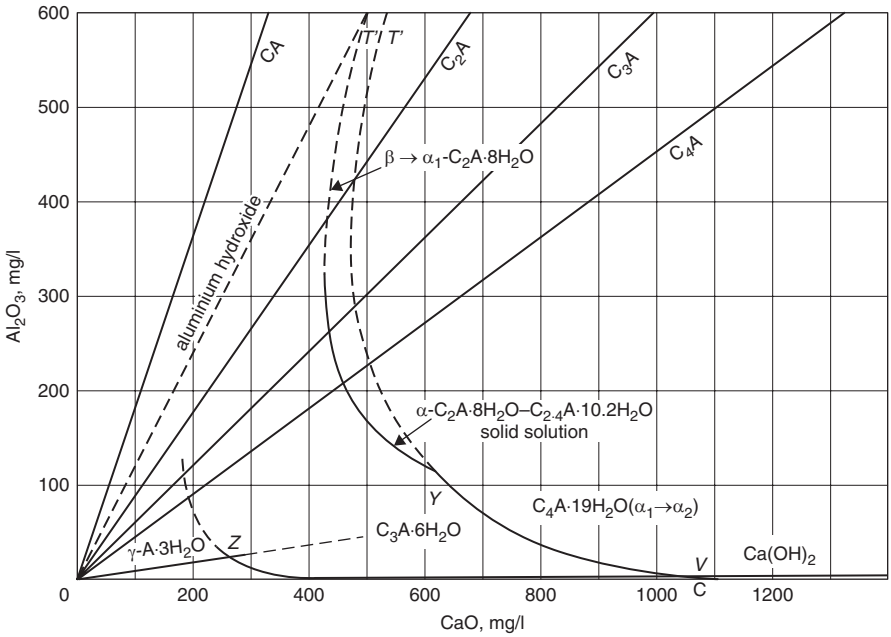


Fig. 3.34 Solubility curves in the $CaO–Al_2O_3–H_2O$ system at 25 °C (According to [84])

the metastable hexagonal aluminates are formed. There are two metastable phases in the $CaO–Al_2O_3–H_2O$ system: C_4AH_{19} and C_2AH_8. They form solid solutions with the limited solubility, of composition given by the formula: $C_{2.0\ldots2.4}AH_{8.0–10.2}$.

At temperatures lower than 20 °C the metastable CAH_{10} phase appears in this system, which is of special importance in case of high calcium aluminate cements (see Chap. 9.1). At temperature higher than 20 °C this phase is transformed into the C_2AH_8 hydrate and amorphous AH_3. According to Jones [84] it is the temperature range from 20 to 25 °C and even at temperature 22 °C the CAH_{10} phase is still formed. Above this temperature the transformation mentioned above takes place. However, during the high calcium aluminate cement hydration and at low w/c ratio the CAH_{10} phase is formed even at 25 °C.

The layer structure of hexagonal hydrates can be derived from their morphology; the thickness of the basic layer corresponds to the largest interplanar spacing on the XRD pattern. These layers are composed of $[Al(OH)_6]^{3-}$ octahedra and $[Ca(OH)_6]^{4-}$ tetrahedra linked with their corners (Fig. 3.35). The composition of the main layer is $[Ca_2Al(OH)_6]^+$ [73]. The structure of these phases is related to the $Ca(OH)_2$ structure in which every third Ca^{2+} ion is substituted by Al^{3+} and Fe^{3+}. The smaller aluminium and iron ions cause the disordering of this structure and influence of some shifting of Ca^{2+} ions and enable their coordination by H_2O molecules from the interlayer plane, beside of the six OH^- ions. Therefore Taylor [62] included these molecules to the main layer composition, which then reveals the composition

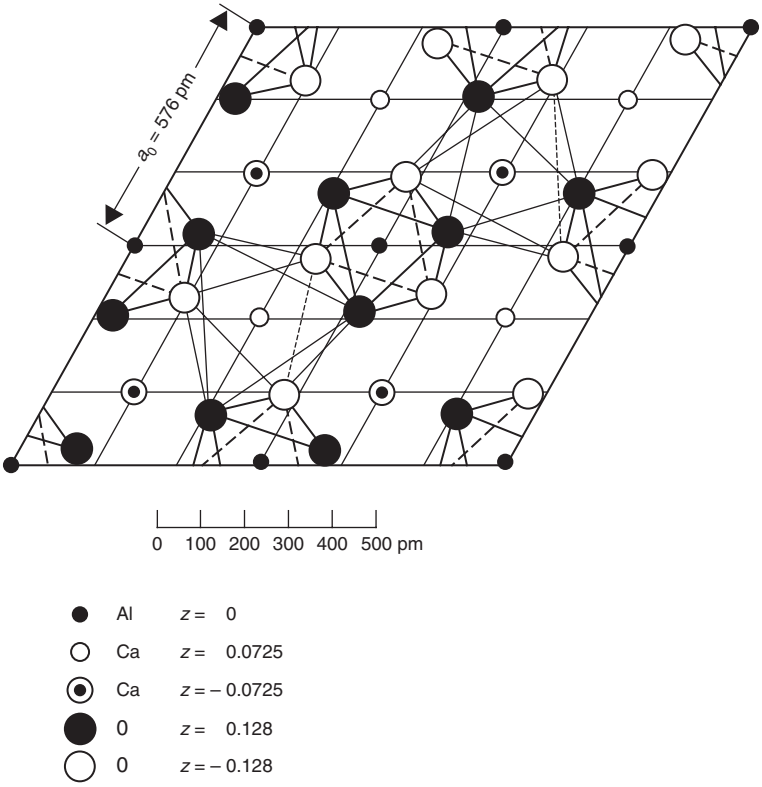


Fig. 3.35 The structure of calcium aluminate hydrate CAH_{19}. (According to [86])

$[Ca_2(Al, Fe)(OH)_6 \cdot 2H_2O]^+$. The hexagonal unit cell of calcium aluminate hydrates has the parameter $a = 570–590$ pm.

The two aluminate phases: C_2AH_8 and C_4AH_{19} are formed at temperature 25 °C, depending on the concentration of $Al(OH)_4^-$ and Ca^{2+} ions in the solution. It is considered that C_2AH_8 three polymorphs is forming: α_1 α_2 and β. The α_1 and α_2 are polytypes and reveal the same peaks of the basic interplanar spacings[4] on the XRD pattern; they differ only with the peaks of remaining planes. However, the β phase has lower *d* value (corresponding to the highest spacing between the basic planes). This is the phase which crystallizes first from the solution and, being in the contact with it, transforms steadily into the α_1 phase. The α_2 phase is obtained by α_1 dehydration to the $5H_2O$ and renewed hydration in the water vapour atmosphere. The XRD patterns of all these phases can be indexed based on the hexagonal unit cell with $a = 580$ pm and $c = 2159$ pm cell parameters.

The C_2AH_8 dried in the atmosphere with gradually decreasing humidity transforms steadily to the hydrate containing $7.5H_2O$ (1.06 nm)[5] at 34 % RH and $5H_2O$ (0.87 nm) at 12 % RH or heating to the temperature 102 °C. Further heating up to the

[4] Basic planes are the (001) planes.

[5] The numbers in brackets are the highest spacing of basic planes.

temperature 120 °C results in the formation of $4H_2O$ containing phase (0.74 nm). The hydrates with 7.5 and $5H_2O$ molecules are rehydrated at 81 % RH, while the C_2AH_4 does not rehydrate [87].

The composition of the tetracalcium aluminate was firstly determined as C_4AH_{13}, however, it appeared finally that at temperature 25 °C only the C_4AH_{19} coexists with the liquid phase. C_4AH_{19} transform into the C_4AH_{13} during drying. At temperatures exceeding 50 °C the latter one can occur in the contact with the solution.

C_4AH_{19} forms also two polymorphs: α_1 and α_2; the latter one is more stable and shows less disordered structure [83]. They both are the polytypes and reveal the hexagonal unit cell—α_1: $a = 577$ pm, $c = 6408$ pm, α_2: $a = 577$ pm, $c = 2137$ pm.

At relative humidity from 12 to 81 % the C_4AH_{13} hydrate occurs as a β polymorph only and reveals the peak from the interplanar spacing $d = 790$ pm. The dehydration of this hydrate proceeds steadily to the water content $11H_2O$ and $7H_2O$; the first one with basal spacing $d = 740$ pm. Hydrate containing $7H_2O$ has only the hydroxyl groups [83, 88]. The rehydration of these hydrates occurs easily to produce C_4AH_{13} at 81 % RH.

The hexagonal hydrates transform, at room temperature, into the C_3AH_6 phase. This reaction occurs by a through–solution mechanism that is the dissolution of hexagonal phases and subsequent crystallization of the cubic one [83]. The rate of the process increases with temperature and with pH too. C_3AH_6 is formed as a product of C_3A hydration in boiling water or in saturated water vapour. The structure of this phase is cubic, the unit cell—space centred, with $a = 1256$–1258 pm, space group Ia_3d; there are eight "molecules" in the unit cell.

The TG curve of C_3AH_6 exhibits only one–step dehydration at temperature 270 °C; there is no intermediate hydrates. At temperatures above 275 °C the $C_3AH_{1.5}$ phase is formed, a metastable relics of C_3AH_6. The XRD pattern of this phase is similar to that for $C_{12}A_7$. At temperature 550 °C the $C_3AH_{1.5}$ phase decomposes to CaO and $C_{12}A_7$.

In hydrothermal conditions, at the temperature range 225–400 °C the C_3AH_6 phase gives $C_4A_3H_3$ and $Ca(OH)_2$ is released (Fig. 3.36). The formula of the product is probably: $Ca_4Al_6O_{10}(OH)_6$.

There are the three phases thermodynamically stable in the system $CaO–Al_2O_3–H_2O$ namely C_3AH_6, $Ca(OH)_2$ and $Al_2O_3 \cdot H_2O$. The *T'TYV* curves correspond to the liquid phase content in metastable equilibrium with the hexagonal hydrates (Fig. 3.34). *V* is the metastable invariant point C_4AH_{19}–$Ca(OH)_2$, *Y* corresponds to the invariant point, in which the hydrates C_4AH_{19} and C_2AH_8 coexist; therefore the C/A molar ration varies from 4 to 2.4. These hydrates are considered as corresponding to the solid solutions α_1– or α_2–C_4AH_{19} with α_1–C_2AH_8; their composition in the *Y* point is close to $C_{2.4}AH_{10.2}$. This sequence of the solid solutions is completed in point *T*. C_2AH_8 can coexist also with the liquid phase of composition corresponding to the *T'T* curve. As one can see, there is one more invariant point possible, as a result of *YV* curve and 0*Z* straight line, that is the curve of stable gibbsite intersection. The invariant points *Z:* for gibbsite–C_3AH_6 and *V*: for $Ca(OH)_2$–C_3AH_6 correspond to the stable equilibrium.

The system at temperature lowered to 21 °C is presented in Fig. 3.37. There is on it the additional curve corresponding to the metastable equilibrium of the CAH_{10}

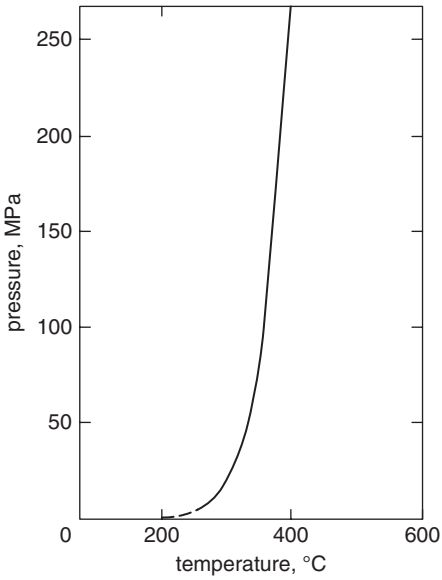


Fig. 3.36 The vapour pressure curve for C_3AH_6 (according to [33]). The decomposition products are: $4CaO \cdot 3Al_2O_3 \cdot 3H_2O$ and $Ca(OH)_2$

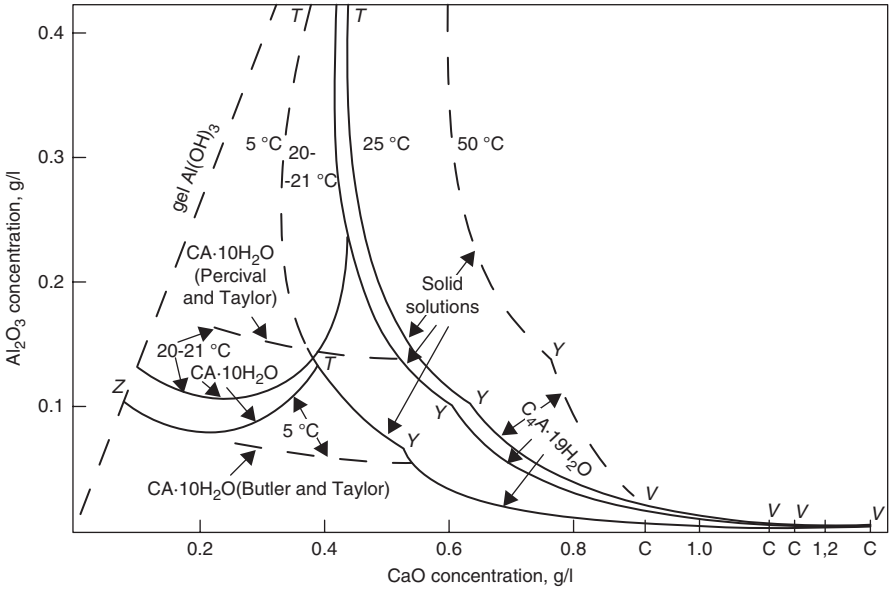


Fig. 3.37 CaO–Al_2O_3–H_2O system at different temperatures. (According to [84])

hexagonal phase. To simplify the image, two curves, corresponding to the stable equilibrium: gibbsite–C_3AH_6 and $Ca(OH)_2$–C_3AH_6 are omitted. Point *Z* is the invariant point for the following phases: aluminum hydroxide gel–CAH_{10}, while the point *T*: for CAH_{10}–solid solutions $C_{2-2.4}AH_{8-10.2}$. Taylor et al. [89] reveal that at temperature 5 °C this point corresponds to the coexistence of CAH_{10}–C_4AH_{19}. At temperature < 5 °C the C_3AH_6 is not stable and transforms into C_2AH_8 or C_4AH_{19} respectively of the liquid phase composition, as it has been reported in some works.

3.3.2 Calcium Sulphoaluminate Hydrates and Other Aluminate Hydrated Phases

The calcium aluminate hydrates can produce the two types of phases in Portland cement paste. At gypsum addition C_3A reacts always at ambient temperature with the sulphate ions and the ettringite $C_3A \cdot 3CaSO_4 \cdot 2H_2O$ is formed. This is the so–called trisulphate, denoted as AFt. When the concentration of sulphates in the solution is low, for example when gypsum is exhausted, the aluminate ions $Al[OH_4]^-$ react with ettringite giving the monosulphate phase $C_3A \cdot CaSO_4 \cdot 12H_2O$ which is known as AFm. Because the $[SO_4]^{2-}$ can be substituted in the structure of these phases by the other anions, simple and complex ones, such as OH^- or Cl^-, the AFt and AFm are the representatives of a large group of compounds. These compounds reveal usually different, rather limited ability of the formation of solid solutions and therefore their identification can be difficult, particularly as their structures, and subsequently the XRD patterns, are very similar.

The structural formula of ettringite is as follows: $[Ca_3(Al, Fe)(OH)_6 \cdot 12H_2O]_2 \cdot (SO_4)_3 \cdot 2H_2O$ [62]. As one can see the aluminum ions can be substituted by the iron(III) ions and simultaneously they are coordinated octahedrally by the OH^- groups. Because, as it has been mentioned earlier, the sulphate anion can be substituted by the other one, the constitutional formula of ettringite can be describe as follows: $[Ca_3(Al, Fe)(OH)_6 \cdot 12H_2O]_2 \cdot X_3 \cdot nH_2O$, where $n \leq 2$, and X means the unit related to the bivalent anion or two units of monovalent one [62]. There is not so many anions which could occupy the position X and the number of monovalent anions entering the Aft structure is limited too [62, 63]. Ettringite occurs in the form of needle–like or rod–like crystals; the latter ones are observed as the crystallization takes place in empty spaces of the paste, for example in the pores. Ettringite is a crystalline phase, detected by XRD as early as after 1 h of hydration [90]. The structure of ettringite is discussed in Chap. 8 relating, among the other, to the expansive cements.

The analogues of ettringite with the CO_3^{2-} and Cl^- ions replacing sulphate are as follows:

$$C_3A \cdot 3CaCO_3 \cdot 32H_2O \text{ and } C_3A \cdot 3CaCl_2 \cdot 32H_2O \tag{3.23}$$

The type and concentration range of the AFt solid solutions are given in many reports by Pöllmann et al. [91–94]. The solid solutions in the ettringite structure can be formed within the following range of compositions [92]:

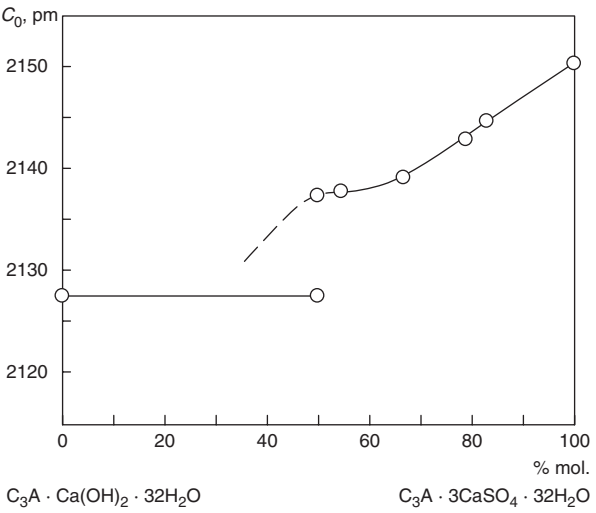


Fig. 3.38 Solid solutions of ettringite and AFt containing $Ca(OH)_2$. (According to [94])

$$\begin{aligned} &Ca_6\left\{Al_2(OH)_{12}\cdot 24H_2O\right\}^{6+}\left\{(x)SO_4\cdot(y)CO_3\cdot(2z)OH\cdot 2H_2O\right\}^{6-} \\ &\quad 0\le x\le 3 \\ &\quad 0\le y\le 2 \qquad x+y+z=3 \\ &\quad 0\le z\le 1.5 \end{aligned} \tag{3.24}$$

It is far easier to follow the compositions of the solid solutions with the two different anions only. These compositions are given by Pöllmann et al. [94]:

$$\left[Ca_6Al_2(OH)_{12}\cdot 24H_2O\right]^{6+}\left[(SO_4)_{(3-2x)}(CO_3)_{2x}\cdot 2H_2O\right]^{6-} \qquad 0\le x\le 1 \tag{3.25}$$

$$\left[Ca_6Al_2(OH)_{12}\cdot 24\,H_2O\right]^{6+}\left[(SO_4)_{(3-1.5x)}(OH)_{3x}\cdot 2H_2O\right]^{6-} \qquad 0\le x\le 1 \tag{3.26}$$

$$\left[Ca_6Al_2(OH)_{12}\cdot 24H_2O\right]^{6+}\left[(CO_3)_{(3-3x)}(OH)_{6x}\cdot 2H_2O\right]^{6-} \qquad 0\le x\le 1 \tag{3.27}$$

In the $C_3A\cdot 3CaSO_4\cdot 32H_2O$–$C_3A\cdot 3CaCO_3\cdot 32H_2O$ solid solutions there is a gap in the range from 100 to 75 % of carbonate phase; in this range the carbonate does not take the sulphate ions to the solid solution. The similar gap is observed in the series $C_3A\cdot 3Ca(OH)_2\cdot 32H_2O$–$C_3A\cdot 3CaSO_4\cdot 32H_2O$ in the range up to 50 mol % of the first component (Fig. 3.38).

Therefore the limiting formulae of these solid solutions with the anions, important for cement chemistry, have the following composition:

$$\begin{aligned} &C_3A \cdot CaSO_4 \cdot 2CaCO_3 \cdot 32H_2O \\ &C_3A \cdot 1.5CaSO_4 \cdot 1.5Ca(OH)_2 \cdot 32H_2O \\ &C_3A \cdot 2CaCO_3 \cdot Ca(OH)_2 \cdot 32\ H_2O \end{aligned} \tag{3.28}$$

Schwiete et al. [95] decribe the $C_3A \cdot 3CaCl_2 \cdot 30H_2O$ phase as stable at temperature below 0 °C, but unstable at 20 °C. This phase reveals the structure identical with that of ettringite. According to Goske and Pöllmann [96] the composition of AFt solid solution with $CaCl_2$ and some amount of $Ca(OH)_2$ is as follows:

$$C_3A \cdot (1-x)CaCl_2 \cdot (x)Ca(OH)_2 \cdot nH_2O, \quad \text{where } 0 \le x \le 0.17 \tag{3.29}$$

There are also the chromium ettringite $C_3A \cdot 3CaCrO_4 \cdot 32H_2O$, and boron which forms two phases: $C_3A \cdot Ca[B(OH)_4]_2 \cdot 2Ca(OH)_2 \cdot 36H_2O$ and $C_3A \cdot 2Ca[B(OH)_4]_2 \cdot Ca(OH)_2 \cdot 30H_2O$ as reported by Pöllmann et al. [94] and Kuzel and Pöllmann [97]. They can form the solid solutions with the sulphate ettringite and the CrO_4^{2-} ion can be substituted not only by the SO_4^{2-} but also by CO_3^{2-}, Cl^- and OH^- [98].

In the four component system $CaO–Al_2O_3–CaSO_4–H_2O$ (Fig. 3.39) only the one sulphoaluminate phase occurs [99]. This is the trisulphoaluminate $3CaO \cdot Al_2O_3 \cdot 3CaSO_4 \cdot 32H_2O$, AFt, known as a natural mineral ettringite. Ettringite is the product of reaction of calcium sulphate [sulphate anions] with calcium aluminate water solutions, forming needle crystals. Ettringite can be easily synthesized by reaction of the aluminum sulphate solution with calcium hydroxide:

$$Al_2(SO_4)_3\ aq + 6Ca(OH)_2 \rightarrow 3CaO \cdot Al_2O_3 \cdot 3CaSO_4 \cdot 32H_2O \tag{3.30}$$

Another method consists in the water processing of calcium aluminate mixture with gypsum and, if it is necessary, with calcium oxide, according to the following reaction schemes:

a. $C_3A + 3CaSO_4 \cdot 2H_2O + aq$
b. $CA + 3CaSO_4 \cdot 2H_2O + 2Ca(OH)_2 + aq$
c. $C_4A_3\overline{S} + 8CaSO_4 \cdot 2H_2O + 6Ca(OH)_2 + aq$

The aforementioned reactions schemes of ettringite formation takes place in reality between ions, in solution:

$$6Ca^{2+} + 2Al(OH)_4^- + 4OH^- + 3SO_4^{2-} + 26H_2O \rightarrow C_3A \cdot 3C\overline{S} \cdot 32H \tag{3.31}$$

The solubility product for this phase can be expressed as follows:

$$K = \left[Ca^{2+}\right]^6 \left[Al(OH)^{4-}\right]^2 \left[OH^-\right]^4 \left[SO_4^{2-}\right]^3 \tag{3.32}$$

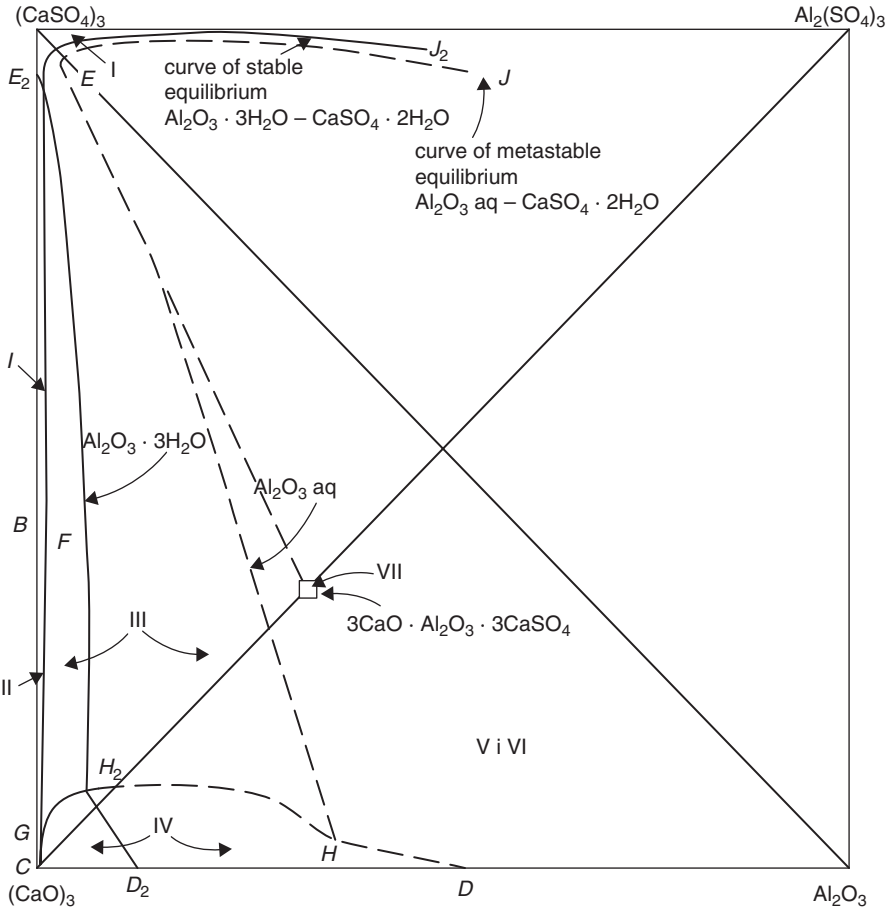


Fig. 3.39 $CaO–Al_2O_3–CaSO_4–H_2O$ system at temperature 25 °C (according to [84]): *I* $C\overline{S}2H$, *II* $Ca(OH)_2$, *III* ettringite, *IV* C_3AH_6, *V* $Al(OH)_3$ gel, *VI* gibbsite, *VII* $C_4A_3\overline{S}$

Ettringite is in equilibrium with the solution containing 0.215 g $CaSO_4$, 0.043 g CaO and 0.035 g Al_2O_3 per litre. In the less concentrated solutions ettringite dissolves incongruently; in water the $Al(OH)_3$ gel and the solution of the composition given earlier is formed. In the calcium hydroxide or gypsum solution the solubility decreases and the decomposition is hampered. In certain range of $Ca(OH)_2$ and $CaSO_4$ concentrations, the ettringite dissolves congruently and, at CaO concentration above 0.15 g/l, the C_3AH_6 precipitates, as a second solid phase.

In Fig. 3.40 the metastable equilibria in the system $CaO–Al_2O_3–SO_3–H_2O$ at room temperature are shown; the solubility planes of different phases are presented [62].

As it has been mentioned earlier, the monosulphate is the second calcium sulphoaluminate phase occurring in cement pastes. The general formula $[Ca_2(Al, Fe)(OH)_6] \cdot X \cdot nH_2O$ is attributed to this phase where *X* means the same as in the

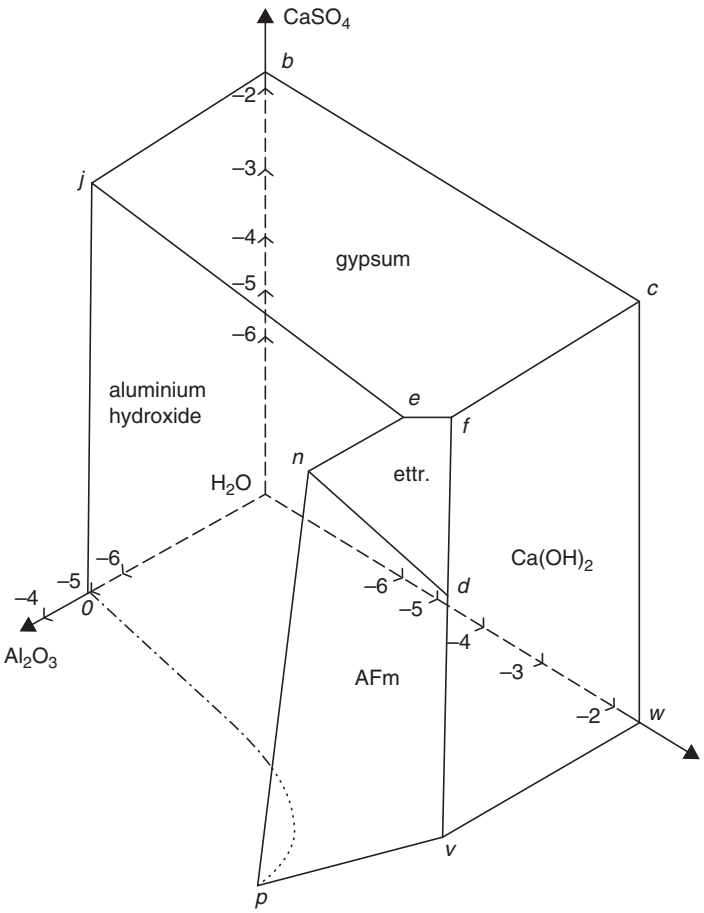


Fig. 3.40 The metastable equilibria in the system $CaO–Al_2O_3–SO_3–H_2O$ at temperature 20 °C; showing the crystallization planes

formula of AFt [62]. In favouring conditions this monosulphate is present in the form of plate–like hexagonal crystals, however, more often in cement pastes AFm is nearly amorphous and is intimately mixed with C–S–H gel [62] (Fig. 3.41).

The monosulphates show a layer structure, which was described earlier in the chapter relating to the C_4AH_{19}. The main layer, together with the H_2O molecules bound with the calcium ions can be given by the formula: $[Ca_2(Al, Fe)(OH)_6 \cdot 2H_2O]^+$ [62]. In more simple AFm structures these units are placed in such a way that the octahedral voids, surrounded by three H_2O from every neighbouring layers, appear. In these voids the *X* anions, water molecules or both these components together, can occur. For example in the $C_3A\ CaCl_2 \cdot 10H_2O$ phase, each void is occupied by the Cl^- ion, while in the monosulphate a half contain SO_4^{2-} anions and the remaining two water molecules H_2O [62]. However, in the C_4AH_{13} structure there are the OH^- anions and one H_2O molecule in each void.

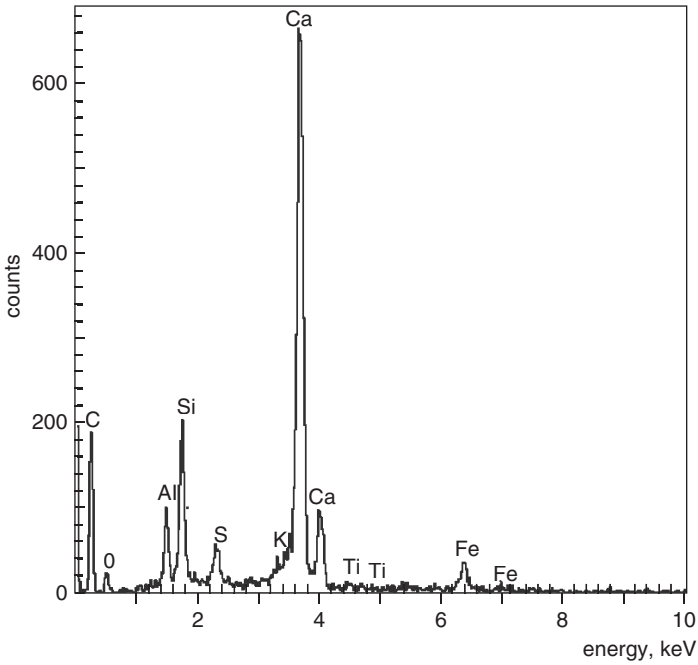


Fig. 3.41 Typical EDS plot of the C–S–H phase

As it results from the aforementioned solid solution ranges, they can contain a very low amount of OH^- ions [96].

$C_4A\bar{S}H_{12}$ forms the solid solutions with the C_4AH_{13} phase in which a half of SO_4^{2-} ions can be substitute by the OH^- ions. Earlier reports about the continuous formation of solid solutions have not been verified [62]. In the case of high sodium or potassium ions concentration in solution, the complex phases can be formed and these ions can be located between the layers [62, 98]. For example Dosch et al. [100, 101] report the formation of the $C_4A_{0.9}N_{0.5}\bar{S}_{1.1}H_{16}$ phase when the concentrations of aluminate, sulphate and sodium ions are high. The structure is close to that of $C_4A\bar{S}H_x$, however, there is a shortage of some Al^{3+} ions and this is balanced by the Na^+ ions in the interlayer positions.

In case of chloride ions in the solution the Friedel's salt is formed readily. This salt does not form the solid solution with monosulphate but a compound having the composition $C_6A_2 \cdot CaSO_4 \cdot CaCl_2 \cdot 24H_2O$ in which the regions of interlayers containing Cl^- ions occur alternatively with those in which SO_4^{2-} ions are placed [102].

In the system containing SO_4^{2-} and OH^- ions the compound having the following formula can occur [102]:

$$C_3A \cdot \frac{1}{2}CaSO_4 \cdot \frac{1}{2}Ca(OH)_2 \cdot nH_2O \tag{3.33}$$

However, when in solution the OH^- and CO_3^{2-} ions are present, the following phase can be formed:

$$C_3A \cdot \frac{1}{2}CaCO_3 \cdot \frac{1}{2}Ca(OH)_2 \cdot 11.5H_2O \tag{3.34}$$

The simultaneous occurrence of the OH^-, SO_4^{2-} and CO_3^{2-} anions in the solutions can result in the formation of phases containing these anions, such as:

$$C_3A \cdot \frac{1}{6}CaSO_4 \cdot \frac{1}{6}Ca(OH)_2 \cdot \frac{4}{6}CaCO_3 \cdot nH_2O \text{ or}$$

$$C_3A \cdot \frac{1}{6}CaSO_4 \cdot \frac{1}{2}Ca(OH)_2 \cdot \frac{2}{6}CaCO_3 \cdot nH_2O \qquad [102]$$

The general formula of these solid solutions has been proposed by Pöllmann et al. [103]:

$$Ca_4\left[Al_2(OH)_{12}\right]^{2+}\left\{(x)SO_4 \cdot (y)CO_3 \cdot (2z)OH \cdot aq\right\}^{2-}$$
$$0.5 \le x \le 1 \qquad 0 \le z \le 0.5 \tag{3.35}$$
$$y = 0 \qquad x + y + z = 1$$

As it is clearly seen from the range of solid solutions given by Pöllmann et al. [103], they are not formed in the system: $C_3A \cdot CaSO_4 \cdot aq$–$C_3A \cdot CaCO_3 \cdot aq$. However, in the system $C_3A \cdot CaCO_3 \cdot aq$–$C_3A \cdot Ca(OH)_2 \cdot aq$ the unlimited solid solutions takes place and a compound with the composition corresponding to the centre of their sequence is formed.

Motzet and Pöllmann [104] report the conditions of formation and the properties of AFm phases containing the sulphate (VI) and sulphite (IV) ions and their solid solutions with C_3AH_{13}. They can be formed in a wide range until 0.7 mol $C_3A \cdot Ca(OH)_2 \cdot 12H_2O$. The release of water from the monosulphite (III) $C_3A \cdot CaSO_3 \cdot 11H_2O$ occurs steadily; every one molecule at temperatures 40, 85 and 110 °C, respectively. The dewatering from the main layer up to the temperature 300 °C proceeds and subsequently the release of crystallization water occurs and the structure collapses already from the temperature 260 °C. Ecker and Pöllmann [105] found also the iron containing AFm and they propose a general formula of solid solutions with the sulphite (IV) ions among the other. This formula is as follows: $4CaO \cdot X_2O_3 \cdot CaY \cdot nH_2O$, where $X = Al^{3+}$, Fe^{3+}, Cr^{3+}; $Y = SO_4^{2-}$, SO_3^{2-}, $(Cl_2)^{2-}$, $(Br_2)^{2-}$, $(I_2)^{2-}$, $(NO_3)_2^{2-}$, $(OH)_2^{2-}$, $S_2O_3^{2-}$. There is also the sulphite (III) containing "ettringite", however it can be produced in special conditions; in cement paste it is not formed at $CaSO_3$ addition [105][6]. Kuzel [106] reports the $CaCl_2$ and $CaBr_2$ containing AFm.

As it can be derived from the compositions proposed by Pöllmann et al. [107], there are also the solid solutions of layer aluminates from the AFm series with chromium and boron. These phases are of significant importance as the immobilization of heavy metals from the waste materials is concerned.

[6] In Poland the system $CaSO_3$–C_3A–H_2O was studied by Lagosz A. and Malolepszy J., Cem. Concr. Res. **33**, 333 (2003).

Table 3.2 Calcium aluminate hydrates with organic cations [113]

A	$[Ca_4Al_2(OH)_{12}]^{2+}\,[(R)_2 \cdot nH_2O]^{2-}$	$R = H–(CH_2)_n–COO^-$ $R = (C_6H_5)–(CH_2)_n–COO^-$
B	$[Ca_4Al_2(OH)_{12}]^{2+}[2x(OH)_2(2–2x)(R)_2 \cdot nH_2O]^{2-}$ $0 < x < 1$	$R = CH_3–(CH_2)_n–SO_3^-$ $R = (C_6H_5)–(CH_2)_n–SO_3^-$

Renaudin et al. [108] investigated the nitrate ions containing AFm phase. The composition of this phase is as follows: $4CaO \cdot Al_2O_3 \cdot Ca(NO_3)_2 \cdot 10H_2O$.

Pöllmann [109, 110, 112–114], as well as Stöber and Pöllmann [111] found the numerous calcium aluminate hydrates with organic cations in the interlayer positions. They can form solid solutions (*A*) or compound of defined composition (*B*). The examples are given in Table 3.2.

Stöber and Pöllmann [111] describe the benzene–sulphonate ions containing AFm of composition $C_3A \cdot Ca(C_6H_5SO_3)_2 \cdot nH_2O$. Meyer et al. [115] report the reaction of calcium aluminates with the citric acid, investigated also by Pöllmann [112]. According to Pöllmann [114] there are also the similar compounds of calcium aluminate hydrates with organic cations related to the AFt phase.

The $C_3A \cdot CaSO_4 \cdot 12H_2O$, denoted briefly as AFm is the second phase present, as a rule, in Portland cement paste. The monosulphate crystallizes in the form of hexagonal plates. This phase can be synthesized from the metastable solution of calcium aluminate by adding saturated solution of calcium hydroxide with gypsum of concentration at which the molar ratio $CaSO_4/Al_2O_3$ in the initial mixture is 1. When this molar ratio is higher, the ettringite is also formed, when it is lower—the solid solution with C_4AH_{13} is produced. To avoid the $Al(OH)_3$ gel precipitation, the CaO/Al_2O_3 molar ratio must exceed 3.

It has been found that at full saturation with water the there is about $16H_2O$ in the monosulphate phase ($d = 959$ pm), while at RH lower than 90% this monosulphate transforms to the hydrate with $12H_2O$ molecules, having $d = 899$ pm [116]. Monosulphate is formed also as a result of reaction between the ettringite and hexagonal aluminates.

In Fig. 3.42 the section of four components system with extended scale of $CaSO_4$ concentrations, is shown. The $CaSO_4$ concentration in the solutions along the H_2R_2 is a metastable prolongation of the E_2H_2 curve from Fig. 3.39. Monosulphate occurs together in metastable equilibrium with ettringite and the solution along the R_2M. Along the $R_2S_2T_2$ curve the solid solution $C_3A \cdot CaSO_4 \cdot 12H_2O$–$C_3A \cdot Ca(OH)_2 \cdot 12H_2O$ co–exists with $Al(OH)_3$ and the liquid phase.

The area of metastable solid solutions $C_3A \cdot CaX \cdot 12H_2O$ has been shown in the four–component system, elaborated by D'Ans and Eick [99] (Fig. 3.43). Although these authors used another AH_3 gel than Jones, the solubility curves and invariant points in both systems do not differ significantly (see Table 3.3). There are the differences as the composition of solid solutions $C_3A \cdot CaX \cdot 12H_2O$ and the fields of its primary crystallization are concerned. According to D'Ans and Eick [99] their composition lies between C_4AH_x and $C_3A \cdot CaSO_4 \cdot nH_2O$. These authors did not found the occurrence neither C_2AH_8 nor CAH_{10} phase. The difference dealing with the field of primary crystallization is related to the continuous reduction of Al_2O_3

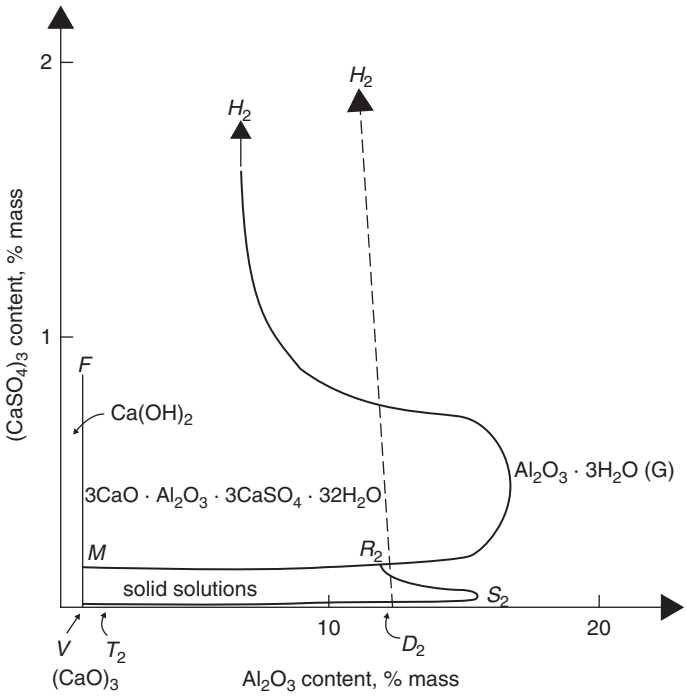


Fig. 3.42 Section of the metastable crystallization field in the $CaO–Al_2O_3–CaSO_4–H_2O$ system at temperature 25 °C, including solid solutions (according to [83]). $Al_2O_3 \cdot 3H_2O$ (*G*) is an intermediate phase between the bayerite and gibbsite; *F, H*$_2$ etc mean the invariant points (see Fig. 3.43, Table 3.3)

concentration with the distance from the $CaO–Al_2O_3–H_2O$ plane. In Fig. 3.43 the *vm* curve represents the composition of the solution in equilibrium with C_4AH_x. The *m* point is an invariant point of this phase in equilibrium with the AH_3 gel, while *v* point with $Ca(OH)_2$. The composition in the point *m* is not consistent with the results reported by Jones for the temperature 21 °C [84]; therefore the further studies are required to elucidate the problem of solid solutions.

The studies of Glasser [117] put a new light on this problem. Basing on them, Brown [118] discussed the C_3A hydration, taking into account the results of D'Ans and Eick too. This will be developed in the next chapter.

3.3.3 C_3A Hydration

The tricalcium aluminate reacts with water at a highest rate among the clinker phases and affects substantially the rheological properties of cement paste. The gel products are formed very rapidly and subsequently crystallize as a mixture of the two phases: C_2AH_8 and C_4AH_{13} respectively. These products cover the C_3A grains and further

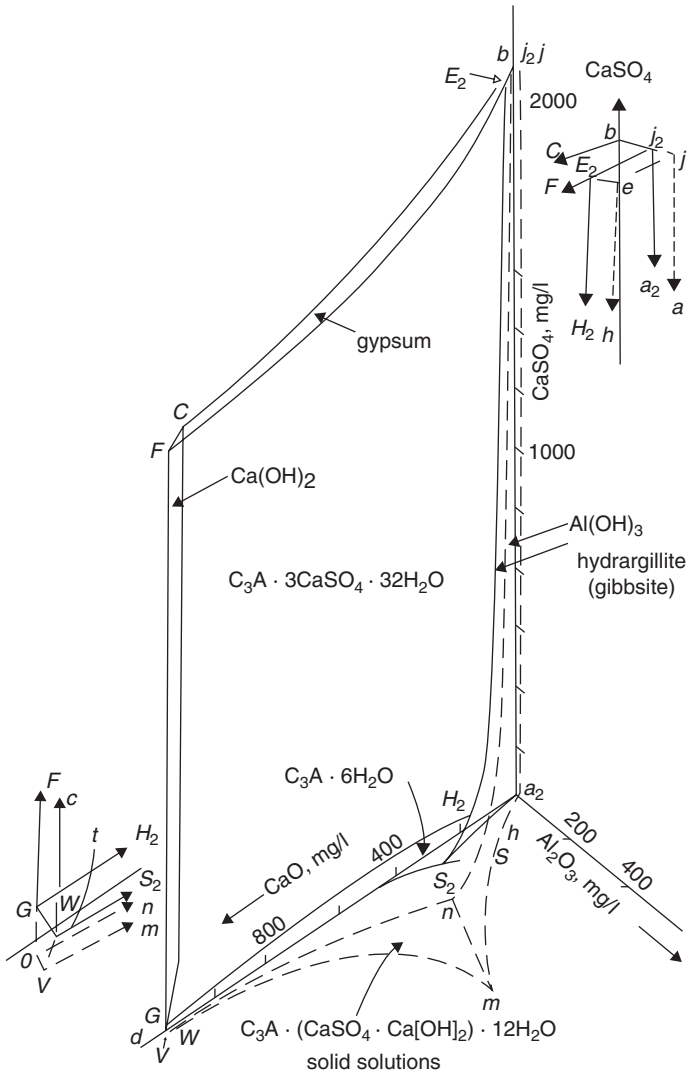


Fig. 3.43 STable (*continuous lines*) and metasTable (*dashed lines*) equilibria of crystallization process in the $CaO–Al_2O_3–CaSO_4–H_2O$ system at temperature 20 °C. (According to [99])

hydration occurs as a result of diffusion of ions through this layer. C_4AH_{13} transforms steadily into the C_4AH_{19}; the latter one can appear independently as a primary one. These hexagonal hydrates in turn transform to the only one stable cubic OH^-_{ad}—this transformation is accelerated at higher temperature, basically over 30 °C:

$$C_4AH_{19} + C_2AH_8 \rightarrow 2C_3AH_6 + aq \tag{3.36}$$

Table 3.3 Invariant points in the four component system at temperature 20 °C [99]

Point	Concentration, mg/l			Phase	Concentration, mg/kg[a]		
	Al_2O_3	CaO	$CaSO_4$		Al_2O_3	CaO	$CaSO_4$
b	–	–	2010	$CaSO_4 \cdot 2H_2O$			
c	–	1105	1683	$CaSO_4 \cdot 2H_2O$ $Ca(OH)_2$			
w	–	1159	–	$Ca(OH)_2$			
t	3.25	1172	–	$Ca(OH)_2$			
			–	$C_3A \cdot 6H_2O$			
S_2	25	315	–	Hydrargilite $C_3A \cdot 6H_2O$			
a_2	0.9	–	–	Hydrargilite			
j_2	0.8	–	2064	Hydrargilite $C_3A \cdot 6H_2O$			
F	2.75	1154	1660	$CaSO_4 \cdot 2H_2O$[b] $Ca(OH)_2$[b]	6.12	1076	1680
G	2.62	1196	14.6	$Ca(OH)_2$[b] $C_3A \cdot 6H_2O$[b]	1.02	1063	24.6
H_2	16.17	159.1	35.75	$C_3A \cdot 6H_2O$[b] Hydrargilite[b]	9.2	174.6	51
E_2	9.23	17.7	2016	Hydrargilite[b] $CaSO_4 \cdot 2H_2O$[b]	2.55	37.75	2040

[a] At temperature 25 °C—according to Jones [84]
[b] Apart from $C_3A \cdot 3CaSO_4 \cdot 32H_2O$

In Fig. 3.44 the microcalorimetric curve, as well as the mechanism of this process are shown schematically according to Skalny [119]. After a rapid reaction with water an induction stage, attributed to the formation of the hexagonal hydrates layer, poorly marked on the calorimetric curve, appears. The theory related to the hampering action of hexagonal hydrates has been proved by the experiments showing that the hexagonal phase stabilizers result in this induction stage elongation [120]. The layer of hexagonal hydrates cannot disturb the C_3A hydration for a longer time because it collapses during the transformation into the cubic C_3AH_6 (Fig. 3.44). This process occurs readily as the heat of C_3A reaction with water is high and as a consequence the temperature of the paste quickly increases.

There were also the hypotheses that the impermeable layer is formed by the AH_3 gel, which appears on the C_3A surface as a result of Ca^{2+} ions deficiency in the liquid phase, between the unhydrous grain and hexagonal hydrates, as a consequence of the C_4AH_{13} formation [121]. According to the hypothesis presented by Skalny [122], the C_3A hydration retardation is due to the formation of the layer rich in Al on the surface of hydrating grains. This is the consequence of incongruent dissolution. The Al rich layer, according to Skalny, transforms to Al_2O_3 or to the complex $[Al_8(OH)_{20}]^{4+}$. Barret [123] in turn, is of the opinion that this hypothesis has low probability, because his studies prove a congruent C_3A dissolution. This dissolution is proved by the composition of solution in which relatively high calcium ions concentration is accompanied by a high $Al(OH)^{4-}$ concentration too.

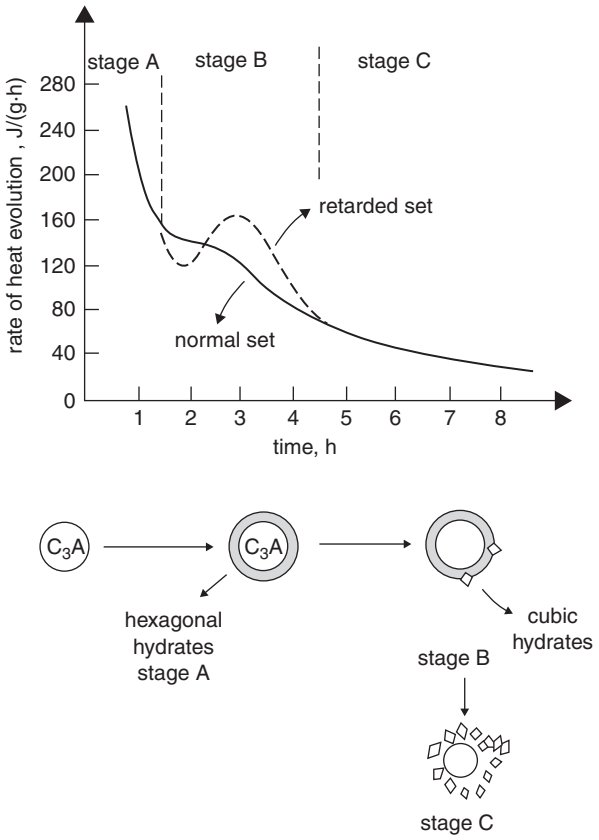


Fig. 3.44 C_3A hydration in water without gypsum. (According to [119])

The rapid formation of the hexagonal hydrates can be easily explained based on the C–A–H system. The dissolution of C_3A results in the molar ratio $CaO/Al_2O_3 = 3$ in the liquid phase (congruent dissolution) or higher than 3 (incongruent dissolution). This solution becomes quickly supersaturated in relation to the hexagonal hydrates (point *M'* in Fig. 3.45).

According to Barret [123] the mechanism of C_3A hydration is similar to the C_3S hydration. The hydroxylation of surface structure elements occurs first:

$$\begin{aligned}&(3Ca_{ca} + 2AlO_{2(AlO_2)} + 2O_O)_s + 4H_2O_l \rightarrow \\ &\rightarrow 3Ca_{ca} + 2Al(OH)_{4(AlO_2)} + 2OH_{Os} + OH^-_{ad}\end{aligned} \tag{3.37}$$

The surface hydroxylation is the effect of the four water molecules combination and protonation reaction, leading to the break of bonds in two water molecules. Immediately after the C_3A surface contact with water it will be privileged the release of one Ca^{2+} ion from the three into the solution, in connection with the formation of two adsorbed OH^-_{ad} ions. It should be manifested as by a temporarily departure from the congruent dissolution; the ESCA should exhibit a few second lasting decrease of C/A ratio on the C_3A surface, immediately after contact with water. Then the

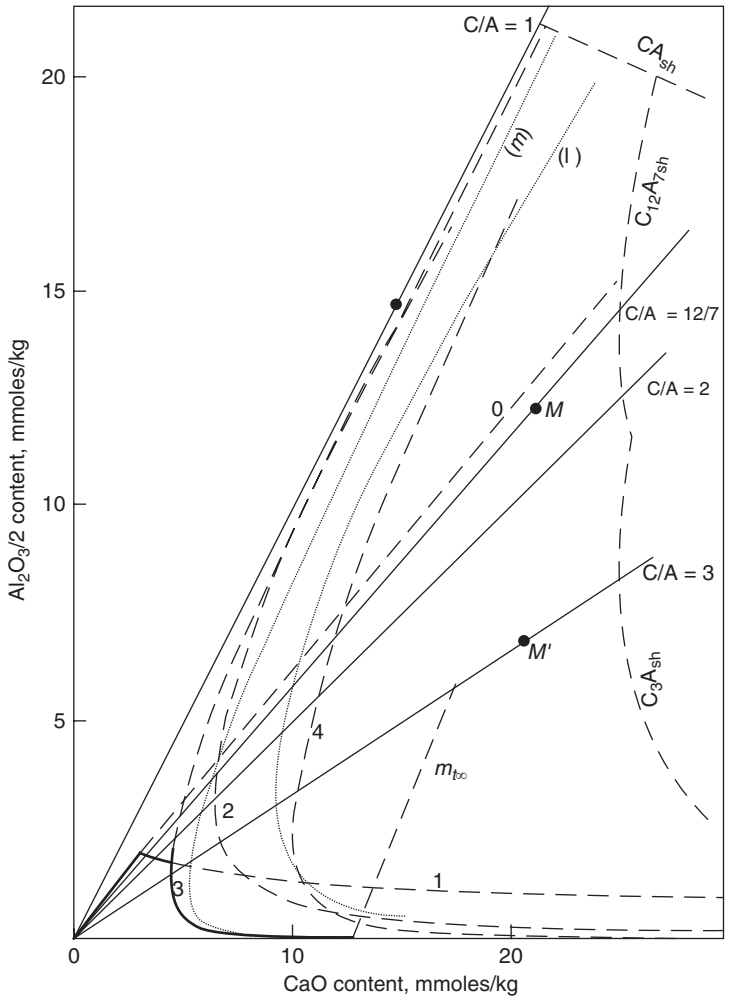


Fig. 3.45 CA_{sh} solubility curve and the solubility curves of hypothetical $C_{12}A_{7sh}$ and C_3A_{sh} phases superposed on the C–A–H system (according to [124]): *0* AH_3, *1* CAH_{10}, *2* C_2AH_8, *3* C_3AH_6, *4* C_4AH_{13}, (*m*) curve of minimum instability, (*I*) curve of the C_2AH_8 oversolubility (the boundary of the unsaturated area), *M* and *M'* points corresponding to the experimental compositions

hydroxylated C_3A layer will be dissolved (a dashed C_3A_{sh} curve in Fig. 3.45) with an exposure of new lattice nodes with oxygen atoms. This process corresponds to the C_3A congruent dissolution. However, this hypothesis has not such experimental support, as it is in the case of C_3S hydration.

The hydration of calcium aluminate is an excellent example of the Le Chatelier model that is the "through solution" reaction. Obviously, as the results of other authors have shown [6, 123, 124], the process is composed of dissolution, followed by nucleation and crystal growth of new phase. This can be well followed on the example of CA hydration.

The CA hydration mechanism is starting similarly as aforementioned phases from the surface hydroxylation. However, opposite to the other aluminates with the higher C/A ratio, the hydroxylation relates only to the transition of AlO^{2-} ions into the $[Al(OH)_4]^-$ ones; thus consists in combination of $2H_2O$, without the formation of two OH^- groups [124]. Applying the Kröger notation we have:

$$Ca_{ca} + 2AlO_{2(AlO_2)s} + 4H_2O_1 \rightarrow \left\{Ca_{Ca} + 2Al(OH)_{4(AlO_2)}\right\}_s \tag{3.38}$$

The hydroxylated $[Al(OH)_4]^-$ ions, behave like an isomorphous admixture occupying the sites of AlO_2^- ions in the structure. This hydroxylation state relates to the one "monomolecular layer", which does not form a separate phase, but a solid solution in the unhydrous aluminate.

The dissolution of the CA_{sh} layer and the formation of saturated solution in relation to this surface layer is the next stage of reaction [6]. The internal layers of CA are exposed and their hydroxylation occurs immediately. Simultaneously, some amount of AH_3 gel is precipitated and therefore the C/A molar ratio in the solution increases insignificantly to the value about 1.1. According to Bertrandie [123], this corresponds to the intersection of CA_{sh} solubility curve with "minimum instability curve" *(m* in Fig. 3.46). This minimum instability curve, from the chemical point of view, corresponds to the transformation of AH_3 gel into the C_2AH_8 phase [6, 124]. The CA_{sh} dissolution is congruent and accompanied by the following reaction:

$$Al(OH)_{4aq}^- \rightleftarrows Al(OH)_{3(gel)} + OH_{aq}^- \tag{3.39}$$

The supersaturation of the solution in relation to the AH_3 gel approaches infinity, when the ratio C/A = 1; it means that the OH^- concentration approaches zero[7]. This reaction is hampered when the ratio $(C/A)_l \approx 1.1$ in the saturated solution is attained.

The occurrence of the saturated solution is proved by its unchanged composition during the many hours period of time, after separation from the solid phase.

Bertrandie and Barret [123] reveal that the formation of hexagonal hydrates in the solution saturated in relation to CA takes place through the homogeneous nucleation. In case of this phase the nucleation occurs initially as a slowest process, illustrated on the calorimetric curve as a long, many hours lasting induction period [125] (Fig. 3.47). After long nucleation, the CAH_{10} phase crystallizes at temperatures below 10 °C; C_2AH_8 and aluminum hydroxide gel appear with increasing temperature.

The nucleation stage is shortened significantly when the calcium monoaluminate phase is contaminated with traces of $C_{12}A_7$ [126]. In the presence of $C_{12}A_7$ the concentration of Ca^{2+} in the liquid phase increases and the metastable region is attained, where the supersaturation in relation to C_2AH_8 (point *M* in Fig. 3.45) takes place and the curve corresponding to the liquid phase composition is intersecting the curve of oversaturation; which causes the instantaneous nucleation. The induction period is then markedly reduced. The similar effect is observed when the

[7] Calculations are given by Barret and Bertrandie [123].

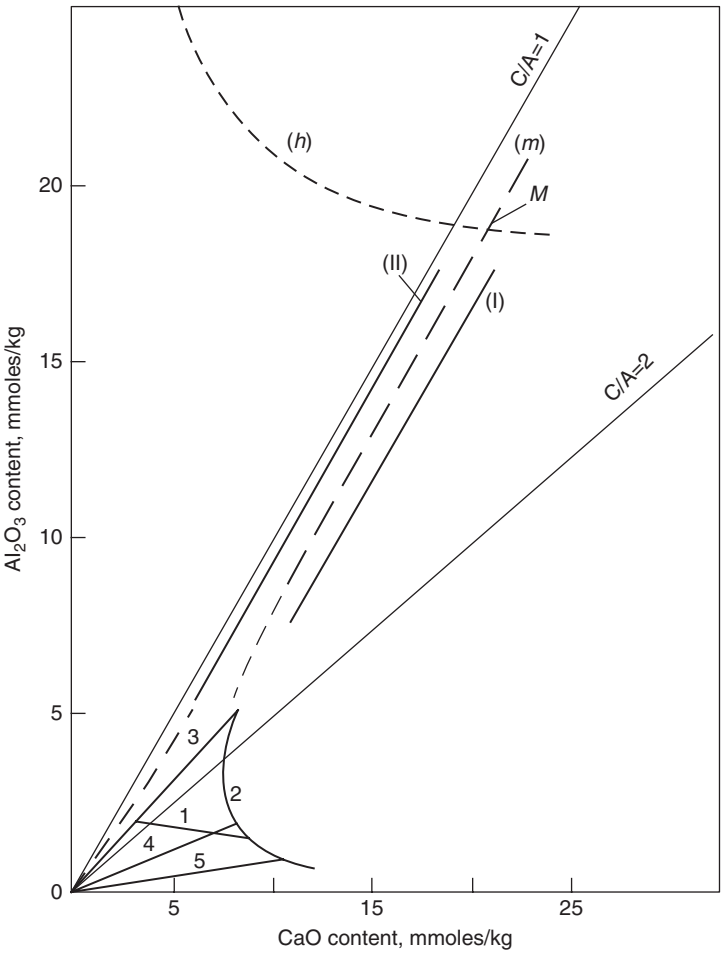


Fig. 3.46 The solubility curves: *1* CAH_{10}, *2* C_2AH_8, *3* AH_3 gel, *4* microcrystalline AH_3, *5* gibbsite. There is also shown the intersection point (*m*) of the curve corresponding to the minimum instability with the one (*h*), corresponding to the CA_{sh} solubility. The supersaturation curves: (*I*) C_2AH_8, (*II*) $Al(OH)_3$ gel are also plotted. (According to [124])

separated solution, saturated in relation to the CA_{sh} is treated with some amount of saturated Ca^{2+} containing solution. Then the rapid crystallization of C_2AH_8 occurs. It should be underlined that simultaneous crystallization of C_2AH_8, C_4AH_{13}, or even the carboaluminate hydrates with the precipitation of AH_3 gel, always result in the return of the liquid phase composition (C/A) to the straight line *m*. The experimental points are situated in a narrow range, called "a corridor" by Barret, between the curves (I) and (II) (Fig. 3.46); which are the C_2AH_8 (I) and AH_3 (II) oversaturation curves.

The concentrations of aluminate and calcium ions in the liquid phase co–existing with the hydrating calcium aluminates can be explained based on the metastable

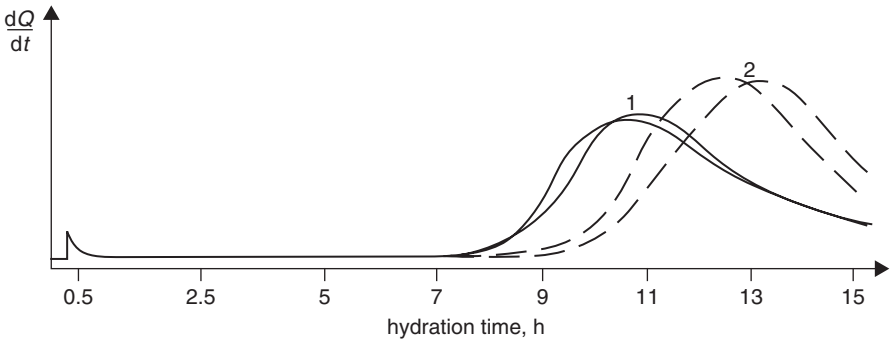


Fig. 3.47 Microcalorimetric curves of CA hydration (according to [125]); temperature 25 °C, W/S = 1; set of curves *1* grain size fraction form 40 to 75 μm, set of curves *2* fraction below 40 μm

equilibrium curves determined by Barret [123, 124]. The following solubility curves can be distinguished (Fig. 3.45): 0—AH_3 gel, 1—CAH_{10}, 2—C_2AH_8, 3—C_3AH_6, 4—C_4AH_{13}. The minimum instability curve (*m*) corresponds to the AH_3 transition into C_2AH_8, (I)—the C_2AH_8 oversolubility curve, (II)—the AH_3 oversolubility curve, $m_{t\infty}$—the straight line corresponding to the C_4AH_{13} transformation into C_2AH_8, on the right—C_4AH_{13} occurs, on the left—C_2AH_8, CA_{sh}, C_3A_{sh}, $C_{12}A_{7sh}$—solubility curves of the hypothetical surface hydroxylated layers.

3.3.4 C_3A Hydration in the Presence of Gypsum

The addition of gypsum is radically modifying the C_3A hydration process. A long induction period appears, followed by the crystallization of ettringite (Fig. 3.48). The preinduction period depends substantially on the rate of sulphate dissolution [127]. As it is commonly known, C_3A reacts with water violently and in the absence of gypsum hemihydrate or sodium and potassium sulphates, a certain amount of hexagonal hydrates is formed in the pre–induction period or even the monosulphoaluminate [128].

In the presence of gypsum ettringite is the only stable phase, covering the C_3A particles with thin layer, is hampering the reaction with water. According to the Skalny's hypothesis [122], there is another retarding mechanism, consisting in the adsorption of sulphate ions on the active sites on the C_3A surface. This hypothesis is rejected by Collepardi [129], who found the weaker retarding effect of Na_2SO_4 than gypsum and it should be quite opposite on the basis of both phases solubility. According to Chatterji [130] the hampering effect is not the consequence of ettringite itself, but it results from the formation of the hexagonal hydrates layer between the ettringite and C_3A grain.

The studies of C_3A hydration under the electron microscope of high resolving power reveal the formation of a gel layer on the surface; this layer corrugates and exfoliates; therefore it cannot be an impermeable membrane retarding the hydration

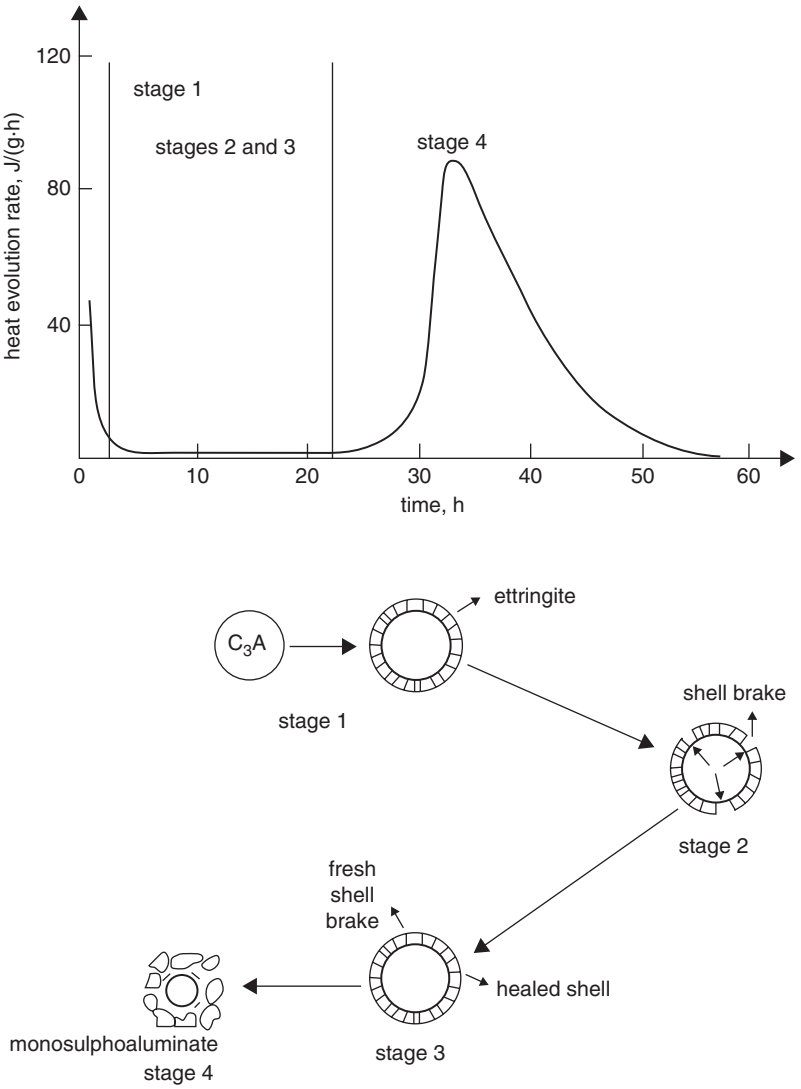


Fig. 3.48 C_3A hydration in the presence of $CaSO_4$. (According to [119])

process [131]. In the presence of gypsum this layer is more compact and on its surface, as well as in the solution, the ettringite small rods start to crystallize [131].

There are the other hypotheses reported, however, the hampering effect of ettringite thin layer is commonly accepted. Further reactions of C_3A with water occur due to the diffusion of SO_4^{2-}, OH^- and Ca^{2+} ions through this layer. The presence of ettringite layer was proved by the electron microprobe studies [132]. It was found that colloidal ettringite formed in the solution saturated with Ca^{2+} ions was causing more intensive retardation of hydration [133]. At the shortage of SO_4^{2-} ions in the

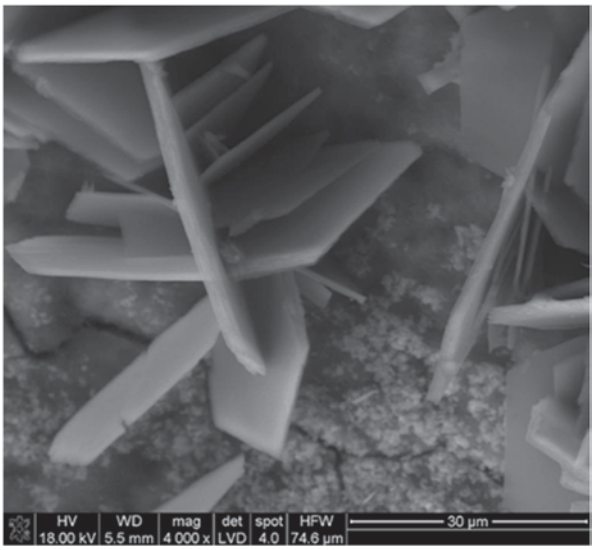


Fig. 3.49 Calcium monosulphate phase $C_3A \cdot CaSO_4 \cdot 12H_2O$. (By the courtesy of B. Trybalska)

solution close to ettringite layer, causes its transformation into monosulphate and its destruction. The other mechanisms of ettringite layer destruction assume its recrystallization, leading to the stresses and cracks formation.

Other hypotheses advance the topochemical ettringite formation on the C_3A/ettringite interface, as a result of ions diffusion. This process is known as an expansive reaction of ettringite formation, leading to the collapse of the ettringite layer. Some authors are of the opinion that the ettringite layer is destroyed by the osmotic pressure [134]. The layer with microcracks has no retarding effect but later, as the gypsum dissolves, these cracks are filled with ettringite and the further hydration is hampered. Finally, when gypsum is exhausted, C_3A hydration proceeds rapidly and simultaneously the ettringite transforms into the monosulphate of pseudo–hexagonal, plate–like morphology (Fig. 3.49).

The solid solutions of $C_4A\bar{S}H_{12}$ with C_4AH_{13} are formed in which the SO_4^{2-} and OH^- ions randomly occupy the sites between the layers [see p. 3.3.2].

3.3.5 Hydration of Different C_3A Polymorphs

The hydration of synthetic C_3A, with variable Na_2O additions, as well as C_3A from Portland cement was investigated. The lower hydration rate in the case of C_3A solid solutions with Na_2O has been reported by most of authors; the highest hydration rate was measured for cubic C_3A [132, 135–137]. The orthorhombic phase, with lower alkali content in the solid solution, reveals higher hydration rate than the monoclinic one [132].

Butt et al. [138] observed a reverse effect. Spierings and Stein [139] did not find any significant difference between the reactivity of various C_3A polymorphs

stabilized with sodium oxide, as compared to the cubic C_3A without foreign elements. Bilanda et al. [140] reported, as the other authors, the retarding effect in case of C_3A+H_2O paste, while the acceleration of reaction between the sodium doped C_3A and gypsum was found (see p. 2.5.3).

The rate of hydration decrease is explained by the densification of the structure, as a result of occupying the voids in the centres of $[Al_6O_{18}]$ rings in C_3A by sodium ions. The transformation of hexagonal hydrates into the cubic C_3AH_6 is also retarded [139].

The next problem relates to the effect of NaOH added to the liquid phase. Spierings and Stein [139] have shown that at low sodium ions content the initial rate of the process is lowering with the increase of Na^+ions concentration. However, at higher concentrations, exceeding 0.4 mol/l, the rate of hydration is increasing. The first effect was related to the drop of Ca^{2+}solubility in the NaOH solution and precipitation of amorphous CH. The second one—with the appearance of $Al(OH)^{4-}$ at higher OH^- concentration which is disturbing AH_3 gel formation. The lowering of the hexagonal hydrates stability with growing NaOH concentration is of importance too. Regourd et al. [141] found that the rate of cubic C_3A hydration in the mixture with C_3S and gypsum did not change practically in the NaOH solution. This is an additional proof that the effect of Na_2O in solid solution with orthorhombic C_3A is caused by the densification of the structure. On the other side, at 3 % K_2SO_4 addition the hydration of the orthorhombic C_3A phase is accelerated in such a way that its hydration degree is equal to the cubic phase [141].

Therefore there is no consistent opinion concerning the effect of Na^+on the rate of hydration, either as solid solution or introduced to the liquid phase. According to Boikova et al. [142] the other foreign ions present in the solid solution, such as Cr_2O_3, TiO_2, Fe_2O_3 and SiO_2, have also a retarding impact. Regourd [141] found also the slower hydration of the iron containing cubic C_3A phase.

Regourd [143] studied the hydration products in the C_3A+C_3S+gypsum mix and found the formation of the tri– and monosilicate–aluminate hydrates: $C_3A{\cdot}3CS{\cdot}31H$ and $C_3A\cdot CS\cdot 12H$. Usually the amount of these silicate–aluminates is generally higher in the case of cubic C_3A. The rate and sequence of their formation depends on the composition of the mixture. They appear with the highest rate in the mixtures with no gypsum. In the mixture with 5 % gypsum only the $C_3A\cdot CS\cdot 12H$ was present, after 8 months. At higher gypsum content (e.g. 16.5 %) the silicate–aluminates are not formed. Moreover, these both forms are instable at higher sulphate ions concentration in the liquid phase, corresponding, for example, to the concentration in the sea water [141]. Then the ettringite is produced. The both silicate–aluminate phases are generally poorly crystallized [141]. Their formation results from an intense diffusion of silicate ions from the C_3S grains toward the C_3A. The flux of aluminum ions in opposite direction is rather limited, however, the C–S–H phase can incorporate from 2 to 3 % Al_2O_3. Regourd [141] reported the formation of ettringite as a first product, then the growth of SiO_2 concentration in this phase and finally the formation of $C_3A\cdot 3CS\cdot 31H$ surrounding the C_3A grains, followed by the transformation into the monosilicate–aluminate, occurring with the decrease of silicate ions flux caused by the growth of C–S–H around the C_3S grains. Then, on the boundary of anhydrous C_3A core the $C_3A\cdot C\overline{S}\cdot 12H$ phase begins to form [141].

A significant initial impact of water vapour on the C_3A phase and on its reaction with water, or with sulphate solutions at later age, is commonly known [144, 145]. C_3AH_6 appears as a first product when the bound water content exceeds 3 %. Wittmann [146] stated that the formation of instable hydration centres are formed first, which could be removed by drying. At longer exposure to the water vapour the stable hydration centres appear. In the light of Barret works it is evident; that the surface hydroxylation of C_3A occurs.

3.4 Hydration of Ferrite Phase

The calcium ferrites react with water more slowly that C_3A does, however, the same hydration products are formed: $C_4(A, F)H_{19}$, $C_4(A, F)H_{13}$, C_3FH_6 [147, 148]. The hexagonal hydrates are relatively stable at low temperatures, but they transform into the cubic C_3FH_6 at temperature as low as about 20 °C. C_3FH_6 is formed directly at temperature exceeding 50 °C [148]. However, this process is much slower than in the case of aluminate phases, probably because of the lower heat of hydration, which causes lower temperature of hydration. The C_3FH_6 phase is formed only as a result of C_2F hydration. However, this phase decomposes quickly to CH and iron hydroxide [147]. The dicalcium ferrite gives, as a result of hydration, C_4FH_{13}, C_4FH_{19} and FH_3 gel. Hexagonal hydrates transform readily into the C_3FH_6, particularly at temperature higher than 38 °C [149].

The reactivity of ferrites toward water changes consecutively: $C_2F \rightarrow C_6AF_2 \rightarrow C_4AF \rightarrow C_6A_2F$ [150]. The calcium aluminate and ferrite hydrates form the unlimited solid solutions. However, in hydrates generally is higher A/F ratio than in the anhydrous phase; therefore some amount of $Fe(OH)_3$ is formed [149], which can be described schematically:

$$C_6A_2F + 3OH^- \rightarrow C_4AH_{19} + C_2AH_8 + FH_3 \tag{3.40}$$

or

$$2C_6A_2F + 6OH^- \rightarrow 3C_4\left[A_{2/3}F_{1/3}\right]H_{19} + FH_3 \tag{3.41}$$

The same authors are evaluating the Fe_2O_3 content in hexagonal hydrates as follows: for C_6A_2F 2.1 ± 1 %, C_4AF 6 ± 3 %, C_6AF_2 30 ± 3 %. In $C_3(A, F)H_6$—from 2 to 3 % with the accuracy ± 2 % [149].

According to Ludwig [151] the C_6A_2F hydration at temperature lower than 15 °C results in the formation of C_2AH_8 and $C_4(A, F)H_x$ phases with high iron(III) ions content. Tenoutasse [152] found the hexagonal hydrates already after 5 min. The latter transforms into the cubic hydrates after one day and $Ca(OH)_2$ appears in the mixture [152]. In the presence of calcium hydroxide the process is significantly modified; C_2F hydration proceeds with higher rate and the transition of hexagonal hydrates into the cubic ones occurs after 4 months. In the case of $C_2(A, F)$ the rate of these hydrates transformation is significantly lower in the presence of $Ca(OH)_2$.

In the presence of gypsum the analogy to the tricalcium aluminate is further maintained. At first, ettringite is formed and subsequently, after exhausting of gypsum, its transforms into monosulphate. The ferrite phase hydration is practically hampered in the liquid phase saturated with calcium hydroxide and gypsum. As a result of C_4AF hydration a gel is formed and after 30 min. it undergoes the recrystallization with the arise of hexagonal hydrates which, in turn, after one day became covered with $Fe(OH)_3$ gel [42, 153].

Therefore the iron (III) ion the phases analogous to the calcium aluminate hydrates in cement pastes is forming, classified to two groups of compounds AFt and AFm. However, in cement paste, the aluminum ions are always present in their composition, because, as it is commonly known, in Portland cement clinker the iron (III) occurs in the form of brownmillerite containing Al^{3+} ions. The iron (III) ion can produce the AFm phases without aluminum ions, but only in the laboratory conditions in the systems of specific composition. C_4FH_{13} forms solid solutions of complete miscibility with C_4AH_{13} phase [62] but $C_4F\bar{S}H_{12}$ occurs in such solid solutions with $C_4A\bar{S}H_{12}$ only at temperature 100 °C; at temperature 25 °C or 50 °C the miscibility is significantly limited [154]. At temperature 25 °C $C_4F\bar{S}H_{12}$ can take to the solid solution 50 molar % $C_4A\bar{S}H_{12}$; the latter one about 10 molar % of its iron analogue [154]. There is also a compound with medium composition in which the Al/Fe ratio is about 0.5 [154]. The similar solid solutions with limited miscibility occur in the case of $C_3F{\cdot}CaCl_2{\cdot}10H_2O$ with its aluminate analogue [154].

The hydraulic activity of C_4AF reveals significant differences in the industrial clinkers; in some cases the peaks of brownmillerite on the XRD patterns remain up the 28 days of hydration [90]. However, there are the clinkers in which brownmillerite exhibits high activity and substantial amount of ettringite is detected in the paste already after 1 hour of hydration and increases significantly after 2 h [90].

3.5 Minor Hydrated Phases in Cement Paste

C_3AH_6 is the only thermodynamically stable phase in the $CaO–Al_2O_3–H_2O$ system at room temperature. This phase does not occur in the Portland cement paste. Some small amounts of this phase can appear in blended cement pastes, usually in the amorphous form. On the other side, this phase is produced in autoclaved pastes, mortars or concretes. This aluminate shows a cubic structure; the silicon, aluminum and calcium cations reveal the tetrahedral, octahedral and disordered cubic coordination respectively [62]. In the hydrogarnets this structure is modified because of the shortage of some or all silicon atoms and the electric charge is balanced by substitution of oxygen atoms bound with silicon by the OH^- ions. The Al^{3+} cation can be partially or totally substituted by Fe^{3+} [62]. The aluminate $Ca_3[Al(OH)_6]_2$ forms the solid solutions with C_3AS_3, known as hydrogrossular. These solid solutions are not probably continuous but in the composition range from C_3AH_6 to about $C_3AS_2H_2$ they can be obtained at relatively low temperatures; those with higher silicon content—only at temperatures above 360 °C [62].

Taylor [62] reports of hydrotalcite appearing having complex composition $[Mg_{0.75}Fe_{0.25}(OH)_2](CO_3)_{0.125}(OH)_{0.5}$ in which the Mg^{2+} ion is substituted by the Al^{3+} or Fe^{3+} ions; the electric charge is balanced by the anions occupying the interlayer positions, together with H_2O molecules. This phase is formed in the slag cement pastes or, as traces, in the Portland cement pastes [62].

In slag cement pastes some amount of the gehlenite hydrate $2CaO \cdot Al_2O_3 \cdot SiO_2 \cdot 8H_2O$ can also be present, but only at high alkalis content [73]. This phase was discovered by Strätling and therefore is also known as strätlingite. This author found it as the product of metakaolinite reaction with $Ca(OH)_2$ [73]. This phase shows a layer structure: the main layer has the composition $[Ca_2Al(OH)_6]^+$ and there is the $[AlSiO_3(OH)_2 \cdot 4H_2O]^-$ between the layers.

3.6 Heat of Hardening

It should be underlined that in case of cement we can measure the heat of hardening; the heat of hydration relates to the situation when the phase composition of hydration products is known. For example, as a result of CaO reaction with water the calcium hydroxide is formed and the heat evolved during this hydration process is 1168 J/g CaO. However, even in this case Lea [83] reports that depending on the physical properties of CaO used and the product obtained, the heat can evolve in the range from 1110 to 1168 J/g. However, in this case it is possible to determine precisely the heat of hydration.

There is quite another problem for example in the case of C_3A. As it is commonly known this phase reacts with a solution and the trisulphoaluminate or monosulphoaluminate is produced, depending on the gypsum content:

$$C_3A + 3C\overline{S}H_2 + 26H \rightarrow C_3A \cdot 3C\overline{S} \cdot 32H + 1453 \text{ J/g } C_3A \tag{3.42}$$

$$C_3A + C\overline{S}H_2 + 19H \rightarrow C_3A \cdot C\overline{S} \cdot 12H + 1097 \text{ J/g } C_3A \tag{3.43}$$

The hydration, or rather hydrolysis, of orthosilicates is more complex. The C–S–H phase is poorly crystallized and reveals variable C/S ratio; this is not a crystalline phase but rather a gel. The heat of adsorption of water on the C–S–H[8] gel interferes with the heat of reaction. Nowadays, it is assumed that the hydration of orthosilicate phases are linked with the following heat of reaction:

$$2(C_3S) + 6H \rightarrow C_3S_2H_3 + 3CH + 238\,833 \text{ J } (523 \text{ J/g } C_3S) \tag{3.44}$$

$$2(C_2S) + 4H \rightarrow C_3S_2H_3 + CH + 90948 \text{ J } (264 \text{ J/g } C_2S) \tag{3.45}$$

[8] Heat of water adsorption on the calcium hydroxide is negligible, while the heat of reaction is reduced by the surface energy of C–S–H gel.

Table 3.4 Heat of hardening of clinker phases (J/g of anhydrous phase) [158]

Phase	Heat of hardening	
	According to Lerch and Bogue	According to Woods, Starke and Steinour
CaO	1168[a]	
MgO	850[b]	
C_3S	502	
C_2S	260	
C_3A to C_3AH_6	867	
C_3A to hexagonal hydrates	1093[c]	569
C_4AF	420	260
$CaSO_4 \cdot 0.5H_2O$	193[d]	837
$CaSO_4$ soluble	142[d, e]	
$C_3A \cdot 3CS \cdot 31H_2O$	624[d, f]	
	1453[g]	
$C_3A \cdot CS \cdot 12H_2O$	783[d, f]	

[a] 1156 J/g according to Thorvaldson, Brown and Parker
[b] Indirect measurement
[c] According to Lea, p. 295 [83]
[d] Per 1 g SO_3
[e] Too low value; according to Jung—243 J/g SO_3
[f] Reaction between C_3AH_6 and $CaSO_4 \cdot 2H_2O$
[g] Reaction between C_3A and $CaSO_4 \cdot 2H_2O$ (according to [83])

In this heat value, apart from the heat of hydration, the heat of water adsorption on a gel product is included. If this heat, evaluated as 84–168 J/g of anhydrous phase, is subtracted, the following values are obtained: for C_3S—404.0 ± 6.3 J/g C_3S and for C_2S 102.6 ± 14.7 J/g C_2S [83]. This problem was discussed with details by Brunauer and Kantro [155]. For the practical purpose the aforementioned total heat of the process is important. Taking into account all the circumstances, apart from some cases dealing with the known crystalline hydration products, we should rather use the term "heat of hardening".

Cement heat of hardening is affected primarily by the phase composition of the clinker. This heat is an additive value and therefore it can be evaluated based on the known composition of Portland cement clinker and the heat of hardening for particular phases, given in Table 3.4.

According to Berman and Newman [156] the C_3A hydration with ettringite formation is accompanied by the heat evolution on the level 816 J/g SO_3; with the monosulphate formation—783 J/g respectively. Applying the Hess rule one can write:

$$C_3A + 6H \rightarrow C_3AH_6 + 867 \text{ J/g } C_3A \tag{3.46}$$

$$C_3AH_6 + 3C\bar{S}H_2 + 24H \rightarrow C_3A \cdot 3C\bar{S} \cdot 32H + 816 \text{ J/g } SO_3 \tag{3.47}$$

thus

$$C_3A \rightarrow \text{ettringite} + 1591 \text{ J/g } C_3A \tag{3.48}$$

Table 3.5 Heat of hardening values (J/g) evaluated per 1% of clinker phases which content was calculated from Bogue's equations (temp. 23 ± 2 °C, w/c = 0.45, Blaine's surface area 3100 ± 200 cm^2/g)

Component	Age, days					
	3	7	28	90	180	360
C_3A	7.1	7.5	7.9	8.4	8.8	9.2
C_3S	3.3	3.8	4.4	4.6	5.0	5.0
C_2S	0.4	0.8	1.3	1.7	2.1	2.5
C_4AF	0.8	1.3	1.7	2.1	2.5	2.9

The value 1591 J/g C_3A result from the addition $867 + 816 \cdot (240/270)$. The measured values are much lower, that is 1453 J/g C_3A. Taking into account the value given by Bogue [157], (p. 455) 624 J/g SO_3, we get $867 + 624 \cdot (240/270) = 1419$ J/g C_3A.

The heat of reaction $C_3AH_6 + C\overline{S}H_2 + 4H \rightarrow C_3A{\cdot}C\overline{S}{\cdot}12H$ equal 783 J/g SO_3 given in Table 3.4, is a little too high. It should be on the level of about 600 J/g SO_3:

$$\begin{aligned} C_3A \xrightarrow{867} C_3AH_6 \xrightarrow{176(230)} C_3A{\cdot}C\overline{S}{\cdot}12H \\ \downarrow \quad 553 - 176 = 377 \\ \downarrow \quad (553 - 230 = 323) \\ C_3AH_6 \xrightarrow{553} C_3A{\cdot}\,C\overline{S}{\cdot}12H \\ C_3A \xrightarrow{1453(1419)} C_3A{\cdot}C\overline{S}{\cdot}12H \end{aligned} \tag{3.49}$$

Therefore we can evaluate that the transformation of monosulphate into ettringite will be exothermic with the heat of about 350 J/g C_3A. Taking into account all the values listed above, together with that evaluated for C_3AH_6, equal 176 J/g C_3A, we get for the reaction:

$$C_3A \cdot C\overline{S} \cdot 12H + 2C\overline{S} \cdot 2H + 18H \rightarrow C_3A \cdot 3C\overline{S} \cdot 32H \tag{3.50}$$

the heat evolved from 323 to 377 J/g C_3A.

In the light of these data there are some doubts as the additional peak on the heat evolution curve is concerned. Jawed [2] attributes this peak to the formation of monosulphate. However, this peak should be rather the effect of the final portion of C_3A hydration, resulting in the formation of hexagonal hydrates [83]. One should remember that the heat of hardening increases with temperature, as it is the case of the rate of hardening. The w/c ratio is also of importance. The heat of cement hardening is affected by the gypsum content because it influence the rate of hydration of clinker phases [33]. Finally, the changes occurring during the storage of cement have some impact on the heat of hardening.

Taking into account all these factors the heat of hardening can be evaluated based on the values given in Table 3.5. A little higher values are given by Kühl [158], according to the measurements by Woods, Steinour and Starke. These data are given in Table 3.6.

Table 3.6 Heat of hardening (J/g)

Component	Age, days					
	3	7	28	90	180	360
C_3A	410	461	477	511	507	569
C_3S	80	75	184	230	222	260
C_2S	712	787	846	787	913	837[a]
C_4AF	121	180	201	197	306	126[b]

[a] 867—according to the other authors, when the C_3AH_6 is formed
[b] According to the other authors—419

Table 3.7 Heat of hardening of clinker phases (J/g) [159]

Component	Age					
	3 days	7 days	28 days	90 days	1 year	6.5 years
C_3A	243 ± 33	222 ± 46	377 ± 4	435 ± 21	490 ± 29	490 ± 29
C_3S	50 ± 21	419 ± 29	105 ± 17	176 ± 13	226 ± 17	222 ± 21
C_2S	888 ± 117	1558 ± 163	1378 ± 96	1302 ± 71	1168 ± 96	1373 ± 105
C_4AF	289 ± 113	494 ± 155	494 ± 92	410 ± 67	377 ± 92	465 ± 100

Verbeck [159] found that the heat of hardening is increasing with w/c ratio (in the range 0.4–0.8) till to 6.5 years. This author established also the correlation coefficients for the calculation of the heat of hardening based on the phase composition of cement. He found also that the data obtained with these calculations led to the results close to those reported by Bogue and Lerch for 13 years of hardening; that means when the hydration is completed [159]. The values calculated by Verbeck are given in Table 3.7. On the other side the rate of heat evolution vs. time depends on cement fineness and increases with it analogously as the rate of hardening. Therefore a very good correlation was found between the heat of hardening and strength of mortars [160]. The heat after 1day hardening contributes to the 3–day strength, while the heat after 3 days—to the 7–day strength respectively.

According to the European Standards recommendation there are two methods of the heat of cement hydration measurements: viz. the dissolution method—EN 196–8 and the semi–adiabatic one—EN 196–9. The latter one is most frequently used because it relates to the early hydration process. Moreover, a good correlation was found between the results obtained by the semi–adiabatic method after 41 h process and the dissolution one relating to the 7–day hydration. The first one can be applied in the studies of all hydraulic binders, except of the rapid setting cements. The low heat Portland cements are assessed based upon the results of the heat measured with this method after 41 h of reaction with water. The standard limit for the low heat (LH) cements is 270 J/g (EN 197–1 standard). The low heat Portland cement without additions is produced, but it is of low class. It is the reason that for these kinds of cements primarily cements with high granulated blastfurnace slag addition belong (see Table 3.8).

In Tables 3.8, 3.9, 3.10, 3.11 and 3.12 the heat of hydration of cements produced in Poland are given, together with the basic properties of these cements [161]. Undoubtedly, the strength of standard mortar is the main feature, however it is defined only very approximately in suitable standard.

Table 3.8 Heat of hardening (J/g) for some types of cements, measured according to PN–EN 196–9 standard

Type of cement	Time, hours				
	12	24	36	41	72
CEM I 32.5R	138	259	299	309	332
CEM I 42.5R	180	286	322	329	349
CEM I 52.5N	222	329	356	362	378
CEM I 52.5R	224	340	374	380	399
CEM II/B–S 32.5 R	126	209	244	253	280
CEM II/B–S 42.5 N	127	245	285	296	330
CEM II/B–S 52.5 N	156	259	294	304	326
CEM III/A 32.5N NA	48	116	165	177	219
CEM III/A 42.5N	94	204	238	247	274
CEM III/B 32.5L	44	101	133	143	183
CEM II/B–V 32.5 R HSR	66	163	197	206	236
CEM V/B (S–V) 32.5N	43	114	148	158	194

Table 3.9 The properties of Portland cements type CEM I

Feature	Type of cement		
	CEM I 32.5R	CEM I 42.5R	CEM I 52.5R
Water demand, %	26.2	26.7	29.8
Initial setting time, min	173	163	138
Le Chatelier test, mm	0.7	0.4	0.3
Compressive strength, MPa, at age			
2 days	23.0	27.0	34.0
7 days	35.6	42.3	50.6
28 days	48.0	51.1	56.8
90 days	51.4	54.2	60.5
Shrinkage of standard mortar, mm/m, at age			
7 days	0.12	0.16	0.19
28 days	0.33	0.40	0.48
Heat of hydration, J/g, after:			
24 h	216	328	373
41 h (semi–adiabatic method)	311	366	415[a]

[a] Relatively high differences, as compared to Table 3.8, result from the origin of cements supplied by different producers

The water demand is a basic property of cement, which is of special practical importance for concrete producers. As it can be derived from the data listed in the tables, the water demand increases with the fineness and consequently with the class of cement strength, analogously as the heat of hydration. Simultaneously, this feature is strongly affected by the mineral additions. The water demand is reduced particularly by the siliceous fly ash, as it is the consequence of physical effect of spherical forms of fly ash grains. However, this effect is in some degree limited by a higher fineness of the CEM II/B–V type cements, resulting from the necessity to

Table 3.10 The properties of Portland cements type CEM II

Feature	Type of cement				
	CEM II/B–V 32.5R	CEM II/B–M(V–LL) 32.5R	CEM II/B–S 32.5R	CEM II/B–S 42.5N	CEM II/B–S 52.5N
Water demand, %	26.7	26.3	28.0	30.0	32.0
Initial setting time, min	26.7	26.7	26.7	26.7	26.7
Le Chatelier test, mm	0.6	0.6	0.3	0.4	0.4
Compressive strength, MPa, at age					
2 days	16.2	15.9	17.9	21.8	26.8
7 days	29.4	27.5	31.8	35.5	39.7
28 days	40.2	38.9	49.9	54.2	58.4
90 days	50.3	45.6	55.2	60.1	64.7
Shrinkage of standard mortar, mm/m, at age					
7 days	0.08	0.06	0.11	0.13	0.16
28 days	0.28	0.27	0.38	0.42	0.47
Heat of hydration, J/g, after					
24 h	250[a]	255	258	266	362[a]
41 h (semi–adiabatic method)	291[a]	293	304[a]	310	413[a]

[a] Relatively high differences, as compared to Table 3.8, result from the origin of cements supplied by different producers

Table 3.11 The properties of cements type CEM III

Feature	Type of cement		
	CEM III/A 32.5N NA/HSR/LH	CEM III/B 32.5N NA/HSR/LH	CEM III/A 42.5N NA/HSR
Water demand, %	30.6	30.8	31.6
Initial setting time, min	226	264	226
Le Chatelier test, mm	0.3	0.5	0.5
Compressive strength, MPa, at age			
2 days	10.2	6.5	15.5
7 days	22.2	19.7	28.8
28 days	45.3	44.0	51.8
90 days	53.6	52.8	61.2
Shrinkage of standard mortar, mm/m, at age			
7 days	0.07	0.04	0.10
28 days	0.30	0.21	0.39
Heat of hydration, J/g, after			
24 h	116	101	243
41 h (semi–adiabatic method)	143	145	283

Table 3.12 The properties of blended cements

Feature	Type of cement	
	CEM V/A(S–V) 32.5N	CEM V/B(S–V) 32.5N
Water demand, %	26.5	29.9
Initial setting time, min	265	285
Le Chatelier test, mm	2	1
Compressive strength, MPa, at age		
2 days	8.1	6.5
7 days	21.1	18.0
28 days	37.9	37.3
90 days	50.1	50.1
Heat of hydration, J/g, after		
24 h	134	114
41 h	176	158
(semi–adiabatic method)		

maintain on adequate level the standard strength after two days of hardening. Cement CEM II/B–M, containing some limestone addition apart from fly ash, reveals lower water demand (Table 3.10).

The shrinkage of mortars produced from different cements increases with their strength class (higher fineness) but decreases in the case of cements with mineral additions, particularly at high granulated blastfurnace slag and siliceous fly ash content.

Finally, it is necessary to discuss the heat of hardening as a source of cracks in the massive concrete structures, resulting from the stresses dealing with the temperature gradient [162]. This problem has been reported with details by Kiernożycki [162] and Neville [163].

The heat of hardening of different cements given in Tables 3.9, 3.10, 3.11 and 3.12 allows to evaluate the temperature rise at early age after concrete placing. It should be remind that up to 10 % or even 20 % of total heat is evolved during the period before the final setting. This is not a remarkable amount; however, the heat evolution takes place during a relatively short period of time and can lead to the significant increase of concrete temperature. The temperature rise in adiabatic conditions can be evaluated based on the experimental data or calculations; taking into account the values given in Tables 3.5 and 3.8; the following formula can be used:

$$\Delta t_b = \frac{C \cdot H}{(C + K) \cdot C_1 + W \cdot C_2} \tag{3.51}$$

where: C is the mass of cement (kg) per m^3 of concrete, H—heat of cement hardening, K—mass (kg) of aggregate per m^3 of concrete, W—mass (kg) of water per m^3 of concrete, C_1—medium specific heat of cement and aggregate [the value 0.8 kJ/(kg · K) can be taken], C_2—specific heat of water [4.2 kJ/(kg · K)]. In practice it

often appears that a concrete beam of cross section 60 × 60 cm should be classified as a massive element.

The assumption of adiabatic condition is quite reasonable because of very low heat conductivity of concrete which is about 0.0126 W/(cm · K).

From the data given in Table 3.5 it can be concluded also that the heat of hardening can be lowered by the C_3A and C_3S content decrease; in the latter case it means the reduction of the lime saturation factor. Unfortunately, this is simultaneously linked with the lowered strength development and reduced class of cement.

Another way is adding granulated blastfurnace slag or fly ash with very low heat of hardening. According to Kühl [158], this heat for slag is from 42 to 63 J/g, depending on the chemical composition and glass content. Therefore the heat of hardening of slag cement can be readily evaluated. It has been proved by the data from Table 3.11 where the heat of hardening of slag cements is about 100 J/g lower after 24 h hydration than this heat for CEM I. This can be derived by a comparison of results in the first column in Table 3.9 (CEM I 32.5R) with those from the last column in Table 3.11 (CEM III/A 42.5 N), for cements of similar compressive strength. The strength of cement CEM III/A is lower, however, in practice, there is seldom concrete structure which need higher strength than 20 MPa after 2 days and the strength on the level of 10 MPa is sufficient. On the other side, cements CEM III/A 42.5R are produced. Moreover, the concretes can be produced at reduced w/c ratio in the case when the high early strength is required, with superplasticizers use.

The heat of hardening can be determined not only by a simplified calculation, but by direct calorimetric measurements, or indirectly applying the Hess rule. According to this rule, the heat of reaction depends only on the initial and final state and this is the basis of the dissolution method. In this dissolution procedure, the heat of hardening is determined as a difference between the heat of neat cement dissolution and heat of hydration products (cement paste) dissolution. The mixture of nitric and fluoric acids is used for this purpose. Only the dissolution method is applied in the case of the longer hydration time. The most accurate, differential calorimetric method has been developed by Zielenkiewicz [164]. The completely hydrated mortar is placed in one container of calorimeter and in the second one—the fresh mortar.

Kamiński and Zielenkiewicz [165] investigated the heat of hardening of cement phases and cements and found a good correlation of calculated heat and experimental data, when the following heat values for particular cement phases (in J/g) are applied:

	72 h	168 h
C_3S	456	565
C_2S	50	113
C_3A+C_4AF	364	528

References

1. Magnan, R., Cottin, B., Gardet, J.: Cement–Wapno–Gips. **30**, 61 (1976) (in Polish)
2. Jawed, L., Skalny, J., Young, J.F.: In: Barnes, P. (eds.) Structure and Performance of Cements, chapter 6 p. 250. Applied Science Publ., London (1983)
3. Kondo, R., Ueda, S.: 5th ICCC Tokyo, vol. II, p. 203. Tokyo (1968)
4. Skalny, J., Jawed, L., Taylor, H.F.W.: World Cement Technol. 9, 183 (1978)
5. Fuji, K., Kondo, R.: J. Am. Ceram. Soc. 57, 492 (1974)
6. Barret, P.: Cim., Betons, Plâtres, Chaux. (485–755), 237 (1985)
7. Barret, P., Bertrandie, D., Menetrier, D.: 7th ICCC Paris, vol. II, pp. II–261. Paris (1980)
8. Barret, P., Menetrier, D., Bertrandie, D.: Cem. Concr. Res. 13, 728 (1983)
9. Barret, P., Menetrier, D.: Cem. Concr. Res. 10, 521 (1980)
10. Vernet, C., Demoulian, E., Gourdin, P., Hawthorn, F.: 7th ICCC Paris, vol. II, pp. II–267. Paris (1980)
11. Jennings, H.M.: J. Am. Ceram. Soc. **69**, 614 (1986)
12. Barret, P., Menetrier, D., Bertrandie, D., Regourd, M.: 7th ICCC Paris, vol. II, pp. II–279. Paris (1980)
13. Chen, J.J., Thomas, J.J., Taylor, H.F.W., Jennings, H.M.: Cem. Concr. Res. **34**, 1499, (2004)
14. de Jong, J.G.M., Stein, H.N., Stevels, J.M.: J. Appl. Chem. **17**, 246 (1967)
15. Barret, P.: 8th ICCC Rio de Janeiro, vol. III, p. 86. Rio de Janeiro (1986)
16. Kurdowski, W., Nocuń, W., Miśkiewicz, K., Szuba, J.: 8th ICCC Rio de Janeiro, vol. III, p. 179. Rio de Janeiro (1986)
17. Young, J.F.: Cem. Concr. Res. **2**, 415 (1972)
18. Tadros, M.E., Skalny, J., Kalyoucu, R.S.: J. Am. Cerom. Soc. **59**, 344 (1976)
19. Menetrier, D., Jawed, I., Sun, T.S., Skalny, J.: Cem. Concr. Res. **9**, 473 (1979)
20. Double, D.D., Thomas, N.L., Jameson, D.A.: 7th ICCC Paris, vol. II, pp. II–256. Paris (1980)
21. Jennings, H.M., Pratt, P.L.: Cem. Concr. Res. **9**, 501 (1979)
22. Bailey, J.E., Chescoe, D.: Proc. Brit. Ceram. Soc. **23**, 165 (1979)
23. Taylor, H.F.W., Mohan, K., Moir, G.K.: J. Am. Ceram. Soc. **68**, 680 (1985)
24. Maycock, J.N., Skalny, J., Kalyoucu, R.: Cem. Concr. Res. **4**, 835 (1974)
25. Fierens, P. J., Verhaegen, I. P.: Il Cemento. **73**, 39 (1976); Cem. Concr. Res. **6**, 287 (1976)
26. Gauffinet, S., Finot, E., Nonat, A.: In: Nonat, A. (ed.) 2nd International RILEM Workshop on Hydration and Setting, 11–13 June 1997. p. 199. RILEM Publications S.A. R.L
27. Kurdowski, W., Nocuń, W.: Cem. Concr. Res. **13**, 341 (1983)
28. Menetrier, D., Cottin, B., Barret, P.: 7th ICCC Paris, vol. II, pp. II–232. Paris (1980)
29. Bellina, G., Hassan, M., Longuet, P.: Cim., Bétons, Plâtres, Chaux, (755), 245 (1985)
30. Bensted, J.: In: Gosh, S.N. (ed.) Advances in Cement Technology, p. 307. Pergamon, Oxford (1983)
31. Regourd, M.: Compt. Rend., Serie C. **290**, 1 (1980)
32. Taylor, H.F.W.: 8th ICCC Rio de Janeiro, vol. I, p. 83. Rio de Janeiro (1986)
33. Taylor, H.F.W. (ed.): The Chemistry of Cements, Academic, New York (1964)
34. Taylor, H.F.W.: J. Am. Ceram. Soc. **69**, 464 (1986)
35. Nonat, A., Courault, A.-Ch., Damidot, D.: Cem. Wapno Beton. **78**, 184 (2001)
36. Diamond, S.: In: Hydraulic Cement Pastes: their structure and properties, University of Sheffield, April 1976, p. 2, Cement and Concrete Ass. Wexham Springs (1976)
37. Jennings, H.M., Dalgleish, B.S., Pratt, P.L.: J. Am. Ceram. Soc. **64**, 567 (1981)
38. Stark, J., Moser, B., Bellmann, F.: 11th ICCC Durban, vol. 1, p. 261. Durban (2003)
39. Nonat, A.: Cem. Concr. Res. **34**, 1521 (2004)
40. Scrivener, K.L., Kirkpatrick, R.J.: 12th ICCC Montreal, Session ST5, Plenary Lecture, Montreal (2007)
41. Richardson, I.G.: Cem. Concr. Res. **34**, 1733 (2004)
42. Henderson, E., Bailey, J.E.: 8th ICCC Rio de Janeiro, vol. III, p. 375. Rio de Janeiro (1986)
43. Taylor, H.F.W.: 5th ICCC Tokyo, vol. II, p. 1. Tokyo (1968)
44. Taylor, H.F.W., Newbury, D.E.: Cem. Concr. Res. **14**, 93 (1984)

45. Richardson, I.G.: In: Bensted, J., Barnes P. (eds.) Structure and Performance of Cements, Chap. 22, p. 500. Spon Press, London (2002)
46. Richardson, I.G.: Cem. Concr. Res. **29**, 1131 (1999)
47. Richardson, I.G., Groves, G.W.: J. Mat. Sci. **28**, 265 (1993)
48. Richardson, I.G.: Cem. Contr. Compos. **22**, 97 (2000)
49. Lachowski, E.E., Diamond, S.: Cem. Concr. Res. **15**, 177 (1985)
50. Rayment, D., Majumdar, A.J.: Cem. Concr. Res. **12**, 753 (1982)
51. Rayment, D., Lachowski, E.E.: Cem. Concr. Res. **14**, 43 (1984)
52. Feldman, R.F.: 5th ICCC Tokyo, vol. II, p. 53. Tokyo (1968)
53. Seligmann, P., Greening, N.R.: 5th ICCC Tokyo, vol. II, p. 179. Tokyo (1968)
54. Dent Glasser, L.S., Lachowski, E.E., Qureshi, M.Y.: Cem. Concr. Res. **11**, 778 (1981)
55. Clayden, N.S., Dobson, C.M., Groves, G. W., Rodger, S. A.: 8th ICCC Rio de Janeiro, vol. III, p. 51. Rio de Janeiro (1986)
56. Grutzeck, M., Benesi, A., Fanning, B.: J. Am. Ceram. Soc. **72**(4), 665 (1989)
57. Mamiedov, S., Bielov, N.W.: Dokł. Akad. Nauk SSSR. **121**, 720 (1958) (in Russian)
58. Greenberg, S.A., Chang, T.N.: J. Phys. Chem. **64**, 1151 (1960)
59. Kantro, D.L., Brunner, S., Weise, C.H.: J. Phys. Chem. **66**, 1804 (1962)
60. Hamid, S.A., Kristallogr, Z.: **154**, 189 (1981)
61. Bonaccorsi, E., Merlino, S., Taylor, H.F.W.: Cem. Concr. Res. **34**, 1481 (2004)
62. Taylor, H.F.W.: Cement Chemistry. Academic Press, London (1990)
63. Taylor, H.F.W.: Adv. Cem. Based Mater. **1**, 38 (1993)
64. Cong, X., Kirkpatrick, R.J.: J. Am. Ceram. Soc. **79**, 1585 (1996)
65. Ping, Yu, Kirkpatrick, R.J., Poe, B., McMillan, P.F., Cong, X.: J. Am. Ceram. Soc. **82**, 742 (1999)
66. Richardson, I.G., Groves, G.W.: Cem. Concr. Res. **22**, 1001 (1992); **23**, 131 (1993)
67. Richardson, I.G.: Cem. Concr. Res. **34**, 1733 (2004)
68. Glasser, F.P., Lachowski, E.E., Macphee, D.E.: J. Am. Ceram. Soc. **70**, 481 (1987)
69. Nachbaur, L., Nkinamubanzi, P.C., Nonat, A., Mutin, J.C.: J. Colloid Interface Sci. **202**, 261 (1998)
70. Viallis–Terrisse, H., Nonat, A., Petit, J.C.: J. Colloid Interface Sci. **244**, 58 (2001)
71. Jennings, H.M.: Cem. Concr. Res. **30**, 101 (2000)
72. Tennis, P. D., Jennings, H.M.: Cem. Concr. Res. **30**, 856 (2000)
73. Locher F.: Cement, Principles of Production and Use. Verlag Bau + Technik, Düsseldorf (2006)
74. Beaudoin, J.J., Ramachandran, V.S., Feldman, R.F.: Cem. Concr. Res. **20**, 875 (1990)
75. Stade, H.: Cem. Concr. Res. **19**, 802 (1989)
76. Hong, S.Y., Glasser, F.P.: Cem. Concr. Res. **29**, 1893 (1999)
77. Divet, L., Randriambololona, R., Leger, D.: Silicates Ind. **70**, 25 (2007)
78. Duchesne, J., Berube, M.A.: Cem. Concr. Res. **24**, 221 (1994)
79. Beaudoin, J.J., Gu, P., Myers, R.E.: Cem. Concr. Res. **28**, 341 (1998)
80. Nonat, A.: 12th ICCC Montreal, TH2–08.1, Montreal (2007)
81. Plassard, C., Leśniewska, E., Pochard, I., Nonat, A.: 12th ICCC Montreal, TH2–03.4, Montreal (2007)
82. Ulm, F., Constantinides, G., Heukamp, F.H.: Materials and Structures/Concrete Science and Engineering. **37**, 43 (2004)
83. Lea, F.M.: The Chemistry of Cement and Concrete, 3rd ed. Chemical Publishing Company, New York (1971)
84. Jones, F.E.: 4th ICCC Washington, t I, p. 205. Washington (1960)
85. Cottin, B., Reif, P.: Rev. Mat. Constr. (661), 293 (1970)
86. Ahmed, S.J., Dent Glasser, L.S., Taylor, H.F.W.: 5th ICCC Tokyo, vol. II, p. 118. Tokyo (1968)
87. Roberts, M.H.: J. Appl. Chem. **7**, 543 (1957)
88. Dent Glasser, L.S., Buttler, F.G., Taylor, H.F.W.: J. Am. Ceram. Soc. **42**, 121 (1959)
89. Percival, A., Buttler, F.G., Taylor, H.F.W.: 4th ICCC Washington, vol. I, p. 277. Washington (1960)

90. Kurdowski, W.: Non published paper
91. Pöllmann, H., Neues Jb. Miner. Abh. 182(2), 173 (2006)
92. Pöllmann, H.: ibid. 182(2), 426 (2006)
93. Pöllmann, H.: LSF Mineralogie. 1999, 363
94. Pöllmann, H., Auer, S., Kuzel, H.J., Wenda, R.: Cem. Concr. Res. 23, 422 (1993)
95. Schwiete, H.E., Ludwig, U., Albeck, J.: Zement–Kalk–Gips. 22, 225 (1969)
96. Goske, J.I., Pöllmann, H.: Environment & Progress, (2), 145 (2004)
97. Kuzel, H.J., Pöllmann, H.: Cem. Concr. Res. 21, 885 (1991)
98. Auer, S., Pöllmann, H., Kuzel, H.: Eur. J. Min. Bh. 7 (1990)
99. D'Ans, J., Eick, H.: Zement–Kalk–Gips. 9, 197, 302 (1953)
100. Dosh, W., Keller, H.: 6th ICCC Moscow, vol. III, p. 141. Moscow (1974)
101. Dosh, W., zur Strassen, H.: Zement–Kalk–Gips. **20**, 392 (1967)
102. Kuzel, H.: Neues Jahrb. Mineral. Monatsh. 193 (1966)
103. Pöllmann, H., Kuzel, H.J., Wenda, R.: Cem. Concr. Res. **20**, 94 (1990)
104. Motzet, H., Pöllmann, H.: Cem. Concr. Res. **29**, 1005 (1999)
105. Ecker, M., Pöllmann, H.: 10th ICCC Goeteborg, vol. II, p. 2ii032. Goeteborg (1997)
106. Kuzel, H.: 5th ICCC Tokyo, II, p. 92. Tokyo (1968)
107. Pöllmann, H., Michaux, M., Nelson, E.B.: Proc. 12th Conf. on Cement Microscopy, p. 303. Canada (1990)
108. Renaudin, G., Rapin, J.-P., Humbert, B., François, M.: Cem. Concr. Res. **30**, 307 (2000)
109. Pöllmann, H.: 9th ICCC New Delhi, vol. VI, p. 198. New Delhi (1992)
110. Pöllmann, H., Stöber, S., Stern, E.: Cem. Concr. Res. **36**, 2039 (2006)
111. Stöber, S., Pöllmann, H.: Cem. Concr Res. **29**, 1841 (1999)
112. Pöllmann, H.: 11th Conf. on Cement Microscopy, p. 324. New Orleans (1989)
113. Pöllmann, H., Stöber, S.: 10th ICCC Goeteborg, vol. III, p. 3iii032. Goeteborg (1997)
114. Pöllmann, H., Kristallogr Z.: **186**, 236 (1989)
115. Meyer, H.W., Pöllmann, H., Kuzel H.J.: Eur. J. Min. Bh. 193 (1992)
116. Turriziani, R.: Ind. Ital. Cemento. **29**, 185, 219, 224, 276 (1959)
117. Glasser, F.P., Marinko, M.B.: Proc. Brit. Ceram. Soc. **35**, 221 (1984)
118. Brown, P.W.: 8th ICCC Rio de Janeiro, vol. III, p. 234. Rio de Janeiro (1986)
119. Jawed, I., Skalny, J., Young, J.F.: In: Barnes, P. (ed.) Structure and Performance of Cements, p. 237. Applied Science Publishers, London (1983)
120. Ramachandran, V.S.: Cem. Concr. Res. **3**, 41 (1973)
121. Carstanje, W.A., Stein, H.N., Stevels, J.M.: Cem. Concr. Res. **4**, 193, 417 (1974)
122. Skalny, J., Tardos, M.E.: J. Am. Ceram. Soc. **60**, 174 (1977)
123. Bertrandie, D., Barret, P.: 8th ICCC Rio de Janeiro, vol. III, p. 79. Rio de Janeiro (1986)
124. Barret, P., Bertrandie D.: 7th ICCC Paris, vol. IV, p. 443. Paris (1980)
125. Galtier, P., Guilhot, B., Murat, M., Bachiorrini, A., Negro, A.: 7th ICCC Paris, vol. II, pp. 11–214. Paris (1980)
126. Cottin, B.: Non published data
127. Locher, F.W., Richartz, W., Sprung, S.: Zement–Kalk–Gips. **29**, 435 (1976)
128. Tenoutasse, N.: 7th ICCC Paris, vol. IV, p. 59. Paris (1980)
129. Collepardi, M., Baldini, G., Pauri, M., Corradi, M.: Cem. Concr. Res. **8**, 571 (1978)
130. Chatterji, S.: 7th ICCC Paris, vol. IV, p. 465. Paris (1980)
131. Scrivener, K.L., Pratt, P.L.: Proc. Brit. Ceram. Soc. **35**, 207 (1984)
132. Regourd, M., Hornain, A., Mortureux, B.: 7th ICCC Paris, vol. IV, p. 477. Paris (1980)
133. Mehta, P.K.: Cem. Concr. Res. **3**, l (1973); **6**, 169 (1976)
134. Birchall, J.D., Howard A.J., Double D.D.: Cem. Concr. Res. **10**, 145 (1980)
135. Boikova, A.L., Grishchenko, L.V., Domansky, A.L.: 7th ICCC Paris, vol. IV, p. 460. Paris (1980)
136. Boikova, A.I., Domansky, A.I., Paramonova, V.A.: Cem. Concr. Res. **7**, 483 (1977)
137. Gupta, P., Chatterji, S., Jeffery, J.W.: Cement Technol. **1**, 159 (1970)
138. Butt, J.M., Kołbasow, W.M., Kozyriewa, N.A.: Trudy Mend. Chim. Tiechnoł. Inst. D. I. Mendelejewa. **57**, 48 (1975) (in Russian)

139. Spierings, G.A.C.M., Stein, H.N.: Cem. Concr. Res. **6**, 265, 487 (1976)
140. Bilanda, N., Fierens, P., Tirlocq, J., Tenoutasse, N.: 7th ICCC Paris, vol. IV, p. 607. Paris (1980)
141. Mortureux, B., Hornain, H., Regourd, M.: ibid. vol. IV, p. 570
142. Boikova, A.L., Paramonova, V.A., Domanski, A.L, Piriutko, M.M.: Cemient. **8**, 20 (1977) (in Russian)
143. Regourd, M.: Il Cemento. **75**, 323 (1978)
144. Breval, E.: Cem. Concr. Res. **7**, 297 (1977)
145. Breval, E.: J. Am. Ceram. Soc. **62**, 394 (1979)
146. Wittmann, F.H.: Schniftenreihe Heft, 290 (1977)
147. Negro, A., Staffieri, L.: Zement–Kalk–Gips. **32**, 83 (1979)
148. Ramachandran, V.S., Beaudoin, J.J.: 7th ICCC Paris, vol. II, pp. II–25. Paris (1980)
149. Rogers, D.E., Aldrige, L.P.: Cem. Concr. Res. **7**, 399 (1977)
150. Malquori, G., Cirilli, V.: 3rd ICCC London, p. 32. London (1955)
151. Ludwig, U.: 6th ICCC Moscow, vol. II/1, p. 104. Moscow (1974)
152. De Keyser, W.L., Tenoutasse, N.: 5th ICCC Tokyo, vol. II, p. 379. Tokyo (1968)
153. Skalny, J., Young, J. F.: 7th ICCC Paris, vol. I, pp. II–1/3. Paris (1980)
154. Kuzel, H.J.: Zement–Kalk–Gips. **21**, 493 (1968)
155. Brunauer, S., Kantro, D.L.: In: Taylor H.F.W. (ed.) w, The Chemistry of Cements, p. 247. Academic, London (1964)
156. Berman, H.A., Newman, E.S.: 4th ICCC Washington, p. 247. Washington (1960)
157. Bogue, R.H.: The Chemistry of Portland Cement. Reinhold Publ. Corporation, New York (1955)
158. Kühl, H.: Zement–Chemie. Verlag Technik, Berlin (1952)
159. Verbeck, G.J., Foster, C.W.: Proc. Am. Soc. Test. Mater. **50**, 1235 (1950)
160. Venuat, M.: Rev. Mat. Constr. (550–551), 333 (1961); (552), 393 (1961); (553), 434 (1961)
161. Kurdowski, W., Garbacik, A., Chłądzyński, S.: 52 Konf. Nauk. Krynica 2006, vol. III, p. 161. Zesz. Nauk. Pol. Gdańskiej, Gdańsk (2006) (in Polish)
162. Kiernożycki, W.: Betonowe konstrukcje masywne, Polski Cement, Kraków (2003) (in Polish)
163. Neville, A.M.: Properties of Concrete, 5th edn., Pearson Education Limited (2011)
164. Zielenkiewicz, W.: Analiza przebiegu efektów cieplnych w kalorymetrach nieizotermiczno–nieadiabatycznych, PWN, Warszawa (1966) (in Polish)
165. Kamiński, M., Zielenkiewicz, W.: Cem. Concr. Res. **12**, 549 (1982)

Chapter 4
Cement Hydration

4.1 Cement Hydration at Room Temperature

Cement hydration is very complex because of the interference of different processes and mutual interaction between different clinker phases entering the reaction with water. Additionally, the image of the process becomes sophisticated as the particular cement grains are poly–mineral. In spite of this fact the clinker phases maintain their specific hydration rate, viz. the tricalcium aluminate phases turns into hydrates rapidly, subsequently the alite and ferrites; the belite phase shows the lowest hydration rate [1]. It is schematically illustrated in Fig. 4.1. The hydration of one phase influences the process of the other cement constituents; this is the consequence of the liquid phase composition or the adsorption of gel–like products on the surfaces of hydrating cement grains. The substantial interaction occurs between the two most rapidly reacting C_3S and C_3A. As Regourd [2] has reported the more rapid reaction of C_3A with gypsum water solution means the acceleration of C_3S hydration. On the other side Cottin [3] explains that the deficiency of SO_4^{2-} ions in the liquid phase, equivalent to the presence of excess aluminate ions, leads to the adsorption of the latter ones on the surface of alite grains and the hydration is thus hampered. As a consequence, the alite hydration is retarded and this is manifested by the modification of the heat evolution and by a low Ca^{2+} ions concentration in the liquid phase (Fig. 4.2). The CH phase detectable by X–ray diffraction appears later, after 5 h hardening. The C_3S hydration, giving a high concentration of the calcium ions in the liquid phase, will contribute, in the presence of SO_4^{2-} ions, to the significant reduction of the C_3A hydration rate. In this case the layer of poorly crystallized ettringite on the surface of C_3A crystals reveals a strong retarding effect on the hydration of aluminate.

After mixing cement with water, the liquid phase is quickly saturated with calcium and SO_4^{2-} ions; the pH value grows to attain the level close to 12.5. The sodium and potassium ions are quickly released to the solution; the maximum of their concentration is observed after 1 day of hardening and it becomes unchanged within

W. Kurdowski, *Cement and Concrete Chemistry*,
DOI 10.1007/978-94-007-7945-7_4, © Springer Science+Business Media B.V. 2014

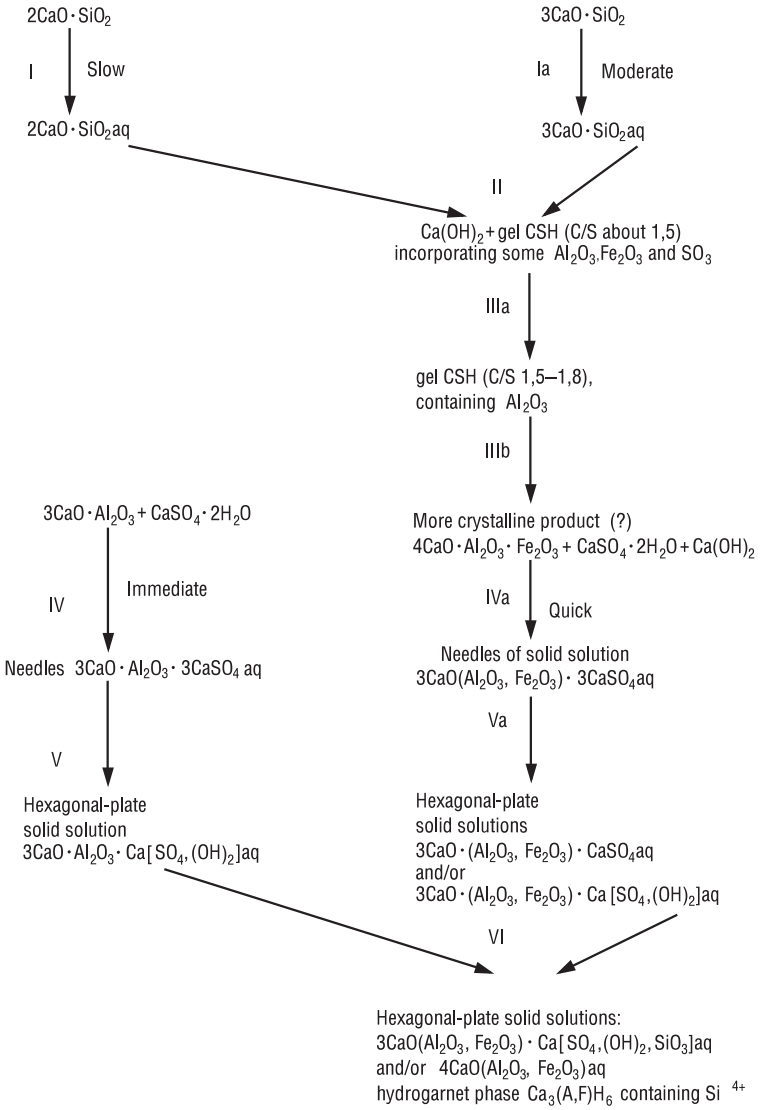


Fig. 4.1 Cement hydration scheme (according to [1])

28 days [4]. The Na^+ and K^+ ions shift the equilibrium in the liquid phase to the left side:

$$CaSO_4 + 2MOH \rightleftarrows M_2SO_4 + Ca(OH)_2 \tag{4.1}$$

Consequently, the lowering of calcium hydroxide solubility together with the increase of gypsum solubility is observed [1, 5, 6].

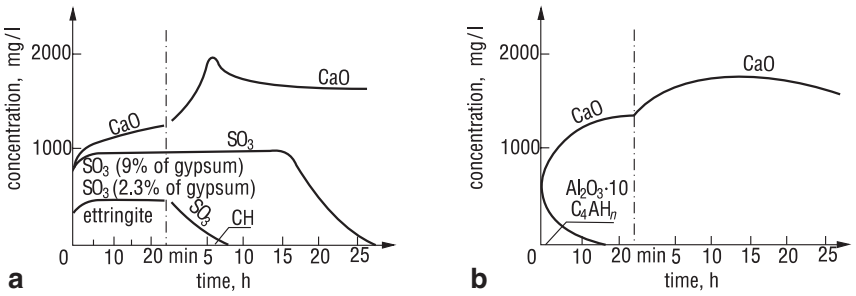


Fig. 4.2 Effect of gypsum addition on the concentration of Ca^{2+} ions in the solution and the formation of new phases during cement hydration (according to [3]): **a** 9 % and 2.3 % gypsum addition. **b** without gypsum

A significant role of the liquid phase has been found in many discussions dealing with the hydration process of particular cement clinker constituents. The changes of concentration, particularly those of Ca^{2+}, SO_4^{2-} and $Al(OH)_4^-$, affect the rate of the process. Simultaneously, the easily crystallized aluminate products, under the influence of the liquid phase, change into the other aluminates having another composition and morphology. For this reason, the liquid phase composition plays a key role in cement hydration.

Numerous studies on the properties of the liquid phase reveal that in the pores of cement paste at water to cement ratio (0.5–0.6) the concentrations of Na^+, K^+, Ca^{2+}, SO_4^{2-} and OH^- attain the level of 0.01 mol/l during 1 h after mixing with water [7]. The concentration of silica and alumina are very low from the beginning. The steady Ca^{2+} lowering is then observed, up to the level 5 mmole/l after 1 day, while the SO_4^{2-} concentration falls down practically to zero. Na^+, K^+, OH^- concentrations are on the high, constant level, so as the liquid phase is basically the solution of sodium and potassium hydroxide. The changes of concentration attributed to the basic constituents of the liquid phase (determined further as pore solution) are shown in Fig. 4.3 [8].

The sodium and potassium concentrations in the liquid phase will be the function of chemical composition of cement and the rate of their release to the solution will be affected by the phase composition of clinker. For example potassium from the potassium sulphate dissolves quickly, while the potassium from the solid solution in belite is liberated to the solution very slowly, during the slow hydrolysis of the host phase. The similar situation is in the case of siliceous fly ash where sodium and potassium occur in the glass which dissolves very slowly—after two weeks hydration in the saturated calcium hydroxide solution their solubility does not exceed a few % of initial content. Taylor [9] and Longuet et al. [10] report that the typical concentrations in the liquid phase of cement paste are as follows: Na^+: 0.05–0.2 mol/l, K^+: 0.2–0.5 mol/l, pH 13.4–13.8 respectively. These concentrations are on the unchanged level for a long time. Assuming that at full cement hydration the bound water content is 0.32 g per 1 g of cement, Taylor estimate that only about 45 % Na and 55 % K are present in the liquid phase for a long time. Glasser and Marr [11, 12] found that Na is incorporated to the hydrates more intensively than K.

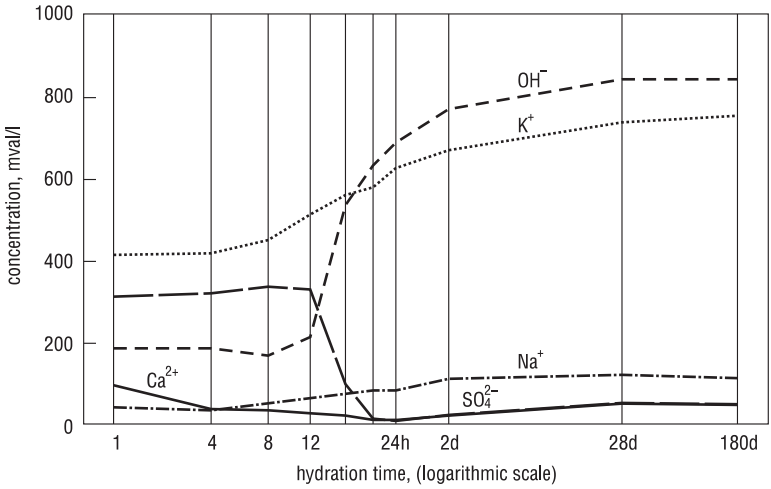


Fig. 4.3 Composition of the liquid phase in cement paste at w/c = 0.65 (according to [8])

The explanation of concentration changes would be possible at the complete knowledge dealing with the phase composition of the paste, the solubility of particular phases and ions activity factors in the multi–component solution formed in cement paste. This was done by Bailey and Hampson [7].

The rate of particular phases reaction with water was investigated by many authors. The alite and C_3A content vs. time and the calcium hydroxide growth in the paste, as determined for many industrial clinkers in the Institute of Cement in Düsseldorf, can be given as a good example [114] (Fig. 4.4). As one can see, at gypsum addition the alite hydrolysis is accelerated, however the tricalcium aluminate reaction with water is not specially affected. The effect of SO_4^{2-} ions on the reaction of alite with water is commonly accepted, while the contradictory reports can be found as the C_3A hydration rate is concerned. For example Tang and Gartner [13] observed the retarding effect of gypsum on the tricalcium aluminate hydration.

The coatings of amorphous, gel–like products, surrounding the cement grains, formed in the pre–induction and on the beginning of the induction period were found under the electron microscope of very high resolution. These coatings are rich in silica and alumina, as well as in the calcium and sulphate ions. Their composition differ significantly from the composition of cement grain on which they are formed. The AFt rods appear after 1 h [14]. They are formed as a result of nucleation in the liquid phase or in the outer layer of gel [15]. During the post–induction acceleration of reaction the C–S–H and CH are intensively formed. The fibrous C–S–H (type I according to Diamond), growing radiantly from the surface of cement grains, as well as the type II "honeycomb" are observed. It is commonly accepted that these forms are derived from the C–S–H thin foils by partial drying of hydrated specimen [9]. C–S–H occurs as a shell with increasing thickness, surrounding the cement grains and AFt rods and it cannot be excluded that the C–S–H nuclei appear on the AFt surfaces.

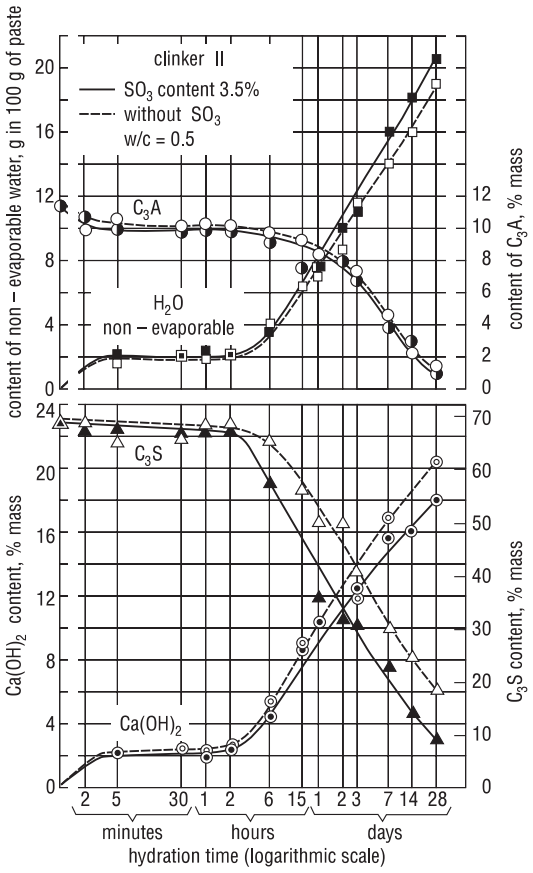


Fig. 4.4 Changes of alite, C_3A, $Ca(OH)_2$ and non–evaporable water content in the paste (according to [8])

There is a strong cohesion between the C–S–H shells, as one can conclude basing on the microcracks formed across this phase but not detectable on the shell boundaries. This is so–called "cohesion point", which agree with the maximum on the calorimetric curve [9]. These linking shells on neighboring larger cement grains control the mechanical properties of paste [9]. After five hours a gap appears between the shell and cement grain; its thickness increases up to 0.5 μm after 12 h. Therefore the shells grow "outside", becomes permeable and process goes through the liquid phase. Scrivener and Pratt [15], as well as Pratt and Ghose [16] observed the formation of C–S–H in the gap between the shell and cement grain before the third stage of the hydration (the decreasing rate) is completed filling it (Fig. 4.5). Filling the gap occurs slowly, so the free space has about 3 μm width after 4 days and disappears after about 7 days.

Cement grains transform in a different way, depending on their size and composition. The finest ones (under 3 μm) are completely dissolved before the II stage and give the outer product, frequently precipitating on the shells of coarse grains. The grains rich in C_3A reveal broader free space between the anhydrous core and

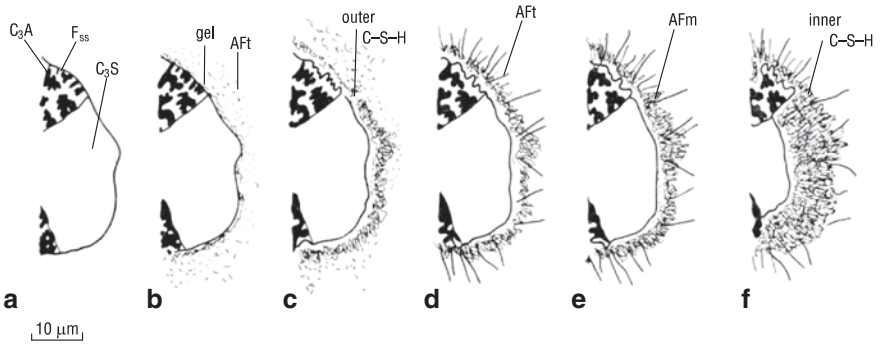


Fig. 4.5 The changes of microstructure during the hydration process (according to [15]): **a** unhydrated cement grain. **b** after 10 min—gel rich in alumina precipitates on cement grains; short AFt rods nucleate in the solution and at edge of gel. **c** after 10 h the C–S–H outer product begins to form on AFt rods leaving a gap between the surface of grain and hydrated shell. **d** after 18 h the renewed hydration of C_3A, [and/or $C_2(A, F)$], producing long rods of AFt, C–S–H inner product starts to form on inside of shell. **e** during the 1–3 days C_3A reacts with AFt inside shell forming hexagonal plates of AFm; the formation of inner C–S–H is continued which reduces separation of anhydrous grain and hydrated shell. **f** after 14 days the inner C–S–H is sufficient to fill the free space, the outer C–S–H became more fibrous

the shell. Small grains, from 15 do 20 µm are completely hydrated up to 7–14 days before the gap is filled by the products; the empty cores of diameter ca. 5 µm appear. CH formed during the stage III crystallizes as hexagonal plates in the space filled with water; therefore the free volume between the shells is significantly reduced [16].

During the stage II and III the crystallization of AFt in the form of long needles is continued. Between the 1 and 3 day the reaction of C_3A with water, and with AFt inside the shell with the formation of AFm starts. This is accompanied by further precipitation of C–S–H inner product. The shells become less and less permeable. AFt continues to crystallize outside them. After about 14 days all the space between the inner residue of grain and the shell is filled with C–S–H, while the outer C–S–H transforms into the more fibrous forms. AFm is produced outside the shells too, giving a intimate mixture with C–S–H [17].

The final stage of hydration begins when the free space between the alite inner part and the shell formed of hydrates is filled with C–S–H. Alite hydration is continued and the interface shifts toward the centre of the grain. In this stage the reaction does not occur presumably through the liquid phase but becomes a topochemical process. The product formed corresponds to the type IV C–S–H according to Diamond.

The shells do not surround the C_3S grains; this could suggest the effect of Si substitution by Al in their formation. Therefore the hydrating C_3S phase is not a good model of hydrating cement [9].

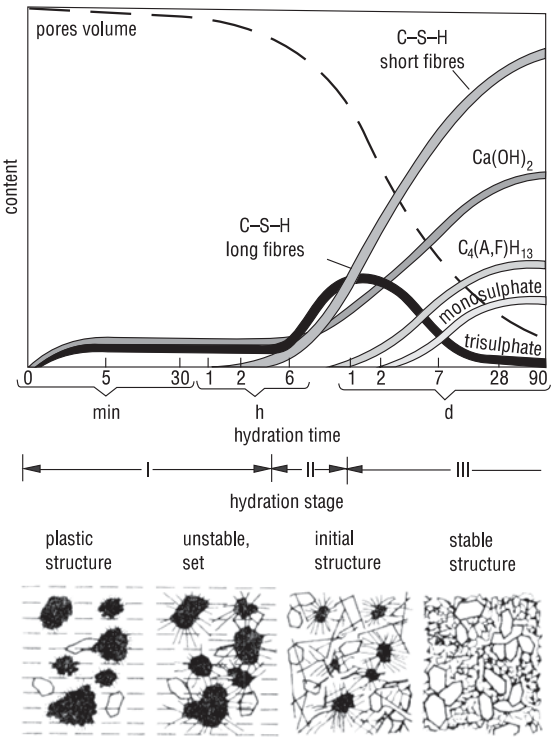


Fig. 4.6 Phase composition of hydrating paste (according to [18])

Belite hydration occurs analogously but this is significantly shifted in time; after 28 days the degree of hydration is approximately 25 %, this corresponds to the hydration degree of alite after 1–1.5 day reaction with water.

The ferrite phase hydration results in the formation of the same products as in the case of C_3A, however, around the relics of ferrite grains the phase rich in iron is observed. Some authors suggested the presence of $Fe(OH)_3$ but this was not proved experimentally.

The phase composition changes of the paste were proposed by Locher and Richartz [18] (Fig. 4.6). Stark et al. [19] reported a little modified composition of the paste, taking into account the presence of syngenite, as a transient phase, too. This could be valid when the potassium sulphate in cement clinker is high and content of ettringite is not decreasing. Obviously, in the pastes and mortars matured for a long time the ettringite is detected, however, it can be attributed to the substantial heterogeneity of the paste. On the other hand the composition found by Locher and Richartz [18] is closer to the equilibrium.

The phase composition change can be easily investigated by XRD. Ettringite appears as the first product, just after 15 min the peak corresponding to $d = 972$ pm, as well as the second one at $d = 561$ pm are detected. The peaks of portlandite are observed soon after the beginning of hydration too; on the XRD pattern there are

those corresponding to $d = 262$ pm and $d = 192$ pm. They can be noticed after 2 h of hydration; after a few days they are visible as the strongest peaks on XRD patterns. C–S–H gives a diffused peak at $d = 270$–310 pm; after a longer time they are sharper at $d = 304$ pm, 280 pm and 183 pm (see Fig. 3.22). However, they can be found only after 2, 3 days. The peak of calcium aluminate C_4AH_{13} at $d = 805$ pm is detectable after 1 day and that of AFm (288 pm)—after two days. When the hardened paste is not protected against the access of air (CO_2), the peaks attributed to carboaluminates, at first $C_4A\overline{C}_{0.5}H_{12}$, further $C_4A\underline{C}H_{11}$ or the solid solutions with the other phases from the AFm group are found. The peaks derived from the clinker phases can be detected after a long time, first these of tricalcium aluminate disappear, but of belite are disappeared very slowly. The brownmillerite behave differently: in some clinkers is not detected after 2 days, while in the other this phase is still present after a few months (peak $d = 745$ pm). The peaks of gypsum disappear usually after 1 day.

4.1.1 Paste Phase Composition

The chemical composition of pastes determined with electron microprobe and electron scanning microscopy revealed that the C/S ratio in C–S–H was between 1.7 and 2.0. In the set of experimental results the local maximum values were 1.75 and 1.95 respectively [20]. The ratios of other atoms to calcium are approximately as follows: Na 0.01; Mg 0.01–0.08; Al 0.04–0.08; S 0.01–0.03; K 0.01–0.02; Fe 0.01–0.03 [21–23]. The composition does not change either with time of curing—except of S/C—or with w/c; it seems to be related to the chemical composition of alite and belite.

Taylor and Newbury [24] presented the results of analysis in the system of coordinates: (Al + Fe)/Ca–Si/Ca and obtained a triangle which is shown in Fig. 4.7. Near the apexes, where there is most of points, the chemical composition corresponds to the following products: CH, C–S–H and hydrogarnets. Taylor and Newbury are of the opinion that the points in middle position, not near the apexes, correspond to the mixtures of phases. In the pastes matured for a short time the AFm phase was found [25]. The differences between the inner and outer C–S–H was not observed, perhaps except of some minor components; their percentage in outer product is a little lower [25, 26]. The Ca/Si ratio higher than 2, results presumably from the presence of C–S–H—AFm mixtures in nanometric scale. This is possible because of the layer structure of both phases: this "perfect mixture" of gels can be thus explained [9]. On the other side the "monophase" mixtures of CH with C–S–H are observed under the microscope only in the pastes with very low w/c [9].

A typical CH content in the pastes produced from Portland cement is in the range 18–25 % after 3 month of hardening. AFt is present only at early age. Using some assumptions and methods Taylor [27] proposed a mass balance for the paste prepared at w/c = 0.5 and stored one year at 11 % RH. The following volume ratios of particular phases were proposed: clinker 0.05; CH 0.11; $CaCO_3$ 0.01; C–S–H

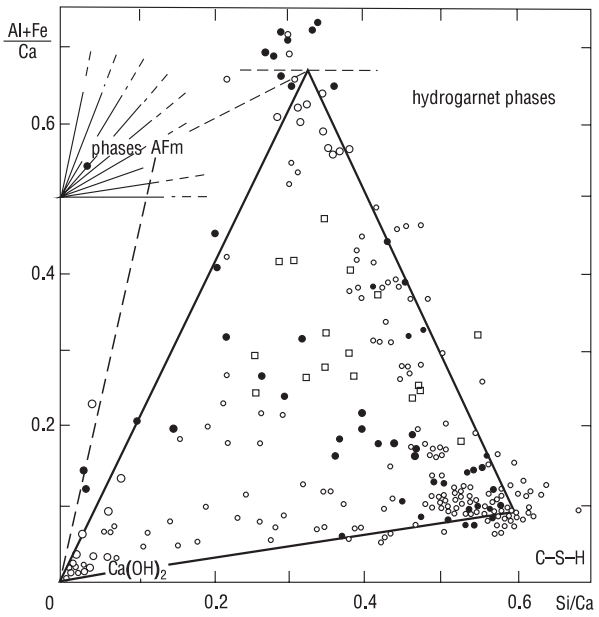


Fig. 4.7 Chemical composition of components of paste matured 3 years, according to [24]: ○ Mg/Ca < 0.20. S/Ca < 0.04, ● Mg/Ca < 0.20. S/Ca ≥ 0.04, □ Mg/Ca ≥ 0.20. S/Ca < 0.04

0.37; AFm 0.15; micropores ≤ 5 nm 0.13; capillary pores 0.18. Taylor [27] analyzed the data relating to the occurrence of iron(III) ions in the paste, other than the high iron content in ettringite and AFm discussed in Chap. 3. Taylor [27] states that the iron(III) ions do not form iron hydroxide in cement paste but they are present as hydrogarnet which is poorly crystalline; the proposed composition of this phase is as follows: $Ca_{2.95}Al_{0.1}Fe_{1.75}Ti_{0.1}Mn_{0.05}Si_{0.4}O_{12}H_{10.4}$.

This is the consequence of low mobility of Fe^{3+} ions which do not migrate but are located in hydrates formed *in situ* from the ferrite phase [27]. Apart from the iron ions in octahedral sites there are the Al^{3+}, Ti^{4+} and Mn^{3+} ions; the latter ones are concentrated in brownmillerite in clinker. The magnesium ions show also a low mobility in pore solution; they do not produce brucite but hydrotalcite $[Mg_{0.75}Fe_{0.2}(OH)_2](CO_3)_{0.125}(OH)_{0.5}$ [27]. The formation of hydrotalcite *in situ* after brownmillerite is promoted by the highest concentration of magnesium in this phase.

4.1.2 Role of Gypsum in Hydration and Disturbances of the Setting Process

The reaction of clinker phases with water, together with the crystallization of hydrates, brings about the substantial changes of rheological properties of the paste. The formation of hydrated phases and, according to Locher [28], the morphology of hydrates crystallized in the liquid phase or on the surface of cement grains, leads to the reduction of distance between them and the viscosity of paste is enhanced. At

the next stage of this process the rigid skeleton structure is built and this structure reveals mechanical strength with ability to carry some load [1, 29]. This early period of hardening, with some strength development, is determined as "setting". The initial setting time is observed approximately together with the end of the induction period on the heat evolution curve; the final set takes place in the middle of the acceleration period.

As it has been mentioned, the hydration of C_3A has a decisive impact on the rheological properties of fresh paste. The high rate of reaction with water leads to the saturation of solution with aluminate and calcium ions and as a consequence to the crystallization of C_4AH_x. This corresponds to the quick stiffening of paste, determined as "flash" set. All the substances modifying the rate of C_3A reaction with water by adsorption on the surface of this phase or by the change of the ions concentration in the liquid phase will have a great impact on the rheological properties of paste.

The disturbing of hydration process at early age affects the strength development at later age and leads even to the reduction of strength. For this reason the optimum conditions of hydration from the beginning of the process are of crucial, technological importance.

Use of gypsum in order to reduce the rate of calcium aluminate ration with water, as a "set controlling agent" is as old as Portland cement production. It is commonly accepted that the C_3A hydration is hampered by the ettringite layer covering the aluminate crystals and forming an impermeable barrier [30]. This old hypothesi s has been proved recently [31–33].

A rapid reaction of C_3A with water is only possible after gypsum consumption; this occurs commonly after 24 h of hydration. Then the hexagonal hydrates are formed and react with ettringite to form AFm. The direct reaction of C_3A with ettringite or rather locally present aluminate ions with ettringite is also possible.

According to Locher [28], the degree of C_3A hydration vs. time is the same with and without gypsum (see Fig. 4.4), while the crystal size is a decisive factor as the setting of paste is concerned. In case of the deficiency of SO_4^{2-} ions in the solution, the C_4AH_x hydrates in the form of large, hexagonal plates from C_3A reaction are produced. They fill the space between the grains and, binding them together, give the effect of flash set [28]. In the presence of gypsum a very small ettringite crystals are formed on the surface of grains and, as a consequence, there is no substantial change of paste viscosity. After certain time these crystals recrystallize and the massive ettringite needles appear, resulting in the setting effect, similarly as at the formation of hexagonal hydrates. However, this concept is not popular; it is generally accepted that in the case of gypsum addition the process of setting occurs as the consequence of C–S–H formation.

A special attention should be paid to the results reported by Cottin [34]. The degree of C_3A hydration in the paste without gypsum is very high—about 35 % after 1 min., with simultaneous C_4AH_{19} phase crystallization. The addition of gypsum causes the hindering of this reaction; after 1 min. the degree of C_3A hydration is not greater than 5 % and the ettringite is formed as a product. Subsequently in both hydrating C_3A pastes the progress of hydration is not observed (Fig. 4.8). Taking

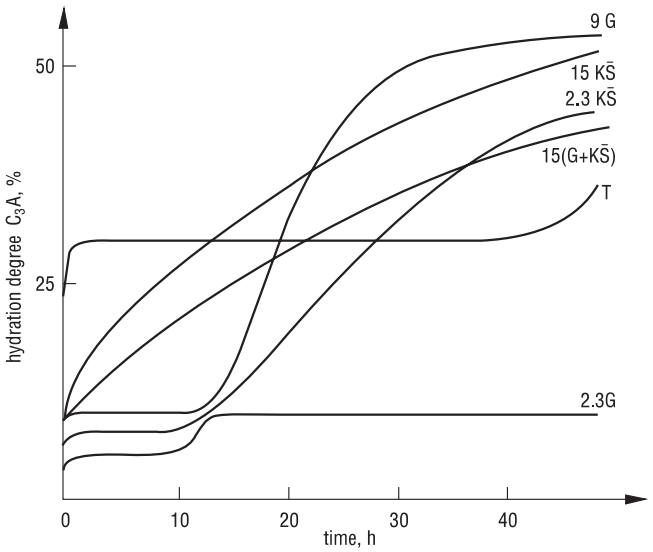


Fig. 4.8 The C_3A hydration rate (according to [34]): *G* gypsum, $K\bar{S} - K_2SO_4$, *T* reference without additive (numbers indicated mass %)

into account these data and having some information about the mean C_3A content in cement clinker (about 16 %), one can estimate the volume of hydration product. In the first case about 6 cm^3 C_4AH_{19}/100 g of cement was produced, in the second one—about 2 cm^3 $C_3A \cdot 3C\bar{S} \cdot 32H$/100 g cement. The paste without gypsum shows flash set. It is not possible to estimate the crystal size which is an important parameter too. In spite of this the evidently higher volume of crystals in the paste without gypsum seems to be convincing. In the studies reported by Cottin [34] there is also valuable information as the liquid phase composition is concerned. In the gypsum or potassium sulphate containing mixture the Ca^{2+} ions concentration curve vs. time reveals a course typical for C_3S (Fig. 4.9).

The calcium hydroxide concentration attains quickly the supersaturation level, with a clear maximum after 6–7 h. The concentration decrease is consistent with the crystallization of CH detectable by XRD. In the paste without gypsum the calcium ions concentration attains quickly the value of about 1600 g CaO/l, then the first "plateau" is observed and after this it increases slowly, up to the concentration of about 1800 g/l after 13 h. After 10 h the concentration of calcium ions is higher than in the sulphates containing samples and is decreasing very slowly. After 48 h there is equal about 1500 mg/l (Fig. 4.9). This is related to the unfavourable effect of aluminate ions on the hydrolysis of alite, as aforementioned in p. 4.1.

The addition of gypsum is related primarily with the C_3A phase content in cement. As it has been widely reported, at the optimum gypsum addition, the maximum strength and minimum drying shrinkage were achieved [3, 35, 36]. One should take in mind, calculating the advantageous gypsum addition, that the retarding effect of

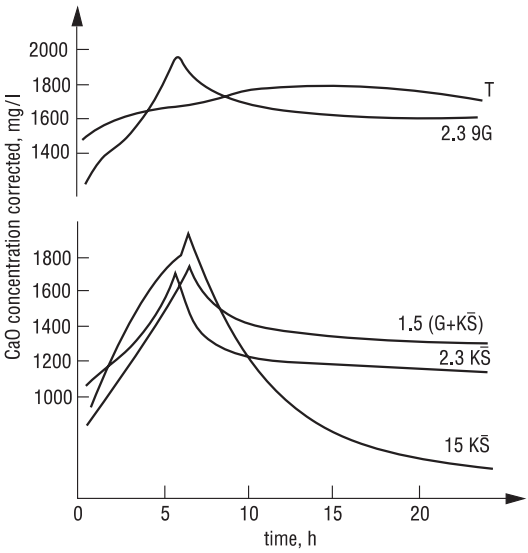


Fig. 4.9 Changes of the Ca^{2+} ions concentration corresponding to the calcium hydroxide content in the liquid phase (according to [34]) (notation as in Fig. 4.8)

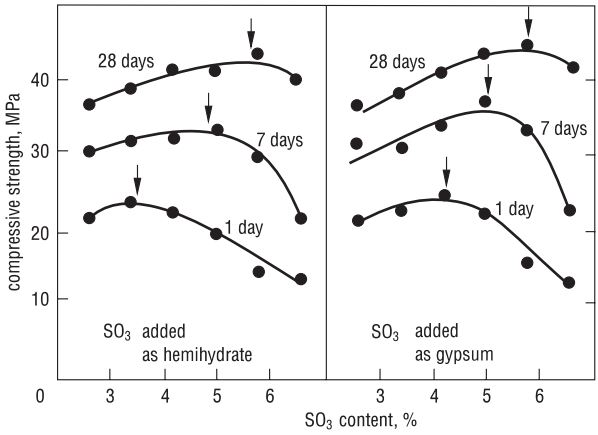


Fig. 4.10 Optimum gypsum addition as a function of compressive strength vs. different period of maturing (according to [35])

gypsum on the C_3A hydration increases with the content of this retarder. Its means that the amount of ettringite formed at early stage of hardening will be reduced with the increase of gypsum content. This phenomenon can be an explanation of growing gypsum optimal content for longer time of maturing (Fig. 4.10).

Cottin [3] tried to explain the beneficial effect of fixed gypsum content in the paste by calculating the total volume of hydrated aluminates and sulphoaluminates (Fig. 4.11).

Jawed et al. [35] remind that the rapid crystallization of ettringite or AFm leads to the reduction of calcium ions concentration in the solution, thus affecting the C_3S hydration. When the crystallization of aluminates takes place before the renewed

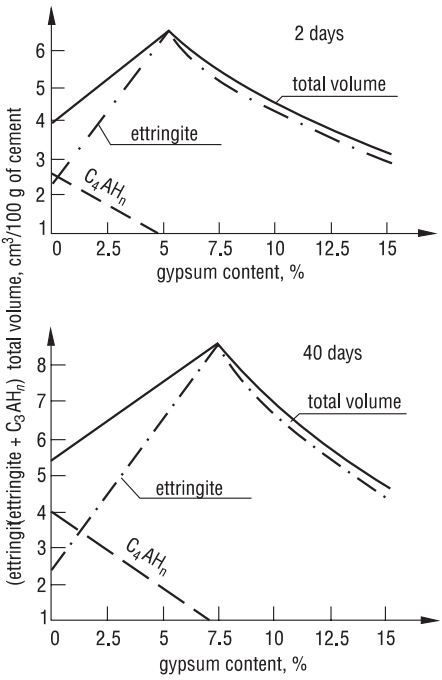


Fig. 4.11 Maximum volume of aluminate phases as a function of gypsum content (according to [3])

acceleration of C_3S hydration (III stage), then the reduction of Ca^{2+} concentration hinders the nucleation of CH and C–S–H and the reaction of C_3S with water is retarded [35]. However, this problem is not fully explained.

The beneficial effect of gypsum consists in the simultaneous acceleration of alite hydration, mainly in the pre–induction period [26, 37]. The transfer of SO_4^{2-} ions to the C–S–H was detected [20]. However, these ions are poorly bound, they are rather adsorbed on the surface of C–S–H gel [38] (see p. 3.2.3). According to Bentur [39] the effect of gypsum on cement hydration should be considered in these two aspects. Gypsum has an impact on the amount and constitution of C–S–H gel. On the other hand, in the presence of gypsum the amount of C–S–H increases but the cohesiveness, being the function of C/S ratio is lowered:

$$W = 522 - 203\,\mathrm{C/S\,[MPa]} \tag{4.2}$$

The effect of gypsum is the resultant sum of these two factors.

The optimum gypsum content is influenced also by the fineness of cement and the content of alkali. The gypsum addition increases with the specific surface area of cement S (by Blaine method, in m^2/kg) and with the Na_2O_e content. The following correlation has been proposed by Ost [40]:

$$\%\,SO_3 = 0.556Na_2O_e + 0.17659S - 0.1072Fe_2O_3 - 3.6004 \tag{4.3}$$

One can also remind the following formulae [41]:
by Lerch

$$\%\,SO_3 = 0.093Al_2O_3 + 1.71Na_2O_e + 0.94K_2O + 1.23 \tag{4.4}$$

by Jirku

$$\%\,SO_3 = 6.8 \cdot 10^{-5} S \cdot C_3A \tag{4.5}$$

S specific surface area is given in cm^2/g.

Haskell [42] proposed the empirical formula being the modified form of Lerch formula, relating to the cement of specific surface equal about 1900 cm^2/g:

$$\%\,SO_3 = 1.1841 + 0.0950C_3A + 1.6364Na_2O_e \tag{4.6}$$

In case of the fineness of about 2800 cm^2/g the constant value in the formula increases from 1.1841 to 1.6841.

These empirical formulae have limited importance, though they take into account the main factors affecting the optimum gypsum addition. In this case the experimental way of determination of the most proper, convenient gypsum content or gypsum replacement by anhydrite, or simultaneous anhydrite and hemihydrate addition, is the best. On the other side, the optimum gypsum corresponds most frequently to the SO_3 content in the range from 2.5 to 3 % for Portland cement, without mineral additions. Apart from the fairly good strength development also the volume stability, with no expansion, even in micro–areas is achieved. A local increase of volume could result in the worsening of the paste microstructure and, as a consequence, in reduction of 28 days and later age strength. Therefore a significant reduction of strength observed in the case of cement with 6 % SO_3 content has probably this cause. The rate of ettringite formation at early age is high, even at significant gypsum addition, corresponding to SO_3 content equal 12 % [43]. This rate decreases as late as after 7 days when the amount of ettringite formed is about 12 %.

The alkali content in clinker is usually on the level of 1 % Na_2O_e; with dominating soluble alkali sulphates. In the solution rich in CH, they increase the solubility of gypsum, while the solubility of calcium hydroxide decreases. In this condition the SO_4^{2-} ions can be bonded with C–S–H. That is why the gypsum addition should be higher. When the specific surface area of cement is high and the reaction of tricalcium aluminate is therefore accelerated, the gypsum addition should be higher too.

The reactivity of C_3A should be considered when the addition and type of calcium sulphate is considered. Locher [28] proposed to designate this reactivity as a ΔC_3A factor, being the part of C_3A hydrated during the pre–induction period, determined by XRD. With help of the diagram establish by Locher it is possible to take into account the SO_3 content in the clinker, as well as the addition of gypsum + anhydrite mixture (Fig. 4.12). Because of the high reactivity of C_3A some amount of hexagonal hydrates and AFm can be formed before gypsum dissolves in

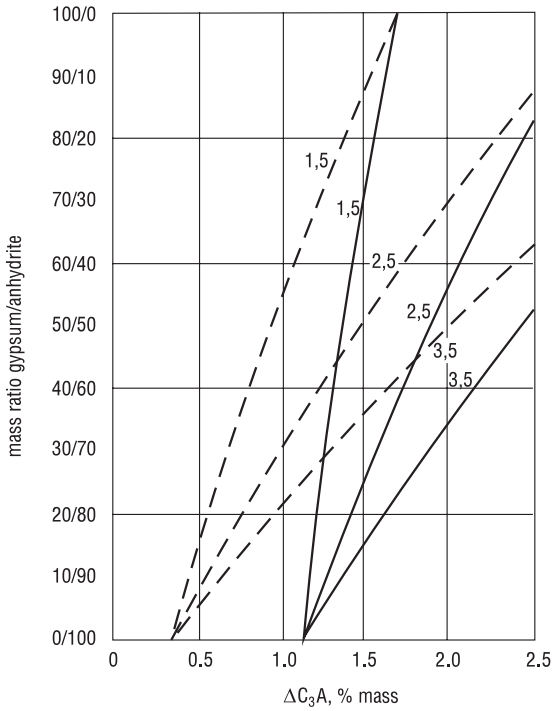


Fig. 4.12 The optimum addition of the mixture of anhydrite with gypsum to clinker against tricalcium aluminate reactivity (ΔC_3A) (after [28]), *broken lines* clinker with 0.3 % SO_3, *full lines* 1.0 % SO_3

the solution. A small, negligible amount of these phases is always observed at early age, as it was mentioned in p. 3.3.4. This effect can be limited with low hemihydrate addition, when there is no sodium and potassium sulphates in clinker. Because of good grindability, gypsum is always present in the finest fractions of cement. The dissolution is therefore accelerated. The rate of calcium sulphate dissolution depends also on the type of calcium sulphate phase: anhydrite III reveals the highest rate of dissolution—during 10 s the solution is supersaturated in respect to gypsum.

Cement with proper gypsum content reveals proper setting. In this case, according to the most of authors, the initial and final setting time is related to the acceleration of alite hydration and the formation of substantial amount of C–S–H. As it was aforementioned, the correlation can be found between the end of induction period and the initial setting time. Other calcium aluminates, particularly $C_{12}A_7$, as well as $C_4A_3\bar{S}$ show high hydration rate in saturated solution of CH and $C\bar{S}H_2$. For this reason cements containing these phases exhibit quick set; their prolonged set requires the presence of organic admixtures, for example citric or tartaric acids. These topic is discussed in Sect. 9.3.

The setting process can be disturbed by undesirable changes of liquid phase composition. The classification of particular cases is illustrated according to Locher [28] in Fig. 4.13.

A high reactivity of C_3A in water, and simultaneously quickly dissolving sulphate phase, giving high SO_4^{2-} ions concentration in solution causes short setting

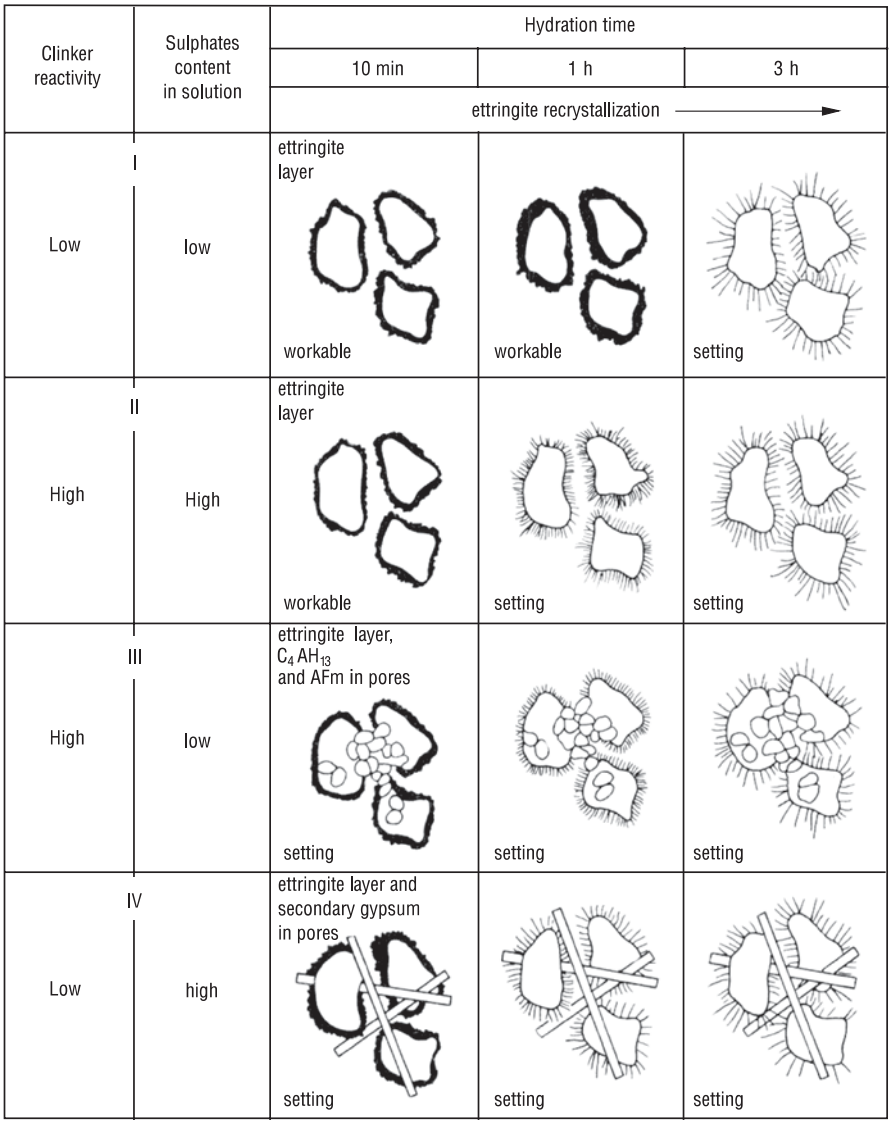


Fig. 4.13 Different set controlling phenomena: *I* and *II* recrystallization of ettringite, *III* hexagonal aluminates, *IV* secondary gypsum (according to [28])

time (case II). The special cements containing $C_{12}A_7$, CA or $C_4A_3\bar{S}$ can be attributed to this case. At too low gypsum content or low dissolution rate of calcium sulphate with reactive aluminate phase the proper setting is not ensured (case III). Case IV corresponds to the false set, resulting from the presence of gypsum hemihydrate. As it is known, the mixing of paste causes the quick dissolution of crystallized

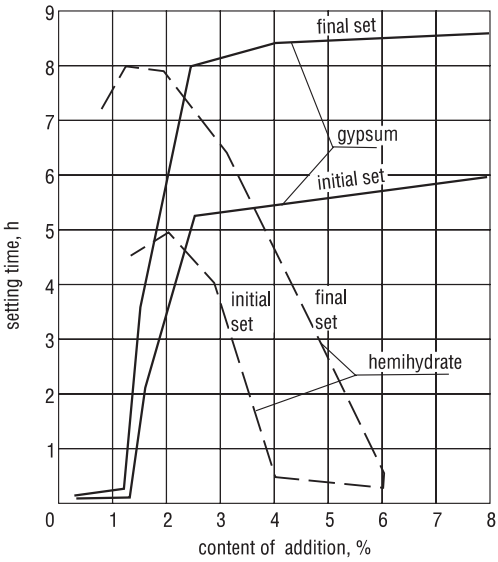


Fig. 4.14 Effect of gypsum and hemihydrate content on setting time (according to [1])

gypsum and the paste exhibits setting and hardening without worsening of properties. The effect of hemihydrate content on the setting time is shown in Fig. 4.14 [1].

According to Locher and Richartz [18], as well as Sprung [44] the formation of syngenite can be also the reason of false set. This phase is produced in cement pastes with higher amount of K_2SO_4 and hemihydrate. The formation of syngenite causes not only flash set but also leads to the consumption of sulphates, and further to the rapid C_3A reaction with water. As a consequence, the stiffening of paste takes place [45].

Frigione [36] distinguished between the two types of false set, resulting from the presence of hemihydrate. This classification is based upon the changes of stress yield value. The first type of false set relates to the cements with the mixture of gypsum and hemihydrate. Is distinguish by quick increase of the stress yield value (Fig. 4.15) and occurs only during very short mixing of paste, not longer than 3 min [36]. The second type of false set occurs when a prolonged mixing is needed for restoring of good viscosity of the paste—at least more than 6 min. or even 10 min. (Fig. 4.16). This false set is linked with the presence of anhydrite III (soluble). In this case the changes of stress yield value are slow. Frigione [36] has proved the effect of calcium hydroxide concentration in the solution as a false set controlling agent. This would be helpful in understanding of the impact of atmospheric conditions on aerated cement during storage. The carbonation, reducing the activity of cement phases and the rate of $Ca(OH)_2$ release to the solution, strengthens the effect of false set. The impact of alkalis, modifying the solubility of gypsum in the liquid phase is significant too (Fig. 4.17) [36].

The best workability or the minimum water content to assure the required consistency of paste (Fig. 4.18) are attributed to such gypsum addition which gives simultaneously a good set controlling effect. Obviously, at too low gypsum content

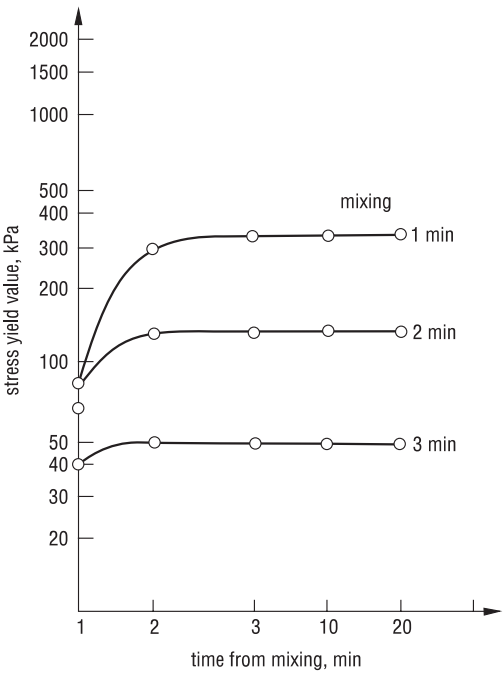


Fig. 4.15 Stress yield value of aerated Portland cement paste heated to the temperature 120 °C (mixture of gypsum and hemihydrate)—false setting type I (according to [36])

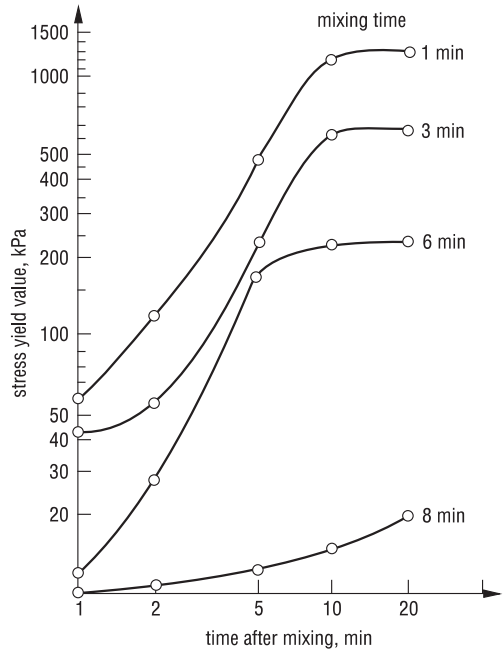


Fig. 4.16 Stress yield value of aerated Portland cement paste heated to the temperature 150 °C (formation of anhydrite III)—false set type II (according to [36])

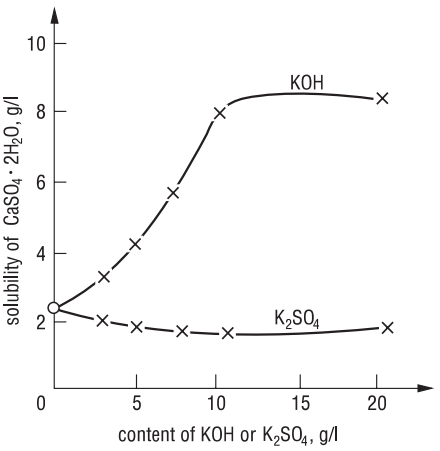


Fig. 4.17 Effect of KOH and K_2SO_4 on the solubility of gypsum (according to [35])

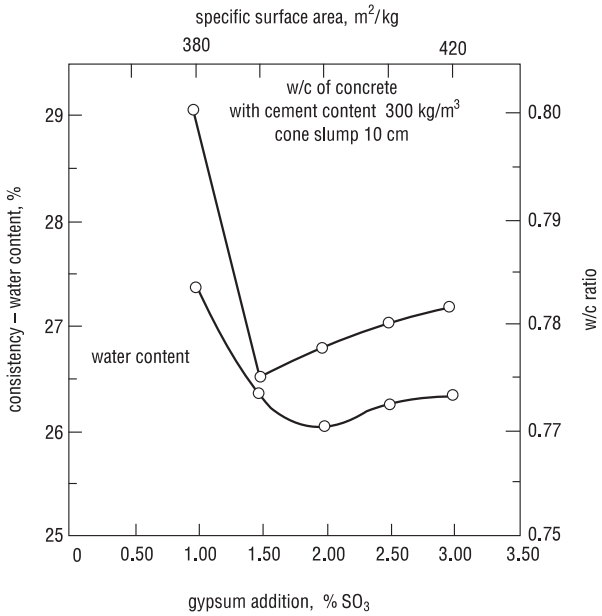


Fig. 4.18 Effect of gypsum on the consistency and w/c of cement paste and concrete (according to [36]) (Blaine specific surface, water content according to ASTM C187)

the formation of hexagonal hydrates will occur. The changes of consistency related to the excess of gypsum, accompanied always by some amount of hemihydrate are attributed by Frigione [36] to the specific surface increase, resulting from the higher content of colloidal gel, in the environment saturated with $Ca(OH)_2$.

Optimum gypsum addition increases with temperature in which the concrete is matured (Fig. 4.19) [41]. The process of C_3A hydration is then accelerated, according to the Arrhenius rule, and the solubility of $Ca(OH)_2$ is reduced (see p. 4.1.3.4).

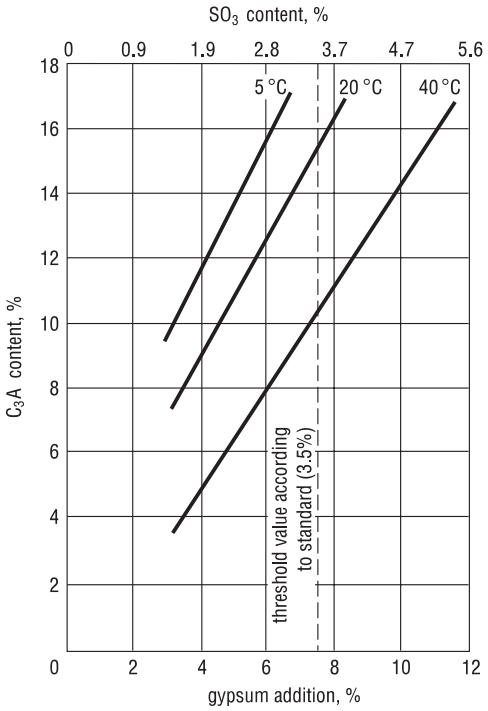


Fig. 4.19 Effect of temperature on the optimum gypsum addition to cement (Kuhs, Oberhausen, according to [41])

With dehydration of gypsum, the phenomena of lumping of cement in silos are related, undesired from the technological point of view. When the temperature of cement during the storage in silo is too high, accompanied with *quasi*–adiabatic conditions, the dehydration of gypsum occurs, and the water vapour condensates on cement grains near the walls, where temperature is lower. It leads to the hydration of aluminates and the crystallization of hexagonal hydrates and ettringite or syngenite, which causes the formation of lumps [46–48]. The analogous mechanism leads to the formation of the layer of hardened cement on the walls of cement silo [46]. These phenomena are dependent primarily on the following factors: temperature of cement, alkalis content, reactivity and content of aluminates, gypsum content [48–50].

There are many reports dealing with the effect of gypsum content on the strength of mortars, because of the practical importance of this problem. The authors are generally of the opinion that the optimum gypsum increases as the later age of hardening is considered (see Fig. 4.10). The similar results are reported by Jelenić [48] for the 90% monoclinic alite and 10% cubic C_3A mixture. This is clearly visible that the maximum of strength shifts toward the higher gypsum contents for later time of hardening and at growing alkali content. The authors attribute effect this to the incorporation of sulphur in the C–S–H [45].

The effect of gypsum fineness was also investigated. Le Jean [49] found a positive role of lower fineness. Frigione [36] did not observe any effect.

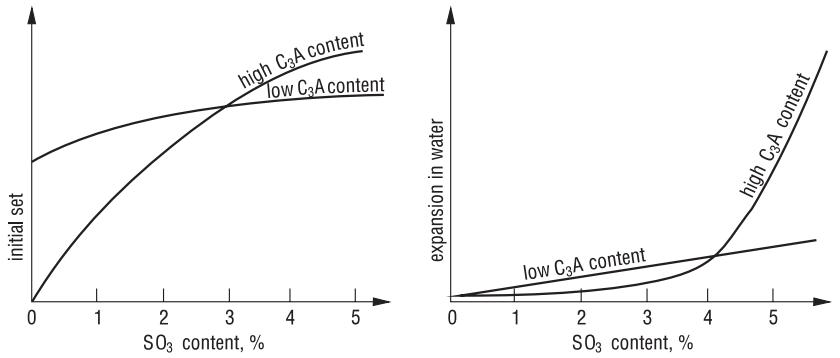


Fig. 4.20 Effect of gypsum content on the initial set and swelling of cement pastes with variable C_3A content (schematically) (according to [41])

Too high gypsum addition causes a risk of paste swelling and consequently, the deterioration of concrete. This is the result of ettringite formation in the period when the plastic deformation of paste, neutralizing the pressure of crystallization cannot occur. The optimum gypsum addition should react completely with the formation of ettringite up to 24 h, however, not later than up to 48 h. High gypsum favours the "internal corrosion" particularly intensive as higher is the C_3A content in cement [50]. It is shown in Fig. 4.20. This phenomenon is particularly dangerous at low fineness of cement, because a substantial amount of non reacted gypsum residue will form the ettringite with C_3A.

4.1.2.1 Set Controlling Agent Without Sulphates

Brunauer [51] proposed to use the complex calcium lignosulphonate and potassium carbonate admixture instead of gypsum or anhydrite; the lowering of water demand was thus obtained. This idea was the subject of numerous studies reported by Brunauer et al. [52]; they were summarized by Odler et al. [53] during the International Congress on Cement Chemistry in Moscow. The optimum addition of these admixtures, depending on the composition of clinker, is as follows: grinding aid 0.1–0.5 %, lignosulphonate 0.25–1.5 %; potassium or sodium carbonate 0.25–1.25 %. By using these admixtures the cement pastes of good workability at w/c 0.3 or even lower can be produced. The phase composition of clinker has no special importance but the properties of fresh and hardened paste (strength) can be controlled by selection of admixture (e.g. lignosulphonate) and its addition. The latter has a great impact on the pore structure in the paste. The grinding aids do not affect significantly the properties of paste, however, their use is necessary in order to obtain cement of high specific surface; this gives the possibility to reach high strength and quick strength development of the paste. Potassium or sodium carbonates induce the formation of carboaluminates hydrates which form the layer on the surface of C_3A and together with lignosulphonate guarantee the proper setting time of cement

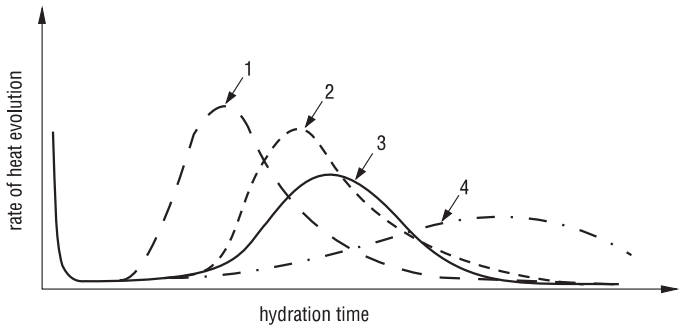


Fig. 4.21 Effect of accelerators on the rate of heat evolution during C_3S hardening (according to [35]): *1* set accelerator ($CaCl_2$) or high temperature of paste, *2* accelerator of hardening (NaCl), *3* reference, *4* set retarder (low temperature)

[53]. Simultaneously, the potassium and sodium ions accelerate significantly the alite reaction with water (see Sect. 4.1.3.5) and the paste early strength increase is thus achieved [53]. Taylor [9] attributes the accelerating effect of potassium on the hydrolysis of alite to the enhanced permeability of the gel layer formed on cement grains.

4.1.3 Effect of Selected Compounds on Cement Hydration

4.1.3.1 Set Accelerators

The set and hardening accelerators have been used for a long time, their application gives several technological and economical effects. Accelerators for example allow concreting works at low temperatures, as well as they are used for some special purposes, where the rapid hardening is required, for example in sealing and repairing works.

Massazza [54] classified the accelerators for two groups: those shortening the setting process and those increasing the strength development. The similar classification was proposed by Jawed et al. [35]. This classification becomes more precise when the changes of induction period and the position of maximum heat evolution peak on the calorimetric curve are considered (Fig. 4.21). As one can see, the classification of accelerators to the two groups:

- accelerators of setting and hardening,
- accelerators of hardening,

would be more rational.

The $CaCl_2$ would be attributed to the first group, together with the higher temperature of concrete curing, (see curve 1 in Fig. 4.21); these two factors shorten the

Table 4.1 Setting time of mortars as a function of triethanoloamine admixture [55]

H_3tea, %	Setting time	
	Initial	Final
0	4.3 h	8.3 h
0.01	4.7 h	8.1 h
0.025	4.9 h	8.1 h
0.05	4.8 h	8.4 h
0.1	2 min	24 h
0.5	6 min	–

induction period and increase the area of the second peak; to the second group—NaCl enlarging the second heat evolution peak (curve 2) can be classified.

In this figure the effect of set and hardening retarders is also shown. The induction period is elongated, the second heat evolution peak is extended, with lower maximum (curve 4).

The inorganic accelerators can be classified to three groups:

- chlorides,
- sodium and potassium salts, particularly the sulphates, incidentally the carbonates,
- nitrides and nitrates.

There is a lot of organic retarders; the number of accelerators is significantly lower and there is no classification of the latter ones. Only the two organic accelerators are mentioned: triethanoloamine and sodium or calcium formate. The effect of some organic accelerators is very surprising—they shorten the initial setting but retard the final setting. The triethanoloamine is a typical example. According to Masazza [54] in this case the hydration of silicates is retarded. Triethanoloamine does not involve visible changes in the early strength development at low addition [55]. However, above some threshold content it shortens radically the initial set and retards the final setting time (Table 4.1). This threshold value depends on the type of cement and therefore some discrepancies, at the same H_3tea admixture to the different cementitious materials, can be explained. For example at the 0.1–1 % addition the set of alite cements is accelerated, while setting time of sulphate resistant ones is retarded.

The other organic accelerators are: carboxyl acids, formaldehyde, cationic polyesters, phenol resins and epoxy resins [54].

Chiesi et al. [57] from Grace company have found that some alkanoloamines, viz. tris(isopropanolo)amine and bis(ethanolo)isopropanoloamine accelerate the hardening of cement by the formation of complex compounds with iron(III) ions thus improving the hydration of brownmillerite [54]. When the alite crystals are covered with brownmillerite, as it takes place in poly–phase cement grains, this leads to the better access of water to the alite crystals beneath and the hydrolysis of alite is accelerated. Higher rate of alite reaction with water results in better strength development and higher 28 day strength.

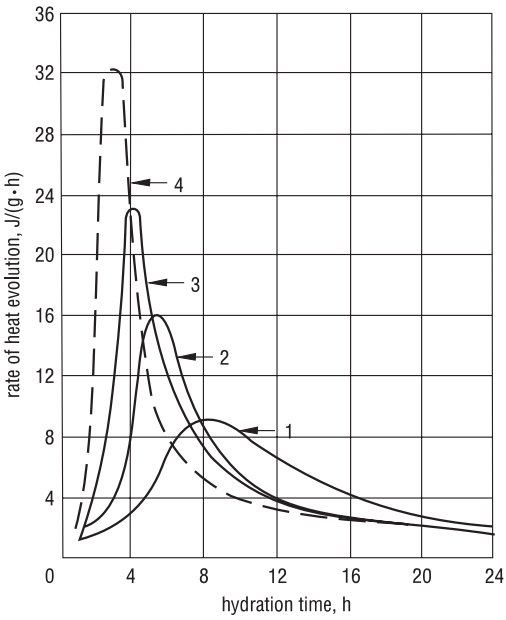


Fig. 4.22 Effect of $CaCl_2$ concentration on the hydration of cement (according to [60]): *1* no admixture, *2* 0.5% $CaCl_2$, *3* 1% $CaCl_2$, *4* 2% $CaCl_2$

The chlorides are the most commonly applied as set accelerators, among the inorganic compounds. $CaCl_2$ improves the rate of hydration and increases the heat evolution, enabling the concreting at low temperature. This admixture has been applied for a long time to accelerate the hardening and therefore the effect of calcium chloride on the properties of concrete has been thoroughly examined [58].

Tenoutasse [59] reported the acceleration of hydration of all clinker phases in the presence of calcium chloride (Fig. 4.22). In the case of silicates no other new phases were found; only at very high content (higher than 20% $CaCl_2$) the basic chloride $CaCl_2 \cdot Ca(OH)_2 \cdot 16H_2O$ is found. Kurdowski and Miśkiewicz [61] revealed the formation of basic chloride $CaCl_2 \cdot Ca(OH)_2 \cdot H_2O$ as a result of reaction of calcium chlorosilicate with water. As Ramachandran [58] reports, the stability of this basic calcium chloride corresponds to the 18% $CaCl_2$ concentration, while $CaCl_2 \cdot 3Ca(OH)_2 \cdot 13H_2O$ at $CaCl_2$ concentration exceeding 34%.

The aluminate and ferrite phases react with calcium chloride with the formation of hydrates analogous to the sulphate phases: $C_3(A, F) \cdot 3CaCl_2 \cdot 30H_2O$ and $C_3A \cdot CaCl_2 \cdot 10H_2O$. In the presence of calcium chloride the reaction of C_3A and brownmillerite with gypsum is significantly accelerated [59, 62]. As first the ettringite is formed. After the consumption of SO_4^{2-} ions the Friedel salt $C_3A \cdot CaCl_2 \cdot 10H_2O$ is produced. The transition of ettringite to AFm begins only after the consumption of $CaCl_2$. The phase composition of hydration products in the mixtures: $C_3A + CaCl_2 + CaSO_4 \cdot 2H_2O$ and $C_4AF + CaCl_2 + CaSO_4 \cdot 2H_2O$ is shown according to Tenoutasse in Figs. 4.23 and 4.24 [59, 62].

The effect of $CaCl_2$ on the constitution of C–S–H gel has been a subject of numerous studies for many years. There is a great impact of chloride, on such

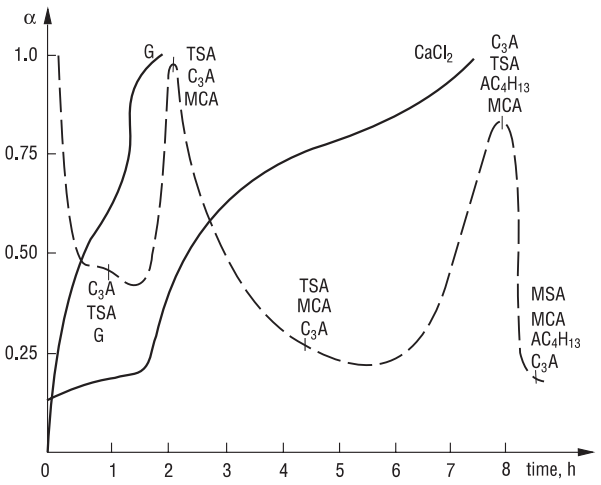


Fig. 4.23 Phase composition of hydrating mixture: $C_3A+20\%$ $CaSO_4{\cdot}2H_2O+12.5\%$ $CaCl_2$ mixtures vs. time (according to [59]). Gypsum (*G*), ettringite (*TSA*), chloroaluminate (*MCA*), monosulphate (*MSA*), w/s = 1.2; t = 25 °C

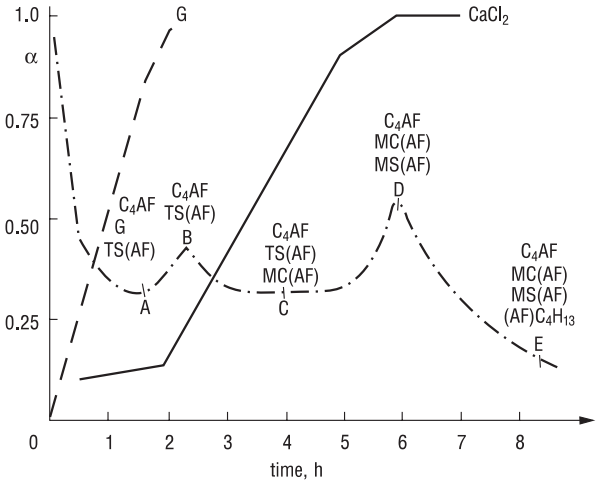


Fig. 4.24 Phase composition of hydrating mixture: $C_4AF+25\%$ $CaSO_4{\cdot}2H_2O+7.5\%$ $CaCl_2$ mixtures vs. time (according to [59]). *G* gypsum, *TS*(*AF*) iron(III) ions containing analogue of ettringite, *MC*(*AF*) iron(III) ions containing analogue of Friedel's salt, *MS*(*AF*) iron(III) ions containing analogue of monosulphate, w/s = 1.0; t = 25 °C

parameters as specific surface area, pore structure and morphology are concerned [63, 64]. The specific surface area determined by BET [with nitrogen] is much higher in the case of $CaCl_2$ addition to C_3S [65]. The surface of C_3S paste grows quickly at early age but after 12 h it reduces (Fig. 4.25). In the pastes with chloride this reduction occurs very quickly and this effect is attributed to the densification of gel as a consequence of physical or chemical changes resulting in the formation of inter–layers bonds [64]. It should, however, be underlined that the application of H_2O in the surface area measurements gives much higher results and there is no differences for the samples with and without $CaCl_2$ addition [66]. These differences of gel specific surface are explained either through the difference in the size of absorbate molecules, that is N_2 and H_2O; the latter ones can more easily enter the

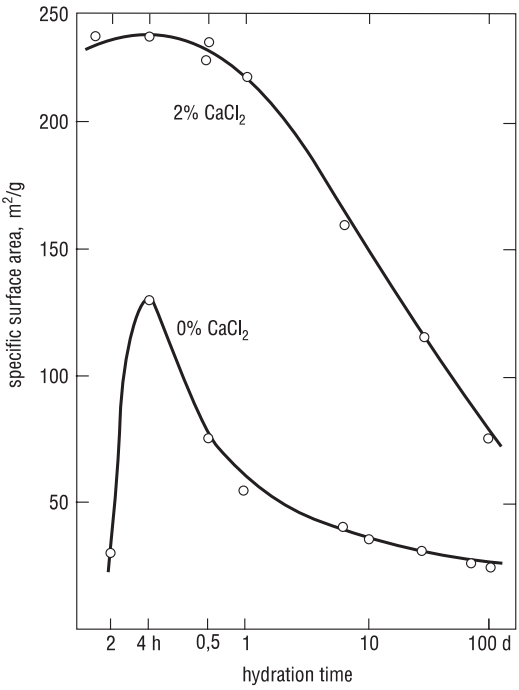


Fig. 4.25 Surface area of C_3S paste vs. hydration time (according to [65])

bottle–neck pores, or by the ability to enter the interlayer space by H_2O molecules [67]. This phenomenon is well known in the case of hydromicas [68]. Last but not least, the hydrophilic properties of C–S–H can be also taken into account. In the previous chapter an attempt to explain these differences was maintained. This was the starting point for Jenning and Tennis who proposed the C–S–H models differing with the density [69].

One cannot forget the modified morphology of C–S–H when the effect of $CaCl_2$ is discussed. The changes are visible particularly at early age of hydration; they are not significant at later period. There is generally accepted that the chlorides cause layer forms to occur while without this admixtures the fibrous C–S–H is dominating. In the opinion of Skalny and Odler [66] the latter one is composed of rolled layers.

Ramachandran [70] found that C–S–H forms flat or crumble foils in the presence of $CaCl_2$. It can be confirmed under the scanning electron microscope that C–S–H with $CaCl_2$ addition is composed of compact mass of high density and this contributes to the compressive strength increase [58]. Moreover, it is considered that at $CaCl_2$ addition the C/S ratio in C–S–H is higher, both in cement and in C_3S or C_2S paste [64, 71, 72].

The modified C–S–H morphology in the presence of $CaCl_2$ is attributed to the chemisorption of chloride on the C–S–H surface. Ramachandran [70] investigated various forms of chloride occurrence in C–S–H gel, applying the washing with alcohol. In Fig. 4.26 the summarized results of his studies are shown. At early age

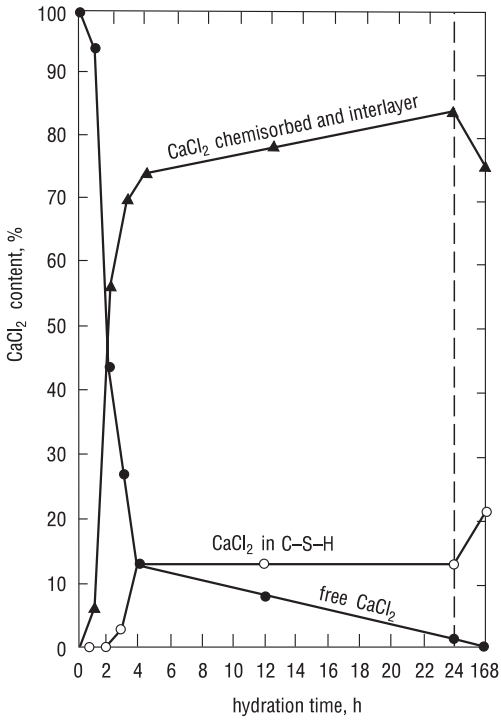


Fig. 4.26 Different forms of $CaCl_2$ occurrence in C–S–H gel (after [70])

during the induction period chloride can produce the surface complex with C_3S, apart from the free chloride. Subsequently the chemisorption on the C–S–H surface takes place; at later age chloride enters the interlayer spaces and finally the solid solution with C–S–H is formed.

The effect of $CaCl_2$ on the porosity of C_3S and cement paste was examined [63, 65, 70, 73]. A higher porosity of pastes with $CaCl_2$ was found, mainly because of the high contribution of small pores, 1–5 nm. This is the consequence of higher degree of hydration and modified C–S–H morphology. After longer period of maturing the porosity of samples with $CaCl_2$ is lower. In the case of H_2O used as an absorbate there is no substantial differences as the porosity of paste is concerned. In Fig. 4.27 the pore size distribution according to Collepardi et al. [73] is shown.

The accelerating mechanism of $CaCl_2$ on the C_3S hydration has not been thoroughly explained. There were several hypotheses under the consideration: catalytic effect, stimulation of C–S–H nucleation, increasing permeability of primary hydrate layer, change of pH value, change of CH solubility. In an interesting study, Garrault et al. [74] reveal that in the presence of calcium chloride the direction of C–S–H growth on C_3S particles is modified. In the case of this admixture the growth perpendicular to the surface of anhydrous phase is dominating. It assures the slower tricalcium silicate surface covering with hydration product and its higher reaction rate with water, in longer period. Sodium chloride, as well as potassium hydroxide increase primarily the formation of higher nuclei amount, but in this case the growth

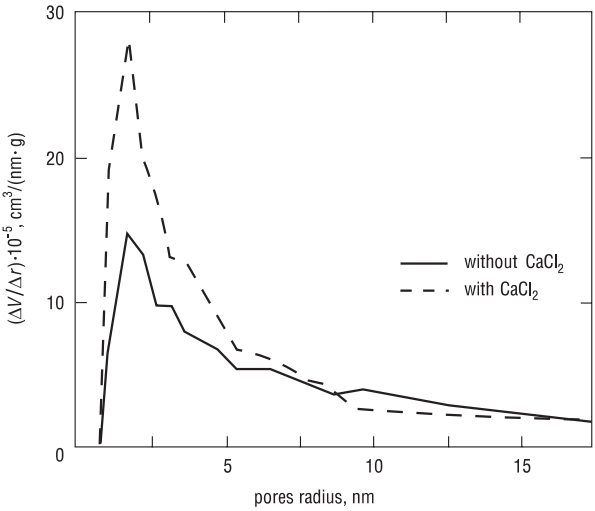


Fig. 4.27 Pore size distribution in cement paste (according to [73])

parallel to the C_3S particle surface is dominating. According to Garrault [74], the adsorption of Ca^{2+} ions on the surface of tricalcium silicate particles takes place, while the sodium and potassium ions reveal lower adsorption ability and therefore they have no impact on the orientation of C–S–H growth on these particles. Simultaneously NaCl and KOH increasing the number of nuclei cause the shortening of the induction period; the effect of the former one is more pronounced. This is not consistent with the data reported by Jawed et al. [35] shown in Fig. 4.21, because these results indicate primarily the effect of NaCl on the rate of C_3S reaction with water during the acceleration period, that is in the area of the main peak on the calorimetric curve.

Jawed et al. [35] indicate that in spite of the initial lowering of CH solubility, a high saturation of the liquid phase with Ca^{2+} ions in the presence of chloride can contribute to the early crystallization of calcium hydroxide and shortening of the induction period. $CaCl_2$ causes the reduction of $Ca(OH)_2$ solubility, as a result of common ion effect, however, this problem is complex because of the basic calcium chlorides formation. As a consequence, the $Ca(OH)_2$ solubility falls to a certain $CaCl_2$ concentration level and then begins to rise. It is shown in Fig. 4.28 according to Guo Chengju [75]. In the presence of chloride the supersaturation of solution in relation to CH is quickly reduced, due to the significantly higher crystallization rate of this phase in the presence of $CaCl_2$ [75]. The mechanism of acceleration by chloride can be therefore explained by the lowering of solution supersaturation to CH (see point 3.1). Each salt producing the supersaturation of the solution in relation to the poorly soluble calcium compounds will promote the low concentration of calcium ions in the liquid phase and higher solubility of C_3S. Na_2CO_3 can be given as an example [35]. The accelerating effect of $CaCl_2$ on the C_3S hydration is attributed to the higher diffusion rate of Cl^- ions in the layer of hydrates covering the C_3S grains, much quicker than the cations in solution and therefore causing the opposite

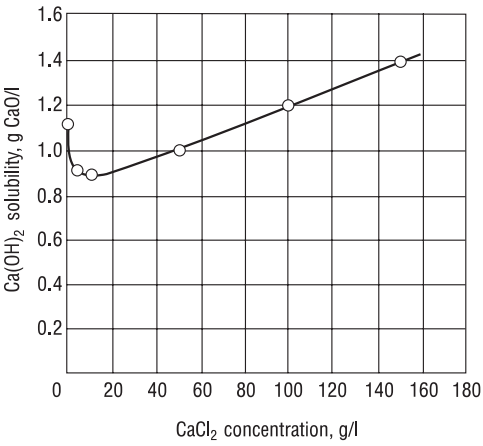


Fig. 4.28 Effect of $CaCl_2$ on the solubility of $Ca(OH)_2$ (according to [75])

diffusion of OH^- ions, to equilibrate the electric charges. The crystallization of calcium hydroxide and further dissolution of silicates is thus accelerated [76].

Kondo et al. [76] discuss the effect of different salts on the C_3S hydration in relation to the mobility of ions and conclude that the accelerating effect of added electrolyte is determined by the rate of diffusion of particular ions. The addition of added electrolyte means the simultaneous impact of both anions and cations on the double electric layer. The ions strongly accelerating the hydration reduce the double layer thickness and the electrokinetic potential; in such a way the coagulation of colloid C–S–H is facilitated. The formation of gel of higher density and smaller pores thus of lower permeability is therefore favoured.

Calcium chloride is among the strongest accelerators. The sequence of cations, as the impact on hydration acceleration is concerned, is as follows: $Ca^{2+} > Sr^{2+} > Ba^{2+} > Li^+ > Na^+ > K^+$, while the sequence of anions—$SO_4^{2-} > OH^- > Cl^- > Br^- > NO_3^-, > J^- > CH_3COO^-$ [77]. There is commonly known that the setting and hardening accelerating cause the 28 days strength decrease, while the retarders give a contrary effect (Fig. 4.29). Calcium chloride is not an exception, however, this is not specially marked after this time of maturing (Table 4.2) [57].

On the other side the addition of calcium chloride or generally the chlorides have a deleterious impact on many concrete properties. The most important is their role in the corrosion of steel reinforcement, favoured by the presence of $CaCl_2$ [78]. This is caused primarily by pH decrease [1] (see also p. 6.4.11).

The corrosion rate is favoured by higher conductivity of the chloride salts containing electrolyte, as it has been underlined by Ramachandran [79]. The corrosion process is intensified only by the well soluble chloride; therefore the compound $C_3(A, F) \cdot CaCl_2 \cdot 10H_2O$ has no detrimental effect. The C–S–H, as it has been shown in Fig. 4.26, bounds some chloride content in solid solution. It is assumed that 75 % of total amount of chloride occurs as soluble matter. On this base the limit of chlorine in cement has been indicated for 0.20 % Cl^- [79]. In the European standards this limit was determined as 0.1 % Cl^-, because some small chloride content

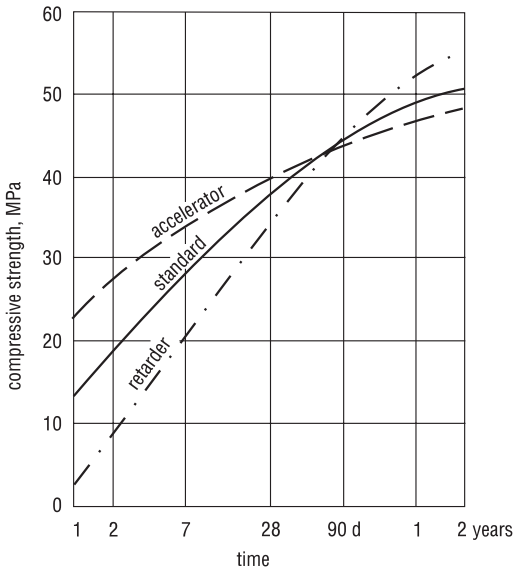


Fig. 4.29 Effect of retarders and accelerators on mortars strength (according to [41])

occurring always in aggregate and in water has been also taken into account. The harmful effect of $CaCl_2$ can be, according to Alimow [80] reduced by the CaO or NH_4NO_3 addition. The first one causes the pH increase, the second is a corrosion inhibitor, like calcium nitrate [54]. The mechanism of chloride ions interaction was discussed in the chapter dealing with corrosion of reinforcement (Sect. 6.4.11).

The increase of shrinkage of 10–50 % is another undesirable effect of $CaCl_2$ admixture [81]. Acceleration of hardening caused by $CaCl_2$ is increasing shrinkage, particularly at early age. However, comparison for the same hydration degree, can give the lower differences [79]. The addition of calcium chloride increases also creep. This effect is attributed to the change in pore size distribution related to the C–S–H morphology [83].

The calcium formate belongs also to the hardening accelerators [79]. This admixture is available as a waste in the production of pentaeritrite (polyhydroxyl alcohol). However, the effect of formate is less pronounced than the effect of chloride (Fig. 4.30).

Justnes and Nygaard [83a, 83b] studied the acceleration effect of technical calcium nitrate (CN) of composition: $x NH_4NO_3 \cdot y Ca(NO_3)_2 \cdot z H_2O$ where $x = 0.092$, $y = 0.500$, $z = 0.826$. They found that the efficiency of CN as set accelerator is strongly dependent on cement type. The optimum addition of accelerator depends also on ambient temperature and at 5 °C was 1.55 and 3.86 % for different cements. The set accelerating efficiency seems to increase with increasing belite content [83a].

4.1.3.2 Retarders of Hardening

The set and hardening retarders are commonly used in practice. At the retardation of setting process the application of ready mix concrete or injection works are easier;

Table 4.2 Effect of $CaCl_2$, $Ca(NO_3)_2$ and CaS_2O_3 on the strength of Portland cement mortars [54]

Admixture	Percentage	Compressive (R_c) and flexural (R_f) strength at age, MPa							
		1		3		7		28	
		R_f	R_c	R_f	R_c	R_f	R_c	R_f	R_c
$CaCl_2$	0	1.6	3.9	3.4	12.0	5.3	22.1	7.9	37.9
	1	2.1	7	4.0	15.0	5.5	29.1	7.6	38.1
	2	2.4	8.3	4.7	17.2	5.2	24.3	7.7	35.2
	3	2.7	8.5	4.6	17.7	5.6	26.5	7.5	36.4
$Ca(NO_3)_2$	2	0.7	1.9	3.4	11.3	4.7	19.3	7.5	31.6
	5	1.5	4.2	4.1	17.3	6.3	26.1	7.7	35.1
CaS_2O_3	1	1.7	4.5	3.5	11.7	5.2	21.0	7.4	34.1
	2	1.8	4.7	3.6	12.7	5.3	20.3	7.6	32.8
	3	1.9	5.6	3.8	13.0	5.3	23.7	7.5	36.6
	5	2.0	5.9	4.1	15.0	5.6	20.5	6.6	31.0
	6.5	2.1	6.9	3.8	14.3	5.1	20.7	6.3	26.8

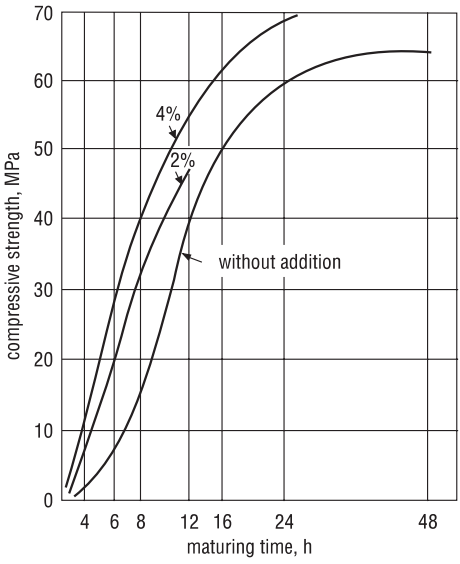


Fig. 4.30 Effect of calcium formate on the early strength of concrete (according to [54])

the uniform, homogenous concrete can be produced by deposition of subsequent layers during longer periods of time, exceeding 24 h. It is known that the joints in the interface between the layers are the weakest parts of concrete structure [84]. Massazza [54] reported the Hungarian method of the rough road pavement placing by covering upper concrete surface with emulsion containing set retarder. This layer should be subsequently removed by washing with water. The retarders are introduced when the concreting at higher temperature. The same problem appears during the cementing works in deep drilling wells. The improving of concrete workability over the wide range of temperatures is an important feature [54].

Table 4.3 The admixtures retarding setting and hardening of cement paste

Group of compounds	Compounds	Percentage by mass of cement, %	Effects
Phosphoric acids and their salts	H_3PO_4, $Na_2HPO_4 \cdot 2H_2O$, Na_3PO_4, $Na_4P_2O_7 \cdot 10H_2O$	0.1–0.6 P_2O_5	Retardation of initial and final set; reduction of initial strength, unchanged 28 days strength; pyrophosphates—the strongest retarders
Heptaoxy–tetraborates	$Na_2B_4O_7 \cdot 10H_2O$	0.1–0.6 B_2O_3	Similar as for pyrophosphates
Fluorides	NaF, KF	0.1–0.5	As above
Metal oxides	PbO, ZnO	0.4–0.5	Strong retardation of setting; reduction of initial strength, unchanged 28 days strength
Lignosul–phonates	calcium, sodium, ammonium	0.1–0.6	Retardation of initial and final set; aerating and plastifying properties reduction of initial strength and 28 days strength; main component of traditional plasticizers used in concrete
Saccharides	glucose, sucrose, saccharase, starch, cellulose	0.0005–0.002	Strong retardation of setting at very low dosage; reduction of initial strength, unchanged 28 days strength; very rapid setting at about 0.2%,
Hydroxycar–boxyl acids and their salts	gluconic acid, sodium, potassium, calcium citric acid, gluconates	0.0005–0.002	As for saccharides
Phosphogypsum (by–product from the phosphoric acid production)		1–3, at P_2O_5 content in phospho–gypsum to 1.5%	Retardation of initial setting time at unchanged setting time; initial and 28 days strength unchanged

There are many organic and inorganic retarding admixtures. The most commonly used inorganic ones are some acids and their salts: boric, phosphate, hydrofluoric, chromic and arsenic; furthermore the zinc and lead oxides, hydroxides and salts [85]. The following sodium salts of the aforementioned acids are among the strong retarders: Na_3PO_4, $Na_2B_4O_7$, Na_3AsO_4, NaF, as well as the calcium salts: e.g. $Ca(H_2PO_4)_2 \cdot H_2O$. The retarders are listed in Table 4.3. The microcalorimetric measurements are the best way to determine their effect—the elongation of induction period on the heat evolution curves is then observed (Fig. 4.31). Their action is particularly intensive when they are introduced in dissolved form to the mixing water. In such a way an early period in which the cement grains react with water with no admixtures is eliminated (the dissolution starts at the same time). However, the exceptions are sometimes observed. For example calcium lignosulphonate gives

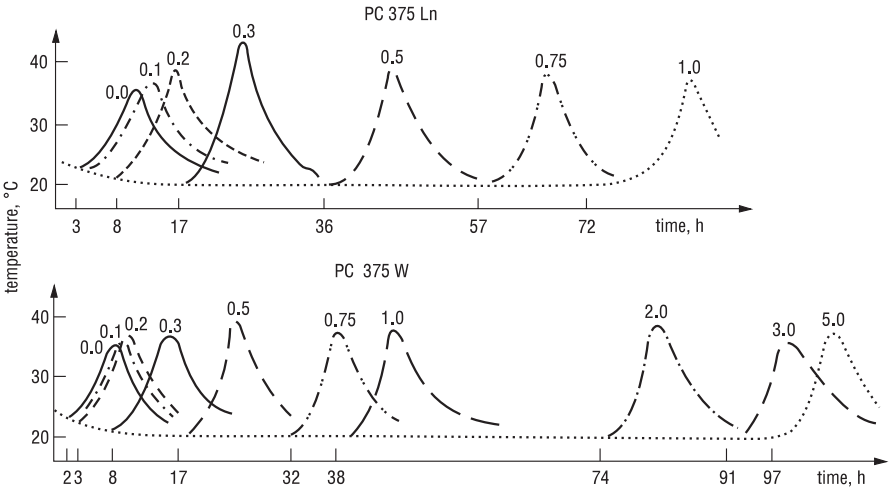


Fig. 4.31 Set retardation of two Portland cements by PbO, w/c = 0.35 (according to [85]) (PbO contents in % by mass. given, on the plots)

higher set retardation when cement is initially for some minutes mixed with water without admixture [86].

According to Bruere [85] this behaviour can be explained by the adsorption of lignosulphonate on the C_3A surface, while when the reaction of this phase with gypsum occurs, lignosulphonate is adsorbed on the C_3S surface and C_3S hydration is hampered. This hypothesis was confirmed by Young [87] who found that the retarding action of lignosulphonate on C_3S hydration can be eliminated by C_3A addition.

This is the rule that retarding effect is proportional to the percentage of admixture, as well as the retardation is significantly stronger at low temperature (Fig. 4.32) [84]. Some organic admixtures loose their properties at higher temperatures. Among them the dicarboxyl acids, amines and aliphatic acids exhibit no retarding action above 60 °C [88].

Finally, the effect of retarders depends on the type of cement. Because they interact with the particular phases, their addition can be reduced either with the hydraulic or pozzolanic components content. The other factors affecting the effectiveness of retarders are: w/c ratio and cement fineness (Fig. 4.33).

The setting retardation is always related to the hydration rate decrease at early age and at same time, the heat evolution is reduced (4.34) [41, 50]. The analogous trends are observed concerning the surface area of hydration product and the non–evaporable water content in the paste which are decreasing [89].

Lieber [85] studied the effect of PbO and ZnO on cement hydration. PbO affects only the C_3S hydration rate: there is no $Ca(OH)_2$ for many hours or even days, depending on its addition. However, after the delay on the beginning, a quite intensive reaction is then continued. The reaction of C_3A with gypsum is retarded but after 24 h there is no soluble calcium sulphate. On the other side, PbO does not affect the

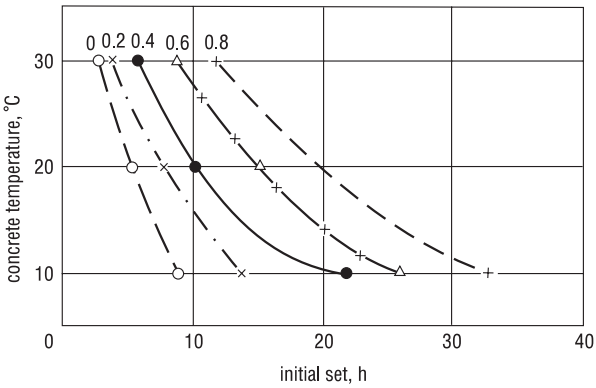


Fig. 4.32 Initial set of concrete mixture as a function of temperature and setting retarder addition (according to [84]) (admixture contents in % by mass given on the plots)

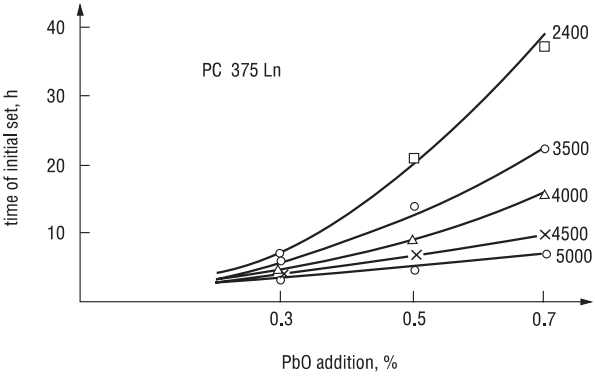


Fig. 4.33 The retarding effect of increasing PbO content on the initial setting time of cements of varying specific surface (indicated on the plots in cm^2/g) (according to [85])

rapid gypsum reactions with cement constituents. The effect of PbO on the strength of cement composites is of "classic" character: the early strength is reduced while just after 3 days it increases, even at PbO content equal 0.4% [85] (see Fig. 4.29). The intensity of delaying influence decreases with increase of cement specific surface (Fig. 4.33). This strong PbO effect on cement hydration has not been explained until now. Undoubtedly, the impermeable coating formation on C_3S surface takes place; however, the factors promoting further hydration remain unknown. The renewed process coincides with the visible reduction of PbO peaks intensity on the XRD pattern. Simultaneously there are no peaks attributed to any lead containing compounds.

Recently Nocuń and Łój [90, 91] studied the effect of PbO and their results comply generally with those of Lieber; they found that in the presence of PbO addition in the alite paste the reaction with water is significantly accelerated. On the other side, in the presence of gypsum a serious delay of the process is found. Therefore the effect of sulphate ions as a hydration rate controlling agent, when lead is added to the cement paste, was proved. PbO has also a great retarding impact on the setting of gypsum [92]. It seems that this effect is the consequence of the formation of amorphous lead sulphate having very low solubility in water.

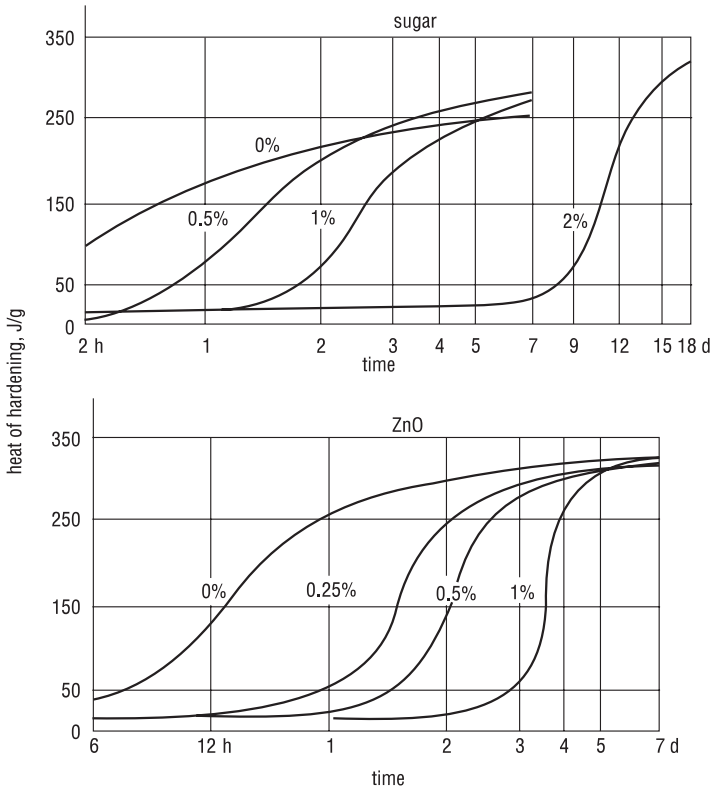


Fig. 4.34 Reduction of heat evolved on hardening as a function of set retarder addition (according to [41])

The similar strong retardation, however, dependent on the type of cement, is observed in case of ZnO [85]. It is particularly well visible for the cements of low specific surface—analogously as for PbO—but with low C_3A content. In spite of the serious retardation of setting, the strength of mortar after 7 days is the same as the strength of reference mortar; after 28 days it is much higher. In case of ZnO the mechanism of delaying action is better recognized. In this case it relates only to C_3S as well [85]. On the other side, neither the reaction of C_3A, nor the reaction of ferrite phase is affected by ZnO (Fig. 4.35). $Zn(OH)_2$ is known because its amphoteric character. In the solution of calcium hydroxide the poorly soluble basic calcium zincate is formed:

$$2ZnO + Ca(OH)_2 + 4H_2O \rightarrow Ca[Zn(OH)_3 H_2O]_2 \tag{4.7}$$

The formation of zincate takes place throughout all the induction period and the beginning of C_3S hydration coincides with the disappearance of this phase [85]. The addition of zincate retards the C_3S hydration only slightly and the intensity of zincate peak on the XRD pattern rapidly decreases as it has been reported by Lieber

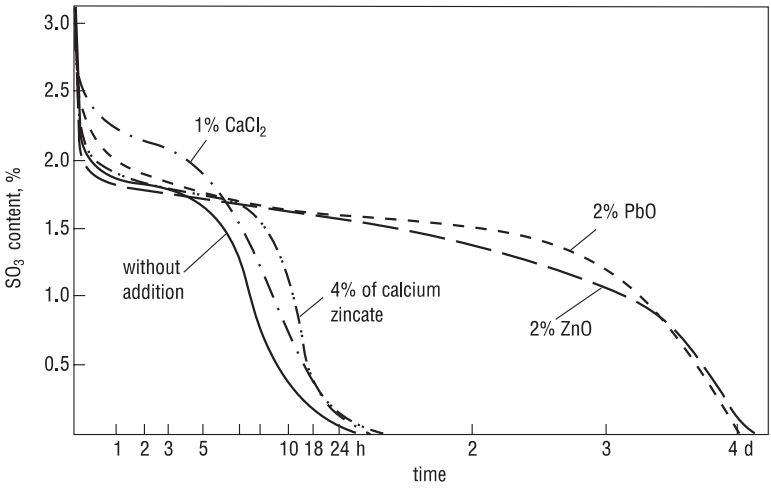


Fig. 4.35 Reaction of gypsum with clinker phases at PbO and ZnO addition (according to [85])

[85]. According to Lieber [85], the zincate decomposes and zinc enters the C–S–H structure. Simultaneously the C/S ratio in C–S–H increases and the long fibres are formed.

According to Jawed et al. [35] the elongation of induction period is the function of calcium ions concentration growth until the required supersaturation in relation to $Ca(OH)_2$ is reached. The zinc hydroxide reaction with calcium hydroxide leads to the formation of complex hydroxyanion; the latter is further precipitated as a calcium salt poorly soluble. As a consequence the concentrations of OH^- and Ca^{2+} ions decrease and the hydration is retarded.

Wenda and Kuzel [93] continued the earlier studies of Lieber [94] on the delaying effect of boric acid. The presence of boric acid results in the deceleration of C_3A reaction with gypsum and ettringite formation. Wenda and Kuzel [93] found the three new phases formed in reaction of boric acid with aluminates. At low oxyborate ion concentration the monoclinic $C_4A \cdot ½B_2O_3 \cdot 12H_2O$, crystallizes as pseudohexagonal plates with excellent cleavage along the plane (0001) [93]. This phase has a layer structure very similar to $C_3A \cdot CaSO_4 \cdot 12H_2O$. Its structural formula can be written as follows:

$$\{Ca_4[Al(OH)_6]_2\} \cdot (HBO_3 \cdot 5.5H_2O)$$

At temperature 20 °C the solid solution with $C_4A \cdot ½CO_3 \cdot 12H_2O$ is formed. Fe^{3+} can substitute totally for Al^{3+} in borate phase: $C_4F \cdot ½B_2O_3 \cdot 12H_2O$. When the concentration of H_3BO_3 is higher [$H_3BO_3/Ca > 0.25$], the $6CaO \cdot Al_2O_3 \cdot 2B_2O_3 \cdot 39H_2O$ is formed and crystallizes as hexagonal prisms. This phase has a XRD pattern similar to that of ettringite. There is second hexagonal phase: $6CaO \cdot Al_2O_3 \cdot B_2O_3 \cdot 42H_2O$.

The formation of borate phases as a result of the reaction between CAH_{10} and C_2AH_8 with H_3BO_3 hampers the transition into the cubic C_3AH_6.

Cussino et al. [95] found a strong delaying effect of V_2O_5 on cement hydration. The hydration of C_3S is retarded as well as the transformation of ettringite into AFm. This is attributed to the formation of amorphous calcium vanadate surrounding the cement grains. The effect increases with percentage of additive. The 28 days strength is not reduced; moreover, at storage in water, it is higher than that of reference.

The mechanism of retardation by soluble phosphates is explained by the precipitation of insoluble tricalcium phosphate layer on the surface of cement grains, impermeable for water [96]. For example the calcium dihydrophosphate $Ca(H_2PO_4)_2 \cdot H_2O$ reacts with $Ca(OH)_2$ in the strongly supersaturated layer surrounding the alite grains and the $Ca_3(PO_4)_2$ is produced.

Similarly influence the soluble fluorides: for example the F^- ions released from NaF to the solution form the insoluble CaF_2 which covers the cement grains. The complex fluorosilicates Na_2SiF_6 and Na_3AlF_6 can additionally result in the precipitation of silicate or aluminate gel on the surface of cement grain poor in calcium. Phosphogypsum, soluble calcium phosphates and sodium fluoroaluminates containing by–products exhibits the retarding effect too [96].

There are many organic retarder of setting (see Table 4.3). Among them the lignosulphonates[1], hydroxyl–carboxylic and carboxylic acids and their salts, amines, amino acids, carbohydrates of general formula $C_n(H_2O)_m$ and the products of their oxidation; that is acids and their salts can be mentioned.

The saccharides and their compounds are also very popular; for example glucose $C_6H_{12}O_6$, saccharose $C_{12}H_{22}O_{11}$, starch $(C_6H_{10}O_5)_n$, cellulose with CH_2OH groups should be mentioned.

Triethanoloamine is generally used to reduce the effect of plasticizers, which retard setting. This compound itself slightly retards the C_3S hydration but the formation of ettringite is accelerated [25]. Triethanoloamine has even lower impact on the C_3S hydration in the $C_3A + C\bar{S}H_2$ mixture and is limited to the first 6 h [26]. In the presence of H_3tea not only the ettringite formation is accelerated but also the conversion to AFm. After finishing of this process the effect of H_3tea becomes practically invisible. The earlier suggestions that H_3tea from the solution is adsorbed by ettringite in such a way that during the first 6 h about 50% initial content is adsorbed (starting from the concentration on the level 0.1%) were verified experimentally. The effect of H_3tea is the function of the phase composition of cement [26].

The organic set retarders have an impact on the strength development similarly as the inorganic ones. In the case of organic compounds the concrete strength increase at later age can be even higher because these admixtures exhibit superplasticizing effect and the w/c ratio can be reduced [97]. The strength development is the function of admixture addition and at higher percentage the strengths achieve the value of reference material at later age of maturing (Fig. 4.36) [94].

[1] It is an opinion that lignosulphonates are rather weak retarders, the strong delaying effect of industrial materials is rather caused by sugar impurities.

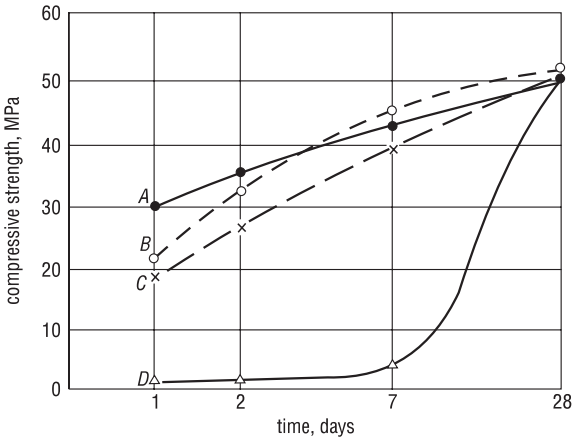


Fig. 4.36 Effect of H_3tea on the strength of mortar produced from Portland cement PZ450F(DIN) (according to [94]): *A* reference, *B* 0.2% H_3tea, *C* 0.5% H_3tea, *D* 1.0% H_3tea

The negative phenomena can be observed in the case of the set retarders application as it has been mentioned by Masazza [54]. The so–called reverse effect consists in the rapid setting and stiffening of the paste, as well as the unsoundness. The origin of these phenomena was not explained; one can conclude that before application of every new retarder it must be thoroughly examined in laboratory [98].

The mechanism of retarding effect has not been explained. There are many hypotheses which highlight this phenomenon only partially. The problem is more complicated and particular retarders differ as the delaying mechanism is concerned. Some of them affect the hydration in many ways. For example in the presence of triethanoloamine the reaction of gypsum with C_3A is accelerated but the hydration of C_3S and calcium hydroxide formation is hampered [94].

The following mechanisms of retardation are generally mentioned:

- the adsorption of large organic molecules on the surface of cement grains (Fig. 4.37)
- formation of chelate complexes,
- precipitation of the layer of poorly soluble calcium compounds (calcium fluoride, calcium propionate) on the surface of cement grains,
- lowering of pH causing the formation of silica gel coating.

The adsorption hypothesis was developed in the works of Previte [99]. According to this author the retarding effect of saccharides depends on the molecule size and its structure. The retarding effect of glucose was explained by an adsorption mechanism in the work of Singh [100]. This effect increases with the concentration of admixture. The retardation relates to the C_3S hydration and consists in the change of potential on the surface of grains, because the molecules of glucose are electrically neutral. On the other side the formation of ettringite is not hindered, as the reaction of C_3A with gypsum can be even accelerated.

Thomas and Birchall [101, 102] studied the concentration of ions OH^-, calcium, silica, aluminum and iron in the solution (w/c = 2) of cement slurries with additions

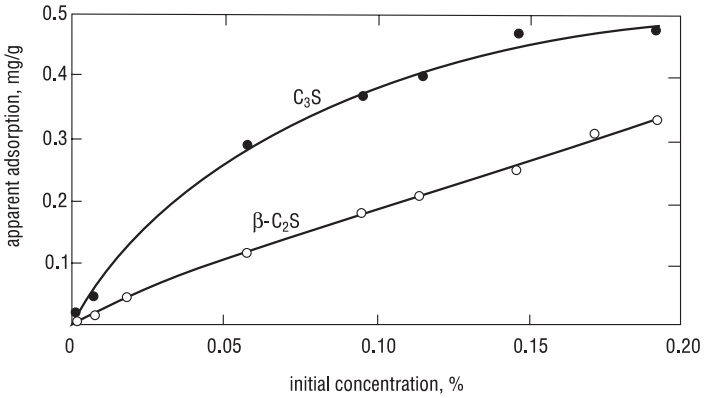


Fig. 4.37 Apparent adsorption of salicylic acid on the C_3S and β–C_2S surface (according to [98])

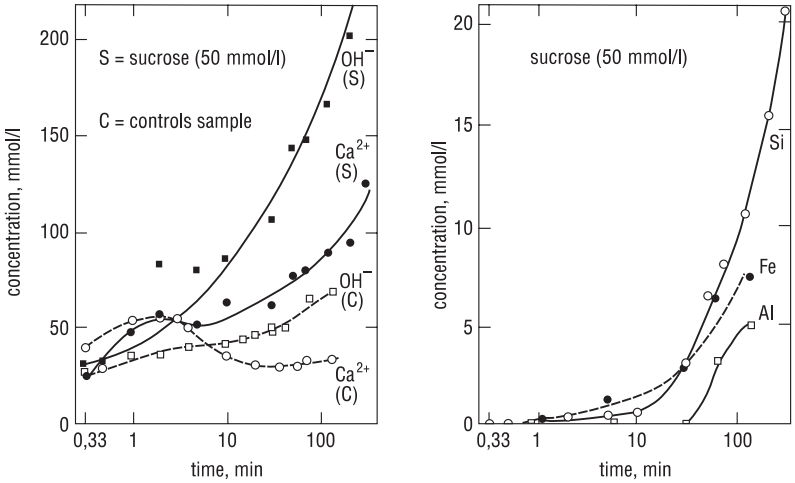


Fig. 4.38 Concentrations of some ions in solution during the Portland cement hydration with sucrose (according to [101])

of sucrose and other sugars and found that the concentration of the three last ions increases significantly at only low changes of Ca^{2+} and OH^- (Fig. 4.38). The C/S ratio which normally is equal 1000 decreased to 2. These effects are explained by adsorption of sucrose molecules on the hydration products; in such a way a high C/S ratio is maintained without precipitation of hydrates, it means without decline from equilibrium conditions. These experiments support strongly the adsorption hypothesis.

According to Milstone [103] the acids being the derivatives of glucose are ten times more intense retarders than the glucose. This was observed earlier by Young

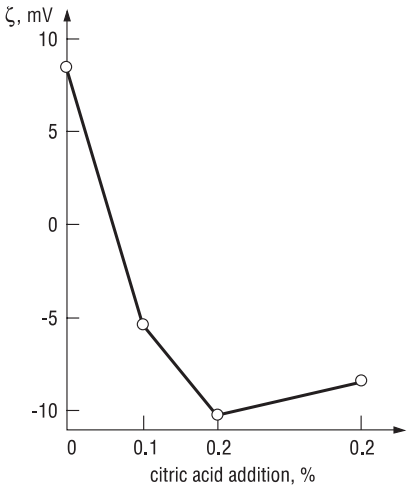


Fig. 4.39 Effect of citric acid addition on the ζ potential of cement particles in the paste (according to [25])

[104] who found the more intensive effect of the products of saccharides degradation to the saccharic acids in the high basic liquid phase, in the paste.

Hypothesis dealing with the formation of chelate complexes, adopted to explain the role of saccharic, urine, aldone acids and their salts, was presented by Mariampolski et al. [105].

However, the hypotheses linking the retarding effect with the adsorption of retarders on the surfaces of clinker phases are the most frequent. This mechanism relates to the carboxyl acids and their salts containing COOH groups. Among others the lignosulphonate and wine acids are classified to this group. It is commonly accepted that the COOH groups are adsorbed on the cement grains. There are some doubts as this hypothesis is concerned. As it has been pointed out by Masazza [28] the amount of substance adsorbed on cement grains is very low while the hydration products, first of all the colloidal C–S–H, can adsorb a huge amount of organic molecules [97].

Singh et al. [25], basing upon the high decrease of ζ potential of cement particles with the increase of citric acid concentration (Fig. 4.39), conclude that the citric anions with negative charge are adsorbed on cement grains in the Stern layer. This layer of big citric ions hinders the access of water to the cement particles. Simultaneously, it has been found that addition of citric acid after ten minutes from cement mixing with water does not affect the initial setting time. It is the proof for the authors that the adsorption of retarder must take place on the anhydrous cement grains [25]. This adsorption on the anhydrous clinker phases seems in some cases to accelerate the hydration process while the reaction of retarder with the hydration products retards the reaction with water [87]. The correlation between the solubility of calcium salts of carboxylic acids and the intensity of their delaying effect has not been found. However, it cannot be excluded that their action is analogous as for zinc, by the formation of insoluble layer on the C_3S surfaces. The formation of this insoluble and nearly impermeable layer is the second, most spread out hypothesis.

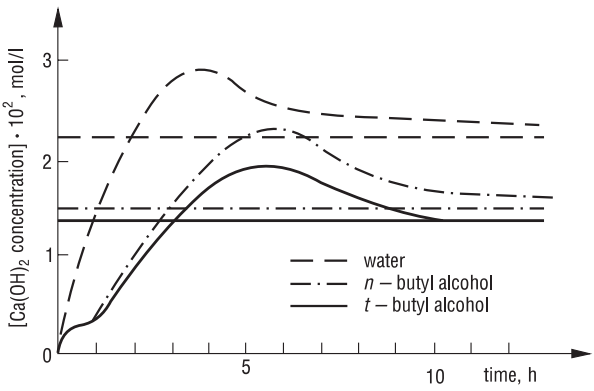
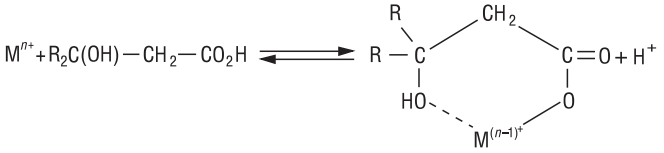


Fig. 4.40 Effect of the *n*- and *t*-butyl alcohol addition to mixing water (1 mol/l) on the CH concentration in the liquid phase vs. time (liquid/$C_3S = 10$) (according to [106])

The third hypothesis assumes the hindered nucleation or crystal growth of hydrates. The hindered $Ca(OH)_2$ nucleation resulted from the favored adsorption on the (001) wall of crystals, by the chelate complex formation was found [35]. The experiments exhibiting that chelate compounds producing acids, such as maleic, glycerin and wine have a strong delaying effect, prove this hypothesis. The fumar, propionate and amber acids do not reveal this effect. The latter ones have no β–hydroxyl groups, producing a stable, six–element chelate ring with metal ions:



(4.8)

The size and number of chelate rings affects the intensity of retarding action; the effects of electrons are important for these complexes formation.

The mechanism of the organic compound interaction on C_3S hydration was discussed by Stadelman and Wieker [106]. Introducing different aliphatic alcohols and ketones to the mixing water 1 mol/l they found the elongation of induction period, as well as reduction of second peak and shifting its maximum to longer time on the heat evolution calorimetric curve. Also the CH concentration in the liquid phase grows slowly and the lower supersaturation is achieved (Fig. 4.40). The authors suggest that the primary hydrate layer on the C_3S surface is stabilized and the reduction of calcium hydroxide solubility is caused by the lower electrical permittivity of the organic compounds containing solutions in comparison with water.

Another effect is observed in the case of propionate acids and their sodium salts. At low concentration the hydration is accelerated but at high–retarded. The complexes with Ca^{2+} ions are formed thus increasing the calcium ions concentration in the solution. This accelerates the decomposition of primary hydrate. At higher concentration the organic anions are adsorbed on the surface of C_3S and the calcium propionate is formed. By hampering the hydration process, α–hydroxy acids (for example lactic acid) and their salts have a very strong delaying effect. This is the

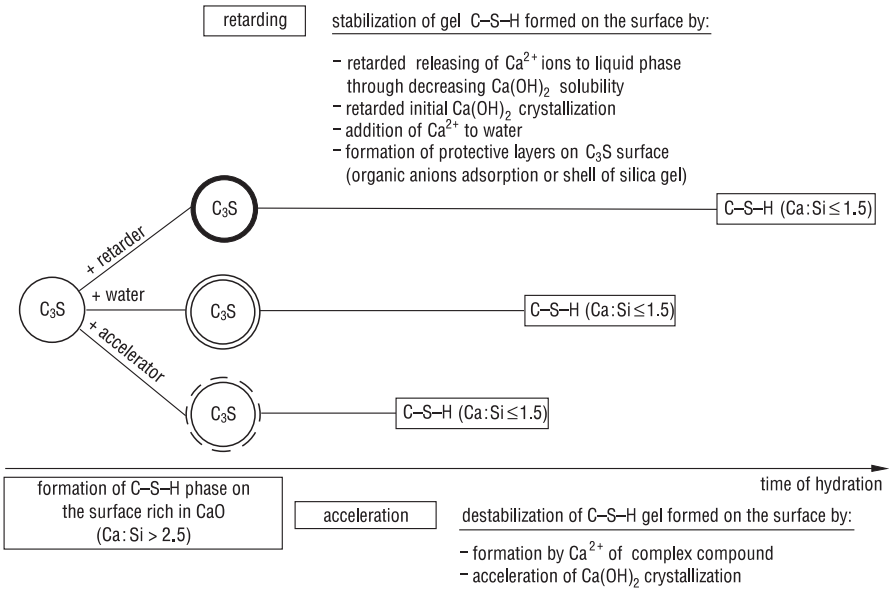


Fig. 4.41 Mechanism of the action of admixtures on C_3S hydration (according to [106])

consequence of the lactic anions ability to form the chelate complexes with Ca^{2+} ions on the C_3S surface, leading to the hampering of hydration.

In the case of cation exchange resin (for example Na containing) there is no possibility of complex anions adsorption on the surface of C_3S because the chemical bonds with the resin are formed. Therefore the resins play only the role of accelerators because they promote the release of calcium ions, from C_3S hydrolysis, to the solution. Opposite to the Na containing resins the hydrogen types retard the C_3S hydration. This is presumably caused by the acidification of the solution as a result of $Ca^{2+} \rightarrow$ proton exchange, favouring the formation of silica gel, covering the C_3S grains. This cover has a retarding impact which is also confirmed by other acids addition to C_3S. Summarizing, according to Stadelman and Wieker [106], the interaction of admixture and primary hydrate has a decisive role: stabilization means the delay of hydration, transformation leads to the acceleration. The formation of chelate complexes and pH changes are also of importance [106]. It is shown in Fig. 4.41.

The effect of retarders on the growth and morphology of crystals was proved. The following examples can be given: a change of ettringite morphology in cement pastes with retarders [94], a change of $Ca(OH)_2$ crystal size and habitus in the C_3S paste with admixtures [107].

It was shown that the effectiveness of organic retarders depends on the number of functional groups in the molecule [108–110]. It relates to the hydroxyl, carboxyl and carbonyl groups, as well as to their position in molecule [110]. The typical examples are: pyrocatechol (1.2–dihydroxybenzene)—set accelerator, rezorcine (1.3–

dihydroxybenzene) with no effect on the hydration process, hydrochinone (1.4–dihydroxybenzene)—retarding agent [88]. In organic compounds the ionic radius and ionic potential of cation has an impact, like in the case of chlorides [103].

4.1.3.3 Effect of Calcium Carbonate

The limestone addition is more and more widely used in cement production, particularly in France [111] and recently in Poland. That is why the effect of this component on cement hydration and the properties of cement paste became the subject of research [112–116]. Previously limestone was considered as an inert filler in the paste, however, the reaction between calcium carbonate and aluminates with the formation of calcium carboaluminate hydrates has been proved [117]. The rate of $CaCO_3$ dissolution is low and therefore the reaction products occur only in the narrow interface area. The $C_3A \cdot ½CO_3 \cdot 12H_2O$ phase is firstly formed and next transforms slowly into the $C_3A \cdot CO_3 \cdot 11H_2O$. The calcium carboaluminate hydrates in the transition zone change the surface of aggregate; it becomes rougher and the bond paste–aggregate is strengthened. In the presence of $CaCO_3$ the C_3S hydration is accelerated; the induction period shortens and the heat evolved in the area of the second peak is increasing (Fig. 4.42) [118]. The mechanism of this $CaCO_3$ action is not explained; perhaps the calcite crystals play a role of heterogeneous nuclei and facilitate the $Ca(OH)_2$ crystallization. It has been proven recently by Nonat et al. [120] (see p. 3.2.3). On the other side there are the hypotheses that the CO_3^{2-} ions can enter the interlayer space in C–S–H.

Ramachandran and Zhang Chun–Mei [118] have confirmed the acceleration of C_3S hydration in the presence of $CaCO_3$ of high fineness, as well as the shortening of induction period and the heat evolved increase in the area of the second peak on the microcalorimetric curve. The formation of C–S–H on the surface of $CaCO_3$ grains with the quicker supersaturation of the liquid phase with Ca^{2+} ions in relation to CH was proved. The morphology of C–S–H changes only slightly. The small $CaCO_3$ crystals play a role of C–S–H nuclei; therefore this phase can be precipitated outside the outer product formed on C_3S surface [118].

According to Vernet [120] in the mixture $C_3A + C\bar{S}H_2 + C\bar{C}$ the ettringite is formed as a first product; subsequently, instead of calcium monoaluminate commonly observed, the carboaluminate and its solid solution with C_4AH_{13} appears when gypsum is consumed. Because of the growth of the second peak on the calorimetric curve, accompanying the gypsum addition, Vernet is stating that these solid solutions contain sulphates [120]. This solid solution is an intermediate product and at the excess of calcite is reacting with it giving the carboaluminates and secondary ettringite [120]. The carboaluminates crystallize mainly on the surface of cement grains (C_3A) where the highest saturation of the liquid phase with $Al(OH)_4^-$ ions occurs. Some practical conclusions can be drawn from these experiments; at low gypsum content limestone plays a role of set controlling agent—this is cement with low hydration heat. The optimum gypsum content, in the case of cement with limestone addition, is a little lower than for cement without addition [120]. It has been

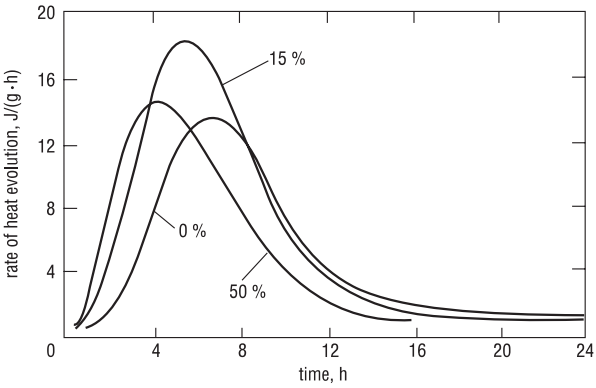


Fig. 4.42 Rate of heat evolution during the C_3S hydration with different $CaCO_3$ addition (according to [118])

proved by Negro et al. [121] who found that at the partial replacement of gypsum by limestone the viscosity of paste is reduced and the strength increase is observed. However, the higher than 50 % gypsum replacement gives the increase of viscosity and the strength decrease. Also in this case the paste shrinkage is higher. All these experiments seem to point out that there is the optimum gypsum to limestone ratio. This problem was discussed earlier by Bensted [122]. However, the carboaluminates in the contact with the sulphate and chloride solutions of high concentration are decomposed. This must be taken in mind applying cement with limestone addition. The following solid solutions of AFt series: $Ca_6Al_2 \cdot (SO_4)_x \cdot (CO_3)_{3-x} \cdot 26H_2O$, where $0 < x < 1.5$ will be formed [123]. The stability of this phase depends on the temperature, as it is shown in Fig. 4.43 that the content of CO_3^{2-} ions is decreasing with temperature.

However, in the presence of limestone the volume of hydrates—mainly AFt—is growing with decrease of temperature, which causes that the empty space in the paste, thus pores, are filled (Fig. 4.44). This has a positive effect on the concrete resistance to aggressive solutions. Consequently, the authors suggest that the increased temperature would have a deleterious impact on the concretes initially cured at lower temperatures, +5–+10 °C [123]. After the ratio CO_3/Al_2O_3 increase, reaching the value of 0.28, the carboaluminate $C_3A \cdot ½\ CaCO_3 \cdot 12H_2O$ content will decrease with simultaneous formation of monocarboaluminate $C_3A \cdot CaCO_3 \cdot 11H_2O$. The maximum of the first calcium carboaluminate content will be correlated with the minimum of the paste porosity.

The blended cements containing apart of limestone also granulated blast furnace slag reveal good properties [125]. The concrete of this cement show low carbonation rate and higher resistance to freezing and thawing, also in the presence of 3 % NaCl solution [125].

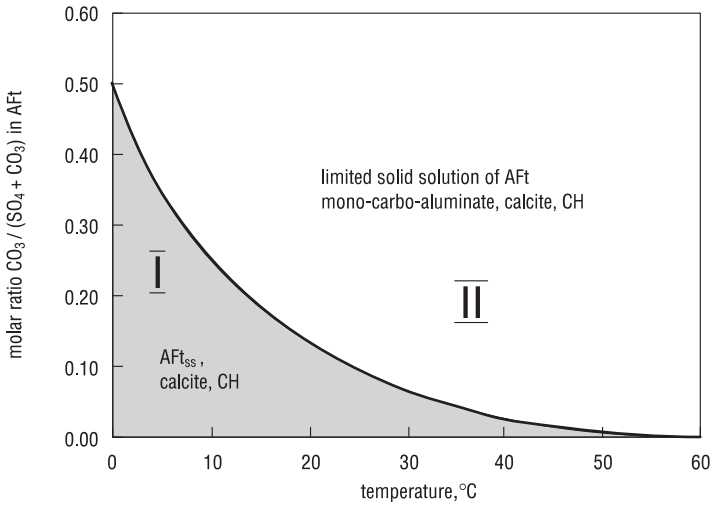


Fig. 4.43 The CO_3^{2-} ions content in AFt vs. temperature, calculated basing on the thermodynamic data; AFt is in equilibrium with the excess of calcite, calcium monocarboaluminate, portlandite and liquid phase (not shown in figure) (according to [123])

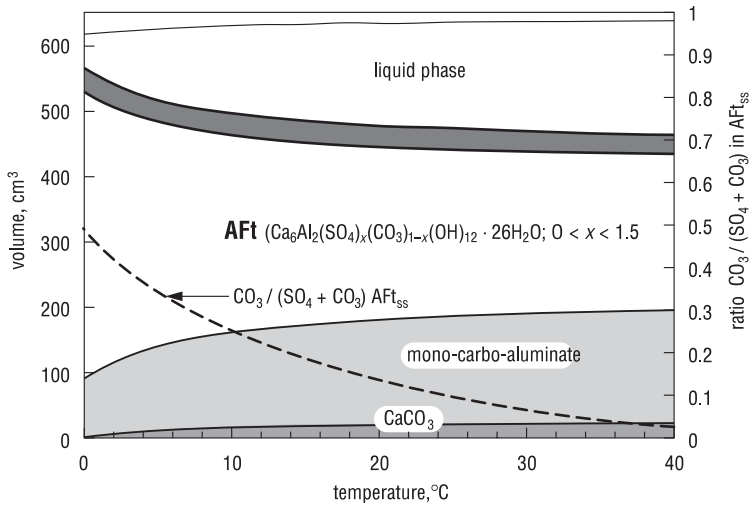


Fig. 4.44 Effect of temperature on the specific volumes of hydrates in the model mixture composed of C_3A, portlandite, $CaSO_4$ and $CaCO_3$ (according to [123]); at constant ratio $SO_3/Al_2O_3 = 1$ and $CO_3/Al_2O_3 = 1.25$ and constant content of solid phases $C_3A + CaSO_4 + CH + CC = 3.25$ moles, reacting with 500 g of water

4.1.3.4 Effect of Potassium and Sodium Sulphates

Potassium and sodium sulphates are the strong accelerators of hardening, but they do not affect specially the induction period and consequently the setting time [60].

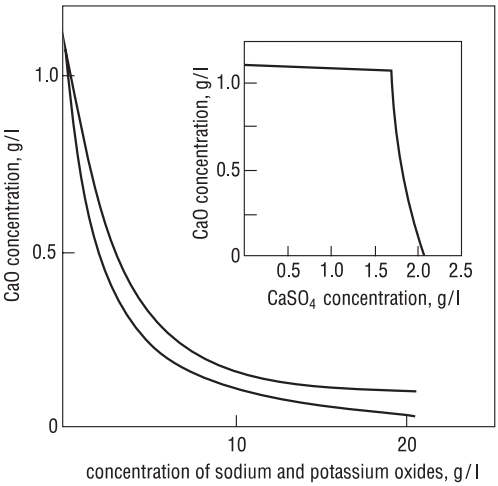


Fig. 4.45 Effect of potassium and sodium sulphates on the solubility of calcium hydroxide. The upper part shows the effect of calcium sulphate which is negligible

The mechanism of their action has not been explained. There are many hypotheses, but primarily those attributing this effect to the liquid phase composition changes should be mentioned [27, 35]. In the presence of alkalis the calcium ions concentration is reduced (Fig. 4.45) and simultaneously the OH^- ions concentration is increased. The increasing ions OH^- concentration is accompanied probably with the higher rate of sulphates bonding by the ettringite formation [126]. This hypothesis is confirmed by the significant effect of NaOH addition on hydration acceleration, similarly of KOH, but somewhat weaker [45].

The effect of K_2SO_4 on the C_3S and β–C_2S hydration was studied, among other, by Shebl and Ludwig [127]. They observed a significant accelerating effect and proved the syngenite formation as a result of secondary gypsum reaction with potassium sulphate. This was the further consequence of K_2SO_4 reaction with $Ca(OH)_2$. Simultaneously, the content of amorphous calcium hydroxide was highly increased. The crystallization of significant part of it occurred in the C_3S paste after 28–90 days and in the β–C_2S after 40–120 days [128]. The effectiveness of K_2SO_4 influence on the C_3S hydration reveals a maximum, attributed to its addition and for higher content is diminishing. In the case of β–C_2S this effect, for 1.39 and 2.78 % of K_2SO_4 was the same [128]. The accelerating effect of both K_2SO_4 and Na_2SO_4 on C_3S and β–C_2S hydration is similar [128, 129]. At the presence of alkalis the specific surface area of hydrated C_3S is lower throughout all the period of maturing; morphology and microstructure of C–S–H is modified [45]. The C–S–H particles are bigger, better crystallized; in the presence of Na_2SO_4 the needle–like forms are observed. Presumably the SO_4^{2-} ions are incorporated in the structure. In the presence of alkalis the microstructure of C–S–H is variable to which the lower strength of cement paste at later ages is attributed [45]. These results are the base of another hypothesis linking the effect of alkalis on cement hydration with the rate of C–S–H and hexagonal calcium aluminate hydrates growth and morphology [45]. Finally the hypothesis of syngenite formation was also developed [127, 130, 131].

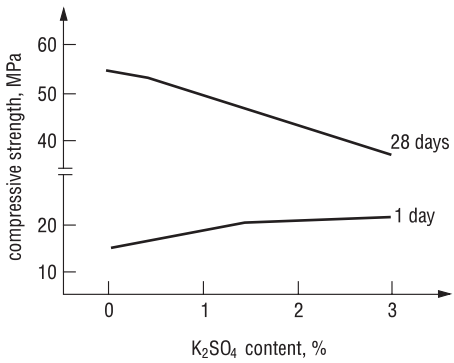


Fig. 4.46 Compressive strength of mortar vs. K_2SO_4 addition to cement

Sprung and Rechenberg [132] state that in the pastes of cements rich in alkalis C_3A dissolves quickly because of the reduced $Ca(OH)_2$ solubility. At low gypsum content the quick set can be observed as a result of the hexagonal calcium aluminate hydrates formation. In the presence of gypsum excess the similar effect can be the consequence of ettringite formation.

The contradictory data relating to the strength development of Portland cement in the presence of sodium and potassium sulphates were obtained. In some reports one can find that the strength decrease take place both at early age and after 28 days [133]. There are also some quite different data showing the strength increase throughout all this period of hardening [134].

The rich experience of cement plants in Poland shows that K_2SO_4 addition together with the properly chosen gypsum content the early strength increase and only slightly lowered 28 days strength can be obtained [135]. It is schematically shown in Fig. 4.46. Recently, the opinion about a higher early and lower 28 days strength in the presence of K_2SO_4 and Na_2SO_4 addition has become a rule. This is the typical effect observed in the case of all the accelerators. Svensen [136] proposed an empirical formula for calculation the 28 days strength lowering (in MPa, as RILEM method):

$$R_{28} = 48.8 - 5.53(\%K_2SO_4) + 0.18(\%C_3S) \tag{4.9}$$

This formula can be applied to cement with Blaine specific surface equal 3000 cm^2/g.

The contradictory data obtained by different authors should be attributed to the effect of many different factors influencing the paste strength. It is difficult to keep them all on the constant level, during the experiments.

Alkalis affect also the technological properties of paste and concrete. Among other they cause the paste shrinkage increase as well as the elasticity modulus of concrete after 14 days, and they reduce the change of concrete mass on drying and increase on wetting [137]. Calleja and Trivino [138] observed the growth of the surface microcracks on the paste with the alkali content and attributed this effect to the higher rate and more effective setting in the surface zone of the paste. However, the swelling of concrete cured in water is significantly lower in the case of cement rich in alkalis, at optimum gypsum content [45].

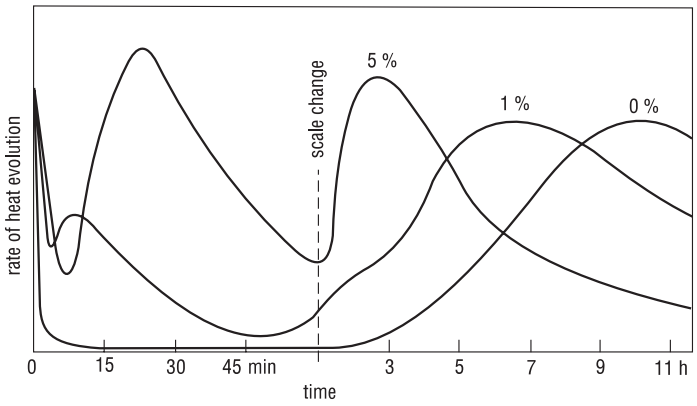


Fig. 4.47 Effect of K_2CO_3 on the C_3S hydration (according to [139])

4.1.3.5 Effect of Sodium and Potassium Carbonates

Sodium and potassium carbonates accelerate strongly the C_3S hydration. The induction period is shortened and on the calorimetric curve the additional peaks of unknown origin appear (Fig. 4.47) [139]. The effect of K_2CO_3 is proportional to the concentration with which the hydration degree and non–evaporable water are increasing [139].

Simultaneously, the C–S–H has "honeycomb" morphology and the C/S ratio remains unchanged. On the other side, according to Kalousek [140], the C/S decrease is the consequence of potassium incorporation into the C–S–H structure. Maycock and Skalny [139] did revealed the presence of potassium in C–S–H with X–ray energy dispersion spectroscopy; however, the source of potassium was not determined. It might be the potassium in C–S–H or in the mixture of C–S–H and potassium containing compound. Stein [141] revealed the acceleration of C_3S hydration in cement paste with simultaneous retarding of ettringite transformation into monosulphate because of the carboaluminates formation.

The effect of sodium and potassium carbonates can be derived from the effect of their hydroxides which appear as a result of reaction between the carbonates and $Ca(OH)_2$. The calcium carbonate is then precipitated. The 0.01 mol/l NaOH solution gives the liberation of 43 and 24.4 % of CH in case of C_3S and β–C_2S respectively, after 24 h of hydration [45]. Yoshi and Sudoh [142] attributed the catalytic effect of NaOH to the sodium silicate formation. This sodium silicate is then reacting with $Ca(OH)_2$ giving the C–S–H. The NaOH liberated during this process can react again with the anhydrous phases.

The accelerated C_3S hydration in the presence of sodium and potassium carbonates is accompanied by the higher SiO_2 concentration in the liquid phase with simultaneous rapid C–S–H (I) formation during the first hour, by the crystallization from the solution [143, 144]. Taking into account the results of Ramachandran [118]

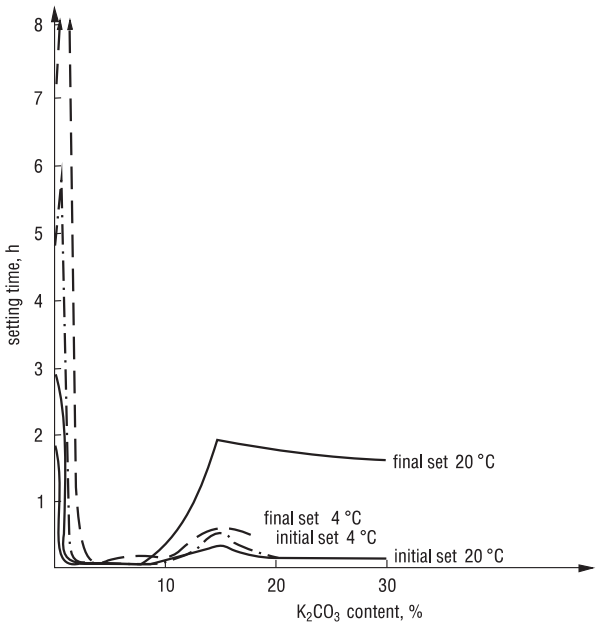


Fig. 4.48 Effect of K_2CO_3 on the setting time of Portland cement (according to [145])

one can presume that the $CaCO_3$ thus formed plays also in this case a role of nuclei for C–S–H.

The influence of K_2CO_3. on cement hydration was studied by Niël [145]. These studies are of great practical importance because, as it is commonly accepted, the alkalis from Portland cement clinker can be liberated during the hydration in humid air and, later on, to react with atmospheric CO_2 giving the carbonates [146, 148]. The false set can be then observed.

Niël [145] found the pronounced retarding effect for the low 0.2 % K_2CO_3 addition. At 2 to 10 % addition a significant shortening of setting time occurs, with the paste workability lost (Fig. 4.48). At higher content, exceeding 10 % the acceleration of set becomes lower. The same changes are found on the curves of consistency and early strength development (Fig. 4.49). The strength after 2 till 28 days at 0.25 % K_2CO_3 is similar, at 1.5 % K_2CO3—lower and at 2.5 % up to 3 days—significantly lower. In the phase composition of paste at 2.5 % K_2CO_3 the $C_4A\overline{C}H_{11}$ vis detected. C_3A and C_4AF react with water very quickly, particularly during the first hour and C_3S—during the 2 to 4 h. The author states that the quick set is the consequence of the formation of poorly soluble $CaCO_3$, $2K_2CO_3 \cdot 2CaCO_3 \cdot 6H_2O$ and syngenite as a result of K_2CO_3 reaction with gypsum [145]. At no gypsum and low Ca^{2+} concentration in the liquid phase there is no retardation of aluminate phases hydration, and these phases react rapidly with water. However, at 0.25 % of K_2CO_3 the ettringite formation is accelerated and the C_3A hydration is hampered.

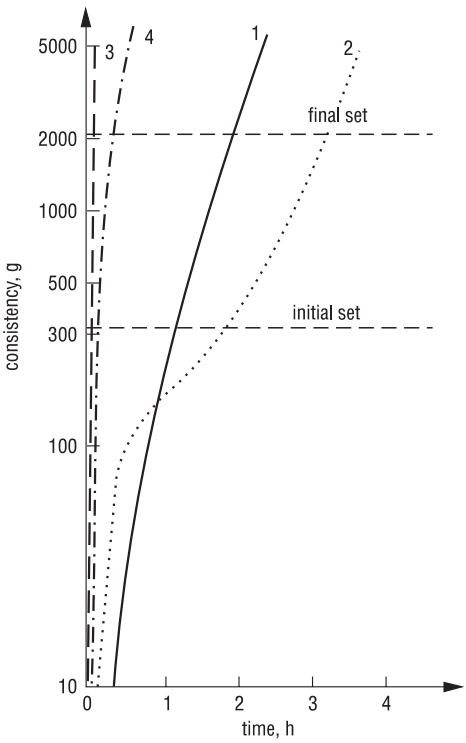


Fig. 4.49 Effect of K_2CO_3 on the consistency of Portland cement paste (measured by Vicat apparatus) (according to [145]): *1* 0%, *2* 0.25%, *3* 2.5%, *4* 20% K_2CO_3

4.1.4 The Effect of Grinding Aids

The agglomeration occurs usually during the cement grinding to the Blaine specific surface exceeding 3000 cm^2/g. The fine cement grains form the agglomerates and the energy consumed in grinding process becomes highly increased; this can be presented on curves illustrating the specific surface growth with time (Fig. 4.50). The belite phase is the most susceptible for agglomeration [148].

The agglomeration process can be eliminated by grinding aids. The most commonly known are different surfactants: triethanoloamine, glycols, alcohols. The lignosulphonates and fatty acids, as well as their salts, for example the sodium stearate are also used. The triethanoloamine and ethylene or propylene glycol were used a time ago. Nowadays, there is a huge amount of grinding aids available. They can be classified into three groups: (1) classic, only grinding facilitating agents, (2) grinding aids improving simultaneously the 28 days strength, (3) admixtures for cements with mineral additions, particularly with fly ash and limestone, which improve their strength. The different one must be used for fly ash and for limestone. The strength modifying effect in the case of Grace products was discussed earlier. In Poland there are, first of all, the products from Grace, Mapei and Chryso, all three types mentioned above, of these producers, are available.

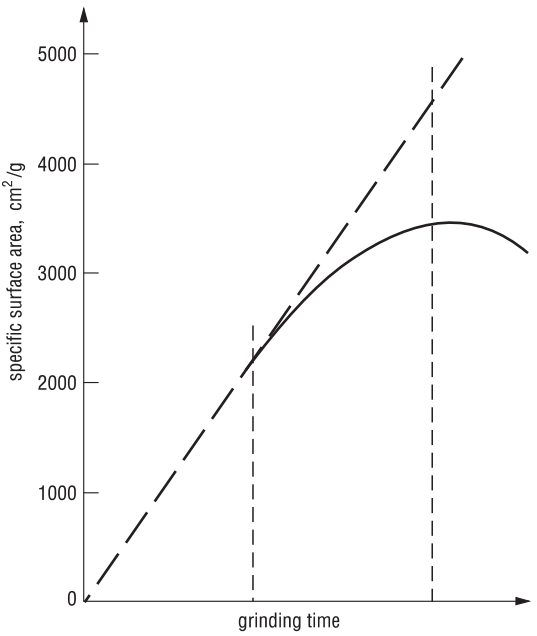


Fig. 4.50 Specific surface of cement vs. time of grinding. The *continuous line*—real curve; the *dashed lines* show the beginning of agglomeration and the end of cement specific surface area increase during grinding

It is commonly accepted that these admixtures are adsorbed on the surface of clinker grains reducing the hardness and prevent the agglomeration. A small addition of grinding agents, usually 0.01–0.1 % rises the output of mills of 15 %, in some cases even of 25 %; the energy consumption lowering is the same.

The mechanism of their action is not definitively explained. According to Rebinder [149] it can consist in the adsorption on the microcracks which leads to the elimination or reduction of valence bonds and the agglomeration becomes difficult. It is assumed that the agglomeration hampering consists in the weakening of the van der Waals and electrostatic forces between the finest cement particles, being its source. Adsorption on grains surfaces of grinding aids eliminates or is weakening these forces. It is assumed that the primarily effect of grinding aids consists in agglomeration prevention [150].

The addition of grinding aids leads to the increased mobility of cement, even of high fineness. The material becomes very transportable, easily flows out from silos and is without difficulties packaged into the bags. On the other side, the fine fraction content in cement increases the dustiness of the air venting the mill and worsening the electrostatic precipitators efficiency by the higher resistivity of cement, which rise from 10^8 to 10^{11} $\Omega \cdot$ cm is observed [151].

In Fig. 4.51 the effect of different grinding aids on the specific surface of cement is presented. As it is shown the poly–glycol–phenol ether and the heptane–phosphonate acid have the strongest impact. The effectiveness of saturated fatty acids and alcohols action grows with the reduction of chains length, the undersaturated acids are more active than the saturated ones [152, 153]. This can be explained by

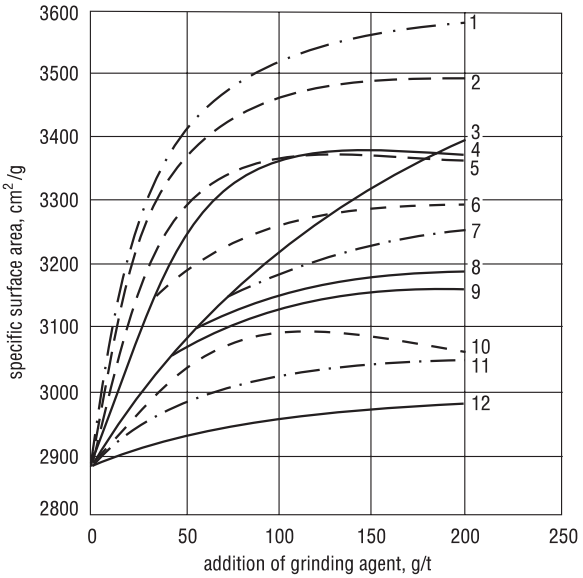


Fig. 4.51 Influence of grinding agents on cement specific surface area (after [150]): *1* polyether glycolic–phenol, *2* hepanophosphonic acid, *3* triethanoloamine, *4* sodium stearate, *5* sodium salt of hydroxamoic acid, *6* decanol, *7* potassium butylxanthogenate, *8* sulphite lye, *9* sodium cetylsulphite, *10* K_2HPO_4, *11* phosphonic acid ester, *12* methylsilicone oil

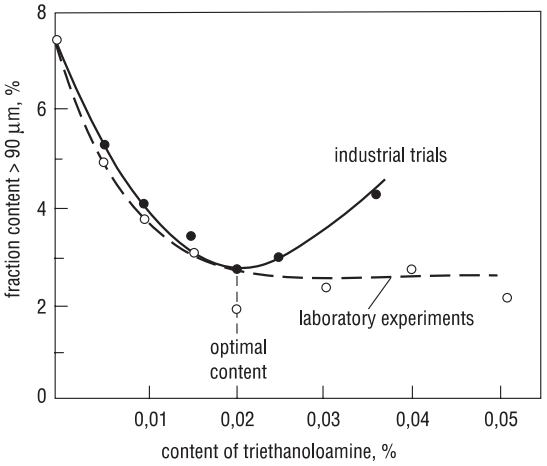


Fig. 4.52 Effect of grinding aids on cement fineness (according to [151])

the polar character of molecules of these substances, because the adhesion occurs between the polar part of molecule and the surface of solid phase.

In the presence of grinding agents the percentage of medium 3–30 µm fraction increases; the grain size distribution of cement is therefore modified [152]. It appeared also that for some admixtures there is an optimum addition and the specific surface decreases when it is exceeded [153]. This can be explained by too fast flow of cement from the mill. In these condition the coarse grains are leaving also the mill. For this reason, the experiments in laboratory mills, working periodically, show that above certain addition of grinding aids the specific surface of cement remains unchanged (Fig. 4.52).

The grinding aids, because of very low content, do not affect practically the hydration process. By some authors a slightly higher water demand and prolonged setting time is reported; it relates to the effect of glycols and ethanoloamine [154]. However, the strength remains practically unchanged. The pore structure and C–S–H specific surface are insignificantly modified [155, 156]. As it has been mentioned earlier, during the last ten years many new grinding agents causing the strength increase after 28 days of hardening were appeared. The mechanism of Grace products effect was discussed in point 4.1.3.1.

4.1.5 Chromium Reducers

On the basis of the European Community regulations (Directive 2003/53/EC) chromium(VI) content in cement must be reduced to the level of 2 mg per 1 kg of cement. The toxicity of soluble chromium compounds brings the skin irritation, causing allergic inflammations and even serious diseases. In cements produced in Poland the total chromium content is in the range from 20 to 100 mg/kg of cement and Cr(VI)—from 5 to 20 mg/kg respectively; this is because of the raw materials composition, particularly the iron–bearing components. The iron(II) sulphate is mainly used as chromium(VI) reducer because of low cost. The iron(II) sulphate occurs in a few modifications differing with crystallization water content: 0, 1, 4, 5, 7 water molecules per one $FeSO_4$ molecule exists. The solubility of hydrated iron sulphates decreases with lower water content; the sulphate $FeSO_4 \cdot 7H_2O$ is hygroscopic and absorbs water vapour transforming into the wet mass. The transformation of seven water molecules containing sulphate into the four containing one occurs at 60 °C; further dehydration to one water molecule needs higher temperature, but in prolonged isothermal heating at 60 °C can take place too. Simultaneously the oxidation of Fe(II) to Fe(III) occurs. One should take into account that the addition of $FeSO_4 \cdot 7H_2O$ to cement mill is associated with the risk of its dehydration to $FeSO_4 \cdot H_2O$. Therefore the latter is frequently introduced to the mill and the former—added to cement just before packaging or loading the car in the case of bulk expedition. Also during storage in silos $FeSO_4 \cdot 7H_2O$ iron is gradually oxidized.

The second reducer tin(II), also often added in the form of sulphate, is stronger reducer and less susceptible to oxidation. Therefore the addition of tin can be lower: in the case of Fe(II) sulphate from 0.2 to 0.3 %, while in the case of Sn(II) sulphate about 0.02 % or sometimes even less. The tin(II) sulphate can be also oxidized during the storage in cement silos, however, this process occurs very slowly. That is why the producers can guarantee the Cr(VI) content below the 2 mg/kg of cement for one year, while in the case of sulphate Fe(II) this period is shortened to two months. Mn(II) sulphate is a good reducing agent which also is difficult for oxidation. However, it did not found industrial application till now.

The reduction of chromium(VI) is an example of “reduction–oxidation” reaction; that means that the reduction of one reactant is linked always with the oxidation of another. Which substance or rather which ion is reduced depends upon

the redox potential of semi–cell composed of ions on different oxidation degree, taking part in the reaction oxidation–reduction. In the discussed reactions there are the semi–cells: Cr(VI)/Cr(III), Fe(III)/Fe(II) and Sn(IV)/Sn(II) which the standard redox potentials in the acid environment are: +1.33 V, +0.77 V and +015 V respectively. From the value of these potentials it results that Cr(VI) will be reduced by both ions: Fe(II) and Sn(II), because their redox potentials are lower than the potential of the system Cr(VI)/Cr(III).

However, the redox potential of semi–cells depends on the pH of the environment in which the reacting ions are located. Because the process of chromium(VI) reduction takes place in cement paste at pH = 12.5–13.4, the potentials of semi–cell are different from those given above, namely: Cr(VI)/Cr(III) = −0.12 V, Fe(III)/Fe(II) = −0.56 V, Sn(IV)/Sn(II) = −0.96 V. However, even in these condition iron(II) and tin(II) are for chromium(VI) strong reducers.

Mapei proposed to apply the antimony(III) which potential is −0.59 V in alkaline solution. The advantage of this reducer, according to the authors, is higher stability of antimony(III) oxide, in comparison with Fe(II) and Sn(II) sulphates, both during cement grinding and storage in silos [158, 159].

4.2 Hydration of Cement in Hydrothermal Conditions

4.2.1 Phases in the $CaO–SiO_2–H_2O$ System

There are numerous phases of hydrated calcium silicates. According to Taylor [156] this can be derived from the properties of calcium atom which can form with oxygen the octahedral coordinated system with different degree of disorder. It has a great impact on the network structure of undergoing condensation [SiO_4] tetrahedra [156, 160]. There are often amorphous phases, but always forming the small 10–20 μm crystals. The crystalline phases are produced in hydrothermal conditions, at temperatures exceeding 100 °C and pressure over 1000 hPa. These syntheses are done in the autoclave, under the saturated water vapour pressure. The natural equivalent of these phases are known; they occur mostly in the contact zones, for example in Crestmore in California, Scawtt Hill in Northern Ireland [156] or in Harturim in Israel [161], as well as in Fuka in Japan [21]. Some of them were not synthesized, for example nekoite or okenite [156].

In Fig. 4.53 the stability ranges of some of calcium silicate hydrates as a function of temperature and pressure are presented [156]. Because of experimental difficulties the $CaO–SiO_2–H_2O$ system has not been elaborated and the liquid phase remaining in equilibrium with the solid phases is not known. However, the research was undertaken to learn the stable, equilibrium phases, formed at variable C/S molar ratio, as a function of temperature and pressure; these problems was studied by Roy [162]. She investigated also the curves of saturated water vapour of many calcium silicate hydrates [163].

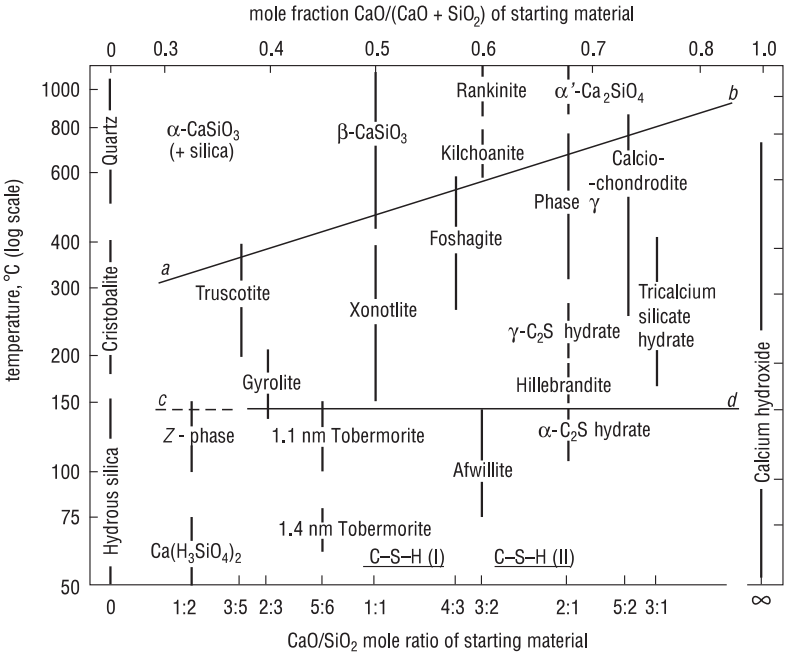


Fig. 4.53 Approximate stability range of known calcium silicate hydrates under hydrothermal conditions. The vertical lines indicate C/S mole ratios, their length is proportional to the temperature stability range; the width of their names gives an approximate range of deviation from their theoretical composition. The horizontal lines mean also the change of composition. At temperature 374 °C the critical point for water is indicated, at higher temperatures the saturated water vapor pressure is about 40 MPa. Above the *ab* line, the anhydrous compounds occur; in the phases marked between the straight lines *ab* and *cd*, water is present as OH^- ions; however, in xonotlite and truscotite there is presumably the molecular water; below the *cd* line there are the Si–OH groups containing phases, as well as the water molecules, OH^- ions and the two types of H_2O. (after [156])

In hydrothermal conditions the solubility of silica rapidly increases while the solubility of calcium hydroxide decreases (Figs. 4.54 and 4.55) [164]. This is undoubtedly the reason of quick reaction of silica with calcium hydroxide or with calcium silicates in these conditions and formation of calcium silicates hydrates. In Table 4.4 the classification of the calcium silicate hydrates according to Taylor [21] is shown; the reference works are also given [9, 63, 154, 155, 161, 165–181].

4.2.2 The Conditions of Formation and Structures of Some Selected Phases

In many calcium silicate hydrated phases the calcium hydroxide layer structure occurs as a base. This structure is shown in Fig. 4.56. The calcium atoms are

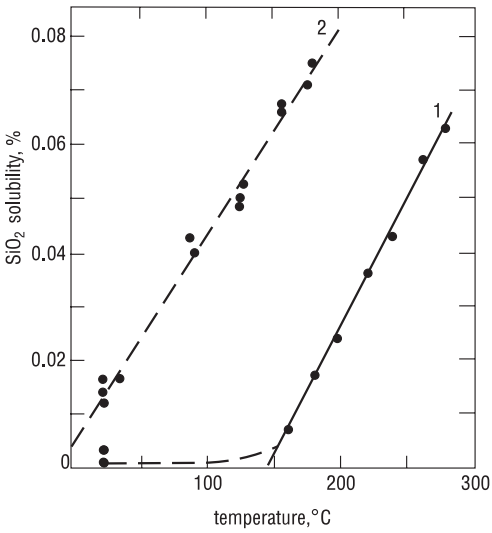


Fig. 4.54 The solubility of silica as a function of temperature (saturated water vapor) (according to [164]): *1* quartz, *2* silica

Table 4.4 The calcium silicate hydrates formed in hydrothermal conditions [21]

Phase	Composition	Structural formula	Remarks
Compounds structurally related to wollastonite			
Nekoite	$C_3S_6H_8$	$3CaSi_2O_5 \cdot 8H_2O$	Naturally occurring mineral; not synthesized
Okenite	$C_3S_6H_6$	$3CaSi_2O_5 \cdot 6H_2O$	Naturally occurring mineral; not synthesized
Xonotlite	C_6S_6H	$Ca_6Si_6O_{17}(OH)_2$	Geothermal cements [165]
Wollastonite	CS	$CaSiO_3$ (β)	
Foshagite	C_4S_3H	$Ca_4[SiO_3]_3(OH)_2$	Geothermal cements [165]
Hillebrandite	C_2SH	$Ca_2[SiO_3](OH)_2$	
Tobermorite group			
1.4 nm tobermorite	$C_5S_6H_9$	$Ca_5[Si_6O_{18}H_2]\ 8H_2O$	[154]
Tacharanite	$C_{12}AS_{18}H_{18}$	$Ca_4[Si_6O_{18}H_2]$ $Al_2O_3 \cdot 5H_2O$?	[155]
1.1 nm tobermorite	$C_5S_6H_5$	$Ca_5[Si_6O_{18}H_2] \cdot 4H_2O$	[154]
1.0 nm tobermorite	$C_5S_4H_5$?		
0.9 nm tobermorite	C_5S_6H	$Ca_5[Si_6O_{18}H_2]$	
C–S–H (I)	$C_5S_{4-6}H_x$?	Complexes 3*n*—1 tetrahedra	[9]
Jennite group			
Jennite	$C_9S_6H_{11}$	$Ca_9[Si_6O_{18}H_2](OH)_8 \cdot 6H_2O$	[161, 166]
Metajennite	$C_9S_6H_7$	$Ca_9[Si_6O_{18}H_2](OH)_8 \cdot 2H_2O$	[166]
C–S–H (II)	$C_9S_{4-6}H_x$	Complexes 3*n*—1 tetrahedra	[9]
Gyrolite group			
Gyrolite	$C_2S_3H_{\sim 2}$	$Ca_8[Si_4O_{10}]_3(OH)_4 \cdot 6H_2O$	Geothermal cements [165–167]

Table 4.4 (continued)

Phase	Composition	Structural formula	Remarks
Compounds structurally related to wollastonite			
Truscottite	$C_7S_{12}H_{\sim 3}$	$Ca_7[Si_4O_{10}][Si_8O_{19}](OH)_4 \cdot \sim 1H_2O$	[168]
Rayerite	$(N, K)C_{14}S_{22}AH_{\sim 8}$	Solid solutions on of truscottite	[169, 170]
Assarson's Z phase	ca. CS_2H_2	$Ca[Si_2O_5] \cdot 2H_2O$?	[170, 171]
C_2S group			
Kilchoanite	C_3S_2	$Ca_6[SiO_4][Si_3O_{10}]$	Geothermal cements, autoclaving [172, 173]
C_8S_5	C_8S_5	$Ca_8[SiO_4]_2[Si_3O_{10}]$	Autoclaving γ–C_2S, C_3S_2, β–CS [173, 174]
Calcio–chondrodite	C_5S_2H	$Ca_5[SiO_4]_2(OH)_2$	[156, 173]
Other calcium silicates			
Phase 0.315 nm	C_4S_5H		[167]
Suolunite	CSH	$Ca_2[Si_2O_7H_2] \cdot H_2O$	
Rosenhahnite	C_3S_3H	$Ca_3[Si_3O_{10}H_2]$	
Afwilite	$C_3S_2H_3$	$Ca_3[SiO_4H]_2 \cdot 2H_2O$	[175, 176]
Killalaite	ca. $C_{3.2}S_2H_{0.8}$	$Ca_{3.2}[Si_2O_7H_{0.6}](OH)$	[177]
α–C_2S hydrate	C_2SH	$Ca_2[SiO_4H](OH)$	[178]
Dellaite	C_6S_3H	$Ca_6[SiO_4][Si_2O_7](OH)_2$	Geothermal cements
Tricalcium silicate hydrate	$C_6S_2H_3$	$Ca_6[Si_2O_7](OH)_6$	[179]
Other calcium silicate hydrates phases occurring in cement paste at higher temperatures			
Scawtite	$C_7S_2\bar{C}H_2$	$Ca_7[Si_6O_{18}](CO_3) \cdot 2H_2O$	Geothermal cements [167]
Flukalite	$C_4S_2\bar{C}H$	$Ca_4Si_2O_6(OH, F)_2[CO_3]$	
Pectolite	NC_4S_6H	$NaCa_2[Si_3O_9H]$	Geothermal cements, sodium activated slags [165, 180]
Rustumite	$C_9S_5H \cdot CaCl_2$	$Ca_{10}[SiO_4][Si_2O_7]_2(8H)_2Cl_2$	Composition, structure [63]
CAS_2 hexagonal	CAS_2	$Ca[Al_2Si_2O_8]$	Geothermal cements [165]
Strätlingite	C_2ASH_8	$[Ca_2Al(OH)_6][AlSiO_5H_2] \cdot 4H_2O$	[165]
Bicchulite	C_2ASH	$Ca_2[Al_2SiO_6](OH)_2$	Geothermal cements
Hydrogarnets	$C_3(A, F)[H_6,S_3]$	$Ca_3[(Al, Fe)_2[SiO_4](OH)_4]_3$	Geothermal cements, autoclaved materials [181]

Many references see Taylor [21]

surrounded by the oxygen atoms in the octahedral co–ordination; the oxygen atoms, in turn are tetrahedrally co–ordinated with three calcium atoms and one hydrogen atom. However, the latter one has no bridging character and the position of adjacent layers permits the hydrogen location in the empty space between the three oxygen atoms from the next layer. The size of calcium octahedra—corresponding to the

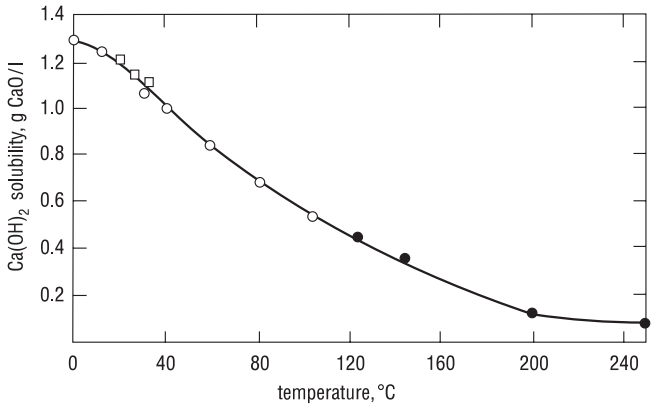


Fig. 4.55 Solubility of calcium hydroxide as a function of temperature (saturated water vapour)

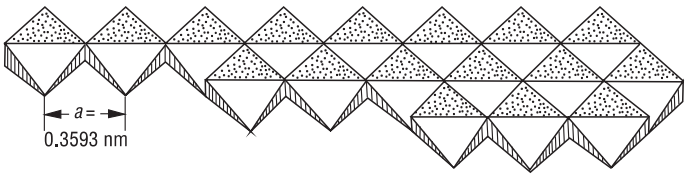


Fig. 4.56 The structure of single CaO_6 layer. The three rows of octahedra are shown. The dotted planes are lying flat. In the center of each octahedron there is a Ca^{2+} cation, each OH^- ion is shared between three CaO_6 octahedra

Si_2O_7 group—allow for fitting to them the anion substructure composed of wollastonite chains (Fig. 4.57) [182].

The silicate group Si_2O_7, ordered along one direction, and having the possibility of wollastonite chains formation, is the basic element of the structure of these silicates. The lack of some individual SiO_4 in this chain does not change the basic structure. This is the source of variable C/S molar ratio not only in the amorphous calcium silicate hydrates but also in the relatively well crystallized tobermorite in which the tendency for increasing C/S ratio is observed [160].

According to Taylor [160] the mechanism of hydrated calcium silicate phases formation is strongly related to the properties of silicate anion substructure. The SiO_4 tetrahedra condensate simultaneously with the calcium–oxygen polyhedral, influencing on one another. Alternatively, the calcium–hydroxide layers can be formed firstly, and the condensation of SiO_4 tetrahedra occurs on this matrix.

Some low amount of ions: CO_3^{2-} or BO_3^{3-} can enter the anion sublattice of silicate chains. Then the Si replacement by C takes place, observed for example in scawtite, with simultaneous interruption of Si–O chain [160].

The xonotlite and hillebrandite reveal the similar basal spacing $d = 0.730$ nm; therefore the conclusion about the presence of wollastonite chains in their structure appeared before their structures were determined. The tobermorite, xonotlite

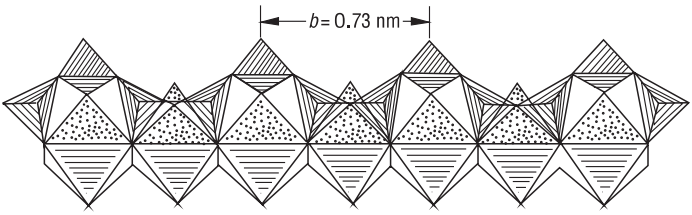


Fig. 4.57 Wollastonite chain linked with one column of CaO_6 octahedra (according to [182])

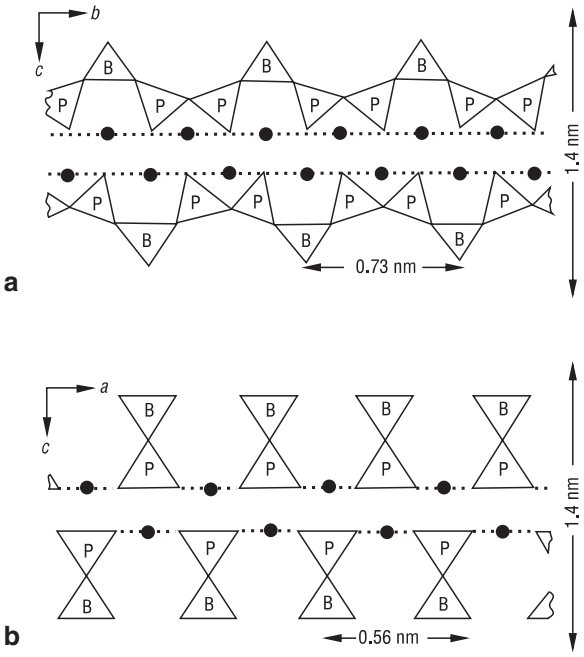


Fig. 4.58 The structure of single 1.4 nm tobermorite layer in *bc* (**a**) and *ac* (**b**) projections; in **b** the chains are seen end–on (according to [27]) (*B* bridging tetrahedra, *P* paired tetrahedra)

and α–C_2SH are the phases of special importance as the composition of silicate phase in hydrothermally cured cement pastes is concerned. Xonotlite is a dominating product in materials autoclaved at higher temperatures (Fig. 4.53), as well as in cement pastes from deep oil wells. Tobermorite is produced in the mixture of cement with silica or calcium hydroxide with silica at temperature not exceeding 140 °C [156]. The structural formula of tobermorite can be written as follows: $Ca_5[Si_6O_{18}H_2] \cdot 4H_2O$ (Fig. 4.58). Predominantly, this is so–called tobermorite 1.1 nm produced from C–S–H phase. However, at higher temperature it is transformed into xonotlite. Tashiro and Kawaguchi [183] found the formation of Cr_2O_3 solid solutions with C–S–H (I), according to the scheme: $2Cr^{3+} \rightarrow Si^{4+} + Ca^{2+}$. With chromium the stability field of C–S–H (I) is enlarged and shifted toward the higher temperatures.

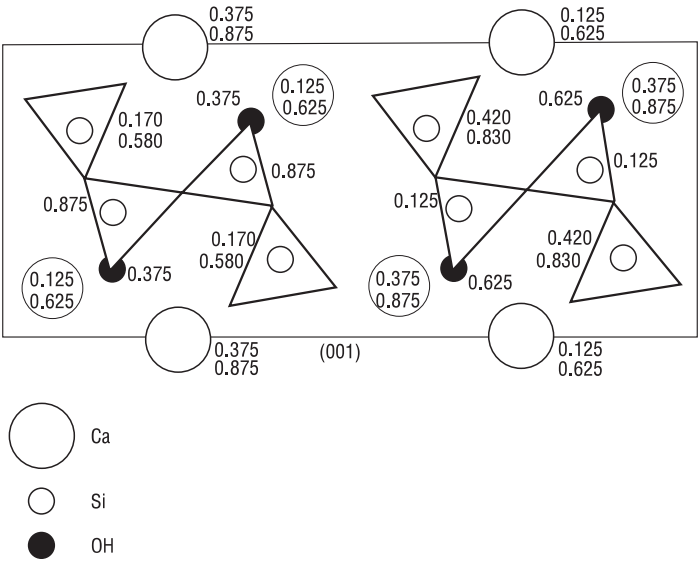


Fig. 4.59 The structure of xonotlite (according to [182]): projection along the b axis (*chain direction*). Tetrahedra are seen as triangles. The position of Ca^{2+}, Si^{4+} and OH^- ions are shown as a part of b = 0.73 nm

C–S–H (I) is transformed into tobermorite only exceptionally, at low addition of Cr_2O_3. Xonotlite is formed at significantly higher temperatures. Because Cr_2O_3 does not form the solid solution neither with xonotlite, nor with gyrolite or truscottite, it occurs at higher temperatures as $Cr(OH)_3$.

The effect of aluminum ions on the transformation of C–S–H into 1.1 nm tobermorite was investigated by Mitsuda and Taylor [184]. The solid solution of aluminum ions in tobermorite enlarges also the stability field of this phase in relation to xonotlite [185]. Diamond [186] found the maximum Al/(Si+Al) ratio in tobermorite to be 0.15; above this value the hydrogarnet phase is appearing. Aluminum is tetrahedrally coordinated and accelerates the formation of 1.1 nm tobermorite. Finally, Mitsuda and Taylor [184] revealed that alkalis (1 % Na_2O + 1.7 % K_2O) are activating the tobermorite formation from zeolite and calcium hydroxide.

Xonotlite $Ca_6Si_6O_{17}(OH)_2$ belongs to the wollastonite group. This phase is built from the three–alternating SiO_3 chains linked to form the bands $[Si_6O_{17}]^{10-}$ (Fig. 4.59) [187]. These bands are parallel to the crystallographic axis b. They reveal a characteristic period of identity 0.730 nm corresponding to the two Ca–O (2 × 0.365 nm) distances in the cation sublattice. This direction corresponds to the direction of xonotlite needle crystals growth.

Xonotlite is an important phase, because it is dominating component in the materials autoclaved at higher temperatures (Fig. 4.53), as well as formed in the pastes in deep wells cementing.

In many calcium silicate hydrated phases the topotactic transformations are observed. According to Taylor [156] this process can be defined as the single crystal

transformation into the product which is also close to single crystal. This is possible when the structures of transformed material and the product are similar and therefore the total deterioration of initial structure and recrystallization does not occur. Dent Glasser et al. [188] numerous examples of topotactic transformations were listed. Some of them are the following: xonotlite at temperature 680–700 °C transforms into β–C_2S, 1.4 nm tobermorite transforms at temperature 55–60 °C into 1.1 nm tobermorite, the latter one at temperature 100–300 °C into the 0.9 nm tobermorite phase. At temperature 800°C tobermorite transforms into β–CS. Both C–S–H (I) and (II) transform into the β–CS at temperature 830–900 °C.

During the xonotlite transition into β–$CaSiO_3$, the $Ca(OH)_2$ layer exhibits only negligible changes [189]. Significant changes take place in the silicon and oxygen consisting layers, not linked directly with calcium.

For the formation of single dreierketten chains of β–CS (the Si–O chains are of a type called dreierketten when they are kinked so as to repeat at intervals of three tetrahedra [27]), Si atoms must migrate from the internal part of tetrahedra to the empty tetrahedra, with which they had a common wall. Additionally some oxygen atoms, those not occurring in the "new" structure must also migrate. These are not the atoms from OH^- groups. Hydrogen atoms migrate separately and in the next stage water molecules are formed.

This mechanism of transition is, according to Taylor [156], a consequence of small Si^{4+} ions size which can migrate easier than large Ca or O atoms. However, there are also the examples of such topotactic transitions, e.g. the formation of γ–C_2S from afwilite, in which the SiO_4 tetrahedra are not transformed but only the Ca^{2+} and H^+ ions, as well as water molecules are migrating [190].

4.2.3 Phase Composition of Cement Hydrated in Hydrothermal Conditions

The hydrothermal treatment of concrete was introduced principally for the acceleration of cement paste hardening process which allowed the curing period shortening. Then after it has been proved that this process gives the possibility of cement replacement by waste materials, practically inert in water at ambient temperature.

It is convenient in practice to separate the two temperature ranges, when the phase composition of cement paste subjected to the thermal treatment is discussed: up to 100 °C in water vapor under the atmospheric pressure, and at higher temperatures and pressures, corresponding to the pressure of saturated water vapor.

The hydration of cement paste in water vapour at atmospheric pressure and temperatures up to 100 °C causes a significant acceleration of the process. Odler and Skalny [191] found the hydration degree of C_3S after 6 h at temperature 50, 75 and 100 °C as 23, 36 and 48 % respectively. At 100 °C the hydration of C_3S was completed after 3 days.

The process runs according the Arrhenius equation in the temperature range from 4 to 110 °C, as it has been proved by Verbeck [192] and the apparent activation

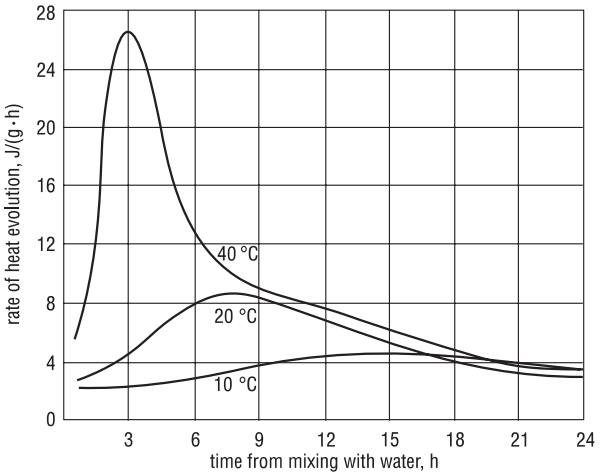


Fig. 4.60 The rate of heat evolution of Portland cement hardening at temperatures: 10, 20 and 40 °C (according to [194]). Composition of cement: C_3S—57%, C_2S—17%, C_3A—7%, C_4AF—8%, gypsum—4%, Na_2O—0.4%, K_2O—0.4%, w/c = 0.4

energy for different cements are very similar. According to Copeland and Kantro [193], the apparent activation energy is dependent on hydration degree.

There are significant changes on the heat evolution curves which consist on the second peak shifting toward shorter times and its height increase. It means that the induction period is shortened and the heat evolved at early age of hydration is increasing (Fig. 4.60). The ratio of non–evaporable water content to the heat of hardening is changing too, being at 80 °C higher than at 20 °C [194].

However, all the authors are unanimous that the phase composition of cement paste hydrated at higher temperatures is little changed as compared to the paste hydrated at ambient temperature. The calcium silicates transform into the C–S–H and calcium hydroxide. The majority of the authors state that the C/S ratio is higher and the H/S ratio is variable [195–199]. However, according to Kantro and some other authors the H/S ratio is higher too [200]. Frequently an opinion is presented that the water vapor treatment of starting mixture the phases with higher C/S and lower H_2O content are produced [1].

Aithen and Taylor [199] found the formation of low amount of C_3S–hydrate. Lach and Bures [201] observed a relatively significant share growth of 1.1 nm tobermorite which content in the temperature range from 60 to 95 °C is increasing. Simultaneously the increasing portlandite content and higher degree of its crystallinity was also found [201]. These observations were not proved by the other authors; that is stated that the formation of tobermorite is starting at temperatures above 100 °C, or as a matter of fact at 120 °C. The changes of morphology of hydrates has not been observed too; however, the appearance of some amount of better crystallized calcium silicate hydrates by some authors were reported [202].

The aluminate and alumoferrite phases are transformed to ettringite, the maximum content of which is rapidly reached and subsequently into solid solutions $C_3A \cdot CaSO_4 \cdot 12H_2O$–$C_4AH_{13}$ is transformed. These solid solutions decompose further and a substantial part of aluminum, iron and sulphate ions the solid solu-

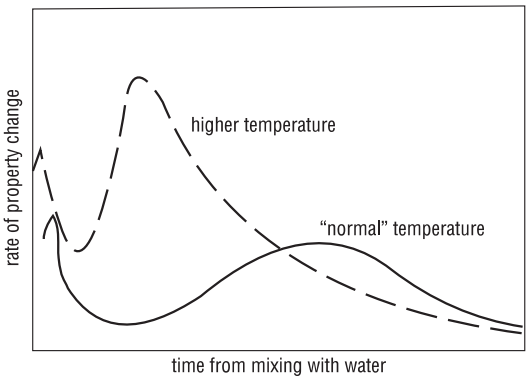


Fig. 4.61 The qualitative effect of increasing temperature on the rate of following parameters changes (according to [194]): heat of hydration, bound water content, shrinkage, strength and elasticity

tions with C–S–H are formed [194–196]. The hydrogarnets were not found [156, 194–196]. However, the formation of this phase in the mixture of C_3A with quartz was found [156, 203]. At room temperature the maximum ettringite content is detected after 18 h, but at temperature 100 °C—after 30 min. At temperature 20 °C the content of solid solutions $C_3A \cdot CaSO_4 \cdot 12H_2O$–$C_4AH_{13}$ even to the 28 days is increasing, while at temperature 100 °C until 4 h [194].

At higher temperature and at the presence of CO_2 from the air the scawtite phase is easily produced. In the CaO–SiO_2–CO_2–H_2O system scawtite is the only four–component phase and it is in equilibrium with the xonotlite, foshagite, tobermorite and calcite [204]. Its structural formula is given in the Table 4.4. In the CaO, quartz and NH_4HCO_3 (or $CaCO_3$) mixtures with water, at proper CaO/SiO_2 ratio equal 7/6, the hydrothermal treatment in autoclave at 205 °C gives practically the monophase product—scawtite [205], while in the mixture containing amorphous silica (Aerosil Degussa) or C–S–H the scawtite is produced as one of the products, (about 50 %), occurring together with tobermorite and calcite. In the mixtures of tobermorite and calcite the xonotlite and calcite are produced; scawtite does not appear [205].

In the industrial practice the strength of hydrothermally treated concrete is a very important feature. Three kinds of water vapour treatments are applied: "short"—not more than 4 h at 80–90 °C; "medium"—7–8 h at 70 °C; "long"—12–18 h at 40–50 °C.

The strength development increases markedly with curing temperature. However, after 28 days the strength and elasticity modulus are higher for the medium (40–50 °C or lower temperatures (Fig. 4.61). This phenomenon is explained by Alexanderson as the effect of microcracks formation in concrete, resulting from thermal expansion of humid air [206].

For this reason it is considered that the pre–maturing has positive effect, increasing the paste tensile strength [50]. This pre–maturing should take at least 5 h. The renewed vibration, before setting, can be also applied. One should remember that initial setting time is markedly shortened at higher temperature. Cement which final setting time at 20 °C is 3.5 h, reveals final set equal 1.5 h at 40 °C and 0.5 h at 80 °C respectively [50].

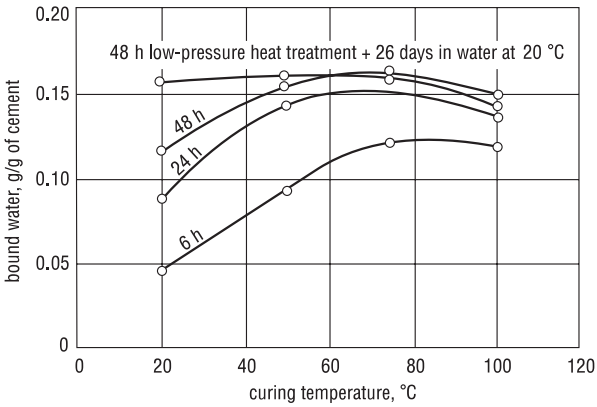


Fig. 4.62 The bound water content in Portland cement pastes measured at different time and curing temperature (according to [194]). Cement composition: C_3S—58 %, C_2S—22 %, C_3A—8 %, C_4AF—5.4 %, gypsum—3.4 %, w/c = 0.25

Many authors found that low pressure heat treatment at temperature 60–80 °C or higher results in the lower hydration degree at later age, as compared with concrete cured at ambient temperature [194, 207]. These data, reported by Idorn [194], are shown in Fig. 4.62. However, there is an exception. Odler and Gebauer [208] did not prove this phenomenon in the experiments with heat treatment of the paste having w/c = 0.3. The chemical shrinkage which can be the measure of hydration degree is higher at 60 °C than at 80 and 90 °C, already after 12 h of paste maturing [209].

There are also some other hypotheses trying to explain this strength lowering. The higher crystalline phase content in relation to the gel–like product can be the reason, according to Budnikov [210]. This can be also derived from the reduced specific surface of the vapour treated pastes [207]. The very anhomogeneous microstructure of heat treated pastes was also mentioned [207]. On the surface of cement grains very compact shells are formed, but the remaining parts of paste reveal more open structure. However, curing at room temperature rather homogenous microstructure assures. This effect can be used to reduce the strength lowering of heat treated pastes. For this aim more compact packing of mixed pastes with lower w/c ratio should be assured, for example by pressing. Then the compact shells give better cohesion between the cement grains [207]. Of this method the advantage was taken in the Danish Research Centre in Karlstrup, where the technology of heat treated cement pastes of high strength was developed [194]. They are composed of densified paste with ground quartz addition.

The mineral composition of thermal treated cement was the subject of numerous studies [50, 211–213]. Cements with high C_3S and low C_3A content are the most suitable. The gypsum content should be higher (see point 4.1.2). The higher fineness is also beneficial, because of the strength improvement immediately after heat treatment. In the case of short–term thermal treatment the rapid hardening cements good results are obtained [214].

The conditions of thermal treatment itself are of importance too. The rate of temperature rise should be relatively slow [156] (Fig. 4.63). The quick temperature increase is leading to the stresses formation in concrete, resulting from the tem-

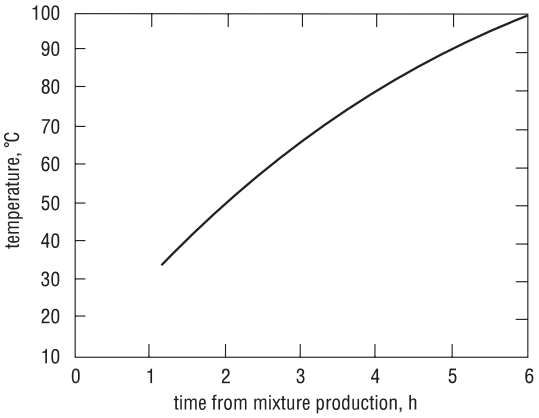
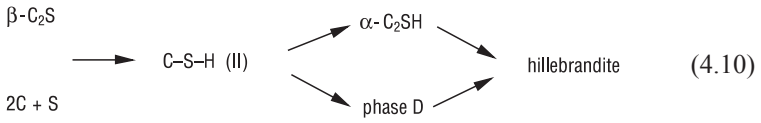


Fig. 4.63 Maximum water vapour heating rate of concrete (according to [156])

perature gradients, these stresses are increasing with the thickness of concrete elements. The difference of temperature in concrete mass should not exceed the value of 20–30 °C which corresponds to the heating rate of 10–20 °C/h [156]. The permissible heating rate depends in some extend on the type of cement used [156]. One should also take in mind that the strength of concrete after 28 days curing decreases with the higher temperature of heat treatment [50]. Taylor [156] underlines that up to 100 °C the reaction of cement paste with aggregate has no practical importance.

The higher differences, in phase composition are observed in the pastes autoclaved in the saturated water vapour at temperature range 120–200 °C. The phase composition of the calcium silicate hydrates is primarily the function of C/S in the starting mixture. In Portland cement paste without additions the C–S–H (I) is transformed quickly to the C–S–H (II) and the latter already at 25 °C into α–C_2SH [194, 199]. The proper addition of the ground quartz gives the 1.1 nm tobermorite. This phase contains aluminium in solid solution, which causes the transition to xonotlite, at temperatures exceeding 160 °C difficult.

The phase composition of cement mixture with quartz of variable fineness and mix proportions, autoclaved at temperature 177 °C during 8 h was investigated by Dyczek [178]. The C–S–H (I) was found as a main component; apart of this phase, the 1.1 nm tobermorite was detected and at 20% quartz addition—α–C_2SH. Basing upon the phase composition of the autoclaved β–C_2S or CaO and SiO_2 mixture of C/S = 2 Dyczek proposed a hypothesis of the of following phase transitions sequence during the hydrothermal process:



(4.10)

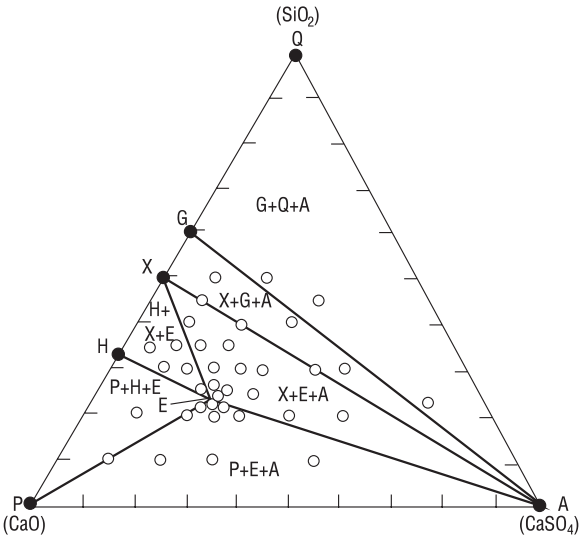


Fig. 4.64 The phases formed in the $CaO–SiO_2–CaSO_4–H_2O$ system at hydrothermal treatment at 235 °C (according to [215]): *Q* quartz, *G* gyrolite, *X* xonotlite, *H* hillebrandite, *E* ellestadite, *P* portlandite, *A* anhydrite

Therefore the author [178] postulates the formation of new, metastable phase belonging to the wollastonite group and containing the silicate groups $[Si_2O_7]^{6-}$, i.e. in rankinite $Ca_3[Si_2O_7]$.

The aluminate and aluminoferrite phases do not transform into the hydrates in the paste, similarly as at the lower temperature range during heat treatment. On the other hand, at substantial addition of quartz the hydrogarnets are formed [199]. One can expect also the formation of hydrogarnets in the autoclaved materials with higher content of fly ash, granulated blastfurnace slag and the other alumina, apart silica, containing wastes [197]. However, at the higher sulphur content the hydroxyl–ellastadite $C_{10}S_3\bar{S}_3H$ can be formed as a result of synthesis at temperature 120–200 °C. Its stability range is shown in Fig. 4.64, according to Takemoto [215].

The conditions of the calcium silicate hydrated phases formation given in Sect. 4.2.2 are of significant importance from the practical point of view. Depending on the temperature, time of thermal treatment, w/c ratio and the composition of initial mixture there are various intermediate phases produced. The reactivity of many phases, inert in relation to water, is markedly increased in the paste hydrothermal treatment [216].

There is a common opinion that the optimum autoclaving temperature should be 175 °C, and the time in the range from 8 to 48 h [50]. At higher temperatures the metastable phases, badly affecting the properties of composite, are formed.

At short hydrothermal treatment, that is up to 6 h, the C–S–H(I) and (II) are the dominating phases in the product. However, the increased heating time to 24 h and temperature to 170 °C results in the higher content of 1.1 nm tobermorite, $\alpha–C_2SH$, xonotlite and gyrolite. The formation of three latter phases depends on the C/S ratio in the initial mixture, whereas the awfilite and hillebrandite form very slowly and their percentage is negligible [1].

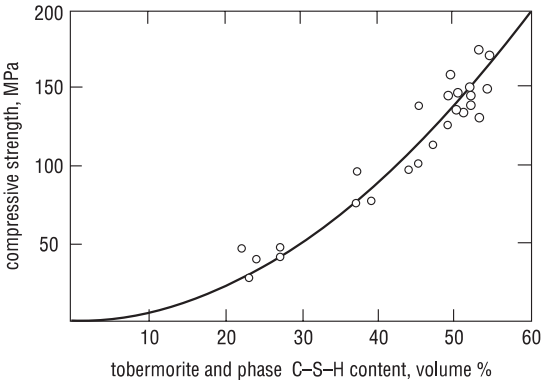


Fig. 4.65 The strength of autoclaved composites vs. the tobermorite and C–S–H phase content (according to [178])

The sequence of the metastable, intermediate phases formation is strongly related to the reactivity of the mixture components, particularly of silica [165, 217, 218]. At higher reactivity of lime the C–S–H (II) appears as a first product, then the C–S–H (I) and tobermorite, irrespectively of the C/S ratio.

At low C/S ratio only in this first stage tobermorite reacts further with quartz giving gyrolite. The latter one is transformed at 200 °C into truscottite, however, this transformation is very slow as compared to the reaction of transformation of tobermorite into xonotlite. The reaction of xonotlite with quartz is very difficult and it is the reason why in the material this phase is present for a very long time. Similarly, according to Luke and Taylor [218], foshagite and the phase 0.315 nm are showing very low reactivity with quartz in the hydrothermal conditions. However, when silica has a high rate of solubility in comparison to quartz, the sequence of phases formation is different: as first the Z phase is formed, which then is transformed into gyrolite and the latter into truscottite. It happens in the case of siliceous acid application, particularly in the mixture with β–C_2S [16].

There is relatively an unanimity opinion about the role of paste phase composition on the strength of concrete. The high strength is attributed to the C–S–H phases, as in the case of ambient temperature, as well to 1.1 nm tobermorite [136, 155]. On the other hand the α–C_2SH is causing the significant strength decrease [1, 156, 178, 199]. For this reason the 10–20 % quartz addition to the paste causes the decrease of the mechanical properties of material, however, the quartz addition of 30–40 % is favourable [1].

Dyczek [178] found a relationship between the strength of autoclaved material vs. the total C–S–H and 1.1 nm tobermorite content, which is shown in Fig. 4.65.

Langton et al. [165] studied the effect of phase composition on the strength of the pastes cured at temperatures 200–400 °C and under high pressure from 7 to 70 MPa. Xonotlite, foshagite, truscottite, hexagonal anorthite, diopside, chrysotile, antigorite and pectolite exhibit high strength [165]. The formation of scawtite does not lower the strength. Particularly good strength properties were observed in the case of xonotlite and foshagite containing mixtures. The effect of crystal habitus was underlined [165]. The needles, fibres, laths and plates contribute to the high

strength. MgO addition up to10% does not change the stability range of phases occurring in the $CaO–SiO_2–H_2O$ system at this condition. Some low Na_2O amount (0.5%) had a great negative impact on the strength of pastes with the composition close to gehlenite; the analcite and triclinic anorthite were then formed [165]. Simultaneously in the case of easily soluble modifications of silica the formation of silica–rich phases: truscottite and wairakite (calcium zeolite) was favoured.

Due to the autoclaving, the composites reveal many useful properties; among them the most important are: high strength, better sulphate corrosion resistance, low drying shrinkage. The lowering of shrinkage is primarily the consequence of the C–S–H replacement by tobermorite [197]. It is also stated that the silicon by aluminum ions substitution in tobermorite is the reason of lower shrinkage of this phase [197]. The improved sulphate corrosion resistance is related to the lowered CH content on one side and to the significantly reduced calcium aluminate hydrates content on the other side. The aluminum ions together with the SO_4^{2-} ions form, as it has been mentioned earlier, the solid solution in the C–S–H and 1.1 nm tobermorite.

Also the hydrogarnets are resistant to the aggressive action of the sulphates water solutions [181]. The replacement of H_2O by SiO_2 in amount to get the SiO_2 content in hydrogarnet structure close to 0.30 of mole ($C_3AS_{0.28}H_{5.44}$) causes practically this phase resistant to sulphates.

The thermal treatment of concrete can cause the detrimental effect of delayed ettringite formation, resulting in the deterioration of concrete elements. The problem of delayed ettringite formation belongs to the internal corrosion of concrete and will be discussed in the chapter relating to this corrosion.

References

1. Lea, F.M.: The Chemistry of Cement and Concrete, 3rd edn. Chemical Publishing Co., Inc., New York (1971)
2. Mortureux, B., Hornain, H., Regourd, M.: 7th ICCC Paris, vol. IV, p. 570. Paris (1980)
3. Cottin, B., Vibert, C.: Cement–Wapno–Gips. **43**, 193 (1976)
4. Delmas, P.: Rev. Mav. Constr. **702**, 291 (1976)
5. Roberts, M.H.: Inv. Symp. On Admixtures for Mortar and Concrete. Brussels, Report II/1, pp. 5–29. (1967)
6. Bombled, J.P.: 7th ICCC Paris, vol. III, pp. IV–164. Paris (1980)
7. Bailey, J.E., Hampson, C.J.: Cem. Concr. Res. **12**, 227 (1982)
8. Locher, F.W.: Cement, Principles of Production and Use. Verlag Bau + Technik GmbH, Düsseldorf (2006)
9. Taylor, H.F.W.: 8th ICCC Rio de Janeiro, vol. I, p. 82. Rio de Janeiro (1986)
10. Longuet, P., Burglen, L., Zelwer, A.: Rev. Mav. Constr. **676**, 35 (1973)
11. Glasser, F.P., Marr, J.: Proc. Brit. Ceram. Soc. **35**, 419 (1984)
12. Glasser, F.P., Marr, J.: Il Cemento. **82**, 85 (1985)
13. Tang, F.J., Gartner, E.M.: Adv. Cem. Res. **1**, 67 (1988)
14. Dalgleish, B.J., Pratt, P.L., Toulson, E.: Mater. J. Sci. **17**(8), 2199 (1982)
15. Scrivener, K.L., Pratt, P.L.: Proc. Brit. Ceram. Soc. **35**, 207 (1984)
16. Pratt, P.L., Ghose, A.: Phil. Tranp. Roy. Soc. London, **A310**, 93 (1983)
17. Harrisson, A., Winter, N.B., Taylor, H.F.W.: 8th ICCC Rio de Janeiro, vol. IV, p. 170. Rio de Janeiro (1986)

18. Locher, F.W., Richartz, W.: 6th ICCC Moskwa, vol. II/1, p. 122. Moscow (1974)
19. Stark, J., Moser, B., Bellmann, F.: 11th ICCC Durban, vol. 1, p. 261. Durban (2003)
20. Raymont, D.L., Lachowski, E.E.: Cem. Concr. Res. **14**, 43 (1984)
21. Taylor, H.F.W., Roy, D.M.: 7th ICCC Paris, vol. I, p. II–2/1. Paris (1980)
22. Ramachandran, V.S.: Cem. Concr. Res. **3**, 41 (1973); **6**, 623 (1976); J. Appl. Chem. Biotechnol. **22**, 1125 (1972)
23. Pauri, M., Monosi, S., Moriconi, G., Collepardi, M.: 8th ICCC Rio de Janeiro, vol. III, p. 125. Rio de Janeiro (1986)
24. Taylor, H.F.W., Newbury, D.E.: Cem. Concr. Res. **14**, 93 (1984)
25. Singh, N.B., Singh, A.K., Singh, P.S.: 8th ICCC Rio de Janeiro, vol. III, p. 101. Rio de Janeiro (1986)
26. Vernet, C., Dermoulian, E., Goudrin, P., Hawthorn, F.: 7th ICCC Paris, vol. II, pp. II–219. Paris (1980)
27. Taylor, H.W.F.:Cement Chemistry. Academic Press, London (1990)
28. Locher, F.W., Richartz, W., Sprung, S.: Zement–Kalk–Gips **33**, 271 (1980)
29. Diamond, S.: 7th ICCC Paris, vol. IV, p. 113. Paris (1980)
30. Collepardi, M., Corradi, M., Baldini, G., Pauri, M.: Il Cemento. **75**, 169 (1978)
31. Hampson, C.J., Bailey, J.E.: Mater. J. Sci. **17**(11), 3341 (1982)
32. Hampson, C.J., Bailey, J.E.: Mater. J. Sci. **18**(2), 402 (1983)
33. Brown, P.W., Libermann, L.O., Frohnsdorff, G.: J. Am. Ceram. Soc. **67**(12), 793 (1984)
34. Cottin, B.: Il Cemento. **75**, 177 (1978)
35. Jawed, L., Skalny, J., Young, J.F: In: Barnes, P. (ed.) w Structure and performance of cements, p. 250. Appl. Science Publ., London (1983)
36. Frigione, G.: In: Ghosh, P.N. (ed.) w Advances in cement technology, p. 485. Pergamon Press, Oxford (1983)
37. Menetrier, D., Jawed, L., Skalny, J.: Cem. Concr. Res. **10**, 697 (1980)
38. Odler, I.: 7th ICCC Paris, vol. IV, p. 493. Paris (1980)
39. Bentur, A.: J. Am. Ceram. Soc. **59**, 210 (1976)
40. Ost, B.W.: Am. Cer. Soc. Bull. **53**, 579 (1974)
41. Venuat, M.: Adjuvants et traitements des mortiers et betons. M. Venuat, Paris (1971)
42. Haskell, W.E.: Rock Products. **62**, 108 (1959)
43. Kurdowski, W., Garbacik, A., Chłądzyński, S.: Cement Wapno Beton. **71**, 81 (2004)
44. Sprung, S.: Zement–Kalk–Gips. **27**, 259 (1974)
45. Jawed, L., Skalny, J.: Cem. Concr. Res. **8**, 37 (1978)
46. Altsed, H.C.: Nielsen Rock. Prod. **77**, 72 (1974)
47. Hallich, K.: Zement–Kalk–Gips. **33**(9), 443 (1980)
48. Jelenić, J., Panowic, A., Bezjak, A.: Cem. Concr. Res. **10**, 463 (1980)
49. Le Jean: 7th ICCC Paris, vol. II, p. 11. Paris (1980)
50. Venuat, M.: 6th ICCC Moskwa, vol. II/2, p. 109. Moskwa (1974)
51. Brunauer, S.: Patent USA, no. 3, 689, 294 (1972)
52. Yudenfreund, M., Odler, I., Brunauer, S.: Cem. Concr. Res. **2**, 313, 331, 463, 577, 731 (1972)
53. Odler, I., Skalny, J., Brunauer, S.: 6th ICCC, vol. II, p. 30. Moskwa (1974)
54. Massazza, F.: In: Gosh, P.N. (ed.) Advances in cement technology. p. 569. Pergamon Press, Oxford (1983)
55. Ramachandran, V.S.: Cem. Concr. Res. **6**, 623 (1976)
56. Dusmuradov, T., Kantsepolski, J.S.: Uzb. chim. Ż. **18**, 55 (1974)
57. Chiesi, C.W., Myers, D.M., Gartner, E.M.: 14th Inv. Conf. On Cement Microscopy, Costa Mesa, USA (1992)
58. Ramachandran, V.S.: Calcium chloride in concrete. Appl. Science Publ., London (1976)
59. Tenoutasse, N.: Zement–Kalk–Gips. 20, 459 (1967); 5th ICCC Tokyo, vol. II, p. 372. Tokyo (1968)
60. Orchard, D.F.: Concrete Technology, vol. l. Applied Science Publ., London (1973)
61. Kurdowski, W., Miśkiewicz, K.: Cem. Concr. Res. **15**, 785 (1985)
62. De Keyser, W.L., Tenoutasse, N.: 5th ICCC Tokyo, vol. II, p. 379. Tokyo (1968)

63. Howie, R.A., Iliushin, W.W.: Nature. **269**, 231 (1977)
64. Ramachandran, V.S., Feldman, R.F.: Il Cemento. **75**, 311 (1978)
65. Collepardi, M., Marchese, B.: Cem. Concr. Res. **2**, 57 (1972)
66. Skalny, J., Odler, I.: Cem. Concr. Res. **2**, 387 (1972)
67. Feldman, R.F., Sereda, P.J.: Mater. Constr. **1**, 509 (1968)
68. Stoch, L.: Minerały ilaste, Wyd. Geologiczne, Warszawa 1974. (in Polish)
69. Tennis, P.D., Jennings, H.M.: Cem. Concr. Res. **30**, 856 (2000)
70. Ramachandran, V.S.: Termochim. Acta. **3**, 343 (1972)
71. Traetteberg, A., Ramachandran, V.S., Grattan–Bellew, P.E.: Cem. Concr. Res. **4**, 203 (1974)
72. Odler, I., Skalny, J.: J. Am. Ceram. Soc. **54**, 362 (1971)
73. Collepardi, M., Marcialis, A., Solinas, V.: Il Cemento. **70**, 83 (1973)
74. Garrault, S., Nachbaur, L., Nonat, A.: In: Przybylski, K. (ed.) w Ceramika, vol. 61. Pol. Tow. Ceram., Kraków (2000)
75. Guo Chengju.: 8th ICCC Rio de Janeiro, vol. III, p. 28. Rio de Janeiro (1986)
76. Kondo, R., Daimon, M., Sakai, E., Oshiyama, H.: J. Appl. Chem. Biotechnol. **27**, 191 (1977)
77. Collepardi, M., Rossi, G., Spiga, M.C.: Ann. Chim. **61**, 137 (1971)
78. Smith, J.R.: J. Am. Concr. Inst. **72**, 607 (1975)
79. Ramachandran, V.S.: Cem. J. Civil. Eng. **5**, 213 (1978)
80. Alimov, P.S., Lelmiezch, N.A.: Izw. Sew–Kawk. Nauczn. Centra Wyp. Szk. Sier. Tiech. Nauk. **3**, 26 (1975). (in Russian)
81. Shideler, J.J.: J. Am. Concr. Inst. **48**, 537 (1952)
82. Hope, B.B., Manning, D.G.: J. Am. Concr. Inst. **68**, 361 (1971)
83. Bentur, A., Milestone, N.B., Young, J.F., Mindess, S.: Cem. Concr. Res. **9**, 161 (1979)
83a. Justnes, H., Nygaard, E.C.: Cem. Concr. Rep. **25**, 1766 (1995)
83b. Justnes, H., Nygaard, E.C.: Adv. Cem. Rep. **8**, 101 (1996)
84. Hallauer, O.: Beton. 119 (1972)
85. Lieber, W.: 5th ICCC Tokyo, vol. II, p. 444. Tokyo (1968)
86. Bruere, G.M.: Nature. **199**, 4888 (1963)
87. Young, J.F.: Cem. Concr. Res. **2**, 415 (1972)
88. Basz, P.M., Rakimbajew Sz, M.: Cemient. **11**, 16 (1973)
89. Simeonow, J., Christowa, J., Zienowa, A.: Baustoffindustrie. 27 (1976)
90. Nocuń–Wczelik, W., Łój, G.: Cement–Wapno–Beton. **73**, 285 (2006)
91. Nocuń–Wczelik, W., Łój, G.: Cement–Wapno–Beton. **73**, 343 (2006)
92. Pichniarczyk, P.: Non published data
93. Wenda, R., Kuzel, H.J.: 8th ICCC Rio de Janeiro, vol. III, p. 307. Rio de Janeiro (1986)
94. Lieber, W., Richartz, W.: Zement–Kalk–Gips. **25**(9), 403 (1972)
95. Cussino, L., Montenero, L., Negro, A.: 8th ICCC Rio de Janeiro, vol. III, p. 114. Rio de Janeiro (1986)
96. Tabikh, A.A., Miller, F.M.: Cem. Concr. Res. **1**, 663 (1971)
97. Diamond, S.: J. Am. Ceram. Soc. **54**, 273 (1971)
98. Schneider, H., Schonfelder, R.: Betonwerk Fertigteiltechnik. **2**, 97 (1972)
99. Previte, R.W.: Cem. Concr. Res. **1**, 301 (1971)
100. Singh, N.B., Ojka, P.N.: 7th ICCC Paris, vol. II, pp. II–100. Paris (1980)
101. Thomas, N.L., Birchall, J.D.: Cem. Concr. Res. **13**, 830 (1983)
102. Thomas, N.L., Birchall, J.D.: Cem. Concr. Res. **14**, 761 (1984)
103. Milestone, N.B.: Cem. Concr. Res. **7**, 45 (1977)
104. Young, J.F.: 5th ICCC Tokyo, vol. II, p. 256. Tokyo (1968)
105. Mariampolski, N.A., Penczow, A.J., Sawaszkin, J.A.: Niefv. Choz. **10**, 27 (1974)
106. Stadelman, C., Wieker, W.: 7th ICCC Paris, vol. IV, p. 199. Paris (1980)
107. Berger, R.L., McGregor, J.D.: Cem. Concr. Res. **2**, 43 (1972)
108. Young, J.F.: J. Am. Ceram. Soc. **53**, 65 (1970)
109. Czerkinski, J.S., Butt, T.S., Slipchenko, G.F., Chmielewska, T.A.: Izw. Akad. Nauk SSSR, Nieorg. Matier. **6**(11), 2038 (1970) (in Russian)

110. Czerkinski, J.S., Slipchenko, G.F., Butt, T.S., Miagkova, M.A., Sirotkina, N.L., Chmelevska, T.A.: Kołłoid. Ż. **34**(5), 738 (1972)
111. Baron, J.: Inv. Sem. On some aspects of admixtures and indust. by–products on the durability of concrete, Chalmers University of Technology, April 28–29 1986, Session IV: "Calcareous additives"
112. Regourd, M.: 8th ICCC Rio de Janeiro, vol. I, p. 199. Rio de Janeiro (1986)
113. Mortureux, B., Hornain, H., Regourd, M.: Colloque International Liaison Pâte de Ciment, Materiaux Associés A 64. Toulouse, France (1982)
114. Jambor, J.: 7th ICCC Paris 1980, vol. IV, p. 487. Paris (1980)
115. Cochet, G., Sorrentino, F.: w Progress In Cement and Concrete. In: Ghosh, P.N. (ed.) Mineral admixtures in cement and concrete, vol. 4, Chap. 7, p. 266. ABI Books, New Delhi (1993)
116. Livesey, P.: In: Swamy, R.N. (ed.) Proc. Inv. Conf. Blended Cements in Construction, p. 1. Sheffield (1991)
117. Grandet, J., Olivier, J.P.: Cem. Concr. Res. **10**, 759 (1980)
118. Ramachandran, V.S., Zhang, Chun–Mei.: Durability of Build. Mat. **4**(1), 45 (1986)
119. Nonat, A., Courault, A.Ch., Damidot, D.: Cement Wapno Beton. **68**, 184 (2001)
120. Vernet, C.: 8th ICCC Rio de Janeiro, vol. III, p. 70. Rio de Janeiro (1986)
121. Negro, A., Abbiati, G., Cussino, L.: ibid., vol. III, p. 109
122. Bensted, J.: World Cement Tech. **11**, 395 (1980); **14**, 383 (1983)
123. Matschei, T., Glasser, F.P.: 17 Intern. Baustofftag., vol. 1, p. 1–0219. Weimar (2009)
124. Matschei, T., Glasser, F.P.: 16 Intern. Baustofftag., vol. 1, p. 1–0389. Weimar (2006)
125. Chłądzyński, S., Garbacik, A.: Cementy wieloskładnikowe w budownictwie. Stowarzyszenie Producentów Cementu, Kraków (2008). (in Polish)
126. Chatterjee, A.K.: In: Ghosh, P.N. (ed.) w Advances in Cement Technology, p. 203. Pergamon Press, Oxford (1983)
127. Shebl, F.A., Helmy, F.M., Ludwig, U.: Il Cemento. **77**, 51 (1980)
128. Shebl, F.A., Ludwig, U.: Il Cemento. **75**, 449 (1978)
129. Gawlicki, M., Nocuń–Wczelik, W.: 8th ICCC Rio de Janeiro, vol. III, p. 183. Rio de Janeiro (1986)
130. Grzymek, J.: Cement–Wapno–Gips. **18**, 45 (1963); Pat. PRL nr. 44998, (1960). (in Polish)
131. Grzymek, J.: Proc. of the 7th Conference on the Silicate Industry, p. 265. Akadémiai Kiadó, Budapest (1965)
132. Sprung, S., Rechenberg, W.: Proc. Symp. Effect of Alkalies on Properties of Concrete, London Sepv. 1976, p. 109. CRCA, (1977)
133. Sudakas, L.G., Zozulja, R.A., Kokurkina, A.W., Sorokina, W.A.: Cemient. **12**, 11 (1978). (in Russian)
134. Czernych, W.F., Azielicka, R.D., Ponomariew, J.F., Mandrykin, J.J.: Cemient. **5**, 7 (1963). (in Russian)
135. Kurdowski, W.: Poradnik technologa przemysłu cementowego. Arkady, Warszawa (1981). (in Polish)
136. Svedsen, J.: Zement–Kalk–Gips. **31**, 281 (1978)
137. Blaine, R.L.: 5th ICCC Tokyo, vol. III, p. 83. Tokyo (1968)
138. Calleja, J.C., Trivino, F.V.: Special Report 90, p. 145. Highway Research Board, Washington (1968)
139. Maycock, J.N., Skalny, J.: Termochim. Acta. **8**, 167 (1974)
140. Kalousek, G.L.: J. Rep. NBS. **32**, 285 (1944)
141. Stein, H.N.: J. Appl. Chem. **11**, 474 (1961)
142. Yoshii, T., Sudoh, G.: Rev. 13th Gen. Meet. Cem. Assoc. Japan, p. 16. Tokyo (1959)
143. Mori, H., Minegishi, K., Ohta, T., Akiba, T.: Rev. 24th Gen. Meet. Cem. Assoc. Japan, p. 26. Tokyo (1970)
144. Ludwig, U.: 6th ICCC Moskwa, vol. II/1, p. 119. Moskwa (1974)
145. Niël, M.M.G.: 5th ICCC Tokyo, vol. II, p. 472. Tokyo (1968)
146. Steinour, H.H.: Portl. Cem. Asp. Rep. Dept. Bull. 98, Chicago (1958)

147. Hansen, W.C.: 4th ICCC Washington, vol. I, p. 387. Washington (1960)
148. Beke, B., Opoczky L.: Zement–Kalk–Gips. **22**, 541 (1969)
149. Rebinder, P.A.: Z. Phys. **72**, 191 (1931)
150. Scheibe, W., Dallmann, W., Rosenbaum, A.: Silikattechnik. **2**, 11 (1970)
151. Dombrowe, H., Drescher, G.: Silikattechnik. **7**, 341 (1975)
152. Raymont, D.L.: Cem. Concr. Res. **12**, 133 (1982)
153. Butt, J.M., Syczov, M.M., Timaszev, W.W.: Chimiczeskaja Tiechnołogija Wiażuszczich Matieriałow. Izd. Wysszaja Szkoła, Moskwa (1980). (in Russian)
154. El–Hemaly, P.A.S., Mitsuda, T., Taylor, H.F.W.: Cem. Concr. Res. **7**, 429 (1977)
155. Cliff, G., Gard, J.A., Lorimer, G.W., Taylor, H.F.W.: Miner. Mag. **40**, 113 (1975)
156. Taylor, H.F.W.: The Chemistry of Cements. Academic Press, London (1964)
157. Atkins, P.W.: Gibbs's Phase Rule Can be Found in Physical Chemistry. Oxford University Press (1998)
158. Magistri, M., Padovano, D.: Int. Cem. Rev. **10**, 49 (2005)
159. Magistri, M., D'Arcangelo, P.: Bud. Technol. Architek. **9**, 68 (2009)
160. Taylor, H.F.W.: 5th ICCC Tokyo, vol. II, p. 1. Tokyo (1968)
161. Gross, S.: Geol. Surv. Israel Bull. 70 (1977)
162. Roy, D.M., Harker, R.J.: 4th ICCC Washington, vol. I, p. 196. Washington (1960)
163. Roy, D.M.: Am. Min. **43**, 1009 (1958)
164. Iler, R.K.: The Chemistry of Silica. Wiley, New York (1979)
165. Langton, C.A., White, E.L., Grutzeck, M.W., Roy, D.M.: 7th ICCC Paris, vol. III, p. Y145. Paris (1980)
166. Gard, J.A., Taylor, H.F.W., Cliff, G., Lorimer, G.W.: Am. Min. **62**, 365 (1977)
167. Luke, K., Taylor, H.F.W., Kalousek, G.L.: Cem. Concr. Res. **11**, 197 (1981)
168. Gard, J.A., Luke, K., Taylor, H.F.W.: Cem. Concr. Res. **11**, 659 (1981)
169. Lachowski, E.E., Murray, L.U., Taylor, H.F.W.: Miner. Mag. **43**, 333 (1979)
170. Assarsson, G.O.: 4th ICCC Washington, vol. I, p. 190. Washington (1960)
171. Gard, J.A., Mitsuda, T., Taylor, H.F.W.: Miner. Mag. **40**, 325 (1975)
172. Brylicki, W.: Tworzywa autoklawizowane ze szlamu poekstrakcyjnego zawierającego gamma C2S. Ph. D. Thesis, AGH, Kraków (1981). (in Polish)
173. Szuba, J.: Hydratacja rankinitu i wolastonitu w warunkach hydrotermalnych. Ph. D. Thesis, AGH, Kraków (1986). (in Polish)
174. Jernejćić, J., Jelenić, I.: Cem. Concr. Res. **4**, 123 (1974)
175. Brunauer, S., Copelard, L.E., Brugg, R.H.: J. Phyp. Chem. **60**, 112, 116 (1956)
176. Bellina, G., Hassan, M., Longuet, P.: Ciments, Betons, Plâtres, Chaux. **4/85–755**, 245 (1985)
177. Taylor, H.F.W.: Miner. Mag. **41**, 363 (1977)
178. Dyczek, J., Zeszyty Naukowe, AGH.: Ceramika Z. 42, Kraków (1979). (in Polish)
179. Gouda, G.R., Roy, D.M.: J. Am. Ceram. Soc. **59**, 412 (1976)
180. Nelson, E.B., Kalousek, G.L.: Cem. Concr. Res. **7**, 687 (1977)
181. Marchese, B., Sersale, R.: 5th ICCC Tokyo, vol. II, p. 133. Tokyo (1968)
182. Mamiedow, Ch.S., Biełow, N.W.: Dokł. Akad. Nauk SSSR. **121**, 720 (1958)
183. Tashiro, C., Kawaguchi, K.: 6th ICCC Moskwa, vol. II/1, p. 227. Moskwa 1974; Cem. Concr. Res. **7**, 69 (1977)
184. Mitsuda, T., Taylor, H.F.W.: Cem. Concr. Res. 5, 203 (1975); Miner. Mag. **42**, 229 (1978)
185. Kalousek, D.: Am. Ceram. Soc. Bull. **40**, 236 (1961)
186. Diamond, S., White, J.L., Dolch, W.L.: Am. Min. **51**, 388 (1966)
187. Gard, J.A.: Nature. **211**, 1078 (1966)
188. Dent Glasser, L.S., Glasser, F.P., Taylor, H.F.W.: Quart. Rev. **16**, 343 (1962)
189. Taylor, H.F.W.: J. Appl. Chem. **10**, 317 (1960)
190. Taylor, H.F.W.: Acta Cryst. **8**, 440 (1955)
191. Odler, J., Skalny, J.: J. Appl. Chem. Biotechnol. **23**, 661 (1973)
192. Verbeck, G.: 4th ICCC Washington, vol. I, p. 453. Washington (1960)

193. Copeland, L.E., Kantro, D.L.: In: Taylor, H.F.W. (ed.) w The Chemistry of Cements, p. 313. Academic Press, London (1964)
194. Idorn, G.N.: 5th ICCC Tokyo, vol. III, p. 411. Tokyo (1968)
195. Clayden, N.J., Dobson, C.M., Growes, G.W., Rodger, P.A.: 8th ICCC Rio de Janeiro, vol. III, p. 51. Rio de Janeiro (1986)
196. Kalousek, G.L.: Mater. Rep. Stand. **5**, 292 (1965)
197. Kalousek, G.L.: 3rd ICCC London, p. 334, London 1955; 5th ICCC Tokyo, vol. III, p. 523. Tokyo (1968)
198. Buckle, E.R., Taylor, H.F.W.: J. Appl. Chem. **9**, 163 (1959)
199. Aithen, A., Taylor, H.F.W.: 4th ICCC Washington, p. 285. Washington (1960)
200. Kantro, D.L., Brunauer, S., Weise, C.H.: Portl. Cem. Ass. Rep. Dep. Bull. 140, Chicago (1961)
201. Lach, V., Bures, J.: 6th ICCC Moskwa, vol. II/2, p. 129. Moskwa (1974)
202. Luke, K., Taylor, H.F.W., Kalousek, G.L.: Am. Ceram. Soc. Bull. **58**, 334 (1979)
203. Butt, M.J., Raszkowicz, L.N.: Cemient. **22**, 21 (1956). (in Russian)
204. Harker, R.: Min. Mag. **34**, 232 (1965)
205. Kurdowski, W., Pilch, M.: 9th ICCC New Delhi, vol. IV, p. 175. New Delhi (1992)
206. Aleksanderson, J.: Swedish Cement and Concrete Research Institute of Technology Stockholm, Proceedings, 43 (1997)
207. Ludwig, N.C., Pence, P.A.: J. Am. Constr. Inst. **52**, 673 (1956)
208. Odler, J., Gebauer, J.: Zement–Kalk–Gips. **55**, 276 (1966)
209. Silchenko, L.A., Michajłov, M.W., Rebinder, P.A.: Dokł. Akad. Nauk SSSR. **167**, 391 (1966). (in Russian)
210. Budnikow, P., Erschler, E.: Special Report 30. Highway Research Board, Washington (1966)
211. Keil, F., Narjes, A.: Zement–Kalk–Gips. **12**, 126 (1959)
212. Kurdowski, W., Peukert, J., Mróz, H.: XXI Konferencja Naukowa Komitetu Inżynierii Lądowej, PAN i KNPZITB, p. 3. Krynica (1979). (in Polish)
213. Peukert, J.: VIII Konferencja Techniczna Przemysłu Betonów, Kruszywo–Cement–Beton, p. 166, Jadwisin (1978). (in Polish)
214. Kurdowski, W., Peukert, J.: Non published data
215. Takemoto, K., Kato, H.: 5th ICCC Tokyo, vol. III, p. 563. Tokyo (1968)
216. Kurdowski, W., Szuba, J.: Il Cemento. **84**, 107 (1987)
217. Hara, N., Inoue, N.: 7th ICCC, Paris, vol. III, p. IV–13. Paris (1980)
218. Luke, K., Taylor, H.F.W.: Cem. Concr. Res. **14**, 657 (1984)

Chapter 5
The Properties of Cement Paste

The properties of cement paste arouse much interest because of their great impact on the fresh concrete quality. The consistency, workability and setting time of concrete mixture are dependent on the rheological properties of fresh cement paste. The heat of hardening and consequently the temperature rise, and the chemical shrinkage are related to the composition of cement as well as the latter governs the strength development and the class of concrete. The knowledge of these properties and their evolution under the influence of several factors gives the possibility to select cement type and its fineness, as well as the composition of concrete mixture. The harmful effect of concrete mixture stiffening could be attributed to the disturbance of cement paste setting. At this early age the rheological properties of cement paste play a decisive role in rheology of concrete. Then the concrete mixture can be considered as a suspension of aggregate in cement paste. In the mixture under stress the displacement of aggregate grains in the surrounding paste takes place. Therefore the rheological properties of concrete are related to the rheological properties of paste and to the paste–aggregate interactions; this effect is more visible in the case of high share of paste in the concrete mixture. The properties of cement has also the decisive effect on superplasticizer type choosing, which finally assures the adequate yield stress value and plastic viscosity of concrete mixture. The last one should be maintained on a constant level during at least two hours, at low w/c ratio. This appropriate interaction between the superplasticizer and cement paste is determined as "cement–admixture compatibility".

At the later age cement paste has a great impact on strength development and the temperature evolution after concrete placement, its drying shrinkage and swelling during wetting. Finally, the phase composition of the paste affects strongly the corrosion resistance and the durability of concrete constructions.

W. Kurdowski, *Cement and Concrete Chemistry*,
DOI 10.1007/978-94-007-7945-7_5, © Springer Science+Business Media B.V. 2014

5.1 The Rheological Properties of Concrete[1]

At the early age cement paste has a form of concentrated suspension of cement grains in water. The structure of this suspension depends on the w/c ratio and fineness of cement. It is also affected by the forces acting between cement grains and water molecules on which in turn the surface charge of cement grains, ions concentration in solution and adsorption phenomena are influencing. These surface charges of cement particles are the result of unsaturated valences of ions on these surfaces, which are formed during grinding of clinker nodules. The crushing of these nodules occurs accidentally and therefore not only on the surface of cement grains different clinker phases are exposed but also these particles have opposite charges. This is shown in Fig. 5.13 where the quartz grains are an example. However, contrary to quartz cement grains are polymineral; it means that different phases can occupy their surface and the isomorphous substitutions, commonly occurring in clinker phases, increase the variety of surface ions.

The presence of opposite charges on the cement grains surfaces is causing their flocculation in diluted suspension, with conglomerates formation and quick sedimentation. As it has been found by Helmuth [1], in diluted suspension these conglomerates will have the w/c ratio of approximately 0.4. In dense suspensions, which are basically cement pastes, the individual conglomerates in standstill show the susceptibility to form a continuous structure. However, the grains are not distributed uniformly in this structure, but they form the aggregates with higher solid phase content and between them the areas filled with water remain. The particles inside these aggregates show the tendency to approach each other at the distance corresponding to the minimum configuration energy [2].

The studies of sedimentation did not show the flocculation effect, only for the grains with diameter higher than 45 μm [3]. The more homogenous distribution of cement grains in water is improved by paste mixing. During mixing the continuous destruction of structure takes place, as the paste reveals tixotropic properties. For every shear rate value an equilibrium (or, according to Helmuth [1], some specific dimension of aggregates), with some constant apparent viscosity during certain period, is attained. This process is associated with re–arrangement of the structure. During mixing break the re–formation process, of the known structure, composed of conglomerates occurs gradually. Due to the paste fluidity (plastic viscosity) during mixing, this structure is week and shows only some limited shear stress value at static state (yield stress value).

The application of plasticizers leads to the complete dispersion of cement grains in water, without conglomerates formation. It is assumed that the molecules of superplasticizer are adsorbed on the surface of cement grains which is neutralizing the

[1] More detailed information of the properties of cement paste and concrete mixture can be find in the following books: Tattersall, G.H. and Banfill, P.F.G. “The Rheology of Fresh Concrete”, Pitman Books, London 1983; Ramachandran, V. S. (Ed.), Concrete Admixtures Handbook, Noyes Publishers, New Jersey 1995.

surface charges and giving all of them the like charge (negative or positive), causing the electrostatic repulsion between these grains.

Several models have been proposed to present the structure of cement paste in which it is commonly assumed that the continuous water layer is formed on the surface of cement grains. A strong attraction of water molecules[2] by the grains surface is a good explanation of this phenomenon. At vigorous mixing or use of plasticizers this water layers tend to have the equal thickness. At first approximation the thickness of this layer is determined by dividing of water volume by the equivalent diameter of cement grain. For example in the paste produced at w/c = 0.5 from cement of specific surface area of 430 m^2/kg, the thickness of water layer will be 1.2 μm; it means about 1/10 weighted average of equivalent grain diameter. In another model the volume of water filling the space between grains is taken into account [4].

The following relationship was proposed by Bombled [4]:

$$d = 2 \times 10^3 \frac{\mathrm{w/c} - 0.12}{S} \tag{5.1}$$

in which

d	distance between the grains (thickness of water layer in μm),
w/c	water to cement ratio,
S	specific surface area of cement (m^2/kg),
0.12	assumed ratio of water in the free space, not belonging to the surface layer.

Cement hydration reactions occur simultaneously and a significant amount of gypsum became dissolved. The liquid phase becomes saturated with the Ca^{2+} and SO_4^{2-} ions and contains the significant part of alkalis, released from cement to the solution (Fig. 4.3). Some amount of ettringite is formed during a few minutes which affects strongly the paste rheological properties, during the induction period. The initial reaction of alite with the formation of C–S–H gel affects also the rheology of cement paste in this period. These topics are discussed in details in Sect. 6.6, focused on the cement–superplasticizer compatibility. The rapid calcium hydroxide crystallization and accelerated hydrolysis of alite after the induction stage results in the significant growth of the paste viscosity. During this period, called the acceleration of cement reaction with water, the rheological properties of paste reveal substantial changes with time.

Several methods were applied in the studies of rheological properties of paste; those based on the acoustic wave velocity, as well as on the measurements of resistance against the force in of penetrator (similar to Vicat apparatus for setting time measurements), also based on the pressure transfer in the paste and different rotation methods: with spindle and finally viscometers with co–axial cylinders [5].

The majority of measurements have been done in dynamical conditions, with the use of co–axial cylinders. However, this method does not give the possibility of precise measurement of the yield stress threshold value. This will be discussed later in this chapter.

[2] The water molecules are dipoles and they can form the bonds: dipole–dipole or ion–dipole.

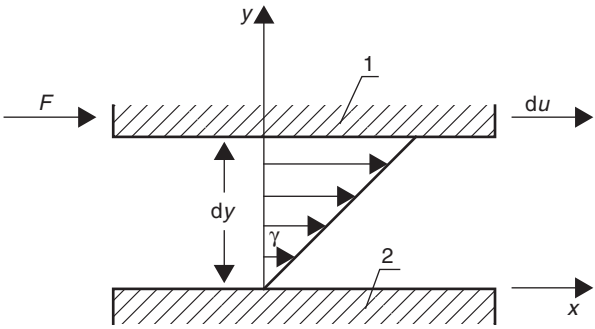


Fig. 5.1 Shear deformation of thin fluid layer: *1* movable–plane, *2* fixed plane

This studies have shown that the rheological parameters are affected by the type of measuring device, composition of the paste and rheological "history" of the sample. The pastes can be attributed to the Newtonian or non–Newtonian types of liquid; between the later the plastic (Bingham), pseudo–plastic or exhibiting the dilatancy phenomena can be differentiated. Moreover, the pastes reveal basically the thixotropy or anti–thixotropy properties.

There are several hypotheses as the rheological properties of cement pastes are concerned. As it is commonly known the rheology deals with the flowing and deformation of materials under stress. The Newtonian fluids show a simple relationship between the shear stress and shear rate. When a thin layer of fluid is placed between the two parallel plates, of which one is fixed and the second will be subjected to the shearing force F, then the shearing of this layer will occur. The dynamic equilibrium will be attained when the force F, in the condition of stationary flow, will be balanced by the viscosity of Newtonian fluid and the relation between the shear stress and shear rate gradient will be linear (Fig. 5.1).

$$\frac{F}{A} = \tau = \eta \frac{\mathrm{d}u}{\mathrm{d}y} = \eta\dot{\gamma} \tag{5.2}$$

where

η means the liquid viscosity,
A the surface of plate,
τ shear stress,
$\dot{\gamma}$ shear rate.

This behaviour is typical for all gases, liquids and solutions of low molecular weight compounds [6]. However, the colloidal suspensions, for example the water suspensions of clay minerals, cement pastes, polymers decline from this rule and they are rated among the non–Newtonian fluids.

The so–called flow curves for some types of non–Newtonian fluids, to which cement pastes belong, are plotted in Fig. 5.2. The hypothesis explaining the properties of Bingham fluid assumes that in standstill it has a three–dimensional structure, which elasticity is strong enough to overcome the shear stress lower than the yield

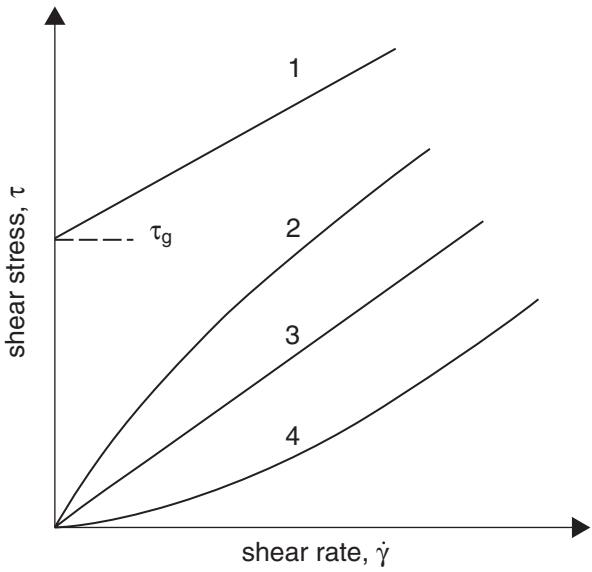


Fig. 5.2 Flow curves of non–Newtonian fluids: *1* Bingham fluid, *2* pseudo–plastic, *3* Newtonian fluid, *4* dilatancy showing fluid, τ_g yield stress value of Bingham fluid (plastic)

stress value τ_g. The structure of fluid is destroyed at the stress exceeding the yield stress value and then the fluid transforms into the Newtonian one, flowing under the τ—τ_g stress. Successively, when the shear stress becomes lower than the yield stress value, the structure will be again rebuilt. The rheological properties of this plastic fluid are represented by the following equation:

$$\tau - \tau_g = \eta_p \dot{\gamma} \tag{5.3}$$

where

η_p means the plastic viscosity.

The pseudoplastic fluids do not show yield stress value. Their apparent viscosity decreases with the shear rate. The flow curve reveals linear character at very high shear rate. The logarithmic plot of shear rate as a function of shear stress of these fluids is often a straight line with the slope between 0 and 1. For the pseudoplastic behaviour description is hence frequently used the power–law equation:

$$\tau = k\dot{\gamma}^n \tag{5.4}$$

where

k and *n* are the parameters typical for the pseudoplastic fluid,
k is representing apparent viscosity,
n a factor describing the departure from the Newtonian fluid.

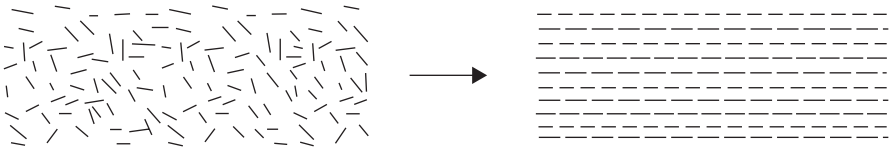


Fig. 5.3 The anisometric particles arrangement in the pseudoplastic fluid under the shear stress

One should remember that k is a function of n. The apparent viscosity η_a of this fluid can be therefore expressed using n as:

$$\eta_a = k\dot{\gamma}^{n-1} \tag{5.5}$$

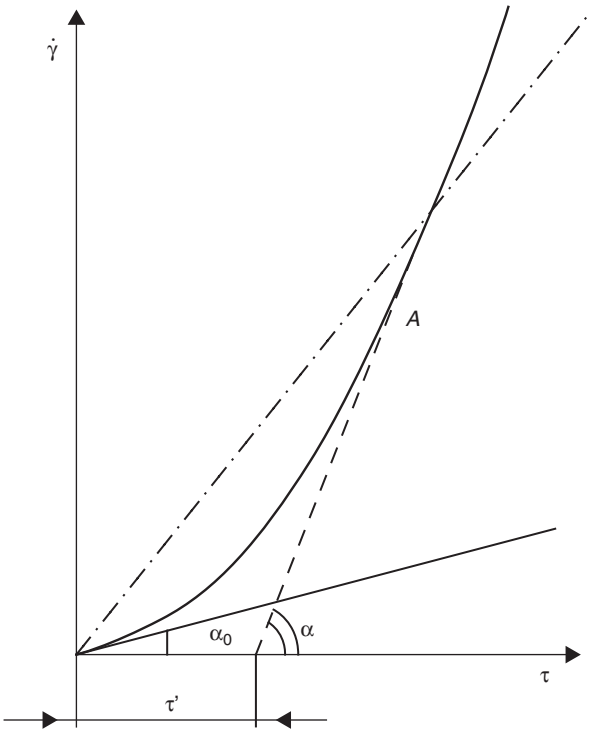
The suspensions with asymmetric particles show the properties of pseudoplastic fluids. This phenomenon can be probably explained by the ordering of these particles with increasing shear rate (Fig. 5.3). Therefore, instead of the random, disordered distribution in the immobile fluid, the progressive flow results in the alignment of particles (crystals) with their longest axis along the direction of flow. Consequently, the apparent viscosity becomes lower with increasing shear rate until the maximum compact distribution of particles is attained. The interruption of flow results in rearrangement of initial disordered distribution of particles. A high apparent viscosity of fluid at standstill can be thus explained. This is a reversible phenomenon and occurs rapidly; the measurements of viscosity do not allow indicating the right time when the structure is formed again. Otherwise this fluid could be a tixotropic one.

The pseudoplastic fluids can be consider as the Bingham fluid with the yield stress value τ'_g and plastic viscosity equal to tg α and it is the reason of their name (see Fig. 5.4).

The dilatancy showing fluids do not have yield stress value. The apparent viscosity of these fluids increases with the rise of shear rate. They generally comply the power law and n constant is higher than 1. The behaviour of these fluids can be explained in the following way [6]: at standstill they have minimum porosity and all pores are filled with liquid phase. At low shear rate the liquid phase plays a role of "grease", reducing the friction of solid grains in the suspension; therefore the shear stresses are relatively low. With growing shear rate the close packing of grains is destroyed. Consequently the suspension is expanded (dilatation) and the porosity becomes higher. The liquid phase (matrix) cannot act as "grease" and the stress required for maintaining the flow significantly increases. The destruction of close packing causes the violent increase of apparent viscosity with the rise of shear rate. The quartz sand water suspension is an example of dilatancy showing fluid.

The thixotropic fluids have an apparent viscosity, dependent not only on the shear rate but also on the shear time. Therefore the flow curve of thixotropic fluids, opposite to the all types of aforementioned fluids, which curves for increasing and decreasing shear rate were superimposed (giving one curve), form a hysteresis loop (Fig. 5.5). As results from these curves the apparent viscosity of tixotropic fluids is decreasing with time (Fig. 5.6), because of the progressive structure destruction.

Fig. 5.4 Pseudoplastic fluids



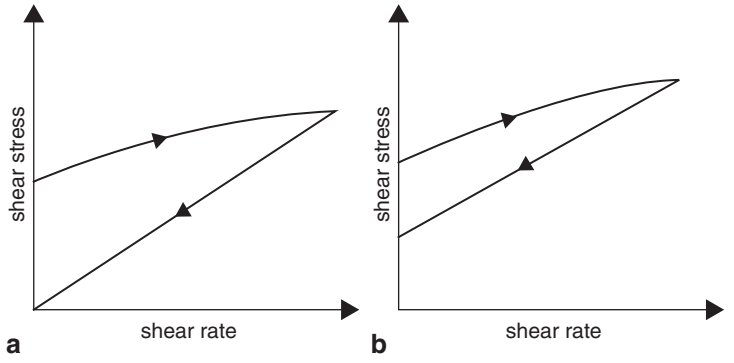


Fig. 5.5 Hysteresis of flow curves for the tixotropic fluids: **a** tixotropic fluid. **b** plastic tixotropic fluid

The rate of structural degradation depends on the number of bonds which can be destroyed. However, the rate of immediate reconstruction of the structure is increasing with time, as the number of potential bonds is rising. Finally, the dynamic equilibrium is attained, in which the rate of structure reconstruction is equal to the rate of decomposition. This equilibrium state is controlled by the shear rate and shifts toward the higher structure disintegration, with the growing shear rate.

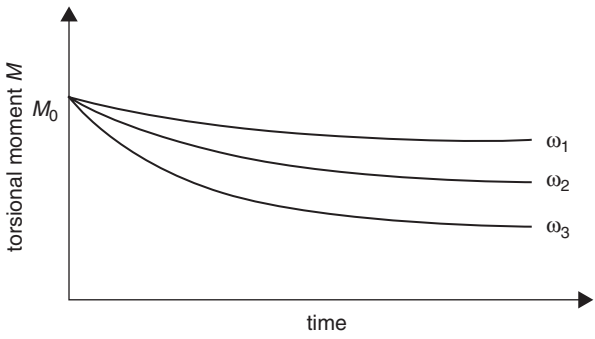


Fig. 5.6 Thixotropy phenomenon; M_0 torsion moment at shear beginning, $\omega_1 < \omega_2 < \omega_3$ angular velocities

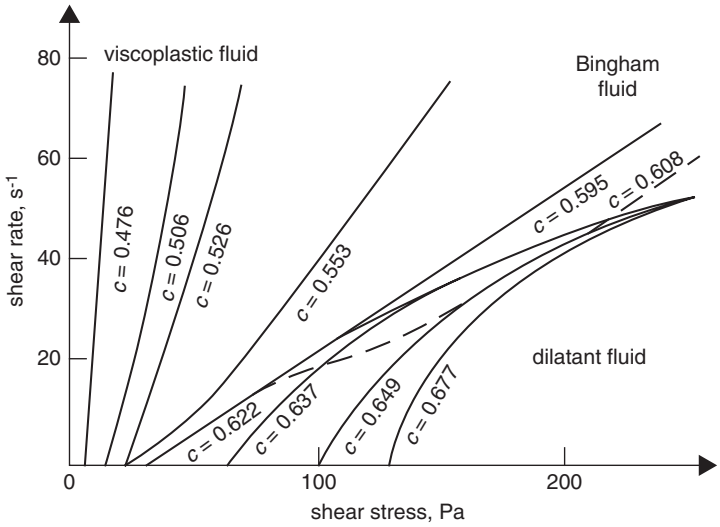


Fig. 5.7 Flow curves of mortars as a function of solid phase content. (according to [7])

Thixotropy is a reversible process and in an immobile state of fluid the continuous, progressive ordering of structure occurs. The one flow curve without hysteresis can be obtained, but the share must continue until the equilibrium is attained. The structure of ordinary tixotropic fluids is totally destroyed at high shear stress. After the shear stress elimination they behave like normal fluids until the structure is rebuilt. There are also the tixotropic plastic fluids (Fig. 5.5) which do not lose totally the features of plastic fluids which is evident from the stable, however, even low yield stress value. Some suspensions show outstanding features; the structure is formed under the shear stress exclusively and without shear it collapses; these fluids show a rheopexy. These properties are appear at moderate shear rate only.

As it was aforementioned, the rheological properties of cement pastes are dependent on many factors. In Fig. 5.7 the evolution of the properties of pastes from the pseudoplastic fluids through the Bingham fluid to the showing dilatancy, at higher

concentration of solid phase [7]. When the volume ratio of solid phase exceeds 0.6, the resistance against shear stress increases with shear rate and simultaneously the increase of volume is occurring. It is the result of cement grains packing change, necessary for these grains mutual movements along the slip plane. The distance between the grains increases perpendicularly to the shear direction. The enlarged distances of grains must be filled with water; therefore the apparent viscosity is the function of shear rate and the permeability of suspension to water flow. This is associated with the intrusion of some air quantity into the paste, as the necessary dilatancy of material under the occurring shear. The limit of solid phase concentration in the suspension is insignificantly raising to 0.62, when the vibration is applied [1].

The water to cement ratio and the fineness of cement are the two important factors determining the properties of cement paste. The thickness of water layer on cement grains and the distance between the grains are dependent upon these parameters, which have the significant effect on the rheological properties of paste, first of all on the yield stress value.

Legrand [7] proposed the following empirical formulae to calculate the threshold stress (yield stress value) of the paste at standstill, before any mixing operation, expressed as a function of the volume share of solid phase:

$$f_0 = A\mathrm{e}^{a(c-0.5)} \tag{5.6}$$

where

A and a are the constants determined experimentally,
c the concentration (by volume) of the solid phase (dissipated). This formula is true for c value in the range from 0.475 to 0.677 (this corresponds to w/c 0.15 and 0.35 respectively).

Another formula, with w/c instead of c can be also used:

$$f_0 = \frac{0.124}{(\mathrm{w/c} - 0.15)^{3.97}} \tag{5.7}$$

The water does not belonging to the layer is defined as 0.15. This formula relates to the cements with constant specific surface area. The effect of surface is taken into account in analogous formula:

$$f_0 = 4.47 \times 10^{-9}\mathrm{S}^{4.01} \tag{5.8}$$

Legrand [7] has shown also that the change of cement grains shape from the prismatic into the spherical one transforms the paste from the pseudoplastic into the Newtonian fluid. It is known simultaneously that this effect—transformation of paste into the Newtonian fluid—can be achieved by use of plasticizing agent [8]. The yield stress value falls also down to zero in the case of vibration. The constant a in the formula (5.6) depends on the shape of grains and type of material but is not related to the specific surface area or the grain size distribution. This constant

changes in the range from 23 to 48; the extreme values correspond to the spherical and prismatic forms respectively. However, the constant A is rising rapidly with the specific surface area, up to the value of 100 Pa. The analogous formula (5.9) is valid for the shear stress measured at constant shear rate, when the paste has been vibrated:

$$\tau = B\mathrm{e}^{b(c-0.5)} \tag{5.9}$$

B and b—are the experimental constants. This formula relates to the c lower than the value corresponding to the transformation of paste from the dilatancy showing fluid to the pseudoplastic one. The constant b depends on the shear rate, type of material and shape of grains but not on the specific surface area and the grain size distribution. The constant B depends on the shear rate and specific surface area of cement.

Long ago it was believed that the rheological properties of cement paste at the beginning of the induction period would not be affected by the phase composition of cement [9]. The similar view, related to the chemical cement composition were also presented by Odler et al. [9], with a remark that this is valid in the case of cements with proper setting. Then it relates to cements containing the sulphates with the rate of solubility corresponding to the reactivity of C_3A phase with water (see Sect. 4.1.2). However, the effect of C_3A becomes clearly recorded after 45 min of hydration [10]. The rheological properties of paste are strongly affected by the content and kind of calcium sulphate added to cement [11]. The influence has particularly the solubility and rate of dissolution of different calcium sulphate phases. In cements with low C_3A content the liquid phase is saturated with calcium sulphate, which acts as a strong flocculating agent, reducing the solubility of calcium aluminate and accelerating the hydration of silicates. At high C_3A content the crystallization of ettringite occurs and the content of sulphate ions is decreasing [11]. In order to improve the rheological properties of the paste gypsum is replaced by a mixture of lignosulphonates and sodium carbonate, which significantly decreases the viscosity and the paste is reaching the properties of *quasi*–Newtonian fluid [12]. This opinion is valid nowadays, however, it should be better presented and this issue will be discussed in Sect. 6.6.

The pastes show always the three–dimensional structure and very often they show tixotropic properties. They change quickly with time as a result of progressive hydration; therefore the same paste can have the tixotropic and anti–tixotropic behaviour [13]. Obviously, it depends on the proportions between the rate of structure destruction and reconstruction. The latter one is directly related to the hydration process. The anti–tixotropic properties are dominating after longer period of hydration and depend upon phase composition and fineness of cement.

Variety of flow curves of cement pastes can be explained basing on the analysis of destruction and reconstruction processes of tixotropic structure, occurring during mixing and the other experimental operations, as well as after their interruption. Bombled [4] attributed the tixotropy phenomena to the degree of flocculation, defined as ratio of the mean size of conglomerates to the weighted average size of

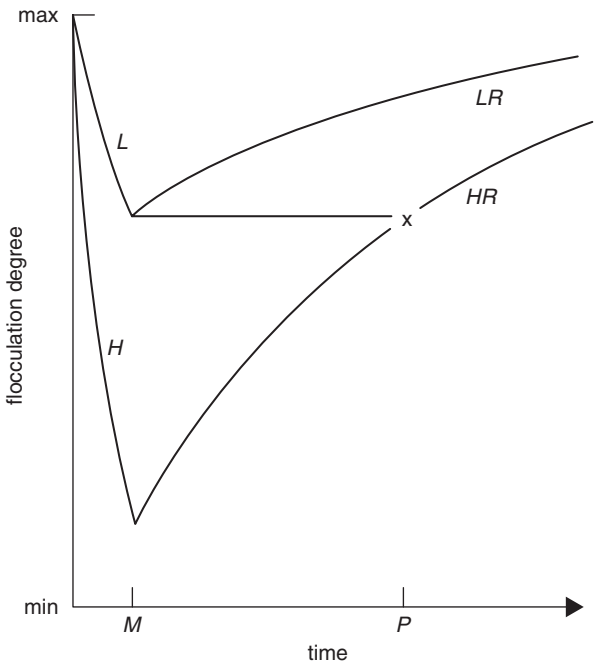


Fig. 5.8 Changes of the degree of cement particles flocculation in the paste during mixing: with high intensity *H* and with low intensity *L*, as well as the growth of degree of flocculation after mixing *HR* and *LR* (according to [1]); *M* end of mixing, *P* time after which the degree of flocculation of the paste vigorously mixed is the same as in the paste mixed with low intensity

cement grains. Bombled [4] assumed afterwards that the degree of flocculation depends on the time of mixing and on the time of storage after mixing; these changes are shown in Fig. 5.8. The first part of the upper curve corresponds to the mixing with low intensity during time *M*, followed by the reconstruction of the structure after mixing interruption. The lower curve represents the changes of the same paste during and after vigorous mixing. It has been presumed that the time constant for the reconstruction is at least ten times higher than the one for the destruction of conglomerates. This is well compatible with the experimental results—the time constant of the structure destruction is approximately 1 minute while the time of reconstruction corresponding to the change of flow curve from that corresponding to the anti–thixotropy to the thixotropy one is 30 to 45 min [9, 10, 14].

The pastes with higher dissipation will show higher rate of structure reconstruction (formation of bonds between the grains), thus favoring the anti–tixotropic behaviour.

The changes of degree of flocculation during the single measurement with rotation viscometer, according to Bombled [11], are shown in Fig. 5.9. The shear rate changes are shown in bottom part of the figure. The dotted line *N* shows the change of flocculation degree of the paste, in which a slow destruction of structure occurs at low shear rate. Then the degree of flocculation is reduced more rapidly, and again shows slower changes during the decreasing share rate. In the immobile paste the degree of flocculation is increasing quickly along the curve 0. The total effect, from superimposing of *N* and 0 curves, gives the changes of flocculation degree presented by the curve *S*. The course of this curve can vary and approach to the limiting

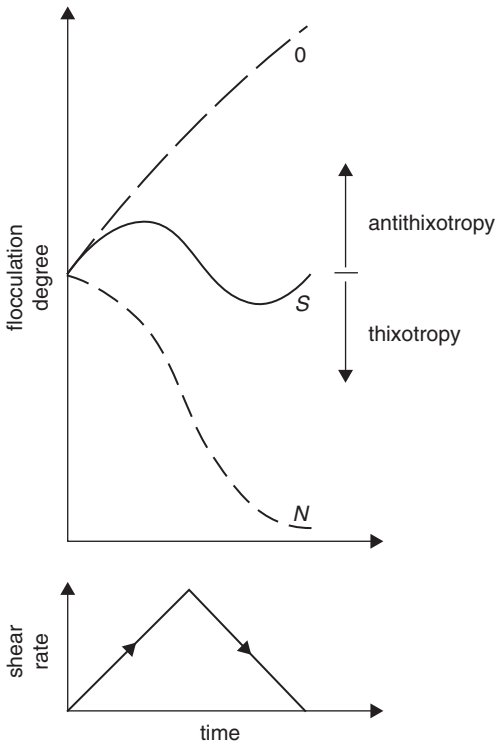


Fig. 5.9 Changes of the flocculation degree of particles in cement paste during the measurements in rotation viscometer at one cycle of increasing and decreasing shear rate. (according to [11])

N and 0 curves, depending on the conditions of measurements; then the paste will reveal the tixotropic or anti–tixotropic properties.

Banfill [13] is distinguishing three types of flow curves for cement pastes showing tixotropic properties, which is presented in Fig. 5.10. The reason of flow curves proceeding, corresponding to the type 1 and 3 was explained earlier. The kind of curve 2 can be considered as an intermediate between 1 and 3. Banfill [13] explains that the curves 2a can be obtained from 2b by cutting the upper *CD* loop and 2c by cutting the lower *AB* loop. These courses are produced at low changes of the rate of structure destruction and reconstruction. The authors are of the opinion that the hysteresis loops are of limited significance in the evaluation of the rheological properties of the paste. In order to obtain the flow curves for the apparent viscosity and yield stress value determination the measurements must be performed in a short time, not longer than 2 min after cement mixing with water [11]. At longer time, because of higher amount of hydrates formation, the curve 3 is obtained (Fig. 5.10). The time of this type of flow curve (anti–tixotropic) is received after a time dependent on the reactivity of cement and the sequence of changes is then 1–2–3. The choice of testing time of given cement can result in obtaining every type of flow curve.

The sample preparation before test, thus it mixing, can cause the changes of paste behaviour. The vigorous mixing during the 5–10 min is usually applied and

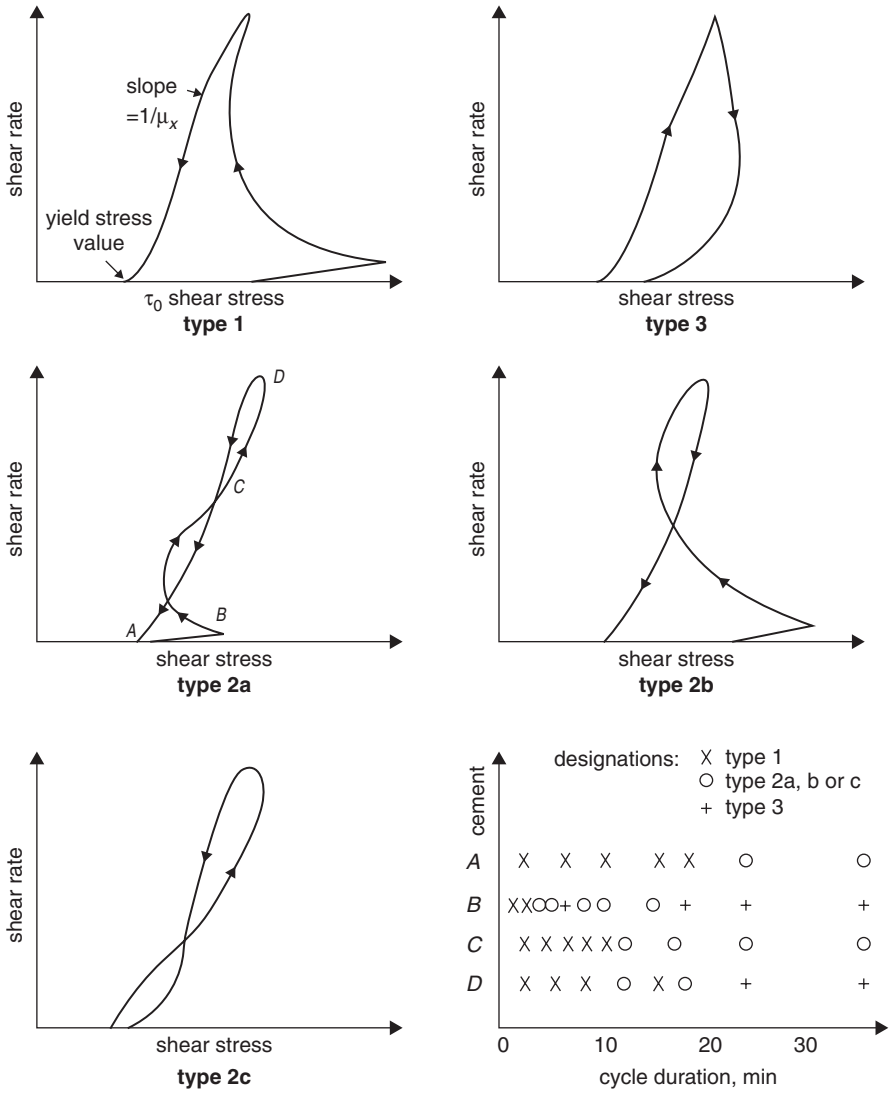


Fig. 5.10 Three types of flow curves for the pastes showing tixotropic properties. (according to [13])

the lowest viscosity of paste is thus achieved. Too weak or too strong mixing results in the viscosity increase. Too short mixing process, up to 1 min, results in the stiffening of the paste, known as a "short mixing setting"; this is caused by the mutual linking of cement grains by hydration products formed on their surfaces during initial reaction. There is an opinion that the 5 min mixing is necessary to remove the symptoms of false setting, derived from the presence, in industrial cements, of some amount of gypsum hemihydrate. At prolonged vigorous mixing during more than 5 min the hysteresis loop became narrow and, as an effect, the *quasi*–Bingham

fluid is produced; the share rate—share stress curves for increasing and decreasing shear rates are interfering.

There are three methods of cement pastes testing with co–axial rotation viscometers:

- at constant shear rate,
- at steadily increasing or decreasing shear rate,
- at shear rate changing continuously.

The equilibrium conditions between the shear stress and shear rate are obtained only in the first method. The two other methods give different flow curves corresponding to the tixotropic or anti–tixotropic fluids. They do not give the quantitative characteristics of the rheological properties of paste [15, 16].

Legrand [15] recommends to apply a constant shear rate and proposes simultaneously the following conditions to obtain the correct measurements with co–axial rotation viscometers:

- the fluid should be homogenous (after 10 min the sedimentation of paste affect the measurements),
- the flow should be laminar, at higher shear rate the disturbances of flow can occur [11],
- the paste should not slide on the surface of cylinder,
- the flow should be stable; it means among others that the rotation velocity of movable cylinder should be constant.

Another group of possible errors arises from the characteristics of apparatus, evaluation of rotation velocity of cylinders and torque, measured as net torque [15]. These problems do not appear in the case of Newtonian or Bingham fluids, while the tixotropic one reveal several problems because the gradient of velocity in the space between the cylinders depends on the paste rheological properties which are to be tested. There are different ways to resolve this problem: Nagataki and Kawano [17] measured directly the distribution of velocity gradient in the space between the cylinders. The assumption that this gradient is linear is not a correct approach, particularly when it appears later that this is not true; it is an error and not the approximation [15].

It has been found that in the case of viscometers with co–axial cylinders, the flow is not homogenous if the distance between cylinders is too wide [1, 18]. The maximum distance should be not higher than 1 mm [1]. At higher distance the flow curves correspond to the pseudoplastic fluids with no clearly marked yield stress value. For low shear rate the flow of paste in the gap between the cylinders is not uniform as long as the stress does not exceed the yield stress value; this can be derived from the Reiner–Rivlin equation:

$$N = \frac{T}{4\pi\eta_p h}\left(\frac{1}{R_b^2} - \frac{1}{R_c^2}\right) - \frac{\tau_g}{\eta}\ln\frac{R_b}{R_c} \tag{5.10}$$

where

N is the rotations per minute,
R_c radius of outer cylinder,
R_b radius of inner cylinder,
T turning moment,
τ_g yield stress,
η_p apparent plastic viscosity,
h cylinder height.

Only for $T/(2\pi R_C^2 h) > \tau_g$ all the volume of paste will flow. However, also in these conditions and even at higher shear stress and shear rate Tattersall [19] found the non–uniform flow. This author states that because of this phenomenon, the results obtained with viscometers with co–axial cylinders are not reliable [19].

Roy [8] has shown that at the distance between the cylinders 0.7 mm it was possible to determine clearly the yield stress value and the ascending curve is basically a straight line. It is important to eliminate the vibrations and shocks during the testes with the rotation viscometer, because the shape of curves can be changed. Finally, at low shear rate a slide of paste along the walls of the cylinder occurs and the yield stress value is thus six times lower. It is assumed that this effect can be eliminated by proper profiling of the cylinder surfaces or applying the grooved surfaces; however, there is not consistent opinion about this in the literature [18]. According to Hanehara and Hamada [20], the slide is observed particularly when the paste shows low plastic viscosity and high yield stress value. However, at high shear rate the centrifugal force can lead to the size segregation of cement grains in the paste [21].

According to Legrand [15], two parameters can be determined using viscometers with co–axial cylinders: initial yield stress value for the paste not subjected to shear previously and final apparent viscosity, corresponding to the steady state flow of the paste. The other indirect data are strongly affected by the test conditions and characteristics of apparatus [15].

The flow of pastes can be relatively well described by the following models:

Bingham model
$$\tau = \tau_g + \eta_p \dot{\gamma} \tag{5.11}$$

Hershel–Bulkely model
$$\tau = \tau_g + A\dot{\gamma}^B \tag{5.12}$$

Robertson–Stiff model
$$\tau = A(\dot{\gamma} + C)^B \tag{5.13}$$

(In the equations A, B and C mean the constants).

The equations (5.12) and (5.13) are composed of two terms, a constant one, corresponding to the yield stress value and an exponential one. The latter relates to the destruction of the structure; as a result the resistance of paste against the shear (shear stress) falls down with the share rate increase. The Hershel–Bulkely's model is transforming into the equation of parabola, for $B=2$. The other models were proposed by Costa and Massazza [21].

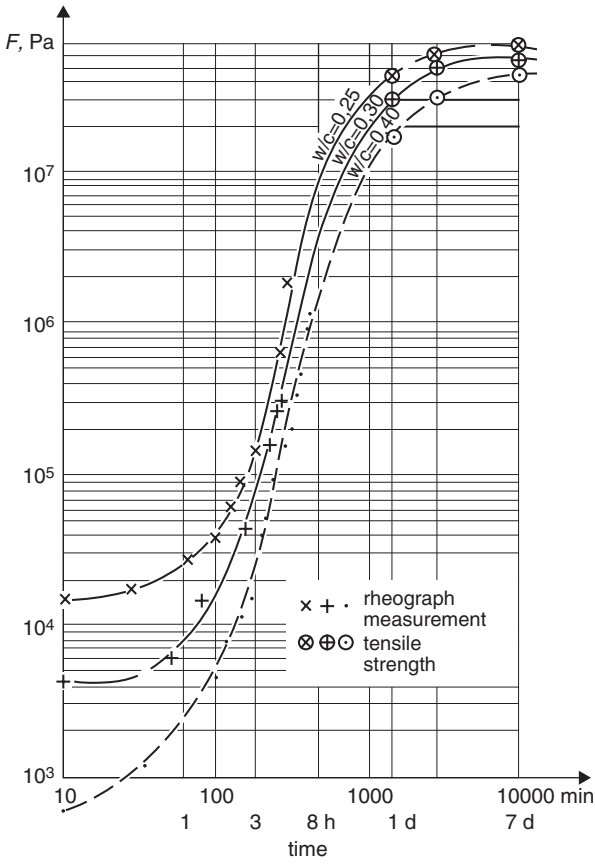


Fig. 5.11 The changes of yield stress value vs time for cement pastes. (according to [5])

Taking into account the reservations about the use of viscometers with co–axial cylinders Bombled [4, 5] proposed the method consisting in the force in of cylindrical penetrator into the paste. The measurements with this method allow rating of cement pastes as *quasi*–Bingham fluids. The resistance to shear stress vs. time, dependent on w/c ratio shows an inflexion occurring in the range from 5 to 15 h (Fig. 5.11). At the same time the elastic properties of paste change, because the measured velocity of acoustic waves propagation is changing [5]. The results thus obtained allow proposing the following relation between the yield stress τ_g, and the distance between the cement grains:

$$\tau_g = k / d^2 \tag{5.14}$$

where

k is a constant,
d distance between the grains.

This distance change vs. time can be also considered:

$$\tau_g \approx \frac{\tau_{g,0}}{(1-t/d_0)^2} \tag{5.15}$$

where

$\tau_{g,0}$ is the initial yield stress,
t time,
d_0 initial distance between the grains.

Introducing to this equation the value of abscissa in the inflexion point Bombled gets the following equation:

$$\tau_g \approx \frac{\tau_{g,0}}{(1-t/T)^2} \tag{5.16}$$

in which

T is the time corresponding to the inflexion point on the curve.

Bombled [4, 5] using constructed device, so–called rheograph, studied the effect of numerous factors on the change of yield stress value. The most important, beside of w/c ratio, is the fineness of cement, as shown in Fig. 5.12. The effect of pozzolanic additions was also studied. The addition of fly ash caused significant rise of yield stress value and apparent viscosity [22]. Nowadays these results are questionable, because of huge amount of experimental data which indicate that in the case of the siliceous fly ash addition the rheological properties of cement pastes are improved; this is explained by the physical effect of spherical fly ash particles. Simultaneously, because of the late pozzolanic reaction occurring in hydration period (see Sect. 7.4), which influences on paste rheology, the paste from cement with fly ash has apparently the "higher" w/c ratio.

The yield stress value, which practically corresponds to the flexural strength of paste, is governing the following properties of fresh paste, primarily: ability to mixing, pompability, workability, sedimentation, stiffening. From the rheology point of view, the hardening process means the *change* of yield stress value vs hydration time. In Fig. 5.12 to the initial setting time and final setting time correspond the yield stress value $2 \cdot 10^4$ and $10 \cdot 10^4$ Pa respectively.

The rheological properties of pastes are strongly affected by the water reducing agents. The pastes behave like the Newtonian fluids with superplasticizers addition [8, 18]. The time of superplasticizer addition is very important. The effect is strong when it is added after longer time from paste producing [3, 23]. This relates to the superplasticizer with the sulphonate groups; this issue will be discussed with details in Sect. 6.6. Petri [24] obtained good correlation with the theoretical model assuming that the paste consists of non–adhesive spherical grains with equal dimensions, and dense packing. The viscosity is given by the following formula:

$$\eta = \eta_0 (1-1.35c)^{-2.5} \tag{5.17}$$

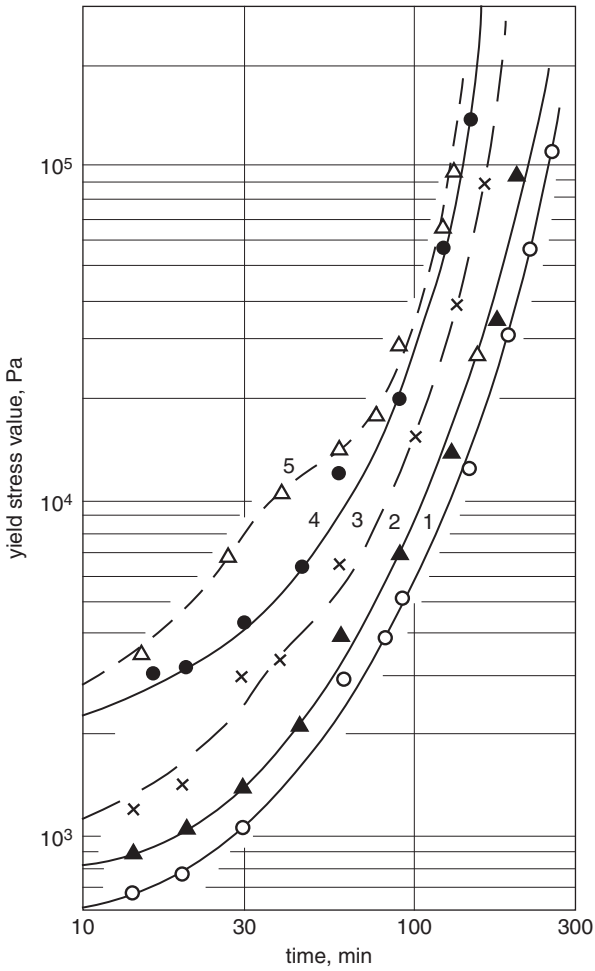


Fig. 5.12 Curves obtained by Bombled with rheograph [4, 5]. Paste with w/c = 0.25 of cements with different specific surface area: *1* 201 m^2/kg, *2* 248.5 m^2/kg, *3* 307 m^2/kg, *4* 403 m^2/kg, *5* 511 m^2/kg

where

c means the volume concentration of the solid phase (dissipated).

The analysis of the rheological properties of cement pastes is complicated additionally by the interaction of solid and liquid phase. In Table 5.1 the approximate size of hydrating cement grains and the distances attributed to the particular types of interactions are shown according to Massazza [21].

The comparatively lowest importance have the hydrodynamic interactions, their role is important at low concentration of the solid phase in the suspension. In the pastes, in which the share of solid phase is substantial, the electrostatic and van der Waals forces are dominating. Moreover, because of the high surface tension of water and the presence of air in the paste, between cement grains the attractive capillary forces appear. They prevail at the grain size from 1 to 0.1 mm. The maximum capillary stress is given by the following Carman formula:

Table 5.1 Interparticle forces. [21]

Forces	Particle size, mm	Interaction	Distance, mm
Capillary	1–0.1	attraction	–
van der Waals	$0.1–10^{-4}$	attraction	$(5–30)\cdot10^{-7}$
Coulomb double layer	$10^{-2}–10^{-6}$	repulsion	$(5–30)\cdot10^{-7}$
Disjoining pressure	$10^{-2}–10^{-6}$	repulsion	$(5–30)\cdot10^{-7}$

$$P_c = \frac{-\lambda F \rho_w / \rho_c}{w / c} \tag{5.18}$$

where

λ is the surface tension of water,
F cement specific surface,
ρ_W, ρ_C density of liquid phase and cement,
w/c water to cement ratio.

The Coulomb and van der Waals forces are of significant importance in the case of colloidal particles: $10^{-2}–10^{-6}$ mm.

On the surface of crystals there are always the non–compensated charges, derived from the non–equilibrated valences of surface atoms, as well as from the isomorphous substitutions. Finally, they can be related to the hydrolysis of amphoteric groups (Figs. 5.13, 5.14).

The non–compensated charges on the surface of solid phase attract the ions from the solution and the electric double layer is formed in the interface. This layer consists of the surface charge of solid particle and the equivalent charge of ions from the liquid phase accumulated near the surface. There are the ions of opposite charge, linked with the strong, rigid bonds to the surface, forming so–called Stern's layer and the so–called diffusion Gouy's layer composed of scattered ions (Fig. 5.15).

The Stern's layer is an internal screen of the electric double layer and stabilizes the charge of colloidal particles. Its thickness corresponds to the one ion diameter and it does not cover the surface completely [25].The thickness is approximately 300 pm; this does not relate to the organic long–chain ions. The external screen is formed by the equivalent number of opposite charged ions. An electric potential of the surface of solid ψ_0, as well as the potentials of internal and external Helmholtz[3] layer are distinguished. The surface potential ψ_0 depends on the concentration in solution of the so–called potential generating ions according to the following Nernst equation:

$$\psi = \frac{kT}{ze} \ln \frac{a}{a_0} \tag{5.19}$$

[3] The outer Helmholtz plane is limiting the Stern's layer and determines the shortest distance available for the hydrated ions from the solution. Inside the internal layer an internal Helmholtz plane is also distinguished which determines the centers of gravity of ions adsorbed on the surface of solid phase.

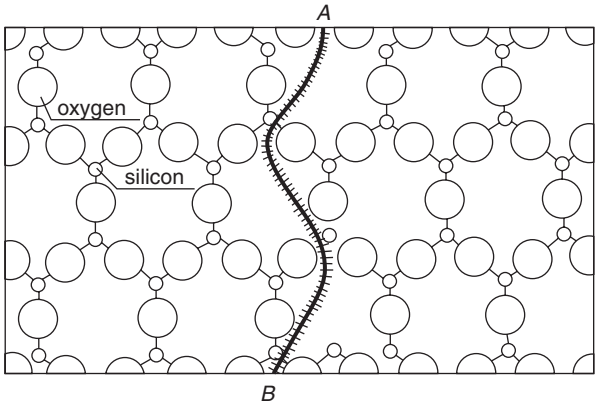


Fig. 5.13 Schematic presentation of the hydrogen and OH^- ions adsorption on the surface of quartz crushed under water (flat image). (according to [25])

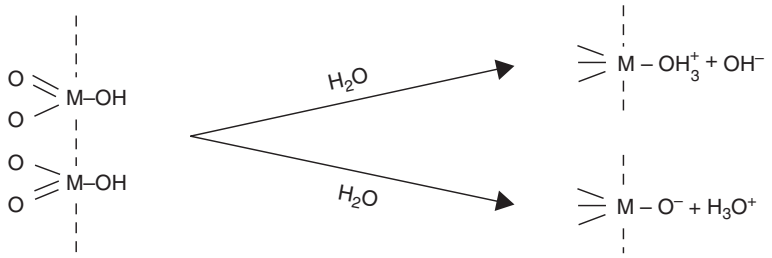


Fig. 5.14 Hydrolysis of OH groups on the surface (according to [21]); the surface of solid phase is marked with the dotted line H_3O^+

where

k	means the Boltzmann constant,
T	temperature
(K), z	valence of potential generating ion,
e	elementary charge,
a	activity of potential generating ion in the solution,
a_0	activity of this ion at $\psi_0 = 0$.

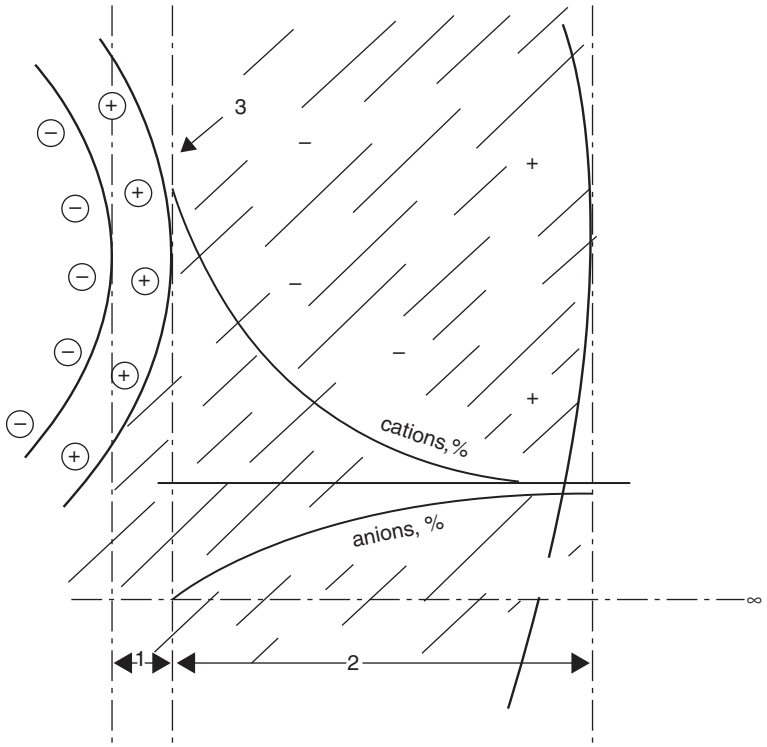


Fig. 5.15 Electric double layer surrounding the particle in the solution; *1* rigid Stern's layer, *2* diffusion layer, *3* shear plane

The external screen is a diffusion layer in which the ions are poorly bonded as the distance from the Stern layer is increasing, and have the tendency to migrate into the solution. Therefore the electric potential in this layer decreases exponentially with the distance from the boundary of Stern layer. On this boundary it is called electrokinetic potential or ζ potential. It can be derived from the measurements of the colloidal particles velocity in the electric field of intensity E. This phenomenon is known as electrophoresis. ζ potential can be determined from the formula given by Smoluchowski:

$$\zeta = \frac{4\pi u \eta}{E \varepsilon} \tag{5.20}$$

where

u is the velocity of particles,
η dynamic viscosity of liquid phase,
E the electric field intensity,
ε specific inductive capacity of the liquid phase.

The thickness of the double electric layer depends on the diffusion layer which is relatively thick. It depends on the concentration of solution and is inversely proportional to the ionic strength of the liquid phase. For the solution with the concentration of 1 mol/l the thickness is close to the diameter of water molecule and it can attain the value of 1000 atomic diameters with the dilution of solution [25]. This thickness is an inverse of the Debye–Hückel function χ:

$$\delta = \frac{1}{\chi} = \sqrt{\frac{1000\varepsilon RT}{8\pi e^2 N^2}} \sqrt{\frac{1}{\mu}} \tag{5.21}$$

where

R is the gas constant,
N Avogadro constant,
μ ionic strength of the solution; the other symbols as in (5.20).

In Fig. 5.15 the important in rheology shear plane, related to the electrokinetic potential, is indicated. It is the potential in the shear plane in relation to the potential of solution, not disturbed by the presence of solid phase. A high potential ζ value is typical for the dissipated colloidal suspension (sol) and the state of coagulation corresponds to the zero value of ζ potential. This potential is reducing with the increasing degree of flocculation.

According to the classic DVLO theory (from the names Deriagin, Landau, Verwey and Overbeck) the stability of colloidal suspension is determined by the equilibrium between the van der Waals attraction forces (V_A) and the electrostatic repulsion, occurring between the electric double layers (V_R). The changes of these forces vs the distance between the colloid particles is shown in Fig. 5.16. The repulsion forces are directly proportional to the product of charges of both particles and decreases with the second power of the distance between them as follows:

$$V_R \approx \frac{q_1 q_2}{\varepsilon r^2} \tag{5.22}$$

where

ε is the permittivity constant of the system.

The van der Waals attractive forces resulted from the appearance and disappearance of instantaneous dipoles in the particles originating from the movement of atom components are as follows:

$$V_A \sim \frac{1}{r^n} \qquad n \approx 6 \tag{5.23}$$

The coagulation occurs when the particles approach on the distance corresponding to the first minimum energy, sometimes to the second minimum. The approach of particles is hampered by the energy barrier, dependent on their size and surface

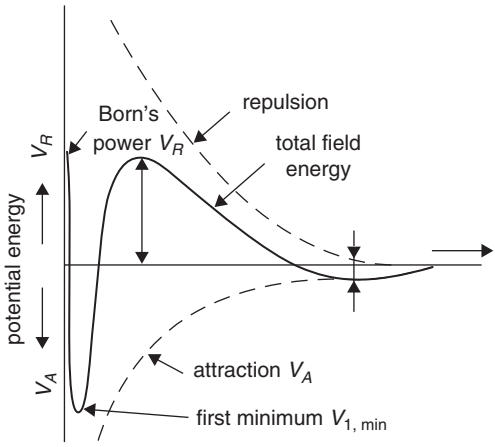


Fig. 5.16 The scheme of potential energy change of two particles

charge. In the case of large particles the resultant potential energy curve reveals a second, significant minimum which can give the flocculation. In the presence of water reducers the surface charge is increasing and subsequently also the ζ potential, and additionally they create the steric effect which counteracts the approach of particles [21].

The changes of electrolyte concentration cause the changes of surface charge and consequently the thickness of diffusion layer. The reduction of this layer favours the coagulation (Fig. 5.17).

The application of classic double layer model to the cement pastes is questionable because the surface in this case is not in thermodynamic equilibrium. The surface of cement grains reacts continuously with water and, as a result, the releasing of different ions into the liquid phase occurs and the surface charge varies all the time. Therefore opposite to the classic double layer its inner part changes continuously. For this reason appeared the concept to replace the classic ζ potential by the dynamic potential, which is changing continuously during the hydration process [26]. However, the ζ potential of hydrating cement is often measured and an example of these measurements results is shown in Fig. 5.18 [27].

On the other side it is difficult to find any relation between the ζ potential and the rheological properties of the paste because the measurements are concerning highly diluted suspensions. Moreover, the rheological measurements relate to the dynamic conditions while the ζ potential is determined in static conditions. In order to give higher practical importance to the electrokinetic measurements, Zelwer [26] recommends to take simultaneously the following parameters:

- dynamic ζ potential,
- pH,
- conductivity, in order to indicate the total ions concentration.

Several structural models have been proposed for cement paste [1, 16]. The model proposed by Legrand[16] seems to be more reliable than the other ones. The irregular shape of cement grains is assumed and the flocculated structure is formed as a

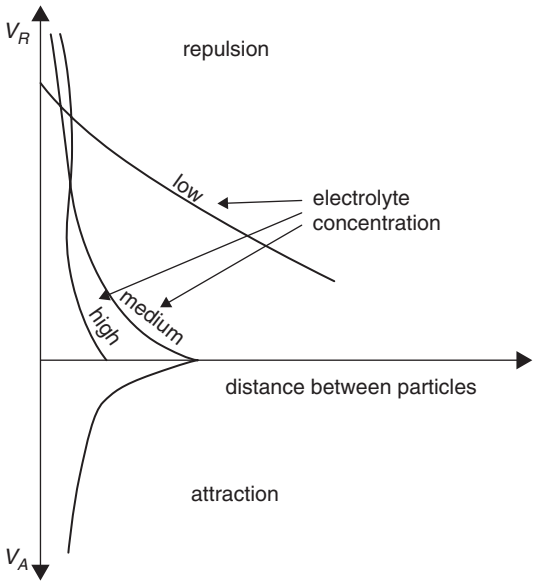


Fig. 5.17 Potential energy of attraction V_A and repulsion V_R as a function of the distance between particles and electrolyte concentration

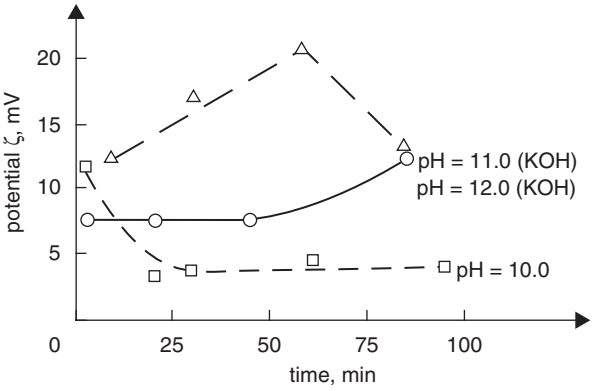


Fig. 5.18 ζ potential of hydrating cement paste as a function of time and initial pH of the liquid phase. (according to [27])

result of bonding by electrostatic attraction, according to the following way: top to top, top to wall (Fig. 5.19).

The bonds are the result of unbalanced totally surface charges on the corners and edges of grains [4]. These bonding forces are supplemented by the van der Waals forces. This results in the "isolated bonding centers" formation and the repulsion appears between the adjacent grain surfaces. This repulsion forces are composed of the repulsion between the double layers and of the disjoining pressure of water layers on the grains. The repulsion forces tend to increase the θ angle (Fig. 5.19), however, the bonding forces are strengthened by the capillary forces. Additionally all the grains are under the gravity force. The flocculated structure thus formed is based upon the local equilibrium of attraction and repulsion forces. This model al-

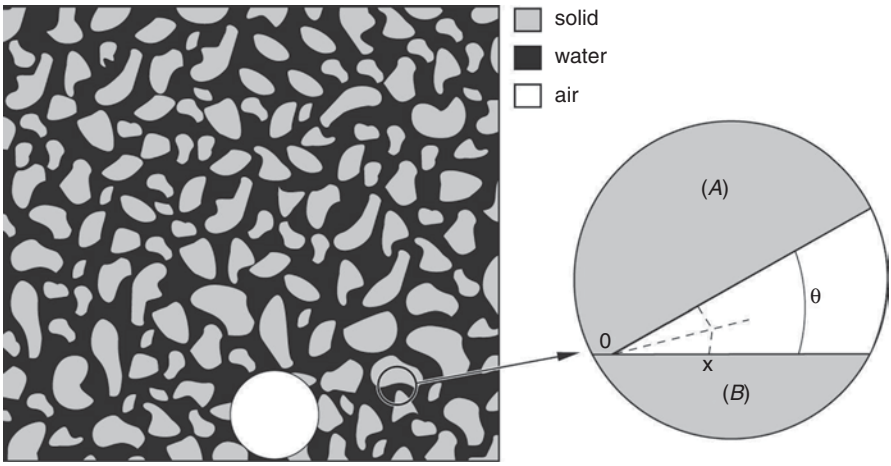


Fig. 5.19 Schematic model of fresh cement paste after flocculation. (according to [16])

lows to explain some rheological properties of the paste, as plasticity, thixotropy and apparent viscosity.

5.2 Relationship Between the Microstructure and Strength of Cement Paste

The knowledge of the relationship between the microstructure of cement paste, the kind of bonds between the components of paste and the strength of material was necessary for the improvement of physical properties of cement paste and concrete. This problem is not easy, because of the amorphous, colloidal form of the most important and dominating paste component, which is the C–S–H phase. Moreover, the porous structure of hydraulic hardened materials is the reason that the strength cannot be simply related to the cohesion forces, without the determination of corresponding to them surface. For this reason the strength has been related to the porosity which gives the characteristics being in some connection with the cohesion forces.

The types of bonds which can occur in cement paste have been analysed by numerous authors [28–32]. There is a common opinion that two types of bonds can be consider: the ionic–atomic bonds, acting only on a very small distance and the van der Waals forces. Initially a significance was attributed to the interlocking of needle–like, fibrous C–S–H particles. However, this was rejected because in the hardened, old pastes there is a very low content of fibrous components. The occurrence of these elongated needle–like C–S–H forms has been questioned recently (see Sect. 3.2.3).

The formation of bonds between the C–S–H crystallites was the subject of numerous discussions. Rebinder et al. [28] presented the hypothesis that the formation of these bonds (the intergrowths) in the contacts of crystallites is controlled by the

liquid phase supersaturation. They stated that there is an equilibrium between the degree of supersaturation of solution and the forces necessary for maintaining the crystals in constant position towards each other. The stresses are linked with the pressure of crystallization and their minimum values contribute to the high strength. The types of bonds occurring between the C–S–H particles were examined by Nonat [33] and are presented in the Sect. 3.2.3.

The particular concepts of structure models of cement paste are based mainly upon the specific surface area measurements and the sorption properties of this material, as well as on the studies of porosity and pore size distribution.

There are the difficult problems because of the amorphous, colloidal nature of cement hydration products; there is no even an electron diffraction pattern for the single crystals [34]. According to Helmuth and Verbeck [34] this is probably the consequence of isomorphous substitutions principally of aluminum and sulphur for silicon, resulting in the modification of gel morphology. The paste cured for 10 years in water does not show the increase of crystalline phases content in hydration products [34]. The curve of water vapour pressure in relation to water content for cement paste is continuous; there are no steps typical for crystalline hydrates [35]. Therefore there is no basis to adopt any "division" pressure of water vapour differentiating the bound water in hydration products from "physical" water, adsorbed by cement paste constituents. There is no possibility to distinguish on this curve, the pressure corresponding to capillary water, gel water, in gel pores, and in gel itself.

The hydration products are produced in the space filled initially by water and in the places occupied by cement grains, forming the pseudomorphoses after these grains. When during hydration the partial drying of samples the partial evacuation of water from the larger pores will occur, which then cannot be filled with hydration products. Therefore the differences of pore structure occur depending on the curing condition of the paste: in water or if it released water during maturing. It must be underlined that the drying causes the irreversible changes of the paste structure. The methods of sample preparation before the examination of sorption properties can result in the different degree of decomposition of colloidal, hydrated calcium silicate hydrates and the change of pore structure [36–38]. The classification of water in the paste for the "evaporable" and "non–evaporable" is quite conventional and should be in every case related to the method of its measurement. Lea [39] is presenting the table in which some drying methods are compared. It does not covered all the methods then some others are added in Table 5.2.

Water in cement paste, considering the relativity of the base of its quantitative division, can be divided as follows:

- water adsorbed on the surface of solid phases (physical sorption, chemisorption),
- water in gel pores and in capillary pores,
- water in hydrates (hydroxyl OH groups), in $Ca(OH)_2$ and crystallization water[4],

[4] The following forms of water incorporated into the crystal lattice can be distinguish: water of crystallization and constitutional (chemically combined) water. The latter one occurs in the form of OH groups [e.g. $Ca(OH)_2$], while the water of crystallization can be divided into coordination and structural. The water of coordination is strongly combined and cannot be removed without the destruction of the structure, however, to the structural the inter–network water is rated,

Table 5.2. Different methods of samples drying

Drying method	Water vapour pressure at temp. 25 °C, Pa	Relative water retention in paste
$Mg(ClO_4)_2$	1.064	1.0
$LiCl{\cdot}H_2O$	359.9705	1.0[a]
P_2O_5	0.00266	0.8
Concentrated H_2SO_4	3.99	1.0
D–drying, temp. −79 °C	0.0665	0.9
Acetone, ether, drying at 40 °C		1.0
Drying at 50 °C		1.2[b]
Drying at 105 °C		0.9[b]

[a] according to Taylor [40] these conditions correspond to the content of bond water
[b] according to Lea [39] rather 1.0 at 50 °C and 0.8 at 105 °C

- water in C–S–H gel structure: in the form of hydroxyl groups, water between the layers,
- free water (in macropores and other voids).

Sierra [41] studied the C–S–H gel using several methods and found the three stages of dehydration (Table 5.3 and Fig. 5.20). According to Sierra, C–S–H gel is composed of three–layer sheets with C/S = 1.72. This author presented also the models of water molecules bonds: for water adsorbed between the layers and the water between the sheets of layers (Fig. 5.21).

Sabri and Illston [42] studied the distribution of evaporable water in hardened cement paste by means of semi–isothermal method. This method includes a heating to reach the peak maximum and next heating at this temperature during 30 min [42]. Obtained curves, plotted in Fig. 5.22, reveal the two types of water which are evolved by the samples in the temperature range 47–54 and 78–90 °C respectively, depending on the time of paste maturing. The first peak is linked with a constant amount of evolved water while the second one—with the amount of water which is increasing with time of sample maturing. The typical, adsorbed water (*A*) evaporates at lower temperature range and forms a classic adsorption isotherm vs. humidity of environment[5]. At higher temperature the hydrated phases, presumably the C–S–H gel, dehydrate (water *B*, between the sheets in the structure).

The physically bound water in the paste, as well as the water in the hydrates can be determined by means of elastic neutron scattering, without sample drying [43, 44]. For this reason it is an very interesting method, and obtained results give the possibility to explain many discrepancies linked with the sorption methods. The results of one study have shown that the free water content (Fig. 5.23) is consistent with that calculated earlier as the capillary water [44].

which is weekly bonded, filling the holes in crystal lattice. It can be easily removed (zeolites). See J. Chojnacki Chemical and physical crystallography, PWN, Warsaw 1961, p. 242 (in Polish).

[5] The adsorption of water is obviously the function of partial water vapour pressure in the gaseous atmosphere surrounding the sample. The authors give only the relative humidity of air to determine this pressure.

Table 5.3. Water loss of two C–S–H samples in thermogravimetric measurements under water vapour pressure [41]

Hydration stage	Drying conditions	C–S–H (I)	C–S–H gel
2	Equilibrium with 100% RH atmosphere at room temperature	$C_{1.52}SH_{2.42}$	$C_{1.75}SH_{2.58}$
1	At water vapour pressure 0.1 Pa (horizontal segment from 40 to 70°C in Fig. 5.20)		$C_{1.75}SH_{1.59}$
	At water vapor pressure 10^{-4} Pa (horizontal segment from 20 to 40°C in Fig. 5.20)	$C_{1.52}SH_{1.56}$	
0	De–watering equivalent to drying at pressure $0.5 \cdot 10^{-5}$ Pa (D–drying)	$C_{1.52}SH_{1.02}$	$C_{1.75}SH_{1.11}$

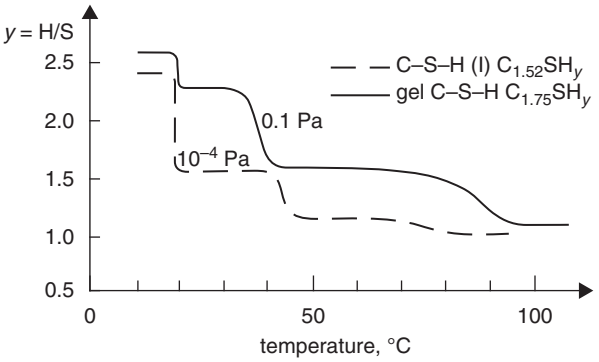


Fig. 5.20 Thermogravimetric curves for the two C–S–H gel samples prepared in the isobaric conditions. (according to [41])

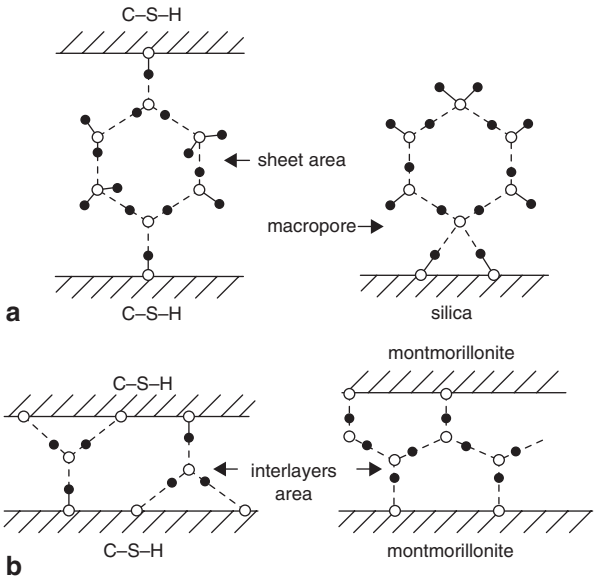


Fig. 5.21 Models of water in the structure of paste (according to [41]): **a** water between the sheets in the C–S–H gel and water adsorbed in the pore of silica gel. **b** interlayer water in C–S–H gel and in montmorillonite

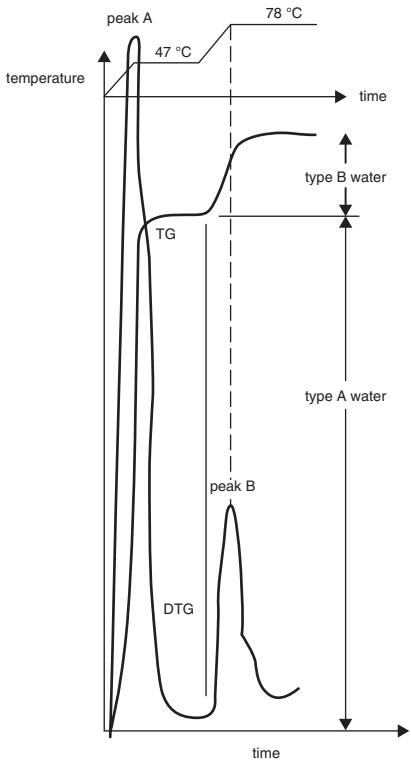


Fig. 5.22 Typical *quasi*–isothermal TG/DTG curves for water saturated Portland cement paste. (according to [42])

Stockhausen et al. [45] differentiated the four types of adsorbed water, condensed in capillaries. The capillaries larger than 100 μm are filled with water only when the sample is in the contact with water. The condensation of water vapour in the pores larger then 10 μm occurs at relative humidity higher than 90 %. In the capillaries with diameter between 3 and 10 μm the structural orientation of water takes place. The condensation is then occurring at 60–80 % RH. This water is frozen at temp. of −43 °C (Fig. 5.24). Finally, the 2.5 molecules thick layer of adsorbed water, belonging to the fourth type, became frozen at temperature lower than −160 °C. These layers are strongly bound to the surface; however, they are movable and behave like a two–dimension van der Waals' gas medium. They can also migrate on the surface [46].

The specific surface is measured based on the adsorption isotherm. As it is known, the experimental data are used for modeling of cement paste.

Specific surface is calculated from the BET isotherm equation. This equation is valid in the range $p/p_0 = 0.05–0.35$; this issue was discussed in the book of Bond [47]. There is a common opinion that this equation use is a serious simplification of the problem. Several better developed modifications of this formula have been proposed; they give a more exact estimation of the "capacity" of the monomolecular layer. However, the practical implementation of these equations is complicating the

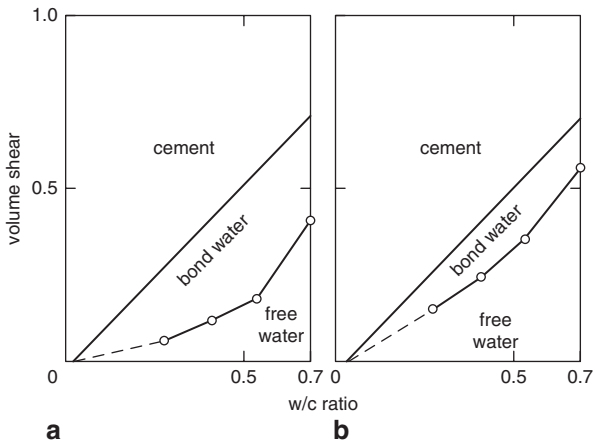


Fig. 5.23 Volume ratio of: cement, combined water and free water in water saturated pastes (according to [44]): **a** composition determined by neutron scattering. **b** composition determined based on the loss on ignition measurements

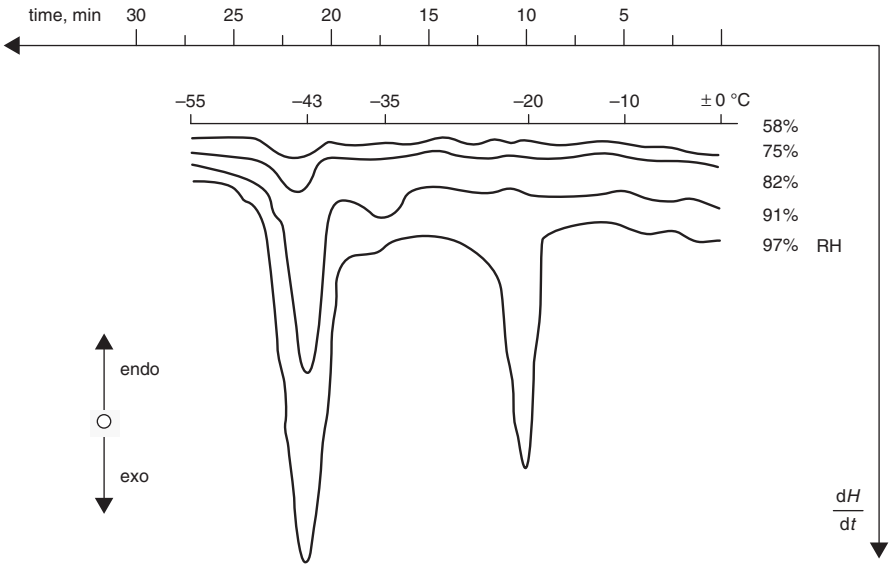


Fig. 5.24 DTA curves of cement paste, hardened in the environment of variable relative humidity. (according to [45])

calculation and does not improve the accuracy without the precise monomolecular layer volume determination.

The specific surface area of cement pastes was investigated applying usually H_2O and N_2 as adsorbates. The values obtained with H_2O are high—about 200 m^2/g. They are proportional to the non–evaporable water content in the paste, and irrespectively also of the porosity [39]. In the case of N_2 application, a significantly lower values are obtained, about 50 m^2/g [35] and they are not proportional to the non–evaporable water content. Use of the other adsorbates gives the results compatible with those for

nitrogen adsorption. A little lower specific surface area was measured with methanol (43 m^2/g [35]). Butane, propane and cyclohexane were also applied [36, 43, and 48]. According to Copeland [38] these differences can be explained as follows: large pores are surrounded by the C–S–H gel acting as a molecular sieve and permeable for water molecules only. Feldman and Sereda [35, 43] attribute this phenomenon of water interaction with the structure of gel; this water is incorporated as an interlayer water in C–S–H. In C–S–H (I) the basic planar spacing is variable indeed [49].

However, the precise sorption measurements were not correlated with the data presented above. The differences associated with the use of different adsorbates can be caused by the mutual interactions between the adsorbate and adsorbent during the sorption process [38]. There are some premises to presume that the energy of interaction of water molecules with the C–S–H surface is significantly higher than in case of the other molecules, for example methanol, and therefore water can intrude to the space inaccessible for these molecules [38]. The hypothesis of Jennings and Tennis [50], as well as their model concerning this issue, is discussed in Sect. 3.2.3.

In the late forties the low–angle X–ray scattering method for the determination of specific surface area was developed. The measurements of the specific surface of condensed colloidal systems became thus possible. This method was applied by Winslow in the measurements of the surface of cement paste in 1973 [51]. The specific surface of the paste dried over the dry ice (*D–drying*) is close to that determined by means of water sorption, while the specific surface of sample saturated with water is three times higher [39]. Applying the low–angle X–ray scattering method Winslow and Diamond [52] found the value of 950 m^2/g. According to Taylor [53], this result can be related to the Ca–O layer and the silicon–oxygen anions attached to it. The reason of these serious discrepancies between the results obtained with H_2O sorption and low–angle X–ray scattering method is not clear.

The surface calculated from the nitrogen adsorption increases with w/c ratio [39] and reduces with the degree of hydration [34, 54]. The specific surface area based on the water sorption is practically stable, irrespectively of w/c ratio; it increases with the degree of hydration [54].

The porosity of samples can be also determined based on the adsorption isotherms. For materials with small pores, as in the case of silica gel and cement paste, the hysteresis loop appears on the isotherms at higher pressure (Figs. 5.25 and 5.26). This departure from the reproducibility of desorption is explained by the capillary condensation.

The pore size distribution can be determined based on the adsorption isotherm, starting from their volume; the suitable formulae are given by Dubinin [55]. The conditions of measurements, which assure the correctness of calculations, can be found in [47] and are discussed by Dubinin [56].

The porosity and pore structure can be also determined with mercury porosimetry, as well as with helium flow method proposed by Feldman [48]. However, a more adequate method of the total porosity measurement is helium pycnometry [57]. The applicability of the mercury intrusion porosimetry covers the pore diameters from 3 nm to about 10^6 nm, while the capillary condensation—from 4 to 50 nm respectively.

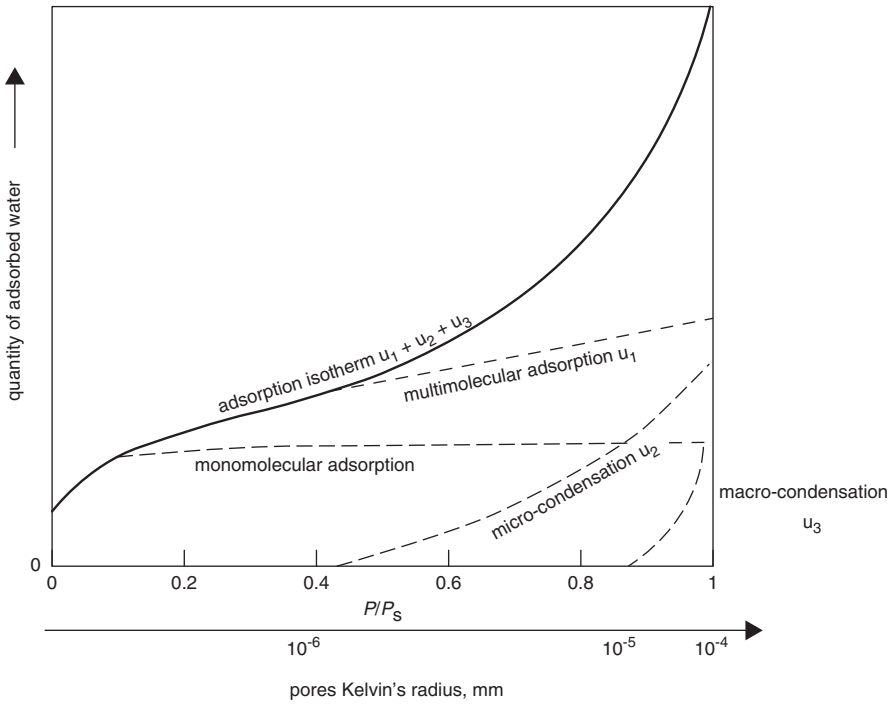


Fig. 5.25 Different adsorption phenomena as a function of relative water vapour pressure and the "Kelvin radius" of pores in the paste

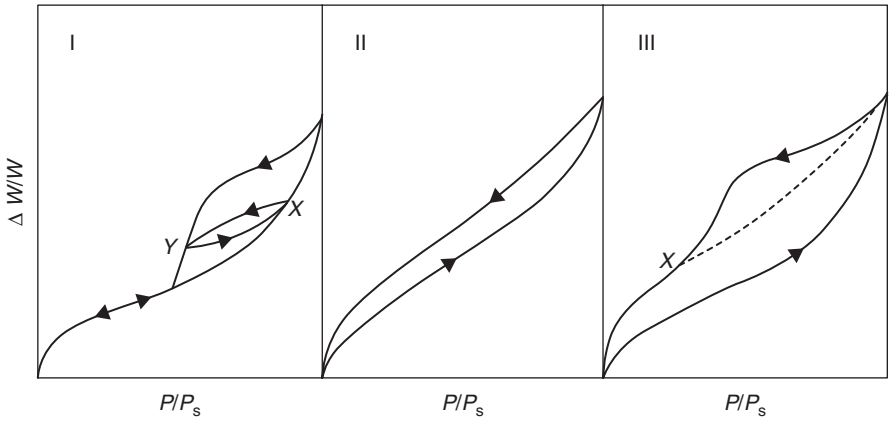


Fig. 5.26 Different forms of sorption hysteresis loops. (according to [48])

A shape of pores should be assumed to calculate the porosity from the Kelvin equation. The result of the pore size distribution calculation is affected by this assumed shape of pores, because the pressure assuring the entire filling the pore depends on the curvature of meniscus, and consequently on the shape of pore. The

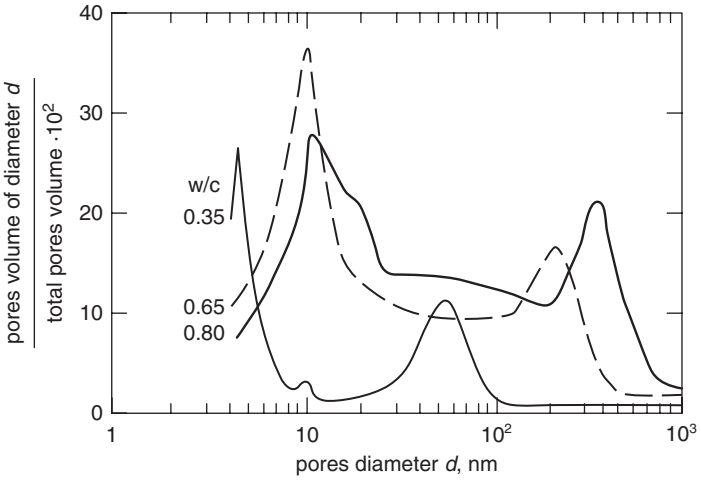


Fig. 5.27 Pore size distribution in cement paste stored in humid environment during 11 years. (according to [34])

two shapes are commonly taken into account: the cylindrical and tubular one [34]. There is another method, ignoring the shape of pores, it is introducing the so–called "hydraulic radius", in which the ratio of pore volume to the surface of pore walls is taken as a measure of pore size [58].

The measurements with mercury porosimetry give two distinct maxima in pores size distribution: the first in the range 4.5–11 nm, and the second one in the range 55–350 nm (Fig. 5.27). The second one corresponds to the capillary pores [34]. This division is conventional; in reality the distribution is continuous. The results of mercury porosimetry are consistent with the measurements of ice propagation during freezing; it is important because the samples prepared for the latter method are not dried [57]. The large pores can be observed directly under the scanning electron microscope.

For the pore size distribution determination the sample must be dried, and as it has been mentioned, the properties of cement paste microstructure strongly depend on the conditions of drying. Marsh [59] studied the pore size distribution for the samples dried at temperature of 105 °C and the samples in which water was replaced by propane. The samples cured one day and those with the fly ash addition after different time of curing reveal the substantial differences (Fig. 5.28). However, the results for Portland cement pastes matured for longer time are relatively similar [59].

The size of pores determined with mercury porosimetry or ice propagation does not mean exactly the size of pores but only the size of "access" to the pores [34].

The correctness of the results for the smallest pores measured with the mercury porosimetry, was questioned because of their possible destruction by intruding mercury. This problem was studied by Winslow [60]. The reduction of pore size during the measurement was proved in the case of the paste; this effect is particularly intensive for the smallest pores (the highest pressure).

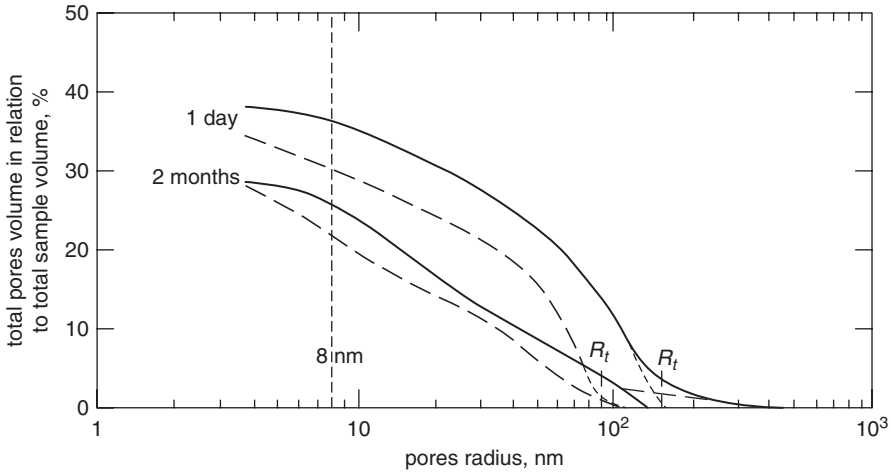


Fig. 5.28 Typical results of the mercury porosimetry measurements for the dried samples (*continuous lines*) and after removal of water by propane (*dashed lines*). (according to [59]), R_t the threshold radius

The structure of pores determination is disturbed also by the distillation of mercury from the paste. The second problem concerns the angle of mercury meniscus in capillary pores; this angle changes from 125 to 135°, depending on the paste curing time—it grows with the porosity and it is affected by the presence of pozzolanic additions to cement. The effect of this angle changes is significant because the cosinus of this angle is a component of Washburn's formula, used in calculations. The result relating to the share of larger pores is significantly affected.

The mercury porosimetry is often applied in the measurements of concrete porosity. There are some doubts concerning the size of concrete samples. The cylindrical concrete specimen for the measurement should have the diameter of about 10 mm and height of about 30 mm and the mass from 3 to 4 g. The aggregate size can attain 20 mm; however, even in the case of aggregate grains equal 8 mm it is not possible to produce the representative specimen with a proper mortar share. Better conditions for the reliable porosity determination are in the GeoPyc apparatus operating with helium, where the cylindrical specimens with diameter of about 48 mm and height of 20 mm are used. In the case of concrete samples the gas (e.g. oxygen) permeability methods can be also applied, however, the evaluation of porosity is only indicatory.

The pore size distribution in cement paste can be also determined from the Defay's relation, linking the radius of meniscus and the freezing point of water in the capillary [61]. The information dealing with the continuity of pores system can be derived from the hysteresis loop between the heating and cooling. However, because of many assumptions, the results are only approximate; the most accurate relate to the larger pores. In Fig. 5.29 the pore size distribution measured with this method, and with mercury porosimetry is shown [61].

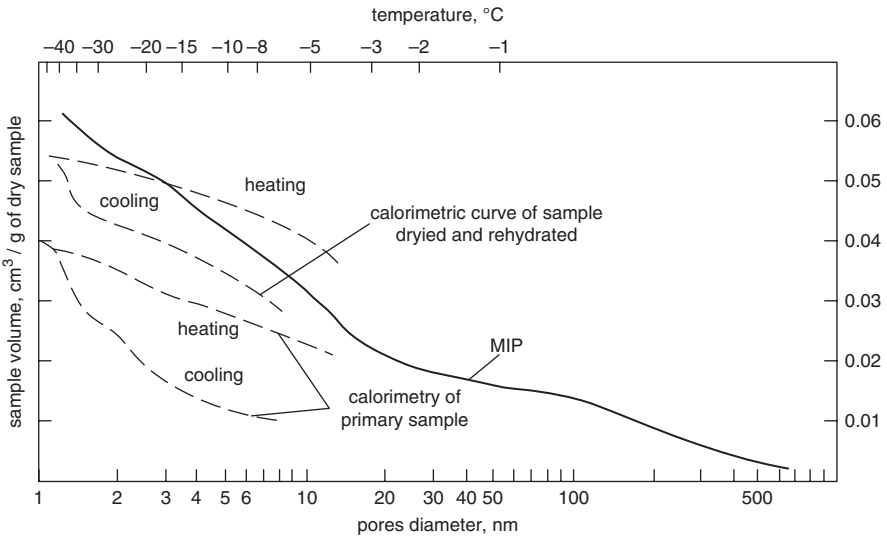


Fig. 5.29 Total pore volume in cement paste determined by mercury porosimetry (*MIP*) and low temperature calorimetry. The amount of water evaporated was identical for all three samples—0.093 g/g of dry material. (according to [61])

The calculation of porosity from the water vapour adsorption isotherm leads to the higher value. Obviously, the porosity becomes higher with increasing w/c ratio because the hydration products cannot fill the rising volume of pores (Fig. 5.30). However, the porosity is substantially lower when nitrogen is applied as an adsorbate. The hydraulic radius of pores, determined from the water vapour isotherm, decreases also with the rise of hydration degree. The ratio of micropores is also increasing [54] with the time of hydration. When the samples are dried only at 11 % RH (over the $LiCl \cdot H_2O$ saturated solution), the porosities from water vapour determination are close to these obtained with helium or methanol [62].

There are "two schools" first of Brunauer and the second one of Feldman and Sereda which, on the basis of different hypotheses, try to explain the differences of cement paste porosity, measured with H_2O sorption or other gases, principally N_2 [35, 43, 48, 54]. These hypotheses are connected rigorously with the proposed structural models for C–S–H phase.

The hypothesis of Brunauer [63] is based on the Powers model with the assumption that the C–S–H gel consists of the small 10 nm particles, separated with the water layers about 0.5 nm thick. The C–S–H particles are composed of the two or three layers; the thickness of one layer is about 1 nm. There are two types of pores in the gel structure: the micropores of the size 0.3–0.4 nm and the larger pores, not exceeding 2 nm [63].

Brunauer's [54] hypothesis assumes that the nitrogen molecules cannot penetrate into the micropores, and even partially to the larger pores. The explanation of Brunauer is the following: (a) the N_2 molecules are larger, (b) the water molecules are dipoles and therefore they are strongly attracted by the surface of hydration

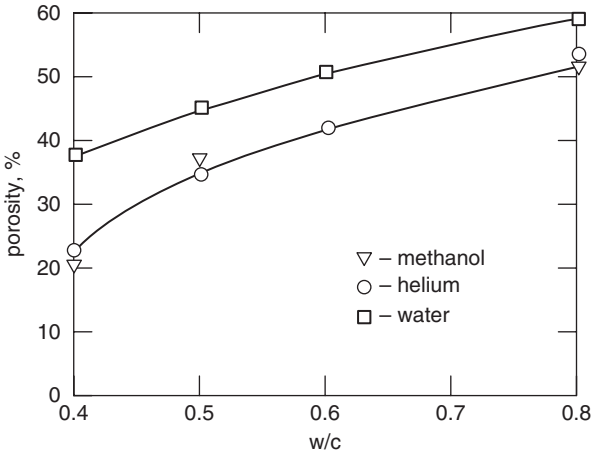


Fig. 5.30 Porosity as a function of w/c ratio in Portland cement pastes. (according to [62])

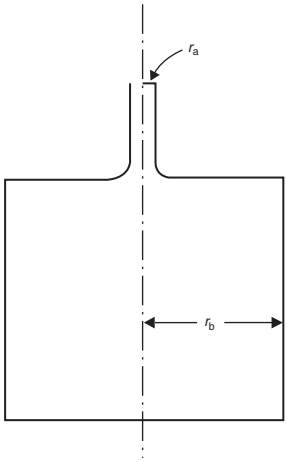


Fig. 5.31 Scheme of an "ink bottle" pore

products, while the N_2 is a poorly attracted quadrupole, (c) the molecules penetrate into the pores with narrow entrance ("ink bottle") (Fig. 5.31) in the process of thermally activated diffusion. This process depends on temperature and that is why the sorption of water at 25 °C occurs with 50 times higher rate than the nitrogen sorption at temperature of − 196 °C.

According to Brunauer, this last cause is the most important; Brunauer is of the opinion that for the equilibrium nitrogen sorption many years will be needed. The model proposed by Jennigs [50] is very similar to this Brunauer's hypothesis.

The Feldman and Sereda hypothesis [35, 43, 48, 57, 62, 64] is based on the assumption that the exchange of interlayer water in the C–S–H phase occurs. The volume of this water is equivalent to the volume of adsorbed water reduced by the volume of adsorbed nitrogen: $V_{H_2O} - V_{N_2}$. The measurements of helium volume

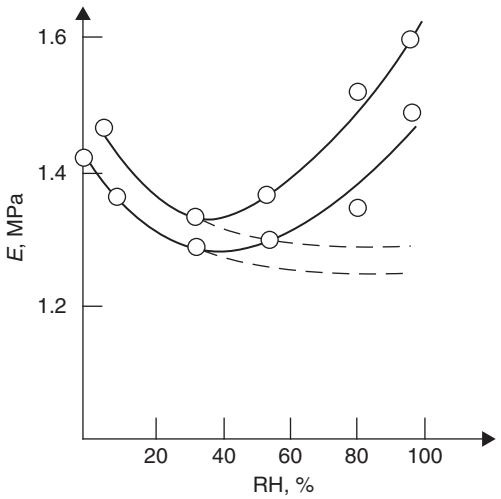


Fig. 5.32 Changes of Young modulus in relation to water content of the paste hardening in equilibrium with the environment of variable relative humidity (according to [37]). The results of two series of experiments; w/c = 0.4

penetrating the interlayer space also allow this volume determination. The hydraulic radii resulting from this hypothesis are also significantly lower: 95–278 pm.

The Young modulus of the paste, raising with the "physically" bound water content, corresponding to the increase of environment relative humidity from 50 to 100 %, is consistent with the Feldman and Sereda hypothesis [43]. This modulus is rapidly reduced for D–dried cement pastes (0.0665 Pa, equal 0.0005 mm Hg). This phenomenon is of basic importance for Feldman and Sereda, proving their hypothesis. From these experimental data the authors conclude that water, entering into the interlayers space takes part in the strengthening of cohesion forces forming the bonds with the calcium ions, present between the layers [43]. Therefore, in the dried samples (Young modulus $17.1 \cdot 10^3$ MPa), the Young modulus increases to the initial value of $33.3 \cdot 10^3$ MPa, after the re–saturation with water at RH 42 %.

The adoption of Wittmann's hypothesis [37, 46], assuming that water entering between the gel particles exerts the disjoining pressure, does not permit to explain the Young modulus increase with the growing moisture of the samples (Fig. 5.32). In the model proposed by Wittmann, so–called Münich model, it is assumed that the properties of paste can be explained with two phenomena: the surface energy of colloidal particles and the disjoining pressure exerted on particles by water. At the relative humidity lower than 50 % the properties of paste are controlled mainly by the surface energy of gel particles. The changes of surface energy linked with the water sorption are the function of the relative humidity of environment. At higher relative humidity the gel particles are separated by a thin water layer. Therefore at high humidity the structure of solid phase (xerogel) is mechanically less durable. The interaction of solid phase with the adsorbed water or condensed in capillary pores has a great impact on the properties of hardened paste. The increase of Young modulus at increasing relative humidity over 50 %, apparently inconsistent with this model, is according to Wittmann, explained by the adhesion linked with chemical bonds, which are not influenced by humidity. Simultaneously Ubelhack [65] showed, with

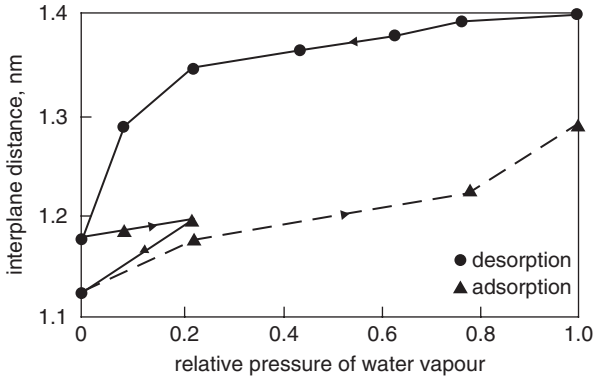


Fig. 5.33 Changes of interplanar space (001) in the C–S–H phase (according to [68])

Mössbauer spectroscopy, that the dependence of Young modulus on the porosity of paste is linked with the interaction of gel particles.

A significant hysteresis loop, ranging up to the very low pressures (Fig. 5.26) is the other experimental result which seems to proof the Feldman hypothesis. These shape of adsorption and desorption curves, resembling that occurring in case of some clay minerals (vermiculite) and the paste, indicates the reversible introducing of water into the structure of solid phase. The increase of interplanar spaces in clay minerals is in this case frequently observed.

Other authors, however, have achieved the experimental results inconsistent with this theory. For example Smith et al. [66] found the irreversible reduction of the interplanar space, from 1.25 to 0.98 nm, in the D–dried C–S–H samples. It proofs the Brunauer's hypothesis [67], which found that the H_2O particles cannot for the second time occupy the interlayer space in the C–S–H gel, after its drying.

The experiments of Smith were undertaken later by Gutteridge and Parrott [68]. The decrease of the basic interplanar space in the synthetic C–S–H (I) from 1.4 nm in water saturated state to 1.13 nm after D–drying during four months, was found. After the full saturation of the sample with water the partial rehydration and the interplanar space rise to 1.28 nm was found, (Fig. 5.33). Gutteridge and Parrott are explaining also the adopted by Smith initial value of 1.25 nm (1.28 nm) [66], as related to the incidental drying of sample before the experiment [68]. There is a general conclusion from all these data that the interplanar water in the C–S–H(I) is not exchangeable and a significant its amount is liberated irreversibly, during the first drying.

There are some discrepancies as the hysteresis loop on the sorption curve is concerned: this loop of H_2O sorption varies in the data of different authors [63]. According to Brunauer [69] this hysteresis is a consequence of non–equilibrium sorption; the sample must be kept in the BET apparatus for 4.5 month to assure the equilibrium.

The detailed studies of the structure of cement paste and its influence on the physical properties we owe to Powers [31, 36]. According to his assumption, the "cement gel", it means the C–S–H phase composed of colloidal particles, is a basic binding component of the paste. This colloidal status of C–S–H is proved by an

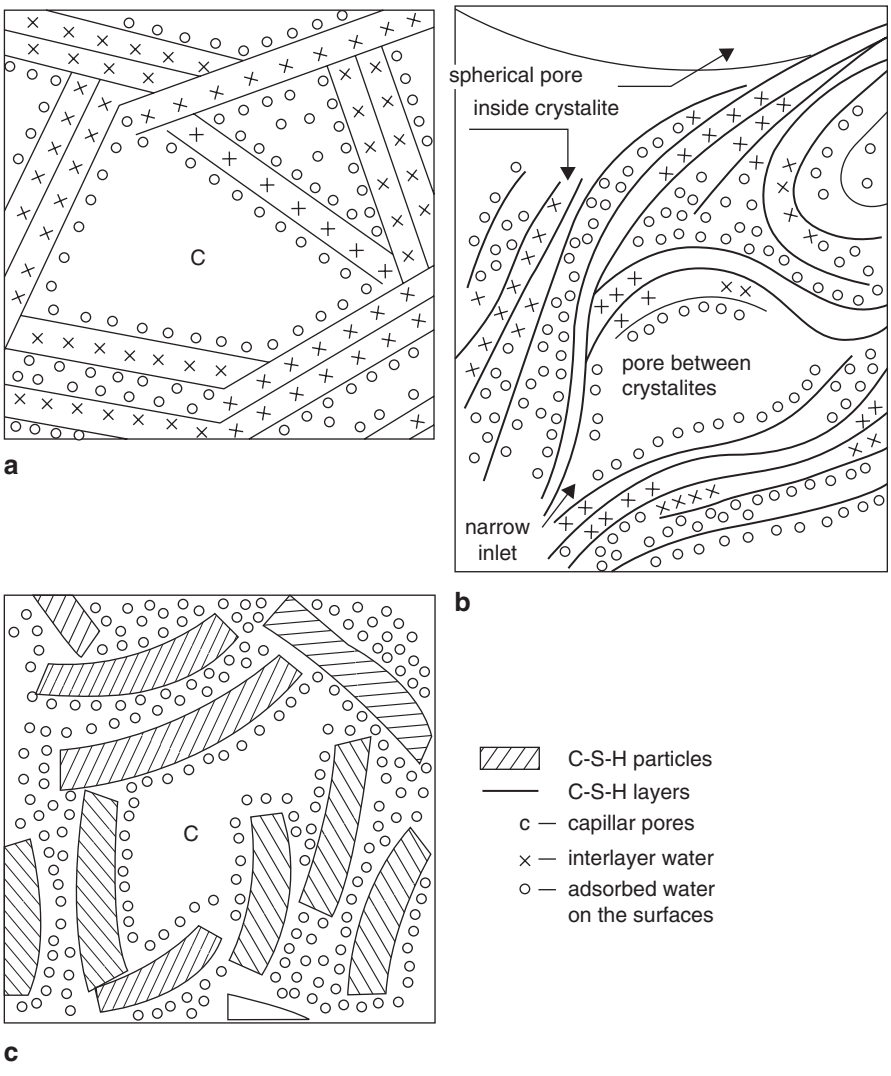


Fig. 5.34 Schemes of different C–S–H models: **a** of Powers and Brunauer. **b** of Feldman and Sereda, modified by Daimon. **c** according to Wittmann

extremely high specific surface area of the paste (200 m^2/g). At present, there are obviously direct methods of the C–S–H particles measurements by means of electron microscopy (for example [70]). In the model of Powers (Fig. 5.34) is assumed that the paste is composed of the gel, in which the gel pores (28% of volume—minimum), capillary pores and incidentally the unreacted cement grains occur. The capillary pores originate from the space between cement grains, initially filled with water. The gel fills gradually these pores. According to Powers, the differences between the pastes relate primarily to the differences in capillary porosity.

In Powers' model it was the assumption that the colloidal C–S–H particles are composed of two or three layers, randomly distributed and bound together with surface forces, similar to the forces occuring in the clay minerals. The stronger ionic–atomic forces, bonding the adjacent particles, occur exceptionally (see the forces between the particles in Sect. 3.2.3). The water vapour can penetrate the spaces between the particles, therefore it can be applied in the specific surface area measurements, while nitrogen, with larger molecules, can penetrate only the larger pores and does not give the possibility to measure the entire specific surface area. The interlayer water is liberated irreversibly during the first, intensive drying.

Based on this model, Powers related the strength of paste with the "cement gel" content. The C–S–H share was determined by Powers as a ratio:

$$X = \frac{\text{gel volume}}{\text{gel volume+capillares volume}} \tag{5.24}$$

This ratio depends therefore on the capillary porosity. The strength can be determined from the following empirical formula:

$$f_{\mathrm{c}} = f_{\mathrm{c}}^{0} X^{\mathrm{n}} \tag{5.25}$$

where

f_c^0 and n	are the empirical constants
f_c^0	is an internal strength of gel, estimated by Powers as 235 MPa,
n	values are in the range from 2.6 to 3; usually 3. In this hypothesis the gel porosity is included in the volume of C–S–H phase.

In order to analyze the effect of humidity on cement paste, Wittmann [71] studied the model of contacting silica glass surfaces. In the atmosphere of relative humidity not higher than 50% these surfaces were in contact. At higher humidity they were separated by a layer of water; which thickness was increasing with relative humidity and attained 50 nm at 100% RH. The same experiment Wittmann repeated with the C–S–H needles, with the same result. To form the chemical bonds between the C–S–H needles the relative humidity should be reduced to 50%; thereby to decrease the thickness of water layer and the distance between the crystals. In this condition the van der Waals forces appeared, which caused further C–S–H needles approaching. In Wittmann's model C–S–H is presented as the three–dimensional network of colloidal particles—"xerogel", in which the ionic–atomic and van der Waals forces occur simultaneously (Fig. 5.34). The share of van der Waals forces depends on the relative humidity of environment; water attracted strongly by the surface of solid phases exerts the disjoining pressure and this can separate the adjacent surfaces decreasing their interaction, particularly at higher RH. According to Wittmann the share of ionic–atomic forces is close to 50%. Chatterji [72] was considering the possibility of the ionic–atomic bonds formation, comparing the force of bonds occurring in the C–S–H particle and the repulsion pressure of water layers. This author concludes that the chemical bonds between the crystals in cement paste do not play a significant role. This is not in accordance with the last results of Nonat [33], relating to the nanoparticles (see Sect. 3.2.3).

Feldman and Sereda [32, 43, 57, 64] developed their model—as aforementioned based on the Young modulus of cement paste measurements at variable relative humidity of the environment. The samples were also prepared by a cold pressing [48]. The Young modulus is increasing if the paste is cured in the environment of relative humidity higher than 50 %. This result is not consistent with the model assuming the presence of water layer between linking particles. The layer of adsorbed water growing with relative humidity causes the decrease of elasticity modulus in case of the system in which hydrogen bonds are occurring. The silver acetate and cellulose can be given as examples [43]. Next, the Young modulus of the porous glass ($F = 172$ m^2/g, 2 nm pores) does not change in the environment with relative humidity from 0 to 100 %. From the comparison of these two materials it results that water adsorbed by cement paste and not weakening the bonds, penetrates presumably the internal structure of colloidal particles, strengthening the bonds inside the particles [43]. This hypothesis was the base of the Feldman and Sereda model of cement paste. This model, shown in Fig. 5.34, explains the increase of Young modulus with growing relative humidity of atmosphere in the range from 50 to 100 %, in which the paste is cured (Fig. 5.32), by a significant impact of water on the bonds inside the structure and a negligible influence on the interaction between the particles.

In the model of Feldman and Sereda is assumed that the C–S–H gel structure is composed of single layers, randomly distributed. These layers, when approach each other, form the interlayer spaces similar to those occurring in the clay minerals, however, they are not ordered as in these minerals, but randomly placed.

The bonds between the layers in the contacts of solid phase surfaces are variable: from the van der Waals forces to the ionic–atomic bonds [64]. This interlayer bond is of exceptional character and cannot be considered only as a bond between the free surfaces. As a consequence, water can reversibly penetrate and leave the interlayer space. For this reason only the measurements with nitrogen give the possibility to determine the proper values of pore surface, because the migration of water into the interlayer spaces causes the distortion of results of measurement with water vapour [43, 64].

An attempt of these hypotheses generalization was undertaken by Kondo and Daimon [73, 74]. These authors differentiate the two types of pores in C–S–H gel: the larger pores, between the gel particles (visible under the scanning electron microscope) and the small pores (invisible under the scanning electron microscope), occurring in the gel particles. Thus there are the pores between the crystallites and inside the crystallites. The latter one, according to Kondo, correspond to the interlayer spaces according to Feldman; however, they cannot be compared to the interlayer spaces in the montmorillonite or vermiculite [73]. The internal pores in gel particles correspond also to the Brunauer's micropores, which according to Kondo are swelling in the presence of water [74]. The classification of different pores proposed by Kondo is given in Table 5.4.

Finally, Wittmann [46] stipulates that the results of sorption measurements cannot be overrated. The hydration products are not stable and transform on drying and rehydration. Many hydrates are losing water when the water vapour pressure falls down, for example C–S–H, C_4AH_{19}. The system is continuously transformed during the experiments. An extremely high surface of gel is reducing substantially when

Table 5.4. Pores classification [74, 75][a]

Class	Diameter	Type of pore	Properties of water	Method, author	Effect on cement paste properties
Macro pores	1000–15 μm [75] 100 nm [74]	Large gaps	As in liquid phase	Brunauer	Strength, permeability
Capi–llary pores [74]	15–0.09 Mm 50–10 nm 2–100 nm [76]	Large capillaries, medium size capillaries; capillary gaps pores between gel particles meso–pores, capillary voids; pores between gel particles	As in liquid phase moderate surface tension	Brunauer, Powers, Kondo, Mihail [73], adsorption of cyclohexane and propane	Strength, permeability, shrinkage at high RH
Gel pores	10–2.5 nm 2.5–0.5 nm 0.5 nm	Small gel pores micropores, gel pores, pores between crystallites interlayer micropores, interlayer spaces, pores inside crystallites	Strong surface tension, strong water adsorption, no meniscus, bonds formed due to structural water	Powers, Daimon Feldman, Diamond	shrinkage to RH 50% shrinkage, creep shrinkage, creep
	0.5–2 nm [76]	Micropores, gel, larger pores inside crystallites interlayer space	Adsorbed water	Brunauer, Powers, Feldman, Mihail, Kondo, mercury porosimetry, methanol adsorption, nitrogen, Feldman water adsorption	
	0.5 nm [74]	Ultrafine, small, between crystallites		Brunauer, Mihail, Kondo, water adsorption	

[a] Pores classification according to IUPAC: micropores to 2 nm, mesopores from 2 to 100 nm (sometimes 150 nm), macropores above 100 nm (sometimes >150 nm)

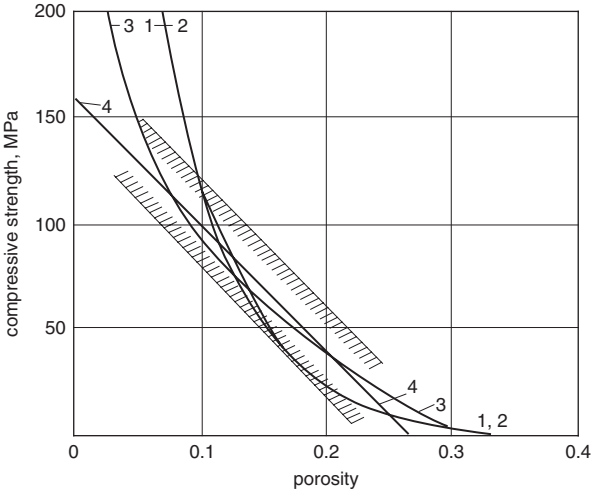


Fig. 5.35 Strength vs. porosity relationship (porosity calculated as a ratio of pore volume to total volume of sample) (according to [80]). Portland cement paste cured at 25 °C; empirical formulas: *1* Balshin: $\sigma_c = 540(1-P)^{14.47}$, *2* Ryshhegitch: $\sigma_c = 636^{-17.04P'}$, *3* Schiller: $\sigma_c = 81.5\ln 0.31/P$, *4* Hasselmann: $\sigma c = 158 - 601P$; the experimental data are enclosed in the dashed area

water evaporates. All these phenomena are the reason of significantly different interpretation of sorption experiments.

Simultaneously with the development of the structural models of the paste numerous data relating the strength of paste with the porosity appeared [75–79]. Verbeck and Helmuth [34] proving the empirical relation provided by Powers paid a special attention to the uniform distribution of hydration products in the paste, because the weakest places have a decisive impact on the strength of material. Therefore, in the formula proposed by Copeland and Verbeck [38], the total porosity instead of the capillary one is included:

$$P_t = P_0 \exp(-Kf_c) \tag{5.26}$$

where

P_t means the total porosity,
P_0 porosity corresponding to the strength equal = 0 (about 60 %),
K constant, equal about $5.37 \cdot 10^{-3}$ MPa^{-1},
f_c strength of the paste.

The other formulas, well conformed to the experimental data, were also used (Fig. 5.35) [80]. The following can be given:

$$R = R_0(1-P)^A \tag{5.27}$$

$$R = R_0 e^{-BP} \tag{5.28}$$

$$R = D\ln\frac{P_{CR}}{P} \tag{5.29}$$

where

R_0 is the strength at zero porosity,
P porosity in % by volume,
P_{CR} porosity at zero strength, *A, B, D* constants.

The formulae (5.27) and (5.28) were often applied to calculate the relation between the Young modulus and porosity.

The later works have shown that the porosity is not the sufficient factor of strength determination, because it is affected also by the pore structure and moreover, of the crystals size and morphology of the solid phase. A significant compatibility of strength and porosity should be attributed to the correlation between these factors strength and total porosity.

Jambor [81] found for example that the relationship between the porosity and strength can be different if it is concerning the pastes of the same w/c ratio and different degree of hydration or with the same degree of hydration and different w/c. This is because the w/c ratio is affecting not only the porosity but also the characteristic of hydration products. The strength depends on the type and volume of hydration products. At low w/c the hydration products have lower content of bound water and higher homogeneity of morphology and size which results in higher binding ability [81].

Apart from the dominating porosity effect, Feldman and Beaudoin [78] paid an attention to the role of bonds between the crystallites and the density of hydration products, as the strength controlling factors,. According to them, the random, disordered arrangement of particles, as well as the poor crystallization degree of hydration products provides the best binding properties. For any given porosity there is an optimum share of well crystallized material with high density and the poorly crystallized one with low density, which assure the maximum strength. Therefore the strength depends on the "internal" strength of particular hydration products, as well as on the bonds between the crystallites. Taylor [82] presented the opinion that at high porosity of paste the forces integrating the particles are important and a high content of the poorly crystallized product is advantageous. At low porosity the bonds between the crystallites are of minor importance; the ratio of high strength component, as a strength controlling agent, is significant. According to this author it is possible to find the iso–strength curves in the system composed of porosity and share of coarse crystals (crystallites) [82] (Fig. 5.36). The simple strength–porosity relationship will be fulfilled only by the limited number of samples [82].

Mindess [83] proved an increase of strength with higher smallest pores share in total porosity. Also Jambor [84] and Zajcew [85] have shown an increase of strength with reduced mean radius of pores, at given porosity. In Fig. 5.37 the relationship between the mean radius of pore and strength found by Jambor [84], is shown. Material composed of tobermorite exhibiting the smallest pores reveals the highest strength (curve I), while the lowest strength is attributed to the hydrogarnets (V). This problem will be discussed later, based on the works of Birchall [97].

According to Zajcew [85], as higher maximum pore size at constant mean size, as lower strength of the paste.

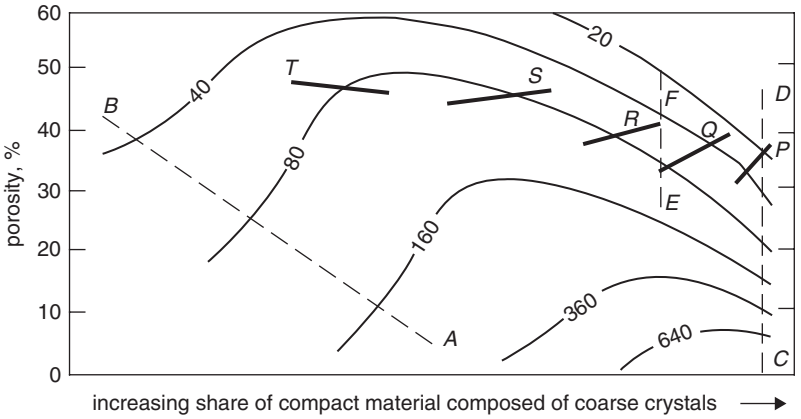


Fig. 5.36 Compressive strength (marked on the curves, in MPa) of paste as a function of porosity and the spatial arrangement of grains. *P–T* lines show the results for the increasing finest fractions of quartz. *AB, CD, EF* lines relate to the pastes cured at room temperature, autoclaved or to the cement–fly ash mixture respectively. (according to [82])

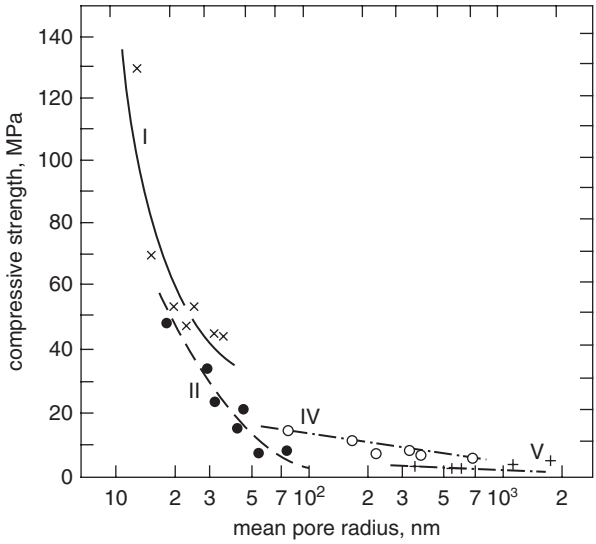


Fig. 5.37 Effect of the mean pore radius in hardened cement paste on strength (different phase composition of materials: *I* mainly tobermorite, *II* mainly C–S–H (I), *IV* 70–80 % hydrogarnets and 20–30 % C–S–H (I), V C_3AH_6 (after [84])

The effect of porosity on the strength of material was studied also by Dyczek and Petri [86], on the pressed samples produced from tobermorite, xonotlite and C–S–H phase.

At present it is not possible to relate the properties of paste to the morphology of hydration products, because of their diversity and variability. Wittmann [46] is of the opinion that the statistical approach to this problem, with help of the computer aided image analysis of microscopic observations, can give the quantitative characteristics of different paste microstructure.

As can be deduced from the analysis of several hypotheses and models, we are still far from the full understanding of binding forces, occurring in cement paste. Undoubtedly, a huge specific surface of particles in C–S–H gel favors the formation of relatively strong bonds between the contacting crystallites. Lea [39] refers to the experiments of Czernin in which high compressive strength was found for the paste produced from quartz, ground to high fineness.

The majority of authors agree that the van der Waals forces occur between contacting gel particles and water films surrounding them [39, 46, 53, 74]; some authors presume that the bridging oxygen Si–O–Si or the O–Ca–O bonds are formed [39, 43]. Kind of bonds between C–S–H shields proposed by Nonat and Plassard are given in Sect. 3.2.3. The idea of intermediary bonds, between the surface atoms of particles, in which the atomic–ionic bonds together with the van der Waals forces are involved, cannot be excluded too. However, there is no regular configuration of atoms in these bonds, as in the classic co–valence, space oriented bonds. The idea presented by Rebinder [28] can be here remembered.

Fortunately, the knowledge of C–S–H gel structure is not necessary in the assessment of physical properties of material. It is commonly known that these properties are determined by the following factors:

- total porosity,
- pore size distribution,
- structural defects,
- degree of structural inhomogeneity.

All experimental results point out a very good correlation between the porosity and strength. However, such an approach is a significant simplification of the problem because the effect of the pore structure cannot be neglected. This has been proved in further studies, in which the strength increase with reduction of pore size was shown.

From the particular relationship between the porosity, pore structure and strength of cement pastes, valid for brittle materials, it was only one step to the application of the Griffith's theory for description of the physical properties of these materials description.

Brittle materials show a significantly lower strength than it would result theoretically from the cohesion calculated basing on the ionic or atomic bond forces. Theoretically this strength should be equal approximately *E/10*, that is the tenth part of Young modulus, but practically is much lower. Griffith [87] assumed that crystals have always defects which cause stress concentration in limited area, sufficient to overcome locally the theoretic fracture toughness. Let us assume that the elliptical crack occurs, which is commonly known as the Griffith crack. It can be proved that in a thin plate with elliptical hole in the middle, subjected to the uniform tensile stress (Fig. 5.38), the highest stress appears in the vertex of the longer axis of ellipse:

$$\sigma_{yy} = 2\sigma_l \sqrt{c / \rho} \tag{5.30}$$

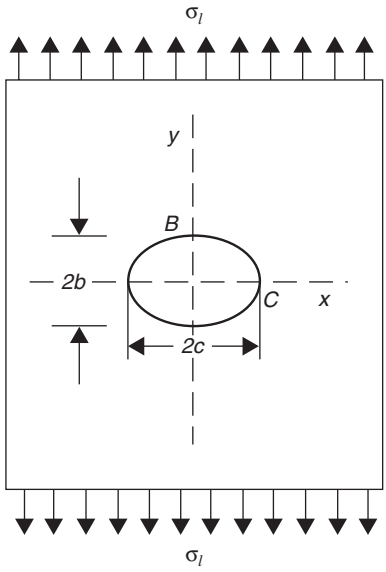


Fig. 5.38 A plate with elliptical hole, subjected to the uniform stress

where

ρ radius of curvature in point *C*,
c half of the longer ellipse axis.

The $2\sqrt{c/\rho}$ ratio corresponds to the stress concentration factor. Assuming that the σ_{yy} stress is equal to the theoretical stress $\sigma_{yy}=\sigma_{th}$ when the cracking takes place, we can conclude that the measured stress is

$$\sigma_{meas.} = \sigma_{th} / 2\sqrt{c/\rho} \tag{5.31}$$

The highest value of stress concentration factor will appear for the narrow failures—hence the Griffith crack. If the microcracks corresponds to the inter–atomic distances and its length is equal 1 μm we have

$$\rho = 200\text{pm} \quad c = 1\mu\text{m} \quad 2\sqrt{c/\rho} \approx 140$$

It allows to evaluate a difference between the theoretical and measured strength. The bonding energy can be calculated only in the case of some simple crystals, thus the theoretical strength. In Fig. 5.39 the theoretical strength of defect–free, filamentary microcrystals—whiskers and the strength of "real" larger crystals are compared [85].

Starting from the energy balance of the process Griffith proposed the following so–called crack propagation criterion, This criterion corresponds to the value of stress causing further crack propagation:

$$\sigma_k = \sqrt{\frac{2EF}{\pi c}} \tag{5.32}$$

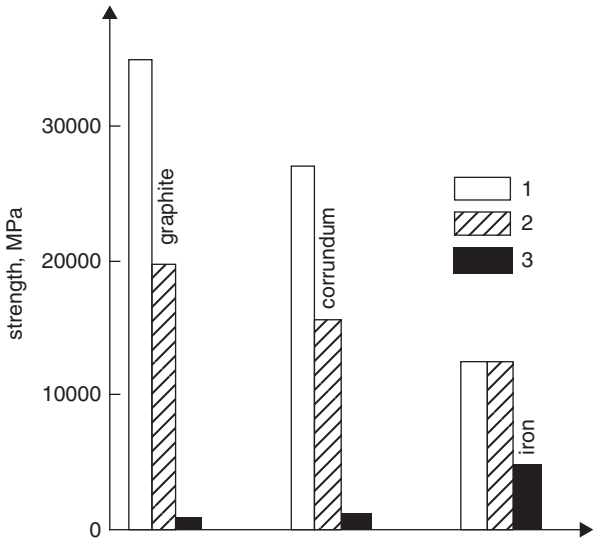


Fig. 5.39 Strength of graphite, corundum and iron: *1* theoretical, *2* whiskers, *3* real crystals. (according to [88])

where

E the Young modulus of elasticity,
F surface energy,
c half of crack length.

Therefore for the brittle elastic materials the fracture toughness depends on the elasticity modulus, surface energy and the length of crack. The energy required for producing of new surface, as a result of cracking, is in practice higher than σ; therefore the fracture energy W is inserted into the Griffith formula. Here fracture energy W, apart from the surface energy, embraces also the plastic deformation, accompanying the crack propagation:

$$\sigma_k = \sqrt{\frac{2WE}{\pi c}} \tag{5.33}$$

Many authors analyzed the applicability of Griffith theory to the hardened cement pastes [89, 90]. Mindess [91] reported the W values for cement paste from 7 to 14 J/m^2. This W value is not necessary in the σ_k calculation; the experimentally determined critical stress intensity factor $K_{IC} = WE$ is sufficient. The stress value is determined when the crack is radically increasing, which means practically the stress causing the cracking of material. For Portland cement pastes the values from 0.4 to 0.5 MN/m$^{3/2}$ are reported [2, 75, 92–94].

The application of classical fracture mechanics in the case of pastes means that the strength is not controlled by total porosity but by a size of largest pores, playing the role of "cracks". This idea was proposed by several authors, for example by Mindess [95] and Wittmann [96].

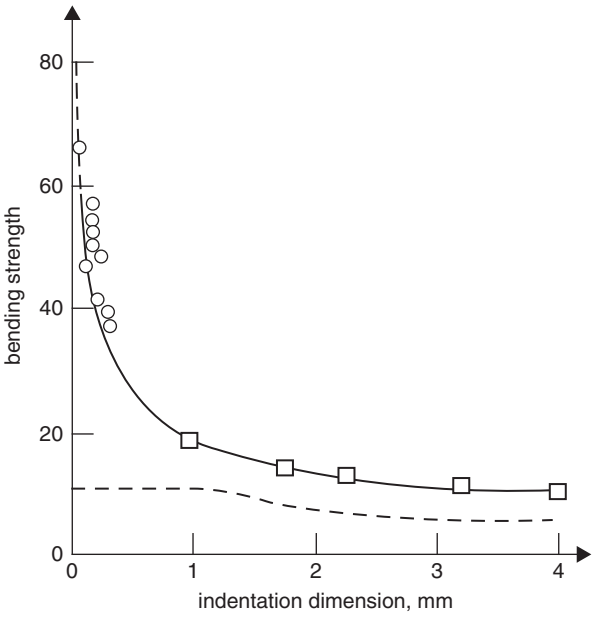


Fig. 5.40 The results for notched MDF cement paste samples (*continuous line*) and classical cement pastes (*dashed line*): *squares* indentations with diamond saw, *circles* defects in the form of air or glass bubbles. (according to [97])

Birchall et al. [97] verified this hypothesis. They measured the tensile strength of paste and compared it to the value calculated from the Griffith's formula, inserting the size of the largest crack, present in the material or produced in it.

The tensile strength of classic cement pastes conforms to the curve plotted on the basis of the Griffith's equation, at the assumption that the width of crack is about 1 mm. The further part of this curve corresponds to the data obtained by Birchall [97], for the specially prepared macro defects free pastes (Fig. 5.40). These pastes are discussed in Chap. 9. They exhibit significantly higher strength because the macropores do not exceed 90 μm.

The compatibility of strength with the total porosity of pastes, proved by all authors, is based on the fact that the factors which reduce the total porosity are diminishing simultaneously the critical size of the "crack". The confirmation of this supposition can be found in the experiments of Alford [98], who shown that the microstructure of classic pastes was very similar to the "macro defect free paste". This is also consistent with all the observations dealing with the beneficial effect of the mean pore size lowering on strength [43, 81–85]. However, the effect of morphology of hydration products can be related to the bonds between the C–S–H crystallites, which affect the surface energy of cracking σ.

There was also presented the hypothesis linking the strength reduction of the paste by the portlandite crystals [99]. This was concluded from the observations of crack propagation in the pastes, surrounded usually the areas rich in CH crystals [100]. However, as it has been shown in recent experiments, the strength of CH is similar to C–S–H strength [101, 102]. Thus, the morphology of calcium hydroxide crystals in the interstitial transition zone, as well as its significant porosity in ordi-

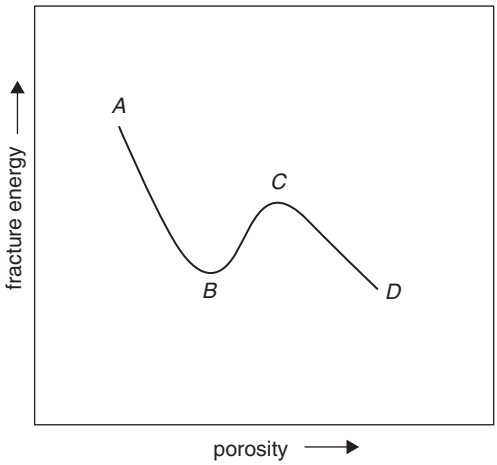


Fig. 5.41 Schematic presentation of general relationship: fracture energy–porosity (after [94]); *A* high strength caused by low porosity and high ratio of unhydrated cement, *B* higher porosity and $Ca(OH)_2$ content, *C* local maximum of strength caused by fracture propagation inhibition on the pores (at porosity = 22.5 %), *D* reduced strength by increased porosity and reduced number of intergranular contacts

nary concrete, favour the formation of cracks running along the CH crystals, which causes the lowering of concrete strength. The silica fume addition or the reduction of w/c, at least to 0.4, is radically changing this situation.

Mindess [89] presented the opinion that the empirical formulae linking the strength with the total samples porosity can be applied to the classical cement pastes. In more precise studies, or in the case of samples with the C–S–H gel modified microstructure (admixtures, hydrothermal treatment), this simple relation is not justified.

The relationship between the cracking energy or the critical stress intensity factor and porosity is more complex, and this relationship was establish qualitatively by Beaudoin [94] (Fig. 5.41). These both parameters depend also on the sample drying procedure, which is understandable in the light of water influence on paste strength, related to the humidity of environment where it was stored.

The reduction of relative humidity of environment from 100 to 0 % causes the growth of W from 7 to 14 J/m^2 and K_{IC} from 0.20 to 0.46 MN/m$^{3/2}$ [2, 94].

Water has a great impact on the paste strength. The water saturated samples have much lower flexural strength than the dry one. However, the compressive strength of paste samples show low increase after drying [46, 103]. Though in the dried samples the microcracks appear, as it has been found under the scanning electron microscope examination, but the adhesion between the surfaces of gel is increasing simultaneously, principally due to the van der Waals forces. The disjoining pressure, exerted by water adsorbed on the walls of crack, is favouring the cracking process, while drying removes the disjoining pressure of water onto the surfaces of crack, close to its boarder. This hypothesis seems to be verified by the experiments with the paste saturated with organic compounds, because such treatment prevents the strength decrease during wetting. Large organic particles cannot penetrate into the microcracks and the disjoining pressure did not appeared [103].

Wittmann [46] determined the tensile strength decrease of the paste specimens dried to the constant mass at temperature 116 °C and subsequently equilibrated with the environment of progressively growing relative humidity. These results are pre-

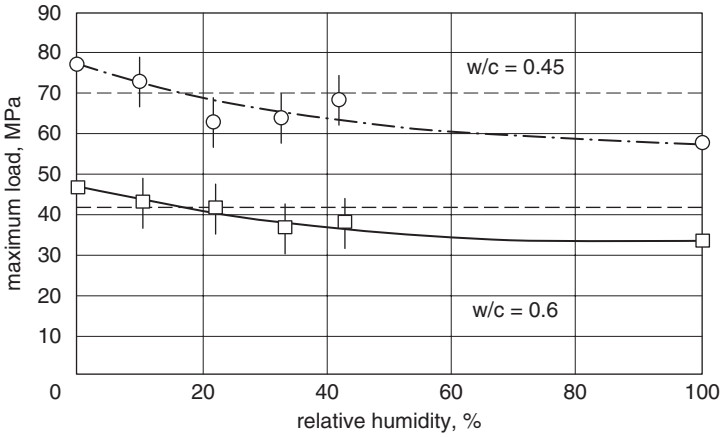


Fig. 5.42 The failure stress of cylindrical pastes specimens vs relative humidity of curing atmosphere in which they were equilibrated. Failure stress of the samples stored 28 days without loss of moisture plotted as dashed lines. (according to [46])

sented in Fig. 5.42. As it is known, the solids reveal a high surface tension, particularly in the case of materials like gel, with very high specific surface area. The surface tension is linked with the surface energy given by Gibbs equation:

$$\sigma = F + A\frac{\mathrm{d}F}{\mathrm{d}A} \tag{5.34}$$

where

A is the specific surface area of a sample.

The water film adsorbed on the surface and neutralizing the charges of surface atoms provides the surface energy lowering of ΔF. The vapour pressure over the solid phase can be calculated from the adsorption isotherm:

$$\pi = \frac{RT}{V_{\mathrm{m}}S}\int_0^{\mathrm{p}}\frac{V}{p}\mathrm{d}p \tag{5.35}$$

where

V_{m} means the mole volume,
S surface,
V volume of gas adsorbed at pressure n,
R gas constant,
T temperature,
p pressure of environment.

Bangham [104] has shown that the surface tension decrease of the solid phase is equivalent to the lowering of surface energy; which is equal to the vapour pressure:

$$\pi = -\Delta F = \sigma_0 - \sigma \tag{5.36}$$

where

σ_0 means the surface tension of solid without water film,
σ the surface tension of solid with adsorbed water film.

Based on the criterion of fracture propagation given by Griffith it can be concluded that with the surface energy decrease the surface tension is decreasing too:

$$\left(\frac{\sigma}{\sigma_0}\right)^2 = \frac{F}{F_0} \tag{5.37}$$

where

σ_0 and F_0 mean the surface tension and surface energy of dry sample,
while σ and F are the same parameters for the wet sample.

After reducing the surface tension the solid which was "compressed" can subsequently expand.

It is known simultaneously [104], that the linear expansion $\Delta l/l$ is related to the surface energy lowering by the formula:

$$\Delta l \,/\, l = \lambda\left(F_0 - F\right) \tag{5.38}$$

From these two relations the next one can be derived:

$$\left(\frac{\sigma}{\sigma_0}\right)^2 = 1 - \frac{l}{\lambda F_0} \cdot \frac{\Delta l}{l} = 1 - \frac{\Delta F}{F} \tag{5.39}$$

λ can be also determined from the following relation:

$$E = \frac{S\rho}{3\lambda} \tag{5.40}$$

where

E is the elasticity modulus,
S internal specific surface area of gel,
ρ density of material without pores.

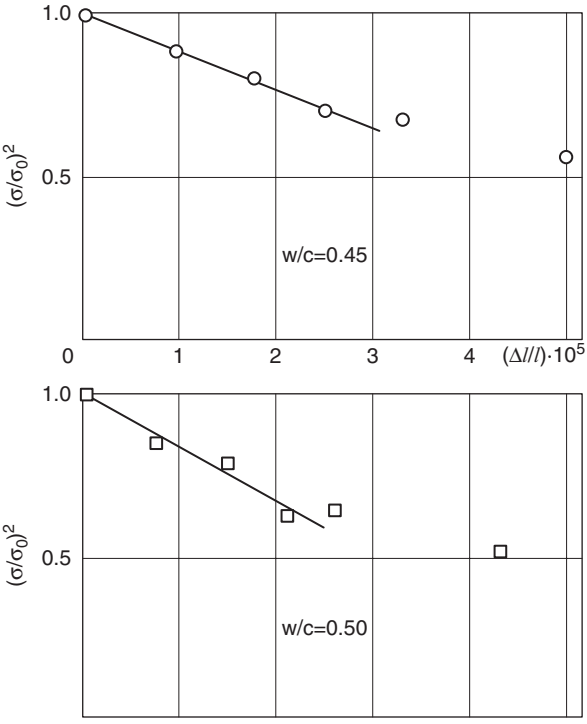


Fig. 5.43 The square of the relative breaking stress vs creep deformation. (according to [46])

The slope of the straight line in the system of coordinates $(\sigma/\sigma_o)^2$—$\Delta l/l$ is as follows:

$$\mathrm{tg}\alpha = -1/\left(\lambda F_0\right) \tag{5.41}$$

This relationship was verified experimentally by Wittmann [46] and the results are presented in Fig. 5.43. As it results from these data, the reduction of relative failure stress vs linear swelling is fulfilling this relation until the relative humidity of 40 %. After the λ value determination the surface energy F_0 can be determined from the slope angle of the straight line.

In Fig. 5.44 the relationship between the square of the relative strength and surface energy is shown [46]. Analogously as in Fig. 5.43, this relationship forms a straight line until the relative humidity of about 40 %.

Also the fatigue strength under the long–term load decreases with the increase of relative humidity of environment in which the samples are equilibrated. It can be concluded that water causes the enlarging of sub–critical microcracks [105].

Feldman and Sereda [43] explain this phenomenon by lower fracture energy of Si–O–Si oxygen bridges, when in samples under load the hydroxyl groups are formed, in the presence of water vapour:

—Si—OH HO—Si—

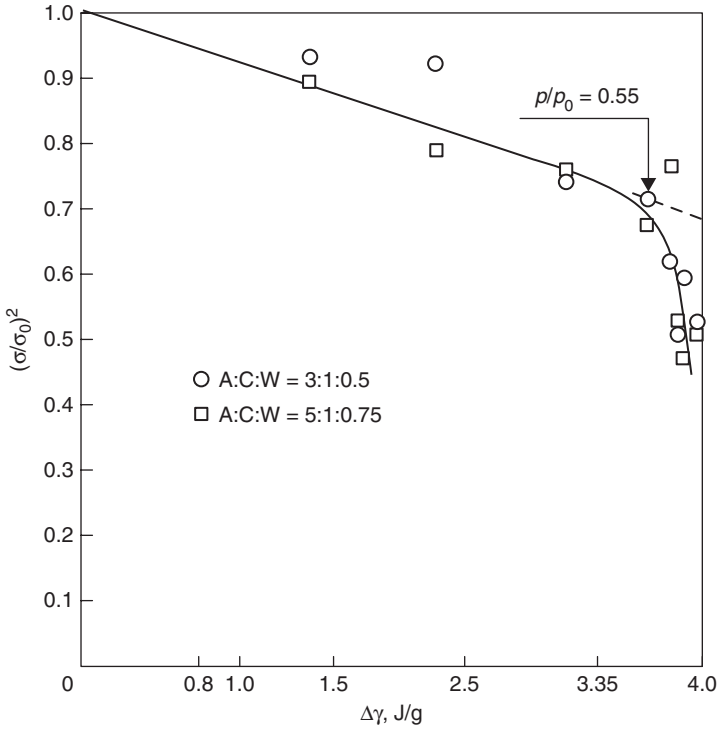


Fig. 5.44 The square of relative compression strength of the paste as a function of surface energy changes (after [46]) (*A*: *C*: *W* aggregate: cement: water ratio); p_0 failure stress

This idea is very similar to the hypothesis explaining the fatigue strength of silica glass under load [106]. There is an opinion that the adsorption of moisture from the environment results in the hydrolysis reaction:

$$\text{H—O—H+Si—O—Si} \rightarrow \text{—Si—OH+HO—Si—} \tag{5.42}$$

which causes a thin layer of silica gel formation on the glass surface.

According to the hypothesis presented by Barrick [107], the solution in the samples under load has a corrosive impact, related to the presence of $Ca(OH)_2$. On the other hand, it is considering that drying of the paste can lead to the crystallization of different phases in the pores (CH, CAH_x), originating from the components occurring in the solution, and hence the strength is improved.

5.3 Deformation of the Paste

In the case of good properties of concrete components and correct mixture proportions the most important is shrinkage of the paste, which can appear at very early age, immediately after concrete placing. There are two groups of reasons resulting

in the shrinkage of the paste. The first one relates to the reactions occurring in the paste (chemical and autogenous shrinkage), as well as to the properties of paste (bleeding), the temperature gradients formation in concrete (heat of cement hardening). To the second group of shrinkage inducing factors the external physical effects are rated (temperature, humidity, insolation, and wind force). The most important process caused by external factors is the reduction of moisture content in concrete, that is its drying. Obviously, these external factors have a great impact on the shrinkage being the result of the former factors and can eliminate or markedly reduce them. For this reason the proper curing of concrete, soon after its placing in construction, has so great importance. It relates particularly to the drying shrinkage of the paste, which can lead to the generation of microcracks or even larger fissures in the concrete composite.

5.3.1 Volume Changes of the Plastic Paste

The reaction of cement with water causes the general reduction of this mixture volume. It can be calculated based on the specific density of substrates and cement hydration products. These volume changes are called the "chemical shrinkage" or contraction and are linked with the lower water volume in the hydrated phases as compared to its volume in the liquid phase. On the base of contraction of cement mixture with water the progress of hydration reaction can be determined and even the strength of concrete [108].

Contraction depends on the phase composition of cement. C_3A has the highest contraction and C_2S—the lowest one. Contraction can be calculated from the molecular mass and densities of the substrates and of hydration products of cement constituents reactions with water. At simplified assumption that the tobermorite $C_3S_2H_3$, with density 2.44 g/cm^3 is the product of C_3S and C_2S reaction with water we have:

For C_3S

$$\begin{gathered} 2C_3S+6H \rightarrow C_3S_2H_3+3CH \\ 2\times\frac{228.33}{3.15}+6\times 18 \rightarrow \frac{342.42}{2.44}+3\times\frac{74.08}{2.23} \\ 145\text{cm}^3+108\text{cm}^3 \rightarrow 140.3\text{cm}^3+99.7\text{cm}^3 \\ 253\text{cm}^3 \rightarrow 240\text{cm}^3 \end{gathered} \tag{5.43}$$

the reduction of volume is 13 cm^3 for 456.66 g C_3S, that is 2.8 %.

For C_2S

$$\begin{gathered} 2C_2S+4H \rightarrow C_3S_2H_3+CH \\ 2\times\frac{172.25}{3.28}+4\times 18 \rightarrow \frac{342.42}{2.44}+\frac{74.08}{2.23} \\ 105\text{cm}^3+72\text{cm}^3 \rightarrow 140.3\text{cm}^3+33.2\text{cm}^3 \\ 177\text{cm}^3 \rightarrow 173.5\text{cm}^3 \end{gathered} \tag{5.44}$$

Table 5.5 Contraction of Portland and calcium aluminate cement [38]

Cement	Reduction of volume in relation to initial volume, %			
	1 day	7 days	28 days	100 days
Portland cement (100 g + 33 g water)	2.8	4.8	6.0	6.9
Calcium aluminate cement (100 g + 33 g water)	11.1	13.8	15.2	16.3

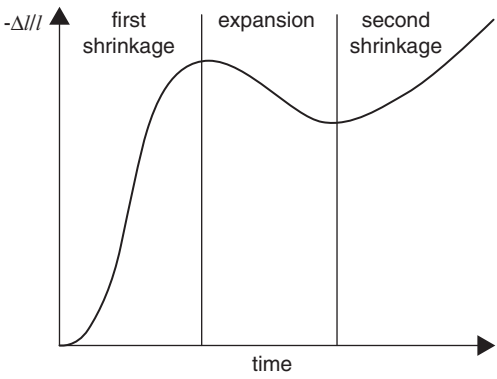


Fig. 5.45 The linear shrinkage of cement paste in a dilatometer. (according to [109])

the reduction of volume is 3.5 cm^3 for 344.5 g C_2S, that is 1 %.

For C_3A

$$\begin{gathered} C_3A+3(CaSO_4 \times 2H_2O)+26H_2O \rightarrow C_3A+3CaSO_4 \times 32H_2O \\ \frac{270.2}{3}+3 \times \frac{172.25}{2.32}+26 \times 18 \rightarrow \frac{1255.13}{1.73} \\ 780.7cm^3 \rightarrow 725.5cm^3 \end{gathered} \tag{5.45}$$

the reduction of volume is 55.2 cm^3 for 786.7 g of anhydrous phase, that is 7 %.

The contraction is linked with the hydration rate, therefore the rate of contraction increases with the C_3A and C_3S share, fineness of cement and w/c ratio. Typical data for Portland cement and calcium aluminate cement are listed in Table 5.5 [38].

The chemical shrinkage was investigated with two methods: in open or in sealed containers. In the first case the paste can exchange water with the environment, which is not possible in sealed container. In this container the paste shrinkage is lower and the shrinkage curve shape is presented in Fig. 5.45 [109]. The three phases can be distinguished: the first shrinkage, expansion and the second shrinkage. The first one occurs before and during setting. Afterwards, some expansion of unknown origin is observed. Buil and Baron [109] suppose that this is the hydration of free lime from cement.

The next shrinkage takes place during hardening and it is known as an autogenous shrinkage or self–drying. It is related—as assumed in the old theory of Davis with the formation of pores in the paste, filled with air. As a consequence, the partial pressure of water vapour being in equilibrium with the paste decreases, resulting in

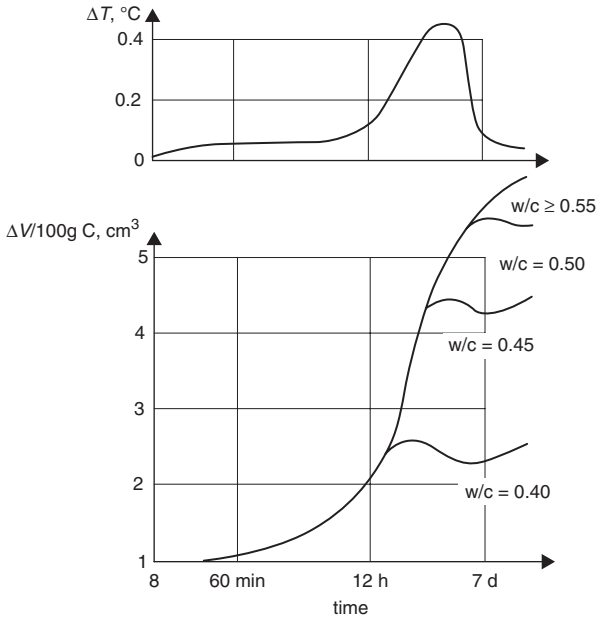


Fig. 5.46 Volume shrinkage of cement paste in sealed containers. (according to [109])

self–drying. From the physical point of view this mechanism is the same as that of drying shrinkage, and the effect is also similar.

Ziegeldorf [110] explained the effect of bleeding on shrinkage, which raised some controversy. As higher bleeding, as higher total shrinkage of the paste, while the absorption of separated liquid by the paste gives some expansion [110]. This author found also that the divergence of shrinkage curves obtained with two aforementioned methods appears more quickly at lower w/c ratio of the paste (Fig. 5.46). At w/c > 0.55 there is no difference between the shrinkage curves obtained with these two methods [110].

The plasticizers decreasing the intensity of bleeding influence simultaneously on the reduction of settlement of solid paste components, which leads to the decrease of shrinkage [109].

The hardening shrinkage, related to the reduction of apparent volume of sample, is much lower than the "chemical" shrinkage, being the reason of the former one. There is an exact relationship between the chemical shrinkage and consequently of the hardening shrinkage and the heat of hardening (Fig. 5.47) [109]:

$$\frac{\mathrm{d}Q}{\mathrm{d}t} \approx 0.5 \frac{\mathrm{d}E_i}{\mathrm{d}t} \tag{5.46}$$

where

Q is the heat of hardening (J/g of unhydrous cement),
E_i contraction (mm^3/g of unhydrous cement),
t time.

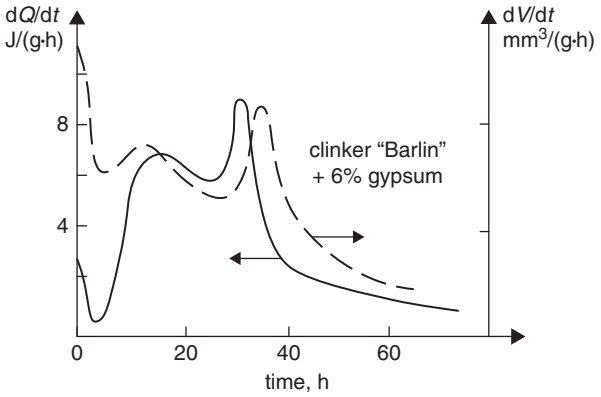


Fig. 5.47 Example of heat evolution and Le Chatelier contraction (chemical, *dashed line*) curves. (according to [109])

Some divergence occurs during the first hours of hydration, attributed to the reduction of water volume, which molecules are attracted by Ca^{2+} cations (solvation), released to the solution [109].

The contraction is significantly affected by the false set, which increase it significantly, during first 3 h [111].

The first shrinkage corresponding to setting is lower than the plastic shrinkage, relating to drying and hence it has no practical importance, while the second one—occurring on hardening, can result in the formation of microcracks in concrete [109]. The latter one takes place in the paste after setting, when a certain strength level is achieved [109]. Its absolute size is very similar to the former one, ranging $1.5 \cdot 10^{-3}$ $\Delta l/l$, that is why the significantly higher stresses in the material are involved. They are more pronounced as the shrinkage changes go faster, particularly as it is coinciding with thermal shrinkage, caused by the temperature fall down in the paste. It depends on w/c ratio and decreases with its increase [109].

In spite of the contraction, the paste matured under water shows the relative volume increase; it means that the external dimensions of sample become higher. This phenomenon is observed after final setting, that is when the increasing volume of solid phases cannot be longer balanced by the plastic changes of the paste. As could be deduced from the calculated examples given earlier, the hydration products exhibit significantly lower density and consequently higher volume than the anhydrous phases. Simultaneously, the hydration products growing on the surface of cement grains, in the space occupied previously by water, is gradually causing the share of capillary pores decrease. The capillary pores ratio decrease vs time is shown in Fig. 5.48 [112].

At early age of cement paste reaction with water the plastic shrinkage occurs, which consists in evaporation of water from the surface layers of concrete [108]. The volume of fresh concrete is thus reduced. This process is not related to the properties of cement itself; however it can also result in the formation of cracks. This situation is the consequence of substantial humidity gradient in concrete. The plastic shrinkage, equal 2.5 mm/m, observed in the 7 cm thick surface layer of concrete, was two times higher than the shrinkage in the core of element [108].

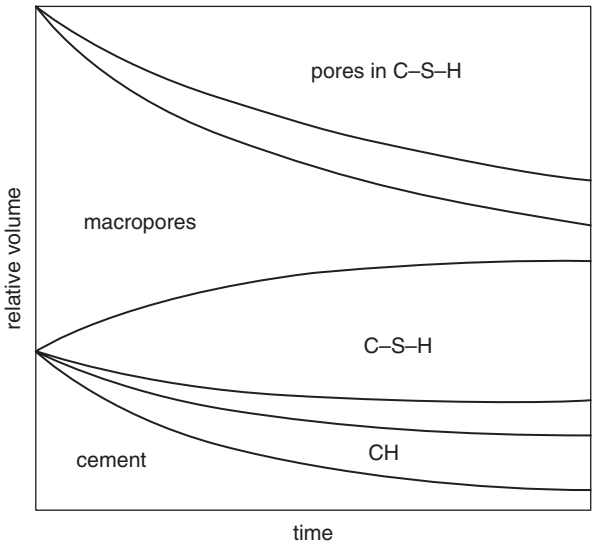


Fig. 5.48 Reduction of capillary porosity vs time of hydration. (according to [112])

In the case of high performance concrete produced at low w/c ratio, the autogenous shrinkage (self–drying) is particularly important. In order to elucidate the causes of this shrinkage, the ratio of water required for completed hydration of cement, estimated by Powers [113] as w/c = 0.38, must be reminded. Powers [113] determined the non–evaporable water and total water content in the paste from several cements with different w/c and matured for different time. These results plotted in the Fig. (5.49) give two straight lines which intersect in a point corresponding to the initial w/c = 0.38, in which the ratio of non–evaporable water is 0.227. Simultaneously, at saturation (capillaries filled with water), the paste contains 0.211 of evaporable gel water, giving the total water content equal $w_t/c = 0.438$. It results that the absorption of water by the paste (sample immersed in water) was 0.058 kg water per 1 kg of cement. The straight lines have the equations: $w_e/c = 0.482 \cdot w_t/c$ (w/c < 0.38) and $w_e/c = w_t/c - 0.227$ respectively.

The volume share of particular cement paste component can be conveniently analyzed on the Rüsch's diagram [108], for the systems with variable w/c (Fig. 5.50). However, the auto–drying must be investigated at constant w/c, lower than 0.38. In the case of closed system, without the external water access, the hydration of cement can be continued for a time after exhausting of free water. Cement drains then water from the coarser capillaries in which menisci will be formed. Simultaneously the progress of hydration will cause the decrease of humidity of the system, thus the lowering of water vapour pressure, which is also enhancing the formation of menisci in capillaries. Then the tensile stress in them will appear causing the shrinkage of the paste. Also the C–S–H phase will lose a part of interlayer water (see Table 5.3). In open system the self–drying will not occur because of the external source of water. These two cases are shown in Fig. 5.51 [114].

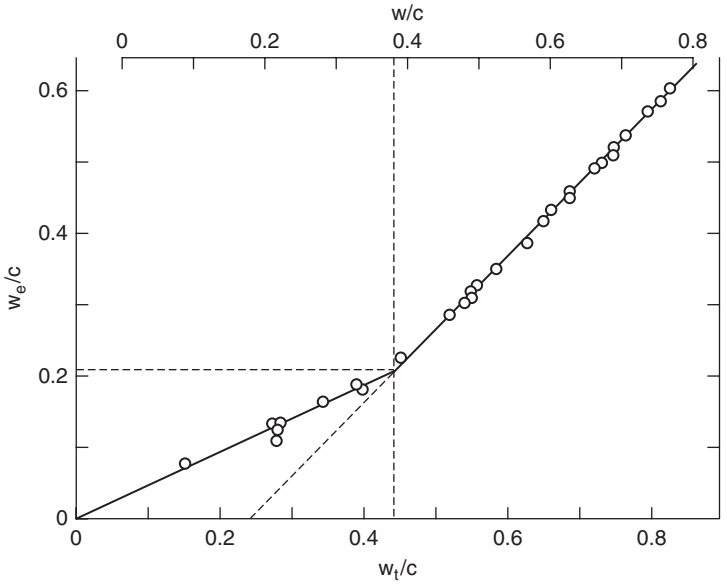


Fig. 5.49 Relations between the initial (w/c), total (w_t/c) and evaporable (w_e/c) water to cement ratios for saturated, mature pastes of a Portland cement. (according to [113])

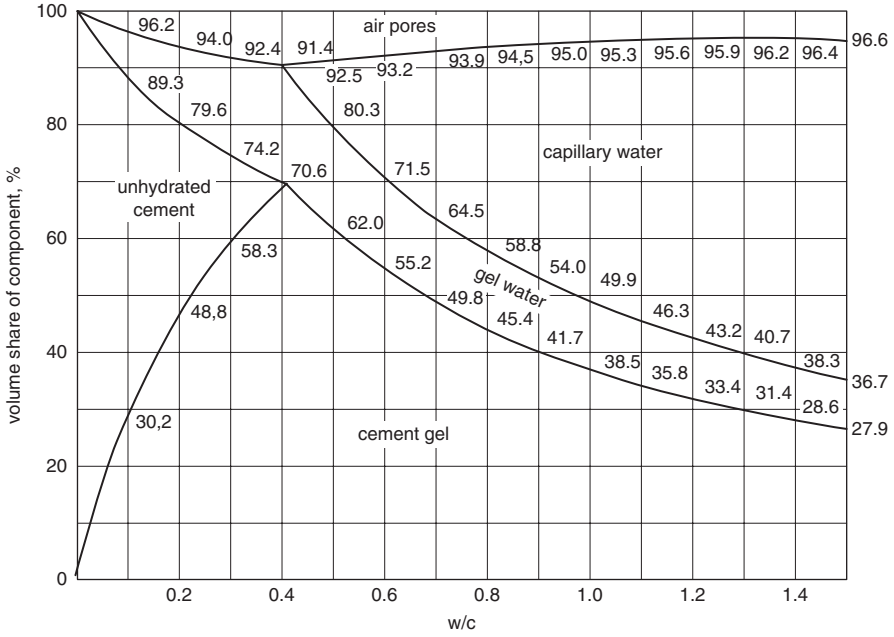


Fig. 5.50 The volume shares of hardened cement paste as a function of w/c ratio. (after [108])

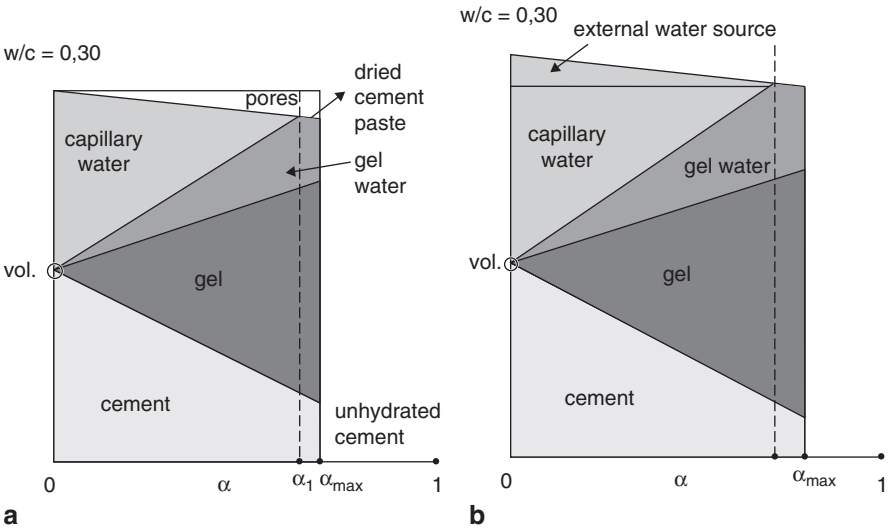


Fig. 5.51 Scheme of the volume changes of cement paste during hydration: **a** closed system **b** open system, access of external water. (according to [114])

In the case of closed system there are two shrinkage increasing factors, a higher amount of cement and less water in the capillary pores, then the higher tensile stresses are induced (smaller radius of menisci). This conditions are typical for high performance concrete and the possibility of cracks formation will be significantly increased. When hydration of cement in the paste of low w/c ratio takes place at the presence of external source of water (case b), the autogenous shrinkage related to the self–drying will be much lower, however, will occur also, because there will be always some microareas in the paste, cut off the external source of water. It means also that the nanopores will be disconnected from the capillary network. The hydration in these microareas will occur as in the paste without external source of water. The autogenous shrinkage will be also higher in the paste of lower w/c, because of the higher cement content; in this case the nanopores formed as a result of chemical shrinkage will absorb more water (Fig. 5.52). Moreover, the capillary water content in initial mix will be reduced, as well as the diameters of these capillaries will be narrower and their tensile stresses will be higher.

Autogenous shrinkage is not harmful in concrete with w/c ratio over 0.5, because in this condition the coarser capillaries volume share is higher and also the content of capillaries with large radius is higher too. Menisci formed in these capillaries generate weak tensile forces and autogenous shrinkage of this concrete is negligible.

The autogenous shrinkage depends on the composition of cement and will decrease in the case of cement with mineral additions and this effect will increase with the rise of the share of these additions. It is obvious, because the hydration or pozzolanic reaction of these additions occurs more slowly and hence they will remain much longer as the anhydrous paste component. The similar effect is observed in

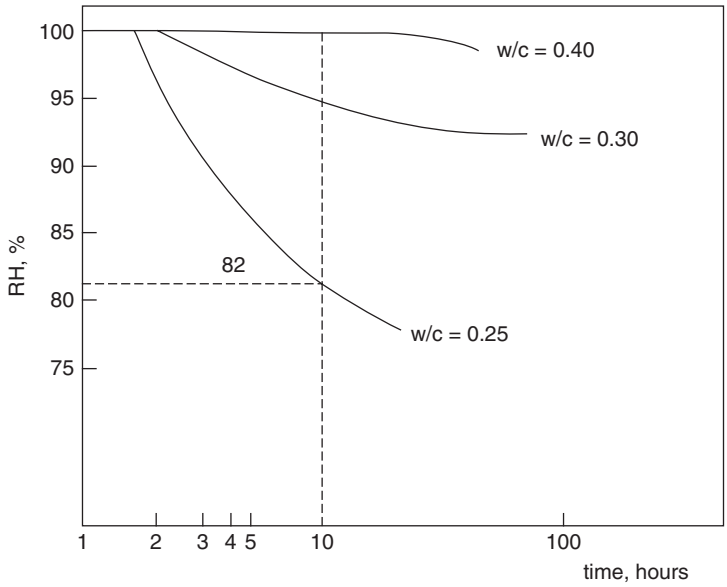


Fig. 5.52 Effect of w/c on the autogenous shrinkage. (according to [96])

concrete in which part of cement will be replaced by mineral additions and the autogenous shrinkage will be reduced.

5.3.2 Drying Shrinkage

Several physical properties of concrete and primarily the volume changes, are strongly related to the moisture content. The close similarity can be noticed when comparing the paste moisture content curves vs water vapour pressure, as well as the shrinkage of sample vs time [39].

The drying shrinkage is beginning very early, immediately after the placing of concrete, and is caused by evaporation of water from its surface. Because of the early loss of water, before and during setting, when the concrete is plastic, this shrinkage is called "plastic shrinkage". Its end coincidence with the final setting time, when a deformation of concrete is markedly reduced [115]. The order of magnitude of this shrinkage is of 1 mm/m, in normal conditions, but is can be much higher (even five times) in the case of strong wind, and at elevated temperature [115].

The effect of this shrinkage phenomenon is of great importance in case of flat concrete surface, for example slab foundations and floors, with a high surface to thickness ratio, where the loss of water may be significant, particularly in summer period and at strong wind (Fig. 5.53). It causes the cracks formation and therefore the curing of concrete, should start immediately after its placing. The loss of water from concrete surface should not exceed 1 kg/(m^{2}h) [115]. The barriers, such as

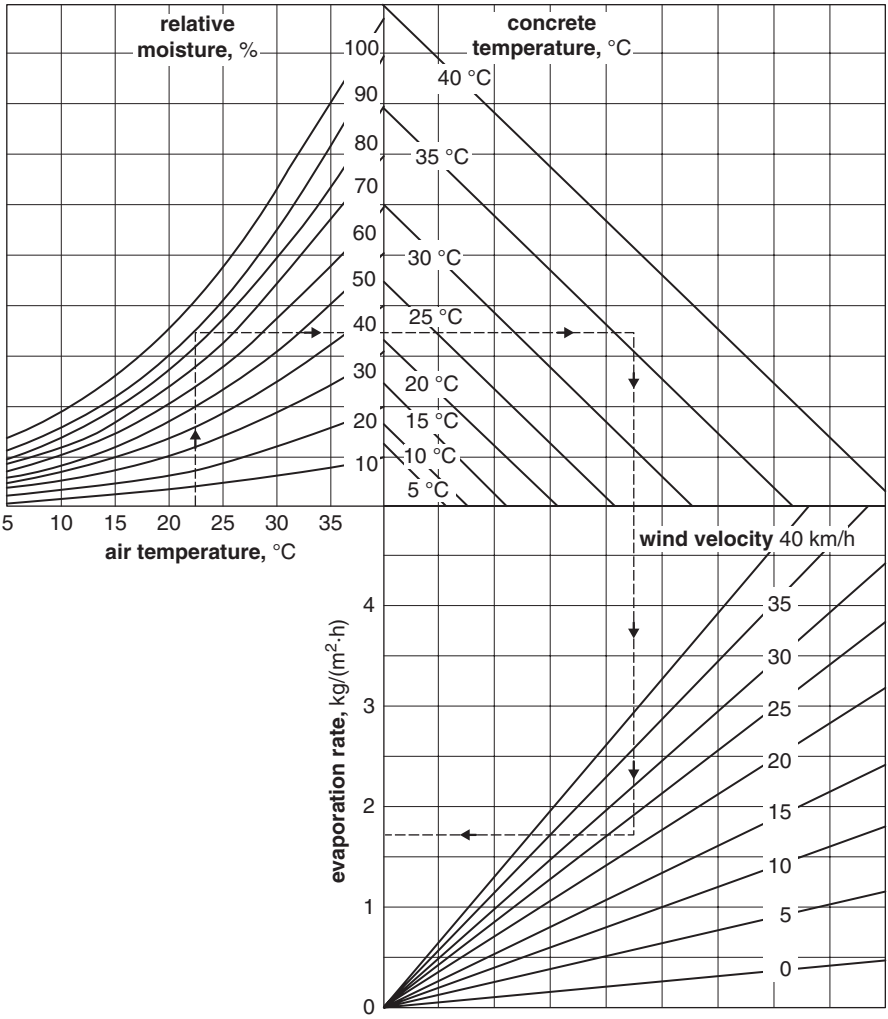


Fig. 5.53 Diagram for evaluation of water evaporated quantity from the concrete surface, as a function of concrete and air temperature, its relative humidity and wind force

reinforcing bars or coarse aggregate grains (Fig. 5.54) [115] can cause so–called incidental shrinkage by counteracting the uniform settlement of concrete (plastic settlement).

As it has been proved, drying shrinkage significantly increases with growing w/c ratio in the paste, as well as slightly with the period of samples curing (Fig. 5.55) [34]. Verbeck and Helmuth [34] conclude that shrinkage is a linear function of primary porosity of samples, while is little affected by the hydration degree. However, it should be remembered that at constant w/c the porosity is a function of hydration degree.

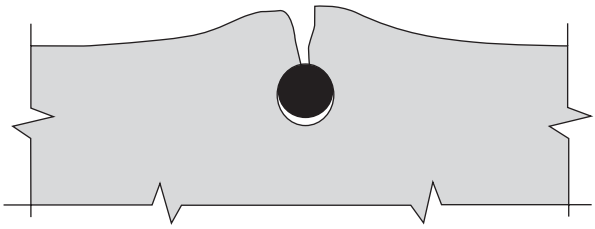


Fig. 5.54 Settlement of concrete in the case of barrier formed by reinforcement. (after [115]) Dėtrichė C. H., Chapter 4 in « La Durabilitė des Bėtons », page 118, fig. 4.7 « Schema montrant le tassement du bėtons bloquė », Published by Presses de l'Ecole Nationale des Ponts et Chaussėes, reproduced with the permission of the Presses de l'Ecole Nationale des Ponts et Chaussėes

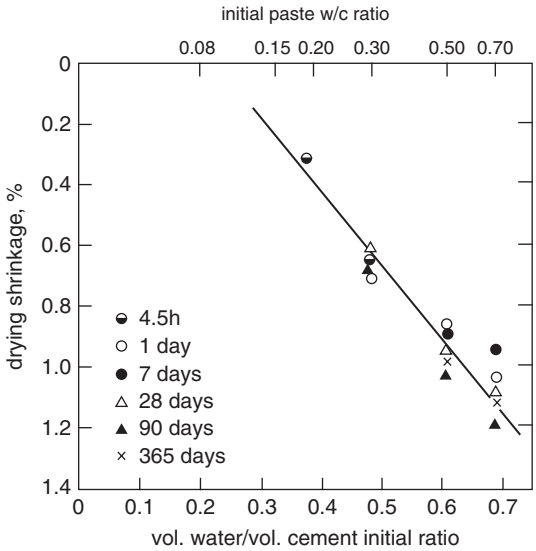


Fig. 5.55 Drying shrinkage of cement paste in air of 0% relative humidity vs initial porosity of pastes. Pastes dried for 2 months. (according to [34])

On the shrinkage curves vs relative humidity the two straight line intervals can be noticed: initial shrinkage, up to the 20–30% loss of water (depending on the previous maturing time) and the second one, for higher loss of water [34]. The first one corresponds to the much slower increase of shrinkage with the water content lowering.

The shrinkage changes are depending on the history of sample, it means on the method of sample drying [52]. The linear dependence between the shrinkage and loss of water is possible only at one drying cycle. The progressive drying with equilibration of paste in relation to the environment[6], through the intermediate steps

[6] The "equilibrium" in term of relative humidity relates to the experimentally determined constant mass of samples in a CO_2 free atmosphere. It does not mean the chemical equilibrium be-

does not result in obtaining this, composed of two sections, broken line mentioned above. At intermediate humidity the irreversible structural changes occur. It should be remembered that the autoclaved paste reveals significantly lower shrinkage.

The mechanism of shrinkage is complex and relates to the following phenomena:

- capillary pressure,
- disjoining pressure of water,
- change of surface energy of gel originated from the desorption of surface adsorbed water,
- exchange of interlayer water.

The phenomena occurring during the adsorption and desorption of water vapour in the paste were discussed in the previous chapter.

The radius of curvature in the capillaries is increasing as the content of condensate decreases; simultaneously the compressive hydrostatic pressure inside the skeleton composed of gel particles increases. The capillary pressure becomes important to the relative humidity of about 40%; at lower humidity water does not form menisci in the capillaries [63].

The liquid in the capillaries of small radius exerts relatively high pressure, inversely proportional to the radius of meniscus:

$$P_{\text{cap}} = \frac{2\sigma}{r} \tag{5.47}$$

where

σ means the surface tension of water.

The shrinkage resulting from the loss of capillary water results in the elastic deformation, depending on the elasticity modulus of the paste. The reduction of elasticity modulus with the increase of w/c ratio leads to the rise of this deformation.

The importance of capillary pressure on shrinkage is variously assessed. According to Powers [113] and Feldman [116] this effect is negligible. On the contrary, Wittmann [117] attributes a decisive role to this effect and it is commonly accepted view.

At relative humidity lower than 40%, particularly below 20%, the effect of decrease of water disjoining pressure, as well as the increase of surface energy of gel becomes significant. The disjoining pressure disappears successively with water evaporation and the van der Waals attractive forces are affecting the neighboring crystallites in gel.

It should be underlined that according to Wittmann [96], the variation of water disjoining pressure has an impact on the paste only at the relative humidity above

cause cement paste is not a stable system from the thermodynamics point of view. Cement paste transformation occurs during many years and aims at the surface energy lowering, first of all through the reduction of very high surface area.

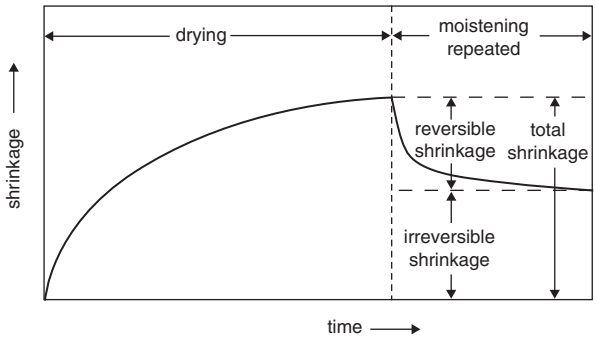


Fig. 5.56 Typical changes occurring in cement paste at first drying and second moistening

50%. This mechanism is rejected entirely by Feldman and Sereda [64], as not consistent with their model.

Simultaneously as a result of water desorption a change of surface energy ΔF occurs, attributed to the paste shrinkage, shown in Figs. 5.45 and 5.46. The changes of surface energy are linked with compressive stress by the following formula:

$$P_F = \frac{2\sigma S}{3} \tag{5.48}$$

where

σ is the surface energy and
S surface.

This effect is significant only at relative humidity of the environment lower than 20%.

According to Wittmann [96] the shrinkage of the paste, occurring with variation of relative humidity under 40%, should be attributed to the change of surface energy. The relation presented in Fig. 5.44, showing the compatibility of stress and energy changes is it confirmation.

Parallel to the capillary shrinkage as well as resulting from the surface energy changes, the shrinkage caused by the interlayer water loss in the paste occurs. The last one is linked with the interplanar space in the C–S–H structure decrease; this problem was discussed in Sect. 3.2.3. The different theories, represented by different research schools, on the possibility of this water reversible loss, are given too.

Feldman [35], opposite to Wittmann, is of the opinion that the surface energy changes have low effect on shrinkage and evaluates it as 20%.

The sample dried for the first time shows an irreversible shrinkage, as shown schematically in Fig. 5.56. The size of this shrinkage is markedly influenced by the porosity of the paste, while of the reversible one is not [34]. The dependence of an irreversible shrinkage vs water loss of the paste is also distinctly dependent on drying time; the shrinkage increases with this time. The slow, progressive structural changes of the paste are hence pointed out [34].

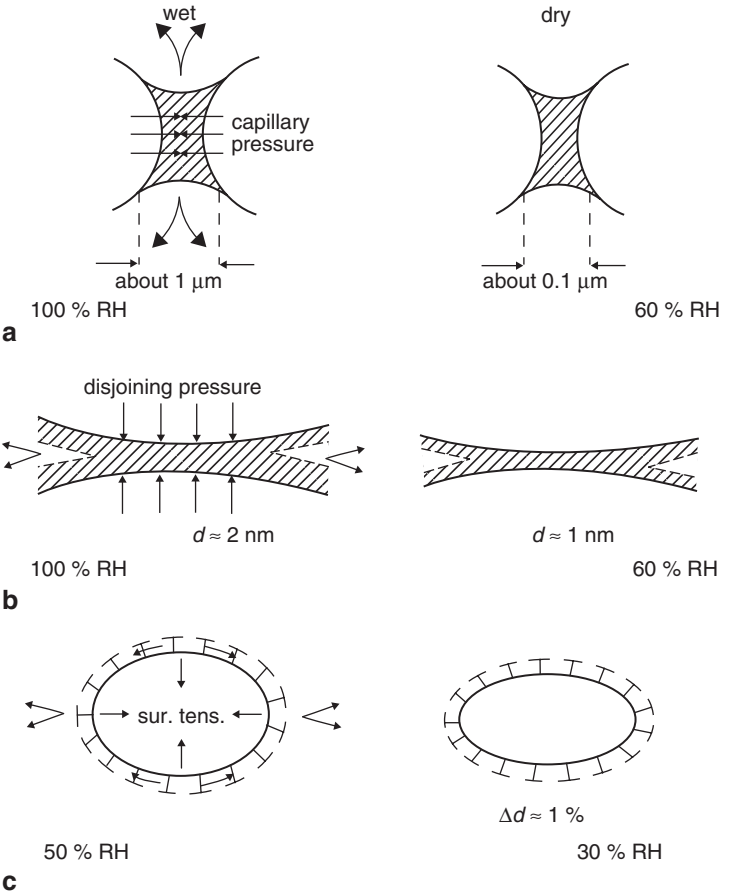


Fig. 5.57 Proposed shrinkage mechanisms of cement paste drying: **a** capillary forces. **b** disjoining pressure. **c** surface tension. (according to [89])

There is some relative humidity threshold value, of the atmosphere surrounding the paste sample, above which the irreversible shrinkage does not occur yet. According to Verbeck [34], it corresponds to the low relative humidity value of 11 %.

Hypotheses concerning the mechanism of irreversible shrinkage assume that the chemical bonds formed between the crystallites of gel are not secondary broken at the renewed moistening of sample [34, 35]. This view is supported by the irreversibility of interlayer water exchange in C–S–H; the basal spacing does not attain its primary value [103].

The mechanism of irreversible shrinkage is not clear; there are presumably all the factors affecting shrinkage involved. The decreasing distance between the gel particles may be considered as irreversible, because it leads to the reduction of free energy of the system. The effect of different factors on irreversible shrinkage is shown in Fig. 5.57.

On the turn of seventies and eighties the hypothesis postulating the two different mechanism of irreversible shrinkage has been proposed [118–120]:

- capillary effect occurring in the porous material containing pores of diameter above 2.5 nm, because the significant capillary pressure can be formed only in mesopores 2.5–3.0 nm,
- gel drying, that means the loss of water by C–S–H, embracing the pores smaller than 2.5 nm (micropores), in which the capillary effect does not occur.

In the paste with low hydration degree the capillary effect is of special importance. The capillary pressure leads to the collapse of pores with diameter in the range from 4 to 10 nm, associated with the specific surface decrease, as measured by nitrogen adsorption.

The gel drying mechanism is always of some importance for the shrinkage formation, but its role becomes significant at higher hydration degree. The distance decrease between the surfaces of C–S–H layers causes the increasing number of Si–O–Si chemical bonds. The condensation of silicate anions in the C–S–H structure causes an irreversible shrinkage. A high degree of silicate anions polymerization in the C–S–H phase in the paste, for example resulting of its thermal treatment, leads to the lower shrinkage. Summarizing, these authors state that shrinkage depends on pore structure (content of pores smaller than 30 nm), on C–S–H share (hydration degree) and its structure. They proposed the following relation:

$$Z = \frac{V^x \cdot S}{N} \tag{5.49}$$

where

Z is shrinkage,
V^x volume of pores under 30 nm; which is a function $\Sigma V_i(D_i)\mathrm{F}(D_i)$ [where $F(D_i) = 300/D_i$, D_i is the mean diameter of pores],
N silicate anions polymerization degree in the C–S–H phase, as determined by trimethylsilylation method,
S specific surface area determined by water vapour adsorption.

The reduction of shrinkage with time of paste maturing would be related not only to the porosity lowering but also to the higher polymerization degree. According to Parrot [121] only the irreversible shrinkage is affected by polymerization degree but not the reversible one.

The authors of the work [120] are of the opinion that the creep and shrinkage are related to the different structural changes. Creep is not affected by porosity, while both creep and shrinkage are the function of the silicate anions polymerization degree of C–S–H phase and decrease with its increase. A significant growth of the specific surface area determined by nitrogen adsorption was found in the samples after the creep measurements [120]. The authors attribute this change to the great "internal dilatancy" of C–S–H phase occurring only at high polymerization degree.

The paste carbonation is an additional component of the shrinkage. This shrinkage is highly dependent on the relative humidity as it is shown in Fig. 5.58 [122].

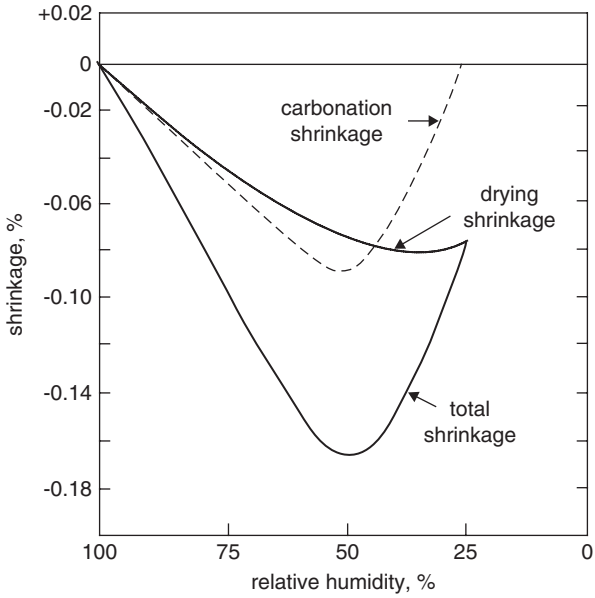


Fig. 5.58 Effect of drying and carbonation on shrinkage. Sample curing: 7 days in water, then 52 days in air without CO_2 and subsequently 60 days in air atmosphere with CO_2

The highest shrinkage corresponds to the relative humidity of 55 %. The plots contribute to the samples firstly dried and subsequently subjected to wetting in the air with increasing relative humidity, CO_2 free or with CO_2. The carbonation shrinkage is occurring also in the pastes without CH, for example produced from calcium aluminate cement or Portland cements autoclaved with silica addition. The depth of carbonation is significantly higher than it would result from the evaluation by means of phenolphthalein test [123, 124].

It should be remember that the carbonation of massive concrete elements of normal density is limited only to the outer surface region. That is why a high carbonation of experimental samples does not express the field conditions encountered in practice. Massive elements, when subjected to drying, reveal a high gradient of moisture and therefore their carbonation occurs at higher humidity than that corresponding to the surrounding atmosphere. Many data concerning the concrete construction are reported by Hamada [123].

The mechanism of shrinkage caused by carbonation is not explained. Lea [39] reminds that the reaction:

$$Ca(OH)_2 + CO_2 \rightarrow CaCO_3 + H_2O \tag{5.50}$$

occurs with the increase of a volume of solid phases. However, in spite of this, the calcium hydroxide carbonation results in the shrinkage similar to that observed in the case of cement paste [39].

At early age of this process in Portland cement pastes, the calcium hydroxide is mainly subjected to carbonation, and 1 mol of H_2O is evolved per 1 mol of CO_2. At later ages of carbonation this ratio is markedly lowered.

Lea [39] is accepting the hypothesis that carbonation shrinkage can be explained by decrease of the non–evaporable water content in cement gel. However, Powers (according to Lea [39]) attributed this shrinkage to the dissolution of $Ca(OH)_2$ in the zone of shrinkage stress caused by drying, and precipitation of calcium carbonate in the zones of lower stress.

Carbonation leads to the reduction of volume changes induced by the moisture changes of concrete matured at ambient temperature or heat treated at normal pressure. However, the volume changes of autoclaved elements, as well as of the lime–sand brick are increased [39]. This stability of volume in the case of non–autoclaved concrete elements was applied in industrial practice [39].

5.3.3 Volume Changes of Concrete

The volume changes of cement paste affect the volume changes of concrete. However, in concrete the presence of more or less interlocked aggregate skeleton can restrain to a certain extent the global deformation of concrete [125]. They will be lower than in a paste, having the same w/c ratio. Certainly the paste shrinkage itself will be not changed, but its restriction by aggregate will possibly result in the microcracking of the hardened cement paste, depending of the tensile strength of the paste and tensile stress generated by the menisci formed due to self–drying of the paste [125].

Aïtcin [125] reminds that the increase of coarse aggregate content and decrease of fine aggregate results in reduction of final shrinkage. However, it should be remember that the coarse aggregate content increase has no effect on the absolute volume change of cement paste. The latter one depends only on the w/c ratio.

A skeleton formed by aggregate plays a main role in the formation and size of microcracks resulting from the volume changes of paste. At a constant w/c ratio, the concretes with lower coarse aggregate content show a tendency to produce a low number of cracks with wide opening, while in those with higher coarse aggregate content a network of small microcracks is formed, however, the total volume of these cracks is similar [125]. From the concrete durability point of view the network of fine microcracks is more convenient than the larger and deeper cracks, which facilitate penetration of corrosive solution into concrete. This results in quick corrosion of reinforcement bars and concrete.

As a result of concrete exposure to dry air or wind, the loss of some water content and decrease of its mass occurs. In the surface capillaries the menisci are produced and consequently the tensile stresses appear, reducing the apparent volume of concrete. This is known as drying shrinkage, accompanied by a loss of concrete mass. As it has been mentioned earlier, as higher w/c ratio as faster and more extensive shrinkage (Fig. 5.52), because water can easily evaporate from wide, joined capillaries system. The final drying shrinkage value is affected by porosity and pore structure, as well as depends on the relative humidity of atmosphere.

Concrete with high w/c ratio can reveal a chemical shrinkage ten times higher than the autogenous one [125]. However, in the case of concretes with low w/c the autoge-

nous shrinkage can be the same as the drying shrinkage of concrete with w/c = 0.5 and occurs during the first days of hydration, when the tensile strength is low. The drying shrinkage develops slowly and begins later, when the tensile strength of concrete is higher. When the concrete with low w/c is not subjected to the proper curing and undergoes drying for a long time in the atmosphere of low humidity, the cracks can appear at longer time after placing, when the tensile stresses induced by autogenous and drying shrinkage will exceed the tensile strength of concrete.

5.3.4 Creep

Cement paste is an elastic material in some extend; it means that the deformations appear and disappear soon after superimposing and removal of the stress. However, at long lasting load the paste exhibits creep. It is shown in Fig. 5.59, where the elastic component is also marked. The creep shows a significant irreversible component, analogously to shrinkage. Therefore the deformation is decreasing after the removal of load, but not totally. In the case of simultaneous drying of loaded sample the creep is higher than for the sample dried before loading. These relations are reported with details by Neville [126] and they are presented schematically in Fig. 5.59.

Neither a model of creep, nor the mechanism of this process is known as well. Obviously, the creep relates to the properties of cement gel and the presence of adsorbed water. The creep growth with moisture content in a paste, while the dried samples do not show this effect [127]. However, this latter statement is not quite sure; perhaps only a substantial reduction of creep occurs [128]. The hypotheses assume the "squeezing" of water from the paste under load.

Powers assumes in his theory that in the case of very thin water layer on the C–S–H particles a disjoining pressure appears. The equilibrium state of adsorbed water depends on the thickness of water layer and of stress.

The application of external stress causes the increase of disjoining pressure and a part of water from micropores must diffuse to the macropores, to maintain the equilibrium. This model is the same as the hypothesis of drying, which is assuming the reduction of adsorbed water layer thickness. Basing on this assumption it can be expected that the creep will grow with the share of capillary pores increase in the paste, then will be inversely proportional to the strength. However, the creep occurs in the samples matured for a long time, even 30 years. Therefore this phenomenon cannot be attributed only to the content of water between the gel particles. For these reasons there must be the other creep generating factors, among the other a hypothesis of the mutual displacement of gel particles is advanced. At the presence of water between them, the slip occurs readily and thus the creep increases with relative humidity of atmosphere with which the samples are in equilibrium.

According to Feldman hypothesis [129], the creep is a symptom of C–S–H gel "ordering", ageing and consequently better regularity of this phase structural arrangement. The mutual translation of layers with interlayer water is required, linked with breakdown of the old bonds and formation of the new one.

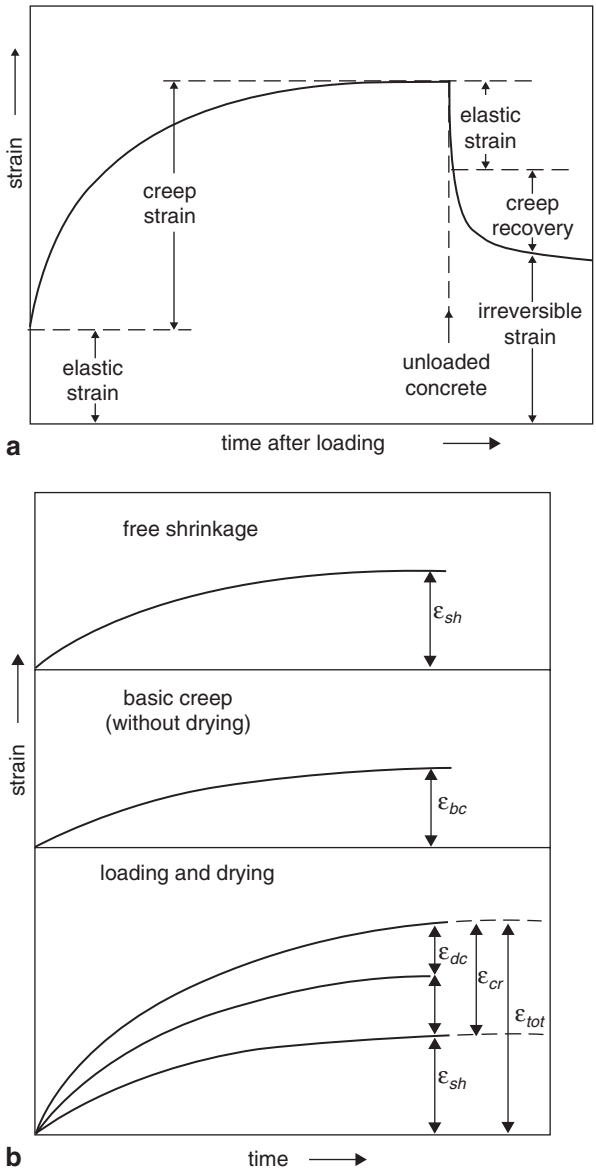


Fig. 5.59. **a** Typical creep curve of cement paste. **b** creep of paste at simultaneous loading and drying: ε_{sh} free shrinkage, ε_{bc} basic creep, ε_{dc} creep at drying, ε_{cr} total creep stress, ε_{tot} total stress (simultaneous loading and drying)

Parrott [130] is considering that the polymerization of silicate anions, occurring with increasing temperature in C–S–H phase, plays an important role in the so–called "thermal" creep. Simultaneously, a coagulation of gel particles with a change of porosity, evidenced its rapid reduction, takes place. The creep is improved by rearrangement of anions. The other materials exhibit creep too, if they undergo the phase transformations under load [130].

The creep of concrete will be related to the presence of C–S–H gel as well; however, in this case the microcracks in the paste–aggregate interface will be also important [130].

Wittmann [96] presents the effect of creep based on the xerogel properties. There are the bonds connecting every gel particle with the surrounding other one. Because of a huge number of particles involved in the deformation of a sample, the probability of particle displacement can be considered using the set theory.

Mindess et al. [131, 132] are of the opinion that the creep is controlled by two factors, namely pore structure and C–S–H phase as well. The microstructure of a paste is modified and the micro–slips between the C–S–H gel particles occur under the load.

Wittmann [96] reminds that the creep of samples, occurring in the conditions without moisture exchange, can be given by a power law equation. However, the controversies appear if the creep is linked with drying shrinkage. These two phenomena, occurring simultaneously, result in the deformation greater than the cumulative effect of these connected components. According to some authors, the creep is increasing as a result of drying. Another approach is to consider this effect as a result of enhanced shrinkage of the element under load.

Wittmann [96] points out that the shrinkage and creep occurring during sample drying is not a simple feature because it is affected by the size and shape of sample. The internal stresses induced during drying process will generate the microcracks in the surface zone. The entire, observed deformation will be dependent on the sample dimensions and the microcracks occurring in the surface layer.

5.3.5 Permeability of Paste

The water permeability of a paste is an important feature because of its decisive role for the resistance of material to the liquid aggressive media. Hence, this is among the most important paste and concrete durability determining factors. The relation between the permeability and diffusion rate and concrete durability, requires to consider more factors that only the porosity and phase composition of the paste; primarily the paste–aggregate interface and the properties of this transition zone must considered.

The permeability coefficient for the liquid medium can be calculated from the modified D'Arcy equation:

$$Q = KA\frac{\mathrm{d}h}{\mathrm{d}x} \tag{5.51}$$

where

Q is the flow of liquid through the sample (m^3/s),
K permeability coefficient of the sample material (m/s),
A cross–section of the flow surface (m^2),
$\mathrm{d}h/dx$ gradient of hydraulic pressure forcing the flow through the sample:

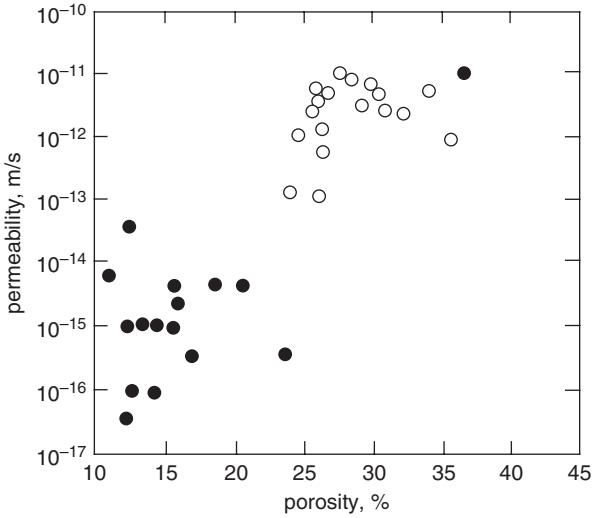


Fig. 5.60 Relation between the total porosity (determined with helium method) and permeability of water saturated pastes (according to [133]); *empty circles*—Portland cement pastes, *black circles*—pastes from cements with mineral additions, cured at 20–80 °C, one year measurements

$P/(\rho g l)$ where P is an applied pressure,
ρ density of sample material,
g acceleration of gravity,
l sample thickness.

It is clear that the permeability of material to water depends mainly on the volume of capillary pores. It is not linked with total porosity but depends rather on the pore size distribution. However, Marsh [133] gives attention to a fairly good correlation between the total porosity, determined by means of helium method, and permeability. This relation is shown in Fig. 5.60 [133]. The "drying" of samples by substitution of water with propan–2–ol and *n*–pentane was applied. Porosity and pore size distribution determined with mercury porosimeter do not correspond to the real structure, because the intrusion of mercury under a high pressure, causes the destruction of hydrates plugging the pores, particularly in the pastes of cements with fly ash.

Illston [134] found a good relation between the maximum continuous pore radius, measured with mercury porosimeter and permeability (Fig. 5.61). The maximum continuous pores radius is defined as a pore size at which the maximum on the pore distribution curve occurs (see Fig. 5.27). This maximum radius of continuous pore system decreases with the time of hydration, as a space between cement grains is filled with hydration products. The term "continuous pores" was firstly used by Winslow and Diamond [135]; they attributed it to the maximum on the pores size distribution curve, as it could be derived from the flow of mercury through the main, continuous pore channels. However below the "peak" mercury is intruding only to the local pore channels [135]. Mehta and Manmohan [136] are considering

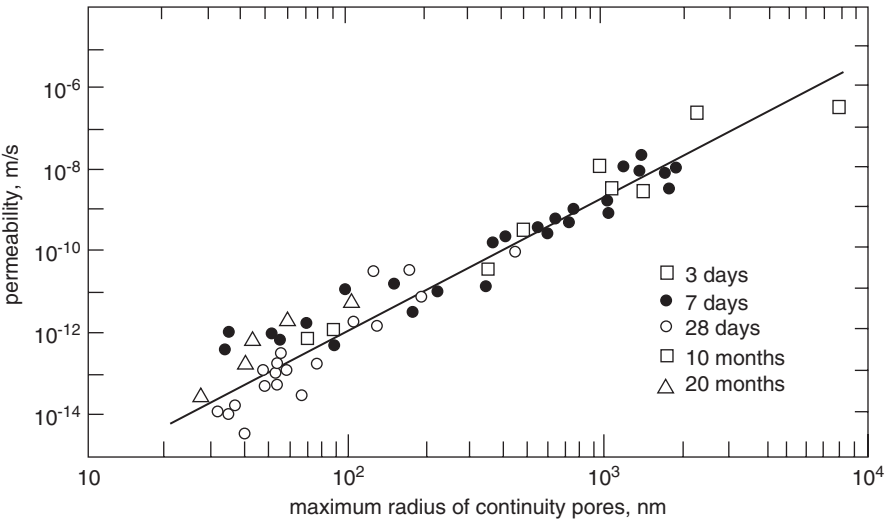


Fig. 5.61 Relation between the maximum pores radius and permeability of hardened cement paste. (according to [134])

that the role of the fine pores in water permeability is negligible. Therefore, with the increase of small pores and decreasing of capillary pores content, after 90 day—or 1 year—paste maturing, the permeability falls down radically. Illston and Mehta [134, 136] were thus proposed to distinguish conventionally the group of large pores, for example bigger than 132 nm, to obtain a good correlation between the share of these pores, determined with mercury porosimeter, and the paste water permeability. The share of large pores is changing with w/c ratio, which is influencing simultaneously the permeability of a paste [136]. Thus the permeability coefficient is increasing exponentially with w/c or decreases with time and hydration degree.

Because of a good correlation between the capillary porosity, i.e. between the large pores and permeability, a relation will also occur between the permeability and strength of concrete. This relation was found experimentally by Torrent and Jornet [137] (Fig. 5.62).

As it has been shown by different authors there is no relation between the total porosity and permeability, because the total porosity can correspond to different pore size distributions [134, 136]. However, Illston [134] found a fairly good correlation between the permeability and a product of total porosity and hydraulic radius, in the following form:

$$\log K = 38.45 + 4.08 \log \varepsilon r_h^2 \tag{5.52}$$

where

K is permeability (m/s),
ε total porosity (cm^3/g),
r_h hydraulic radius.

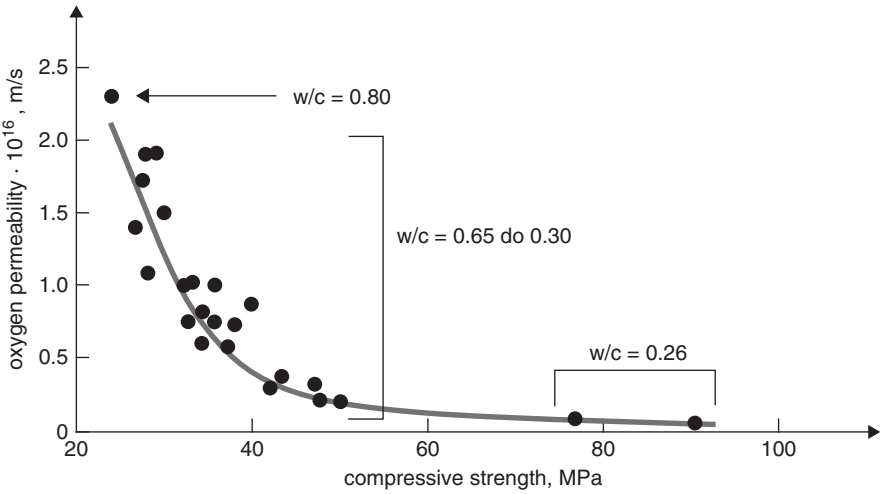


Fig. 5.62 Permeability vs strength of concrete. (according to [137])

There are many controversies concerning the time of measuring period, needed to obtain a stable water flow under a high pressure [133, 138]. In some cases an inversion of flow is observed. There are many hypotheses explaining this phenomenon: progress of hydration during experiments, crystallization of calcium hydroxide in larger pores and their plugging, formation of calcite in the pores, effect of water pressure on the stability of structure. Thus there is a proposal to determine this "stable flow" as a state in which the changes do not exceed the value $0.1 \cdot 10^{-12}$ m/s [138]. The samples should be filled with water before the measurements, however, according to Feldman [139], this operation cannot be executed at pressure below atmospheric, as it was proposed by some authors. The caution must be kept to avoid the cracks formation in the sample.

Marsh [133] investigated the permeability of water in the pastes matured at different temperatures, while Illston [134]—the effect of hydration time (Fig. 5.63). The decrease of permeability with paste maturing time results from the lowering of capillary pores share, as well as continuous one (Fig. 5.64) [115]. Simultaneously the decrease rate of porosity (capillary pores) is higher as the w/c ratio is lower (Fig. 5.65) [136]. After 28 days of hydration at w/c = 0.4 only the pores in hydrates remain, to which the pores smaller than 125 nm are included [136].

Paste of cements with fly ash addition show much lower permeability to water [134]. The pastes of these cements become less permeable, as compared to Portland cements with no mineral additions, particularly at shorter period as higher is temperature of their maturing. Therefore the permeability of paste from cement with fly ash cured at 20 °C becomes lower after 28 days, while cured at 50 and 65 °C already after 7 days. There are the two permeability controlling factors involved: significant reduction of capillary pores and reduction of continuity of pore system, as a consequence of pozzolanic reaction. The effect of ground granulated blastfurnace slag and siliceous fly ash on concrete porosity at different curing time was studies

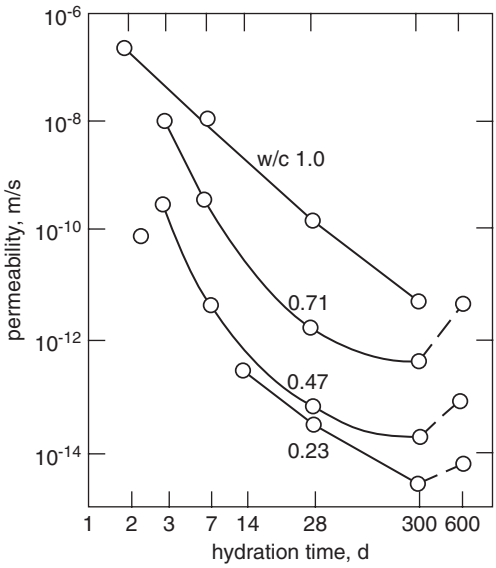


Fig. 5.63 Effect of cement paste hydration progress on its permeability at different w/c. (according to [134])

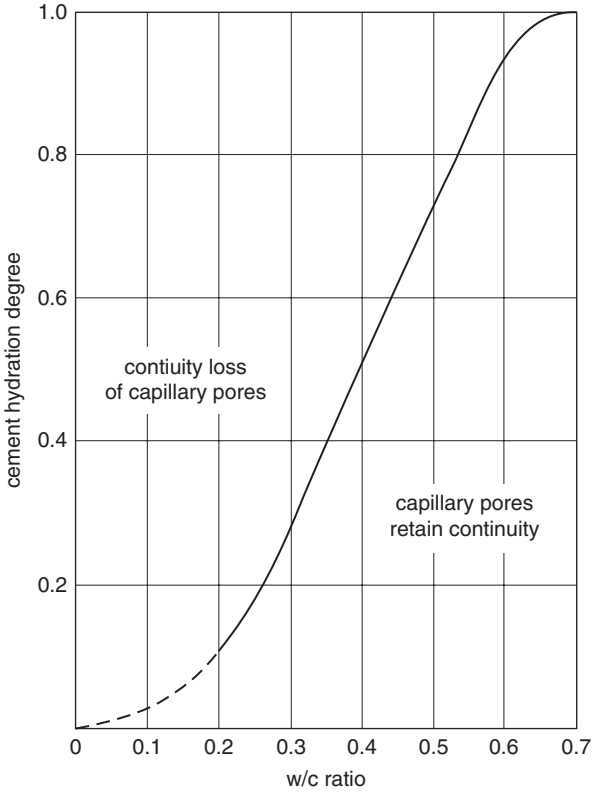


Fig. 5.64 Hydration degree required to break the continuity of pores. (according to [115])

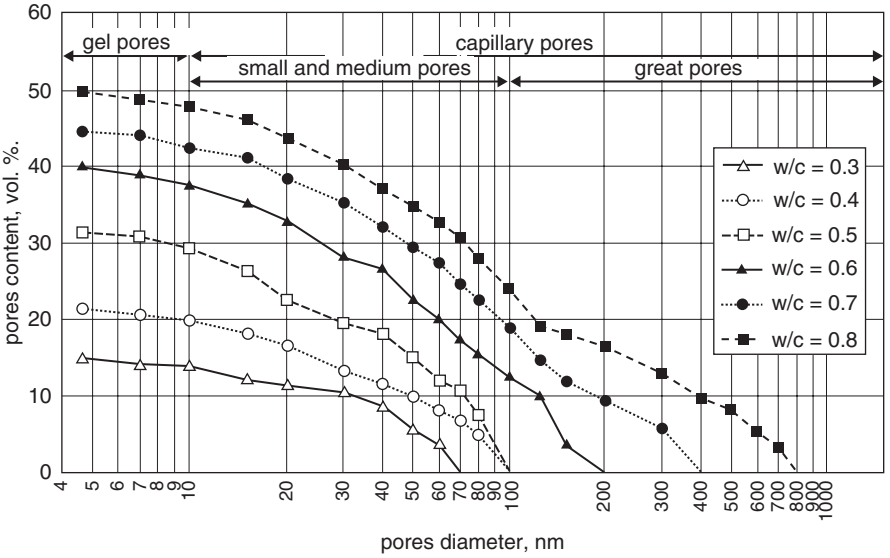


Fig. 5.65 Effect of w/c on the porosity of Portland cement paste after 28 days of hardening. (according to [136])

by Feldman [139]; the results are shown in Fig. 5.66. These changes can be satisfactorily explained based on the scheme presented by Massazza [140] (Fig. 5.67). After prolonged curing the smaller capillary pores became filled with C–S–H phase formed as a result of pozzolanic reaction, which is also breaking their continuity, as well as the larger capillaries became narrower (Fig. 5.67b).

The similar reduction of water permeability was found in the case of a paste from cement with silica fume, rice hush ash and slags [138, 141]. Also concretes produced of cement with 35% fly ash addition show 2–5 times lower permeability, as compared to concrete from cement with no mineral additions [139].

There were attempts to relate the permeability of concrete to the properties of interfacial transition zone. However, the unambiguous results were not obtained. According to Roy [142], the construction of interfacial transition zone surface does not play important role in concrete permeability, while Valenta [143] has quite opposite opinion. This problem will be discussed in Chap. 6 where the construction and properties of interfacial transition zone will be presented [144]. In the light of the studies by Richet and Oliver [145] it is evident that the porosity of interfacial transition zone in traditional concretes (w/c = 0.5 or more) has a significant influence on the permeability of concrete; this permeability is a hundred times higher than in the case of cement paste and rises with the size of aggregate (Fig. 5.68). However, the effect of the transition zone on the diffusion of ions is not so evident, because the locally increased water content in this zone, decrease the w/c ratio in cement matrix outside it, which consequently limits the diffusion, thus a total effect can be negligible [145].

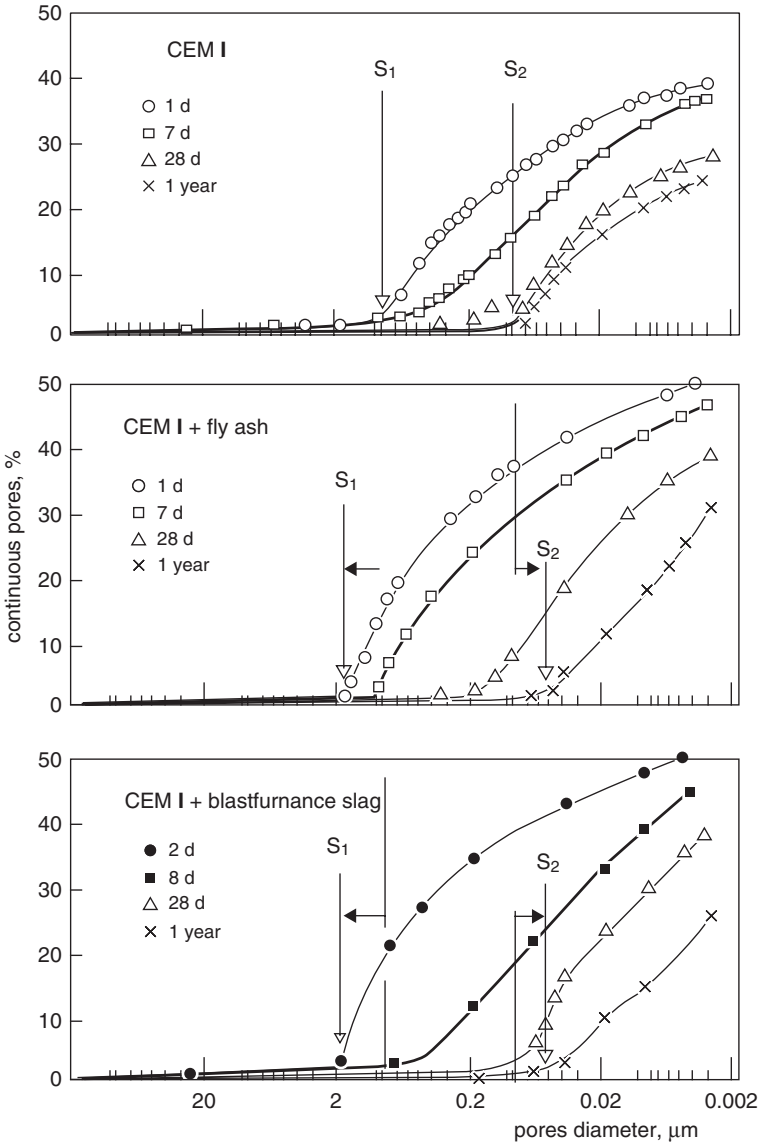


Fig. 5.66 Effect of slag and fly ash addition on the pore structure in the pastes after different time of curing at constant w/c = 0.45 (according to [139]). *S1, S2* maximum pores

Porosity and then permeability of concrete contribute to the transport of gaseous or liquid media, as well as ions through this material. The latter one is of basic importance for the corrosion processes.

There are the two mechanisms of ions the transport in concrete. The first one consists in the flow of liquid in capillaries because of the difference of hydraulic

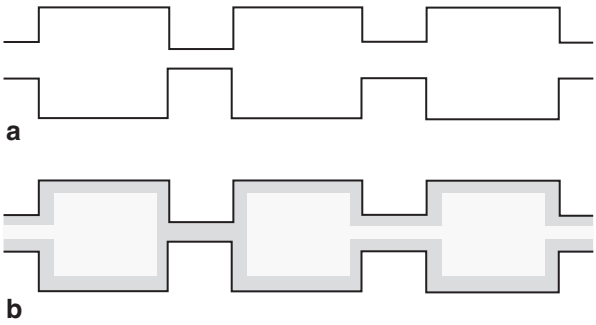


Fig. 5.67 Reduction of capillary porosity in the paste as a result of C–S–H phase formation, at addition of slag or fly ash (schematically); **a** capillary pores in cement paste after 15 day of hydration. **b** modification of pore structure as a result of C–S–H phase formation after longer time. (according to [140])

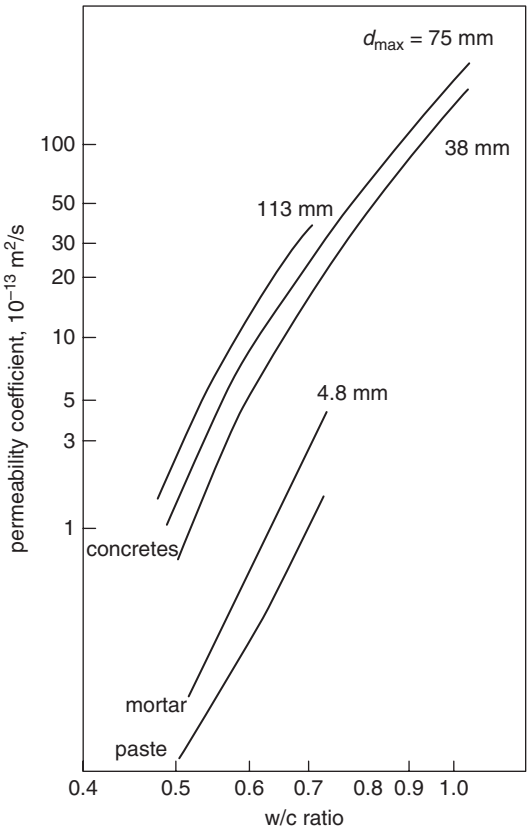


Fig. 5.68 Effect of w/c ratio and aggregate size on permeability of concrete. (according to [145]) Buil P., OllivierJ. P., Chapter 3 in « La Durabilitė des Bėtons », page 66, fig. 3.4 « Transport par diffusion dans un capillaire avec adsorption», Published by Presses de l'Ecole Nationale des Ponts et Chaussées, reproduced with the permission of the Presses de l'Ecole Nationale des Ponts et Chaussées

pressure or capillary–rise resulting from the surface tension of liquid, mainly water and water solutions. This mechanism is determining the permeability of paste and concrete. The second mechanism is a diffusion which can occur in all states of matter: liquid, gaseous and solid. Transport of ions in the solutions migrating in capillary pores occurs with the highest rate; also the diffusion in liquids is of several orders of magnitude higher than in solids.

Transport of liquid in the continuous network of capillaries, as well as in the microcracks, is forced by the hydraulic pressure or by the capillary action. The latter one is the effect of surface tension of water causing the pressure in capillaries, which can be expressed by Laplace formula:

$$P_{\mathrm{c}} = \frac{2\sigma}{r_{\mathrm{m}}} \tag{5.53}$$

where

σ surface tension of water,
r_{m} radius of meniscus.

Radius of liquid meniscus, that is the Kelvin radius, depends on the capillary diameter and wetting angle θ. It can be calculated from the formula:

$$r_{\mathrm{m}} = \frac{r_{\mathrm{c}}}{\cos\theta} \tag{5.54}$$

In case of a good wetting ability of concrete by a liquid, as it relates to water solutions, one can take approximately that $r_{\mathrm{m}} = \mathrm{r_c}$.

On the other side, if there is no continuous network of capillaries in concrete, the transport of ions occurs by diffusion; this process is several orders of magnitude slower than the capillary flow. Diffusion takes place under the difference of concentration and can be expressed by a Fick's first law:

$$J = \frac{\mathrm{d}m}{\mathrm{d}t} = -\mathrm{D} \cdot \frac{\mathrm{d}c}{\mathrm{d}x} \tag{5.55}$$

where

J means a flux of ions (mass/time),
$\mathrm{d}c/\mathrm{d}x$ concentration gradient along the $\mathrm{d}x$ segment in the direction of diffusion.

Opposite to flow, the diffusion is not theoretically affected by the pore size. However, in the case of very small pores, for example the gel one, an impact of pore surface on diffusion is observed. Then the adsorption as the most important factor (Fig. 5.69), as well as the "tortuous" of channels in the micropores and the variable pore radius will disturb the diffusion. These factors are considering by several authors which are adopting the so–called effective diffusion coefficient in the following form:

$$D_{\mathrm{ef}} = D\tau\frac{p}{K} \tag{5.56}$$

where

τ frequency of pore diameter change,
p porosity,
K tortuosity.

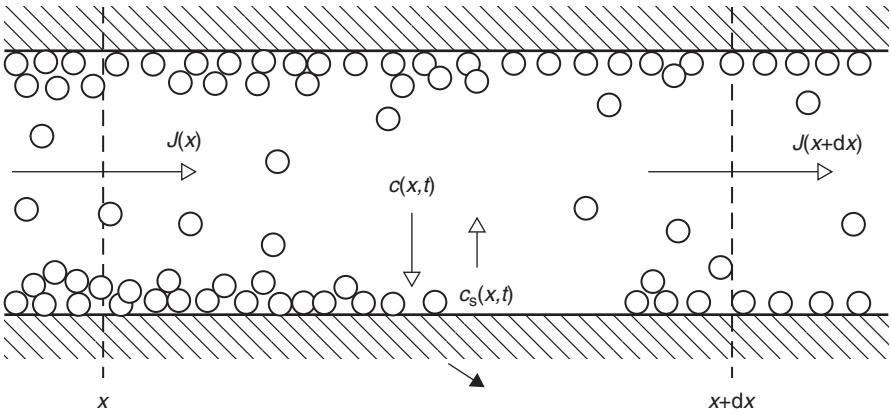


Fig. 5.69 Adsorption of ions in the capillary during the diffusion transport. (according to [145]) Buil P., OllivierJ. P., Chapter 3 in « La Durabilitė des Bėtons », page 57, fig. 3.4 « Transport par diffusion dans un capillaire avec adsorption», Published by Presses de l'Ecole Nationale des Ponts et Chaussėes, reproduced with the permission of the Presses de l'Ecole Nationale des Ponts et Chaussėes

There are numerous studies of the diffusion rate of ions, principally the chlorides, in water saturated paste [138, 145–149]. Migration of ions in hardened cement paste is not a simple diffusion. Ions are adsorbed on the surface of hydrated phases, in pores, or even react with hydrates. Therefore the diffusion coefficients cannot be considered in a classic manner. Their values derived from the Fick's equation should be considered as apparent or "effective" diffusion coefficients. For example it is known that $CaCl_2$ reacts with aluminates and $C_3(A, F)\cdot CaCl_2\cdot 10H_2O$ phase is formed. The basic calcium chloride $Ca(OH)_2\cdot CaCl_2\cdot H_2O$ can be also formed in some conditions.

The problem of chloride ions diffusion is discussed in details in Sect. 6.4.4, relating to the chloride corrosion.

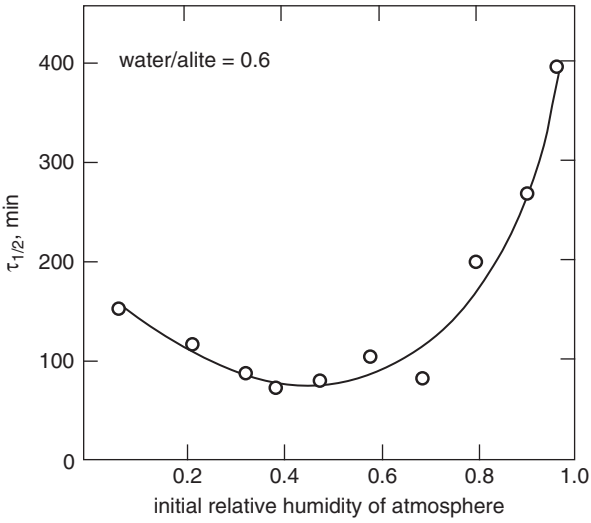
According to Ushiyama [150], the diffusion of SO_4^{2-} ions is 10–100 times slower than Cl^- (see Fig. 6.50); moreover, the effective diffusion coefficient of sulphate ions depends on pH of the liquid phase and it seems that its value is affected by the formation of ettringite.

There are numerous studies focused on the water replacement in the paste by different organic liquids [151–154]. This was mentioned earlier as a method of paste drying, because the organic liquids, having relatively high vapour pressure, are readily removable from cement paste by drying at temperature 30 °C [133]. According to Parrott [152] the replacement of half amount of evaporable water in hydrated alite (half–change period) is approximately a linear function of liquid viscosity. Applying different organic liquids, such as: propan–1–ol, propan–2–ol, *n*–pentane, benzene, Parrott [153] came to the conclusion that this exchange is a simple physical diffusion process.

In Table 5.6 the time needed to replace a half of water content in hydrated alite pastes of varying porosity, according to Parrott [154] is presented. The porosity decreases and this period of half–change increases as the alite hydration proceeds,

Table 5.6. Diffusion and porosity measured by replacing water by methanol in hydrated alite [154]

Time of hydration, days	1	3	10	28	203
$\tau_{1/2}$, min.	30	32	74	142	271
Porosity (water)	0.613	0.583	0.554	0.532	0.495
Porosity (methanol)	0.612	0.566	0.551	0.523	0.479



.Fig. 5.70 Effect of preliminary drying in the atmosphere at various relative humidity on the rate of water replacement in the paste by methanol in hydrated C_3S, w/c = 0.6. (according to [152])

because the content of smaller pores in a paste is simultaneously increasing. The effect of moisture content, up to which the alite samples were preliminary dried, on the period of half–change determined in the experiment, was also explained by Parrot [152]. From the curve plotted in Fig. 5.70 it can be conclude that this period is several times shorter at more intensive drying [152]. Less pronounced differences were found by Feldman [139], as well as by Day and Illston [155].

Parrott et al. [153] found an exact relationship between the rate of water replacement by methanol and the ratio of pores greater than 50 nm. With lowering of this ratio to the level of about 0.4, the diffusion becomes extremely low (Fig. 5.71); the authors attribute this to the filling of pore channels by some amount of hydration products. However, Feldman [138] remarks that there are some questions as the water replacement by methanol is concerned. The reactivity of methanol towards $Ca(OH)_2$ and C–S–H, resulting in the formation of calcium methoxide or a methylated complex compounds was reported by some authors [138, 156]. These reactions occur very quickly and a substantial amount of products appears, modifying the paste microstructure. The swelling of paste, observed by Feldman [138] was about 0.1 % after 14 days when the paste absorbed 85 % methanol as water replacement. This effect can be attributed to the intrusion of methanol between the layers in C–S–H structure and the calcium methoxide formation. At extended distance between C–S–H layers the specific surface of paste markedly increases, as it has been proved by Winslow and Diamond [135]. In turn, the water replacement by propan–2–ol, re-

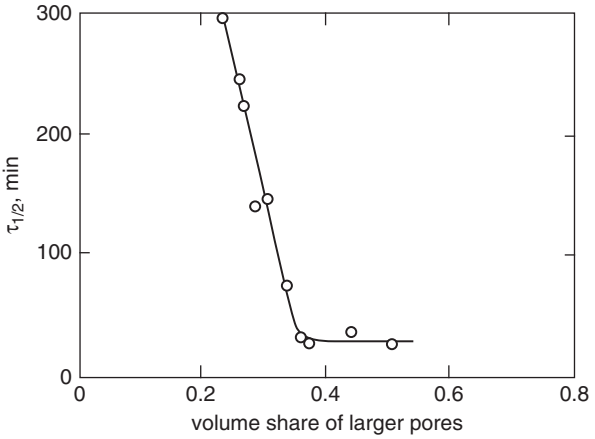


Fig. 5.71 Rate of water replacement in the paste by methanol, as a function of larger pores (>50 nm) share. (according to [153]) Parrot L.J., Patel R.G., Killch D.C., Jennings H.M., "Effect of Age on Diffusion in Hydrated Alite Cement", J. Am Ceram. Soc. 67, 233 (1984), published by John Wiley & Sons Ltd, reproduced with the permission of Wiley & Sons

sults in about 0.14 % shrinkage, attributed by Feldman [138] to the different interaction of water and propan–2–ol with the surface of cement paste. Besides, Feldman [129] prefers applying propan–2–ol as a drying medium in the case cement paste.

The diffusion of oxygen is of particular importance as the corrosion of steel reinforcement in concrete is regarded. Ludwig [157] was among the first authors who initiated the studies focused on this problem. The linear relation between the permeability and oxygen diffusion rate was found, as presented in Fig. 5.72 [138]. It has been proved in the same experiments that the CO_2 diffusion can be evaluated based on the oxygen diffusion coefficient.

The formula proposed by D'Arcy should be modified when applied to gaseous phase diffusion. Hence, the compressibility of gas must be taken into account, by introducing the mean value of pressure to the equation—½ (P_2+P_1), where P_1 is an atmospheric pressure, and P_2—pressure under which the gas is forced. Therefore the gradient of pressure along the sample thickness L will be P_2-P_1. Substituting with the oxygen viscosity as $2.02\cdot10^{-5}$ N s/m^2 at temperature 20°C, we get the permeability coefficient from the following formula:

$$K = \frac{0.04\cdot10^{-16}\,RP_1L}{A\left(P_2^2 - P_1^2\right)} \qquad [\mathrm{m}^2/\mathrm{s}] \tag{5.57}$$

In order to calculate the effective oxygen diffusion coefficient an equation based on the Fick's law is usually applied:

$$Q_A = \frac{D_{\mathrm{ef}}S\left(C_1 - C_2\right)P}{LRT} \tag{5.58}$$

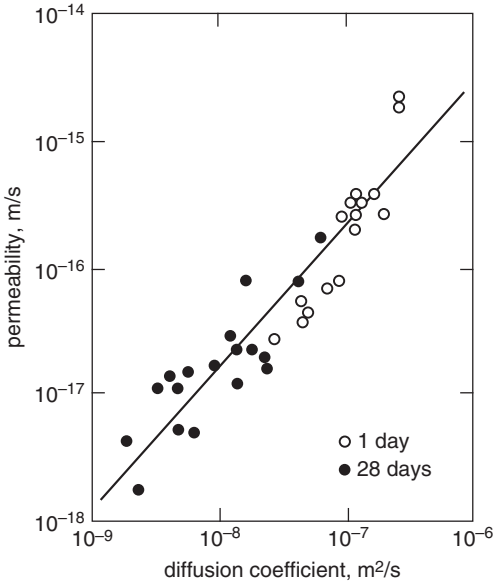


Fig. 5.72 Relation between the permeability of mortar and oxygen diffusion coefficient. (according to[138])

where

Q_A	is the flow of oxygen (mol/s),
S	surface of the flow cross section (m^2),
C_1, C_2	molar share of oxygen in gaseous phase, being in the contact with both sides of the sample,
P	applied pressure (MPa),
L	sample thickness (m),
R	gas constant [$m^3 \cdot MPa/(K \cdot mol)$],
T	absolute temperature.

The oxygen permeability measurements are quick and steady state is attained quickly. However, the sample must be dried before the measurement and, undoubtedly, the pore structure is then modified [158]. Different methods of sample drying cause the different permeability values; the difference is the lowest in the case of water replacement by the isopropyl alcohol and drying at temperature 38 °C [158]. A substantial decrease of fly ash containing concrete permeability should be underlined. After one series of measurements the samples were dried at temperature 105 °C and subjected to the permeability measurements again. The permeability was then three times higher. It is probable that this effect should be attributed to the microcracks formation in concrete. Concrete produced with fly ash shows low permeability, however, in the case of cements with mineral additions this question is unambiguous as yet. For example Oberholster [75] reports, the results of Gräf and Grube, that the oxygen permeability of slag cement concrete is higher than that produced from Portland cement. Nevertheless, after prolonged curing in humid condition the permeability of slag cement concrete is lower. Similarly, fly ash in

concrete does not reduce the permeability; this is even higher than for the control Portland cement concrete samples, however, only in the case of the wrong or insufficient curing of containing fly ash samples.

Plasticizers and superplasticizers improve radically the pore structure (effect of w/c) and concrete becomes less permeable to air and water [159]. Collepardi and Massida [159] found a capillary porosity and pore size lowering with decreasing permeability of concretes in which water reducers were used. The resistance to the sulphate attack was also improved [159].

Obviously, the diffusion of gas in concrete is largely controlled by the degree of pore filling with a liquid phase; it relates also to the diffusion of oxygen. The oxygen diffusion in dried or in water saturated concrete corresponds approximately to the rate ratio of oxygen diffusion in the air and in liquid water [75].

Diffusion of oxygen depends markedly on the technology of concrete element production, as well as on the time and conditions of curing. Curing in the condition of high relative humidity, prolonged from one to three days, reduces the oxygen permeability 5 times, and further curing—up to 28 days, 9 times [75]. The effect of w/c ratio is somewhat less; w/c lowering equal 0.05 gives 1.6 times lower permeability. At increasing cement content in concrete from 240 to 300 kg/m^3, the permeability, at constant w/c = 0.7, is 2.1 times higher [160].

References

1. Helmuth, R.A.: 7th ICCC Paris, vol. III, p. VI–0/16. Paris (1980)
2. Powers, T.C.: Rheology of Freshly Mixed Concrete. The Properties of Fresh Concrete. Wiley, New York (1968)
3. Paillere, A.M., Briquet, Ph.: 7th ICCC Paris, vol. III, p. VI–186. Paris (1980)
4. Bombled, J.P.: Rev. Mat. Constr. (688), 137 (1974)
5. Bombled, J.P.: Rev. Mat. Constr. (673), 256 (1971)
6. Wilkinson, W.L.: Non–Newtonian Fluids. Pergamon Press Ltd., England (1960)
7. Legrand, C.: Cem. Concr. Res. 2, 17 (1972)
8. Roy, D.M., Asaga, K.: Cem. Concr. Res. 9, 731 (1979)
9. Odler, I., Becker, Ch., Weiss, B.: Il Cemento. 75, 303 (1978)
10. Ish–Shalom, M., Greenberg, S.A.: 4th ICCC Washington, vol. II, p. 731. Washington (1960)
11. Bombled, J.P.: 7th ICCC Paris, vol. III, p. VI–164. Paris (1980)
12. Diamond, S.: World Cement Technology. 11, 116 (1980); 7th ICCC Paris, vol. II, p. II–148. Paris (1980)
13. Banfill, P.F.G., Saunders, D.C.: Cem. Concr. Res. 11, 363 (1981)
14. Lapasin, R., Longe, V., Rajgelj, S.: Cem. Concr. Res. 9, 309 (1979)
15. Legrand, C.: 7th ICCC Paris, vol. IV, p. 124. Paris (1980)
16. Legrand, C.: Le Béton Hydraulique, p. 99. Presses de L'Ecole Nationale des Ponts et Chaussées, Paris (1982)
17. Nagataki, S., Kawano, S.: 7th ICCC Paris, vol. III, p. IV–120. Paris (1980)
18. Banfill, P.F.G., Gili, S.M.: 8th ICCC Rio de Janeiro, vol. VI, p. 223. Rio de Janeiro (1986)
19. Tattersall, G.H.: 8th ICCC Rio de Janeiro, vol. VI, p. 228. Rio de Janeiro (1986)
20. Hanehara, S., Yamada, K.: Cem. Concr. Res. 21, 175 (2008)
21. Costa, V., Massazza, F.: 8th ICCC Rio de Janeiro, vol. VI, p. 248, Rio de Janeiro (1986)
22. Ivanov, J., Zacharieva, S.: 7th ICCC Paris, vol. III, p. VI–103. Paris (1980)

23. Collepardi, M., Corradi, M., Baldini, G., Peuri, M.: 7th ICCC Paris, vol. III, p. VI–20. Paris (1980)
24. Petri, E.M.: Ind. Eng. Chem. Prod. Res. Dev. 15, 242 (1976)
25. Gaudin, A.M.: Flotation, 2nd edon. Mc Graw–Hill Book Company Inc., New York (1957)
26. Zelwer, A.: Ciment Bétons Plâtres Chaux. (749), 213 (1984)
27. Nägele, D.: Cem. Concr. Res. 15, 453 (1985)
28. Rebinder, P.A., Siegałova, J.J., Amelina, J.A., Andreieva, E.P., Kantorowich, S.J., Lukjanova, O.J., Solovieva, J.S., Shchukin, J.D.: 6th ICCC Moscow, vol. II/1, p. 58. Moscow (1974). (in Russian)
29. Sychev, M.M.: ibid., vol. II/1, p. 42
30. Setzer, M.J., Wittmann, F.H.: Appl. Phys. 3, 403 (1974)
31. Powers, T.C.: 4th ICCC Washington, vol. II, p. 577. Washington (1960)
32. Sereda, P.J., Feldman, R.F., Swenson, E.G.: Special Report 90, p. 58. Highway Research Board, Washington (1966)
33. Nonat, A.: 12th ICCC Montreal, TH2–08.1, Montreal (2007)
34. Verbeck, G.J., Helmuth, R.A.: 5th ICCC Tokyo, vol. III, p. 1. Tokyo (1968)
35. Feldman, R.F.: 5th ICCC Tokyo, vol. III, p. 53. Tokyo (1968)
36. Powers, T.C.: In: Taylor, H.F.W. (ed.) The Chemistry of Cements, p. 391. Academic Press, London (1964)
37. Wittmann, F.H.: 7th ICCC Paris, vol. I, p. VI–2/l. Paris (1980)
38. Copeland, L.E., Verbeck, G.J.: 6th ICCC Moscow, vol. II/1, p. 258. Moscow (1974). (in Russian)
39. Lea, F.M.: The Chemistry of Cement and Concrete, 3rd edn., p. 271. Chemical Publ. Com., New York (1971)
40. Taylor, H.F.W.: Cement Chemistry. Academic Press, London (1990)
41. Sierra, F.: 7th ICCC Paris, vol. III, p. VI–201. Paris (1980)
42. Sabri, S., Illston, J.M.: ibid., vol. III, p. VI–52
43. Sereda, P.J., Feldman, R.F., Ramachandran, V.S.: ibid., vol. I, p. VI–1/3
44. Harris, D.H.C., Windsor, C.G., Lawrence, C.D.: Mag. Concr. Res. 26, 65 (1974)
45. Stockhausen, N., Dorner, H., Zech, B., Setzer, M.J.: Cem. Concr. Res. 9, 783 (1979)
46. Wittmann, F.H.: Mat. Constr. 1, 547 (1968)
47. Bond, R.L.: Porous Carbon Solids, p. 24. Academic Press, London (1967)
48. Feldman, R.F.: Cem. Concr. Res. 2, 375 (1972)
49. Smith, H.H., Bayliss, P.: Cem. Concr. Res. 2, 643 (1972)
50. Tennis, P.D., Jennings, H.M.: Cem. Concr. Res. 30, 856 (2000)
51. Winslow, D.N.: Ph. D. Thesis, University La Fayette. Indiana USA. (after [50])
52. Winslow, D.N., Diamond, S.: J. Am, Ceram. Soc. 57, 193 (1974)
53. Taylor, H.F.W., Roy, D.M.: 7th ICCC Paris, vol. I, p. II–2/1. Paris (1980)
54. Odler, I., Hagymassy, J., Bodor, E.E., Yudenfreund, M., Brunauer, S.: Cem. Concr. Res. 2, 577 (1972)
55. Dubinin, M.M.: Ż. fiz. chim. 30, 1692 (1956). (in Russian)
56. Dubinin, M.M., Zukovska, E.G.: Ż. fiz. chim. 30, 1840 (1956). (in Russian)
57. Feldman, R.F.: 8th ICCC Rio de Janeiro, vol. I, p. 336. Rio de Janeiro (1986)
58. Brunauer, S., Mikhail, R.S., Bodor, E.E.: J. Coloid Interface Sci. 24, 451 (1967)
59. Marsh, B.K., Day, R.L., Bonner, D.G., Illston, J.M.: RILEM Symp. on Principles and Appl. of Pore Struc. Char. Milan (1983)
60. Deciang, Ski, Winslow, D.N.: Cem. Concr. Res. 15, 645 (1985)
61. Sellevold, J., Bager, H.: 7th ICCC Paris, vol. IV, p. 394. Paris (1980)
62. Feldman, R.F.: Cem. Technol. 3, 5 (1972)
63. Brunauer, S., Skalny, J., Odler, I.: Proc. RILEM/IUPAC Int. Symp. “Pore Structure and Properties of Materials”, p. C3–26. Prague (1973)
64. Sereda, P.J., Feldman, R.F.: J. Appl. Chem. 13, 150 (1974)
65. Ubelhack, H.: Proc. of a Conf. “Hydraulic Cement Pastes”, p. 166. University of Sheffield (1976)

66. Smith, R.H., Bayliss, P., Gamble, B.R., Mills, R.H.: Cem. Concr. Res. 2, 559 (1972)
67. Brunauer, S., Kantro, D.L., Copeland, L.E.: J. Am. Chem. Soc. 80, 761 (1958)
68. Gutteridge, W.A., Parrott, L.J.: Cem. Concr. Res. 6, 357 (1976)
69. Brunauer, S.: 4th ICCC Washington, vol. I, p. 149. Washington (1960)
70. Henderson, D., Barley, J.E.: 8th ICCC Rio de Janeiro, vol. III, p. 376. Rio de Janeiro (1986)
71. Wittmann, F.H.: J. Am. Ceram. Soc. 56, 409 (1973)
72. Chatterji, S.: 7th ICCC Paris, vol. III, p. VI–5. Paris (1980)
73. Kondo, R., Daimon, M.: 6th ICCC Moscow, vol. II/1, p. 244. Moscow (1974). (in Russian)
74. Daimon, M., Abo–El–Enein, S.A., Hosaka, G., Goto, S., Kondo, R.: J. Am. Ceram. Soc. 60, 110 (1977)
75. Oberholster, R.E.: 8th ICCC Rio de Janeiro, vol. I, p. 323. Rio de Janeiro (1986)
76. Hornain, H., Mortureux, B., Regourd, M.: Coll. Int. Liaisons Pâtes de Ciment Materiaux Associés, p. C–56. Toulouse (1982)
77. Schiller, K.K.: Cem. Concr. Res. 1, 419 (1971)
78. Feldman, R.F., Beaudoin, J.J.: Cem. Concr. Res. 6, 389 (1976)
79. Beaudoin, J.J., Ramachandran, V.S.: Cem. Concr. Res. 5, 617 (1975)
80. Rossler, M., Odler, I.: Cem. Concr. Res. 15, 320 (1985)
81. Jambor, J.: Proc. of a Conf. “Hydraulic Cement Pastes”, p. 175. University of Sheffield (1976)
82. Taylor, H.F.W.: Cem. Concr. Res. 7, 465 (1977)
83. Mindess, S.: J. Am. Ceram. Soc. 53, 621 (1979)
84. Jambor, J.: Proc. RILEM/IUPAC Int. Symp. “Pore Structure and Properties of Materials”, vol. II, p. D–75. Prague (1973)
85. Zaitsev, Y.: 7th ICCC Paris, vol. III, p. VI–176. Paris (1980)
86. Dyczek, J., Petri, M.: 6th ICCC Moscow, vol. II/2, p. 159. Moscow (1974). (in Russian)
87. Griffith, A.: Phil. Trans. Roy. Soc. A221, 163 (1920)
88. Dereń, J., Haber, J., Pampuch, R.: Chemia ciała stałego. PWN, Warszawa (1979). (in Polish)
89. Mindess, S.: In: Barnes, P. (ed.) Structure and Performance of Cements, p. 319. Appl. Science Pub., London (1983)
90. Baggot, R., Sarandily, A.: In: Young, J. (ed.) Very High Strength Cement–Based Materials, vol. 42, p. 69. Materials Research Society, Pittsburgh (1985)
91. Mindess, S.W.: In: Wittmann, F.H. (ed.) Fracture Mechanics of Concrete, p. 481. Elsevier, Amsterdam (1983)
92. Brown, J.H., Pomeroy, C.O.: Cem. Concr. Res. 3, 475 (1973)
93. Hillemeier, B., Hilsdorf, H.K.: Cem. Concr. Res. 7, 532 (1977)
94. Beaudoin, J.J.: Cem. Concr. Res. 12, 705 (1982)
95. Nadean, J.S., Mindess, S.W., Hay, L.M.: J. Am. Ceram. Soc. 57, 51 (1974)
96. Wittmann, F.H.: In: Skalny, J. (ed.) Cement Production and Use, p. 143. Eng. Foundation, New York (1979)
97. Birchall, J.D., Howard, A.J., Kendall, K.: Nature. 289, 388 (1981)
98. Alford N, Mc N., Rokman, A.A.: J. Mater. Sci. 16, 3105 (1981)
99. Massazza, F.: Il Cemento. 83, 259 (1986)
100. Berger, R.L.: Science. **175**, 626 (1972)
101. Beaudoin, J.J.: In: Skalny, J., Gebauer, J., Odler, I. (eds.) Materials Science of Concrete, Special Vol.: Calcium Hydroxide in Cement Matrices, p. 131. American Ceramic Society, Westerville (2000)
102. Mindess, S.: ibid., p. 143
103. Robertson, B., Mills, R.H.: Cem. Concr. Res. **15**, 225 (1985)
104. Bangham, D.H., Fakkoury, N.J.: J. Chem. Soc. **1324** (1931)
105. Mindess, S., Nadean, J.S., Hay, J.M.: Cem. Concr. Res. **4**, 953 (1974)
106. Zarzycki, J.: Les Verres et l’Etat Vitreux. Masson, Paris (1982)
107. Barrick, J.E., Krokosky, E.M.: J. Testing and Evaluation. **4**(1), 61 (1976)
108. Czernin, W.: Cement Chemistry and Physics for Civil Engineers. Bauverlag, Wiesbaden (1980)

109. Ziegeldorf, S., Hilsdorf, H.K.: 7th ICCC Paris, vol. IV, p. 333. Paris (1980)
110. Buil, M., Baron, J.: ibid., vol. III, p. VI–37
111. Sulikowski, J.: 4th ICCC Washington, vol. I, p. 527. Washington (1960)
112. Parrott, L.J.: In: Gartner, E.G. (ed.) Advances in Cement Manufacture and Use. Trout Lodge, Potosi, Missouri 1988, United Eng. Trustees (1989)
113. Powers, T.: Proc. Conf. "Structure of Concrete and its Behaviour under Load", p. 319. Cem. and Concr. Ass. London (1968)
114. Jensen, OM., Hansen, PF.: After Cem. Concr. Res. **31**, 647 (2001)
115. Détriché, C.H.: In: La Durabilité des Bétons, chapter 4, p. 107. Presses Ponts et Chaussées, Paris (1992)
116. Feldman, R.F., Sereda, P.J.: Eng. J. (Canada). **53**, 509 (1968)
117. Wittmann, F.H.: Cem. Concr. Res. **6**, 49 (1976)
118. Young, J.F., Berger, R.L., Bentur, A.: Il Cemento. **75**, 391 (1978)
119. Bentur, A., Berger, R.L., Lawrence, F.V., Milstone, N.B., Mindess, S., Young, J.F.: Cem. Concr. Res. **9**, 83 (1979)
120. Bentur, A., Kung, J.H., Berger, R.L., Young, J.F., Milstone, N.B., Mindess, S., Lawrence, F.V.: 7th ICCC Paris, vol. III, p. VI–26. Paris (1980)
121. Parrott, L.J.: Mag. Concr. Res. **25**, 197 (1973)
122. Venuat, M., Alexandre, J.: Rev. Mat. Constr. (638), 421 (1968); (639) 496 (1968); (640), 5 (1969)
123. Mineru Hamada.: 5th ICCC Tokyo, vol. III, p. 342. Tokyo (1968)
124. Smolczyk, H.G.: ibid., vol. III, p. 369
125. Aïtcin, J.P.: Cement Wapno Beton, **70**, 115 (2003), Binders for Durable and Sustainable Concrete. Taylor & Francis, New York (2008)
126. Neville, A.M.: Properties of Concrete, 5th edn. Pearson Education Limited (2011)
127. Pihlajavaara, S.E.: Cem. Concr. Res. **4**, 761 (1974)
128. Gamble, B.R.: In: Skalny, J. (ed.) Cement Production and Use, p. 163. Proc. Engineering Foundation Conf. Rindage, New York (1979)
129. Feldman, R.F.: Cem. Concr. Res. **9**, 521 (1979)
130. Parrott, L.J.: 7th ICCC Paris, vol. IV, p. 817. Paris (1980)
131. Mindess, D., Young, J.F., Lawrence, F.V.: Cem. Concr. Res. **8**, 591 (1978)
132. Bentur, A., Milstone, N.B., Young, J.F., Mindess, S.: Cem. Concr. Res. **9**, 161 (1979)
133. Marsh, B.K., Day, R.L.: In: Young, J.F. (ed.) Very High Strength Cement–Based Materials, p. 113. Materials Research Society, Pittsburgh (1985)
134. Nyame, B.K., Illston, J.M.: 7th ICCC Paris, vol. III, p. VI–181. Paris (1980)
135. Winslow, D.N., Diamond, S.: J. Am. Ceram. Soc. **57**, 193 (1974)
136. Mehta, P.K., Manmohan, D.: 7th ICCC Paris, vol. III, p. VII–1. Paris (1980)
137. Torrent, R.J., Jornet, A.: In: Malhotra, V.M. (ed.) Proc. of 2nd Int. Conf. "Durability of Concrete", ACI SP–126, p. 1147. Montreal (1991)
138. Feldman, R.F.: 8th ICCC Rio de Janeiro, vol. I, p. 336. Rio de Janeiro (1986)
139. Feldman, R.F.: In: Malhotra, V.M. (ed.) Proc. 1st Int. Conf. "On the use of fly ash, silica fume, slag and other mineral by–products in concrete", ACI, SP–79, p. 415. Montebello (1983)
140. Massazza, F., Oberti, G.: In: Malhotra, V.M. (ed.) Proc. of 2nd Int. Conf. "Durability of Concrete", ACI SP–126, p. 1259. Montreal (1991)
141. Manmohan, D., Mehta, P.K.: Cem. Concr. Aggregates. **3**, 63 (1981)
142. Wakely, L.D., Roy, D.M.: Cem. Concr. Res. **12**, 533 (1982)
143. Valenta, O.: 5th ICCC Tokyo, vol. III, p. 193. Tokyo (1968)
144. Scrivener, K.L., Bentur, A., Pratt, P.L.: Adv. Cem. Res. **1**, 230 (1988)
145. Buil, P., Ollivier, J.P.: In La Durabilité Des Bétons, chapter 3, p. 57. Presses Ponts et Chaussées, Paris (1992)
146. Midgley, H.G., Illston, J.M.: Cem. Concr. Res. **14**, 546 (1984)
147. Goto, S., Roy, D.M.: Cem. Concr. Res. **11**, 751 (1981)
148. Page, C.L., Skart, N.R., El Farras, E.: Cem. Concr. Res. **11**, 395 (1981)

149. Midgley, H.G., Illston, J.M.: 7th ICCC Paris, vol. III, p. VII–101. Paris (1980)
150. Ushiyama, H., Goto, S.: 6th ICCC Moscow, vol. II/1, p. 331. Moscow (1974)
151. Patel, R.G., Parrott, L.J., Martin, J.A., Killch, D.C.: Cem. Concr. Res. **15**, 343 (1985)
152. Parrott, L.J.: Cem. Concr. Res. **11**, 651 (1981)
153. Parrot, L.J., Patel, R.G., Killch, D.C., Jennings, H.M.: J. Am. Ceram. Soc. **67**, 233 (1984)
154. Parrot, L.J.: Mat. Struct. **17**, 131 (1984)
155. Day, R.L., Illston, J.M.: Cem. Concr. Res. **13**, 7 (1983)
156. Day, R.L.: Cem. Concr. Res. **11**, 341 (1981)
157. Darr, G.M., Ludwig, U.: Proc. RILEM–IUPAC Int. Sym. "Pore Structure and Properties of Materials", vol. IV. p. C–249. Prague (1973)
158. Day, R.L., Joshi, R.C., Langan, B.W., Ward, M.A.: Proc. 7th Int. Ash. Utilization Symp., vol. 2, p. 811. Orlando (1985)
159. Collepardi, M., Massida, L.: Proc. of a Conf. "Hydraulic Cement Pastes", p. 256. University of Sheffield (1976)
160. Mills, R.H.: Cem. Concr. Res. **15**, 74 (1985)

Chapter 6
Concrete Properties

6.1 Effect of Cement Paste on Concrete Properties

Cement paste has a great impact on the properties of concrete, however, these properties are related to the three concrete components: cement, aggregate and water. The effect of cement paste should be discussed under the assumption that all these components are of high quality and their proportions in the concrete mixture are fairly well selected.

There is an opinion that the effect of paste is visible at the very beginning, soon after the concrete components mixing, based upon the strong relationship between the properties of cement paste and fresh concrete. Cement water demand, giving the proper consistency of the paste, should correspond to the water content and required workability of concrete mixture. The rheological properties of concrete are strongly dependent on the rheological properties of cement paste. The hardening process, that is setting time and strength development, is also the function of the loss of workability and rate of concrete stiffening. However, a simple adaptation of these phenomena from cement paste to concrete mixture is a complex problem, because of the effect of aggregate.

According to Gebauer [1], the water demand of cement paste is the function of the C_3A and alkali content, as well as the function of cement fineness. However, in the same report [1] this author also found no relation between the water demand of cement and water content in concrete mixture, to produce the composite of stable consistency. It appears in practice that this parameter is strongly affected by aggregate, particularly by its porosity and sand fraction content. Therefore the exceptional caution is required as the results are transferred from cement paste to concrete mixture.

Locher [2] investigated the effect of cement fineness, determined by the parameters of RRSB equation, such as: *x'*—particle size (determining such a diameter that 63.2 % particles are smaller than *x'*), *n*—slope of the straight line determining the half of width of normal distribution, on the water demand of cement. At constant *n*, the reduction of *x'* parameter from 20 to 13 μm in the *n*–*x'* system leads to the significant growth of water demand (Fig. 6.1). The C_3A reactivity, as well as the specific surface of cement are shown in Fig. 6.1 too.

W. Kurdowski, *Cement and Concrete Chemistry*,
DOI 10.1007/978-94-007-7945-7_6, © Springer Science+Business Media B.V. 2014

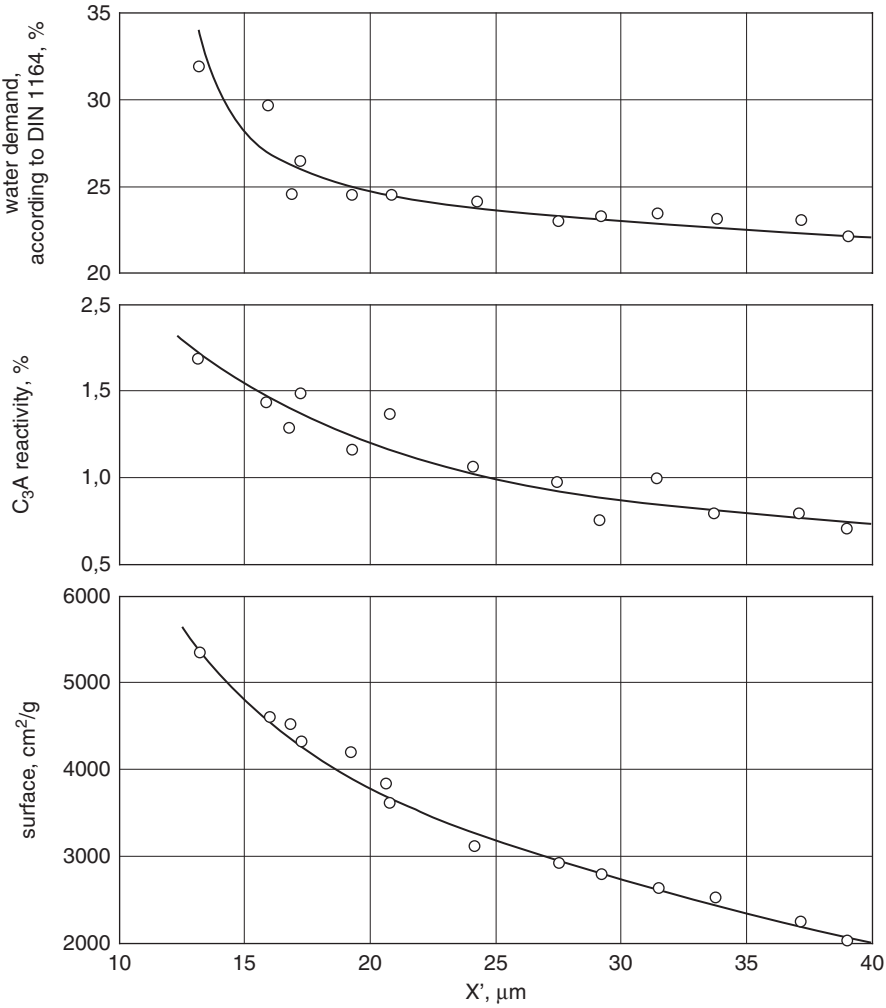


Fig. 6.1 Effect of *x'* parameter on the water demand of cement, $n = 0.86$. (According to [2])

The state of the art of the relation between the properties of cement paste and concrete, has been summarized by Bombled [3]. The effect of cement fineness and cement content in 1 m^3 of concrete was particularly well recognized (Figs. 6.2 and 6.3) [4].

Moreover, the effect of mineral and chemical composition of cement on setting and stiffening of concrete is known, as well as on its strength.

The effect of mineral additions (slag, fly ash, pozzolanic materials) on the same properties of concrete has been also determined. However, there are still some problems to be resolved as yet. Amongst them, the role of cement phases as concrete corrosion resistance controlling factors has been pointed out by Bombled [3], though

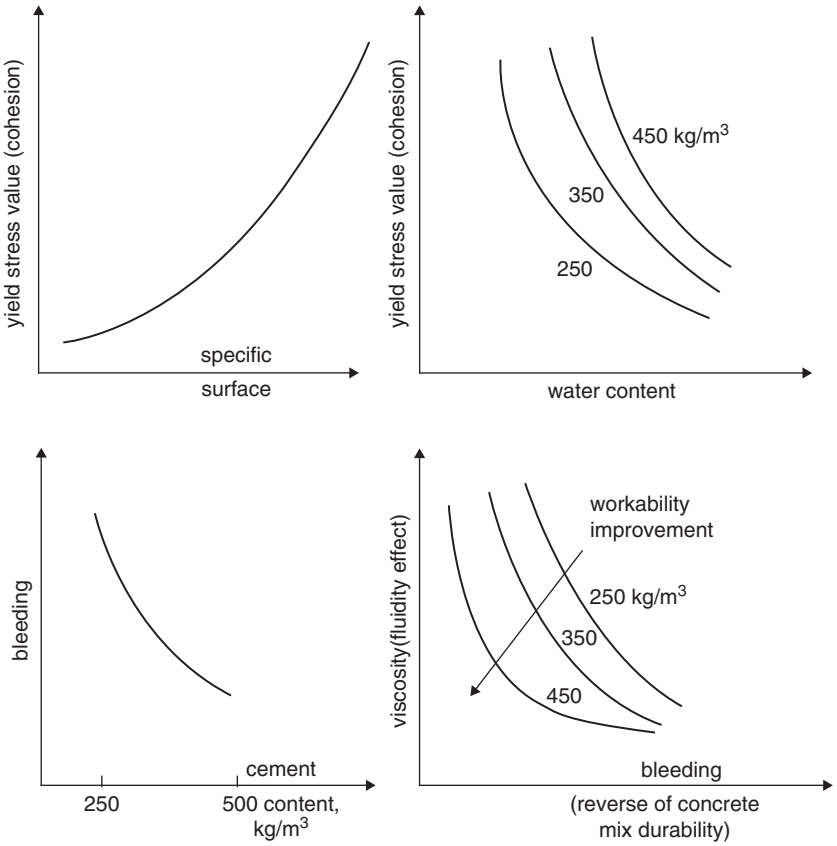


Fig. 6.2 The influence of cement content in concrete on the properties of concrete mix. (According to [4])

there is a huge amount of experimental data dealing with this problem, which will be discussed in Sect. 6.4.

There are some paste properties which influence the behaviour of fresh concrete. The workability of concrete mixture is the function of the rheological properties of paste which depend on the fine fraction content in cement. The yield stress value, being the measure of concrete mixture consistency at final stage of mixing, is increasing with the rise of cement specific surface area (Fig. 5.12). The initial setting time is significantly shorter in the case of this cement property.

The rheological properties of concrete mixture, which control the workability, are affected by C_3A content in clinker. The content of gypsum and its rate of dissolution is also very important; this problem is discussed in Sect. 4.1.2.

At early age the role of alkalis is significant and the two reciprocal effects are observed: the fluidizing action on one side and the set accelerating on the other side. The latter one causes the quick loss of workability. At high alkali content the second effect is dominating.

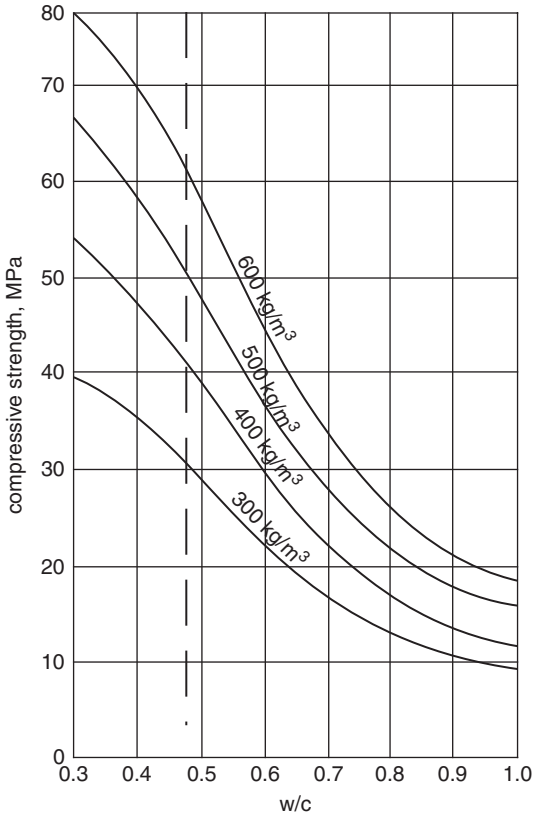


Fig. 6.3 Effect of w/c ratio and cement content in concrete on its strength after 28 days. (According to [4])

Every disturbance of cement setting, primarily the false set, linked with hemi–hydrate content, results in the rapid stiffening of concrete. It causes the additional water supply to automated concrete mixer, in the ready mix plant. The problem of optimum gypsum content and the effect of particular calcium sulphate phases dissolution rate on setting process have been presented in Sect. 4.1.2. The role of some ions from admixtures added to cement paste for set regulation has been discussed in Sect. 4.1.3. Cement setting is greatly affected by temperature; the process can be shortened with temperature because of higher solubility of cement clinker components, as well as by increasing the diffusion rate in the liquid phase. The early, preliminary stiffening of concrete has not been well recognized as yet [4].

The relations between the strength development of the paste or primarily of mortar and concrete are among the best recognized problems. It should be briefly reminded that the strength development of concrete is directly proportional to the strength of mortar. At early age, during the first 24 h this is a simple function of cement fineness, as well as the C_3S and C_3A content.

The profits of the rapid–hardening cements, that means:

- cements with high, fine alite crystals content [5],
- cements with high silica modulus [6],
- with low barium oxide admixture [7]

are significant. These cements are used in precast plants and in quick concreting, for example in constructions of silos and other structures with climbed shuttering, as well as in all cases when the accelerated maturing of concrete is needed. In 1963 the airstrip at the Orly airport in Paris was put into operation as soon as 24 h after the concrete placing. However, then the calcium aluminate cement of Lafarge was used.

The use of rapid–hardening cements in concrete production is a specific problem. As it is known, there are the two important parameters, as the short thermal curing (8 h or less) in the production of precast elements is concerned: the strength immediately after thermal treatment (f_{cti}) and further, the strength after 28 days of subsequent maturing ($f_{ct}28$). The latter one should not be significantly lower than the strength of concrete cured in standard conditions for 28 days (f_c28). Rapid–hardening cements usage give the possibility to limit the thermal treatment, to avoid the strength decrease of concrete after this treatment ($f_{ct}28$) as compared to the standard strength (f_c28) [8]. The usage of rapid–hardening cements give serious economic advantage in precast elements, produced with short heat treatment.

Cement and consequently the cement paste should acquire an assumed durability of concrete in normal environment. Finally, the cement paste constitutes an effective protective layer of reinforcing steel. Particular cases of concrete corrosion in different aggressive media will be discussed in Sect. 6.4. Some general remarks are presented below.

It should be underlined that the durability of concrete depends primarily on concrete composition (mix proportions) correctly designed, then on the production conditions of concrete mixture which is important (the dosage of components, particularly the dosage of water, should be free of any errors); the mixture should be well compacted and fresh concrete properly cured, after placing. Apart from the limited porosity (permeability), a fairly good durability is achieved in concrete with neither micro–cracks nor fissures. Elimination of segregation phenomena is very important too. Only when the concrete complies with the aforementioned requirements, the carbonation is negligible and is limited only to the thin surface layer. The concretes with higher cement content are better (see Fig. 6.72). There is a common opinion that the cement pastes with higher calcium hydroxide content have better resistance to carbonation, as well as are better protecting the steel reinforcement [4]. At low permeability the leaching of relatively easily soluble components [$Ca(OH)_2$] is seriously reduced and concrete is protected against the loose microstructure formation. Finally, properly produced concrete has higher resistance to freezing–thawing cycles. As it has been shown in Sect. 5.3.4. the properties of concrete are highly controlled by porosity. For this reason the macropores share should be as low as possible and low content of capillary pores should be assured. Therefore the vibration treatment of concrete mixture, with low w/c ratio (due to the superplasticizers),

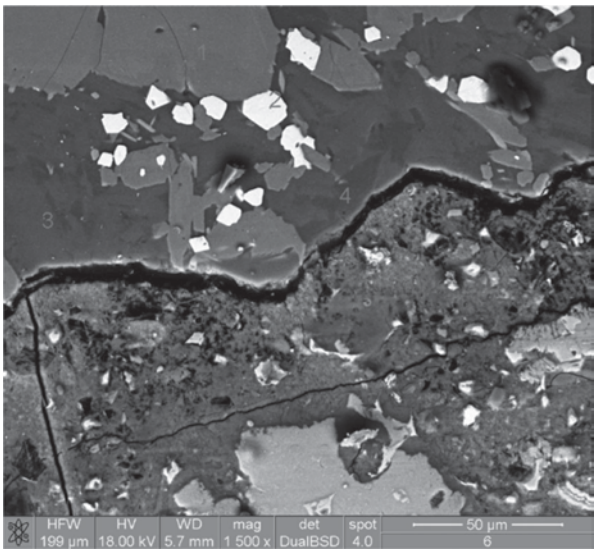


Fig. 6.4 Microcracks running around the surface of aggregate. (According to [9])

is of special importance. The effect of superplasticizers, as well as air entraining agents will be discussed in Sect. 6.6.

There are many controversial opinions as the origin of microcracks is concerned, because this phenomenon depends on many factors related both to the properties of concrete and to the environmental. Particularly the significance is attributed to the shrinkage affecting factors; therefore the number of microcracks grows with fineness, as well as with the cement soluble alkali content, and presumably, with C_3A content, particularly above 8% [3].

6.2 Cement Paste–Aggregate Bond

The properties, particularly the mechanical strength of concrete considered as a composite material, are strongly influenced by the properties of particular components, that is cement paste and aggregate, as well as by the binding forces acting between them. In a traditional concrete the aggregate component is the lowest deformable; therefore the stresses are concentrated in aggregate and are transferred to the interfacial transition zone paste–aggregate. As a result, the breaking of paste–aggregate bonds occurs. These cracks run around the surface of aggregate grains, through the paste which reveals lower strength (Fig. 6.4) [9]. Obviously, when the matrix (paste)–aggregate bond shows high strength, the crack propagation is hampered, while at low strength this propagation is favored. In concretes with weak aggregate, for example a light one, the cracks through the aggregate grains are observed; therefore the strength of material, as a whole, is reduced.

Maso [10] has shown experimentally that at weak paste–aggregate bond its cracking does not imply the cracking of whole material, because in this case the strength of composite is only the function of the strength of cement matrix.

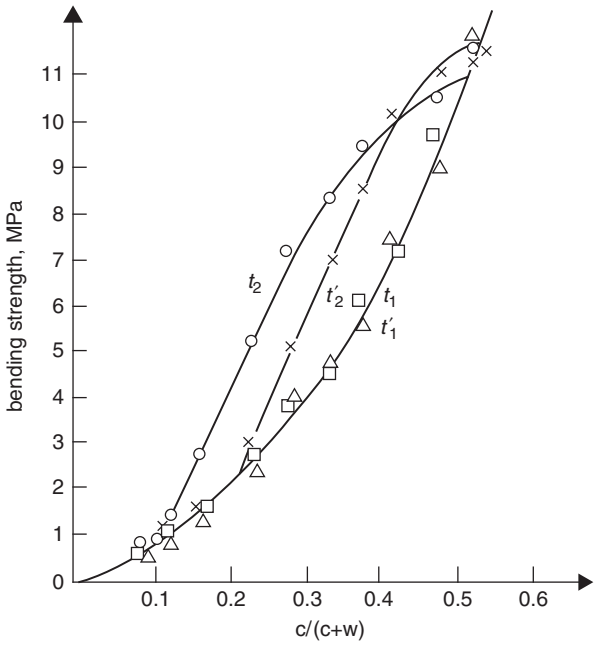


Fig. 6.5 Flexural strength of mortar with calcite and quartz: t_1 (*triangles*)—mortar with calcite covered with silicon resin, t'_1 (*squares*)—mortar with quartz covered with silicon resin, t_2 (*circles*)—mortar with calcite without modification, t'_2 (*obelisks*)—mortar with quartz without modification. *c* and *w* are the volume cement and water concrete in a paste respectively. Strength determined after 28 days. (According to [10])

Above some level of adhesion force, the cracking of paste–aggregate bonds results in cracking of material; then the matrix cannot transfer all load. This can be demonstrated based on an example (Fig. 6.5). The paste–aggregate bond is hence of substantial importance and the strength of concrete is thus determined [10].

The following formula for concrete strength was derived by Alexander and Taplin [11] from the regression analysis:

$$\sigma = \sigma_0 + b_0 + b_1 M_1 + b_2 M_2 \tag{6.1}$$

where M_1 means the flexural strength of cement paste, M_{2-} strength of paste–aggregate bond, b_0, b_1, b_2—constants; $b_1/b_2 \approx 2$. One can conclude from the formula presented above that the strength of paste ratio is two times higher than the paste–aggregate bonding force. Simultaneously, the critical stress intensity factor for the paste–aggregate interface is three times lower than for the hardened cement paste as it has been found by Hillmeier and Hilsdorf [12]. The stress—deformation (σ–ε) curves are of linear character both for the paste and aggregate[1], but they are not liner for concrete. This is the consequence of some imperfection of paste–aggregate bonds and, partially, the role of progressively propagating microcracks at increasing loading. The cracks occur usually in the interfacial zone before the load is applied. The cracking process was investigated under the microscope by Mindess and Diamond [13, 14]. The microcracks propagation was not observed up to 30 % total load

[1] Cement paste can be considered as a concrete with micro—aggregate in the form of unhydrated cement grains. Its high strength is attributed to the occurrence of strong bonds between these unhydrated cement grains and C–S–H.

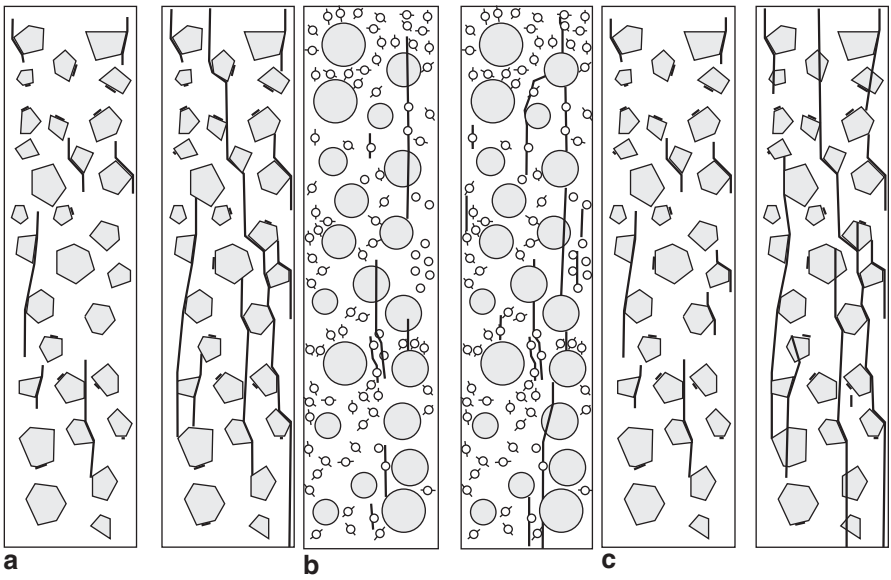


Fig. 6.6 Computer simulation of crack propagation: **a** in fractured concrete (around *aggregate grain*), **b** in lightweight concrete (through *aggregate grain*), **c** in high strength concrete (through *aggregate grain*). (According to [15])

value. At higher stress the propagation of microcracks occurs. For this reason the σ–ε relationship declines from a straight line more and more. When the stress level increases up to 50 % maximum total load value, the microcracks appear in the paste, which joined together the neighboring aggregate grains. After exceeding 75 % total load value the number of cracks increases. Finally, they attain a critical length and, as a consequence the destruction of material takes place.

Zaitsev and Wittmann [15] proposed a model of fracture, presented in Fig. 6.6. The authors assume in this model that the cracks start in the interfacial transition zone.

The XRD studies of the interfacial transition zone (material produced by abrasion of paste layers) [16], as well as the SEM observations with EDS analysis [16] revealed the presence of transition zone surrounding the aggregate grains, determined by Maso as an "aureole" [10]. This relates to the former water film around the aggregate. This area shows higher w/c ratio and subsequently cement components can readily dissolve, as well as the hydration products crystallize from the solution. Calcium hydroxide crystallizes in this interfacial transition zone and the crystals are oriented in such a way that their (001) axis is perpendicular to the surface of aggregate, as it was reported by Barnes et al. [17]. The C–S–H is then formed and the two products occur together as a duplex film about 1 μm thick (Fig. 6.7).

Outside this duplex film there is a porous zone where the following components are observed: primary—coarse and secondary—fine crystalline $Ca(OH)_2$, C–S–H particles and hydrated cement grains; the latter ones are present often in the forms

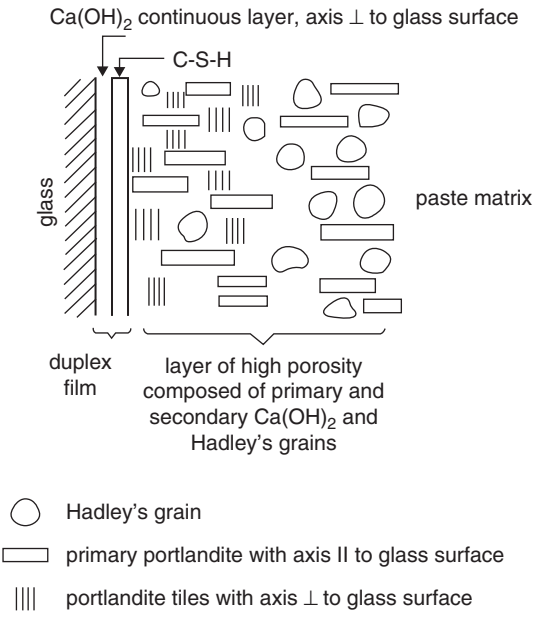


Fig. 6.7 Scheme of the paste–glass surface bond formation. (According to [15])

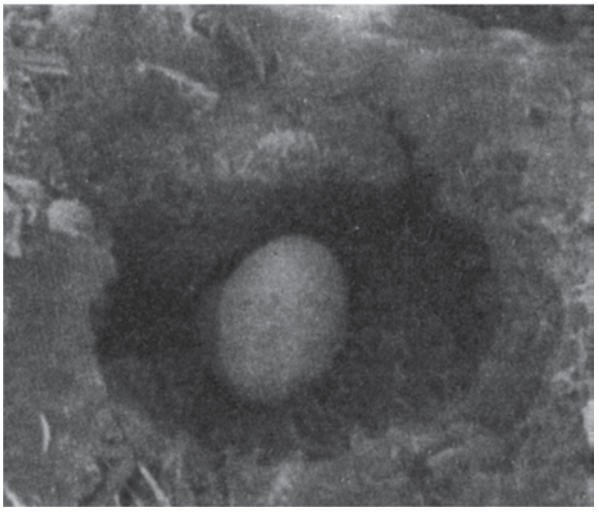


Fig. 6.8 Hadley's grain in the paste produced at w/c = 0.5, 7 days of hydration. (Photo of B. Trybalska)

of so–called Hadley's grains. Hadley's grains are composed of hydrate layer, mainly C–S–H, of 1 μm thick with empty space in the middle, sometimes more or less filled with hydration products or relics of unhydrated cement (Fig. 6.8).

The orientation of portlandite crystals was proved by Grandet and Olivier [16] in the XRD studies. This orientation is less evident with growing distance from the surface of aggregate grain and disappears as far as 40 μm from the grain, at w/c

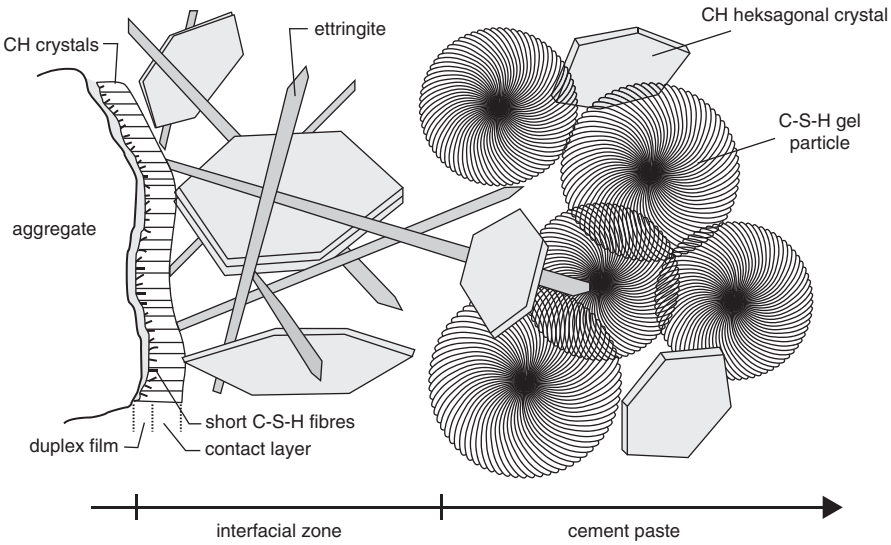


Fig. 6.9 Scheme of the interfacial transition zone. (According to [28])

0.29, irrespectively of the type of aggregate. According to Grandet and Olivier [16] the thickness of oriented CH crystals zone increases proportionally with w/c$\leq$0.33 and then reduces. At high w/c (about 0.5) a significant amount of calcium aluminates are randomly crystallizing on the surface of aggregate [18]. C–S–H in duplex film is fibrous and transforms gradually into the "honeycomb" form with time [17]. The calcium hydroxide crystals orientation degree is reduced in the case of aggregate reacting with the paste, for example for marble. Therefore the strength of such an interfacial zone, and consequently the strength of concrete increase, hence the "aureole"—porous and composed of large, oriented portlandite crystals—is the weakest part of material. All these factors favor the fracture formation and propagation. The shrinkage cracks appear in this zone as well [10].

Neither the duplex film, nor the oriented portlandite crystals in the interfacial zone were found by all the authors [19, 20]. However, there is a common opinion that this area is enriched with calcium hydroxide crystals and exhibits higher porosity. Consequently, it will have a great impact on the corrosion resistance of concrete. The transition zone of high porosity is the weakest micro–area where the corrosion of concrete will begin [21]. For this reason, the interfacial transition zone became a subject of numerous studies [16, 17, 22–28]. The constitution of this zone can be easily observed on the model proposed by Rooij et al. [28] (Fig. 6.9).

A layer composed of CH and C–S–H gel is formed on the aggregate surface immediately after mixing of concrete components with water [17]. However, Zimbelman [29] found the presence of small ettringite crystals. After the duplex film, the layer of portlandite crystals oriented perpendicularly with c axis to the aggregate surface is present [30, 31]. This is an interlayer between the duplex film and cement matrix, and is formed during 1–2 days after mixing of concrete components with

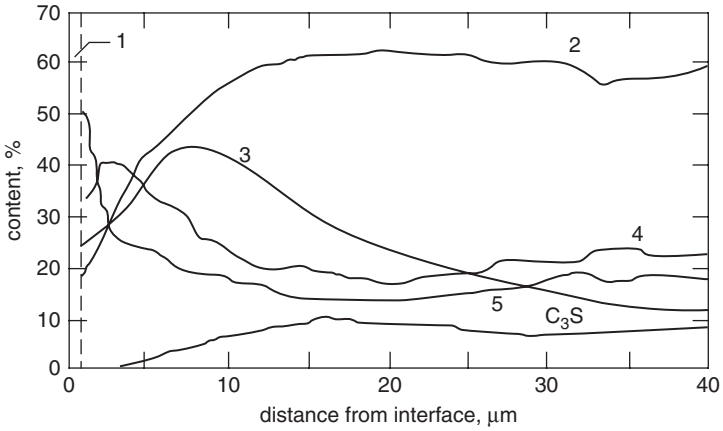


Fig. 6.10 Phase composition as a function of the distance from interface. (according to [35]): *1*—duplex film on the aggregate surface, *2*—C–S–H, *3*—ettringite, *4*—portlandite, *5*—porosity

water [32]. After interface a zone of higher porosity is present, in which frequently larger portlandite and ettringite crystals are formed, however, the first with very low thickness [27]. These crystals interpenetrate the basic cement matrix [33].

The following features have been attributed by Diamond and Huang [34] to the interfacial transition zone, as compared to the bulk paste matrix:

- a significantly higher number of capillary pores, often in a form of continuous network (Fig. 6.10),
- less unhydrated cement grains (Fig. 6.11),
- higher portlandite and ettringite content (Fig. 6.12),
- lower strength and brittleness.

Numerous hypotheses explaining the interfacial transition zone formation were proposed. The most frequently reported is of Olivier et al. [37], which explain the mineral grains content decrease with simultaneous water content increase by the so–called "wall effect". This term was firstly used by Mehta and Monteiro [38], who discussed the packing density of grains in the transition zone, consisting in filling the spaces between the larger cement grains by smaller ones. This could explain the transition zone of 10 μm thickness, while it has in reality 50 μm. Some authors attribute the formation of interfacial transition zone to the water layer surrounding the mineral grains in concrete immediately after mixing with water. Scrivener and Pratt [39] attribute it to the local bleeding and concentration of water under the coarser aggregate grains. However, the transition zone occurs around aggregate grains and this hypothesis does not refer to this fact. In turn, Hunter [40] proposes a hypothesis based on the effect of syneresis: in the colloidal particles containing system, the rapid coagulation of sol occurs and a conglomerates composed of some particles with high water content are formed. Because of the system tendency to minimize its free energy—particularly the surface energy—the number of contacts between the particles increases, the shrinkage of gel occurs and the excess water primarily

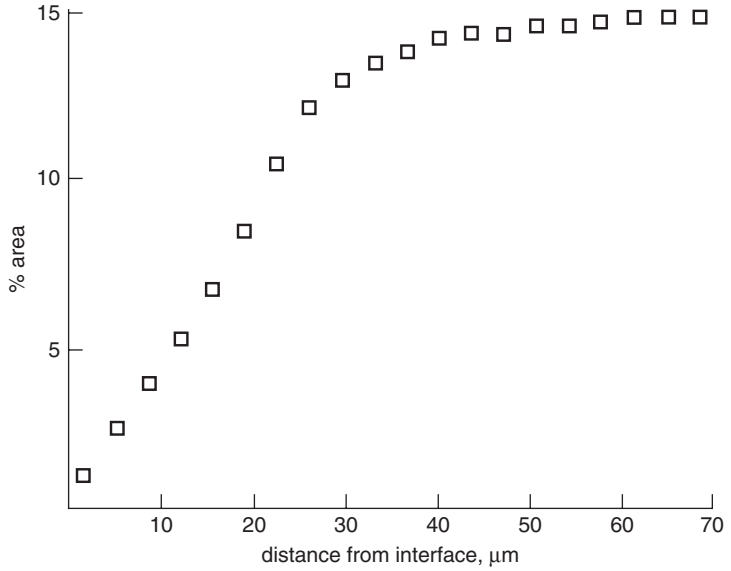


Fig. 6.11 Unhydrated clinker content in the interfacial transition zone. (According to [35])

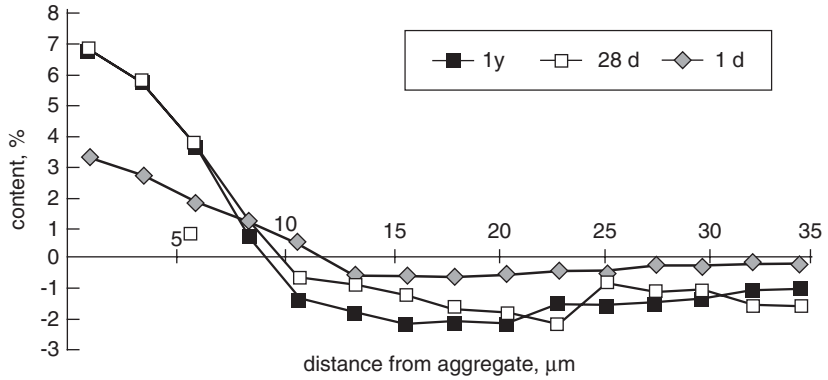


Fig. 6.12 $Ca(OH)_2$ content as a function of a distance from aggregate surface. (According to [36])

encapsulated in the conglomerates is pushed outside. The contraction linked with hydration reactions is added to the shrinkage induced by syneresis of gel.

Quite another conditions occur in the case of concrete with porous aggregate, particularly a dry one, which will significantly absorb water. However, the construction of interfacial transition zone has not been studied in such a concrete as yet [10]. One can even suppose, based upon the model studies, that the growth of calcium hydroxide content around the aggregate grains will not be formed. There are some premises indicating the enrichment in ettringite [10]. In case of dry, porous

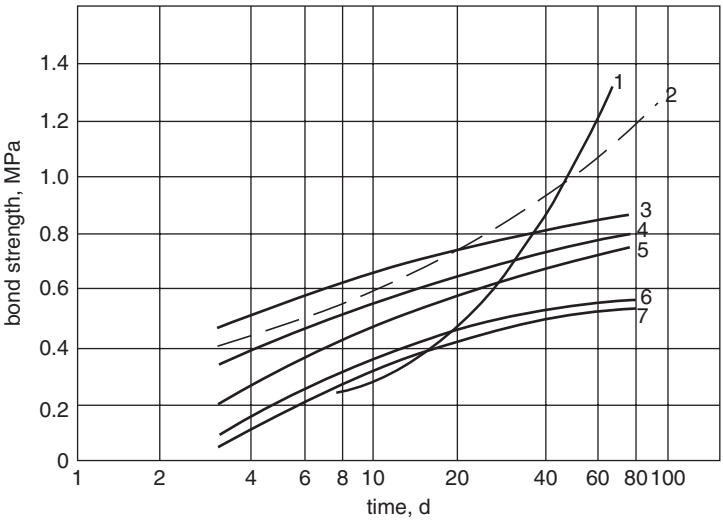


Fig. 6.13 Cement paste–aggregate bond in concretes with different aggregates of natural origin, with rough and polished surfaces. (according to [18]): *1*—polished limestone, *2*—cracked limestone, *3*—polished quartz, *4*—quartz, natural gravel, *5*—polished calcite, *6*—polished feldspar, *7*—polished granite

aggregate not only water but also cement paste will penetrate the macropores with a strong bond formation and an interfacial transition zone will be quite different. In Fig. 6.13 the effect of aggregate on the paste–aggregate bond is shown [18].

According to Langton and Roy [19] the occurrence or absence of CH crystals orientation can be an indication of aggregate reactivity with the paste. On the surface of inactive aggregate firstly a film enriched in calcium, but not in silica, is formed, called as C–H(C–S–H) by Roy, which consists the first zone. Subsequently the C–S–H gel particles grow outside from this film, consisting the second zone (II). These zones correspond to the duplex film. Larger CH crystals and C–S–H layer forming the interface binding the aggregate and paste run across the zones mentioned above. Therefore, the aggregate surface is covered with a layer of C–S–H gel and hexagonal portlandite crystals. This two layers zone is modified in case of reactive aggregate, for example an opal one (Fig. 6.14). The surface is then covered with a S–C–K–H film and larger crystals grow outside towards the paste, constituting the first zone. This layer is covered with C–S–H particles, binding the transition area with the paste (zone II). Therefore, one can distinguish here the four zones. The shrinkage cracks occur in both zones I and II (Fig. 6.14) [19].

The authors are not consistent as the construction of duplex film is concerned; however, there is a commonly accepted opinion that this transition zone is enriched with calcium hydroxide crystals, well developed and oriented in relation to the aggregate surface [10, 16, 41, 42].

The orientation of CH crystals is disturbed when some irregularities occur, such as rough aggregate surface, as well as the formation of calcium aluminate hydrate

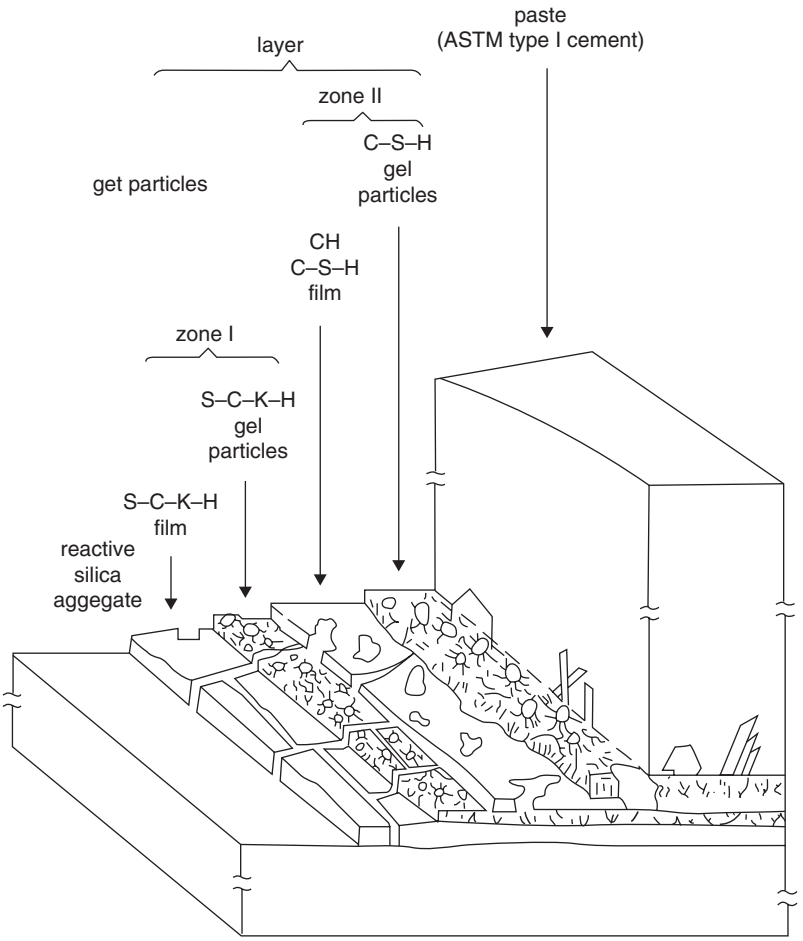


Fig. 6.14 Binding of cement paste with reactive silica. (According to [19])

phases or ettringite takes place [10, 18, 41]. The "aureole" is shaped during setting. More disordered orientation is observed in the presence of fine $Ca(OH)_2$ added to cement and playing the role of nuclei of this phase crystallization; then the growth of calcium hydroxide crystals occurs randomly [41]. The strength of mortar is thus improved. It was found that the ettringite content decreases with growing distance from aggregate surface [43].

The interfacial transition zone in concretes from cement with hydraulic or pozzolanic additions is considerably changed. In the case of slag addition the interfacial transition zone is thicker, presumably because of the higher water to ground clinker ratio, before the initial setting occurs [43]. In the pastes with fly ash there is much more water around the fly ash grains and the crystallization of $Ca(OH)_2$ and ettringite is favored [44]. However, with silica fume addition the porosity of

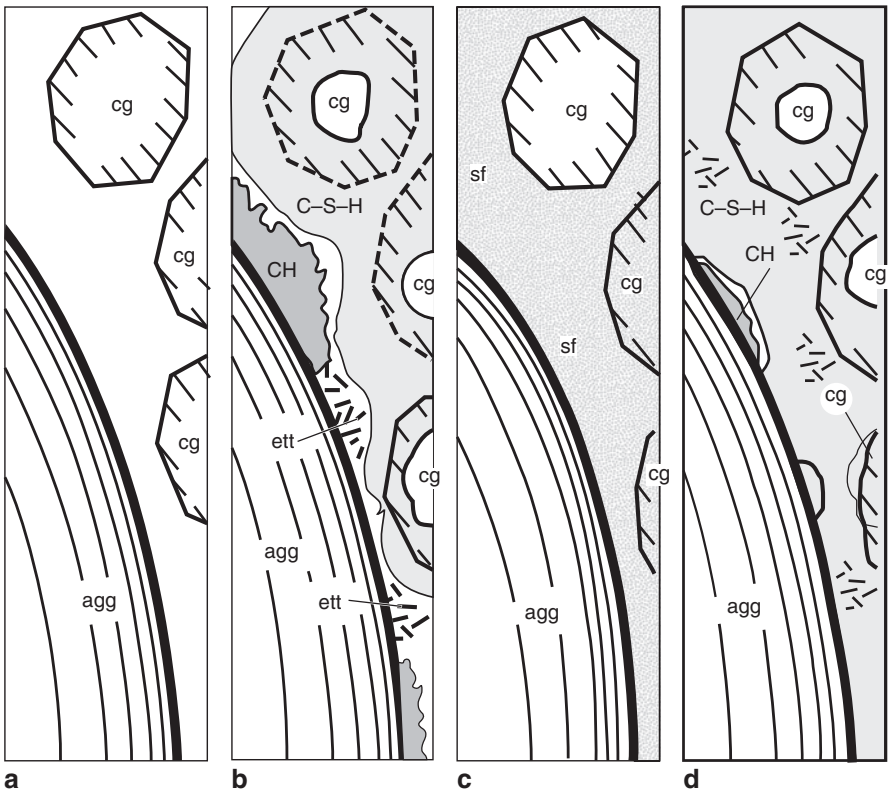


Fig. 6.15 Effect of silica fume addition on the construction of paste–aggregate transition zone; *cg*—cement grains, *sf*—silica fume, (**a**, **b**); **c**, **d** hydration progress. (According to [23])

interfacial transition zone is several times lower [23]. This is the consequence of very fine particles of this powder (0.1–0.2 μm) on one side and very high pozzolanic activity on the other side, resulting in C–S–H formation at the expense of calcium hydroxide. It is the reason of mechanical properties of concrete improvement, because the silica fume addition causes the removal of microstructural discontinuities, which normally are related to the porosity and high number of portlandite crystals (Fig. 6.15) [23, 45].

The paste–aggregate adhesion is significantly affected by the irregularity (roughness) of aggregate surface, while the reaction of aluminates and calcite, with the formation of carbo–aluminates hydrates is of minor importance and hence the strength of concrete from Portland cement with limestone or quartz aggregate is very similar [20]. The strength of concrete increases clearly with the ratio of sharp, crushed aggregate with rough surface, improving the adhesion to cement paste. In some circumstances the reaction occurring in the mixture can modify the "roughness" of aggregate surface and lead to the increasing strength of concrete. It should be mentioned, however, that some deformability of interfacial transition zone may in some

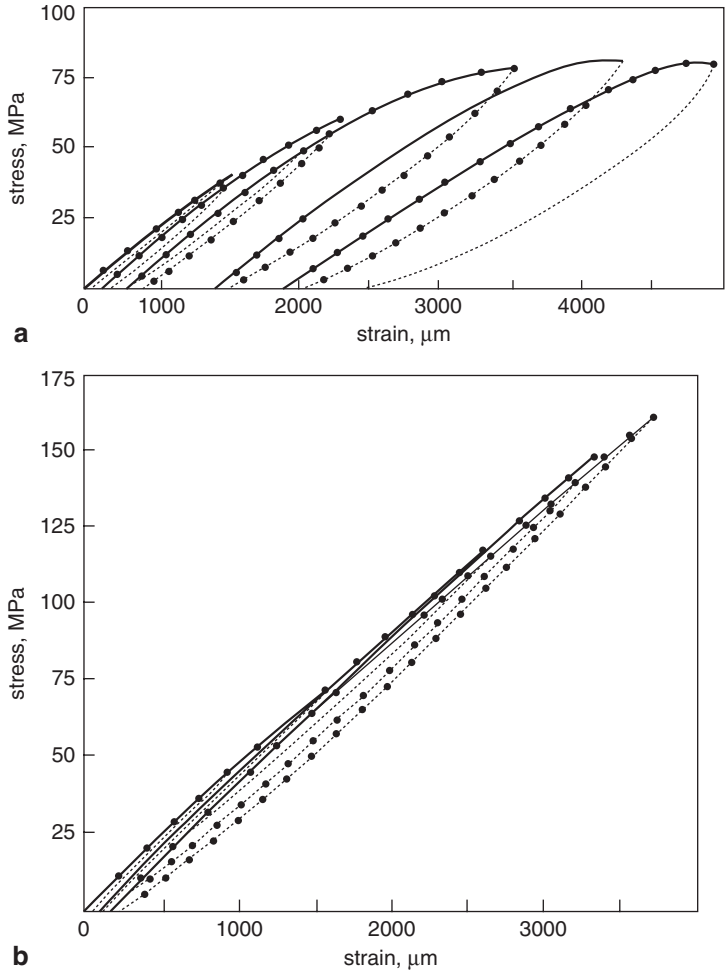


Fig. 6.16 Stress–strain curves for loading cycles: **a** concrete with basalt aggregate, cured in standard conditions, **b** autoclaved concrete with quartz aggregate. (According to [47])

cases enhance the concrete resistance against the formation of shrinkage cracks, linked with drying [46].

The strength of concrete with quartz aggregate can be significantly improved by autoclaving. The strength of interfacial transition zone is then higher than the strength of paste [41]. The epitaxial[2] growth of hydrated phases on the surface of aggregate grains occurs and the aggregate becomes the weakest component in such a concrete. The tangent elasticity modulus increases and the hysteresis of concrete deformations on cyclic applying and removal loading decreases [47] (Fig. 6.16).

[2] Epitaxy—oriented crystallization; growth of crystal of one phase on a crystal of other one occurring at mutual crystallographic orientation of these lattice planes on which the crystals intergrowth occurs. Geometric condition of its occurring is such similarity of lattice structure of both phases that they can, at least approximately, be compatible forming one common wall of two crystals.

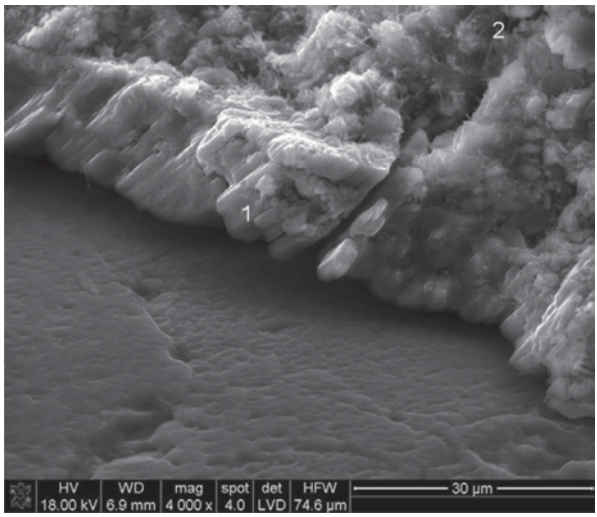


Fig. 6.17 Interfacial transition zone in concrete with high w/c. The crack is running along the aggregate surface, portlandite (*1*), C–S–H (*2*) and ettringite crystals. (Photo of B. Trybalska)

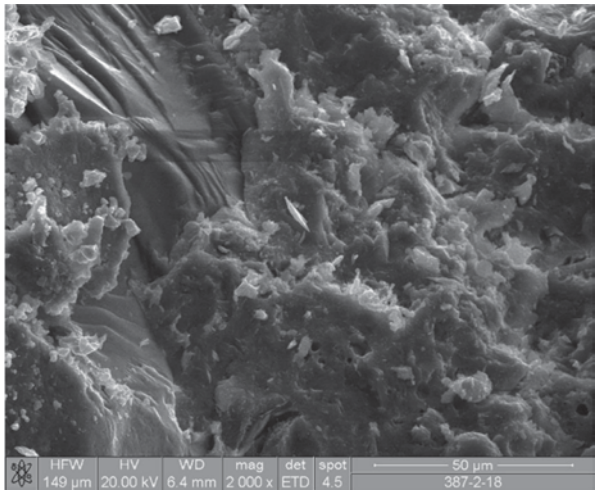


Fig. 6.18 Aggregate grain and dense cement matrix with C–S–H in an interfacial transition zone. (Photo of B. Trybalska)

The reduction of water content in high performance concretes, even below w/c = 0.4, results in the modification of interfacial transition zone construction. Porosity in this zone significantly decreases and the microstructure of the matrix surrounding the aggregate grains is the same as in the bulk material, not adjacent to the aggregate. The structure of interfacial transition zone in ordinary and high performance concrete is shown in Figs. 6.17 and 6.18. It was also presented by Aïtcin [48].

Considering the aggregate surface as "one mineral component" is a simplification, when the properties of interfacial transition zone are discussed. The rocks being the raw materials in aggregate production are composed of minerals having frequently large dimension 200–500 µm, thus ten times larger than cement grains. That

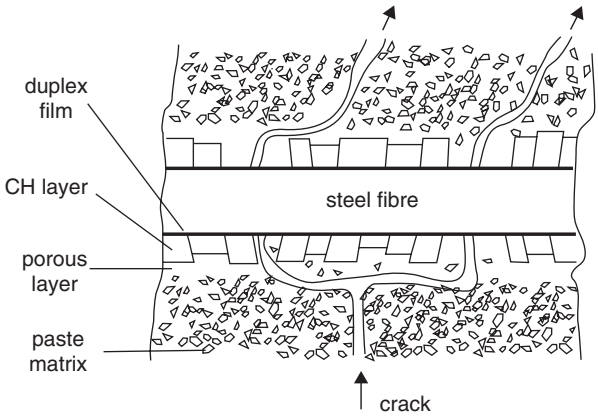


Fig. 6.19 Structure of interfacial transition zone and microcracks propagation (schematically). (According to [50])

is why the paste is in contact with the minerals of various chemical composition and properties; therefore in a concrete there are numerous interfacial transition zones.

6.3 Paste–Reinforcement Bond

The construction of interfacial transition zone around the reinforcement in concrete is very similar to the aggregate paste interface. This is presumably the consequence of locally occurring higher w/c ratio, promoting dissolution of cement components and crystallization of cement hydration products from the liquid phase. This interfacial transition zone reveals also higher porosity and lower strength than the bulk cement matrix.

This interfacial transition zone is enriched with portlandite crystals of hexagonal shape, with the *c* axis perpendicular to the surface of aggregate [49]. This layer is not continuous and there are in the formed "pockets" the C–S–H particles, surrounding sometimes the portlandite crystals [50, 51], as well as the ettringite is present too [52]. In Fig. 6.9 the construction of paste—reinforcement interface is shown [50]. The three zones can be noticed:

- duplex film, 1–2 μm thick, adjacent to the reinforcement,
- zone composed of large CH crystals, 10–30 μm thick,
- zone of high porosity, parallel to the interface.

The thickness of interfacial transition zone is determined by the range of oriented portlandite crystals and equals 50–100 μm [16]. However, only a 10–20 μm thick layer of this zone shows clearly different mechanical properties, as compared to the bulk cement matrix. The microstructure of interfacial transition zone is variable and depends on the type and properties of cement and reinforcement, presence of admixtures, concrete maturing regime, as well as the other factors (Fig. 6.19).

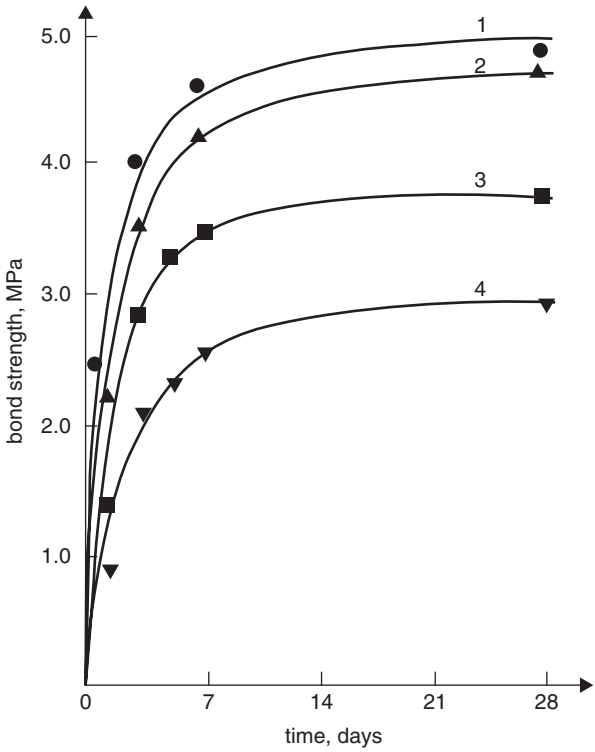


Fig. 6.20 Strength of cement paste bond with different metal reinforcement. (according to [51]): *1*—brass, *2*—copper, *3*—soft steel, *4*—stainless steel

There are no chemical reactions between the reinforcing steel and cement paste; however, they can occur in the case of copper, brass and zinc. As a consequence, the bonding forces between the paste and a reinforcement are increasing [49, 53]. In Fig. 6.20 the strength of bonds between cement paste and different metals are shown, according to Al Khalaf and Page [51].

The chemical reactions of cement paste with zinc (galvanized steel) result in the release of zinc to the solution and the formation of calcium zincate, $CaZn_2(OH)_6 \cdot 2H_2O$, covering the surface of metal [49]. Simultaneously, there is no portlandite crystals in this transition zone because in the presence of zinc alite hydration is delayed (see Sect. 4.1.3.2). The coating of hydrated calcium zincate crystals on the surface of metal increases the bonding forces between paste and reinforcement by the roughness formation on its surface.

In a paste cured for a short period of time, the cracks induced during bending occur in the vicinity of the paste interface with reinforcement, while in the old samples—along the contact plane [51]. This observation is not fulfilled for copper and brass, which proofs a better cement paste adhesion, of chemical nature, to these metals (Fig. 6.20).

The adhesion of steel to cement paste consists primarily in the mechanical interpenetrating of both materials and hence the so–called elastic component of shear strength is produced. At low load the plastic deformation occurs and subsequently

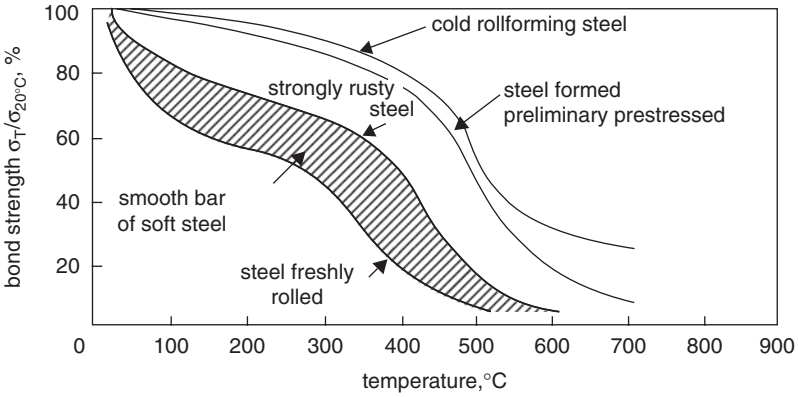


Fig. 6.21 Reduction of steel–paste bond for different types of steel as a function of increasing temperature. (According to [55])

disappears with loading removal. After overcoming of this stress, only the frictional resistance component remains.

The steel–paste bond is deteriorated progressively under the repeated cycles of reinforced concrete loading; the mechanism of load transfer is destroyed and the strength of composite decreases [41].

The bonding force of paste with ordinary reinforcing steel, measured as flexural strength, is the same as for the aggregate and equal about 5 MPa after 28 days [53, 54]. This bonding force increases with decreasing w/c of a paste, with time of maturing and degree of concrete compacting. Superplasticizers as well as silica fume improve the bond. The casting and compacting technology are also of importance; the horizontal placement of element is favourable.

The bonding force of paste with reinforcing steel depends on temperature and decreases at increasing temperature [55]. Reduction of steel–paste bond is clearer in the case of polished steel than of rusted or ribbed bars (Fig. 6.21). The steel–paste bond weakening in the case of ribbed bars vs. temperature is equivalent to the decrease of concrete flexural strength.

Covering of reinforcing bars with resin, applied as an anti–corrosion protection, can lower their adhesion to cement paste. Worsening of adhesion occurs in the case of vinyl polychloride, but it does not occur if the epoxy resins are used. However, some epoxy resins reveal the creep effect [56].

As it is commonly known and applied for a long time, the properties of paste can be improved by reinforcement with the fibres. For example, the production of asbestos–cement materials started 80 years ago. The fiber reinforcement technology has been developed extensively for the last 20 years and the other fibres has been taken into account, first of all the steel fibres, but also the carbon, glass, resin, polypropylene and cellulose fibres as well. The fibres reinforcement gives the possibility to enhance the flexural and tension strength, as well as the impact resistance. The fibre composite modifies the properties of concrete by control cracking and the mode of failure by means of post—cracking ductility.

The improvement of concrete properties by fibre reinforcement is primarily attributed to markedly higher fibre resistance to rupture, as it is shown in Table 6.1 according to Hannant [57].

The properties of fibre reinforced composites are more intensively affected by the bonding force between the fibres and the matrix than in the case of concrete with and without reinforcement. Mindess at al. [54] consider that we do not know exactly how the increase of bonds force of paste with aggregate and reinforcement improve concrete properties. The higher bonds force in the case of these materials increase their brittleness and consequently, the lowering of stress value, at which the microcracks appear. At increasing bonds force between the paste and reinforcement, the probability of reinforcing bars deterioration under the impact load is higher [54]. Finally, Mindess et al. [54] are of the opinion that the modification of adhesion forces is of minor importance, while the properties of composite are controlled basically by the type of cement (matrix strengthening), aggregate and reinforcing steel.

However, in the case of fibres reinforced composites, strengthening of their bonding force with the paste enhance their properties [54]. By modifying of fibres geometry and increasing of the compactness degree of composite the materials with extremely high tensile strength and showing post–cracking ductility, can be produced. However, the fibres transfer better the tensile stress when they are pull out of the matrix rather than broken together with it.

Weaker bond between fibre and matrix is a fracture arrestor, which has been explained by Cook and Gordon hypothesis [58]. In the stress field the tensile component (σ_x) shows a maximum value at some distance before the crack tip (Fig 6.22). A weaker bond in the interfacial plane is broken under this stress before the propagating crack approaches and cross this plane. At this point the crack propagation is ended, which can eventually change a direction of 90°.

Hannant [57] points out that cement paste has several properties which limit the possibility of modification by the addition of fibres. They are as follows:

- small deformation before the cracking begins,
- high elasticity modulus, which, although playing an advantageous role in limitation of concrete construction deflection, is decreasing the possibility to exploit the ability of fibres to transfer load,
- the workability requirement of the concrete mixture is limiting the fibres content which could be introduced [57, 59],
- the relatively low bonding forces of paste with different fibres,
- high alkalinity of environment; this is beneficial in the case of steel but deleterious for glass fibres.

The fibres content is relatively low because of the properties of cement matrix and the share of 8 % is seldom exceeded. According to Hannant [57], the application of fibres does not increase the stresses at the very moment of composite cracking, but the merit of fibre inclusion must lie in the load carrying ability of the fibres after matrix cracking has occurred. The cracked composite may carry a lesser or greater load after cracking than the uncracked material as shown in Fig. 6.23. Both curves may have practical value although multiple cracking is more likely to occur for the

Table 6.1 Properties of fibres [57]

Type of fibre	Fibre diameter (μm)	Fibre length (mm)	Density (g/cm^3)	Young's modulus (GN/m^2)	Poisson's ratio	Tensile strength (MPa)	Elongation at break (%)[a]	Percent by volume (%)
Chrysotile asbestos (white)	0.02–30	40	2.55	164	0.3	200–800	2–3	10
Crockidolite (blue)	0.1–20	–	3.37	196	–	3,500	2–3	–
Carbon fibre type 1 (high modulus)	8	10	1.90	380	0.35	1,800	0.5	2–12
Carbon fibre type 2 (high strength)	9		1.90	230		2,600	1.0	10–20
Cellulose			1.2	10		300–500		10–20
Glass fibre	12.5	10–50		80	0.22	3,300	4.8	2–8
204 filament strand	110 × 690		2.7	70	–	1,250	–	
Kevlar PRD 49	10	6.65	1.45	133	0.32	2,900	2.1	2
Kevlar PRD 29	12	6.65	1.44	69	–	2,900	4.0	
Polypropylene (single fiber)	100–200	5–50	0.9	to 5	–	400	18	0.1–6
Fiber with high rupture strength	100–600			200		700–2,000	3.5	0.5–2
Stainless steel	10–330	10–60	7.68	160	0.28	2,100	3	

[a] *Note*: 1 % elongation = 10.000×10^{-6} strain

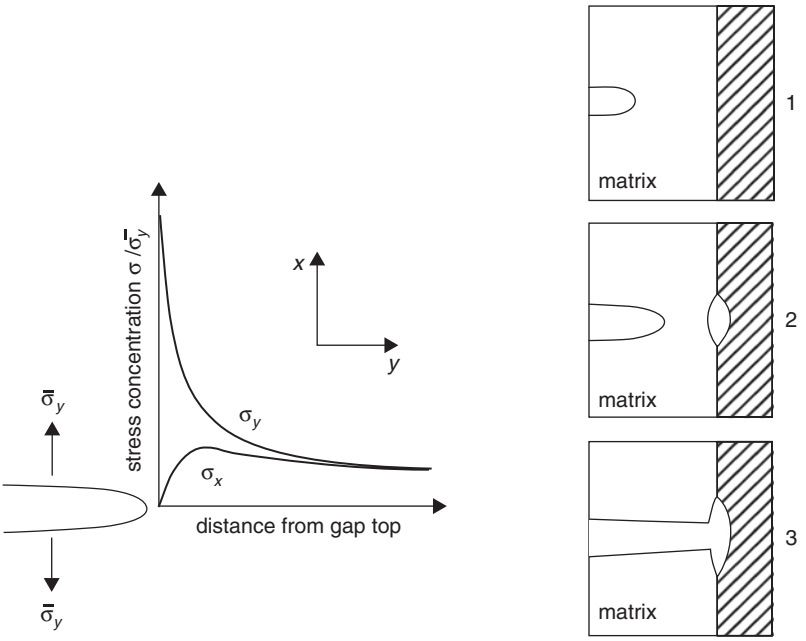


Fig. 6.22 Distribution of stress as a function of distance from crack tip and locking of crack propagation in the interface with weak bonds. (According to [58])

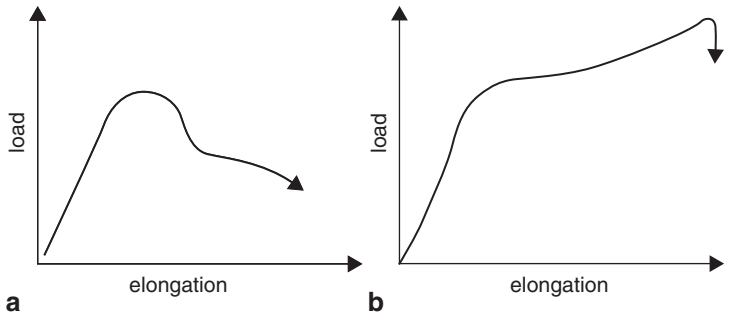


Fig. 6.23 Typical load–extension curves in direct tension. (According to [57])

material described by Fig. 6.23b and this endows the composite with greater apparent ductility [57].

In order that the material may follow the curve in Fig. 6.23b, it is necessary for the critical fibre volume to be exceeded. The critical fibre volume is defined as the volume of fibres which, after matrix cracking will carry the load which the composite sustained before cracking. In such a way, a brittle material in which one cracking surface could be formed with low energy, transforms into the pseudo–plastic body, which can carry momentary the overload with no visible damage. Therefore, the

goal of paste strengthening by an addition of fibres is thus the obtaining of composite in which a huge number of small cracks < 0.1 mm wide and placed in close neighbourhood will be formed.

In spite of the many years of practice, the composites with cement matrix are still the subject of numerous investigations, because their properties are worsening with time, and the main cause are the detrimental changes occurring in the paste–fibre interface [60]. The extensive studies to create a theoretical model which would allow predicting their properties are carried out simultaneously [61–63].

There is also a shortage of data on the impact of the transition zones both paste–aggregate and paste–reinforcement on concrete properties. The correlation between concrete durability and strength of bond has not been found as yet. Mindess et al. [54] propose some methods of paste with aggregate or reinforcement bond strengthening. The silica fume addition can be applied very easily.

Mindess et al. [54] are stating that the strength of concrete is only in moderate degree dependent on the strength of paste–aggregate bond. It is commonly known that the cracks in high strength concrete run across the aggregate but not around its grains.

6.4 Concrete Corrosion

Durability of concrete is defined as an ability to ensure, with required factor of safety and for assumed period of time, the functions predicted in the design of concrete structure. There is no need to explain that the durability has a capital practical meaning. Therefore numerous works were focused on the mechanism of concrete deterioration; hence this knowledge is a starting point toward the invention of methods aimed in prevention or retardation of the durability threatening processes.

Durability of concrete is the most important feature of this material; its importance has increased since the idea of "sustainable development" appeared. As a main rule, the effectively using of natural resources, to save them for future generations, is generally accepted. On the other side, however, one should remember that concrete is not stable material in Earth conditions, as it results for example from the free enthalpy of paste components reactions with CO_2. The iron and aluminum hydroxides are stable, as well as calcium carbonate and silica gel. The natural aggregates, as well as those produced from different type of rocks, undergo similar transformations to those occurring in nature, for example in the case of silts or clays, being the sedimentary rocks, formed by transformations mainly of magmatic and metamorphic rocks. These sedimentary rocks are composed of clay minerals and with high quartz sand content; quartz being one of the most stable rock forming minerals.

Durability of concrete can be attained first of all by producing material of low permeability, which causes the migration of aggressive solution into this composite very difficult. The tightness of concrete will be the result of low porosity, which can be assured by low w/c ratio; it should be generally lower than 0.4. That is why the high performance concretes are produced in majority with w/c of about 0.35. In case

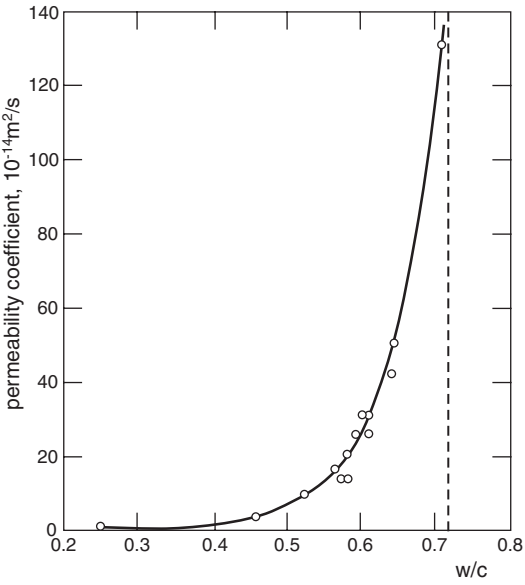


Fig. 6.24 Permeability coefficient of hardened cement paste vs w/c, for entirely hydrated cement clinker. (According to [64])

of lower strength concretes w/c is usually on the level of 0.5, which causes the capillary pores, as well as the aggregate–paste (cement matrix) interfacial transition zone formation. This zone reveals high porosity and hence it is the weakest part of concrete. At improper curing of concrete at early age the microcracks can appear which, apart from capillary pores, are the quick access paths for aqueous media inside the mass of composite. The occurrence of continuous system of capillaries in concrete is controlled not only by w/c, but also by cement hydration degree (Fig. 6.24).

A very good relationship is obtained between the porosity, from mercury porosimetry measurements, and permeability of hardened pastes. However, this method cannot be recommended in the case of concretes, as it has been mentioned in Chap. 5. A representative concrete sample cannot be satisfactorily reduced to the small specimen for mercury porosimetry measurements. Therefore different methods of concrete "enrichment" in paste component are used; the last one being the concrete porosity controlling factor. The concretes with lightweight aggregate are an exception in this case. There is usually too much paste in these small samples of concrete and the methods of concrete "enrichment" in paste worsen additionally the situation.

In the opinion of experts, expressed during the workshop on the sulphate corrosion resistance, a low permeability of concrete is more important than the use of high sulphate resistant cement, in the case of sulphate corrosion hazard [65]. Therefore the w/c ratio maintained on a low level, together with higher cement content and proper curing of concrete at the early age of hardening, are of basic significance.

The internal and external concrete corrosion are distinguish. The internal concrete corrosion results from the concrete components themselves, first of all the

reactive aggregates and too high sulphate content. In the case of reactive aggregates, the mechanism consists in the reaction of reactive silica with sodium and potassium hydroxides with the formation of non–stoichiometric, hydrated silicate gel, with varying Na^+, K^+ and Ca^{2+} cations content. Therefore for this phase the formula: Na–K–Ca–Si–aq is often used. Swelling of this phase leads to the deterioration of concrete. The second case i.e. the over–sulphated cement results in ettringite formation when the paste in concrete loses its plasticity and it leads to concrete destruction. One should rather exclude the non–standard content of sulphates in cement; however, gypsum or, more scarcely anhydrite, can be present, in exceptional cases, in aggregate.

The delayed ettringite formation is rated among the internal corrosion of concrete, which is induced by a heat treatment of concrete, and thus occurring mainly during the precast concrete elements production. However, one cannot exclude the temperature rise up to 70 °C in the interior of massive concrete structure, as a consequence of heat evolution process in hardened cement paste, and in this condition ettringite can be unstable.

The external corrosion takes place when concrete is exposed to the attack of hazardous liquids; among them one should mention first of all the sulphate, sulphide and chloride solutions, as well as gaseous CO_2, acid rains and variable temperatures, falling down frequently below zero point.

There is a common opinion that corrosion of concrete needs the liquid environment or at least an atmosphere of high humidity. The transport of liquid through the concrete causes the sequence of processes, including at first the concrete components of the highest reactivity: calcium hydroxide and calcium aluminate hydrates. One can thus conclude that the phase composition of cement has a great impact on the behavior of concrete in any aggressive environment.

The causes of concrete deterioration are usually very complex and occur simultaneously or successively. However, frequently it can be distinguish one or few basic processes, from which the destruction of material is beginning. Among the most important causes of paste destruction, based on chemical reactions which can occur in an aggressive environment, the three principal corrosion mechanisms can be distinguish. They are the following.: the dissolution of cement matrix components, expansive reactions and decomposition of hydrates, first of all C–S–H, in the case of which the formation of phases showing no binding properties can occur. Dissolution of paste components and subsequent leaching process results in concrete microstructure loosening and therefore the further deterioration, for example by freezing of water, is accelerated.

On the other side the expansive reactions can cause the cracking and destruction of concrete as a result of formation of compounds with low solubility, which precipitate from the liquid phase and exert a crystallization pressure. The sulphate corrosion is a typical case and leads to the crystallization of gypsum and ettringite. There are much more compounds evoking expansion, for example the chlorides: $CaO \cdot CaCl_2 \cdot 2H_2O$, $MgO \cdot Mg(OH)Cl \cdot 5H_2O$ [66] or the sodium carbonate hydrate $Na_2CO_3 \cdot 10H_2O$ [67], which crystallization cause the destruction of concrete. As a result of complex sulphate corrosion, occurring together with carbonation process, the C–S–H phase is decomposed with the formation of thaumasite, a product without binding properties.

Different types of corrosion are classified formally, taking into account the following factors:

- pH value: acid corrosion, basic corrosion,
- type of anion: sulphate, chloride, multi–component,
- kind of environment: soft water, sea water, sewage, de–icing salts (chlorides), plant and animal fat, sugar solutions, gases.

This classification has a long tradition and reflects rather the problems to be resolved by the specialists in the field of cement chemistry, with aim to improve the durability of concrete in the more frequently occurring aggressive environments. The sulphate corrosion is here a typical, common example, which led to the invention of calcium aluminate cement by Bied (*ciment fondu*). The deterioration of concrete by de–icers, used in millions tons (for example in the USA in winter 1966/1967 6.3 million t [62]), became a serious problem. The cost of bridges repairs in USA in 1975 was 200 million $ [63].

In reality the mechanism of concrete deterioration as a consequence of acid corrosion, if it is sulphuric acid, is the same as in case of sulphate corrosion. For this reason in both environments the matrix based on Portland cement with reduced C_3A content is more resistant. This example shows the imperfection of kind of corrosion classification, presented above.

On the other side the distinguishing of acid corrosion has the justification; Portland cement paste is not stable in water solution with pH lower than 10, or even 10.5 [68]. Therefore the concrete in such an environment is readily corroded. However, concrete from calcium aluminate cement is stable with no special protection, at pH of water solution reduced to 4 [69]. As it was aforementioned, beside of pH value there are the other factors involved: diffusion rate (permeability) and, as in all the chemical reactions, the solubility of products.

The basic aggression can be, in principle, due to the action of sodium and potassium carbonates, particularly to the sodium compounds [67]. This can be considered as promoted by sodium lye together with carbonation of concrete. In this condition the sodium carbonate hydrates are formed and concrete is damaged by their crystallization.

In practice, the aggressive solutions of salts are the most frequently occurring corrosive solutions; they will be discussed later. On the other side the nitrate promoted corrosion is the untypical example. In this case the calcium nitrate–aluminate crystals are formed in the pores of cement paste [70]. The pastes from metallurgical cements show a significantly higher resistance to nitrates; the slag content should exceed 70%.

A special case of corrosive action was reported by Oberholster [71]. The components of Carboniferous shale aggregate were the iron sulphide minerals, such as pyrrhotite, pyrite, chalcopyrite. The first was oxidized pyrrhotite:

$$4FeS + 9O_2 + (4+n)H_2O \rightarrow 4H_2SO_4 + 2Fe_2O_3 \cdot nH_2O \tag{6.2}$$

The bacteria play an important role in this reaction. The further corrosion process consists in reaction of sulphuric acid with calcite, also present in this aggregate, with the formation of expansive gypsum. The sulphuric acid reacts also with

calcium hydroxide from the paste to form gypsum. Gypsum can also react with aluminates to form expansive ettringite. In Sect. 6.4.5 the details of the sulphate attack are presented.

6.4.1 Paste–Aggregate Reactions

Some reactions of the paste with aggregate have been mentioned in Sect. 6.2. It relates to the calcium aluminate reaction with calcite, which promotes the strength of concrete and proceeds in two stages. In the first stage the $C_3A \cdot \frac{1}{2} CaCO_3 \cdot 12H_2O$ is quickly formed and in the second stage it transforms progressively into $C_3A \cdot CaCO_3 \cdot 11H_2O$. The reaction rate increases with the fineness of calcium carbonate, therefore it is faster in the case of limestone co–ground with clinker [72, 73]. The rate of these reactions is reduced with lowered w/c ratio.

The transformation of aluminates into the carboaluminate phase prevents the transition of ettringite into monosulphate phase [72].

There is no reason to presume that in standard conditions of paste curing it could react with quartz, however, during thermal curing at 60 °C the surface of quartz grains reveals some symptoms of reaction [41]. At low pressure steam curing at 80 °C the reactions of paste with quartz, albite and anorthite occur with moderate rate [41]. As aforementioned, the reaction with siliceous aggregate is significantly accelerated by autoclaving. Quartz reacts with calcium hydroxide, formed as a result of cement hydrolysis, to give tobermorite crystals [74].

Application of limestone aggregate in concrete of calcium aluminate cement causes a significant strength increase [75]. A continuous strength development is observed during the whole research period, up to 5 years. A significant strength increase was noted for the concrete with corundum aggregate, in which the chemical bonds between the paste and aggregate were found [18].

The paste–aggregate reactions resulting in the destruction of concrete are a specific problem. Primarily the reactions of aggregate with alkalis from cement, resulting in expansion and cracking of concrete should be discussed. This internal corrosion relates to the aggregates containing reactive silica, mainly opal and siliceous glass. Strength development of concrete with these aggregates are shown in Fig. 6.25 [76].

There are also the other reactive aggregates, namely gneiss and mica containing shales [41]. In the interfacial transition zone, in the vicinity of aggregate surface—kaolinite and hydromicas, while from cement paste side—gel of sodium–calcium silicate hydrate, respectively are formed. However, in the case of serpentine concrete deterioration is due to the formation of brucite [75]. The clay minerals, such as chlorites, vermiculite, as well as micas and feldspars, are also included to reactive aggregate components.

The decomposition of dolomite aggregate in the reaction with alkalis from cement, is also ranked among the cause of concrete destruction. On the other side, the

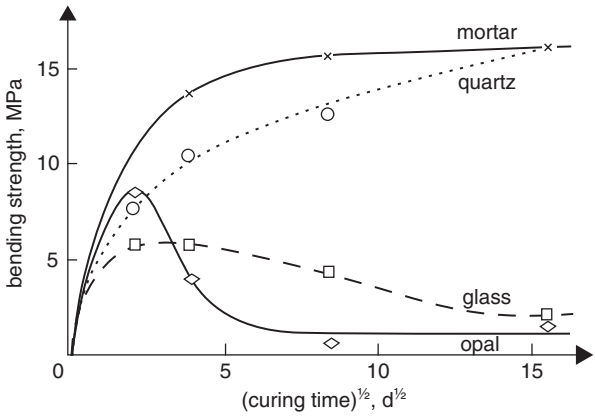


Fig. 6.25 Strength development of concrete with glass, opal and quartz aggregate within 8 months experiments (curing conditions: 95–100 % RH, temperature 23 °C). (According to 76])

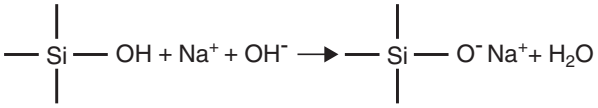
decomposition of dolomite was found by Deloye et al. [75] in a 30 years matured concrete, however, without any symptoms of its destruction.

The deterioration of concrete can be the consequence of the presence of some aggregates components which, for example, as iron sulphide, decompose to give iron(III) hydroxide and sulphuric acid [71]. This phenomenon will be presented later. Let us discuss now the studies of concrete deterioration mechanism caused by alkali silica reaction, the most important in practice. The two types of reactions can be distinguish:

- reaction of alkalis with silica–rich aggregate,
- reaction of alkalis with carbonate aggregate.

In the case of silica–rich aggregates the two groups of materials can be distinguish: the aggregates containing reactive forms of silica, to which belong: opal, tridymite, cristobalite, acidic volcanic glass. They react rapidly with alkalis to cause expansion in a short period of time. The aggregates produced from the hornstones, clay–mica shales, granites, granite gneiss and granite–diorite, greywacke and quartzite rocks can be classified as another group. The reactive component of these rocks are chalcedony, crypto–crystalline quartz or quartz under stress.

Amorphous or poorly crystallized silica contained in aggregate reacts with sodium or potassium hydroxide in aqueous solution, and, as it is commonly known, in concrete pore solution, a significant amount of these hydroxides can be present. To this reactive silica belong the most frequently opal, tridymite with defected structure [77] or siliceous glass. The two–stage process occurs: the first stage is the typical acid–base reaction, in which the acidic silanol groups react with sodium or potassium hydroxide:



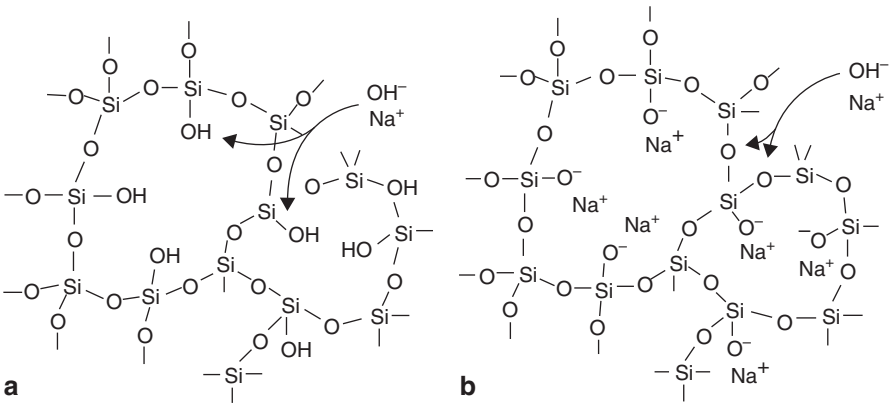


Fig. 6.26 Neutralization of acidic silanol groups (**a**) and negative charge of non–bridging oxygen ions (**b**) in gel by sodium hydroxide. (According to [78])

The second reaction stage occurs at high pH and consists in breaking of oxygen bridges:

$$\equiv Si-O-Si\equiv + 2Na^+ + 2OH^- \rightarrow 2(\equiv Si-O^-Na^+) + H_2O$$

The negative charge of non–bridging oxygen ions are equilibrated by the sodium and potassium cations as it is shown in Fig. 6.26 [78]. In the progressive process, at sufficient alkali concentration in the liquid phase, as a result of high number of oxygen bridges broken, the reactive silica is transformed into sodium silicate. This sodium silicate contains monomers and partially more polymerized silicate anions [78, 79]. This is a gel relatively well soluble in water.

The advancement of aggregate decomposition process depends on the degree of silica phases structural disorder and on the conditions in which the process occurs, primarily of the alkalis concentration in the liquid phase, temperature, as well as of their diffusion condition to reaction site.

The humidity and temperature are of high importance as the properties of gel are regarded. The strongest expansion was observed at room temperature and at RH 80 % [80].

The effect of temperature on the reaction progress and expansion was studied by Diamond et al. [81]. As it is shown in Fig. 6.27, at early age the rate of reaction is higher at temperature of 40 °C than at temperature of 20 °C, but after 30 days the progress of reaction is the same. The expansion proceeds in the same way, however, after 90 days is higher at temperature of 20 °C. Ludwig [82] has also found that at establishing dynamic osmotic equilibrium the higher temperature accelerates the reaction, but simultaneously diminishes the expansion, after longer period.

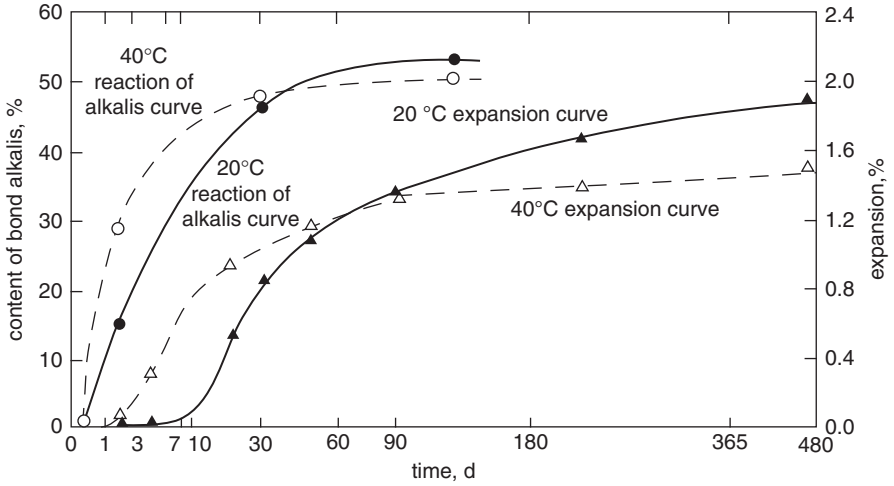


Fig. 6.27 Comparison of the curves of alkalis reaction and expansion of mortars with 8 % addition of opal aggregate, cured at two temperatures. (According to [81])

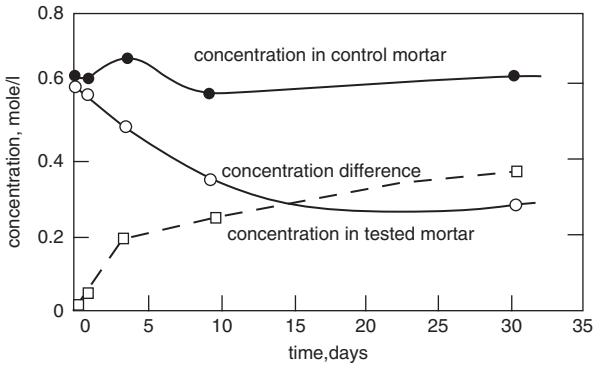


Fig. 6.28 Comparison of combined Na^+ and K^+ ions content (together with bound water contents) in pastes with reactive and non–reactive (quartz sand) aggregate as a function of maturing time at temperature of 20 °C. (According to [81])

The $Na^+$and K^+content in the concrete pore solution became lower, as compared with the quartz sand containing reference sample (Fig. 6.28). The stationary state is achieved after 1 month when the ratio of combined alkalis is about 35 % [81].

Formerly there was an opinion that the reaction of aggregate would be accompanied by the increase of volume, for example as in the case of CaO hydration. Nowadays, a more significant importance is attributed to the properties of reaction products. The hypothesis of the mechanism of concrete destruction assumes that the sodium silicate gel absorbing water swells [78]. Another type of expansion occurs when the sodium and potassium silicate gel transforms to sol. There is an opinion that this liquid of high viscosity exerts pressure after filling the pores in concrete [78, 80]. According to many authors, the osmotic pressure is causing expansion [80].

It is assumed that cement paste plays a role of semi–permeable membrane which is impermeable for the silicate anions formed as a result of reaction. Some authors postulate that this semi–permeable membrane is composed of sodium and potassium silicates gel formed during reaction. A concentration gradient appears and linked with him the osmotic pressure. Recently, the difference in discussions of swelling mechanism, attributed to the sorption of water or to the osmotic pressure, became insignificant. There is a view that sodium and potassium ions can diffuse through the semi–permeable membrane more easily than the calcium ions.

The expansion of synthetic sodium silicate gel was measured by Struble and Diamond [83]. The two types of gel have been differentiated: a gel exerting high swelling pressure of 4–11 MPa and a second with low, of about 0.5 MPa. There is no substantial difference between their chemical composition. They found that the significant free expansion is not always linked with high pressure. The calcium containing gel is causing the moderate expansion [83]. The same authors [84] found the highest swelling pressure for the gel with Na_2O/SiO_2 ratio about 0.35.

According to Dent Glasser [79] the swelling process does not require the semi–permeable membrane formation, separating the areas with different ions concentration. Gel itself behaves like a semi–permeable membrane. A gel formed around aggregate is enriching in sodium and potassium ions and swells with moisture absorption. From the thermodynamic point of view the separation of this system by a semi–permeable membrane is not a necessary condition for water movement. The difference of water free energy in the two parts of the system is a driving force of water movement in such direction to diminish this difference. Therefore the osmotic mechanism or swelling of gel are the manifestation of the same phenomenon.

It is not a simple task to find the causes of concrete damage, they are generally very complex. The process can begin by concrete structure loosening by the expansive alkali–aggregate reaction; further destruction can occur for example by freezing and thawing. The beginning—at least—of destruction by the alkali–aggregate reaction is proved by the presence of silica gel exuded from the concrete, as well as the gel coating around the aggregate grains.

Nowadays, a significant importance is attributed to the delayed ettringite formation, associating the alkali–aggregate reaction and causes the prolonged, and higher expansion of concrete at later age (Fig. 6.29) [85, 86]. The question of delayed ettringite formation was studied by Owsiak [87–89], which came to the conclusion that the delayed ettringite formation, irrespectively on the cause of this phase crystallization, results in a higher expansion due to the alkali—siliceous aggregate reaction. According to Collepardi and Ogoumah Olagot [90], the delayed ettringite formation occurs only in the presence of microcracks in concrete (see point 6.4.3). It is the another justification of the occurring of delayed ettringite formation in concretes, after the expansion caused by alkalis reaction with aggregate.

In a porous aggregate or concrete there is more space and the swelling processes may not cause the destruction of material. For this reason there is frequently no correlation between the degree of silica reaction in aggregate and the scale of expansion.

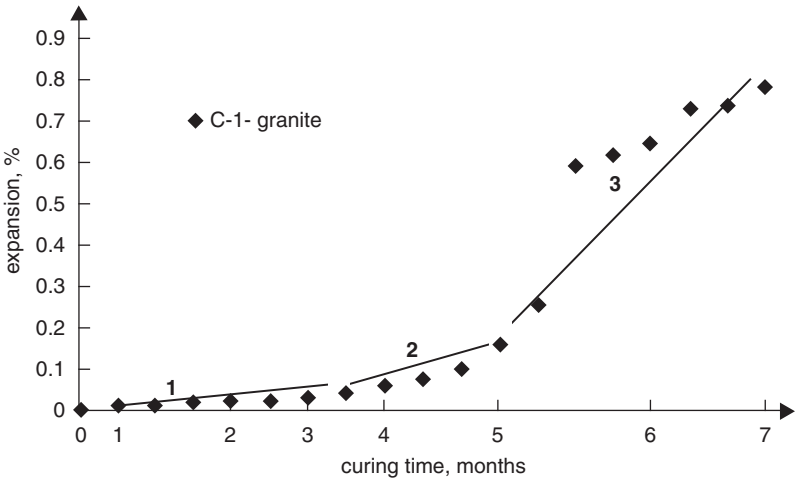


Fig. 6.29 Expansion of mortar from cement with high alkali content and granite aggregate vs time. Segment 3 results presumably from the delayed ettringite formation. (According to [85, 86])

Considering the different studies, Diamond et al. [81] point out that the expansion can occur without the sorption of moisture from the environment; therefore water absorbed by sodium–potassium silicate gel can be only the capillary solution.

Struble and Diamond [83, 84] studied the expansion of sodium and sodium–calcium silicate gel and noted a very untypical phenomenon. Some gels have shown higher swelling under load than free expansion (Fig. 6.30), and then were transformed into sol. The other gels, after the initial shrinkage, which can occur if the expansion pressure is lower than the applied load, have shown swelling. The authors attribute this unexpected behaviour to the molecular structure of gel.

There is an opinion that gel is composed of polymerized particles and monomers which are subjected to the structural transformations under the load, as a consequence of water absorption. These structural changes are proved by an effect of gel ageing, after which the swelling and pressure became substantially lower [83]. There was also establish that gels containing no calcium do not transform to sol.

Dent Glasser and Kataoka [78, 91] postulate that the pressure accompanying the sorption of NaOH aqueous solution by the sodium silicate gel is equivalent to the osmotic pressure of surrounding solution, because there are major differences of concentration between this liquid and gel, before the equilibrium is reached [78, 91] (Fig. 6.31). Maximum pressure is found for the gel with the molar ratio SiO_2/Na_2O from 3 to 5 which is corresponding to the most destructive reactive aggregate content in concrete [78].

The studies of the phase composition of interfacial transition zone were also developed. A white layer of reaction products is formed on the reactive aggregate surface, sometimes surrounded by a black gel. The crystalline thaumasite is often formed this white layer [60, 71]. Regourd et al. [92] found the two types of gel; the

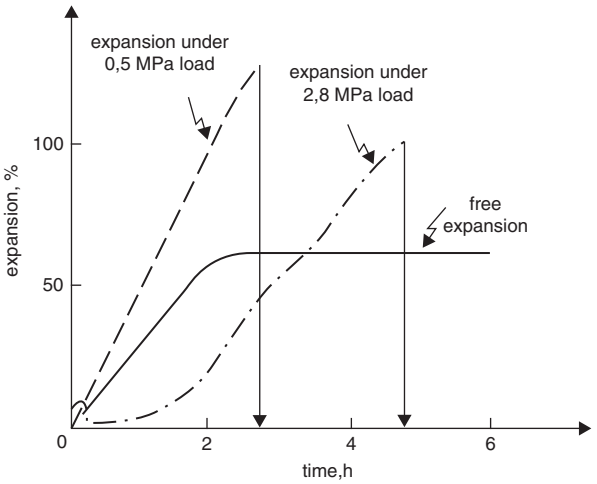


Fig. 6.30 Free swelling and swelling under load of the gel with molar composition: 0.42 Na_2O, 1.0 SiO_2, 1.57 H_2O, which expansion pressure was 3.1 MPa. (According to [83, 84])

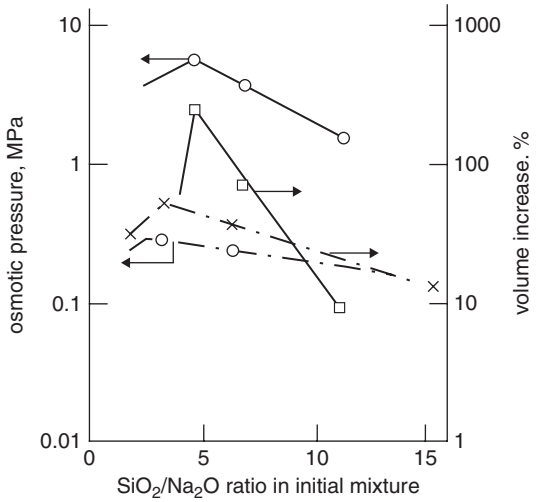


Fig. 6.31 Free swelling of solid phase and osmotic pressure of solutions as a function of molar SiO_2/Na_2O ratio in a initial sample [78, 91]; *continuous lines*—NaOH concentration 0.7 mol/l, *dashed lines*—NaOH concentration 0.05 mol/l

one with high silica content (C/S 0.2–0.4) surrounding the aggregate and the second with higher lime content (C/S 1.8) in the pores. The crystallization of secondary C–S–H on the aggregate surface, in contact with gel, as well as also in this zone, the accumulation of ettringite and $Ca(OH)_2$ crystals, was observed. There is an opinion that the ettringite crystals are formed as a result of the liquid phase migration in concrete and their crystallization is rather not harmful [93].

Some authors [94, 95] found in the reaction layer on aggregate grains, a poorly crystallized material, showing the strong XRD peak corresponding to $d = 1.2$ nm. This product is stable only in humid conditions. This phase transforms into okenite on drying. In a damaged concrete with quartzite or agglutinated sandstone or

hornfels[3] aggregate Oberholster et al. [71] found a crystalline calcium–potassium silicate.

This silicate has a XRD peak characterized by a d = 1.2 nm spacing and this is presumably the semi–crystalline phase reported by Cole [94]. A progressive transformation of gel into a crystalline product can occur as it is postulated by some authors [60, 92]. Apart from the 1.2 nm phase, Davis [96] found the two other compounds with the XRD peaks at d = 0.87 nm and 0.28 nm. Calcium is always a constituent of the sodium and potassium silicate gels, as it has been proved in several works [60, 92]. According to Regourd et al. [92] cement paste is penetrated by a "mobile" sodium and potassium silicate sol reacting with $Ca(OH)_2$ and C–S–H imbibing the Ca^{2+} ions by diffusion. It is stated that the reaction of $Ca(OH)_2$ is promoted by dissolution of this phase in a sodium and potassium silicate sol, at lowered pH [60]. The alkali–aggregate reaction is accelerated by chloride ions; this effect is particularly visible at low temperatures [60].

It should be underlined that the composition of concrete samples damaged as a result of alkali–aggregate reaction is very complex. Apart from aforementioned crystalline phases there is an amorphous gel and the products of concrete constituents carbonation by atmospheric CO_2, as well as aggregate residue. In the approximative chemical composition of reaction products silica is a dominating component: from 60 to 80%, there is a significant amount of CaO: from 12 to 20% and K_2O: from 6 to 19% [97].

When the reactive aggregate must be applied in concrete, there are the two ways recommended to protect the composite against the destructive expansion. They are as follows:

- use of low alkali cement,
- use of cement with pozzolanic or hydraulic additions.

According to Lea [98], Davis already in 1951 proposed to limit the alkali content in cement to the level 0.6% Na_2O_e, to prevent a destructive expansion. Nevertheless, the expansion was observed in some cases in spite of the low alkali content [98]. Moreover, as it has been reported by Stark [99], the alkalis needed in this reaction can originate from the aggregate. Stark found this phenomenon also in the case of glass with composition corresponding to andesite or ryolite tuff. The cracks appeared as late as after 5–8 years. Owsiak [100] studied the effect of saturated $Ca(OH)_2$ solution on the leaching of alkalis from granite and found the releasing of substantial amount of these components to the liquid phase.

As it has been proved by Way and Cole [101], a ground granite and basalt release a significant amount of alkalis to the aqueous $Ca(OH)_2$ solution at temperature of 50 °C, as a result of feldspar decomposition. The sandstones are less reactive; the quartz sand presents the lowest reactivity. However, the relation between the leaching of alkalis from the mineral constituents in a rock and the quality/applicability

[3] Hornfels is a metamorphic rock with some characteristic minerals, such as andalusite, cordierite, garnet; the main constituents are as follows: quartz, micas, and feldspars. Hornfels is a product of sedimentary rock or magmatic rocks transformation, occurring as a result of intrusions.

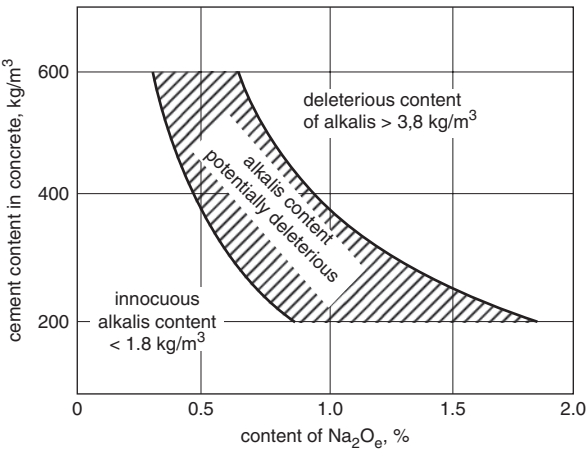


Fig. 6.32 Relationship between the active alkalis content in cement and cement content in a concrete vs. the alkali–silica reaction susceptibility. (According **to [71])**

of this rock as the aggregate was not found [60, 101]. Granites and basalts give generally a very good aggregate, in spite of their susceptibility for alkali releasing to the liquid phase. However, Deloye et al. [102] found the deterioration of concrete when the aggregates were the source of alkalis. This relates to the gneiss, granite and serpentinite materials. As one can see these results are ambiguous, however, there is an opinion that only the weathered granite or basalt can be the aggregate of poor quality.

On the other side the aggregate of poor quality are produced from the sedimentary rocks with no alkalis soluble in $Ca(OH)_2$ solution. Malek and Roy [103] presented a hypothesis that the simultaneous releasing of aluminum, sodium and potassium ions does not cause any harmful swelling. The calcium aluminates hydrates formed are binding in their structure high quantity of the OH^- ions, reducing the aggressiveness of liquid phase towards the reactive silica from the aggregate. Grattan–Bellew [104] studied the effect of phlogopite scales addition to cement mortar. As it is known, a part of potassium in phlogopite is exchangeable. This additive accelerated the reaction of dolomitic limestone aggregate and consequently the expansion of concrete was accelerated too.

The expansion of concrete is generally a slow process. The 0.05% expansion level is attained, depending on the type of aggregate and alkali content, after a period of one to 14 months [99]. This is a threshold value, because above it the microcracks propagation from the reactive aggregate to the surrounding mortar takes place. The curves plotted in Fig. 6.32 also show that the alkali content lower than 0.6% Na_2O_e is not sufficient to ensure the durability of concrete [99].

The alkali limiting criterion, for example 0.6% Na_2O_e in cement, is linked with the aim to reduce the concentration of sodium and potassium ions in the concrete pore solution. Simultaneously, these ions cause a substantial decrease of $Ca(OH)_2$ concentration in the capillary solution. Some doubts arouse as the calculation of alkali content in the form of sodium equivalent is concerned hence it is known that the potassium silicate gel reveals lower expansion that the sodium silicate.

The limit content 0.6 % Na_2O_e in cement relates to the average cement content in concrete, that is 400 kg in 1 m^3. This corresponds to the alkali content 2.4 kg in 1 m^3 of concrete. Locher and Sprung [105] estimate the limit content of sodium equivalent for 3 kg Na_2O_e in 1 m^3 of concrete; that is 500 kg of 0.6 % Na_2O_e containing cement. Obviously, the Na_2O_e content in cement can be raised to 1 %, as cement content in concrete is 300 kg/m^3. Oberholster et al. [71] postulate the 1.8 kg Na_2O_e/m^3 as a safe limit. These authors distinguish the three range of alkali content in concrete [71] (Fig. 6.32): at alkali content exceeding 3.8 kg Na_2O_e/m^3 the destructive expansion occurs in every case, at the content less than 1.8 kg Na_2O_e/m^3 the expansion due to alkali–silica reaction is not observed. Finally, at the intermediate alkali content range the expansion depends on the reactivity of aggregate and the concentration of soluble alkalis in cement. However, because for the determination of aggregate reactivity and soluble alkali content the long–term laboratory experiments are necessary, this intermediate range is considered as potentially harmful [71]. One should remember that the relationships shown in Fig. 6.32 are concerning the aggregates from Malmesbury in South Africa, produced from greywacke and hornfels of high reactivity to alkalis.

As aforementioned, the source of alkalis in concrete can be the aggregate and mixing water too. The possibility of alkali intrusion to concrete from the external sources should be also under control. Among other the most popular are the de–icing salts used in winter on roads. They are exceptionally detrimental, because in the presence of sodium or potassium chlorides the OH^- ions concentration in concrete increases at the expense of $Ca(OH)_2$, from the paste [106].

Different methods are used in order to evaluate the reactivity of aggregate. Some of them are the following:

- petrographic examination [49, 107],
- examination of concrete or mortar cubes according to ASTM C227,
- accelerated chemical method, ASTM C289,
- examination of cubes cut off from the rock according to ASTM C586, in air at temperature 38 °C and 100 % RH.

The method of testing 25 × 25 × 285 mm mortar prisms, stored at temperature 38 °C and 100 % RH cannot be applied for the aggregates which are showing late expansion [60].

The accelerated chemical method consists in the determination of soluble silica and lowering of NaOH solution alkalinity. This method is based on the assumption that any reactive aggregate is releasing the amount of silica higher than the equivalent decrease of the solution alkalinity. The results thus obtained allow classifying the aggregate to the one of three groups: non–reactive, potentially reactive or destructive one (Fig. 6.33).

Turriziani [60] points out that the limit values used to classify the particular types of aggregate relate only to the American materials. It has been underlined by Lea [98] that the results of tests for some expanding aggregates allow to classify them as the non–reactive ones and there are the inverse cases too. Sorrentino et al. [108] found that the classification of aggregate to any reactivity class (Fig. 6.33) is more

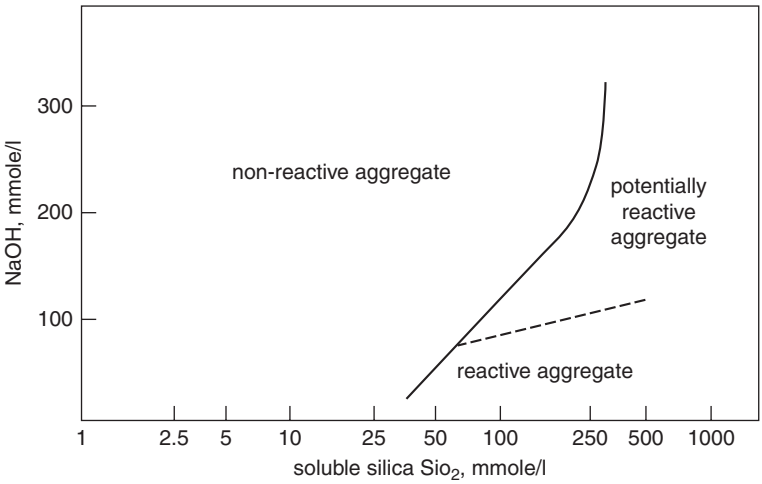


Fig. 6.33 Assessment of the aggregate reactivity based on the accelerated chemical method. (According to ASTM C289)

accurate when the leaching is carried out for 48 h, not for 24 h, as it is recommended by ASTM C289. Simultaneously, the doubts submitted by Turriziani [60] to the applicability of this method to the aggregates other than the rocks of American origin, were not confirmed. The correctness of accelerated chemical method and its compatibility with the other tests was proved by Kurdowski et al. [109]. In the former Czechoslovakia[4] the method consisting in the observation of smooth surface of the aggregate specimen immersed in 1–mole NaOH solution at temperature of 38 °C for 72 h was used. The presence of exuded gel was the proof of aggregate reactivity.

The soluble alkali content in cement is of great importance for the aggregate expansion reaction. Sodium and potassium occur in cement in the form of sulphates and form the solid solutions in C_3A and C_2S (see Sect. 2.5.5.3). Sodium and potassium sulphates are very quickly dissolved. Alkalis from C_3A solid solution are easily soluble too, while those from C_2S are practically inactive, because of the slow C_2S hydration. The release of alkalis is also affected by distribution of particular phases in the polymineral cement grain; one can imagine C_3A encapsulated in brownmillerite coating; its reaction with water will be retarded.

Therefore, taking into account all these aforementioned peculiarities, one can differentiate, apart from the total alkali content in cement, the content of soluble alkalis[5] and so–called "active" alkalis, which correspond to the Na_2O_e released to the solution after varying period of the reaction. Many data concerning the alkali content in cements produced in different countries can be found in technical literature [71]. Substantial differences can occur between the total and soluble alkali content.

[4] According to the former Czechoslovak standard CSN72 1162, 1981.

[5] The content of water soluble alkalis is usually determined according to the former British standard BS 4550 part II (the suspension produced by introducing 1 g cement sample to 250 ml distilled water is stirred at temperature 20°C for 24 h).

There are numerous experimental results showing the effectiveness of pozzolanic additions in reducing expansion, which can be thus lowered to the admissible level. The slag and pozzolanic cements have been used for many years to produce concretes containing the reactive aggregate, to control their expansion [110–112]. Different authors recommend varying additions percentage [60, 80, 105, 113–118]. However, the range 25–40 % for fly ash and 50–70 % for the ground granulated blastfurnace slag addition is most frequently reported. According to many authors, the ground granulated blastfurnace slag is more effective, however, its addition must be a little higher [80, 110]. Fly ash, particularly with high alkali content, for example 4 %, gives no satisfactory results [119]. The effect of silica fume is particularly intensive [60] and its content can be significantly lower [120]. There is an opinion that the silica fumes addition is protecting even the glass fibres against the corrosive action of the paste [80].

Expansion is practically eliminated if 15–40 % of pozzolana co–ground with Portland cement clinker is used [98]. Some authors recommend 20 % of diatomite addition, the others 30–35 %. of volcanic glass. The effectiveness of natural pozzolanas is rather variable [98]. The method of verifying their effect is given by Lea [98].

Hobbs [110] concludes that the expansion occurs only when the water soluble alkalis, expressed as Na_2O_e, is higher than 2.5 kg/m^3 of concrete. It relates to the total alkali content, introduced with all concrete components. In this context, if cement replacement by fly ash does not allow reducing alkali content below this value, or even it becomes higher, then the addition of this pozzolana will not decrease the expansion, but even it can be increased [110].

There are generally more alkalis in fly ash than in Portland cement. Most of these alkalis occur in the vitreous phase and hence only a part is water soluble, usually about 0.1 % Na_2O_e [60]. On the other side one should remember that the glass is the most reactive component of fly ash in cement paste. It is not clear what part participate in the pozzolanic reaction and what is released to the pore solution. However, there is a dominant opinion that the release of alkalis to the solution from fly ash occurs slowly and hence they cannot participate in the reaction with aggregates [60]. Therefore Hobbs [110] proposes to take only 0.2 % Na_2O_e as an income of alkalis from fly ash, when the total alkalis content in concrete is calculated. However, better effect are showing fly ash with low alkalis and CaO content [60, 121].

Because of the significantly lower expansion in the case of cement with mineral additions, in the case of these cements the higher threshold Na_2O_e value was establish in the standards and directives, in many countries. In the German former standard DIN 1164 the admissible content was raised to 0.9 % for slag cements with 50 % slag and to 2 % at 65 % slag content [122]. In England, the 1.1 % Na_2O_e content in cement with 50 % granulated blast furnace slag is admissible[6].

[6] Introduced in 2003 the PN–B–19707 standard the maximum Na_2O_e values for all types of cements, which can be classified as low alkali cements are given. They are as follows: for CEM I, II, IV and V $Na_2O_e \leq 0.60$ %, in the case of slag cements the sodium equivalent increases up from 0.95 % through 1.10–2 % for CEM II/B–S and CEM III/A, as well as CEM III/B and CEMIII/C respectively.

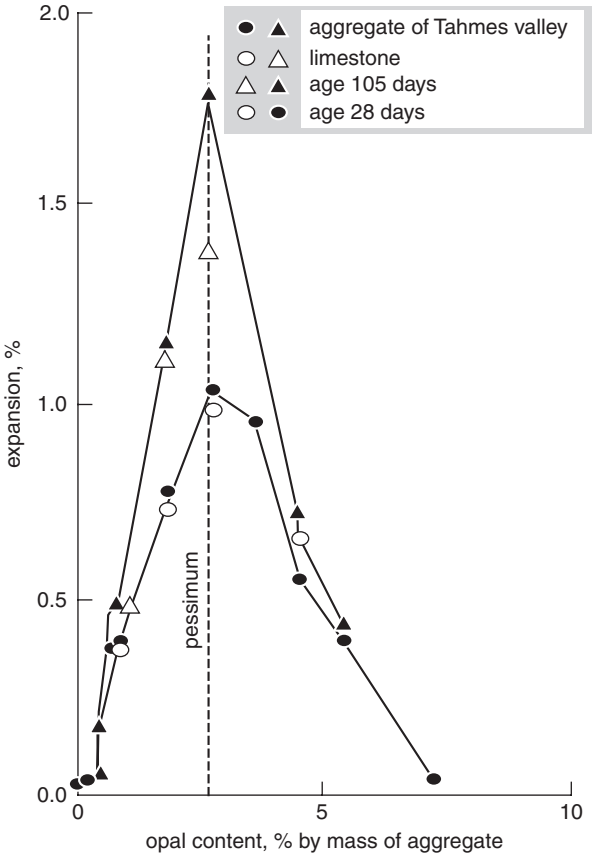


Fig. 6.34 Expansion vs opal content after 200 days of concrete maturing; w/c = 0.41 [123]

One should remember that in some cases the expansion depends on the fineness of reactive forms of silica. According to Hobbs [123], the expansion is the highest at the particle size of reactive component, for example opal, in the range from 0.1 to 1 mm. At the fineness lower than 10 μm the expansion is eliminated and the reactive silica reveals the nature of pozzolanic material. The behaviour of chalcedony is not typical; despite of the presence of active form of silica (cristobalite) the expansion is not always observed.

Hobbs [123] found the highest expansion at some highly reactive silica content, for example at the presence of opal in aggregate, however, at lower silica reactivity the maximum expansion can increases even to 100 % of this component. The phenomenon of passing the expansion through a maximum is defined as pessimum (Fig. 6.34).

There are three following hypotheses explaining the mechanism of the effect of pozzolanic additions:

- reduction of permeability resulting in the effective ionic diffusion coefficients decrease,

- bonding of alkalis and calcium hydroxide as a result of pozzolanic reaction,
- uniform distribution of calcium hydroxide in the paste.

These three mechanisms have been proved by the experimental data, however, their significance change depending on many peculiarities.

The hypothesis dealing with the permeability is based on the observations that the destructive expansion occurs only in the moist concrete and the "source" of liquid phase is required. As it has been mentioned in Sect. 5.3.4, the pozzolanic addition to cement change the structure of pores in a paste; the share of micropores is significantly higher and the ratio of pores greater than 132 nm, which are the permeability controlling factor, is low [113, 124, 125]. The effect of granulated blastfurnace slag on cement paste porosity and permeability has been presented in numerous papers [113, 117, 126, 127]. As it has been shown by Bakker [113, 117, 127] the permeability of the paste from slag cement containing 70% of granulated blastfurnace slag is significantly lower as compared to the permeability of Portland cement. According to Bakker, the reduction of expansion attributed to the reactive aggregate is caused by the markedly lower ions mobility in this paste. The diffusion of OH^- ions and alkalis, which is seriously reduced is also mentioned [113, 117]. It is caused by filling the pores with C–S–H, formed in higher quantity. Regourd et al. [92] have found that the C–S–H phase in slag cement pastes is much more compact and the micropores in this phase have lower dimensions; moreover, the C/S ratio is substantially reduced. The decrease of C/S ratio in the C–S–H phase from 1.71 to 1.55 was also shown by Rayment [128].

It has been pointed by several authors that the conditions of aggregate reaction with slag containing cement paste are different, because the content of soluble compounds of sodium and potassium and $Ca(OH)_2$ content are lowering during the hydration process [97, 107, 129]. Regourd et al. [92] found a substantial potassium content increase in C–S–H in the paste with silica fume. The K_2O content increases from 0.2 to 1.1% in the case of the same cement, but with 30% of silica fume addition. Glasser and Marr [130] explain that this change of gel properties results from different charge of C–S–H gel particles (see Sect. 3.2.3). At high C/S ratio this is a positive charge and at low—a negative one. Tong Ming–Shu et al. [131] proved these conclusions experimentally, by CaO addition to cement.

As it has been shown by Roy [80] the alkalis content in the pore solution of cement paste was significantly lower at 50% slag addition (Fig. 6.35). It should be underlined that this phenomenon is observed irrespectively of the alkali content in mineral additions, which can be higher than in cement. Similarly, the sodium and potassium content decrease in pore solution occurs in case of fly ash cement paste [115]. The effect of fly ash is, however, not clear, because in some cases Diamond [129], as well as Glasser and Marr [130], observed the increase of these ions concentration in the liquid phase of cement paste. However, these authors are of the opinion that silica fume and, after longer period of time, fly ash, reduce the sodium and potassium soluble compound content [129, 130].

Though the mechanism of pozzolana effect is not clear, one should agree with a view that at increased, uniformly distributed, fine silica powder content in concrete,

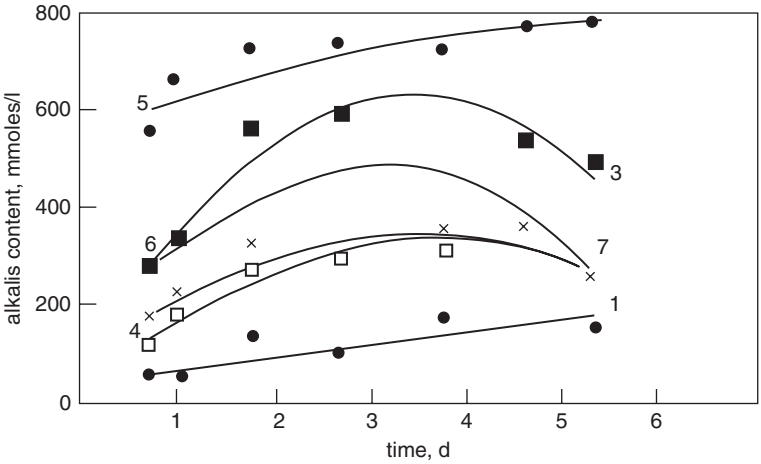


Fig. 6.35 Alkali content in the pore solution of cement paste, 50% of slag addition. (according to [80]); *1*—cement with 65% of slag addition; 0.97% Na_2O_e in clinker, *3*—cement without slag, 0.97% Na_2O_e in clinker *1*, *4*—cement with 5% of slag addition, 0.97% Na_2O_e in clinker *1*; slag as in 1, 5—cement without slag, 1.47% Na_2O_e in clinker, *6*—cement with 50% of slag, slag as in *1*, clinker as in *5*, *7*—cement with 50% of two slags (35% as in *1*, 15% of the second), clinker as in *1*

the Na_2O_e/SiO_2 ratio in silica gel will be reduced and the susceptibility to swelling decreases as well. Moreover, the pozzolanic additions promote the uniform distribution of Na^+ and K^+ ions in the concrete, thus the concentration of these ions around the aggregate grains does not occur and the osmotic pressure does not appear.

However, according to Glasser and Marr [130], slags and natural pozzolanas reduce only the sodium content but they have no influence on potassium content. Natural pozzolanas, because of their high potassium content, will cause the potassium concentration increase in the liquid phase of the paste [60].

Linking of the preventing action of mineral additions, with the sodium and potassium concentration lowering in the liquid phase, is obvious. The progress of alkali silica reaction is strongly dependent on this concentration, as well as on the related pH of this solution. Low alkali content is a warrant of the lack of concrete expansion with reactive aggregate.

Chatterji is of the opinion that the presence of calcium hydroxide in a paste is the necessary factor for expansion to occur. With the lack of $Ca(OH)_2$ the destructive expansion of concrete with active aggregate, even at high alkali level, is not produced [106].

According to the hypothesis of Kawamura et al. [132] the expansion of concrete is limited when $Ca(OH)_2$ in the paste "is available". These authors found that the sodium or potassium silicate formed as a result of alkali–silica reaction, in the presence of fly ash contains much more lime. This complies with much earlier view presented by Verbeck and Gramlich [133] that the availability of Ca^{2+} ions on the

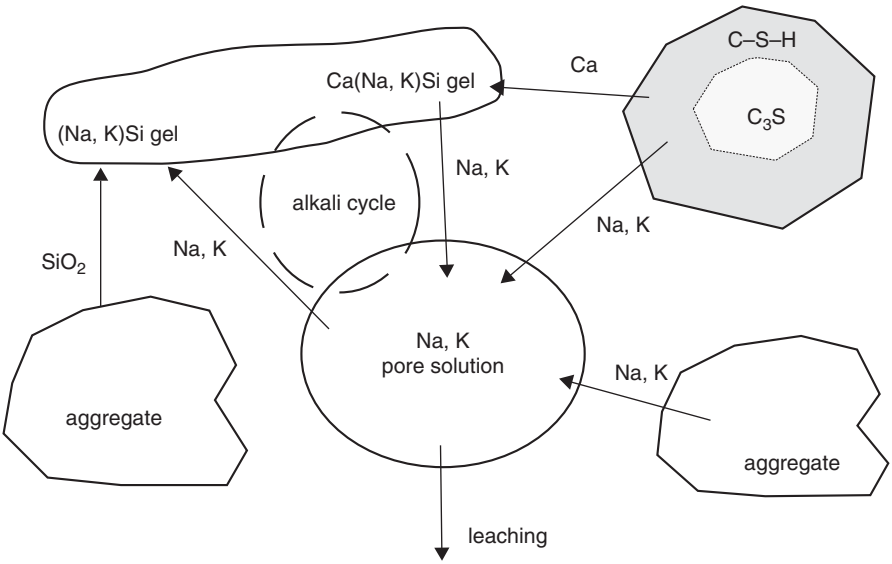


Fig. 6.36 Scheme of alkali cycle in concrete. (According to [135]) Thomas T.C.H. "The role of calcium hydroxide in alkali recycling in concrete" in Materials Science and Concrete, Special volume: Calcium Hydroxide in Concrete (J. Skalny, J. Gebauer and J. Odler eds.), p.234, Fig. 9, Published by The American Ceramic Society, 735 Ceramic Place, Westerville, Ohio 43081, 2001, reproduced with the permission of The American Ceramic Society

surface of reactive aggregate grains is the main factor promoting the progress of alkali–silicate reaction.

It is assumed in this hypothesis that the sodium or potassium silicate transforms rapidly into the compact, non–expanding C–N–S–H gel. This hypothesis refers to the long time ago established view showing that calcium silicate gels as well as calcium, sodium and potassium silicate gel, have relatively low solubility and show extremely low susceptibility to swelling. The susceptibility to swelling is thought to increase continuously from calcium silicate gel with low alkalis content, through the sodium–potassium gels with low calcium content up to the sodium gels with the highest expansion. The composition of formed gel is controlled by the calcium concentration in the liquid phase, in the place of reaction.

The hypothesis supporting the decisive role of $Ca(OH)_2$ was advanced by Hansen [134], as early as in 1944. According to Hansen the Ca^{2+} ions can replace alkalis in a reaction product and hence they promote their further reaction with silica, with the new batch of expansive gel formation. This problem was then developed by Chatterji [106], as it has been mentioned earlier. Recently, Thomas returned to the Hansen's hypothesis (see Fig. 6.36) [135]. Studying experimentally gel in the concrete samples from an old dam, he found the proves of potassium ions by calcium ions replacement. This process occurs when the gel is migrating to the areas occupied by rich in calcium hydroxide cement matrix.

It results from the thermodynamic calculations that the magnesium ions containing minerals will not be stable in the solution of high sodium, potassium and calcium hydroxides concentrations [136]. As it is known, sodium and potassium hydroxides concentration in concrete pore solution is generally in the range from 0.5 to 1 mol/l and can be even higher in high performance concretes, produced with w/c ratio of 0.4 or less. Therefore the pore solution in this concrete will be highly reactive to the aggregate [137]. As it has been shown experimentally anthophyllite is a component of aggregate reacting with KOH with the formation of expansive gel [138]. It should be remembered the Mather's [139] opinion expressed in 1975: "every aggregates react with alkalis; they differ only in the type and rate of reaction, as well as the transformation degree".

6.4.2 Limestone Aggregates

At the end of forties several cases of limestone aggregate concretes destruction have been documented in North America. Initially this was attributed to the poor aggregate resistance to freezing and thawing. However, already in 1957 Swenson [140] proved that the limestone aggregate swelling was the result of reaction with alkalis from cement.

All reactive carbonate rocks in the world have similar composition and texture. These are the dolomitic limestones contaminated with clays, showing very fine texture. They are composed of dolomite crystals scattered in a matrix built of clay minerals and calcite pelite. Most of them reveal good physical properties, primarily high strength, low absorbability, high density and hence they can be used in the production of high quality aggregate.

There are various hypotheses explaining this aggregate expansion mechanism. The most wide spread refer to the swelling of clay minerals and of osmotic pressure formation [141, 142]. All these hypotheses agree that this phenomenon relates to the reaction of soluble alkalis from cement with the aggregate leading to the decomposition of dolomite:

$$\mathrm{CaMg(CO_3)_2 + 2(Na,K)OH \rightarrow Mg(OH)_2 + CaCO_3 + (Na,K)_2CO_3} \qquad (6.3)$$

However, Swenson [140] had shown that the decomposition of dolomite alone does not cause expansion.

The osmotic mechanism of expansion was proposed by Hadley [142], and Swenson and Gillot [141]. This mechanism is assuming that the osmotic pressure would be generated around the dolomite crystals, in the rock matrix [142, 143]. The sodium and potassium ions in the cement paste solution migrate through the aggregate pores to the dolomite crystal, causing its decomposition. This reaction products, which are sodium, potassium and calcium carbonates and brucite are formed around the dolomite grain. The calcium carbonate crystallizes as calcite, while the magnesium

ions—partially, as well as the total content of the sodium and potassium carbonates remain in solution. They form a highly concentrated solution around the dolomite crystals. The matrix, composed of clay minerals play a function of semi–permeable membrane, surrounding these crystals. This membrane is permeable for the water molecules, but is impermeable for the magnesium ions; the sodium and potassium ions are immobilized, to maintain the electroneutrality. It is assumed that the ions over 0.8 nm cannot pass through the membrane, and the magnesium ions, as a result of solvation, have a diameter of about 1.1 nm. The osmotic pressure is generated by substantially higher concentration of ions in solution around the dolomite grains, in comparison with the concentration in the concrete pore solution [143].

Swenson and Gillot [141] elaborating their hypothesis were based on the observation of clay intrusions in dolomite. Montmorillonite, when present in these intrusions, is absorbing water and swells exerting a significant pressure[7]. According to Swenson, the decomposition of dolomite leads to the formation of pores and fissures, which facilitate the access of water to further montmorillonite inclusions. Lea [98] reminds a view that the inclusions of clay minerals in dolomite grains are "moisture–free" and they hydrate in the presence of water.

These hypotheses were verified by Pagano and Cady [143]. They added Li_2CO_3 to the liquid phase in the paste, thus the lithium cation with so great ionic radius that it cannot migrate to dolomite grains but equilibrates the concentration differences in both sides of semipermeable membrane. Simultaneously it results from the double layer theory that the expansion of montmorillonite can be diminished by introducing cation with great charge and small ionic radius. Such cations can migrate in the pores of paste to the montmorillonite surface. Pagano and Cady [143] used $FeCl_3$. The addition of each of two salts caused a significant decrease of expansion, which was supporting the osmotic mechanism, but gives no possibility to distinguish between the mechanisms proposed in the Hadley and in Swensen hypotheses. The authors [143] came to the conclusion that probably both the mechanisms play an important role in the expansion of reactive carbonate rocks.

Tang et al. [144], basing on the observations under the scanning electron microscope, advanced a hypothesis that the growth of brucite crystals around the dolomite grains is the cause of expansion, whereas the clay minerals form coatings, through which the alkali rich solution is migrating.

These experiments, though the further studies and observations are required, can have a serious practical importance, because the expansion of carbonate aggregates is more difficult to control. The pozzolanic additives moderate this effect only in the case when the Na_2O_e in cement is lower than 0.4 [98].

The methods applied to assess the reactivity of silica containing aggregates cannot be directly adapted for the reactivity of carbonate aggregates determination [98]. The measurement of concrete expansion, stored in air at temperature of 23 °C and 100 % RH, with the use of alkali–rich cement, is the best method [98].

[7] See L. Stoch, "Clay minerals", Ed. "Wyd. Geologiczne", Warszawa 1974, s. 441 (in Polish).

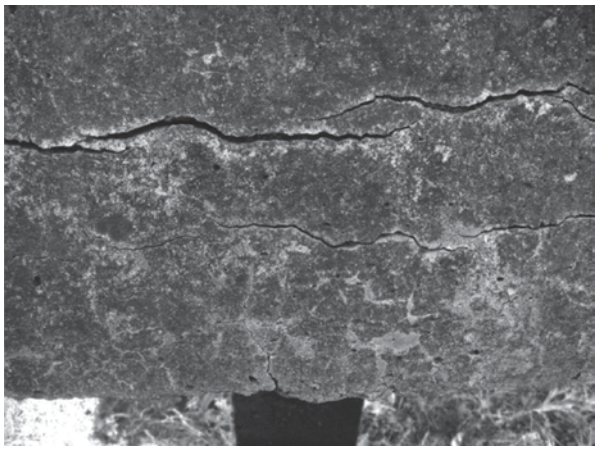


Fig. 6.37 Prestressed concrete railway sleeper with cracks caused by the delayed ettringite formation

6.4.3 Delayed Ettringite Formation

The destruction of concrete sleepers due to the delayed ettringite formation was detected for the first time in Germany in early eighties [145, 146]. Numerous studies have been carried out since this time to elucidate the mechanism of delayed ettringite formation and deterioration of concrete structures, as well as the effect of cement clinker composition and thermal treatment on concrete expansion. Delayed ettringite formation (DEF) is concerning mainly the production of precast concrete elements, using heat treatment to accelerate the hardening of concrete. In Fig. 6.37 a pre–tensioned prestressed concrete railway sleeper with cracks caused by the delayed ettringite formation is shown. The cracking of heat treated precast concrete elements, at low steam pressure, was the subject of investigations in the field of cement and concrete chemistry. Most of reports appeared during 20 years—from the beginning of eighties up to 2003. Ten reports referring to this question were presented during the International Congress on Cement Chemistry in Göteborg, in 1997. It cannot be exclude that in the case of massive concrete structures, because of temperature rise caused by heat of cement hardening, there are the similar conditions as in the case of thermal treatment, and the delayed ettringite formation can occur. Divet and Pavoine [147] have shown that the severe damages of five bridges were caused by DEF, resulting from the self–heating of massive elements in bridge constructions.

In spite of numerous experimental works there are several unresolved questions and many controversial opinions dealing with this problem. Some authors support a view that the deterioration of concrete is the effect of alkali–aggregate reaction and the crystallization of ettringite occurs later, in the microcracks thus produced [148].

There is a relatively good accordance as the chemical and phase composition, as well as the fineness of cement is concerned. Very well documented results in this field have been presented by Kelham [149, 150]. Expansion increases with rise of alite and tricalcium aluminate content. The chemical composition of cement is of

importance too—expansion increases with higher sodium, potassium and magnesium content. Finally, expansion increase with increased fineness of cement.

There is a commonly accepted view concerning the effect of heat treatment temperature. As higher temperature of thermal treatment, as higher and faster the expansion [151].

The question of expansion mechanism excites most controversies. There are the two contradictory hypotheses:

- the first, older one, is assuming that expansion is caused by the formation of coatings surrounding the aggregate grains and composed of dense, large ettringite crystals, known as "massive ettringite" [145],
- the second one, is attributing the expansion to the formation of nanometric ettringite crystals in C–S–H gel [152]. The formation of ettringite shells around the aggregate grains is considered as the secondary process, occurring in the voids produced as a result of C–S–H matrix expansion. Thus it will be the secondary ettringite, and not the delayed ettringite formation.

The effect of pessimum—the highest expansion at about 4% SO_3 content in cement—is the further not quite clear phenomenon. The SO_3 level corresponding to the highest expansion can vary for different cements [149].

The other stormy discussed problem refers to the role of anhydrite present in cement clinker, which slow dissolution is the cause of delayed ettringite formation [153]. In this case the delayed ettringite formation will be not linked with the heat treatment of concrete.

It is worth to note the threshold level of alkalis, at which the expansion of concrete is occurring. Kelham [154] is supposing that it is near the alkalis content equal 0.7% Na_2O_e.

As it is commonly known, that the formation of ettringite in a paste (concrete) cured at ambient conditions is completed within one to 2 days; in the same time the crystallization of monosulphoaluminate hydrate or calcium aluminate C_4AH_{13} is begining (Fig. 4.6). Simultaneously the sulphate ions concentration in the solution decreases to the very low level and next is increasing slowly, to 50 moles/l (Fig. 4.3). However, the delayed ettringite formation, together with expansion of concrete is known, even in the case of not heat treated concretes but caused by oversulphated cement i.e. with not standard, too high gypsum content. In this condition the reaction of C_3A with the solution containing sulphate ions is dramatically longer and occurs after cement hardening, leading to its destruction, caused by ettringite expansion [155]. This is a "classic example" of internal sulphate corrosion.

At ambient temperature the equilibrium between the sodium or potassium sulphates and calcium hydroxide is shifted to the right side of the equation:

$$Na_2SO_4 + Ca(OH)_2 + 2H_2O \rightarrow CaSO_4 \cdot 2H_2O + 2NaOH \tag{6.4}$$

However, at temperature of 90 °C the ionic equilibrium in the paste (concrete) solution is changing and the calcium hydroxide becomes stable. The equilibrium of calcium hydroxide with sodium and potassium sulphates at elevated temperature will

Table 6.2 Sulphate phases in equilibrium with NaOH solution as a function of its concentration and at different temperature [151]

NaOH concentration (mmoles/l)	Detected phases		
	25 °C	75 °C	100 °C
0	Ettringite	Ettringite	Ettringite
400	Ettringite	$Ca(OH)_2$, C_4AH_{13}	AFm, $CaSO_4$, $Ca(OH)_2$
700	Ettringite	$Ca(OH)_2$, C_4AH_{13}	$Ca(OH)_2$, $CaSO_4$
1,000	Ettringite	$Ca(OH)_2$, amorphous phases	C_3AH_6, $Ca(OH)_2$, $CaSO_4$

be shifted to the left side (Table 6.2). Wieker and Scrivener [156] use the following form of the equation:

$$Ca(OH)_{2s} + 2M_l^+ + SO_4^{2-} \rightleftarrows \{CaSO_4\}_s + 2M_l^+ + 2OH_l^- \tag{6.5}$$

where $\{CaSO_4\}_s$–AFt, AFm, gypsum and C–S–H, M–K and Na, s–solid phase, l–liquid.

The cause of delayed ettringite formation was elucidated based on the ettringite stability in concrete. As it is known, ettringite is stable at least at temperature 100 °C, in saturated water vapour [157]. However, Wieker et al. [151] found that ettringite is not stable at higher temperatures in the presence of alkalis. The results of these studies are presented in Table 6.2.

At NaOH concentration of 400 mmoles/l ettringite is not stable already at temperature of 75 °C, and in this condition C_4AH_{13} as an aluminate phase is formed. At NaOH concentration equal 1 mol/l the aluminate ions form the amorphous phases, and at temperature of 100 °C the hydrogarnet C_3AH_6 is formed.

The same results were obtained by Ghorab and Kisher [158]. Also Sylla [159] found the reduction of ettringite content in cement pastes after 3 h of thermal treatment at temperature of 60 °C; this phase disappears almost entirely after this period when the temperature of curing rises to 80 °C. The same results were found by Odler et al. [160]. It found also good relation with the composition of solution, which in the pastes subjected to thermal treatment at temperature of 90 °C have a different sulphate ions concentration (Fig. 6.38). The concentration of these ions is maintained on the high level after 28 days of paste matured in water and is quicker reduced after this period [151]. However, even after 90 days it is four times higher than in the paste cured all the time in water at ambient temperature.

These experimental results were confirmed theoretically by the thermodynamic calculations presented by Glasser et al. [161]. The most important conclusion drawn from these calculations is that the ettringite is stable at temperature of 85 °C only at a very high sulphate ions concentration in the liquid phase. The increasing alkali content in cement causes the necessity to rise the sulphate ions concentration in cement paste solution, required for ettringite stabilization. Ettringite is in equilibrium with monosulphate when the molar ratio of SO_4^{2-}/Na^+ is higher than 0.31, and with gypsum—when this ratio is higher than 0.43. The gypsum share will be, in turn, related to the ratio of aluminate to sulphate ions concentration. Collepardi and Ogoumagh Olagot [90] state that at total SO_3 content in cement (from clinker

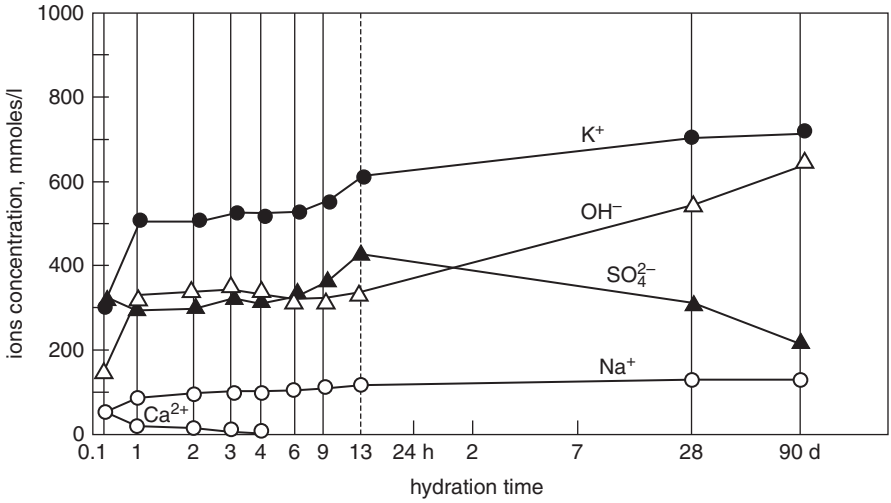


Fig. 6.38 Composition of the liquid phase in Portland cement paste subjected to thermal treatment at 90 °C and then cured in water at 20 °C, plotted as a function of time. (According to [151])

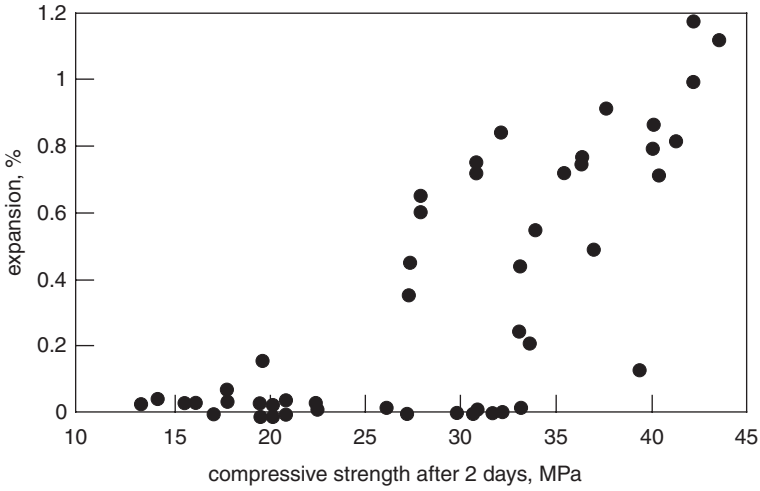


Fig. 6.39 Expansion of mortar as a function of cement strength after 2 days. (After [149])

and sulphates added to cement) on the level not exceeding 2 %, the expansion will not occur.

The studies by Kelham [149, 150, 154] have shown that the expansion of mortars depends on the alite and C_3A content in cement and is increasing with the share of these phases, thus with the rise of early strength of mortar (Fig. 6.39). The expansion is affected also significantly by SO_3 content in cement; the highest expansion

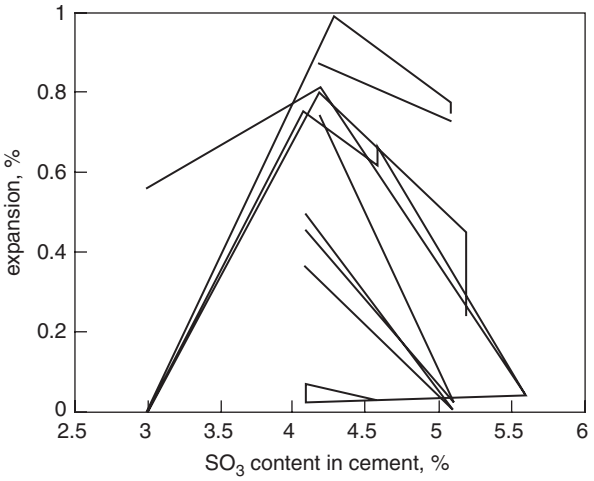


Fig. 6.40 Effect of SO_3 content in cements from industrial clinkers on the expansion of mortars subjected to the heat treatment at temperature of 90 °C, and next matured in humid atmosphere at temperature of 20 °C for a long period of time. (According to [149])

Table 6.3 Calculated composition of the $Ca(OH)_2$ saturated solution in equilibrium with solid phases in the system $CaO–Al_2O_3–SO_3–Na_2O–H_2O$ at temperature of 20 °C. (After [161])

Phases	$[SO_4]$ (mmoles/l)	[Ca] (mmoles/l)	[Al] (mmoles/l)	[Na] (mmoles/l)
C_3AH_6–AFm	13.58	0.549	3.23	250
C_3AH_6–AFm	54.87	0.325	5.20	500
C_3AH_6–AFm	193.1	0.202	6.90	1,000
AFm–AFt	76.65	2.478	0.283	250
AFm–AFt	183.9	2.058	0.354	500
AFm–Aft	420.7	1.699	0.377	1,000
AFt–gypsum	108.51	9.5	0.011	250
AFt–gypsum	226	8.22	0.255	500
AFt–gypsum	373.7	6.76	0.90	1,000

was observed by Kelham [149] at 4 % sulphate content, as it is shown in Fig. 6.40; Table 6.3.

The expansion is affected by the content of sodium and potassium and increases markedly at K_2SO_4 addition to cement or KOH addition to the mixing water [150]. Lawrence [162, 163] proposed an empirical equation to calculate the expansion of mortar after 800 days of maturing, as follows:

$$\begin{aligned} \mathrm{Eksp}_{800} &= 9.51 + 0.304\mathrm{SO}_3 + 0.00085\mathrm{SSC} \\ &\quad + 1.728\,\mathrm{ar\,Na_2O_e} - 0.162\mathrm{CaO} - 0.040\mathrm{C_3A} \end{aligned} \tag{6.6}$$

where: SO_3, CaO, C_3A (Bogue's formulae)) is the contents of these components in cement, %, SSC—specific surface of cement, cm^2/g, ar Na_2O_e—sodium equivalent of alkali residue in cement, after leaching with water within one hour.

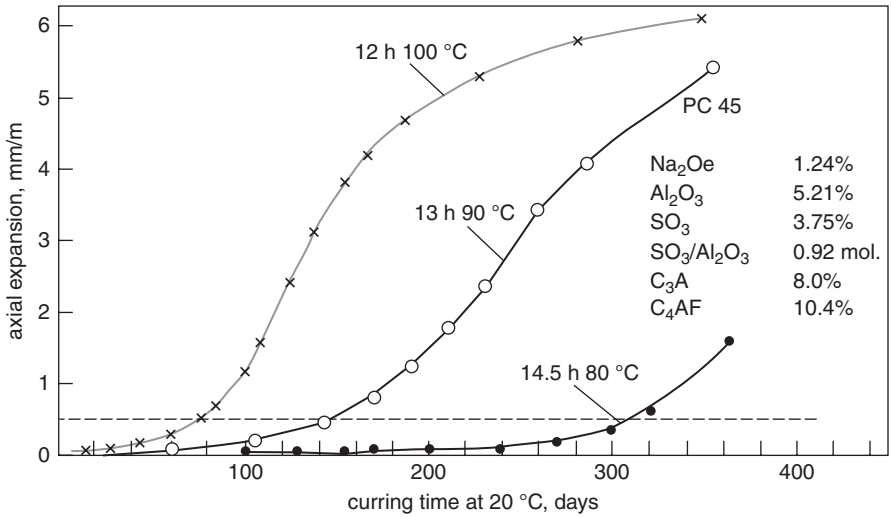


Fig. 6.41 Expansion of mortars from Portland cement with $Na_2O_e = 1.24$, subjected to thermal treatment at different temperatures (time of curing given on the *plots*), and subsequently matured at humid atmosphere at temperature of 20 °C. (According to [151])

The other empirical relationships [145, 149, 164] were not verified experimentally in the case of 55 cements investigated by Lawrence [162]. However, in these studies the effect of SO_3 and C_3A in cement has been proved once again.

The data referring to the effect of heat treatment temperature on the magnitude of concrete expansion are compatible. As typical relation, the results of Wieker [151] can be given, which, are shown in Fig. 6.41. From these results the conclusion can be drawn that the rise of heat treatment temperature increases the expansion and accelerates and its occuring.

All authors basically agree that the expansion of concrete is the effect of delayed ettringite formation. However, there are significant discrepancies as the mechanism of expansion is concerned. As it has been pointed out earlier, the two contradictory hypotheses were proposed. The first one was advanced by Heinz and Ludwig [145] which assumed that the shells of massive ettringite, formed around the aggregate grains, exerted the crystallization pressure and consequently led to the expansion. This theory is supported nowadays too, among the others by Yang et al. [165, 166]. They present the view that at least a part of ettringite shells is not formed by recrystallization in the voids around the aggregate grains, but causes expansion and cracks. Also according to Diamond [167] the shells of massive ettringite exert pressure, and consequently the expansion during ettringite crystallization.

On the other hand Johansen et al. [168] were the first to propose the hypothesis assuming the uniform swelling of cement paste, however, without establishing the cause of its appearing. The cement paste free–voids around the aggregate grains appear as a result of this swelling and their width is approximately proportional to the grain size. Some of them can be next filled with recrystallized ettringite; this

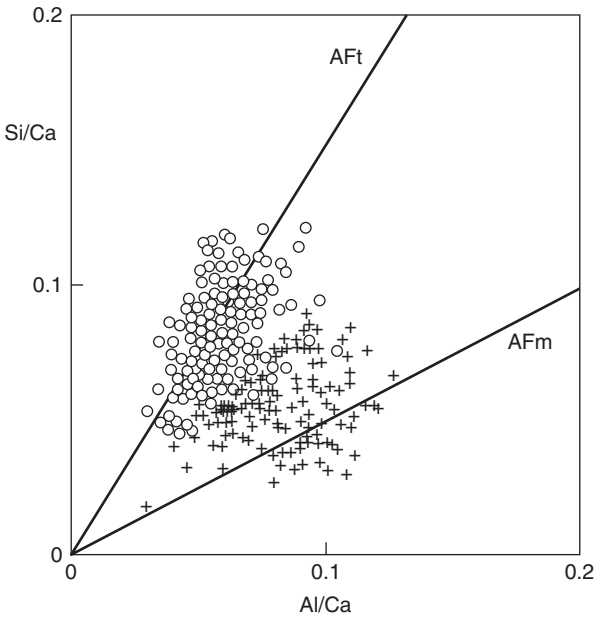


Fig. 6.42 Comparison of Si/Ca and Al/Ca molar ratios of C–S–H phase, in expanding (o) and non–expanding (+) mortar. (According to [170])

recrystallization is caused by dissolution of primary small ettringite crystallites with large crystals formation in the free void spaces in concrete (so–called Ostwald's ageing effect). Therefore the crystallization of ettringite around the aggregate grains is the secondary process, following the former swelling of cement matrix, which caused expansion. That only some voids around the aggregate grains are filled with ettringite, is supporting this hypothesis.

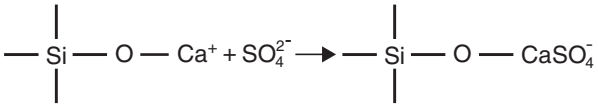
The hypothesis of Johansen et al. [168] was further developed in the microstructural studies by Scrivener and Taylor [169], as well as by Scrivener and Lewis [170]. In the pastes showing expansion Scrivener [169, 170] found that a brighter external C–S–H phase on the alite crystals, expanded and was exfoliated from the dark core, with a gap formation between these two areas. In the pastes which not showed swelling, the EDS analysis of brighter external C–S–H did not reveal any defined sulphate to aluminate ions ratio. This proves that they do not form any defined phase, but that they are only absorbed by the C–S–H gel. After longer periods of paste curing the results of analysis are more and more close to the C–S–H—AFm line; it means that the product is a calcium monosulphate intimately mixed with C–S–H phase. However, immediately after the heat treatment, in the pastes showing swelling, the brighter, outer C–S–H gel contains absorbed sulphate and aluminate ions, in concentration corresponding to the ettringite and C–S–H mixture (Fig. 6.42) [170].

On the base of these EDS studies, a hypothesis was advanced that the formation of ettringite, inside this bright outer C–S–H gel, would result in expansion [170]. The crystallization of massive ettringite is a secondary process and is not related with expansion.

This question was then investigated by Pade et al. [171], as well as by Famy [152, 172] and the results reported by Scrivener [169, 170] has not been proved. The sulphate and aluminate ions concentrations in the brighter outer C–S–H gel, as found immediately after the thermal treatment, do not correspond to ettringite, but in fact they are the sulphate and aluminate ions absorbed; the latter ones substitute silicon in the C–S–H phase [169]. The sulphate ions absorption level was decreasing during later paste maturing, while the amount of aluminum remained unaltered. There was an argument disproving the hypothesis formed by Scrivener and Lewis [170].

As it has been shown by Famy [152], the participation of outer C–S–H gel in the mechanism of expansion was supported by the observations under the scanning electron microscope. This outer C–S–H product is formed in the space filled initially by water, as a result of silicate phases dissolution and precipitation of the products of their hydrolysis. Primarily the finest grains of cement take part in this process. However, the remaining sulphates are adsorbed on the C–S–H gel adherent to cement grains, and only 7% sulphate ions are in the paste pore solution [152]. During the paste storing in water the sulphate ions adsorbed by C–S–H are released into the solution and react with calcium monosulphoaluminate and ettringite is formed. This ettringite formation can cause expansion, because it crystallizes in a limited space from the monosulphate occurring as nanoparticles in a mixture with C–S–H. These ettringite crystals are submicroscopic and cannot be observed under SEM. However, their decisive role in expansion was proved by Scherer [173]. The swelling of paste caused by submicroscopic ettringite crystals formation leads to the formation of gaps around the aggregate grains in which the massive ettringite by recrystallization is formed later [152]. This model of expansion mechanism, proposed by Famy [152], is shown in Fig 6.43.

The sulphate ions sorption ability of C–S–H is important for the Famy's hypothesis [152]. The experiments linked with this problem were carried out by Barbulo et al. [174]. They studied the sorption of sulphate ions of C–S–H phase and found the dependence between sorption and Ca/Si ratio. According to these authors [174] the sulphate ions are adsorbed on the sites occupied by Ca^{2+} ions, on the C–S–H surface. It can be expressed by the formula:



This mechanism of sorption was proved by increasing content of adsorbed sulphate ions as a function of growing Ca/Si content in C–S–H, as it is shown in Fig. 6.44.

The sorption does not increase with temperature. The results reported by Barbulo et al. [174] put some new light on the role of siliceous fly ash and silica fume; these additives reduce the Ca/Si ratio of C–S–H and hence reduce the sorption ability of this phase. The sorption ability of C–S–H was discussed with more details in Chap. 3.

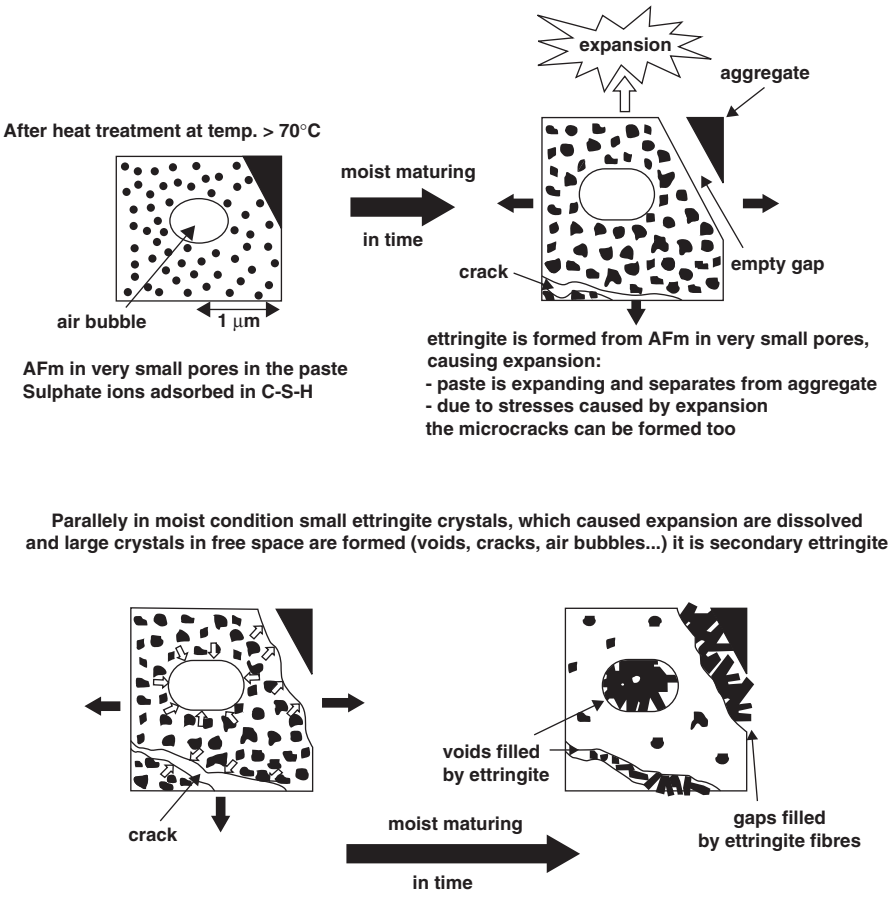


Fig. 6.43 Famy's model of expansion mechanism, related to the delayed ettringite formation. Concrete treated at temperature > 70°C (According to [152])

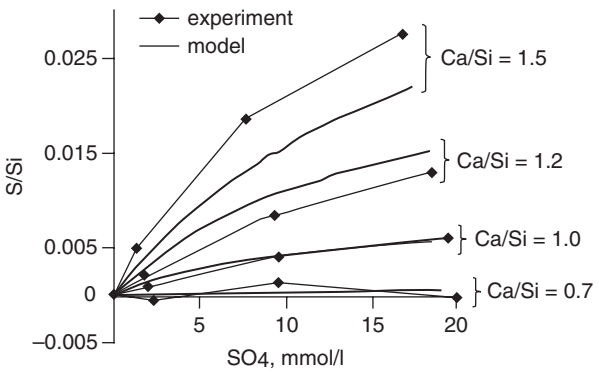


Fig. 6.44 S/Si ratio in C–S–H as a function of sulphate ions concentration in the liquid phase, for the C–S–H samples of different Ca/Si molar ratio. (According to [174])

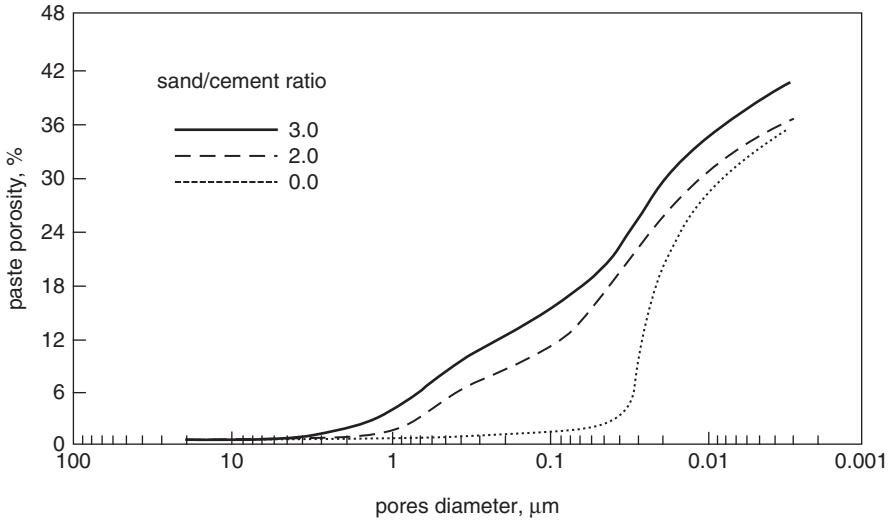


Fig. 6.45 Change of porosity structure with sand addition to cement paste. (According to [180])

The delayed ettringite formation is strongly affected by the humidity of atmosphere, in which the concrete elements, earlier steam cured, are matured. According to Heinz et al. [145, 146] the humid environment is the obligatory condition for the delayed ettringite formation. This view has been verified by many authors [171, 175]. However, Taylor [176] was of the opinion that in the case of moisture shortage ettringite can be formed imbibing water from C–S–H.

The correlation between the linear expansion of concrete and aggregate grains size and the width of the gaps around the aggregate grains, was examined too [171, 177]. It was found that the gaps are increasing with the size of aggregate grains and that the linear concrete expansion was showing good correlation with the width of gaps. The authors of these experiments are of the opinion that this is additional indirect proof for the validity of Famy's hypothesis [152], concerning the paste expansion mechanism.

The effect of sand and aggregate properties was investigated too by Fu et al. [178], as well as by Grattan–Bellew et al. [179]. They found the growth of expansion with lowering of aggregate size, that is with higher aggregate surface. This effect relates presumably to the growth of the share of the porous interfacial transition zones in concrete, which enhance the migration of liquid and transport of ions (Fig. 6.45). This can be proved by an observation that the expansion occurs earlier in the mortars or concretes that in pastes, produced from the same cements [166, 180]. In the case of limestone aggregates the formation of calcium carboaluminate hydrates on the surface of aggregate grains can be of great importance; this product will be participating in changes of the construction of interfacial transition zone. The question of carboaluminate formation will be discussed in point 7.7, concerning the properties of cement with limestone addition. The lack of ettringite shells on

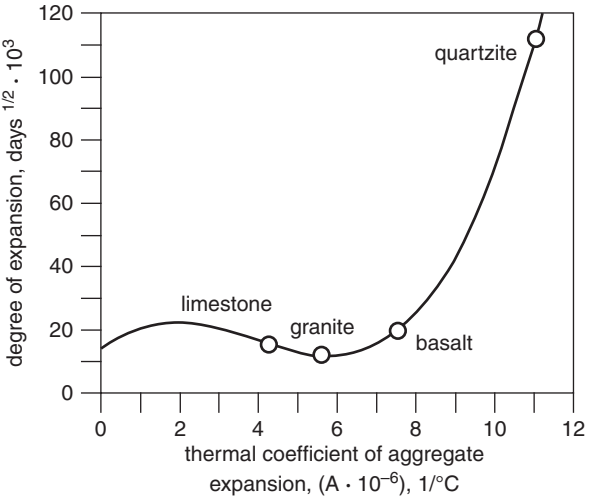


Fig. 6.46 Rate of linear expansion of mortar bars vs. thermal conductivity of aggregate. (According to [179])

the surface of limestone aggregate, as opposed to quartz or quartzite, for example according to Yang et al. [166], can be the consequence of carboaluminate hydrates formation on limestone grains.

Application of limestone sand results in a substantial decrease of expansion [165, 180]. According to Kurdowski and Duszak [181], expansion does not occur practically at 30% of limestone addition. However, as it has been shown by Kelham [182], the expansion is only seriously delayed and can start after about 1,000 days. Finally, it is identical as in a concrete with quartz sand. However, 30% of fly ash addition eliminate expansion [175, 181].

The thermal expansion coefficient for various types of aggregate has a great impact on the expansion resulted from the delayed ettringite formation, as it has been pointed out in some reports. This problem was investigated by Grattan–Bellew et al. [179] who proved the relationship mentioned above (Fig. 6.46).

Mielenz et al. [153], as well as Hime [153] advanced a hypothesis relating the expansion of concrete to the anhydrite content in clinker and SO_4^{2-} ions content in belite structure. Very slow release of SO_4^{2-} ions from these phases to the solution retards the reaction with aluminate phases and the delayed ettringite formation takes place, even in not thermal treated concrete. According to Klemm and Miller [183] the industrial clinkers reveal generally low anhydrite content and, moreover, this anhydrite reacts rapidly with water. The similar results were reported by Michaud and Suderman [184]. Moreover, Herfort et al. [185] found that the sulphates occurring in the silicate phases were associated with aluminum, which content is rising in this condition. Simultaneously the Al_2O_3/SO_3 ratio is higher than one. When assuming the release of aluminate ions into the solution at the same rate as the sulphate ions, the formation of calcium monosulphoaluminate hydrate, rather than ettringite will occur. Herfort et al. [185] investigated the solubility of anhydrite from the clinker with 1.5% anhydrite content and the consumption of this phase within 7 days was found (XRD peak disappeared).

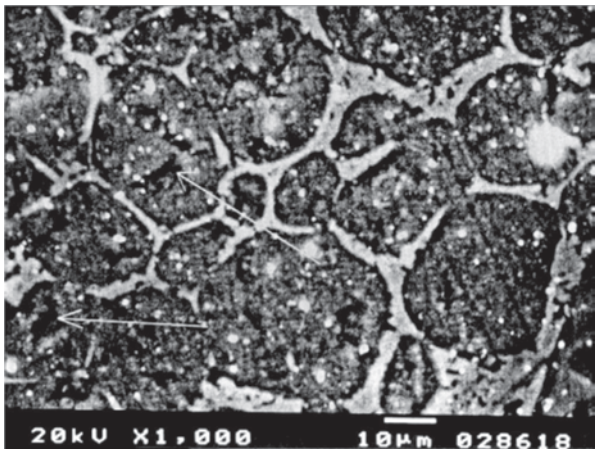


Fig. 6.47 Anhydrite inclusions in belite, in 6% SO_3 containing clinker [187]

The hypothesis assuming that the anhydrite occurring in industrial clinkers contributes to the delayed ettringite formation was turned down during the International RILEM Conference in Villars [186]. However, Kurdowski [187], found that cement from the 6% anhydrite containing clinker shows expansion when subjected to the thermal treatment, which extend and rate is the function of Na_2O_e content, in the form of sulphate. At 2% Na_2SO_4 a serious expansion, as soon as after 70 days of mortar maturing in water, occurs. It should be underlined that cement used in these experiments contained only 3% C_3A, but 13% of brownmillerite. The results show that brownmillerite can give an expansive ettringite too [187]. The clinkers used were burned in a semi–industrial scale, in small rotary kiln, and anhydrite was present in clinker in the form of inclusions in belite phase. The sulphate spurrite was the source of these inclusions; it decomposed at the temperature of clinker sintering, giving small anhydrite particles, forming the inclusions in belite (Fig. 6.47). One cannot exclude that in special clinkers, for example in the belite–sulphate ones, anhydrite will occur in the form of inclusions in belite, causing the expansion of mortar, even without heat treatment. In Portland cement clinkers there is rather impossible.

Application of thermal treatment at temperature not exceeding 70 °C can counteract the delayed ettringite formation. In the case of the necessity of higher temperature application, the use of slag cement, with at least 50% slag content should be considered [183]. At the 8% of silica fume addition the expansion is prevented as well [180]. Ghorab et al. [188] found no expansion not only in the case of slag cement, but also at 30% of fly ash addition to cement. The similar effect was found for the Bavarian trass (30%) [188]. The role of fly ash was confirmed in another work [182].

The problem of simultaneous occurrence of delayed ettringite formation, associating the alkali–aggregate reaction, occurring always with some delay, should be discussed separately. According to many authors, in some cases of concrete corrosion attributed to the delayed ettringite formation, the alkali–aggregate reaction is

responsible for concrete damage [148]. The formation of ettringite is a secondary process and results in the crystallization of this phase in the micropores and fissures linked with the previous reaction. In the later work Shayan and Ivanusec [189] came to the same conclusion. In the numerous studies Owsiak [85, 190] proved that the two processes could occur together. It means that the alkali–aggregate reaction initiates the corrosion of concrete and is next followed by delayed ettringite formation, promoting further expansion. It is indicated primarily if the expansion caused by the alkali–aggregate reaction increases markedly in the case of cement usage with higher sulphate content [85] (see Fig. 6.40).

6.4.4 Corrosion of Concrete in the Chlorides Solutions

Chlorides are among the most aggressive salts which cause the rapid corrosion of concrete. In the highly basic environment of concrete, the pore solution, being in a quasi–equilibrium with the hydrates and aggregate, has the pH value of about 13. The sodium and potassium hydroxide content in this solution is generally higher than 500 mmoles/l, often close to 1 mol/l, because of the low w/c ratio, particularly in the high performance concretes. It is one of the reason of high aggressiveness of chlorides, which usually have the acid reaction. The rate and range of attack will be influenced by the concentration of chloride salt of solution in contact with concrete and on the type of cation bonded with chlorine.

The corrosion process consists in migration of chloride ions into the concrete with simultaneous OH^- ions diffusion in an opposite direction, from the leached cement hydrates. Therefore the porosity, and consequently the permeability of concrete is of fundamental importance. Cement matrix is a part of concrete which is subjected to the destructive action as a first one. The attack of chloride ions on cement paste will be then discussed first. However, some information concerning the effect of aggregate on the chloride ions diffusion is needed for comprehensive presentation of phenomena occurring in concrete.

The importance of studies focused on the problem of chloride attacks, in the recent 30 years is constantly increasing, especially because of the increasing maintenance and repair costs of road concrete pavements, particularly on highways, bridges and viaducts. The destruction is due first of all by the use of de–icing salts, causing scaling and surface damages of concrete and, as a consequence, the corrosion of reinforcing steel. Better knowledge of the mechanisms of chloride corrosion is one of the directions to find the methods to resolve this problem.

6.4.4.1 Diffusion of Chloride Ions in Cement Paste

The chloride ions are highly mobile (the highest effective diffusion coefficient) and that is why the corrosion of concrete, due to the attack of chloride containing solution, occurs so rapidly. The rate of diffusion is of significant importance when the durability of concrete is considering. Therefore this property is often examined.

Different testing methods are used [191–196]:

- the measurements of the thickness of paste layer, on which boundary the diffusing ions achieve the established concentration,
- the concentration profile across the longitudinal cross–section is determined,
- the amount of ions diffusing through the paste plate specimen is determined.

In the former method, for the chloride ions measurements two methods can be used:

- at the stationary state,
- in dynamic conditions.

In the first one, the measuring stand consists of the horizontal cylinder divided in two chambers by separation with plate paste specimen, in which the diffusion is to be determined. One chamber is filled with NaCl or $CaCl_2$, the second one with deionized water or $Ca(OH)_2$ saturated solution. For these solution the following requirements are recommended by Marchand et al. [197]:

- the disarrangement of pores structure in the sample by leaching during measurement should be restrained to minimum,
- the ionic force of the chloride solution should not be changed during the measurement; it means that the chemical composition of solutions in both chambers should be close to the composition of pore solution in concrete.

In these conditions the chemical activity gradient of chlorides in the first chamber should be decreased to minimum, and consequently the disarrangement of pores structure in the specimen should be negligible. However, the conditions of experiments do not comply generally with these requirements and in the most cases the pure chloride and calcium hydroxide solutions are used in the first and in the second chamber or their mixture in the first one (e.g. [198], [199]).

The effective diffusion coefficient is calculated generally from the equation derived by Page et al. [191] from the first Fick law:

$$J = \frac{V}{A} \cdot \frac{\mathrm{d}c_2}{\mathrm{d}t} = \frac{D}{e} \cdot (c_1 - c_2) \tag{6.7}$$

where: J is the flux of ions traversing the sample (mol cm^{-2} s^{-1}), V—volume of NaCl solution in the first chamber (cm^3), A—surface of plate specimen (cm^2), e—thickness of plate concrete specimen (cm), D—effective diffusion coefficient (cm^2 s^{-1}), c_1—concentration of chloride ions in the chloride salt containing chamber (mole cm^{-3}), c_2—concentration of chloride ions in the solution, to which the chloride ions diffuse (mole cm^{-3}).

By integration of the equation (6.10) we have:

$$\ln(1 + c_2 / c_1 - c_2) = DA / V\mathrm{e} \cdot (t - t_0) \tag{6.8}$$

where t_0 is time required to get a constant diffusion rate.

When c_1 is significantly lower than c_2, the (6.10) equation can be replaced by approximate (6.12) for $t > t_0$:

$$c_2 = \frac{DAc_1}{V} \cdot e \cdot (t - t_0) \tag{6.9}$$

Then we can calculate D from the equation:

$$D = \frac{V\mathrm{e}}{A} \cdot \frac{c_2}{c_1} \cdot \frac{1}{(t - t_0)} \tag{6.10}$$

Calculation of D from the equation (6.13) can be done at following assumptions:

- diffusion is *quasi*–stationary,
- flux of diffusing ions is constant along the total diffusion length,
- concentration of chloride ions is constant in the whole volume of sample.

In the calculation of diffusion coefficient the Ernst–Planck correction for the reduced mobility of ions should be taken into account.

At variable conditions applied in the second method mentioned above, the samples in the form of elongated cylinders or cubes, immersed in the chloride solution are examined. All the surfaces of samples, beside of the one, are sealed to prevent the chloride ions penetration. Only one surface is thus subjected to the penetration of chlorides.

The apparent diffusion coefficient is calculated in the approximate way from the second Fick law for the unidirectional flow. It gives little information on the mechanism of chloride ions intrusion [197]. Moreover, these calculations have low accuracy, because the solution of the second Fick law is based on the assumption that this apparent diffusion coefficient is constant along the whole sample length; however, the latter statement is not true [197].

One should remember, when comparing these both methods, that the results obtained with every of them are affected by different binding potential of chlorides. In the case of the method with variable conditions the reactions of chloride ions with cement phases will occur and the penetration of ions will be reduced; hence the measured apparent diffusion coefficient will be lower. When the measurements are carried out in constant conditions majority of reactions will be completed, and their effect on the diffusion of chloride ions will be markedly lower, as well as the apparent diffusion coefficient will be consequently higher.

In both methods of the apparent diffusion coefficient measurements the acceleration of diffusion process in an electric field is frequently applied. Sometimes this method is called as the “studies of migration”. The interpretation of measurement results is based on the assumption that the migration mechanism in cement paste is analogous to the diffusion. However, there are seldom experimental works comparing the results obtained with these two methods. Tang and Nilsson [200] found a good correlation between the results of measurements in variable conditions and by migration method; the latter one in variable conditions too. Contradictory data

were reported by Delagrave et al. [201], which found that the measurements of migration in variable conditions give too low values of effective diffusion coefficient.

It was assumed simultaneously that the application of electric field accelerate only the transport of ions through the paste without effect on the microstructure of hardened cement paste. However, the experimental results do not support this assumption. On the contrary, at long term action of electric field the microstructure of paste is altered [197]. Application of electric field will also cause the effect of electroosmosis, consisting in the flow of ions towards an electrode being the source of electric current, with the double layer formation on the gel surfaces [197]. According to some authors this phenomenon can accelerate the transport of chloride ions through cement paste with microcracks [197].

Diffusion of chloride ions is influenced by numerous factors, which affect the experimental results. Primarily the chloride ions can react with calcium aluminates and the Friedel's salt $C_3A \cdot CaCl_2 \cdot 10H_2O$ is formed. When the concentration of chloride ions is high the chloride analogue of ettringite $C_3A \cdot 3CaCl_2 \cdot 30H_2O$ can be also formed [202] (see Sect. 4.3.3).

It results that the amount of bound chlorides depends on the C_3A (and C_4AF) content in cement. The structure of pores in the paste is one of the factors influencing the formation of calcium chloroaluminate hydrates. According to Marchand et al. [197], and later, Delgrave et al. [201], the chloroaluminate hydrates were not detected till now in cement matrix of the high performance concretes (w/c = 0.25), even in the presence of chloride ions in the paste.

Many authors proved experimentally that the ability of chloride ions binding in cement paste is not only associated with C_3A content but is embracing also the ferrites, hence it depends upon the total $C_3A + C_4AF$ percentage [203, 204]. This could be presumed, because the occurrence of the $C_3F \cdot CaCl_2 \cdot 10H_2O$ phase, analogous to chloroaluminate, is known [36]. There are also the solid solutions of aluminate phases in the pastes with the iron(III) ions substituting the aluminum ions; their composition is analogous to the Friedel's salt: $Ca_3(Al, Fe) \cdot CaCl_2 \cdot 10H_2O$ [36, 205]. However, because the reaction of brownmillerite with water is much slower than the reaction of C_3A, the ability of the chloride ions binding by brownmillerite will be much more affected by the hydration degree of the paste.

C–S–H gel is participating in chemisorption and adsorption of chloride ions too. According to Beaudoin [206] and Ramachandran [207], the three types of chloride ions can be distinguish: the free ions easily extracted in an alcohol, the chemisorbed ones on the gel surface, and in the interlayers area—they cannot be extracted by alcohol and, finally—the strongly bound chlorides, presumably occurring as a solid solution in C–S–H. The latter cannot be leached by water. The C–S–H ability of chloride ions binding depends on the H/S and C/S ratio and increases with them [207].

These results are important as the ability of chloride ions binding in the pastes from cements with mineral additions is discussed. For example Diamond [208], as well as Page and Vennesland [209] found that the silica fume addition is significantly increasing the free chloride ions concentration in the paste pore solution. In the

Table 6.4 Effective chloride ions diffusion coefficients at temperature of 25 °C in different cement pastes with w/c = 0.5 [191, 211]

Type of cement	$D \cdot 10^9$ (cm^2/s)
Portland cement	44.7
Portland cement + 30 % FA	14.7
Portland cement + 65 % GGBS	4.1
Portland HSR cement	100.0

light of results reported by Beaudoin [206] this can be explained as a consequence of the C/S ratio lowering in C–S–H gel, in the presence of silica fume.

The granulated blastfurnace slag and siliceous fly ash addition will have a similar effect on the ability of chloride ions binding in cement pastes, because they will also decrease the C/S ratio in C–S–H gel. Uchikawa and Okamura [210] report the following C/S ratio: 1.7 for Portland cement, 1.6 in case of 40 % slag addition and 1.2 at 40 % of siliceous fly ash addition. Simultaneously, these additions will cause the aluminates content decrease in favor of calcium silicate hydrates.

In Table 6.4 the effective chloride ions diffusion coefficients in the pastes from various cements, determined by Page et al., are presented [191, 211]. The NaCl molar solution in saturated $Ca(OH)_2$ solution, as well as the saturated $Ca(OH)_2$ solution were applied in two chambers of measuring stand. As can be concluded from these data, the chloride ions diffusion coefficient is ten times lower in slag cement paste and three times lower at 30 % fly ash addition. As it can be concluded, the resistance of slag and pozzolanic cements to the attack of aggressive water solutions is significantly higher. This relates undoubtedly to the much lower capillary porosity of these cement pastes.

As it results from experiments of several authors [197, 212], the composition of pore solution has an impact on the chloride ions binding ability. Byfors [212] studied the effect of the OH^- and SO_4^{2-} ions concentration in mixing water on this chloride ions binding ability. He found the lowered ability of chloride ions binding at increasing concentration of OH^- and SO_4^{2-}. According to Tenoutasse [213], aluminates and ferrites react in the first place with SO_4^{2-} ions and, when the latter are exhausted, C_3A and C_4AF begin to react with the chloride ions. Moreover, as it has been proved by Richartz [214], chloroaluminate hydrates are dissolved in the solutions of sulphates with the increasing of chloride ions concentration in the solution. However, this process depends on the concentration of chloride ions in pore solution and then it depends on pH of this solution; it means that the ability of chloride ions binding is the function of their concentration. This question will be discussed in the Sect. 6.4.4.2. focused on the mechanism of cement paste destruction by chlorides attack.

In the light of a great impact of the pore solution composition on the chloride ions binding ability, a significant effect of cement composition on this process, through the influence on the composition of solution, is evident.

The cations which form the chloride salt have the important influence on Cl^- ions binding ability. This question was studied by many authors [215–219] and their results were summarized by Marchand et al. [197]. The conclusion from these data are that the sequence of cations, ordered according to the increasing chloride ions

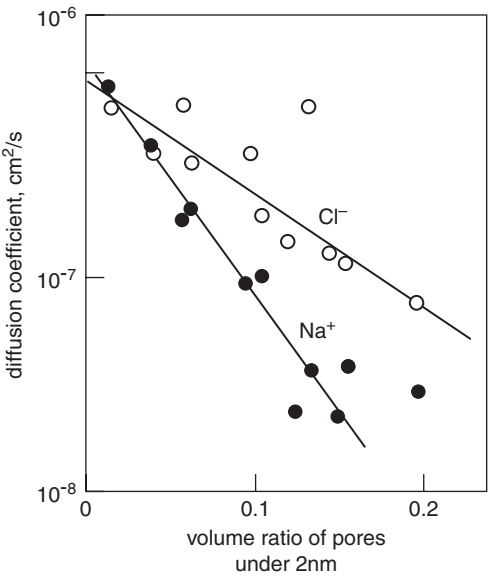


Fig. 6.48 Effective diffusion coefficient as a function of pores under 2 nm. (According to [196])

binding ability in cement paste is as follows: Na^+, K^+, Ca^{2+}, Mg^{2+}. This complies also with the results of Byfors [219], who found that the growing OH^- concentration in the pore solution lowered the chloride binding ability of paste. Tritthart [218] found also, that of solubility of hydroxide formed by the cation linked with chloride ion is one of the factor influencing the binding ability of these ions.

Porosity and permeability of the paste are the main factors determining the diffusion of chloride ions. The microstructure of paste has a direct impact on the diffusion of these ions, as it results from several works. The rate of diffusion is reduced with decreasing w/c ratio [191, 218, 220]. This questions have been discussed in Sect. 5.3.4.

The structure of pores plays an important role in diffusion process, and particularly the share of gel pores, smaller than 2 nm and capillaries, up to 100 nm. Numerous studies show a substantial reduction of the effective diffusion coefficient at growing ratio of gel pores. This effect was confirmed, among the others, by Goto and Daimon [196], as it is shown in Fig. 6.48.

The condition increasing gel pores content in the paste will reduce the diffusion coefficient. It corresponds to the higher content of C–S–H phase in the paste. The increase of gel content is strongly dependent upon the two following factors:

- time of hydration,
- the share of hydraulic and pozzolanic additions, from which the most commonly used are: granulated blastfurnace slag and siliceous fly ash.

Mineral additions reduce the maximum pore radius and effective diffusion coefficient (Fig. 6.49) [221]. The rate of chloride ions diffusion in the paste increases in the following order: slag cement < cement with siliceous fly ash < Portland

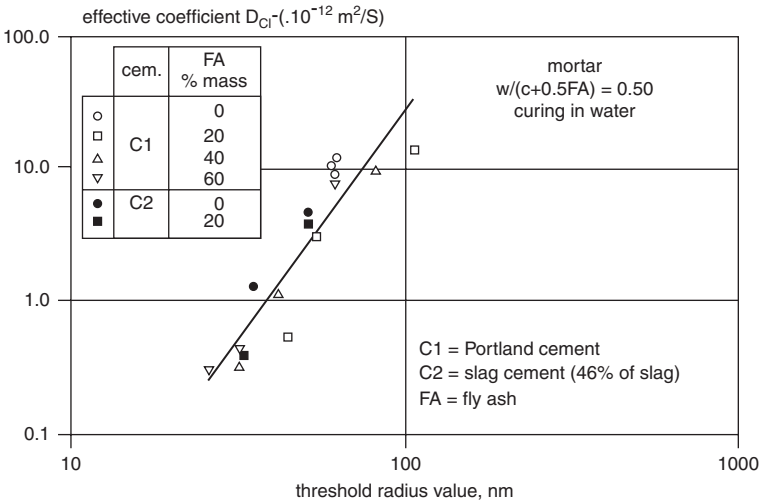


Fig. 6.49 Effective Cl^- diffusion coefficient in the paste as a function of maximum pore radius. (According to [221])

cement without additions < sulphate resistance Portland cement [222]. According to Regourd [223], in the case of the granulated blastfurnace slag and siliceous fly ash additions the pore size distribution and pores structure is changed. This effect is discussed in Sect. 5.3.4. Due to the pozzolanic reaction the fine pores share and the discontinuity of capillary pores occurs, because of the increasing C–S–H content in the paste. Obviously, the rate of diffusion will become lower.

The diffusion of chlorides occurs with higher rate as the Cl^- bonding cation is bivalent, not monovalent. According to Ushiyama and Goto [192] the sequence of salts, in the order of decreasing chloride ions diffusion rate is as follows: $MgCl_2$ > $CaCl_2$ > LiCl > KCl > NaCl. Moreover, the same authors [192] found that the cement paste behaved as an electropositive semi–permeable membrane The surfaces of hydrates are positively charged, as a result of Ca^{2+} ions adsorption. The electric double layer is formed, to which the anions can migrate and penetrate the micropores, and the cations are repulsed. Therefore the effective diffusion coefficients of cations are lower (Fig. 6.50) [192, 196]. The role of the electric double layer, inhibiting the diffusion, was discussed also by Chatterji [224].

Midgley [225] found that the concentration of chlorides vs depth of diffusion complies a power law. As aforementioned, the chlorides react with the calcium aluminate hydrates in the paste. However, a part of chloride ions are remaining as free, in the small capillary pores. Chlorides affect the pore size distribution in the paste; the small pores share is increasing with their concentration [225].

The diffusion coefficient of ions is well correlated with the ratio of fine pores, smaller than 2 nm, irrespectively on the type of cement used to produce the paste, and of curing conditions. The relation between the porosity and diffusion is obvious, because the ions diffusion takes place in the pore liquid. The proportion between

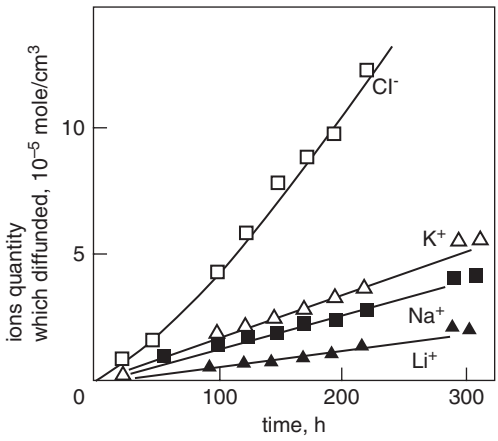


Fig. 6.50 Effect of different ions on the diffusion rate. (According to [196])

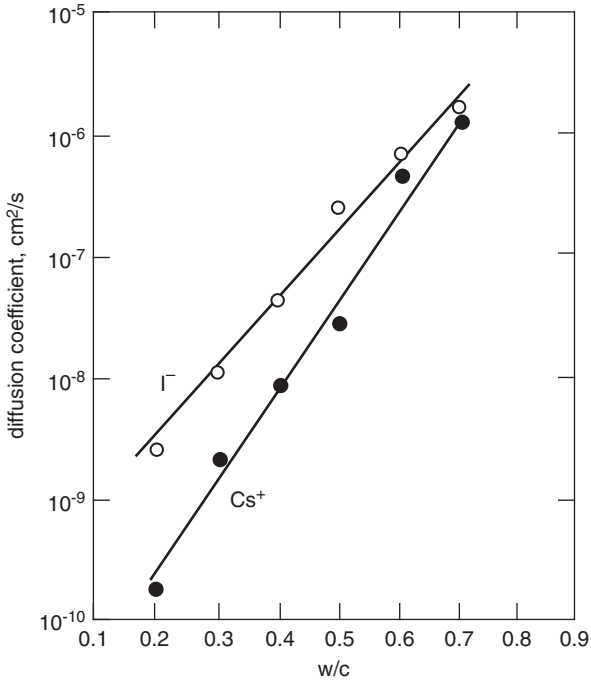


Fig. 6.51 I^- and $^{137}Cs^+$ diffusion coefficients at temperature of 80 °C as a function of cement paste w/c ratio. (According to [193, 227])

the ions occurring in the liquid phase generally and those present in the pores corresponds to the ratio of pores below 2 nm. The apparent diffusion coefficient in relation to the ratio of pores smaller than 2 nm is shown in Fig. 6.48 [196].

The diffusion is increasing with the w/c ratio of the paste, that means with the increasing capillary porosity [192, 226]. There is a close correlation between the w/c ratio (porosity) and the rate of diffusion in the paste, as it is shown in Fig. 6.51

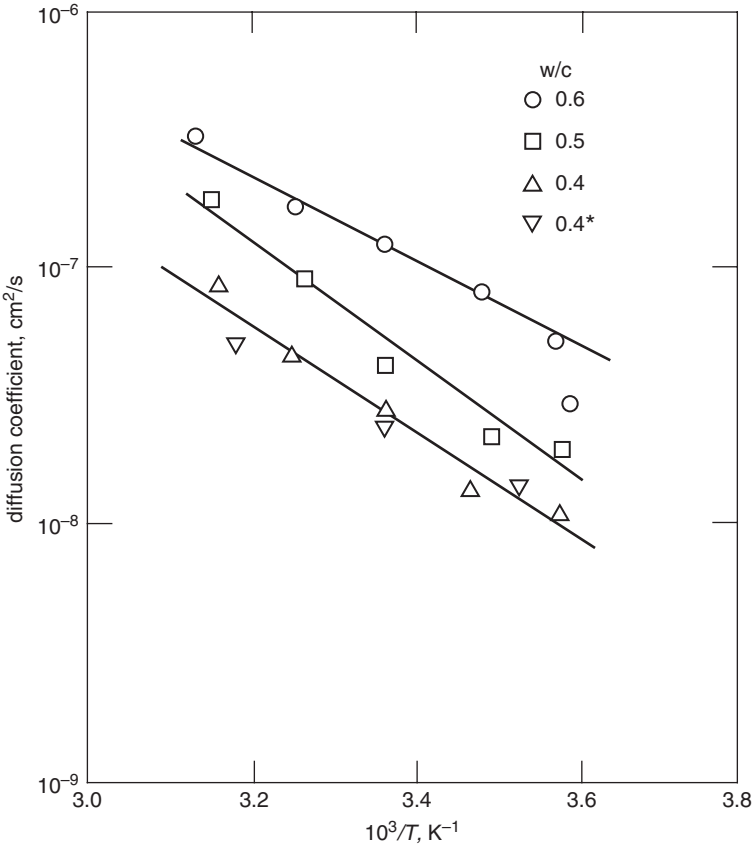


Fig. 6.52 Arrhenius law for the effective Cl^- ions diffusion coefficient in the Portland cement paste with different w/c ratio. (According to [191])

[227]. As early, as in 1946 Powers and Brownyard [228] established the relation between the permeability and porosity of hardened cement paste. Simultaneously, diffusion is fulfilling the Arrhenius law and its rate is increasing with temperature (Fig. 6.52) [191].

The difference between the microstructure of cement paste and concrete should be taken into account when the diffusion conditions are compared. The paste (cement matrix in concrete)—aggregate interfacial transition zone is of special importance. This transition zone is formed of the thin layer of cement paste, about 50 μm wide, which has different microstructure than the bulk cement matrix in this concrete (see Sect. 6.2). The porosity of this interfacial transition zone is significantly higher; the portlandite content is higher as well. In the case of high performance concrete with low w/c ratio the microstructural difference between the interfacial region and the matrix is negligible or none.

The aggregate in concrete will have two inverse impact on the ions transport [229]. In the presence of large, non–porous grains the diffusion occurs in the pores

which are more tortuous. On the other side, the porous, interconnected interfacial transition zones will promote the transport of ions or solution through the material. The significance of the transition zones for the transport properties of concrete was confirmed by several authors [229–232]. Brenton et al. [232] and Bourdette [233] found that the effective chloride ions diffusion coefficient was 6–12 time higher in the interfacial transition zone than in the bulk cement matrix. In Fig. 5.68 the effect of grain size of aggregate and w/c ratio on the permeability coefficient of concrete is shown [229].

The lowering of w/c ratio and addition of silica fume are the most often applied methods in order to eliminate the negative effect of the interfacial transition zone. There is a common opinion that the high performance concretes have considerably reduced chloride ions penetration and higher resistance to the attack of corrosive solutions.

6.4.4.2 Mechanism of Cement Paste Deterioration in Chlorides Environment

The three following mechanisms of concrete destruction as a result of chloride corrosion are reported:

- "acid" corrosion at lowered pH, resulting in the $Ca(OH)_2$ dissolution and leaching of calcium from the phases of cement paste,
- formation of expansive phases, namely the basic calcium and magnesium chlorides,
- osmotic pressure.

As it is known, the phases of cement paste are stable in the strongly alkaline pore solution in concrete, which has a relatively high concentration of potassium and OH^- ions. Moreover, this solution is saturated with respect to the hydrates, which are stable in these conditions. Therefore, the migration of chloride ions into cement paste (concrete) will disturb this thermodynamic equilibrium and, by pH lowering, will cause the dissolving of the hydrates, which will release the OH^- ions. This will be simultaneously the "defensive" action of cement paste to the external attack of corrosive medium. As it results from Fig. 6.53, where the calculated solubility of some phases are shown, the portlandite presents the lowest stability and it will dissolve at pH 11 (first buffer), together with C_4AH_{19} [234]. Ettringite is the most stable phase; however, its stability will depend on the presence of gypsum. At the absence of gypsum ettringite decomposes at pH falling down below 10.7.

At low calcium ions concentration the progressive C–S–H decomposition and the de–calcification of this phase will occur, with simultaneous decrease of C/S molar ratio (Fig. 3.16). When the calcium ions concentration will decrease below 2 mmes/l, that is corresponding to the C/S ratio below 0.63, the transformation of C–S–H into the silica gel will take place. In the range of CaO from 20 to 2 mmoles/l, C–S–H phase will release calcium ions to the solution. Therefore after $Ca(OH)_2$ exhausting, C–S–H will be a second buffer, supporting the pH of pore solution in concrete. Due to the buffering role of hydrated phases in cement matrix, the pH

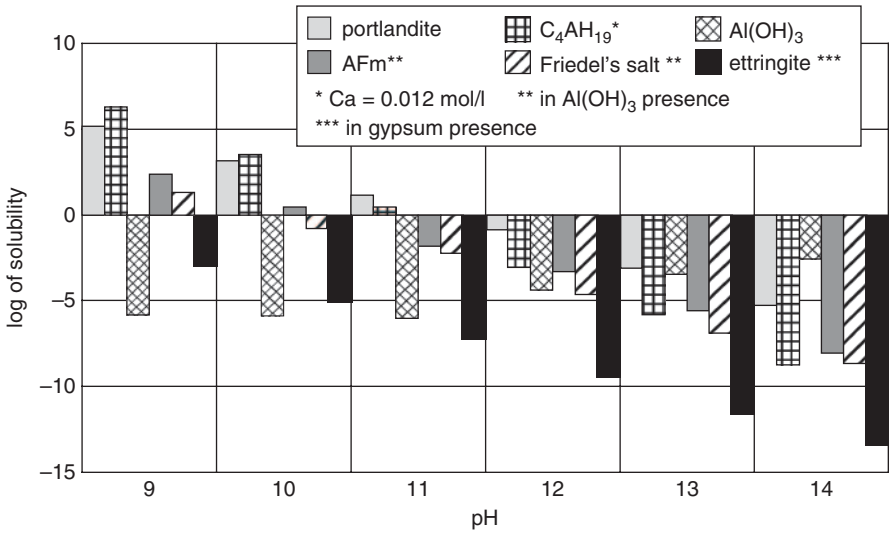


Fig. 6.53 Solubility of hydrates (mmoles/l) as a function of pH of saturated $Ca(OH)_2$ solution. (According to [234]) Vernet C., Chapter 5 in « La Durabilitė des Bėtons », page 142, fig. 5.2 « Echelle de solubilitė de quelques hydrates en fonction du pH », Published by Presses de l'Ecole Nationale des Ponts et Chaussėes, reproduced with the permission of the Presses de l'Ecole Nationale des Ponts et Chaussėes

decrease below 11 of pore solution in concrete occurs very slowly and is strongly dependent on the permeability of concrete [234]. The analysis of solubility products reveals that the precipitation of the $C_3A \cdot CaCl_2 \cdot 10H_2O$ phase will occur simultaneously to the migration of chloride ions in concrete; however, ettringite will be stable even at high chloride ions concentration. The stability of Friedel's salt will depend on the type of cation, binding chloride anion in corrosive solution and this phase will decompose in the case of $MgCl_2$ and NH_4Cl. The rapid corrosion of concrete in the latter solution was studied by Słomka [235]. The stable phases at long term corrosion in the $MgCl_2$ and NH_4Cl solutions are gypsum, gibbsite, iron(III) hydroxide and gel SiO_{2aq}.

Because of the high chloride ions diffusion rate, higher than in the case of cations, the diffusion of OH^- to the concrete surface layers will simultaneously occur, which will be connected with pH lowering. As a consequence, the chloride ions, migrating through the paste, substitute the OH^- groups, moving in solution in the opposite direction. The effective diffusion coefficients, determined for lithium and the other alkali metal cations, are considerably lower than for chloride ions, which prove, according to Ushiyama and Goto [192], that the simultaneous diffusion of Cl^- and OH^- in reverse direction occurs in this case too.

The diffusion of OH^- ions will cause, in the case of $MgCl_2$, the precipitation of brucite; therefore a protective barrier on the surface of concrete, known in the case of concrete corrosion in sea water, will be formed.

In solution with high concentration of chloride ions, the formation of basic calcium chloride or, in $MgCl_2$ solution, the basic magnesium chloride will occur, after long concrete corrosion process. The formation of basic chlorides $Ca(OH)_2 \cdot CaCl_2 \cdot H_2O$

Table 6.5 Molar volumes of various aluminate and calcium phases

Phase	Molar volume (cm^3/mole)
$C_3A \cdot 3CaSO_4 \cdot 32H_2O$	725
$C_3A \cdot CaSO_4 \cdot 12H_2O$	319
$C_3A \cdot Ca(OH)_2 \cdot 12H_2O$	263
$C_3A \cdot CaCl_2 \cdot 10H_2O$	263
$CaSO_4 \cdot 2H_2O$	74
$CaSO_4$	46
$Ca(OH)_2$	33

and $Mg_3Cl_2(OH)_4 \cdot 2H_2O$ was found for the first time by Smolczyk [236], in highly concentrated chloride solutions. These phases are expansive and their crystallization cause the microcracks formation, leading to the destruction of concrete.

There are opposing opinions as the expansive action of Friedel's salt is concerned [237, 238]. Riedel [237] did not find any negative effect of this phase on the strength of paste. In the paste stored in NaCl saturated solution the Friedel's salt formation is associated with some decrease of strength, however, this decrease is considerably lower than in the case of the samples stored in $CaCl_2$ or $MgCl_2$ solutions[237]. On the other side, Conjeaud [238] is stating that the precipitation of this phase resulted in the deterioration of mortar. Kurdowski et al. [239] studied the corrosion of aluminate cement in the concentrated solution of chlorides and found the formation of Friedel's salt in the external layers of samples, however, with no destruction phenomena or even the microcracks formation. In Table 6.5 the calculated volumes of different aluminate and calcium phases are given. Consideration of the volume changes caused by the following reaction:

$$C_3A \cdot Ca(OH)_2 \cdot 12H_2O + CaCl_2 \rightarrow C_3A \cdot CaCl_2 \cdot 10H_2O + Ca(OH)_2 + 2H_2O \quad (6.11)$$

is showing that the volume increase should not occurs. However, the $Ca(OH)_2$ release favors its further reaction with $CaCl_2$ and the formation of basic calcium chloride, giving an expansion. The next possible reaction is as follows:

$$C_3A \cdot CaSO_4 \cdot 12H_2O + CaCl_2 \rightarrow C_3A \cdot CaCl_2 \cdot 10H_2O + CaSO_4 \cdot 2H_2O \quad (6.12)$$

This reaction is linked with a decrease of volume; however, as the crystallization of gypsum is taken into account, the overall volume is increasing and can be estimated as 18 cm^3/mole of AFm. But the crystallization of gypsum is less probable in the concentrated solution of chlorides and rather the formation of anhydrite will be more probable, with the decrease of total volume. These examples are showing that the effect of chloroaluminate hydrate on the formation of microcracks and deterioration of concrete is negligible.

A significant volume increase can occur, when the sulphate anions released in the reaction (6.12) will react with the monosulphate or C_4AH_{19}, to form secondary ettringite. In this case the increase of volume will be 406 and 462 cm^3/mole of these phases respectively.

There are not so many papers dealing with the osmotic pressure, as a potential mechanism of cement paste destruction in chloride solutions [240–242]. There are

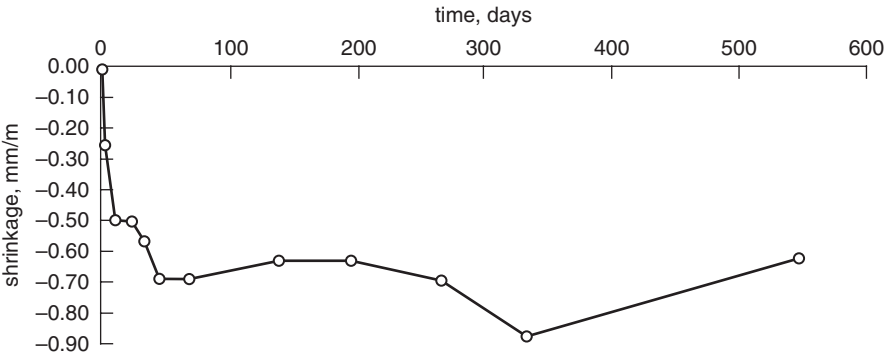


Fig. 6.54 Shrinkage of the samples from alkali activated slag cement paste without Portland cement clinker, with Na_2SiO_3 addition in concentrated $MgCl_2$ solution. (After [246])



Fig. 6.55 Basic magnesium chloride crystals in a microcrack after 23 months of curing in the magnesium chloride solution. (According to [245])

some controversies between the authors of these works and Chatterji [242]; the latter one rejects this mechanism at all. On the other side, Kurdowski et al. [243–245] obtained the results indicating the importance of the osmotic pressure in chlorides corrosion. This mechanism was proved in the case of highly concentrated chloride solution and presumably could not be found at lower concentrations. These experiments were embracing the pastes from various cements, as well as from individual clinker phases [243–246]. The corrosion process was always initiated by the shrinkage of cement paste bars, occurring very early, after a few days and was lasting within about 60 days (Fig. 6.54). The microcracks appeared, as a consequence of this shrinkage, and the diffusion of chloride ions or even the migration of corrosive solution inside the samples was thus promoted.

The basic magnesium chloride crystallizes in these microcracks (in the case of $MgCl_2$ solution), but without the increase of volume, because the gaps give enough space for the crystal growth (Fig. 6.55) [243, 245]. However, on the shrinkage curve for the paste composed mainly of C–S–H, a hampering of the shrinkage development after about 20 days can be noticed (Fig. 6.54) [245]. Therefore the shrinkage

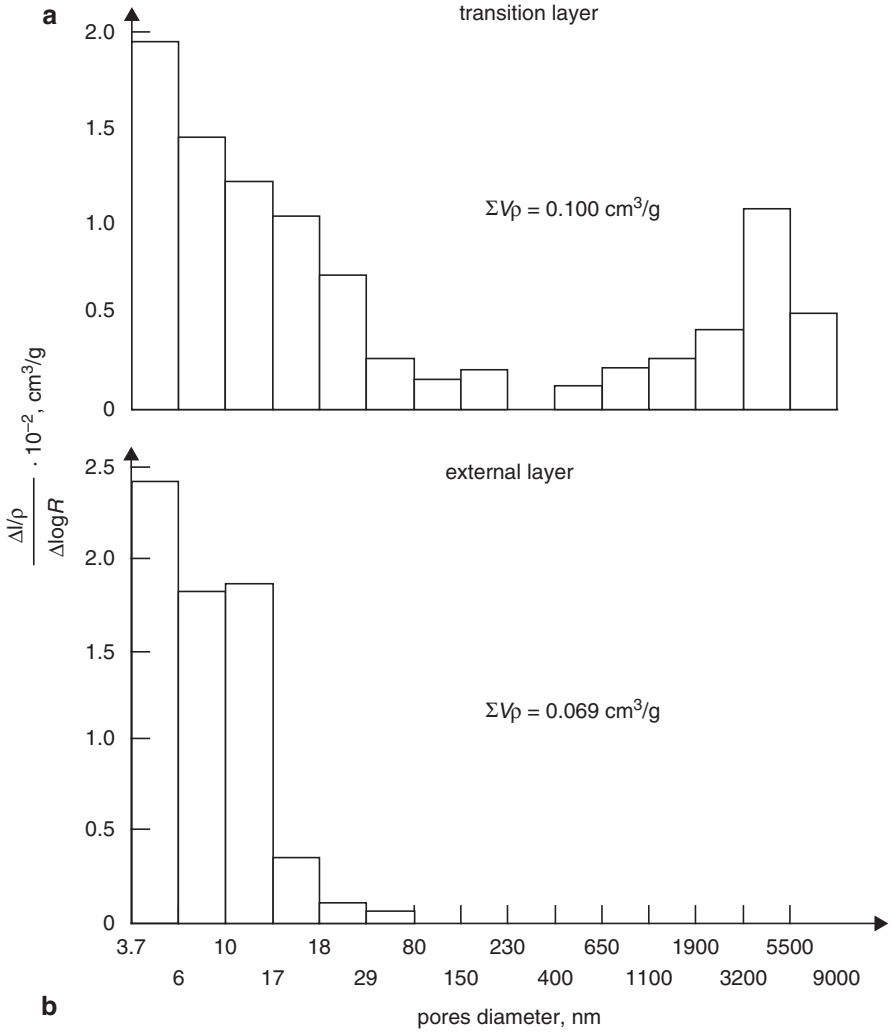


Fig. 6.56 Pores size distribution in the alkali activated slag cement paste after 2 years of curing in the magnesium chloride solution of high concentration. (According to [245])

due to the consolidation of gel is dominating. The outer layer on the surface of samples became very compact, with extremely low porosity (Fig. 6.56). The Portland cement paste bars reveal analogous volume changes; the highest durability can be attributed to those produced from cement with low aluminates content and high silica modulus [246]. The samples containing principally tobermorite, without C–S–H gel, do not show shrinkage, but a progressively occurring expansion, due to the formation of basic magnesium chloride [246].

The process of C–S–H gel consolidation occurs practically before the initiation of corrosion reactions and can be observed under the scanning electron microscope



Fig. 6.57 Irregular domains of compact C–S–H gel in the paste after 1,200 days of curing in the chloride solution. (According to [246])

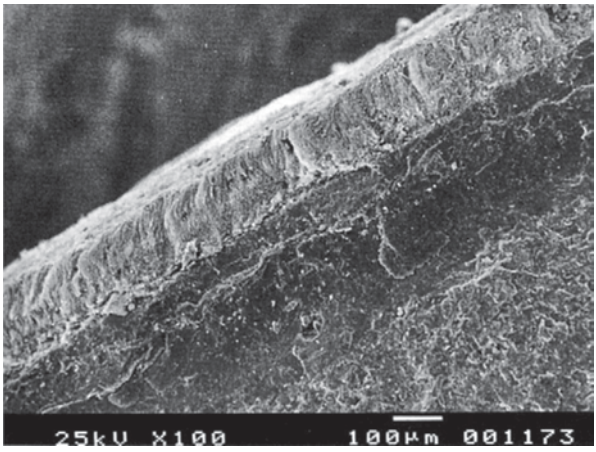


Fig. 6.58 Protective barrier composed of brucite and basic magnesium chloride on the surface of paste after 23 months of curing in the magnesium chloride solution. (according to [240])

(Fig. 6.57) [246]. In dense, compact gel the diffusion of ions is slowed down significantly.

The alkali activated slag cement with sodium silicate shows a high durability in the magnesium chloride solution, which is caused among others by the slow slag hydration. The shrinkage microcracks are filled with C–S–H formed as a hydration product of slag which reacts gradually with chloride solution. In this paste, like in the calcium aluminate cement paste, also of high durability, the diffusion of chloride ions occurs more rapidly than the diffusion of magnesium ions and hence the diffusion of OH^- toward the corrosive solution takes place, followed by the precipitation of a barrier composed of brucite and basic magnesium chloride (Fig. 6.58) [239, 244]. The diffusion of chloride ions is therefore restricted and the durability of paste is enhanced as well. After longer period of time (5 years) this protective barrier collapses and the corrosion process proceeds rapidly, to the destruction of paste.

As it can be concluded from the experimental aforementioned data, in the corrosion of pastes in the chloride solutions the physical transformations and chemical reactions are included. The cations bonding the chloride ions have a great impact on the corrosion process. The most rapid concrete destruction occurs in the presence of magnesium and ammonium cations.

6.4.5 Sulphate Attack

The sulphate attack has been known from a long time, and already in 1858 Vicat [247] studied the chemical causes of hydraulic compounds corrosion in sea water [247]. Bied [248] invented the technology and developed the production of calcium aluminate cement, as a remedy for rapid destruction of concrete in France, caused by the sulphate ground water attack, from the dissolution of gypsum and anhydrite.

During the last 70 years many papers dealing with the sulphate corrosion appeared, aimed in the determination of the corrosion mechanism and looking for the methods of anti–corrosion protection. The harmful effect of calcium aluminate higher content was also found a long time ago. Kuhl [249] was writing that Michaelis already in 1901 proposed to replace aluminum by iron. The production of sulphate resistant, iron containing Portland cements started (cement Ferrari 1928 [249]). Simultaneously, basing on the experiences derived from the ancient Romans, the pozzolanic additions came into use, with aim to enhance the sulphate resistance [250]. The granulated blastfurnace slag was the first addition used on a large scale for slag cement production as early as in 1880 in France, and next in Germany, in 1892 [249]. The slag cement was initially applied in the case of works in marine environment, in foundations and the other underground structures, without contact with air [250]. The reason was that there was an opinion that this cement did not hydrate in air.

The opinion of favourable effect of pozzolanic additions, particularly blastfurnace slag and siliceous fly ash against the sulphate corrosion, is maintained to the present days and has the universal, rich documentation [251]. However, some authors are of the opinion, that the physical effect of reduced porosity and capillary adsorption (permeability), in the case of high performance concrete with superplasticizers addition is more important than the influence of pozzolanic additions [252]. Analogous opinion was supported by Skalny and Pierce [65].

There are two methods of corrosion progress investigation: the examination of expansion of the bars immersed in the sulphate solution of given concentration and the measurements of strength changes of the samples cured in the similar solution. It should be remember that in the latter case at the beginning of corrosion process the higher rate of strength development can be found, as compared with the reference samples cured in water, due to the improvement of microstructure initiated by corrosion (Fig. 6.59). The corrosion products, primarily ettringite, cause the reduction of porosity and hence the strength increases, which is followed by a rapid strength decrease. Therefore the rapid strength development, occurring until the pores in concrete will be filled, is a proof of considerable corrosion progress.

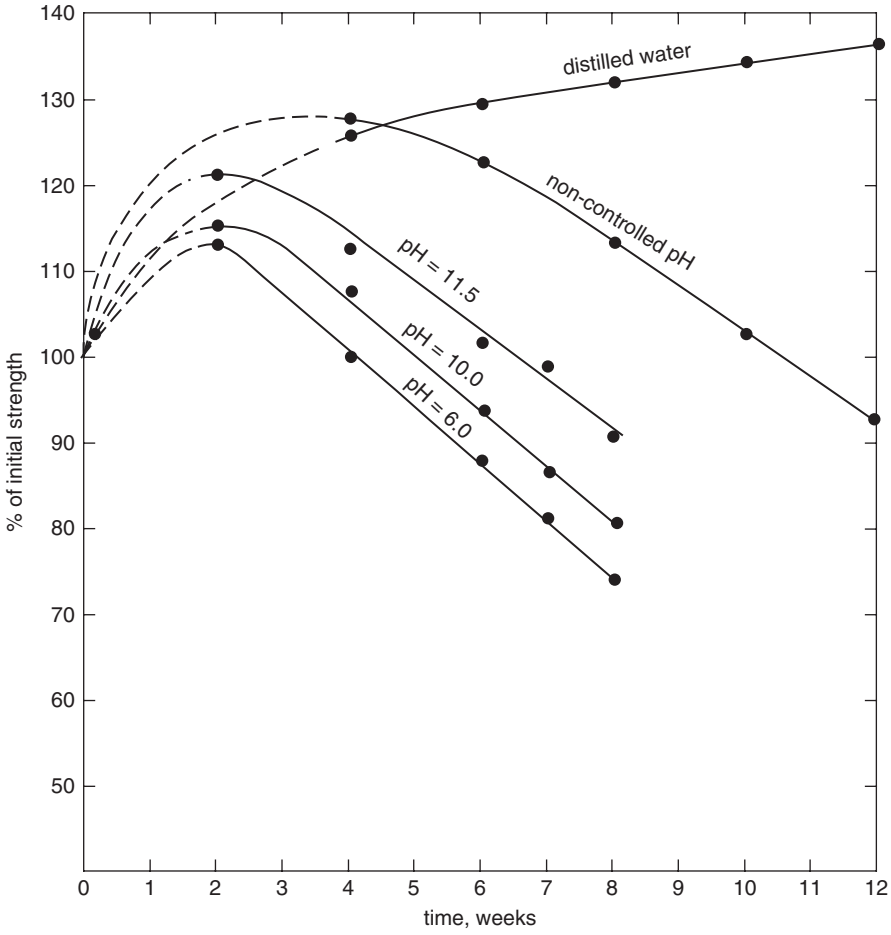


Fig. 6.59 Relative strength of concrete placed in corrosive medium, in respect to the early strength after 2 days of storage in % in relation to pH of solution. (According to [176])

The European standard establishing the sulphate resistance of cement determination, nowadays in preparation, will be based on the French standard NF P 18–837. The linear changes are measured on the standard mortar $2 \times 2 \times 16$ cm bars, immersed in the Na_2SO_4 solution of concentration equal 16 g of SO_4^{2-} per liter. The expansion of sulphate resistant cement should not exceed 0.5 % after 1 year of immersion in this solution. The C_3A content in the sulphate resistant Portland cements is generally lower than 3 % and the $C_4AF + C_3A$ total is lower than 25 %. In the ASTM C 150–94 standard the C_3A content is restricted to 5 %, and the total $C_4AF + C_3A$ to 25 %. In the British BS 4027:1991 standard the C_3A content was restricted to 3.5 % and SO_3 to 2.5 % respectively. The slag cements have a high sulphate resistance and Locher [253] was of the opinion that at slag content above 65 % the Al_2O_3 percentage would be out of importance, while at a lower slag addition the aluminum oxide

content should be restricted. Similar view was presented by Regourd et al. [254]; these authors related this limit to the clinker component only and postulated the 8 % C_3A limit at the slag content lower than 60 %. From the numerous studies of cement pastes with high slag addition, or cements without clinker component, the conclusion can be drawn that the corrosion resistance of these cements is also caused by very slow slag hydration. The reaction between the slag and pore solution, occurring simultaneously with the corrosion process, results in the formation of C–S–H gel filling the voids generated due to the corrosion process.

In spite of numerous research there are still many unresolved and controversial problems inspiring the intensive discussions. A good example is the problem of ettringite and the mechanism of its expansive action. There are many hypotheses concerning this problem, but they all are at least doubtful [176]. On the basis of considerations presented by Scherer [173], Brown and Taylor [176] are willing to accept the crystallization pressure of micrometric particles as a main cause of ettringite expansive effect. Simultaneously, as a rule the expansion of concrete due to the sulphate attack is always linked with the formation of ettringite.

Similarly, as in the case of the other types of corrosion, the inner and outer concrete corrosion can be distinguish, as it has been mentioned earlier, and, in the case of sulphate attack, this classification can be considered as a classic one.

The sulphate corrosion of concrete is a complex process, in which the physical and chemical factors are involved and one unique mechanism cannot be distinguish. This process is composed of chemical reactions, often very complex, linked with physical transformations. The physical changes are the most frequently the consequence of chemical reactions, but they can be induced by other factors, not necessary directly related to the sulphate attack, for example the microcracks caused by freezing. However, they have generally a serious impact on the rate of sulphate corrosion itself. They promote the transport of ions inside the concrete; this transport can be maintained through the migration of solution either as a result of capillary–rise or hydraulic pressure. This mechanism of transport has several orders of magnitude higher rate than the diffusion, occurring as a result of concentration difference in the pores of various size. However, the most significant effect of diffusion is observed in the micropores. The most important physical transformations are those relating to the microstructure and the strength changes and softening of material, linked with them. Therefore the modification of physical properties of concrete results from the modification of hardened paste microstructure, mainly from the change of its phase composition, including the C–S–H decay.

The complexity of chemical reactions was underlined by Taylor [255]. There are several mutually related processes, including not only the formation of ettringite and gypsum, decomposition of C–S–H phase through decalcification, but also the precipitation of brucite, occurring in the case of magnesium sulphate; they all lead to the destruction of material [176].

The sulphate attack is more severe as the concrete is subjected to cyclic wetting and drying. Therefore the laboratory expansion measurements do not reflect completely the field conditions. Mehta [251], basing on the observations of various concrete structures, found that the decrease of adhesion and strength, as well as the

transformation of material into a loosen, cake–like mass, were the symptoms of sulphate corrosion. These phenomena, however, without disregarding the microcracks originating from ettringite expansion, would indicate mainly the deterioration of C–S–H.

There are few works relating to the rate of reaction fronts shifting, during sulphate corrosion. Gollob and Taylor [256] found these changes of paste phase composition at w/c = 0.35 on a depth of 0.5–1 mm after 6 months of immersion in Na_2SO_4 or $MgSO_4$ solution of concentration of 0.25 mol/liter, at temperature of 20 °C. The surface layer was formed of gypsum and the second under it, was enriched in ettringite [256].

The attack of sulphate solution depends on the type of cation bound with SO_4^{2-}. The barium and lead sulphates do not exhibit aggressive action, first of all because of their very poor solubility, while the other sulphates react with cement paste constituents and, depending on the conditions, they cause the expansion and destruction of concrete. The calcium, sodium, magnesium and ammonium sulphates are ordered according to the increasing harmful effect on concrete durability. The reactions accompanying their interaction with cement paste are significantly differentiated. Calcium sulphate reacts only with the aluminates and ferrite phases with ettringite formation. However, sodium sulphate reacts firstly with calcium hydroxide with gypsum formation, but moreover also with C–S–H. In the past there was a certainty that Na_2SO_4 does not react with C–S–H (for example Lea [98]), however, Gollob and Taylor [256] found a slow decalcification of C–S–H by sodium sulphate with the formation of NaOH. This process is initiated after the calcium hydroxide consumption, or when calcium hydroxide is not easily available, for example encapsulated in the C–S–H gel. The sequence of reactions is as follows:

$$Na_2SO_4 + Ca(OH)_2 + 2H_2O \rightarrow 2NaOH + CaSO_4 \cdot 2H_2O \tag{6.13}$$

When the concentrations of calcium and sulphate ions in the liquid phase exceed the gypsum solubility product, the crystallization of this phase takes place. The sulphate and calcium ions react then with AFm phases and ettringite is formed:

$$\begin{aligned} 2Ca^{2+} + 2SO_4^{2-} + Ca_4Al_2(OH)_{12}SO_4 \cdot 6H_2O + 20H_2O \\ \rightarrow Ca_6Al_2(OH)_{12}(SO_4)_3 \cdot 26H_2O \end{aligned} \tag{6.14}$$

$$\begin{aligned} 2Ca^{2+} + 3SO_4^{2-} + Ca_4Al_2(OH)_{14} \cdot 6H_2O + 20H_2O \\ \rightarrow Ca_6Al_2(OH)_{12}(SO_4)_3 \cdot 26H_2O \end{aligned} \tag{6.15}$$

The progressive decalcification of C–S–H can be written as follows:

$$\begin{aligned} 1.75CaOSiO_2 \cdot nH_2O + xNa_2SO_4 + 2xH_2O \\ \rightarrow (1.75 - x)CaOSiO_2 \cdot nH_2O + 2xNaOH + xCaSO_4 \cdot 2H_2O \end{aligned} \tag{6.16}$$

Gypsum thus produced is expansive, but can subsequently reacts with aluminates to form ettringite. However, there is no good correlation between the amount of ettringite and gypsum on one side and the degree of expansion on the other side.

From the stoichiometry of reactions (6.14) and (6.16) results that in some conditions the calcium hydroxide can be formed, which is the potentially substrate of the reaction (6.14), increasing the amount of gypsum formed. Ettringite produced according to the equation (6.16) is expansive too. The reaction (6.16) is dominating in the soluted gypsum containing solutions, it means at limited sodium content. The calcium sulphate shows a weaker corrosive effect because of the lower solubility in water.

It should be remember that the high gypsum content in the mixture is causing the rate of ettringite formation lowering. This relation was discussed in Sect. 4.1.2, dedicated to cement setting. Therefore in some cases, in the samples corroded in sulphate environment, a continuous gypsum content increase is observed, while the ettringite content goes through a maximum and decreases. As it is known, the sodium and potassium hydroxides affect significantly the solubility of calcium hydroxide. Therefore the corrosion in the presence of sodium or potassium sulphate occurs more slowly than in the case of magnesium sulphate. Very often this is explained by the increase of pH in the liquid phase in the case of the corrosion process, induced by sodium and potassium sulphates.

The reactions of magnesium sulphate occur analogously, but the reaction (6.19), that is the decalcification of C–S–H, occurs more rapidly. This is due to a very poor solubility of magnesium hydroxide, known as brucite. This hydroxide is precipitated as a white gel, forming a layer of corrosion products, mainly on the concrete surface. This layer, when dense and compact, plays a role of a barrier, impeding the diffusion of sulphate ions into the concrete. However, a crystalline brucite can be occasionally formed [80].

In the case of magnesium sulphate a hydrated magnesium sulphate can be produced or poorly crystallized serpentine [256]. Because of the low solubility of these phases as well as of brucite, the penetration of magnesium ions inside the concrete is very slow, however, it can be accelerated in the case of porous material, linked with high w/c ratio. On the other side, the precipitation of magnesium phases results in a significant decrease of OH^- ions content in the solution and the decalcification of C–S–H is accelerated [reaction (6.16)]. The pH decrease causes the loss of durability of the other phases, for example ettringite decomposes at pH below 9 [234]. This low pH value is observed in a final stage of concrete destruction.

In the presence of magnesium hydroxide the pH decreases to 10.5 and C–S–H is not stable. $MgSO_4$ reacts with calcium sulphoaluminate hydrates; they decompose with the formation of gypsum and $Al(OH)_3$.

The thaumasite $CaSO_4 \cdot CaSiO_3 \cdot CaCO_3 \cdot 15H_2O$ [257, 258] appears often, apart from gypsum and aluminum hydroxide or silica gel, in the deteriorated concrete. The formation of this phase takes place when the sulphate attack occurs at low temperature and together with an intensive carbonation process.

The aggressive effect of ammonium sulphate was discussed by Oberholster [71]. This compound reacts with calcium hydroxide, with the formation of gaseous ammonia:

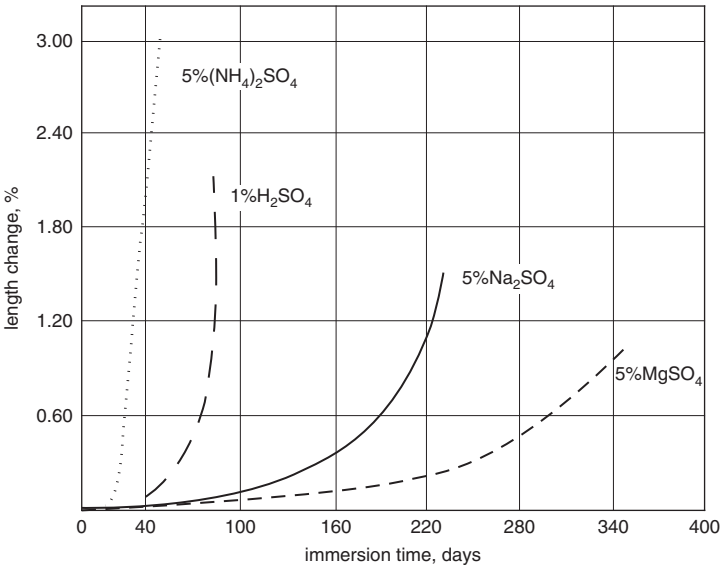


Fig. 6.60 Linear expansion of mortar cubes immersed in various sulphate solutions. (According to [71])

$$Ca(OH)_2 + (NH_4)_2SO_4 \rightarrow CaSO_4 \cdot 2H_2O + 2NH_3 + 2H_2O \qquad (6.17)$$

The ammonium sulphate is very hazardous; gaseous ammonia volatilizes from the reaction site and hence the process occurs rapidly. The consumption of calcium hydroxide causes the decomposition of C–S–H with $Ca(OH)_2$ release. This was concluded from the expansion of mortars placed in aggressive solutions (Fig. 6.60). The expansion appeared as a result of gypsum and ettringite formation; the latter one was also decomposed under the influence of $(NH_4)_2SO_4$ [71].

The role of the ferrite phase, generally identified as brownmillerite, should be mentioned too. In the case of sulphate attack this phase can be the source of aluminate ions [237]; moreover the ferrite ions can form the analogue of ettringite or to substitute the aluminate ions in all calcium aluminate phases [222]. The latter case is undoubtedly the most common one in the Portland cement paste. However, the reaction of sulphate ions with ferrites is slower. There is a view that the F/Al ratio in the hydrated phases is lower than in brownmillerite; hence, some amount of iron(III) hydroxide is always present [222] (see also Sect. 4.1.1.). This hydroxide occurs in the gel–like form and therefore the diffusion of ions through the gel layer is slowed down. Therefore, the corrosion process is hindered. The other phases containing the Fe^{3+} ions can be produced too, it is discussed in Chap. 3.

As it has been mentioned earlier, during the sulphate attack, as in the case of the other corrosion processes, the zonal phase composition changes of the paste, with the decreasing concentration of sulphate ions, in the direction to the concrete interior along the diffusion path, is observed. Gollob and Taylor [256] studied the

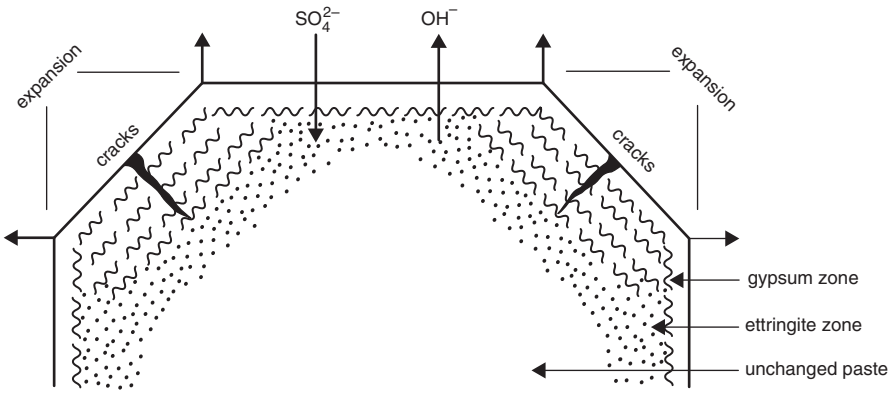


Fig. 6.61 Reaction zones in the sample of cement paste placed in Na_2SO_4 or $MgSO_4$ solution. (According to [256])

phase composition in these zones and found a significant amount of gypsum in the outer layer, and beneath—the zone enriched in ettringite, occurring in the form of micrometric particles mixed with C–S–H (Fig. 6.61). The monophase ettringite area was not found. However, Wang [259] detected the ettringite–rich region. Yang et al. [260] examined the interfacial transition zone in the concrete during sulphate attack and have shown that the SO_4^{2-} ions transport occurred principally through this zone; gypsum was the only corrosion product present in this concrete. Diamond and Lee [261] found zonal gypsum formation, parallel to the concrete surface. Brown and Badger [262] examined "*in situ*" the concrete in the structure exposed to the sulphate attack and found that in the outer layers, carbonated and poor in calcium, gypsum was stable; in the regions with higher pH, far from the surface, ettringite was the stable phase. In the light of results presented above, several authors are questioning if ettringite formation is therefore a main destructive process in sulphate corrosion. However, in some cases the serious impact of ettringite was proved; the microcracks formed in concrete as a result of ettringite crystallization are the ways of rapid ions transport and the corrosion of concrete is accelerated [176].

Vernet [234] submitted the example of reaction fronts modeling, in which the precipitation of CD compound firstly occurred, and then of ABn; firstly the product with the lower solubility is formed (Fig. 6.62). The $CaCO_3$ and $Mg(OH)_2$ layers on the surface of concrete exposed to the sea water attack are the examples.

In the favourable kinetic condition, in the reaction front the precipitated product is continuously consolidated and plays a role of a "trap" for the diffusing ions, and these ions cannot cross this impermeable barrier [234].

As a result of sulphate corrosion the major changes of concrete microstructure occurs. In the absence of any corrosion processes, cement matrix in concrete shows some specific features; the most important ones are listed below (Fig. 6.63) [261]:

- coarse cement grains are surrounded by compact hydrate shell, so–called inner product,

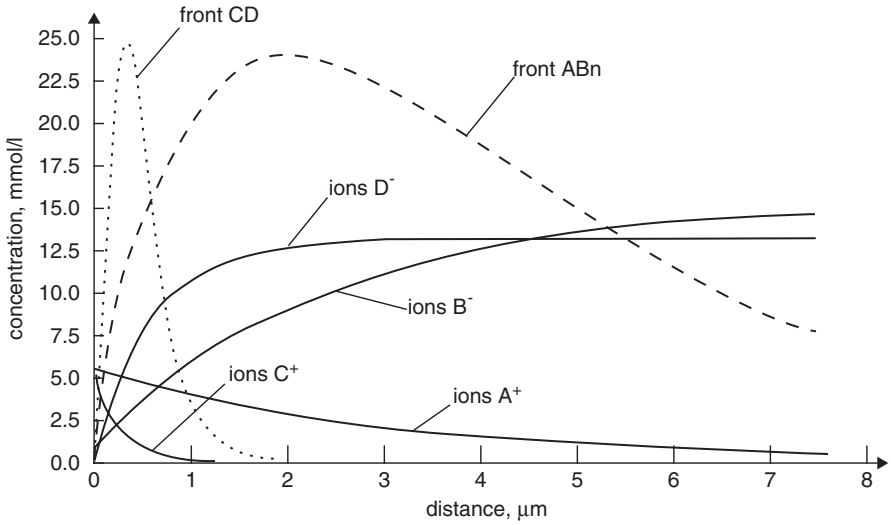


Fig. 6.62 Reaction fronts calculated with "Gradif" model. (According to [234]) Vernet C., Chapter 5 in « La Durabilitè des Bètons », page 154, fig. 5.6 « Modèle Gradif. Calcul simplifiè d'un front de prècipitation », Published by Presses de l'Ecole Nationale des Ponts et Chaussèes, reproduced with the permission of the Presses de l'Ecole Nationale des Ponts et Chaussèes

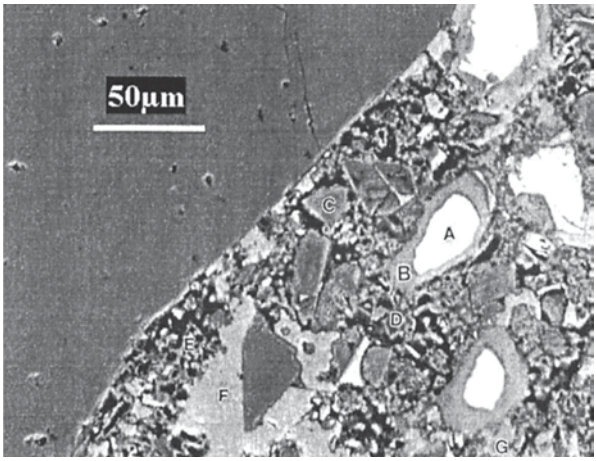


Fig. 6.63 Appearance of normal features not subjected to sulphate attack: *A*—unhydrated cement, *B*—dense inner C–S–H gel surrounding unhydrated cement, *C*—inner C–S–H gel constituting fully hydrated cement grain, *D*— region of small hollow shell hydration grains, *E*—groundmass or outer product C–S–H gel, *F*—$Ca(OH)_2$ surrounding a sand grain chip, *G*—deposit of calcium hydroxide within the groundmass (After [261]) Diamond S., Lee R.J. in Materials Science and Concrete, Special volume: Sulfate Attack Mechanisms (J. Marchand amd J. Skalny eds.), p. 138, Fig. 1, 1999, published by The American Ceramic Society, 735 Ceramic Place, Westerville, Ohio 43081, 2001, reproduced with the permission of The American Ceramic Society

- C–S–H gel of the similar morphology to the outer product, occurring as pseudomorphoses of cement grains hydrated entirely,
- sporadically occurring gaps surrounded by hydrate layers, composed mainly of C–S–H (Hadley's grains),
- vast regions of cement matrix filled with higher porous C–S–H gel; so–called outer product,
- portlandite crystals grown on the surface of sand or aggregate grains, as well as occurring sporadically in cement matrix,
- small ettringite crystals occurring sporadically in cement matrix or present as small clusters; the monosulphate crystals are very scarce,
- larger air pores, more or less filled with large portlandite crystals or sporadically with ettringite.

Sulphate attack causes the irreversible changes in cement matrix: phases occurring normally are disappearing or their composition and microstructure is significantly altered, the new phases, being the corrosion products appear [261]. The principally changes are the replacement of portlandite by gypsum, forming frequently massive deposits on sand and aggregate grains, or crystals layer in the corroded matrix. This gypsum crystallization with portlandite replacement is associated with generation of stresses and microcracks. In the case of magnesium sulphate brucite is precipitated, principally in the surface layers of concrete.

The transformations occurring in C–S–H gel are of major importance as the durability of concrete is concerned. Normally it contains a few quantity of aluminum and sulphur (see Fig. 3.41), because it is intimately mixed with amorphous calcium monosulphoaluminate which, as a rule, does not form detectable crystals, even under SEM. In the corroded concrete the darker and brighter regions of C–S–H gel are observed. This dark gel is after the profound transformations resulting in the C/S ratio lowering caused by decalcification and has significantly higher content of aluminum, sulphur and magnesium [261]. The transformation of bright C–S–H are much less pronounced. C–S–H gel is replaced by ettringite in some regions; this ettringite is the product of hexagonal hydrates or AFm reaction with sulphate ions. There are the stresses and microcracks generated in these regions too. Ettringite does not occur in the surface layers of concrete because it is susceptible for carbonation and, as a result, the thaumasite is formed [261]. Ettringite occurs generally in the form of larger crystals in the pores or as a massive deposits around the aggregate. There are always the microcracks in these regions.

Unhydrated cement grains lose calcium mostly, due to leaching process and the siliceous acid gel as residue remains. Therefore the strong bonds, found previously between these grains and inner C–S–H gel, are lost. The substitution of calcium with the magnesium ions with the formation of magnesium silicates can also occur [256]. Occasionally, the brownmillerite relics, as a marker of cement grains remains [261].

The following transformations due to the corrosion process are found [261]: transition of portlandite into gypsum, decalcification of C–S–H gel, leaching of calcium from the large cement grains, deposition of gypsum and ettringite within the framework of the cement paste, as well as the microcracks formation with significant

Table 6.6 Aggressiveness of sulphate containing waters with respect to Portland cement [71]

SO_4^{2-} concentration (mg/l)	Aggressiveness
<300	Very low
300–600	Low
601–1,500	Moderate
1,501–5,000	Strong
>5,000	Very strong

increase of concrete porosity and simultaneous weakening of bonds between the components of the groundmass.

In spite of the numerous research, there are many discrepancies as the threshold, permissible sulphate content in the concrete pore solution is concerned. Obviously, there is a huge amount of factors affecting the corrosion rate and many of them were discussed in previous chapter. Therefore, it is not surprising that in the concrete with high cement content, even of higher C_3A percentage, the corrosion in the $CaSO_4 \cdot 2H_2O$ solution occurs more slowly than in the concrete poorer in cement of low C_3A content [263].

There is a surprising effect observed when the mixture of sulphates is consisting a corrosive solution. The Na_2SO_4 addition to $MgSO_4$ solution or inversely, $MgSO_4$ to the Na_2SO_4 solution, causes the attack less intensive as in the presence of the one, single salt [61].

The process of corrosion is affected by so many factors that the determination of threshold concentration of sulphate solution has a relative significance. However, irrespectively of these comments it can be remember a rather common view that at the sulphate concentration exceeding 1,000 mg/l (Table 6.6) the distinct attack is initiated. However, the corrosion once commenced can develop with a considerable rate.

The sulphate corrosion resistance of concrete is strongly affected by the phase composition of cement. A high resistance is assured with low C_3A and moderate C_3S content in cement; the latter one is producing a substantial amount of $Ca(OH)_2$ in the paste (Fig. 6.64) [264]. According to the requirements of ASTM standard sulphate resistant cement should contain no more than 5 % C_3A and less than 50 % C_3S, calculated with Bogue's formulae. Moreover, the total $C_4AF + 2C_3A$ should not exceed 20 %. $CaSO_4$ reacts more slowly with $C_4(A, F)aq$, and the rate of reaction lowers with decreasing A/F ratio. The role of iron(III) hydroxide gel, surrounding the aluminate hydrates cannot be also excluded.

The enhanced resistance of concrete to aggressive sulphate solutions can be achieved by the use of hydraulic or pozzolanic additions. These additives should not contain too much aluminum compounds, because they will produce the calcium aluminate hydrates in the paste.

The effect of pozzolanic additions is due to the reduction of $Ca(OH)_2$content with simultaneous increase of C–S–H phase share in the paste and hence the noticeable decrease of capillary pores.

The question of permeability growing with the decrease of cement content in concrete (Fig. 6.65), as well as with increasing w/c ratio should not be neglected, when the sulphate resistance is assessed [264].

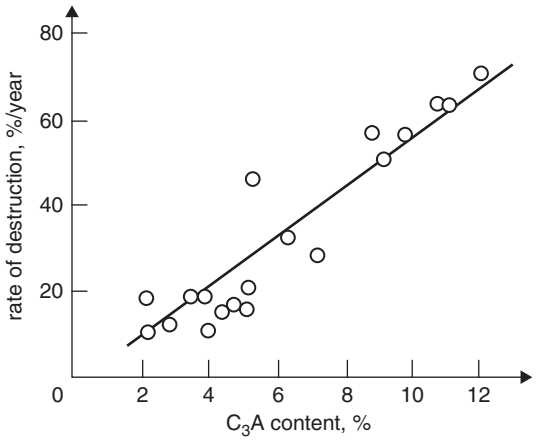


Fig. 6.64 Effect of C_3A content in cement on the rate of concrete destruction. (According to [264])

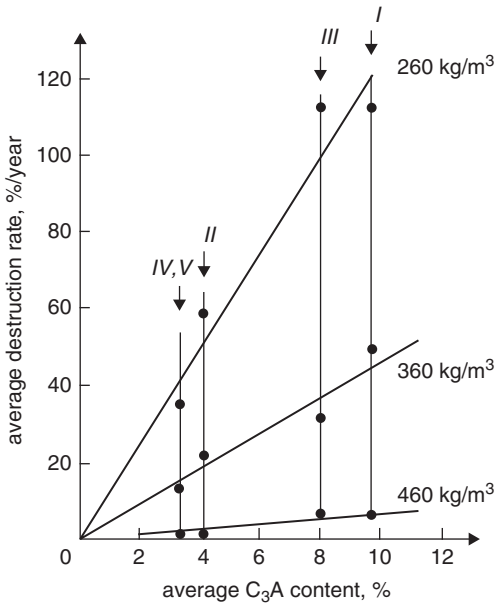


Fig. 6.65 Effect of C_3A content in cement and cement content in concrete on its rate of destruction in sulphate solution. (According to [264])

It is also known that the sulphate attack can be caused by aggregates, particularly when they contain the calcium–rich feldspar [265]. Then, in the presence of $CaSO_4$ and $Ca(OH)_2$ the expansive ettringite is formed. Van Aardt and Visser [265] found that at temperature 80 °C the hydrogarnet appeared, showing no expansion and resistant to the sulphate attack. The resistance of hydrogarnet to the sulphate corrosion was reported earlier by Marchese et al. [266]. The C_3AH_6 solid solution with C_3AS_3, with the composition corresponding to $3CaO \cdot Al_2O_3 \cdot zSiO_2 \cdot (6–2z)$ H_2O, where $z \geq 0.35$, has a sulphate resistance, increasing with SiO_2 content.

The concrete resistance is highly influenced by proper curing. Primarily the permeability of material is controlled and the infiltration of harmful ions is hindered.

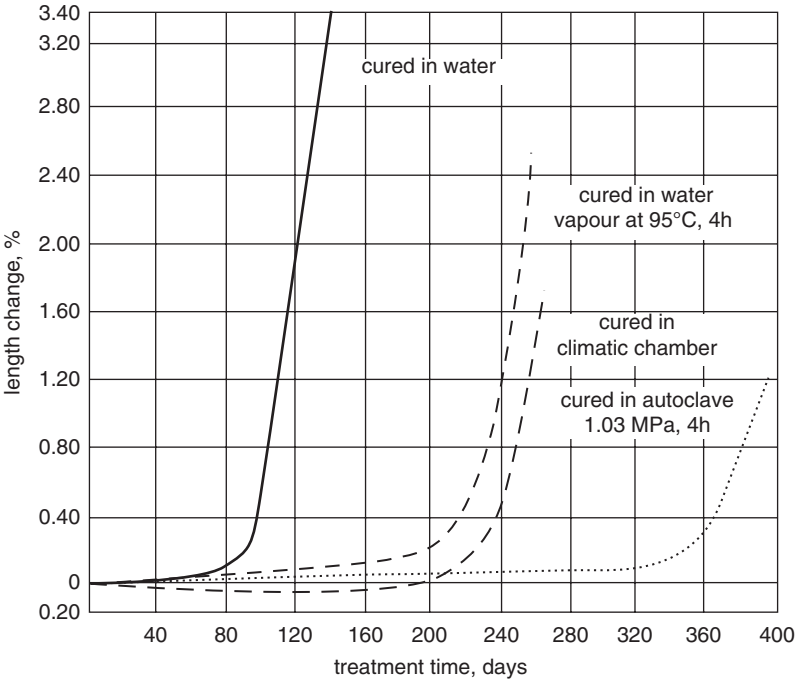


Fig. 6.66 Linear expansion of samples immersed in the 1 % H_2SO_4 solution. (According to [71])

The underwater maturing is not good in this case, because presumably the surface carbonation and the formation of poorly permeable surface layer is prevented.

The autoclaved concrete elements have the best sulphate resistance (Fig. 6.66) [71].

This is an interesting feature that the sulphate attack is less severe at higher temperatures. Taking the expansion as a measure of aggressiveness one can note that it has the highest value at the temperature of + 5 °C and subsequently is decreasing; at 80 °C is quite low [71].

The destruction of concrete due to the formation of thaumasite replacing the C–S–H phase is a special case of sulphate corrosion. This process is promoted by the simultaneous intensive carbonation, or by use of limestone Portland cement, together with the low temperature. In Poland the destruction of concrete structures due to the thaumasite formation has not been reported, however, this can arise from the multicomponent paste composition of damaged concrete and very similar XRD pattern of thaumasite and ettringite.

Thaumasite was discovered by Nordenskiold [267] in 1878, in Sweden. The name of this mineral can be derived from the Greek “thaumazein”, which means to be surprised. In the next years the occurrence of thaumasite was found in many geological systems, as a result of rock mineralization. The number of concrete structures damaged as a result of thaumasite formation were later increasing too. Relatively recently in 1965 Erlin and Stark [268] identified thaumasite in the destructed sewage channels. Subsequently in England, in Stoke on Trent in 1969 thaumasite was



Fig. 6.67 Thaumasite sulphate attack in a structural beam—the bridge support in the motorway (Photo courtesy of Halcrow Group Ltd, U.K.). (According to [273])

detected in plaster of building houses, which was reported by Bensted and Varma [269]. In this case the gypsum plaster covered the walls, which were built up using masonry cement with limestone addition [270]. Since this time several examples of thaumasite formation in the damaged concrete structures has been found in the world.

Thaumasite is the untypical compounds with the following structural formula: $Ca_6[Si(OH)_6]_2(CO_3)_2(SO_4)_2 \cdot 24H_2O$, in which the silicon has an octahedral coordination. The untypical silicon coordination causes the exceptionality of this compound. For the first time it was determined by Moenke [271] with infrared spectroscopy and subsequently verified in the XRD studies, by Edge and Taylor [272].

Thaumasite is readily formed at a relatively low temperature, at the range from 0 to +5 °C, and certainly below 10 °C. The temperature below 15 °C was reported too. It is attributed to the favorable conditions for the formation of intermediate phase, containing groups $[Si(OH)_6]^{2-}$, which make possible the thaumasite nuclei formation [273]. However, thaumasite already formed is stable at temperature up to about 110°C, at which it is decomposing with a disordered structure formation, so–called thaumasite glass. In this glass the silicon reveals tetrahedral coordination [273].

The formation of thaumasite occurs as a result of sulphate corrosion of cement matrix in concretes or in mortars, with simultaneous participation of $CaCO_3$, eventually at easily access of CO_2. Thaumasite is then present in the form of white powder (Fig. 6.67), without binding properties. This is harmful for concrete destruction of the basic phase of cement matrix, the calcium silicate hydrate. C–S–H became decomposed being the source of silicate ions indispensable for thaumasite formation.

This special case of sulphate corrosion, occurring together with the carbonation of cement matrix, is called frequently thaumasite corrosion. The limestone Portland cement matrix is particularly susceptible for this type of corrosion, because all the necessary components, beside of the external source of sulphates, are present.

The two following routs of thaumasite formation are known:

- C–S–H reaction with Ca^{2+}, SO_4^{2-}, CO_3^{2-} ions in water,
- C–S–H and ettringite decomposition under CO_2 influence.

The processes attributed to these two routs can be written as follows:

$$\begin{aligned} &"Ca_3Si_2O_7 \cdot 3H_2O" + 2(CaSO_4 \cdot 2H_2O) + CaCO_3 + CO_2 + 23H_2O \\ &\rightarrow Ca_6[Si(OH)_6]_2(CO_3)_2(SO_4)_2 \cdot 24H_2O \end{aligned} \tag{6.18}$$

$$\begin{aligned} &Ca_6[Al(OH)_6]_2(SO_4)_3 \cdot 26H_2O + "Ca_3Si_2O_7 \cdot 3H_2O" + CaCO_3 + CO_2 + xH_2O \\ &\rightarrow Ca_6[Si(OH)_6]_2(CO_3)_2(SO_4)_2 \cdot 24H_2O + CaSO_4 \cdot 2H_2O + [Al(OH)_3]_2 + 3Ca(OH)_2 \end{aligned} \tag{6.19}$$

The latter reaction scheme shows that in the process of thaumasite formation the access of external sulphate ions is not required. Simultaneously, the possibility to some amount of aluminum ions incorporation into the thaumasite structure in the form of partial solid solution is not taken into account in the last equation, though this occurrence is known.

As one can conclude from the thaumasite formula given above, its structure is similar to that of ettringite and therefore the solid solution of these phases can be easily formed. This solid solution is known as woodfordite and therefore the formation of thaumasite from ettringite is determined as a “woodfordite route” [273]. Abundant information dealing with the thaumasite was reported by Bensted [273]. The effect of variable C/S ratio of C–S–H on thaumasite formation was studied by Małolepszy and Mróz [274].

The sulphate attack with C–S–H gel decomposition and thaumasite formation is particularly harmful for the durability of concrete, because it occurs with the destruction of the most important binding constituent of concrete and leads to the collapse of this material. Because of the relatively low temperatures of thaumasite formation, the concrete foundations, and elements of the underground sewage systems, as well as the concrete road elements are especially susceptible for this type of destruction. In order to prevent thaumasite formation the classic approach should be applied, first of all the permeability of concrete should be reduced, and the use of cement with mineral additions should be considered. Bensted [273] suggested the lowering the C_3A and alite content in cement.

6.4.6 Corrosion in Sea Water

The corrosion induced by sea water is a complex process, in which the physical factors, mainly the temperature and erosion are important, apart from the chemical

Table 6.7 Composition of sea water [278]

Sea area	Degree of salinity (g/l)	Mean composition of Atlantic ocean (%)	
Baltic sea	3.0–8.0	Cl^-	55.3
Black sea	18.3–22.2	Br^-	0.2
White sea	26.0–29.7	SO_4^{2-}	7.7
Atlantic ocean	33.5–37.4	CO_3^{2-}	0.2
Pacific ocean	34.5–36.4	Na^+	30.6
Indian ocean	35.5–36.7	K^+	1.1
Mediterranean sea	38.4–41.2	Ca^{2+}	1.2
Red sea	50.8–58.5	Mg^{2+}	3.7
Caspian sea	126.7–185		
Dead sea	192.2–260		

conditions, such as the concentrations of ionic species, mainly chlorides and sulphates, as well as CO_2 content. Mehta [275] is of the opinion that low pH is responsible for accelerated corrosion of concrete in sea water. In sea water the CO_2 concentration has a significant impact on the pH level, which can be reduced from the normal 8.2–8.4 range to 7. To prove this opinion Mehta [275] reports the studies of Feld [276], who attributed the damages of concrete piles and capitals of columns (elements of the bridge over the James River, Newport News, Virginia, USA) after 21 years of exploitation to the low pH of sea water. The same cause was reported by Mehta [275] in the case of damage of the beams after 25 years of exploitation of the bridge near Ocean City, in New Jersey. In these both cases the pH of sea water was close to 7, because of the high CO_2 concentration. Lea [98] is of the same opinion that the attack of sea water becomes more intensive with decreasing pH and at $pH < 7$ the aggressive CO_2 is present [98]. However, is simultaneously stating that the solubility of CO_2 in sulphate solutions or in sea water is low and therefore these two cases mentioned above are an exception [98].

From the chemical point of view the corrosion caused by sea water is the simultaneous, chlorides and sulphates attack, with high ratio of magnesium salts (Table 6.7). However, it occurs in this case some weakening of sulphates attack in the presence of chlorides, in spite of the high SO_4^{2-} concentration [277]. The weaker attack of sea water than of the $MgSO_4$ solution of the same concentration is caused by a higher solubility of ettringite and gypsum in chloride solutions. This can result, at least partially, to the formation of non–expansive ettringite [278]. However, on the other side Locher [279] found that the NaCl addition to sulphates solution did not hamper the sulphate attack, but even in some cases increased it. The effect of sulphates was reduced at $NaHCO_3$ addition; according to Locher [279] this could be the cause of weaker attack of sea water on concrete, as compared with $MgSO_4$. Presumably this would be the effect of calcite layer formed on the surface of paste and in the pores near the surface. The rate of corrosion is well correlated with the amount of ettringite formed. In the less damaged samples there is more chloroaluminate hydrates as the effect of reaction of chlorides containing liquid phase and monosulphoaluminate [279]. However, ettringite formed from chloroaluminate is

a stable phase in the presence of sulphate ions as it was aforementioned, while trichloroaluminate hydrate is stable in sulphates solution.

It should be mentioned that in a warm, dry climate the chlorides improve the sulphate attack [280]. Presumably, it is the reason, apart from the known effect of temperature on the rate of chemical reactions (Arrhenius rule), that in a warm climate the concrete corrosion occurs more rapidly than for example in the North Sea. The examples of disastrous quick concrete corrosion in the warm seas in the Middle East are known, as well as the excellent durability of drilling platforms situated on the North Sea [278]. The conditions governing in different geographic zones: temperature, erosion, biological environment, are highly variable and therefore the mechanisms of concrete deterioration are greatly modified [61].

From the biological factors the important role have bacteria, which are oxidizing sulphur and hydrated sulphides to the sulphates [98]. These mechanisms are not fully elucidated. The ammonium carbonate evolving mollusks can contribute in concrete deterioration too.

There is no full consensus of the importance of expansive ettringite formation. According to Mehta [275] it is out of importance, while Regourd [281] is of the opinion that ettringite is among the factors promoting the concrete corrosion. The basic role in concrete corrosion is attributed by Mehta to the chlorides and magnesium ions [275]. Particularly the chlorides ions are the cause of reinforcement corrosion and in the case of reinforced concretes they are the main cause of their destruction.

According to Mehta [275], the resistance of concrete against the sea water attack is controlled by concrete permeability and primarily by cement content. This author refers to the excellent performance of concrete structure in San Pedro Harbour, near Los Angeles after 67 years of exploitation, erected from concrete with high cement content, about 350 kg/m^3, in spite of Portland cement application with high C_3A content. Mehta compared it with the severe damage of concrete produced at about 230 kg/m^3 of cement content. In the damaged concrete layers the brucite, gypsum, ettringite, thaumasite, aragonite and carboaluminate hydrates were found [281]. The similar results were reported by Regourd [281, 282]: the concrete cubes from Portland cement with high C_3A content (15 %) and cement share of 600 kg/m^3, placed in sea water were not damaged after 66 years, while those contained 300 kg/m^3 of cement were destructed. Idorn [283] and Gjörv [284] came to the same conclusion.

The magnesium ions content is another very important factor, as it has been discussed in Sect. 6.4.4 and 6.4.5, and is linked with the very low solubility of brucite. Apart from brucite, the aragonite, calcite, gypsum and thaumasite are the phases stable in sea water. The formation of magnesium silicate hydrate $4MgOSiO_2 \cdot 2H_2O$, without binding properties, is also mentioned by Mehta [275]. The typical for the chloride attack exchange of calcium by the magnesium ions and leaching out of the former ones is observed simultaneously. The removal of calcium occurs by decomposition of calcium hydroxide and decalcification of C–S–H (see Sect. 6.4.4). The sea water attack leads often to the formation of barriers, composed of aragonite and brucite on the surface of concrete. An advantageous effect of the calcium carbonate barrier, slowing down the corrosion process, was underlined by Locher [279] and Regourd [281].

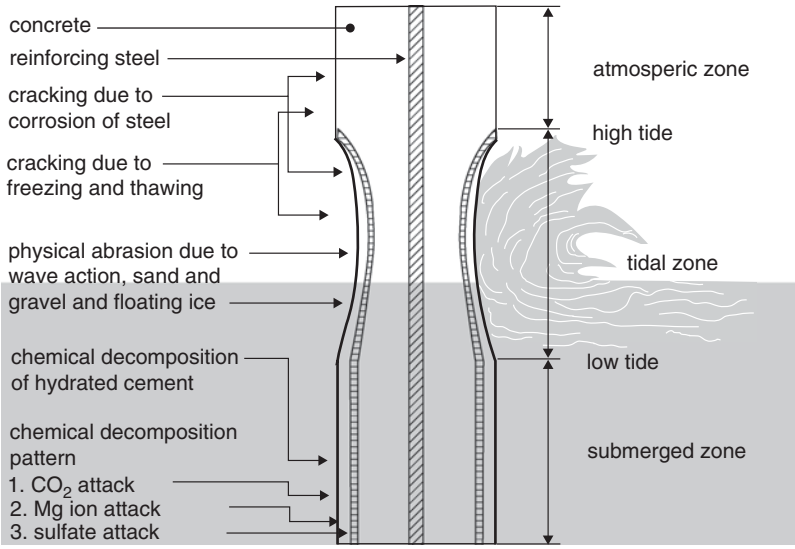


Fig. 6.68 Concrete degradation by sea water. (According to [275])

The corrosion of concrete under sea water attack is a complex process and depends upon many physical and chemical factors, as well as upon the climate conditions. The placement of structure in relation to the sea is very important and the following situations can occur in practice (Fig. 6.68) [275]:

- the zone of the sea water drops range, transported with the wind,
- the partial structure immersion in sea water,
- the total structure immersion in the sea, without the possibility of partial emerging during falling tide.

When the structure is kept under water the chemical processes are dominating, while at cyclic submerging and emerging the destruction is complicated; the physical and chemical factors superimpose each other. After the emerging and reduction of concrete moisture content, the crystallization of various salts, for example $Na_2SO_4 \cdot 10H_2O$ is expected; the expansion of these salts, similar to that induced by ettringite is observed [67]. During the rising and falling tide the severe erosion by sand grains, or even larger rock pieces and ice in winter occurs. As huge amount of chlorides can penetrate the concrete in these conditions was shown by Berke et al. [285], which were reporting 0.8–0.9 kg/m^3 within 1 year.

The physical factors: erosion, freezing and thawing, crystallization of salts superpose on the corrosive attack of chlorides and sulphates. There are the conditions favoring the osmotic pressure mechanism too.

Regourd et al. [254] point out that the sea water effect on the cement paste is very often surprising, quite different than expected.

The corrosion of concrete exposed to sea water becomes significantly intensive with lowering pH of the liquid phase below 7, with the aggressive CO_2 in solution

[98, 275], as it was mentioned earlier. However, one should take in mind that the CO_2 solubility in the sulphate solutions or in sea water is very low. On the other side the HCO_3^- ion, together with Mg^{2+} one are involved in the formation of aragonite layer on the surface of concrete submerged in sea water [222].

At cyclic concrete submerging and emerging in sea water the conditions are different and the carbonation becomes an important, effective process [286]. There is an opinion that the carbonation does not improve the corrosion resistance against the sea water attack [61]. The corrosion of concrete in this environment is more severe as shorter is the time of maturing before the exposure to the aggressive medium. The following processes are involved in the chemical action of sea water:

- calcium hydroxide leaching,
- intermediate $C_3A \cdot CaCl_2 \cdot 10H_2O$ formation followed by transformation into the expansive ettringite,
- crystallization of secondary expansive ettringite and expansive gypsum,
- long term corrosion process, accompanied generally with carbonation, leading to the ettringite transformation into thaumasite, as well as the formation of aragonite and brucite [286]. Brucite can form the magnesium–calcium silicate hydrates at the expense of C–S–H. The sodium and potassium silicates appear too [61].

As it can be concluded from the information relating to the chemical mechanism of cement paste corrosion under sea water, its resistance depends primarily on the $Ca(OH)_2$ and calcium aluminates content; it means that the resistance increases with the C–S–H phase content in the paste. Therefore cements poor in C_3A, with low C_3S/C_2S ratio, that is those with high silica ratio and low lime saturation factor show the best resistance. Cements with high slag and pozzolana content are extremely resistant, particularly when they are produced from clinker poor in C_3A. Very good results were assured by the three component cements, with 30% pozzolana addition, beside of slag [98]. Calcium aluminate cement reveals, as in the case of sulphate attack, the highest corrosion resistance in marine environment (see Chap. 9).

Considering the low C_3A content one should remember that the resistance of this phase in marine environment depends on polymorph, which is present in cement clinker [286]. Cement with cubic C_3A gives more ettringite than chloroaluminate hydrates in sea water, while the inverse behaviour is observed in the case of cement with rhombohedral or monoclinic C_3A. Beside of the errors attributed to the Bogue calculation method, the occurrence of various C_3A polymorphs can be the source of inadequate correlation between the C_3A content and resistance of concrete to the attack of aggressive solutions.

The slag cement with high content of the granulated blastfurnace slag, that is CEM III/B according to the European standard, is particularly recommended for the production of concrete applied in the structures exposed to the sea water attack. Regourd et al. [254] are of the opinion that slag cement should have the slag content higher than 60%, and then the mineral composition of clinker is not important. The similar view was reported by Locher [253] and Wang [259], however, these authors state that the Al_2O_3 content in slag should be restricted.

6.4.7 Miscellaneous Corrosive Media

6.4.7.1 Sewage

The sewage sludge is generally of basic character and has not a significant corrosive impact on concrete. The corrosion mechanism is as follows: the microorganisms reduce sulphur to sulphides; part of them is expelled to the atmosphere in the form of H_2S [71]. Hydrogen sulphide condensates on the upper surfaces of sewer and dissolves in the water layer on the walls. Then it is oxidized to the sulphuric acid in the presence of bacteria. Due to the destructive action of H_2SO_4 on cement matrix its peeling off the aggregate takes place and the corrosion of sewer walls are occurring. Decisive factors are the following: concentration of sulphur, temperature, the oxidation—reduction potential of sludge components and the concentration of hydrogen ions [71]. The most severe, destructive conditions occur in the following cases [71]:

- the sludge is discharged into the sewer under pressure,
- concentrated carbonaceous wastes i.e. night–soil or conservancy–tank inlets are discharged into the sewer,
- certain industrial effluents of low pH are discharged into the sewer,
- – at low gradient that the flow rate is less than the minimum required for scouring the sewer. Under this condition the sewage turns septic and slime accumulates on the walls below the water level. This provides an excellent breeding ground for sulphite–producing organisms.

In order to improve the resistance of sewers the use of concrete with limestone aggregate is recommended [71]. The oxidation of sulphides with chlorine and whitewash, to raise the pH value over 10, is another remedial method [222]. The systematic removal of slime and mud to accelerate the flow, but with maintaining its laminar character, is recommended too [222]. Surface sewer walls treatment, particularly with gaseous SiF_4 can be also used [222].

6.4.7.2 Fire Resistance

Concrete has high specific heat and low thermal conductivity, therefore the protection of reinforcing steel against fire is very good. However, concrete itself can be destructed due to the stresses induced by temperature gradient and different thermal expansion of aggregate and cement matrix. Under fire action the extreme temperature gradients are formed, and the external layers shows the tendency for spalling of from the internal ones, having lower temperature [287]. At temperature rise up to about 300 °C the paste shows expansion. However, at this temperature shrinkage of paste due to the loss of water occurs, but the expansion of aggregate is continued [222]. The expansion of quartz at temperature of about 570 °C, due to the polymorphic transformation $\beta \rightarrow \alpha$ occurs, and at temperature of about 650 °C the subsequent shrinkage, linked with the decomposition of $CaCO_3$ to CaO, commences. Piasta et al. [288] reported the transformations of the matrix under the fire attack,

as occurring principally due to the carbonation at temperature below 500 °C, and during the further heating up to 900 °C—consisting in the porosity and macropores ratio increase.

The blastfurnace lump slag is a fairly good aggregate for concrete exposed to high temperature hazard [222], limestone can be used too, and dolomite is very good for this condition [287]. However, quartz containing aggregate should be avoided (see Sect. 5.3.2) of the aforementioned reason. The strength decrease due to the higher temperature impact is given by Neville [287]. This author [287] is stating that temperature of 600 °C can be considered as the upper limit for the Portland cement concrete structures[8].

Some problems can appear in the case of rapid temperature rise as a consequence of the fire attack on the high performance impermeable concrete structure. In such a concrete the water evaporates rapidly and exerts a high pressure resulting in spalling; the exposure of reinforcement is frequently observed [289, 290]. The problem of fire resistance was widely reported; 50 works were publish in the RILEM Workshop Proceedings (Leipzig 2009)[9]. Concrete with polypropylene fibres addition of 1–3 kg/m^3 (0.1–0.2 % by volume) [291] can improve the fire resistance of HPC. When melting, they produce a network of pores through which the water vapour can be released. The internal pressure in HPC is then four times lower than in HPC without fibres [291]. The 0.9–1.8 kg/m^3 fibres addition do not cause the particular lowering of HPC mechanical properties.

6.4.8 Carbonation of Concrete

Carbon dioxide reacts with cement paste phases and these reactions occur in the liquid phase in which gaseous carbon dioxide dissolves. The rate of carbonation depends upon the rate of CO_2 migration to the pores in concrete; this is significantly affected by the moisture content in the environment. The effective CO_2 diffusion coefficient in air is 10^4 times higher than in water and this is the decisive factor in carbonation process [292]. In the concrete saturated with water the capillaries are filled with the solution, the diffusion is slowed down and the carbonation practically does not occur. In the case of concrete in equilibrium with dry atmosphere the amount of water in the capillaries is not sufficient to dissolve CO_2 and the carbonation is very slow too (Fig. 6.69). The most convenient conditions occur when the water forms a layer on the walls of capillaries in which CO_2, quickly migrating in air, dissolves and reacts with calcium ions. According to Venuat [293], Verbeck found the maximum carbonation rate at relative humidity in the range from 40 to 80 %, in equilibrium with the moisture of concrete (Fig. 6.69).

[8] The fire resistant concretes are discussed in the monographic book by Nadachowski F., "Refractory materials technology", Editor: Śląskie Wydawnictwo Techniczne, Katowice 1995. (in Polish).

[9] First International RILEM Workshop on Concrete Spalling Due to Fire Exposure (ed. F. Dehn, E.A.B. Koenders 3–5 September 2009, Leipzig, Germany.

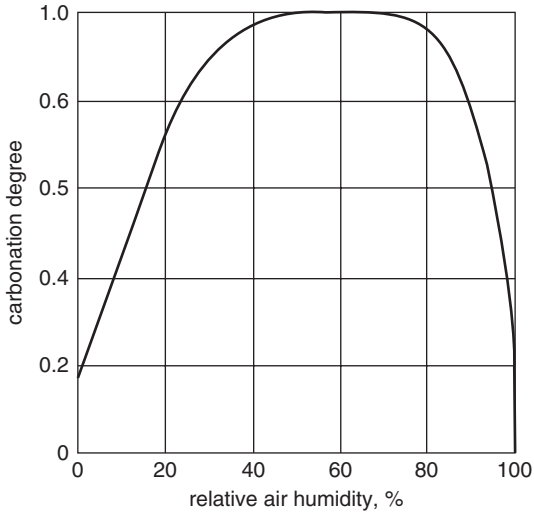


Fig. 6.69 Carbonation rate vs. humidity of environment with which concrete is in equilibrium

The rate of carbonation depends on concrete permeability, then it decreasing with low w/c ratio, and with cement content increase. Therefore, the rate of carbonation is inversely proportional to the strength of concrete.

All paste components are subjected to carbonation [293–295]:

$$Ca(OH)_2 + CO_2 \rightarrow CaCO_3 + H_2O \tag{6.20}$$

$$4CaO \cdot Al_2O_3 \cdot 13H_2O + 4CO_2 \rightarrow 4CaCO_3 + 2Al(OH)_3 + 10H_2O \tag{6.21}$$

$$\begin{aligned} &3CaO \cdot Al_2O_3 \cdot 3CaSO_4 \cdot 31H_2O + 3CO_2 \rightarrow \\ &\rightarrow 3CaCO_3 + 2Al(OH)_3 + 3(CaSO_4 \cdot 2H_2O) + 22H_2O \end{aligned} \tag{6.22}$$

$$3CaO \cdot 2SiO_2 \cdot 3H_2O + 3CO_2 + nH_2O \rightarrow 3CaCO_3 + 2SiO_2aq + 3H_2O \tag{6.23}$$

Thus AFm and AFt decompose also under CO_2 action. Unhydrated clinker phases are carbonated too, but the rate of this process is higher in the case of silicates than for aluminates. The carbonation of paste phases has thermodynamical justification, because at ambient temperature and in the presence of CO_2 the stable phases are: $CaCO_3$, quartz and gibbsite [296]. In Table 6.8 the free enthalpy changes, for carbonation reactions, calculated by Babushkin and Mchedlov–Petrossian are given [296]. Although the prevailing opinion is that portlandite is carbonated first, some data point out the quick, effective C–S–H carbonation [61]. Various polymorphs of calcium carbonate are produced, presumably the vaterite is formed first and subsequently transforms into calcite; aragonite can occur as an intermediate phase too.

Table 6.8 Free enthalpy and equilibrium pressure of CO_2 during carbonation of paste components [296]

Reaction	ΔG^{o}_{298} (kJ/mol)	Equilibrium pressure CO_2 (MPa)
$\frac{1}{5}(5CaO \cdot 6SiO_2 \cdot 5.5H_2O)(s)+CO_2(g) =$ $= CaCO_3(s)+\frac{5}{6}SiO_2(s)+1.1H_2O(c)$	−47.27	$10^{-7.28}$
$\frac{1}{4}(4CaO{\bullet}Al_2O_3{\bullet}19H_2O)(s)+CO_2(g) =$ $= CaCO_3(s)+\frac{1}{2}Al(OH)_3(am)+4H_2O(l)$	−61.55	$10^{-9.78}$
$\frac{1}{3}(3CaO{\bullet}Al_2O_3{\bullet}3CaSO_4{\bullet}32H_2O)(s)+CO_2(g) =$ $= CaCO_3(s)+CaSO_4{\bullet}2H_2O(s)+\frac{2}{3}Al(OH)_3(am)+\frac{23}{3}H_2O(l)$	−42.96	$10^{-6.52}$
$\frac{1}{3}(3CaO{\bullet}Fe_2O_3{\bullet}CaSO_4{\bullet}32H_2O)(s)+CO_2(g) =$ $= CaCO_3(s)+CaSO_4{\bullet}2H_2O(s)+\frac{2}{3}Fe(OH)_3(am)+\frac{23}{3}H_2O(l)$	−58.91	$10^{-9.31}$
$Ca(OH)_2(s)+CO_2(g) = CaCO_3(s)+H_2O\ (l)$	−74.61	$10^{-12.1}$

Lach and Matousek [297] studied the C_3AH_6 carbonation and found the formation of $C_3A \cdot CaCO_3 \cdot 11H_2O$ as a first products. Subsequently, this phase decomposes to $Al(OH)_3$ and $CaCO_3$. Calcium carbonate appears in the form of vaterite sometimes aragonite and then is transformed to calcite. pH of the solution seems to have a great impact on the $CaCO_3$ phase produced as a result of carbonation process. The carbonation of hydrogarnet $3CaO \cdot Al_2O_3 \cdot SiO_2 \cdot 4H_2O$ is much slower.

The well crystallized, autoclaved calcium silicate hydrates show low carbonation rate in spite of the higher lime content, than the amorphous forms of tobermorite, poorer in calcium [298]. However, Roy [80] found that the C–S–H richer in calcium than tobermorite, was readily carbonated and the equilibrium CO_2 partial pressure was lower.

The following properties are altered as a consequence of concrete carbonation: shrinkage (see Sect. 5.3.2), strength, porosity, susceptibility to deformations, and resistance to the environmental impact. However, the pH of pore solution in concrete decreases and the passive film on steel is deteriorated; therefore, the reinforcement is exposed to corrosion. This corrosion is probably the most frequent reason of concrete deterioration, because the rust formation causes the surrounding concrete to crack and spall (see Sect. 6.4.11.).

The pores structure is affected by carbonation too. The total porosity decreases and the pores size distribution is shifted towards larger dimensions. The larger pores are not specially altered, but the volume of smaller became lower. The diffusion rate in carbonated concrete becomes low, as well as the permeability, particularly at low w/c ratio. On the other hand the increased porosity was found in the case of slag

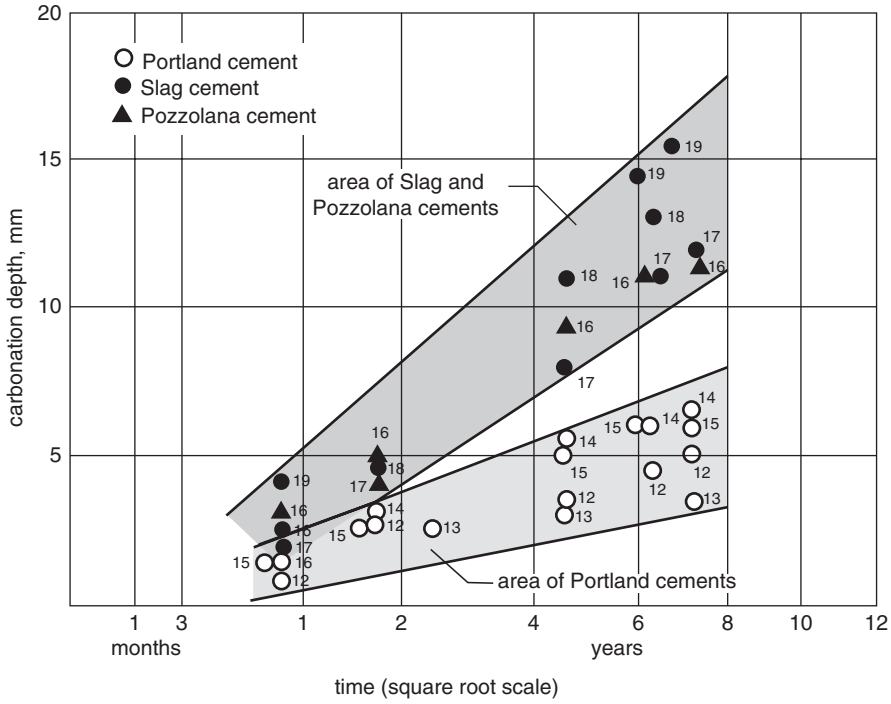


Fig. 6.70 Effect of cement type on the depth of concrete carbonation. (According to [301])

cement paste with high, 75% slag content [299]. The carbonation depth increases for cement pastes with fly ash too [299]. The curing conditions affect this process considerably. Finally, one should not prove the obvious effect of the degree of concrete mixture compacting.

There are, however, the contradictory opinions as the impact of particular mineral additions are concerned. According to many authors the progress of carbonation was higher in concretes produced from cements with slag and fly ash addition [300–304]. The carbonation is significantly accelerated in the case of cements with more than 50% slag and 30% fly ash [292], while the limestone Portland cements require the finely ground cement clinker component (see Chap. 7). The results obtained by Meyer [301] for a large number of cements and shown in Fig. 6.70, are a good example. From these results it can be concluded that the carbonation is slower in the case of Portland cement pastes without additions. Additionally Litvan and Meyer [302] found the reduction of total porosity and small pores share in concretes of Portland cement, while in the granulated blastfurnace slag containing concrete the total porosity was unaltered, but the fraction of large and medium pores became higher.

Analyzing these data it should be remember that the carbonation rate depends on the permeability of concrete, it means that is decreasing with lowering of w/c ratio

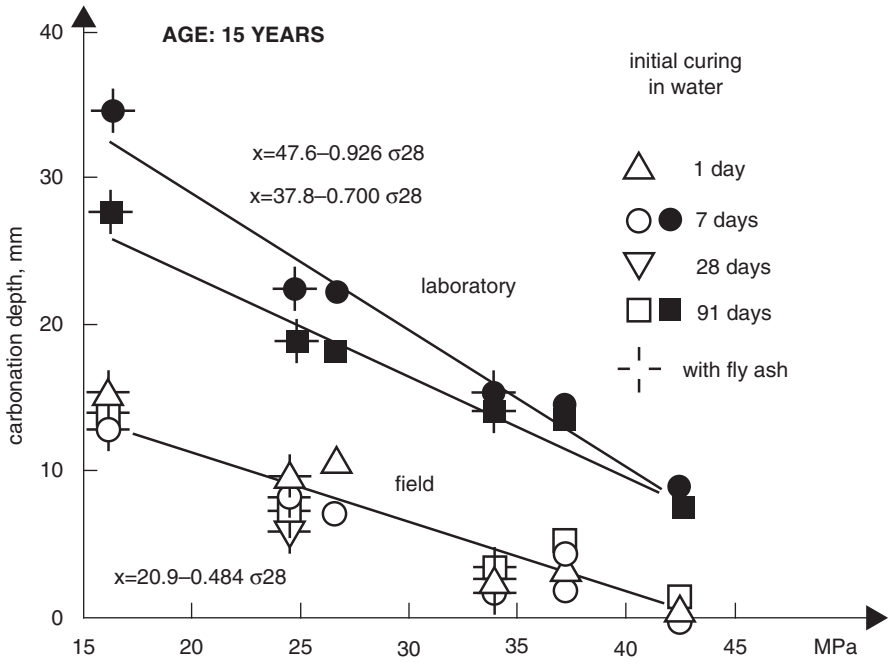


Fig. 6.71 Carbonation depth as a function of concrete strength [307]

and with increase of cement content in concrete [303]. Therefore the carbonation rate is inversely proportional to the strength of concrete. It is known that the hydration of mineral additions occurs more slowly than the hydration of clinker phases and the beneficial changes of porosity and permeability of paste (cement matrix) can occur after longer period of maturing. After this age the strength increase occurs, which exceeds strength of reference concrete, produced of Portland cement without mineral additions. Basing upon this observation the authors are of the opinion that the carbonation of concrete proceeds slowly when the high strength is attained, irrespectively of the type of cement used for concrete production [305–307]. The importance of proper curing should be underlined particularly in the case of cements with mineral additions at early age, up to 7 days after concrete placing. The proper treatment of fresh concrete is beneficial for concretes with silica fume [292].

The depth of carbonation as a function of concrete strength is shown in Fig. 6.71 [307]. There is a large number of data indicating no special difference in carbonation process of Portland and other cements, as their strength is similar [301, 308, 309]. Only in the case of low quality concrete with high w/c ratio and porosity, these concretes produced from Portland cement show better resistance to carbonation. One can explain the difference by higher total porosity of concrete with mineral additions at early age; however, their permeability after longer period of time is markedly improved (Table 6.9) [310].

Table 6.9 Relative permeability of concrete with and without fly ash [310]

Fly ash source	Content (kg/m^3)	w/c + FA[a]	Relative permeability (%)	
			After 28 days	6 months
None	0	0.75	100	26
Chicago	30	0.70	220	5
Chicago	60	0.65	1,410	2
Cleveland	30	0.70	320	5
Cleveland	60	0.69	1,880	7

[a] FA—Fly ash

Berry and Malhotra [118] conclude that in any high quality concrete with fly ash the carbonation process is comparable to this in concrete without mineral additions. Concrete with low cement content, not subjected to the proper curing at early age (stored at low humidity) will be undoubtedly susceptible for the action of various corrosions; physical and chemical, including carbonation [118].

Many different empirical formulae were proposed to determine the progress of carbonation. The thickness of carbonated layer as a function of carbonation time is the most frequently given by the following relation:

$$x = a\sqrt{t} \tag{6.24}$$

According to Venuat [293], Verbeck was the first to propose the following formula:

$$x = kt^{1/2} \tag{6.25}$$

where x is in cm, time in years; at constant value $k = 0.5$ the 0.5 cm thick layer is formed after 1 year and 5 cm after 100 years.

Kishitani (according to [293]), taking into account the w/c ratio, proposed the following empirical formulae:

a) $\mathrm{w/c} \geq 0.6$ $$t = \frac{0.3(1.15 + 3\mathrm{w/c})}{R^2(\mathrm{w/c} - 0.25)^2}x^2 \tag{6.26}$$

b) $\mathrm{w/c} < 0.6$ $$t = \frac{7.2}{R^2(4.6\mathrm{w/c} - 1.76)}x^2 \tag{6.27}$$

where t is given in years, x in cm; R means the constant equal from 0.2 to 6.4; for ordinary concrete from Portland cement $R = 1$.

Venuat [293] proposed the following empirical formula:

$$x = a\sqrt{t} + b \tag{6.28}$$

The constants a and b depend on the cement content in 1 m^3 of concrete; $a = 5$ for 350–500 kg/m^3, 12 for 300 and 15 for 200 kg/m^3 respectively. Constant $b = -2$ for

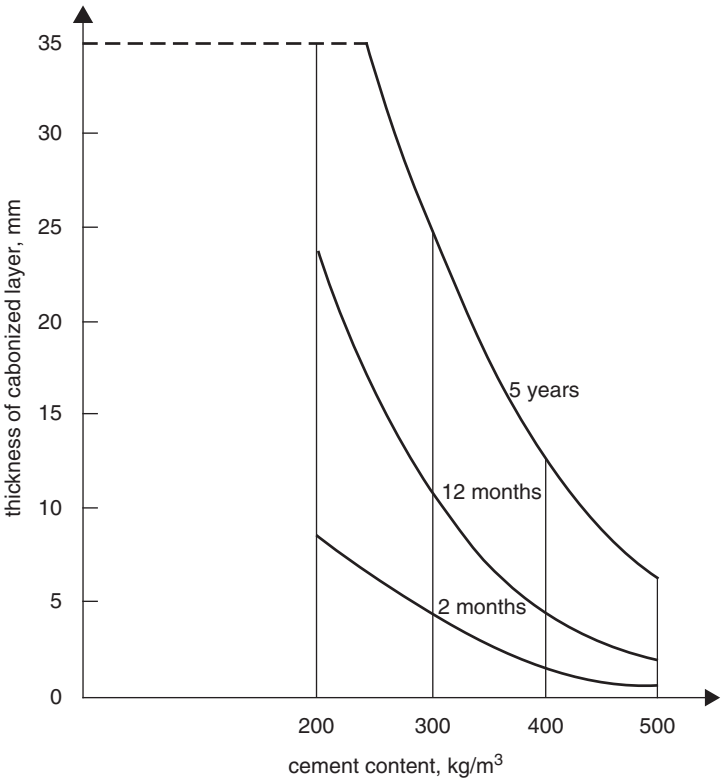


Fig. 6.72 Carbonation depth as a function of cement content. (According to [293])

500, 0 for 400, +2 for 350, 300 and 200 kg/m^3. Effect of cement content on the carbonation depth is shown in Fig. 6.72; carbonation is inversely proportional to this factor.

Duval [292] proposed the following formula, taking into account the strength of concrete:

$$x = \sqrt{365c}\left(\frac{1}{2.1\sqrt{f_{c28}}} - 0.06\right) \tag{6.29}$$

where x is the carbonation depth, in mm; c—time in years; f_c28—compressive strength after 28 days, MPa.

The carbonation depth markedly decreases at reduced w/c ratio, as it is shown in Fig. 6.73 [311].

In slag cements the slag fineness has a great impact on carbonation. In the case of Portland cement the thickness of carbonated layer was 15.5 cm after 5 years, and with 50% of slag ground to the specific surface 300 m^2/kg attained 20 cm after 2

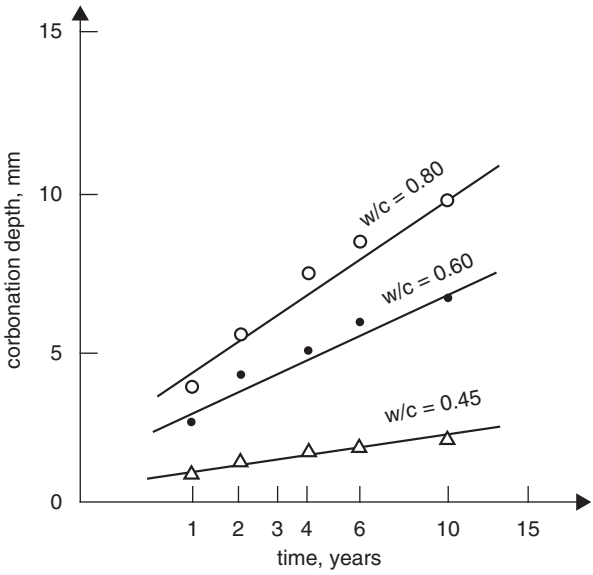


Fig. 6.73 Carbonation depth as a function of w/c ratio. (According to [311])

years. However, with the same slag addition, but with its fineness corresponding to the specific surface area equal 400 m^2/kg the thickness of carbonated layer was 14.5 cm after 5 years [293].

Carbonation can have a positive influence on the strength of concrete, and it has been used for a long time in practice [289, 312]. Carbonation is not effective in the case of fresh, poorly hardened concrete because it results in softening of concrete surface [61]. However, the surface carbonation of hardened concrete can improve the resistance to the attack of aggressive media, for example of sulphates [61].

The impact of atmospheric CO_2 on unhydrated cement, particularly at high relative humidity of air, leads to the calcium hydroxide and alite carbonation and even to the ettringite formation [61]. The formation of sodium and potassium carbonates or hydrogen–carbonates can be observed too. The significant advancement of these processes, worsen the properties of cement, enhancing water demand [61]. The formation of sodium and potassium carbonates is possible even as a result of $(N_2K)C_8A_3$ and $(N, K)C_{23}S_2$ decomposition, and their content of 0.2–0.5 % can cause false setting [61].

6.4.9 Soft Waters

The soft water attack occurs in the case of mountain torrents, and for example in the Scandinavian countries the water dams were destroyed by this process. The calcium hydroxide and other hydrates dissolution are involved in this corrosion mechanism. $Ca(OH)_2$ is dissolved before the other phases; sodium and potassium hydroxides are quickly leached out, because of their high solubility. However, according to Taylor

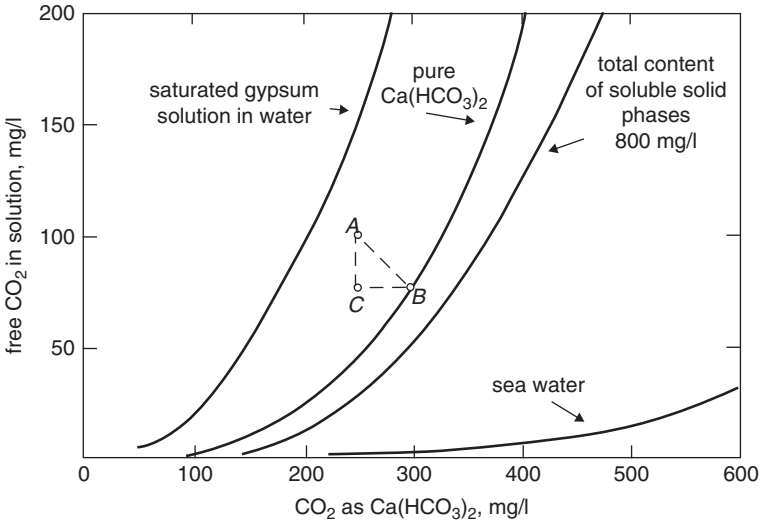


Fig. 6.74 Equilibrium curves of CO_2 and calcium bicarbonate concentration in the solution. (According to [98])

[222], the dissolution of paste components can occur at the same time, because of the high specific surface areas of the hydrates, particularly C–S–H. The $Ca(OH)_2$ dissolution process is markedly influenced by CO_2. Aggressive influence has only free CO_2, present in excess in relation to the amount necessary to form calcium bicarbonate and maintain it in solution, according to the formula:

$$CaCO_3 + CO_2 + H_2O \rightleftarrows Ca(HCO_3)_2 \tag{6.30}$$

According to Lea [98], CO_2 reacting with $Ca(OH)_2$ in solution gives $CaCO_3$, which subsequently transforms to bicarbonate. The CO_2 necessary to the $Ca(HCO_3)_2$ stabilization is not aggressive, because it cannot dissolve further parts of $CaCO_3$. Therefore more CO_2 is required in the solution. In the presence of other ions in the solution the equilibrium changes, as it is shown in Fig. 6.74. The amount of free CO_2 necessary for stabilization decreases and only in the presence of gypsum it is increasing. The following example shows how to apply the diagram plotted in Fig. 6.74: when the CO_2 and $Ca(HCO_3)_2$ contents in the solution are given by point *A*, CO_2 reaction with $CaCO_3$ in the solid phase causes the bicarbonate increase to the concentration given by point *B*; the amount of consumed, aggressive CO_2 corresponds to the segment *AC*. It means that the amount of aggressive CO_2 is 22 g only from the total content equal 100 g. The *AB* segment is sloped to the X–axis at angle of 45°. The CO_2 scale is two times greater than the $Ca(HCO_3)_2$ scale, because two moles of bicarbonate are formed from one CO_2 mol.

Portland cements of various phase composition do not give special differences in amount of calcium leached, while the slag cements do [98]. At paste surface carbonation the leaching of calcium is greatly reduced. This process results in gradual

strength decrease; however a significant reduction of strength is occurring when a significant amount of lime is leached [98]. For example at 18% lime decrease of the mortar, the strength lowering is 15%, but at 27% lime deficiency the strength reduction is 40%. In the pH range from 6 to 7 the leaching of lime is inversely proportional to pH.

The removal of components from the paste, as a result of exchange with liquid phase surrounding concrete, can proceed basically by two mechanisms:

- leaching as a result of water filtration through the paste under the difference of pressure,
- diffusion of components in the liquid phase, as a result of concentration gradient of the paste solution and surrounding liquid medium.

It is obvious that the same mechanisms can operate in opposite directions; it means that the introduction of ions from the surrounding liquid medium inside the paste can be possible. The mechanisms mentioned above are controlled by pores structure and permeability of cement paste.

Leaching, as well as diffusion is mainly dependent on the solubility of compounds in which the removed components occur. The basic information can be provided by the concentration of different ions in cement paste solution. On this basis conclusion can be drawn that among the components present in Portland cements the most readily will be leached sodium, subsequently slower calcium, and silicon significantly more slowly. This presumption are proved experimentally.

The rate of leaching of various untypical ions from cement paste has become the subject of interest, because of paste application for the stabilization of industrial sludge and storage of nuclear waste [80, 313]. The chlorides, iodides and sodium ions are rapidly leached from the paste. The rare earth and uranium compounds show low solubility in the pastes and their removal occurs with very low rate [80].

In the case of easily removable components of cement paste better immobilization can be attained by their transformation into the compounds less soluble in water, or by utilization of surface adsorption. The C–S–H in the paste is of significant importance in the last aspect. According to Barnes and Roy [314] after the portlandite leaching, C–S–H is the component which controls the removal of ions from the paste. Well known example of leaching ability reduction can be chlorides which are significantly lower leachable from the pastes with high C_3A content. All the permeability reducing factors, for example silica fume addition, will improve the immobilizing capacity. It was found that partial carbonation of paste causes the reduction of calcium and strontium leaching [315].

The studies on the immobilization of heavy metals in concrete have been developed for the last 20 years [316–320]. It has been found that the concrete is a very effective heavy metals immobilizing matrix. The combinations with AFm phases are formed; these phases have a layer structure and the exchange of OH^- ions with monovalent and bivalent anions is possible [317]. The strong adsorption on C–S–H gel is an important factor, and morphology of this phase is markedly modified [318]. Cement with zeolites addition can be applied to immobilize the radioactive elements [319]. Special cement with high aluminates content has shown high effectiveness for heavy metals immobilization [320].

6.4.10 Action of Frost on Concrete[10]

Damage of concrete in aggressive media is accelerated by ice formation. There are several factors affecting the destruction of concrete as a result of capillary water freezing. Water does not freeze in the gel pores, because they are too small for stable ice nuclei formation. The monomolecular layer of adsorbed water, bound with the surface forces, does not freeze too. The temperature of water freezing in capillaries varies with capillary diameter; it is assumed as equal of about −15 °C. The permeability of concrete is an important factor, because water is penetrating into it as a result of capillary action. The process occurs significantly more rapidly when concrete is under the unilateral hydrostatic water pressure.

One should remember that in concrete resistant to freezing and thawing the aggregate must be resistant and, taking into account its porosity, should not crack during freezing. However, as it has been pointed out by Pigeon [321], it is not a sufficient condition, since the aggregate can have an open system of pores and a significant amount of water is forced out into the paste during freezing; the destructive tensile stresses are thus generated. Such an aggregate cannot be used in concrete which should be freeze–thaw resistant.

The action of frost on concrete mixture and fresh concrete is specific, because it is concerning setting and hardening processes. The stresses generated in material do not cause damage because the concrete is still plastic, but at lower temperature the setting process, as well as the strength development, is retarded (Fig. 6.75) [278]. The deleterious effect of low temperature is compensated by use of warm mixing water and heat exchange reducing cover. The use of cement with high heat of hydration is recommended. The reactions in the mixture after freezing of water are stopped. The following factors are important when the concreting must be done at low temperature:

a) water content in the mixture (low w/c ratio),
b) type and content of cement,
c) initial curing conditions (covers).

In Fig. 6.75 the relative rate of hydration is shown in respect to the rate of hydration at temperature of 20 °C. According to the authors [278] this curve showing the hydration rate can be described with Arrhenius equation. However, it seems that too high simplifications were assumed. However, the experimentally derived relation, in which the heat of hydration will be used, is well adjusted to this curve.

In the case of hardened concrete the saturation with water is a very important as a factor of frost resistance. Some authors propose the following relation for the degree of critical water saturation of concrete:

$$\frac{\text{freezable water content in concrete}}{\text{free space available for water}} < 0.9 \tag{6.31}$$

[10] This question is discussed in details in a book by M Pigeon and R. Pleau, "Durability of Concrete in Cold Climates", Taylor & Francis, London and New York 1995.

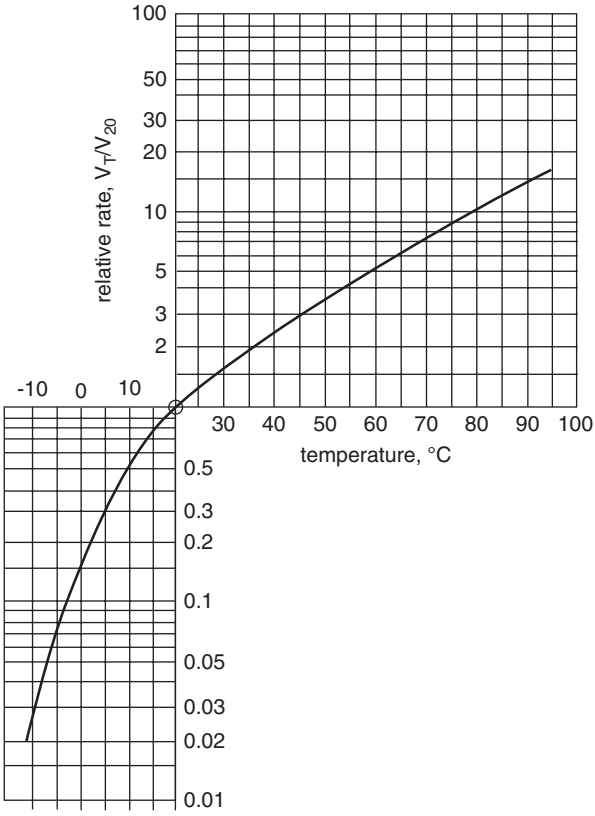


Fig. 6.75 Effect of temperature on cement hydration. (According to [278]) Duval R., Hornain H., Chapter 9 in « La Durabilitè des Bètons », page 383, fig. 9.13 « Influence de la tempèrature sur la rèaction d'hydratation du ciment Portland », Published by Presses de l'Ecole Nationale des Ponts et Chaussèes, reproduced with the permission of the Presses de l'Ecole Nationale des Ponts et Chaussèes

Fagerlund [322] presented a method for determination of the critical degree of saturation (S_{cr}) based on modulus of elasticity measurement after six freezing and thawing cycles (Fig. 6.76a).

The resistance of concrete to freezing and thawing is dependent, primarily on its porosity and absorbability [323]. Low quality concrete has high absorbability [324].

The determination of total concrete porosity is not sufficient. The pores structure should be taken into account. The following types of pores can be distinguished:

a) pores in aggregate;
b) air pores always present in concrete in some amount or entrained specially by use of air entraining admixtures. The pore diameters are in the range from 10 μm to 1 mm, their volume ratio can be from 1 to 6%;
c) capillary pores resulting from excess water, not used in cement hydration. They play a decisive role in concrete permeability and their diameters are in the range from 1 to 10 μm;
d) gel pores occurring in the cement gel and constituting usually 26% of its volume; they are smaller than 2.5 nm.

This classification is very important for understanding the phenomena occurring at the action of freezing, since the freezing of water occurs gradually, starting from

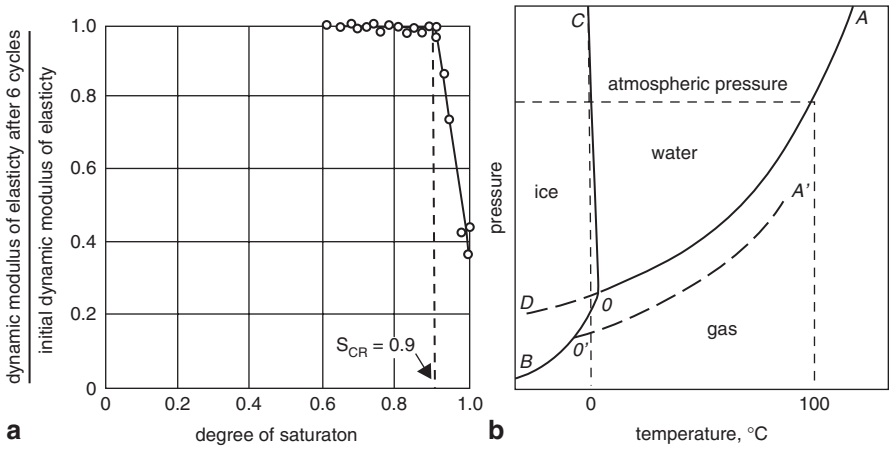


Fig. 6.76 **a** Relationship between the relative dynamic modulus of elasticity and the degree of saturation of concrete after six freezing and thawing cycles. (After [322]). **b** H_2O system; O'A' curve corresponding to the vapour pressure of solution, OD curve corresponds to the vapour pressure of the supercooled water

the largest pores and, as a temperature falls down, is continued in the smaller one (see Fig. 5.24). In gel pores water does not freeze at all, because the nuclei of ice cannot be formed in them, in any case not at temperature higher than −78 °C [287]. Simultaneously, it should be remember that the liquid phase in the paste occurs as a solution, less or more saturated with various soluble salts, primarily with sodium and potassium hydroxides. According to the Raoult law this lowers freezing temperature, because of the water vapour pressure decrease of the solution (Fig. 6.76b).

There are the three main hypotheses explaining the mechanism of concrete destruction under the action of freezing and thawing:

- hydraulic pressure hypothesis of Powers [325],
- osmotic pressure hypothesis of Powers and Helmuth [326],
- thermodynamic hypothesis of Litvan [327].
- These three hypotheses correspond well to the experimental data.

Powers [325] assumed that water is freezing gradually, and in remaining solution the concentration of soluble salts is increasing. As the temperature decreases, the ice content in capillary pores augments and because water freezing increase its volume of 9 %, it is forced out from the capillaries. It causes water flow to the air pores. The flow and the pressure increase with the rate of freezing (rate of temperature decrease) and with the amount of freezing water. The pressure is increasing also with the distance of water travel to the air pore. The cracks appear when this pressure is higher than the tensile strength of concrete. This hypothesis explains well the importance of air entraining of concrete, and air–void critical spacing factor, equal to the half of distance between the pores walls.

In further experiments Powers and Helmuth [326] found that water is moving to the capillaries in which ice is produced, that is towards the colder zones. Basing on

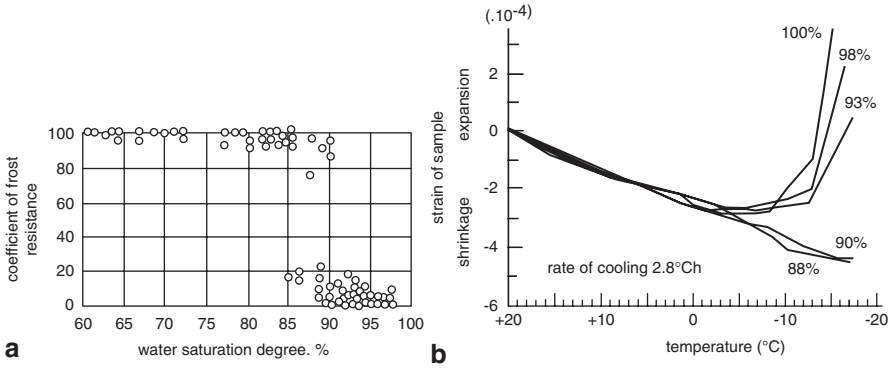


Fig. 6.77 **a** Effect of concrete saturation with water on the freeze–thaw resistance. (according to [287]). **b** Effect of concrete saturation with water on dimension change of concrete, in the case of slow cooling. (After [417])

these observations they proposed the osmotic pressure hypothesis. Because of the effect of surface tension, increasing with decreasing capillary radius, the freezing of water occurs at first in the larger pores. Simultaneously, the concentration of salts in water being in equilibrium with ice grows up continuously and is much higher than the "initial" concentration in smaller pores, in which the ice is not formed. The osmotic pressure is generated as a result of this concentration gradient and water moves from the smaller to the larger pores. However, in the latter ones there is no place and the pressure increases. This osmotic pressure associating the freezing of water in concrete augments with increasing concentration of salts in the paste pore solution.

Litvan [327, 328] paid an attention to the fact that over the supercooled water the vapour pressure would be higher than over ice (OD section of vapour pressure curve in Fig. 6.76b). Because of the surface tension effect the ice will be formed firstly on the walls of air bubbles and water will be moving toward these pores or toward the surface of concrete, to compensate the difference of vapour pressure. Basing on the Kelvin law one can presume that water will be transferred at first from the larger pores and, as the temperature falls down, from the smaller and smaller ones. Similarly as in previous hypotheses high rate of cooling and the amount of water potentially freezable, promote the transport of water. The pressure augments too with the distance to be overcome by water. All these factors accelerate the destruction of concrete.

It has been found in many experiments that the deleterious action of frost depends on the concrete saturation with water, as aforementioned, and became dangerous above the value of 85 %.

The degree of concrete saturation with water is influencing also by the dimension change of concrete during freezing (Fig. 6.77a) [417]. Thermodynamical analysis shows that water should freeze outside porous material (concrete) and when freezing is proceeding slowly, close to equilibrium condition, it causes the shrinkage of concrete, when water saturation is below the critical value [417]. Higher water

saturation is causing expansion (Fig. 6.77b) [417]. However, high rate of cooling is causing expansion of concrete [334].

It is difficult to find a simple correlation between the freeze–thaw resistance and concrete saturation with water, because there are many factors involved. These factors have an impact on the porosity and they are as follows: pores in aggregate grains, paste–aggregate interfacial transition zone, capillary pores ratio in the paste, gel pores, air–voids entrapped during concrete mixture production[11]. However, the microstructure and porosity of cement paste is of principal importance.

The decrease of freeze–thaw resistance with increasing rate of temperature changes, as well as a better freeze–thaw resistance tested in humid air than in water, was proved in laboratory experiments [98]. The concrete samples are deteriorated more rapidly when dried between the cycles of freezing and thawing.

Air entrainment is the best way to improve concrete frost resistance. The air pores surrounded by gel are filled with water with difficulty, particularly when their surface tension is lowered by use of air entraining agents. These admixtures and ways of their action are discussed in Sect. 6.6.4. They are surfactants, composed of non–polar hydrocarbon chains or the other hydrophobic groups, linked with the following hydrophilic groups: $-COO^-$, $-SO_3^--NH_3^+$. On the gaseous and liquid phase interface the polar groups are turned to water—they reduce its surface tension and decrease the pressure in air bubbles. The formation of these air bubbles is therefore promoted and their agglomeration is hampered. On the liquid–solid interface the polar groups are linked with the surface of solid and the non–polar "ends" are turned to water; therefore the cement grains become hydrophobic and the air bubbles can be attached to them (see Fig. 6.89). It causes the best condition for regular air bubbles distribution in concrete mixture. Small air bubbles system formation in concrete reduce the distance for water to travel, and the possibility to generate a high hydraulic pressure is restricted. Therefore, the mean distance between the air bubbles, the so–called air–void spacing factor, is very important. It is accepted that this spacing factor should be equal 250 μm (Fig. 6.78a) [329]. According to Helmuth [330], the travel of water to the air bubbles occurs in non–saturated condition, therefore, in this case hydraulic pressure does not depend on the flow distance and the spacing factor is not important. However, the spacing factor, or rather uniform distribution of air bubbles in cement matrix, are important in this sense that they allow the formation of micro–areas, in which the volume and pressure changes, generated during water freezing in pores, can be unloaded. Pigeon and Lachance [331] proved once again the importance of spacing factor and suggested its minimum value as 680 μm at w/c = 0.5. However, experiments of Okada et al. [333] are proving that the critical air–void spacing factor should be lower, not exceeding 200 μm, and only for concrete with very low w/c ratio can be higher (Fig. 6.78b).

[11] The term "critical degree of water saturation of concrete " was introduced by G. Fagerlund; this factor allows to evaluate the freeze–thaw resistance of concrete [322]. The RILEM method of concrete frost resistance is based upon this definition (Matér. Constr. RILEM, 1977, 10, 58, 217).

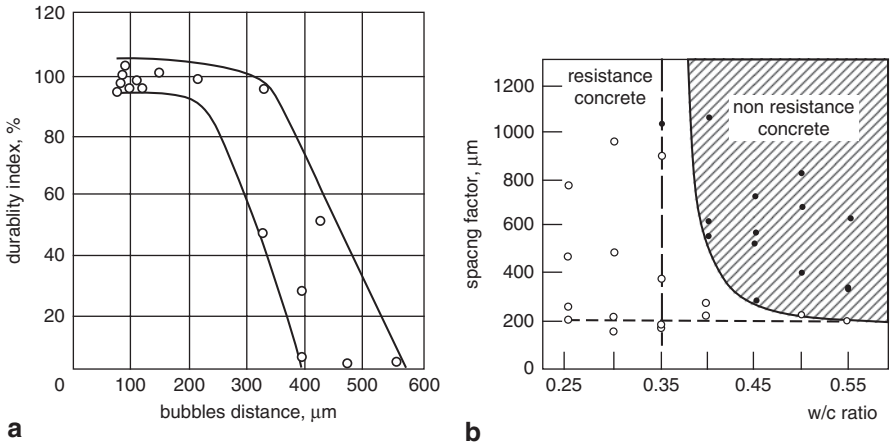


Fig. 6.78 **a** Effect of air–void spacing factor on the durability of concrete. (According to [287]). **b** Relationship between the air–void spacing factor and w/c ratio of concrete; the curve fixes the critical air–voids spacing factor. (After [333])

It is the opinion that air content in concrete should be kept on the level 4–5 % by volume. However, at extremely severe conditions of concrete freezing in sea water this value should be two times higher [98].

The freeze–thaw resistance of high performance concrete is a controversial problem. According to some authors, the HPC over the 80 MPa class are resistant to the action of frost and deicers, without the air entrainment, mainly because of the low w/c ratio in the range 0.25–0.30 [332, 333]. However, many of them conclude that the air entraining agent should be applied "in any case". In a review contribution Carles–Gibergues and Pigeon [334] agree with this conclusion because of the relatively short period of time since when the HPCs have been applied in constructions and relatively not too long experience with these composites. Finally, these authors [334] are of the opinion that in the case of concretes with $w/c \leq 0.25$ and showing the strength ≥ 100 MPa the air entrainment is not required. Also Aïtcin [406] states that HPC from Portland cement with w/c ratio in the range 0.26–0.30 is resistant to freeze–thaw cycles without air entrainment. This conclusion is valid for HPC with or without silica fume [406].

Many research were focused on the effect of fly ash, silica fume and granulated blast furnace slag addition on the concrete freeze–thaw resistance. All these additions improve the freeze–thaw resistance, as compared with the concrete from Portland cement, however, on condition that all these concretes are air entrainment [80]. Freeze–thaw resistance of concrete with fly ash can be lowered in the case when it has high coal content. The limit value, increased recently to 9 % (according to the European standard EN 197–1:2002/A3:2007), is too high and the 5 % level should be maintained, as it was recommended by the elder directives (previous standard EN 197–1:2002). The effect of non–combusted coal on the applicability of fly ash is discussed in details in Sect. 7.4.

Special cements with silica fume, giving condensed, compact pastes (DSP) with high content of ultra–fine particles, have very good freeze–thaw resistance [80]. It is caused by extremely low capillary porosity and hence very low content of freezable water in these pastes. The same remark can be related to the reactive powder concrete (RPC), for example the Ductal type composite [335]. This question will be discussed in Chap. 10.

Observations of field concrete structures and many experiments have shown the acceleration and strengthening of concrete destruction process during freezing and thawing in the case of additional action of de–icing salts. They cause primarily surface scaling of concrete, however, in unfavorable conditions cracking and damage of the concrete elements can occur. It is enough to remind that in the USA the cost of bridge repairs in 1975 was 200 million $; this was the consequence of the large scale application of de–icing salts on roads, in the sixties [63]. Cracking due to internal pressure generated by the action of frost in hardened cement matrix is not very common nowadays, probably because most concrete are sufficiently protected by the use of air entrainment agents.

There is no general theory explaining the destruction mechanism of concrete in the presence of de–icing salts. As it results from the huge amount of experimental data this mechanism is very complex. Various physical and chemical processes are overlapping, however, the opinion of dominating role of physical factors prevails.

The effect of frost and de–icing salt cannot be separated; there are even numerous experimental proofs that the harmful consequences of freezing and thawing cycles are strengthened. However, typical chemical reactions cannot be excluded; such an approach would be misleading. The hypotheses related to concrete deterioration as a result of freezing of water, particularly that one based on the role of osmotic pressure, allows more precisely presenting the effect de–icing agents.

Numerous experimental data allow to distinguish main factors, having the principal importance in the process of concrete destruction under the action of frost, associated with de–icers impact. The two chlorides: calcium and sodium, are mainly used as de–icing salts[12]. Discussing the effect of de–icing salts on concrete it should be remember that the migration of ions from these salts will cause the increase of ionic power of concrete pore solution. This would result in significantly lower vapour pressure and higher concrete saturation with moisture (Fig. 6.76b). Simultaneously, the drying of concrete through evaporation of moisture to the surrounding atmosphere will be significantly lower. The growth of the osmotic pressure, proportional to the concentration of the solution, will be the second factor. Water from the deeper concrete parts, due to the osmotic pressure, will be raised toward the surface concrete layers, in which the concentration of salts is higher. These surface layers will be not able to absorb this water and simultaneously water cannot take out to the surface through the layer of ice; hence the pressure is generated and the outer concrete layer is raised up. In such a way the scaling of concrete occurs [336].

[12] Nowadays the organic compounds are widely used as de–icers; for example those based on acetates; on the airports the glycol de–icer has been put into use long time ago.

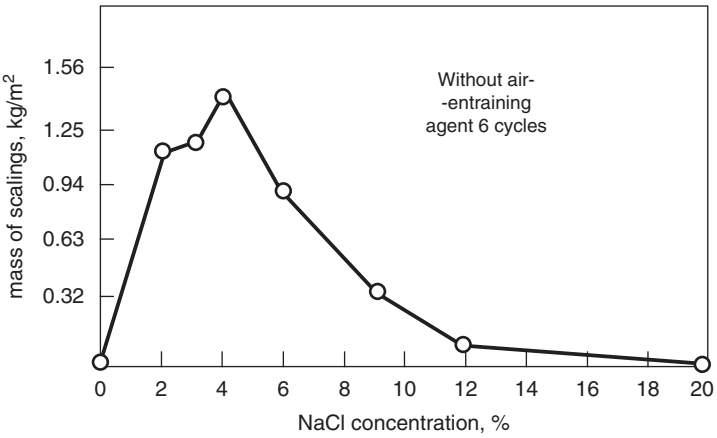


Fig. 6.79 Effect of NaCl concentration on the degree of surface scaling of concrete. (According to [339])

There are the other factors involved in this process too. Rösli and Harnick [337] paid an attention that the covering of frozen concrete with de–icing salts will cause thermal shock, as more intensive as temperature of environment is lower. For the ice layer melting on the concrete surface heat supply of 330 J/g of ice is required. Melting of 1 mm thick ice layer on the 1 m^2 concrete surface requires 330 kJ of heat; this energy must be taken from the concrete mass under the ice cover. Therefore the application of de–icing salts on concrete surface results in thermal shock and, as a consequence, the microcracks can appear. In these conditions the infiltration of salt solutions inside the concrete occurs easily.

The most severe scaling was observed by many authors for medium concentration of salts (Fig. 6.79) [338, 339]. Though the osmotic pressure increases with salt concentration, but simultaneously temperature of water freezing in concrete is decreasing. As a result of these two opposing factors, the most intensive scaling occurs at the medium salt concentration, equal 2–4 %. According to many authors this is the proof for predominant physical mechanism of this process [287].

Summarizing it can be stated that the use of de–icers on the concrete road pavements can generate the following phenomena:

- surface scaling due to the osmotic pressure,
- microcracks due to thermal shocks,
- chemical reactions.

The corrosion of concrete in chloride solutions was discussed in Sect. 6.4.4; here it can be only remained that the basic calcium chlorides formed in this process are expansive. Yang et al [339] measurements of samples length changes, with increasing number of cycles of wetting and drying, are very instructive. They found (Fig. 6.80) the continuous length increase for the samples stored in salt solutions; the samples after drying were longer than after wetting, that was contrary to the water storage. Length increase was rising with solution concentration.

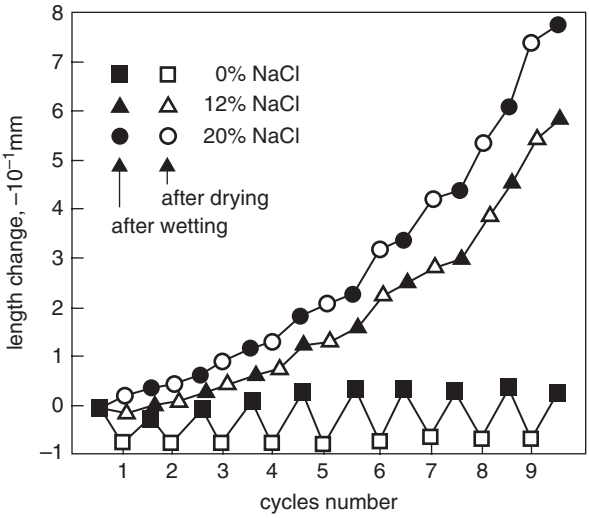


Fig. 6.80 Effect of NaCl concentration on the length change of concrete specimens during wetting and drying. (According to [339])

Numerous research allowed the determination of factors controlling the durability of concrete highway pavements. The highway should be properly protected against water access, because water is strongly destructive agent for every road pavement. At sufficient drainage the critical degree of concrete water saturation will be not attained. Simultaneously, the porosity of road concrete pavements should be low; the w/c ratio on the level of 0.4 or less is suggested. The high cement content in concrete should be maintained. The high quality aggregate, with low dust fraction content, must be used. Moreover, air entraining agents should be added to concrete. The resistance to scaling is related to the 200 μm air–void spacing factor value; internal microcracking of concrete is also simultaneously hampered. Finally, the concrete on the road pavement should be matured in proper conditions, subjected to careful curing. When the concrete complies with the requirements listed above, the excellent durability will be ensured, for 50 years or more, even at high intensity of road traffic. It should be mentioned that the Gliwice–Opole highway in Poland, built of concrete slabs by Germans, was in very good condition for 75 years, and now was demolished only because the change of this road location.

6.4.11 Corrosion of Steel in Concrete

In a good quality concrete the reinforcing steel is protected against corrosion[13], because it is in cement paste covering of pH from 12.5 to 13.5, or at least 11.5. Steel is then covered by a passive film of the thickness from 1 to 100 nm, composed of

[13] The corrosion of reinforcement is discussed in details in a book by Grzegorz Wieczorek, "Concrete corrosion initiated by chlorides or carbonation of concrete cover", Editor: Dolnośląskie Wydawnictwo Edukacyjne, Wrocław 2002. (in Polish).

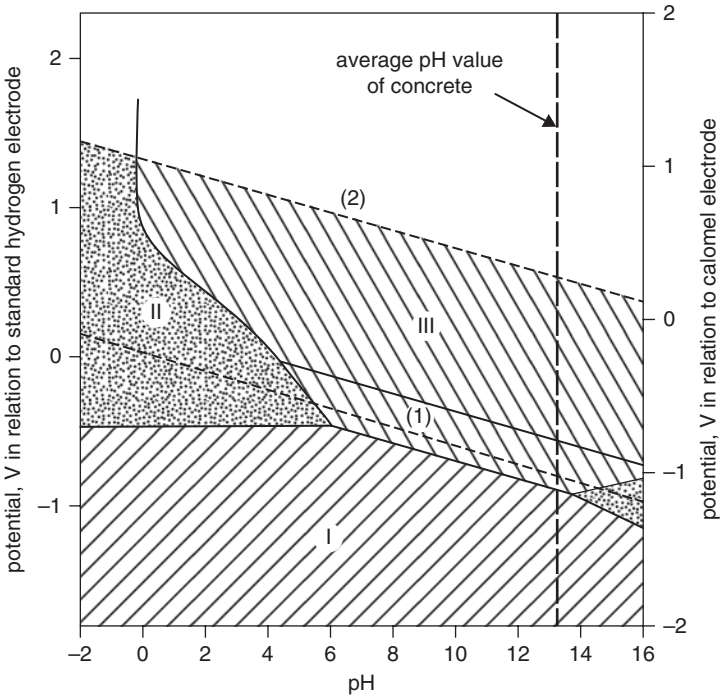


Fig. 6.81 Fe–H_2O diagram in the pH–E coordinates system. (According to [341])

γ–Fe_2O_3 and Fe_3O_4 [340]. This passivation role of paste in concrete is maintained as long as the concrete complies with the following requirements:

- lower permeability and higher homogeneity,
- greater thickness of paste cover surrounding the reinforcement,
- higher calcium hydroxide content.

However, concrete is exposed to the action of external factors, primarily of CO_2, SO_2, chloride and sulphate solutions which causes pH decrease below 11. The analysis of the influence of pH changes on the durability of reinforcement in concrete can be done based on the equilibrium system elaborated by Pourbaix [341] for iron (Fig. 6.81). This is a diagram in the coordinate system: pH—potential of metal, in relation to its salts. The thin, horizontal line represents the potential of semi–cell Fe^{2+} |Fe, which is independent of pH of solution.

Three areas relating to the various state of iron can be distinguish on this Fe–H_2O diagram: the first one (I) in which iron is inert, and cannot be corroded (Fe), the second one (II) corresponding to the formation of $Fe^{2+} = FeOOH^-$; it means that the corrosion of iron occurs, and the third one (III) in which iron became covered with Fe_3O_4film (straight line 1) or Fe_2O_3 (straight line 2) i.e. became passive and corrosion process does not occur.

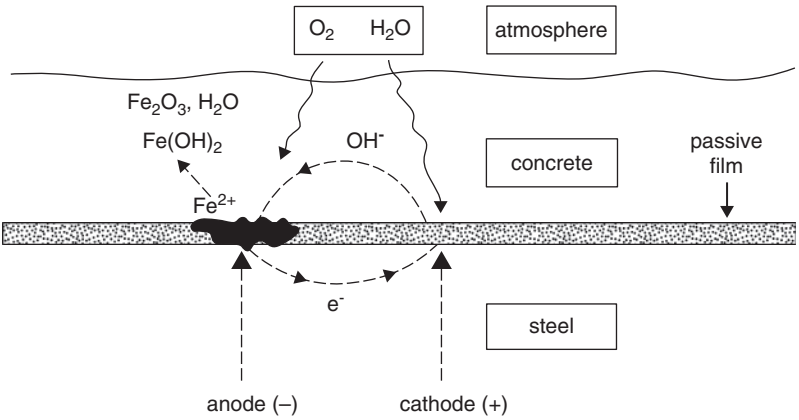


Fig. 6.82 Scheme of reinforcement corrosion in concrete. (According to [343])

Conclusion from this diagram is that in the case of pH 13, typical for concrete, iron is in equilibrium with Fe_3O_4 or Fe_2O_3, at a potential of −900 mV; below this value corrosion does not occur. At higher potential the oxides, Fe_3O_4 or Fe_2O_3 are formed and the passive film on reinforcement is thus produced, effectively decreasing the rate of corrosion, which became negligible low.

From the Pourbaix diagram [341] results that the potential of iron in the passive state can vary in a wide range, from −900 mV to +200 mV, depending on the availability of oxygen. In the surface of concrete in contact with air at ambient conditions, the measured values of corrosion potential are between −200 mV and +100 mV (the reference scale for the calomel electrode), that is clearly above the passivation range indicated on the Pourbaix diagram [341].

The studies of passive film on steel in concrete have shown that it is composed of Fe_3O_4–γ–Fe_2O_3 solid solution. In the case of passive film damage and initiation of corrosion process potential is changing to the more negative values: from −400 mV to even −1,000 mV.

In the presence of chloride ions passivation of steel needs higher pH value. Several hypotheses were proposed to explain the mechanism of passive film destruction in the presence of chlorides [342]. Possibility of chloride ions penetration to passive film, the effect of electric field generated around the adsorbed chloride ions, promoting of Fe^{2+} ions diffusion from the surface of metal are listed. Other factors will be discussed farther.

The corrosion of iron is an electrochemical process occurring in the presence of electrolyte and with access of oxygen (Fig. 6.82) [343]. As a result of different ions concentration in solution and inhomogeneity of steel formed by the grain boundaries, and regions in which the stresses occur—the local electrical cells are formed in the form of anodic and cathodic micro-areas on the surface of metal. On anode the process of iron oxidation is occurring:

$$2Fe \rightarrow 2Fe^{2+} + 4e^{-} \tag{6.32}$$

while on cathode:

$$2H_2O + O_2 + 4e^- \rightarrow 4OH^- \tag{6.33}$$

The anode and cathode on the surface of metal are connected by a metallic conductor which allows the passage of electrons, while in the surrounding medium, being an electrolyte, assures the transport of ions by diffusion and is closing the circuit of cell (Fig. 6.82).

Then the iron(II) ions will react with the OH^- ions with the soluble iron hydroxide formation:

$$Fe^{2+} + 2OH^- \rightarrow Fe(OH)_2 \tag{6.34}$$

In the presence of oxygen the process will be continued:

$$2Fe(OH)_2 + \frac{1}{2}O_2 \rightarrow 2FeOOH + H_2O \tag{6.35}$$

The hydroxide $Fe(OH)_3$ and oxide Fe_2O_3 will be produced too.

The rust is composed of the mixture of the following phases: $Fe(OH)_3$, Fe_2O_3, $Fe_2O_3 \cdot H_2O$ (gëthite and lepidocrockite), as well as magnetite.

The rate of corrosion process will depend on the conductivity of electrolyte and the difference of potential between the anode and cathode. Particularly the oxygen access, necessary for the cathodic reaction, can be the factor limiting the rate of corrosion [98]. Simultaneously, as a result of corrosion current, the polarization of electrodes occurs (their potentials increase in respect to the equilibrium potential values) and the dynamically maintained potential value has the deciding effect on the corrosion rate. In the case of steel in paste environment strong polarization of anodic microareas occurs, which increase anodic potential, decreasing the difference of potential in respect to cathode; therefore, as it results from the curves in *E*–pH system, the passivation of steel due to the oxides film occurs [98].

The steel corrosion rate in concrete will be higher in the presence of chloride ions, which reduce the anodic polarization and enhance the conductivity of the paste [226]. Other factors are influencing also concrete resistivity, namely the low w/c ratio, low humidity and temperature decrease, all result in resistivity increase. Therefore, in dry concrete or immersed in water, its corrosion is negligible.

Chlorides are initiating the corrosion on the surface of metal, however, the mechanism of this process is not fully understood. The catalytic effect of chlorine is considered. Depassivation of film on the steel surface can occur by its dissolution or by diffusion of chloride ions through this film.

Very low concentration of chloride ions, on the level of 0.01 %, can modify the morphology of passive film causing the compound FeOOH and then unstable complex $FeCl_3^-$ formation, which is bonding OH^- ions according to the reactions:

$$Fe + 3Cl^- \rightarrow FeCl_3^- + 2e^- \tag{6.36}$$

$$FeCl_3^- + 2OH^- \rightarrow Fe(OH)_2 + 3Cl^- \tag{6.37}$$

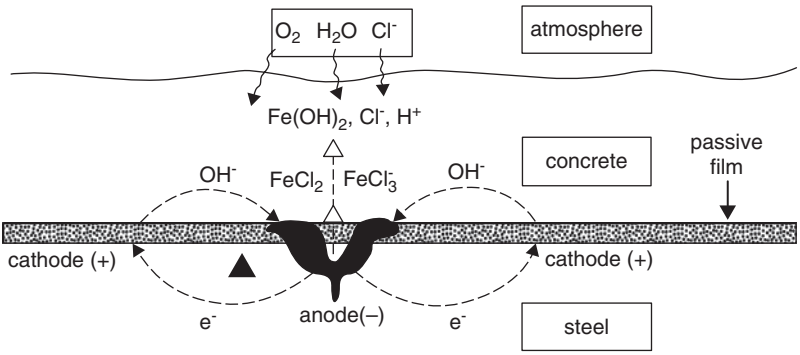


Fig. 6.83 Effect of chloride ions on the reinforcement corrosion in concrete. (According to [343])

Electrons, liberated by oxidation reaction, are transported in metal to the cathode microareas. As a result of these reactions, the pH lowering occurs and the chloride ions are recovered (Fig. 6.83).

Corrosion of metal is localized in small pits, which are the anodic microareas, and surrounding passive film forms cathodic great surfaces. A high cathode/anode surface area ratio gives locally a high density of corrosion current. At pH increase due to the OH^- ions generated in the cathode areas, the possible external aggression is restricted in these areas. For further reaction occurring, Cl^- ions should be formed at the expense of OH^- ions and maintain Cl^-/OH^- ratio higher than the critical value of depassivation. At high Cl^-/OH^- ratio rapid depassivation of steel occurs and the effective diffusion coefficient is violently increasing. According to Raharinaivo [344] this coefficient increases from 12×10^{-12} in the case of concrete in which corrosion of reinforcement does not occur, through the value of 49×10^{-12} in concrete with microcracks of low width (≤ 0.3 mm) to 80×10^{-12} cm^2/s in the concrete with microcracks width above 0.5 mm. The direction of microcracks run has a great impact on the corrosion progress: when their run is perpendicular then the reinforcement corrosion is localized in small areas; when their run is parallel to the reinforcement the process occurs rapidly and the spalling of paste from the reinforcement occurs.

It is assumed that the critical Cl^-/OH^- ratio, above which corrosion commences is 0.6. When the concentration of Cl^- is lower, a stable iron (II) hydroxide is formed, and in inverse case, this hydroxide is not stable and transforms into an intermediate product, so–called "green rust" and finally the chlorine containing $Fe_2O_3 \cdot H_2O$ is formed.

Various factors affecting the Cl^-/OH^- ratio in the paste and controlling the period of time, after which the threshold value 0.6 is exceeded and the corrosion process begins are searching. It has been known for a long time that the chloride ions which react with calcium aluminate to form the Friedel's salt: $C_3A \cdot CaCl_2 \cdot 10H_2O$, do not accelerate the corrosion of steel [209, 214, 344]. However, it is difficult to find a relation between the total chloride content in concrete and the amount of free chloride

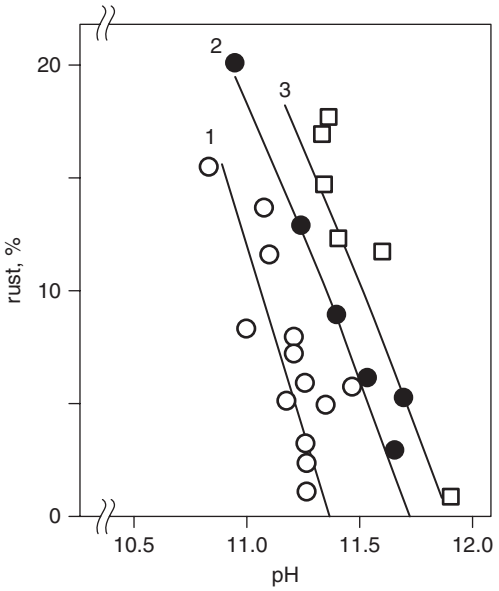


Fig. 6.84 Effect of pH on the corrosion of steel in carbonated concrete (*1*) or in the presence of chlorides: 0.12 % NaCl (*2*) and 0.18 % NaCl (*3*). (According to [346])

ions which react with the passive oxide film. As it was proved experimentally there is no relation between the C_3A content in cement and the concentration of harmful chlorides [63]. On the contrary, in some cases at lower C_3A content the higher chloride concentration is admitted. In the presence of chlorides the final result depends upon the pH and on their acidic interaction with iron to form the iron(II) chloride [345]. The latter can subsequently generate the hydrochloric acid in the other microareas, according to the following reaction scheme:

$$FeCl_2 + 2H_2O \rightarrow Fe(OH)_2 + 2HCl \tag{6.38}$$

Deep pits in the reinforcement are formed as a result of this reaction [60, 342].

According to the recommendation of American Concrete Institute the content of chlorine in cement should be as follows: 0.06 % for the pre–stressed concrete, 0.10 % for the reinforced concrete structure in humid environment, exposed to the external attack of chlorides, 0.15 % for the concrete in the same conditions but without chlorides access. There are no restrictions for the dry reinforced concrete without contact with the ground.

The progress of corrosion is beginning from the chloride ions concentration equal 0.5 % in relation to the mass of cement, and its rate is proportional to the increasing concentration up to 2 %. Simultaneously in the presence of chlorides the process commences at higher pH than it would occur without chlorides [346] (Fig. 6.84).

Very important information on steel passivation in concrete can be assessed from the measurements of anode and cathode polarization potential in the function of current density [60, 63].

The specific resistivity of concrete is of special importance in the corrosion process, as can be derived from the presented discussion. This property is influenced

by the moisture content in concrete, concentration of ions in concrete pore solution, pores structure and temperature [226].

Chlorides concentration of 0.6% by mass of concrete is reducing the resistivity two times [60]. Therefore, the progress of reinforcement corrosion in concrete can be assessed from measurements of surface resistivity [60].

The initiation of reinforcement corrosion causes the destruction of concrete, as a result of expansion, because iron is increasing six times its volume by oxidation if it is assumed that rust is composed mainly of $Fe(OH)_3 \cdot 3H_2O$. As a result microcracks and fissures are generated in concrete, which increase significantly its permeability for liquid and gaseous media.

The mathematical models were elaborated which give the possibility to calculate the rate of reinforcement corrosion and to evaluate the life time of concrete structure, depending on various factors [80].

The comprehensive study of reinforcing steel corrosion and methods of concrete protection against this process can be found in Ściślewski [347] book.

The most important methods of reinforcing steel protection are the following:

- covering of reinforcement with the protective coatings (epoxy resins, cement suspensions with addition of some bitumen compounds, asphalt solution in toluene,
- electroplating,
- application of corrosion inhibitors: inorganic—i. e. sodium nitrate(III) (nitrite), organic—sodium benzoate [348],
- proper choosing of concrete composition,
- covering of concrete with the protective coatings.

The electrochemical methods of chloride ions removal from concrete have been proposed more recently [349], as well as the cathode protection of reinforcement [286]. The question of electrochemical methods application to the reinforced concrete repairs was discussed in detail by Zybura [350]. This author is recommending primarily cathodic protection in the case of chloride corrosion and for chlorides removing from concrete. The electrochemical methods are successfully used to recover the high pH value in the strongly carbonated concrete [350, 351]. Under the action of direct current which positive pole is the steel net immersed in an electrolyte covering concrete surface, and reinforcing bars are a negative pole, the reduction of hydrogen ions and electrolysis of water, with the formation of OH^- ions occurs (Fig. 6.85). This method allows the reconstruction of passive film on steel and hampering of corrosion process [350]. However, the electrochemical methods of concrete renovation are expensive and can be applied in the case of structures of great economical or cultural value.

The application of so called “wandering” corrosion inhibitors is among the modern methods of the damaged structure repair. The sodium monofluorophosphate is used for this purpose [USA patent no 5071579], as well as the potassium monofluorophosphate, patented in Europe by Domtar Inc. The clean dry surface of concrete is covered by the monofluorophosphate water solution or in the form of gel; the phosphate ions infiltrate the concrete and reconstruct the passive film on reinforcement.

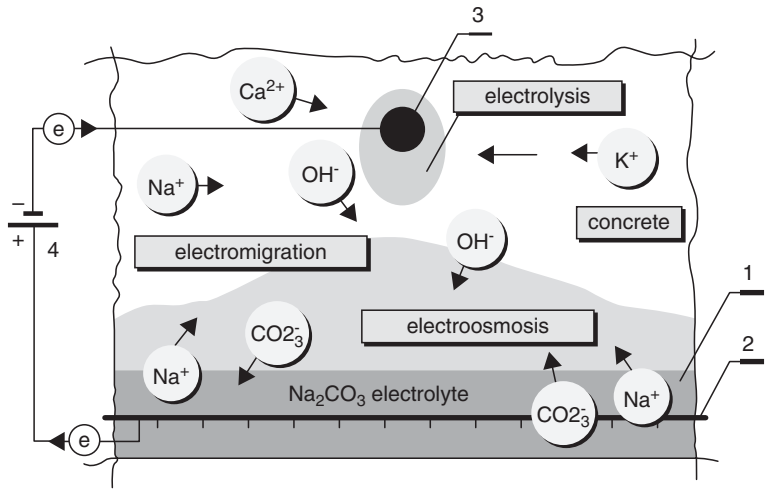


Fig. 6.85 Scheme of the electrochemical pH value recovery in concrete. (according to [350]): *1*—electrolyte, *2*—anodic net, *3*—reinforcing bar, *4*—direct current source

There are "traditional" prejudices against the use of slag cement or Portland cement with fly ash addition in reinforced concretes, however, they have not been proved experimentally [311, 352]. On the contrary, a quite different behaviour of these materials was reported; presumably this can be the consequence of reduced permeability of concrete and the resulting lower diffusion (see Table 6.9). However, application of higher content and higher class cement has a positive influence on the durability of reinforcement.

6.5 Efflorescence of Concrete

The efflorescence on the surface of concrete have no practical importance from the durability point of view; however, they affect badly the appearance of external decorative façades of concrete buildings and other structures. They are particularly noticeable when the colored or white cement plasters are employed. From the aesthetic reasons the remedies for minimizing this phenomenon are needed. In the case of concrete pavers, very often colored, the efflorescence are particularly undesired. The producers of pavers are familiar with this problem and look for the new remedial treatments to avoid it.

The efflorescence is not a phenomenon noticeable only in the case of concrete or mortar; it means occurring in cement paste. It is also known in the case of ceramics, especially bricks and roof tiles, which are not bonded with cement mortar. Efflorescence relates generally to the porous materials in which the transport of mass, primarily of liquids, can occur. The presence of compounds easily water soluble in this porous material is a factor promoting this process. The mechanism of efflores-

cence concerns the transport of soluble components to the external surface where the evaporation of water and crystallization of soluble compounds from the solution occurs. Such process is known, for example in the case of gypsum, crystallizing on the surface of ceramic materials. One should remind the gypsum "desert blooms" or white halite deposits on sand in Africa.

On the surface of concrete, finishing plaster or the other building materials the processes generated by the impact of gaseous air components or rain component occur. Apart from the corrosion phenomena due to the acid rains, the carbonation of calcium hydroxide influenced by CO_2, is of highest importance. This process refers especially to concrete, mortar and cement plasters.

Transport of liquid from the internal part of concrete to the surface is necessary to initiate efflorescence and hence the capillary phenomena play a decisive role. Diffusion of ions from dissolved compounds can also occur through the absorption of external water, for example from rain. In concrete being in contact with water the so–called capillary action occurs; it means water penetration to mesopores, under the action of water surface tension. This question is discussed in Chap. 5.

Obviously, maximum height of liquid in capillary (l) will be equivalent to its hydrostatic pressure, which is as follows:

$$p_H = \rho g l \sin \alpha \tag{6.39}$$

where ρ is density of liquid, *g*–earth acceleration, α–capillary to horizontal plane slope angle.

The porosity and pores structure will be of special importance for liquids transport in concrete. These both properties relate directly to w/c ratio and the degree of hydration, because porosity of concrete is affected mainly by cement paste; the porosity of aggregate is generally very low. Continuous pores volume is increasing with w/c ratio and decreases with degree of cement hydration. There are the permeability controlling factor, because the transport of liquids in concrete composite occurs principally in continuous pores.

The pores structure is affected by the presence of mineral additions in two different ways. At first, the addition particles reduce the voids of granular skeleton, and secondly, due to pozzolanic properties they cause C–S–H content increase in cement paste. As a consequence, mesopores i.e. capillary pores content decreases and the ratio of gel pores, which belong to micropores, is increasing. The micropores contribute marginally to the flow of liquid through the paste, but they participate in diffusion. Diffusion is concerning the transport on the level of ions and molecules. This process depends on the effective diffusion coefficient and was discussed in Chap. 5.

In transport of liquid through concrete the flow of water under the hydrostatic pressure is important. This transport is typical in the case of barrages and dams, and can also occurs in foundations. In the case of fissures presence in concrete they can cause effluents, noticeable in the form of deposits of great thickness. However, this phenomenon cannot be considered as typical efflorescence. White or grey deposits on the concrete surface, when abundant, can be generated due to the corrosion pro-

cesses (thaumasite or alkali—silica reaction) and obviously they also are not linked with efflorescence.

The content of concrete component readily soluble is the other efflorescence controlling factor, beside permeability. This refers generally to the cement paste, from which the sodium, potassium and calcium ions are released to the pore solution in concrete.

Concentration of these ions in pore solution of concrete plays a decisive role in the formation of efflorescence. Pore solution, in the case of ordinary cements, is always saturated with calcium hydroxide—the basic source of efflorescence. The concentration of potassium and sodium is important too; the potassium content is always several times higher. These both components occur in pore solution in the form of hydroxides, as a result of reaction with calcium ions. Particularly sodium is a very mobile ion and in the case of concrete produced from alkali activated slag cement, with sodium compound addition and without Portland cement clinker, Na^+ ions migrate to the surface and the white sodium carbonate efflorescence is formed.

Cement pastes and consequently mortars and concretes do not suffer of sulphates efflorescence. Sulphates transform in cement paste into the calcium sulphate and react rapidly with calcium aluminate to form ettringite. At low alkali content, the calcium monosulphoaluminate phase will be produced. According to Bensted [353], gypsum and syngenite $K_2Ca(SO_4)_2 \cdot H_2O$ can crystallize from the solution after water evaporation from large concrete surface. Mirabilite $Na_2(SO_4)_2 \cdot 10H_2O$ can be detected in efflorescence too [354]. However, this efflorescence is basically generated in the contact of concrete with sea water, for example on breakwaters. Apart from constructions in coastal areas, mirabilite can be formed also in desert areas; this compound has been found in southern Australia. Mirabilite occurs in the form of thin layers under the concrete surface and then on the surface the microcracks are generated. These cracks appear due to the transition of unhydrous sodium sulphate into mirabilite in the case of moisture absorption by concrete, because mirabilite has higher specific volume. A few cases of concrete structures destruction as a result of this process were reported [355].

Calcium hydroxide is relatively well soluble in water, and when water evaporates from the concrete surface a layer of portlandite can be produced. The carbonation of portlandite occurs easily in reaction with atmospheric CO_2; therefore the calcium carbonate is the main component of efflorescence. The calcium ions can react with CO_2 in the liquid phase of paste and calcium carbonate precipitates because of its low solubility:

$$Ca(OH)_2 + H_2CO_3 \rightarrow CaCO_3 + 2H_2O \tag{6.40}$$

As aforementioned efflorescence formation is promoted by a high content of sodium and potassium hydroxides. A coefficient K is applied, being the total of calcium, sodium and potassium present in the liquid phase. Though the influence of lime content seems to be obvious, the effect of sodium and potassium is not. As it is known, these components minimalize the solubility of calcium hydroxide and there must be other reasons causing their advantageous effect of efflorescence formation.

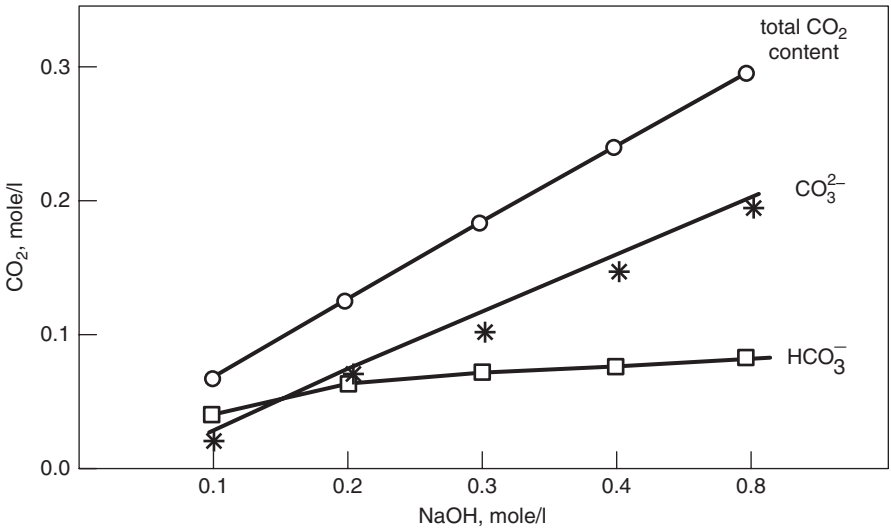


Fig. 6.86 Different ions of carbonic acid solution as a function of NaOH concentration. (According to [357])

The problem of sodium and potassium hydroxides effect on the formation of efflorescence was explained by Dow and Glasser [356]. Solubility of CO_2 in water is increasing with pH, that means with the concentration of sodium and potassium. CO_2 in solution at pH slightly higher than 10 occurs mainly in the form of CO_3^{2-} ion. In the carbonic acid solution, the main component of its dissociation is HCO_3^-:

$$H_2CO_3 \rightarrow H^+ + HCO_3^- \tag{6.41}$$

However, in alkaline solutions the hydrogen carbonate is subjected to the further dissociation according to the reaction:

$$HCO_3^- + OH^- \rightarrow CO_3^{2-} + H_2O \tag{6.42}$$

In Fig. 6.86 the concentrations of various carbonate ions in solution, as a function of NaOH concentration, are shown. The ions formed as a result of carbonic acid dissociation will relatively quickly react with the calcium ions and calcium carbonate will precipitate from the solution.

In pure water CO_2 sorption from gaseous phase is slow because the formation of carbonic acid is slow too. The presence of OH^- ions in liquid phase exerts double effect: they increase the carbonate ions concentration and accelerate the hydrolysis of CO_2 molecules and then CO_2 dissolution. According to Payne and Dodge [357], at temperature of 30 °C CO_2 sorption in KOH solution of concentration 0.2 mol/l is ten times faster than in pure water. One should underline that the effect of KOH is

much stronger than the effect of NaOH. Simultaneously, the viscosity of KOH solution is lower than that of NaOH and diffusion is thus accelerated.

Solubility of CO_2 depends also on its partial pressure in the atmosphere surrounding concrete and on temperature. These relations, as it is known, will have an inverse effect; it means that the CO_2 solubility will decrease with temperature and increase with rising partial pressure of this gas.

Dow and Glasser [356] advance a hypothesis that the water layer on a concrete surface is indispensable for carbonate efflorescence formation. Therefore they propose the following model: the process is initiated when moisture appears on the surface of concrete in which alkalis will dissolve. Sorption of CO_2 is then accelerated and its solubility markedly increased. CO_3^{2-} removed from solution by $CaCO_3$ precipitation is supplemented rapidly.

As aforementioned, the efflorescence is not harmful for the durability of concrete. When the mechanism involved in efflorescence formation is known, the remedies of effective preventing its occurrence are also possible. For example cements with mineral additions can be used in the production of concrete elements. Silica fume has particularly beneficial effect, which prevents efflorescence already from 5% addition. The ground granulated blastfurnace slag or siliceous fly ash are good additives too. The latter one should be ground when added to concrete or taken from the last section of electrical precipitator, where the finest fractions are collected.

6.6 Admixtures Modifying Paste and Concrete Properties

Application of admixtures in concrete technology has significantly increased in the last 30 years. They allow producing high strength and high durability concretes, as a result of reduced w/c ratio. Production of HPC, as well as the self-compacting or reactive powder concretes would not be possible without superplasticizers. These concretes have generally w/c ratio not exceeding 0.4 or even 0.35. Production of high strength concretes was based earlier on the use of high strength cements and higher cement content. However, the wonderful development of concrete properties in recent years is inseparably linked with the application of superplasticizers which allow producing of good workability concrete mixtures at w/c ratio of about 0.3. Nowadays concretes with strength of 300 MPa or higher and w/c of about 0.25 are produced, which can be classified as low temperature ceramics. The reactive powder concretes, for example Ductal, are among these composites [335].

Edmeades and Hewlett [358] classify the admixtures as soluble and insoluble in water; the latter are applied in the form of emulsion. The soluble admixtures: set and hardening accelerators and retarders, plasticizers and superplasticizers, air entraining agents, permeability or shrinkage reducing agents, are more spread out. The accelerators, retarders and shrinkage reducing agents react usually with cement hydration products, mainly with calcium ions to form the products giving the required effect.

In Sect. 4.1.3 the setting and hardening controlling admixtures have been discussed; this section refers to the rheological properties and influencing concrete performance after hardening.

Application of admixtures is as old as the history of mortars and concrete is. The ancient Romans used the animal blood, which was popular also in India. According to Chandra [359], about 3,000 years BC the natural admixtures of various type were in use in India, for example molasses, fruit juices, bananas, olive oil, eggs, milk products and many others. The natural admixtures to lime mortars in India can be classified, based on their specific role, as follows:

- accelerators of setting and hardening—egg protein, fig juice, starch from blood, soured milk,
- sealing agents—mainly milk products,
- air entraining substances—malt, beer, animal skin,
- plasticizers—sugar, olive oil, glycerol, mineral oils, protein, pine resin,
- modifiers—animal blood, hemp grains, protein, casein,
- shrinkage reducing agent—bee wax.

The sealing admixtures were very important because they allowed to produce hardened lime mortar resistant to the action of water.

The following admixtures: bull blood, soured milk, egg protein, Fig juice and rye cake are mentioned by Vitruvius in his work "De Architectura" (46 A.D.). As one conclude from this concise review, these natural, various polymers containing products, were used with the same purpose as the contemporary admixtures.

6.6.1 Water Reducing Admixtures (Plasticizers)

The lignosulphonates, byproducts, from the paper industry, were used first, about 1930. Their role of slurry thinners in Portland cement clinker production by wet method was well known.

It can be derived, from the standard definition of plasticizers, that they reduce the water content of about 5–15 %, at the same workability of concrete mixture. The improvement of workability can be also achieved at constant w/c ratio, with lower admixture addition. The molecules of plasticizers are adsorbed on the surface of cement grains, giving them like charges. As a result, the Coulomb repelling forces cause the dispersion effect. At the same time the neutralization of opposite electric charges on cement grains occurs and prevents their flocculation. The addition of conventional, organic surfactant type plasticizers is usually 0.2 % by mass of cement. At higher content the properties of paste are altered; primarily hydration is strongly retarded, paste is aerated or even the false set can be observed. As one can conclude, these water reducers retard hydration and aerate simultaneously the paste. However, as Hanehara and Yamada [360] report, there are special methods of filtration, allowing elimination of set retardation effect.

These plasticizers can be used as air entraining admixtures because they are adsorbed on the air bubbles, on the air–liquid phase interface in paste. The authors

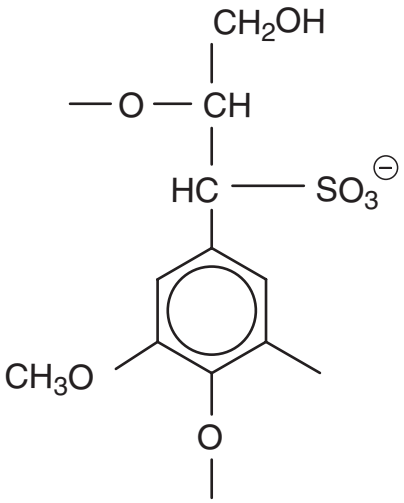


Fig. 6.87 Typical structure of lignosulphonate anion

of work [360] classify lignosulphonates as typical air entraining and plasticizing admixtures. Calcium, magnesium or sodium lignosulphonates (Fig. 6.87) are applied as retarders and plasticizers. Their plasticizing effect is due to the lubricating ability, as a consequence of the presence of hydrophilic groups on the outer surface of adsorbed plasticizer.

The carboxylic acids (containing carboxylic groups –COOH), hydrolyzed carbohydrates and hydrolyzed proteins are used as plasticizing agents too. They are generally more efficient when applied a few minutes after mixing cement with water, as well as in the case of low tricalcium aluminate and low alkali content in cement [222]. In the case of plasticizers addition the decrease of workability occurs later but at higher rate.

Adequate classification of plasticizers is difficult because of their diversity. The following, traditional classification is generally accepted [98, 360]:

- anionic surfactants,
- non–ionic substances,
- other ones, e.g. polysaccharides, dextrin, water soluble derivatives of cellulose, silicones.

Anionic surfactants are the most commonly used; they dissociate in water to form the surface active anion, composed of hydrocarbon radical and hydrophilic group and inactive cation. The substances from this group can be classified further as follows [98]:

- lignosulphonate acids and their salts (Ca, Na, Mg, NH_4),
- hydroxycarboxylic acids and their salts (Ca, Na, triethanoloamine), for example gluconic acid,
- saponified or non–saponified abietic resins and sodium or potassium abietates,
- alkylarylsulphonates.

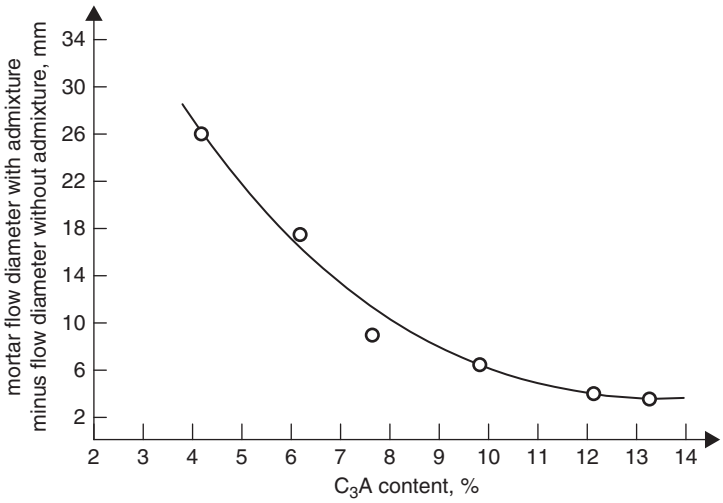


Fig. 6.88 Loss of workability of cement paste with 2% calcium lignosulphonate as a function of C_3A content in cement, at constant C_3S/C_2S ratio. (According to [361])

The two latter ones act primarily as air entraining agents.

The water reducer from the first sub–group introduce usually low quantity of air (on the level 2–3% by mass of cement) and are retarders; those from the second sub–group have no air entraining effect but they retard setting too. The retarding action increases markedly when the addition of plasticizer is too high and attains for example 0.6% by mass of cement [362].

To water reducers from the first and second sub–group modifying their effect admixtures are added, namely intensifying the air entrainment or accelerating setting. High air entrainment is not advantageous because it results in strength lowering. To overcome this effect tributyl phosphate can be added [361]. Triethanoloamine or Na_2CO_3 for setting acceleration are added [363]. As it has been mentioned in Sect. 4.1.3.2, the retarding action of lignosulphonates is attributed to the presence of sugar; it can be removed in the process of plasticizer treatment [364].

The optimum addition of plasticizers depends on many factors, primarily of the paste composition. As it is commonly known, the kind of calcium sulphate phase and its content, as well as the C_3A percentage and properties are of great importance for the paste fluidity (Fig. 6.88) [361]. Plasticizer addition increases with C_3A content. Massazza [361] is reminding that the lignosulphonates can in some cases cause false set, particularly at high C_3A and alkali content in cement. However, when these admixtures are added 2 min after cement mixing with water, or if sulphate content is increased, this effect can be counteracted [286]. Type of aggregate, its grain size distribution and surface properties are of importance too.

The workability of concrete without plasticizer decreases with temperature, however, at the presence of admixture the effect of temperature can be various. At some of them there are no workability changes with temperature increase. To these

belong sodium carboxylates or sodium polyacrylates [361]. It is possible to modify their composition and to produce a plasticizer which shows workability increase with temperature rise. Finally, some plasticizers do not affect paste workability, it means that workability is inversely proportional to the temperature.

Plasticizers affect also indirectly the properties of hardened concrete, giving the possibility of w/c ratio change. Strength increase from 2 to 20% after 28 days of concrete hardening, when the identical workability of the mixture is taken as a basis feature, but at lower w/c ratio, due to plasticizers addition. The early strength can be a little lower because of retarded hardening but the reverse situation can happen too. The example is calcium formate. However, to high plasticizers addition results in strength decrease. Moreover, some plasticizers addition, for example lignosulphonates, causes the drying shrinkage increase, but calcium sucrose decreases it [362]. It is important that at optimum addition the increase of drying shrinkage is negligible [365]. This effect is lower in the case of slag cement and cement with pozzolanas addition [366]. There are some information about the creep increase, however, this question has not been fully explained so far [361]. Finally, it should be reminded that the use of plasticizers is resulting of durability improving, as a consequence of reduced porosity and permeability (effect of w/c ratio). The capillary pores structure in cement paste is not specially affected in the presence of plasticizers; only by the effect of reduced w/c ratio.

The morphology of cement hydration products is very little affected by plasticizers [349]. In some works the reduction of ettringite crystal size [367] and of calcium hydroxide [368] in the presence of lignosulphonates is reported. This effect can be attributed to frequently long lasting adsorption of plasticizer particles on the surface of crystals [367].

According to Ramachandran [367], lignosulphonates are not only adsorbed on the surface of crystals but also are occupying the interlayer positions in their structure. This leads to the shrinkage increasing, though this effect could be attributed to the increased share of macropores due to the air entrainment of the paste.

The mechanism of plasticizers action is linked with the structure of organic molecules [369]. The organic ions are composed of long carbon chains without electric charge, and with electrically charged or polar part. Water dipole, of opposite charge, is attracted by this polar part of organic ion. Usually the carbon chains as hydrophobic stand out from water and the hydrophilic polar groups are immersed. In anionic surfactants the polar part is negatively charged. In the case of non–ionic admixtures the polar groups have dipole properties. The carbon chains can be composed in both cases of polar groups as well.

The behaviour of surfactant in cement, aggregate, water and air mixtures is presented in Fig 6.89 [369]. Plasticizer molecules, when adsorbed on cement grains, cause their deflocculation, by giving to their surface like charges, which assure their repulsion. The change of surface charge and ζ potential takes place. The active groups in organic molecules are mainly: CHO, OH, COOH, HO–C–C=O. They assure the hydrophilic properties of cement grains and therefore these grains are readily wetted by water. Simultaneously, water trapped in conglomerates is released, due to cement particles deflocculation.

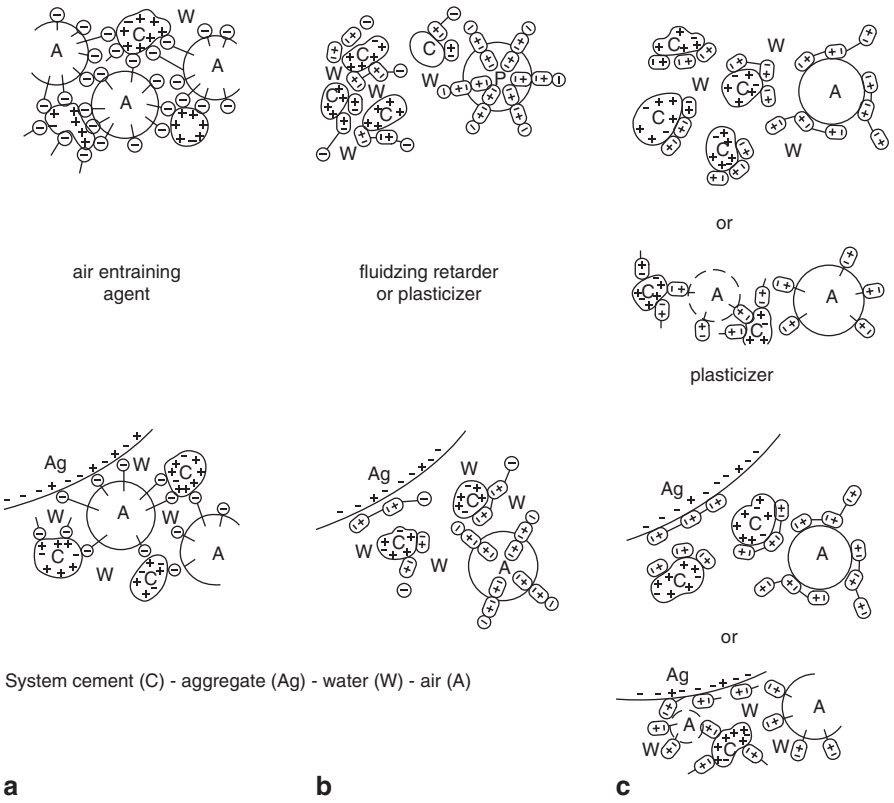


Fig. 6.89 Scheme of the system: cement–water–(admixture, air) and the system: aggregate–water–cement–(admixture, air). (according to [369]); **a** anionic type surfactant addition resulting in hydrophobic cement properties—air bubbles are attaching to cement and aggregate; **b** anionic type surfactant addition resulting in hydrophobic cement properties—air bubbles are isolated from cement grains and aggregate; **c** non–ionic admixture causing hydrophobic cement properties—air bubbles are isolated from cement grains and aggregate

Too high addition of plasticizer does not involve such negative effects as in the case of air entraining agents [360]. The air bubbles are isolated and irregularly distributed; therefore they do not improve the paste freeze–thaw resistance. Moreover, they have somewhat higher volume as the voids formed in the case of air entraining admixtures.

Polar parts of organic molecules are primarily adsorbed on C_3A and C_4AF phases, on cement grains. Therefore cement setting is retarded, unless the special accelerator is used simultaneously. Viscosity decreases due to deflocculation and in some extend under air bubbles influence. The latter reduce also bleeding.

Addition of non–ionic surfactants to the paste cement grains acquire hydrophilic properties, analogously as under the influence of anion active plasticizers. Hence the hydration process is not affected. Only the macromolecular compounds, among them for example saponins, can act at high concentration as shields on the surfaces

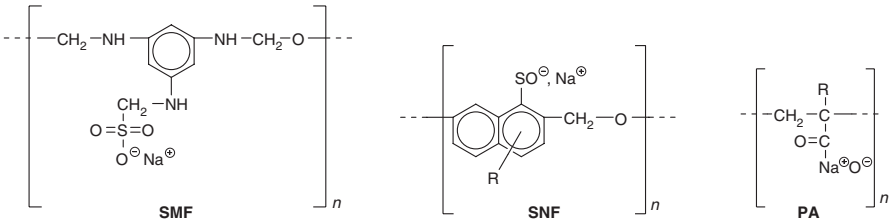


Fig. 6.90 Structure of polyarylsulphonate and polycarboxylate polymer molecules. (According to [371])

of cement grains. Polymers provide the best fluidizing effect at certain molecular mass and number of functional groups [370]. The changes of the hardened concrete properties with addition of non–ionic fluidifiers are very similar to the effect of anion active agents.

6.6.2 Superplasticizers

Superplasticizers (SP) reveal analogous effect as plasticizers; it means that they improve the workability of cement mixture at constant w/c ratio or give the possibility to reduce w/c at constant workability. Therefore the strength can be improved; as early as in 1984 Paillere [371] reported the concrete class of 60 MPa. The melamine resins act more effectively than the naphthalene–formaldehyde condensates [361]. The concrete subjected to thermal treatment or autoclaving shows much better strength, with respect to the reference, with superplasticizers addition. The difference between plasticizers and superplasticizers is only one: the latter can be used in higher concentrations without causing excessive retardation or air entrainment.

The most commonly used superplasticizers can be classified to the four groups [361]:

- sulphonated melamine formaldehyde polymers, SMF,
- salts of sulphonated naphthalene formaldehyde polymers, SNF,
- modified lignosulphonates,
- other substances.

Beside from the polyarylsulphonate polymers—SMF and SNF, the polycarboxylate (e.g. polyacrylates) polymers PA belong nowadays to the most commonly used superplasticizers (Fig. 6.90) [372]. All these polymers dissociate in water; in the case of the first anions with the sulphonate groups $-SO_3^-$ and the second—carboxylate $-COO^-$ groups are formed.

However, to the latter group (other substances) polymers of not fully recognized properties, which properties are given only by producers, are included. They are, among other, the multi–ring sulphonates, alkylarylsulphonates acids, sulphonated polystyrene, sulphonated creosote—formaldehyde condensates and many others [373].

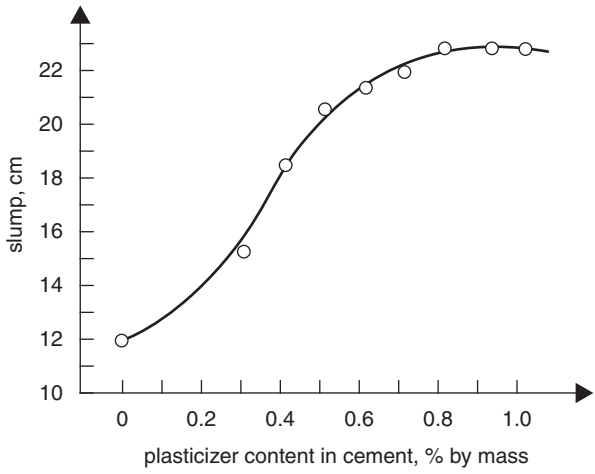


Fig. 6.91 Effect of superplasticizer (acryloarylsulphonate–formaldehyde polymer) on the workability of concrete with cement content 300 kg/m^3, w/c = 0.6. (According to [361])

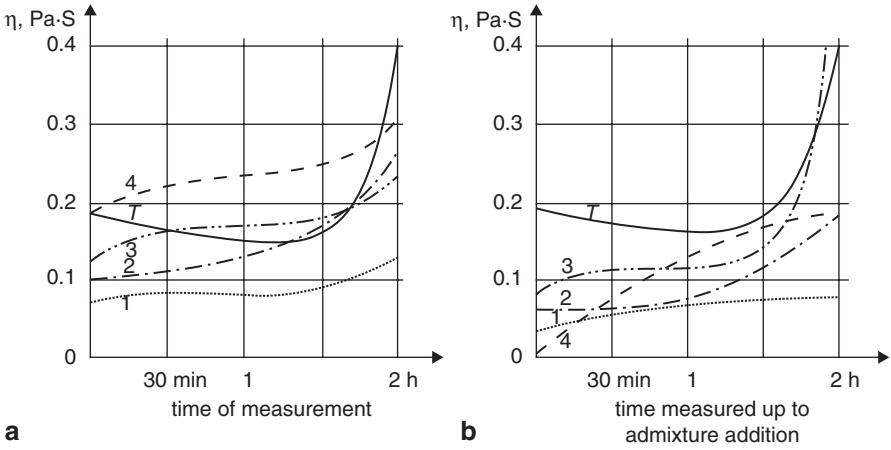


Fig. 6.92 Viscosity of cement pastes (w/c = 0.40) with plasticizers added: **a** to the mixing water, **b** at various time after mixing. (according to [374]): *1*—melamine resin, *2*—calcium naphthalene sulphonate, *3*—sodium lignosulphonate + phosphate ester, *4*—sodium lignosulphonate + sulphonated naphthalene (traces), *T*—no admixture

Superplasticizer addition should be much higher, in the range from 1 to 3 % by mass of cement than that of plasticizer. The fluidizing effect is increasing, from certain threshold content, proportionally to superplasticizer addition (Fig. 6.91) [361].

Paillere [371] paid an attention that superplasticizers behave similarly to fluidifiers, when they are added to the concrete mixture with mixing water. Superplasticizers give a better fluidization when introduced at the end of mixing, however, their higher effectiveness is manifested when they are added a certain time after the end of concrete mixing. Superplasticizers added after 30, 60, 120 min to the paste result in viscosity lowering to 0.04–0.16 Pa s (Fig. 6.92) [374]. Fluidifiers do not improve

paste fluidity in a visible degree when added after one hour, and the fluidity is even lower than that of reference paste when they are added after two hours from paste producing.

The effect of superplasticizer varies with type of cement and gypsum content. For example the fluidizing action of melamine resin is enhanced with gypsum content [375]. The fluidity increase is also higher in the case of cements with fly ash [361]. However, the loss on ignition of fly ash should be taken into account. This loss corresponds to the uncombusted coal content; coal occurs as quick–coke of high specific surface, adsorbing the SP and lowering its effectiveness. Fluidity is changing with the fineness of cement; for example the fluidity caused by sulphonated naphthalene increases almost two times when specific surface area of the same cement is rising from 320 to 400 m^2/kg. These examples show that superplasticizer addition should be verified experimentally.

There are some data indicating that superplasticizers should be used at cement content in concrete on the level of 300–350 kg/m^3 and the aggregate size should be limited to 32 mm [376]. Then the best results are obtained.

There is a serious drawback of superplasticizers application—it concerns the reduction of concrete fluidity with time [371]. It is an opinion that the rate of this process decreases with superplasticizer addition [361].

At the addition of lignosulphonate workability of concrete is maintained practically on constant level within 30 min, while in the case of melamine resin or sulphonated naphthalene, added with mixing water, the reduction of workability occurs already after 15 min and after 30 min achieves significant value. These changes are less intensive when superplasticizer is added at the end of mixing; in this case the workability is equal to initial value of control mix after 30 min, but higher than the workability of reference mix after 60 min.

Higher rate of slump loss in the case of melamine superplasticizers, as compared to the lignosulphonates, is observed even if they are added in the best moment, that is 30 min after concrete mixture production (Fig. 6.93).

Repeated superplasticizer addition to the concrete mixture is sometimes proposed when placing of concrete for some reasons is delayed. This leads to the renewed high fluidity of concrete (Fig. 6.94) [371]. In the case of melamine resin the higher rate of plastic viscosity increase is observed again [371].

Setting is not observed even after 54 h when the addition of superplasticizer is repeated for the third time [371]. At the second and third lignosulphonate addition the viscosity is decreasing too, but the stiffening occurs practically immediately. Thus the method of repeated admixture addition should be verified experimentally before its application in common practice [371]. The mechanism of this phenomenon is not explained, particularly that the melamine resins do not retard setting.

The use of set retarders is recommended in order to restrict the quick stiffening in the case when superplasticizer is added several times [377]. The special compositions of superplasticizers are examined too [361].

It should be reminded that concrete flowability decreases with temperature. Surprisingly, the stiffening occurs more rapidly in the case of mixing concrete mixture than with no mixing [378].

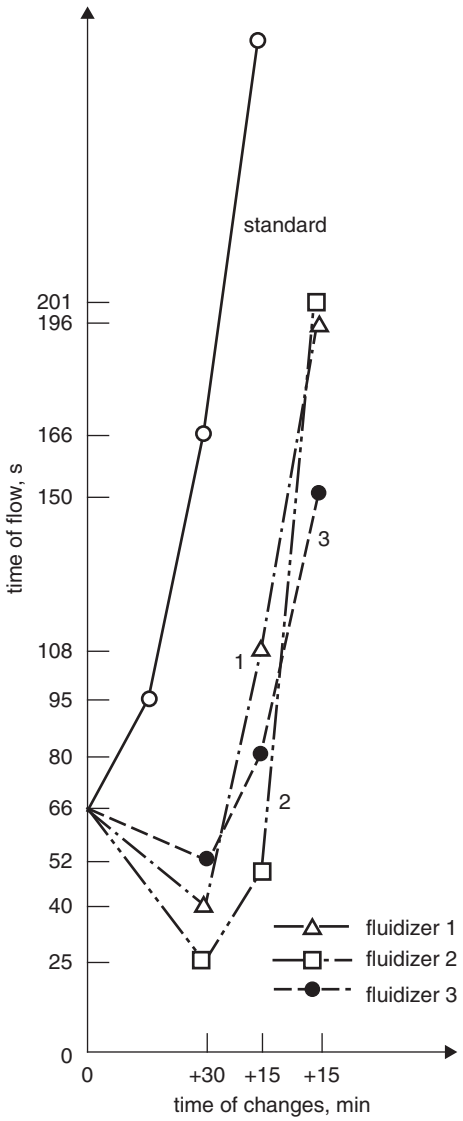


Fig. 6.93 Workability of mortar change with time; superplasticizer added after 30 min. (according to [371]). Kind of superplasticizers as in Fig. 6.92

The effect of superplasticizers on the properties of concrete is similar to that of plasticizers. The strength and durability increase as a result of water content lowering. Superplasticizers do not affect creep [297], but improve the freeze–thaw resistance [376]. However, the use of air entraining agents is recommended in several cases [361].

The mechanism of superplasticizers action consists in the adsorption of their molecules on cement grains, as it is in the case of plasticizers. The adsorption occurs

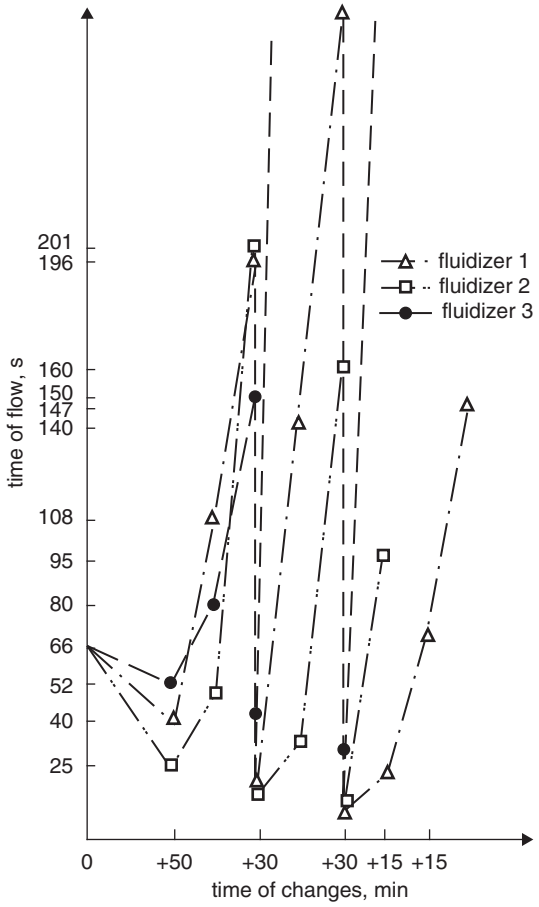


Fig. 6.94 Workability change of mortar with time; superplasticizer added repeatedly (after 30 min., 60 min., 90 min.). (according to [371]). Kind of superplasticizers as in Fig. 6.92

primarily on the surface of hydrated calcium aluminates and sulphoaluminates [374]. The type of superplasticizer and its polymerization degree affect adsorption [379]. Due to the adsorption of cement particles are repulsing each other. Simultaneously with superplasticizer addition the electrokinetic potential decreases significantly to the value from −35 to −45 mV [380]. The water film surrounding cement particles is readily formed. Moreover, the steric effects due to the presence of superplasticizer molecules, which counteract the adhesion of cement particles and, as a consequence the significant deflocculation of suspension is obtained [371]. This deflocculation is different for various cement grain size fractions; it is particularly high for coarse grains [371]. Cement grains are covered with 40 layers of polymers, thus the thickness of this layer is 40 nm [381].

The poly–aryl sulphonate type superplasticizers have been widely used. However, for the last 20 years many new types of superplasticizers have been put into use. They are the derivatives of acrylic, methacrylic and maleic acids. Acrylate–based

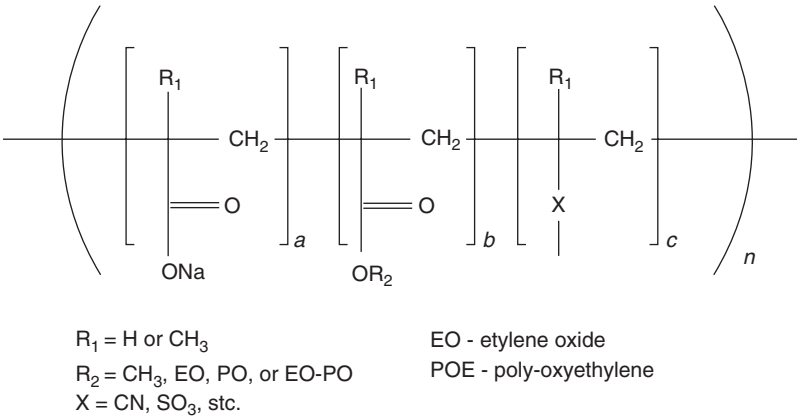


Fig. 6.95 Structure of polyacrylate copolymer. (According to [382])

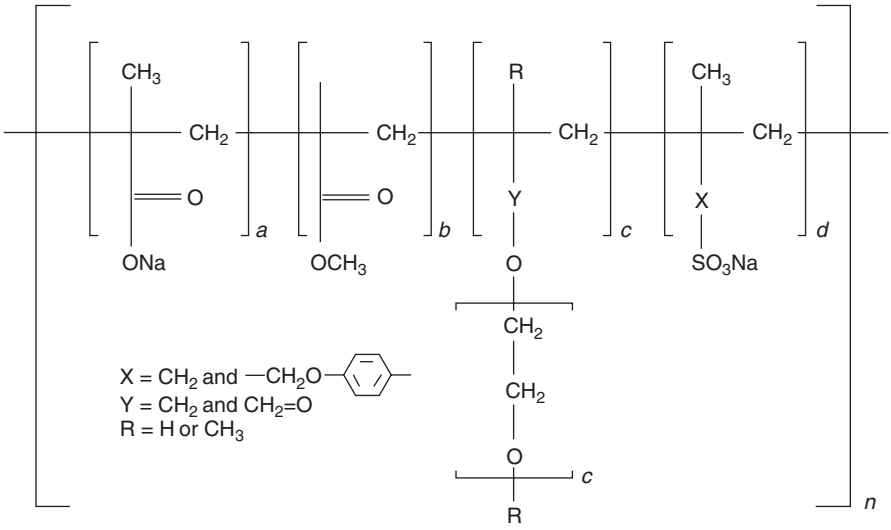


Fig. 6.96. Structure of the acrylic ester copolymer molecule. (According to [382])

polymers are commonly used; they are built of the three types of acid derivative mers:

- carboxylate,
- alkylester,
- polyetherester.

In the most of these polymers the polyacrylate or polymetacrylate main chain is present with a number of side chains. The poly–oxy–ethylene, poly–oxy–propylene, as well as the poly–ether and ether–ester mers or their mix occurs mainly as the side chains (Figs. 6.95 and 6.96). These side chains are plotted as perpendicular to

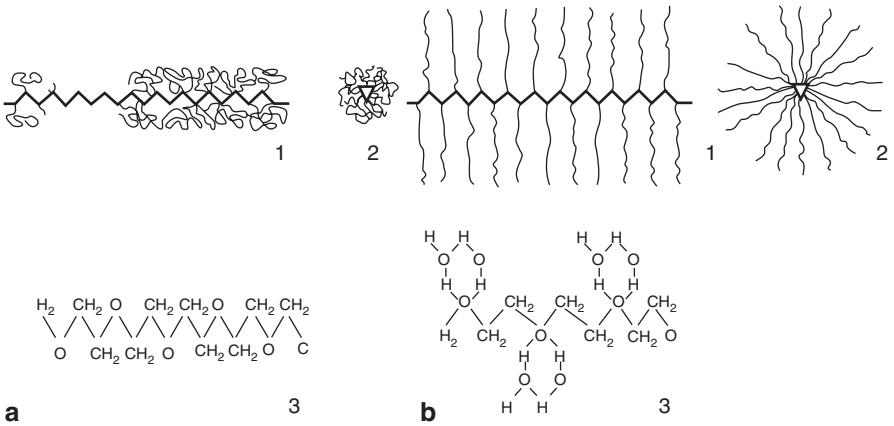


Fig. 6.97 Arrangement of polyether chains in polymer molecule: **a** unhydrated, **b** hydrated; *1*—orthogonal projection, *2*—axial projection, *3*—magnification of polyether chain unit. (According to [372])

the main chain and therefore the polymer structure is determined as the "*comb–like*" one (Fig. 6.97). The polyether chains have the hydrophilic properties and due to the hydration process they produce the hydrogen bridges between the oxygen atoms from ether unit and dipole water molecule [372]. As a consequence, the change of volume and structure of chains is caused (Fig. 6.97).

According to Hanehara and Yamada [360], in the polycarboxylate superplasticizers the main chain is built of polyethylene and the side chains are the poly–oxyethylene (POE) and carboxylane groups. Modifying this basic structure admixtures with various properties are produced, resulting in dispersion of cement grains immediately after mixing with water, good retention of workability, controlled setting and the others.

In these polymers, apart from the electrostatic repulsion, resulting from like charges occurring on the surface of cement grains, the so–called steric hindrance is produced, due to the presence of side chains. This steric repulsion is very important as a dispersive interaction in cement water suspension (see Fig. 6.99).

In Fig. 6.98 the molecular structure of the two polymers, according to Hanehara and Yamada [360] is shown, which are the base of frequently used superplasticizers. The first one is a typical polycarboxylate polymer; the second one has a more complex structure, with the cross linked main chains.

The dispersive properties of these polymers are the function of polymerization degree of mers forming the main chain (its length), as well as of the density and length of side chains. The longer side chains are expected to contribute to the improved fluidity, particularly at low w/c, while is a certain optimum in relation to the length of main chain [360]. Yamada et al. [383] report the structural factors controlling the fairly good dispersive properties of superplasticizers and their stability over longer period of time (Table 6.10). However, there are some experimental results which do not comply with these rules. One can conclude that the properties of superplasticizers depend on the raw materials and conditions of SP manufacturing.

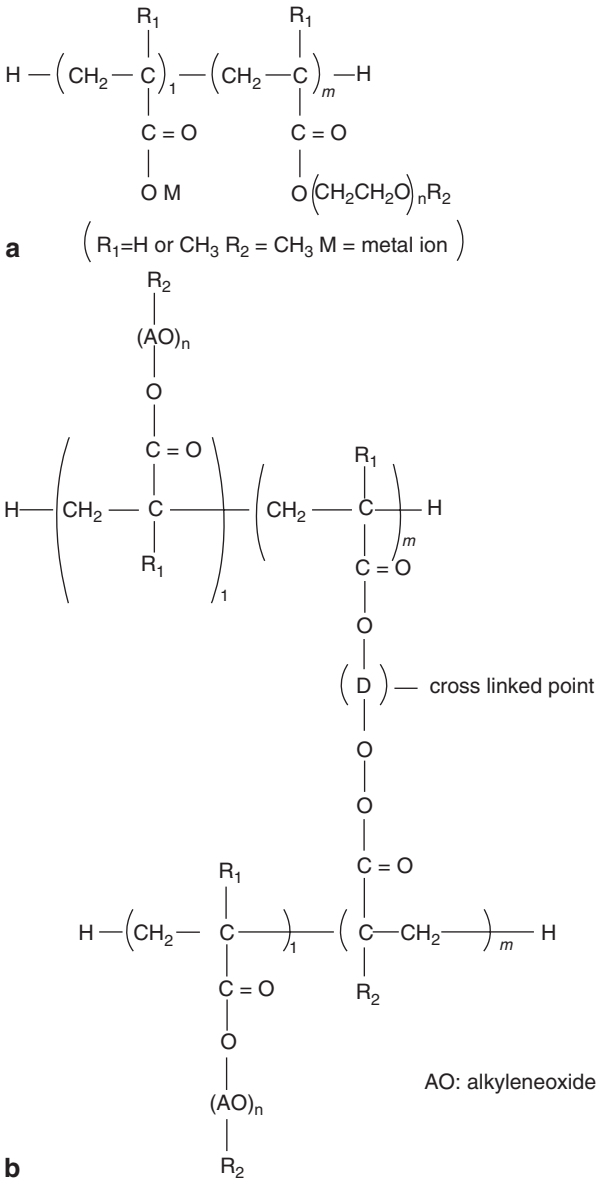


Fig. 6.98 Structure of superplasticizer molecule: **a** polycarboxylate, **b** polycarboxylate polymer with the cross–linked main chains. (According to [360])

Table 6.10 Structural factors causing high dispersibility and its retention [383]

Dispersibility and retention	Relative chain length of trunk polymer	Relative grafts length	Relative number of grafts
Low dispersibility and short its retention	Long	Short	Large
High dispersibility	Short	Long	Low
Long dispersibility retention	Shorter	Long	Large

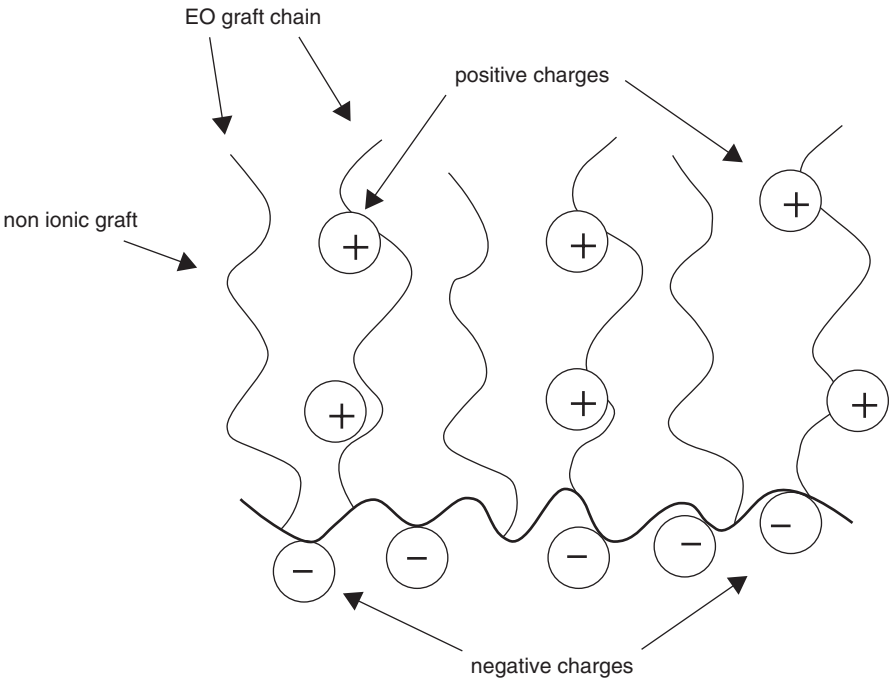


Fig. 6.99 Schematic image of the new low–stickness type superplasticizers. (According to [360])

It means that the chemical structure of SP molecules on their properties from different producers can vary, in spite of the same basic structure and mechanism of interaction with concrete mixture. The fluidity of paste increases with time in some cases, as the polycarboxylate superplasticizers, composed of mullein anhydride, poly–oxyethylene and aryl ether, are used.

It should be underlined that the precise determination of polymer structure is extremely difficult; the illustrations relating to the SP structures show only an approximate image; the commercial products are virtually the mixtures of several polymers.

However, the basic mechanism of superplasticizers action is very similar. The carboxylate groups are adsorbed on the surface of cement grains, on the sites occupied by calcium ions [360]. Their dispersive action is generally attributed to the electrostatic repulsion, due to the presence of negative charge induced on the surface of cement grains, originating from the sulphonate or carboxylate groups present in the side chains. These side chains show simultaneously the steric hindrance, strengthening the dispersive action. In Fig. 6.99 the molecular structure of the mains chain and side chains together with the electrostatic charges in the new type SP, highly reducing the viscosity of paste, is shown schematically [360].

Yamada and Hanehara [384] assume that the adsorption of polymer complies with the Langmuir equation and the amount of adsorbed polymer is in equilibrium

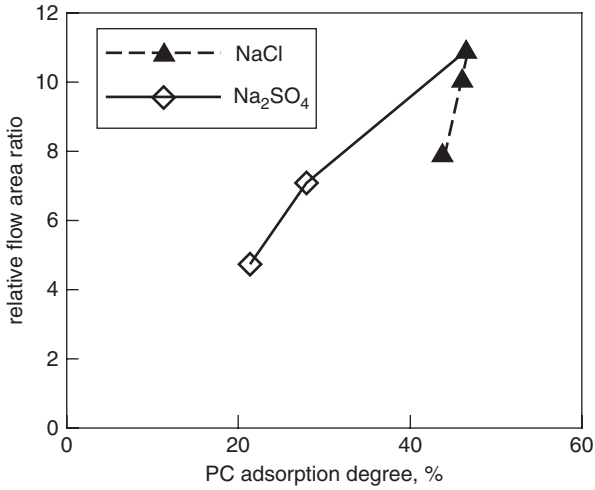


Fig. 6.100 Relationship between PC adsorption and paste fluidity. (According to [384])

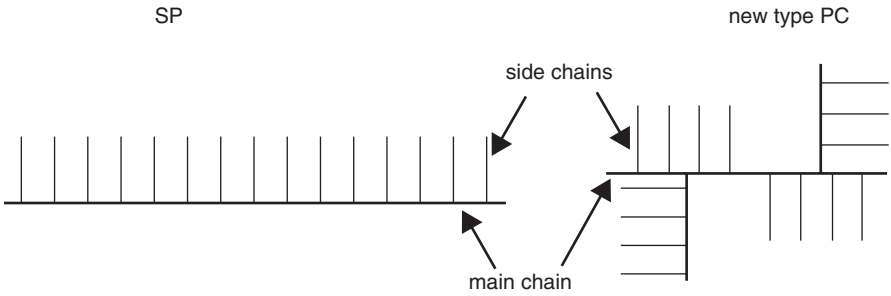


Fig. 6.101 Chemical structure and schematic image of traditional PC and new branched PC. (according to [360])

with the sulphate ions. Based on this equation they calculated the amount of adsorbed polymer admixture and found a good correlation of adsorption degree with the relative flow area ratio determined experimentally (Fig. 6.100) [384].

In Fig. 6.100 the decreasing ratio of adsorbed superplasticizer with increasing sulphate ions concentration in the liquid phase is shown. According to Hanehara and Yamada [360] the concentration of sulphate ions in the solution contributes to the loss of compatibility between cement and carboxylate superplasticizer.

The polymers used recently have branching structure, including the main chain (Fig. 6.101). They are highly effective dispersants. They allow reducing the apparent viscosity at constant shear stress [360]. In other words, when the concrete mixtures of the same workability are compared, those with these admixtures are more readily available to transport, pumping and concreting. This group comprises also the multifunctional agents (Fig. 6.102); the carboxylic units introduce the shrinkage reducing component [360].

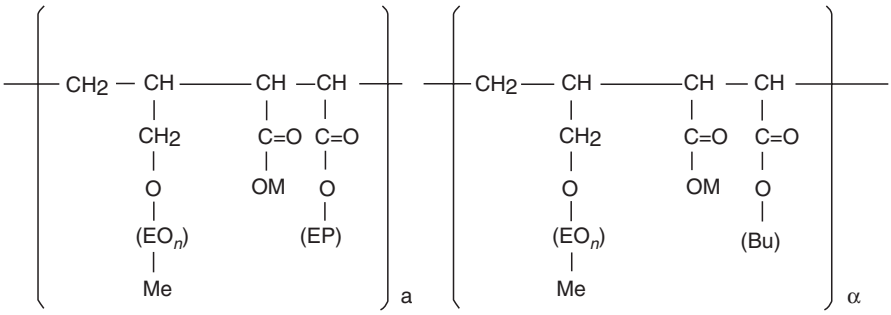


Fig. 6.102 Molecular structure of multifunctional polycarboxylate superplasticizers. (According to [360])

In spite of the many years experiences in use of superplasticizers in modern concrete technology there are many unresolved questions. The most important is the conformity of the system cement–superplasticizer, determined as "compatibility" [385–393]. It is known that at any given admixture the concrete mixture, produced from any given cement, reveals required properties (good, stable workability), while the results are not satisfactory for another cement. A situation which happened in Toulouse in 1989, where the loss of workability followed 5 min after concrete mixture producing and another superplasticizer was necessary, would be a good example.

The determination which cement properties are controlling cement–admixture compatibility is of the key importance in resolving this problem. Therefore many studies dealing with this question have been carried out recently [385–393].

There are many factors affecting the rheological properties of concrete; among them the C_3A, sodium and potassium sulphate content, fineness of cement, type of sulphate set retarder, degree of gypsum dehydration during grinding and finally the free CaO in Portland cement clinker. These factors influence the superplasticizer adsorption and rheological properties by the change of concrete pore solution composition and the rate of hydration process, as well as the nature of hydration products. A particularly major adsorption is due to tricalcium aluminate; it occurs very quickly, within a few seconds [393, 394]. However, on the other side Ramachandran et al. [392] are of the opinion that the adsorption of superplasticizer is occurring rather on the hydration products than on the unhydrated cement phases. The rate of C_3A hydration is influenced by the type of calcium sulphate phase; an adequate sulphate concentration in solution is required to retard the C_3A hydration. Anhydrite dissoluting slower than gypsum will not assure the ettringite shell formation on C_3A surface at fairly high rate, after cement mixing with water. Gypsum will be much better, however, in the case of very active C_3A, its rate of dissolution will be also to low. Therefore, some hemihydrate content would be required (see Sect. 4.1.2). From this point of view the potassium sulphate, from cement clinker, will be of special importance. At potassium content higher than 0.5 % (approximately) and the SO_3/K_2O molar ratio close to 1, a sufficient sulphate ions concentration level will be

assured, due to the high dissolution rate of K_2SO_4 the sufficient sulphate ions concentration in solution will be assured; in this case the type of calcium sulphate phase in cement will be of minor importance. An advantageous effect of hemihydrate on the flow diameter was reported by Hanehara and Yamada [360], concluding that this phase will also retain the paste fluidity for required period of time. According to Hanehara and Yamada [360], the surface of hydrates is determined by the C_3A hydration rate, therefore, the ratio of polyacrylate superplasticizer adsorbed on the surface of hydrating cement is determined too [360].

Aïtcin [387] discussed in detail the problem of sulphonated polymers, which $-SO_4^{2-}$ groups are adsorbed on the C_3A surface active sites, competing with SO_3^- anions from dissoluted sulphates of cement. Therefore, this author proposes to add later superplasticizers containing these groups, while those with $-COO^-$ anions to add immediately, with mixing water. Fernon et al. [395] assume that the differences consist in SNF adsorption on the hydrates formed directly after mixing cement with water. However, Nawa and Eguchi [390] found that in the system C_3A–gypsum the SMF adsorption was lower when the superplasticizer was added after certain time, in which the hydration of this mixture occurred. Bonen and Sarkar [391] found a good correlation between the adsorption and the product of C_3A content and fineness of cement. Assuming that the interaction of sulphonated superplasticizer with C_3A plays a decisive role in the rheology of mortars and concretes from Portland cement, Bonen and Sarkar [391] come to the conclusion that the initial plasticity of cement paste will depend of C_3A content and cement fineness. However, the reduction of flow diameter is more extensively influenced by the ionic force of concrete pore solution. Therefore, they conclude that C_3A and ettringite content has little effect on concrete mixture fluidity.

According to Jiang et al. [385] sodium and potassium sulphate content is the main factor determining the fluidity and decrease of fluidity of cement pastes, with polynaphthalene sulphonate admixture. The advantageous alkali content, from the fluidity and its retention point of view, is 0.4–0.5 % Na_2O_e. In the case of cements with this optimum soluble alkali content C_3A does not affect practically the decrease of fluidity. Kim et al. [393] studied the adsorption ability of analogous cements and found that those not compatible with superplasticizer have higher adsorption ability of SNF superplasticizer, because did not contain the soluble alkali sulphates. Na_2SO_4 addition causes the increase of concrete mixture flow diameter reducing the amount of SNF which has been adsorbed. This experimental result is inconsistent with the general opinion that the adsorption of superplasticizer has a positive influence on cement paste rheology, due to the enhanced electrostatic repulsion of cement particles. The authors [393] explain this discrepancy assuming that SNF molecules remaining in solution can play a role of additional barrier repulsing cement particles and increasing paste fluidity. Moreover, with hydration development SNF molecules adsorbed on the surface of solid phases are less effective being implemented into the formed hydration products. SNF remaining in solution is subsequently progressively adsorbed on the surface of hydrates formed. The SNF molecules still continuously available in solution assure the retention of electrostatic repulsive forces as well as the steric hindrance; therefore, the paste fluidity is maintained. The advantageous effect of polymer present in so-

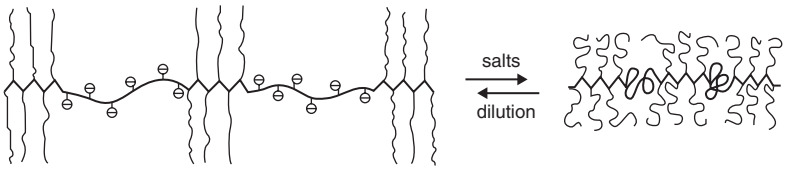


Fig. 6.103 Arrangement of carboxylate side chains as a result of the ionic force change of the solution. (According to [372])

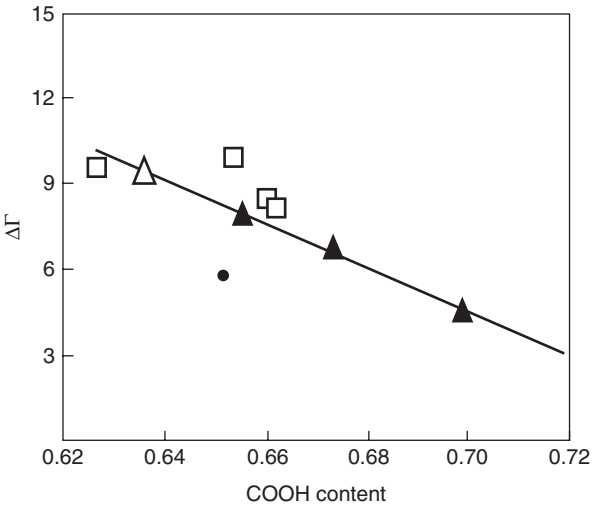


Fig. 6.104 The effect of carboxylate groups in a truck chain of superplasticizers on the influence of sulphate ions. *Triangles*—increase of NaCl concentration (on the *right*), *squares*—Na_2SO_4. (According to [360])

lution was also mentioned by Hanehara and Yamada [360], however, without any explanation.

The results consistent partially with those of Kim [393] were obtained by Yamada et al. [396], who found the reduction of adsorption of superplasticizer on cement grains and the reduction of flow diameter with higher concentration of sulphate ions in the paste. Na_2SO_4 was added to the paste for this purpose and the degree of "saturation", corresponding to the minimum flow diameter which did not decreased further, was 1 mol/l. The amount of adsorbed carboxylate superplasticizer lowered slowly, starting from 0.5 mol/l, however, "saturation" at 1 mol/l was not attained [396]. However, opposite to Kim [393] results, the flow surface area was increasing with admixture adsorption (Fig. 6.100). Hamada and Yamada [360], based upon the results reported by Ota and Uomoto, attribute the reduction of PA adsorption, as a function of ionic force of liquid phase in the paste, to the corrugation of the polymer backbone and, as a consequence, to the reduction of steric hindrance. In Fig. 6.103 the effect of ionic force on the arrangement of carboxylate mers is shown, according to Grzeszczyk and Sudol [372].

According to Hanehara and Yamada [360] the adsorption of carboxylate admixtures is influenced by sulphate ions too and is diminishing with SO_4^{2-} concentration increasing. In Fig. 6.104 the effect of sulphate ions on the flow surface area at various number of carboxylate groups in a truck chain of PC is shown.

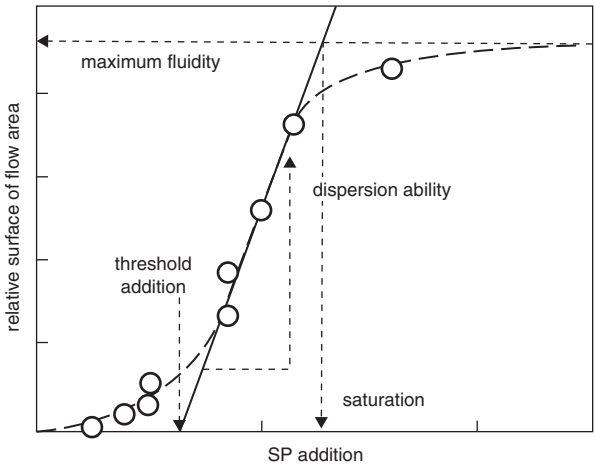


Fig. 6.105. Critical addition and dispersing ability of superplasticizers. (According to [400])

The experiments of Bundyra–Oracz et al. [397–399] on the pastes from model mixtures (alite, C_3A, calcium sulphoaluminate—Klein complex compound), as well as on the industrial clinkers with various C_3A content and with Klein complex addition have shown that the rheological properties of paste are basically dependent on the amount of hydration products formed. The yield stress value shows very good compatibility with the amount of ettringite formed, while the plastic viscosity—with the total amount of hydrates; the C–S–H content is significant. The magnesium lignosulphonate and $NaHCO_3$ used as set controlling agents, as in the studies by Brunauer (see Sect. 4.3.3), allowed producing the paste with very low yield stress value and plastic viscosity, though the C_3A content in cement was 9 %. Because the flow diameter is well correlated with the yield stress value [400], one can conclude that the reduction of flow diameter of paste with Na_2SO_4 addition [396] is associated with an increase of ettringite content.

Hanehara and Yamada [360] studied the effect of PA admixture addition on the flow diameter and found an exact relationship in the case of w/c = 0.4; however the results are not always good for w/c = 0.3 because of the effect of cement with water mixing procedure. This problem was resolved by addition of limestone powder. According to these authors there is no general method of cement–admixture compatibility establishment, but it is possible to settlement certain experimental conditions, which permit to determine it. It is moderate fineness of cement and suitable w/c. Moreover, the proper conformity criteria should be selected, because the plastic viscosity, yield stress value and flow diameter can give various results [400]. In Fig. 6.105 the effect of SP on the relative flow area, chosen as cement–SP compatibility determining parameter, after Yamada [400] is shown. SP does not affect the relative flow area below the threshold value, above this value the flow area is increasing proportionally with admixture, but above the "saturation" level this parameter is not influenced by an admixture content.

Uchikawa et al. [24] obtained very interesting results measuring the thickness of polymer layer adsorbed on cement grains by Auger electron spectroscopy. Thick-

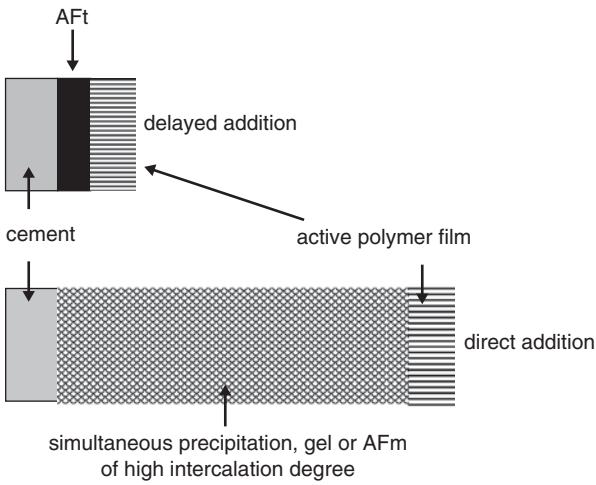


Fig. 6.106 Adsorption of polymer on cement grains. (according to [402])

ness of this layer, which contained carbon, was 10 times greater than the length of polymer side chains, when the admixture was added together with mixing water, but when the admixture was added later, this thickness corresponded only to the length of side chains. These results were consistent with atomic force microscopy measurements of repulsive force between the paste and platinum wire [401]. Simultaneously Fernon et al. [395] found the formation of the organic–mineral phase in the case of SNF and AFm. According to Flatt and Horst [402], due to the intercalation[14] of AFm by SNF, part of SNF is immobilized and cannot participate in dispersive action. This process, which after these authors is embracing also C–S–H, and basically polymers with linear chains, is influenced by the availability of SO_4^{2-} ions. These ions cause the precipitation of AFt which drastically reduces the intercalation of hydration products with polymer molecules [402] (Fig. 6.106). It should be reminded that the possibility of various organic groups incorporation to the AFm structure was presented by Pöllmann [403], as it has been discussed in Sect. 3.3.3.

The composition of superplasticizers is as a rule very complex. They comprise generally, beside of the main polymer (so–called "base"), many others components, such as the anti–foaming agents, because most of superplasticizers reveal air entraining effect, as well as set retarders or accelerators of hardening. The latter one cannot contain chlorides. According to Hanehara and Yamada [360] a typical multi–components admixture is composed of polyol(gluconic acid)—lignosulphonate—polycarboxylate—air entraining agent. The hydration is retarded by lignosulphonate and this contributes to the good workability of concrete mixture over longer period of time. This is advantageous also because the carboxylate groups accelerate the C_3A hydration immediately after mixing cement with water [360]. On the other side a significant air entrainment observed in the laboratory experiments

[14] Intercalation—the incorporation of one compound into the structure of the other during its precipitation.

and then controlled by use of anti–foaming agents, does not occur in the production of ready mix concrete; therefore the air entraining admixture should be used. The latter one is particularly important because in the presence of some polycarboxylates the freeze–thaw resistance is markedly lowered [360].

According to Hanehara and Yamada [360], the diethyl glycol containing grinding aids accelerate the loss of workability with time in the case of mortars with PA admixture, which is reacting with Ca^{2+} ions; hence the C_3A reactivity is enhanced immediately after mixing cement with water. It is possible to prevent this process by increasing the hemihydrate to gypsum ratio in cement. The reduction of SP effectiveness, especially the loss of fluidity with time [360], occurs in the presence of montmorillonite in the aggregate; in this case the absorption of polyether side chains in the interlayer space of montmorillonite takes place.

Park et al. [404] studied the effect of granulated blastfurnace slag ($F = 600$ m^2/kg), siliceous fly ash (370 m^2/kg, 4 % carbon content) and silica fume on the rheological parameters of Portland cement ($F = 330$ m^2/kg) with SNF. The yield stress value and plastic viscosity decrease with granulated blastfurnace slag addition was found, while at the presence of fly ash these parameters were slightly higher and drastically increased with silica fume addition. At simultaneous silica fume and slag addition the rheological properties of paste were improved too. The effect of fly ash is not advantageous when it contains uncombusted coal (loss on ignition), but at low loss on ignition and high fineness the rheological properties of cement paste are positively modified [405].

6.6.3 Shrinkage Reducing Admixtures

In order to diminish the chemical and drying shrinkage the surface tension of water reducing agents, that is the surfactants, are used. Therefore the pressure in the capillaries, causing shrinkage, is lowered. The non–ionic molecules of shrinkage reducing admixtures are placed at the gaseous and liquid phase interface, that means at the air–water interface and hence they act analogously as air entraining agents. According to Aïtcin [406] the autogenous shrinkage does not occur in high performance concrete when the formworks are removed as soon as possible and the concrete is cured in moist condition for at least 7 days.

These admixtures are based on the 2.2–dimethyl–propane–1.3–diol (neo–pentyl glycol) of the formula $(CH_3)_2C(CH_2OH)_2$, or similar chemical compounds. They are added in amount about 4 kg/m^3 of concrete.

The shrinkage reducing admixtures do not reduce the evaporation of water amount in the atmosphere of low humidity. In the case of these admixtures applying the air content and air pores distribution in cement matrix are of crucial importance. Nowadays the compositions of admixture and expansive additive are used. The latter one can be based on the calcium oxide or calcium sulphoaluminate (Klein complex compound), linked with ettringite formation [407]. This method permit the total shrinkage elimination, while the admixture alone allows reducing shrinkage of about 40 %; according to Collepardi et al. [407] this is a synergic effect.

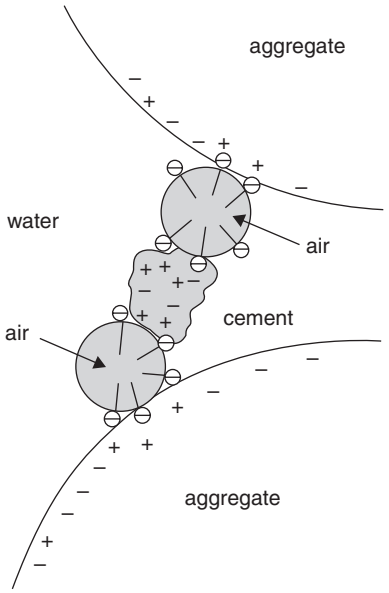


Fig. 6.107 Distribution of air entraining agent molecules in concrete: the non–polar chain is attached to the air bubble, the anionic group is adsorbed on the surface of cement grains and aggregate. (According to [358])

6.6.4 Air Entraining Agents

The air entraining agents are the surfactant adsorbed on the surface of air bubbles, that is on the air–liquid phase interfacial surface in concrete (Fig. 6.107).

Air entraining agents can be classified as follows:

- animal or plant fats and oils, as well as fat acids,
- natural resins, giving with lime the resin acid salts, soluble in water, or with NaOH addition—the saponified compounds of resin acid,
- sodium and potassium salts of sulphonic or alkylsulphate acids.

The sodium abietate, the salt of abietic acid produced from natural pine tree resin, was used as the air entraining agent. The anionic admixtures, mainly alkylarylsulphonates, sodium oleate, as well as the non–ionic surfactants such as nonylphenolethoxylate are more and more frequently used. This surfactant is efficient air entrainer but does not perform well in freeze-thaw durability tests [358].

Among the anionic surfactants the sodium dodecylbenzenesulphonate, sodium sodium oleate sulphate and sodium oleate are the most widely used (Fig. 6.108). The sodium dodecyl–benzene–sulphonate and sodium abietate are very effective and a very low content, about 0.005 % by mass of cement is sufficient to give the air content on the level about 5 %.

Air entraining agents are composed of the non–polar hydrocarbon chains or the other hydrophobic units, linked with the following hydrophilic groups: —COO^-, —COO^-, —SO_3^- On the gaseous and liquid phase interface these polar groups are directed to water—they lower its surface tension, and facilitate the formation of air

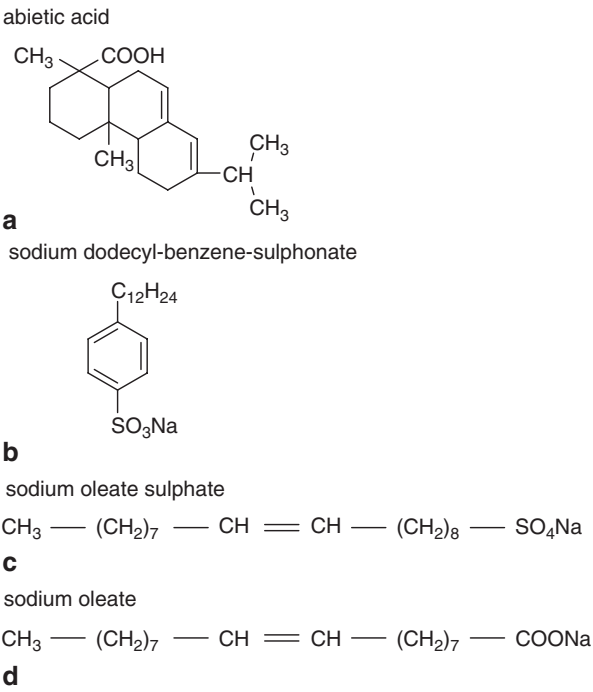


Fig. 6.108 Molecular structure of air entraining admixtures. (According to [358])

bubbles and counteract their integration. On the solid and liquid phases interface the polar groups are linked with the solid phase, while the non–polar ones are directed to water, assuring to cement grains hydrophobic properties. As a consequence, to cement grains the air bubbles are attached and the "tails" of non–polar chains are gathered inside these bubbles. It assures the best condition for the uniform distribution of air bubbles in cement mixture (Fig. 6.107). In the case of concrete correct air entrainment the air bubbles should have the diameter from 0.02 to 1.0 mm. The effect of these admixtures on the concrete resistance to freezing and thawing is discussed in Sect. 6.3.11.

The too high addition of air entraining agent is disadvantageous because primarily the hydration is slowed down (the surface of cement grains becomes hydrophobic), and secondly too high air content is introduced to the paste.

The air entraining agents reduce slightly the content of mixing water, necessary to assure the same workability of concrete mixture. This effect is the consequence of increased volume of cement paste and the resulting lubrication, reducing the friction caused by aggregate grains. According to Lea [98], the hydrophobic layer of air entraining agent, adsorbed on cement grains, can be involved in this effect. The air entraining agents affect the structure of capillary pores in the paste and, as they are hydrophobic, they reduce the capillary action. The action of air entraining agents is little affected by the type of cement but the grading of aggregate is important. However, the admixture addition should be higher with increasing cement fineness, but lower at higher alkali content, which is presumably the effect

of higher pH [368]. Also with the rise of sand fineness the higher addition of admixture is required. Simultaneously it should be remember that the stability of air entrainment degree depends on superplasticizer used. SMF and SNF reduce the air content [358].

The plastic viscosity of concrete mixture is increasing generally with air entrainment which is caused by adsorption of admixture molecules on cement grains; the hydrophobic properties are thus obtained [358]. Simultaneously, the bleeding is diminished [358].

The mechanism of air entraining agent action consists in the reduction of over–pressure, occurring in air bubbles. This over–pressure can be expressed as follows:

$$\Delta P = 2\sigma / R \tag{6.43}$$

where σ is the surface tension of air bubble, R—radius of air bubble.

The reduction of surface tension causes the stabilization of air bubbles, thus the bubbles introduced during mixing are remaining in concrete (paste).

6.6.5 Permeability Reducing Admixtures

In order to lower the permeability of concrete the addition of very fine powders to concrete mixture is used, which reduce the capillary porosity. They are the materials insoluble in water and hence they are applied in the form of emulsion, as water suspension. They are usually added together with a superplasticizer, to maintain the stable workability level. The silica fumes are often used for this purpose. The other materials used are: quartz flour, bentonite, slag, fluorosilicates and colloidal silica [358]. One should remember that, in concretes with high cement content, the addition of powders can cause inverse effect, increasing the water demand and reducing the degree of concrete consolidation. For this reason, if the heat of hydration is not important and the shrinkage cracks can be restrained, the best method of water permeability reduction is to increase cement content. In this case the lignosulphonate addition is advantageous, because this admixture favors the formation of smaller pores at the expense of larger ones [358].

The reduction of concrete permeability can be achieved by use of hydrophobing agents, such as oils and wax, applied usually in the form of emulsion. The precipitation of their insoluble calcium salts, producing the layers on the walls of capillary pores, is often occurring. The soaps produced from fatty acids, for example the stearates, oleates and palmitates are good hydrophobing admixtures. Advantageous have also the asphaltic emulsions or sulphonated naphthalene–formaldehyde resin (superplasticizer). These admixtures significantly lower the capillary action of dry concrete. Some organic silicon compounds act also as effective hydrophobing agents [408].

As aforementioned, the hampered transport of water through concrete with hydrophobing agents addition counteracts also the formation of efflorescence.

6.6.6 *Viscosity Modifying Admixtures*

In some cases in practice it is necessary to enhance the viscosity of paste to comply with special requirements of the concrete mixture placing. In the underwater concreting the application of viscosity enhancing agent counteracts washing–out of the paste from the mixture. In the plaster mixtures these agents enhance the adherence to the wall. They are used in the production of self–compacting concrete mixture to improve the rheological properties.

Viscosity modifiers give the stability of rheological properties and at the same time improve the quality of concrete mixture. The mechanism of their action involves the crosslinking of cement grains and fine aggregate fractions by long chains of admixture molecules. Simultaneously, due to the functional groups occurring in their structures they act as "liquid glue" and can easily move in the paste [409].

Viscosity modifiers can be divided in several groups, taking into account the type of chemical compound and the mechanism of their action [409]:

Class A—synthetic and natural organic polymers soluble in water, increasing the viscosity of mixing water; these are the following groups of compounds: cellulose ethers, poly(ethylene oxide), polyacrylamides, polyvinylalcohol and others.

Class B—organic flocculants soluble in water, adsorbed on cement grains and increasing viscosity by electrostatic attraction. To class B belong styrene copolymers with carboxylate groups, synthetic polyelectrolytes and natural rubbers.

Class C—emulsions of various organic substances, increasing the electrostatic attraction and introducing ultra–fine particles to cement paste. The following compounds, among many others, are in this group: acryl emulsions and water dispersions of clay.

Class D—inorganic materials diluted with water, of very high specific surface area; they improve the water retention of the paste. Typical examples: bentonite, silica fume.

Class E—inorganic materials of very high specific surface area; they increase the content of fine particles in the paste and therefore its thixotropic properties. The examples are: siliceous fly ash, hydrated lime and kaolin.

When these admixtures are added to concrete for under water works the resistance for washing–out is the key parameter, determining their applicability. In Fig. 6.109 the data relating to the two different viscosity modifying agents (VMA), used at various w/c ratios, are shown. As one can conclude, even at addition on the level 0.10% by mass of cement, the cement paste washing–out is nearly 10 times lower.

The viscosity modifying agents used in the self–compacting concretes production allow reducing of fine grained fraction. The SCC production costs can be greatly lowered too. The impact of various viscosity modifying agents on the properties of fresh SCC mixture is shown in Table 6.11. The results relate to the concrete mixture of the following composition: 380 kg CEM II/A–LL 42.5; 185 l of water; aggregate of maximum grain size 20 mm and the polycarboxylate based superplasticizer used as 0.8% by mass of cement. The most important feature of the viscosity modifying agents used in SCCs is that they do not affect the yield stress value at significant growth of viscosity.

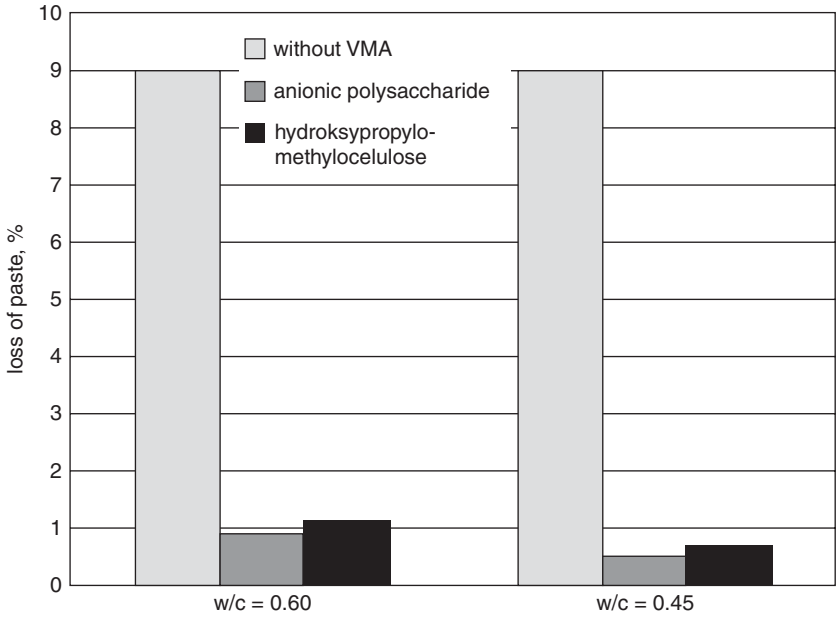


Fig. 6.109 Loss of concrete mixture mass after three times placing in water. (According to [409])

Table 6.11 Effect of two various viscosity modifying agents on the properties of SCC [409]

Type of VMA	Flow diameter cm	T_{50} s	V–funnel[a] S	Remarks
No VMA	71	2	Blocking	Segregation and bleeding
Modified cellulose (3 %)	67	3	9	Segregation after addition of water+ 10 l/m^3
Nanosilica (5 %)	54	3	Blocking	
Polysaccharides (150 g/m^3)	66	4	26	Segregation after addition of water + 10 l/m^3; flow diameter reduced at higher addition
Xantane gum	68	3	28	Segregation and bleeding; flow diameter reduced at higher addition
Modified polyacryloamides (2 %)	56	12	Blocking	Segregation after addition of water + 10 l/m^3
Modified polyacryloamides (1 %)	68	4	11	No changes after addition of water + 10 l/m^3

[a] Funnel flow test; time of concrete mixture flow from the funnel is measured

6.7 Mineral and Chemical Composition of Aggregates

In the concrete mix design relatively little attention is paid to the chemical and mineral composition of aggregate. Obviously, grading and physical properties, mainly the compressive strength, abrasion resistance, porosity and freeze–thaw resistance are of the highest importance [287, 410]. Only in the case of potential risk of alkali

silica reaction the mineral composition of aggregate is determined by microscopic methods or the chemical composition is analyzed according to the ASTM C289 standard.

This question has not been thoroughly studied, presumably because of the traditional approach to the assessment of aggregate, as aforementioned [287, 409]. Neville [287], in his excellent monographic book, giving a concise classification of minerals according to the ASTM C294–86. Neville [287] is writing: " Even small amounts of minerals or of rocks may have a large influence on the quality of aggregate". This statement underlines the need of petrographical examination of aggregate. It is important particularly when the aggregate is deriving from new deposits, primarily in the case of gravel aggregates which have very complex and variable mineral composition. These materials are composed of the chips of various rocks. The crushed aggregate originating from one deposit and one rock is much more uniform. However, even in this case a various degree of weathering or geological transformation of rock from one deposit can occur, changing the mineral composition and properties of the rock material.

In the Polish standard PN–87/B–01 1000 the classification, names and determination of particular types of aggregates are given. In the PN–EN 932–3 standard the simplified method of aggregate petrographic constitution verification is recommended, and eventually the chemical composition analyzing. In the PN–G–11010 Polish standard the methods of some hazardous components determination in water leachates are given. Finally, in the PN–EN 1744 standard a group of methods of harmful components (chlorides, fluorides, sulphates), as well as the reactive silica determination is recommended.

Some harmful components of aggregate are mentioned in Sect. 6.3.2, where the alkali–aggregate reaction and the construction of aggregate–cement matrix interfacial transition zone are discussed. It should be underline once again that the properties of concrete are not badly influenced by all reactions of aggregate with basic hydroxides contained in concrete pore solution. The reaction of calcium hydroxide with albite is a good example of advantageous process [411]. Albite $Na[AlSi_3O_8]$ forms solid solutions with anorthite $Ca[Al_2Si_2O_8]$, in which the sodium and calcium ions can be mutually substituted. As it has been proved experimentally, the diffusion of calcium ions to the surface layer of albite takes place readily with the substitution of sodium ions in albite structure. It facilitates the occupation by calcium ions of active sites on the albite surface and the further diffusion into the inner parts of its structure. This process leads successively to the transformation of surface albite layer into the C–S–H phase and has advantageous influence on the properties of aggregate–cement matrix interfacial transition zone [411]. One should underline that the plagioclases reveal a low degree of stability on the scale of mineral stability according to Goldich [412] and this accounts for their reactivity in the calcium hydroxide saturated solution. The sodium ions are released in the form of sodium hydroxide, the second product of this reaction; this process can be written as follows:

$$\begin{aligned} &Na_{1-2x}[Al_{1-x},Si_{3-x}O_8] + xCa(OH)_2 + nH_2O \rightarrow \\ &\rightarrow \frac{x}{3}\{Ca_3 \cdot Si_2O_7 \cdot nH_2O\} + 2x\text{NaOH} \end{aligned} \tag{6.44}$$

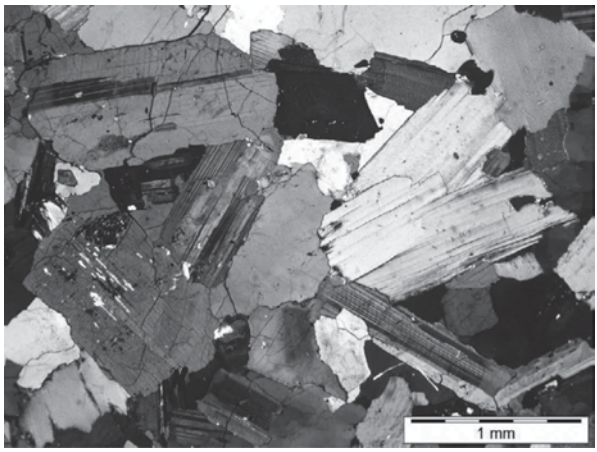


Fig. 6.110 Granite from Nadziejów near Nysa (Poland). Large biotite crystals seen in different cross sections, in the neighborhood of xenomorphic quartz grains and feldspars (plagioclases). Polaroid×

Table 6.12 Standard content of the rock forming[a] and accessory minerals in certain rocks in % by mass [414]

Mineral	Basalt	Gabbro	Granite[b]	Melafire	Syenite
Quartz	1	0	39–49	7–18	9–15
Orthoclase	3–8	8–10	15–25	12–17	17–27
Anorthite	14–19	about 40	6–17	7–22	15–21
Albite	5–29	5–7	10–24	29–34	About 26
Diopside	30–36	about 15	0	3–10	0–6
Olivine	0	15–17	0	0	0
Hematite	0–3	0	0–1	7–13	0–1
Hyperstene	0	0	0–6	0	0–13
Enstatite	0	0	0–2	4–12	0–8
Magnetite	7–11	4–6	1–3	0	2–6
Nefeline	5–18	5–6	0	0	0
Apatite	0–3	About 1	0	1–1.5	about 1
Ilmenite	3–7	About 2	0	1–3	1–2

[a] See the Figs. 6.110 and 6.111
[b] Corundum α–Al_2O_3 1–8

However, the magnesium ions containing minerals can react with concrete pore solution and, as a consequence, the harmful swelling occurs, due to the formation of poorly soluble $Mg(OH)_2$, precipitating in the form of brucite. One should remember that magnesium is a constituent of the rock forming minerals, such as pyroxenes and olivines.

Mineral composition of rocks used in aggregate production in Poland can be found in the Catalogue of Aggregate (Road and Bridge Research Institute Warsaw, Poland [413]. Mineral composition of magmatic and metamorphous rocks from the Lower Silesia in Poland is given according to the report of Geological Institute (1959, [414]). On the base of these data the content of the most important minerals in some rocks, used for aggregate production, is given in the Table 6.12. There

Table 6.13 Chemical composition of selected rocks [414]

Component	Basalt	Gabbro	Granite	Melafire	Syenite
SiO_2	44–48	43–44 (52)	70–77	58–60	55–63
Al_2O_3	11–13	15–19	11–17	13–17	12–17
Fe_2O_3	6–9	3–4 (2)	0.6–2	7–9	3
FeO	4–7	7–8	0.3–1.5	0.4–1.3	4–8
CaO	10–12	9–12	1–4	2–7	5–7
MgO	8–12	8	0.5–2	3–5	2–5
TiO_2	2–3	0.8–1	——[d]	1.5	1
Na_2O	2.4–3	2–4	1.3–2	4	1–3
K_2O	1–1.5	1–2	1.5–4	2–3	3–6
MnO	traces–0.05	—— (0.05)[a]	——	0.01–0.04	traces–0.6
P_2O_5	0.2–0.3	0.2–0.4	——	0.5–0.6	traces
CO_2	0	——	——	1[b]	0
H_2O^-	0.5–1	2.3[c]	1–2[c]	2–2.5	1–3
H_2O^+	0.3–1			1–3	0
S	0	——	——	0	0

[a] Sowia Kopa near Lądek Zdrój in Poland
[b] Only in one case
[c] Total
[d] No data

are so–called "rock forming minerals", which occurrence in certain types of rocks is unquestionable, however less certain is the content of accessory minerals. Their content should be verified experimentally on the rock samples currently used for aggregate production.

Several important data and information concerning aggregates in the United Kingdom can be found in Chap. 16, in Lea's Chemistry of Cement and Concrete [358].

In Table 6.13 the chemical composition of some selected rocks is shown, because these data are rather less known among the specialist working in building industry. The variability range of chemical composition for the magmatic rocks presented in Table 6.13 has been taking account of data given by Polanski [415].

It should be underlined that the sodium and potassium content in the majority of rocks which serve for aggregate production is high, in the range from 5 to 7%. This is an important feature because, as it was found many years ago, the sodium and potassium hydroxides reacting with active silica, could be released from aggregate [99, 101]. Way and Cole proved the leaching of alkalis in the $Ca(OH)_2$ solution, from the crushed granite or basalt, as a result of feldspar decomposition. The leaching of alkalis from aggregate is not basically the equivalent to the occurring of harmful expansive reactions. As it is known, the granites and basalts are the highest quality aggregates. However, Deloye at al. [75] report the examples of concrete destruction due to the alkalis from aggregate, such as gneiss, granite and serpentine.

The following conclusions can be drawn from the mineral composition data:

There is neither quartz and, consequently, nor active silica in basalt and gabbro. It does not mean, however, that silica will be not present in chemical composition

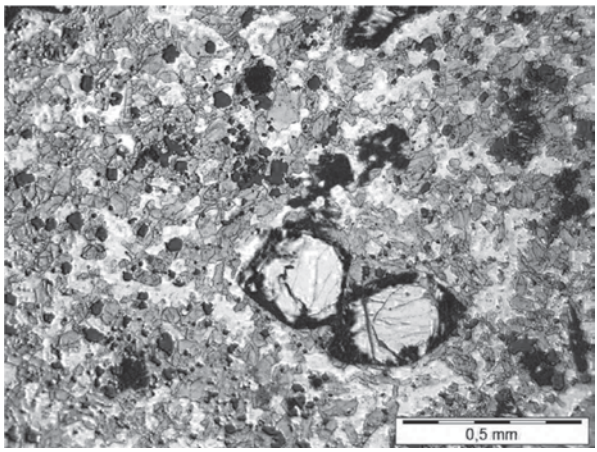


Fig. 6.111 Basalt from Sulików in Poland. Olivine crystals with iddingsite rims (*black*), surrounded by the rocky groundmass built of plagioclase laths, small pyroxene grains and opaque magnetite. One polaroid

of these rocks, because most of the rock forming minerals belong to silicates or aluminosilicates, with lower or higher aluminum content (Si/Al ratio from 1:3 to 1:1). The structural formulas of sodium–calcium aluminosilicates—plagioclases, with 3–dimensional frameworks structure, were given earlier. This group of aluminosilicates, known as feldspars, includes the orthoclase $K[AlSi_3O_8]$; the diopside $CaMg[Si_2O_6]$ is rated to the pyroxenes, the silicates having chain structure. Olivine is the magnesium and iron(II) orthosilicate, with isolated $[SiO_4]^{4-}$ groups, have the formula $(Mg, Fe)_2[SiO_4]$. Its various composition results from the unlimited substitution of magnesium and iron(II) ions. The water suspension of olivine shows the pH = 10–11, the same as wollastonite [416]. Among the silicate rock forming minerals one should mention the enstatite and nepheline. The first one $MgSiO_3$ (with some Fe^{2+} substitution) of chain structure, the second one with single aluminosilicate anions: $KNa_3[Al_4Si_4O_{16}]$. The hypersthenes—$(Mg, Fe)[Si_2O_6]$ solid solution is close to enstatite. The nepheline is relatively unstable in the concrete pore solution and can release easily the potassium and sodium ions. In invaluable monograph of Görlich [416] one can find not only the comprehensive data concerning the minerals but also the silicate occurring in cement and, generally, in ceramics.

Hematite and magnetite are the iron(II) and iron(III) oxides respectively. Magnetite belongs to the spinel group. Illmenite is iron titanate $FeTiO_3$, apatite contains the admixtures of fluorine and chlorine (Fig. 6.115). It reacts with the concrete pore solution, with precipitating of $Ca_3(PO_4)$ [411].

The mineral composition of gravel is very complex. The incidental studies of gravel originating from the deposits in northern Poland reveal that this aggregate is of limestone–siliceous type, with various characteristics. The variability of mineral composition of naturally occurring gravels is clearly visible in Figs. 6.112, 6.113 and 6.114.

From the microscopic studies it can be concluded that the fragments of the following rocks occur in the gravel: sandstone, limestone and feldspar. In two ag-

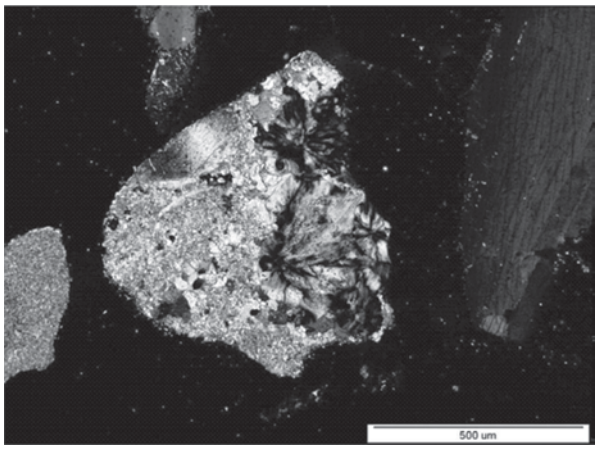


Fig. 6.112 Limestone with the chalcedony spherolites in gravel

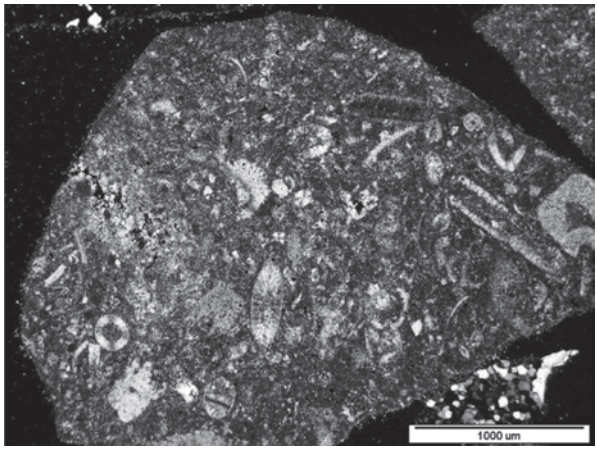


Fig. 6.113 Organic micrite limestone in the gravel

gregate samples the chalcedony, presumably originated from the opal recrystallization, was found (Fig. 6.112). In one aggregate sample the apatite was detected (Fig. 6.115). The following minerals were also found: quartz, calcite, plagioclases, dolomite, amphiboles (antophyllite), and muscovite. There is also some amount of kaolinite, occurred mainly as a product of feldspar transformation.

Gravel can provide the harmful components, for example: chalcedony (mentioned above), cryptocrystalline quartz or dolomite with the clay minerals inclusions. The magnesium anthophyllite can be reactive too.

The following conclusions can be drawn from the mineral composition data:

Silicon is the component with the higher content among the aggregate chemical constituents. The further are: aluminum, iron, magnesium and calcium. The latter one is as the third component in basalt and gabbro rocks. One should underline that the amount of sodium and potassium is relatively high in the aggregate produced

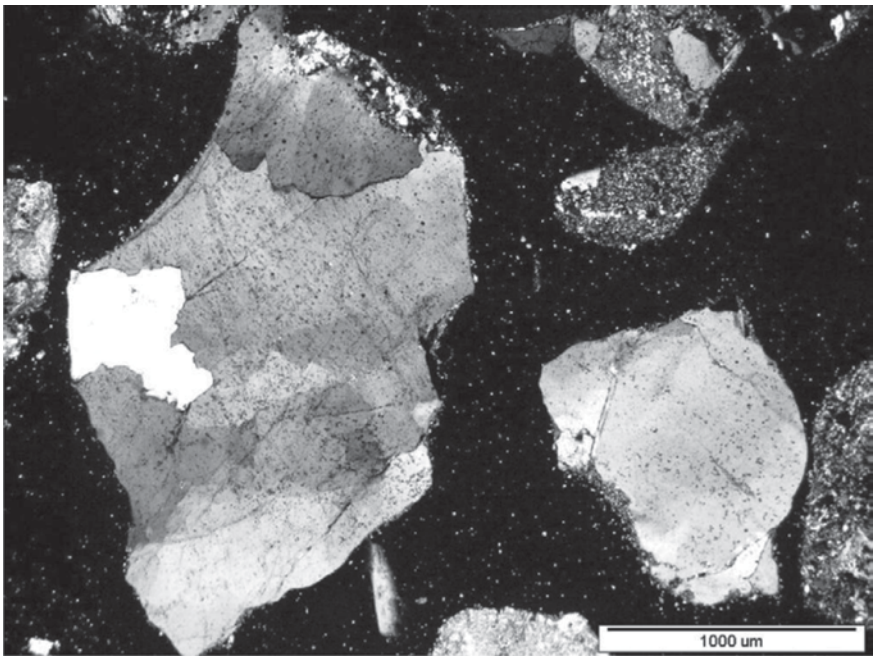


Fig. 6.114 Grain of the quartz–chalcedony rock with the microcline in the gravel

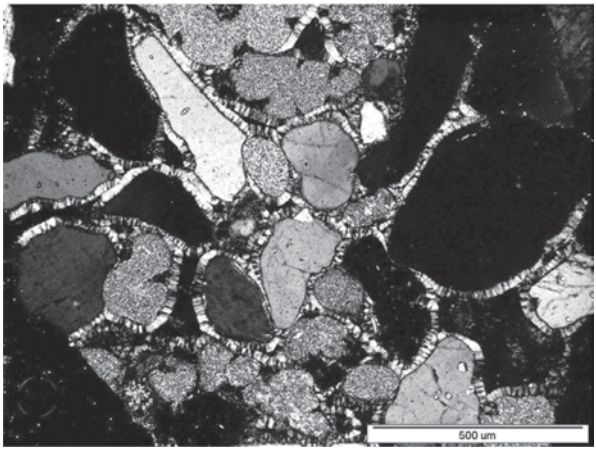


Fig. 6.115 Quartz grains with the apatite rims in the gravel

from the magmatic and metamorphous rocks. Obviously, in the limestone rocks the content of calcium is high and in the dolomite—the percentage of calcium and magnesium respectively. In some magmatic rocks a substantial amount of chlorine can be found (Table 6.14).

Table 6.14 Chemical variability of magmatic rocks, % by mass [415]

Component	Content (% by mass)	Component	Content (% by mass)	Component	Content (% by mass)
SiO_2	32–80	Na_2O	0–19	Cl	0–5
Al_2O_3	0–30	K_2O	0–12	F	0–1
Fe_2O_3	0–8	H_2O	0–5	Cr_2O_3	0–1
FeO	0–17	TiO_2	0–5	BaO	0–5
MgO	0–49	P_2O_5	0–4		
CaO	0–18	MnO	0–0.4		

References

1. Gebauer, J.: 7th ICCC Paris, vol. IV, p. 760. Paris (1980)
2. Locher, F.W.: Influence of the Grinding Process on Cement Properties, w Advances in Cement Manufacture and Use. In: Gartner, E. (ed.) Engineering Foundation, New York (1988).
3. Bombled, J.P.: 7th ICCC Paris, vol. IV, p. 756, Paris (1980)
4. Venuat, M.: Rev. Mat. Constr. **553**, 434 (1961), **629**, 59 (1968)
5. Grzymek, J.: Silikattechnik. **6**, 296 (1955), **10**, 81 (1959)
6. Peukert, J.: 6th ICCC Moscow, vol. III, p. 27. Moscow (1974)
7. Kurdowski, W.: Wpływ dodatku baru na własności klinkieru portlandzkiego, „Ceramika", No. 18, PAN. Kraków (1972). (in Polish)
8. Peukert, J.: Materiały VIII Konferencji Technicznej Przemysłu Betonów, p. 166. Jadwisin, March 30–31th (1978). (in Polish)
9. Grzeszczyk, St., Starzyk, K.: Cement Wapno Beton. **75**, 89 (2008)
10. Maso, J.C.: 7th ICCC Paris, vol. I, p. VII–l/3. Paris (1980)
11. Aleksander, K.M., Taplin, J.H.: Austr. J. Appl. Sci. **13**, 277 (1962), **15**, 160 (1964)
12. Hillemeier, B., Hilsdorf, H.K.: Cem. Concr. Res. **7**, 532 (1977)
13. Mindess, S., Diamond, S.: Cem. Concr. Res. **10**, 509 (1980)
14. Mindess, S., Diamond, S.: Mat. Concr. **15**, 107 (1982)
15. Zaitsev, Y.B., Wittmann, F.H.: Mat. Concr. **14**, 357 (1981)
16. Grandet, J., Ollivier, J.P.: 7th ICCC Paris, vol. III, p. VII–63, VII–85. Paris (1980)
17. Barnes, B.D., Diamond, S., Dolch, W.L.: Cem. Concr. Res. **8**, 233 (1978)
18. Conjeaud, M., Bonin, A., George, C.M., Montgomery, R., Sorrentino, F.P.: Coll. Int. Liaisons Pâtes de Ciment Materiaux Associés, p. C 12. Toulouse (1982)
19. Langton, C.A., Roy, D.M.: 7th ICCC Paris, vol. III, p. VII–127. Paris (1980)
20. Conjeaud, M., Lelong, B., Cariou, B.: 7th ICCC Paris, vol. III, p. VII–6. Paris (1980)
21. Petri, E.M.: Ind. Eng. Chem. Prod. Res. Dev. **15**, 242 (1976)
22. Ping, X., Beaudoin, J.J.: Cem. Concr. Res. **22**, xxx (1992)
23. Scrivener, K.L., Bentur, A., Pratt, P.L.: Adv. Cem. Res. **1**, 230 (1988)
24. Uchikava, H., Savaki, D., Hanehara, S.: Cem. Concr. Res. **25**, 353 (1995)
25. Barnes, B.D., Diamond, S., Dolch, W.J.: J. Am. Ceram. Soc. **62**, 21 (1979)
26. Scrivener, K.L., Gartner, E.M.: Proc. Conf. „Bonding in Cementiteous Composites", p. 77. In: Mindess, S., Shaw, S.P. (eds.) Pittsburgh, USA (1987)
27. Scrivener, K.L., Pratt, P.L.: 8th ICCC Rio de Janeiro, vol. III, p. 466. Rio de Janeiro (1986)
28. De Rooij, M.R., Bijen, J.M., Fens, G.: RILEM 2nd Int. Conf. on Interfacial Transition Zone in Cementiteous Composites, p. 4949. In: Katz, A. (ed.) Haifa, Israel (1998)
29. Zimbelman, R.: Cem. Concr. Res. **15**, 801 (1985)
30. Struble, L., Skalny, J., Mindess, S.: Cem. Concr. Res. **10**, 277 (1980)
31. Zimbelmann, R.: Betonwerk und Fertigteil–Technik. **2**, 89 (1978)
32. Diamond, S.: Mater. Res. Soc. Symp. **85**, 21 (1987)
33. Hoshino, M.: ACI Mater. J. **86**, 125 (1989)

34. Diamond, S., Huang, J.: RILEM 2nd Int. Conf. on Interfacial Transition Zone in Cementiteous Composites, p. 1. In: Katz, A. (ed.) Haifa, Israel (1998)
35. Scrivener, K.L.: The microstructure of concrete. In: Skalny, J. (ed.) Materials Science of Concrete, p. 127. The American Ceramic Society (1989)
36. Uchikava, H., Savaki, D., Hanehara, S.: Cem. Concr. Res. **25**, 353 (1995)
37. Ollivier, J.P., Maso, J.C., Bourdette, B.: Adv. Cem. Based. Mater. **2**, 30 (1995)
38. Mehta, P.K., Monteiro P.J.M., Mater. Res. Soc. Symp. **114**, 65 (1988)
39. Scrivener, K.L., Pratt, P.L.: 8th ICCC Rio de Janeiro, vol. III, p. 466. Rio de Janeiro (1986)
40. Hunter, R.J.: Introduction to Modern Colloid Science. University Press, Oxford (1993)
41. Massazza, F., Costa, V.: 8th ICCC Rio de Janeiro, vol. I, p. 158. Rio de Janeiro (1986)
42. Monteiro, P.J., Maso, J.C., Ollivier, J.P.: Cem. Concr. Res. **15**, 953 (1985)
43. Monteiro, P.J., Mehta P.K.: Cem. Concr. Res., **15**, 378 (1985)
44. Kokuba, M., Yamada, J.: 6th ICCC Moscow, vol. III, p. 83. Moscow (1974)
45. Carles–Gibergues, A., Grandet, J., Ollivier, J.P.: Coll. Int. Liaisons Pâtes de Ciment Materiaux Associés, p. B.11. Toulouse (1982)
46. Nagataki, S., Takuada, M.: 7th ICCC Paris, vol. III, p. VII–90. Paris (1980)
47. Tognon, G.P., Ursella, P., Coppetti, G.: 7th ICCC Paris, vol. III, p. VII–75. Paris (1980)
48. Aïtcin, P.C.: Cement Wapno Beton. **70**, 115 (2003)
49. Arlignie, G., Grandet, J., Ollivier, J.P.: Mat. Constr. **18** (106), 263 (1985)
50. Bentur, A., Diamond, S., Mindess, S.: Cem. Concr. Res. **15**, 331 (1985)
51. Al Khalaf, M.N., Page, C.L.: Cem. Concr. Res. **9**, 197 (1979)
52. Pinchin, D.J., Tabor D.: Cem. Concr. Res. **8**, 15 (1978)
53. Page, C.L., Al Khalaf, M.N., Rotchie, A.G.B.: Cem. Concr. Res. **8**, 481 (1978)
54. Mindess, D., Odler, I., Skalny, J.: 8th ICCC Rio de Janeiro, vol. I, p. 151. Rio de Janeiro (1986)
55. Diederichs, U., Schneider, U.: Mag. Concr. Res. **33**, 75 (1981)
56. Clifton, J.R., Mathey, R.G.: J. Am. Concr. Inst. **80**, 288 (1983)
57. Hannant, D.J.: Fibre Cements and Fibre Concretes. Wiley, Chichester (1978)
58. Cook, J., Gordon, J.E.: Proc. Roy. Soc. **A282**, 508 (1964)
59. Nayeb Haskani, H., Cohen, M.D.: Cem. Concr. Res. **15**, 879 (1985)
60. Turriziani, R.: 8th ICCC Rio de Janeiro, vol. I, p. 388. Rio de Janeiro (1986)
61. Calleja, J.: 7th ICCC Paris, vol. I, p. VII–2/1. Paris (1980)
62. Litvan, G.G.: 6th ICCC Moscow, vol. H/2, p. 40. Moscow (1974)
63. Dehghanian, C., Locke, C.E.: Corrosion **39**, 299 (1983)
64. Powers, T.C., Copeland, L.E., Hayes, J.C., Mann, H.M.: J. Amer. Concr. Inst. **51**, 285 (1954)
65. Skalny, J., Pierce, J.S.: In: Marchand, J., Skalnyw, J. (eds.) Materials science of concrete: Sulphate attack mechanisms, p. 49. The American Ceramic Society, Westerville, USA (1999)
66. Smolczyk, H.G.: 5th ICCC Tokyo, vol. III, p. 274, Tokyo (1968)
67. Skalny, J., Marchand, J.: In: Kurdowski, W., Gawlicki, M. (eds.) Sulphate attack on concrete revisited, w Kurdowski Symposium, Kraków June 2001, p. 171. Akapit, Kraków (2001)
68. Dutruel, F., Gayader, R.: Monographie n°7. du CERIB (France) (1975)
69. Alegre, R.: Ann. Inst. Techn. Bat. Tran. Publ. (374), 12 (1978)
70. Żivika, V.: Zement Kalk Gips. **24**, 175 (1971)
71. Oberholster, R.E., Wan Aardt, J.H.P., Brandt, M.P.: In: Barnes, P. (ed.) w Structure and Performance of Cements, p. 365. Appl. Science Publ., London (1983)
72. Mortureux, B., Hornain, H., Regourd, M.: Coll. Int. Liaisons Pâtes de Ciment Materiaux Associés, p. A.64. Toulouse (1982)
73. Grandet, J., Ollivier, J.P.: Cem. Concr. Res. **10**, 759 (1980)
74. Massaza, F., Pezzuoli, M.: 7th ICCC Paris, vol. III, p. VII–16. Paris (1980)
75. Deloye, F.X., Le Roux, A., Lesage. R., Coll. Int. Liaisons Pâtes de Ciment Materiaux Associés, p. B.1. Toulouse (1982)
76. Perry, C., Gillott, J.E.: Durability Build. Mater. **1**, 305 (1983)
77. Gutteridge, W.A., Hobbs, D.W.: Cem. Concr. Res. **10**, 183 (1980)
78. Dent Glasser, L.S., Kataoka, N.: Cem. Concr. Res. **11**, 1 (1981)

79. Dent Glasser, L.S.: Cem. Concr. Res. **9**, 515 (1979)
80. Roy, D.M.: 8th ICCC Rio de Janeiro, vol. I, p. 362. Rio de Janeiro (1986)
81. Diamond, S., Barneyback, R.S., Struble, L.J.: Proc. 5th Int. Conf. on Alkali–Aggregate Reaction in Concrete, p. 252/22. Cape Town (1981)
82. Ludwig, U.: ibid., p. 525/24
83. Struble, L.J., Diamond, S.: Cem. Concr. Res. **11**, 611 (1981)
84. Struble, L.J., Diamond, S.: J. Am. Ceram. Soc. **64**, 652 (1981)
85. Owsiak, Z.: Cem. Concr. Res. **34**, 7 (2004)
86. Grattan–Bellew, P.E.: Cem. Concr. Res. **35**, 1868 (2005)
87. Owsiak, Z.: Wewnętrzna korozja siarczanowa betonu. Pol. Świętokrzyska. Kielce (in Polish) (2008)
88. Owsiak Z.: Cement Wapno Beton. **67**, 241 (2000)
89. Owsiak, Z.J.: Civil Eng. Manag. **13**, 201 (2007)
90. Collepardi, M., Ogoumagh Olagot, J.J.: In: Scrivener, K., Skalny, J. (eds.) w Internal Sulphate Attack and Delayed Ettringite Formation. Proc. Int. RILEM TC 186–ISA Workshop, p. 212. Villars (2002)
91. Dent Glasser, L.S., Kataoka, N.: Proc. 5th Int. Conf. on Alkali–Aggregate Reaction in Concrete, p. 252/23. Cape Town (1981)
92. Regourd, M., Hornain, H., Mortureux, B., Poitevin, P., Peupatier, H.: Coll. Int. Liaisons Pâtesde Ciment Materiaux Associés, p. B.17. Toulouse (1982)
93. St. John, D.A.: Cem. Concr. Res. **11**, 801 (1981)
94. Cole, W.F., Lanuchi C.J., Sandy M.J.: Cem. Concr. Res. **11**, 443 (1981)
95. Cole, W.F., Lanuchi, C.J.: Cem. Concr. Res. **13**, 611 (1983)
96. Davis, C.E.S.: Aust. J. Appl. Sci. **9**, 52 (1958)
97. Roy, D.M., Idorn, G.M.: Mortars and Concrete ACI J. **79**, 444 (1982)
98. Lea, F.M.: The Chemistry of Cement and Concrete, 3rd edn. Chemical Publ. Comp., New York (1971)
99. Stark, D.: Cem. Concr. Aggregates. **2**, 92 (1980)
100. Owsiak, Z.: Cement Wapno Beton. **68,** 61 (2001)
101. Way, S.J., Cole, W.F.: Cem. Concr. Res. **12**, 611 (1982)
102. Deloye, F.X., Le Roux, A., Lesage, R.: Bull. Liaison Lab. Pont. Chauss. **126**, 37 (1983)
103. Malek, R.A., Roy, D.M.: Proc. 6th Int. Conf. on Alkalis in Concrete, p. 223. Copenhagen (1983)
104. Grattan–Bellew, P.E.: Durability Build. Mater. **1**, 363 (1983)
105. Locher, T.W., Sprung, S.: Beton. (7), 302 (1973), (8), 349 (1973)
106. Chatterji S.: Cem Concr. Res. **9**, 185 (1979)
107. Smolczyk, H.G.S.: Symp. on Alkali–Aggregate Reaction, p. 183. Reykjavik (1975)
108. Sorrentino, D., Sablo, S., Junique, D.: Ann. ITBTP. (499), 89 (1991)
109. Kurdowski, W., Garbacik, A., Trybalska, B.: Cement Wapno Beton. **72**, 339 (2005)
110. Hobbs, D.W.: Mag. Concr. Res. **34**, 82 (1982)
111. Gaze, M.E., Nixon, P.J.: Mag. Concr. Res. **35**, 107 (1983)
112. Tang, M.S., Ye, Y.F., Yang, H.Q., Zhen, S.H.: Cem. Concr. Res. **13**, 171 (1983)
113. Bakker, R.F.M.: Silicates Ind. **47**, 91 (1982)
114. Metso, J.: Silicates Ind. **47**, 123 (1982)
115. Diamond, S.: Cem. Concr. Res. **11**, 383 (1981)
116. Frigione, G., Marotta, R.: World Cem. Technol. **12**, 73 (1981)
117. Bakker, R.F.M.: Ciment, Bétons, Plâtres, Chaux. (734), 49 (1982)
118. Berry, E.E., Malhotra, V.M.: In: Malhotra, V.M. (ed.) w Supplementary Cementing Materials for Concrete, p. 37. Canadian Government Publishing Centre, Ottawa (1987)
119. Kawamura, M., Takemoto, K., Hasaba, S.: Rev. 38th Gen. Meet. Cem. Assoc. Japan, p. 92. Tokyo 1984.
120. Aïtcin, P.C., Regourd, M.: Cem. Concr. Res. **15**, 711 (1985)
121. Dunston, E.R.: Cem. Concr. Aggregates. **3**, 101 (1981)

122. Wischers, G.: Widerstand gegen die Alkalireaktion, w Zement Taschenbuch 1976/77, p. 94. Verein Deutscher Zementwerke. Bauverlag GmbH, Wiesbaden–Berlin (1976)
123. Hobbs, D.W.: Mag. Concr. Res. **33**, 208, (1981)
124. Mehta, P.K., Manmohan, D.: 7th ICCC Paris, vol. III, p. VII–1. Paris (1980)
125. Feldman, R.F.: 8th ICCC Rio de Janeiro, vol. I, p. 336: Rio de Janeiro (1986)
126. Smolczyk, H.G.S.: 7th ICCC Paris, vol. I, p. III–1/3. Paris (1980)
127. Bakker, R.F.M.: Proc. 5th Int. Conf. on Alkali–Aggregate Reaction in Concrete. Cape Town, p. S252/29. (1981)
128. Rayment, P.L.: Cem. Concr. Res. **12**, 133 (1982)
129. Diamond, S.: Proc. 6th Int. Conf. on Alkalis in Concrete, p. 155. Copenhagen (1983)
130. Glasser, F.G.: Marr, J.: Il Cemento. **82**, 85 (1985)
131. Tong Ming–Shu, Ye Yu–Feng, Yuan Mei–qi, Zen Ski–hua: Cem. Concr. Res. **13**, 171 (1983)
132. Kawamura, M., Takemoto, K., Hasaba, S.: Proc. 6th Int. Conf. on Alkalis in Concrete, p. 167. Copenhagen (1983)
133. Verbeck, G.J., Gramlich C.: ASTM Proc., **55**, 1110 (1955)
134. Hansen, W.C.: J. Amer. Concr. Inst. **15**, 213 (1944)
135. Thomas, M.: The role of calcium hydroxide in alkali recycling in concrete. In: Skalny, J., Gebauer, J., Odler, I. (eds.) w Materials Science of Concrete: Calcium Hydroxide in Concrete, p. 225. The American Ceramic Society, Westerville (2000)
136. Kurdowski, W.: Non Published Paper
137. Glasser, F.P.: 11th ICCC Durban, vol. I, p. 19. Durban (2003)
138. Kurdowski, W., Garbacik, A., Baran, T.: Gospodarka Surowcami Mineralnymi. **22**, 87 (2006). (in Polish)
139. Mather, B.: Symp. on Alkali–Aggregate Reaction, p. 17. Reykjavik (1975)
140. Swenson, E.G.: ASTM Bull. **226**, 48 (1957)
141. Swenson, E.G., Gillot, J.E.: Transp. Res. Record. **45**, 21 (1964)
142. Hadley, D.W.: Transp. Res. Record. **45**, 1, 196 (1964)
143. Pagano, M.A., Cady, P.D.: Cem. Concr. Res. **12**, 1 (1982)
144. Tang, M.S., Liu, Z., Han, S.F.: In: Grattan–Bellew, P.E. (ed.) w Concrete Alkali–Aggregate Reactions, p. 275. Noyes Publ., Park Ridge (1987)
145. Heinz, D., Ludwig, U.: 8th ICCC Rio de Janeiro, vol. V, p. 189. Rio de Janeiro (1986)
146. Heinz, D., Ludwig, U., Rudger, L.: Concrete Pecasting Plant and Technology. **11**, 56 (1989)
147. Divet, L., Pavoine, A.: In: Scrivener, K., Skalny, J. (eds.) w Internal Sulphate Attack and Delayed Ettringite Formation, Proc. Int. RILEM TC 186–ISA Workshop, p. 98. Villars (2002)
148. Shayan, A., Quick, G.W.: Adv. Cem. Res. **4**, 149 (1991)
149. Kelham, S.: Cem. Contr. Composites. **18**, 171 (1996)
150. Kelham, S.: 10th ICCC Göteborg, vol. IV, paper 4IV059. Göteborg (1997)
151. Wieker, W., Herr, R., Schubert, H.: In: Kurdowski, W. (ed.) Proc. Int. Coll. Corrosion of Cement Paste, Mogilany 16–17 November, p. 3. Kraków (1994)
152. Famy, C.: Ph. D. Thesis, Imperial College, Materials Departament, London (1999)
153. Mielenz, R.C., Marusin, S., Hime, W.G., Jugowic, Z.T.: Concr. Intern. **17**, 62 (1995)
154. Kelham, S.: Conf. Cement and Concrete Science, Keele University. 2–3 September 1999
155. Kurdowski, W., Garbacik, A., Chladzynski, S.: Cement Wapno Beton. **71**, 81 (2004)
156. Wieker, W., Scrivener, K.L.: 9th ICCC New Delhi, vol. I, p. 449. New Delhi (1992)
157. Bensted, J.: Il Cemento. **76**, 117 (1976)
158. Ghorab, H.Y., Kisher, E.: 8th ICCC Rio de Janeiro, vol. V, p. 105. Rio de Janeiro (1986)
159. Sylla, H.M.: Beton. **38**, 449 (1988)
160. Odler, I., Adbul–Maula, S., Zhougya, L.: In: Struble, L.J., Brown, P.W. (eds.) Materials Research Society Symposium Processings, vol. 85, Microstructural Development During Hydration of Cement, p. 139. (1987)
161. Glasser. F.P., Damidot. D., Atkins. M.: Adv. Cem. Res. **26**, 57 (1995)
162. Lawrence, C.D.: In: Skalny, J., Mindess, S. (eds.) Materials Science of Concrete IV, p. 113. The American Ceramic Society, Westerville (1995)
163. Lawrence, C.D.: Cem. Concr. Res. **25**, 903 (1995)

164. Hime, W.G.: In: Dhir, R.K., Dyer, T.D. (eds.) w Concrete for Environment Enhancement and Protection, p. 387. E & FN Spon, London (1996)
165. Yang, R., Lawrence, C.D., Sharp, J.H.: Cem. Concr. Res. **26**, 1649 (1996)
166. Yang, R., Lawrence, C.D., Sharp, J.H.: Adv. Cem. Res. **11**, 119 (1999)
167. Diamond, S.: In: Scrivener, K., Skalny, J. (eds.) w Internal Sulphate Attack and Delayed Ettringite Formation, Proc. Int. RILEM TC 186–ISA Workshop, p. 178. Villars (2002)
168. Johansen, V., Thaulow, N., Skalny, J.: Adv. Cem. Res. **5**, 23 (1993)
169. Scrivener, K.L., Taylor, H.F.W.: Adv. Cem. Res. **5**, 139 (1993)
170. Scrivener, K.L., Lewis, M.C.: 10th ICCC Göteborg, vol. IV, paper 4IV061. Göteborg (1997)
171. Pade C., Jakobsen U. H., Johansen V., International Baustofftagung, Bauhaus–Universität, Weimar 1997, vol. 1, p. 1
172. Famy, C., Scrivener, K.L., Atkinson, A., Brough, A.R.: Cem.Concr. Res. **31**, 795 (2001).
173. Scherrer, G.W.: In: Scrivener, K., Skalny, J. (eds.) Internal Sulphate Attack and Delayed Ettringite Formation, Proc. Int. RILEM TC 186–ISA Workshop, p. 139. Villars (2002)
174. Barbarulo, R., Peycelon, H., Prane, S.: In: Scrivener, K., Skalny, J. (eds.) The role of C–S–H and temperature in delayed ettringite formation, Proc. Int. RILEM TC I86–ISA Workshop, p. 155. Villars (2002)
175. Odler,, I., Chen, Y.: Cem. Concr. Res. **25**, 853 (1995)
176. Brown, P.W., Taylor, H.F.W.: In: Marchand, J., Skalny, J.P (eds.) The Role of Ettringite in External Sulphate Attack, p. 73 in Materials Science of Concrete, Sulfate Attack Mechanisms. The American Ceramic Society, Westerville (1999)
177. Skalny, J., Johansen, V., Thaulow, N., Palomo, A.: Materiales de Constructión. **46**, 5 (1996)
178. Fu, Y., Xie, P., Gu, P., Beaudoin, J.J.: Cem. Concr. Res. **24**, 1015 (1994)
179. Grattan–Bellew, P.E., Beaudoin, J.J., Vallée, V.G.: Cem.Concr. Res. **28**, 1147 (1998)
180. Feldman, R.F.: In: Malhotra, V.M. (ed.) Fly ash, silica fume, slag and natural pozzolanas in concrete, Proc. 2nd Int. Conf. Madrid, ACI, SP–91, 2, p. 973. (1986)
181. Kurdowski, W., Duszak, S.: In: Scrivener, K., Skalny, J. (eds.) Proc. RILEM TC 186–ISA Workshop, p. 229. Villars (2002)
182. Kelham, S.: ibid., p. 197.
183. Klemm, W.A., Miller, F.M.: 10th ICCC Göteborg, vol. IV, paper 4IV059. Göteborg (1997)
184. Michaud, V., Suderman, R.: 10th ICCC Göteborg, vol. II, paper 2ii11. Göteborg (1997)
185. Herfort, D., Soerensen, J., Coulthard, E.: World Cem. Res. Dev. **28**, 77 (1997)
186. Scrivener, K., Skalny, J. (ed.): Internal Sulphate Attack and Delayed Ettringite Formation, Proc. RILEM TC 186–ISA Workshop, Villars (2002)
187. Kurdowski, W.: Cem. Concr. Res. **32**, 401 (2002)
188. Ghorab, H.Y., Heinz, D., Ludwig, U., Meshendahl, T., Wolter, A.: 7th ICCC Paris, vol. IV, p. 496. Paris (1980)
189. Shayan, A., Ivanusec, I.: Cem. Concr. Comp. **18**, 161 (1996)
190. Owsiak, Z.: Cement Wapno Beton. **66**, 40 (2007)
191. Page, C.L., Short, N.R., El Tarras, A.: Cem. Concr. Res. **11**, 395 (1981)
192. Ushiyama, H., Goto, S.: 6th ICCC Moscow, vol. II/1, p. 331. Moscow (1974)
193. Collepardi, M., Marcialis, A., Turriziani, R.: J. Am. Ceram. Soc. **55**, 514 (1972)
194. Collepardi, M., Marcialis, A., Turriziani, R.: Il Cemento. **69**, 143 (1972)
195. Gjörv, E., Vennesland, O.: Cem. Concr. Res. **9**, 229 (1979)
196. Goto, S., Daimon, M.: 8th ICCC Rio de Janeiro, vol. VI, p. 405. Rio de Janeiro (1986)
197. Marchand, J., Gerard, B., Delgrave, A.: In: Skalny, J., Mindess, S. (ed.) w Material Science in Concrete p. 307. The American Ceramic Society, Westerville (1998)
198. Andrade, C.: Cem. Concr. Res. **23**, 724 (1993)
199. Hornain, H., Marchand, J, Duhot, V., Moranville–Regourd, M.: Cem. Concr. Res. **25**, 1667 (1995)
200. Tang, L., Nilsson, L.O.: Cem. Concr. Res. **25**, 1133 (1995)
201. Delagrave, A., Pigeon, M., Revertegat, E.: Cem. Concr. Res. **24**, 1433 (1994)
202. Schwiete, H.F., Ludwig, U., Albeck, J.: Zement Kalk Gips. **22**, 225 (1969)

203. Theissing, E.M., Mebius–van, De Laar T., De Wind, G.: 7th ICCC Paris, vol. IV, p. 823. Paris (1980)
204. Glasser, F.P., Luke, K., Angus, M.J.: Cem. Concr. Res. **18**, 165 (1988)
205. Ecker, M., Pöllmann, H.: 10th ICCC Göteborg, vol. II, p. 2ii032. Göteborg (1997)
206. Beaudoin, J.J., Ramachandran, V.S., Feldman, R.F.: Cem. Concr. Res. **20**, 875 (1990)
207. Ramachandran, V.S.: Mater. Constr. Struct. **4**, 312 (1971)
208. Diamond, S.: Cem. Concr. Aggregates. **18**, 97 (1986)
209. Page, C.L., Vennesland, O.: Mater. Constr. Struct. **16**, 19 (1983)
210. Uchikawa, H., Okamura, T.: Binary and ternary components blended cement. In: Sarkar, L., Ghosh, S.N. (eds.) w Progress in Cement and Concrete, vol. 4, p. 1. ABI Books, New Delhi (1993)
211. Short, N.R., Page, C.L.: Silicates Ind. **47**, 237 (1982)
212. Byfors, K.: Nordic Concr. Res. **5**, 27 (1986)
213. Tenoutasse, N.: Zement Kalk Gips. **22**, 459 (1967)
214. Richartz, W.: Zement Kalk Gips. **24**, 447 (1969)
215. Theissing, E.M., Hest–Wardernier, P.V., De Wind, G.: Cem. Concr. Res. **8**, 683 (1970)
216. Blank, G., Gunkel, P., Smalczyk, H.G.: 8th ICCC Rio de Janeiro, vol. I, p. 85. Rio de Janeiro (1986)
217. Arya, C., Buenfeld, N.R., Newman, J.B.: Cem. Concr. Res. **20**, 291 (1990)
218. Tritthart, J.: Bundesministerium für Wirtschaftige Angelegenheiten Strassenforschung. Heft, Vienna (1988)
219. Byfors, K.: CBI Report No. 190. Swedish Cement and Concrete Institute. Stockholm (1990)
220. Midgley, H.G., Illston, J.M.: Cem. Concr. Res. **14**, 546 (1984)
221. Uchikawa, H., Uchida, S., Ogawa, K.: 8th ICCC Rio de Janeiro, vol. IV, p. 251. Rio de Janeiro (1986)
222. Taylor, H.F.W.: Cement Chemistry. Academic Press, London (1990)
223. Regourd, M., Hornain, H., Aïtcin, P.-C.: Mater. Res. Soc. Symp. Proc. Boston. **85**, 185 (1987)
224. Chatterji, S.: Adv. Cem. Bas. Mat. **7**, 102 (1998)
225. Midgley, H.G., Illston, J.M.: 7th ICCC Paris, vol. III, p. VII–101. Paris (1980)
226. Hansson, C.M., Frølund, Th., Markussen, J.B.: Cem. Concr. Res. **15**, 65 (1985)
227. Atkinson, A., Nitkerson, A.K.: Matrs Sci. **19**, 3068 (1984)
228. Powers, T.C., Brownyard, T.L.: J. Am. Concr. Inst. **18**, 1946 (1947)
229. Buil, M., Olivier, J.P.: w La Durabilité des Bétons, p. 57. In: Baron, J, Ollivier, J.-P. (eds.) Presses Ponts et Chaussées, Paris (1992)
230. Garboczi, E.J., Schwartz, L.M., Bentz, D.P.: Adv. Cem. Bas. Mat. **2**, 169 (1995)
231. Bourdette, B., Ringot, E., Ollivier, J.P.: Cem. Concr. Res. **25**, 741 (1995)
232. Brenton, D., Ollivier, J.P., Ballivy, G.: Diffusivite des Ions Chlores dans la Zone de Transition entre Pâte de Ciment et Roche Granitique. In: Maso, J.C. (ed.) Interfaces in Cementiteous Composites, p. 278. Spon, London (1992)
233. Bourdette, B.: La Durabilité de Mortier. Ph. D. Thesis, INSA–Toulouse (1994)
234. Vernet, C.: w La Durabilité des Bétons, p. 129. In: Baron, J., Ollivier, J.-P. (eds.) Presses Ponts et Chaussées, Paris (1992)
235. Słomka–Słupik, B.: Cement Wapno Beton. **75**, 61 (2009)
236. Smolczyk, H.G.: 5th ICCC Tokyo, vol. III, p. 274. Tokyo (1969)
237. Riedel, W.: Zement Kalk Gips. **26**, 286 (1973)
238. Conjeaud, M.: Int. Seminar on Calcium Aluminates, p. 171. In: Murat, M. (ed.) Torino (1982)
239. Kurdowski, W., Taczuk, L., Trybalska, B.: In: Mangabhai, S. (ed.) w Calcium Aluminate Cement, p. 222. Spon, London (1990)
240. Boies, D.B., Bortz, S.: National Cooperative Highway Research Program. **19**, 19 (1965)
241. Van Aardt, J.H.P.: 4th ICCC Washington, vol. II, p. 835. Washington (1960)
242. Chatterji, S.: Cem. Concr. Res. **8**, 461 (1978)

243. Kurdowski, W., Trybalska, B., Duszak, S.: In: Richardson, I.G., El Tarras, A. (eds.) Proc. 16th Int. Conf. on Cement Microscopy, p. 80. Int. Cem. Microscopy Assoc., Richmond (1994)
244. Kurdowski, W.: Advances ceramics glass and mineral binding materials. In: Stoch, L. (ed.) Proc. of 5th Polish–German Seminar, Zakopane, Ceramika, No. 42, p. 35. PAN, Kraków (1992)
245. Kurdowski, W., Duszak, S., Trybalska, B.: In: Krivienko, P.V. (ed.) 1st Int. Conf. Alkaline Cements and Concretes, vol. II, p. 961. Kiev (1994)
246. Kurdowski, W., Duszak, S.: Adv. Cem. Res. **7**, 143 (1995)
247. Vicat, L.J.: Recherche sur les causes chimiques de la destruction des composés hydrauliques par l'eau de mer. (1858)
248. Bied, J.: Recherches industrielles sur la chaux, ciments et mortiers. Dunod, Paris (1926)
249. Kuhl, H.: Zement–Chemie, vol. II, p. 561. Verlag Technik, Berlin (1951)
250. Lea, F.M., Desh, C.H.: Die Chemie des Zements und Betons. Zementverlag GmbH, Berlin (1937)
251. Mehta, P.K.: Sulphate Attack on Conrete—A Critical Review. In: Skalny, J. (ed.) Sulphate Resistance of Concrete III. The American Ceramic Society, Westerville (1992)
252. Mehta, P.K., Schiessl, P., Raupach, M.: 9th ICCC New Delhi, vol. I, p. 571. New Delhi (1992)
253. Locher, F.W.: Zement Kalk Gips. **19**, 395 (1966)
254. Regourd, M., Hornain, H., Mortureux, B.: Silicates Ind. **42**, 13 (1977)
255. Taylor, H.F.W.: In: Marchand, J., Skalny, J. (eds.) Discussion in Materials Science of Concrete: Sulphate Attack Mechanisms, p. 46. The American Ceramic Society, Westerville (1999)
256. Gollob, R.S., Taylor, H.F.W.: Cem. Concr. Res. **24**, 735 (1994)
257. Van Aardt, J.H., Visser, S.: Cem. Concr. Res. **5**, 225 (1975)
258. Lukas, W.: Cem.Concr. Res. **5**, 503 (1975)
259. Wang, J.G.: Cem. Concr. Res. **24**, 735 (1994)
260. Yang, S., Zhongyi, X., Mingshu, T.: Adv. Cem. Bas. Mater. **4**, 1 (1996)
261. Diamond, S., Lee, R.J.: Microstructural alterations associated with sulphate attack in permeable concretes. In: Marchand, J., Skalny, J. (eds.) w Materials Science of Concrete: Sulphate Attack Mechanisms, p. 123. The American Ceramic Society, Westerville (1999)
262. Brown, P.W., Badger, S.: Cem. Concr. Res. **30**, 1535 (2000)
263. Schrämli, W.: World Cement Technol. **9**, 35 (1978), **10**, 75 (1979)
264. Verbeck, G.J.: Research and Development Laboratories of PCA Bull. **227** (1967)
265. Van Aardt, J.H.P., Visser, S.: 7th ICCC Paris, vol. IV, p. 400. Paris (1980)
266. Marchese, B., Mascob, G., Sersale, R.: J. Am. Conr. Inst. **55**, 146 (1972)
267. Vogt, T.: Norsk Geologisk Tidsskrift. **18**, 291 (1938)
268. Erlin, B., Stark, D.C.: Highway Research Record. **113**, 108 (1965)
269. Bensted, J., Varma, S.P.: Cem. Concr. Res. **6**, 321 (1976)
270. Bensted, J.: Thaumasite sulphate attack. In: Kurdowski, W., Gawlicki, M. (eds.) w Kurdowski Symposium, Kraków June 2001, p. 189. Akapit, Kraków (2001)
271. Moenke, H.: Naturwissenschaften. **51**, 239 (1939)
272. Edge, R.A., Taylor, H.F.W.: Nature. **224**, 363 (1969)
273. Bensted, J.: Cement Wapno Beton. **74**, 165, 248 (2007)
274. Małolepszy, J., Mróz, R.: Cement Wapno Beton. **73**, 93 (2006)
275. Mehta, P.K.: Sulphate attack in marine environment. In: Marchand, J., Skalny, J. (eds.) w Materials Science of Concrete: Sulphate Attack Mechanisms, p. 295. The American Ceramic Society, Westerville (1999)
276. Feld, J.: Construction Failures. John Wiley, New York (1968)
277. Kind, W.W.: Cemient. **56**, 3 (1956). (in Russian)
278. Duval, R., Hornain, H.: La durabilité du béton vis–à–vis des eaux agressives. In: Baron, J., Ollivier, J.-P. (eds.) w La Durabilité des Bétons, p. 351. Presses Ponts et Chaussées, Paris (1992)
279. Locher, F.W.: 5th ICCC Tokyo, vol. III, p. 328. Tokyo (1968)

280. Ben Yair, M.: Cem. Concr. Res. **4**, 405 (1974)
281. Regourd, M.: Carbonatation accélérée et résistance des ciments aux eaux agressives. Cement and Concrete Association (1976). In: Symp. Int. RILEM sur la carbonatation du béton, Slough, 5–6 April 1976
282. Regourd, M.: Ann. Inst. Tech. Bat. Trav. Publ. **329**, 86 (1975)
283. Idorn, G.M.: Durability of Concrete Structures in Denmark. Technical University of Denmark (1967)
284. Gjörv, O.E.: Durability of Reinforced Concrete Wharves in Norvegian Harbors. Ingenior Plaget A/S, Oslo (1968)
285. Berke, N.S., Pfeifer, D.W., Weil, T.G.: Concr. Intern. **10**, 45 (1988)
286. Regourd, M., Hornain, H., Levy, P., Mortureux, B.: 7th ICCC Paris, vol. I, p. 4, pp. 4–1, 1/21. Paris (1980)
287. Neville, A.M.: Properties of Concrete, 5th edn. Pearson Education Limited (2011)
288. Piasta, J., Sawicz, Z., Rudziński, L.: Matér. Contr. (Paris). **17**, 291 (1984)
289. Śliwiński, J., Ehrenfeld, W.: Cement Wapno Beton. **65**, 103 (1998)
290. Hager, I.: Ph. D. Thesis, Ecole Nationale des Ponts et Chaussées. Paris (2004)
291. Hager, I., Pimienta, P.: Cement Wapno Beton. **70**, 263 (2003)
292. Duval R.: La durabilité des armatures et du béton d'enrobage. In: Baron, J., Ollivier, J.-P. (eds.) w La Durabilité des Bétons, p. 173. Presses Ponts et Chaussées, Paris (1992)
293. Venuat, M., Alexandre, J.: Rev. Mat. Concr. **638**, 421 (1968), **639**, 496 (1968), **640**, 5 (1969)
294. Majumdar, A.J., Stuck, M.S.: Cem. Concr. Res. **11**, 781 (1981)
295. Suzuki, K., Nishikawa, T., Ito, S.: Cem. Concr. Res. **15**, 213 (1985)
296. Babuszkin, W.J., Matwiejew, G.M., Mczedłow–Petrosjan, O.P.: Tiermodinamika Silikatow. Strojizdat, Moscow (1986). (in Russian)
297. Lach, V., Matousek, M.: In: Murat, M. (ed.) Int. Seminar on Calcium Aluminates, p. 11. Torino (1982)
298. Mayers, S.L.: Rock Products. **52**, 96 (1949)
299. Oberholster, R.E.: 8th ICCC Rio de Janeiro, vol. I, p. 323. Rio de Janeiro (1986)
300. Hamada, M.: 5th ICCC Tokyo, p. 343. Tokyo (1968)
301. Meyer A., ibid., p. 394.
302. Litvan, G.G., Meyer, A.: In: Malhotra V.M. (ed.) Proc. 2nd Int. Conf. on Fly Ash, Silica Fume, Slag and Natural Pozzolanas in Concrete, ACI SP–91, p. 1446. Madrid (1986)
303. Skjolsvold, O.: ibid., p. 1031
304. Fattuhi, N.I.: Matér. Costr. RILEM. **19**, 131 (1986)
305. Massazza, F., Oberti, G.: Proc. Third NCB Int. Sem. Cem. Build. Mater., vol. IV, p. VIII/13. New Delhi (1991)
306. Ho, D.W.S., Lewis, R.K.: In: Malhotra V.M. (ed.) Proc. 2nd Int. Conf. on Fly Ash, Silica Fume, Slag and Other Mineral By–products in Concrete, ACI SP–79, p. 333. Montebello (1983)
307. Nagataki, S., Ohga, H., Kyum, K.E.: In: Malhotra, V.M. (ed.) Proc. 2nd Int. Conf. on Fly Ash, Silica Fume, Slag and Natural Pozzolanas in Concrete, ACI SP–91, p. 521. Madrid (1986)
308. Kokubu, M., Nagataki, S.: Proc. Symp. on Durability of Concrete, RILEM, Final. Rep., Part II, D71–79, (1986)
309. Schubert, P., Von Berg, W.: Betonwerk Technik. **11**, 692 (1979)
310. Davis, R.E.: Tech. Memo. American Concrete Pipe Association (1954)
311. Schiessl, P.: Deutscher Ausschuss für Stahlbeton. **255**, 39 (1976)
312. Sauman, Z., Lach, V.: Cem. Concr. Res. **2**, 435 (1972)
313. Roy, D.M., Scheetz, B.E., Wakeley, L.D., Barnes, M.R.: Nucl. Chem. Waste Mat. **3**, 35 (1982)
314. Barnes, M.W., Roy, D.M.: In: Douglas, C. (ed.) Materials Research Society Symposium Preceedings: Scientific Basis for Nuclear Waste Management, vol. VI, p. 159. Brookins North Holland, New York (1983)
315. Komarneni, S., Roy, D.M.: Cem. Concr. Res. **11**, 759 (1981)
316. Glasser, F.P.: Cem. Concr. Res. **22**, 201 (1992)

317. Göske, J., Pöllmann, H., de Villiers, J.P.: 11th ICCC Durban, vol. IV, p. 2174. Durban (2003)
318. Nocuń–Wczelik, W., Małolepszy, J.: 10th ICCC Gothenburg, vol. IV, paper 4iv043. Gothenburg (1997)
319. Nicolas, G., Lequeux, N., Prene, S., Boch, P.: 11th ICCC Durban, vol. IV, p. 2199. Durban (2003)
320. Auer, S., Kuzel, H.J., Pöllmann, H., Sorrentino, F.: Cem. Concr. Res. **25**, 1347 (1995)
321. Pigeon, M.: The Frost Durability of Concrete. In: Ghosh, S.N. (ed.) w Cement and Concrete Science & Technology, vol. 1, p. 417. ABI Books, New Delhi (1992). Pigeon, M., Plean, R.: Durability of Concrete in Cold Climates. Taylor & Francis, London (1995)
322. Fagerlund, G.: Matériaux et Constructions/Materials and Structures. **10** (58), 231, (1977)
323. Mamillan, M.: Annales de ITBTP. **235–236**, 1019 (1967)
324. Mamillan, M., Simonneti, C., Cuendet, R.: ibid., **246**, 865 (1968)
325. Powers,T.C.: Proc. Highway Res. Bd. **29**, 184 (1949)
326. Powers, T.C., Helmuth, R.A.: ibid., **32**, 285 (1953)
327. Litvan, G.G.: J. Amer. Ceram. Soc. **55**, 38 (1972)
328. Litvan, G.G.: ibid., **58**, 38 (1975)
329. Powers, T.C.: J. Am. Concr. Inst. **50**, 741 (1954)
330. Helmuth, R.A.: 4th ICCC Washington, vol. III, p. 829. Washington (1960)
331. Pigeon, M., Lachance, M.: J. Am. Concr. Inst. **77**, 282 (1981)
332. Gagne, R., Pigeon, M., Aïtcin, P.C.: Matér. Constr. RILEM. **23**, 103 (1990)
333. Okada, E., Hisaka, M., Kazama, Y., Hattori, K.: In: Malhotra, V.M. (ed.) Developments in the use of superplasticizers, p. 215. ACI Sp–68 (1981)
334. Carles–Gibergues, A., Pigeon, M.: In: Baron, J., Ollivier, J.–P. (eds.) La durabilité des bétons en ambiance hivernale rigoureuse, Chapter 7. w La Durabilité Des Bétons. Presses Ponts et chaussées, Paris (1992)
335. Lukasik, J., Acker, P., Vernet, Ch., Behloul, M.: Conf Dni Betonu, p. 111. Polski Cement, Kraków (2004). (in Polish)
336. Klieger, P.: ASTM Special Tech. Publ. **691**, 282, (1980)
337. Rösli, A., Harnik, A.B.: ibid., p. 464
338. Verbeck, G., Klieger, P.: Highway Res. Bd. Bull. **150**, 1 (1957)
339. Yang, Q.B., Wu, X.L., Huang, S.Y.: 9th ICCC New Delhi, vol. V, p. 282. New Delhi (1992)
340. Sagoe–Crentsil, K.K., Glasser, F.P.: In: Page, C.L., Treadaway, K.W., Bamforth, P.B. (eds.) w Corrosion of Reinforcement in Concrete, p. 74. Elsevier, London (1990)
341. Pourbaix, M.: Wykłady z korozji elektrochemicznej. PWN, Warszawa (1978). (in Polish)
342. Foley, R.T.: Corrosion. **26**, 58 (1970)
343. Bukowiecki, A.: Schweizerische Bauzeitung. **66**, 856 (1968)
344. Raharinaivo, A., Brevet, P., Pannier, G., Grimaldi, G.: Bull. Liaison Lab. Ponts et Ch. **145**, 31 (1986)
345. Ramachandran, V.S., Seeley, R.C., Polamark, G.M.: Mat. Constr. **17**, 100, 285 (1984)
346. Saeki, N., Takada, N., Fujita, Y.: Trans. Jap. Contr. Inst. **6**, 155 (1984)
347. Ściślewski, Z.: Korozja i ochrona zbrojenia. Arkady, Warszawa (1981). (in Polish)
348. Wieczorek, G.: Wpływ inhibitorów korozji na trwałość zbrojenia w betonie. Habilitation Thesis, ITB, Warszawa (1977). (in Polish)
349. Slater, J.E., Lankard, D.R., Moreland, P.J.: Mat. Performance. **15**, 21 (1976)
350. Zybura, A.: Zabezpieczanie Konstrukcji Żelbetowych Metodami Elektrochemicznymi. Wyd. Pol. Śląskiej, Gliwice (2003). (in Polish)
351. Jaśniok, M., Zybura, A.: Inżynieria i Bud. **7–8**, 434 (1999)
352. Thomas, M.D.A., Matthews, J.D., Haynes, C.A.: In: Page, C.L., Treadaway, K.W., Bamforth, P.B. (eds.) w Corrosion of Reinforcement in Concrete, p. 198. Elsevier, London (1990)
353. Bensted, J.: Cement Wapno Beton. **68**, 133 (2001)
354. Marusin, S.L.: Proc. Twenty Second Int. Conf. on Cement Microscopy, Montreal, Canada, p. 154, April 29–May 4, 2000. Cement Microscopy Association, Illinois (2000)
355. Skalny, J., Marchand, J.: Science of Cement and Concrete. In: Kurdowski, W., Gawlicki, M. (eds.) w Kurdowski Symposium Kraków, p. 171, (2001)

356. Dow, C., Glasser, F.P.: Cem. Concr. Res. **33**, 147 (2003)
357. Payne, J.W., Dodge, B.F.: Ind. Chem. Eng. **24**, 630 (1932)
358. Emeades, R.M., Hewlett, P.C.: In: Hewlett, P.C. (ed.) w Lea's Chemistry of Cement and Concrete, 4th edn, Chapter 15. Arnold, London (1998)
359. Chandra, S.: Architecture and Ancient Building Materials in India. Tech. Books International, New Delhi (2003)
360. Hanehara, S., Yamada, K.: Cem. Contr. Res. **38**, 175 (2008)
361. Massazza, F.: In: Ghosh, S.N. (ed.) in Advances in Cement Technology, p. 596. Pergamon Press, Oxford (1983)
362. Depke, F.M.: Betonwerk + Fertigteil–Technik. **3**, 124 (1975)
363. Odler, I., Duchstein, U., Becker, Th.: Cem. Concr. Res. **8**, 469 (1978)
364. Kobayashi, K., Ito, T., Mari, T., Nishiyama, K.: Rev. 23rd Gen. Meet. Cem. Assoc. Japan, p. 193. Tokyo (1970)
365. Feldman, R.F., Swenson, E.G.: Cem. Concr. Res. **5**, 25 (1975)
366. Collepardi, M., Marcialis, A., Salinas, V.: Il Cemento. **70**, 3 (1973)
367. Ramachandran, V.S.: Cem. Concr. Res. **2**, 179 (1972)
368. Thormann, P.: Betonwerk + Fertigteil–Technik. **10**, 621 (1980)
369. Kreijger, C.J.: Int. Symp. on Admixtures for Mortar and Concrete, Brussels, RILEMABEM, vol. II, p. 33 (1967)
370. Sakai, E., Raina, K., Asaga, K., Goto, S., Kondo, R.: Cem. Concr. Res. **10**, 311 (1980)
371. Paillere, A.M.: Ann. Inst. Techn. Bat. Trav. Publ. **424**, 38 (1984)
372. Grzeszczyk, S., Sudol, M.: Cement Wapno Beton. **70**, 325 (2003)
373. Massazza, F., Testolin, M.: Il Cemento. **77**, 73 (1980).
374. Massazza, F., Costa, V., Barrila, A.: VIII Conference on Silicate Science, Budapest, p. 177 (1981)
375. Aigensberger, A., Fok, N.L., Rey, T.: J. Am. Concr. Inst. **68**, 608 (1971)
376. Bonzel, J., Siebel, E.: Beton. **20**, 59 (1974)
377. Whiting, D.: Cem. Concr. Aggregates. **2**, 31 (1980)
378. Lewandowski, R., Peterfy, P.: Betonwerk + Fertigteil–Technik. (8), 546 (1974), (9), 597 (1974)
379. Kondo, R., Daimon, M., Sakai, E.: Il Cemento. **75**, 225 (1978)
380. Daimon, M., Roy, D.M.: Cem. Concr. Res. **9**, 103 (1979)
381. Massazza, F., Costa, V.: 7th ICCC Paris, vol. IV, p. 529. Paris (1980)
382. Spiratos, N., Page, M., Mailvaganam, N.P., Malhotra, V.M., Jolicoeur C.: Superplasticizers for Concrete. Marquis, Quebec (2006)
383. Yamada, K., Ogawa, S., Hanehara, S.: Cem. Concr. Res. **31**, 375 (2001)
384. Yamada, K., Hanehara, S.: 11th ICCC Durban, vol. II, p. 538. Durban 2003.
385. Jiang, S., Kim, B.–G., Aïtcin, P.–C.: Cem. Concr. Res. **29**, 71 (1999)
386. Erdogdu, S.: Cem. Concr. Res. **30**, 767 (2000)
387. Aïtcin, P.–C.: Cement Wapno Beton. **73**, 269 (2006)
388. Prince, W., Edwards–Lajnef, M., Aïtcin, P.–C.: Cem. Concr. Res. **32**, 79 (2002)
389. Prince, W., Espagne, M., Aïtcin, P.–C.: Cem. Concr. Res. **33**, 635 (2003)
390. Nawa, T., Eguchi, H.: 9th ICCC New Delhi, vol. IV, p. 603. New Delhi (1992)
391. Bonen, D., Sarkar, S.L.: Cem. Concr. Res. **25**, 1423 (1995)
392. Ramachandran, V.S., Malhotra, V.M., Jolicoeur, C., Spiratos, N.: Superplasticizers Properties and Applications in Concrete. Minister of Public Works and Government Services, Canada 1998.
393. Kim, B.–G., Jiang, S., Jolicoeur, C., Aïtcin, P.–C.: Cem. Concr. Res., **32**, 79 (2002)
394. Andersen, P.J., Kumar, A., Roy, D.M., Wolfe–Confer, S.: Cem. Concr. Res. **16**, 255 (1986)
395. Fernon, V., Vichot, A., Le Goanvie, N., Combet, P., Corazza, F., Costa, U.: Proc. 5th CANMET/ACI Int. Conf. SP Oth. Chem. Adm. Concr., SP–173. Am. Concr. Inst., Farmington Hills, p. 225 (1997)
396. Yamada, K., Takahashi, T., Hanehara, S., Masuhisa, M.: Cem. Concr. Res. 30, 197 (2000)
397. Byndyra–Oracz, G.: Ph. D. Thesis, ITB, Warszawa (2006). (in Polish).

398. Bundyra–Oracz, G., Garbacik, A., Grzeszczyk, S., Kurdowski, W.: Silicates Ind. **73**, 241 (2008)
399. Bundyra–Oracz, G., Kurdowski W.: Materiales et Construction, w druku.
400. Yamada, K., Sugamata, T., Nakanishi, H.: J. Adv. Contr. Technol. **4**, 241 (2006)
401. Uchikawa, H., Hanehara, S., Sawaki, D.: Cem. Concr. Res. **27**, 37 (1997)
402. Flatt, R.J., Horst, Y.F.: Cem. Concr. Res. **31**, 1169 (2001)
403. Pöllmann, H., Stöber, S., Stern, E.: Cem. Concr. Res. **36**, 2039 (2006)
404. Park, C.K., Noh, M.H., Park, T.H.: Cem. Concr. Res. **35**, 842 (2005)
405. Giergiczny, E., Giergiczny, Z.: Cement Wapno Beton. **77**, 157 (2010)
406. Aïtcin, J.–C.: Bétons Haute Performance, Eyrolles, Paris
407. Collepardi, M., Borski, A., Collepardi S., Ogoumah Olagot J. J., Troli R.: Cem. Concr. Comp. **27**, 704 (2005)
408. Najduchowska, M., Pichniarczyk, P.: Cement Wapno Beton. **77**, 141 (2010)
409. Khayat, K.H.: ACI Materials J. **92**(2), 164 (1995)
410. Śliwiński, J.: Beton zwykły. Polski Cement, Kraków (1999). (in Polish)
411. Garbacik, A., Grzeszczyk, S., Kurdowski, W.: 54 Conf. KILW PAN, vol. 5, p. 283. Krynica Zdrój (2008). (in Polish)
412. Konta, J.: Keramicke a Sklařské Suroviny. Univerzita Karlova, Praha (1982)
413. Ogólnopolski Katalog Kruszyw, Instytut Bad. Dróg, Oddz. Wrocław (2003). (in Polish)
414. Pendias, H., Maciejewski, S.: Zbiór analiz chemicznych skał magmowych i metamorficznych Dolnego Śląska, Prace Inst. Geologicznego, vol. 24. Wyd. Geologiczne, Warszawa (1959). (in Polish)
415. Polański, A.: Geochemia i surowce mineralne, Wyd. Geologiczne, Warszawa (1974). (in Polish)
416. Görlich, E.: Chemia krzemianów, Wyd. Geologiczne, Warszawa (1956). (in Polish)
417. Ramachandran, V.S., Feldman, R.F., Beaudoin J.J.: Concrete Science, Treatise on Current Research. Heyden and Son Ltd, London (1981)

Chapter 7
Mineral Additions for Cement Production

7.1 Classification

The history of mineral additions to cement is as long as the history of cement. In Chap. 1 the original applications of natural pozzolanas are mentioned. According to Smolczyk [1], the usage of granulated blastfurnace slag as binder became important in 1862, when Emil Langen found the hydraulic properties of this material. The production of slag binder activated with lime, started in Germany as early as in 1865. The production of slag cement in Germany began in 1892, while in France this cement has been manufactured since 1880.

The following classification of cement mineral additions is commonly accepted:

- hydraulic materials,
- pozzolanic materials,
- fillers.

This classification is based upon the chemistry of hardening process, however, some reservations, as it will be further mentioned, should be pointed out.

The granulated blastfurnace slag is primarily reckoned among the hydraulic additions. These materials exhibit latent hydraulic properties which means that activated are setting and hardening under water, analogously to Portland cement. As a result of slag reaction with water the same hydrated phases as in the case of Portland cement are formed, with dominating C–S–H. As the activators can be used:

- basic compounds, e.g. $Ca(OH)_2$, NaOH, Na_2SiO_3,
- low acidic materials: $CaSO_4$, $Al_2(SO_4)_3$,
- physical factors: higher temperature and pressure.

Granulated blastfurnace slag can hydrate without activation too [2]. The calcium hydroxide necessary to activate the reaction of slag glass is probably formed as a result of calcium sulphide hydrolysis:

$$2CaS + 2H_2O \rightarrow Ca\left(HS\right)_2 + Ca\left(OH\right)_2 \tag{7.1}$$

W. Kurdowski, *Cement and Concrete Chemistry*,
DOI 10.1007/978-94-007-7945-7_7, © Springer Science+Business Media B.V. 2014

Among the pozzolanic materials active silica containing additions are ranked. This silica is reacting with calcium hydroxide in water at ambient temperature and the reaction products with hydraulic properties are formed, primarily C–S–H phase. The lime content in pozzolanas is generally low, as compared with blastfurnace slags, therefore for their hardening the $Ca(OH)_2$ or cement addition is required, the latter one is releasing the calcium hydroxide from alite and belite hydrolysis.

It should be remember that the granulated slags, because of the significant silica content, reduce the calcium hydroxide content in the paste and contribute to the C–S–H phase formation. For this reason they can be considered simultaneously as pozzolanas. On the other hand, some fly ashes from the brown coal combustion contain a substantial CaO amount, occurring mainly as anhydrite, but sometimes as free lime, and can harden after mixing with water. It is typical for such waste materials, particularly having variable composition, that their classification in unequivocal groups is difficult.

Finally, the so–called fillers constitute the last group of additives, which are, as a rule, inert and do not react in cement paste. The limestone, added on a large scale in Italy and in France was classified to this group a time ago [3]. As it is commonly known, the limestone cannot be considered as an inert concrete component; however, as compared with mineral additions from the former two groups, degree of $CaCO_3$ reaction in cement paste is rather poor. Nowadays, however, limestones are recommended in the EN 197–1 standard as mineral additions, together with pozzolanic additives (see types of cements, Table 1.3). In 2007 the ratio of limestone cements produced in Europe and Turkey was 21.4% (members of Cembureau); this corresponded to the annual output on the level of 56.2 million tons, in majority class 42.5[1]. The ground quartz sand can be considered as typical filler, which does not react practically with calcium ions in cement paste, at ambient temperature.

It should be realized that the tendency of energy consumption, as well as the CO_2 emission lowering will imply the application of mineral additions on increasing scale. This is reflected in the European standard (Chap. 1). The ratio of cements with mineral additions in Europe was 62% in 1999 and in 2007 already 72.7%[1]. It should be mentioned that in Poland there are cement plants where the mean cement clinker content is below 60%, despite that the type CEM I is also produced. The purposefulness of cement production with mineral additions development is caused primarily by the necessity of CO_2 emission lowering, which is justified by the environment needs, and is simultaneously related to the European Union Emission Trading Scheme. The energy consumption lowering is of importance too. The usage of some alternative fuels is particularly developed, because for example CO_2 from biomass combustion is out of restrictions mentioned above. Production of cement with mineral additions is therefore advantageous; for example the slag cement production with 50% of slag gives the reduction of electric energy and heat consumption, more or less of the same range. All the factors presented above are the basis of continuous growth of mineral additions application. Moreover, the higher

[1] Cembureau data

durability of concrete produced from blended cements is also important, as it was discussed in Chap. 6.

There are two mineral additions which are used on a large scale for cement production all over the world: granulated blastfurnace slag and siliceous fly ash. Also in Poland their contribution is the highest among the mineral additions, and their total consumption in 2009 was 2.644 million tons, including 1.269 million tons of granulated blast furnace slag[2]. However, in some countries, primarily in France, in Italy and in Germany, there is also an old tradition to produce the pozzolanic cements with the natural pozzolanas. The two following groups of these materials can be classified:

- the volcanic rocks,
- the organogenic rocks.

The pyroclastic rocks, in the form of loosen deposits or consolidated formations, produced as a result of diagenetic cementations belong to the first group. They originate from the eruption of magma and include sands, volcanic ash and fragments of rocks, carried away from the crater of volcano. The loosen deposit rocks from Naples and Rome, the Santorin earth from the Santorin Island, as well as the consolidated rocks: the Rhine, Naples and Bavarian tuffs, so–called trass, are among the most commonly known.

Only those pyroclastic rocks which are acidic, with high vitreous component or zeolite content exhibit pozzolanic properties.

The organogenic rocks composed of diatoms deposits are known as diatomitic earths or diatomites. The radiolarian and sponge shells occur as radiolarites, gaizes or spongiolites. These formations are cemented with opal or chalcedonite binder. The deposits of these rocks occur in Poland in Beskidy and Tatra Mountains; the diatomites occur in Podkarpacie Region [4]; tuffs are present near Cracow (Filipowice).The latter ones are rich in potassium (about 8 %). Because of the contamination with clay minerals they are not exploited. The other deposits, beside of tuffs, are not too large in Poland; however, they are important as raw materials for chemical industry.

The glass, opal silica and zeolites are the components of pozzolanas active in the presence of calcium hydroxide. However, pozzolanas contain also a large amount of inert components, to which the crystalline phases, such as quartz, feldspars, dolomite, magnetite, pyroxenes and calcite belong. Pozzolanas can also contain harmful for concrete durability components i.e. organic substances and swelling clays (montmorillonite).

The active natural pozzolanas, for example diatomites, about 4 % CaO, if their addition is 20 %, and about 6 % CaO at 30 % addition are bonding in C–S–H [5]. According to Massazza [5], this process is very slow and the effect is visible as late as after 28 days, and the strength development after 3 months of cement paste hardening (Fig. 7.1). Hence the recommended percentage of addition to cement is on the level 20–30 % [5]. According to Massazza [5] the standard method CEN EN 196.V allows fairly good assessment of pozzolanic activity. This method consists in the determination of Ca^{2+} and OH^- concentrations after 8–days conditioning of suspension of 20 g

[2] Polish Cement Association data

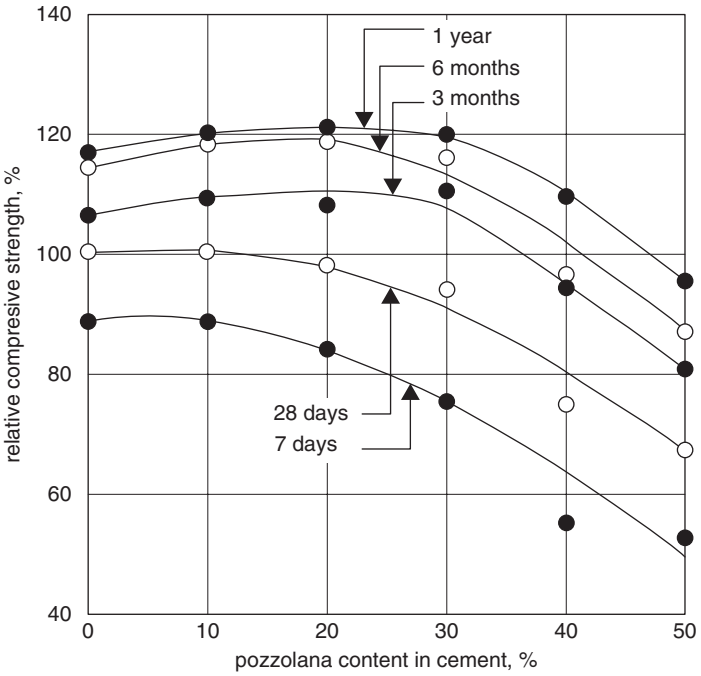


Fig. 7.1 Content of pozzolana in Portland cement and the compressive strength of standard mortar (according to [5])

cement in 100 ml distilled water in sealed vessel, stored at temperature of 40 °C. The results thus obtained should be situated below the $Ca(OH)_2$ solubility curve.

The Chapelle method [6] of pozzolanic activity determination, applied in France for many years, is similar to that proposed by Massazza [5]. This method consists in boiling 1 g of pozzolana with 1 g of CaO in 250 cm^3 of distilled water, during 16 h [6]. The combined CaO content is then determined.

The concretes produced from cements with natural pozzolana addition are particularly resistant to the chemical corrosion, but the resistance to physical factors is only slightly changed. However, they should be cured for a longer time in humid condition than the concrete produced from Portland cement without mineral additions. They are useful in these conditions where a low heat of hardening and high resistance to chemical corrosion is required [5].

In Poland the artificial pozzolana i.e. fly ash is the most important among the pozzolanic additions, application of which in cement production is rational both from the economic and ecological reasons.

The zeolites[3], which are the components of natural pozzolanas are the subject of great interest too. According to Taylor [7] the activity of zeolites is not lower than the

[3] The structure of zeolites is presented in details in M. Handke book: "Crystalochemistry of Silicates", AGH Kraków 2006

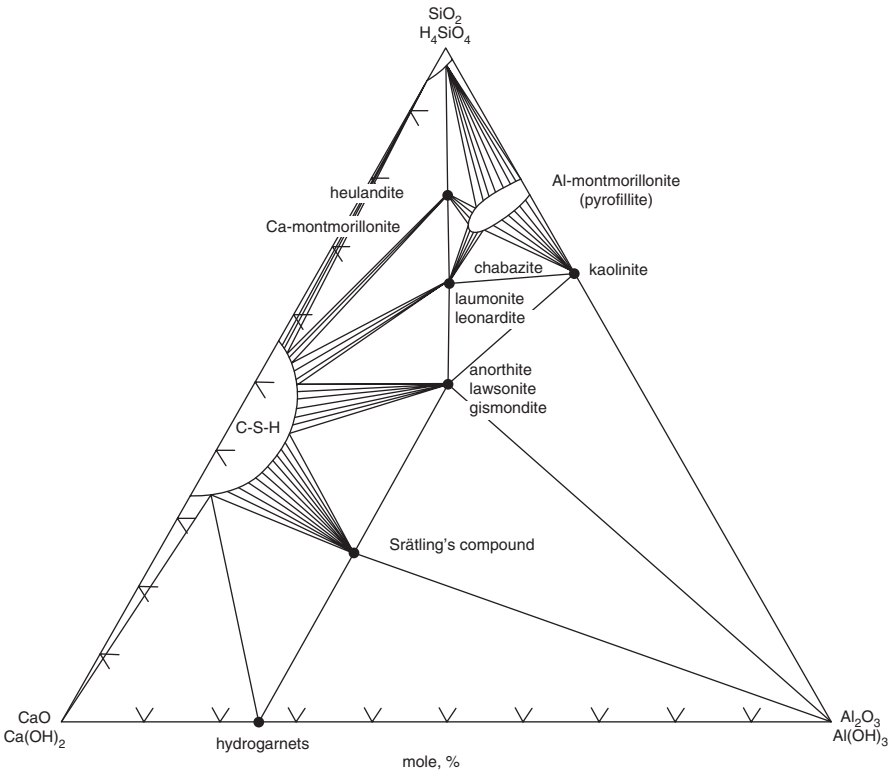


Fig. 7.2 Zeolites fields in the $CaO–Al_2O_3–SiO_2–H_2O$ system (according to [12])

activity of vitreous pozzolanic materials. Zeolites are aluminosilicates composed of 3–dimentional frameworks in which tetrahedra share four vertices. However, their structure is open in which the gaps can be occupied by cations of lithium–type or beryllium–type elements, as well as by water, more molecules loosely bound. The most commonly known zeolites are: chabazite $Ca[Al_2Si_4O_{12}] \cdot 6H_2O$ and philipsite $K_2(Ca, Na)_2[Al_6Si_{10}] \cdot 12H_2O$, occurring in the deposits of volcanic ash in Italy [8]. They were formed as a result of transformation of volcanic ash rich in aluminosilicates at moderate temperature and pressure increase. Nowadays the synthesis of zeolites from basalt or ryolite were studied [9], as well as from fly ash rich in silica and alumina [10, 11], in reaction with NaOH or KOH. Voinovitch and Dron [12] were shown the zeolite stability fields in the C–A–S–H system, from which can be concluded that C–S–H are associated by zeolites in a broad range of compositions, particularly in a silica rich region. However, they are not stable in cement paste rich in CH (Fig 7.2) [12]. Oberholster et al. [13] made a supposition that a white gel of hydrated sodium and potassium silicate, formed in reaction of aggregate with sodium and potassium hydroxide, is zeolite similar to A ($Na_{12}[Al_{12}Si_{12}O_{48}] \cdot 27H_2O$), however, with much lower aluminum content. Also Marfil and Maiza [14] found

that the gel product of silica reaction with sodium and potassium hydroxide gives on the XRD pattern peaks attributed to the clinoptilolite.

According to Feng Naiqian [15] the clinoptilolite (Na, K)$[Al_2Si_{10}O_{24}] \cdot 6H_2O$ and mordent $Na[AlSi_5O_{12}] \cdot 3H_2O$ are the zeolites the most often used in the production of building materials in China. Their absorption capacity is very high, exceeding 150 mg CaO/g, and in the case of clinoptilolite from some deposits even 200 mg/g [15]. These zeolites are used in cement production (usually the addition is 30%, or 40%), and directly in concrete production, replacing 5–10% by mass of cement [15]. The concretes from cement with 40% zeolite reveal significantly higher strength after 7 days of hardening and about 10 MPa higher after 28, 90 and 180 days respectively, than the concrete from slag cement [15]. The interfacial transition zone is advantageously modified too which has positive influence on strength and durability of concrete. Simultaneously zeolites absorb a part of mixing water which is preserved during concrete transport, placement and vibrating operation [15]. This water is a carrier of plasticizers, dissolved and partially occurring in the form of suspension [15]. Thanks to this method the plasticizer action is extended and the rheological properties of concrete mixture are maintained during transport, placement and even pumping [15].

In some countries in Easter Asia the rice husk ash, a very good pozzolanic material, is used [16, 17].

7.2 Metallurgical Slags

Two groups of metallurgical slags can be distinguished: the slags from iron production and the slags from non–ferrous metals production (in Poland primarily the copper slags). The chemical composition of these metals is given in Table 7.1.

In metallurgical plants, apart from the blastfurnace slags, a huge amount of slags, from steel production is obtained. The composition of converter slags is interesting from the point of view of their disposal as a binder [18], because they are rich in lime. The following mineral components are present in these slags: C_2F, C_2S, (Mn, Mg, Fe, Ca)O. Because of substantial periclase content the mortars produced from converter slag disintegrate after some period of hardening, usually after 28 days [18]. George and Sorrentino [18] propose the addition of modified flux to the steel making process, containing, apart from lime (50% CaO) and magnesium (5% MgO), high amount of Al_2O_3 (25%). This would result in bounding of calcium and iron in slag in aluminoferrite $(Ca_{1.8}Fe^{II}_{0.2})(Al_{1.32}Fe^{III}_{0.59})O_5$ [18]. In Poland the slags from steel production were investigated by Stabrawa [19] and Gustaw [20]. The applicability of these slags is limited, they contain the oxide phases and sometimes high chromium content [21]. Huge amount of copper slag is produced in metallurgical plant in Legnica, in Lower Silesia. This slag is highly acidic and is not suitable for cement production [22].

Table 7.1 Chemical composition (% by mass) of metallurgical slag (analytical data obtained by R. Skomorowska)

Component	Granulated blast furnace slag from metallurgical plant:				Other slags			
	"Sendzimir"	"Pokój"[a]	"Kościuszko"[a]	"Katowice"		nickel	copper 1	copper 2
SiO_2	40.6	37.2	34.8	40.0		65.8	43.9	39.0
Fe_2O_3	0.3	0.4	0.6	1.7		3.2	4.1	3.6
Al_2O_3	6.3	9.0	8.4	7.6		4.7	14.8	12.8
CaO	40.9	42.8	39.5	41.0		5.2	19.6	19.0
MgO	7.5	6.0	7.8	7.0		12.5	9.6	10.0
Other	4.4	4.6	5.3	2.7	FeO	2.0	0.9	5.0
Z[b]	1.35	1.55	1.45	1.39	SO_3	0.3	0.5	0.2
					S		0.2	0.1
G[c]	0.15	0.24	0.22	0.19	MnO	0.2	0.1	0.1
					Na_2O	0.2	0.7	0.8
Glass[d]	87	68	86	98	CuO	–	1.3	4.9
					L.o.i.	4.9	–	–
					K_2O	0.2	3.1	2.8

[a] metallurgical plants now closed; [b] $Z=(CaO+MgO+Al_2O_3)/SiO_2$; [c] $G=Al_2O_3/SiO_2$; [d] % by volume

Undoubtedly, the increase of glass content in slag is assuring their best hydraulic properties. The water granulation, additionally under pressure, is the best method, assuring the glass content exceeding 90 % [1].

However, there are always some crystalline phases in slags, primarily the melilites, merwinite and monticellite. Melilites are the solid solutions of gehlenite $Ca_2Al[Al, SiO_7]$ and akermanite $Ca_2Mg[Si_2O_7]$, which belong to silicates with structure containing cyclic groups $[Si_2O_7]^{6-}$. The structure of merwinite $Ca_3Mg[SiO_4]_2$ and monticellite $CaMg[SiO_4]$ is composed of isolated groups $[SiO_4]^{4-}$. A substantial amount of magnesium oxide is combined in these phases and MgO never occurs as periclase. At higher MgO content, about 8 %, the spinel $MgO \cdot Al_2O_3$ is formed. This phase is inert and does not react with water.

The potential mineral composition of slags used in cement industry was calculated by Gourdin [23]. He has shown that the potential phases: C_3S_2, C_2AS and C_2MS_2 constitute 95 %, and the remaining: CS, C_3MS_2 and C_2S—5 % of slag respectively. Then he verified this composition experimentally through the devitrification of slag glass. The other components occurring in slags are: calcium sulphide CaS and at higher titanium content—perovskite, $CaO\ TiO_2$. The low contents of rankinite $Ca_3[Si_2O_7]$, pseudo– wollastonite $Ca_3[Si_3O_9]$, sometimes larnite α'–$Ca_2[SiO_4]$ can be found too.

Numerous tests were taken to find a relationship between the properties and chemical composition of slag. This approach was based on the common conviction that the hydraulic activity of slag is increasing with alkalinity, thus with lime content. As first the alkalinity modulus $(CaO+MgO)/(SiO_2+Al_2O_3)$ was introduced, which was used in former Soviet Union until 1990 [24]. Subsequently, taking into account the beneficial effect of aluminum, the modulus in the form: $(CaO+MgO+1/3Al_2O_3)/(SiO_2+1/3Al_2O_3) \geq 1$ was proposed in Germany. This formula was based on the amphoteric nature of aluminum, which substituting silicon, will be acidic. Finally, in some countries (in Poland, Japan, Germany) the activity modulus $Z=(CaO+MgO+Al_2O_3)/SiO_2$ was used. The limit Z values are: in Japan above 1.4 and in Germany more than 1.6 respectively. In Poland these Z values are in the range from 1.35 to 1.55 (see Table 7.1), partially because of the medium MgO content. The positive opinion of the effect of MgO on hydraulic activity is not plausible because, as it has been mentioned earlier, at the MgO content exceeding 5 % the formation of spinel is found [25]. This was taken into account in the following modified formula:

$$\frac{Ca + CaS + \frac{1}{2}MgO + Al_2O_3}{SiO_2 + MnO} \geq 1.5 \tag{7.2}$$

However, this form of modulus was not accepted. As one can see, in this formula the presence of sulphide was also included. In the paste the hydrolysis of sulphide occurs with the evolution of hydrogen sulphide.

The reactions of CaS with sulphur from slag result in the formation of calcium multi–sulphide and thiosulphate [26]:

$$\mathrm{CaS} + 3\mathrm{S} \rightarrow \mathrm{CaS_4} \tag{7.3}$$

$$4\mathrm{S} + 2\mathrm{Ca(OH)_2} \rightarrow \mathrm{CaS_2O_3} + \mathrm{Ca(HS)_2} + \mathrm{H_2O} \tag{7.4}$$

Then the multisulphide can react with CO_2 from the liquid phase in the paste with evolution of hydrogen sulphide:

$$\mathrm{CaS_4} + \mathrm{CO_2} + \mathrm{H_2O} \rightarrow \mathrm{CaCO_3} + 3\mathrm{S} + \mathrm{H_2S} \tag{7.5}$$

This reaction occurs at $pH < 9$.

At the access of air to concrete, which has substantially higher O_2 content than CO_2 (0.02–0.04 %), the oxidation of sulphides to the sulphates will be the predominant reactions:

$$\mathrm{CaS} \xrightarrow{\mathrm{O_2}} \mathrm{CaS_2O_3} \xrightarrow{\mathrm{O_2}} \mathrm{CaSO_3} \xrightarrow{\mathrm{O_2}} \mathrm{CaSO_4} \tag{7.6}$$

The incompatible effect of magnesium on the strength of mortars was found. In the case of high Al_2O_3 (about 27 %) and low lime content ($C/S \approx 1.16$), the MgO increase at the expense of CaO and SiO_2 results in the lowering of strength, particularly over the 2.5 % content of this component [27]. Quite different data are reported by Bergt [28], who found the strength increase up to 14 % MgO. It seems that this effect is strongly dependent upon the glass content in slag and the form of magnesium in slag, in this aspect.

This only partially positive effect of MgO has found its reflection in the quality coefficient of slag proposed by Langavant [29]:

$$i = 20 + \mathrm{CaO} + \mathrm{Al_2O_3} + 0.5\mathrm{MgO} - 2\mathrm{SiO_2} \tag{7.7}$$

In this formula the contents of particular oxides present in a slag as % by mass should be introduced, as it is in the formulae of modules.

According to Langavant [29], slag can be attributed to the one of the following classes of hydraulic activity: poor, when $i < 12$, fairly good, when $12 < i < 16$, and excellent when $i > 16$. On the other side, MgO has a great impact on the properties of vitreous phase in slag [4]. Therefore the effect of MgO is strongly dependent upon the rate of cooling, determining the distribution of MgO between the glass and crystalline phases. There is a common opinion that MgO content up to 12 % in vitreous phase has a beneficial influence on strength [1]. Some authors relate this effect to the content of Al_2O_3 in slag [29, 30]. At 5–6 % MgO the Al_2O_3 content should be on the level 5–7 %, and at 10–12 % MgO should be higher, that is 15–18 % Al_2O_3.

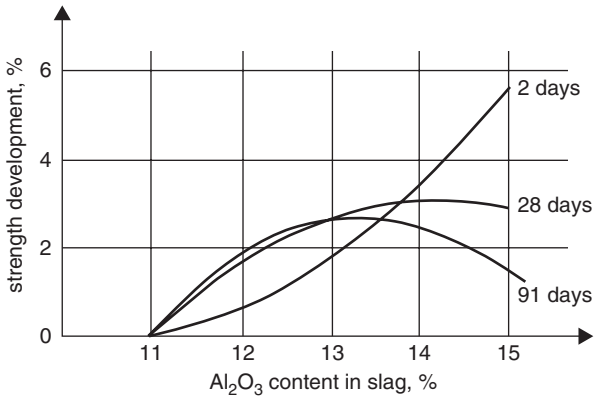


Fig. 7.3 The mean strength of slag cement mortar as a function of Al_2O_3 content in slag; 75% slag with specific surface area 3850 cm^2/g (according to [1]); $(CaO+MgO)/SiO_2=1.4$

Among the other components TiO_2 has an unfavorable effect on the strength of slag cement, particularly at percentage higher than 4% [31]. This impact can be moderated by Na_2O added to the slag melt before granulation [32].

The other coefficient of slag the hydraulic activity, thus linked with the strength of slag cements, were formulated too. Two examples are presented below [33, 34]:

$$Z' = \frac{CaO + 0.5MgO + Al_2O_3}{SiO_2 + FeO + (MnO)^2} \tag{7.8}$$

$$Z'' = \frac{CaO + MgO + Al_2O_3 + BaO}{SiO_2 + MnO} \tag{7.9}$$

Johansson [35] studied the correlation of various modules with the strength of 50% slag containing cement. He found no relationship with the strength after 3 days of hardening; on the other side the coefficient: (C+M+A)/S as well as (C+0.5 M+A+CaS)/(S+MnO) give a fairly good correlation after 7 and 28 days of hardening.

Based on the numerous experimental data Smolczyk [1] found a week suitability of these modules. Even those very complex have no advantage over the simple ones, which take into account only the silica content, as for example:

$$Z = \frac{100 - SiO_2}{SiO_2} \tag{7.10}$$

Smolczyk [1] found a good empirical formula in which, instead of the simple proportional relations, he introduced some functions. Based on the experimental data he concluded that the Al_2O_3 content exceeding 13% would favor, first of all, the early strength (Fig. 7.3).

Al_2O_3 is the component having a strong impact on the increase of hydraulic activity, as one can include from the other reports [36, 37]. The role of MgO content up to 11% is the same as the role of CaO. MnO has an unfavorable effect on the

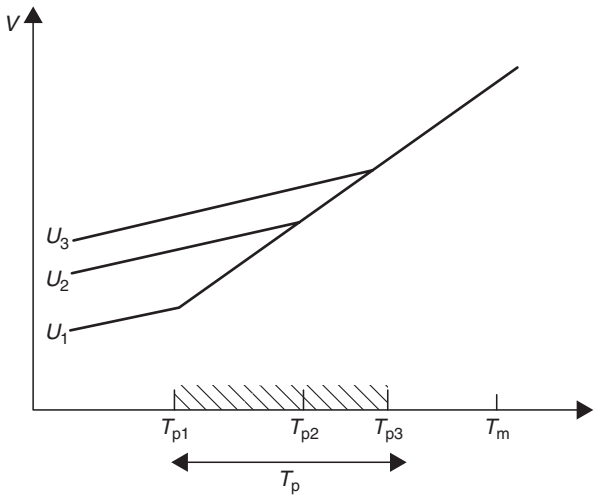


Fig. 7.4 The influence of rate of cooling on the specific volume of glass (according to [42]); $U_3 > U_2 > U_1$, T_p—temperature range of transformation, T_m—melting point

strength of slag pastes [1], as it was proved by Rojak too [38]. However, cements with good strength can be obtained at significant MgO content, when the Al_2O_3 [39] or BaO ratio is high [34].

According to Solacolu [40], the effect of MnO on the hydraulic activity of slag depends on its alkalinity. In the case of basic slags MnO has a negative impact, while in the case of acid ones MnO affects advantageously the hydraulic activity.

The role of P_2O_5 depends on the type of slag; however, this compound has always a beneficial influence on 28–day strength.

Further studies of slag hydraulic properties include the effect of glass reactivity as a function of chemical composition [40, 41], because the construction of this phase depends on its chemical composition. The temperature of melt granulating and the conditions of this process that is the rate of cooling and the access of oxygen are very important as well. It is commonly known that the temperature of transformation and consequently the volume of vitreous phase are affected by the rate of cooling [42]. As higher the rate of cooling as higher is the temperature of transformation and more defects are formed in glass network, which will have lower specific gravity (Fig. 7.4).

Solacolu [40], Locher [43] and Tanaka [44] found that the highest hydraulic activity have slag glasses with the composition corresponding to the fields of primary crystallization of gehlenite, akermanite and merwinite. The glasses with the composition: 50 % CaO, 31 % SiO_2 and 19 % Al_2O_3 (Fig. 7.5), activated with anhydrite and Portland cement clinker (2 %), revealed the highest strength. This composition varied depending on the type of activator; for the Portland cement clinker it was: 51.5 % CaO, 33 % SiO_2, 13.5 % Al_2O_3, while for anhydrite: 49–50 % CaO, 31–33 % SiO_2 and 18–19 % Al_2O_3 [44]. Therefore, as one could expect, the sulphate activation required higher Al_2O_3 content.

Solacolu [40, 41] was the first who proposed the hypothesis that the activity of glass will increase with the volume of micro–areas in which the crystallization

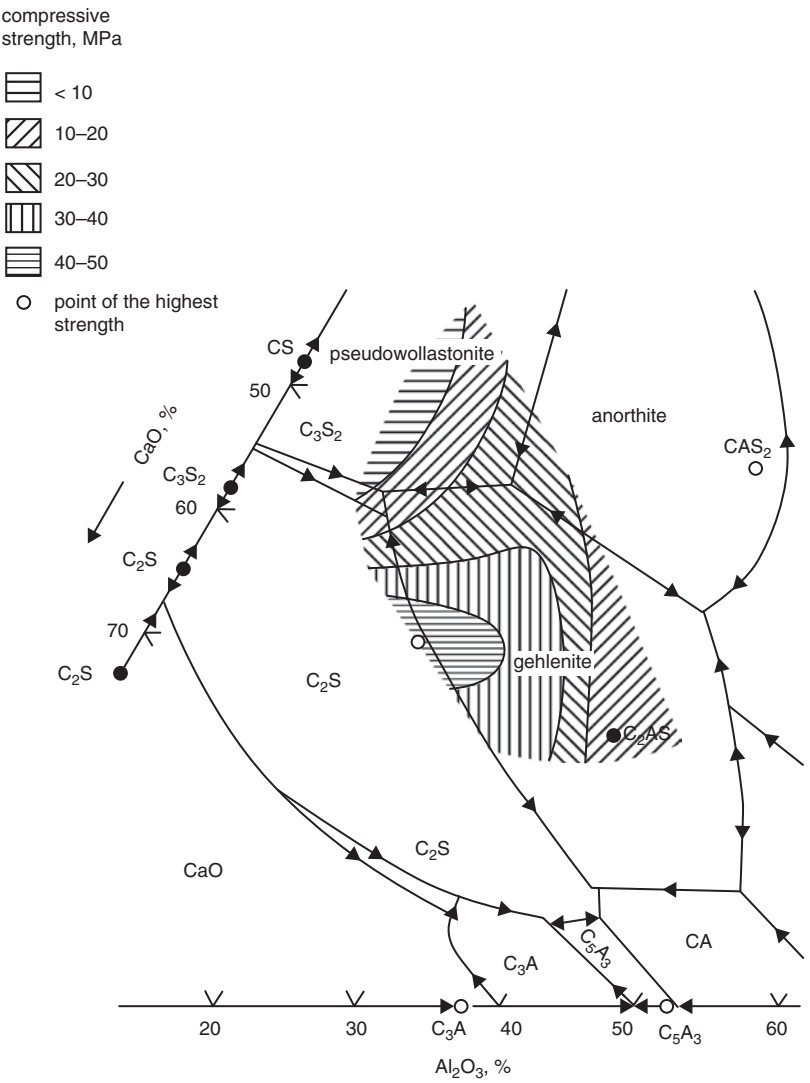


Fig. 7.5 Compressive strength of mortars from slag glasses of composition given by the dashed area (+5% MgO), activated with $Ca(OH)_2$ (according to [43])

process was beginning, it means in which the nuclei of crystalline phases have appeared. As it is known, the crystallization of glass is promoted by separation of melt to two phases of various structures, which is called liquation [45]. The liquation occurs when the surrounding of modifying ions in the network by oxygen atoms does not correspond to their coordination number, related to the ionic radius. The susceptibility to liquation increases with the ionic potential of cation (z/r, where z—ionic charge, r—ionic radius).

The liquation leads to the formation of some micro–heterogeneities in the structure of glass. The application of microprobe analysis gives the possibility to found these heterogeneities due to the differences in their chemical composition [16]. The observations under SEM show the presence in glass of domains containing microcrystals, most frequently of dendritic morphology [46]. The chemical composition shows that there were merwinite crystals. Their content up to 5% caused the strength increase of mortar containing 76% of slag and 4% of Portland cement. The merwinite content up to 35% has a negligible effect on strength as well. These results were proved by Frearson and Uren [47], which observed the thicker rims of hydrates around the slag grains in this case when slag contained inclusions of merwinite dendritic microcrystals. Simultaneously, the strength of slag cements with 50% addition of this slag increases significantly with merwinite content at the expense of glass up to 25%, after 28 days of hardening [47].

Another approach to the positive effect of the beginning of crystallization of slag glass on the hydraulic activity can assume the favorable changes of its chemical composition, which improve the reactivity with water.

The studies with more precise methods, that is with low angle X–Ray scattering and thermo luminescence, reveal the occurrence of micro–heterogeneities and defects modifying the energy of glass and increasing its hydraulic activity [48, 49].

A good method, basing on defects presence in slag glass, is using fluorescence for its reactivity evaluation, by slag exposing to the ultraviolet radiation [1, 50]. The highly reactive slags reveal fluorescence in the range of red light. For one type of slag this method is sufficient, for various types it should be applied together with the C/S ratio determination [1, 50].

The glass content in slag can be measured by microscopic or XRD methods; in the latter case the 10% CaF_2 should be added as an internal standard [16]. There is also the microscopic method in reflected light, with etching specimens with nitric acid solution in ethyl alcohol [47].

Slag content in cement, apart from the microscopic method, can be measured by selective dissolution in the mixture of H4edta, triethanoloamine and sodium hydroxide [51]. Kondo and Oksawa [52] proposed another solvent, composed of salicylic acid, methanol and acetone [53]. The methods of slag content determination in cement are given in the Polish standard PN–B–19707.

The silicon which exhibits tetrahedral coordination is the basic glass forming element of slag glass. The silica tetrahedra are not form distributed in a ordered manner, but they form a irregular network i.e. with no long–range order. The degree of $[SiO_4]^{4-}$ anions polymerization in glass depends on the content of modifying cations, such as Ca^{2+}, Mg^{2+}, Na^{+}, K^{+}…, which form non space–oriented ionic bonds. These ions are occupying the gaps in glass network (Fig. 7.6). From these ions the dissolution of glass in water is beginning; first react with water those with the highest coordination number and, as a consequence, the lowest strength of M–O bond.

The aluminum ion has a great impact on the properties of slag glass. Because of its amphoteric properties it can play a role of glass–forming element, when it occurs in tetrahedral coordination, or as a modifier—in octahedral coordination respectively. Aluminium share in one of these coordination depends on the alkaline

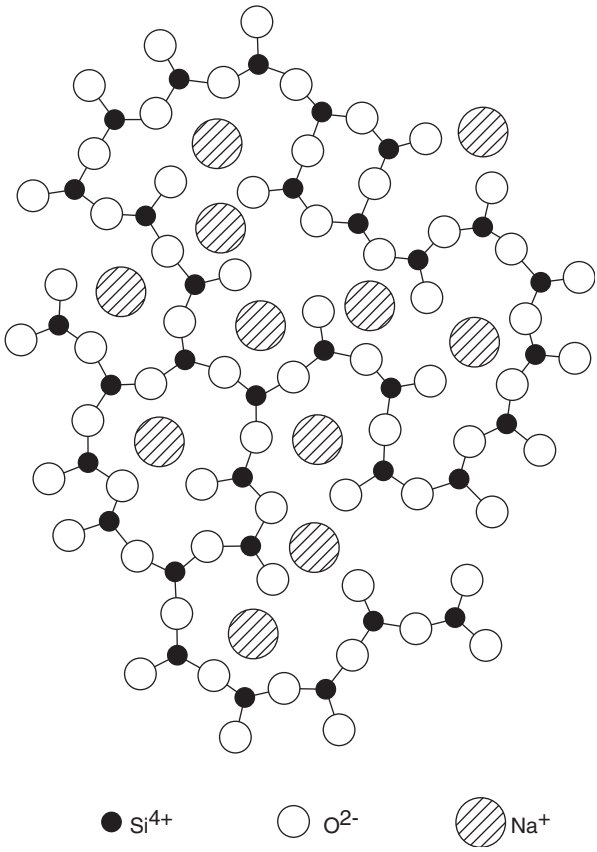


Fig. 7.6 The 2D scheme of glass structure

ions content in glass, primarily sodium and potassium (see Sect. 2.3). The role of magnesium ions, which can occur in coordination 4 or 6, is similar [50].

The ratio of aluminum and magnesium in tetrahedral or octahedral coordination in the slag glass depends not only on the chemical composition of glass but on the conditions of cooling operation too [1, 24, 54]. The studies of slags used in the production of slag cements in former Soviet Union allowed to Satarin [24] to find the relation between the hydraulic activity and MO_6/MO_4 ratio. Those glasses with $MO_6/MO_4 = 0.35$ revealed the best hydraulic activity [24].

Because the Al–O bond is weaker in the octahedral than in tetrahedral coordination it can be concluded that the hydraulic activity of slag glasses will increase with the content of aluminum in octahedral coordination. On the other hand, the higher amount of aluminum in tetrahedra corresponds to the higher content of modifying cations, to assure the electric charge equilibration. Therefore aluminum can replace silicon in the glass network for example according to the following scheme:

$$(\mathrm{Al}, \mathrm{Na})^{4+} \rightarrow \mathrm{Si}^{4+} \tag{7.11}$$

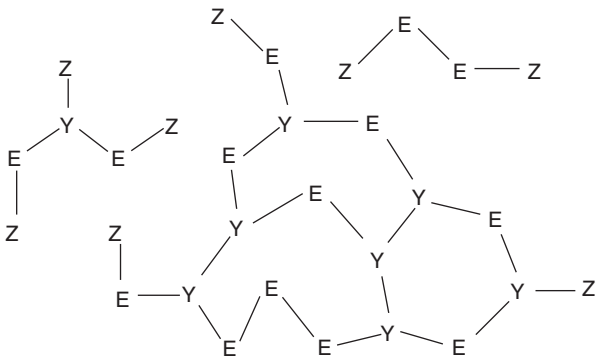


Fig. 7.7 The network of glass with average silica content (according to [57]); $Y=[SiO_{2.5}]^{-}$; $E=[SiO_3]^{2-}$; $Z=[SiO_{3.5}]^{3-}$

For this reason, with increasing content of aluminum in tetrahedral coordination the ratio of bridging oxygen atoms in glass is rising, thus the polymerization degree of the glass–forming anions decreases too, and the share of so–called active oxygen atoms increases.

There are the opinions that the $[AlO_4]^{5-}$ tetrahedra are poorly attached to the glass structure than the $[SiO_4]^{4-}$ ones and hence they are more readily released to the water solution [54].

The role of bridging and non–bridging oxygen atoms and the related $[SiO_4]^{4-}$ anions polymerization degree was discussed by Toop and Samis [55], as well as by Masson [56], which introduced the notion of environment alkalinity P_F. This alkalinity is linked with the modifying ions content, which break down the Si–O–Si bonds and augment the ratio of active oxygen: $P_F = \sqrt{[O^{2-}]\cdot[O^0]}$. $P_F > 1$ corresponds to the structure composed of isolated silicates tetrahedra [57]. This problem was developed by Dron [57, 58], who determined the polymerization degree of $[SiO_4]^{4-}$ anions basing on the studies by the Raman spectroscopy. According to Dron [58] hypothesis, the probability that there are the silicates tetrahedra in slag glass, in which all the oxygen atoms will be bridging or there will be no bridging at all, is low. This leads to the conclusion that the of slag glass network is built of single or branched chains (Fig. 7.7).

The three types of silicate tetrahedra can be thus distinguished:

- occupying branching positions: $Y=[SiO_{2.5}]^{-}$,
- belonging to single chain: $E=[SiO_3]^{2-}$,
- ending the chain: $Z=[SiO_{3.5}]^{3-}$.

However, $[AlO_4]^{5-}$ tetrahedra will be surrounded by four bridging oxygen atoms and thus they will be the elements of spatial network of glass. This hypothesis is founding prove in the composition of solution obtained from dissolution of slag [58]. In this solution the molar ratios $C/S \approx 1.63$ and $A/S \approx 0.425$, which corresponds to the situation as if will be "dissoluted" $2C_3S_2$ and CA. Therefore, the dissolution of slag occurs in such a way, as if structural units of higher alkalinity (Z) will be selectively released to the liquid phase and the elements of glass network of lower alkalinity (Y and E respectively) will be remaining in the solid phase. They can

subsequently participate in the pozzolanic reaction with Ca^{2+} and OH^- ions, which occurs topochemical.

The C–S–H phase thus formed will have lower calcium content than slag and the concentration of aluminate ions will increase initially in the liquid phase, because the crystallization of aluminates will occur in later period [58].

According to Dron [58], the aluminum ions are governing the slag hydraulic activity and they are first released to the liquid phase. However, he consider that magnesium oxide presents always a properties of strong base, thus analogously as the calcium oxide.

The coordination of Al^{3+} and Mg^{2+} ions, as well as the degree of silicate anions polymerization investigated Goto et al. [59] and concluded that aluminum was always present in tetrahedral coordination. However, Run–Zhang et al. [60] proved the occurrence of aluminum and magnesium both in tetrahedral and octahedral coordination. Glasses in which the ratio $MO_6/MO_4 = 0.5$ were assuring the highest strength of slag cements. The effect of silicate anions polymerization on the hydraulic activity of slag glasses was proved by Run–Zhang and Qiong–Ying [61]. The structure of silicate anions in glasses was discussed by Görlich [45].

MacDowell [62] has shown that the synthetic gehlenite glass, molten at high temperature, not lower than 1600 °C, and cooled rapidly, has very high hydraulic activity. The binding material thus produced shows high strength [62, 63]; moreover this is extremely durable in corrosive media, for example in $CaCl_2$ solution [64, 65]. The paste of this glass contains only the gehlenite hydrate C_2ASH_8 and unhydrated glass. The Friedel's salt and silica rich hydrogarnet $Ca_3Al_2[SiO_4](OH)_8$ appear as the corrosion products in chloride solutions [64]. The resistance of gehlenite paste is caused by its low porosity and by the presence of unreacted glass, which undergoing hydration is additionally sealing the paste and forms silica rich hydrogarnet, showing very high corrosion resistance [65].

7.3 Slag Cements

There is a consensus that the composition of Portland cement clinker has a great impact on the hardening and strength level of slag cements [24, 61, 66]. This problem was studied by Kubicki [67], but no quantitative relationship was found [1]. There is a common opinion that the clinkers with high C_3S content and high early strength are the best. The effect of high C_3A content is mentioned too [68]. High C_3A content in clinker is required particularly in the case of acidic slags [69]. However, the opinions are ambiguous. According to Satarin [24], the C_3A content should not exceed 10 %. The free lime content has a positive impact too [24, 67]. The higher K_2SO_4 content in the case of mean fineness of slag is advantageous, at higher (6000 cm^2/g) there is an inverse effect [70]. Analyzing the mutual relations between the quality of clinker and the properties of slag cement, one should remember that the slag and particularly the minor components of slag can have high effect on clinker strength development [1].

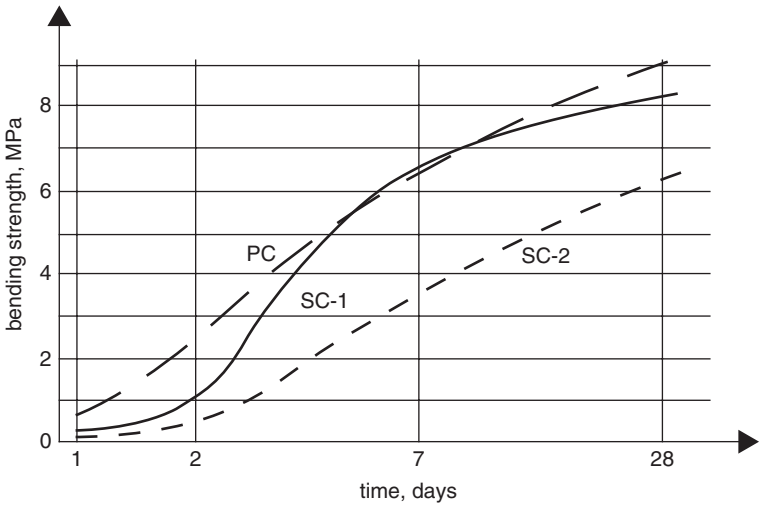


Fig. 7.8 Flexural strength of mortar from slag cement (SC) with the fineness 350 m^2/kg (SC-2) and 630 m^2/kg (SC-1) respectively, in comparison to the strength of Portland cement mortar (PC) (according to [72])

There is an opinion that the early strength of cement, after 3 or even 7 days depends primarily on the properties of cement clinker and its fineness, even in the case of high slag content, about 50 % [36]. On the other side, at high slag content, over 75 %, this is the slag, which contributes to the early strength of cement and clinker only after 28 days [70].

The other question deals with the common or separate grinding of slag and clinker. As a matter of fact the fineness of every component of binder is important, because at common grinding slag, as having lower grindability, will be always collected in a coarser fraction.

There is no doubt that the fine grinding of slag has a positive impact on the strength development of mortar [50, 71] (Fig. 7.8). Slag cement with 80 % of slag, with the specific surface area of this component on the level of 630 m^2/kg, contributes in strength increase not lower than Portland cement, even at temperature of 5 °C (Fig. 7.8), as well as similar shrinkage [72]. Therefore the technology of separate slag and clinker grinding, followed with mixing of these components, is more advantageous and allows of producing slag cement (CEM III/A and CEM III/B) even class 52.5 (in Poland Eko–Cem grinding plant).

Comparing the chemical composition of slags in Poland with the composition of slag glass of high hydraulic activity one can conclude that the quality of these slags is rather poor. The high SiO_2 content and low alumina content are the decisive factors. Slags in France SiO_2 content is on the level 33–35 % and the Al_2O_3 content is 12–15 % respectively [57]. The C/S ratio is 1.20–1.35, while in slags in Poland—1.01–1.03. Therefore the strength decrease caused by slag addition is significant. However, in the case of slag from “Katowice” metallurgical plant, with high amount of glass the strength reduction is much lower than the percentage of

addition [37]. The other domestic slags cause the reduction of strength, even after 28 days of hardening, practically equal to the slag addition, therefore, for slag cement production of class 32.5, with about 45 % addition of slag, clinker of class 42.5 should be used. Only after 90 days the strength of slag cement paste became close to the strength of Portland cement and at longer period of hardening is markedly higher.

Very low variability of granulated blastfurnace slag quality, in the case of material originated from one metallurgical plant, is the major advantage.

In some European countries the quality of slags is very good; the strength development of slag cements is therefore similar to that for Portland cements attributed to the same class [1]. At slag addition setting time of cement is delayed. 40 % slag allows reducing gypsum content; in the case of some clinkers gypsum can be eliminated. However, gypsum is always used in slag cement production, not only from economical reason, but because SO_4^{2-} ions are the activators of slag hydration. For this reason a higher calcium sulphate addition is frequently advantageous, particularly in the form of anhydrite.

This longer setting time of slag cement can be turned to account in the ready mix concrete technology; the concrete mixture should have delayed set adjusted to the transport period.

In order to improve the properties of slag cements the finer grinding should be used as compared with the Portland cements of the same strength. The significant amendment of strength development can be obtained by the use of grinding aids, particularly of triethanoloamine [24].

Slag cements reveal numerous advantageous properties, as it has been pointed out in Chap. 6. A low permeability of concretes produced of this cement, resulting from the reduction of capillary porosity of the paste and lower calcium hydroxide content, are the most important [1]. For this reason slag cements present much higher resistance in the sulphate, chloride solutions and hence in the sea water environment. Regourd et al. [73] report that the durability of slag cement is not influenced by the phase composition of clinker when the slag content exceeds 60 %. However, at lower slag addition the C_3A content in clinker should not exceed 8 %.

In Fig. 7.9 the expansion in sulphate solutions is shown for three following cements: Portland cements with 13 % C_3A (1) and 3 % C_3A (2) respectively and the slag cement one with 65 % slag and 13 % C_3A content in clinker (3) [53].

Slag cement shows also a fairly good resistance to the attack of acid waters, as it has been proved in many years experiments with mortars blocks immersed in the solution of 100 mg carbonate acid per liter [53].

Low permeability of concretes produced from slag cements significantly decrease the diffusion of chlorides, irrespectively on the w/c ratio (Fig. 7.10) [1, 53] (see also Table 6.4). Only 2 cm thick concrete layer is practically impermeable for chlorides during two years exposition.

High resistance of slag cements to the attack of aggressive media is also related to the low $Ca(OH)_2$ content in the paste of these cements (Fig. 7.11). At low $Ca(OH)_2$ content the secondary gypsum and ettringite cannot be formed or only in negligible amount. Moreover, aluminum forms with C–S–H solid solution which conserves

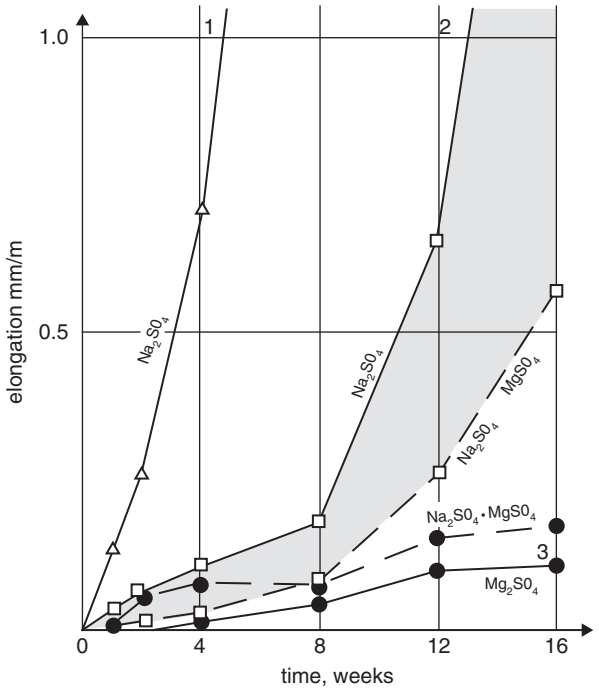


Fig. 7.9 Expansion of bars stored in the sulphate solution of concentration of 0.31 mol/l (after [53])

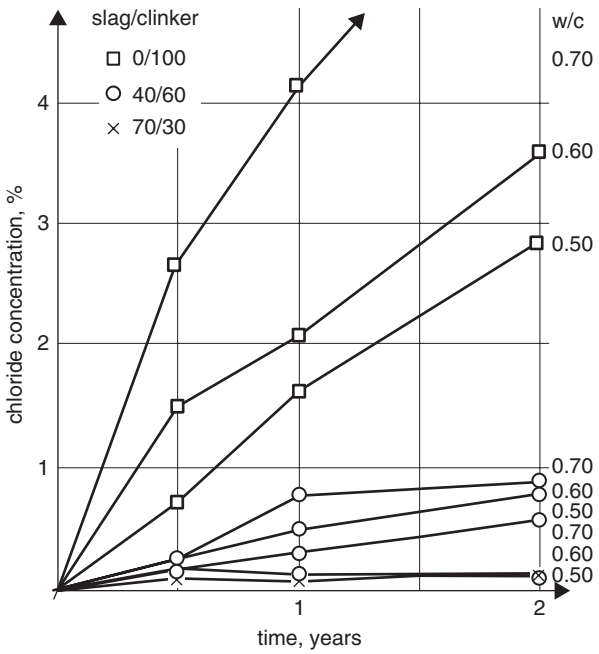


Fig. 7.10 Diffusion of chlorides in concrete beam. NaCl solution of concentration of 3 mol/l; 2–4 cm thick layer (according to [53])

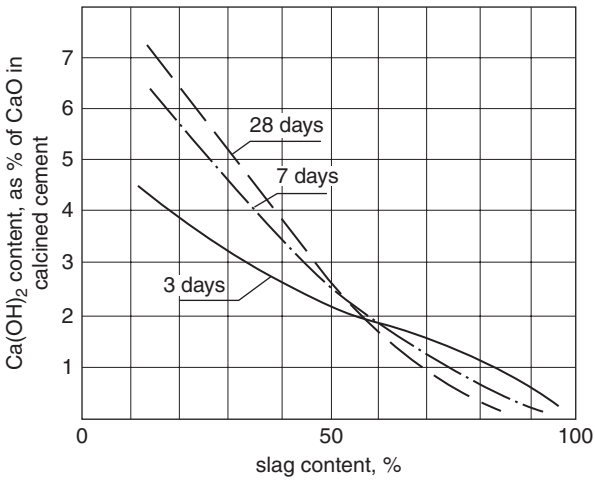


Fig. 7.11 $Ca(OH)_2$ content in metallurgical cement paste

compact morphology with low permeability for a long time [73]. Low calcium hydroxide content should be, at least theoretically, the base for the presumption, as the corrosion of steel in concrete with metallurgical cement is considered [1, 36, 53, 74]. This presumption was not proved neither during the long lasting observations of samples stored in field conditions, nor during the examinations of concrete structures in Germany [1, 53, 75]. In Germany the slag cements are used for the production of all types of concrete, not only for the reinforced ones but in the prestressed concrete too. The bridge in Köln over Rhine is an example of modern construction entirely built of slag cements (so–called HOZ 35 L and HOZ 45 L, at present CEM III 32.5N and 42.5N, according to the European Standards) prestressed concrete [1]. It must be also reminded that in slag cement concrete the pore solution is saturated with calcium ions and pH is always about 12.5, at least.

The 23 years lasting observations of reinforced concrete beams from slag cement, exposed to the attack of sea water, prove fairly good protection of reinforcement in this concrete [74].

The results of long studies of Smolczyk [53] excluded also the corrosive attack of H_2S, evolved as a result of sulphides hydrolysis, contained in slag. In the most severe conditions, it means at the access of gas with the composition: 3 % CO_2, 10 % O_2 and 87 % N_2 (% by volume), there is 10^{-6} H_2S % by mass of cement in slag cement concrete and this is not hazardous situation for steel. It can be reminded that the reaction of H_2S with steel occurs according to the following equation:

$$H_2S + Fe \rightarrow FeS + 2H \tag{7.12}$$

Atomic hydrogen causes the micro–cracks formation in the reinforcing steel as a result of reaction $2H \rightarrow H_2$ (hydrogen "brittleness") [76].

According to the document published by RILEM Committee, the formation of H_2S is not possible in the case of compact, non–permeable concrete [77]. Mather [78] did not found the corrosive action of sulphides too. However, high concen-

tration of chlorides, often found in concrete are detrimental, and in this case the low permeability of concrete from slag cements is the best protection against corrosion [53].

Low permeability of concrete from slag cement is also the good protection against carbonation, which progress is not higher than in the case of Portland cement [53]. However, carbonation occurs quickly when concrete becomes dry. This is, according to Smolczyk [53], the main cause of negative results of laboratory investigations, in which small and quickly drying samples are used. On the other hand the long lasting field studies reveal good performance of slag cement concretes [79].

The first results of observations, twenty years after building the experimental houses of Portland and slag cements (former HOZ 275, nowadays CEM III 32.5N) were published by Litvan and Mayer [80]. They are not positive for slag cement because, in spite of the fact that the carbonation is similar as in the case of Portland cement, the depth of carbonation increases proportionally with time; it means it occurs at higher rate. The authors are of the opinion that this is the consequence of unfavorable large and mean pores ($\geq$18 μm and 0.35–0.019 μm respectively) share increase in concrete of slag cement. The flexural strength decreases too [77, 80]. The positive effect of slag on the alkali–aggregate reaction is known too (see Chap. 6). Smolczyk [81] formulated the empirical formula for reactive alkali content as a function of slag addition to cement:

$$N_{ra} = N\left[1 - \left(\frac{H}{72}\right)^2\right] \tag{7.13}$$

where N_{ra} is reactive alkalis content in slag cement (Na_2O_e soluble), N—total alkali content in slag cement (Na_2O_e), H—slag content in cement.

On the other hand, slag cements reveal similar to the Portland cements freeze–thaw resistance in the presence of de–icers, if to the first air entraining agents are added [53]. Without air entraining agents Portland cement concrete shows better freeze–thaw resistance, while slag cement is better with air entrainment [82].

The usage of slag cements is particularly favourable in the case of massive concrete structures, dams and barrages [1, 36], because of the low heat of hardening. However, slag cement concrete should be cured in moist condition at early age in order to prevent scaling [1].

Slag cements 32.5N should not be used when concreting proceed at low temperatures, particularly below 5 °C, because of very slow strength development, as compared to Portland cement concrete. This is related also to the Portland cement class 32.5 with mineral additions (Table 7.2) [83].

Apart slag cements, in the past two kinds of slag cements were produced: with lime and anhydrite addition. The latter was based on the Kuhl's invention [84], which found the activating effect of sulphate ions on the reaction of slag with water. The so–called supersulphated cement contained 80–85 % of granulated slag, 10–15 % of anhydrite and 5 % of Portland cement clinker, and was produced according

Table 7.2 Strength of concrete from various cements, matured at temperature + 5 °C [83]

Kind of cement	Compressive strength at 5 °C as % of strength at 20 °C		
	3 days	7 days	28 days
550, rapid hardening 450[a]	60–75	75–90	80–105
450, rapid hardening 350[b]	45–60	60–75	75–90
350	30–45	45–60	60–75
250[c]	15–30	30–45	45–60

After 2 days the standard strength is equal:
[a] 20 MPa (class 42.5 R), [b] 10 MPa (class 32.5R), [c] now not produced

to Kuhl's patent DRP 237777 [5]. This cement was standardized in Germany and also in France, Great Britain and Belgium [36]. A good slag with minimum 15% Al_2O_3 and alkalinity modulus $(C+M+A)/S \geq 1.6$ was required. The strength of concrete from supersulphated cements is the function of lime and alumina content in slag [86] (Fig. 7.12) and they should be very finely ground. Ettringite and C–S–H are the hydration products. Ettringite content is increasing relatively quickly, reaching maximum content in the period between 3 and 7 days. However, Taylor [87] found that anhydrite is completely reacted up to 3 days and the content of ettringite does not change, while the C–S–H content is increasing [87]. Because of the too high Al_2O_3 content in relation to gypsum, after longer time of hydration, cement paste contains ettringite, calcium monosulphoaluminate hydrate and $Al(OH)_3$, apart from C–S–H [85].

The phase composition of a paste from this cement, after 3 days of hydration at w/c = 0.5, assessed by Taylor [87], is shown in Fig. 7.13. Ca/Si is about 0.7 [87].

The supersulphated slag cement was produced in the period 1940–1960; production was abandoned presumably because of lower Al_2O_3 content in slag [84]. According to Gebauer [88], production started in 1932 and was finished in 1977.

The supersulphated cement mortars and concretes are resistant to the sulphate waters, week organic acids, chlorides and hence to sea water too [36]. The concretes of supersulphated cement were generally of very good quality and durability. As an example Gebauer [88] gives the Beervlei dam in South Africa, built in the years 1954–1956; the concrete samples from this dam have in year 2000 strength of 124 MPa. Cement paste was composed of small ettringite crystals, surrounded by $Al(OH)_3$ gel and C–S–H matrix. The carbonation was found only in the surface layer, to the depth 2–5 mm, and from the new phases only gypsum and calcite appeared, however, the microstructure remained compact [88].

The importance of supersulphated cements decrease during the last fifty years and their production on a large scale was abandoned. In some countries, for example in France, a significant amount of granulated blastfurnace slag with low lime addition is used in road construction [89]. For example in 1974 almost a half of annual blastfurnace slag output was used for this purpose [90].

Kühl [84, 85], as early as in 1907 found the possibility to produce cement from slag activated with sodium hydroxide. Various sodium compounds as slag activators can be used, however, they react rapidly with calcium hydroxide transforming, at ambient temperature into the sodium hydroxide. Industrial production was developed as a result of Glucchovsky [92] works and it took place after 1965 [88].

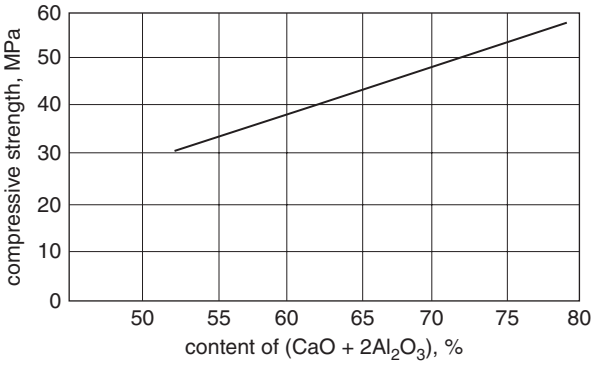


Fig. 7.12 Strength of supersulphated slag cements as the function of CaO and Al_2O_3 content in slag (after [86])

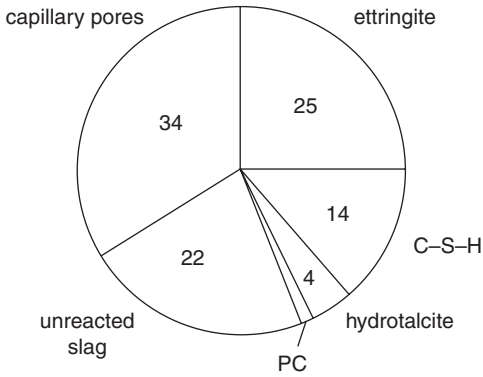


Fig. 7.13 Phase composition of supersulphated slag cement paste after 3 days of hydration at w/c = 0.5 (after [87])

In the production of these slag cements three sodium activators can be used: NaOH, Na_2CO_3 and Na_2SiO_3. There is no experimental data which of them is the best. Theoretically sodium silicate should be the best, because the $[H_3SiO_4]^-$ ions evolved in the reaction of this compound with $Ca(OH)_2$ will produce at once C–S–H gel. This was proved experimentally by Baran [93] who found this process, when K_2SiO_3 was added to Portland cement.

The alkali activated slag cements were produced in relatively huge amount in the former Soviet Union and used particularly in the production of concrete pipes, resistant to the aggressive environment, primarily acidic. They were also used in the foundations, as well in the oil well cementing [94, 95]. The alkali activated slag cements technology was developed in Poland by Malolepszy [96, 97]. These cements show a very high strength after heat treatment. High shrinkage, being presumably the consequence of high gel content, and efflorescence caused by sodium ions migration, should be mentioned as major disadvantage of these materials. Efflorescences are composed of the white sodium carbonate, precipitated on concrete surface. Main component in pastes of alkali activated slag cement is C–S–H phase, however, zeolites can be sometimes formed, favored by heat treatment [97, 98].

The alkali activated slag cements are successfully used in the sealing works in hydrotechnical constructions, particularly the underwater ones [99], as well for cutting of water outflow from the rock deposit [100]. They can be used in shotcreting in hydraulic engineering and geotechnics because of their advantageous rheological properties. The manufacturing of anti–filtration screens, cutting off the outflow of water, with application of alkali activated slag cements, is the subject of Polish Patent no PL 162731 B1, 1994.

Also in other countries alkali activated slag cements, with Na_2SiO_3 and gypsum [101], as well as cement F with 5–8 % sodium activator and lignosulphonate as a plasticizer [102] are produced.

The structure of C–S–H phase formed in alkali activated slag cements was studied by Deja [98]. He found the elongation of silicate chains, that is the ordering of the structure with its transformation closer to tobermorite, as a function of hydration time. [98]. The aluminate ions occur in the paste of this cement primarily in C–S–H (even about 7 % Al_2O_3), however, they can form also hydrogarnet phase rich in silicon [98].

In cement pastes rich in NaOH the U phase can occur, particularly at higher temperatures [103]. Moranville and Li [103] synthesized this phase in the mixture of C_3A with gypsum, in 0.6 mol/l of NaOH solution. This phase can be also formed in cement pastes under Na_2SO_4 attack [104]. U phase was found by Dosh and zur Strassen [105] in 1967. This is the defected AFm phase, in which the vacancies of Al^{3+} occur and the charge is balanced by Na^+ and SO_4^{2-} ions in the interlayer positions. It has a structural formula $\{Ca_4Al_{2(1-x)}(OH)_{12}[SO_4]^{6x-}\{yNa_2SO_4 \cdot 6xNa \cdot aq\}^{6x+}$. The typical XRD peaks are 100 pm and 50 pm. U phase can be formed in the alkali activated slag cements pastes, when the pore solution becomes enriched in SO_4^{2-} ions or in Portland cement pastes exposed to the Na_2SO_4 solution [103]. The formation of U phase means that the corrosion is initiated, because this phase is not stable in contact with the solution of lower alkalinity and transforms into ettringite, which is expansive in $Ca(OH)_2$ containing paste [103].

7.4 Fly Ash

The total annual output of fly ash in Poland is about 20 million tons (in 2008 over 26 million tons) of fly ash from the black coal combustion and about 9 million tons of fly ash from the brown coal combustion respectively. The production of fly ash cements started in XX c. in late sixties. The annual fly ash consumption attains 1400 thousands tones. The three types of fly ash generated in the pulverized fuel combustion (frequently determined as conventional ones) can be distinguished (Table 7.3): those from the black coal, from the brown coal in Turoszów coal–field as well as from the Konin and Bełchatów coal–field.

Table 7.3 Chemical composition of fly ash (contents given in mass %) (analyses of R. Skomorowska)

Component	Fly ash from black coal combustion from power plant:			Fly ash from brown coal combustion from power plant:		
	"Jaworzno"	"Miechowice"	"Rybnik"	"Turoszów"	"Bełchatów"	"Konin"
L.o.i.	2.7	5.2	8.2	3.0	6.4	2.4
SiO_2	44.0	47.6	49.1	51.6	56.5	47.9
Fe_2O_3	17.0	9.5	10.6	4.6	4.4	5.6
Al_2O_3	25.9 [a]	23.9 [a]	22.8 [a]	33.5	17.9	11.8
CaO	5.5	6.6	4.3	1.8	12.2	20.4
MgO	1.7	3.1	1.8	1.3	0.2	5.3
SO_3	0.7	0.9	0.9	0.5	1.3	4.4
K_2O	1.9	2.2	1.3	2.0	0.5	0.6
Na_2O	0.4	0.7	0.3	0.7	0.2	0.4
TiO_2	0.02 [b]	0.0 [b]	0.0 [b]	0.03 [b]	0.5	0.9
insoluble	76.0	76.5	82.9	76.8	–	–
Pozzolanic activity	13.4	13.5	16.2	18.9	–	–
Blaine specific surface cm^2/g	2000	3000	3600	4300		

[a] Total $Al_2O_3 + TiO_2$. [b] sulphur in sulphides. [c] Determined as total $SiO_2 + Al_2O_3$ dissolved in NaOH 1 mol/l solution, after boiling during 0.5 h.

In the Polish BN–79/6722–09 Standard fly ash is classified into the following categories:

- siliceous fly ash,
- aluminous fly ash,
- calcareous fly ash.

This classification is not perfect, unlike the other classifications; for example the calcareous fly ash is not distinguished regarding the differences of anhydrite content (SO_3). As it results from the analysis presented in Table 7.3, the fly ash from Bełchatów could be even used in the production of CEM II/B–V cement, after CaO transformation into the calcium hydroxide, while the fly ash from Konin only in a limited range, because of the SO_3 content. The transition of CaO to $Ca(OH)_2$ is necessary, because in the PN–EN 197–1 standard the reactive CaO content in fly ash is restricted to 10%. The aforementioned classification rates Polish fly ash from the hard coal combustion to the siliceous ash and that from the brown coal combustion in Turoszów coal–field—to the aluminous ones respectively.

The chemical composition of fly ash from the hard coal does not show considerable scatter. The SiO_2 content is mostly in the range 46–50% and Al_2O_3 content varies in the range 22–25%. Fly ash from Jaworzno has higher content of Fe_2O_3 and lower of SiO_2. Obviously, the chemical composition of fly ash can substantially scatter; this relates particularly to the fly ash of Konin coal–field. According to Giergiczny [106] the silica content can vary from 23 to 70%, CaO from 18 to 50%, SO_3 from 2 to 11% and MgO from 2 to 9% respectively. These ranges can change if the desulphurization products are present in fly ash, as it will be discussed further.

Table 7.4 Chemical composition of siliceous fly ash from the Upper Silesia coal–fields and Lublin coal–field [112]

Component	Content in % by mass	
	Upper Silesia Coal Field	Lublin Coal Field
L.o.i.	2.7	2.5
SiO_2	53.3	52.4
Al_2O_3	25.2	31.8
Fe_2O_3	7.4	7.0
CaO	3.9	1.0
MgO	2.8	1.4
Na_2O	1.2	0.5
K_2O	3.0	2.6
SO_3	0.5	0.8

One should mention that in the fly ash from different sources in Poland, in general alkali content Na_2O_e exceeds 1.5 %, which value is recommended by the American Standard ASTM C618–84 [107]. Only the fly ash from power plant in Rybnik fulfills this requirement. However, Tenoutasse [108] is of the opinion that the alkalis from fly ash are released to the liquid phase very slowly and they are not harmful (see also Sect. 5.6).

The grain size distribution of fly ash varies significantly; they show specific surface area in the range from 200 to 450 m^2/kg. It is not important in cement production, because fly ash is mostly ground together with clinker. Addition of fly ash to the end chamber of the ball mill seems to be the best solution; it can be applied easily in the mills with the two–sides feeding [37]. Cements produced by mixing with fly ash separately ground to the very high specific surface assures rapid strength development [109]. Therefore, fly ash from coal powder fired furnace, and collected in the third section of electro–filter, shows very good pozzolanic properties [110, 111].

In Table 7.4 the chemical composition of siliceous fly ash from the Upper Silesia coal–fields and Lublin coal–field is given; the ratio of the latter one is significant [112].

In specific surface area of fly ash measurement it should be remember that the higher carbon content, because of its high porosity, can have a great impact on the results, being the source of major errors [113]. There are the suggestions to limit this method of testing to the fly ash with loss on ignition lower than 5 % [113]. The grain size distribution of fly ash gives Gauss curve type [113]. Fly ash particles are generally of spherical shape with smooth, glassy surface (Fig. 7.14). Many fly ash particles occur as “bubbles” filled with the mixture of gases, so–called cenospheres. The composition of gases was determined by Courtault [114]; their composition contains, in decreasing series: H_2,N_2, CO, H_2O, Ar, CO_2.

There is a relationship between the grindability of fly ash and hydrogen content; this is presumably the effect of OH^- ions absorption by melted ash, with the increase of its brittleness [114].

The chemical composition of fly ash is the same as the composition of clays. The most important components are SiO_2 and Al_2O_3; the pozzolanic activity of material augments with increasing amount of silica and alumina [115]. The pozzolanic activ-

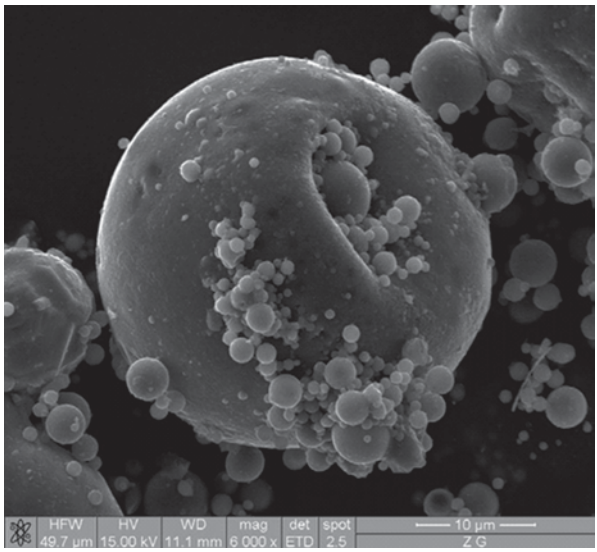


Fig. 7.14 Fly ash grain in the area rich in cenospheres (photo of B. Trybalska)

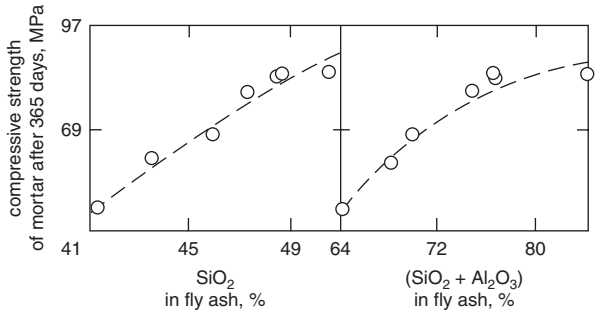


Fig. 7.15 Strength of mortar after 365 days of hardening as a function of SiO_2 and Al_2O_3 content in the fly ash (after [115])

ity, determined as the strength of lime–fly ash mortar, is increasing with percentage of these components (Fig. 7.15).

Carbon is a noxious component; it gives irregular dark patches on the surface of concrete, because it reveals a tendency to flow out [116]. It can be counteracted by addition of surfactants. The absorption of chemical admixtures added to concrete by carbon grains is also unfavourable. Carbon is generally present in coarser fraction of fly ash, above 100 µm [109].

The limits of carbon content in different standards or recommendations were in the range from 2.5 to 6% [37, 107, 109]. PN–EN 196–2 Standard is increasing this limits in fly ash for concrete production, expressed as "loss on ignition", to 9% in type C fly ash and to 7% and 5% for type B and A respectively. The uncombusted carbon content (Fig. 7.16) in fly ash used in cement and concrete production should not exceeds 5%, because of the increasing water demand and necessary superplasticizers addition; the rheological properties of concrete mixture become worsened as well [117, 118]. Giergiczny and Giergiczny [118] found that in fly ash fraction below 45 µm the uncombusted carbon content is usually very low, thus this fraction

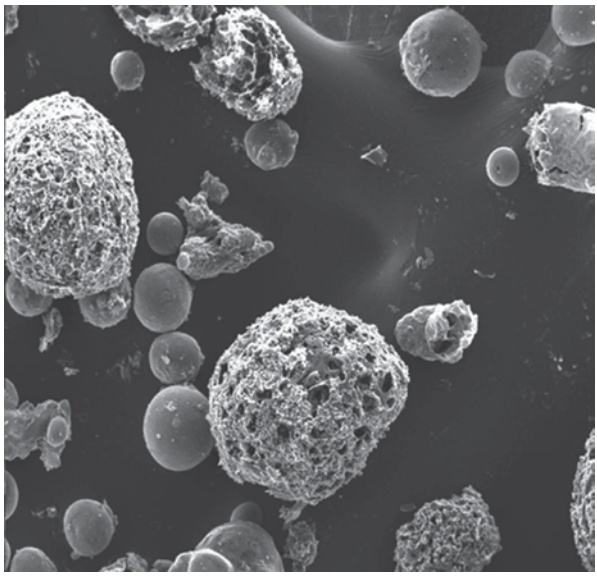


Fig. 7.16 Particles of uncombusted carbon in siliceous fly ash (after [112])

added to cement decreases water demand and shows good pozzolanic properties. On the other hand, fly ash with high content of fraction above 45 μm exhibits significantly poor quality. In order to characterize quickly the quality of fly ash these authors recommend to determine loss on ignition and residue on the 45 μm sieve (these parameters should be as follows: L.o.i≤5%, residue≤40%). Irrespectively of the poor quality of fly ash with high carbon content, the acceptation of so high limits in PN–EN 196–2 Standard is surprising and does not match with the sustainable development rules. Primarily, admitting of so bad coal combustion technology in power plant, which gives such high level of uncombusted carbon equal 9%, is the waste.

MgO is the next component, restricting in fly ash. It can occur as periclase and the limit of its content is 4% or 5% [36]. High presence of sulphur is not advantageous as well, because this component can causes the concrete volume change, after longer period of maturing (ettringite). Therefore the SO_3content is limited to 5%, or even to 2.5% in British Standard [36]. In the PN–EN 196–2 Standard the threshold value for SO_3 is 3% and chlorine 0.1%.

The phase composition of fly ash can be very different even in particular grains. Glass is a main constituent; its content in the siliceous fly ash is generally higher than 80%. The crystalline phases are: quartz, mullite, hematite and magnetite. In Table 7.6 some examples of different fly ash composition are shown.

For the quantitative determination of ash phase composition XRD or XRD and ash extraction with hydrofluoric acid are used [113, 114, 123].

The constitution of fly ash glass is similar to the silica glass or the alumina–silica one, remembering the slag glass [16]. Tkaczewska and Malolepszy [111]. studied the siliceous fly ash glass. They found that the glass in fly ash from the third, end section of electrical precipitator has higher aluminum and modifiers content which

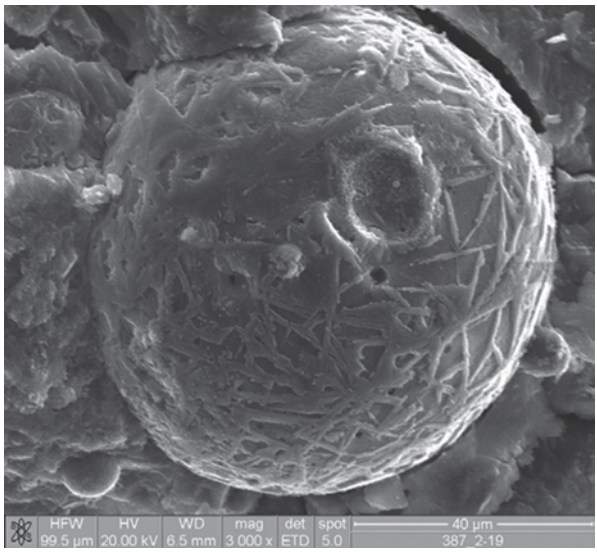


Fig. 7.17 Fly ash grain with magnetite crystals on the surface. The cenospheres are visible (photo B. Trybalska)

presumably is causing its higher pozzolanic activity. According to Hubbard [122], the glass phase is mainly formed by partial illite melting, while the transformation of kaolinite, occurring in the solid state, results in the formation of mullite or amorphous metakaolinite. Therefore it is the silica–alumina–potassium glass, which is proved by analyses. Iron in high degree forms own iron–rich phases: hematite and magnetite (Fig. 7.17), and in minor degree is included in glass [115]. The other elements present in the glass are calcium, magnesium and alkalis; the latter ones can be absorbed by the melt from the gaseous phase [124]. Sulphur forms anhydrite or is included in glass too [36].

Glass in the fly ash from the brown coal combustion is much more differentiated [125]. Apart from glass rich in silica and alumina there are the alumina–rich one, as well as the glasses poor in alumina, belonging to the C–F–S system. The lime rich glass are closer to melilite and have good hydraulic properties. First Diamond [126] and then Uchikawa et al. [120], on the basis of XRD tests, distinguished the following types of fly ash glass: siliceous similar to cristobalite, alumina–silica one (mullite), closer to $C_{12}A_7$ and melilite.

As components of fly ash from the brown coal, apart from the phases listed above, are also: C_2S, $C_{12}A_7$, C_2F, $C_4A_3\overline{S}$, CaO and periclase. The example of phase composition of fly ash is given in Table 7.5 [119].

The pozzolanic properties of fly ash are undoubtedly related to the glass and they are improved with increasing content of this phase and of the fineness of fly ash. The following factors are crucial for fly ash of good quality:

- low carbon content,
- high glass content,
- low alkali content,
- high fineness.

Table 7.5 Phase composition of fly ash (% by mass)

Phase	Polish fly ash					Japanese fly ash						French fly ash [72, 121]		English fly ash [122]
	"Blachownia"	Jaworzno II"	"Łagisza"	"Turoszów"	"Połaniec"	1	2	5	6	Average [a]	Coarse grains			
Glass	78	61	64	79	62	64	70	72	86	83	72	63	34[b]	83
Quartz	12	29	19	11	21	17	14	7	5	8	13	12	5	4
Mullite	10	10	17	10	12	19	16	6		8	13	21	4[d]	13
Magnetite					5			15[c]				4		
Spec. Surface cm^2/g	3500	3100	1900	3700	3900	3200	3800	2800	3700			0		

[a] average, [b] from brown coal, [c] 21–9% iron calculated as Fe_2O_3, [d] moreover CaO—28%, hematite—4%, C_2S—14%, $CaSO_4$– 15%.

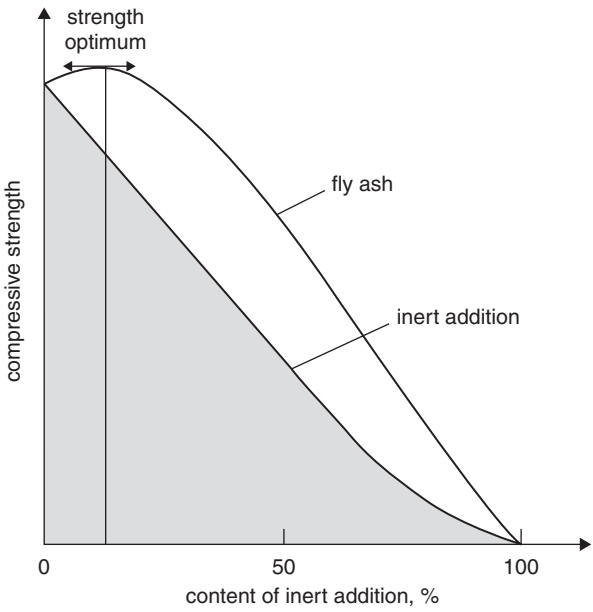


Fig. 7.18 Assessment of fly ash pozzolanic activity based on the strength measurements

The higher glass content and fly ash fineness and higher pozzolanic properties the higher was the coal fineness, combusted in boiler furnace. However, it should be underlined that the properties of fly ash can vary substantially, even in the case of the same coal [1]. Therefore, to use in cement production fly ash, with quality is controlled rigorously in production process, is the best solution.

There are different methods of pozzolanic activity of fly ash or natural pozzolanas determination. The best, however long, are the measurements of strength development of mortars produced from ground Portland cement clinker with chosen addition of fly ash. These strength development is compared with mortar produced from cement with ground sand, used as inert additive (Fig. 7.18).

This method reflects well the practical conditions because the pozzolanic reaction depends on the mineral composition of cement.

Another method consists on the measurement of mortars strength, composed from two parts of sand, 2.5 parts of fly ash and one part of lime, which after mixing with water are compacted in the moulds under the pressure of 10 MPa and the cubic specimens are obtained [114].

There are many quick, chemical methods. Three can be mentioned: the Feret–Florentino test, the Chapelle method and the ASTM one.

In the Feret–Florentino test the dissolution in HCl of the following fly ash samples is measured: fly ash sample without treatment, second fly ash sample hydrated with lime for 7 days at temperature of 20 °C, the third one hydrated for 4 days at temperature of 50 °C. The difference between the solubilities is the measure of fly ash pozzolanic activity.

In the Chapelle method the mixture of 1 g of fly ash and 1 g of lime is boiled in 250 cm^3 of distilled water during 16 h. Then the amount of bound lime is determined [127].

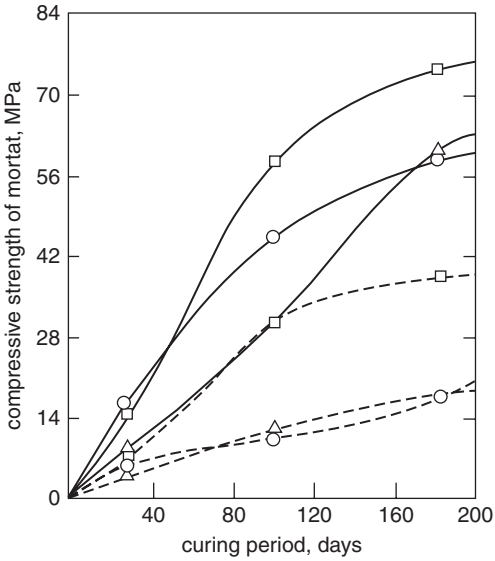


Fig. 7.19 Effect of fly ash extraction with water on the strength of mortars (according to [115]); continuous lines—after extraction, dashed lines—without extraction

Raask [128] proposed to determine the fly ash solubility in the HF of concentration 0.1 mol/l.

Fly ash—in spite of significant fineness—is ground together with Portland cement clinker in order to improve the properties of produced cement. During grinding microcracks are induced in the glass shell on fly ash particles and their reactivity in cement paste solution is increasing. Moreover, the grinding process results in reactive glass surface liberation and generation of microstresses in glass particles, which enhance their reactivity [27]. Simultaneously fly ash became well homogenizes with Portland cement clinker. The big, irregular fly ash grains are primarily disintegrated, while the small spheres remain less disrupted [113].

Pozzolanic cement strength increase can be also achieved by application of grinding aids: triethanoloamine and glycol. Heating of fly ash to the temperature 40–80 °C results in better reactivity too [109].

The extraction with water improves the pozzolanic properties of fly ash which was not preciously ground [115]. The results are presented in Fig. 7.19. Wett and Thorne [115] are of the opinion that the increased reactivity is the consequence of the fly ash conglomerates disintegration by water and increased specific surface.

It should be remembered that the pozzolanic activity properties determined with different methods are not comparable and have no universal meaning. The amount of bound lime is not always well correlated with the strength of mortars, and similarly the degree of fly ash which has reacted. The found pozzolanic activity is affected by the properties of lime and cement used in the test. There are some approaches to resolve this problem. Hubbard [122] formulated the pozzolanic potential index including the calcium ions binding ability with the strength increase after longer period of maturing. This index is expressed as a ratio $(K_2O/Al_2O_3)\cdot 10$.

The three classes of English fly ash were distinguished:

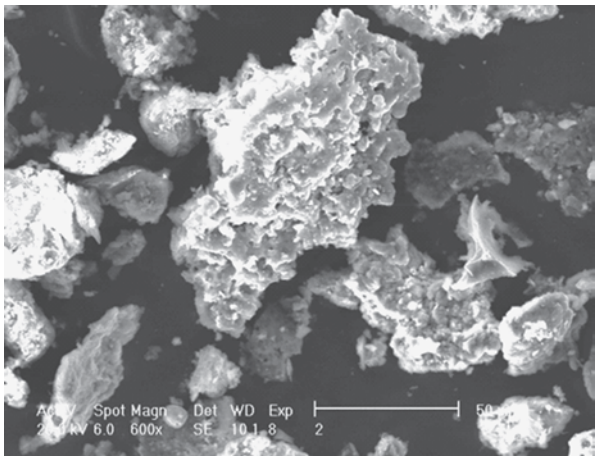


Fig. 7.20 Fluidized bed fly ash under the scanning electron microscope (according to [112])

- class 1: (K/A) 10 > 1.0 high reactivity
- class 2: 0.5 < (K/A) 10 < 1.0 mean reactivity
- class 3: (K/A) 10 < 0.5 poor reactivity

In the PN–EN 450–1 Standard the method of fly ash index activity determination, for their use in concrete production, is given. In the measurements of strength of the mixture of cement CEM I 42.5 with 25 % of fly ash is used. The C_3A content in cement should be in the range from 6 to12 % and Na_2O_e in the range of 0.5–1.2 %. The compressive strength after 28 days should be not lower than 75 % of cement strength and after 90 days—85 %. It should be notice that the range of Na_2Oe content is wide, which will have great impact on the pozzolanic properties of fly ash and consequently on strength, particularly after 28 days of hardening. It was shown by Giergiczny and Rajczyk [129], who found major differences of siliceous fly ash activity: this index was near the limit value in the case of cement $Na_2O_e = 0.7$ (76 %), but the use of cement with $Na_2O_e = 1.02$ resulted in the value of 84 %. One can expect that in the case of cement with Na_2O_e content close to the standard value (i.e. 0.55) this fly ash would not attain the value fulfilling standard requirements. This standard gives also the determination of reactive SiO_2 in fly ash, which should be obtained as a difference between the total residue insoluble in hot HCl and that insoluble in KOH (16 h extraction at ambient temperature and subsequent 4 h boiling). It seems that this method will give the results far from real pozzolanic activity evaluated from the strength of mortar.

The new technology of coal combustion in fluidized bed has been implemented in some power plants, recently. The temperature of this process is much lower, about 900 °C, thus its phase composition and properties are totally different. At low combustion temperature only the dehydroxylation of clay minerals occurs and the produced amorphous substance is one of the main components of fluidized bed ash [106] (Fig. 7.20). Simultaneously with coal combustion the flue gas desulphurization is performed and the sorbent, usually calcium carbonate, is introduced into the fluidized bed. Because that the excess amount of sorbent must be added (Ca/S

Table 7.6 Chemical composition of fly ash from boilers with the fluidized bed furnaces [130]

Component	Content, % by mass					
	fluidized bed combustion fly ash			bottom waste		
	min.	max.	average	min.	max.	average
L.o.i.	1.55	3.68	2.69[a]	0.26	3.53	1.37
SiO_2	35.3	49.5	44.18	28.3	85.7	40.73
Al_2O_3	18.30	26.50	23.02	2.16	27.40	14.65
Fe_2O_3	5.24	8.59	7.19	1.84	5.24	3.27
MnO	0.05	0.13	0.08	0.03	0.20	0.07
TiO_2	0.74	0.98	0.90	0.09	1.95	0.64
CaO	5.08	28.02	10.95	2.75	43.40	22.46
CaO	0	6.57	2.18	1.89	15.38	8.14
MgO	0.81	2.75	2.03	0.49	2.41	1.47
SO_3	2.90	10.70	5.58	0.11	21.13	14.56
P_2O_5	0.18	0.72	0.44	0.05	0.48	0.16
Na_2O	0.61	2.20	1.29	0.27	0.98	0.56
K_2O	1.66	2.98	2.40	1.10	3.56	1.78
BaO	0.06	0.17	0.09	0	0.17	0.05
SrO	0.03	0.06	0.04	0.01	0.07	0.03
TOC	0.16	5.18	1.54	0.17	3.81	0.73

[a] Giergiczny [106] found 5–7%

molar ratio is mostly 1.5), the fluidized bed ash is significantly enriched in anhydrite and CaO, as well as in $CaCO_3$.The chemical composition of this ash is highly variable; the use of so–called biomass, apart from coal, contributes to the variability of this byproduct (Table 7.6 [130]). The three types of fluidized bed ash can be distinguished: fly ash carried by the stream of combusting gases, ash from the fluidized bed and the bottom ash (in amount about 75%, 15% and 10% respectively). The fluidized bed ash exhibits hydraulic and pozzolanic properties, related primarily to the amorphous phase content, which example is metakaolinite; this phase will react with CaO to form C–S–H [106]. The reaction of this phase with anhydrite leads to the formation of ettringite [106]. Therefore the paste produced from fluidized bed fly ash reveals, after 7 days of hardening, the compressive strength of about 5 MPa, however, without further strength increase [106].

The fluidized bed fly ash does not comply with the PN–EN 197–1 Standard as cement component and can be used only as filler, in amount not exceeding 5%. However, the fluidized bed fly ash can used as set controlling agent, because of anhydrite content. This ash does not fulfill also PN–EN 450–1 Standard requirements as an addition to concrete. In Table 7.6 the contents of particular components in fluidized bed fly ash and bottom ash are given [130].

The significant amounts of fluidized bed ashes are generated; in 2000 the annual output was 723 thousand tones [131]. Some part is used in cement industry, as a raw material in Portland cement clinker production. They are also added to concrete on the base of technical approvals. They can be easily distinguished from the ash of pulverized–coal fired furnace, because they do not give the mullite peak on XRD pattern.

7.5 Cements with Fly Ash Addition

Fly ash addition to cement is diminishing shrinkage and creep, as well as heat of hardening. This latter feature is an advantageous one because, as it is pointed out by Owens [132], the self–heating of concrete has a negative effect on the strength after 28 days of hardening. It is caused by weakening of cement matrix bond with aggregate and with microcracks formation, due to high thermal expansion of air and water in the concrete. The temperature rise in concrete up to 60 °C brings about the strength decrease of 32 % [132]. These unfavorable phenomena can be eliminated by the fly ash addition. The mortars produced from cement with fly ash addition, cured at 60 °C have much higher strength. At 30 % fly ash addition the mortars show higher strength after 28 days when cured at temperature of 60 °C and 80 °C, even compared to the mortar from cement without addition, cured all the time at temperature of 20 °C.

The mortars produced from cements with fly ash show, however, lower strength development at early age. Simultaneously, one should take into account the inevitable rise of concrete temperature, which favors the pozzolanic reaction and improves the strength. At 20 °C the pozzolanic reaction commences not before 10–14 days [132, 133].

There is an opinion that the reaction of glass with calcium hydroxide begins late and C–S–H phase is visible under the electron microscope till after 28 days [134]. However, a view is advanced, that the pozzolanic reaction starts immediately, but affect the properties of paste after relatively long time [113, 135]. On the other side the formation of ettringite in the fly ash mixture with lime or in the paste from the brown coal ash is observed already after one to some hours [135, 136]. Curing of mortar at temperature of 40 °C results in considerably higher strength after 28 days maturing [137]. After 180 days maturing at temperature of 20 °C the mortars reveal even higher strength. However, the progress of the pozzolanic reaction is slowed down significantly in the case of curing at temperature of 8 °C; after 90 days the strength of mortar attains no more than 50 % of the reference mortar without fly ash (Fig. 7.21).

Hence, another drawback of fly ash cements becomes evident—the very low strength increase at low temperatures. The improvement of strength development can be achieved by very fine fly ash grinding.

Taking into account the properties of fly ash cements, as well as the acceleration of pozzolanic reaction at higher temperature, many authors recommend to apply this cement in the production heat treated precast elements,. For example Dalziel [138] found that the thermal treatment of cement with 20 % of fly ash at temperature of 65 and 85 °C result in higher strength of mortar already after three days and this trend is continued during all studied period. The flexural strength increase was particularly evident (Fig. 7.22). This behaviour was proved by the other authors [113].

Concretes from cements with fly ash addition exhibit a higher sensitivity to the moisture deficiency at early age. They should be carefully cured protected against the moisture loss, because of the shrinkage cracks risk.

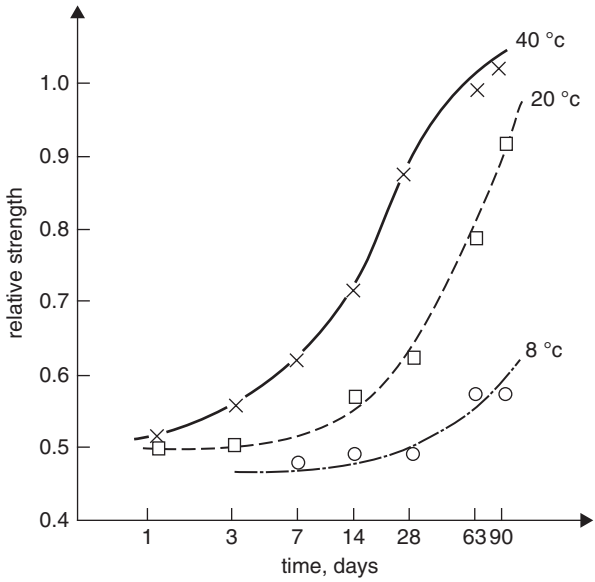


Fig. 7.21 Relative strength of cement pastes with 30% fly ash addition (according to [137])

The increased resistance to the aggressive environment is an advantageous feature of these materials. It is linked with $Ca(OH)_2$ content lowering in the paste, but primarily to the reduction of larger pores share, that means the permeability decrease. The ion exchange ability decreases and this counteracts the corrosion reactions progress. Obviously, these properties are developing with the fly ash content increase, and in the case of sulphate attack—with C_3A content decrease in cement clinker. The apparent diffusion coefficient of Na^+ and Cl^- decrease with siliceous fly ash addition is shown in Fig. 7.23 [139].

Fly ash addition is diminishing also the risk of reaction of alkalis from cement with aggregate, which was discussed in Sect. 6.4. The fly ash addition, which allows the reduction of OH^- ions concentration in the liquid phase of the paste to 0.3 mol/l is protecting concrete against destruction [140]. This corresponds to about 40% of fly ash addition to cement with average alkalis content ($Na_2O_e = 0.92\%$) or about 30% in the case of cement with lower alkalis content ($Na_2O_e = 0.68\%$).

The modification of concrete mixture properties in the presence of fly ash, primarily its workability, is important too. The improvement of workability is attributed to the spherical shape, as well as the smooth surface of fly ash grains [113]. The workability augments with the fineness of fly ash and this allows w/c ratio lowering (Fig. 7.24). However, there are some cases of workability worsening in the presence of fly ash [141].

The three component cements with fly ash addition, apart from granulated blast-furnace slag {CEM II/B–(S–V)}, have the advantageous properties; first of all fairly good strength development.

A part of cement in concrete production can be replaced by siliceous fly ash. The quantity of fly ash addition is then determined according to PN–EN 206–1 Standard, which is introducing *k* coefficient and the maximum fly ash/cement ratio cannot be higher than 0.33. The water/binder ratio can be calculated using this

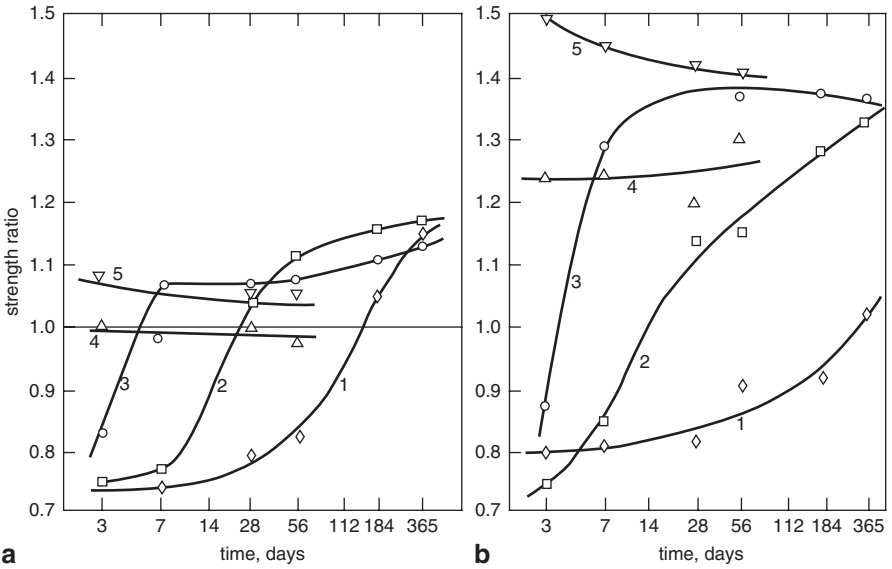


Fig. 7.22 Relation of mortar strength produced from cement with fly ash to the strength of reference mortar without fly ash as a function of time and temperature (according to [138]): a) compressive strength, b) flexural strength, temperature of 1–20 °C, 2–35 °C, 3–50 °C, 4–65 °C, 5–80 °C

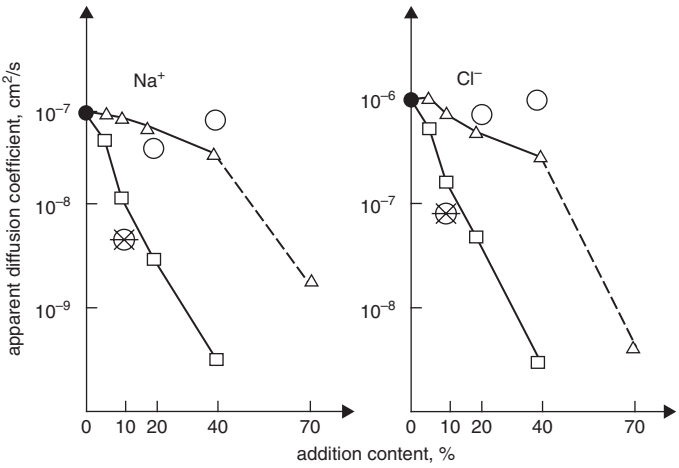


Fig. 7.23 Na^+ and Cl^- apparent diffusion coefficients in the pastes produced from cement with siliceous fly ash (temperature of 45 °C, w/c = 0.40) (according to [139])

coefficient as: water/(cement + k fly ash). In the case of concrete produced from CEM I cement, fulfilling the PN–EN 197–1 Standard coefficient k should be equal:

- $k = 0.2$, when CEM I 32.5 is used,
- $k = 0.4$, when CEM I 42.5 or 52.5 is used.

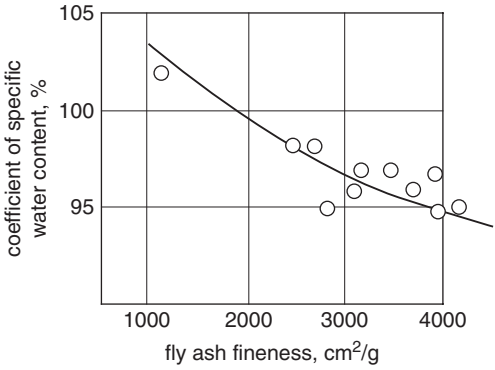


Fig. 7.24 Water demand in the case of mortars with addition of fly ash of various fineness (after [113])

Simultaneously, the minimum cement content in concrete, required in the particular exposition classes (according to the PN–EN 206–1:2003 Standard) can be reduced maximally (in kg/m^3) of amount fulfilling the relation: k (C_{min}—200). For example in the case of CEM I 32.5, in which k=0.2 and for the exposition class XC2 determining minimum cement content as C_{min}=280 kg/m^3, the maximum reduction of cement is: 0.2 (280 − 200)=16 kg/m^3, that is about 20 kg/m^3. Moreover, because, by mass, FA/C≤0.33, the fly ash to cement ratio will be FA/260=0.33, it means FA=0.33 260=86, that is about 90 kg/m^3. The fly ash share can be higher but it cannot be accompanied by further reduction of cement content; therefore fly ash will play a role of an inert filler i.e. micro–aggregate. Obviously, the fly ash share can be lower and it is frequently equal to cement content lowering by mass, thus in the given example it will be about 20 kg/m^3. Polish standard PN–B–06265 (national supplement to the PN–EN 206–1 Standard) contains Table 2, giving the minimum cement content in 1 m^3 of concrete, with and without siliceous fly ash addition. Simultaneously, this standard excludes the possibility of fly ash addition, as a part of binder—thus cement replacement—in concretes produced from Portland fly ash cements. In 2009 the consumption of siliceous fly ash in concrete production in Poland was 790 thousand tons.[4]

In Unites States and in Canada, as well as in India in numerous constructions concretes with high fly ash content are used [142]. In Table 7.7 the physical and chemical properties of fly ash, which can be used for concretes production with high fly ash content, are given.

The authors [142] are reporting that the same advantage can be achieved in concrete production using cement with fly ash addition, with simultaneous warranty of its quality and optimum properties, which are under constant control. These authors are reminding also that the new ASTM C 1157 Standard edited in 1998, does not restrict the type and percentage of mineral addition, under the condition that cement complies with other standard requirements [142].

Giaccio and Malhotra [143] introduced the term "high–volume fly ash concrete" in 1980, however, F or C class fly ash should replace at least 50 % of cement and the

[4] Data from the Association of Ready Mix Concrete Producers in Poland

Table 7.7 Standard requirements for the fly ash used in concrete production [142]

Chemical composition, class F[a]	ASTM C 618	Physical properties	ASTM C 618
Free water, max., %	3.0	residue on the 45 μm sieve, max, %	34
L.o.i., max. %	6.0	water demand	105
($CaO+Al_2O_3+Fe_2O_3$), min. %	70	expansion in autoclave, max, %	0.8
		density and fineness in the range, max. %	5
CaO, max. %	–		
SO_3, max., %	5.0	pozzolanic activity	75[b]

[a] In the paper the requirements for class C is also given, but without any examples of their use for concrete production with high ash content.
[b] In the mixture with Portland cement after 7 or 28 days, in relation to cement without ash.

Table 7.8 Typical composition of high–volume fly ash concrete mixture, kg/m^3 [142]

Component	Compressive strength at age 28 days, MPa		
	20 MPa	30 MPa	40 MPa
Water	120–130	115–125	115–200
Cement[a], kind I/II	125–130	155–160	180–200
Fly ash class F[a]	125–130	215–220	220–225
Coarse aggregate[b]	1170 ± 10	1200 ± 10	1110 ± 10
Fine aggregate	800 ± 10	750 ± 10	750 ± 10
Admixtures[c]	c	c	c

[a] Cement and fly ash according to ASTM, if high early strength is required, use rapid hardening cement III
[b] Maximum 19 mm
[c] To assure 5–7% of air entraining agent should be, depending on sand grading, 200 ml/m^3 (concrete of low strength) up to 300 ml/m^3 (high strength concrete). Superplasticizer additions is low in the case of acrylic admixtures from 100 to 200 ml/m^3

last one content in concrete does not exceed usually 200 kg/m^3. The water content in these concretes is low (generally lower than 130 liters/m^3) to give the water to binder ratio not higher than 0.4, or even lower. Therefore the superplasticizer is applied to maintain the workability of concrete mixture, in the range from 150 to 200 mm according to flow test. When the high early strength is not required (at higher water to binder ratio) the superplasticizer is not necessary [142]. This concrete reveals excellent workability, low drying shrinkage, very good durability, high strength, particularly at later age and therefore Malhotra classified it to the high performance concretes [142]. A typical composition of concrete mixture is given in Table 7.8.

Because of the low w/c ratio Malhotra and Mehta [142] recommend to start early with the concrete proper curing, to avoid the crack formation, resulting from the plastic shrinkage. Because of the low heat of hardening, the high–volume fly ash concretes are free of the temperature gradient induced as well as of drying shrinkage microcracks [142]. They are resistant to the various forms of corrosion, primarily of sulphate and chloride attack, as well as of alkali silica reaction, or even they assure

a good protection of reinforcing steel [142]. Therefore the high–volume fly ash concrete technology allows the production of the high performance concrete [142].

Many works focused on the fly ash binders activated with relatively high concentrated NaOH solutions, analogously as in the case of the slag alkali–activated cements, were conducted based on the studies inspired by Glukchovsky [144]. LaRosa et al. [145] have shown that the series of zeolites can be obtained, starting from the siliceous fly ash and NaOH or KOH water solutions with concentration 2.8 mol/l, at elevated temperature from 80 °C to 200 °C. The $Al(OH)_3$ and colloidal silica were added too [145]. The formation of two zeolites was found: $Na_6Al_6Si_{10}O_{32} \cdot 12H_2O$, so–called zeolite NaP and zeolite Y with composition $Na_{2.06}Al_2Si_{3.8}O_{11.63} \cdot 8H_2O$. The studies in this field were conducted by Barth and Höller [9] as early as in 1976 and later on there were many research works in this field [146–148]; in Poland by Derdacka and Malolepszy [149] in 1975. Because zeolites present high ion exchange ability, they are primarily used for water purification from heavy metals. However, they can also be applied as binders for concrete with special properties, for example for heavy metals immobilization [150]. There are primarily binders containing amorphous sodium–aluminosilicate gel, which can be used for production of high strength and high resistant concrete, in different corrosion environments [151, 152]. The use of higher NaOH concentration and longer thermal treatment (temperature 40–90 °C) can give better crystallized [153] zeolites. The silica–alumina glass is the raw material of good quality to produce them and the siliceous fly ash complies well with this requirement. The NaOH or Na_2SiO_3 are mostly used as activators [154], the potassium hydroxide is used occasionally [155]. According to Palomo et al. [156] the sodium and potassium silicates are the best activators. It is assumed that to the binder matrix has the following formula [157]:

$$M_n\left(-\left[SiO_2\right]_z - AlO_2\right)_n - wH_2O$$

where M is the sodium or potassium cation, $z = 1$, 2 or 3, n is the polymerization degree.

In this gel aluminum has tetrahedral coordination, similarly as silicon [158]. Only a very low part of silicon and aluminum dissolves and is participating in polymerization.

In concretes produced from NaOH activated fly ash, subjected to the heat treatment at temperature of 60 °C or 75 °C during 24 h or longer, the coarse aggregate below 9.5 mm and sand are used. The optimum content of paste, assuring the advantageous strength was evaluated as 18 % by volume, which corresponds to the fly ash content of about 445 kg/m^3 [159]. The ratio of NaOH solution of 8 moles/liter to fly ash equal 0.4 and curing temperature of 75 °C assure the highest strength. The observations of microstructure matrix have shown that the degree of fly ash reaction is low and the gel reaction products were formed a shell surrounding the fly ash grains [159]. The hydroxysodalite was the only crystalline product.

Currently the intensive studies are developed with aim to find the most rational ways of these concretes application, primarily in Spain and in China [156, 160,

161]. One can presume that there will be the applications in environment, in which a very high resistant to corrosion and additionally at higher temperatures will be demanded.

7.6 Silica Fume[5]

Silica fume is a byproduct from manufacturing of metallic silicon or various silicon alloys with iron (ferro–silicon) or other metals in electrical arc furnaces. They are formed by oxidation of SiO vapour in the gaseous phase and are precipitated in the dust collectors.

Silica fume, because of the high specific surface area (700 m^2/kg according to Blaine) and glass composition, has a very good pozzolanic properties. Their specific surface, as measured by nitrogen adsorption, is between 13 and 23 m^2/g [16]. They are devitrified after heating to the temperature of 100 °C linked with cristobalite crystallization, and in the case of Fe–Si50 alloy with enstatite crystallization [16]. Simultaneously the morphology of silica fume particles, which are glass spheres with diameter from 0.1 to 0.2 μm is important. They agglomerate readily. Therefore, they should be added to concrete together with superplasticizers and vigorously mixed. In this condition the powder spheres will be uniformly distributed between cement grains and play a role of excellent microfiller. Moreover, because of the high pozzolanic activity, their reaction with lime is marked already after one day [16]. The strength gain of cement mortar with silica fume addition is observed already after ten days, and the profitable addition is in the range from 5 to 15% (mostly 10%). Regourd [16] found that the silica fume addition improves the properties of fly ash cements. The rapid reaction of silica fume is causing the strength increase while the effect of fly ash is marked after longer period. The similar phenomenon is observed in the case of slag cements. The content of silica fume in this case should be carefully determined, because the rapid lime consumption can have a negative impact on cement strength after 28 days of hardening [16].

The total annual output of silica fume is low, about 1.2 million tons, from which 30% is delivered by USA, Japan and Norway [16] (in Poland—about 10,000 tons). Therefore this material is expensive. Moreover, because of the high fineness and low density (2.1–2.25 g/cm^3) their handling and transport are troublesome. Hence, their practical application is focused in the production of special cements and concretes. This problem will be discussed in Chap. 10.

Silica fume reduces markedly the porosity of concrete, as well as improves the other properties. The permeability of gaseous media and diffusion of ions, for example the chloride ones, is strongly diminished. The resistance of concrete with silica fume becomes higher [162–164]. The porosity of interfacial transition zone in concrete, also cement matrix–steel reinforcement interface is strongly reduced, as

[5] The monographic book „Silica fume" (in Polish) by W. Nocuń–Wczelik was edited by Polski Cement, Kraków 2005.

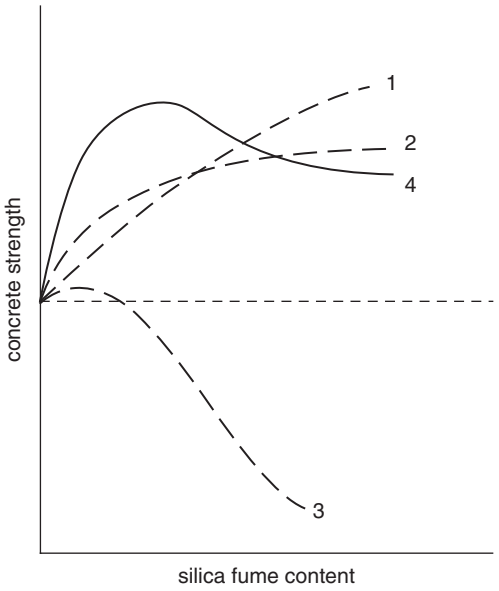


Fig. 7.25 Effect of silica fume on the strength of concrete as the resultant (4) of three factors: pozzolanic reaction (1), effect of micro-filler (2), water demand (3) (according to [165]).

it was discussed in Chap. 6. The effect of silica fume on the strength of concrete is very well summarized in Fig. 7.25, according to Khayat and Aïtcin [165].

The granulated silica fume, when used in concrete production, can be a source of reactive silica, causing the reaction with sodium and potassium hydroxides and leading to the deterioration of concrete [166].

7.7 Fillers

Limestone is used first of all as filler. The application of this material has a long tradition in many countries, where the masonry cement was produced. The mortars and plasters are produced from the lime and cement mixed at the ratio from 3:1 to 2:1 with sand addition. In many countries this material was replaced by masonry cement with the ground limestone and air entraining agent. The maximum limestone content was 60% in Sweden, about 50% in USA, Canada and in France; in Great Britain it was 25% [37]. The masonry cement shows very good plasticity and workability; it should exhibit high retention of water and low shrinkage.

Since 1979 in French new standards for cement were introduced, which allowed the 3% dosage of filler for all types of cements [167]. European Standard EN 197–1 introduced in 2000 increased the content of filler to 5%.

The main goal of fillers addition is, due to their physical properties and fineness, to improve the concrete mixture workability, the increase of compactness, thus the reduction of permeability, primarily due to capillary pores volume decrease, as well as the reduction of trend to microcracks formation.

Contrary to their name fillers are not quite inert and their impact on the properties of paste can be reduced to three following mechanisms (it relates to limestone) [168, 169]:

- the effect of microfiller, consisting in the dispersion of clinker grains and filling the free spaces between them,
- the effect on the epitaxial crystallization of C–S–H,
- the chemical reaction with aluminates and the formation of carboaluminate hydrates.

Limestone addition is accelerating the hydration of C_3A due to the formation of carboaluminates [170]. The hydration of C_3S is accelerated as well, as it was discussed in Chap. 4 [169].

Limestone used as a filler should be free of the organic compounds—French Standard limits their content to 0.5%. The clay admixture should be as low as possible, it is determined from the methylene blue absorption test, which should not exceed 1.5 g per 100 g of filler with the fineness below 80 μm [16]. Simultaneously, cement with limestone addition should give the paste of standard consistency, at water content lower than 30% [171].

The content of grain size fraction coarser than 80 μm should not exceed 3% to give the required fineness of the filler. Because of the significantly higher grindability of limestone than that of clinker, cements with this filler have higher specific surface area and limestone is principally contained in the finest fractions [171].

However, in PN–EN 197–1 Standard the limestone is specified as a mineral addition, therefore it is classified as main component of cement, like slag or fly ash, (see Table 1.3 in Chap. 1) and distinguishes two types of limestone: L and LL, as it was discussed in Chap. 1.

The examination of industrial cement CEM II/B–LL 32.5R has shown that limestone is present mainly in the finest fractions, principally below 32 μm [172]. 90% of total limestone amount is present in this fraction and in 0–10 μm fraction 55% [172]. Simultaneously, the fineness of clinker component is worsened. Ranc and Carious [173] found very good properties of cements with 15% and 30% limestone content, which did not differ in no way from CEM I cements of the same class. However, there were cements produced by mixing cement clinker of high fineness (in cement of class 42.5 the specific surface of clinker was 397 m^2/kg, and limestone—540 m^2/kg; the same fineness of components was in the case of class 32.5) with limestone [173]. Chłądzyński and Garbacik [174] in similar studies produced cements starting from the clinker with specific surface area of 330 m^2/kg and limestone of 850 m^2/kg. This cement showed the lowest strength after 28, 91 and 364 days (CEM I—52, 56 and 60 MPa, CEM II/B–LL with 33% limestone—34, 37 and 39 MPa respectively) and consequently the lowest properties, as compared to the other cements examined in this work {amongst the others: CEM II/B–V, CEM II/B–S as well as CEM II/B–M, including CEM II/B–M (V–LL)—produced of the same clinker} [174]. Concretes produced of these cements were matured at 3 different temperatures and subjected to sulphate corrosion, corrosion in sea water and carbonization, as well as the freeze–thaw cycles. CEM II/B–LL presented only the lowest shrinkage [174].

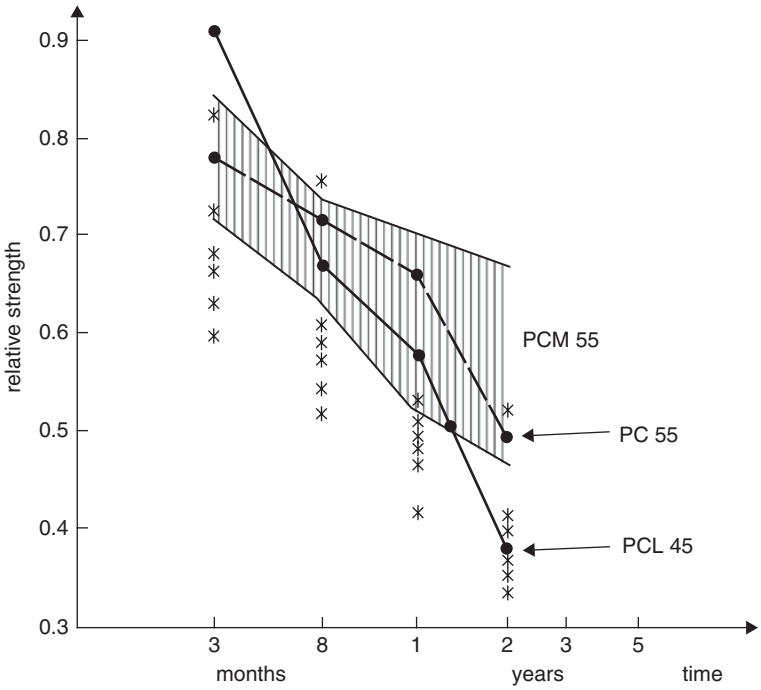


Fig 7.26 Relative strength (strength of samples cured in sea water to the strength of samples cured in standard conditions) (according to [171]). Dashed area corresponds to 6 cements PC 55, cements PC 45 with additives marked with crosses; PC 55 – Portland cement without additives; PCM 55 – special Portland cement without additives used in the sea environment (*prise mer*); PCL 45 – cement with limestone

It is evident from these data, that the best properties of Portland limestone cement can be achieved by separate Portland cement clinker and limestone grinding and subsequent mixing of these components. Because the C_3A phase is reacting with limestone, the lower gypsum addition, reduced of about 50%, can be used [175].

Many years of French experience with about 30% limestone containing cements allowed the evaluation of concretes manufactured from these cements [171, 176]. These cements do not differ, in traditional application, from Portland cements of the same class, without mineral additions. Concrete has identical freeze–thaw resistance, if only the proper air entraining agent is used. The critical air–void spacing factor is in this case significantly smaller and equal about 200 μm, while in the case of Portland cement concrete without additions—about 400 μm [171]. The durability of concretes from these cements is good too; they are resistant as compared to concrete of other cements, even in the aggressive environment of seawater (Fig. 7.26). In the latter case clinker fulfilled the requirements of old French standards for cement used in marine constructions; the C_3A content was lower than 10% and the total ($C_3A + 0.27C_3S$) lower than 23.5% respectively.

7.8 Metakaolinite[6]

Metakaolinite is produced by heating of kaolinite at temperatures between 700 °C and 900 °C; however, the temperature should not exceed 800 °C. At prolonged heating at 900 °C mullite, the inert component, is formed. Obviously there are the other factors influencing the optimum temperature, as the pozzolanic properties of kaolinite are concerned. Primarily the time of thermal treatment at maximum temperature and hence the type of kiln (temperature regime) and the fineness of used kaolinite should be pointed out. Metakaolinite can be produced by burning even at temperature 1000 °C, if the so–called "flash calcining" is applied [177]. The excellent pozzolanic properties of metakaolinite can be attributed to the dehydroxylation of kaolinite, occurring at temperature of 550 °C [178]. The structure of kaolinite is composed of silicate layer linked with the gibbsite layer in such a way that the one oxygen atom from the $[SiO_4]$ tetrahedron belongs simultaneously to the octahedron of the gibbsite layer $AlO(OH)_2$ (two–layers sheets). The general formula is $Al_2[Si_2O_5](OH)_4$. In the product of dehydroxylation there is no the long–range order, the sequence of layers is strongly disturbed and the aluminum transforms into the tetrahedral coordination [179]. This change of aluminum coordination is frequently considered as a proof of metakaolinite formation. The metakaolinite is highly reactive, particularly in alkaline solutions, as well as in the solutions of weak acids [180]. Therefore it is used for the production of mortars and concretes [181]. Special applications of these composites, such as rapid hardening mortars for repairs of concrete, high temperature resistant concretes, concretes used in the construction of hazardous wastes storage containers, are reported by Davidovits [182].

Metakaolinite is the high quality mineral addition to cement or concrete because of the excellent pozzolanic properties. In reaction with calcium hydroxide C–S–H, C_4AH_{13} and gehlenite hydrate are produced [183]. These reactions are rapid and as soon as after 3 days these phases are detectable by XRD [184]. The gehlenite hydrate is unstable in the presence of calcium hydroxide, while C_3AH_6 is the stable phase, however, the rate of CH reaction with C_2ASH_8 is low and the non–equilibrium state is existing [185].

Metakaolinite reacting with calcium hydroxide in cement paste is strongly modifying the properties of mortars and concretes, primarily increasing the resistance to various aggressive media. The role of metakaolinite in the alkali–aggregate reaction and sulphate corrosion protection was discussed by Jones [180]. The addition of metakaolinite decreases the permeability of concrete, as well as the rate of chloride ions diffusion and reinforcement steel corrosion [186]. This is the consequence of advantageous change of pore structure, increasing volume of smaller pores, below 0.01 μm, and reduction of larger ones, above 0.1 μm [187, 188]. The significant calcium hydroxide content lowering is of importance too.

[6] The commonly used term „metakaolin" is not correct; this pozzolana should be determined as „burned kaolin". The term metakaolinite is brief and relates to the component controlling the pozzolanic properties of material.

The rheological properties of concrete are strongly modified by metakaolinite addition, because of its high specific surface area, usually between 10 and 25 m^2/kg. At 5 % of cement replacement the thixotropy of concrete becomes higher, however, without higher effect on the workability [180]. The bleeding is reduced and the surface of concrete becomes smoother. At higher metakaolinite dosage superplasticizer should be applied, however, the amount of admixture is lower than in the case of silica fume [180].

According to Hobbs [188] metakaolinite addition accelerates markedly the flexural strength development, during the first six hours from producing of concrete mixture. The early compressive strength of concrete at 10 % cement replacement is not influenced; however, after 28 days and after longer period, the compressive strength becomes higher [188]. Because the strength of cement paste with metakaolinite is not changed, Larbi and Bijen [186] conclude that the increase of concrete strength should be attributed to the modification of microstructure in the interfacial transition zone; the bonding force between cement matrix with metakaolinite and aggregate is significantly higher.

References

1. Smolczyk, H.G.: 7th ICCC Paris, vol. I, p. III–1/3, Paris (1980)
2. De Jong, Y.A.: Silicates Ind. **42**, 5 (1977)
3. Baron, J., Dourve, Ch.: World Cement. **18**, 100 (1987)
4. Kotlarczyk, J., Kawalec, B.: Zeszyty Naukowe AGH. **138**, 335 (in Polish) (1966)
5. Massazza, F.: Properties and applications of natural pozzolanas. In: Bensted, J., Barnes, P. (eds.) Structure and Performance of Cements, Chap. 13, p. 326, 2nd edn. Spon Press, London (2002)
6. Venuat, M., Papadakis, M.: Fabrication et utilisation des Liants hydrauliques. M. Venuat, Paris (1964)
7. Taylor, H.F.W.: Cement Chemistry. Academic Press, London (1990)
8. Sersale, R.: Occurances and uses of zeolites in Italy. In: Sand, L.B., Mumpon, F.A. (eds.) Natural Zeolites—Occurrence, Properties, Use, p. 537, Pergamon Press, Oxford (1978)
9. Barth–Wirsching, U., Höller, F.: Eur. J. Miner. **1**, 489 (1989)
10. LaRosa, J.L., Kwan, S., Grutzeck, M.W.: J. Am. Ceram Soc. **72**, 1574 (1992)
11. Grutzeck, M.W.: Zeolite–cement composites. In: Sarkar, L., Ghosh, S.N. (eds.) Progress in Cement and Concrete, vol. 4, p. 368. ABI Books, New Delhi (1993)
12. Voinovitch, I.A., Dron, R.: Bull. Liaison Lab. Ponts et Chauss. **83**, 55 (1976)
13. Oberholster, R.E., van Aardt, J.H.P., Brant, M.P.: In: Barnes, P. (eds.) Structure and Performance of Cements, p. 365. Appl. Sci. Publ., London (1983)
14. Marfil, S.A., Maiza, P.J.: Cem. Concr. Res. **23**, 1283 (1993)
15. Feng Naiqian: Properties of zeolitic mineral admixture concretes. In: Sarkar, L., Ghosh, S.N. (eds.) Progress in Cement and Concrete, vol. 4, p. 398. ABI Books, New Delhi (1993)
16. Regourd, M.: 8th ICCC Rio de Janeiro, vol. I, p. 199. Rio de Janeiro (1986)
17. Uchikawa, H.: 8th ICCC Rio de Janeiro, vol. I, p. 249. Rio de Janeiro (1986)
18. George, C.M., Sorrentino, F.P.: 7th ICCC Paris, vol. II, p. III–140. Paris (1980)
19. Stabrawa, S.: Cement–Wapno–Gips. **33**, 233 (1980) (in Polish)
20. Gustaw, K., Roszczynialski, W., Ptak, A.: Cement–Wapno–Gips. **33**, 274 (1978) (in Polish)
21. Wang, Yu–Ji., Xie, Gong–Xin.: 7th ICCC Paris, vol. II, p. III–19. Paris (1980)
22. Derdacka, A., Paluch, E., Gawlicki, M.: Cement–Wapno–Gips. **30**, 229 (1975) (in Polish)

23. Gourdin, P.: Ciment, Bétons, Plâtres, Chaux. **727**, 363 (1980)
24. Satarin, W.I.: 6th ICCC Moscow, vol. III, p. 45. Moscow (1974)
25. Sobczuk, R.: Cement–Wapno–Gips. **26**(2), 38 (1971) (in Polish)
26. Kämpfe, F.: Zement. **24**, 317 (1935)
27. Taneja, C.A.: 6th ICCC Moscow, vol. III, p. 60. Moscow (1974)
28. Bergt, K.: Proc. of the Seventh Conf. on the Silicate Industry, p. 661. Budapest (1965)
29. Cleret de Langavant, J.: Rev. Mat. Constr. **401**, 38 (1949); **411**, 425 (1949); **448**, 1 (1953); **453**, 175 (1953)
30. Rojak, S.M., Chkolnik, J.: 7th ICCC Paris, vol. II, p. III–74. Paris (1980)
31. Dowgopot, W.J., Rojak, S.M., Czebukow, M.F., Szkolnik, J.S.: Cemient. **7**, 11 (1971)
32. Rojak, S.M., Szkolnik, J.S., Orininski, N.W., Slejepcow, Ż.J., Adamakin, F.K., Fiebrowa, T.N.: Stroitielnyje Matieriały. **2**, 33 (1972)
33. Sopora, H.: Silikattechnik. **10**, 361 (1959)
34. Wyłkowa, J.S., Dogandzijewa, R.G.: 6th ICCC Moscow, vol. III, p. 69. Moscow (1974)
35. Johannson, S.E.: Silicates Ind. **43**, 139 (1978)
36. Lea, F.M.: The Chemistry of Cement and Concrete. Chemical Publ. Comp., New York (1971)
37. Kurdowski, W.: Poradnik Technologa Przemysłu Cementowego. Arkady, Warszawa (1981) (in Polish)
38. Rojak, S.M., Kryłow, W.F., Klementiewa, W.S.: Stroitielnyje Matieriały. **3**, 37 (1965)
39. Taneja, C.A., Theri, S.P., Singh M.: 7th ICCC Paris, vol. II, p. 111–48. Paris (1980)
40. Solacolu, S., Balta, P.: Rev. Mat. Const. Trav. Publ. **583**, 95 (1964)
41. Solacolu, S.: Zement–Kalk–Gips. **11**, 125 (1958)
42. Zarzycki, J.: Les Verres et l'Etat Vitreux. Masson, Paris (1982)
43. Locher, F.W.: 4th ICCC Washington, vol. I, p. 267. Washington (1960)
44. Tanaka, T.: Rock Prod. **59**, 106 (1956); **60**, 100 (1957); **60**, 107 (1957)
45. Görlich, E., w Dereń, J., Haber, J., Pampuch, R.: Chemia ciała stałego, p. 163. PWN, Warszawa (1975) (in Polish)
46. Demoulian, E., Gourdin, P., Hawthorn, F., Vernet, C.: 7th ICCC Paris, vol. II, p. 111–89. Paris (1980)
47. Frearson, J.P.H., Uren, J.M.: Proc. 2nd Int. Conf. on the Use of Fly Ash, Silica Fume, Slag and Natural Pozzolanas in Concrete, vol. 2, p. 1401. Madrid (1986)
48. Vernet, C., Demoulian, E., Gourdin, P., Hawthorn, F.: 7th ICCC Paris, vol. II, p. III–128. Paris (1980)
49. Fierens, P., Poswick, P.: *ibid*., vol. II, p. Ul–112
50. Schröder, F.: 5th ICCC Tokyo, vol. IV, p. 149. Tokyo (1968)
51. Demoulian, E., Vernet, C., Hawthorn, F., Gourdin, P.: 7th ICCC Paris, vol. II, p. III–151. Paris (1980)
52. Kondo, R., Oksawa, S.: 5th ICCC Tokyo, vol. IV, p. 255. Tokyo (1968)
53. Smolczyk, H.G.: Rev. de Métallurgie. 275 (May 1978)
54. Pokh, W.: Nauka. 354 (1971) (in Polish)
55. Toop, G.W., Samis, G.S.: Trans. Met. Soc. AITM. **106**, 147 (1983)
56. Masson, C.R.: J. Am. Ceram. Soc. **51**, 134 (1968)
57. Dron, R.: 8th ICCC Rio de Janeiro, vol. IV, p. 81. Rio de Janeiro (1986)
58. Dron, R., Brivot, F.: 7th ICCC Paris, vol. II, p. Ul–134. Paris (1980)
59. Goto, S., Yoshii, T., Daimon, M.: Cem. Concr. Res. **15**, 964 (1985)
60. Run–Zhang, Y., Shi–Xi, O., Qiong–Ying, G.: Silicates Ind. **48**(1), 3 (1983)
61. Run–Zhang, Y., Qiong–Ying, G.: Silicates Ind. **47** (12), 279 (1982)
62. MacDowell, J.F.: 8th ICCC Rio de Janeiro, vol. IV, p. 423. Rio de Janeiro (1986)
63. MacDowell, J.F., Sorrentino, F., Capelle, M.: Cem. Concr. Res. **32**, 208 (2002)
64. Kurdowski, W., Duszak, S., Sorrentino, F.: Corrosion of Gehlenite Hydrate in strong choride solution. In: Mangabhai, R.J., Glasser, F.P. (eds.) Calcium Aluminate Cements, p. 371. IOM Communications, London (2001)
65. Kurdowski, W.: Cement–Wapno–Beton. **70**, 131 (2003) (in Polish)
66. Smolczyk, H.G.: Zement–Kalk–Gips. **31**, 294 (1978)

67. Kubicki, R.: Cement–Wapno–Gips. **15**, 1 (1959) (in Polish)
68. Pankratow, W.L., Ignatowa, W.P., Cernes, R.L.: Naucznyje Soobszczenia NII Cemienta. **23**, 79 (1968)
69. Kryłow, W.F., Pankratow, W.L., Kołosowska, W.M.: Cemient. **30**(3), 15 (1965)
70. Hawthorn, F., Demoulian, E., Gourdin, P., Vernet, C.: 7th ICCC Paris, vol. II, p. III–145. Paris (1980)
71. Regourd, M.: *ibid*., vol. I, p. III–2/3
72. Regourd, M.: *ibid*., vol. I, p. III–2/9
73. Regourd, M., Hornain, H., Mortureux, B.: Silicates Ind. **42**, 19 (1977)
74. Nurse, R.W.: In: Taylor, H.F.W. (red.) The Chemistry of Cements, p. 37. Academic Press, London (1964)
75. Vanden Bosch, V.: Silicates Ind. **42**, 145 (1977)
76. Keil, F.: Zement Herstellung und Eigenschaften. Springer–Verlag, Berlin (1975)
77. ICCRC Committee: Matér. Constr. **9**, 187 (1976)
78. Mather, B.: J. Am. Ceram. Ind. **29**, 205 (1957)
79. VDZ–Komission: “Carbonatisierung”, “Carbonatisierung des Betones”. Beton. **22**, 296 (1972)
80. Litvan, G.G., Mayer, A.: Proc. 2nd Int. Conf. on Fly Ash, Silica Fume, Slag and Natural Pozzolanas in Concrete, vol. 2, p. 1445. Madrid (1986)
81. Smolczyk, H.G.: 6th ICCC Moscow, vol. III, p. 57. Moscow (1974)
82. Bozel, J., Siebel, E.: Beton. **27**, 153, 203, 237 (1977)
83. Zement Taschenbuch: Bauverlag, Berlin 1976/1977
84. http://www.uni–weimar.de/Bauing/fib/forschung/eng–fo_shz.thm
85. Kühl, H.: Zement Chemie. Verlag Technik, Berlin (1952)
86. Lou Zonghan: 7th ICCC Paris, vol. IV, p. 82. Paris (1980)
87. Taylor, H.F.W.: Ettringite – Friend or Foe. In: Materials Science and Concrete, Special volume: Calcium hydroxide in concrete. Skalny, J., Gebauer, J., Odler, J. (eds.), p. 215. Fig. 2A, Published by The American Ceramic Society, 735 Ceramic Place, Westerville, Ohio 43081, reproduced with the permission of The American Ceramic Society (2001)
88. Gebauer, J.: *ibid*., p. 1
89. Ponteville, M.: Silicates Ind. **42**, 193 (1977)
90. Ponteville, M.: Silicates Ind. **41**, 193 (1976)
91. Purdon, A.O.: J. Soc. Chem. Indus. **59**, 191 (1940)
92. Gluckovsky, V.D., Rostoyskaya, G.S., Rumyna, G.V.: 7th ICCC Paris, vol. III, p. V–164. Paris (1980)
93. Baran, T.: Wpływ szkła wodnego potasowego na proces hydratacji cementu portlandzkiego. Ph. D. Thesis, University of Science and Technology, Kraków (2003) (in Polish)
94. Głuchowski, W.D., Zajtsew, W., Pachomow, W.: Silicates Ind. **48**, 197 (1983)
95. Roy, D.M.: Cem. Concr. Res. **29**, 249 (1999)
96. Małolepszy, J.: 8th ICCC Rio de Janeiro, vol. IV, p. 104. Rio de Janeiro (1986)
97. Małolepszy, J.: 8 Int. Baustoff und Silikattagung, Weimar, vol. l, p. 158 (1982)
98. Deja, J.: Trwałość Zapraw i Betonów Żużlowo–alkalicznych, Ceramika, Nr 83. PAN, Kraków (2004) (in Polish)
99. Brylicki, W., Małolepszy, J., Stryczek, S., Gonet, A., Dziewański, J.: VII Konf. Techn. Kontrola Zapór, p. 41. Rytro (1996) (in Polish)
100. Dziewański, J., Olszamowski, Z.: Likwidacja filtracji wody przez masyw skalny prawego przyczółka zapory Wisła–Czarne, Studia, Rozprawy, Monografie, No. 41. Ed. Centrum Podst. Prob. Gosp. Sur. Mineral. i Energią. PAN, Kraków (1996) (in Polish)
101. Voinovitch, J., Raverdy, M., Dron, R.: 7th ICCC Paris, vol. II, p. III–122. Paris (1980)
102. Forss, B.: Int. Conf. on Slag and Blended Cements. Univ. of Alabama, Birmingham, 12–19 Febraury 1982 (after [16])
103. Moranville, M., Li, G.: The U–phase: Formulation and Stability. In: Marchand, J., Skalny, J. (eds.) Sulfate Attack Mechanisms, p. 175. The American Ceramic Society, Westerville (1999)

104. Li, G., Le Bescop, P., Moranville, M.: Cem. Concr. Res. **29**, 759 (1989)
105. Dosch, W., zur Strassen H.: Zement–Kalk–Gips. **9**, 392 (1967)
106. Giergiczny, Z.: Rola popiołów wapniowych i krzemionkowych w kształtowaniu właściwości współczesnych spoiw budowlanych i tworzyw cementowych. Pol. Krakowska, Kraków (2006) (in Polish)
107. Aïtcin, P.C., Antefage, F.: Carles–Gibergues A., Vaquier A.: Proc. 2nd Int. Conf. on Fly Ash, Silica Fume, Slag and Natural Pozzolanas in Concrete, vol. l, p. 91. Madrid 1986
108. Tenoutasse, N., Marion, A.M.: *ibid*., vol. 1, p. 51
109. Alsted Nielsen, H.C.: 7th ICCC Paris, vol. III, p. IV–72, Paris (1980)
110. Rajczyk, K.: Mikropopioły jako nowy aktywny dodatek mineralny", VI Międzyn. Konf. Naukowo–Techniczna "Popioły z energetyki". Licheń Stary k/Konina (1999) (in Polish)
111. Tkaczewska, E., Małolepszy, J.: Cement–Wapno–Beton. **75**, 148 (2009)
112. Gawlicki, M., Galos, K., Szluga, J., Gawlicki, M.: p. 139, 196. In: Ney, R. (red.) Mineralne surowce odpadowe. Inst GSMiE PAN, Kraków (2009) (in Polish)
113. Kobuku, M., Jamede, D.: 6th ICCC Moscow, vol. III, p. 83. Moscow (1974)
114. Courtault, B.: 7th ICCC Paris, vol. II, p. Ul–117. Paris (1980)
115. Wett, J.D., Thorne, D.J.: J. Appl. Chem. **15**, 585 (1965); **15**, 595 (1965); **16**, 33 (1966)
116. Sersale, R.: 7th ICCC Paris, vol. I, p. IV–1/3. Paris (1980)
117. Garbacik, A., Baran, T.: Conf. "Dni Betonu", Wisła 2008, p. 513. Wyd. Polski Cement, Kraków (2008) (in Polish)
118. Giergiczny, E., Giergiczny, Z.: Cement–Wapno–Beton. **77**, 157 (2010)
119. Kurdowski, W., Poleszak, M.: Tonin. Ztg. **102**, 696 (1978)
120. Uchikawa, H., Uchida, S., Hanekara, S.: 8th ICCC Rio de Janeiro, vol. IV, p. 245. Rio de Janeiro (1986)
121. Carles–Gibergues, A., Thenoz, B., Vaquier, A.: 7th ICCC Paris, vol. III, p. IV–36. Paris (1980)
122. Hubbard, F.H.: J. Mater. Sci. Letters. **3**, 938 (1984)
123. Saumann, Z.: llth Conf. on the Silicate Industry, p. 461. Budapest (1973)
124. Massazza, F., Pezzuoli, M.: 8th ICCC Rio de Janeiro, vol. II, p. 180. Rio de Janeiro (1986)
125. Liu, Haukun., Lu, Zhongya., Lin, Shengjie.: 7th ICCC Paris, vol. III, p. IV–53. Paris (1980)
126. Diamond, S.: Cem. Concr. Res. **13**, 452 (1983)
127. Reverdy, M., Brivot, F., Pailler, A.M., Dron, R.: 7th ICCC Paris, vol. III, p. IV–36. Paris (1980)
128. Raask, E.: *ibid*., vol. III, p. IV–1
129. Giergiczny, E., Rajczyk, K.: Cement–Wapno–Beton. **71**, 307 (2004) (in Polish)
130. Jarema–Suchorowska, S., Kurczak, B.: "Właściwości popiołów z kotłów fluidalnych pracujących w energetyce zawodowej", Mat. Conf. "Popioły z energetyki". Zakopane (2009) (in Polish)
131. Jarema–Suchorowska, S., Szczygielski, T.: "Perspektywy gospodarowania ubocznymi produktami spalania w świetle krajowego planu gospodarki odpadami", IX Międzyn. Konf. "Popioły z energetyki". Ustroń (2002) (in Polish)
132. Owens, P.W., Buttler, F.G.: 7th ICCC Paris, vol. III, p. IV–60. Paris (1980)
133. Guillaume, L.: Silicates Ind. **28**, 297 (1963)
134. Diamond, S.: 7th ICCC Paris, vol. III, p. IV–19. Paris (1980)
135. Vaquier, A., Carles–Gibergues, A.: Rev. Mat. Constr. Trav. Publ. **662**, 331 (1970)
136. Carles–Gibergues, A., Thenoz, B., Vaquier, A.: 7th ICCC Paris, vol. III, p. IV–53. Paris (1980)
137. Hales, Y., Jensen, H.V., Pratt, P.L.: 8th ICCC Rio de Janeiro, vol. IV, p. 176. Rio de Janeiro (1986)
138. Dalziel, J.A.: 7th ICCC Paris, vol. III, p. IV–93. Paris (1980)
139. Uchikawa, H., Uchida, S., Ogawa, K.: 8th ICCC Rio de Janeiro, vol. IV, p. 231. Rio de Janeiro (1986)
140. Kollek, J.J., Varma, S.P., Zaris, C.: *ibid*., vol. IV, p. 183
141. Braun, H., Gebauer, J.: Zement–Kalk–Gips. **36,**254 (1983)

142. Malhotra, V.M., Mehta, P.K.: High–Performance, High–Volume Fly Ash Concrete. Supplementary Cementing Materials for Sustainable Development Inc., Ottawa (2005)
143. Giaccio, G.M., Malhotra, V.M.: ASTM Journal of Cement, Concrete, and Aggregates. **10**, 88 (1988)
144. Glukhovski, V.D.: Soil Silicates. Kiev (1959)
145. LaRosa, J.L., Kwan, S., Grutzeck, M.W.: J. Am. Ceram. Soc. **75**, 1574 (1992)
146. Mondragon, F., Rincon, F., Sierra, L., Escobar, M., Ramirez, J., Fernandez, J.: Fuel. **69**, 263 (1990)
147. Berkgaut, V., Singer, A.: Appl. Clay Sci. **10**, 369 (1996)
148. Park, M., Choi, J.: Appl. Clay Sci. **9**, 219 (1995)
149. Derdacka, A., Małolepszy, J.: Cement–Wapno–Gips. **41**, 291 (1975) (in Polish)
150. Palomo, A., de la Furente, J.: Cem.Concr. Res. **33**, 281 (2003)
151. Duxson, P., Provis, J.–L., Luckey, G.C.: J. Coll. Surf. A: Physicochem. Eng. Aspects. 47 (2005)
152. Bakharev, T.: Cem. Concr. Res. **35**, 658 (2005)
153. Criado, M., Fernandez–Jimenez, A., de la Torre, A., Aranda, M., Palomo, A.: Cem. Concr. Res. **37**, 671 (2007)
154. Yang, K.H., Song, J.K., Ashour, A.F., Lee, E.T.: Constr. Build. Mater. **22**, 1981 (2009)
155. Kong, D.L., Sanjayan, J.G.: Cem. Concr. Comp. **30**, 986 (2008)
156. Palomo, A., Grutzeck, M.W., Blanco, M.T.: Cem. Concr. Res. **29**, 1323 (1999)
157. Alvarez–Ayuso, E., Querol, X., Plana, F., Alastuey, A., Moreno, N., Izquierdo, M.: J. Hazard Mater. **154**, 175 (2008)
158. Mozgawa, W., Deja, J.: J. Mol. Struct. **924–926**, 75 (2009)
159. Ravikumar, D., Peethamparan, S., Neithalath, N.: Cem. Concr. Comp. **32**, 399 (2010)
160. Querol, X., Umana, J.C., Plana, F., Alastuey, A., Lopez–Soler, A., Medinaceli, A., Valero, A., Domingo, M.J., Garcia–Rojo, E.: Fuel. **80**, 857 (2001)
161. Palomo, A., Glasser, F.P.: Brit. Ceram. Trans. J. **91**, 107 (1992)
162. Feldman, R.F.: Proc. 2nd Int. Conf. on Fly Ash, Silica Fume, Slag, Natural Pozzolanas in Concrete, vol. 2, p. 973. Madrid (1986)
163. Gantefell, O.: *ibid*., vol. 2, p. 991
164. Nagatali, S., Vjike, J.: *ibid*., vol. 2, p. 1049
165. Khayat, K.H., Aïtcin, P.C.: Chap. 6, Silica fume a unique supplementary cementiteous material. In: Sarkar, S.L., Ghosh, S.N. (ed.) Progress in Cement and Concrete, vol. 4, p. 226. ABI Books, New Delhi (1993)
166. Erhenfeld, W., Fiertak, M., Śliwiński, J.: Cement–Wapno–Beton. **70**, 251 (2003) (in Polish)
167. Charreton, Ch.: Int. Sem. "Some Aspects of Admixtures and Industrial By–Products on the Durability of Concrete", April 28–29, Chalmers University of Technology, Gothenburg (1986)
168. Conjeaud, M., Lelong, B., Cariou, B.: 7th ICCC Paris, vol. III, p. VII–6. Paris (1980)
169. Ramachandran, V.S., Zhang, Chu–Mei.: Durability Build. Mat. **4**, 45 (1986)
170. Jambor, J.: 7th ICCC Paris, vol. IV, p. 487. Paris (1980)
171. Menetrier, D., Sorrentino, F.: 8th ICCC Rio de Janeiro, vol. IV, p. 60. Rio de Janeiro (1986)
172. Kurdowski, W.: non published paper
173. Ranc, R., Cariou, B., after Buil, M., Ollivier, J.–P.: In: Baron, J., Ollivier, J.–P. (ed.) La Durabilité Des Bétons, Chap. 3, p. 57. Presses Ponts et Chaussées, Paris (1992)
174. Chłądzyński, Sł., Garbacik, A.: Cementy wieloskładnikowe w budownictwie. Polski Cement, Kraków (2008) (in Polish)
175. Bensted, J.: World Cement. **11**, 395 (1980); **14**, 383 (1983)
176. Cochet, G., Sorrentino, F.: Limestone filled cements: Properties and uses. In: Sarkar, S.L., Ghosh, S.N. (eds.) Progress in Cement and Concrete, vol. 4, p. 266. ABI Books, New Delhi (1993)
177. Dunham, A.C.: Proc. Yorkshire Geol. Soc. **49**, 95 (1992)
178. Stoch, L.: Minerały ilaste. Wyd. Geologiczne, Warszawa (1974) (in Polish)
179. Justnes, H., Meland, I., Björgum, J.O., Krane, J., Skjetne, T.: Adv. Cem. Res. **3**, 105 (1990)

180. Jones, T.R.: Metakaolin as a pozzolanic addition to concrete. In: Bensted, J., Barnes, P. (red.) Structure and Performance of Cements, p. 372, 2nd edn. Spon Press, London (2002)
181. Palomo, A., Blanco–Varela, M.T., Granozo, M.L., Puertas, F., Vazquez, T., Grutzeck, M.W.: Cem. Concr. Res. **29**, 997 (1999)
182. Davidovits, J.: Proc. Symp. "Concr. Tehnol. Past, Present, and Future." Mehta, P.K. (ed.), vol. V, p. 383. ACI (1994)
183. Malquori, G.: 4th ICCC Washington. Ntl. Bur. Std. Monograph. 43 (2), 983. Washington (1962)
184. Kurdowski, W., Pomadowski, H.: Silicates Ind. **66**, 85 (2001)
185. de Silva, P.S., Glasser, F.P.: Cem. Concr. Res. **23**, 627 (1993)
186. Larbi, J.A., Bijen, J.M.: Proc. 4th Conf. On Fly Ash, Silica Fume, Slag and Natural Pozzolanas in Concrete, p. 655. Istanbul (1992)
187. Chadbourn, G.A.: Chloride resistance and durability of cement paste and concrete containing metakaolin. Ph. D. Thesis, University of Aston (1997)
188. Hobbs, M.: after [179]

Chapter 8
Hydration of Cements with Mineral Additions

8.1 Hydration of Slag

Dissolution is an important process of slag hydration, particularly at early age. The sodium, potassium and aluminum ions, as well as the other basic elements of glass silicate network are released first to the solution [1, 2]. The concentration of calcium ions, silica and alumina in the liquid phase is low (Fig. 8.1) [2].

However, Kondo [3] is of the opinion that the hydrolysis of the glass in water occurs and the calcium ions are released initially to the liquid phase. Simultaneously on the surface of slag grains an acid, colloidal shell of silica–alumina gel is formed. This shell has low permeability and hence the further slag reaction with water is hindered. In the presence of $Ca(OH)_2$, added as alkaline activator, the silicon and aluminum from the shell are released to the solution (Fig. 8.2). The solubility of aluminum compounds becomes considerably increased in the solution of pH higher than 12.5 because in this condition the $Al(OH)_4^-$ ions are formed [4]. The concentration of aluminum in the liquid phase is increasing because the calcium aluminates crystallize a little later, primarily the C–S–H (I) is formed. Simultaneously the solubility of hydrates formed in this condition is reduced.

According to De Jong [5] the transition of primary hydrate to the liquid phase is also promoted by the SO_4^{2-} ions. Therefore the notice is taken that gypsum is a strong slag hydration activator. The mixture of $Ca(OH)_2$ and gypsum is a good activator too [2]. In the lack of gypsum the hydration is badly affected by the increased solubility of alumina.

The examination of chemical composition of slag glass surface at the early age of hydration has shown that it is modified immediately after the contact with the liquid phase [6]. As the result of incongruent dissolution of slag grains on their surface the layer of C–S–H is formed, with, however, lower C/S ratio than in the Portland cement paste. When the hydration of slag is activated by alkalis, this phase contains the Na^+ or K^+ ions.

The "through–solution" mechanism of C–S–H formation, it means with previous releasing of ions to the liquid phase as an effect of slag dissolution, is proved additionally by the precipitation of this phase not only on the surface of slag grains but also on the glass stand [powder specimen], under the light microscope [7]. The

W. Kurdowski, *Cement and Concrete Chemistry*,
DOI 10.1007/978-94-007-7945-7_8, © Springer Science+Business Media B.V. 2014

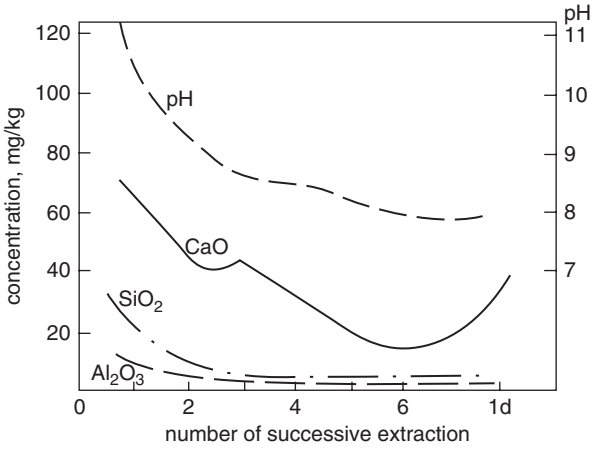


Fig. 8.1 The multiple extraction of C_2AS glass (5 g glass in 100 ml of water) (according to [2]) (the last point on the *y* axis means the extraction after 1 day)

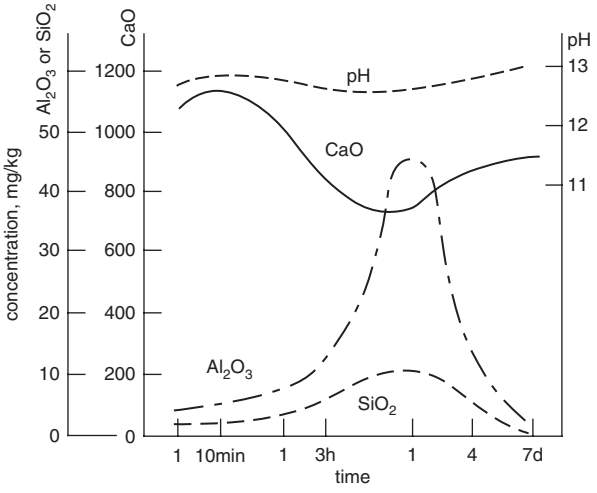


Fig. 8.2 Solubility of C_2AS glass with 2 moles $Ca(OH)_2$ addition (1 g of solid in 100 ml of water) (according to [3])

gehlenite hydrate C_2ASH_8, formed in the case of sodium activation, is crystallizing also far from the slag glass surface, in the space occupied by liquid phase [7].

According to Dron [8], the hydration of vitreous slag consists in its dissolution and crystallization of hydrates from the liquid phase. The dissolution occurs in the alkaline environment and the OH^- ions play a decisive role. The change of free enthalpy of this system is depending on the solubilities of the anhydrous phase and of the hydrates–reaction products.

It can be presented by the formula:

$$\Delta G^o = RT \log \frac{P_2}{P_1} \tag{8.1}$$

where: P_1 and P_2 are the solubility products of substrates and products of the reaction.

Because the solubility products of activators [$Ca(OH)_2$, $CaSO_4 \cdot 2H_2O$] and hydrates (C–S–H, ettringite, C_4AH_x) are constant at given temperature, the change of

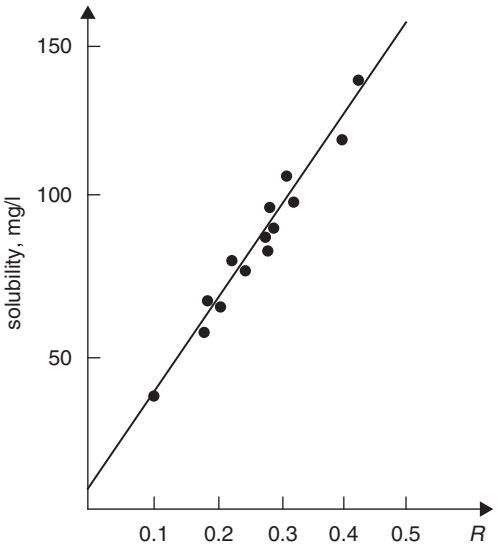


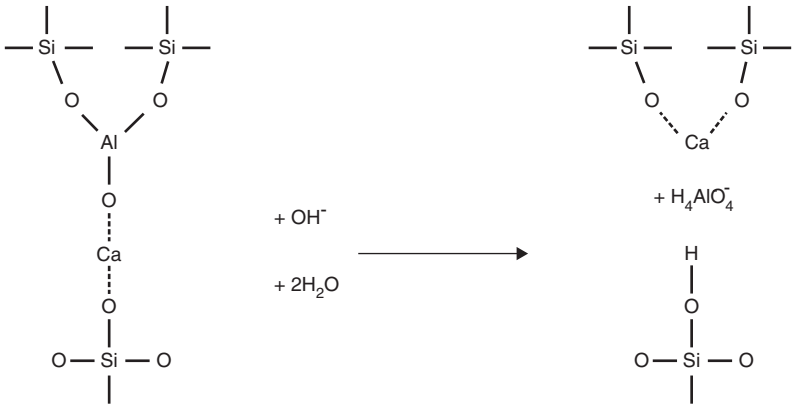
Fig. 8.3 Solubility of slag as a function of *R* (according to [8])

free enthalpy is depending only on slag solubility. Therefore the hydraulic activity of slag can be determined from the measurements of its solubility in the liquid phase, of constant pH. The classification of slags proposed by Dron [8] is based on the solubility of slag in the NaOH water solution of concentration 0.04 mol/l. This solubility is changing proportionally to the following relation:

$$R = \frac{[Al][Ca]}{([Al]+[Si])^2} \tag{8.2}$$

where: [Al], [Ca], [Si] are the concentrations of particular atoms in % by mole (Fig. 8.3).

Based on these experiments Dron [8] concludes that the reactivity of slag is the function of AlO^+ cations content, which have significant chemical affinity to the OH^- ions. The hydrolysis, causing the formation of $H_4AlO_4^-$ ions occurs on the surface of slag:



(8.3)

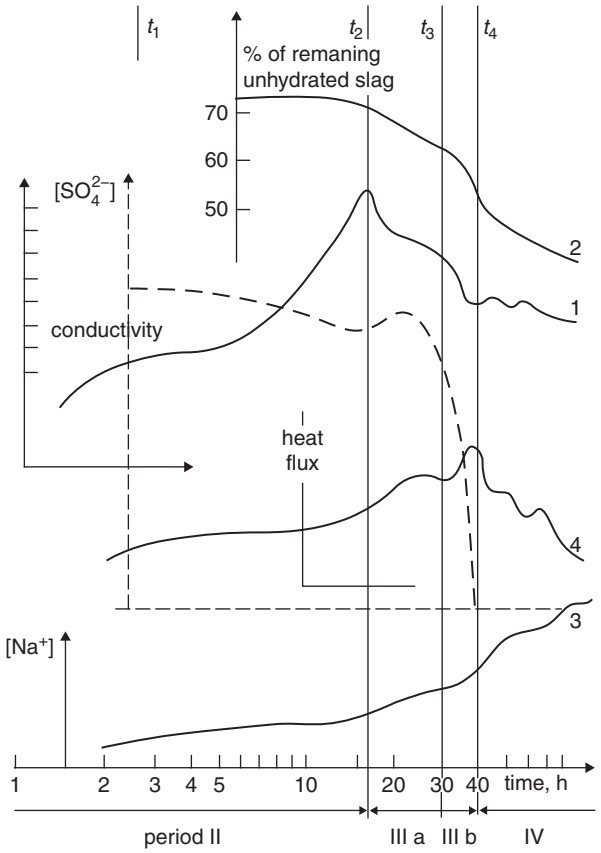


Fig. 8.4 Hydration process of slag cement (w/c = 0.4) (according to [10]), pre–induction period is omitted

The silicon ion on the end–position of the chain, forming the silanol group SiOH, tends to pass to the solution with the ion $H_2SiO_4^{2-}$ formation, which is disturbing the equilibrium in solution, causing the releasing of Ca^{2+} ions to the liquid phase. The process is interrupted on the structural element Y (see Fig. 7.7).

The hydration is accelerated when there are structural defects on the surface of vitreous slag grains, which act as active sites on which the C–S–H nuclei are formed [9].

However, Fierens [9] has shown, that the hydroxylation of the slag glass surface layer, as a result of water molecules chemisorption, which is enhanced by the surface electron defects (trapped electrons), can be considered as a topochemical process. The topochemical processes became important also at later hydration stage, when the pozzolanic reaction of slag glass network, impoverishes of the majority of alkaline elements, with calcium ions is occurring, and calcium ions are chemisorbed on the active sites of solid phase.

Vernet [10] has shown that there is a good correlation of the heat flux, linked with the exothermic hydration processes and the SO_4^{2-} ions concentration lowering, caused by ettringite formation, and the increasing hydration degree of slag. At the same period the maximum rate of C–S–H formation is occurring too (t_3) (Fig. 8.4).

The maximum rate of slag reaction with water is found in the t_4 period, in which the transition of ettringite into monosulphoaluminate occurs simultaneously, as a result of gypsum consumption.

The highest amount of C–S–H will be formed in the vicinity of slag grains, where the concentration of silica in the liquid phase is the highest. C–S–H will be also formed in the pores in the paste. In the later it will have better developed morphology, and will reduce the porosity of the paste, particularly in the range of larger pores, from 30 to 100 nm. The microstructure of slag cement paste confirms the formation of C–S–H phase of different morphology. This phase is generally worse crystallized than in the Portland cement paste, generally more compact [11], and richer in MgO and Al_2O_3. The ettringite crystals occur in the form of thin needles [11].

On the basis of thermodynamical considerations Voinovitch and Dron [12] have concluded that the activation with NaOH results in the formation of the following slag hydration products: C–S–H, C_4AH_{13} and C_2ASH_8. The $Ca(OH)_2$ addition gives the following products: C–S–H and C_4AH_{13}. The activation with gypsum gives C–S–H, ettringite and $Al(OH)_3$.

Locher [13] found that the gehlenite hydrate is not stable in the calcium hydroxide containing mixture and is transformed into hydrogarnet C_3ASH_4. C_2ASH_8 is not the stable phase in the gypsum and calcium hydroxide solutions and in this condition is transformed into ettringite. However, the gehlenite hydrate is stable in the presence of gypsum and Na_2SO_4 [13].

Mascolo [14] found that in the hydration products of slag glass rich in magnesium this ion is substituting for calcium in C_4AH_{13}. The (C, M)AH_{13} phase shows the continuous shifting of the XRD peak, with increasing Mg ions content [15]. At high MgO content in slag the $Mg_6Al_2CO_3(OH)_{18}\cdot 4H_2O$ can also be formed [16].

In the slag cement paste the hydration is initiated by reaction of the ground clinker phases with water. The slag grains became covered with C–S–H, however, the adhesion of this phase to the glass surface is weak [17]. The slag grains are surrounded by the compact, poorly crystallized shell of hydrates. C–S–H reveals lower C/S ratio and higher Mg and Al content than in Portland cement paste.

In cements with high slag content, about 80 %, the ettringite plays an important role as the concrete early strength controlling phase. With time, also in this cement paste this phase transforms into monosulphoaluminate and its solid solution with C_4AH_{13}. However, in contradistinction to the Portland cement paste, the ettringite content after 7 days of hardening is rather high [17]. The final ettringite content depends on the Al_2O_3 percentage in slag, as well as gypsum addition. It has been found that the high amount of fibrous ettringite has a positive impact on the flexural strength [17].

The C_4AH_x transforms into hydrogarnet with time and the sodium and potassium ions promote this transition [17].

The C_3S hydration degree increases with slag addition after 1 and 3 days, however, after longer period, is the same as without slag [18]. It is assumed that it can be the consequence of the C–S–H crystallization on the slag grains. The lowering of calcium ions concentration in the liquid phase is of importance too. This effect is visible particularly in the case of very high fineness of slag. [18].

The effect of slag on C_3A and C_4AF hydration is negligible, because the concentrations of Ca^{2+}, Al^{3+} and SO_4^{2-} ions in the liquid phase are not changed significantly by the presence of slag. However, because the calcium aluminate hydrates and ettringite are well crystallized and, moreover, they form rather the porous than the compact microstructure, it can be concluded that the hydration rate will be somewhat reduced [18]. On the other hand, some amount of calcium hydroxide and SO_4^{2-} ions is adsorbed on the slag glass surface and bounded in the pozzolanic reaction; in such a way the reaction of aluminates should be accelerated. There is a good correlation between the degree of slag hydration and the strength of cement [11]. However, as it has been pointed out by Fierens [19], sometimes at the same hydration degree of different slag, various strength can be obtained. This is the proof that there are the other factors influencing the strength development, for example the microstructure of hydrates, related to the conditions of their crystallization.

Autoclaving of slag cement pastes with high slag content (about 75 %) at temperature of 180 °C gives the product of untypical phase composition [20]: hydrogarnets $C_3(A, F)SH_4$, hydroksyellastadite $Ca_{10}(SiO_4)_3(SO_4)_3(OH)_2$, γ–$C_2SH$ are formed. At higher temperature the amount of dicalcium silicate hydrate is increasing. The heat treatment is improving also the pore structure, by decreasing the ratio of capillary pores, which is not observed in the case of Portland cements [21].

8.2 Fly Ash Hydration

There is a common opinion that the hydration of fly ash and natural pozzolanas is initiated by dissolution of these material, releasing initially of sodium and potassium ions, and then the aluminum and silica, to the liquid phase. Two hypotheses are proposed explaining the mechanism of this process. According to the first one, the reaction begins by the protonation of glass surface in alkaline solution, due to which the Si–OH groups are formed, as a result of one surface oxygen valence bonding of the glass network. Further protonation leads to the oxygen bridges breaking and the H_3SiO_4 ions are continuously released to the solution [18, 22].

In the second hypothesis is assumed that the glass surface has a negative charge, due to the presence on this surface of oxygen atoms with non–equilibrated charge: $–Si–O^-$ therefore the adsorption of Ca^{2+} ions from the liquid phase is promoted. The chemisorption of calcium ions provide for the sodium and potassium ions release from glass to the liquid phase [23]. Gradually, the surface layer of glass becomes richer in silicon and aluminum which form the amorphous shell around the pozzolana grains [23, 24]. The release of aluminum and silicon ions from the this shell to the liquid phase is significantly facilitated. They react with calcium ions in the solution with C–S–H phase formation, which both in the pores and on the surface of pozzolana particles is precipitating [23, 24].

This hypothesis is based upon the studies of Greenberg [25, 26], which has shown in his works that the silanol groups are the active sites on the surface of silica on which the calcium ions from the liquid phase are chemisorbed. Only the second elementary event is the release of silicon ions to the liquid phase and

their reaction with calcium ions with the formation of the nuclei of C–S–H phase $H_4SiO_4aq + Ca^{2+}aq + 2OH^-aq = n_1CaO{\cdot}SiO_2 \cdot n_2H_2O_{(s)}$. The growth of these nuclei leads to the crystallization of C–S–H. The factor determining the rate of the whole process is the release of silica to the solution [26]. The product of silica reaction with water is the monosilicic acid H_4SiO_4 [26]. The solubility of silica is increasing with pH because of the $H_3SiO_4^-$ and $H_2SO_4^{2-}$ ions formation.

In the NaOH solution the solubility of silica is the function of its specific surface area *S*:

$$dc / dt = k_1 S \tag{8.4}$$

where *c* is the monosilicic acid concentration (mole/l), $k_{1\_}$ rate constant.

Finally, the mechanism of the process can be reduced to the dissolution of fly ash glass or crystalline zeolite, in the case of natural pozzolana. There is an opinion that the pozzolanas composed of zeolites are more reactive than the vitreous ones [27]. This can be related to the high porosity of zeolites and their ion exchange ability [41]. Therefore the bonding of calcium ions occurs very quickly and pozzolana is transformed into the alumina–silica gel.

The hypotheses relating to the mechanism of pozzolana reaction with calcium hydroxide water solution, are similar to the slag glass reaction with the liquid phase. The components of pozzolana in highly alkaline environment undergo the hydrolysis, with release of silicon and aluminum ions to the liquid phase. In the solution they react with calcium ions, and C–S–H as well as calcium aluminate hydrates, and in the case of gypsum ettringite are formed [27]. Low solubility of these phases results in the rapid decrease of silicon and aluminum ions concentration in solution which increase the rate of these ions release to the liquid phase. In relation to the significant amount of aluminium in fly ashes the addition of gypsum provide for the acceleration of their hydration analogously as in the case of slags, because the formation of ettringite causes the decrease of alumina ions concentration.

The C–S–H formed has lower C/S ratio than in the Portland cement paste. Takemoto and Uchikawa [23] studied the chemical composition of C–S–H phase binding C_3S crystals with fly ash particles. They found a significant decrease of C/S ratio from approximately 2 in the vicinity of C_3S to the very low value near the fly ash grain surface (Fig. 8.5).

Uchikawa [18] determined the composition of C–S–H phase in the Portland cement paste and in the pastes with 40% fly ash and slag addition after 4 years of hydration. The results are given in Table 8.1.

Ettringite, similarly as in Portland cement pastes, is gradually transformed into the solid solution: $C_3A{\cdot}Ca[SO_4,(OH)_2]{\cdot}12H_2O$. In the fly ash rich in Al_2O_3 ettringite can be detected even during a year [23]. The carboaluminates: $C_3A{\cdot}CaCO_3{\cdot}11H_2O$ are always appearing too.

In the mixtures of lime and natural pozzolana Sersale [27] found the hydrogehlenite C_2ASH_8. It was formed, apart from hydrogarnet at later age, from 70 to 150 days, when the amount of combined calcium hydroxide changed from 46 to 60% [28]. The formation of hydrogarnets was found also by Takemoto and Uchikawa [23].

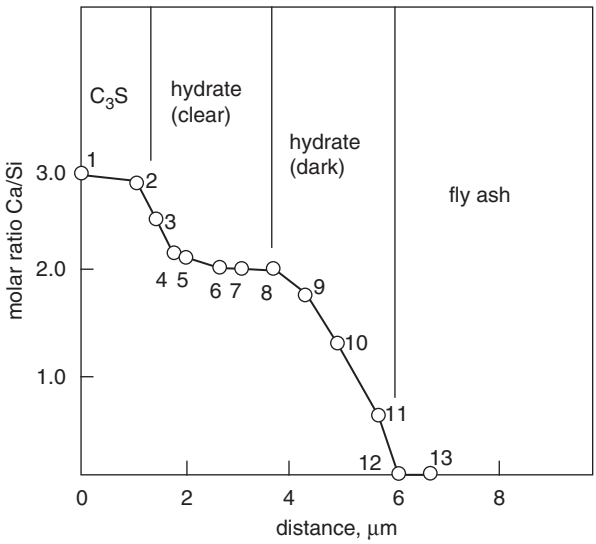


Fig. 8.5 Chemical composition change of hydrates layer from the C_3S crystal to the fly ash particle (according to [23]) (1–13 points of analyses)

Table 8.1 Chemical composition of C–S–H phase in the paste with and without 40 % of additives (w/c = 0.40, 20 °C, 4 years of maturing) [18]

Cement	Molar ratio			Content, %	
	C/S	A/C	C/(S+A)	Na_2O	K_2O
Portland	2.03	0.06	1.81	0.03	0.11
With fly ash	1.01	0.21	0.84	0.24	0.33
With slag	1.62	0.44	0.96	0.23	0.30

It can be concluded, that the phase composition of pastes from cements with fly ash is very similar to that of Portland cements, which is linked with significant similarity of chemical composition of both cements.

Uchikawa [18] has shown that the reaction of fly ash glass with calcium ions commences just after 1 day or at latest after 3 days, at room temperature. The hydration of fly ash is slow; the reacted depth of the large fly ash grains after 10 years is about 2 μm [29]. However, the small grains are consumed completely and the layers of reaction products shift to the centers of grains. This can be explained by the higher active glass content in small grains. A very low thickness of the outer shell in the fly ash bubbles, from 30 nm to 1/4*d* (*d*—diameter of bubble) is of importance too [29]. The small spheres inside the larger grain are hydrated and the large grain is filled with hydration products; the outer shell is reacted too.

The observations under the scanning electron microscope revealed the occurrence of water film, 0.5 to 1 μm thick and free of hydrates, between the surface of fly ash grain and the layer of hydrates. This water film is filled up gradually with the hydration products; however, this process is slow and not completed even after two years [29].

In Fig. 8.6 the hydration process of fly ash grain in the mixture with C_3S is shown schematically, according to Takemoto and Uchikawa [23]. The calcium hydroxide from the liquid phase is adsorbed on the surface of fly ash grain negatively charged.

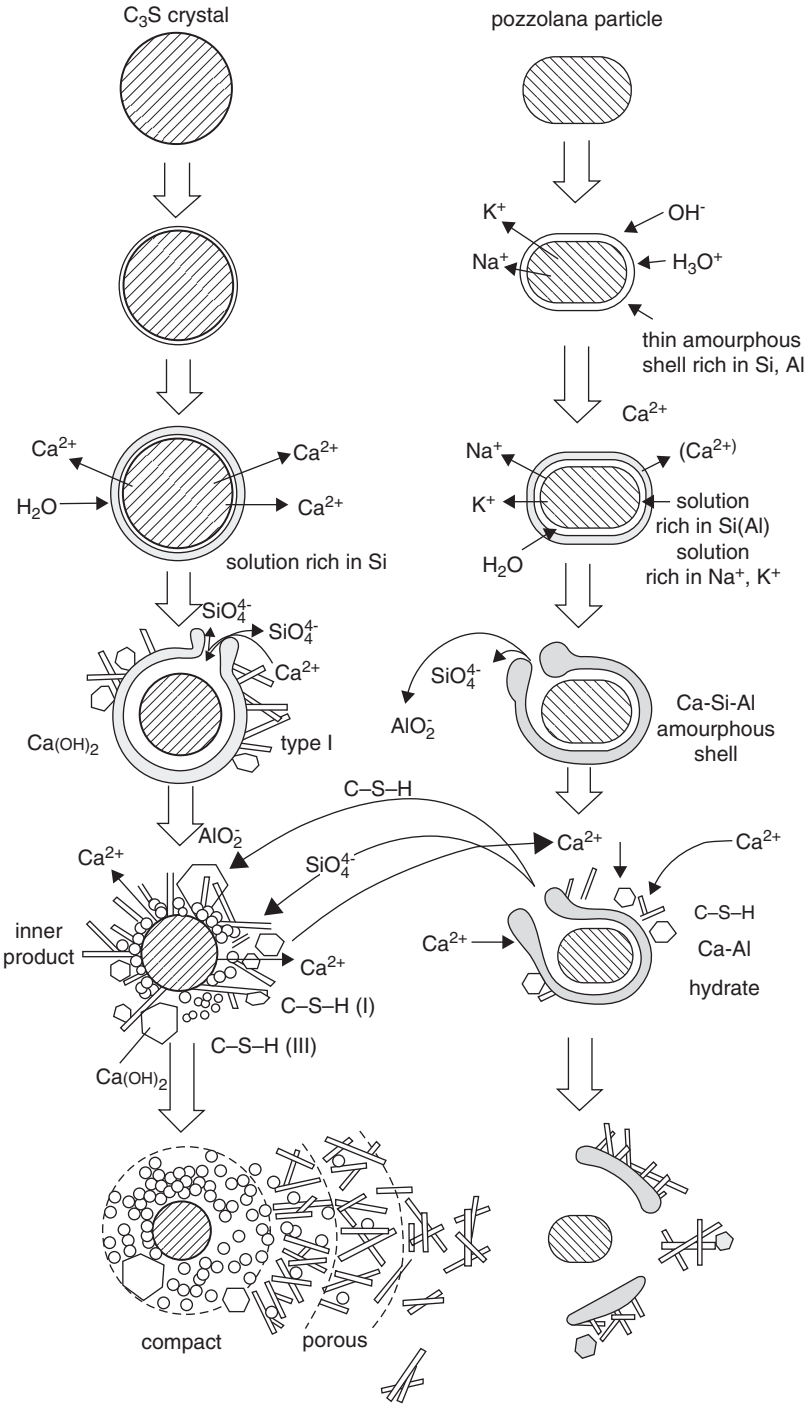


Fig. 8.6 Scheme of hydration mechanism in the C_3S–pozzolana mixture (according to [23])

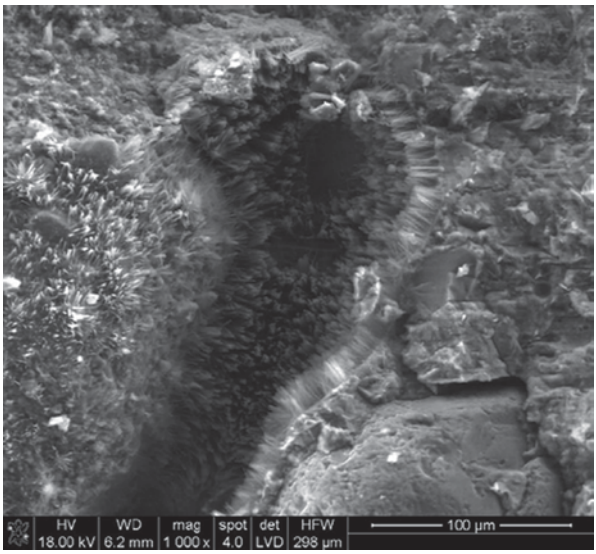


Fig. 8.7 Shell of fibrous C–S–H crystals formed on the fly ash grain, decorticated during specimen preparation (photo B. Trybalska)

C–S–H phase produced as a result of hydration on the C_3S surface has higher C/S ratio and lower on the surface of fly ash, where it is more porous (Fig. 8.5). The fly ash grains interact with the H_3O^+ ions and release gradually the Na^+ and K^+ ions to the solution, and simultaneously on their surface the amorphous shell rich in silica and alumina is formed. The Na^+ and K^+ ions augment the alkalinity of liquid phase which is increasing the content of silica $H_3SiO_4^-$ and alumina $H_4AlO_4^-$ ions. These ions react with Ca^{2+} with the hydrates formation which are increasing the thickness of the products shell. As a result of differences between the concentrations of basic ions, as well as SO_4^{2-} and AlO_2^-, in the shell and in solution, the osmotic pressure is generated. Therefore the swelling of the shell occurs and a free space between the adsorbed shell and the grain of pozzolana appears. This space is filled gradually with the silicate, aluminate, sodium and potassium ions. When the critical value of pressure is attained the shell became disrupted and the diffusion of silicate and aluminate ions to the solution is possible. It causes the further grows of outer C–S–H on the C_3S grains and the calcium aluminates formation. The concentration of potassium and sodium ions in solution surrounding the fly ash grains beside the destroyed shell is decreasing, and further C–S–H as well as calcium aluminates formation became possible. However, the amount of these products is negligible as compared to that on the C_3S grains. Therefore the free space around the fly ash grains is remaining, in regions of high sodium and potassium concentration, in which the crystallization of hydrates is hindered. As the processes leading to the destruction of shells surrounding the grains of pozzolana are repeated, and the reduction of sodium and potassium ions concentrations, the free spaces around the fly ash grains are filling successively with the hydrates. In Fig. 8.7 the shell of fibrous C–S–H crystals formed on the fly ash grain are shown; this grain was decorticated during specimen preparation.

The strength of concrete is increasing as the shells are moderately filled with the hydration products. However, throughout the period as they will be not filled,

it means till the strong bonds between the bulk paste and fly ash grains will be not formed, the pozzolanic reaction contributes relatively slightly to the concrete strength development.

Some authors are of the opinion that the pozzolanic reaction consists in the binding of calcium ions with the amorphous silicate–aluminate gel and thus it is a topochemical process [30]. As a result, a C–S–H shell, poorly permeable for ions, is formed on the surface of pozzolana. It is referred to the former hypothesis of the mechanism of C_3S reaction with water. C_3S undergoes the hydrolysis with the release of calcium ions, which are diffusing to the liquid phase. These ions are adsorbed on the formed acidic layer, enriched in silica, and react "*in situ*" with the formation of C–S–H, as a result of topochemical process [31].

The fly ash or natural pozzolana addition is influencing simultaneously on the clinker phases hydration. Quite similarly as slag also fly ash addition is increasing the alite hydration rate, particularly in the post–induction period [18]. Presumably it is linked with the chemisorption of Ca^{2+} ions on the fly ash grain and subsequent crystallization of C–S–H on these grains. For example if in comparable condition the C_3S hydration degree after 1 day is 35 %, then in the mixture with 30 % fly ash, of specific surface 370 m^2/kg, is increased to 45 %.

On the other hand, the problem of fly ash effect on the early rate of clinker phases reaction with water has not been elucidated as yet. Because of the set retardation of cements with fly ash, there is an opinion that the chemisorption of Ca^{2+} ions on the fly ash grains surface mentioned above, is causing retardation of nucleation and crystallization of portlandite [32]. The retardation of alite reaction with water can be also caused by uncombusted porous coal particles in fly ash. [33]. The hydration of C_3A is also slowed down by fly ash which is attributed to the formation of C_4AH_x hydrates layer on the surface of this phase and its stabilization by the sulphate ions [34]. The delayed reaction of tricalcium aluminate with water is caused by the sodium and potassium sulphates occurring as precipitates on the fly ash grains [33]. This distribution of these compounds is known in the case of Portland cement clinker and is linked with their crystallization from the gaseous phase. Finally, there is general opinion that the significant effect on these phenomena have the phase composition of cement and in the case of cement with high C_3A content the hydration of this phase is accelerated, while the alite hydrolysis is retarded [33].

The fly ash with low SO_3 and alkali content and high calcium ion adsorption ability is promoting the hydration of C_3A and accelerate the transition of ettringite into the monosulphoaluminate. On the other hand, fly ash, as well as natural pozzolana, rich in sodium and potassium sulphates lowers the rate of C_3A hydration [18]. It is assumed that SO_3 from fly ash hinders C_3A hydration more intensively than gypsum, which is linked with other components of fly ash released to the solution at the same time. In this condition also the transformation of ettringite into the monosulphoaluminate is delayed [18].

As it can be concluded from aforementioned considerations, the quality of fly ash is determined by the alkali and sulphate content. These components have a great impact on the C_3A and C_3S hydration and consequently on setting and other properties of cement paste.

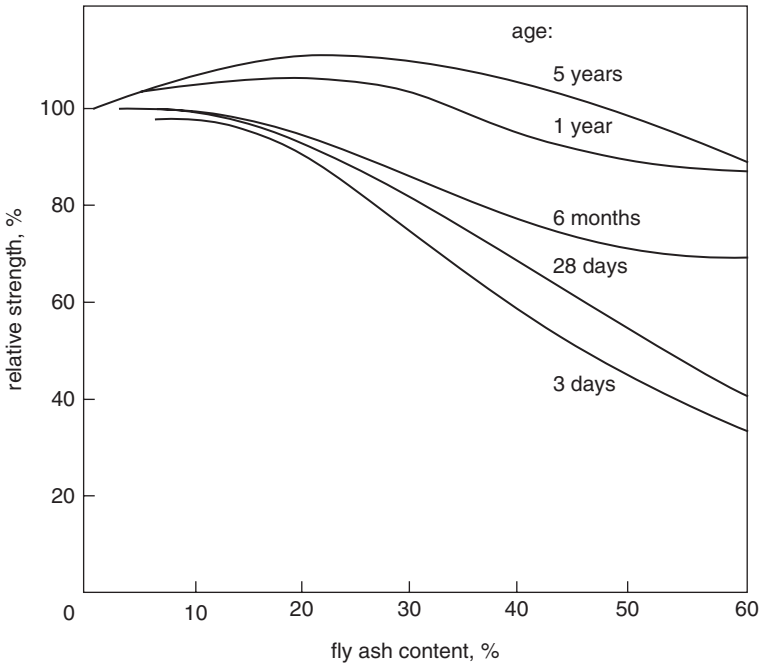


Fig. 8.8 Strength of concrete as a function of cement replacement by fly ash, % by mass (according to [36])

During the International Congress on Cement Chemistry in Rio de Janeiro Regourd [35] proposed the classification of fly ash on the basis of these two components content. It is as follows:

- three categories on the basis of sodium and potassium sulphate content: 0.5 %, 0.5–1.5 %, > 1.5 %,
- three classes basing on the total sulphate content: 0.1 %, 1–3 %, > 3 %,
- three groups on the basis of carbon content: 0–3 %, 3–6 %, > 6 %,
- three groups basing on the CaO content: 0–5 %, 5–15 %, > 15
- Moreover, Regourd [35] proposed to take into account the content of empty grains (cenospheres); which gives the additional three groups: 0–5 %, 5–10 %, > 10 %.

The fly ash Portland cement reveals the lower compressive strength after 2 and 7 days, while the strength development after longer period of hardening, over 90 days, is better. The concrete, in which some part of cement is replaced by siliceous fly ash, shows similar strength development; the data reported by Odler [36] should be recognized as representative (Fig. 8.8). These results show the usefulness to keep cement replacement by fly ash on the level of 30 % by mass.

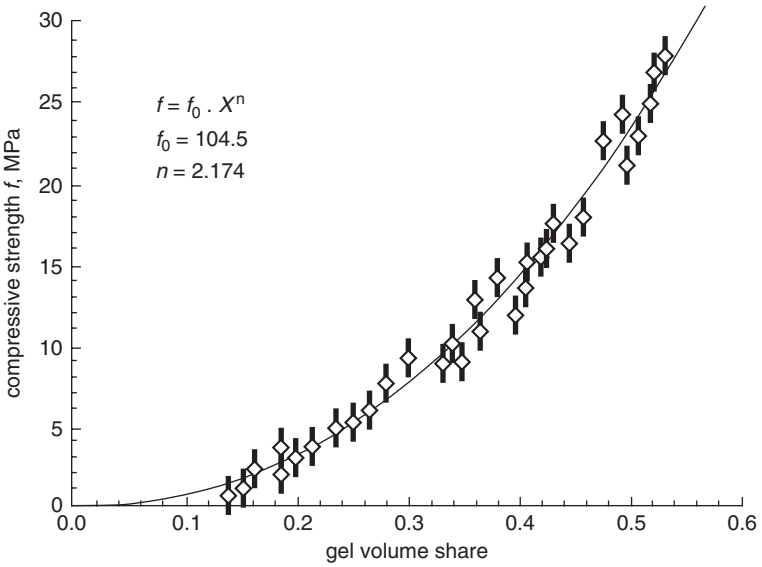


Fig. 8.9 Strength development of the mortar as a function of increasing C–S–H gel content in the paste (according to [37])

The very convincing results, dealing with the effect of fly ash and even generally of pozzolanas on the strength of mortars due to the pozzolanic reaction, were reported by Mehta [37]. They are shown in Figs 8.9 and 8.10. In Fig. 8.9 the effect of the C–S–H gel increasing content in the paste on the strength of mortar is presented; these data can be related to the Powers formula (5.25). On the Fig. 8.10 the strength development of concrete is plotted as a function of the pozzolanic reaction progress, which is equivalent to the increase of C–S–H gel content. It results from the curves on this figure that the most advantageous percentage of cement replacement by fly ash is on the level of 30–35 % by mass.

The siliceous fly ash is also used in the production of cellular concrete, according to the original Polish technology "Unipol" [38, 39]. The mixture of Portland cement and lime is used as binder[1], sand and fly ash as an aggregate. There are two methods of the raw mixture production: sand is ground separately with water to obtain the slurry, or the binder is ground with sand to produce a dry mixture. The binder content is about 20 % by mass of sand. The third important component is aluminum powder, applied as porosity generating agent. In the alkaline environment composed of cement, lime and water aluminium reacts with calcium hydroxide and the gaseous hydrogen is formed:

$$2\mathrm{Al} + 3\mathrm{Ca}\left(\mathrm{OH}\right)_2 + 6\mathrm{H_2O} \rightarrow 3\mathrm{CaO} \cdot \mathrm{Al_2O_3} \cdot 6\mathrm{H_2O} + 3\mathrm{H_2} \uparrow \qquad (8.5)$$

[1] In the so–called PGS technology the binder is composed of lime and fly ash mixture.

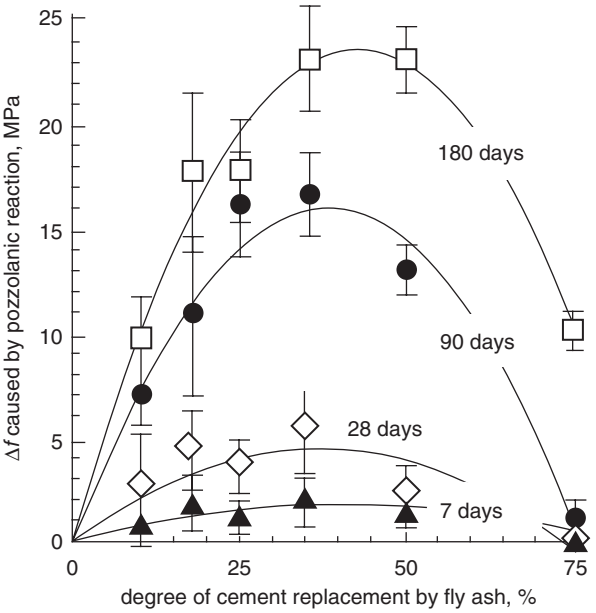


Fig. 8.10 Strength of mortar with various fly ash content as a function of time (according to [37])

The two alternative variants can be used in "Unipol" technology. In the first one cement is co–ground with lime and sand addition in dry condition (the approximate composition: sand—38 %, lime—35 %, cement—27 %) to the specific surface from 400 to 600 m^2/kg. In second variant the sand with 2 % of lime (to prevent the sedimentation) is ground with water to produce a slurry; the specific surface area of the mixture is from 170 to 220 m^2/kg. The fly ash can be used instead of sand, without grinding. The suspension of aluminum powder in water is prepared with surfactant addition to assure homogeneity. These three components are subsequently fed to the mixer: first the sand slurry, then the binder in amount of 260 kg/m^3 of concrete and finally the aluminum powder suspension, each time with 2–3 min mixing. The green cake thus produced is cast in the moulds and conditioned in the chambers for 1.5–2.5 h, at temperature 50 °C, for hardening and simultaneously expansion occurs. The hardened mass is demoulded and cut into blocks. Then the elements are placed in the autoclaves for the final hardening, in the saturated water vapour under the pressure of 1.1–1.3 MPa (at temperature about 180–200 °C) [39]. The low pressure curing in autoclave for 20 min before final heat treatment has a beneficial effect on autoclaving process [40]. After autoclaving the elements are cooled during 1–2 h and stored. The maturing of ready concrete elements during about 7 days is recommended [40]. The main properties of autoclaved cellular concrete are: a very low thermal conductivity coefficient $K \approx 0.4$ W/(m^2K) and low bulk density in the range 400–900 kg/m^3. There are the varieties with density 300 kg/m^3 and K about 0.3 [40]. The production of concrete with lower bulk density requires higher aluminum powder addition. The compositions of mixtures are given in the monographic books of Paprocki [38] and Jatymowicz et al. [39].

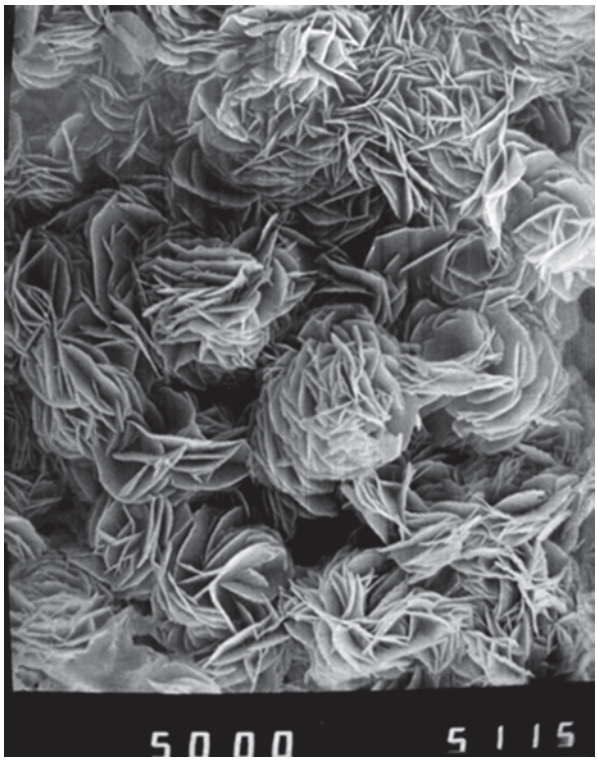


Fig. 8.11 Plates crystals of tobermorite, forming rosettes (photo B. Trybalska)

The cellular concrete hardening and strength development is mainly assured by the C–S–H phase. C–S–H is binding the grains of sand or fly ash, which are fine aggregate. Therefore the SiO_2/CaO ratio, as a result of binder content in concrete, is important. In the case of sand filler this ratio is about 3, and with siliceous fly ash is about 1.8. The activity of lime, determined as t_{60} i.e. the time in which the temperature of hydrating material attains 60 °C, should be higher than 15 min. The SO_3 content, important in the case of siliceous fly ash, should not exceed 2 % and the uncombusted coal content—7 % respectively [39].

The reaction of calcium hydroxide with silica is significantly accelerated by autoclaving, because the rate of reaction increases exponentially with temperature (Arrhenius equation). Simultaneously, at higher temperature the solubility of silica is higher (Fig. 4.54), which is of significantly importance for the rate of reaction with calcium ions. In these conditions C–S–H is formed relatively quickly, and its CaO/SiO_2 molar ratio is below 1.

The transformation into tobermorite will be also occurring, which will have characteristic plate–morphology, sometimes as elongated crystals (Figs. 8.11 and 8.12). The formation of gyrolite and truscotite is also possible; the composition of these phases is shown in Table. 4.4.

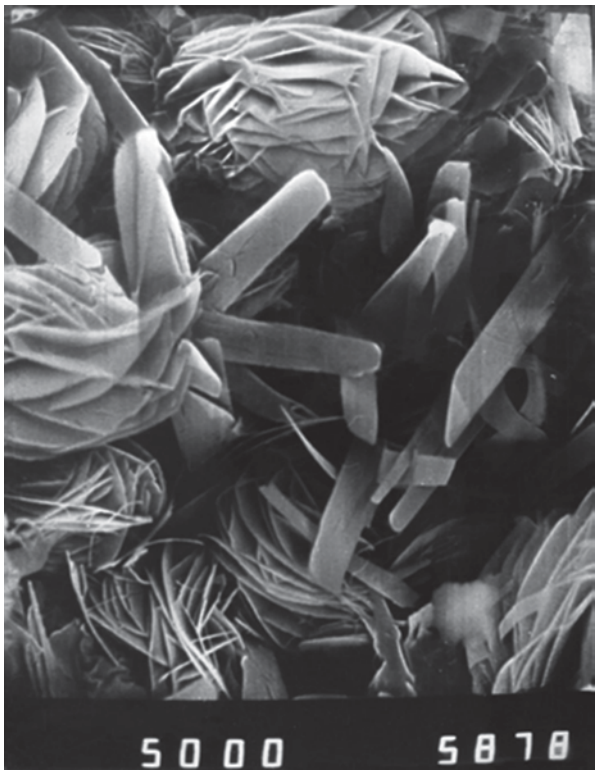


Fig. 8.12 Elongated morphology of tobermorite crystals (photo B. Trybalska)

References

1. Dron, R., Brivot, R.: 7th ICCC Paris, vol. II, p. 3–134. Paris (1980)
2. Daimon, M.: *ibid*., vol. I, p. III–2/1
3. Kondo, R.: Fundamental study on the manufacture of slag cement. Ph. D. Thesis in Tokyo Institute of Technology (1958)
4. Voinovitch, I., Raverdy, M., Dron, R.: 7th ICCC Paris, vol. II, p. III 122. Paris (1980)
5. De Jong, Y.A.: Silicates Ind. **42**, 5 (1977)
6. Regourd, M., Thomassin, J.H., Baillif, P., Touray, J.C.: Cem. Concr. Res. **13**, 549 (1983)
7. Regourd, M.: 7th ICCC Paris, vol. IV, p. 63, Discussion du Panel, Thème III. Paris (1980)
8. Dron, R.: 8th ICCC Rio de Janeiro, vol. IV, p. 81. Rio de Janeiro (1986)
9. Fierens, P., Poswick P.: Silicates Ind. 42, 235 (1977)
10. Vernet, C.M.: 7th ICCC Paris, vol. IV, p. 63, Discussion du Panel, Thème III. Paris (1980)
11. Regourd, M., Mortureux, B., Gautier, D., Hornain, H., Volant, J.: ibid., vol. II, p. 3–105
12. Voinovitch, I.A., Dron, R.: Silicates Ind. 41, 209 (1976)
13. Locher, F.W.: 4th ICCC Washington, vol. I, p. 267. Washington (1960)
14. Mascolo, G.: Cem. Concr. Res. 3, 207 (1973)
15. Taneja, C.A.: 6th ICCC Moscow, vol. III, p. 60. Moscow (1974)
16. Mascolo, G., Marino, D.: 7th ICCC Paris, vol. II, p. III–59. Paris (1980)
17. Regourd, M.: ibid., vol. I, p. III–2/9
18. Uchikawa, H.: 8th ICCC Rio de Janeiro, vol. I, p. 249. Rio de Janeiro (1986)
19. Fierens, P., Poswick, P.: 7th ICCC Paris, vol. II, p. III–112. Paris (1980)

20. Kropp, J., Seeberger, J., Hilsdorf, N.K.: Proc. 2nd Int. Conf. on Fly Ash, Silica Fume, Slag and Natural Pozzolanas in Concrete, vol. 1, p. 201. Madrid (1986)
21. Elola, A.L., Szteinberg, A.S., Torrent, R.I.: 8th ICCC Rio de Janeiro, vol. IV, p. 145. Rio de Janeiro (1986)
22. Dron, R.: Bull. Liaison Lab. Ponts Chauss. **99**, 66 (1978)
23. Takemoto, K., Uchikawa, H.: 7th ICCC Paris, vol. I, p. IV–2/1. Paris (1980)
24. Dent Glasser, L.S., Lachowski, E.E., Taylor, H.F.W.: Cem. Concr. Res. **8**, 733 (1978)
25. Greenberg, S.A.: J. Phys. Chem. **60**, 325 (1956)
26. Greenberg, S.A.: J. Phys. Chem. **65**, 12 (1961)
27. Sersale, R.: 7th ICCC Paris, vol. I, p. IV–1/3. Paris (1980)
28. Sabatelli, V., Sersale, R., Amicarelli, V.: Rend. Accad. Sci. Fis. Mat. **34**, 243 (1967)
29. Kokubu, M., Jamade, D.: 6th ICCC Moscow, vol. III, p. 83. Moscow (1974)
30. Držaj, B., Hoćevar, S., Slokan, M., Zajc, A.: Cem. Concr. Res. **8**, 711 (1978)
31. Magnan, R., Cottin, B., Gardet, J.J.: Ciment, Bétons, Plâtres, Chaux. **692**, 41 (1975)
32. Jawed, I., Skalny, J.: Materials Research Society Symp. N. Diamond, S. (ed.), p. 60. (1981)
33. Luke, K.: Pulverized fuel ash as a cement extender. In: Bensted J., Barnes, P. (eds.) Structure and Performance of Cements, p. 353, 2nd edn. Spon Press, London (2002)
34. Wei, F.–J., Grutzeck, M.W., Roy, D.M.: Cem. Concr. Res. **15**, 174 (1985)
35. Regourd, M.: 8th ICCC Rio de Janeiro, vol. I, p. 199. Rio de Janeiro (1986)
36. Odler, I.: Mater. Struct. **24**, 143 (1991)
37. Mehta, P.K.: Cem. Concr. Res. **15**, 669 (1985)
38. Paprocki, A.: Betony komórkowe. Arkady, Warszawa. (1966) (in Polish)
39. Jatymowicz, H., Siejko, J., Zapotoczna–Sytek, G.: Technologia autoklawizowanego betonu komórkowego. Arkady, Warszawa. (1980) (in Polish)
40. Soboń, M.: oral information
41. Handke, M.: Crystalochemistry of Silicates. AGH, UWN–D, Kraków. (2005) (in Polish)

Chapter 9
Special Cements

According to Kurdowski and Sorrentino the special cements are these, which properties are outside the limits included in standards, relating to the ordinary cements [1, 2]. They are devoted to the special applications and are frequently produced with unconventional methods or from atypical raw materials. This definition based on use is restrictive, because it does not take into account that it is possible to produce concrete with special properties from ordinary cements by using various additives and admixtures or by thermal treatment, during the hydration stage e.g. autoclaving.

Recently, higher and higher amounts of special cements are manufactured, which is the result of technological progress in all branches of building engineering. The shrinkage compensation cements for the waterproof concrete coatings, or fast–setting cements for the cut off the water leakages, are the typical examples. The energetic crisis and necessity of CO_2 emission reducing, increased significantly the searching of new, untypical belite cements. These so–called low energy cements have been occupying many place in the chemistry of cement, since the Cement Congress in Paris [3]. Large amount of sulphate–aluminate cement are produced in China (over 2 million t in 1990) [4]. Belite, calcium sulphoaluminate (3[CA] $CaSO_4$) and brownmillerite are the main components of these cements [4].

One can expect that the properties of some special cements will be standardized and these materials will join the group of conventional binders. However, other will remain for the long time in the group of untypical, special cements. The examples of the latter are white and calcium aluminate cements.

In Polish Standard PN–B–19707 the following special cements are distinguished:

- sulphate resistant cement, which linear expansion after placing 52 week in Na2SO4 solution should be lower than 0.5 %,
- low heat cement, which, tested with semi–adiabatic method, should evolve after 41 h heat of hardening lower than 270 J/g, and in the case of CEM IV and V the same value after 7 days,
- low alkali cement; in the case of CEM I, II, IV and V Na2Oe $\leq$ 0.60 %, in the case of slag cements Na2Oe in the range from 0.95 % through 1.10 to 2 % for CEM II/B–S and CEM III/A, to CEM III/B and C respectively.

W. Kurdowski, *Cement and Concrete Chemistry*,
DOI 10.1007/978-94-007-7945-7_9, © Springer Science+Business Media B.V. 2014

Table 9.1 Types of calcium aluminate cements. [7]

Type	Chemical composition, %				Raw alumina material	Technology
	Al_2O_3	Fe_2O_3	SiO_2	CaO		
1	37–40	11–17	3–8	36–40	Red bauxite	Melting
2	48–51	1–1.5	5–8	39–40	Red bauxite	Melting[a]
3	51–60	1–2.5	3–6	30–40	White bauxite	Sintering & melting
4	78–80	0–0.5	0–0.5	17–27	Alumina	Sintering

[a] in reducing conditions with metallic Fe separation

The requirements for low heat (heat of hydration details are given in EN–196–8 and 9) and sulphate resistant (SR) cements are given in the standard EN–197–1, introduced in 2011.

These cements will be not discussed in this chapter because of aforementioned reasons.

9.1 Calcium Aluminate Cement

Calcium aluminate cement technology was developed in France by Bied, in the Lafarge laboratory [5]. Calcium aluminate cements are produced by sintering or melting of the limestone with bauxite or aluminum hydroxide mixtures, depending on the impurities acceptable level in the product. Sintering is difficult at higher Fe_2O_3 content. In the world the technology of calcium aluminate cement producing by melting, developed by Lafarge Company (French *ciment fondu*) is the most popular.

The second technology, popular particularly in the United States is applying clinker sintering in the rotary kilns. This technology is used in Poland in Mapei plant, in Górka near Trzebinia. The properties of these cements have been reported by Sawków [6]. There are also technologies of yellow phosphorus and aluminate clinker production in arc furnace or rotary kilns [7]. Calcium aluminate clinker produced with this technology contains usually some amount of the $C_{11}A_7{\cdot}CaF_2$ phase, because fluorine is introduced with the phosphorites. Leary [8] found also in this clinker the new phase $3CaO \cdot 3Al_2O_3 \cdot CaF_2$. This phase is formed in a short burning, at temperature of 1,400 °C.

Robson [7] is distinguishing the four types of calcium aluminate cements, depending on the iron(III) oxide and alumina content (Table 9.1). The production of aluminate cement with 11–17 % Fe_2O_3 (calculated amount, because of the high FeO content) is the least widespread; this cement belonging to the type I is manufactured from the cheapest, red, rich in iron bauxite. From the practical point of view the calcium aluminate cements can be divided to the two groups: ordinary containing mainly CA (more often over 60 %), C_4AF and in lower amount C_2AS, C_2S and wüstite, and also white cements with CA as a main component and in low quantities CA_2 and α–Al_2O_3. The latter is the Robson type 4 called by him white. White calcium aluminate cements, with low impurities content, mainly the iron oxides and silica, are applied chiefly for the production of refractory concretes.

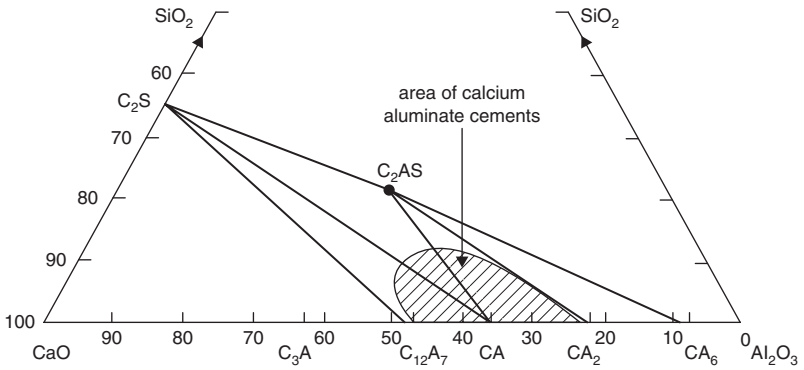


Fig. 9.1 Calcium aluminate cements field in the part of $CaO–Al_2O_3–SiO_2$ system. (according to [5])

The SiO_2 content, not higher than 6%, exceptionally 8% in calcium aluminate clinker, is the basic criterion of bauxite applicability. The bauxites, in which the SiO_2 content, calculated in relation to the ignited substance does not exceed 5%, are generally used. Fe_2O_3 content in melted cements can be high. Therefore bauxites in which the Fe_2O_3 content approaches 30% are used. The TiO_2 content is not an obstacle, but the limestone, which is the raw material significantly cheaper, should be distinguish by high purity. The limestones with CaO content over 50%, and in which SiO_2 is not exceeding 1.5% and MgO 1%, are generally used.

Mineral composition of calcium aluminate cements can be assessed based on the three component $CaO–Al_2O_3–SiO_2$ system and the following phases can occur: CA, CA_2, $C_{12}A_7$, C_2S, C_2AS (Fig. 9.1) [5]. However, the mineral composition is variable and depends primarily on the chemical composition, in which iron plays the main role and the atmosphere: oxidizing (rotary kilns) or reducing one (blast furnaces, L furnaces), thus the Fe^{2+}/Fe^{3+} ratio. It should be also remembered that the calcium aluminate cements composition is rather closer to the C–A–F system.

The main phase which is the calcium monoaluminate contains from 0.55 to 4.7% Fe [9]. In this phase the iron Fe (III) ions are occuring. The iron content in CA is related to its content in clinker and to the degree of Fe^{3+} reduction to Fe^{2+}. The solubility limit in CA is 4.8% of Fe [7].

According to Robson [7], the hydraulic activity is improved by iron admixture. However, Talaber [10] is of the opinion that iron admixture reduces the rate of reaction with water. Suzuki [11] has shown, that the strength of CA paste doped with Fe_2O_3, and particularly with the $SiO_2+Fe_2O_3$ mixture, is substantially higher than the strength of CA paste without admixtures. The ferrite phase is generally much richer in iron than C_4AF and its formula is close $C_{10}AF_4$. Hence it is composed of 80% C_2F and 20% "C_2A" [9]. It is so–called "grey interstitial matter" which can contain high titanium content and the replacement occurs according to the scheme: $Fe_2O_3 \rightarrow 2TiO_2$.

Jeanne [9] is proposing the following formula: $Ca_{10.1}A_{1.2}(xFyT)_{3.9}$. In this phase, rich in titanium $x=0.4$, $y=1.2$, while in the iron rich one $x=0.9$, $y=0.2$.

This isomorphous substitution of iron by titanium does not imply the XRD pattern changes, due to the similarity of ionic radii [9]. Jeanne [9] does not find any other titanium containing phases, while George [12] and Talaber [10] mention the monocalcium titanate, at higher TiO_2 content.

The white interstitial matter is composed of wüstite—FeO. Iron oxide is included in pleochroite composition, which is frequently in form of fibrous or needle–like crystals. Midgley [13] presented the opinion that this phase is composed of the following anionic groups $[Al_2O_7]^{8-}$, $[AlO_4]^{5-}$, $[SiO_4]^{4-}$: $Ca_{22}Fe^{II}_3Al_{14}(Al_2O_7)_8(AlO_4)_4(SiO_4)$. Finally it is assumed that its composition corresponds to the formula [2, 12]:

$$22CaO \cdot 13Al_2O_3 \cdot 3MgO \cdot SiO_2$$

MgO is substituted by FeO, which is leading to the following compositions [14]:

$$22CaO \cdot 13Al_2O_3 \cdot 3FeO \cdot 4SiO_2$$

$$23CaO \cdot 13Al_2O_3 \cdot 3FeO \cdot 3.5SiO_2$$

$$23CaO \cdot 13(Al_2O_3 \cdot Fe_2O_3) \cdot 3FeO \cdot 4SiO_2$$

Midgley [15] proposed the following general formula for pleochroite occurring in industrial clinkers:

$$(Ca, Na, K, Fe^{II})_A(Fe^{III}Al)_B(Al_2O_7)_8$$
$$(AlO_4)_{6-x}(SiTiO_4)_x$$

in which the values attributed to A and B should give the crystal electrical neutrality; usually $A=28$, $B=13$.

At higher silica content, besides of β–C_2S, the gehlenite phase appears. Gehlenite is the phase of very low reactivity to water and simultaneously it is bonding some part of Al_2O_3. Hence the higher amount of silica in the raw material used for calcium aluminate cement production is not required.

MgO occurs first of all in pleochroite, but it can form the solid solutions with the other phases, however, in very low concentration. Talaber [10] mentions also that the formation of akermanite and magnesium spinels is possible too.

In calcium aluminate clinkers there are some amounts of sulphides, particularly when they are produced in blastfurnace. These compounds have a negative impact on the properties of cement paste [10].

Alkalis are the undesirable components too; this will be explained by discussing the hydration processes. However, they are always present in the raw materials and then in low amounts in clinker, usually from 0.1 to 0.3 %; they are concentrated in the glass phase.

In calcium aluminate clinkers the lower or higher $C_{12}A_7$ amounts are present, which causes set acceleration of cement paste. Sometimes in the sintered clinkers even the C_3A phase can be present, due to the local inhomogeneity of the raw mixture, in which the larger limestone grains can occur. Calleja [16] proposed the simplified formulae for the calculation of calcium aluminate cement phase composition.

There is a substantial difference between the phase composition of Portland and calcium aluminate cement. In the first one the phase composition does not change significantly at the variable content of minor components.

Hydration of CA leads to the formation of two hexagonal hydrates: CAH_{10} and C_2AH_8. CAH_{10} is formed at lower temperatures, not exceeding 20 °C; the ratio of C_2AH_8 increases with temperature. At temperature above 30 °C both hexagonal hydrates transform to the only stable cubic C_3AH_6 phase.

The hydration process can be thus schematically presented in the following way:

$$\begin{aligned} &CA \rightarrow CAH_{10} \\ &\quad\downarrow > 20^{\circ}C \\ &\quad C_2AH_8 + AH_3 \\ &\quad\downarrow > 30^{\circ}C \\ &\quad C_3AH_6 + AH_3 \end{aligned} \tag{9.1}$$

Usually in the process of CA hydration the mixture of the two hexagonal hydrates together with the colloidal aluminum hydroxide are formed. It is all the more probable that calcium aluminate cement contains always some amount of $C_{12}A_7$ phase, which hydrating gives at once these two hexagonal phases:

$$C_{12}A_7 + 60H \rightarrow 2CAH_{10} + 5C_2AH_8 \tag{9.2}$$

At temperature exceeding 23 °C, the C_2AH_8 is principally formed, but its content is very variable and depends probably on the alkali and $C_{12}A_7$ percentage in cement [5]. Ferrites form $C_2(A, F)H_8$, however, the $C_4(A, F)H_x$ can appear too. The possibility of C_3AH_6 formation was reported too.

The mechanism of CA and $C_{12}A_7$ hydration consists in the congruent dissolution, nucleation of hydrates and further crystals growth. The hydration process can be easily followed taking as an example the reaction of monocalcium aluminate with water, without admixture of $C_{12}A_7$ or other phases with $C/A > 1$. Due to the low nucleation rate in this condition, in the liquid phase a high concentration of calcium and aluminium ions is maintained for a long time (Fig. 9.2).

The C/A molar ratio is usually 1.06 because of low amount of AH_3 precipitation [17]. Exceeding the ratio of $C/A \geq 1.2$, for example in the presence of very low $C_{12}A_7$ content, causes the rapid crystallization of hydrates, due to solution supersaturation in relation to the hexagonal hydrates (Fig. 9.3).

The hexagonal hydrates are unstable and transform into C_3AH_6 at temperature range 35–45 °C in cubic C_3AH_6. It is the only stable hydrate in the $CaO–Al_2O_3–H_2O$ system. The rate of conversion depends mainly on three factors: temperature, humidity and pH. In the dry concrete the conversion does not occur. At higher pH in the presence of alkalis the conversion is accelerated [18].

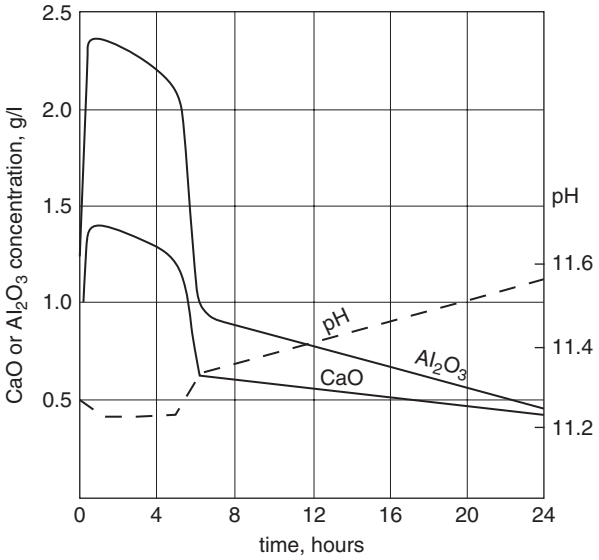


Fig. 9.2 Composition and pH of the solution obtained by shaking 50 g CA in 1 L of water. (after [5])

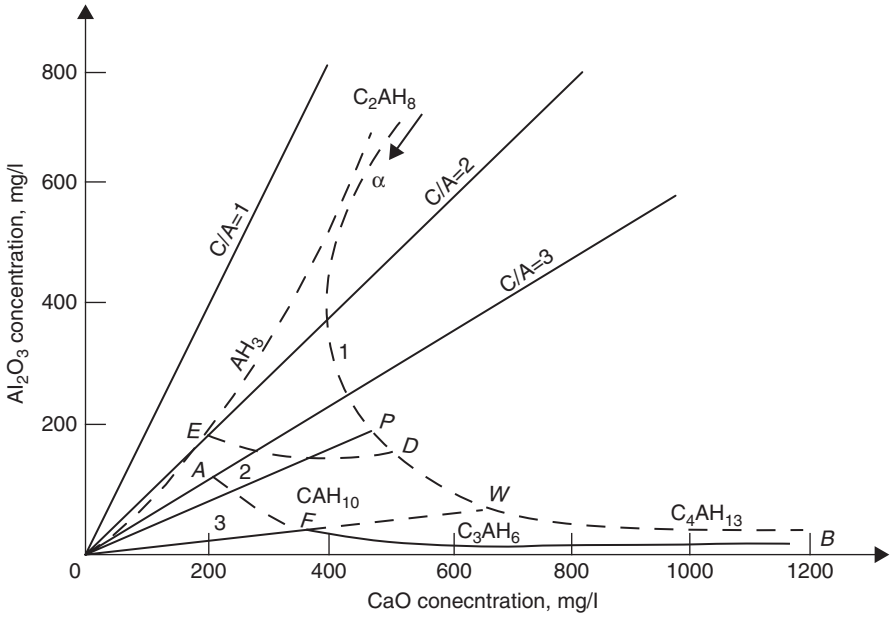


Fig. 9.3 The system CaO–Al_2O_3–H_2O at 21 °C; 1 hexagonal hydrates, 2 micro–crystalline compounds, 3 gibbsite

The conversion of unstable hexagonal hydrates into the cubic C_3AH_6 is associated with elution of high water amount according to the reactions:

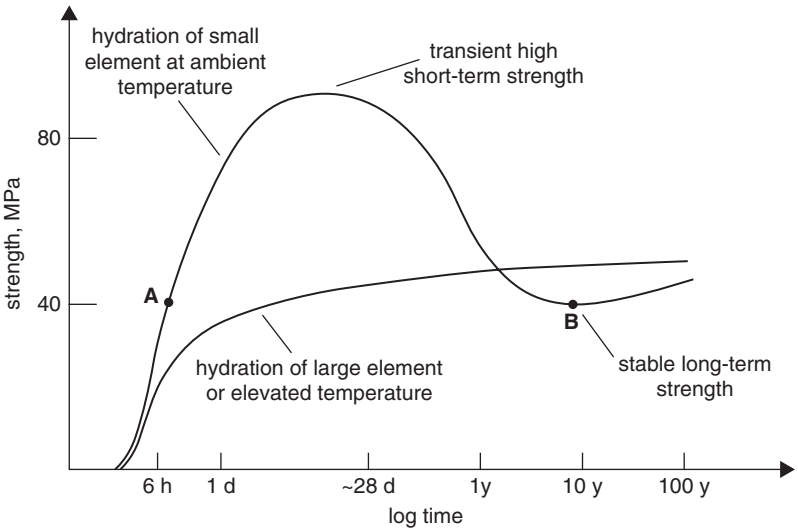


Fig. 9.4 Schematic strength development curves for calcium aluminate cement concrete at w/c ≈0.4 and cement content of 400 kg/m^3. (according to [20])

$$3CAH_{10} \rightarrow C_3AH_6 + 2AH_3 + 18H \tag{9.3}$$

$$3C_2AH_8 \rightarrow 2C_3AH_6 + AH_3 + 9H \tag{9.4}$$

Simultaneously, the density of hexagonal hydrates is significantly lower: CAH_{10}—1.78, C_2AH_8—1.95 in comparison to C_3AH_6—2.53 and AH_3—2.40 g/cm^3. Therefore it can be calculated that, as a result of these reactions, the volume of solid phases will be reduced of 50 and 25 % in the first and second case respectively. As a consequence, a high porosity increase together with strength decrease of concrete will occur. For this effect preventing the low w/c ratio should be assured. The CA hydration with C_3AH_6 formation requires 46 % of water; hence the critical w/c value is 0.4 and should not be exceeded.

Simultaneously high cement content in concrete should be maintained, on the level of 400–450 kg/m^3 [19]. The curing of concrete could be performed at temperature close to 38 °C or higher, which assures the cubic hydrate direct formation, during calcium aluminate cement reaction with water [12]. This situation is well presented by the schematic strength development shown by Scrivener and Capmas [20] (Fig. 9.4).

There are also the hypotheses indicating the possibility to counteract the conversion by $CaCO_3$ addition, which causes the carboaluminates formation [21]. Simultaneously the application of limestone aggregate leads to the significant strength increase of calcium aluminate cement concrete; the strength development is then observed over the 5 years period of time (Fig. 9.5). However there is no proof that at the presence of $C_3A{\cdot}CaCO_3{\cdot}11H_2O$ the conversion of hexagonal hydrates in C_3AH_6

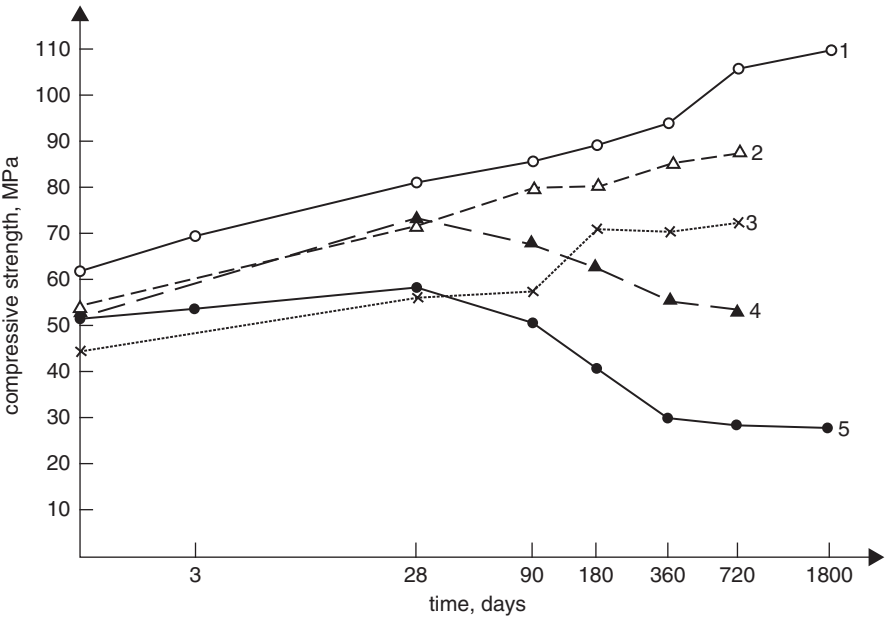


Fig. 9.5 Compressive strength of calcium aluminate cement concretes (according to [21]); 1 limestone aggregate, cement content 350 kg/m^3, w/c = 0.5, 2 crushed limestone aggregate, w/c = 0.6, 3 siliceous aggregate with ground limestone, 4 siliceous boulders, w/c = 0.54, 5 siliceous aggregate, w/c = 0.54

is hindered [12]. On the other hand, the results reported by Cussino and Negro [21] indicate that the formation of carboaluminates allows the compensation of strength decrease caused by conversion.

The calcium aluminate cement pastes, particularly those with low minor components content (white cements) show the setting time shortening with temperature up to 40 °C. However, the pastes produced from some C_2S containing cements reveal longer setting when the temperature is increasing from 20 to 30 °C. This phenomenon cannot be explained by slower C_2AH_8 crystallization, which is formed at temperature of 30 °C, in comparison with the crystallization of CAH_{10} at temperature 20 °C, which is occurring with higher rate [2]. Cottin [19], has shown that this effect is related to the presence of SiO_2, however, the mechanism of retardation was not explained.

CA phase has a decisive effect on high strength and rapid strength development of calcium aluminate cement paste. However, these pastes can be strongly modified depending on temperature in which the hydration occurs [22]. At low temperature, up to 20 °C, the CAH_{10} is formed. At higher temperature, particularly above 45 °C, C_3AH_6 and gibbsite are formed. Setting period is a little shorter than in the case of Portland cements and generally does not exceed ½ h. Therefore the calcium aluminate cements belong thus to the slow setting but rapid hardening cements. Slow setting is caused by AH_3 gel formation, which probably decrease the ions diffusion

rate in the liquid phase, and CH addition, providing to the hexagonal hydrates formation, significantly shortens this period.

Calcium aluminate cements do not show the strength decrease at high temperatures, because the dehydrated grains of hydrates are sintered quickly and react with fine fractions grains of aggregate, producing the ceramic bonds[1]. It is the main advantage of these cements, which are used in the manufacturing of refractory concretes. In order to ascertain fairly good refractoriness, cements with low iron and other accessory component content are used, which contain only calcium aluminates: CA and CA_2 and corundum. α–Al_2O_3 is often added during cement grinding [23].

The white calcium aluminate cements, with special aggregate (for example corundum) can be used for production of refractory concretes resistant even up to 2,000 °C (Super Secar 250). Refractory castables have also good resistance to thermal shock.

The heat of hardening of calcium aluminate cement is in the range 460–500 J/g that is similar to Portland rapid hardening cement. However, 70–90 % of total heat is evolved during 24 h at temperature of 20 °C, while in the case of Portland cement at the same time only 25 to 50 %, due to the lower hydration rate. This is characteristic property of calcium aluminate cements, very well correlated with rapid strength development, which is assuring their hardening even at temperature of 0 °C [12]. The calcium aluminate cement concretes must be cured in moisture, otherwise the superficial dehydration occurs, which can lead to the disintegration of this layer. In the core of concrete the temperatures can increase up to 70–80 °C, after 8–10 h hydration. It causes the conversion of hexagonal hydrates into cubic and the strength decrease at later age is prevented (Fig. 9.4). Therefore the curing of calcium aluminate cement concrete at higher temperature is recommended [12].

There is an opinion that the concrete should be matured for at least 24 h at the temperature of 20 °C or close to 20 °C. The calcium aluminate cement concrete shows the lowest strength at the temperature of 800–900 °C, because the calcium aluminate hydrates are decomposed and the ceramic bond has not sufficient strength. The $C_{12}A_7$ phase is detected as a first dehydration product, and at temperature of about 600 °C CA_2, formed as a result of active Al_2O_3 (*in statu nascendi*) reaction; this Al_2O_3 is the product of AH_3 decomposition [12]. The sintering is greatly accelerated at temperatures above 800 °C.

Calcium aluminate cements are extremely highly resistant to various aggressive media. They were invented as a result of concrete searching, resistant to sulphate solutions attack. Besides the sulphates, they are resistant also in the acidic waters environment (see Chap. 6) as well as in sea water. This was proved by examination of calcium aluminate cement concretes after many years of exploitation in different conditions. For example Lea [5] reports that the concrete samples, moreover those with anhydrite aggregate, stored many years in gypsum water, do not show any symptoms of destruction. The other concrete samples were successfully stored for 20 years in Medicine Lake in Dakota, where the concentration of sulphates was

[1] See F. Nadachowski, "Basal technology of refractory materials", edited by Śląskie Wyd. Techniczne, Katowice 1995 (in Polish).

high. In another case the calcium aluminate cement concrete containers were stable being in contact with 5 % $MgSO_4$ solution for 8 years. Long lasting studies proved the calcium aluminate cement paste resistance to the attack of chlorides [24].

The calcium aluminate cement concrete is resistant to the attack of weak solutions of mineral acids too. The resistance to organic acids is limited to the pH value of about 4. However, the porous calcium aluminate cement concrete is not stable in the soft water, if permeable.

This good resistance of calcium aluminate cement paste to the attack of aggressive media is not clear and cannot be explained by the properties of hydrated aluminate phases. George [12] is reminding that the ground paste of calcium aluminate cement dissolves more rapidly than that of Portland cement in mineral acids. However, the situation is quite different in the case of concrete element. Nowadays there is an opinion that the resistance of concrete depends on the porosity, pore structure (large pores ratio) and permeability. George [12] pays an attention that the porosity of calcium aluminate cement concrete is considerable lower than that of Portland cement, at the same w/c ratio. It seems that this is a consequence of higher water content in the calcium aluminate hydrates than in C–S–H, as well as of the presence of aluminum hydroxide gel.

The lack of $Ca(OH)_2$ has a great impact on the chemical resistance of aluminate cement paste. The AH_3 gel is not soluble at pH decreasing to 3.5–4.0 and therefore the paste from calcium aluminate cement is stable in acidic solutions in this pH range.

The calcium aluminate cements are not resistant to the attack of alkalis, because the aluminum hydroxide is soluble in the water solutions of sodium and potassium hydroxides, with which the calcium aluminates are also reacting with. The alkali metals carbonates react with calcium aluminate hydrates and these reactions cause destruction of concrete:

$$K_2CO_3 + CaO \cdot Al_2O_3 aq \rightarrow CaCO_3 + K_2O \cdot Al_2O_3 \tag{9.5}$$

$$2K_2CO_3 + 2CaO \cdot Al_2O_3 aq \rightarrow 2CaCO_3 + K_2O \cdot Al_2O_3 + 2KOH \tag{9.6}$$

The potassium or sodium aluminates dissolving in alkaline solution, are transformed in $Al(OH)^{4-}$ ions [25]. Due to the low permeability of concrete corrosion occurs slowly. Though the experiments show that that the rapid deterioration of calcium aluminate cement concrete occur at pH higher than 13, however, these concretes should not be used in environment of high pH. Aggregate containing soluble alkalis should also be avoided.

There are controversial opinions about the corrosion of reinforcing steel in the calcium aluminate cement concretes. This is linked with the less basic paste in comparison with the Portland cement one. However, it appeared in practice, that in the good quality concrete there was no difference related to the stability of steel reinforcement in comparison with Portland cement. The destruction of reinforced concrete was linked with high w/c, in which the conversion of hexagonal hydrates into cubic caused the porosity and rapid carbonation increase [12].

Table 9.2 Fe_2O_3 and FeO content in white cements

Country/cement producer	Fe_2O_3[a] content, %	FeO content, %	Degree of whiteness
Germany	0.30	0.15	82
Great Britain	0.26	0.08	86
France (Lafarge)	0.29	0.08	85
Italy (Italcementi)	0.18	0.10	89
Poland (Wejherowo)[b]	0.60	0.10	77

[a] Total Fe content calculated as Fe_2O_3, [b] Now closed

Due to the absence of $Ca(OH)_2$ in the calcium aluminate cement paste a higher durability of glass fibers was expected in fiber reinforced composites. Majumdar [26] proved that the calcium aluminate cement composites had much better mechanical properties, but only the case of alkali resistant glass.

9.2 White and Coloured Cements

The color of cement is the result of light absorption in the visible part of spectrum, due to the presence of transition metal ions.

In the case of white cement the most important are iron oxides. The Fe^{3+} ions occurring in the tetrahedral coordination in C_4AF give an intense gray color. The change of tetrahedral coordination into the octahedral one in C_6AF_2 is improving the whiteness of cement [27]. The reduction of $Fe3^{+}$ also improves whiteness, because Fe^{2+} substitutes calcium in calcium orthosilicates and has octahedral coordination [28]. Therefore clinker should be burned in the slightly reducing atmosphere, in order to lower the oxidizing degree of the part of iron (Table 9.2).

Teoreanu [27] reminds that the TiO_2 admixture improves the whiteness because the Ti^{4+} ions displace Fe^{3+} ions from tetrahedral positions, causing to occupy by them the positions with octahedral coordination. The similar positive effect has vanadium.

The boron ions can improve the whiteness, substituting Fe^{3+} in tetrahedral coordination [29]; however, their action can lead to the increase of light absorption. Teoreanu [27] states that it is linked with the cation vacancies formation in the lattice of orthosilicates, caused by the substitution of silicon by boron. Manganese is frequently among the minor components in the white cement clinker. However, opposite to the previously discussed elements, the Mn^{3+} ions give strong coloring, that is the worsening of whiteness even at low content. The Mn^{3+} ions reduce also the possibility of changing the Fe^{3+} ions coordination from tetrahedral to the octahedral one by titanium, vanadium, chromium and cobalt [30].

Cobalt and chromium, in spite of the changing the Fe^{3+} ions coordination to the octahedral, reduce the whiteness, because they absorb the light stronger than the iron (III) ions [27, 30].

Quick determination of the cement whiteness degree is based on the comparison with the standard; now it is MgO, formerly it was $BaSO_4$. Munsell and Hunter [31]

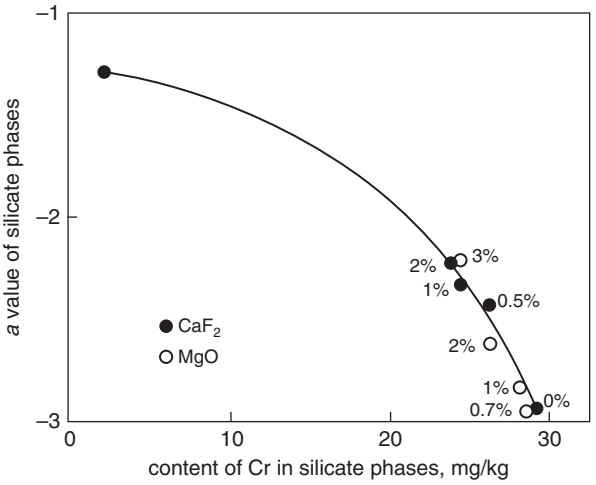


Fig. 9.6 Effect of Cr content in calcium silicates on the intensity of green shade of cement (values of *a* index) in the case of MgO and CaF_2 addition. (according to [31])

methods can be applied for more precisely cement color determination. Munsell, for more precise color expression, introduced three components: the shade (*H*), brightness (*V*—numerical scale) and saturation (*C*—color saturation). For measurement and expression of color the *Yxy* system or Hunter method is applied. The brightness of white cement should be at least 80 %, which gives a visual effect of white color.

Uchikawa et al. [31] studied the effect of coloring admixtures on the whiteness of cements, applying the Hunter method. It results from these investigations, that the color of white cement is controlled mainly by Cr, Mn, Fe, and the most intensive coloring gives chromium. These three elements are responsible for cement coloring on green, green–blue and yellow respectively. Titanium, vanadium, cobalt, nickel, copper and zinc almost have no effect on cement color. The effects of Cr and Fe on whiteness, Cr, Mn and Fe on brightness, Cr on green, Fe on yellow and Mn on blue colors, are very strong. The green coloring of white cement is primarily dependent on green color of calcium orthosilicates and yellow coloring of the interstitial matter. Color of the latter is closely connected with the Fe^{3+} content. The gaseous atmosphere during clinker burning controls not only the oxidization degree of Cr, Mn and Fe but also their distribution in the clinker phases. In the reducing atmosphere Fe and Cr are concentrated mainly in the interstitial matter and form very often the metallic inclusions in this matter. In this conditions the green or blue coloring does not appear.

The initial cooling temperature causes only low change of elements oxidation degree. However, the higher temperature of quick cooling the higher whiteness degree and decrease of intensity of green and yellow coloring, due to the Cr and Fe content decrease in clinker phases. The water cooling is diminishing the yellow coloring due to the prevention of the oxidation of Fe^{2+} ions to Fe^{3+}. MgO and CaF_2 is influencing the distribution and content of transition metals in clinker phases. Some addition of CaF_2 and MgO is preventing the green color appearing, due to the reduction of Cr content in orthosilicates phases. CaF_2 displaces chromium from the silicates; therefore the *a* value (Fig. 9.6) is approaching zero. However, the MgO addition to 2 % strengthen the coloring of C_4AF phase and reduce the brightness *V*

[32]. Simultaneously it displace Fe from the silicate phases increasing its content in interstitial matter [31]. Kawashima et al. [33] found that in the industrial clinkers, produced in the conditions far from the equilibrium, the solid solutions of MgO and Fe_2O_3 in silicates lower the whiteness.

Apart fluorite $CaCl_2$ addition has also a positive impact on the whiteness due to the sublimation of the part of iron and increasing the phase C_6AF_2 content at the expense of C_4AF [34].

The white cement clinker should be produced from the pure raw materials, first of all with very low content of Fe_2O_3 and Mn_2O_3, which are the most commonly occurring coloring oxides.

The lack of iron and high silica ratio causes the sintering of clinker difficult and the mineralizers must be applied. The fluorite is commonly used, but the more effective fluorosilicates and aluminates, for example Na_3AlF_6 can also be applied. The $CaCl_2$ appears in some reports, because there is an opinion of iron volatilization possibility, in the form of $FeCl_3$ [35]. In spite of the mineralizers addition, the free CaO content in white cements is generally higher, on the level from 2 to 3 %.

Mineral composition of white clinkers is variable; the C_3S ranges from 40 to 65 %, C_2S from 15 to 40 %, C_3A from 5 to 16 %, while C_4AF from 0.6 to 1.5 %.

The cooling of clinker from the temperature of 1,400 °C in reducing atmosphere is of special importance; otherwise the clinker grains will have a green shell. For this purpose the mazout or water is injected on the layer of clinker in the rotary kiln. The further cooling without access of air, at least to the temperature of 600 °C is also very beneficial [36].

There are methods of clinker bleaching in the reducing gaseous atmosphere at temperature range 1,400–600 °C (Lafarge technology). The generator gas can be used, which subsequently is introduced to the rotary kiln.

As it has been mentioned above the quick cooling from the temperature of 1,400 °C is important. In this condition the ferrite phase content is decreasing, as the C_6A_2F is replaced by lower amount of C_6AF_2 and the colorless tricalcium aluminate is formed [35]. At slow cooling also in belite solid solution the iron oxide content is increasing and its whiteness is decreasing. Generally, from the two calcium silicates in clinker C_3S has higher whiteness.

The colored cements can be produced from the white clinker. The technology consists in mixing white cement with mineral dyes, most often the metal oxides, added from 1 to 3 % by mass. There are some reports dealing with alternative colored cements technology, consisting on the production of colored clinkers [37].

9.3 Expansive Cements

The drying shrinkage caused from water loss and consolidation of gel is a serious drawback of Portland cement concretes. Shrinkage generates the microcracks formation, when the stresses are higher than the tensile strength of concrete, which significantly increases the permeability of this composite. The volume changes, discussed in Chap. 5 include, besides of the contraction of paste called the hydraulic

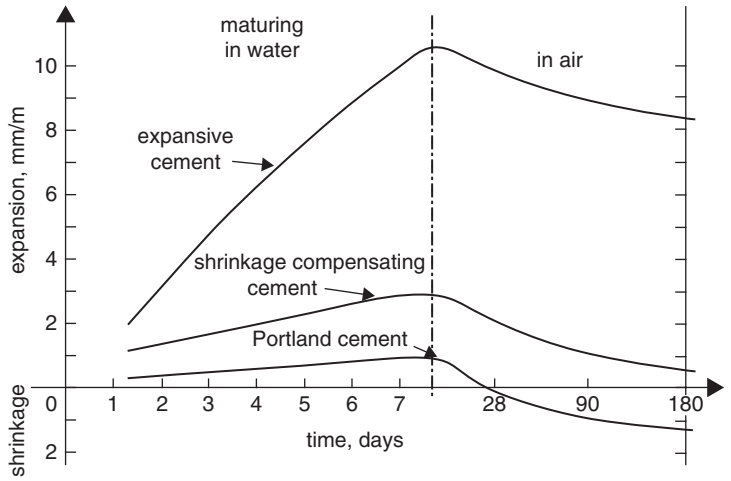


Fig. 9.7 Volume changes of expansive, shrinkage compensation and classic Portland cement

shrinkage, the swelling in water too. This swelling is caused by cement hydration progress and reduction of paste porosity, due to the filling of pores by colloidal C–S–H. However, this swelling of concrete cured in water is not equivalent to the drying shrinkage and therefore concrete shows the absolute volume decrease (Fig. 9.7).

The conception of expansive cement technology is based upon such swelling increase of the paste[2] which equilibrates or is exceeding the drying shrinkage (Fig. 9.7). Two types of these cements are distinguished: the shrinkage compensating, if the absolute volume change is close to zero, and the expansive, in which the absolute volume change is positive.

In order to increase the swelling of concrete during the maturing in water the advantage is taken of the reactions causing the volume increase. Several such reactions are known, but the most important, from the practical point of view, are two of them: the formation of ettringite and the formation of portlandite. Among the other, well known the formation of brucite should be mentioned:

$$MgO + H_2O \rightarrow Mg(OH)_2 \tag{9.7}$$

There are the other reactions or processes linked with volume increase of the mixture, in which they proceed. Some of them are mentioned in Chap. 5. For many reasons these reactions cannot be used in the production of expansive cements.

The reaction of ettringite formation is the most important because it is very easy influence on the rate of this phase formation, by changing the composition of cement and thereby the liquid phase composition.

These advantageous properties do not show calcium and magnesium oxides, which hydration rate depends primarily on the reactivity of initial substrates phases towards water. Their reactivity is primarily the function of burning temperature

[2] The concrete volume increase is directly dependent of the cement paste volume change.

and the fineness of oxides. The calcination temperature influence the oxide crystal growth (recrystallization), with the reduction of their porosity [38]. It is difficult in practice to maintain the constant properties of oxides and hence CaO can be only an auxiliary factor, raising the volume increase linked with ettringite formation [39].

The technology of expansive cements which would produce bursting of the paste after relatively short time of hydration, usually not exceeding 24 h, is a special problem. There are cements used in loosening of the rock blocks, applied in manufacturing of large stone plates for buildings facade, giving a decorative architectural effect. As it is known, the rock blocks producing with explosives causes the cracks formation and large part of material are lost. Such expansive cements can be useful in demolishing of old concrete building in the vicinity of the other buildings or in every cases where the use of explosives in not possible. These expansive cements could be based on ettringite formation, but in this case the use of calcium oxide, which gives rapid increase of expansion and higher tensile stresses, is more favorable. This CaO is hardly burned, and produced in shaft kilns with coke as fuel. The properties of CaO can be determined, according to the PN–EN 459–2 Standard, by measuring of t_{60}, it means the time after which the lime slaked in Dewar vessel attains the temperature of 60 °C. The lime which t_{60} is equal 20 min, or at least is over 15 min can be used. The addition of lime is high, on the level of 40 % and Portland cement should have very rapid strength development, during the first 12 h. The accelerators of hardening, for example $CaCl_2$, can be used.

The expansive reaction occurring in classic expansive cements should be adjusted to the paste properties; in the plastic paste the volume changes are accumulated and the swelling will not occur, only the plastic deformation of material takes place. On the other side the paste should reveal some deformability, to be adapted to the limited volume increase without greater cracks. In practice, in the case of Portland cement matrix it means that the expansive reaction should occur principally between 24 and 72 h of paste hardening. The earlier processes will not contribute to the volume increase of concrete, but the reactions occurring after 72 h should show the decreasing tendency. The paste volume stabilization should be achieved after about 190 h; otherwise the deterioration or at least weakening of concrete will be expected.

During the further continuation of cement hydration, the macropores formed as a result of swelling will be filled gradually with the colloidal phases: with C–S–H in the case of Portland cement and with AH_3 in the case of calcium aluminate one, and the porosity of concrete will decrease.

The strength development and volume increase with time for expansive cement of good quality (a) and for cement, which was destructed due to the retarded swelling (b) are shown in Fig. 9.8 [40].

The production of expansive cement in the industrial scale was initiated by Lossier in the thirties of XX c, in France; the technology was based on the ettringite formation [41]. The expansive cement technology was significantly developed by Klein, who proposed in 1966 to apply the calcium sulphoaluminate, as a source of aluminum ions [42]. This technology is the most popular in the world till now.

The $C_4A_3\overline{S}$ phase is identical with the naturally occurring mineral haüynite, first synthesized by Rogozina [43]. This compound is a stable phase, which is formed in the system $CaO–Al_2O_3–SO_3$ at temperature range 1,250–1,300 °C and

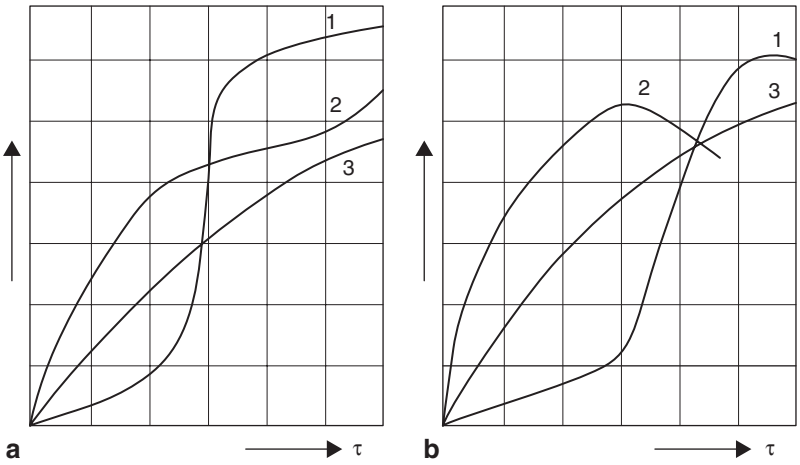


Fig. 9.8 The changes of: 1 expansion, 2 compressive strength, 3 self–tensioning of paste as functions of time. (according to [40])

is decomposed at 1,350 °C. $C_4A_3\overline{S}$ is usually one component of expansive clinker, together with belite, brownmillerite, some amount of anhydrite and free CaO. In practice the expansive additives of different composition are used; the details of their composition are known only to the producers. The sulphoaluminate (Klein's compound) and anhydrite may constitute such a material. Kondo et al [44] studied the structure of $C_4A_3\overline{S}$ phase and proved their affinity to haüynite: $(Ca_2Na_6)[Si_6Al_6O_{24}](SO_4)_2$. In the $C_4A_3\overline{S}$ phase there is a continuous network of $[AlO_4]^{5-}$ tetrahedra and separated $[SO_4]^{2-}$ tetrahedra. The calcium ions have an irregular coordination with the number of 8 [44] (Fig. 9.9).

Various aluminate phases can be used as a source of aluminate ions in reaction of ettringite formation. From the practical point of view the two anhydrous phases: $CaO{\cdot}Al_2O_3$ and $3CaO{\cdot}3Al_2O_3{\cdot}CaSO_4$, as well as the calcium aluminate hydrates, are the most important. The two last one are usually the mixture of hexagonal hydrates, mainly C_2AH_8 and cubic C_3AH_6. They are produced as a result of calcium aluminate cement hydration.

All these phases react with the SO_4^{2-} ions to form ettringite, but some content of $Ca(OH)_2$ is necessary to avoid the formation of aluminum hydroxide:

$$CAH_{10} + 2Ca(OH)_2 + 3(CaSO_4 \cdot 2H_2O) + 14H_2O \rightarrow C_3A \cdot 3CaSO_4 \cdot 32H_2O \quad (9.8)$$

$$C_4A_3\overline{S} + 8C\overline{S}H_2 + 6CH + 37H \rightarrow 3C_3A3C\overline{S}H_{32} \quad (9.9)$$

The process of ettringite formation depends first of all on the liquid phase composition. This can be investigated basing on the $CaO–Al_2O_3–CaSO_4–H_2O$ system, from which it results that the ettringite is stable in a wide range of concentrations [45]. The liquid phase at temperature of 25 °C should contain at least 0.215 g $CaSO_4$,

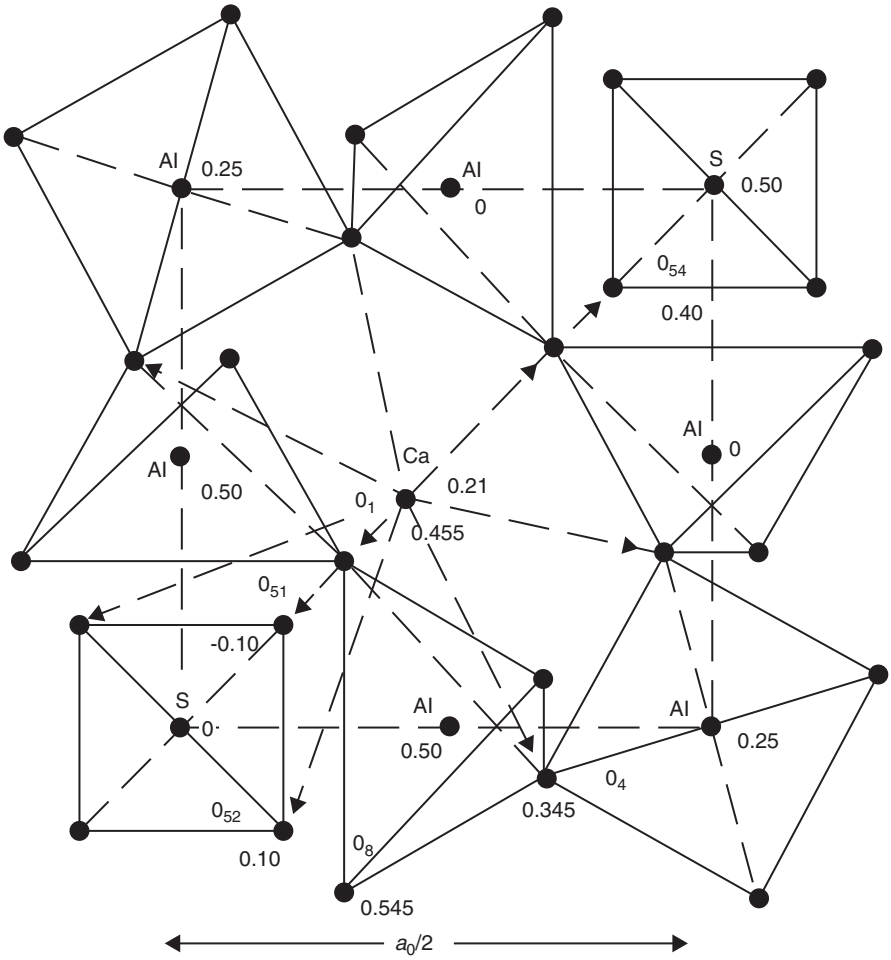


Fig. 9.9 Positions of atoms in $a_0/2$ of $Ca_8Al_{12}O_{24}(SO_4)_2$ unit cell projection on the 001 plane. (according to [44])

0.043 g CaO and 0.035 g Al_2O_3 per liter. $C_3A{\cdot}3CaSO_4{\cdot}32H_2O$ dissolves incongruently in water producing the AH_3 gel and the liquid phase with the composition given above. From the equilibrium system it results that at temperature of 25 °C ettringite dissolves congruently in the solution containing 0.027 g CaO per liter and it is stable until the CaO concentration 0.15 g/l, while at higher calcium hydroxide concentrations is in equilibrium with another solid, that is with C_3AH_6.

As it was shown by Mehta [46], the rate of ettringite formation in the mixture of anhydrous calcium aluminates, calcium hydroxide and gypsum was the highest in the case of CA. The reaction in the mixture with $C_4A_3\overline{S}$ was slower, while the reaction of C_3A was hampered, because of the impermeable ettringite layer formation (see Sect. 3.3). The $C_{12}A_7$ is also not a good source of ettringite, because it reacts

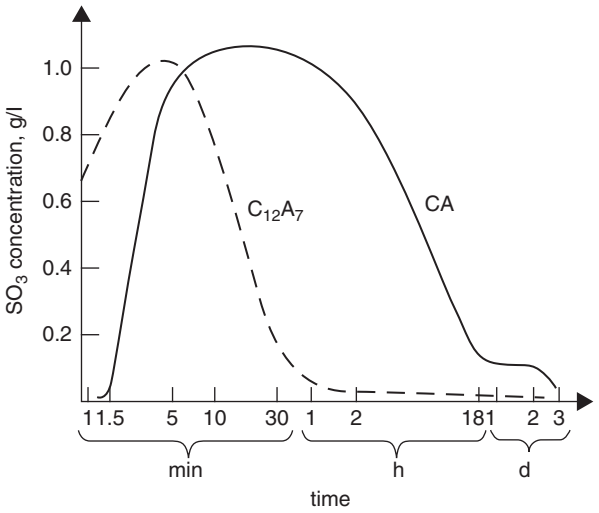


Fig. 9.10 Gypsum bonding during CA and $C_{12}A_7$ hydration. (according to [47])

rapidly with water and setting process cannot be controlled, even at very high gypsum addition (Fig. 9.10) [47].

The rate of CA and $C_4A_3\overline{S}$ reaction is advantageous also in the light of earlier remarks, because these phases are hydrated completely during the 72 and 180 h respectively. This rate is reduced at $Ca(OH)_2$ addition, while at no calcium hydroxide, in the presence of gypsum only, it is higher (Fig. 9.11) [46]. The retarding effect results from the crystallization degree of ettringite. As it was proved by Mehta [48], in the presence of CH, in the solution saturated with calcium ions the colloidal forms of ettringite were produced. Similarly, Xue et al. [49] observed the formation of very fine ettringite crystals, not exceeding 1 μm, in saturated calcium hydroxide solutions.

Retardation of hydration process augments with the C/A ratio of the anhydrous clinker phase; that is in order: $C_3A > C_{12}A_7 > C_4A_3\overline{S} > CA$ [50]. According to Bonin and Cariou [50], when the composition of mixture corresponds to the calcium monosulphoaluminate formation, the hampering of reaction is not observed. The formation of $C_3AC\overline{S}H_{12}$ occurs rapidly and some amount of ettringite formed on the beginning of reaction, does not affect the kinetics. However, low retarding effect is occurring in the case of AH_3 formation, as it was mentioned in Sect. 9.1.

Chatterji [51, 52] puts forward several times the hypothesis that the sulphate expansion is caused by monosulphate formation. However, the results reported by Alunno Rossetti et al. [53] disprove this hypothesis; the compacted $C_4A\overline{S}H_{12}$ and $C\overline{S}$ mixtures revealed high expansion due to the ettringite formation.

Apart from the reaction of ettringite formation, the CaO and MgO are also applied as expansive components. The technology with CaO application, is more developed, particularly in Japan. In order to avoid the unfavorable properties of CaO, due to its rapid or retarded hydration, the methods consisting in the anhydrite or C_3S mixture manufacturing, as the matrix with calcium oxide inclusions, were developed. Dissolution or hydration of the matrix causes the gradual exposure of CaO crystals, which then can react with water. Kawano et al. [54] invented the

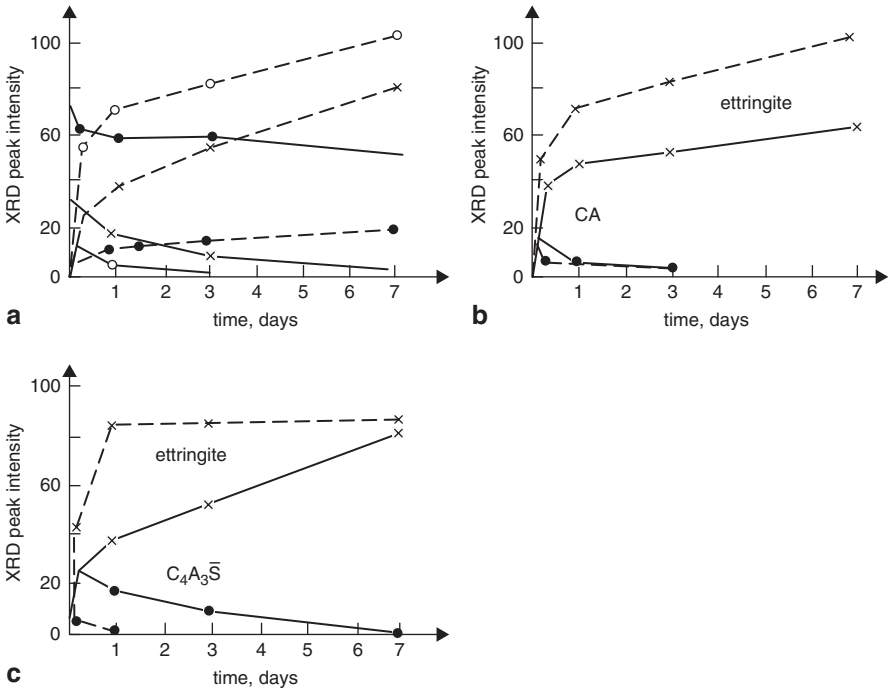


Fig. 9.11 Rate of ettringite formation (*dashed lines*) and decrease of initial phase content: **a** CA (*bright circles*), $C_4A_3\overline{S}$ (*crosses*) and C_3A (*black circles*) in the gypsum and lime containing pastes. **b** CA with gypsum without lime (*dashed line*) and with lime (*continuous lines*). **c** the same for $C_4A_3\overline{S}$. (according to [46])

technology in which the limestone, clay and anhydrite are sintered together. Composition of the sinter is as follows: alite—38 %, CaO—44 to 47 %, $CaSO_4$ 6 to 10 %. CaO occurs mainly in the form of 10–30 μm inclusions in the large 100 ÷ 900 μm alite crystals. The similar additive composed of fine CaO crystals dispersed in the alite or anhydrite matrix is patented [1]. The methods of CaO based expansive cements manufacturing are given by Pollitt and Brown [55], Allen [56], Collepardi [57] and Daugherty [58]. The expansive component synthesized by Collepardi [57] is composed of CaO and MgO.

Mehta [59] developed the method of expansive cement production, containing MgO grains. In order to obtain good expansion magnesite should be decarbonated 1 h at temperature of 900 ÷ 950 °C and the size of MgO grains should exceed 300 μm. The addition of such prepared expansive agent should be 5 ÷ 10 % by mass of cement.

The expansion mechanism has been the subject of numerous studies for many years. It is caused by the known contradiction consisting in the lowering of absolute volume of the system, due to ettringite or other hydrates formation; this problem is discussed in Chap. 5. The oldest hypothesis was presented by Lafuma [60], which already in 1929 suggested that the formation of ettringite as a result of reaction in the solid state (topochemical reaction) will cause expansion, while occurring

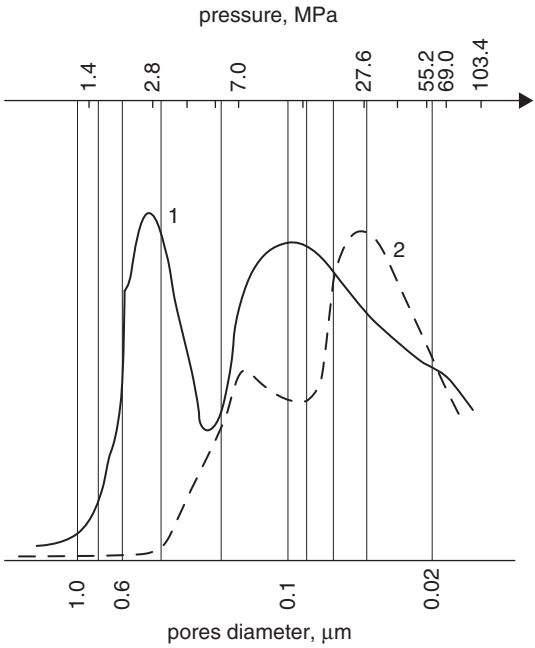


Fig. 9.12 Pore size distribution in the expansive (1) and Portland cement (2) pastes. (according to [1])

"through the liquid phase"—will not. It merits the remark that this hypothesis has been presented up to now [61].

From many reports, first of all presented by Mehta [62, 63], the opinion was preserved that ettringite is formed by the crystallization from the liquid phase. Therefore the hypothesis of Lafuma lost much of its actuality.

The four hypotheses are the most frequently proposed to explain the expansion mechanism:

1. crystallization pressure resulting from the anisotropic crystals growth,
2. "*in situ*" hydration of unhydrous phase with the formation of hydrated phases,
3. absorption of water by colloidal ettringite,
4. osmotic pressure formation.

The hypothesis of crystallization pressure is based on the well known phenomenon of anisotropic crystal growth in certain direction which develops significant tensile stresses. This hypothesis is proved in the studies of gypsum hemihydrate hardening [64, 65]. The swelling linked with crystallization is well known in ceramics [66]. The crystallization pressure can found its natural explanation in the needle morphology of ettringite crystals, which form the radial placed spherulite units.

The hypothesis of crystallization pressure finds also justification in the higher porosity of expansive cement paste in the range of macropores, from 0.2 to 0.8 μm, typical for ettringite formation. These pores appear in the paste after 1 day of hardening, but they are not found in the classic Portland cement paste (Fig. 9.12). Expansive cement pastes are distinguished by generally higher porosity than the Portland cement pastes. However, one should underline that the expansive cements of good

quality show the porosity decrease of the pastes with time, caused by the increasing amount of gel products, filling the capillary pores. These products are C–S–H and AH_3, in the case of Portland and calcium aluminate cement pastes respectively.

The hypothesis related to the crystallization pressure is proved by very well known high susceptibility to crystallization of portlandite and ettringite, which are very easy detected and quickly formed crystalline phases of cement paste. The results reported by Chatterjee and Jeffery [67] seem to comply well with this hypothesis and show that the $Ca(OH)_2$ crystallization causes the repulsion of grains; the growth of pores and the formation of the new one is thus promoted.

There were some other works supporting the crystallization hypothesis. Ogawa and Roy [68] examined systematically the microstructures of pastes and found the irregularly distributed ettringite crystals around the $C_4A_3\overline{S}$ grains at early age of hydration. However, in later age the ettringite crystals were growing radially from the sulphoaluminate particles and the reaction zone became more consolidated. The change of ettringite crystals orientation from the random distribution to the radial one is, according to the authors [68], an important stage in the process of expansion initiation. Alunno Rossetti [53] observed the formation of consolidated ettringite crystals around the monosulphoaluminate grains; the thickness of this layer was increasing. These crystals fill the voids in the paste and initiate swelling, as a result of mutual "pushing out". This explanation is almost identical with previous model presented by Bentur [69] and Chatterji [67] (Fig. 9.13).

Rossetti [53], as well as Chen [70] found that the electrokinetic potential of ettringite crystals increased markedly in the saturated calcium hydroxide solutions. These authors are stating that, apart from the crystallization pressure, the growth of electrokinetic potential causing the repulsion forces, contributes to the expansion. This can also explain the advantageous CaO addition effect on the expansion increase [39]. Ettringite formation from $C_4A_3\overline{S}$ is rapidly consuming calcium hydroxide and the CH concentration in the solution decreases. When CH is added, the constant supersaturation of the solution can be maintained.

Wang Shanba [71] studied various mixtures in which ettringite was produced and concluded that the crystallization pressure, attributed to the growth of ettringite crystals was the decisive factor.

Clastres and Murrat [72] found the correlation between the expansion and the growth of ettringite content, as determined by DTA (Fig. 9.14). On the other side the expansion is increasing after the calcium sulphate consumption. Therefore the authors [72] are of the opinion that this process is in agreement with hypothesis proposed by Mehta [73]; in this hypothesis the expansion occurs due to the water absorption by the colloidal ettringite.

The weak side of the hypothesis of crystallization pressure is the well known phenomenon that crystals growing in the supersaturated solution cannot exert a pressure when the other crystals can grow free, with no obstacles. To elucidate this discrepancy the hypothesis explaining the expansion as the effect of *in situ* hydration of anhydrous phases was proposed. It is assumed that the crystals of anhydrous phase are surrounded by the colloidal hydration products. The solution of electrolyte can migrate through the pores in colloidal gel to the surface of anhydrous phase, but there is no empty space for the crystallization of hydrates formed. The

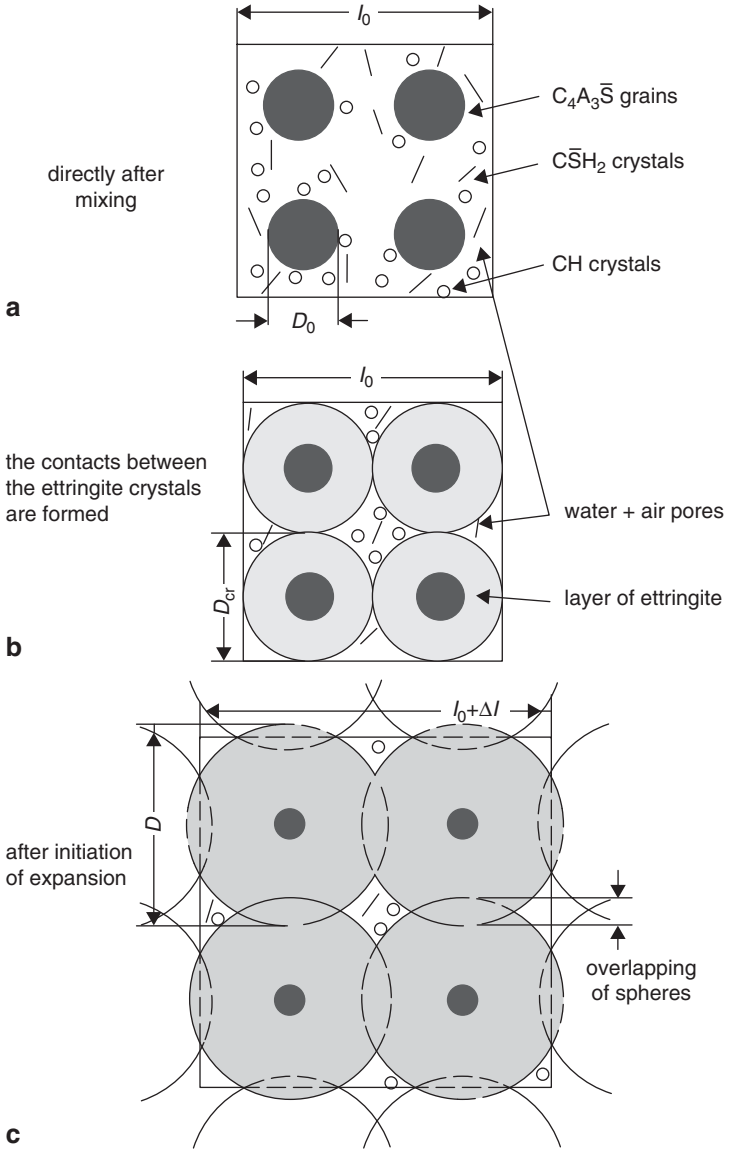


Fig. 9.13 Model of expansion (according to [69]): **a** directly after mixing with water. **b** the contacts between the ettringite crystals are formed. **c** after initiation of expansion

hydrates have always many times greater volume than the anhydrous phases. For example the transformation of CaO to $Ca(OH)_2$ is accompanied with the 95 % volume increase, C_3A and $C\bar{S}H_2$ reacting to $C_3A{\cdot}3CaSO_4{\cdot}32H_2O$ give 132 % increase. Thus the *in situ* transformation of anhydrous phase into the hydrates causes the significant stresses leading to the increase of material volume. The local hydration

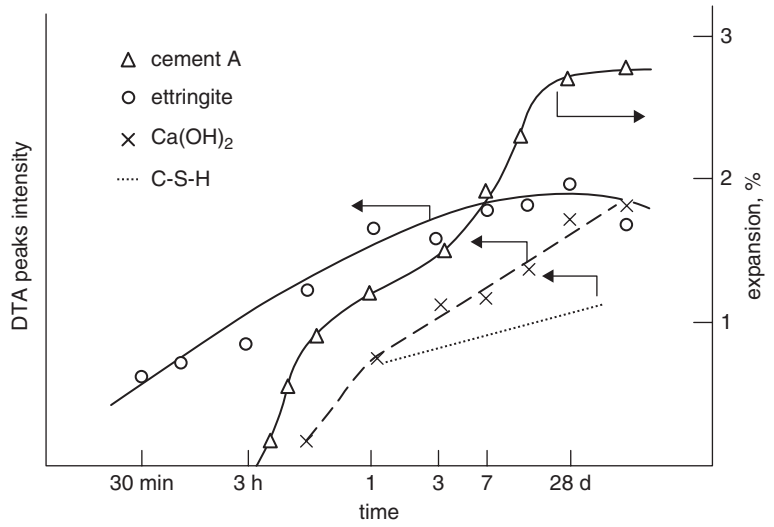


Fig. 9.14 Expansion as a function of ettringite content. (after [72])

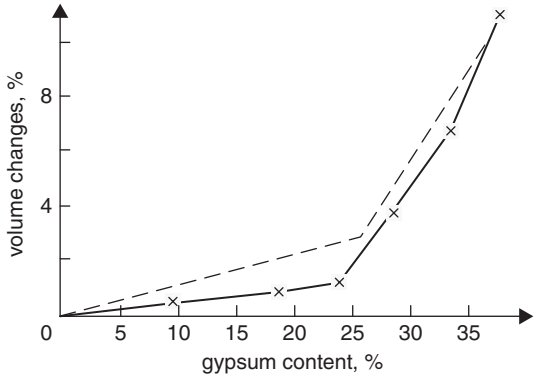


Fig. 9.15 Expansion of calcium aluminate cement and gypsum mixture: measured (*continuous line*) and calculated (*dashed line*). (according to [76])

of unhydrous grains leads to swelling, irrespectively of the crystallization degree of formed hydrated phases. The *in situ* transformation as mechanism of expansion was proposed by Mather [74] and Hansen [75].

A important experimental support of *in situ* hypothesis was presented by Cottin [76]. The mixture of calcium aluminate cement and gypsum is hydrating with too low water content. The change of volume calculated from the phase composition of the paste corresponds very well to the measured value.

In the late seventies Mehta [73] proposed the expansion hypothesis assuming that the negatively charged colloidal ettringite particles of high specific surface area attract water dipoles, which surrounding the crystals, are inducing the repulsive forces—presumably linked with the double layer. It caused the general paste vol-

ume increase. Simply, water is absorbed by the colloidal ettringite composed of small hydrophilic crystals and, as a consequence, swelling is observed. According to Mehta [73] access of external water is necessary to initiate the expansion of colloidal ettringite. In order to verify experimentally this hypothesis, Mehta [73] assured the total hydration with ettringite formation of the mixture of $C_4A_3\overline{S}$, gypsum and lime. The conditions of hydration prevented the mixture against the loss of water and carbonation. The ettringite formed was then exposed to the action of water and the volume change was measured after different period. On the other side Collepardi [77] found that the access of external water is not necessary for expansion, however, in the closed system the expansion is lower [77]. The hypothesis proposed by Mehta was proved in the studies of corrosion process, in which the formation of cracks was linked with the occurrence of compact, amorphous ettringite, undetectable by XRD [78]. There is a common opinion that the higher expansion of paste is linked with the fine, colloidal ettringite crystals formation in the saturated calcium hydroxide solutions [79]. At lower saturation with lime compounds ettringite occurs in the form of larger crystals, mainly in pores, far from the calcium aluminate grains surface.

Dron and Brivot [80] prepared the tablets of ground ettringite pressed under the pressure of 50 MPa, with low porosity, of about 17%. The tablets treated with water do not practically swell—swelling is on the level 0.4%, while *in situ* ettringite formation from calcium sulphoaluminate gives the volume increase of 40% and the destruction of samples. The authors [80] state that the Mehta hypothesis is not valid and the crystallization pressure is the cause of expansion. Simultaneously Dron and Brivot [80] calculated the approximate crystallization pressure based upon the change of free enthalpy of reaction:

$$C_4A_3\overline{S} + 6CH + 8C\overline{S}H_2 + 74H \rightarrow 3C_6A\overline{S}_3H_{32} \tag{9.10}$$

Yamazaki and Sakakibara [81] measured the pressure of expansion associated with the CaO hydration. The force of expansion achieved after 4 h the value close to 9 kN. The authors [81] state that the expansion is caused by the increasing thickness of the hydrate shells, formed on the larger CaO grains. As one could presume, the porosity of samples increases with expansion.

The last hypothesis, supported by many authors, is assuming that the osmotic pressure is the cause of expansion [82]. The semi–permeable membranes of hydration products are formed around the unhydrated grains, through which the ions migrate from the solution to the surface of these grains, which causes the substantial differences of concentration from both sides of the membranes. The osmotic pressure resulting from the concentration gradient can attain the values exceeding 50 MPa [83, 84]. This hypothesis has been developed to explain the concrete destruction mechanism due to the alkali–aggregate reactions (see Chap. 6).

One should remember that the crystallization pressure will depend on the supersaturation of solution in relation to ettringite. It can be expressed by the following formula:

$$P = \frac{RT}{V} \ln \frac{K}{K_S} \tag{9.11}$$

where P is the pressure, in MPa; T is the temperature in K, R—the gas constant (8.3 $J \cdot K^{-1}$ $mole^{-1}$), V—the volume of one mole (m^3 $mole^{-1}$), K/K_S—the supersaturation degree given as the activity of ions ratio. The precipitation of ettringite can be given by the following equation:

$$6Ca^{2+} + 2Al(OH)_4^- + 3SO_4^{2-} + 4OH^- + 26H_2O \rightarrow C_6A\bar{S}_3H_{32} \tag{9.12}$$

The solubility product will be as follows:

$$K = Ca^{2+6} \cdot AlOH_4^{-2} \cdot OH^{-4} \cdot SO_4^{2-3} \tag{9.13}$$

For example, for $K/K_S = 2.4$ P = 3 MPa.

Recently, Sherer [85] analyzed in details the formation of crystallization pressure, arriving to the conditions in which this pressure can be high. From this analysis it results that these conditions are fulfilled when the pore diameter does not exceed 100 nm and the growing crystal is of similar size. In these conditions the propagation of microcracks of similar diameter can occur. Taking into account the supersaturation equal 3.0 as calculated by Damidot and Glasser [86], Sherer [85] calculated the tensile stress on the level of about 6 MPa. This is the serious arguments supporting the hypothesis of crystallization pressure as the cause of expansion.

During the seminar dedicated to the sulphate corrosion mechanisms Brown and Taylor [87] analyzed the hypotheses dealing with ettringite expansion. At first they discussed the hypothesis of Lafuma [60] assuming the topochemical reaction *in situ*, without any passage of ions through the solution. Apart from the commonly accepted view that ettringite is crystallizing from the solution, the substantial difference between the C_3A and ettringite structures are against this hypothesis. Therefore this hypothesis has been rejected by Brown and Taylor [87]. In Mehta [73] hypothesis it was suggesting that the small ettringite crystals of colloidal size imbibed water and thereby caused expansion. Generally imbibition of water and resultant swelling involve gel–like materials of indefinite composition, which have the flexibility to expand without breaking. This features cannot be attributed to ettringite. Therefore three possibilities might be considered [87]:

- separate ettringite microcrystals attract water to their surfaces,
- aggregates of ettringite crystals similarly attract water (or in this case, imbibe),
- ettringite crystals take up water internally.

None of these hypotheses were verified experimentally [87]. The specific surface area of ettringite crystals is much lower than the surface of C–S–H and the latter one does not shows swelling [87]. Finally, there is no room for more water in the crystal structure of ettringite (there are 26 molecules in the structure) [87].

However, according to Brown and Taylor [87] there is the possibility to “reverse” the phenomenon of local drying, that is to modify Mehta hypothesis. Formation

of ettringite entails the incorporation of a substantial portion of water into a solid product. If this water cannot be supplied rapidly enough from an external source then ettringite is formed in a partly dehydrated condition; expansion occurs when it subsequently takes up water from external source. As it is known, ettringite can be easily dehydrated from 32 to 12 water molecules with simultaneous reduction of unit cell parameters *a* and *b* from 1.12 to 0.84 nm, however, the crystallinity normally deteriorates greatly. Brown and Taylor [87] admit even a variant that ettringite takes some of its water from the surrounding C–S–H and the expansion occurs when the later regains its water from the external source. Finally, these authors [87] summarize their considerations and conclude that the further studies are necessary. However, they comply with the crystallization pressure.

Taylor [88] pointed out that the ettringite formation would not result in expansion and it depends on the conditions in which the process occurs. For example a high amount of this phase is produced in the hydrated supersulphated cement paste and expansion is not occurring. Therefore the problem of "good" and "bad" ettringite appeared [88]. pH of the liquid phase in the paste is of main importance; this is provided first of all by the calcium hydroxide. Addition of lime to the belite–sulphate cement change the properties of this binder, transforming it into the expansive cement. According to Taylor [89] the problem must be analyzed in the microareas in which the aluminate $Al(OH)_4^-$ ions diffusion can occur. Their concentration in the liquid phase is low; if the concentrations of the other ions necessary for ettringite formation will be high, then the aluminate ions cannot diffuse on larger distance from the solid phases being their source (C_3A, $C_4A_3\overline{S}$). In the case of saturated calcium hydroxide solution these conditions are fulfilled and ettringite is formed in the region of high supersaturation, near the sources of aluminate ions. Therefore the crystallization pressure can be high. At shortage of $Ca(OH)_2$, aluminate ions diffuse on larger distances, to the areas where the supersaturation is low, and the crystallization pressure will be low too [89].

The progress of works on the development of expansive cements technology allowed the better understanding of the factors influencing expansion. The most important are as follows:

- phase composition of cement,
- reactivity of components.

These two factors affect the composition of the liquid phase, which plays a decisive role in the ettringite formation process. The fineness of calcium aluminate, added as expansive agent, improves the expansion because its reactivity with water is enhanced. There is no difference between gypsum and anhydrite II. In the case of the latter the secondary gypsum is detected in the M type cement [90]. High CA fineness is advantageous, and it is not a problem, because of its good grindability. $C_4A_3\overline{S}$ shows similar properties and these two components can be co–ground with the Portland cement clinker.

In Fig. 9.16 the effect of fineness of Portland cement and calcium aluminate cement added as expansive component, is shown [90]. The specific surface area increase of Portland cement has a disadvantageous influence, because its rapid

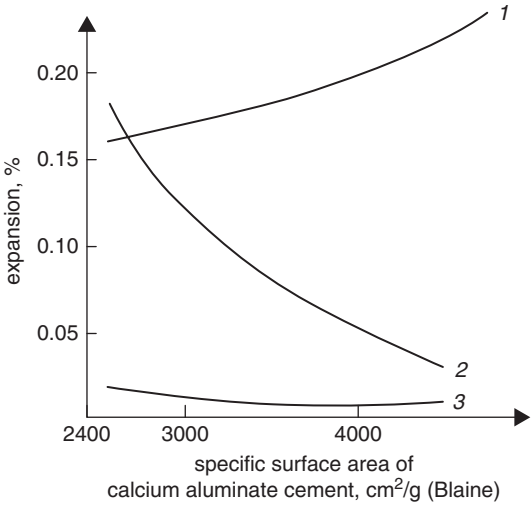


Fig. 9.16 Effect of fineness of expansive cement type M two components on expansion. (according to [90]). The Blaine specific surface area of Portland cement: *1* 2,600 cm^2/g, *2* 3,300 cm^2/g, *3* 4,500 cm^2/g

hardening restricts the expansion. The low alkali and C_3A contents in Portland cement are important too. At high alkali content the Ca^{2+} ions concentration is reduced, which has the negative effect on the formation of ettringite. C_3A is always a potential swelling possibility, after a longer period; it is difficult to control this effect. Gaspar [90] paid an attention to the positive role of CO_2, because carbonation is increasing expansion.

Cohen and Mobascher [91] has presented the interesting studies, aimed in the determination of the best proportions of Portland cement, Klein complex and gypsum in the expansive cement type K. These authors concluded that the ratio of $CaSO_4$ available to $CaSO_4$ required to produce ettringite should be in the range between 65 and 70 %. They found simultaneously that in the case of reinforced concrete from expansive cement, the expansion should occur between the fourth and seventh day.

The effect of expansive cement phase composition on its properties of was widely studied by Szeląg [92]. This author proved the significant role of the gypsum/Klein complex and gypsum/CA ratio; the properties of expansive cements can be controlled by changing these proportions. As higher gypsum/Klein complex or gypsum/CA ratio as higher expansion and stresses generated in the mortar (Fig. 9.17) [92].

Expansion is highly dependent on the curing conditions, because they have an impact on the reaction of ettringite formation, which consumes considerable water amount and its rate increases with temperature. Therefore the highest expansion is achieved when the concrete is cured in water, at temperature exceeding 25 °C [1].

Calcium oxide is an important component of expansive cements and all the authors are unanimous of its positive effect, causing expansion increase. The optimum free CaO content is 3–4 % in the K type expansive cement [93].

CaO addition is decreasing the ettringite quantity formed at early age, particularly during the first hours of hydration. Therefore the rate of ettringite producing phases with water at early age, when the paste is still plastic, is low. Lime addition is increasing expansion not only at early but also at later ages, until the process is completed (Fig. 9.18) [39, 93, 94]. At CaO addition to cement the calcium ions

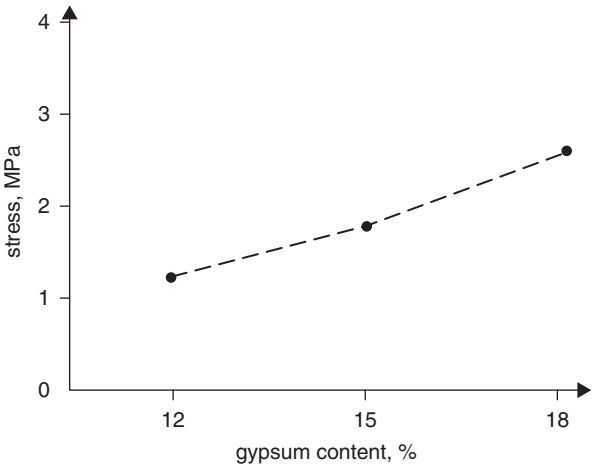


Fig. 9.17 Stresses generated in the expansive cement mortar with 8 % Klein complex of specific surface area equal 300 m^2/kg, lime content—5 %, cement of specific surface area of 250 m^2/kg. (according to [92])

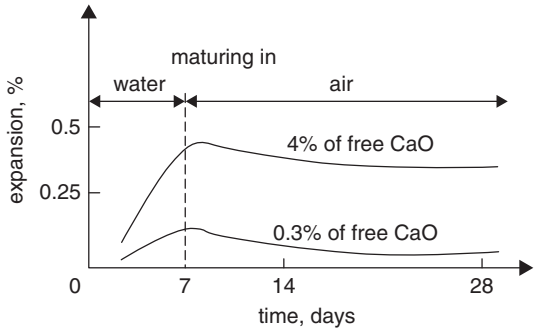


Fig. 9.18 Effect of free CaO content on the K type cement expansion. (according to [93])

concentration in the liquid phase is noticeably higher (Fig. 9.19), which shows that the calcium hydroxide released by alite hydrolysis does not compensate the rapid Ca^{2+} ions consumption for ettringite formation from the calcium sulphoaluminate. It is possible that at later age CaO contributes directly to the expansion increase, through the formation of calcium hydroxide [58]. According to Thiel [93], this can be proved by increasing expansion of pastes as the temperature of the lime admixture burning is higher (Fig. 9.20).

As aforementioned, the expansion is dependent on the paste curing conditions, because ettringite formation is consuming considerable water amount and its rate increases with temperature. Therefore the stability of ettringite in the paste at higher temperature and at drying condition is very important. The instability of this phase during thermal treatment or concrete drying would exclude the possibility of applying expansive cements in the conditions. This problem is related to the structure and stability of ettringite, especially with the conditions in which the release of crystallization water occurs.

The structure of monoclinic ettringite was determined by Taylor and Moore [95]. This is formed of columns of empirical formula $\{Ca_3[Al(OH)_6]\cdot 12H_2O\}^{3+}$, parallel to the *c* axis. There are the channels between the columns with SO_4^{2-} ions and other

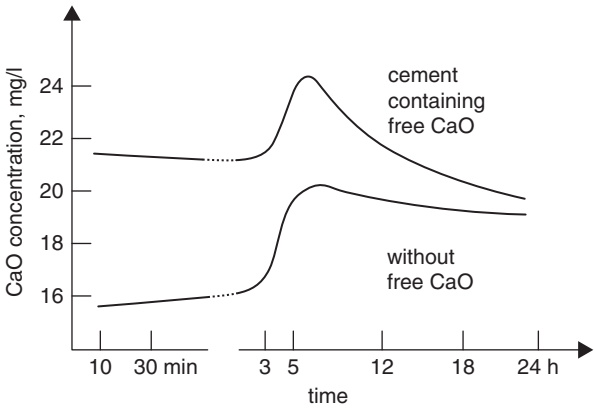


Fig. 9.19 Concentration of calcium hydroxide in the liquid phase of paste as a function free CaO in the K type expansive cement. (according to [93])

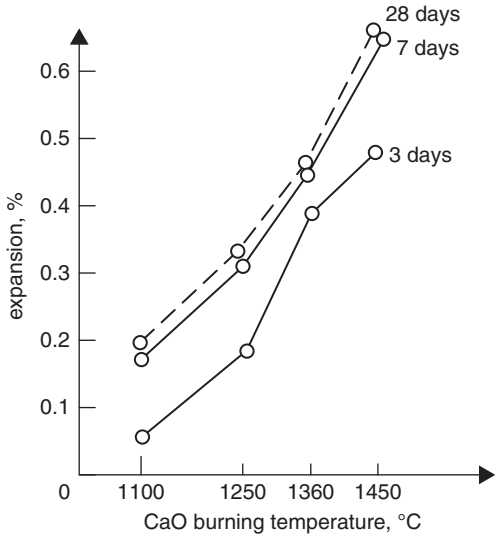


Fig. 9.20 Effect of temperature of the lime admixture burning on the K type cement expansion. (according to [93])

H_2O molecules (Fig. 9.21). Per two units („molecules" according to formula) forming the columns the channels contain four sites, of which three are occupied by SO_4^{2-} ions, and one by one or two water molecules, giving the structural formula:

$$\{Ca_6[Al(OH)_6]_2 \cdot 24H_2O\}[3SO_4](2H_2O)$$

corresponding to the chemical formula: $C_3A{\cdot}3CaSO_4{\cdot}32H_2O$

In Fig. 9.22 the structure of one unit of column is shown, in which the periods of identity along the *c* axis is 1.07 nm [96]. As it results from the structural formula, the Al coordination number is 6, while calcium is surrounded by 8 groups: 4OH and $4H_2O$ (edge–sharing of neighbors octahedra). The SO_4^{2-} ions can be substituted by OH^-, CO_3^{2-}, or even by $H_2SiO_4^{2-}$, while the Al^{3+} ions by Fe^{3+}. It gives the variable composition of ettringite, often designed as AFt phase.

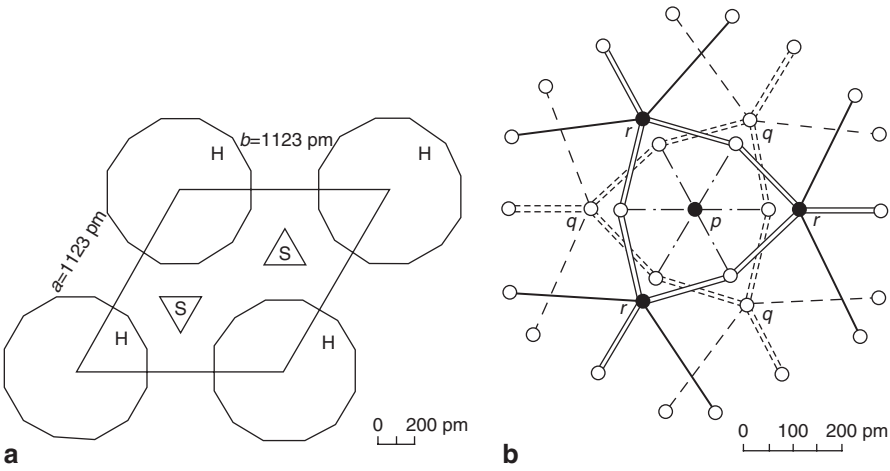


Fig. 9.21 Crystal structure of ettringite (according to [95]): **a** projection along the *c* axis: columns (*H*) and tetrahedra SO_4^{2-} (*S*). **b** details of column structure: *p*—Al^{3+} ions at $z=0$ and 1/2 (superposition), *q* and *r*—Ca^{2+} for $z=1/4$ and ¾ respectively. *Empty circles*—OH^- ions coordinated around Al^{3+} ions or Ca^{2+} ions or water molecules coordinated only with Ca^{2+} inside the column. Ca—O bond at $z=1/2$ plotted with *continuous lines*; at $z=-1/2$ with *dashed lines*. All the coordinates *z* are given as a fraction of the pseudo–cell height (4,072 pm)

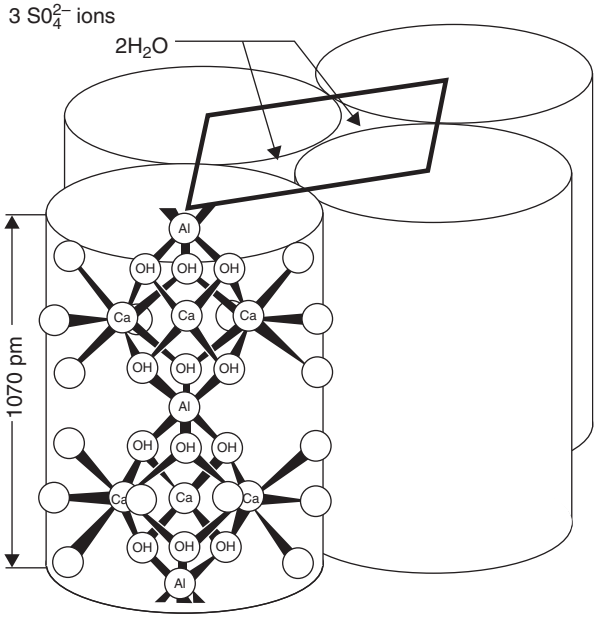


Fig. 9.22 Structure of one unit of ettringite column. (according to [96])

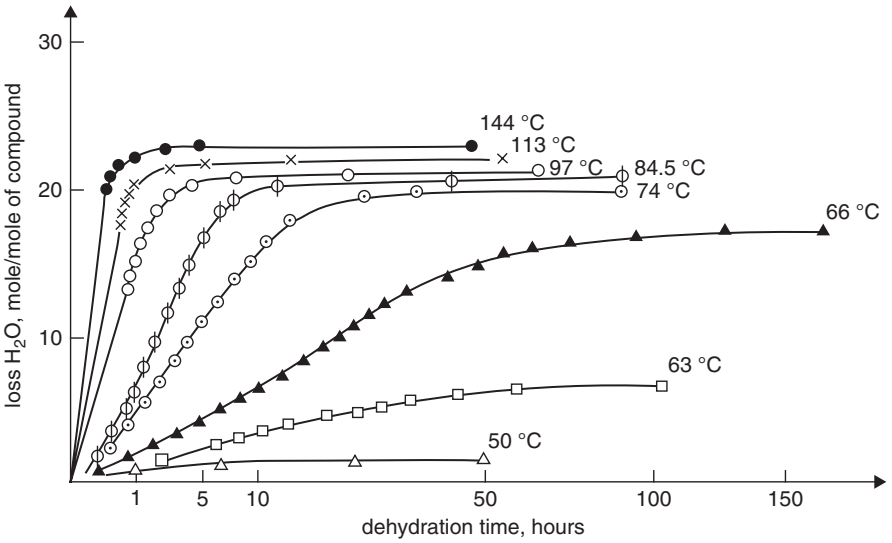


Fig. 9.23 Dehydration of ettringite in isothermal conditions in air under normal pressure. (according to [103])

Mehta [97] established that the synthetic ettringite is stable at temperature of 65 °C in dry atmosphere. However, in the air of RH close to 100% ettringite does not change even at temperature of 93 °C. The similar results were obtained by Satava and Veprek [98], who found that ettringite is decomposing in the saturated water vapour atmosphere at temperature of 111 °C to form $C_4A\bar{S}H_{12}$ and $C\bar{S}H_{0.5}$. Ludwig [99] and 4 years later Skoblinskaya and Krasilnikov [100] obtained the water vapour desorption isotherms and XRD patterns of ettringite. Ludwig [99] found that the crystal structure of ettringite did not change, in degree, which can be found by XRD, up to 12% RH. At this RH level ettringite releases 10 water molecules. Berman and Newman [101] found also that the XRD pattern did not change after releasing by ettringite of 9 H_2O. Finally, Mehta and Klein [102] did not observed any changes on the ettringite XRD pattern after this losses 15 water molecules.

Ludwig et al. [103] reported in 1980 the additional data relating to the dehydration of ettringite (Fig. 9.23). At temperature range 45–50 °C ettringite looses 1.4 H_2O molecule, at temperature range 55–125 °C further 22 molecules and the residual 8 molecules at temperature above 146 °C. In the temperature range 160–180 °C the hydrate with 6 water molecules is stable. Dehydration product is maintaining the morphology of ettringite crystals and its porosity is 46%. It very easily undergoes carbonation.

Skoblinskaya and Krasilnikov [100] analyzed the desorption isotherms of water vapour lost by ettringite, on the basis of ettringite structure determined by Moore and Taylor. They found that the 2 water molecules, from 32, did not belong to the ettringite structure.

These two molecules are easily detached in the wide interval of vapour pressure; this is typical for the water molecules trapped by structural defects, as well as for adsorbed water. Therefore, there are 30 water molecules in ettringite structure.

In the first stage of dehydration ettringite looses 12 water molecules. The XRD studies do not reveal any change; however, the microscopic observations allow detection of two hydrates containing $30H_2O$ and $18H_2O$ respectively. 12 water molecules loss relates presumably to the calcium polyhedra, which are the additional apexes of trigonal prisms. During the second dehydration stage 12 following water molecules are released—at first the third one from the main apex of trigonal prism then after the last water molecule lives the calcium polyhedron and the number of water molecules is reduced to 6. When water molecules reach 16 the destruction of hydrate with $18H_2O$ takes place and the cubic crystal structure became decomposed. In the final third dehydration stage 12 hydroxyl groups strongly bound, are released.

Summarizing the data of these works it can be concluded that ettringite is stable in low pressure steam curing even at temperature of 90 °C. However, the autoclaving of paste leads to decomposition of ettringite as early as at temperature of 110 °C. In this condition the c monosulphate is stable in these conditions because it decomposes, in the saturated water vapour atmosphere at the temperature of 190 °C [98].

Ettringite can be unstable also in the conditions of the low pressure vapour heat treatment, if the sulphate content is not sufficient. This question was discussed in details in Sect. 6.4.3.

As aforementioned expansive cements produced industrially are based on the formation of ettringite. The technologies differ only with the type of calcium aluminates and of the matrix material. The types of expansive cements are shown in Table 9.3. Two types of matrix are used: Portland cement and calcium aluminate cement. The following phases are used as the source of aluminum ions: C_3A, CA (as calcium aluminate cement), $C_4A_3\overline{S}$ and the calcium aluminate hydrates: C_4AH_x or CAH_{10}. The second technology is the oldest one, and was implemented by Lossier in forties XXc [60].

Three types of expansive cements, based on the expansive reaction of ettringite formation, known as K, M and S cements are produced. In cement K the $C_4A_3\overline{S}$ phase, so—called Klein complex, is added as a source of aluminate ions, and matrix is composed of Portland cement. Cement M is produced as a mixture of Portland cement with calcium aluminate cement or aluminous slag and gypsum. Application of refractory cement Secar (Ciment fondu), with high aluminum content is recommended [90]. The 1.5 % of this cement addition is sufficient to obtain significant expansion. Finally, type S is composed of Portland cement with high C_3A content and gypsum addition.

To the separate subgroup belong cements, in which the untypical aluminous compounds are used: alunite[3] or aluminum sulphate. In the former USSR, in China and Bulgaria production of expansive cements, based on the natural [104] or calcined [105, 106] alunite was developed.

[3] Alunite—potassium–aluminum sulphate with the formula $KAl_3(OH)_6(SO_4)_2$.

Table 9.3. Expansive cements

Type of cement	Matrix–cement	Additives			Mixing of the components during grinding	Remarks
		Aluminates phases	Sulphates phases	Lime		
M	Portland	Aluminate Cement	Gypsum	-	Cement	Former USSR[a]
M	Portland	Alumina slag	Gypsum	+	Cement	Former USSR
K	Portland	$C_4A_3\overline{S}$[b]	Gypsum or gypsum + andhydrite	-	Cement	USA[c]
K	Portland	$C_4A_3\overline{S}$	Gypsum or gypsum + andhydrite	-	Concrete	Japan
S	Portland		Gypsum	-	Cement	USA
AlE*x*[d]	Calcium aluminate	C_4AH_{13}	Gypsum	-	Cement	Former USSR
AlE*x*	Calcium aluminate		Gypsum	-	Cement	Former USSR
AlE*x*	Calcium aluminate		Gypsum	-	Cement	China[e]
PE*x*	Portland	Alunite	Gypsum	-	Cement	Former USSR Bulgary
PE*x*	Portland	$Al_2(SO_4)_3$		-	Cement	Former USSR
PE*x*	Portland			+	Cement	Japan, CaO inclusions in C_3S and/or $CaSO_4$ matrix

[a] In former USSR expansive cements were divided into 3 classes: 20, 40 and 60; their potential of self–prestressing was 2, 4 and 6 MPa respectively, [b] Expansive clinker containing $C_4A_3\overline{S}$, Portland cement phases, CaO_{free} and anhydrite, [c] The first producer; nowadays this cement is manufactured in many countries; among them in significant amount in Russia, [d] AlE*x*—calcium aluminate expansive cements, PE*x*—Portland expansive cements, [e] Very similar to that patented by Lafarge

The second group consists of calcium aluminate expansive cements, in which calcium aluminate cement is a matrix and the source of aluminate ions. The latter one can originate also from the calcium aluminate hydrate C_4AH_x, added in the grinding process. Obviously, gypsum is the constituent of all these cements.

Finally, there is the third group of cements based on the expansive reaction of portlandite formation.

There are the three technologies of the K type cements production. Expansive clinker can be produced composed of alite, $C_4A_3\overline{S}$, C_4AF and $C\overline{S}$; however, it is not convenient because the calcium sulphoaluminate is decomposed in rotary kiln already at temperature of 1,350 °C. The better solution is to produce expansive

clinker composed of $C_4A_3\overline{S}$, C_2S, C_4AF, $C\overline{S}$ and C, burned at temperature of about 1,300 °C.

The raw mix for clinker production should contain some excess of gypsum, because the vapour pressure of $CaSO_4$ is higher than of $C_4A_3\overline{S}$ which decomposition is thus prevented. The presence of anhydrite in the clinker is not unfavorable, only lower amount of this compound must be added to the grinding process. Some amount of free CaO is beneficial too, as it was discussed earlier. The sulphate spurrite $(C_2S)_2C\overline{S}$ phase is sometimes produced at low temperature and at about 1,300 °C this phase decomposes [40]. At higher content of spurrite the expansive properties of clinker are reduced. The amount of $C_4A_3\overline{S}$ in clinker can be determined by XRD or by chemical method. This method consists in the extraction of the other clinker components with the solution of maleic acid in methanol and subsequent with the ammonium chloride water solution [107].

In Japan the expansive additive has the following composition: 15–20 % $C_4A_3\overline{S}$, 45–50 % $C\overline{S}$ and 20–30 % CaO. The belite content is low [62, 108, 109]. In the USA the clinker having the composition close to $C_4A_3\overline{S}$, with some amount of C_2S and C_4AF are produced [62, 63]. The composition can be highly variable, depending on the alumina–bearing raw materials.

Boikova et al. [110] examined the composition of sulphoaluminate clinkers. $C_4A_3\overline{S}$ can incorporate to 1 % MgO, 2 % SiO_2 and 3.5 % Fe_2O_3; moreover—0.5 % Na_2O, 1 % K_2O and 0.2 % TiO_2. This complies well with the data referring to the $C_4A_3\overline{S}+C_4AF$ mixture, in which the composition of ferrite phase changed toward the C_6A_2F in such a way that "the excess" of 3.3 % Fe_2O_3 formed solid solution with sulphoaluminate with the formula: $C_4(A_{0.979}F_{0.021})\overline{S}$ [111]. Much higher iron(III) ions content in the solid solution is reported by Ogawa and Roy [112].

Expansive clinker is ground together with Portland cement and gypsum or anhydrite. This technology has been applied, among the others, in the USA, former USSR and in Poland. In Japan expansive additive is ground separately and delivered as a commercial product, mixed with Portland cement in the concrete mixture manufacturing.

Various type of expansive cements: M, K and with calcium aluminate cement matrix, were produced in former USSR [40, 47, 113]. The two M type cements were produced: SCT—waterproof expansive cement, composed of Portland cement, aluminous slag, gypsum and lime mixed at 66:20:14 ratio, as well as SCN cement, composed of Portland cement, calcium aluminate cement and gypsum mixed at 67:22:9:2 ratio. SCT cements are subjected to the thermal treatment and cured in water at room temperature. According to Mikchailov [113], during heat treatment the AFm phase is produced and transforms later to ettringite; ettringite formation causing swelling. This technology was applied in the production of precast elements. Among cements with calcium aluminate cement matrix the waterproof WPC cement, composed of calcium aluminate cement, gypsum and C_4AH_x, mixed at 65:22:13 ratio should be mentioned.

The two groups of expansive cements can be distinguish, based on the tensile stress produced: to 2 MPa and to 4, or even 6 MPa. They are used in the self–prestressed concrete manufacturing. There is an opinion that the tensile stress should

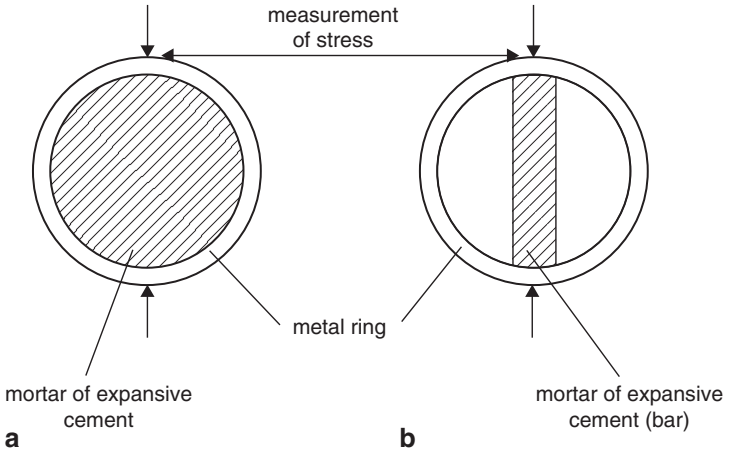


Fig. 9.24 Measurements of stress due to the expansion pressure—scheme: **a** biaxial restricted expansion. **b** uniaxial restricted expansion

not exceed in practice 3.5 MPa, to avoid the damage of concrete coating surrounding the reinforcement [114, 115]. The expansion pressure is most often measured with American method, in the steel ring (Fig. 9.24). The stress is calculated from the measured deformation of the ring, at known steel elasticity modulus.

The shrinkage–compensated concrete mixture is designed in the same way as in the case of ordinary concrete. Their properties, such as strength, elasticity modulus, drying shrinkage, creep, and freeze–thaw resistance are very similar.

However, concrete from expansive cements have higher loss of workability, particularly at higher temperature and set more rapidly. It is the caused by significant amount of ettringite formed. Their negative properties can be minimized designing the concrete mixture with higher fluidity (w/c ratio should be increased of 0.05) or the set retarders can be applied. Mehta [62] recommended to add 0.05 % of citric acid, Collepardi [116] the other carboxylic acids or polyalcohols. The expansive cement concretes should be protected against drying at early age, because the shrinkage before setting has an extremely disadvantageous impact on expansion and can contribute to the appearance of shrinkage fissures.

Obviously, the expansion of concrete will depend on cement content in 1 m^3 of concrete, as well as on the w/c ratio (Fig. 9.25) [62]. One should remember that the type of aggregate affects the expansion too. Temperature, humidity during concrete maturing and the reinforcement are the other important factors.

The resistance of expansive concrete to the sulphate solutions attack depends on the type of cement. Only the concrete of K cement type has high sulphate resistance [64].

The self–prestressed concretes should be very carefully designed, basing on laboratory experimental results. The type and amount of reinforcement must be taken into account. Polivka [117] has shown that successful applications of self–prestressed concretes required the three–axial reinforcement, restricting the expansion.

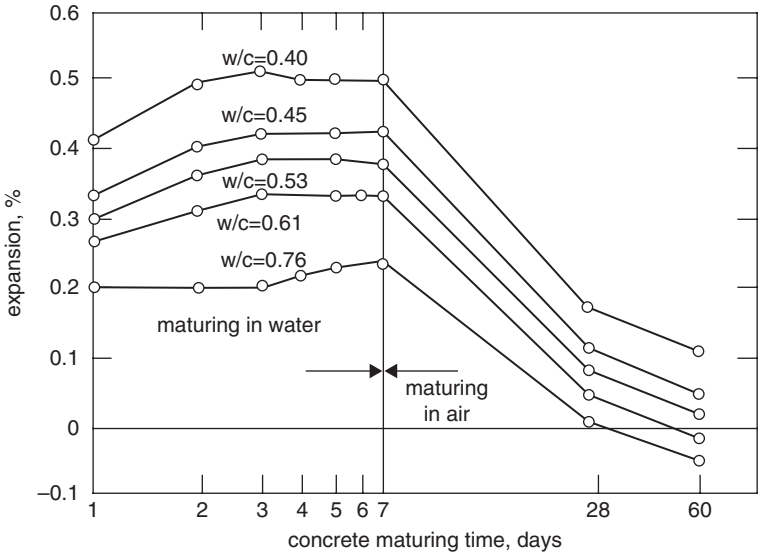


Fig. 9.25 Effect of w/c on the linear expansion of concrete. (according to [62])

Only in the case of flat, plate elements the two–axial reinforcement is sufficient, if concrete was designed for prestressing at low stress.

The application range of expansive cement concretes is increasing—apart from the known, traditional, such as tanks, leak proof coatings, shells, the new one appeared. Smirnow et al. [118] proposed the technology of fibers containing sealing and isolating layer materials. Michajłow [119] and Kuzniecowa [40] proposed the use of expansive cement in the low temperature concreting works, in the areas of permafrost. Michajłow [119] recommends the sodium nitride addition.

As it was mentioned earlier, the highly expansive cements can be used in loosening the rock blocks in the building stone manufacturing [120].

9.4 Rapid Hardening and Fast–Setting Cements

The classic approach to the cement strength development was to increase the alite and C_3A content, as well as the fineness of cement. The increase of silica modulus to about 3 and use of some minor components, mainly barium and boron results in further cement properties enhancement. The rate of hardening of these cements [121–123] is increasing with their specific surface in the range 4,400–4,600 cm^2/g and with K_2SO_4 addition (1.5 %), according to Grzymek's patent [124].

At early seventies the new technology of rapidly hardening cements, with the fluorine stabilized $C_{12}A_7$ phase, was developed. The two modifications of this

technology are known: in the first one the $C_{11}A_7CaF_2$ phase is produced separately and mixed during grinding with clinker and anhydrite. In the second one clinker is burned with CaF_2 addition, which causes the $C_{11}A_7CaF_2$ phase formation at the expense of C_3A, being decomposed, as a phase with incongruent melting [125, 126]. The Al_2O_3 content in this clinker should be of about 7 %. To this clinker anhydrite is added during grinding. Cement thus produced contains 6–15 % $C_{11}A_7CaF_2$ and 10–20 % anhydrite, apart from the Portland cement clinker. The fineness of cement corresponds to the Blaine specific surface area of 550 m^2/kg.

This method was the beginning of various technologies development, applying ettringite content increase, which improves the strength at early stage of rapid hardening cements. However, the fast–setting of cement is a disadvantage of this technology, because the $C_{12}A_7$ hydration cannot be controlled by gypsum addition. Therefore the two variants of technology were individuated: the fast–setting and rapid hardening cements as well as the rapid hardening one. In the latter case the classic set retarders, for example the tartaric or citric acid, should be used.

Several groups of fast–setting cements are known; their setting time is in the range from 30 to 3 min [1]. It can be also distinguish three groups of cements on the basis of strength development; they are presented schematically in Fig. 9.26. The very fast–setting cements have relatively low strength, on the level of 10–15 MPa, corresponding to their application, such as anchors installation or blockage of water outflow. The fast–setting cements from the second group (setting 8–60 min) are used in sealing of inspection covers and manholes, and installation of thin dividing walls as well as door or window frames, moulding of window ledges, setting walls, finishing and facades. All these applications do not require high strength. A time ago these cements were produce by burning of natural marl at temperature range 800–1,000 °C and prolonged storage of ground material. Nowadays the cements with higher Al_2O_3 content, from 6 to 12 % and Fe_2O_{3-} about 6 % are also manufactured [1]. There are also cements composed of β–C_2S and $C_{12}A_7$ mixture [127]. $C_{12}A_7$ can be produced in a rotary kiln form pure raw materials, however, when Fe_2O_3 content is higher, the raw mixture melting should be recommended.

The fast–setting cements can be produced by mixing cements: calcium aluminate with Portland. In Fig. 9.27 the setting time curves for these cements mixtures are shown as a function of time. The processes occurring during their setting were investigated by Cottin [128], who found the rapid formation of hexagonal aluminates and, in the case of gypsum ettringite. In the simpler case without gypsum addition the liquid phase is very quickly supersaturated in respect to the hexagonal aluminates, because at the presence of calcium hydroxide, in the solution, as a result of CaO hydration and alite hydrolysis, the C/A ratio is increased.

Ghosh et al. [129] proposed to add the calcium aluminate cement to Portland cement, together with calcium chloride and anhydrite. This mixture has the properties of expansive cement with setting time of about 15 min and strength: 20 MPa after 2 h, 40 MPa after 7 h and 70 MPa after 1 day. Further strength increase is slight.

The rapid hardening cements are known, which are composed of $C_4A_3\overline{S}$ in the mixture with C_2S, C_4AF, $C_{12}A_7$ and anhydrite. The hardening of these cements

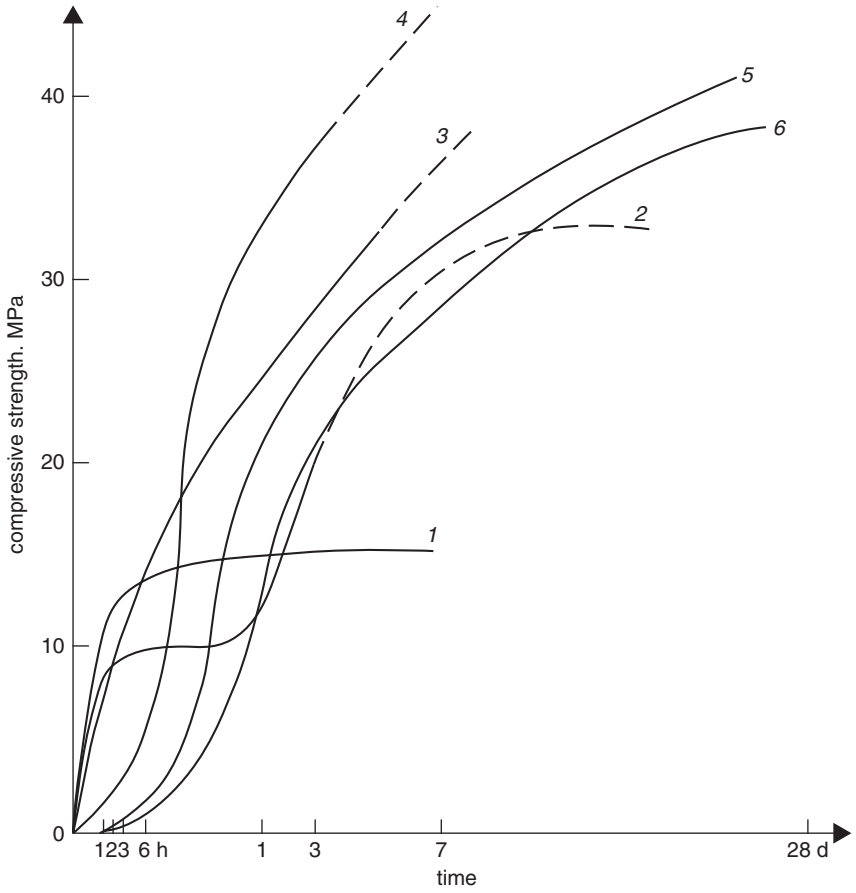


Fig. 9.26 Strength development of special cements (schematically): *1*, *2* fast–setting or very fast–setting, *3*, *4* very–high–early–strength, *5*, *6* high–early–strength

corresponds to the curve 3 in Fig. 9.26. Further strength development of these cements, after longer hydration time, depends upon the C_2S hydration progress. The technologies of these cements are described in Sect. 9.5.

It is known, that the monoclinic tricalcium aluminate with alkalis in solid solution reacts with water slowly (see Chap. 2). Therefore this phase can be used as a source of aluminate ions in reaction of ettringite formation. The fast–setting cements are known which contain 35 % $NC_{14}A_5$, apart from the high belite content of 57 % or calcium orthosilicate phases: belite and alite (C_2S—38 %, C_3S—21 %) [1].

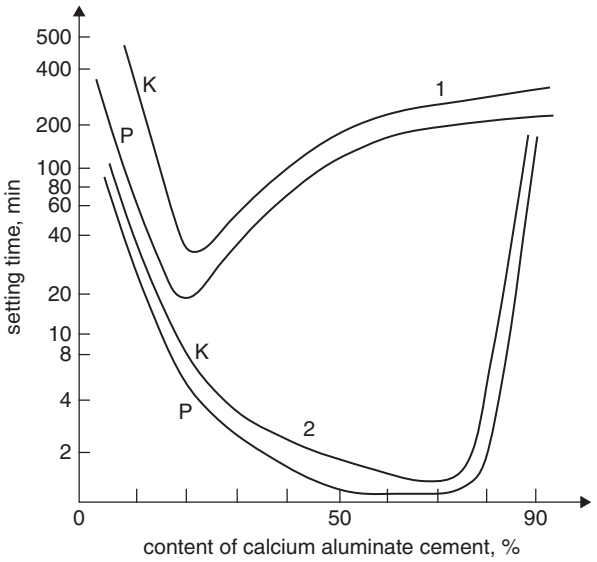


Fig. 9.27 Effect of calcium aluminate cement content in the mixture with Portland cement containing less than 1% CaO_{free} (*curve 1*) and 2.7% CaO_{free} (*curve 2*) on setting; *P* initial setting time, *K* final setting time. (according to [1])

9.5 Low Energy Cements

The increasing costs of fuel, as well as, quite recently, the restrictions of CO_2 emission, increased the use of mineral additions and accelerated. the studies aimed with the searching of binders having the properties corresponding to Portland cement, but produced with lower energy consumption. The investigations tent to the following materials:

- belite Portland cements,
- slag cements or slag–fly ash cements with different activators.

The second group of binders was discussed in Chap. 7; it should be mentioned that their production and use have long tradition. The Roman cements, composed of lime and natural pozzolanas, are good example.

Belite cements are not a technological novelty too. Portland cements produced in thirties, in XXc, had a considerably lower lime saturation factor and high belite content. It was linked with much slower strength development and therefore it caused the gradual changes of cement phase composition, with the increase of alite content.

As it is known, that the heat consumption of the clinkering process is mainly due to the calcium carbonate decomposition and the long period (about 20 min) of clinker heating in sintering zone at maximum temperature, to assure full alite formation. Therefore the energy consumption increases with lime saturation factor (see Chap. 2).

In seventies, XXc, the studies aimed in the improvement of belite cements strength development were undertaken. The two methods are applied: the first consists in the acceleration of belite hydration, while the second one—in enhancing the content of ettringite formed. As it was explained in Sect. 9.3, the application of

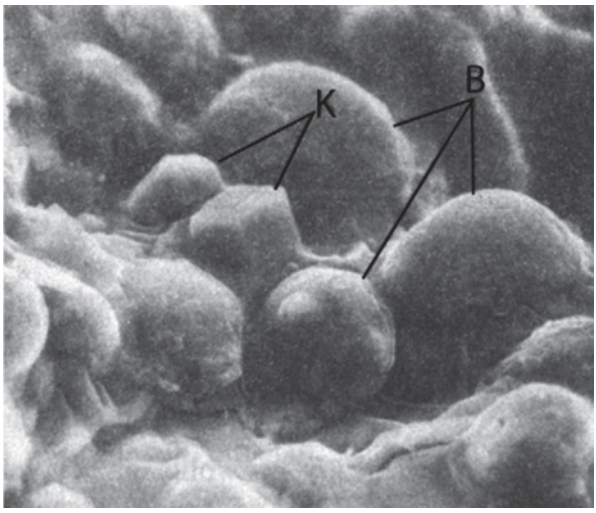


Fig. 9.28 Expansive clinker *K* $C_4A_3\overline{S}$ phase, *B* belite. (photo of B. Trybalska)

Table 9.4. Phase composition of low energy clinkers

Type of clinker					
I	II[a]	III	IV	V	VI
C_3S 40%	C_2S	C_2S	C_2S	C_2S	C_2S
C_2S 40%	$C_4A_3\overline{S}$	$C_{12}A_7$	CA	$C_4A_3\overline{S}$	$C_4A_3\overline{S}$
C_3A 10%	C_4AF	C_4AF	C_4AF	CA	$C_{12}A_7$
C_4AF 10%	$C\overline{S}$	–	–	–	$C\overline{S}$

[a] Main phases; C_3S, C_3A and C can occur as minor components

calcium aluminates of lower CaO content than C_3A, for example CA, $C_{12}A_7$ and $C_4A_3\overline{S}$, results in changing the paste hydration process, and the ettringite content will grow rapidly at early period of hardening. It is convenient to use CA or $C_4A_3\overline{S}$ phase; the latter one is more convenient, because it can be produced from the raw materials with higher minor components content, first of all SiO_2 (Fig. 9.28). CA phase is in practice added in the form of aluminate cement.

Finally, it is known that the increase of ferrite phases content in clinker is advantageous. They are formed at low temperatures and produce the melt, which promotes the calcium oxide reaction with silica. The ferrite phases react quickly with water, giving with lime the hydrated compounds, analogous to the aluminate hydrates.

Numerous experimental works concerned very different clinker phase compositions, which are presented in Table 9.4.

The clinker composition of the first group is a classic belite Portland cement. However, as it was proved experimentally in the case of raw materials, composed of chalk with high silica ratio, the high strength cements can be produced [130].

The results of investigations of the second group of belite cements properties, allowed to choose of the most advantageous compositions, given in Table 9.5. Beside

Table 9.5 Phase composition of sulphate–aluminate cements and the strength of mortars

Phase content, % by mass						Compressive strength at age (days), MPa				Reference
C_2S	$C_4A_3\overline{S}$	C_4AF	CA	$C\overline{S}$	C	1	3	7	28	
41	29	–	20	8	2	28	32	38	55	[131]
33	39	–	19	8	1	31	50	58	80	[132]
16	64	–	–	20	–	25	30	35	36	[133]
25	20	40	–	15	–	35	37	37	52[a]	[134]
30	20	30	–	20	–	28	34	35	54[a]	[135]
39	28	8	6	12	6	38	39	62	72	[136]
20	54	10	–	–	10[b]	40	56	–	70[c]	[137]
33	23	44	–	–	–	30	71	80	86	[138]
34.5	19	49.5	–	–	–	34	66	78	82	[138]
7	48	45	–	–	–	30	55	122	133	[138]

[a] After 120 days, [b] $C_{12}A_7$, [c] after 1 year—102 MPa

of the clinkers II, the two compositions corresponding to type V (Table 9.4) are shown.

Opposite to the cements type II (Table 9.4), the cement type V does not generally originate from the one clinker only but it is a mixture of sulphate–aluminate and aluminate clinkers. The same method is concerning the type IV cement production.

In the papers [129–137] many examples of the sulphate–aluminate cements compositions one can find, very similar to those given in Table 9.5.

According to Mudbhatkal et al. [133], the most advantageous A/S and $A/\overline{S}$ ratios in the clinkers, which allow producing the high strength cements are: for burning temperature 1,200 °C: A/S = 2.5, $A/\overline{S} = 3.8$, LSF = 1.0; for burning temperature 1,300 °C: A/S = 2.0, $A/\overline{S} = 3.8$, LSF = 1.0. The lime saturation factor was calculated from the formula:

$$M_N = \frac{C}{0.7(F + T + \overline{S}) + 0.55A + 1.87S} \tag{9.14}$$

The main advantage of this technology is a relatively simple belite clinker production with high $C_4A_3\overline{S}$ content (Fig. 9.28). This can be related to the significant amount of the liquid phase, which is formed as early as at temperature of 1,200 °C.

The strength development of sulphate–aluminate cement mortars is strongly influenced by the SO_3/Al_2O_3 ratio. This ratio affects the phase composition of paste, as well as the rate of hydration products formation. Klein and Mehta [136] examined the phase composition of hydration products, formed in the mixture: $C_4A_3\overline{S} + CaSO_4 + CaO + H_2O$. The results are shown in Fig. 9.29.

The compositions of the $C_4A_3\overline{S}$, C_2S, $CaSO_4 \cdot 2H_2O$ mixture was also studied with the aim to find the best strength of mortars. In Fig. 9.30a the results of Deng et al. are presented [132]. Mehta [138] reported the similar results (Fig. 9.30b). The other authors give only the optimum $\overline{S}/A$ molar ratio which, for example

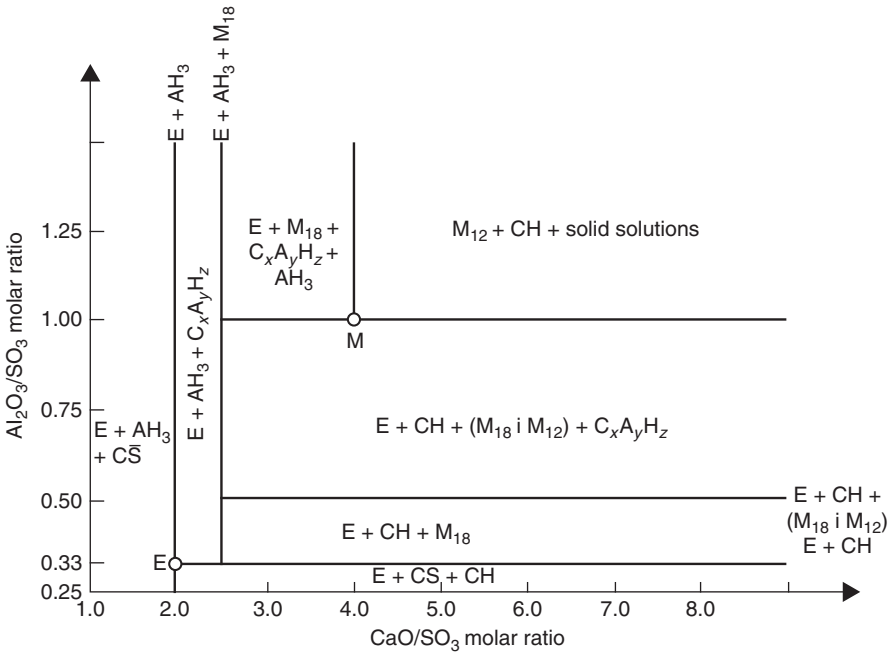
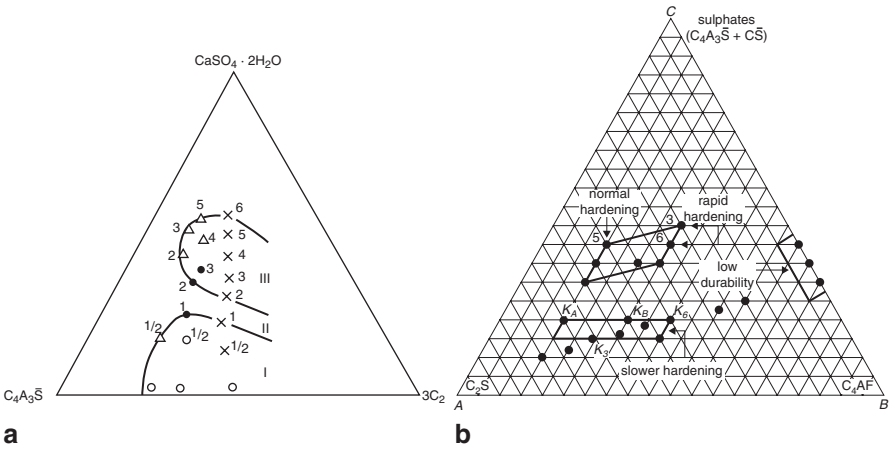


Fig. 9.29 Ultimate composition of $C_4A_3\bar{S}$, $C\bar{S}$ and lime hydration products. (according to [136])



a **b**

Fig. 9.30 **a** Effect of the three main phases proportions on the physical properties of cements (according to [132]): *I* rapid hardening cements field, *II* slightly expansive cements field, *III* field of expansive cements and cements applied in the self–prestressed concretes production; the number correspond to the approximate $3C_2S/C_4A_3\bar{S}$ ratio. **b** Three–components system showing the composition of sulphate–belite cements. (according to [138])

according to Sudoh [137], should be in the range 1.3–1.9. According to Zacharov [139], the most advantageous lime saturation factor of the sulphate–aluminate clinker should be 1.2.

Numerous studies goal was to produce active belite [133, 140–146]. These works can be divided in three groups:

a. low–temperature belite synthesis,
b. searching of stabilizers increasing the belite phase hydraulic activity,
c. improving belite hydraulic activity by very rapid cooling.

The research related to the first group are based on the assumption that the belite synthesis at low temperature is increasing the number of structural defects of this phase and augments its hydraulic reactivity; simultaneously, this phase is produced at low energy consumption.Struillou and Arnould [144] invented the method of C_2S production at temperature of 750 °C, based on the calcium nitrate as a source of calcium. $Ca(NO_3)_2$ is particularly good starting material because it is molten at 561 °C, and the reaction of formed *in statu nascendi* CaO with silica occurs quickly:

$$Ca(NO_3)_2 \rightarrow CaO + (2-x)NO + xNO_2 + \frac{3-x}{2}O_2 \tag{9.15}$$

$$2CaO + SiO_2 \rightarrow Ca_2SiO_4 \tag{9.16}$$

The volatilized nitrogen oxides can be used in the HNO_3 synthesis and then to the calcium nitrate production, therefore the process will form closed circuit. However, the belite thus produced revealed poor hydraulic properties and, as a next step, 6% of gypsum was added to the mixture. As a result, the very active "sulphate belite" was obtained, particularly when the spongiolite was used as a source of silica, instead of quartz. The authors found the substitution of silicon by sulphur with the formation of solid solution with the formula

$$Ca_{2-x}S_xSi_{1-x}O_4 \qquad x < 0.10$$

β–C_2S can be synthesized at temperature of 1,000 °C when 5–10% of $CaCl_2$ is added to the $CaCO_3 + SiO_2$ mixture [147, 148]. However, the closed circuit for the chlorides must be used. For these reasons the nitrate and chloride methods are troublesome for industrial application. The method of β–C_2S producing, proposed by Shibata et al. [146], consisting in the repeated γ–C_2S heating to the temperature of 1,000 °C or 1,500 °C and rapid cooling, is not economical as well. However, in this method the possibility of β–C_2S phase stabilization without admixtures is original.

The second group of studies focused on searching stabilizers of the β–C_2S which ensure high hydraulic activity of this phase, has long history (see Chap. 2).

The two questions appear linked with the stabilization of different C_2S polymorphs: hydraulic activity of different phases and the relation between the properties of stabilizing ions and the stabilized phase reactivity with water [149].

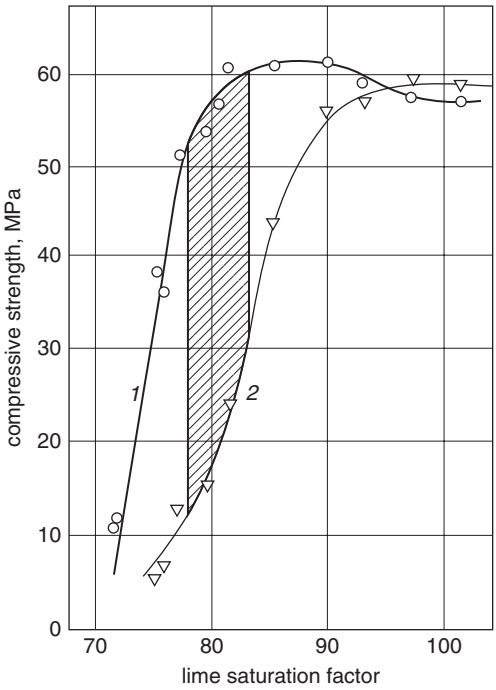


Fig. 9.31 Effect of cooling rate on the strength of cements with various lime saturation factor. (according to [141])

These problems have not been elucidated until now, because the very different synthesized specimens were compared. It is obvious, that the stabilizer content must increase with the higher temperature polymorph stabilization. Also the same polymorph stabilization with various stabilizers needs generally their very different additions.

It was earlier an opinion that the highest rate of hydration has β–C_2S polymorph. However, recently many experimental data were obtained proving the significant reactivity of α and α' phases [142, 145, 149, 150].

The solubility of hydroxides (or acids) of stabilizers elements in water can be an indication, of their effect on the C_2S hydraulic activity. Much better solubility of these elements than that of calcium hydroxide or silicic acid improves the C_2S reactivity in respect to water [151]. Ba instead of Ca and Al instead of Si are the examples. Boron, which is known as a retarder, lowers the C_2S hydration rate.

Suzuki et al. [145] synthesized the α–, α'—and β–C_2S phases, stabilized with two component admixtures: Na_2O–Al_2O_3 (or Fe_2O_3) and K_2O–Al_2O_3 (or Fe_2O_3). The phase stabilized with Na_2O (or K_2O) and Fe_2O_3 showed the highest hydration rate. The solid solution has the formula $Ca_{1.75}Na_{0.25}Si_{0.75}Fe_{0.25}O_4$. The samples synthesized at temperature of 1,360 °C had the highest reactivity. Al_2O_3 addition only α'+β phases is stabilizing and the strength of specimens is much lower.

Stark et al. [141–143] studied the possibility of belite cement activity improvement by quenching. A great impact of the cooling rate on the strength of mortar was proved, of clinker lime saturation factor below 90 % (Fig. 9.31).

The lime saturation factor, proposed by different authors, for typical belite clinkers is in the range from 80 to 82 and silica modulus is higher than 2.5. Usually they contain the following amount of phases: 50% C_2S, 30% C_3S and 20% $C_3A+C_2(A, F)$. C_2S is essentially in the form of α' polymorph and in low amount as β phase. Simultaneously it was found that the reactivity of C_3A, in the rapidly cooled clinker, is quickly reduced; therefore the required SO_3 content should be lowered with the increasing rate of cooling [152]. The soluble alkalis affect the strength of belite cements analogously as in alite cements; the strength after 3 days is higher, while after 28 days is decreasing [152]. However, the alkalis in solid solution in clinker phases improve the strength of mortar; both after 3 and 28 days of hardening.

9.5.1 Alinite Cements

The chlorides are the known mineralizers accelerating significantly the reaction of lime with silica [147, 148, 153]. The chlorides addition causes the intermediate phases formation, spurrite and chlorosilicate, and the acceleration of the process is due to the liquid phase formation (see Chap. 2). The chloroaluminate decomposes at temperature exceeding 1,000 °C; chlorine is volatilized as the gaseous phase. Nudelman [154], has shown that a part of chlorine is combined in the basic calcium silicate of composition close to alite. This phase was called alinite: $Ca_{11}(Si, Al)_4O_{18}Cl$ [155]. Alinite has variable composition; however, beside of the chlorine atoms, it should also contain aluminum and magnesium [156, 157]. The following composition of alinite was given by Massazza [156]:

$$3[CaO_{0.875}MgO_{0.07}(CaCl_2)_{0.055}](SiO_2)_{0.885}(Al_2O_3)_{0.115}$$

In the structure of alinite there are the $(Si, Al)O_4$ tetrahedra and the Ca polyhedra. The latter occur in the three forms [158]:

- Ca_1 shows the octahedral coordination, is surrounded by five oxygen atoms and one chlorine atom; the latter one is situated on larger distance,
- Ca_2 is surrounded by eight oxygen atoms and situated in the center of regular cube,
- Ca_3 is in the center of flattened octahedron, in which the Ca–O closed distance is 215 pm.

There are eight Ca octahedra placed around each chlorine atom; they are joined together with walls and form a symmetrical tetragonal cluster around the quaternary axis. The clusters are joined along the *c* axis with Ca_2 cubes and form a column (Fig. 9.32).

Using $CaBr_2$ addition the bromine alinite was synthesized. The composition of this phase is as follows: $3[CaO_{0.89}MgO_{0.055}(CaBr_2)_{0.055}][(SiO_2)_{0.88}(Al_2O_3)_{0.05}(Fe_2O_3)_{0.07}$ [159] (Fig. 9.33).

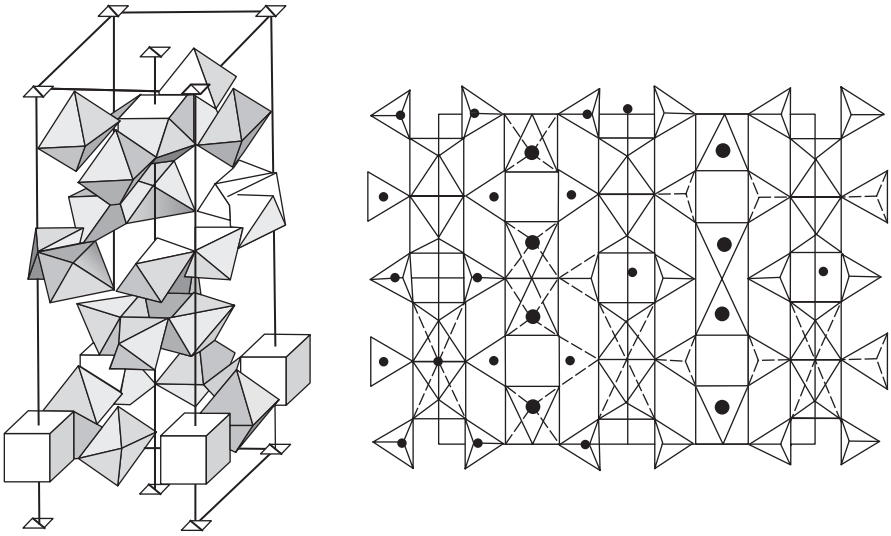


Fig. 9.32 Alinite structure (according to [155]). Axonometry of the half unit cell (left side). Cross section of the alinite unit cell $y = 1/4$. The channels with SiO_4 tetrahedra are shown

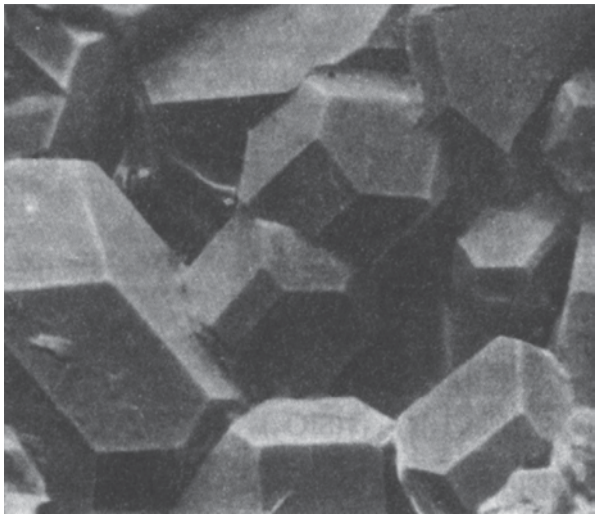


Fig. 9.33 Bromine alinite. (photo B. Trybalska)

The high calcium chloride content in the raw mixture is facilitating the clinkering process and it can be produced at temperature of 1,250 °C. The phase composition of alinite clinker can vary in the following range [154]:

alinite	60–80 %
belite	10–30 %
$C_{11}A_7 \cdot CaCl_2$	5–10 %
C_4AF	5–10 %

At higher burning temperature the alinite content in clinker decreases, as well as the chlorine content; chlorine is combined in aluminate phase only [160].

The production of alinite clinker, which has the properties of rapid hardening cement, due to high hydraulic activity of alinite, is, however, linked with two problems. The first one is the HCl emission from the rotary kiln; HCl is formed in reaction of chlorine with water vapour, contained in the kiln gases. Nudelman [154] proposed the closed chlorine cycle with the calcium chloride recovery, in reaction between HCl and $CaCO_3$. However, it would complicate seriously the functioning of kiln installation. Another problem relates to the very high chlorine content in alinite clinker and consequently in cement, which will cause the corrosion of reinforcement in concrete. These questions are discussed in Chap. 6. However, the alinite cement can be applied in special cases, in the concreting works at lowered temperature, principally in permafrost area.

9.6 Oilwell Cement

Various types of oilwell cements are distinguished. The most important is the phase composition of cement, primarily the C_3A phase content, which is causing quick paste thickening. The main feature of oilwell cement is that it must remain sufficiently fluid for a long period, needed for its pumping to deep well. Simultaneously, the temperature in the bore–hole is increasing with depth, with the rate depending on the geothermal degree, which in Europe is about 33 m/°C. The bore–holes in the case of oil wells are up to 6,000 m and then the temperature is achieving 200 °C and the pressure 140 MPa. In these conditions the cement slurry with w/c from 0.4 to 0.6 must be pumped to the bottom of the bore hole.

The oilwell cements should have several properties, from which the most important are the following [161]:

- low permeability after the slurry hardening,
- good adhesion to the hole casing and surrounding rocks,
- protection of steel casing against the aggressive liquids,
- protection of casing against squeezing due to the thrust of the rock mass surrounding the hole.

At the temperatures and pressures not exceeding 80 °C and 30 MPa the Portland cement with up to 3 % C_3A can be used. At higher pressures, up to 44 MPa and at temperatures up to 100 °C, the Portland cement without C_3A and with ferrite phase up to 24 % C_4AF is recommended [162, 163]. The C_3S content is in the range from 48 to 65 % with average from 50 to 60 %. Only this phase composition of cement (at w/c 0.5) provides the required fluidity, below 500 Pa s, during the period of at least 1.5 h, in the conditions given above. In the ISO 10426–1 Standard the oilwell cements class D, E, F are specified as cements with the mean and with high sulphate resistance, the C_3A content should be lower than 8 and 3 % respectively. Moreover, the $C_4AF + 2xC_3A$ content in the latter one should not exceed 24 %; these

two cements mentioned above correspond to the class G and H oilwell cements, according to the American Petroleum Institute classification [164].

The fineness of oilwell cements is not too high and corresponds to the Blaine specific surface in the range from 240 to 280 m^2/kg. The Blaine specific surface of cement class G is in the range from 280–340 m^2/kg, and class H—200–260 m^2/kg. According to the American Petroleum Institute directives the strength development in hydrothermal conditions should be as follows: after 8 h from 1.4 to 3.5 MPa; after 24 h from 6.9 to 13.8 MPa for particular cement classes [164]. The properties of oilwell cements must be modifies by use of various additives[4]. The lignosulphonates, cellulose derivatives, tartaric acid, saccharates and inorganic borax are employed as set retarders; at lignosulphonate additive water demand is simultaneously reduced. The sulphonated melamine resins and naphthalene–formaldehyde resins are mainly used as water reducers, as well as the polycarboxylates [165]. According to Taylor [166] the saturated NaCl solution is often used as an effective retarder up to temperature of 130 °C, while the modified lignosulphonates to the temperature of 150 °C. The bentonite (3–4 %), diatomites, expanded perlite and pozzolanas, which belong to the additives of low density, allow to raise the water content and fluidity of the slurry. Bentonite improves the resistance of slurry to cracking, prevents the sedimentation of cement grains and improves the ability to seal the cracks in the surrounding rock mass[165]. The bulk density of the slurry is often an important parameter; the high density additives: in this purpose hematite, magnetite, barite or manganese oxides are used [165]. The fibrous oilwell cement is added to the bore hole to prevent the effluents of drilling mud. The fibrous cement contains 2–3 % addition of different organic fibers, for example the polypropylene [165].

Among the other additives the anti–foaming agents [propylene poly–glycol, lauryl alcohol] are also used. Finally, the expansive oilwell cements, for example those with MgO addition, are used to close the gas effluence [165].

The properties of oilwell cement can be modified by addition of siliceous fly ash in amount of 30–35 % [163]. As it was mentioned in Sect. 4.2, the pastes with CaO/SiO_2 molar ratio below 2 or even close to 1 assure higher strength in hydrothermal conditions. It is linked with the fact that the α–C_2SH and $C_6S_2H_3$ phases have low strength and simultaneously raise the permeability of hardened paste. To prevent the formation of these phases of disadvantageous relatively higher density, increasing porosity and decreasing strength of hardened paste, the quartz flour is added to the oilwell cement, used for cementing of the deep bore holes. This flour can be mixed directly with cement, or ground with expansive clinker [165]. The tobermorite, formed in cement paste at lower CaO/SiO_2 ratio, gives much higher strength; the strength decrease due to the transformation of tobermorite into xonotlite and gyrolite is negligible [161].

There are the other hydrated phases produced in geothermal conditions: kilchoanite, dellaite $\{Ca_6[SiO_4][Si_2O_7](OH)_2\}$, pectolite and scawtite [167]. The aluminate phases transform into hydrogarnets and the sulphates to hydroxyellastadite [168]; at very high pressure the hexagonal $Ca[Al_2Si_2O_8]$ is formed [167].

[4] In the case of oilwell cements the term “admixture” is not used.

In special cases, for very deep bore holes cementing, the lime with quartz sand mixtures, metallurgical slags, as well as the dicalcium silicate with sand mixtures can be used [169]. In Russia the slag activated with sodium compounds is used [165].

In some cases to the oilwell cement gypsum hemihydrate, or the aluminum with iron(II) sulphates mixture can be added in order to increase the thixotropy of the slurry, due to gypsum formation. It gives the possibility for tight sealing of the ring space, even when the bore hole is surrounded by permeable rock mass [165]. This slurry can be pumped but gels rapidly when stationary. The detailed information dealing with the oilwell cements can be found in the series of Bensted papers [165].

9.7 Sorel Cement

Sorel cement does not have hydraulic properties, however, because of its special properties it is worthwhile to pay an attention to this material. Primarily it is single out for high strength, high elasticity modulus, abrasion resistance and refractoriness [1, 170].

Sorel cement, more precisely the Sorel cement paste, is produced by mixing MgO with magnesium chloride solution:

$$5MgO + MgCl_2 + 3H_2O \rightarrow 2\{Mg_3(OH)_5Cl \cdot 4H_2O\} \tag{9.17}$$

$$3MgO + MgCl_2 + 11H_2O \rightarrow 2\{Mg_2(OH)_3Cl \cdot 4H_2O\} \tag{9.18}$$

The phase formed in reaction (9.17) is called as 5 1 8 or 5 and can be written using the following formula

$$5Mg(OH)_2 \cdot MgCl_2 \cdot 8H_2O$$

The product formed in the process (9.18) can be written as:

$$3Mg(OH)_2 \cdot MgCl_2 \cdot 8H_2O$$

The latter one is determined as 3 1 8 or 3. They both dissolve in water.

Under the influence of CO_2, or in the presence in the system of $MgCO_3$, they transform into the carbonate phases; there are two carbonate compounds:

$$Mg_2OHClCO_3 \cdot 3H_2O\,(\text{phase A}) \text{ and } Mg_5(OH)_2(CO_3)_4 \cdot 4H_2O\,(\text{phase B})$$

As in the case of Portland cement the hydration of Sorel cements proceed simultaneously. The formation of low soluble A phase is advantageous, because it contributes to the improved durability of the Sorel cement paste. The soluble phosphates added to the Sorel cement paste raise the resistance to water, due to the insoluble complexes formation. Phosphate is adsorbed on the surface of phase 5 and the layer

of insoluble phosphate is formed [1]. The phosphates can also precipitate in the pores and the access of water is then restricted.

The Sorel cements are used to produce the industrial floors. They can be also used in special materials, in which they form the metal–glass bond. They can serve, in dry atmosphere, as a material for decorative plasters, because of the high esthetic value (artificial ivory) [170]. They can be also applied in the salt mines.

The disadvantage of these cements, apart of the susceptibility to water, is their volume instability [170].

The magnesium phosphate cements are also known, which can be used for quick repairing of various constructions, including roads [1]. They very rapid hardening, permits the road traffic opening just after 45 min. On the other hand, the numerous magnesium oxysulphates, for example [$Mg(OH)_2 \cdot MgSO_4 \cdot 5H_2O$] have no practical importance because of the poor durability [1].

9.8 Very High Strength Pastes

Huge amounts of empirical data, indicating the decisive effect of porosity on the strength and the other concrete properties, were essential for development of various methods aimed in the reduction of capillary pores content. Among them is the impregnation of concrete with different substances [171, 172][5].

The technology of concrete impregnation with organic polymers is the most commonly known [173]. The sulphur impregnated concrete was also studied, however, the durability of this material was poor, because of the instability of sulphur in the highly basic cement matrix.

The technology of concrete soaking with monomeric substance and subsequent "*in situ*" polymerization is relatively new. According to Idorn [171], it was initiated by Steinberg in 1968. Beside of the polymer impregnated concretes, there are also the polymer concretes (resin concretes)[6], without cement and the polymer–cement concretes; in the latter case cement is mixed with monomer and water to produce the concrete mixture[7]. This question will be discussed in Chap. 10.

The manufacturing of concrete impregnated with polymers is relatively restricted though this technology creates some new possibilities. Rather small concrete elements can be subjected to impregnation because of the complexity of this method. The following steps are included: drying of elements, degassing at lowered pressure, immersion in monomer, separation of excess monomer from the surface,

[5] The term "impregnation" is sometimes wrongly used, to define the addition of water repellents (such as oleic, lauryl, stearic acids or their salts added as about 0.5 % by mass), which are adsorbed on the surface of cement grains. This cement is hence hydrophobic and can be exposed to the humid air, e.g. during transport or storage, with no detrimental effects.

[6] Resin concrete is the subject of comprehensive study by L. Czarnecki "Betony żywiczne", Edited by Arkady, Warszawa 1982. (in Polish)

[7] See T. Hop, "Betony modyfikowane polimerami", Edited by Arkady, Warszawa 1976. (in Polish).

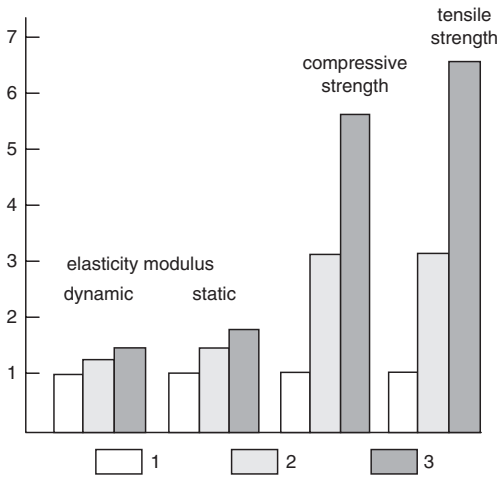


Fig. 9.34 Comparison of mechanical properties of normal concrete and polymer impregnated concrete (according to [171]): *1* normal concrete, *2* soaked with methyl metacrylate, *3* soaked with ethyloacrylonitryl. The coefficients illustrating the strength increase and the elasticity increase due to impregnation are scaled on the axis of ordinates

covering of element surface with 10–15 % polymer solution, lagging with aluminum or polyethylene foil, the polymerization of monomer under the γ radiation or due to the thermo–catalytical effect. In spite of the complexity, this technology found some applications because of major improvement of concrete properties: the strength of concrete increases two to six times and the elasticity modulus two times (see Fig. 9.34); the creep is reduced as well [171, 172]. The porosity decrease increase the durability because the impact of environment is restricted; the freeze–thaw resistance is improved too.

There are many questions to resolve as the technology of concrete impregnation is concerned. They relate mainly to the durability of polymers in the basic environment of concrete and the formation of stresses [171].

The technology of concrete pressed at low w/c ratio has been developed simultaneously with the impregnation. The superplasticizers addition allows to produce the paste at w/c = 0.20 [173]. Gypsum can be also replaced by 1 % calcium lignosulphonate addition with 0.5 % K_2CO_3 [174]. The porosity in this technology is minimized to 5 %, while in normal concretes it equals 25 to 30 %. The hot pressing is also used and in this case porosity is below 2 % [175].

In eighties of twentieth century the two new technologies of very high strength cement pastes were developed: the DSP—Densified Systems containing homogeneously arranged ultra–fine Particles (in Denmark), and the MDF—Macro Defects Free Cements.

The DSP technology is based on the high silica addition, very quick reacting with calcium hydroxide [176, 177]. This silica, in the form of silica fume, plays a dual role: as the pores filling material (micro–filler), as well as the calcium hydroxide bonding reagent; calcium hydroxide is released as a product of cement hydration.

In the paste, the very fine silica particles (two orders of magnitude finer than the cement grains) are homogeneously distributed, together with cement grains, due to the addition of superplasticizer (deflocculation). The intensive mechanical homogenization is very important too, allowing the formation of paste with minimum

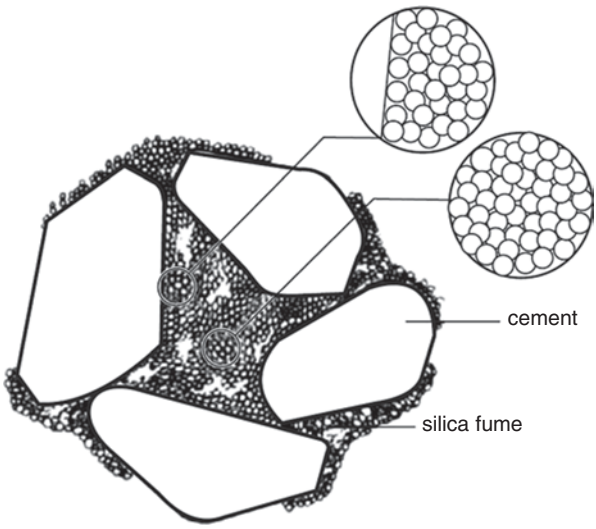


Fig. 9.35 DSP cement paste. (Densified system containing homogeneously arranged ultra–fine particles)

water content (w/c = 0.12–0.20). As a consequence, the space between the cement grains is filled in maximum degree with very fine silica particles (Fig. 9.35). A part of cement is never hydrated because of the low w/c ratio.

C–S–H gel, forming homogeneous, consolidated structure, is the main component of the hardened paste. This gel has a low C/S ratio but the alkali content is higher, for example 1.3% K_2O [178]. The $Ca(OH)_2$ crystals are observed sporadically in the gel. There is no air bubbles and the volume of capillary pores is very low. The drying shrinkage is limited, as the percentage of hydration products is low. The shrinkage microcracks should not appear because the structure is homogeneous and the strength is very high. Unhydrated cement grains cores play the role of microfiller with high strength. In the industrial practice various fillers can be added, like fibers or aggregates, as well as the curing conditions, basically the temperature, can be changed; hence the products of various special properties can be obtained. In Denmark the material called Densit is produced; its high strength and resistance to abrasion allow replacing steel or the other metals in linings, facings and tools. The compressive strength of DSP materials is in the range 350–400 MPa, and the elasticity modulus is 80 GPa. The Dash 74 is the special material produced of DSP paste in hydrothermal conditions and with steel aggregate, beside of silica. It can be used in rocket engineering [179].

The other class of very high strength pastes was obtained by Birchall and co–workers [180–182] and called macro–defect–free (MDF) cements. This is a group of MDF materials are composed of cements and polymers. As it was reported in Chap. 5, the strength of cement paste is controlled by the pores greater than 40 nm and hence this material complies well the Griffith theory. Birchall developed the technology of these materials production, which is based on addition of water soluble polymer to cement paste. The following polymers can be used: hydroxypropyl methylcellulose, polyacrylamide and poly(vinyl acetate). Cement is mixed with these polymers and with low water addition in a special device, for example roller mill. The polymer addition prevents the cavitation during the high shear stress, as

well as reduces the friction between cement grains. As a result, a very dense packing is obtained. Some amount of air occurring in cement paste (called mass) can be readily removed under low pressure.

At very low air pores cement grains in the paste have dense arrangement, close to regular, and occupied by them volume equals about 0.6 of total volume. After removal of air bubbles the ratio of cement increases up to 0.7, that is to the value corresponding to the densest hexagonal packing.

These pastes can are easily shaped by extrusion or pressing, giving the products with the properties similar to those of steel. The polymer chains are adsorbed on the surface of cement grains and hence these grains are covered with hydration products which are cross–linked with these chains. Because of the limited amount of water the polymer chains undergo dehydration and exert very strong compressive stresses inside the material. Consequently the shrinkage of material occurs and the residual porosity is reduced to 1 %. Portland cement can be used in MDF production and in this case the polyacrylamide is added, and in the case of calcium aluminate cement, poly(vinyl acetate) is used. The properties of composite can be modified by addition of various fillers, such as steel and glass or organic fibers. The hydrothermal treatment is included in this technology too. The flexural strength of MDF pastes is in the range 100–1,500 MPa, the elasticity modulus—50 GPa. However, this material is not resistant in water, which is dissolving the organic components and causing the destruction of the product.

References

1. Kurdowski, W., Sorrentino, R.: w Structure and Performance of Cements, p. 471. In: Barnes, P. (ed.) Appl. Science Publishers, London (1983)
2. Kurdowski, W., George, C.M., Sorrentino, F.P.: 8th ICCC Rio de Janeiro, vol. I, p. 292. Rio de Janeiro (1986)
3. Cements Research Progress, yearbooks 1980–1986, American Ceramic Society
4. Muzhen, S., Kurdowski, W., Sorrentino, F.: 9th ICCC New Delhi, vol. I, p. 317. New Delhi (1992)
5. Lea, F.M.: The Chemistry of Cement and Concrete, 3rd edn. Chemical Publ. Comp., New York (1971)
6. Sawków, J.: Cement–Wapno–Gips. **32**, 348 (1978). (in Polish)
7. Robson, T.D.: 5th ICCC Tokyo, vol. I, p. 349. Tokyo (1968)
8. Leary, J.K.: Nature. **194**, 79 (1962)
9. Jeanne: Rev. Mat. Constr. **629**, 53 (1968)
10. Talaber, L.: 6th ICCC Moscow, vol. III, p. 124. Moscow (1974). (in Russian)
11. Suzuki, K.: 6th ICCC Moscow, vol. II/1, p. 232. Moscow (1974). (in Russian)
12. George, C.M.: w Structure and Performance of Cements. In: Barnes, P. (ed.) p. 415. Appl. Science Publ., London (1983)
13. Midgley, H.D.: Trans. Brit. Ceram. Soc. **67**, 1 (1968)
14. Sorrentino, F.P.: Studies in the system CaO–Al2O3–SiO2–Fe–O2. Ph. D. Thesis, University of Aberdeen (1973)
15. Midgley, H.D.: Cem. Concr. Res. **9**, 623 (1979)
16. Calleja, J.: 7th ICCC Paris, vol. III, p. V–102. Paris (1980)
17. Barret, P., Bertrandie, D.: 7th ICCC Paris, vol. III, p. V–134. Paris (1980)
18. Robson, T.D.: High Alumina Cements and Concretes. Contractors Record Ltd, London (1962)

19. Cottin, B.: Sem. Int. Alluminate Calcic, p. 236. Torino (1982)
20. Scrivener, K.L., Capmas, A.: Chapter 13. In: Hewlett, P.C. (ed.) Lea's Chemistry of Cement and Concrete, 4th edn. p 709. Arnold, London (1998)
21. Cussino, L., Negro, A.: 7th ICCC Paris, vol. III, p. V–62. Paris (1980)
22. Cottin, B., Reif, P.: Rev. Mat. Constr. **661**, 219 (1971)
23. Sawków, J.: Cement–Wapno–Gips. **30**, 317 (1976). (in Polish)
24. Kurdowski, W., Taczuk, L., Trybalska, B.: Proc. 2nd. Int. Sem. Durability of Concrete, p. 85. Swedish Council for Buil. Res., Gothenburg (1989)
25. Nikuszczenko, W.M., Kotimczenko, W.S., Rumiancev, P.F., Kalinin, A.I.: 6th ICCC Moscow, vol. III, p. 136. Moscow (1974). (in Russian)
26. Majumdar, A.I.: J. Mater. Sci. **16**, 2597 (1981)
27. Teoreanu, I.: 6th ICCC Moscow, vol. III, p. 255. Moscow (1974). (in Russian)
28. Zubiekin, A.P., Kitajev, W.W.: Izw. Sew. Kawk. Nauczn. Centra Wys. Szk. Sier. Tiechn. Nauk. 10, 78 (1982). (in Russian)
29. Graczjan, A.N., Rotycz, N.W.: Ż. prikl. chim. **43**, 1894 (1970). (in Russian)
30. Ponomariew, I.F., Graczjan, A.N., Rotycz, N.W.: Silikattechnik. **19**, 69 (1968)
31. Uchikawa, H., Uchida, S., Ogawa, K., Hanekera, S.: Il Cemento. **83**, 153 (1986)
32. Miyazawa, K., Tomita, K.: Zement–Kalk–Gips. **19**, 82 (1966)
33. Kawashima, A., Sate, S., Myazawa, Y., Omammda, K.: Rev. 33rd Gen. Meet. Cem. Assoc. Japan, Paper 4, (1979)
34. Graczjan, A.N., Kalitnikowa, A.N., Mandrykin, J.: Ż. prikł. chim. **42**, 1006 (1969). (in Russian)
35. Graczjan, A.N., Gajdżurow, P.P., Zubiedin, A.P., Rotycz, N.W.: Tiechnollogia bielogo portland cemienta, Izd. Lit. Po Str. Moscow (1970). (in Russian)
36. Kupper, D., Wiemer, K.H.: Zement–Kalk–Gips. **39**, 531 (1986)
37. Okushima, M., Kondo, R., Muguruma, H., Ono, Y.: 5th ICCC Tokyo, vol. IV, p. 419, Tokyo (1968)
38. Wührer, J.: Rev. Mat. Constr. **519**, 339 (1958), **520**, 16 (1959)
39. Kurdowski, W., Thiel, A.: Cem. Concr. Res. **11**, 29 (1981)
40. Kuzniecowa, T.W.: Aluminatnyje i sulfoaluminatnyje cemienty. Strojizdat, Moscow (1986). (in Russian)
41. Lafuma, H.: 3rd ICCC London, p. 581. London (1955)
42. Klein, A.: U.S. Patent 3251701 (1966)
43. Rogozina, T.A.: Ż. prikł. chim. **30**, 1682 (1957)
44. Okushima, M., Kondo, R., Muguruma, H., Ono, Y.: 5th ICCC Tokyo, vol. IV, p. 419. Tokyo (1968)
45. Jones, F.E.: J. Phys. Chem. **48**, 311 (1944)
46. Mehta, P.K.: Effect of Lime on Hydration of Pastes Containing Gypsum and Calcium Aluminates or Calcium Sulfoaluminate. J. Am. Ceram. Soc. **56**, 315 (1973). (published by John Wiley & Sons Ltd, reproduced with the permission of Wiley & Sons)
47. Budnikow, P.P., Krawczenko, I.W.: 5th ICCC Tokyo, vol. IV, p. 319. Tokyo (1968)
48. Mehta, P.K.: Cem. Concr. Res. **3**, 1 (1973)
49. Xue, J.G., Chem Wen, H., Tong Xue, L., Zhao Yu, P., Xu Ji, Z.: 7th ICCC Paris, vol. III, p. V–33. Paris (1980)
50. Bonin, A., Cariou, B.: ibid., vol. III, p. V–158
51. Chatterji, S., Jeffery, J.W.: Mag. Concr. Res. **19**, 185 (1963)
52. Chatterji, S.: 7th ICCC Paris, vol. IV, p. 586. Paris (1980)
53. Alunno Rossetti, V., Chiocchio, G., Paolini, A.E.: Cem. Concr. Res. **12**, 577, 667 (1982)
54. Kawano, T., Chitocja, K., Mori, T.: 6th ICCC Moscow, vol. III, p. 179. Moscow (1974)
55. Pollitt, H.W.W., Brown, A.W.: U.S. Patent 3883361 (1975)
56. Allen, J.H., Klemm, W.A., Luker, J.P.: U.S. Patent 3884710 (1975)
57. Collepardi, M.: U.S. Patent 4046583 (1971)
58. Daugherty, K.E., Luker, J.P., Allen, J.H., Klemm, W.A.: U. S. Patent 4002483 (1977)
59. Mehta, P.K., Pirtz, D., Komandant, G.I.: 7th ICCC Paris, vol. III, p. V–6. Paris (1980)
60. Lafuma, H.: Rev. Mat. Constr. **243**, 441 (1929)

61. Teoreanu, I., Dumitrescu, C.: Cem. Concr. Res. **12**, 141 (1982)
62. Mehta, P.K., Polivka, M.: 6th ICCC Moscow, vol. III, p. 158. Moscow (1974)
63. Monteiro, P.M., Mehta, P.K.: Cem. Concr. Res. **15**, 378 (1985)
64. Jorgensen, K.G.: Silicates Ind. **26**, 522 (1961)
65. von Kronert, W., Hanser, P.: Tonind. Ztg. **99**, 238 (1975)
66. Nadachowski, F.: Zarys technologii materiałów ogniotrwałych. Śląskie Wyd. Techniczne, Katowice (1995). (in Polish)
67. Chatterji, S., Jeffery, J.W.: Mag. Concr. Res. **15**, 83 (1963)
68. Ogawa, K., Roy, D.M.: Cem. Concr. Res. **12**, 101 (1982)
69. Bentur, A.: Cem. Concr. Res. **4**, 709 (1974), **5**, 139 (1975)
70. Chen, S.: Cem. Concr. Res. **12**, 257 (1982)
71. Wang, S.: Symposium of Cement and Concrete, p. 161. China Acad. Publ., Beijing (1985)
72. Clastres, A., Murrat, M.: Sem. Int. Alluminat Calcic, p. 334. Torino (1982)
73. Mehta, P.K.: J. Am. Ceram. Soc. **51**, 179 (1978)
74. Mather, B.: Cem. Concr. Res. **3**, 651 (1973)
75. Hansen, W.: Cem. Concr. Res. **6**, 595 (1976)
76. Cottin, B.: Ann. Chim. Res. **4**, 139 (1979)
77. Collepardi, M., Baldini, G., Pauri, M., Corradi, M.: Cem. Concr. Res. **8**, 571 (1978)
78. Regourd, M.: Oral Information
79. Soustelle, M., Cottin, B.F.: 7th ICCC Paris, vol. IV, p. 110. Paris (1980)
80. Dron, R., Brivot, F.: 8th ICCC Rio de Janeiro, vol. V, p. 115. Rio de Janeiro (1986)
81. Yamazaki, Y., Sakakibara, Y.: ibid., vol. IV, p. 395
82. Thorvaldson, T.: 3rd ICCC London, p. 463. London (1955)
83. Szeikin, A.E., Jakub, T.J.: Biezusadocznyj portlandcemient, p. 20. Strojizdat, Moscow (1966). (in Russian)
84. Babuszkin, W.L., Mokricka, Ł.P., Novikova, S.P., Zinov, W.G.: 6th ICCC Moscow, vol. III, p. 187. Moscow (1974). (in Russian)
85. Sherer, G.W.: Cem. Contr. Res. **29**, 1347 (1999)
86. Damidot, D., Glasser, F.P.: Cem. Concr. Res. **23**, 1195 (1993)
87. Brown, P.W., Taylor, H.F.W.: The role of ettringite in external sulfate attack. In: Marchand, J., Skalny, J. (eds.) Materials Science of Concrete, Sulfate Attack Mechanisms, p. 73. The American Ceramic Society, Westerville (1999)
88. Taylor, H.F.W.: Ettringite – Friend or Foe? In: Skalny, J., Gebauer, J., Odler, I. (eds.) Materials Science of Concrete: Calcium Hydroxide in Concrete, p. 211. The American Ceramic Society, Westerville (2001)
89. Taylor, H.F.W.: In: Gartner, E., Uchikawa, H. (ed.) Cement Technology, p. 61. The American Ceramic Society, Westerville (1994)
90. Gaspar, J.P.: Internal report. Lafarge, Francja (1979)
91. Cohen, M.D., Mobascher, B.: Cem. Concr. Res. **24**, 267 (1991)
92. Szeląg, H.: Cement–Wapno–Beton. **75**, 315 (2008), **76**, 11 (2009)
93. Thiel, A.: Czynniki wpływające na zmiany objętości cementów ekspansywnych. Ph. D. Thesis, University of Science and Technology, Kraków (1982). (in Polish)
94. Kurdowski, W.: 7th ICCC Paris, vol. I, p. V–2/1. Paris (1980)
95. Moore, A.E., Taylor, H.F.W.: Acta Cryst. **326**, 386 (1970)
96. Taylor, H.F.W.: 6th ICCC Moscow, vol. II/1, p. 192. Moscow (1974)
97. Mehta, P.K.: J. Am. Ceram. Soc. **55**, 55 (1972)
98. Satava, V., Veprek, O.: J. Am. Ceram. Soc. **58**, 357 (1975)
99. Ludvig, H.: Tätegkeitsbericht des Forschungs Institute der Zementindustrie, p. 80. (1969–1971)
100. Skoblinskaya, N.N., Krasilnikov, K.G.: Cem. Concr. Res. **5**, 381, 419 (1975)
101. Berman, H.A., Newman, E.S.: 4th ICCC Washington, p. 247. Washington (1960)
102. Mehta, P.K., Klein, A.: Special Report 90, p. 328. Highway Research Board, Washington (1966)

103. Ghorab, H.Y., Heinz, D., Ludwig, U., Meskendahl, T., Wolter, A.: 7th ICCC Paris, vol. IV, p. 496. Paris (1980)
104. Kutateladze, K.S., Gabadadze, T.G., Niergadze, H.G.: 6th ICCC Moscow, vol. III, p. 189. Moscow (1974)
105. Wu Chung, W., Wang Yan, S.: 7th ICCC Paris, vol. III, p. V–27. Paris (1980)
106. Wolkov, W.W., Kolovski, W.P., Janev, J.D.: 6th ICCC Moscow, vol. III. p. 182. Moscow (1974). (in Russian)
107. Fukuda, N.: 5th ICCC Tokyo, vol. IV, p. 341. Tokyo (1968)
108. Kawano, T., Hitotsuya, K., Mori, T.: 6th ICCC Moscow, vol. III, p. 179. Moscow (1974)
109. Kokubu, M.: ACI Publication, SP–38, p. 353. (1973)
110. Krivobrodov, Y., Fomitcheva, O.J., Boikova, A.J.: 8th ICCC Rio de Janeiro, vol. II, p. 240. Rio de Janeiro (1986)
111. Kurdowski, W.: Non published paper
112. Ogawa, K., Roy, D.M.: Cem. Concr. Res. **11**, 741 (1981)
113. Michajlov, W.W., Litver, S.L.: Ekspansiwnyje cemienty i samoupragajuszczije bietony. Strojizdat, Moscow (1974). (in Russian)
114. Klein, A.: Expansive Cements Concrete. Publ. SIT–38, Detroit (1973)
115. Polivka, M., Wilson, C.: ACI Publication, (SP–38), 227 (1973)
116. Collepardi, M., Marciali, A., Massida, L., Turiziani, R.: Cemento. **72**, 53 (1975)
117. Polivka, M.: ACI Publication, (SP–38), 483 (1973)
118. Smirnow, B.L., Biełowa, I.F., Diewiatkow, E.A., Żylin, A.S.: Bieton i żelezobieton. **4**, 17 (1981). (in Russian)
119. Michajlov, W.W., Korolewa, G.P., Biejlina, M.I., Kuzniecowa, T.W.: Bieton i żelezobieton. **4**, 13 (1981). (in Russian)
120. Dowding, C.H., Labuz, J.F.: Proc. Am. Soc. Civ. Eng. 108 (GT 10), 1288 (1982)
121. Kurdowski, W.: Poradnik Technologa Przemysłu Cementowego. Arkady, Warszawa (1981). (in Polish)
122. Kurdowski, W.: Cement–Wapno–Gips. **24**, 253 (1979). (in Polish)
123. Peukert, J.: 6th ICCC Moscow, vol. III, p. 27. Moscow (1974)
124. Grzymek, J.: Patent polski nr 43443 i 43444, Warszawa (1959). (in Polish)
125. Chvatal, T.: Zement–Kalk–Gips. **26**, 385 (1973)
126. Greening, N.R., Copeland, L.E., Verbeck, G.J.: U. S. Patent 3628973 (1971)
127. Sorrentino, F.P.: French patent 7423137 (1974)
128. Cottin, B.: 7th ICCC Paris, vol. III, p. V–113. Paris (1980)
129. Laxim, S., Mandel, P.K., Ghosh, R.: 8th ICCC Rio de Janeiro, vol. IV, p. 357. Rio de Janeiro (1986)
130. Kurdowski, W., Garbacik, A.: Symposium of Cement and Concrete, p. 4. Beijing, China Acad. Publ. (1985)
131. Mejling, J.: Thermochim. Acta. 349 (1985)
132. Deng Jun, A., Ge Wen, M., Su Mu, Z., Li Xiu, Y.: 7th ICCC Paris, vol. IV, p. 381. Paris (1980)
133. Mudbhatkal, G.A., Parmeswara, P.S., Heble, A.S., Pai, B.V.B., Chatterjee, A.K.: 8th ICCC Rio de Janeiro, vol. IV, p. 364. Rio de Janeiro (1986)
134. Kulikowa, T.G., Zozulia, P.V., Korniejew, W.L., Chołod, T.G.: Cemient. (7), 11 (1982)
135. Kuzniecowa, T.W.: Cemient. (9), 17 (1982).(in Russian)
136. Klein, A., Mehta, P.K.: 5th ICCC Tokyo, vol. IV, p. 336. Tokyo (1968)
137. Sudoh, G., Ohta, T., Harada, H.: 7th ICCC Paris, vol. III, p. V–152. Paris (1980)
138. Mehta, P.K.: World Cem. Techn. **11**, 166 (1980)
139. Zacharow, Ł.A.: 6th ICCC Moscow, vol. III, p. 153. Moscow (1974)
140. Nakamura, T., Sudoh, G., Akaiwa, S.: 5th ICCC Tokyo, vol. IV, p. 351. Tokyo (1968)
141. Stark, J., Mühller, A., Schrader, K., Rümpler, K., Dahn, B.: Silikattechnik. **30**, 357 (1979), **31**, 50 (1980), **31**, 168 (1980)
142. Stark, J., Mühller, A., Schrader, K.: Zement–Kalk–Gips. **34**, 476 (1981)
143. Müller, A., Stark, J., Rümpler, K.: Zement–Kalk–Gips. **38**, 303 (1985)

144. Struillou, R., Arnould, M.: 7th ICCC Paris, vol. III, p. V–75. Paris (1980)
145. Suzuki, K., Ito, S., Fugii, N.: ibid., vol. II, p. 11–47
146. Shibata, S., Kishi, K., Asaga, K., Daimon, M.: Cem. Concr. Res. **14**, 323 (1984)
147. Kurdowski, W.: Silicates Ind. **30**, 500 (1965)
148. Garbacik, A.: Przyspieszenie procesu syntezy krzemianu dwuwapniowego przez dodatek chlorku wapniowego. Ph. D. Thesis, University of Science and Technology (1980). (in Polish)
149. Pritts, J.M., Daugherty, K.E.: Cem. Concr. Res. **6**, 783 (1976)
150. Ono, Y., Kawamura, S., Soda, Y.: 5th ICCC Tokyo, vol. I, p. 275. Tokyo (1968)
151. Kurdowski, W.: Ceramika. nr 18, PAN, Kraków (1972). (in Polish)
152. Müller, A., Stark, J.: Silikattechnik. 37, 301 (1086), **38**, 301 (1987)
153. Shrestka, P.R.: 8th ICCC Rio de Janeiro, vol. III, p. 148. Rio de Janeiro (1986)
154. Nudelman, B.I.: 6th ICCC Moscow, vol. I, p. 217. Moscow (1974). (in Russian)
155. Nudelman, B.I., Bikbau, M., Swientitski, A., Ilukhine, W.: 7th ICCC Paris, vol. III, p. V 169. Paris (1980)
156. Massazza, F., Gilioli, C.: Il Cemento. **80**, 101 (1983)
157. Bojkowa, A.T., Jesajan, A.K., Sokołowa, R.A., Domanski, A.J., Piriżko, M.A.: Cemient. (6), 13 (1981). (in Russian)
158. Bikbau, M.: 7th ICCC Paris, vol. IV, p. 285. Paris (1980)
159. Kurdowski, W., Moryc, U.: Cem. Concr. Res. **19**, 657 (1989)
160. Kurdowski, W., Garbacik, A.: 7th ICCC Paris, vol. IV, p. 702. Paris (1980)
161. Bensted, J.: World Cement. **18**, 72 (1987)
162. Kurdowski, W., Kot–Książkiewicz, B., Stępień, K., Gumułczyński, L.: Polish patent No. 71148 (1976). (in Polish)
163. Kurdowski, W., Kot–Książkiewicz, B.: Sprawozdanie z Posiedzenia Kom. Nauki PAN Oddz. Kraków, XVI/2, 5537, 1972, PAN Warszawa–Kraków (1973). (in Polish)
164. API Specification 10: 3rd edn. Am. Petroleum Inst., Washington DC (1986)
165. Bensted, J.: Cement Wapno Betonl. **69**, 249 (2002), **71**, 61 (2004). (in Polish)
166. Taylor, H.F.W.: Cement Chemistry. Academic Press, London (1990)
167. Taylor, H.F.W., Roy, D.M.: 7th ICCC Paris, vol. I, p. II–2/1. Paris (1980)
168. Kropp, J., Seeberger, J., Hilsdorf, H.: Proc. 2nd Int. Conf. on Fly Ash, Silica Fume, Slag. and Natural Pozzolanas in Concrete, vol. I, p. 201. Madrid (1986)
169. Rojak, S.M.: 6th ICCC Moscow, vol. III, p. 231. Moscow (1974)
170. Bensted, J.: Cement Wapno Beton. **73**, 297 (2006)
171. Idorn, G., Fördös, Z.: 6th ICCC Moscow, vol. III, p. 287. Moscow (1974)
172. Czarnecki, L.: Cement Wapno Beton. **77**, 63 (2010)
173. Thaunlow, N.: Cem. Concr. Res. **4**, 269 (1974)
174. Judenfreund, M., Skalny, J., Mikhail, R.S., Brunauer, S.: Cem. Concr. Res. **2**, 313 (1972), **4**, 463 (1974)
175. Roy, D.M., Gouda, R.R.: J. Am. Ceram. Soc. **50**, 549 (1973)
176. Hiorth, L.: Phil. Trans. Roy. Soc. A310, 167 (1983)
177. Bache, H.H.: Second Int. Conf. on Superplasticizers in Concrete. Ottawa–Ontario–Canada, p. 33 (10–12 June, 1981)
178. Regourd, M.: In: Young, J.F. (ed.) Very High Strength Cement Based Materials vol. 42, p. 3. Materials Research Society, Pittsburgh (1985)
179. Riezer, J.M., Mackenzie, M.L., Double, D.D.: ibid., p. 253
180. Birchall, J.D., Howard, A.J., Kendall, K.: Nature. **289**, 388 (1981)
181. Birchall, J.D.: Phil. Trans. Roy. Soc. A310, 31 (1983)
182. Birchall, J.D., Howard, A.J., Kendall, K.: Proc. Brit. Ceram. Soc. **32**, 25 (1982)

Chapter 10
New Concretes

10.1 Introduction

First of all the title of this chapter should be explained. There is in this chapter a short section dealing with high performance concrete, which cannot be rated among a "new" kind of composite. It is assumed that the first works on this technology started in Chicago in 1960 and as early as in 1965 concrete having the strength exceeding 50 MPa was used in the construction of skyscrapers (Lake Point Tower 1965) [1]. The progress was fast, because in 1977 the next skyscraper in Chicago (River Plaza) was erected and the concrete used in this construction achieved compressive strength of 77 MPa. To finish these examples it should be mentioned the skyscraper in Seattle (Two Union Square, 1988) and in this case concrete has the strength of 131 MPa [1]. This technology development is concerning only high strength concrete, which is not equivalent to the high performance concrete, defined as a material of special properties, however, there was no doubt that it was the beginning of HPC. The possibility of higher and higher strength concrete manufacturing, due to reduced w/c ratio, indicated one of the direction of technological development and the trends in the investigations aimed in the improvement of the other concrete properties.

There is no doubt that the self compacting concrete (SCC) and the reactive powder one (RPC) will be categorized as the "new" concretes, because they are the products of quite unique, new technologies. The latter one is classified as a low temperature ceramics. Such an approach to the RPC was presented for the first time in the Roy's paper [2].

It should be underlined that the base of rapid concrete technology development was the use of superplasticizers. They allow the w/c lowering to 0.25 or, in the case of RPC, even to 0.20. The progress in concrete technology was initially attributed mainly to the cement production development, especially to the gain of cement strength, by increasing alite content and the fineness of material. However, in about 1965 the superplasticizers came into use. About ten years later Scandinavians begin to use silica fume, which solved the problem of interfacial transition zone in concrete. According to Aïtcin [1], it was an important step in the high performance concrete technology. The development of concrete composites has been very well

W. Kurdowski, *Cement and Concrete Chemistry*,
DOI 10.1007/978-94-007-7945-7_10, © Springer Science+Business Media B.V. 2014

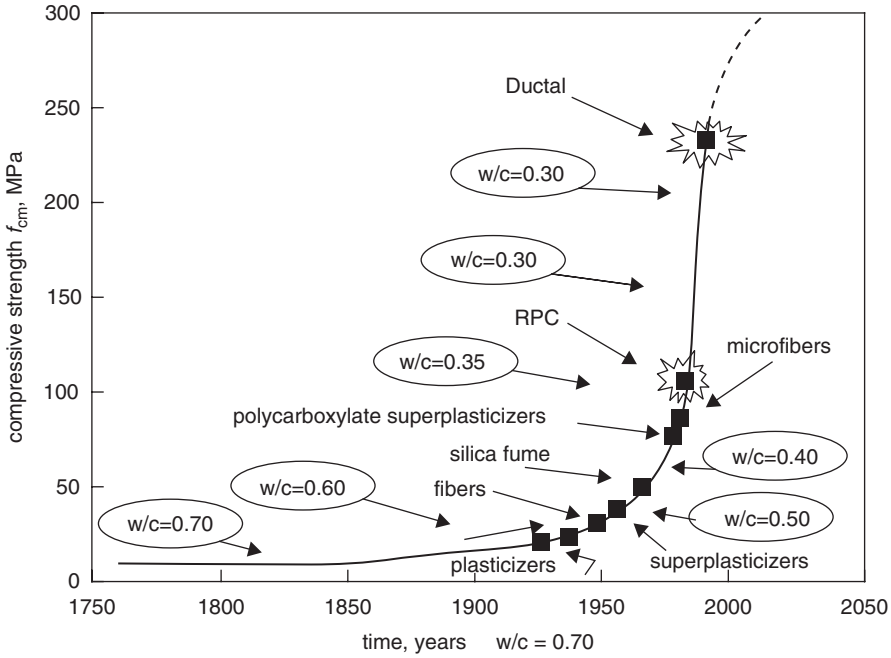


Fig. 10.1. The base of concrete technology development (after [3])

illustrated by the curve presented by Czarnecki [3]; this curve includes the RPC and the recent achievements in concrete technology (Fig. 10.1).

In the end of this chapter the polymer–cement concretes are briefly discussed. This technology is not "new" as well, because it was proposed by Steinberg in 1968 [4]. However, the polymer–cement concretes reveal so unique properties that they can be classified as special concrete composites [5].

10.2 High Performance Concretes

As it has been mentioned earlier, the HPC should exhibit, apart from the high strength, the other special properties, primarily the durability. Low w/c ratio is the first step to the reduction of porosity, mainly in the range of capillary pores and this problem was discussed in chapters 5 and 6. At the absence of connected capillary pores the permeability of concrete is lowered, which is the obligatory condition to assure durability. As it has been explained in the two chapters mentioned above, the migration of solutions inside concrete constitutes the fastest mechanism of destruction by ions causing the corrosive reactions (see chapter 6). However, the diffusion transport of these ions, though a several orders of magnitude slower, leads finally to the reactions resulting in concrete corrosion. In these detrimental for concrete pro-

cesses the phase composition of cement matrix and the role of unhydrated cement are significant. Olek and Lu [6] studied the effect of binder composition on the rate of chloride ions diffusion and found that the addition of 97.5 kg per 1 m3 of concrete of fly ash or ground granulated blastfurnace slag, apart from the silica fume in amount 23.4 kg / m3 of concrete, provided lower effective diffusion coefficient than in the case of Portland cement (366.6 kg/m3) with silica fume only (see also Table 6.4).

The type and composition of binder for HPC production will be discussed later. At first the question of unhydrated cement should be explained. A time ago there was the false opinion that unreacted cement presents a hazard for concrete durability. It was thus forgotten that hydration is linked with contraction, which means the reduction of volume occupied by the products in respect to the volume of substrates (see Chap. 3). This problem should be explained because from time to time the false opinion are presented that cement hydration process can result in microcracks formation and destruction of concrete. Reassuming this problem it should be underlined that unhydrated cement grains have a positive impact because they are hard, resistant micro–aggregate, which are strongly bounded with cement matrix. Simultaneously they are the potential source of hydration products which can fill up the microcracks ("self–healing") being the routes of pore solution transport, formed by unfavourable corrosion processes. The CaO hydration in hardened concrete is another problem, as the free lime in clinker is too high. The hypotheses explaining this expansion are presented in Chap. 3.

The criteria of component selection for high performance concrete production are of interest, however, they are very similar to these for ordinary concrete. Most of authors agree that in the manufacturing of HPC having the strength of 100 MPa, the ordinary Portland cements type CEM I class 42.5R, 52.5 and 52.5R should be used [1]. According to Aïtcin [1], in some cases the use of cement CEM II/B S–V 42.5R is more favourable. There are many examples in technical literature proving that the production of 80–85 MPa compressive strength concrete is possible with CEM I 42.5 N, or even with CEM II/B–V 32.5R [7, 8]. However, Aïtcin [1] was of the opinion that the 100 MPa compressive strength HPC should be produced using high class cement. Aïtcin [1] underlines that clinker with low C_3A content and the higher percentage of sodium and potassium sulphates (Na_2O_e about 1 and simultaneously Na_2O_e/SO_3 about 1) shall be more appropriate in the light of concrete mixture workability, as well as the cement–superplasticizer compatibility. The same opinion was presented by Neville [9].

There are few data dealing with the mineral additions to cement used in HPC, most of them relates to the silica fume, which effect on interfacial transition zone and other concrete properties was described in Chap. 6 and 7. As it has been stated earlier, silica fume is one of the basic HPC components, improving not only the strength and durability, due to the substantial modification of interfacial transition zone, but also enhancing the resistance of concrete as a result of pozzolanic reaction and change of pore structure characteristics [10]. The effect of silica fume on the freeze–thaw resistance is positive too [11]; however, it is better if this component is included in cement [8]. On the other side the drying shrinkage is disadvantageously increasing [12].

The maximum size of coarse aggregate should be limited to 10–12 mm, in exceptional cases to 20–25 mm, when the parent rock material is sufficiently strong and homogeneous [1]. In larger size aggregate the occurrence of strength reducing cracks and pores is generally more probable. Simultaneously, the surface area of smaller particles is higher and the concentration of stress in the aggregate–cement matrix interface is lower and the hazardous microcracks appearing is less probable [9].The required aggregate strength was determined by Grodzicka [8] as 150 MPa. It should be reminded that the reduction of w/c ratio will increase concrete strength as long as the strength of hardened cement matrix will not exceed the strength of aggregate. Moreover, as it is underlined by Aïtcin [1], large coarse aggregate grains introduce to the system the heterogeneity, which can increase shrinkage and creep, and the elasticity modulus may be lowered. The same opinion presents Neville [9]. As in the case of ordinary concrete, the flat and elongated aggregate grains are not favourable, because they worsen the workability of concrete mixture and generally have lower strength; the best are rounded grains. Simultaneously the grains surface should be rough, which improves adhesion to the matrix, but the workability is worsened. Therefore one should look for the compromise. Additionally the dust fraction content should not exceed 1.5 % and this parameter is standardized.

The fine aggregate fraction is selected according to the standards for ordinary concrete, however, it can have coarser graining, because clinker grains act as a fine aggregate which is heighten by high cement content, usually 450–550 kg/m^3 [8]. According to Neville [9] the sand fraction should equal from 28 to 32 %. The similar values, from 27 to 30 % are given by Aïtcin [1].

The selection and addition time of superplasticizer to a concrete mixture should be based on the experimental verification performed on the mixture composed of the same components that will be used in HPC production. However, it can be presumed in advance that the carboxylate ether based superplasticizer will provide the best rheological properties. The properties of superplasticizers were discussed in Sect. 6.6.

An important for HPC durability and still discussed problem is the resistance to freezing and thawing cycles. This issue was discussed in Sect. 6.5, however, because of its exceptional importance, some additional comments, should be added. It will concern the application of air entraining agents in the case of HPC. The low w/c and high cement content concretes exhibit compact microstructure and profitable pore structure, it means a high content of gel pores and small capillaries, in which water freezes at low temperature (see Sect. 5.2). Simultaneously, the free water content in the matrix is low. The problem of high performance concrete air entrainment was investigated by many authors; the important conclusions can be drawn from the works of Aïtcin [1]. Aïtcin [1] is of the opinion that the concrete produced at low w/c, lower than 0.3, must be air entrained. However, Pigeon and Pleau [13], basing on numerous works, are concluding that air entrainment is generally not required for high–strength concrete, having a water/binder ratio smaller than about 0.25. The exception is in the case of fly ash or slag added as partial replacement of Portland cement, particularly as aforementioned authors [13] state, there is not enough data available in this case. Non air entrainment high strength concretes have generally

a good scaling resistance and it seems that it is linked with their good resistance to internal microcracking [13].

As it results from the experiences acquired in Canada and related to the concrete structures, the best high performance concrete resistance to freezing and thawing, in the case of air entrainment, is achieved at air content from 4 to 6 % and spacing factor from 200 to 350 μm [1]. The non air–entrained concrete contains from 1.5 to 2.5 % entrapped air [1]. Simultaneously, the 5 % strength decrease corresponds to 1 % air content increase, it means the same relation as in ordinary concrete [1]. Therefore some additional amount of cement should be added to the mixture. On the other hand, air entrainment has a positive impact on workability.

Neville [9] also recommends the air entrainment of HPC, however, he pays attention that the adequate execution of this process is difficult. In practice, in the case of road and bridge pavements, the coarse aggregate can cause the occurrence of cracks. In the bottom part of bridge pavement the moisture is retained causing aggregates saturation, which freezing cause the destruction of surrounding mortar [9]. These phenomena occur though the aggregate, used in HPC production, had a standard resistance to freezing and thawing (loss of mass ≤ 1 %) and low absorbability (≤ 1 %).

The question of microcracks formation in HPC due to temperature gradient, caused by heat of hydration of high class and content of cement, is controversial too. This fear was presented by Flaga and Mierzwa [14], while Hegger [15] and Cook [16] did not prove it experimentally; the temperature rise was not higher than in the case of ordinary concrete. Lachemii and Aïtcin [17] found temperature of 77 °C, during the concreting of bridge near Montreal. Almost identical temperature was measured by Mirambel et al. [18]. Kaszyńska proved neither the significant temperature rise, nor the HPC strength decrease after 28 days hardening, in laboratory condition. On the other hand, these fears were repeated [17]. Finally, Aïtcin [1, 20] does not presume the higher temperature rise in HPC than in ordinary concrete due to the lower hydration degree of cement in the former one. However, it was forgotten that in massive concrete elements, at temperature higher than 70 °C, the delayed ettringite formation can occur with all the consequences attributed to this phenomenon (see Sect. 6.4.3).

In Table 10.1 the compositions of HPC with advantageous properties, according to Neville [9] are shown. A very high strength of concrete E, with low Portland cement content and high slag addition is worse to mention. Presenting the USA experience in this field Olek [21] quoted the most often used HPC compositions. The binder content is generally in the range 350–400 kg/m^3; it means that the values given by Neville, 450–500 kg/m^3, are somewhat higher (average 443). The coarse aggregate content is 1,100–1,200 kg/m^3 (significantly higher) and the fine aggregate—700–800 kg/m^3 (significantly higher). The composition of binder is shown in Fig. 10.2, in which

Portland cement and silica fume are the major components. The slump values are in the range 150–200 mm; strength after 28 days is in the range 75–100 MPa [21].

Polish contribution in HPC technology was reported by Ajdukiewicz and Radomski [22].

Table 10.1 Composition of high performance concretes of good quality, kg/m^3 (only 4 from 9 compositions have been chosen). [9]

Component	A	B	D	E
CEM I	534	500	513	163
Silica fume	40	30	43	54
	59	0	0	0
Slag	0	0	0	325
Fine aggregate	623	700	685	730
Coarse aggregate	1,069	1,100	1,080	1,100
Water	139	143	139	136
w/b	0.22	0.27	0.25	0.25
Flow, mm	255	–	–	200
f_c after 28 days, MPa	124[a]	93	119	114

[a] after 56 days

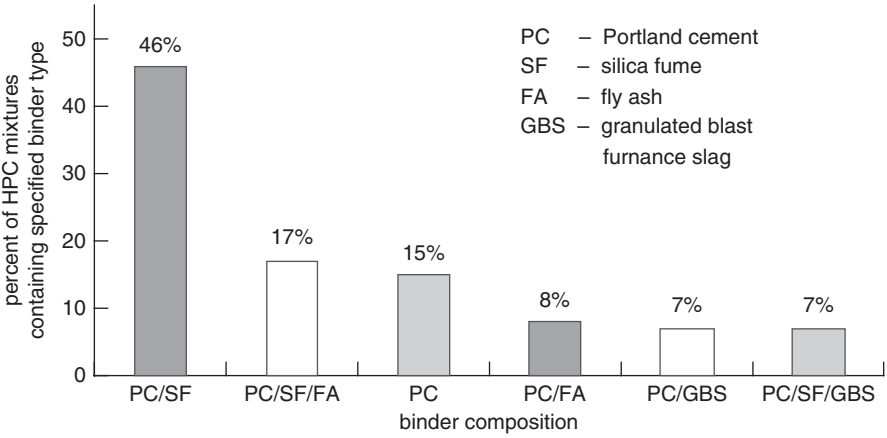


Fig. 10.2 Composition of the most often used binders in HPC. (according to [21])

In some HPC application the abrasion resistance is important. The important studies and field experiments carried out by Gjørv et al. [23] contribute much to this question. The authors examined abrasion on the specially made highway pavement exposed to heavy traffic with studded tyres. The results are shown in Fig. 10.3.

The abrasion resistance research data of HPC have been summarized by Aïtcin [1] in the following way:

- the abrasion resistance of concrete having 150 MPa strength is equal to that of granite,
- the service life of this class concrete is 10 times longer than that of ordinary concrete pavement under abrasion by studded tyres,
- the abrasion resistance is lowered in wet conditions as compared with dry conditions but the higher the compressive strength the less the difference (Fig. 10.3),

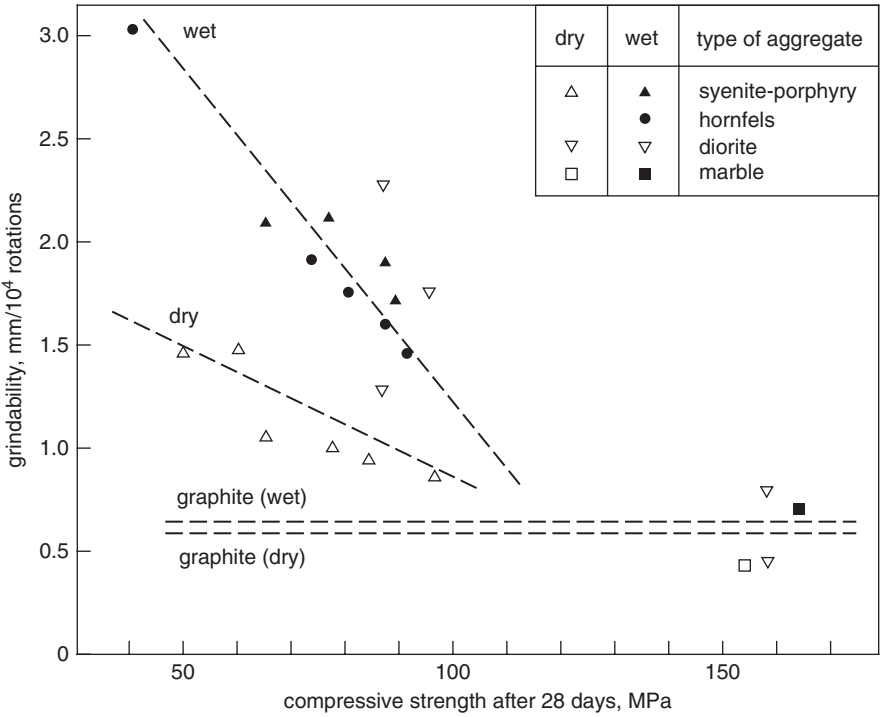


Fig. 10.3 Abrasion resistance as a function of concrete compressive strength. (according to [23])

- the quality of coarse aggregate plays is very important,
- the quality of sand is important too; the natural sand replacement by a sand produced from ground hard rocks causes the concrete strength decrease but increase the abrasion resistance.

HPC fire resistance is rather poor, as it was discussed in Sect. 6.4.7.2; however, it is necessary to remind the important differences of HPC microstructure with and without silica fume [24]. In binder matrix with silica fume, the volume of gel pores increases at the expense of capillary pores. It causes the serious differences of HPC properties with this addition [14, 25, 26]. HPC with silica fume addition, matured in water for 28 days when exposed at temperature of 400 °C explosive failure has occurred [24]. It was caused by rapid water vapour pressure rise in compact concrete microstructure. The high performance concrete without silica fume was not damaged in these conditions, but strength decrease of about 25 % was found [24]. The similar phenomena were described by other authors [26–28]. Addition of polypropylene fibres in amount from 1 to 2 kg/m^3 can be a remedy, minimizing the deleterious effect of high temperature on the high performance concrete. These fibers are melted at temperature of 170 °C and produce a network of channels, providing the water vapour decrease throughout the material [29].

One can mention briefly of the possibility of manufacturing the very high strength HPC by increasing cement content, reduction of maximum coarse aggregate grains and improving packing of the granular skeleton. This is the step toward the reactive powder concrete technology.

10.3 Self Compacting Concrete

The self compacting concretes (SCC) are obtained from the concrete mixtures that reveal the following special properties: it is the ability to flow and compact under the gravity force, thus to fill all space within the formwork without segregation and expel entrapped air. SCC is an excellent material for the constructions of complicated shape, with closely spaced reinforcement, including the underwater structures. The major advantage of SCC technology is that vibration compacting is not necessary. Therefore, it is applied in all cases where the vibration cannot be used, for example where vibrations or noise are inadmissible. The self—leveling of the mixture occurs after placement which thus can be considered as "self—leveling" one. Moreover, SCC is an excellent architectural material, ensuring the smooth surface of elements. The properties of SCC mixture allow elongation of transporting time and shortening the placement time.

The self compacting concretes were invented by Okamura and Ozawa [30] and after two years of studies the first constructions with SCC applications: Akashi Kaikyo Bridge and Trans Tokyo Bay Bridge were erected in 1988.

The flow of concrete mixture is essentially influenced by the coarse aggregate content, which is increasing the internal friction with the remaining mix components and the resistance of flow decreasing its rate. Therefore SCC contains aggregate with less coarse fractions of limited maximum size; simultaneously the mortar and sand contents are higher. Okamura [30] quantified the water to fine powder fraction ratio as equal 1. The coarse aggregate to fine aggregate and to cement matrix ratio by mass should be 50 % : 20 % : 30 % [31].

Cement is the main powder component of SCC and, as in the other types of concretes, is governing the strength and strength development. Cement has also the decisive influence on the rheology of self compacting concrete mixture.

The other fine powder components, added to control the workability of concrete mixture are: fly ash, limestone flour and ground granulated blastfurnace slag. The content of these mineral additions can be substantially high when cement type CEM I is used; they substitute up to 50 % cement, particularly that of class 42.5. One can conclude that the Portland cements with mineral additions can be also applied. The effect of limestone flour on the properties of concrete mixture was studied, among the others, by Grzeszczyk [32].

The self compacting concrete mixture should have high plastic viscosity and low yield stress value. It is ensured by the high content of fine powder fraction (Fig. 10.4) and low w/c ratio [33], but the use of superplasticizers is essential too. It must be the polycarboxylates or polycarboxylic ethers admixtures. SCC technology

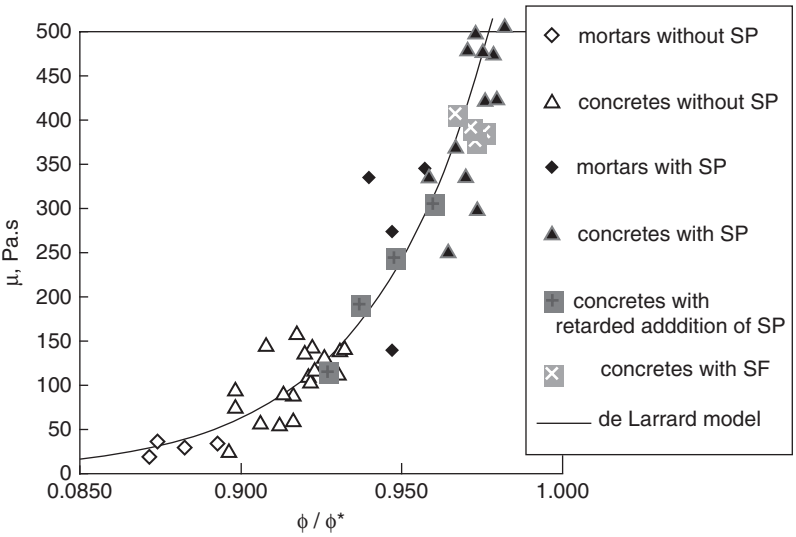


Fig. 10.4 Plastic viscosity as a function of relative concentration of solid phase Φ/Φ. (SP—superplasticizer, SF—silica fume) (according to [33])

was developed due to the availability of these high range water reducers. The viscosity enhancing admixtures, which are not adsorbing on cement grains, thus do not disturb the superplasticizers effect, provided a significant improvement of SCC technology. This admixtures, based generally on the poly–saccharides, control the viscosity by the cross–linking of mixture, with the long chains occurring in their molecules (see Sect. 6.6).

10.4 Reactive Powder Concretes

The reactive powder technology has been developed on the basis of so–called DSP (densified systems containing homogeneously arranged ultrafine particles) technology. They have been obtained using Portland cement with silica fume, at very low w/c ratio in the range from 0.12 to 0.20. Silica fume plays a double function: fills the pores and reacts with calcium hydroxide, released as a result of calcium orthosilicates hydrolysis [34, 35]. In the industrial practice various fillers, such as fibers or aggregates, can be added, as well as the curing conditions, mainly temperature can be changed to obtain the numerous products with different properties. The product called Densit has been produced in Denmark for a long time. This material can be considered as a precursor of reactive powder concrete.

According to Aïtcin [20] the reactive powder concrete (RPC) was invented by Richard from Bouygues company to resolve the problem of HPC, which attained strength of 150 MPa. The best aggregates have to low strength and generate the defects in these concrete. The efforts to reduce the maximum size of coarse

aggregate and the resistance forces provided by this component, which grains are contacting, inspired Richard to the concept of this fraction removal from the composite [20].

There are a considerable number of works concerning RPC and numerous papers on this subject can be found [36–54]. Much attention should pay to the works of Cheyrezy et al. [36], as well as Richard and Cheyrezy [37], which in one series of mixtures used only silica fume, and in the second series the ground quartz sand with $d_{50}=10$ μm, and in some experiments the steel fibers. The proportions of components in these mixtures were the following: in the first series—cement 1, silica fume 0.25, sand 1.1; in the second series the content of silica fume was lowered to 0.23, and quartz flour was added equal 0.39, the share of water was 0.17 (w/b = 0.14). The proportions of components in "granular skeleton" were 74/26. In order to obtain the most convenient packing the authors applied de Larrard and Sedran model [38]. The volume ratio of aggregate and binder was 52/48 respectively. All mixtures were pressed before and during setting, as well as subjected to the low pressure heat treatment.

Apart from the high cement content, RPC contains reactive powders, primarily the quartz flour and lower content of mineral additions with pozzolanic or hydraulic properties. All these mineral additions are very finely ground, and their specific surface area is about 1 m^2/g. Silica fume has much higher specific surface area, about 20 m^2/g. The quartz sand, usually with grading below 600 μm or even 400 μm is used as aggregate. The proportions of powder or several powders and sand should be so selected to ensure the excellent tightness of granular skeleton. Several powders are used primarily to ensure the good tightness of granular skeleton, however, frequently one powder can assure close packing which markedly simplify the technological process [55].

Heat treatment, as well as autoclaving is one of the methods improving strength [36, 37, 55]. The application of heat treatment has a great impact on the acceleration of pozzolanic reaction, which causes the formation of chemical bonds between the hydrates in the paste and the powder particles. The reactivity of quartz is, as it is known, very low in cement paste at ambient temperature, is enhanced significantly at elevated temperatures, and is very high in condition occurring in autoclave. It is confirmed by the strength increase of RPC submitted to this treatment [36, 55, 56]. Simultaneously, the experimental results indicate that the powder of higher pozzolanic activity and particularly with the hydraulic properties (granulated slag) ensure better strength of composite [57]. The suspensions of colloidal silica are sometimes used too.

The assumed high strength of RPC causes the high content of cement and is generally in the range from 800 to 1,000 kg in 1 m^3. Simultaneously high class cement should be used, it means CEM I 52.5R. Silica fume addition is usually 20 % by mass of cement, and water to solid ratio should be close to 0.20 or even lower, hence the effective polycarboxylate—based superplasticizers must be used.

In order to ensure the maximum packing of granular skeleton, composed of powders and sand aggregate, the formulas proposed by de Larrard and Sedran [38] or Funka and Dinger [39] may be applied. Particularly the latter model is frequently used [40]. It can be written as formula

$$Y_i = \frac{(D_i^n - D_{\min}^n)}{(D_{\max}^n - D_{\min}^n)} \cdot 100\,\% \tag{10.1}$$

where Y_i is the cumulative % of i—fraction content, D_i—diameter of i—fraction grains in μm, $D_{\max}$—maximum diameter of grains in μm, $D_{\min}$—minimum diameter of grains in μm, n—constant equal 0.37.

This relation can be plotted in the form of parabolic curve.

The selection of concrete mixture composition should ensure fairly good workability. There are cases that in this aim the best packing, the closest to the Funk's curve cannot be selected, and the proportions of powders and sand are a little different from that established by formula (10.1) [58].

In order to increase RPC tensile and bending strength, as well as to cause some plastic properties under load the steel or sometimes the polypropylene fibers are added [36, 37, 55, 58]. The steel fibers with 0.16–0.18 mm diameter and 6–15 mm length [58] are generally added in quantity of 2–2.5 %, because at higher content the workability is worsened markedly. Obviously, the shorter fibers have less negative impact on workability. The detailed studies of Zdeb and Śliwiński [55, 56, 58] on fibers addition effect were shown that 3 % addition of steel fibers with 0.16 mm diameter and 6 mm length cause a significant strength increase. This effect was observed in the case of composites cured in various conditions: in water at temperature of 20 °C, in water vapour at 90 °C under normal pressure, as well as autoclaved at temperature of 250 °C, and under pressure of about 4 MPa. The compressive and tensile strength increase was similar and practically did not differ for various curing conditions [56]. The work of cracking, calculated from the stress—deformation curves, was the highest in the case of autoclaved samples [58].

The Ductal composite, produced by Lafarge Company, is the only reactive powder concrete material manufactured on an industrial scale [59]. Ductal was used to construct several bridges: for road traffic in Australia, for pedestrians in Sherbrooke, Canada, in Seonyu, Corea, Sermaises in France, Sakata Mirai and Akakura in Japan [59]. There are many bridge investments in USA, linked with Ductal composite [59]. Ductal achieves extremely high strength and resistance against various aggressive media [59]. A high unhydrated Portland cement content contributes to the "self–healing" of microcracks, originating due to the various physical or chemical factors [59].

The research works and practical applications of Ductal in different constructions will undoubtedly contribute to the development of RPC technology, as well as to the increase of this material importance.

10.5 Polymer–Cement Concretes

The polymer–cement concretes are produced by addition of polymer to the concrete mixture. The following modification of this technology can be specified:

- the monomer or prepolymer are added to the mixture which polymerize simultaneously with hydration of cement (*post mix*); the amine hardeners added provide the space cross–linking of polymer component,
- the non–reactive polymers, exerting the physical effect only, are added to the concrete mixture (*pre–mix*).

The polymer addition is generally higher than 5% and can even reach 30% by mass of cement, because this content is assuring the formation of continuous phase in concrete [5]. In the majority of cases the polymer content is in the range from 8 to 12%.

Different forms of polymers are introduced to concrete mixture, as follow [5]:

a. dispersions—the 200–1,000 nm polymer particles are dispersed in the liquid, in most cases in water; water dispersions are known as latexes. They are the most commonly available polymer forms added to concrete, for examples the synthetic rubber latexes, as butadiene–styrene rubber latex, acryl poly(esters), vinyl acetate–ethylene copolymers, styrene–acryl copolymers. The butadiene–styrene copolymer, poly(vinyl acetate) are polymerized before addition to concrete mixture. In the case of additives, which are used before polymerization, the epoxy resins are among the most often applied;
b. emulsions which are the immiscible liquid systems, the microdroplets (1,000–5,000 nm) of liquid macromolecular compounds (resins) constitute the dispersed phase. The epoxy resins are applied in this form;
c. the redispersible powders, it means the powders which can produce dispersion again, after evaporation of dispersant—liquid from the dispersed suspension. There are powders composed of larger particles, usually in the range from 1 to 10 μm. They are vinyl acetate–ethylene copolymers, styrene–acryl copolymers, poly(vinyl acetate) carboxylate and polyacrylates;
d. water solutions of polymers, such as poly(vinyl alcohol), cellulose derivatives: methylcellulose, poly(acrylamide) and some poly(acryl esters);
e. liquid synthetic resins, added to the concrete mixture with hardeners, e.g. epoxy resins.

The majority of polymers, used as additions to concrete, contain the stabilizing admixtures, being the non–ionic surfactants. They may include also the anti–foaming agents. It should be additionally remembered that the polyesters, as poly(vinyl acetate) may hydrolyze in the strongly alkaline environment of concrete.

Kotwica and Malolepszy [60] studied the hydration of cement with 10% addition of redispersible vinyl acetate–ethylene copolymer powder and found that this copolymer is hydrolyzing and changes radically the liquid composition in the paste. The potassium ions concentration is increasing, accompanied by analogous ions

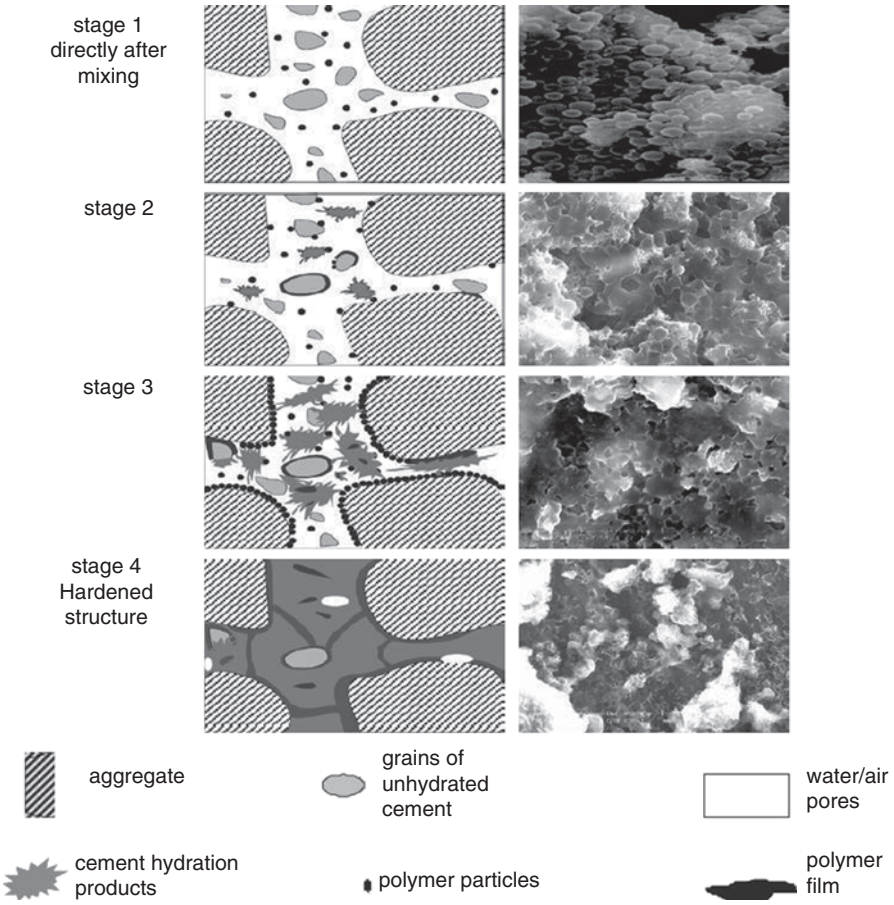


Fig. 10.5 Model of polymer–cement composite microstructure formation for the pre–mix polymer addition. (according to [5])

CH_3COO^- content, which causes the significant increase of ionic force of solution in the paste [60].

The addition of polymer to the concrete mixture causes the significant change of concrete properties [5]. However, for these concretes quite different curing conditions are required, mainly initially in water or in very humid air and then in dry air. Therefore they cannot be used in under water concreting [5]. In practice these polymer–cement concretes are cured in the same way as cement concretes and for this reason they do not attain the assumed properties [5].

In the case of technology in which the structural hardening of additive is occurring during cement hydration, these two processes interact and very important is maintaining of conditions so that the hydration will precede polymerization (Fig. 10.5). Since the premature formation of continuous polymer film disturbs or even hampers the reaction of cement with water [61, 62]. In case of regular

occurrence of these two processes the microstructure composed of two mutually percolating components—polymer and cement hydrates is generated. The most commonly used epoxy resins provide the most convenient conditions of microstructure formation.

In some cases the hardener is not used and it is taken advantage of calcium hydroxide the catalytic effect, evolved as a product of calcium silicates hydrolysis, at the initial period of alite [61]. At resin content not exceeding 20 % by mass of cement the properties of polymer–cement concrete do not differ significantly from those of polymer hardened by traditional method.

At higher resin content, the structural hardening covers only about 50 % of polymer. This can be beneficial when the microcracks appear in concrete the rest of polymer can participate in the "self–healing" process [61].

There is a long, good tradition of concrete application with the styrene–butadiene copolymer for bridge pavements. The polymer to cement ratio (p/c) in most cases equals 0.15 (dry polymer mass) [61].

Czarnecki and Lukowski [61] mention the acryl polymers added at p/c = 0.1, which provide the better abrasion resistance, important for bridge pavements and industrial floors and improve the other properties typical for these polymer–cement concretes. The authors [61] mention also the epoxy–cement concrete, the only practically used composite, in which the polymer structural hardening occurs simultaneously with cement hydration [61].

The polymer–cement concrete reveal, apart from the higher compressive strength—better adhesion to aggregate and lower porosity of the interfacial transition zone in comparison with traditional concrete. The propagation of cracks in concrete is thus changed [61, 62]. The tightness of polymer–cement concrete and resistance to the attack of corrosive environment, including the acidic one, are generally improved. In the latter case the epoxy resin is recommended. In the two papers by Czarnecki (one with Lukowski) [5, 61] the recent achievements in the area of polymer–cement concrete are presented.

The polymer–cement and polymer concretes are widely used in repairing works in reinforced constructions and in their surface protection [5]. The excellent cohesion to various materials, high tightness and resistance to freezing and thawing cycles are the main technical advantages of polymer–cement concretes. These questions are discussed in details in monographic book by Czarnecki and Emmons [63].

References

1. Aïtcin, P.-C.: Béton Haute Performance. Eyrolles, Paris (2000)
2. Roy, D.L.: 9th ICCC New Delhi, vol. I, p. 357. New Delhi (1992)
3. Czarnecki, L.: Materiały Budowlane, XLVII Konferencja Naukowa KILiW PAN i KN PZITB Problemy naukowo–badawcze budownictwa, vol. I, p. 65. Opole–Krynica (2002). (in Polish)
4. Idorn, G., Fordos, Z.: 6th ICCC Moskwa, vol. III, p. 287. Moscow (1974)
5. Czarnecki, L.: Cement–Wapno–Beton. **77**, 63 (2010)
6. Olek, J., Lu, A.: Cement–Wapno–Beton. **71**, 271 (2004)

7. Starzyk K., Influence of intersticial transition zone of HPC with bazalt aggregate, PhD Thesis, Opole University of Technology (2008). (in Polish)
8. Grodzicka, A.: Odporność betonu wysokowartościowego na działanie mrozu. Prace Naukowe Instytutu Techniki Budowlanej. Warszawa (2005). (in Polish)
9. Neville, A.M.: Properties of Concrete, 5th edn. Pearson Education Limited (2011)
10. Byfors, K.: Cem. Concr. Res. **17**, 115 (1987)
11. Malhotra, V.M., Carette, G.G., Sivasundaram, V.: Role of silica fume in concrete. In: Malhotra, V.M. (ed.) Advances in Concrete Technology. Ottawa (1994)
12. Cohen, M.D., Olek, J., Dolch, W.L.: Cem. Concr. Res. **20**, 103 (1990)
13. M. Pigeon and R. Pleau, "Durability of Concrete in Cold Climates", Taylor & Francis, London and New York 1995.
14. Flaga, K., Mierzwa, J.: Przegląd Budowlany. (8–9), 342 (1992). (in Polish)
15. Hegger, J.: High–Strength Concrete for a 186 m High Office Building in Frankfurt, Germany, w Proc. Symp, p. 504. High–Strength Concrete, Lillehammer (1993)
16. Cook, W.D., Miao, B., Aïtcin, P.-C., Mitchell, D.: ACI Mater. J. **89**, 61 (1992)
17. Lachemii, M., Aïtcin, P.-C.: ACI Mater. J. **94**, 102 (1997)
18. Mirambell, E., Calmon, J.L., Aguado, A.: Heat of Hydration in High–Strength Concrete: Case Study, w Proc. Symp, p. 554. High–Strength Concrete, Lillehammer (1993)
19. Kaszyńska, M.: Właściwości BWW w początkowym okresie dojrzewania, Conf. Dni Betonu, p. 49. Polski Cement, Szczyrk (2002). (in Polish)
20. Aïtcin, P.-C.: Trwały wysokowartościowy beton—sztuka i wiedza. ibid., p. 7. (in Polish)
21. Olek, J.: Betony wysokowartościowe—przegląd technologicznych doświadczeń w USA. ibid., p. 91. (in Polish)
22. Ajdukiewicz, A., Radomski, W.: Cem. & Comp. **24**, 243 (2002)
23. Gjørv, O.E., Baerland, T., Ronning, H.R.: Concr. Int. **12**, 45 (1990)
24. Śliwiński, J., Ehrenfeld, W.: Cement–Wapno–Beton. **65**, 103 (1998)
25. Kucharska, L.: Przegląd Budowlany. **8–9**, 351 (1992) (in Polish)
26. Sanjayan, G., Stocks, L.J.: ACI Mater. J. **90**, 170 (1993)
27. Riley, M.A.: Concr. Int. **13**, 60 (1991)
28. Hager, I., Tracz, T.: Cement–Wapno–Beton. **76**, 3 (2009)
29. Walraven, J.C.: Beton o szczególnych właściwościach. Conf. Dni Betonu, p. 20. Wisła (2004). (in Polish)
30. Okamura, H., Ozawa, K.: Mix Design for Self–Compacting Concrete. Concrete Library of JSCE, No. 25. (1995)
31. Walraven, J.C., Takada, K.: Cement + Beton. 23 (1999)
32. Grzeszczyk, S., Jankowska–Renkas, E.: Silicates Ind. **74**, 229 (2009)
33. de Larrard, F.: Naukowa metoda ustalania składu mieszanki betonowej, Conf. Dni Betonu, p. 81. Wisła (2004). (in Polish)
34. Hiorth, L.: Phil. Trans. Roy. Soc. **A310**, 167 (1983)
35. Bache, H.H.: Second Int. Conf. on Superplasticizers in Concrete. Ottawa, Canada, 10–12 June 1981
36. Cheyrezy, M., Maret, V., Frouin, L.: Cem. Concr. Res. **25**, 1491 (1995)
37. Richard, P., Cheyrezy, M.: Cem. Concr. Res. **25**, 1501 (1995)
38. de Larrard, F., Sedran, T.: Cem. Concr. Res. **24**, 997 (1994)
39. Funk, J., Dinger, D.: Predictive Process Control of Crowded Particulate Suspensions Applied to Ceramic Manufacturing. Kluver Academic Publ., Boston (1994)
40. Inter. Symp.: Ultra High Performance Concrete. Kessel (2004)
41. Bonneau, O., Vernet, C., Moranville, M., Aïtcin, P.-C.: Cem. Concr. Res. **30**, 1861 (2000)
42. Chan, Y., Chu, S.H.: Cem. Concr. Res. **34**, 1167 (2004)
43. Coppola, L., Troli, R., Cerulli, T., Collepardi, M.: L'Industria Italiana del Cemento. 112 (1996)
44. Corinaldesi, V., Morconi, G.: Proc. 9th CANMET/ACI Intern. Conf., p. 63. Warszawa (2007)
45. Feylessoufi, A., Crespin, M., Dion, P., Bergaya, F., Van Damme, H.: Adv. Cem. Based Mat. **6**, 21 (1997)
46. Cwirzen, A., Penttala, V., Vornanen, C.: Cem. Concr. Res. **38**, 1217 (2008)

47. Droll, K., Inter. Symp.: Ultra High Performance Concrete, p. 285. Kessel (2004)
48. Heinz, D., Forst–Michael, L.: ibid., p. 685
49. Jungwirth, J., Muttoni, A.: ibid., p. 533
50. Korpa, A., Trettin, R.: ibid., p. 155
51. Low, N.M.P., Beaudoin, J.J.: Cem. Concr. Res. **23**, 905 (1993)
52. Shaheen, E., Sheive, N.G.: ACI Mater. J. **103**, xxx (2006)
53. Toutanji, H.A., El–Korchi, T., Katz, R.N., Leatherman, G.L.: Cem. Concr. Res. **23**, 618 (1993)
54. Bonermann, R., Schmidt, M.: 6th Inter. Symp. HS/HPC, p. 863. Leipzig (2002)
55. Zdeb, T.: Wpływ składu i technologii wykonania na wybrane właściwości betonów z proszków reaktywnych. Ph. D. Thesis, Politechnika Krakowska (2010). (in Polish)
56. Zdeb, T., Śliwiński, J.: Inżynieria i Budownictwo. 693 (2008). (in Polish)
57. Kurdowski, W., Garbacik, A., Szeląg, H.: Cement–Wapno–Beton. **76**, 292 (2009)
58. Zdeb, T., Śliwiński, J.: The influence of steel fibre content and curing conditions on mechanical properties and deformability of reactive powder concrete at bending. In: Brandt, A.M., Olek, J., Marshall, I.H. (eds.) Proc. of the 9th Int. Symp. Brittle Matrix Composites 9, p. 33. Warszawa (2009)
59. Lukasik, J., Hacker, P., Vernet, C.: Conf. Dni Betonu, p. 111. Wisła (2004)
60. Kotwica, Ł., Małolepszy, J.: Cement–Wapno–Beton. **76**, 282 (2009)
61. Czarnecki, L., Łukowski, P.: Cement–Wapno–Beton. **77**, 198 (2010)
62. Czarnecki, L.: Concr. Int. **7**, 47 (1985)
63. Czarnecki, L., Emmons, P.H.: Naprawa i ochrona konstrukcji betonowych. Polski Cement, Kraków (2002). (in Polish)

Index

A
Abietate, 492, 511
Abrasion of concrete, 666
Absorption
  of concrete
    influence on freezing resistance, 487
  of water, 338, 401
Accelerators of Portland cement
  chlorides, 227, 228, 233
  of hardening, 226, 248, 490, 509, 617
  inorganic, 227
  mechanisms, 226–234
  non–chloride, 234, 248
  organic, 227
  of setting, 226, 490
Acid–basicity equilibrium
  effect of alkalis, 50
    of sulphate anions, 50
Acid resistance, 550, 612
Acids
  α–hydroxy, 245
  abietic, 511
  acetic, 108
  acrylic, 499
  aldone, 244
  aliphatic, 237
  alkylarylsulphonates, 495
  alkylsulphate, 511
  amber, 245
  arsenic, 236
  boric, 108, 236, 240
  carbonic, 488
  carboxylic, 241, 244, 491, 637
  chromic, 236
  citric, 178, 219, 244, 637, 639
  dicarboxyl, 237
  fatty, 254, 255, 513
  fluoric, 199, 236, 560
  fumar, 245
  gluconic, 491, 509
  hepanophosphonic, 256
  hydrochloric, 483
  hydrofluoric, 560
  hydroxamoic, 256
  hydroxycarboxylic, 491
  lactic, 245
  lignosulphonate, 491
  maleic, 107, 109, 122, 245, 499, 636
  methacrylic, 499
  monosilicic, 591
  nitric, 199, 545
  phosphoric, 236
  propionate, 245
  saccharic, 244
  salicylic, 107, 545
  silicic, 122, 646
  sulphuric, 395–397, 459
  tartaric, 219, 639, 650
  urine, 244
  wine, 244, 245
Acrylamide polymers, 514, 654, 655, 672
Activation of slag, *see* Slag
Activator
  of hardening, 533
  selection, 533, 543, 572
  sodium, 555, 556
Adhesion
  of steel to paste, 387
Admixtures, *see also* Polymers
  accelerators, 489
  air entraining, 471, 490, 494, 510
  anti–shrinkage, 510
  anti–washout, 514
  in antiquity, 6
  classification, 490
  compatibility, 279
  dispersing agents, 511
  effectiveness, 496, 497, 510

W. Kurdowski, *Cement and Concrete Chemistry*,
DOI 10.1007/978-94-007-7945-7, © Springer Science+Business Media B.V. 2014

grinding aids, 510
hydrophobic, 512
influencing factors, 491, 497, 505–507
mechanism of action, 498
molecules structure, 491, 495, 500–505, 512
permeability reducers, 513
plasticizers, 490–510
retarders, 489, 491, 492, 497, 509
secondary effects, 497
shrinkage reducers, 510
steric effect, 499
surface adsorption on cement grains, 469
superplasticizers, 489, 495–510
viscosity modifiers, 514
water reducers, 490, 492
Adsorbents
differences in measured surface, 309
Adsorption
of nitrogen, 163, 309, 345, 347, 573
of chloride ions, 164, 430
of methylene blue, 575
of plasticizer, 280
of potassium, 164, 232
Adsorption hysteresis
isotherms, 310
AFm phases
solid solutions
with $CaCl_2$, 177
with $Ca(NO_3)_2$, 177
transformation in ettringite, 444
AFt phases
solid solutions
with boron, 173
with $CaCl_2$, 171, 173, 175
with $CaCO_3$, 171, 177
with $CaCrO_4$, 173
with organic cations, 178
Afwilite, 265
Agglomeration
silica fume, 573
Aggregate
chemical composition, 515–521
fine, 348, 515, 599, 664, 665, 668
freeze–thaw resistance, 515
mineral composition, 515–521
porosity, 515
reactive, 381, 394, 396, 397, 401–408, 410, 411
reactivity determination, 413
reactivity test, 405
for self–compacting concrete, 514
Aggregate–cement paste interface, 386, 387, *see also* Interfacial Transition Zone
Air
accidentally entrapped, 474, 665, 668
bubbles, 52, 473, 474, 490, 494, 511–513, 654, 655
content, 475, 510–513, 665
entrapped, 665, 668
influence of strength, 492, 665
spacing, 474, 478, 576, 665
Air–entrained concrete
effect on scaling resistance, 665
workability, 512, 665
Air entraining agents
mode of action, 512
spacing factor, 472, 474, 478, 576, 665
Akermanite, 36, 540, 543, 606
Alabaster, 1
Albite, 396, 516
Alcohols
aliphatic, 245
ethylic, 545
Alinite
bromine analogue, 647
Alite
C_3A effect on hydration, 205
content of Al, 83
content of Mg, 53, 83
crystallization, 48, 54, 112
crystals corrosion, 48
crystals shape, 53
C–S–H shell, 595
C/S ratio, 86
decomposition, 64, 65, 86, 87, 107
dendrites, 53, 54
gas bubbles inclusions, 52
heat of hydration, 193–195
inclusions of interstitial matter, 54, 117
polymorphism, 53, 94–101
recrystallization, 53, 54
solid solution, 53, 63, 65, 76, 82–87, 111
structure, 77–80
zonal crystals, 53, 117–119
Alkali
dolomite reaction, 397
hydroxides, 394, 397, 412, 445, 467, 472, 487, 488, 518, 574, 612
silica gel, 400
influence
on clinkering process, 61–63
on CH solubility, 231, 232
on gypsum solubility, 206, 444
sulphates, 218, 506
Alkalinity of pore solution, 435

Alkalis
adsorption from gaseous phase, 562
all–in aggregate, 400, 403, 414, 425, 426, 516, 553, 577, 626
carbonization, 575
in cement soluble, 374
in concrete, 405
condensation from gaseous phase, 67
cycles in rotary kiln, 61
effect on setting, 221, 250, 251, 281
effect on strength, 224, 250, 251, 397
forms in clinker, 61, 62
from aggregate (basalt, granite), 404, 518
from fly ash, 558
influence on melt viscosity, 30, 49, 62
on clinkering, 49–51
in pore solution of slag cement paste, 409
in Portland cement clinker, 253
sulphur compounds, 109
water soluble, 407
vapour pressure, 61
Alkali–silica reaction, *see* Corrosion alkali–silica reaction
mechanism of alkali–silicate gel formation, 394
composition and expansion, 402
temperature and expansion, 399
$Al(OH)_3$
gel, 174, 178, 554
Altshuller's formula, 49
Aluminate
anions in solution, 519
hydrates, 451, 642, *see also* Calcium aluminate hydrates
Aluminium
hydroxide, 171, 184, 392, 445, 604, 607, 612, 618, *see also* Al(OH)3; Gibbsite
powder, 597, 598
sulphate, 173, 634
Alumino–ferritic modulus, 73
Aluminosilictes, 519, 537
Aluminous cement, *see* Calcium aluminate cement
Amines, 237, 241
Amino–acids, 241
Ammonium
dimethyl–citrate, 116
salts, attack on concrete, 444–446
Amorphous phases, 258, 416
Amphiboles, 520
Amphoteric components, 50
Ancient mortars, 1, 7
Andesite, 403
Anhydrite
C_3A reactivity, 218
effect on cement hydration, 415
inclusions in belite, 425
Anorthite, 36, 271, 272, 396, 516
Anthophyllite, 412, 520
Antigorite, 271
Apatite, 519, 520
Aphthitalite, 109
Aragonite, 456, 458, 461, 462
Arcanite, 69, 109
Arrhenius rule, 223, 456
Artificial pozzolanas, 2
Autoclaved
aerated concrete, 221
calcium silicate hydrates, 462
Autoclave test, 12
Autogenous shrinkage
control, 340
influence of w/c, 338, 340
Avrami's formulae, 86

B

Bacteria sulphate reducing, 396, 456, 459
Ball mill, 558
BaO, 82, 85, 89, 543
Barite, 650
Barium
solid solutions in alite, 82, 83, 85
Basalt, 404, 518, 520, 537
Bauxite, 604, 605
Belite, *see also* Dicalcium silicate; C_2S
composition in Portland cement clinker, 88–98
crystallization, 56
dendritic habitus, 118
heat of hydration, 211, 641
hydraulic activity, 645
hydroxylation of the surface, 138, 182, 184, 190
rate of reaction with water, 214
strength, 647
solid solutions
with C_3P, 615
types I, II, III, 98
Belitic cement, 603, 641, 642, 646, 647
Benzene sulphonate ions, 178
Bentonite, 513, 514, 650
Binders
development, 1–10
history, 1–10
hydraulic, 10, 195
latent, 533

Bingham's model
of non–Newtonian fluid, 282, 283
Blastfurnace slag, *see* Slag and slag cement
Bleeding, 332, 335, 379, 494, 513, 578
Blended cement, *see* Composite cement
B_2O_3, 89
Bogue's formulae
Taylor's modification, 115
Bond
between crystals, 319
between C–S–H sheets, 304, 305, 319, 324
in concrete, 381
covalence, 76, 77
ionic, 166, 324, 545
potassium by silanol groups, 164
Si–O, 77
length, 88–90, 152
van der Waals, 255, 296, 297, 300–303, 308, 319, 324, 328, 344
Boron, 51, 115, 173, 177, 613, 638, 646
Bound water, 190, 207, 304, 307, 314, 322
Bredigite, 97
Brownmillerite, *see also* C_4AF
in Portland cement clinker, 212, 213
manganese analogous, 111
structure, 120
Brucite, 213, 396, 412, 413, 436, 440, 443, 445, 449, 456, 458, 517, 616

C

CA
hydration, 183, 184, 607, 609
CA_2, 25, 36, 60, 605
CA_6, 25, 36, 605
C_3A
chemical composition in clinker, 104
compatibility of the system admixture–cement, 505, 506, 508
effect on strength, 215, 216
effect on sulphate resistance, 11, 15, 442, 450, 649
Friedel's salt formation, 429
heat of crystallization, 74
of hydration, 192–195
hydration 179–190
influence of Cr_2O_3, 189
Fe_2O_3, 189
K_2SO_4, 189
SiO_2, 189
TiO_2, 189
mechanism of retardation, 181, 186
influence on rheology, 214, 505, 506, 508
polymorphism, 100, 101, 188, 458
solid solution
composition, 104
sodium, 76, 99–103
structure, 98–103
C_5A_3, 44–46, 544
$C_{12}A_7$, 25, 31, 36, 38, 41, 44, 60, 71, 183, 605, 620
$C_{12}A_{7ss}$, 60
$C_{11}A_7{\cdot}CaCl_2$, 60, 648
"$C_3A{\cdot}CaCl_2{\cdot}H_{10}$", 175, 228, 233, 360, 429, 436, 437, 458, 482
"$C_3A{\cdot}3CaCl_2{\cdot}H_{30}$", 173, 228, 429
"$C_3A{\cdot}CaCO_3{\cdot}11H_2O$", 247, 248, 396, 462, 591, 609
"$C_3A{\cdot}0.5CaCO_3{\cdot}12H_2O$", 247, 248, 396
"$C_{11}A_7{\cdot}CaF_2$", 36, 59, 60, 604, 639
"$C_3A{\cdot}CaSO_4{\cdot}H_{12}$", 180, *see also* Monosulphate
"$C_3A{\cdot}3CaSO_4{\cdot}H_{32}$", 180, *see also* Ettringite
$CaCl_2$, *see also* Calcium chloride
as mineralizer, 56, 59
$CaCO_3$, *see* Calcium carbonate
CaF_2, 56–59, 107, 241, 545, 614, 639
$C_2(A,F)$
heat of crystallization, 73
solid solution, 105–107
A/F ratio, 107
with Cr, 106
with Mg, 105, 106
with Mn, 106
with SiO_2, 106
with Ti, 106
structure, 103, 105
influence of $CaCl_2$, 107
of CaF_2, 107
C_4AF, 13, 41, 44–46, 71, 106, 419
C_6AF_2, 41, 45, 46, 106
C_6A_2F, 41, 45, 46, 106, 190
$C_4(A,F)H_{13}$, 190
$C_4(A,F)H_{19}$, 190
CAH_{10}, 115, 167, 169, 171, 178, 183, 185, 186, 240, 607, 609, 610, 634
C_3AH_6, 180, 194, 608
C_4AH_{13}, 169, 175, 176, 178–181, 183, 185, 186, 212, 247, 415, 577, 589, 635
structure, 169
C_4AH_{19}, 180, 190, 436
Calcite
hetero–nuclei of C–S–H, 142
Calcium
aluminate, *see* Cement calcium aluminate
hydrates, 166–171
hexagonal, 166–169, 171, 178, 180–182, 189–191, 193, 214, 220, 250, 607–609

structure, 162, 167
carbonate
decomposition, 21, 30, 55, 641
efflorescence, 487
reaction with aluminate hydrates, 247
secondary formation, 66
as set regulator, 247
chloride, basic, 228, 360, 436, 437
formate, 227, 234, 493
hydroxide, *see also* CH; Portlandite
corrosive solutions attack, 435
importance in alkali–silica reaction, 411
in cement with fly ash, 382
in slag cement, 552
leaching, 403, 435, 458, 518
pozzolanic reaction, 408, 548
reaction with silica, 411
solubility, 206, 245
strength, 327
langbeinite, 109
nitrate, 94, 234, 645
oxide, 21, 24, 30–32, 38, 39, 48, 49, 55, 107, 173, 510, 548, 617, 620, 629, 642, see also CaO
sulphide, 533, 540
sulpho–aluminate
hydrated, 171–179
structure, 619
sulphate, 173, 218–220, 237, 288, 372, 444, 445, 487, 492, 505, 506, 550, 623
titanate, 85, 112, 606
vanadate, 241
Calorimetry
of Portland cement phases, 16, 132, 133, 199
of different cement types, 373
CaO
crystallization, 37, 39, 42
heat of hydration, 192
maximum in clinker, 42, 43
primary, 107
reaction with Al_2O_3, 537
reaction with SiO_2, 55
secondary, 107
solubility, 85
structure, 107
volume stability, 12, 218
Ca–O, bond length
disruption, 91
Ca–OH bond
in C–S–H, 136
Capillary pores in concrete
continuous, 354
permeability, 352, 574, 662
shrinkage, 340
Capillary water
freezing of, 470
influence on, 340
shrinkage, 344
Carboaluminate hydrates, 185, 247, 423, 424, 456, 575
Carbonation of cement paste
formula of progress, 465, 466
influence of cement type, 463
of mineral additions, 463
of moisture, 461
of w/c, 466
of strength, 464
on shrinkage, 347
Carbon content in fly ash cement, 559, 560, 562, 596
Carbon dioxide
aggressive, 455, 457, 468
presence in sea water, 455
solubility in water, 458
C_2AS, 31, 544, 605
$C_4A_3\overline{S}$, 219, 220, 562, 617–621, 623, 626, 628, 634, 636, 640, 642, 643
C_2ASH_8, 548, 577, 586, 589
Celite, 12, 13
Cellulose, 241, 319, 388, 491, 514, 650, 672
Cement
additives
classification, 534
hydraulic, 403, 533
mineral, 11, 16, 164, 198, 254, 340, 363, 407, 429, 454, 464, 533–535, 615, 663, 668
pozzolanic, 413
agglomerates formation in silo, 224
alinite, 647–649
alkalis, soluble, 406, 412
aluminate, *see* Calcium aluminate
anhydrite, 8
belite, 603, 641, 642, 646, 647
belite–ferrite, 13
blended, 151, 191, 248, 535
calcium aluminate
corrosion, 612
durability, 613
heat of hydration, 611
hydration, 166–190
interstitial matter, 605
kinds, 604
phase composition, 605–607
strength development, 609

calcium sulphoaluminate, 174, 445, 510, 603, 617, 626, 630, 636
classification, 10–18
coloured, 613–615
composite, 238, 613
expansive
clinker, 63, 618, 636, 650
components, 620, 621, 628
expansion hypotheses, 625
factors influencing expansion, 628
gypsum addition and stress, 630
K, M, S types, 634
lime influence, 630
grains, surface charge, 490
history, 1–10
hydration, 9, 114, 167, 195, 205, 207, 247, 250, 253, 281, 304, 333, 386, 471
effect of $CaCl_2$, 226
at low temperatures, 228, 237, 553
hydrophobic, 494
interstitial material, *see* Portland cement clinker
low alkali, 403, 603
low–energy, 641–649
low heat, 195, 603
lump formation in silo, 224
masonry, 453, 574
oilwell, 649–651
Portland
history, 1–10
with fly ash, *see* Fly ash
hydration, 205–212
strength, 116
pozzolanic, 2, 407, 430, 535, 564
rapid hardening, 10, 16, 18, 268, 373, 610, 611, 639, 640, 649
reaction with humid air, 253
regulated set
requirements, 16
Roman, 2, 641
shrinkage compensated, 637
slag
alkali activated, 9, 164, 440, 487, 555, 556, 572
carbonation, 463, 466
efflorescence, 487
sulphate resisting, 15, 16, 393, 432, 441, 442
supersulphated, 9, 554, 628
very high strength, 653
water ratio influence on strength, 541
on durability, 392
on porosity, 392
with fly ash, 567–573
with limestone, 247, 248, 383, 423, 453, 459, 575, 576
with silica fume, 356, 476, 669
oilwell, 649–651
oil well cementing, 649–651
white, 37, 485, 604, 610, 613–615
without gypsum, 115
Cement paste
autogeneous shrinkage, 332, 335, 338, 340, 341, 349
bond kinds, 303, 304
chemical shrinkage, 268
crack propagation, 327, 374, 389
deformability, 383, 617
Densified System containing ultra–fine Particles, 653
drying shrinkage, 341–348
heat treatment, *see* Heat treatment
Macro Defects Free, 653
microstructure, 303
model, 304, 309, 319
permeability, 351
effect with fibres, 389
of gas, 573
hydration development, 356
interfacial transition zone, 506
of strength, 354
plastic shrinkage, 337, 571
with reinforcement, 386–388
rheology, 279, 281, 295
specific surface area, 10, 162, 163, 217, 218, 229, 309, 317
stress–strain relation, 384
tixotropic, 280, 284, 286, 288, 289, 290, 292
swelling of, 362, 419
very high strength, 653, 654
volume changes, 348
Cenospheres, 558, 559, 562, 596
Ceramics
low temperature, 489, 661
CF, 29, 39
CF_2, 39
C_2F
polymorphic transformation, 105
structure, 103, 105
C_3FH_6, 9, 109
CH, *see also* Calcium hydroxide; Portlandite
amorphous, 189
crystallization, 142
Chain of wollastonite, *see* Dreierkette
formation, 260
Chalcedony cement, 535
Chapelle's method, 536, 563

Charge, *see under* Surface charge
surface on cement grains, 244, 280, 490
Chelate complexes, 242, 244, 246
Chemical attack on concrete
chlorides, 426, 430, 456, 572, 612
sea water, 447, 455, 456, 458, 552
sulphates, 364, 396, 441, 443–445, 451, 452, 456, 458, 568
Chemical shrinkage, 268, 279, 333–335, 340, 349
Chemically bound water, *see* Bound water
Chemisorption
water, 144, 304, 588
Chloride ions
accelerator or retarder
cement phases formation, 428
corrosion of cement paste, 426–441
mechanism of corrosion, 426–441
Chloride–sulphate attack interaction, 456
Chlorosilicate
in calcium silicate formation, 228
in cyclones preheater, 112
Chromium
reducers
antimonium, 258
iron sulphate, 257
Mn (II) sulphate, 257
substitution in clinker phases, 614
Ciment Fondu, 395, 604, 634, *see also* Calcium aluminate cements
Clay, expansion
in limestone, 3, 70,
heated, as pozzolanic materials, *see also* Metakaolinite
swelling, 154, 412
Clinker
density, 13
influence on strength, 549
melt
content, 112
peritectic, 38, 42, 44
viscosity, 50, 51
nodulising, 69
phase composition, 11, 46, 64, 103, 121
phases formation, *see* System(s) from acid slag
reduction, 64
white, 64, 615
Clinker, Portland cement, *see* Portland cement clinker
Clinkering process
departure from equilibrium, 46–48
effect of fluxes
mineralizers, 55, 56
in industry
influence of alkalis
of chlorine, 59, 60
of fluorine, 56
of sulphur, 63
of phosphorous, 63
melt migration, 49
melt surface tension (nodulising effect), 69
melt viscosity, 49, 51
effect of alkalis, 50, 51
Cl, F, P, 51
MgO, 50, 51
sulphates, 50, 51
in rotary kiln, 63–69
Cluster, 117, 449, 647
CO_2, *see* Carbon dioxide
Coal in fly ash
effect on colouring, 559
on specific surface area determination, 557
limit, 560
Coefficient of activity (slag), 541
Cohesion
forces, 303, 315
Compatibility of superplasticizer–cement system, 505
effect of potassium sulphate, 505, 506
Composite cements
alkali silica reaction, 397, 404, 410, 411, 487, 572
composition, 17
Concrete
aerated autoclaved, 597, 598
air entrained, 511, 513
capillary action, 359, 470, 586, 512, 513
carbonation, 460–467
cement paste
alkali silica reaction, 396–412
chlorides attack, 426–441
corrosion, 392–485
delayed ettringite formation, 414–426
resistance, 11, 450, 451, 456, 458, 471, 612
sulphates attack, 441–454
sea water attack, 454–459
slag cement effect, 364, 431, 442, 458, 463, 538
with limestone, 412–414
cracking
and curing, 341
under autogenous shrinkage, 340
under drying, 328
under temperature gradient, 198
Ductal, 671

durability, 351, 392, 444, 663
effect of cracks on frost resistance, 470
from fly ash cement, 567, 568
from reactive powders, 661, 669–671
from slag cement, 548–556
chloride ions diffusion, 550
corrosion, 550
expansion, 550
alkali silica reaction, 553
carbonation, 553
frost action, 553
history, 6–10
interfacial transition zone, 376–384
influence of silica fume, 383
in high performance concrete, 385
bond with aggregate, 374–386
with reinforcement, 386–392
permeability, 351–364, 393, 408, 426
polymer–cement, 672–674
polymer impregnation, 652, 653
porosity, 351–364
and durability, 351
and strength, 353, 354
resistance to corrosion, 11, 450, 451, 456, 458, 471, 612
main factors, 272, 279, 370, 378, 450, 458
to fire, 459, 460
self–compacting, 489, 514
self–heating, 414
influence on strength, 567
shrinkage, 348, 349
Concreting under water, 514, 673
Condensation
of SiO_4 tetrahedra, 260
Conduction thermal, 459, 598
Conductivity, 199, 233, 302, 459, 481, 598
Conglomerates, 121, 280, 288, 289, 379, 380, 493, 564
Congruent dissolution
of C_3S, 133, 141
melting, 141
Connectivity of silicate tetrahedra, 88, 547
Conversion, in calcium aluminate cement pastes, 440
Cooling of Portland cement clinker
reactions during, 47, 48, 64, 65, 117
studied by light microscopy, 116122
Coordination number
of calcium ions, 90, 91
of silicon, 76
Copolymer of vinyl acetate with ethylene, 653, 655
styrene–acrylic, 672
Corrosion, alkali–silica reaction
carbonate aggregate, 412
effect of pozzolanic additions, 408
on soluble alkalis in cement, 408
influence of delayed ettringite formation, 400
mechanism, 398
Corrosion of concrete reinforcement, 478485
chloride ions influence, 480483
Cracks, formation, 188, 340, 341, 354, 617
Creep, 349
Cristobalite, 24, 48, 118, 397, 408, 562, 573
CS, 24, 265, 540
$(C_2S)_2CaF_2$, 56, 57
C_2S, *see also* Belite
dissolution, 49
polymorphic transformation, 65
resorption, 37
solid solutions with La, Nd, Y, 96
stabilization of polymorphs, 96
structure, 8890
C_3S, *see also* Alite
calorimetry, 132
crystallization, 37, 52, 63
decomposition, 87
heat of hydration, 16
hydroxylation of the surface, 138, 140, 182
polymorphic transformation, 80
polymorphs stabilisation, 79
resorption, 37, 38, 46, 47
solid solution, 63, 82, 83, 85
structure, 7788
X–ray powder diffraction patterns, 81
$(C_3S)_3CaF_2$, 56, 57
$C_{10}S_3\overline{S}_3H$, 270
C–S–H
α, β, γ, 149
I, II, III, IV, 134, 135, 149152
adsorption properties, 469
bonds, 166, 327
bridging tetrahedra, 157
$CaCl_2$ influence on morphology, 231, 234
calcium ions bond, 166
chemisorption, 231, 429
concentration data, 166
crystallization, 133, 134, 140, 141
crystallinity ratio, 152
crystals dimension, 151
degree of crystallinity, 166
densifying, 147
E, 147
epitaxial growth, 140, 384, 575
equilibrium curve, 186, 468

forms, fibres, 146, 149, 151, 240, 378
foils, 147, 149, 152, 208, 230
honeycomb, 150, 208, 252, 378
spheres, 142, 147, 150, 151, 163
H/D ratio, 163
hydrophilic properties, 230
inner products, 143, 144, 147, 149–151, 210, 212, 448, 449
interplanar distance, 316, 317, 344
minor components content, 212
model of Cong and Kirkpatrick, 158
of Feldman and Sereda, 163, 318, 319
of Jennings, 162, 163, 230
of Kondo and Daimon, 320
of Richardson and Groves, 158, 159, 163
of Taylor, 157
of Viallis, 162
modelling of the phase, 157–165
morphology, 147–151, 247, 252
influence of $CaCl_2$, 230, 231, 234
of sulphate, 250
nucleation, 142, 208, 217, 591
influence of $CaCl_2$, 231
of $CaCO_3$ (calcite), 247, 253
octahedra CaO_6, 156, 157
outer product, 149, 151, 209, 210, 212, 247, 420, 441, 448, 594
particles, dimension, 151
pores, 151, 163, 164, 231, 233, 309, 214, 217, 218
primary hydrate, 142, 231, 245, 585
ratio of C/S, 132–138, 142, 148, 149, 153, 154, 157–160, 163, 164, 192, 212, 217, 230, 240, 243, 402, 409, 429, 430, 585, 591, 592
influence of autoclaving, 259, 261, 262, 269–271
on Al solid solution, 153, 589
on morphology, 151, 240, 252
shrinkage in chloride solution, 234
silicate anions, 148, 155–157, 165, 265, 345, 347, 351
specific surface area, 163, 256, 377, 468, 627
absorbate influence, 229
hypothesis of Brunauer, 314
of Jennings, 162
of Feldman and Sereda, 314, 319
solid solution
substitution of Ca by Al, 153, 164
by Fe, 153, 164
by K, 164, 165
by Mg, 153
by Na, 164, 165
of Si by B, 262
by C, 262
by Cr, 263, 264
by S, 153
with CaCl2, 230, 231
with CO_3^{2-}, 164, 262
with Zn_{2+}, 239
strength
Powers formula, 317
structure, 154–156
almost amorphous, 152
hypothesis of Nonat, 149, 151, 153, 159
of Taylor, 153, 154
pseudo–hexagonal, 151
semi–crystalline, 149
transformation II to I and III to IV forms, 146, 147
water interlayer, 154
X–ray microanalysis, 153
Cuprum, 112, 115
Cuspidine, 60
Cyclone preheater, 61, 65, 66, 69

D

Dams
effect of soft water, 467
D–drying
definition, 309
Decarbonisation
precalcination, 69
Deceleratory period, 240
Defects
in C3S structure, 85, 144, 146
of crystal structure, 85, 131
on the surface, 588
Defloculation, 493, 494, 499, 653
Defoamers, 509, 510, 650, 672
Degree of hydration
at elevated temperatures, 266, 268
Dehydroxylation, 29, 30, 70, 566, 577
De–icing salts, 395, 405, 426, 476, 477, *see also* Frost action
Delayed ettringite formation, 272, 394, 400, 414–426, 665
Dellaite, 650
Densit, 654, 669
Deriagin, Landau, Vervey's theory, 300
Design life of concrete, 392
Diatomaceous earth, 535
Dicalcium ferrite, 39, 190, *see also* Ferrite (phase)

Dicalcium silicate, *see also* Belite
enthalpy of polymorphic transformation, 91
hydration, 147, 148
hydraulic activity, 96
in calcium aluminate cements, 21
polymorphs
structures, 93
stabilization of polymorphs
α–dicalcium silicate hydrate, 590
Diffusion
chloride ions, 426–435
Fick formulae, 359, 360, 362, 427
methods of measurement, 427
Dimers, 49, 141, 155, 157–159, 162, 166
Diopside, 271, 519
Disjoining pressure, 303, 315, 319, 328, 343, 344, 349
Dispersing agents, 503
Dissolution
incongruent, 133, 181, 182, 585
congruent, 133, 141, 182, 183, 607
selective (of slag), 108, 545
Dolomite
aggregates, and expansion in concrete, 397
Dreierkette, 156, 265
Drying of C–S–H
effect on silicate anion structure, 157
Dry process, 6, 598, 666
DSP materials, 654
Ductal, 476, 489, 671
Duplex film, 376, 378, 381, 386
Durability of concrete
in chlorides solution, 426, 427
influencing factors, 373
in sulphates solution, 4
in sea water, 576
relation with cement type, 373

E

Early product
Portland cement pastes, 77
tricalcium silicate pastes, 131, 146
Effective coefficient of diffusion, 359, 360, 427, 429, 436, 482, 486, 663
Efflorescence, 485–489, 513, 555, 556
Elasticity modulus, 166, 251, 267, 319, 327, 344, 637, 653, 664
Electrical double layer, 297, 300, 432
Electrokinetic potential, 233, 299, 300, 499, 623
Electron diffraction
alite, 304
C–S–H, 304
Electron spectroscopy for chemical analysis (ESCA), 148, 182
calcium silicate pastes, 139
Ellestadite
fluoric, 57, 58
hydroxyl, 270
Energy
activation, 49, 50, 266
free, 51, 345, 379
hydration, 486
Enstatite, 519, 573
Enthalpy changes, *see* Thermochemistry
Entropy, 27
Epitaxial crystallization, 575
Equation
of Avrami, 86
of Bingham, 293
of Carman, 297
of Debye–Hückel, 300
exponential, 293
of Gibbs–Helmholtz, 27
of Hershel–Bulkely, 293
of Legrand, 287, 293
of Nernst, 297
of Petri, 323
of Reiner–Rivlin, 292
of Robertson–Stiff, 293
of Smoluchowski, 299
of strength, 300
Equilibria, 174, *see under* System:phases concerned
Etching
of clinker for microscopy, 116
Ether, 499, 501, 564
Ettringite, *see also* AFt phases
bad, 628
in concrete attacked by sulphates, 457
dehydration, 633, 634
delayed formation, 665
dissolution, 628
effect of elevated temperatures, 634, 636
enthalpy of crystallization, 627
expansion hypotheses, 627
in expansive cements, 455
good, 628
influence on C_3A hydration, 629, 642
morphology, 454
relation to alkali–silicate reaction, 508
solubility product, 633
stability in heat treated cement paste, 630
structure, 631, 633, 634
in supersulphated cements, 595
Eutectic
curve, 38, 42, 47, 59

local, 48
melt, 31, 58, 103
Evaporable water, 237, 305, 361
Expanding agents, 406
Expansion, *see also* Alkali silica reaction; Sulphate attack; Expansive cements
of concrete containing reactive aggregates, 419
from excessive gypsum content in cement, 550
of sodium–potassium silicate gel, 401
Expansive cements, *see* Cement expansive

F

False set, 15, 220, 221, 253, 291, 336, 372, 467, 490, 492
Fatty acid salts
as air entraining agents, 254
Fe^{2+} in clinker phases
influence on C_3S decomposition, 87
Feldman hypothesis, 316, 350
Feldman–Sereda model, 163, 319, 344
Feldspar reaction,
in concrete, 397, 518
Fe_2O_3 in solid solution
in C_3A, 101
in C_2S, 96
in C_3S, 77
Feret–Florentin's method
of pozzolanic activity assessment, 563
Ferrari cement, 441
Ferrite cement, 636, 642
Ferrites, *see also* C_2F; C_6AF_2; C_4AF
colour, 205
compositions in clinkers, 30
enthalpy of crystallization, 446
factors affecting reactivity, 30
hydration, 190
under heat treatment, 30, 56
in calcium aluminate cement, 55
solid solution, 55
A/F ratio, 30
with Cr, 106
with Mg, 431
with Mn, 106
with Si, 29
with Ti, 106
influence of $CaCl_2$, 60
of CaF_2, 60
structure, 205
FH_3, 190
influence on $C_2(A,F)$
on clinker melt viscosity, 190
Field of primary crystallization, 178, 543
Fillers
effect on concrete properties
on hydration, 575
mechanism of action, 574
Fire damage of concrete
of high performance concrete, 667
quartz noxious effect, 63
Flash set, 214, 215, 221
Floc structure
effect of water reducers and superplasticizers, 302, 303
Floculation, *see* Floc formation
Flowing of concrete mix, 506
Fluorellestadite, 57, 58
Fluorescency, 545
Fluoride, 57, 58, 241, 516
Fluoride phases
in Portland cement clinker formation, 241
Fluorosilicates, 241, 513, 615
Fluxes in Portland cement making
system $CaSO_4$–CaF_2–Ca_2SiO_4, 55
system CaO–SiO_2–CaF_2, 55
Fly ash
alkali–silica reaction, 404, 411
calcareous, 557
effect of ettringite formation
on hydration, 599
of SiO_2 and Al_2O_3 on strength, 31
of temperatures on strength, 356
siliceous, 196, 597
chemical composition, 557
from fluidized bad combustion, 65
glass composition, 571
influence on concrete, 576
pozzolanic activity, 407
phase composition, 560
uncombusted coal, 497, 510, 599
Foshagite, 267, 271
Fracture mechanics, 327
Free lime, 115, *see also* CaO
determination, 107
in cement making, 107
in expansive cement, 334
volume stability, 218
Free water porosity
comparison with mercury porosities, 312
in pastes of composite cements, 307
Freeze–thaw attack
aggregate, 470
air–void spacing factor, 474, 478
damage, 576
freezing rate, 472
fly ash, calcerous effect, 475
siliceous, 430

hypotheses of destruction, 476, 626
influencing factors, 590
mechanism of de–icers action, 426
resistance of HPC, 475
scaling, 426, 476
spacing factor, 576
water saturation, 478
and dynamic modulus of elasticity, 471
Freezing resistance
cooling rate, 471
dynamic modulus of elasticity, 470
Friedel's salt, *see* $C_3A{\cdot}CaCl_2{\cdot}H_{10}$

G

Gabbro, 518, 520
Gaize, 535
Garnet, 403
Gases
in cenospheres, 558, 596
Gehlenite
hydrate, see C_2ASH_8
Gel
alkali–silicate, 404
calcium influence on expansion, 404
of cement, 471
strength, 474
factors, 474
formed in early period of hydration, 354
formed in alkali silica reaction, 397
pores, 304, 317, 431, 470–474, 486, 664, 667
Powers formula, 597
of silica, 134, 142, 310, 410, 445
bonds, 246
space ratio, 353
of tobermorite, 266
water, 304, 338
Geothermal well cementing, 261, 262
Germania tricalcium, 85
Gibbsite, 169, 171, 436, 461, 577, 610, *see also* Aluminium hydroxide
Gibbs phase rule, 33
reduced, 51
Ginstling–Brounstein formula, 25
Glass
aluminium coordination, 546
in clinker, 110, 115
determination, 413
dissolution, 199, 415
in fly ash, 475
of gehlenite composition, 272
in granulated blast furnace slag, 430–432, 441, 553–535
in natural pozzolanas, 410, 535, 536, 563, 590
in Portland cement clinkers, 107, 425
in silica fume, 538, 573
magnesium coordination, 546
MO_6/MO_4 ratio influence on strength, 546, 548
network of silica tetrahedra, 543
Glucose, 241–243
Glycol, 254, 256, 510, 564
Gneiss, 396, 397, 404, 518
Granite, 397, 403, 404, 518
Granulated blastfurnace slag, *see* Blast furnace slag; Slag cement; Super–sulphated cement
Griffith theory, 654
propagation of crack, 327
Grinding aids, 225, 254
and dust in ventilation air, 255
mechanism of action, 255
Groups hydrophilic, 474, 491
silanols, 588
Gypsum
attack on concrete, 194
behaviour on grinding and storage of cement, 194
effects on cement hydration, 653
formation during sulphate and chloride attack, pH importance, 426, 456
hemihydrate content, importance of, 221
hydration, 505
influence on alite hydration, 205, 219
hydration, 550
optimum content in Portland cement, 611
reactions with calcium aluminate cements, 611
secondary, 250, 552, 628
Gyrolite, 264, 270, 271, 599, 650

H

Hadley grains, 377, 412, 413, 448
Halite, 69, 486
Hardening
accelerators, 226, 248
classification, 226
K_2SO_4 and Na_2SO_4, 82
influence on strength, 195
calcium aluminate cements, 77
effect of $CaCl_2$, 234, 617
of $CaCO_3$, 348
of NaCl, 226
Portland cement, 114, 212
relation to hydration reactions, 281, 380

retarders, 234
lead oxide, 236
organic, 236, 237
zinc oxide, 237
Heat evolution, 214, 228, 236, 394, *see also* Calorimetry
calcium aluminate cement, 373
Portland cement, 214
Heat treatment of concrete
strength after 28 days, 112, 565, 567, 573, 665
bond kinds, 414
permeability of gases
bond with aggregate, 567
with fibres, 573
effect of hydration development, 506
of w/c, 364
effect on paste composition, 266, 268–270
on set, 492
on specific surface area, 549
on strength, 542
fresh paste, 214, 295
influence of interfacial transition zone, 447
hydration degree, 146, 183, 265, 313, 341
quartz addition, 268, 269, 271
Heavy metals
in Portland cement making, 66, 112
zinc influence on Portland cement hydration, 112
Helmholtz plane, 297
Hematite, 39, 519, 560, 562, 650
Hemihydrate, 130, 221, *see also* Gypsum
effect on admixtures compatibility, 279
cement hydration, 281
Hess rule, 193, 199
Hexagonal aluminate hydrates, *see* $C_4[A,F]H_{13}$
High alumina cements, *see* Calcium aluminate cement
High performance concrete
fire resistance, 459, 460
freezing resistance, 248, 412
ingredients, 661
High strength concrete, 392, 489, 661, 664
High temperatures
in autoclave, 263, 269, 671
influence on heat of hydration evolution
on hydration, 228
on strength, 198
in oilwell cementing, 649–651
Hillebrandite, 263, 270
Hysteresis, 284, 286, 290, 291, 310, 313, 316, 384
Honeycomb, 150, 208, 252, 378
Hot water concreting, 470
Hydrate primary, 142, 231, 245, 246, 585
Hydrates containing organic anions, 245
Hydration
of calcium aluminate, 166–189
of cement activation energy, 30, 49, 50
influence of accelerators, 145, 146, 148, 189, 226
of calcium chloride, 617
of retarders, 489
mechanism, 144, 182
reactions and products
of clinker phases, 129–196, *see under* Phase names
definition, 8
induction period, 86, 129, 142–145
topochemical reaction, 133
of tricalcium silicate, 131
mechanism, 131
induction period, 146
Hydraulic
activity of slag, 540, 542, 543, 545, 546, 548, 549, 587
modulus, 540, 543, 546, 548
cements, 649
definition
latent, 533
lime, *see* Lime hydraulic
pressure in freezing, 472
Hydrogarnet phases, 264, *see also* C_3AH_6
compositions, 416
formation, 270, 591
durability, 272
from aluminate or ferrite phase, 191
in autoclave processes, 270, 590
Hydrogen
sulphide, 459, 540, 541
Hydrolysis, 131, 146, 192, 208, 215, 226–228, 281, 297, 396, 421, 488, 534, 552, 595, 630, 669, 674
Hydrophilic groups, 474, 491, 511
Hydrophobic
admixtures, 513
Portland cement, 512
Hydrotalcite, 192, 213
composition, 555
formation in hydration of slag cements, 549
Hydrothermal treatment
cement selection, 265
conditions, 654

influence of quartz addition, 268
on contraction, 333
on dormant period, 266
on heat evolution, 228
on hydration degree, 234
on paste phase composition, 270
on set, 237
on strength, 279
on surface, 114
Hydroxylation of tricalcium silicate surface, 231
Hydroxyl–ellestadite, 57
Hyposulphite, 444, 603
Hysteresis loop, 284, 290, 291, 310, 313, 316

I
Ice crystal formation and freeze thaw damage, 475
Illite, 29, 73, 562
enthalpy of dehydroxylation, 138
effect on heat of clinkering, 70
Inclusions of CaO and C_2S in alite, 52
of C_2S in C_3A, 208
Incongruent dissolution
melting, 133, 182, 595
Induction period, 142
after, 146, 147, 595
before, 186, 217, 218
calcium aluminate cements, 604, 605, 610, 611
calcium silicate pastes, 430, 453, 462, 647
of C_3S, 86
amorphous silica effect, 146, 267
defect effect, 327
mineral additions
CH concentration, 166, 245, 623
Portland cement pastes, 171, 395
Inner product
Portland cement pastes, 151
Inorganic salts
effect on Portland cement hydration, 34
Intercalation, 509
Intercrystalline pores
water, 171
Interfacial transition zone, cement paste and aggregate
model, 474
Intergrinding
fly ash, 553
gypsum, 576
limestone, 576
slag, 553
Interlayer
calcium ions, 158, 159
water, 154, 309, 314, 317, 338, 344, 345, 351
Interlocking, 150, 303
Intermolecules forces, 49, 304
Interstitial matter in Portland cement clinkers
composition, 48, 120
effects of cooling rate, 64
Interstitial sites, 106
Invariant point, 39, 42–47, 57, 59, 134, 169, 171, 178, 180
Ionic radius, 75, 93, 108, 247, 413, 545
Ionic substitutions
polymorph stabilization, 91, 646
reactivities of clinker phases, 213
Ions
aluminate, 171, 205, 214, 215, 416, 420, 421, 424, 446, 548, 556, 594, 618, 628, 634, 635, 641
aluminium, 83, 607
bensosulphonic, 178
carbonic acid, 488
chloride, 164, 165, 234, 360, 426–432, 435–441, 480–484, 577, 663
diffusion in Portland cement pastes, 556
potassium, 164, 176, 205, 232, 400, 404, 412, 413, 580, 594, 672
potential forming, 165
sodium, 99, 176, 189, 226, 489, 516, 519, 555, 594
sulphate, 49, 186, 189, 208, 238, 267, 288, 360, 415–417, 421, 424, 444–446, 456, 504–507, 554, 595
Iron
compounds, 227
sulphite, 177
Iron(II) oxide, *see* Wüstite
in clinker phases, 55
influence on C_3S decomposition, 85–87
Iron(III) hydroxide as product from ferrite phase hydration, 191, 211

J
Jander formula, 22, 24, 28
Jennite structure, 157, 158

K
Kaolinite, 396, 520, 562, 577
heat of dehydroxylation, 29, 577
influence on heat of clinkering, 51, 55, 63, 66, 112, 113
Kilchoanite, 650
Kiln rings, 59, 66
Kinetics of hydration

of calcium silicates formation, 6, 258, 266
of Portland cement clinker formation, 191, 192, 253
Klein's compound, 618
K_2O, 109
$K_2O{\cdot}Al_2O_3$, 109
K_2SO_4, 50, 109, 186, 207, 215, 219, 250, 251, 406, 415, 445, 505, 506, 595, 596, 663, *see also* Potassium sulphate
influence on belite hydration, 211, 641

L

Lafarge, 6, 373, 604, 615, 671
Langbeinite calcium, 109
Larnite, 97, 540
Latent hydraulic
material, 533
slag (definition), 533
Late product, 151
in Portland cement paste, 151
Latex, 672
Leaching of concrete by water, 418
Lead, 112
effect on Portland cement hydration, 236–239
oxide, 236–240
Le Chatelier shrinkage, 8, 9, 11
Legrand formula for yield stress value calculation, 286, 287
Lepol grate, 65
Light microscopy
etching method, 545
of Portland cement clinker, 97
Lignosulphonates, 241, 254, 288, 490–497, 650
as retarders, 491
as water reducers, 650
Lime
for autoclaved aerated concrete, 599
for expansive cement, 617
free, see CaO; Free lime
primary, 87
secondary, 87
history, 1
hydraulic, 2, 3, 7
saturation factor, 42, 69, 107, 121, 199, 458, 641, 643, 645, 646
Limestone
as addition to Portland cement, 115
reactions with calcium aluminate hydrates, 334
Liquation, 32, 51, 544, 545
Liquid phase (in formation of Portland cement clinker), *see also* Clinker melt
composition, 31
pore solution, 207
quantity, 21
solidification, 38
viscosity, 31, 48, 49
Lithium
salts, 436
Loss on ignition of fly ash, 497
Low–alkali cement and admixtures, 403, 408, 603
Low temperatures
effects on Portland cement hydration, 395
relation of concrete strength of cement type, 328

M

Macro Defect Free cement paste, 327, 654
Macropores (definition), 617
Magnesium
carbonate, 70, 651
decomposition enthalpy, 70
chloride, basic, 435, 436, 438, 439
chloride solutions, attack on concrete, 394
hydroxide, *see* Brucite
oxide, *see* Periclase
in Portland cement clinker, 60
oxychloride cement *see also* Sorel cement, 10
sulphate solutions, attack on concrete, 455
Magnetite, 481, 519, 535, 560, 562, 650
Manganese
in clinker, 111, 613
influence on strength, 541
solid solutions in brownmillerite
in C_3S, 105
in slag, 111, 538
Marl, 2, 21, 29, 39, 48, 639
Mayenite, 35
Melamine formaldehyde sulphonate polymers, 495
Melaphyre, 517, 518
Melilite, 540
Melt in clinkering process, *see* Portland cement clinker melt
Melting temperature, 30, 33
Mercury intrusion porosimetry 311
concrete, 312
Portland cement paste, 312
Mercury porosity, 311, 312
Merwinite, 540, 545

Mesopores, 486
Metakaolin
application, 577
as mineral addition to cement and concrete, 577
pozzolanic properties, 562, 566, 577
production, 566, 577
reactivity, 29
structure, 29, 577
Methanol, reactions with C_3S or cement pastes, 309, 361, 362
Methyl cellulose, 654, 672
MgO, *see also* Periclase
in alite, 54, 108
in belite, 108
in C_3A, 108
in $C_2(A,F)$
in clinker, 108
in fly ash, 560
influence on melt viscosity, 30, 51
on strength, 541
in slag, 538, 541
structure, 108
Micro–heterogenity in glass, 545
Micropores (definition), 486
Microscopy
light, 13, 97, 120
scanning electron, 149, 212
transmission electron, 159
Microsilica, *see* Silica fume
Microstructure
calcium aluminate cement paste
paste–aggregate interfaces, 385, 434
paste– steel reinforcement interfaces, 386
Portland cement paste, 210, 218, 303–332
after carbonation, 554
sulphate attack, 447, 448
Middle product, 147
Mineralizers, in Portland cement making, 55, 56, 615, 647
transition phases, 614
Mirabilite and expansion, 487
Mix, concrete
slump loss, 497
workability, 235, 279, 369, 371, 389, 489, 490, 492, 493
fly ash addition, 568
Mix proportions, 269, 373
Modulus of elasticity
composite cement pastes, 389
Portland cement pastes, 267, 344
Molybdate method, *see also* Silicate anion structure
Monocalcium aluminate, 25, 607
hydrate
Monocarboaluminate, 248
Monoclinic, 53, 79–82, 90, 93, 99, 100, 103, 120, 188, 224, 240, 458, 631, 640
Monosulphate (monosulphoaluminate), 171, 174–178, 186–188, 191–194, 229, 252, 396, 415, 420, 421, 424, 437, 449, 455, 487, 554, 589, 595, 620, 623, 634, *see also* $C_4A\bar{S}H_x$ phases; AFm phases
Monticellite, 540
Montmorillonite, 320, 413, 510, 535
Mortars
development, 2, 3
history, 490
Munich model, 315

N

Nagelschmidtite, 63
Na_2O
solid solution in alite, 82, 86, 87
in belite, 86, 93, 94, 98
in C_3A, 99–103
influence on C_3A reactivity, 103
in slag, 542
Naphthalene formaldehyde sulphonate polymers, 495
$NaSO_4 \cdot 10H_2O$, *see* Mirabilite
Nekoite, 258
Newton's liquids, 282, 283, 287, 288, 292, 295
Nitrogen sorption isotherms, 314
Nodulization, in clinker formation, 21, 65
Non evaporable water
Powers–Brownyard model, 338
definition, 304
in Portland cement pastes, 237
Non–gypseous Portland cement, 115
Nuclear magnetic resonance, 9, 137, 155, 163
Nucleation
aluminates, 182, 183
CH, 142, 148
C_2S, 86, 91
C_3S, 51–53
C–S–H, 142, 144, 231
gypsum, 131
heterogeneous, 51, 131, 144
homogenuous, 52, 144, 184
rate, 91, 607
solution alcalinity, 258
surface, 87

Nuclei
CaO, 86
CH, 142
C_2S, 86
C_3S, 144
C–S–H, 144, 208, 247, 253, 591

O
Oilwell cement, 649–651
Okenite, 258, 403
Ono's method (light microscopy), 13, 97, 120
Opal
as aggregate, 397, 408
cement, 535
Organic
acids, 554, 612
cations in AFt phase, 178
Orthoclase, 519
Outer product
definition, 151, 448
in Portland cement paste, 448
Over–solubility curve, 186
Oxygen
active (non bridging), 398, 547
bridging, 49, 324, 547

P
Passivation of steel, 480, 481, 482
Paste, *see under* Starting material, e.g. Portland cement paste, slag cement paste)
Pectolite, 271, 650
Periclase (magnesium oxide)
in Portland cement clinkers, 108, 109
structure, equilibria, 108
volume stability, 12
Permittivity, 245, 300
Perovskite, 540
Pessimum
in alkali silica reaction, 408, 415
Phase
composition, potential, 540
equilibria, high temperature U, 556
Phenolphthalein test, for carbonation, 347
Pyroclastic rocks, 535
Plagioclase, 516, 519, 520
Plasticizers, 241, 280, 281, 335, 364, 489–495, 498, 538
Pleochroite, 606
P_2O_5
in Portland cement making, 111
in slag, 543
solid solution in belite, 63, 98
Polish cement industry development, 5
Polyacrylamides, 514
Polymer–cement
concrete, 672–674
microstructure model, 672
properties, 672
paste, 672
Polymer concrete, 652, 674
Polymerisation
of anions, 49, 345–347, 351, 398, 547, 548
glass–forming, 545, 547
Polymers
adsorption on cement grain, 507, 509
polyacrylic, 500
polyarylosulphonic, 495
polycarboxylanic, 495, 501
influence of ionic strength of solution on side chains configuration, 507
new kinds, 503, 504
structure, 495, 500–505
resins, 492, 495–497, 511, 513, 650, 672, 674
steric effect, 499
Polyol (polyhydroxy alcohol), 509
Pores and porosities, definition
capillary, 151, 213, 304, 311, 312, 317, 337, 340, 349, 352–356, 358, 359, 364, 373, 379, 393, 430, 432, 454, 471, 474, 476, 486, 493, 512, 513, 550, 555, 574, 590, 623, 652, 654, 662, 667
classification, 321
continuous, 352, 353, 357, 486
free water, 305, 307, 308, 338, 664
gel, 304, 317, 321, 356, 431, 470–472, 474, 486, 664, 667
mercury, 311–313, 321, 352, 353, 393
micro, meso, macro, 321
strength
total, total water, 338
water freezing temperature, 470, 477
Pore solution
alkali silica reaction, 397, 399, 404, 411, 412
delayed ettringite formation, 421
Porosity
calculated, 322
of "cement gel" (Powers–Brownyard), 434
Portland cement, *see* Cement
chemical analysis, 14
constituent phases, 72–123
high early strength, 199, 548

hydration
at high temperatures, 258–272
at low temperatures, 226
in autoclave process, 258–272
low alkalis, 403, 408, 603, 629
low heat, 16, 195, 553, 571, 603, 604
phase compositions of particle size fractions, 256
rapid hardening, 638–641
reactions during silos storage, 224, 257, 258
specific surface area, 10, 116
sulphate resisting, 15, 16, 116, 393, 432, 441, 442, 450, 452, 603, 604, 637
types of, 17, 18
unsoundness, 242
water demand, 14, 196–198, 369, 370
white, *see* White portland cement
Portland cement clinker
calculation of phase composition, 15
clinkering process, 48–69
of reducing conditions, 35, 39, 65, 101, 613–615
influence of minor components, 52, 55, 64, 70, 93, 94, 111–115
enthalpy of clinkering formation, 75
light microscopy, 116–122
melt
content, 21, 112
peritectic, 38
quantity, 21
viscosity, 28, 49–51, 112, 117
minor components, 111–115
reactions during formation, 21–77
phosphates, 51, 96
reactivities of individual phases, 77, 85, 96, 103, 111
typical compositions of phases, 116
Portland cement paste
calorimetry, 16, 132, 133, 199
chemical composition, 212
constituent phases, 129–191, 205–271, 334
creep, 349–351
effects of admixtures
enthalpy changes during hydration, 138
heat treatment, 265–272
quartz addition, 268
effect on hydration degree, 265, 266
on strength, 267–269, 271, 272
resistance to sulphate attack, 272
microstructure, 303–332
models of structure, 315–320, 324
pore structure, 320–322
relations to physical properties, 369–374
setting
effect of difference calcium sulphate phases, 213–225
very high strength, 652–655
Portland cement with mineral additions, *see also* Composite cement
with fillers, 574–577
with fly ash, 567–573, *see also* Fly ash
coefficient of ions diffusion in paste, 568
influence of temperature on hydration, 567, 569
on strength, 567, 569
with limestone, 17, 514, 575
with metakaolin, 577, 578
with silica fume, *see* Silica fume
with slag, *see* Slag cement
Portlandite, *see* Calcium hydroxide
Potassium
calcium sulphate, *see* Calcium langbeinite
hydrated, *see* Syngenite
carbonate, 225, 252, 395, 413, 467
chloride, 405
oxide, 109
sodium sulphate, *see* Aphthitalite
solid solution in C_3A, 100, 103
in Portland cement clinker, 109
sulphate, 50, 109, 186, 207, 211, 215, 219, 250, 251, 406, 415, 445, 505, 506, 595, 663, *see* also K_2SO_4; Arcanite
Potential
electric of the surface, 297
electrokinetic, 233, 299, 300, 499, 623
ionic, 247, 545
Pourbaix diagram, 480
Powers–Brownyard model, 434
Powers formula, 597
Pozzolanas
natural, 2, 407, 410, 533, 535, 536, 563, 590, 641
influence on strength, 535, 536, 563
Pozzolanic
activity, 14, 383, 535, 536, 557, 558, 562–565, 576
cements, 2, 17, 407, 430, 535, 564
resistance to alkali silica reaction, 407, 408, 410, 413
to corrosion, 407, 408, 430, 441, 451, 458, 463
siliceous fly ash, 148, 196, 198, 207, 271, 295
test methods, 535, 536, 559
Precalciners in rotary kilns, 6
Preheaters in rotary kilns, 66, 109

Pre–induction period, 186, 217, 218
Primary flue gas desulphurization, residues from, 566
Proto C_3A, 101, 103
Protonation, 138, 158, 159, 182, 590
Pseudo–wollastonite, 540
Pyrite, 395
Pyrocatechol, 246
Pyrrhotite, 395
Pyroxene, 517, 519, 535

Q
Quantitative X–ray diffraction analysis
  Portland cement clinker, 76
Quartz, 25, 26, 29, 48, 117, 120, 121, 268–271, 280, 324, 397, 517, 520, 561, 670
  reactions in cement making, 48, 68
    polymorphism, 24, 29, 118
Quick set, 219, 251, 253

R
Radiolarians, 535
Radius, *see* Ionic radius
Rankinite, 21, 32, 35, 270, 540
Raoult's law for vapour pressure, 472
Rare earth, 85, 96, 469
Rate equations, in calcium silicate formation, 132
Reaction
  meritectic, 32, 34, 37
  through solution, 183, 581
Reactive sites
  on alite surface, 87
Reactivities of phases
  calcium aluminate cements, 604–613
  Portland cements, 10, 72–122, 195, 347, 353, 465, 547, 573, 586, 588, 605, 636, 657
Recrystallization
  of alite, 53, 54, 64
  of belite, 64, 636
  of C_4AF gel, 191
  ettringite layer, 188
Reducing conditions, in making Portland cement clinker, 101
Reducers of chromium(VI), *see* Chromium reducers
Rezorcine, 246
Resorption, 37, 38, 42, 46, 47
Retarders
  calcium aluminate cements, 233
  of hardening, 234–247, 506
  oilwell cementing, 49–51
  organic, mechanism, 241–247, 476, 493, 513, 514, 575
    K_2CO_3 effect, 612
  of setting, 234, 236, 242
    calcium phosphates, mechanism, 241
    inversion effect, 162
    sodium fluoride, 241
Rheology
  Bingham's formula, 282, 283
  effects of water reducers and superplasticizers, 295
  Hershell–Bulkely's formula, 293
  models 281, 295
Ring in rotary kilns, 66
Roman buildings, 7
Roman cement, 2, 641
Rotary kiln, flash, 21, 212, 213, 219, 574
Ryolite, 400, 534

S
Saccharides hydrolized, 241, 242, 244, 491
Saccharose, 241
Salt scaling, 426, 476, 477
Sand
  quartz, 284, 392, 399, 403, 404, 424, 513, 534, 651, 664
Santorin Earth, 1, 535
Saturation factor, *see also* Lime saturation factor, 42, 69, 107, 121, 199, 458, 641, 643, 645–657
Scanning electron microscopy
  concrete, 147
    at aggregate–cement paste interface, 369
    fly ash, 147, 148
  from fluidized bed combustion, 563
  siliceous, 599
  Portland cement paste, 622
  attacked by sulphates, 445
  C–S–H after chloride solution attack, 445
Scawtite, 262, 267, 271, 650
Sea water
  attack, 11, 441, 447, 454–458, 550, 552, 556, 568, 572, 611
    calcium aluminate cements, 611
    concrete, 395, 436, 441, 447, 454–458, 475, 487, 550–556, 559, 560, 565–576
  composition, 11, 398, 447, 454–459, 467, 468, 611
Self–drying, 335, 338, 339, 340, 348
Separation of phases in Portland cement, 32

Set
correlation with induction period, 214, 219, 227, 239, 247, 591
regulator without gypsum, 215, *see also* On–gypseous Portland cement
trietanolamine effect, 227, 241
Setting
calcium aluminate cement, 334, 603, 610, 641
definition, 10, 12, 603
effect of hemihydrate, 221
of temperature, 238, 248, 492
Portland cement paste, 222, 268
false set, 220, 221, 253, 291, 336, 372, 467, 490, 492
flash set, 214, 221
Sewage, attack on concrete, 459
Shrinkage
autogeneous, 332, 335, 338, 340, 341, 349, 510
carbonation, 347, 348, 462
chemical, *see* Contraction
drying of Portland cement paste, 348, 439
plastic, 279, 333, 336, 337, 341, 510, 513, 571
Silanol groups, 159–165, 397, 398, 590
Silica
active, 145, 382, 394, 396–398, 404, 408, 516, 518, 534, 574
solubility, 599
fume, 17, 328, 356, 382, 383, 388, 392, 407, 409, 410, 421, 425, 429, 430, 435, 464, 469, 475, 476, 510, 513, 514, 573, 574, 661, 663, 665–667, 669, 670
formation, composition, physical properties, 647
influence on cement paste–aggregate bond, 383
on concrete properties, 356
on pore structures, 356
in high performance concrete, 392
influence on water demand, 467
ratio (silica modulus) and strength, 439, 638
reactive, *see* Alkali–silica reaction
Silicate anion structure
calcium silicate pastes, 258
with admixtures, 255
C–S–H(I), 157
Portland cement pastes, 192
pozzolanic cement pastes, 312
1.4 nm tobermorite and jennite, 262
Silicate anions, species in solution, 165
Siliceous aggregates, potentially reactive
Siliceous fly ash, *see* Fly ash
Silicosulphate, *see* Spurrite silicate
Slag blastfurnace granulated
activators of hydration, 533, 550
classification, 533, 534, 535
composition, 36, 148, 195, 199, 270, 430, 458, 510, 534, 538, 539, 550, 554, 606, 663
effect on clinker phases hydration
of composition on properties, 595
on glass content on strength, 199
on setting, 550
of MO_6/MO_4 ratio, 50
exothermic effect of clinkering, 69, 70
glass, 199, 407, 489, 535, 550, 606
aluminium effect, 70, 60, 76, 83, 101, 106, 111, 167, 269, 546, 591, 597, 607
composition, 36, 148, 195, 199, 270, 430, 458, 510, 534, 538, 550, 554, 606, 663
grindability, 219, 549, 558, 575, 628
hydration, 114, 148, 195, 198, 199, 270, 406, 407, 431, 489, 509, 554, 606, 663
mechanism, 146, 358, 408, 430, 441, 458, 489, 607, 662
hydraulic activity, 549
influence on clinker hydration, 112
phases formed, 270
solubility, 271, 431, 458, 489
Slag cement
heat of hydration, 115, 192, 199
hydration at low temperatures, 191, 553
hydration chemistry, microstructure, 589, 590
paste resistance to corrosion, 612
to chloride attack , 426, 456, 572
pore structures and physical properties, 192, 574
sea water attack, 456–458
sulphate attack, 361, 441, 458
Slump, 496, 497, 665
Slump loss, 497
SO_3 (as oxide component; *see also* Individual phases), 52, 215, 418, 620
in clinker formation, 69, 70, 103
in Portland cement hydration products, 243
Sodium
carbonate, hydrated, *see* Mirabilite
chloride, in oilwell cementing, 649–651

equivalent, 12, 404, 408, 418
fluoride, 236, 241
silicate, 103, 398, 399, 555
sulphate, 248, 250, 444, 487
solutions, attack on concrete, 572
Soft water
attack on concrete, 395, 467–469, 612
Solid solutions, *see under* Phases names
CH in tobermorite, 158
by extraction, 76, 636
by substitution, 53, 76, 83–85, 93–96, 100–103, 158, 164, 272, 516, 519, 606, 645
testing method, 427
Solid–state reactions
formulae of Jander and Ginstling, 26
Solubility curves
$CaO–Al_2O_3–H2O$ and related systems, 24, 25, 31, 32, 35, 36, 167, 178
$CaO–SiO_2–H_2O$ system, 24, 31–34, 41, 134,
Solubility product, 173, 436, 444, 586, 627
Soluble salts
and damage to concrete, 472
Sorption isotherms, 310, 633
Specific surface areas
calcium silicate and cement pastes, 468
cements, 468
effect on hydration kinetics, 217, 218
Spinel, 519, 540, 606
Spurrite
formation in cement kiln, 66–69, 425, 636
in kilns preheater, 61, 66, 69
chromate, 56
sulphate, 66
in rotary kiln, 66, 67, 69, 425, 636
Starch, 241, 490
Steam curing
high pressure, 393, 629
low pressure, 268, 316, 396, 598, 634, 670
Steel
corrosion, 481, 484, 577
interface with paste, 235, 375, 386, 387, 573
Stern's layer
diffusion, 297
duplex, 297
external, 165
internal, 165
Strätlingite, *see* C_2ASH_8
Strength
and pore structure, 441
calcium aluminate cements, 396
development, 10–12, 16, 199, 214, 218, 225
microsilica cements, 557
Portland cements, 251, 550, 641
slag cement, 553
of paste, 372
correlation with heat of hydration, 604
heat treatment, Na_2O effect, 603
effect of crystals dimensions
of crystals shapes, 599
of tobermorite, 650
Strontium, 469
Sucrose and other organic compounds, as retarders, 236, 243, 493
Sulphate
attack, 456
calcium aluminate cements, 438, 458
composite cements, 454
internal, 415
Portland cements, 454
supersulphated cement, 455
corrosion, 447 *see under* Corrosion
tests, 449
thaumasite formation, 452
zonal composition changes of paste, 446
ions in C–S–H phase, 449
phases in Portland cement clinker
on cement compatibility with admixtures, 372
estimation from bulk analysis, 650
formation, 620
light microscopy, 97
resisting Portland cements, 432
mechanism of resistance, 441
Sulphates
paste resistance, 612
as solid solutions in C_3A, 506
in C_2S, 506
in C_3S, 506
influence on rheology, 281
Sulphide ion
attack on concrete, 397
in cement hydration, 533
in slag and slag cement, 541
Sulphites in aggregate, 177
Sulphospurrite ($C_5S_2\overline{S}$), *see* Spurrite; Sulphate
Sulphuric acid
attack on concrete, 395–397, 459
Superplasticizers, 199, 295, 364, 373, 374, 388, 441, 489, 495–510, 559, 573, 653, 661, 664, 668–670
Supersulphated cements
resistance to sulphate attack, 554
Surface, 10, 11, 22, 29, 31, 33 passim

Surfactants, 254, 274, 291, 493, 494, 510, 511, 559, 672
Swelling
of air, 251, 320, 616
effect on surface energy, 315
Syngenite
formation and effects on cement hydration, 221
formation during cement storage, 66
Synthetic resins
cations changeable, 227
epoxyde, 227
phenol, 227
System(s)
"CaO–Al_2O_3", 35
"CaO–Al_2O_3–Fe_2O_3", 40, 41, 605
"CaO–Al_2O_3–Fe_2O_3–SiO2", 41–45
"CaO–Al_2O_3–SiO_2", 35–39, 47, 48, 59, 60, 83, 605
"CaO–C_2S–C_4AF", 47
"CaO–C_2S–$C_{12}A_7$–C_2F", 43–46
"CaO–C_2S–$C_{12}A_7$–C_4AF", 42
"CaO–Fe_2O_3", 39
"CaO–Fe_2O_3–SiO_2", 39, 40
"CaO–MgO–Al_2O_3–SiO_2", 83, 84
"CaO–SiO_2", 32–35, 55
"CaO–SiO_2–$CaSO_4$", 63
"$CaSO_4$–CaF_2–Ca_2SiO_4", 58
System(s), hydrated
"CaO–$CaSO_4$–SiO_2–H_2O" (heat treated at 235oC), 270
"CaO–Al_2O_3–H_2O", 31, 166–171, 182, 183, 191, 607, 608
"CaO–Al_2O_3–SiO_2–H_2O", 537
"CaO–Al_2O_3–SO_3–H_2O", 174, 175

T

Temperature
effect on cement hydration kinetics, 167, 205, 207, 226, 237, 238, 250, 471, 493, 616–618, 653
Tetracalcium aluminoferrite, *see* Ferrite (phase)
Tetrahedra, paired and bridging
in glass, 547
aluminates, 546, 547
silicates, 546, 547
Thaumasite
route of formation, 452, 453
structure, thermal behaviour, 445
from sulphate attack with carbonation, 452
Thermal
gradient, 69, 198, 269, 332, 459, 571, 665
insulation materials, autoclaved, 271
shock, 477, 611
treatment, 96, 265, 269–272, 345, 373, 414–421, 425, 495, 567, 572, 577, 603, 630, 636, *see also* Heat treatment
conditions, 259, 269, 271
influence of quartz addition, 268
effect on contraction, 333, 334, 336
on hydration degree, 663
on paste phase composition, 615
on specific surface area, 334
on strength, 334
phases transformation, 351
transition phases, 269
Thermochemistry
aluminate and ferrite phase hydration, 211
calcium hydroxide dissolution, 215
calcium silicate hydration, 131, 147
clinker formation, 69
Portland cement hydration
phases hydration, 253
Thermodynamics, 341
Thixotropy, 285, 286, 289, 290, 303, 578, 651
Titanium
in clinker, 111
oxide, 111
solid solution in C_3A, 111
influence on C_3A hydration, 189
on C_4AF hydration, 111, 540
in slag, 540, 606
Tobermorite
1.1 nm, 264–266, 269–272
1.4 nm, 152, 153, 157–159, 265
formation, 263
shrinkage, 272
solid solutions
with Al, 272
with SO_4^{2-}, 262
Tobermorite gel, 152
Topochemical reaction, 133, 621, 627
Topotactic reaction, 265
Total (water) porosity, 320, 328, 352, 353, 354, 464
Toughness, 325, 327
Transformation degree
protonation, 412
Transition phases
and Portland cement making, 269
Transitional zone, *see* Interfacial transition zone
Trass, 2, 425, 535
Tributhyl phosphate, 492
Tricalcium aluminate, *see* C_3A
Tricalcium silicate, *see also* Alite

heat of hydration, 192
hydration, 131, 146
surface composition, 85
thermal stability, 82
X–ray powder patterns, 79
Tricalcium silicate hydrate, 131–141, 146, 262
Tridymite, 24, 33, 40, 397
Triethanoloamine, and cement hydration, 492, 545, 546
strength, 241, 242, 252
Trimer, 154
Trimethylsilylation, *see also* Silicate anion structure, 154, 346
Truscottite, 261, 264, 271, 272
Tuff, 1, 2, 7, 403, 535

U
Unsoundness of cement, 242
U phase, 556

V
Vacancy
calcium, 84, 94, 144
cationic, 76
octahedral, 83
oxygen, 95, 97, 140
silicon, 85
tetrahedral, 95
Vanadium111, 613, 614
van der Waals attracting bonds, 225, 296, 297, 300–303, 308, 319, 324, 328, 344
Vaterite, 461, 462
Vegard's rule, 76
Vermiculite, 316, 320, 397
Vicat, 3, 14, 15, 254, 281, 346, 441
Viscometer, 14, 281, 289, 292–294
Viscosity
modifiers, 514
plastic, 279, 280, 283, 497, 508, 510
Void spacing factor, 474, 475, 478, 576
Volatiles
circulation in cement kiln, 59, 64, 66
Volcanic deposit, 1
Volume changes, in concrete on freezing, 339, 341, 348, 437, 439, 615–617

W
Wall effect, 379
Washburn equation, 312
Waste material utilization
composite cements, 265
low energy cements, 603, 641–647
Portland cement clinker production, 566
Water
adsorbed, 154, 305–308, 314, 315, 319, 349, 470
freezing temperature, 470
bleed, 332, 335, 379, 494, 578
bond in hydrates, 158
bound, 470
capillary, 304, 307, 344, 470
to cement ratio, minimum for complete hydration, 207, 286
of crystallization, 305
demand for Portland cement, 196–198
porosity, 196
effect of fly ash, 196, 198
evaporable, 305, 360
free, 305, 307, 338
substitution by propanol, 338
by organic fluids, 305
in gel, 304
layer on cement grains, 286
non–evaporable, 237, 252, 266, 309, 338, 348
physical, 304
reducers, 301, 364, 490, 492, 650, 669
desorption isotherms, 633
vapour influence on C3S decomposition, 190
workability of concrete mix, 515
Water–repellent admixtures, 652
Weathering, 516
White Portland cements, 610, 613
Wollastonite, 32, 35, 118, 156, 158, 260, 263, 264, 270, 519, 540
Workability
effect of fly ash, 568
of water reducers, 492
of superplasticizers, 490–493
Wüstite, 604, 606

X
Xonotlite, 259, 263–265, 267, 269–271, 323, 650
X–ray microanalysis
C_3S, 9
Portland cement pastes, 101
X–ray powder diffraction
C_3S, 76, 205
C–S–H, 152
X–ray scattering
small angle, 163, 309, 545
Xerogel
definition, 315, 319, 351
Xonotlite
structure, 263, 264

Y
Yield stress value, 280, 283, 284, 286, 287, 290–295, 371, 508, 510, 514, 668
Young's modulus, *see* Elasticity
Ytr, 85, 96

Z
Zeolites, as pozzolanic materials
  synthesis from fly ash, 270, 537
Zeta potential, 244, 299–301, 493
Zinc
  in cement hydration, 387
  in clinker making
  oxide, 114, 239
  phases formation, 113, 114
  retarding mechanism, 113
  substitution in alite, 236
Zoning
  in alite, 65